Evaluation of Analytical Tools for Determining the Seismic Response of Reinforced Concrete Shear Walls

Paul Erling Oyen

A thesis submitted in partial fulfillment
of the requirements for the degree of

Master of Science in Civil Engineering

University of Washington

2006

Program Authorized to Offer Degree: Civil & Environmental Engineering

Volume One

University of Washington
Graduate School

This is to certify that I have examined this copy of a master's thesis by

Paul Erling Oyen

and have found that it is complete and satisfactory in all respects,
and that any and all revisions required by the final
examining committee have been made.

Committee Members:

_____
Laura Lowes

_____
Dawn Lehman

_____
Gregory Miller

Date: _____

In presenting this thesis in partial fulfillment of the requirements for a master's degree at the University of Washington, I agree that the Library shall make its copies freely available for inspection. I further agree that extensive copying of this thesis is allowable only for scholarly purposes, consistent with "fair use" as prescribed in the U.S. Copyright Law. Any other reproduction for any purpose or by any means shall not be allowed without my written permission.

Signature_____

Date_____

University of Washington

Abstract

Evaluation of Analytical Tools for Determining the Seismic Response of Reinforced Concrete Shear Walls

Paul Erling Oyen

Co-Chairs of the Supervisory Committee:
Professor Laura Lowes
Department of Civil and Environmental Engineering

Professor Dawn Lehman
Department of Civil and Environmental Engineering

Recent advances in computational capabilities, both hardware and software, have made nonlinear analysis a viable tool for seismic structural engineering. However, to fully realize these capabilities, data management tools and analysis parameter recommendations are required and have not been developed for reinforced concrete shear walls. Therefore, a study was conducted to evaluate commonly available nonlinear analysis techniques to predict wall response to lateral loading including the development of an object-oriented framework in MATLAB to manage analyses. The following models were considered: (1.) distributed plasticity push-over, (2.) lumped plasticity push-over, (3.) 2D continuum analysis utilizing the modified compression field theory (MCFT), and (4.) distributed plasticity push-over utilizing the MCFT. Comparison of the analytical to experimental data reveals that the inclusion of bar-slip and shear deformation effects improve the prediction of wall behavior. The study concludes with the calibration of a linear shear model for inclusion with the distributed plasticity analysis method.

TABLE OF CONTENTS

List of Figures vi

List of Tables lxi

Volume One **1**

Chapter 1 Introduction 1
- 1.1 Objectives 1
- 1.2 Methods 1
- 1.3 Outline of the Thesis 2

Chapter 2 Background 4
- 2.1 Previous Experiments of Structural Walls 4
  - 2.1.1 Compiled Experimental Wall Data 4
  - 2.1.2 Reduced Data Set for Evaluation of MCFT-based models 18
- 2.2 Previous Analyses of Structural Walls 22
  - 2.2.1 Martinelli 23
  - 2.2.2 Ile and Reynouard 23
  - 2.2.3 Palermo 24
  - 2.2.4 Kwan and He 24
- 2.3 OpenSees 25
- 2.4 Data Management in Finite Element Analysis 25

Chapter 3 Preprocessor 29
- 3.1 Preprocessor Overview 30
- 3.2 General Formulation 31
  - 3.2.1 Data Types 31
  - 3.2.2 Transformation of Data 32
  - 3.2.3 Functionality Associated with Data Types 32
  - 3.2.4 Parts of the Preprocessor 33

3.3 Specific Implementation 36
3.3.1 Solver – OpenSees 36
3.3.2 OpenSees Tcl Script Writing Classes 37
3.3.3 Processed Data – Processed_OpenSees 37
3.3.4 Data Processor – DataProcessor_SW 42
3.3.5 Data Processor Generator 45
3.3.6 Raw Data – WallData 45
3.3.7 Raw Data Generator – WallDataGenerator_WallInfo050922 45
3.3.8 Global Driver 46
3.4 Using the Preprocessor 46
3.5 Summary 46

Chapter 4 Evaluation of Beam-Column Elements for Simulation of Structural Walls 47
4.1 Introduction/Overview 47
4.1.1 Research Impetus 47
4.1.2 Approach 47
4.1.3 Organization of Chapter 48
4.2 Description of Simulation Elements and Constitutive Models 48
4.2.1 Cross Section Analysis 49
4.2.2 Lumped Plasticity Beam-Column Element 52
4.2.3 Distributed Plasticity Beam-Column Element 53
4.2.4 Typical Predicted Force-Displacement Response Curves 53
4.3 Description of Evaluation Method 54
4.3.1 Description of Wall Characteristics 54
4.3.2 Description of Measured Response Quantities 57
4.3.3 Description of Simulated Response Quantities 58
4.3.4 Method of Determining Quality of Results 59
4.4 Flexural Strength Analysis 59
4.4.1 Comparison of Experimental and Analytical Results 59
4.4.2 Influence of Wall Parameters on Strength Prediction 61
4.4.3 Summary 68
4.5 Initial Stiffness and Yield Displacement Capacity 69
4.5.1 Comparison of Experimental and Predicted Results 69
4.5.2 Influence of Wall Parameters 72
4.5.3 Summary 86

4.6 Maximum Displacement Capacity 86
4.6.1 Comparison of Experimental and Predicted Results 86
4.6.2 Influence of Wall Parameters 89
4.6.3 Summary 103
4.7 Comparison of Lumped-Plasticity and Distributed-Plasticity Analytical Results 103

Chapter 5 Response-2000 105
5.1 Sectional Analysis in Response-2000 105
5.2 Full Member Analysis in Response-2000 109
5.3 Response-2000 Results 112
5.4 Response-2000 Discussion 112
5.5 Response-2000 Summary 116

Chapter 6 VecTor2 117
6.1 Modeling Decisions 117
6.2 Analysis Output Evaluation Method 119
6.3 Description of Results 119
6.3.1 Oesterle B1 119
6.3.2 Oesterle B6 127
6.3.3 Pilakoutas SW7 133
6.4 Discussion and Comparison of Results 141

Chapter 7 Enhanced Beam-Column Element 142
7.1 Description of Evaluation Method 142
7.2 The Bar-Slip Model 143
7.2.1 Implementation with Distributed Plasticity Model 143
7.2.2 Theoretical Bar-Slip Model 146
7.2.3 Results Using Bar-Slip Model 149
7.2.4 Typical Response Curves of Bar-Slip Model 154
7.2.5 Effect of Bar-Slip on Secant Stiffness and Yield Displacement Prediction 156
7.2.6 Effect of Bar-Slip on Maximum Displacement Prediction 157
7.3 Elastic Shear Model 159
7.3.1 Theoretical Model and Implementation 159
7.3.2 Typical Response Curves of Elastic Shear Model 165
7.3.3 Effect of Elastic Shear on Prediction of Displacements 165
7.4 Calibration of the Elastic Effective Shear Modulus Model 165

7.4.1 Method . . . 167
7.4.2 Calibrated Parameters . . . 167
7.4.3 Results of Example Walls . . . 183
7.4.4 Displacement Prediction Using Shear Models Calibrated to Yield Displacement . . . 185
7.4.5 Displacement Prediction Using Shear Models Calibrated to Maximum Displacement . . . 185
7.5 Conclusions . . . 186

Chapter 8 Discussion and Conclusions . . . 187
8.1 Summary of Research Program . . . 187
8.2 Recommendations for Future Preprocessor Implementations . . . 189
8.3 Recommendations for Nonlinear Analysis of Shear Walls . . . 190
8.4 Recommendations for Future Development of Analysis Methods . . . 191

Bibliography . . . 193

Volume Two **198**

Appendix A The Modified Compression Field Theory . . . 198
A.1 MCFT Assumptions . . . 198
A.2 MCFT Steps . . . 199
A.3 Material Model for Average Tensile Stress in Concrete . . . 199
A.4 Material Model for Concrete in Compression . . . 200
A.5 Material Model for Average Stress in Reinforcement . . . 201
A.6 The Crack Check . . . 202
A.7 Applicability of the MCFT . . . 202

Appendix B Moment Curvature Analysis Figures . . . 203

Appendix C Moment Curvature Analysis Figures – Compare Programs . . . 234

Appendix D Strength Prediction Versus Design Parameter Figures . . . 265

Appendix E Beam-Column Element Push Over Analysis Figures . . . 276

Appendix F Lumped Plasticity Predictions Versus Design Parameter Figures . . . 307

Appendix G Distributed Plasticity Predictions Versus Design Parameter Figures . . 323

Appendix H Calibrated Linear Shear Coefficients Versus Design Parameter Figures 339

Appendix I Bar-Slip Push Over Analysis Figures 360

Appendix J Bar-Slip Predictions Compared to Design Parameter Figures 391

Appendix K Bar-Slip Change in Error Compared to Design Parameter Figures . . . 407

Appendix L Effective Shear Model Predictions Compared to Design Parameter Figures 438

Volume Three **514**

Appendix M Elastic Effective Shear Push Over Analysis Figures 514

Appendix N Effective Shear Model Prediction Error Change Compared to Design Parameter Figures 665

LIST OF FIGURES

Figure Number Page

2.1 Experimental Behavior of Oesterle B1 19
2.2 Experimental Damage of Oesterle B1 19
2.3 Experimental Behavior of Oesterle B6 21
2.4 Experimental Damage of Oesterle B6 21
2.5 Experimental Behavior of Pilakoutas SW7 22
2.6 Experimental Damage of Pilakoutas SW7 23

3.1 Transformation of Data in the Preprocessor 33
3.2 The Global Processor Run Command 35
3.3 Preprocessor Top Level Classes and Associations 36
3.4 Processed Data Organization and Associations 40
3.5 General Data Processor Organization and Associations 43

4.1 Lumped Plasticity Force Based Element 49
4.2 Force Based Distributed Plasticity Element 50
4.3 Wall Cross Section Definitions for Sectional Analysis 51
4.4 Cyclic Example of Giuffré Menegotto Pinto Model 52
4.5 Comparison of Experimental and Analytical Force-Displacement Curves - Oesterle B1 54
4.6 Comparison of Experimental and Analytical Force-Displacement Curves - Oesterle B6 55
4.7 Comparison of Experimental and Analytical Force-Displacement Curves - Pilakoutas SW7 55
4.8 Maximum Moment Prediction Ratio v. Normalized Thickness 62
4.9 Maximum Moment Prediction Ratio v. Aspect Ratio 63
4.10 Maximum Moment Prediction Ratio v. Axial Load Ratio 64
4.11 Maximum Moment Prediction Ratio v. Horizontal Reinforcement Ratio . . 65
4.12 Maximum Moment Prediction Ratio v. Longitudinal Reinforcement Ratio in the Boundary Element 66
4.13 Maximum Moment Prediction Ratio v. Maximum Shear Stress Ratio 67

4.14 Maximum Moment Prediction Ratio v. Maximum Shear Demand Ratio . . 68
4.15 Lumped-Plasticity Secant Stiffness Up To Yield v. Normalized Thickness . 72
4.16 Distributed-Plasticity Secant Stiffness Up To Yield v. Normalized Thickness 73
4.17 Lumped-Plasticity Secant Stiffness Up To Yield v. Aspect Ratio 74
4.18 Distributed-Plasticity Secant Stiffness Up To Yield v. Aspect Ratio 75
4.19 Lumped-Plasticity Secant Stiffness Up To Yield v. Axial Load Ratio 76
4.20 Distributed-Plasticity Secant Stiffness Up To Yield v. Axial Load Ratio . . 77
4.21 Lumped-Plasticity Secant Stiffness Up To Yield v. Horizontal Reinforcement Ratio 78
4.22 Distributed-Plasticity Secant Stiffness Up To Yield v. Horizontal Reinforcement Ratio 79
4.23 Lumped-Plasticity Secant Stiffness Up To Yield v. Longitudinal Reinforcement Ratio in the Boundary Element 80
4.24 Distributed-Plasticity Secant Stiffness Up To Yield v. Longitudinal Reinforcement Ratio in the Boundary Element 81
4.25 Lumped-Plasticity Secant Stiffness Up To Yield v. Shear Stress Ratio at Yield 82
4.26 Distributed-Plasticity Secant Stiffness Up To Yield v. Shear Stress Ratio at Yield 83
4.27 Lumped-Plasticity Secant Stiffness Up To Yield v. Shear Demand Ratio at Yield 84
4.28 Distributed-Plasticity Secant Stiffness Up To Yield v. Shear Demand Ratio at Yield 85
4.29 Lumped-Plasticity Maximum Displacement Prediction Ratio v. Normalized Thickness 89
4.30 Distributed-Plasticity Maximum Displacement Prediction Ratio v. Normalized Thickness 90
4.31 Lumped-Plasticity Maximum Displacement Prediction Ratio v. Aspect Ratio 91
4.32 Distributed-Plasticity Maximum Displacement Prediction Ratio v. Aspect Ratio 92
4.33 Lumped-Plasticity Maximum Displacement Prediction Ratio v. Axial Load Ratio 93
4.34 Distributed-Plasticity Maximum Displacement Prediction Ratio v. Axial Load Ratio 94
4.35 Lumped-Plasticity Maximum Displacement Prediction Ratio v. Horizontal Reinforcement Ratio 95

4.36 Distributed-Plasticity Maximum Displacement Prediction Ratio v. Horizontal Reinforcement Ratio . . . 96
4.37 Lumped-Plasticity Maximum Displacement Prediction Ratio v. Longitudinal Reinforcement Ratio in the Boundary Element . . . 97
4.38 Distributed-Plasticity Maximum Displacement Prediction Ratio v. Longitudinal Reinforcement Ratio in the Boundary Element . . . 98
4.39 Lumped-Plasticity Maximum Displacement Prediction Ratio v. Maximum Shear Stress Ratio . . . 99
4.40 Distributed-Plasticity Maximum Displacement Prediction Ratio v. Maximum Shear Stress Ratio . . . 100
4.41 Lumped-Plasticity Maximum Displacement Prediction Ratio v. Maximum Shear Demand Ratio . . . 101
4.42 Distributed-Plasticity Maximum Displacement Prediction Ratio v. Maximum Shear Demand Ratio . . . 102

5.1 Differential Element for Determination of Shear at Cross Section . . . 107
5.2 Free Body Diagram for Concrete Layer k . . . 108
5.3 Shear and Moment in Wall Assumed by Response-2000 . . . 110
5.4 Flexural Failure in Response-2000 . . . 111
5.5 Shear Influenced Failure in Response-2000 . . . 111
5.6 Oesterle B1 - Shear Stress Ratio v. Drift from Response-2000 . . . 113
5.7 Oesterle B6 - Shear Stress Ratio v. Drift from Response-2000 . . . 114
5.8 Pilakoutas SW7 - Shear Stress Ratio v. Drift from Response-2000 . . . 114

6.1 VecTor2 Predicted Response of Oesterle B1 . . . 121
6.2 Initial Cracking of Oesterle B1 by VecTor2 . . . 122
6.3 First Yield of Oesterle B1 by VecTor2 . . . 123
6.4 Onset of Reduced Convergence of Oesterle B1 by VecTor2 . . . 124
6.5 Oesterle B1 at Observed Maximum Displacement by VecTor2 . . . 125
6.6 Predicted Maximum Drift of Oesterle B1 by VecTor2 . . . 126
6.7 VecTor2 Predicted Response of Oesterle B6 . . . 128
6.8 Initial Cracking of Oesterle B6 by VecTor2 . . . 129
6.9 First Yield of Oesterle B6 by VecTor2 . . . 130
6.10 Oesterle B6 Halfway Between Yield and Max Drift by VecTor2 . . . 131
6.11 Predicted Maximum Drift of Oesterle B6 by VecTor2 . . . 132
6.12 VecTor2 Predicted Response of Pilakoutas SW7 . . . 134
6.13 Initial Cracking of Pilakoutas SW7 by VecTor2 . . . 135

6.14 Pilakoutas SW7 at Observed Diagonal Cracking Displacement by VecTor2 . 136
6.15 Pilakoutas SW7 Experimental Crack Patterns at Three Levels of Drift . . . 137
6.16 First Yield of Pilakoutas SW7 by VecTor2 138
6.17 Pilakoutas SW7 Halfway Between Yield and Max Drift by VecTor2 139
6.18 Predicted Maximum Drift of Pilakoutas SW7 by VecTor2 140

7.1 Implementation of Bar Slip Model with Distributed Plasticity Element . . . 144
7.2 Definition of Bar Slip Material Model 145
7.3 Assumed Compressive Depth 146
7.4 Stress and Strain Distribution of an Anchored Bar 148
7.5 Pushover of Beam-Column Element with Bar-Slip – Oesterle B1 154
7.6 Pushover of Beam-Column Element with Bar-Slip – Oesterle B6 155
7.7 Pushover of Beam-Column Element with Bar-Slip – Pilakoutas SW7 155
7.8 Initial Stiffness Absolute Difference in Error v. Aspect Ratio Using Beam-Column Element with Bar-Slip Enhancement 156
7.9 Initial Stiffness Absolute Difference in Error v. Longitudinal Reinforcement Ratio in BE Using Beam-Column Element with Bar-Slip Enhancement . . . 157
7.10 Maximum Displacement Absolute Difference in Error v. Aspect Ratio Using Beam-Column Element with Bar-Slip Enhancement 158
7.11 Maximum Displacement Absolute Difference in Error v. Longitudinal Reinforcement Ratio in BE Using Beam-Column Element with Bar-Slip Enhancement 158
7.12 Pushover of Beam-Column Element with Elastic Shear – Oesterle B1 165
7.13 Pushover of Beam-Column Element with Elastic Shear – Oesterle B6 166
7.14 Pushover of Beam-Column Element with Elastic Shear – Pilakoutas SW7 . 166
7.15 Comparison of predicted behavior of Oesterle B1 using each calibrated parameter 183
7.16 Comparison of predicted behavior of Oesterle B6 using each calibrated parameter 184
7.17 Comparison of predicted behavior of Pilakoutas SW7 using each calibrated parameter 184

A.1 Average Concrete Tensile Stress Strain Relationship 200
A.2 Concrete Compressive Stress Strain Relationship 201

B.1 Moment Curvature Analysis – Lefas SW11 204
B.2 Moment Curvature Analysis – Lefas SW12 204
B.3 Moment Curvature Analysis – Lefas SW13 205

B.4 Moment Curvature Analysis – Lefas SW14 205
B.5 Moment Curvature Analysis – Lefas SW15 206
B.6 Moment Curvature Analysis – Lefas SW16 206
B.7 Moment Curvature Analysis – Lefas SW17 207
B.8 Moment Curvature Analysis – Lefas SW21 207
B.9 Moment Curvature Analysis – Lefas SW22 208
B.10 Moment Curvature Analysis – Lefas SW23 208
B.11 Moment Curvature Analysis – Lefas SW24 209
B.12 Moment Curvature Analysis – Lefas SW25 209
B.13 Moment Curvature Analysis – Lefas SW26 210
B.14 Moment Curvature Analysis – Lefas SW30 210
B.15 Moment Curvature Analysis – Lefas SW31 211
B.16 Moment Curvature Analysis – Lefas SW32 211
B.17 Moment Curvature Analysis – Lefas SW33 212
B.18 Moment Curvature Analysis – Oesterle B1 212
B.19 Moment Curvature Analysis – Oesterle B2 213
B.20 Moment Curvature Analysis – Oesterle B3 213
B.21 Moment Curvature Analysis – Oesterle B4 214
B.22 Moment Curvature Analysis – Oesterle B5 214
B.23 Moment Curvature Analysis – Oesterle B6 215
B.24 Moment Curvature Analysis – Oesterle B7 215
B.25 Moment Curvature Analysis – Oesterle B8 216
B.26 Moment Curvature Analysis – Oesterle B9 216
B.27 Moment Curvature Analysis – Oesterle B10 217
B.28 Moment Curvature Analysis – Oesterle R1 217
B.29 Moment Curvature Analysis – Oesterle R2 218
B.30 Moment Curvature Analysis – Pilakoutas SW4 218
B.31 Moment Curvature Analysis – Pilakoutas SW5 219
B.32 Moment Curvature Analysis – Pilakoutas SW6 219
B.33 Moment Curvature Analysis – Pilakoutas SW7 220
B.34 Moment Curvature Analysis – Pilakoutas SW8 220
B.35 Moment Curvature Analysis – Pilakoutas SW9 221
B.36 Moment Curvature Analysis – Salonikios LSW1 221
B.37 Moment Curvature Analysis – Salonikios LSW2 222
B.38 Moment Curvature Analysis – Salonikios LSW3 222

B.39 Moment Curvature Analysis – Salonikios MSW1 223
B.40 Moment Curvature Analysis – Salonikios MSW2 223
B.41 Moment Curvature Analysis – Salonikios MSW3 224
B.42 Moment Curvature Analysis – Salonikios MSW6 224
B.43 Moment Curvature Analysis – Sittipunt W1 225
B.44 Moment Curvature Analysis – Sittipunt W2 225
B.45 Moment Curvature Analysis – Tasnimi SHW1 226
B.46 Moment Curvature Analysis – Tasnimi SHW2 226
B.47 Moment Curvature Analysis – Tasnimi SHW3 227
B.48 Moment Curvature Analysis – Tasnimi SHW4 227
B.49 Moment Curvature Analysis – Thomsen RW1 228
B.50 Moment Curvature Analysis – Thomsen RW2 228
B.51 Moment Curvature Analysis – Vallenas SW3 229
B.52 Moment Curvature Analysis – Vallenas SW4 229
B.53 Moment Curvature Analysis – Vallenas SW5 230
B.54 Moment Curvature Analysis – Vallenas SW6 230
B.55 Moment Curvature Analysis – Wang SW1 231
B.56 Moment Curvature Analysis – Wang SW2 231
B.57 Moment Curvature Analysis – Yanez S1 232
B.58 Moment Curvature Analysis – Zhang SW7 232
B.59 Moment Curvature Analysis – Zhang SW8 233
B.60 Moment Curvature Analysis – Zhang SW9 233

C.1 Moment Curvature Analysis Comparison – Lefas SW11 235
C.2 Moment Curvature Analysis Comparison – Lefas SW12 235
C.3 Moment Curvature Analysis Comparison – Lefas SW13 236
C.4 Moment Curvature Analysis Comparison – Lefas SW14 236
C.5 Moment Curvature Analysis Comparison – Lefas SW15 237
C.6 Moment Curvature Analysis Comparison – Lefas SW16 237
C.7 Moment Curvature Analysis Comparison – Lefas SW17 238
C.8 Moment Curvature Analysis Comparison – Lefas SW21 238
C.9 Moment Curvature Analysis Comparison – Lefas SW22 239
C.10 Moment Curvature Analysis Comparison – Lefas SW23 239
C.11 Moment Curvature Analysis Comparison – Lefas SW24 240
C.12 Moment Curvature Analysis Comparison – Lefas SW25 240
C.13 Moment Curvature Analysis Comparison – Lefas SW26 241

C.14 Moment Curvature Analysis Comparison – Lefas SW30 241
C.15 Moment Curvature Analysis Comparison – Lefas SW31 242
C.16 Moment Curvature Analysis Comparison – Lefas SW32 242
C.17 Moment Curvature Analysis Comparison – Lefas SW33 243
C.18 Moment Curvature Analysis Comparison – Oesterle B1 243
C.19 Moment Curvature Analysis Comparison – Oesterle B2 244
C.20 Moment Curvature Analysis Comparison – Oesterle B3 244
C.21 Moment Curvature Analysis Comparison – Oesterle B4 245
C.22 Moment Curvature Analysis Comparison – Oesterle B5 245
C.23 Moment Curvature Analysis Comparison – Oesterle B6 246
C.24 Moment Curvature Analysis Comparison – Oesterle B7 246
C.25 Moment Curvature Analysis Comparison – Oesterle B8 247
C.26 Moment Curvature Analysis Comparison – Oesterle B9 247
C.27 Moment Curvature Analysis Comparison – Oesterle B10 248
C.28 Moment Curvature Analysis Comparison – Oesterle R1 248
C.29 Moment Curvature Analysis Comparison – Oesterle R2 249
C.30 Moment Curvature Analysis Comparison – Pilakoutas SW4 249
C.31 Moment Curvature Analysis Comparison – Pilakoutas SW5 250
C.32 Moment Curvature Analysis Comparison – Pilakoutas SW6 250
C.33 Moment Curvature Analysis Comparison – Pilakoutas SW7 251
C.34 Moment Curvature Analysis Comparison – Pilakoutas SW8 251
C.35 Moment Curvature Analysis Comparison – Pilakoutas SW9 252
C.36 Moment Curvature Analysis Comparison – Salonikios LSW1 252
C.37 Moment Curvature Analysis Comparison – Salonikios LSW2 253
C.38 Moment Curvature Analysis Comparison – Salonikios LSW3 253
C.39 Moment Curvature Analysis Comparison – Salonikios MSW1 254
C.40 Moment Curvature Analysis Comparison – Salonikios MSW2 254
C.41 Moment Curvature Analysis Comparison – Salonikios MSW3 255
C.42 Moment Curvature Analysis Comparison – Salonikios MSW6 255
C.43 Moment Curvature Analysis Comparison – Sittipunt W1 256
C.44 Moment Curvature Analysis Comparison – Sittipunt W2 256
C.45 Moment Curvature Analysis Comparison – Tasnimi SHW1 257
C.46 Moment Curvature Analysis Comparison – Tasnimi SHW2 257
C.47 Moment Curvature Analysis Comparison – Tasnimi SHW3 258
C.48 Moment Curvature Analysis Comparison – Tasnimi SHW4 258

C.49 Moment Curvature Analysis Comparison – Thomsen RW1 259
C.50 Moment Curvature Analysis Comparison – Thomsen RW2 259
C.51 Moment Curvature Analysis Comparison – Vallenas SW3 260
C.52 Moment Curvature Analysis Comparison – Vallenas SW4 260
C.53 Moment Curvature Analysis Comparison – Vallenas SW5 261
C.54 Moment Curvature Analysis Comparison – Vallenas SW6 261
C.55 Moment Curvature Analysis Comparison – Wang SW1 262
C.56 Moment Curvature Analysis Comparison – Wang SW2 262
C.57 Moment Curvature Analysis Comparison – Yanez S1 263
C.58 Moment Curvature Analysis Comparison – Zhang SW7 263
C.59 Moment Curvature Analysis Comparison – Zhang SW8 264
C.60 Moment Curvature Analysis Comparison – Zhang SW9 264

D.1 Maximum Moment Prediction Ratio v. Maximum Shear Stress Ratio 266
D.2 Maximum Moment Prediction Ratio v. Maximum Shear Demand Ratio . . 266
D.3 Maximum Moment Prediction Ratio v. Normalized Thickness 267
D.4 Maximum Moment Prediction Ratio v. Aspect Ratio 267
D.5 Maximum Moment Prediction Ratio v. Longitudinal Reinforcement Ratio in the Boundary Element 268
D.6 Maximum Moment Prediction Ratio v. Horizontal Reinforcement Ratio . . 268
D.7 Maximum Moment Prediction Ratio v. Volumetric Transverse Reinforcement Ratio 269
D.8 Maximum Moment Prediction Ratio v. Axial Load Ratio 269
D.9 Maximum Moment Prediction Ratio v. Yield Shear Demand Ratio 270
D.10 Maximum Moment Prediction Ratio v. Yield Shear Stress Ratio 270
D.11 Yield Moment Prediction Ratio v. Maximum Shear Stress Ratio 271
D.12 Yield Moment Prediction Ratio v. Maximum Shear Demand Ratio 271
D.13 Yield Moment Prediction Ratio v. Normalized Thickness 272
D.14 Yield Moment Prediction Ratio v. Aspect Ratio 272
D.15 Yield Moment Prediction Ratio v. Longitudinal Reinforcement Ratio in the Boundary Element 273
D.16 Yield Moment Prediction Ratio v. Horizontal Reinforcement Ratio 273
D.17 Yield Moment Prediction Ratio v. Volumetric Transverse Reinforcement Ratio 274
D.18 Yield Moment Prediction Ratio v. Axial Load Ratio 274
D.19 Yield Moment Prediction Ratio v. Yield Shear Demand Ratio 275

D.20 Yield Moment Prediction Ratio v. Yield Shear Stress Ratio 275

E.1 Push Over Analysis – Lefas SW11 277
E.2 Push Over Analysis – Lefas SW12 277
E.3 Push Over Analysis – Lefas SW13 278
E.4 Push Over Analysis – Lefas SW14 278
E.5 Push Over Analysis – Lefas SW15 279
E.6 Push Over Analysis – Lefas SW16 279
E.7 Push Over Analysis – Lefas SW17 280
E.8 Push Over Analysis – Lefas SW21 280
E.9 Push Over Analysis – Lefas SW22 281
E.10 Push Over Analysis – Lefas SW23 281
E.11 Push Over Analysis – Lefas SW24 282
E.12 Push Over Analysis – Lefas SW25 282
E.13 Push Over Analysis – Lefas SW26 283
E.14 Push Over Analysis – Lefas SW30 283
E.15 Push Over Analysis – Lefas SW31 284
E.16 Push Over Analysis – Lefas SW32 284
E.17 Push Over Analysis – Lefas SW33 285
E.18 Push Over Analysis – Oesterle B1 285
E.19 Push Over Analysis – Oesterle B2 286
E.20 Push Over Analysis – Oesterle B3 286
E.21 Push Over Analysis – Oesterle B4 287
E.22 Push Over Analysis – Oesterle B5 287
E.23 Push Over Analysis – Oesterle B6 288
E.24 Push Over Analysis – Oesterle B7 288
E.25 Push Over Analysis – Oesterle B8 289
E.26 Push Over Analysis – Oesterle B9 289
E.27 Push Over Analysis – Oesterle B10 290
E.28 Push Over Analysis – Oesterle R1 290
E.29 Push Over Analysis – Oesterle R2 291
E.30 Push Over Analysis – Pilakoutas SW4 291
E.31 Push Over Analysis – Pilakoutas SW5 292
E.32 Push Over Analysis – Pilakoutas SW6 292
E.33 Push Over Analysis – Pilakoutas SW7 293
E.34 Push Over Analysis – Pilakoutas SW8 293

E.35 Push Over Analysis – Pilakoutas SW9 294
E.36 Push Over Analysis – Salonikios LSW1 294
E.37 Push Over Analysis – Salonikios LSW2 295
E.38 Push Over Analysis – Salonikios LSW3 295
E.39 Push Over Analysis – Salonikios MSW1 296
E.40 Push Over Analysis – Salonikios MSW2 296
E.41 Push Over Analysis – Salonikios MSW3 297
E.42 Push Over Analysis – Salonikios MSW6 297
E.43 Push Over Analysis – Sittipunt W1 298
E.44 Push Over Analysis – Sittipunt W2 298
E.45 Push Over Analysis – Tasnimi SHW1 299
E.46 Push Over Analysis – Tasnimi SHW2 299
E.47 Push Over Analysis – Tasnimi SHW3 300
E.48 Push Over Analysis – Tasnimi SHW4 300
E.49 Push Over Analysis – Thomsen RW1 301
E.50 Push Over Analysis – Thomsen RW2 301
E.51 Push Over Analysis – Vallenas SW3 302
E.52 Push Over Analysis – Vallenas SW4 302
E.53 Push Over Analysis – Vallenas SW5 303
E.54 Push Over Analysis – Vallenas SW6 303
E.55 Push Over Analysis – Wang SW1 304
E.56 Push Over Analysis – Wang SW2 304
E.57 Push Over Analysis – Yanez S1 305
E.58 Push Over Analysis – Zhang SW7 305
E.59 Push Over Analysis – Zhang SW8 306
E.60 Push Over Analysis – Zhang SW9 306

F.1 Initial Stiffness Prediction v. Aspect Ratio 308
F.2 Initial Stiffness Prediction v. Axial Load 308
F.3 Initial Stiffness Prediction v. Horizontal Reinforcement Ratio 309
F.4 Initial Stiffness Prediction v. Longitudinal Reinforcement Ratio 309
F.5 Initial Stiffness Prediction v. Maximum Shear Demand Ratio 310
F.6 Initial Stiffness Prediction v. Maximum Shear Stress Ratio 310
F.7 Initial Stiffness Prediction v. Normalized Thickness 311
F.8 Initial Stiffness Prediction v. Volumetric Transverse Reinforcement Ratio . 311
F.9 Initial Stiffness Prediction v. Yield Shear Demand Ratio 312

F.10 Initial Stiffness Prediction v. Yield Shear Stress Ratio 312
F.11 Yield Displacement Prediction v. Aspect Ratio 313
F.12 Yield Displacement Prediction v. Axial Load 313
F.13 Yield Displacement Prediction v. Horizontal Reinforcement Ratio 314
F.14 Yield Displacement Prediction v. Longitudinal Reinforcement Ratio 314
F.15 Yield Displacement Prediction v. Maximum Shear Demand Ratio 315
F.16 Yield Displacement Prediction v. Maximum Shear Stress Ratio 315
F.17 Yield Displacement Prediction v. Normalized Thickness 316
F.18 Yield Displacement Prediction v. Volumetric Transverse Reinforcement Ratio 316
F.19 Yield Displacement Prediction v. Yield Shear Demand Ratio 317
F.20 Yield Displacement Prediction v. Yield Shear Stress Ratio 317
F.21 Maximum Displacement Prediction v. Aspect Ratio 318
F.22 Maximum Displacement Prediction v. Axial Load 318
F.23 Maximum Displacement Prediction v. Horizontal Reinforcement Ratio . . . 319
F.24 Maximum Displacement Prediction v. Longitudinal Reinforcement Ratio . . 319
F.25 Maximum Displacement Prediction v. Maximum Shear Demand Ratio . . . 320
F.26 Maximum Displacement Prediction v. Maximum Shear Stress Ratio 320
F.27 Maximum Displacement Prediction v. Normalized Thickness 321
F.28 Maximum Displacement Prediction v. Volumetric Transverse Reinforcement Ratio 321
F.29 Maximum Displacement Prediction v. Yield Shear Demand Ratio 322
F.30 Maximum Displacement Prediction v. Yield Shear Stress Ratio 322

G.1 Initial Stiffness Prediction v. Aspect Ratio 324
G.2 Initial Stiffness Prediction v. Axial Load 324
G.3 Initial Stiffness Prediction v. Horizontal Reinforcement Ratio 325
G.4 Initial Stiffness Prediction v. Longitudinal Reinforcement Ratio 325
G.5 Initial Stiffness Prediction v. Maximum Shear Demand Ratio 326
G.6 Initial Stiffness Prediction v. Maximum Shear Stress Ratio 326
G.7 Initial Stiffness Prediction v. Normalized Thickness 327
G.8 Initial Stiffness Prediction v. Volumetric Transverse Reinforcement Ratio . 327
G.9 Initial Stiffness Prediction v. Yield Shear Demand Ratio 328
G.10 Initial Stiffness Prediction v. Yield Shear Stress Ratio 328
G.11 Yield Displacement Prediction v. Aspect Ratio 329
G.12 Yield Displacement Prediction v. Axial Load 329
G.13 Yield Displacement Prediction v. Horizontal Reinforcement Ratio 330

G.14 Yield Displacement Prediction v. Longitudinal Reinforcement Ratio 330
G.15 Yield Displacement Prediction v. Maximum Shear Demand Ratio 331
G.16 Yield Displacement Prediction v. Maximum Shear Stress Ratio 331
G.17 Yield Displacement Prediction v. Normalized Thickness 332
G.18 Yield Displacement Prediction v. Volumetric Transverse Reinforcement Ratio 332
G.19 Yield Displacement Prediction v. Yield Shear Demand Ratio 333
G.20 Yield Displacement Prediction v. Yield Shear Stress Ratio 333
G.21 Maximum Displacement Prediction v. Aspect Ratio 334
G.22 Maximum Displacement Prediction v. Axial Load 334
G.23 Maximum Displacement Prediction v. Horizontal Reinforcement Ratio . . . 335
G.24 Maximum Displacement Prediction v. Longitudinal Reinforcement Ratio . . 335
G.25 Maximum Displacement Prediction v. Maximum Shear Demand Ratio . . . 336
G.26 Maximum Displacement Prediction v. Maximum Shear Stress Ratio 336
G.27 Maximum Displacement Prediction v. Normalized Thickness 337
G.28 Maximum Displacement Prediction v. Volumetric Transverse Reinforcement Ratio 337
G.29 Maximum Displacement Prediction v. Yield Shear Demand Ratio 338
G.30 Maximum Displacement Prediction v. Yield Shear Stress Ratio 338

H.1 Alpha Calibrated to Yield v. Aspect Ratio 340
H.2 Alpha Calibrated to Yield v. Axial Load Ratio 340
H.3 Alpha Calibrated to Yield v. Horizontal Reinforcement Ratio 341
H.4 Alpha Calibrated to Yield v. Longitudinal Reinforcement Ratio 341
H.5 Alpha Calibrated to Yield v. Max Shear Demand Ratio 342
H.6 Alpha Calibrated to Yield v. Max Shear Stress Ratio 342
H.7 Alpha Calibrated to Yield v. Aspect Ratio 343
H.8 Alpha Calibrated to Yield v. Volumetric Transverse Reinforcement Ratio . 343
H.9 Alpha Calibrated to Yield v. Shear Demand Ratio at Yield 344
H.10 Alpha Calibrated to Yield v. Shear Stress Ratio at Yield 344
H.11 Alpha Calibrated to Max Displacement v. Aspect Ratio 345
H.12 Alpha Calibrated to Max Displacement v. Axial Load Ratio 345
H.13 Alpha Calibrated to Max Displacement v. Horizontal Reinforcement Ratio . 346
H.14 Alpha Calibrated to Max Displacement v. Longitudinal Reinforcement Ratio 346
H.15 Alpha Calibrated to Max Displacement v. Max Shear Demand Ratio 347
H.16 Alpha Calibrated to Max Displacement v. Max Shear Stress Ratio 347
H.17 Alpha Calibrated to Max Displacement v. Aspect Ratio 348

H.18 Alpha Calibrated to Max Displacement v. Volumetric Transverse Reinforcement Ratio . . . 348
H.19 Alpha Calibrated to Max Displacement v. Shear Demand Ratio at Yield . . 349
H.20 Alpha Calibrated to Max Displacement v. Shear Stress Ratio at Yield . . . 349
H.21 Alpha Calibrated to Yield with Bar Slip v. Aspect Ratio . . . 350
H.22 Alpha Calibrated to Yield with Bar Slip v. Axial Load Ratio . . . 350
H.23 Alpha Calibrated to Yield with Bar Slip v. Horizontal Reinforcement Ratio 351
H.24 Alpha Calibrated to Yield with Bar Slip v. Longitudinal Reinforcement Ratio 351
H.25 Alpha Calibrated to Yield with Bar Slip v. Max Shear Demand Ratio . . . 352
H.26 Alpha Calibrated to Yield with Bar Slip v. Max Shear Stress Ratio . . . 352
H.27 Alpha Calibrated to Yield with Bar Slip v. Aspect Ratio . . . 353
H.28 Alpha Calibrated to Yield with Bar Slip v. Volumetric Transverse Reinforcement Ratio . . . 353
H.29 Alpha Calibrated to Yield with Bar Slip v. Shear Demand Ratio at Yield . 354
H.30 Alpha Calibrated to Yield with Bar Slip v. Shear Stress Ratio at Yield . . . 354
H.31 Alpha Calibrated to Max Displacement with Bar Slip v. Aspect Ratio . . . 355
H.32 Alpha Calibrated to Max Displacement with Bar Slip v. Axial Load Ratio . 355
H.33 Alpha Calibrated to Max Displacement with Bar Slip v. Horizontal Reinforcement Ratio . . . 356
H.34 Alpha Calibrated to Max Displacement with Bar Slip v. Longitudinal Reinforcement Ratio . . . 356
H.35 Alpha Calibrated to Max Displacement with Bar Slip v. Max Shear Demand Ratio . . . 357
H.36 Alpha Calibrated to Max Displacement with Bar Slip v. Max Shear Stress Ratio . . . 357
H.37 Alpha Calibrated to Max Displacement with Bar Slip v. Aspect Ratio . . . 358
H.38 Alpha Calibrated to Max Displacement with Bar Slip v. Volumetric Transverse Reinforcement Ratio . . . 358
H.39 Alpha Calibrated to Max Displacement with Bar Slip v. Shear Demand Ratio at Yield . . . 359
H.40 Alpha Calibrated to Max Displacement with Bar Slip v. Shear Stress Ratio at Yield . . . 359

I.1 Pushover of Beam-Column Element with Bar-Slip – Lefas SW11 . . . 361
I.2 Pushover of Beam-Column Element with Bar-Slip – Lefas SW12 . . . 361
I.3 Pushover of Beam-Column Element with Bar-Slip – Lefas SW13 . . . 362
I.4 Pushover of Beam-Column Element with Bar-Slip – Lefas SW14 . . . 362

I.5 Pushover of Beam-Column Element with Bar-Slip – Lefas SW15 363
I.6 Pushover of Beam-Column Element with Bar-Slip – Lefas SW16 363
I.7 Pushover of Beam-Column Element with Bar-Slip – Lefas SW17 364
I.8 Pushover of Beam-Column Element with Bar-Slip – Lefas SW21 364
I.9 Pushover of Beam-Column Element with Bar-Slip – Lefas SW22 365
I.10 Pushover of Beam-Column Element with Bar-Slip – Lefas SW23 365
I.11 Pushover of Beam-Column Element with Bar-Slip – Lefas SW24 366
I.12 Pushover of Beam-Column Element with Bar-Slip – Lefas SW25 366
I.13 Pushover of Beam-Column Element with Bar-Slip – Lefas SW26 367
I.14 Pushover of Beam-Column Element with Bar-Slip – Lefas SW30 367
I.15 Pushover of Beam-Column Element with Bar-Slip – Lefas SW31 368
I.16 Pushover of Beam-Column Element with Bar-Slip – Lefas SW32 368
I.17 Pushover of Beam-Column Element with Bar-Slip – Lefas SW33 369
I.18 Pushover of Beam-Column Element with Bar-Slip – Oesterle B1 369
I.19 Pushover of Beam-Column Element with Bar-Slip – Oesterle B2 370
I.20 Pushover of Beam-Column Element with Bar-Slip – Oesterle B3 370
I.21 Pushover of Beam-Column Element with Bar-Slip – Oesterle B4 371
I.22 Pushover of Beam-Column Element with Bar-Slip – Oesterle B5 371
I.23 Pushover of Beam-Column Element with Bar-Slip – Oesterle B6 372
I.24 Pushover of Beam-Column Element with Bar-Slip – Oesterle B7 372
I.25 Pushover of Beam-Column Element with Bar-Slip – Oesterle B8 373
I.26 Pushover of Beam-Column Element with Bar-Slip – Oesterle B9 373
I.27 Pushover of Beam-Column Element with Bar-Slip – Oesterle B10 374
I.28 Pushover of Beam-Column Element with Bar-Slip – Oesterle R1 374
I.29 Pushover of Beam-Column Element with Bar-Slip – Oesterle R2 375
I.30 Pushover of Beam-Column Element with Bar-Slip – Pilakoutas SW4 375
I.31 Pushover of Beam-Column Element with Bar-Slip – Pilakoutas SW5 376
I.32 Pushover of Beam-Column Element with Bar-Slip – Pilakoutas SW6 376
I.33 Pushover of Beam-Column Element with Bar-Slip – Pilakoutas SW7 377
I.34 Pushover of Beam-Column Element with Bar-Slip – Pilakoutas SW8 377
I.35 Pushover of Beam-Column Element with Bar-Slip – Pilakoutas SW9 378
I.36 Pushover of Beam-Column Element with Bar-Slip – Salonikios LSW1 378
I.37 Pushover of Beam-Column Element with Bar-Slip – Salonikios LSW2 379
I.38 Pushover of Beam-Column Element with Bar-Slip – Salonikios LSW3 379
I.39 Pushover of Beam-Column Element with Bar-Slip – Salonikios MSW1 . . . 380

I.40 Pushover of Beam-Column Element with Bar-Slip – Salonikios MSW2 . . . 380
I.41 Pushover of Beam-Column Element with Bar-Slip – Salonikios MSW3 . . . 381
I.42 Pushover of Beam-Column Element with Bar-Slip – Salonikios MSW6 . . . 381
I.43 Pushover of Beam-Column Element with Bar-Slip – Sittipunt W1 382
I.44 Pushover of Beam-Column Element with Bar-Slip – Sittipunt W2 382
I.45 Pushover of Beam-Column Element with Bar-Slip – Tasnimi SHW1 383
I.46 Pushover of Beam-Column Element with Bar-Slip – Tasnimi SHW2 383
I.47 Pushover of Beam-Column Element with Bar-Slip – Tasnimi SHW3 384
I.48 Pushover of Beam-Column Element with Bar-Slip – Tasnimi SHW4 384
I.49 Pushover of Beam-Column Element with Bar-Slip – Thomsen RW1 385
I.50 Pushover of Beam-Column Element with Bar-Slip – Thomsen RW2 385
I.51 Pushover of Beam-Column Element with Bar-Slip – Vallenas SW3 386
I.52 Pushover of Beam-Column Element with Bar-Slip – Vallenas SW4 386
I.53 Pushover of Beam-Column Element with Bar-Slip – Vallenas SW5 387
I.54 Pushover of Beam-Column Element with Bar-Slip – Vallenas SW6 387
I.55 Pushover of Beam-Column Element with Bar-Slip – Wang SW1 388
I.56 Pushover of Beam-Column Element with Bar-Slip – Wang SW2 388
I.57 Pushover of Beam-Column Element with Bar-Slip – Yanez S1 389
I.58 Pushover of Beam-Column Element with Bar-Slip – Zhang SW7 389
I.59 Pushover of Beam-Column Element with Bar-Slip – Zhang SW8 390
I.60 Pushover of Beam-Column Element with Bar-Slip – Zhang SW9 390

J.1 Initial Stiffness NLBC v Max Shear Stress Ratio 392
J.2 Initial Stiffness NLBC v Max Shear Demand Ratio 392
J.3 Initial Stiffness NLBC v Aspect Ratio 393
J.4 Initial Stiffness NLBC v Normalized Thickness 393
J.5 Initial Stiffness NLBC v Long Reinf Ratio in BE 394
J.6 Initial Stiffness NLBC v Horiz Reinf Ratio 394
J.7 Initial Stiffness NLBC v Vol Trans Reinf Ratio 395
J.8 Initial Stiffness NLBC v Yield Shear Stress Ratio 395
J.9 Initial Stiffness NLBC v Yield Shear Demand Ratio 396
J.10 Initial Stiffness NLBC v Axial Load Ratio 396
J.11 Yield Displacement NLBC v Max Shear Stress Ratio 397
J.12 Yield Displacement NLBC v Max Shear Demand Ratio 397
J.13 Yield Displacement NLBC v Aspect Ratio 398
J.14 Yield Displacement NLBC v Normalized Thickness 398

J.15 Yield Displacement NLBC v Long Reinf Ratio in BE 399
J.16 Yield Displacement NLBC v Horiz Reinf Ratio 399
J.17 Yield Displacement NLBC v Vol Trans Reinf Ratio 400
J.18 Yield Displacement NLBC v Yield Shear Stress Ratio 400
J.19 Yield Displacement NLBC v Yield Shear Demand Ratio 401
J.20 Yield Displacement NLBC v Axial Load Ratio 401
J.21 Maximum Displacement NLBC v Max Shear Stress Ratio 402
J.22 Maximum Displacement NLBC v Max Shear Demand Ratio 402
J.23 Maximum Displacement NLBC v Aspect Ratio 403
J.24 Maximum Displacement NLBC v Normalized Thickness 403
J.25 Maximum Displacement NLBC v Long Reinf Ratio in BE 404
J.26 Maximum Displacement NLBC v Horiz Reinf Ratio 404
J.27 Maximum Displacement NLBC v Vol Trans Reinf Ratio 405
J.28 Maximum Displacement NLBC v Yield Shear Stress Ratio 405
J.29 Maximum Displacement NLBC v Yield Shear Demand Ratio 406
J.30 Maximum Displacement NLBC v Axial Load Ratio 406

K.1 Initial Stiffness Absolute Error v Max Shear Stress Ratio 408
K.2 Initial Stiffness Absolute Error v Max Shear Demand Ratio 408
K.3 Initial Stiffness Absolute Error v Aspect Ratio 409
K.4 Initial Stiffness Absolute Error v Normalized Thickness 409
K.5 Initial Stiffness Absolute Error v Long Reinf Ratio in BE 410
K.6 Initial Stiffness Absolute Error v Horiz Reinf Ratio 410
K.7 Initial Stiffness Absolute Error v Vol Trans Reinf Ratio 411
K.8 Initial Stiffness Absolute Error v Yield Shear Stress Ratio 411
K.9 Initial Stiffness Absolute Error v Yield Shear Demand Ratio 412
K.10 Initial Stiffness Absolute Error v Axial Load Ratio 412
K.11 Initial Stiffness Relative Error v Max Shear Stress Ratio 413
K.12 Initial Stiffness Relative Error v Max Shear Demand Ratio 413
K.13 Initial Stiffness Relative Error v Aspect Ratio 414
K.14 Initial Stiffness Relative Error v Normalized Thickness 414
K.15 Initial Stiffness Relative Error v Long Reinf Ratio in BE 415
K.16 Initial Stiffness Relative Error v Horiz Reinf Ratio 415
K.17 Initial Stiffness Relative Error v Vol Trans Reinf Ratio 416
K.18 Initial Stiffness Relative Error v Yield Shear Stress Ratio 416
K.19 Initial Stiffness Relative Error v Yield Shear Demand Ratio 417

K.20 Initial Stiffness Relative Error v Axial Load Ratio 417
K.21 Yield Displacement Absolute Error v Max Shear Stress Ratio 418
K.22 Yield Displacement Absolute Error v Max Shear Demand Ratio 418
K.23 Yield Displacement Absolute Error v Aspect Ratio 419
K.24 Yield Displacement Absolute Error v Normalized Thickness 419
K.25 Yield Displacement Absolute Error v Long Reinf Ratio in BE 420
K.26 Yield Displacement Absolute Error v Horiz Reinf Ratio 420
K.27 Yield Displacement Absolute Error v Vol Trans Reinf Ratio 421
K.28 Yield Displacement Absolute Error v Yield Shear Stress Ratio 421
K.29 Yield Displacement Absolute Error v Yield Shear Demand Ratio 422
K.30 Yield Displacement Absolute Error v Axial Load Ratio 422
K.31 Yield Displacement Relative Error v Max Shear Stress Ratio 423
K.32 Yield Displacement Relative Error v Max Shear Demand Ratio 423
K.33 Yield Displacement Relative Error v Aspect Ratio 424
K.34 Yield Displacement Relative Error v Normalized Thickness 424
K.35 Yield Displacement Relative Error v Long Reinf Ratio in BE 425
K.36 Yield Displacement Relative Error v Horiz Reinf Ratio 425
K.37 Yield Displacement Relative Error v Vol Trans Reinf Ratio 426
K.38 Yield Displacement Relative Error v Yield Shear Stress Ratio 426
K.39 Yield Displacement Relative Error v Yield Shear Demand Ratio 427
K.40 Yield Displacement Relative Error v Axial Load Ratio 427
K.41 Max Displacement Absolute Error v Max Shear Stress Ratio 428
K.42 Max Displacement Absolute Error v Max Shear Demand Ratio 428
K.43 Max Displacement Absolute Error v Aspect Ratio 429
K.44 Max Displacement Absolute Error v Normalized Thickness 429
K.45 Max Displacement Absolute Error v Long Reinf Ratio in BE 430
K.46 Max Displacement Absolute Error v Horiz Reinf Ratio 430
K.47 Max Displacement Absolute Error v Vol Trans Reinf Ratio 431
K.48 Max Displacement Absolute Error v Yield Shear Stress Ratio 431
K.49 Max Displacement Absolute Error v Yield Shear Demand Ratio 432
K.50 Max Displacement Absolute Error v Axial Load Ratio 432
K.51 Max Displacement Relative Error v Max Shear Stress Ratio 433
K.52 Max Displacement Relative Error v Max Shear Demand Ratio 433
K.53 Max Displacement Relative Error v Aspect Ratio 434
K.54 Max Displacement Relative Error v Normalized Thickness 434

K.55 Max Displacement Relative Error v Long Reinf Ratio in BE 435
K.56 Max Displacement Relative Error v Horiz Reinf Ratio 435
K.57 Max Displacement Relative Error v Vol Trans Reinf Ratio 436
K.58 Max Displacement Relative Error v Yield Shear Stress Ratio 436
K.59 Max Displacement Relative Error v Yield Shear Demand Ratio 437
K.60 Max Displacement Relative Error v Axial Load Ratio 437

L.1 Beam-Column With Shear Initial Stiffness v Max Shear Stress Ratio 439
L.2 Beam-Column With Shear Initial Stiffness v Max Shear Demand Ratio . . . 439
L.3 Beam-Column With Shear Initial Stiffness v Aspect Ratio 440
L.4 Beam-Column With Shear Initial Stiffness v Normalized Thickness 440
L.5 Beam-Column With Shear Initial Stiffness v Long Reinf Ratio in BE 441
L.6 Beam-Column With Shear Initial Stiffness v Horiz Reinf Ratio 441
L.7 Beam-Column With Shear Initial Stiffness v Vol Trans Reinf Ratio 442
L.8 Beam-Column With Shear Initial Stiffness v Yield Shear Stress Ratio 442
L.9 Beam-Column With Shear Initial Stiffness v Yield Shear Demand Ratio . . 443
L.10 Beam-Column With Shear Initial Stiffness v Axial Load Ratio 443
L.11 Beam-Column With Shear Yield Displacement v Max Shear Stress Ratio . . 444
L.12 Beam-Column With Shear Yield Displacement v Max Shear Demand Ratio 444
L.13 Beam-Column With Shear Yield Displacement v Aspect Ratio 445
L.14 Beam-Column With Shear Yield Displacement v Normalized Thickness . . . 445
L.15 Beam-Column With Shear Yield Displacement v Long Reinf Ratio in BE . 446
L.16 Beam-Column With Shear Yield Displacement v Horiz Reinf Ratio 446
L.17 Beam-Column With Shear Yield Displacement v Vol Trans Reinf Ratio . . 447
L.18 Beam-Column With Shear Yield Displacement v Yield Shear Stress Ratio . 447
L.19 Beam-Column With Shear Yield Displacement v Yield Shear Demand Ratio 448
L.20 Beam-Column With Shear Yield Displacement v Axial Load Ratio 448
L.21 Beam-Column With Shear Maximum Displacement v Max Shear Stress Ratio 449
L.22 Beam-Column With Shear Maximum Displacement v Max Shear Demand Ratio 449
L.23 Beam-Column With Shear Maximum Displacement v Aspect Ratio 450
L.24 Beam-Column With Shear Maximum Displacement v Normalized Thickness 450
L.25 Beam-Column With Shear Maximum Displacement v Long Reinf Ratio in BE 451
L.26 Beam-Column With Shear Maximum Displacement v Horiz Reinf Ratio . . 451
L.27 Beam-Column With Shear Maximum Displacement v Vol Trans Reinf Ratio 452

L.28 Beam-Column With Shear Maximum Displacement v Yield Shear Stress Ratio . . . 452
L.29 Beam-Column With Shear Maximum Displacement v Yield Shear Demand Ratio . . . 453
L.30 Beam-Column With Shear Maximum Displacement v Axial Load Ratio . . . 453
L.31 Beam-Column With Shear Modulus Calibrated to Yield Displacment - Initial Stiffness v Max Shear Stress Ratio . . . 454
L.32 Beam-Column With Shear Modulus Calibrated to Yield Displacment - Initial Stiffness v Max Shear Demand Ratio . . . 454
L.33 Beam-Column With Shear Modulus Calibrated to Yield Displacment - Initial Stiffness v Aspect Ratio . . . 455
L.34 Beam-Column With Shear Modulus Calibrated to Yield Displacment - Initial Stiffness v Normalized Thickness . . . 455
L.35 Beam-Column With Shear Modulus Calibrated to Yield Displacment - Initial Stiffness v Long Reinf Ratio in BE . . . 456
L.36 Beam-Column With Shear Modulus Calibrated to Yield Displacment - Initial Stiffness v Horiz Reinf Ratio . . . 456
L.37 Beam-Column With Shear Modulus Calibrated to Yield Displacment - Initial Stiffness v Vol Trans Reinf Ratio . . . 457
L.38 Beam-Column With Shear Modulus Calibrated to Yield Displacment - Initial Stiffness v Yield Shear Stress Ratio . . . 457
L.39 Beam-Column With Shear Modulus Calibrated to Yield Displacment - Initial Stiffness v Yield Shear Demand Ratio . . . 458
L.40 Beam-Column With Shear Modulus Calibrated to Yield Displacment - Initial Stiffness v Axial Load Ratio . . . 458
L.41 Beam-Column With Shear Modulus Calibrated to Yield Displacment - Yield Displacement v Max Shear Stress Ratio . . . 459
L.42 Beam-Column With Shear Modulus Calibrated to Yield Displacment - Yield Displacement v Max Shear Demand Ratio . . . 459
L.43 Beam-Column With Shear Modulus Calibrated to Yield Displacment - Yield Displacement v Aspect Ratio . . . 460
L.44 Beam-Column With Shear Modulus Calibrated to Yield Displacment - Yield Displacement v Normalized Thickness . . . 460
L.45 Beam-Column With Shear Modulus Calibrated to Yield Displacment - Yield Displacement v Long Reinf Ratio in BE . . . 461
L.46 Beam-Column With Shear Modulus Calibrated to Yield Displacment - Yield Displacement v Horiz Reinf Ratio . . . 461

L.47 Beam-Column With Shear Modulus Calibrated to Yield Displacment - Yield Displacement v Vol Trans Reinf Ratio 462
L.48 Beam-Column With Shear Modulus Calibrated to Yield Displacment - Yield Displacement v Yield Shear Stress Ratio 462
L.49 Beam-Column With Shear Modulus Calibrated to Yield Displacment - Yield Displacement v Yield Shear Demand Ratio 463
L.50 Beam-Column With Shear Modulus Calibrated to Yield Displacment - Yield Displacement v Axial Load Ratio 463
L.51 Beam-Column With Shear Modulus Calibrated to Yield Displacment - Maximum Displacement v Max Shear Stress Ratio 464
L.52 Beam-Column With Shear Modulus Calibrated to Yield Displacment - Maximum Displacement v Max Shear Demand Ratio 464
L.53 Beam-Column With Shear Modulus Calibrated to Yield Displacment - Maximum Displacement v Aspect Ratio 465
L.54 Beam-Column With Shear Modulus Calibrated to Yield Displacment - Maximum Displacement v Normalized Thickness 465
L.55 Beam-Column With Shear Modulus Calibrated to Yield Displacment - Maximum Displacement v Long Reinf Ratio in BE 466
L.56 Beam-Column With Shear Modulus Calibrated to Yield Displacment - Maximum Displacement v Horiz Reinf Ratio 466
L.57 Beam-Column With Shear Modulus Calibrated to Yield Displacment - Maximum Displacement v Vol Trans Reinf Ratio 467
L.58 Beam-Column With Shear Modulus Calibrated to Yield Displacment - Maximum Displacement v Yield Shear Stress Ratio 467
L.59 Beam-Column With Shear Modulus Calibrated to Yield Displacment - Maximum Displacement v Yield Shear Demand Ratio 468
L.60 Beam-Column With Shear Modulus Calibrated to Yield Displacment - Maximum Displacement v Axial Load Ratio 468
L.61 Beam-Column With Shear Modulus Calibrated to Maximum Displacment - Initial Stiffness v Max Shear Stress Ratio 469
L.62 Beam-Column With Shear Modulus Calibrated to Maximum Displacment - Initial Stiffness v Max Shear Demand Ratio 469
L.63 Beam-Column With Shear Modulus Calibrated to Maximum Displacment - Initial Stiffness v Aspect Ratio 470
L.64 Beam-Column With Shear Modulus Calibrated to Maximum Displacment - Initial Stiffness v Normalized Thickness 470
L.65 Beam-Column With Shear Modulus Calibrated to Maximum Displacment - Initial Stiffness v Long Reinf Ratio in BE 471

L.66 Beam-Column With Shear Modulus Calibrated to Maximum Displacment - Initial Stiffness v Horiz Reinf Ratio 471
L.67 Beam-Column With Shear Modulus Calibrated to Maximum Displacment - Initial Stiffness v Vol Trans Reinf Ratio 472
L.68 Beam-Column With Shear Modulus Calibrated to Maximum Displacment - Initial Stiffness v Yield Shear Stress Ratio 472
L.69 Beam-Column With Shear Modulus Calibrated to Maximum Displacment - Initial Stiffness v Yield Shear Demand Ratio 473
L.70 Beam-Column With Shear Modulus Calibrated to Maximum Displacment - Initial Stiffness v Axial Load Ratio 473
L.71 Beam-Column With Shear Modulus Calibrated to Maximum Displacment - Yield Displacement v Max Shear Stress Ratio 474
L.72 Beam-Column With Shear Modulus Calibrated to Maximum Displacment - Yield Displacement v Max Shear Demand Ratio 474
L.73 Beam-Column With Shear Modulus Calibrated to Maximum Displacment - Yield Displacement v Aspect Ratio 475
L.74 Beam-Column With Shear Modulus Calibrated to Maximum Displacment - Yield Displacement v Normalized Thickness 475
L.75 Beam-Column With Shear Modulus Calibrated to Maximum Displacment - Yield Displacement v Long Reinf Ratio in BE 476
L.76 Beam-Column With Shear Modulus Calibrated to Maximum Displacment - Yield Displacement v Horiz Reinf Ratio 476
L.77 Beam-Column With Shear Modulus Calibrated to Maximum Displacment - Yield Displacement v Vol Trans Reinf Ratio 477
L.78 Beam-Column With Shear Modulus Calibrated to Maximum Displacment - Yield Displacement v Yield Shear Stress Ratio 477
L.79 Beam-Column With Shear Modulus Calibrated to Maximum Displacment - Yield Displacement v Yield Shear Demand Ratio 478
L.80 Beam-Column With Shear Modulus Calibrated to Maximum Displacment - Yield Displacement v Axial Load Ratio 478
L.81 Beam-Column With Shear Modulus Calibrated to Maximum Displacment - Maximum Displacement v Max Shear Stress Ratio 479
L.82 Beam-Column With Shear Modulus Calibrated to Maximum Displacment - Maximum Displacement v Max Shear Demand Ratio 479
L.83 Beam-Column With Shear Modulus Calibrated to Maximum Displacment - Maximum Displacement v Aspect Ratio 480
L.84 Beam-Column With Shear Modulus Calibrated to Maximum Displacment - Maximum Displacement v Normalized Thickness 480

L.85 Beam-Column With Shear Modulus Calibrated to Maximum Displacment - Maximum Displacement v Long Reinf Ratio in BE 481
L.86 Beam-Column With Shear Modulus Calibrated to Maximum Displacment - Maximum Displacement v Horiz Reinf Ratio 481
L.87 Beam-Column With Shear Modulus Calibrated to Maximum Displacment - Maximum Displacement v Vol Trans Reinf Ratio 482
L.88 Beam-Column With Shear Modulus Calibrated to Maximum Displacment - Maximum Displacement v Yield Shear Stress Ratio 482
L.89 Beam-Column With Shear Modulus Calibrated to Maximum Displacment - Maximum Displacement v Yield Shear Demand Ratio 483
L.90 Beam-Column With Shear Modulus Calibrated to Maximum Displacment - Maximum Displacement v Axial Load Ratio 483
L.91 Beam-Column With Shear Modulus Calibrated to Yield Displacment With Slip - Initial Stiffness v Max Shear Stress Ratio 484
L.92 Beam-Column With Shear Modulus Calibrated to Yield Displacment With Slip - Initial Stiffness v Max Shear Demand Ratio 484
L.93 Beam-Column With Shear Modulus Calibrated to Yield Displacment With Slip - Initial Stiffness v Aspect Ratio 485
L.94 Beam-Column With Shear Modulus Calibrated to Yield Displacment With Slip - Initial Stiffness v Normalized Thickness 485
L.95 Beam-Column With Shear Modulus Calibrated to Yield Displacment With Slip - Initial Stiffness v Long Reinf Ratio in BE 486
L.96 Beam-Column With Shear Modulus Calibrated to Yield Displacment With Slip - Initial Stiffness v Horiz Reinf Ratio 486
L.97 Beam-Column With Shear Modulus Calibrated to Yield Displacment With Slip - Initial Stiffness v Vol Trans Reinf Ratio 487
L.98 Beam-Column With Shear Modulus Calibrated to Yield Displacment With Slip - Initial Stiffness v Yield Shear Stress Ratio 487
L.99 Beam-Column With Shear Modulus Calibrated to Yield Displacment With Slip - Initial Stiffness v Yield Shear Demand Ratio 488
L.100 Beam-Column With Shear Modulus Calibrated to Yield Displacment With Slip - Initial Stiffness v Axial Load Ratio 488
L.101 Beam-Column With Shear Modulus Calibrated to Yield Displacment With Slip - Yield Displacement v Max Shear Stress Ratio 489
L.102 Beam-Column With Shear Modulus Calibrated to Yield Displacment With Slip - Yield Displacement v Max Shear Demand Ratio 489
L.103 Beam-Column With Shear Modulus Calibrated to Yield Displacment With Slip - Yield Displacement v Aspect Ratio 490

L.104 Beam-Column With Shear Modulus Calibrated to Yield Displacment With Slip - Yield Displacement v Normalized Thickness 490
L.105 Beam-Column With Shear Modulus Calibrated to Yield Displacment With Slip - Yield Displacement v Long Reinf Ratio in BE 491
L.106 Beam-Column With Shear Modulus Calibrated to Yield Displacment With Slip - Yield Displacement v Horiz Reinf Ratio 491
L.107 Beam-Column With Shear Modulus Calibrated to Yield Displacment With Slip - Yield Displacement v Vol Trans Reinf Ratio 492
L.108 Beam-Column With Shear Modulus Calibrated to Yield Displacment With Slip - Yield Displacement v Yield Shear Stress Ratio 492
L.109 Beam-Column With Shear Modulus Calibrated to Yield Displacment With Slip - Yield Displacement v Yield Shear Demand Ratio 493
L.110 Beam-Column With Shear Modulus Calibrated to Yield Displacment With Slip - Yield Displacement v Axial Load Ratio 493
L.111 Beam-Column With Shear Modulus Calibrated to Yield Displacment With Slip - Maximum Displacement v Max Shear Stress Ratio 494
L.112 Beam-Column With Shear Modulus Calibrated to Yield Displacment With Slip - Maximum Displacement v Max Shear Demand Ratio 494
L.113 Beam-Column With Shear Modulus Calibrated to Yield Displacment With Slip - Maximum Displacement v Aspect Ratio 495
L.114 Beam-Column With Shear Modulus Calibrated to Yield Displacment With Slip - Maximum Displacement v Normalized Thickness 495
L.115 Beam-Column With Shear Modulus Calibrated to Yield Displacment With Slip - Maximum Displacement v Long Reinf Ratio in BE 496
L.116 Beam-Column With Shear Modulus Calibrated to Yield Displacment With Slip - Maximum Displacement v Horiz Reinf Ratio 496
L.117 Beam-Column With Shear Modulus Calibrated to Yield Displacment With Slip - Maximum Displacement v Vol Trans Reinf Ratio 497
L.118 Beam-Column With Shear Modulus Calibrated to Yield Displacment With Slip - Maximum Displacement v Yield Shear Stress Ratio 497
L.119 Beam-Column With Shear Modulus Calibrated to Yield Displacment With Slip - Maximum Displacement v Yield Shear Demand Ratio 498
L.120 Beam-Column With Shear Modulus Calibrated to Yield Displacment With Slip - Maximum Displacement v Axial Load Ratio 498
L.121 Beam-Column With Shear Modulus Calibrated to Maximum Displacment With Slip - Initial Stiffness v Max Shear Stress Ratio 499
L.122 Beam-Column With Shear Modulus Calibrated to Maximum Displacment With Slip - Initial Stiffness v Max Shear Demand Ratio 499

L.123 Beam-Column With Shear Modulus Calibrated to Maximum Displacment With Slip - Initial Stiffness v Aspect Ratio 500
L.124 Beam-Column With Shear Modulus Calibrated to Maximum Displacment With Slip - Initial Stiffness v Normalized Thickness 500
L.125 Beam-Column With Shear Modulus Calibrated to Maximum Displacment With Slip - Initial Stiffness v Long Reinf Ratio in BE 501
L.126 Beam-Column With Shear Modulus Calibrated to Maximum Displacment With Slip - Initial Stiffness v Horiz Reinf Ratio 501
L.127 Beam-Column With Shear Modulus Calibrated to Maximum Displacment With Slip - Initial Stiffness v Vol Trans Reinf Ratio 502
L.128 Beam-Column With Shear Modulus Calibrated to Maximum Displacment With Slip - Initial Stiffness v Yield Shear Stress Ratio 502
L.129 Beam-Column With Shear Modulus Calibrated to Maximum Displacment With Slip - Initial Stiffness v Yield Shear Demand Ratio 503
L.130 Beam-Column With Shear Modulus Calibrated to Maximum Displacment With Slip - Initial Stiffness v Axial Load Ratio 503
L.131 Beam-Column With Shear Modulus Calibrated to Maximum Displacment With Slip - Yield Displacement v Max Shear Stress Ratio 504
L.132 Beam-Column With Shear Modulus Calibrated to Maximum Displacment With Slip - Yield Displacement v Max Shear Demand Ratio 504
L.133 Beam-Column With Shear Modulus Calibrated to Maximum Displacment With Slip - Yield Displacement v Aspect Ratio 505
L.134 Beam-Column With Shear Modulus Calibrated to Maximum Displacment With Slip - Yield Displacement v Normalized Thickness 505
L.135 Beam-Column With Shear Modulus Calibrated to Maximum Displacment With Slip - Yield Displacement v Long Reinf Ratio in BE 506
L.136 Beam-Column With Shear Modulus Calibrated to Maximum Displacment With Slip - Yield Displacement v Horiz Reinf Ratio 506
L.137 Beam-Column With Shear Modulus Calibrated to Maximum Displacment With Slip - Yield Displacement v Vol Trans Reinf Ratio 507
L.138 Beam-Column With Shear Modulus Calibrated to Maximum Displacment With Slip - Yield Displacement v Yield Shear Stress Ratio 507
L.139 Beam-Column With Shear Modulus Calibrated to Maximum Displacment With Slip - Yield Displacement v Yield Shear Demand Ratio 508
L.140 Beam-Column With Shear Modulus Calibrated to Maximum Displacment With Slip - Yield Displacement v Axial Load Ratio 508
L.141 Beam-Column With Shear Modulus Calibrated to Maximum Displacment With Slip - Maximum Displacement v Max Shear Stress Ratio 509

L.142 Beam-Column With Shear Modulus Calibrated to Maximum Displacment With Slip - Maximum Displacement v Max Shear Demand Ratio 509
L.143 Beam-Column With Shear Modulus Calibrated to Maximum Displacment With Slip - Maximum Displacement v Aspect Ratio 510
L.144 Beam-Column With Shear Modulus Calibrated to Maximum Displacment With Slip - Maximum Displacement v Normalized Thickness 510
L.145 Beam-Column With Shear Modulus Calibrated to Maximum Displacment With Slip - Maximum Displacement v Long Reinf Ratio in BE 511
L.146 Beam-Column With Shear Modulus Calibrated to Maximum Displacment With Slip - Maximum Displacement v Horiz Reinf Ratio 511
L.147 Beam-Column With Shear Modulus Calibrated to Maximum Displacment With Slip - Maximum Displacement v Vol Trans Reinf Ratio 512
L.148 Beam-Column With Shear Modulus Calibrated to Maximum Displacment With Slip - Maximum Displacement v Yield Shear Stress Ratio 512
L.149 Beam-Column With Shear Modulus Calibrated to Maximum Displacment With Slip - Maximum Displacement v Yield Shear Demand Ratio 513
L.150 Beam-Column With Shear Modulus Calibrated to Maximum Displacment With Slip - Maximum Displacement v Axial Load Ratio 513

M.1 Pushover of Beam-Column Element with Elastic Shear – Lefas SW11 515
M.2 Pushover of Beam-Column Element with Elastic Shear – Lefas SW12 515
M.3 Pushover of Beam-Column Element with Elastic Shear – Lefas SW13 516
M.4 Pushover of Beam-Column Element with Elastic Shear – Lefas SW14 516
M.5 Pushover of Beam-Column Element with Elastic Shear – Lefas SW15 517
M.6 Pushover of Beam-Column Element with Elastic Shear – Lefas SW16 517
M.7 Pushover of Beam-Column Element with Elastic Shear – Lefas SW17 518
M.8 Pushover of Beam-Column Element with Elastic Shear – Lefas SW21 518
M.9 Pushover of Beam-Column Element with Elastic Shear – Lefas SW22 519
M.10 Pushover of Beam-Column Element with Elastic Shear – Lefas SW23 519
M.11 Pushover of Beam-Column Element with Elastic Shear – Lefas SW24 520
M.12 Pushover of Beam-Column Element with Elastic Shear – Lefas SW25 520
M.13 Pushover of Beam-Column Element with Elastic Shear – Lefas SW26 521
M.14 Pushover of Beam-Column Element with Elastic Shear – Lefas SW30 521
M.15 Pushover of Beam-Column Element with Elastic Shear – Lefas SW31 522
M.16 Pushover of Beam-Column Element with Elastic Shear – Lefas SW32 522
M.17 Pushover of Beam-Column Element with Elastic Shear – Lefas SW33 523
M.18 Pushover of Beam-Column Element with Elastic Shear – Oesterle B1 523

M.19 Pushover of Beam-Column Element with Elastic Shear – Oesterle B2 524
M.20 Pushover of Beam-Column Element with Elastic Shear – Oesterle B3 524
M.21 Pushover of Beam-Column Element with Elastic Shear – Oesterle B4 525
M.22 Pushover of Beam-Column Element with Elastic Shear – Oesterle B5 525
M.23 Pushover of Beam-Column Element with Elastic Shear – Oesterle B6 526
M.24 Pushover of Beam-Column Element with Elastic Shear – Oesterle B7 526
M.25 Pushover of Beam-Column Element with Elastic Shear – Oesterle B8 527
M.26 Pushover of Beam-Column Element with Elastic Shear – Oesterle B9 527
M.27 Pushover of Beam-Column Element with Elastic Shear – Oesterle B10 . . . 528
M.28 Pushover of Beam-Column Element with Elastic Shear – Oesterle R1 528
M.29 Pushover of Beam-Column Element with Elastic Shear – Oesterle R2 529
M.30 Pushover of Beam-Column Element with Elastic Shear – Pilakoutas SW4 . 529
M.31 Pushover of Beam-Column Element with Elastic Shear – Pilakoutas SW5 . 530
M.32 Pushover of Beam-Column Element with Elastic Shear – Pilakoutas SW6 . 530
M.33 Pushover of Beam-Column Element with Elastic Shear – Pilakoutas SW7 . 531
M.34 Pushover of Beam-Column Element with Elastic Shear – Pilakoutas SW8 . 531
M.35 Pushover of Beam-Column Element with Elastic Shear – Pilakoutas SW9 . 532
M.36 Pushover of Beam-Column Element with Elastic Shear – Salonikios LSW1 . 532
M.37 Pushover of Beam-Column Element with Elastic Shear – Salonikios LSW2 . 533
M.38 Pushover of Beam-Column Element with Elastic Shear – Salonikios LSW3 . 533
M.39 Pushover of Beam-Column Element with Elastic Shear – Salonikios MSW1 534
M.40 Pushover of Beam-Column Element with Elastic Shear – Salonikios MSW2 534
M.41 Pushover of Beam-Column Element with Elastic Shear – Salonikios MSW3 535
M.42 Pushover of Beam-Column Element with Elastic Shear – Salonikios MSW6 535
M.43 Pushover of Beam-Column Element with Elastic Shear – Sittipunt W1 . . . 536
M.44 Pushover of Beam-Column Element with Elastic Shear – Sittipunt W2 . . . 536
M.45 Pushover of Beam-Column Element with Elastic Shear – Tasnimi SHW1 . . 537
M.46 Pushover of Beam-Column Element with Elastic Shear – Tasnimi SHW2 . . 537
M.47 Pushover of Beam-Column Element with Elastic Shear – Tasnimi SHW3 . . 538
M.48 Pushover of Beam-Column Element with Elastic Shear – Tasnimi SHW4 . . 538
M.49 Pushover of Beam-Column Element with Elastic Shear – Thomsen RW1 . . 539
M.50 Pushover of Beam-Column Element with Elastic Shear – Thomsen RW2 . . 539
M.51 Pushover of Beam-Column Element with Elastic Shear – Vallenas SW3 . . . 540
M.52 Pushover of Beam-Column Element with Elastic Shear – Vallenas SW4 . . . 540
M.53 Pushover of Beam-Column Element with Elastic Shear – Vallenas SW5 . . . 541

M.54 Pushover of Beam-Column Element with Elastic Shear – Vallenas SW6 . . . 541
M.55 Pushover of Beam-Column Element with Elastic Shear – Wang SW1 542
M.56 Pushover of Beam-Column Element with Elastic Shear – Wang SW2 542
M.57 Pushover of Beam-Column Element with Elastic Shear – Yanez S1 543
M.58 Pushover of Beam-Column Element with Elastic Shear – Zhang SW7 543
M.59 Pushover of Beam-Column Element with Elastic Shear – Zhang SW8 544
M.60 Pushover of Beam-Column Element with Elastic Shear – Zhang SW9 544
M.61 Pushover of Beam-Column Element with Elastic Shear Calibrated to Yield – Lefas SW11 545
M.62 Pushover of Beam-Column Element with Elastic Shear Calibrated to Yield – Lefas SW12 545
M.63 Pushover of Beam-Column Element with Elastic Shear Calibrated to Yield – Lefas SW13 546
M.64 Pushover of Beam-Column Element with Elastic Shear Calibrated to Yield – Lefas SW14 546
M.65 Pushover of Beam-Column Element with Elastic Shear Calibrated to Yield – Lefas SW15 547
M.66 Pushover of Beam-Column Element with Elastic Shear Calibrated to Yield – Lefas SW16 547
M.67 Pushover of Beam-Column Element with Elastic Shear Calibrated to Yield – Lefas SW17 548
M.68 Pushover of Beam-Column Element with Elastic Shear Calibrated to Yield – Lefas SW21 548
M.69 Pushover of Beam-Column Element with Elastic Shear Calibrated to Yield – Lefas SW22 549
M.70 Pushover of Beam-Column Element with Elastic Shear Calibrated to Yield – Lefas SW23 549
M.71 Pushover of Beam-Column Element with Elastic Shear Calibrated to Yield – Lefas SW24 550
M.72 Pushover of Beam-Column Element with Elastic Shear Calibrated to Yield – Lefas SW25 550
M.73 Pushover of Beam-Column Element with Elastic Shear Calibrated to Yield – Lefas SW26 551
M.74 Pushover of Beam-Column Element with Elastic Shear Calibrated to Yield – Lefas SW30 551
M.75 Pushover of Beam-Column Element with Elastic Shear Calibrated to Yield – Lefas SW31 552

M.76 Pushover of Beam-Column Element with Elastic Shear Calibrated to Yield – Lefas SW32 552
M.77 Pushover of Beam-Column Element with Elastic Shear Calibrated to Yield – Lefas SW33 553
M.78 Pushover of Beam-Column Element with Elastic Shear Calibrated to Yield – Oesterle B1 553
M.79 Pushover of Beam-Column Element with Elastic Shear Calibrated to Yield – Oesterle B2 554
M.80 Pushover of Beam-Column Element with Elastic Shear Calibrated to Yield – Oesterle B3 554
M.81 Pushover of Beam-Column Element with Elastic Shear Calibrated to Yield – Oesterle B4 555
M.82 Pushover of Beam-Column Element with Elastic Shear Calibrated to Yield – Oesterle B5 555
M.83 Pushover of Beam-Column Element with Elastic Shear Calibrated to Yield – Oesterle B6 556
M.84 Pushover of Beam-Column Element with Elastic Shear Calibrated to Yield – Oesterle B7 556
M.85 Pushover of Beam-Column Element with Elastic Shear Calibrated to Yield – Oesterle B8 557
M.86 Pushover of Beam-Column Element with Elastic Shear Calibrated to Yield – Oesterle B9 557
M.87 Pushover of Beam-Column Element with Elastic Shear Calibrated to Yield – Oesterle B10 558
M.88 Pushover of Beam-Column Element with Elastic Shear Calibrated to Yield – Oesterle R1 558
M.89 Pushover of Beam-Column Element with Elastic Shear Calibrated to Yield – Oesterle R2 559
M.90 Pushover of Beam-Column Element with Elastic Shear Calibrated to Yield – Pilakoutas SW4 559
M.91 Pushover of Beam-Column Element with Elastic Shear Calibrated to Yield – Pilakoutas SW5 560
M.92 Pushover of Beam-Column Element with Elastic Shear Calibrated to Yield – Pilakoutas SW6 560
M.93 Pushover of Beam-Column Element with Elastic Shear Calibrated to Yield – Pilakoutas SW7 561
M.94 Pushover of Beam-Column Element with Elastic Shear Calibrated to Yield – Pilakoutas SW8 561

M.95 Pushover of Beam-Column Element with Elastic Shear Calibrated to Yield – Pilakoutas SW9 . . . 562
M.96 Pushover of Beam-Column Element with Elastic Shear Calibrated to Yield – Salonikios LSW1 . . . 562
M.97 Pushover of Beam-Column Element with Elastic Shear Calibrated to Yield – Salonikios LSW2 . . . 563
M.98 Pushover of Beam-Column Element with Elastic Shear Calibrated to Yield – Salonikios LSW3 . . . 563
M.99 Pushover of Beam-Column Element with Elastic Shear Calibrated to Yield – Salonikios MSW1 . . . 564
M.100 Pushover of Beam-Column Element with Elastic Shear Calibrated to Yield – Salonikios MSW2 . . . 564
M.101 Pushover of Beam-Column Element with Elastic Shear Calibrated to Yield – Salonikios MSW3 . . . 565
M.102 Pushover of Beam-Column Element with Elastic Shear Calibrated to Yield – Salonikios MSW6 . . . 565
M.103 Pushover of Beam-Column Element with Elastic Shear Calibrated to Yield – Sittipunt W1 . . . 566
M.104 Pushover of Beam-Column Element with Elastic Shear Calibrated to Yield – Sittipunt W2 . . . 566
M.105 Pushover of Beam-Column Element with Elastic Shear Calibrated to Yield – Tasnimi SHW1 . . . 567
M.106 Pushover of Beam-Column Element with Elastic Shear Calibrated to Yield – Tasnimi SHW2 . . . 567
M.107 Pushover of Beam-Column Element with Elastic Shear Calibrated to Yield – Tasnimi SHW3 . . . 568
M.108 Pushover of Beam-Column Element with Elastic Shear Calibrated to Yield – Tasnimi SHW4 . . . 568
M.109 Pushover of Beam-Column Element with Elastic Shear Calibrated to Yield – Thomsen RW1 . . . 569
M.110 Pushover of Beam-Column Element with Elastic Shear Calibrated to Yield – Thomsen RW2 . . . 569
M.111 Pushover of Beam-Column Element with Elastic Shear Calibrated to Yield – Vallenas SW3 . . . 570
M.112 Pushover of Beam-Column Element with Elastic Shear Calibrated to Yield – Vallenas SW4 . . . 570
M.113 Pushover of Beam-Column Element with Elastic Shear Calibrated to Yield – Vallenas SW5 . . . 571

M.114 Pushover of Beam-Column Element with Elastic Shear Calibrated to Yield – Vallenas SW6 . . . 571
M.115 Pushover of Beam-Column Element with Elastic Shear Calibrated to Yield – Wang SW1 . . . 572
M.116 Pushover of Beam-Column Element with Elastic Shear Calibrated to Yield – Wang SW2 . . . 572
M.117 Pushover of Beam-Column Element with Elastic Shear Calibrated to Yield – Yanez S1 . . . 573
M.118 Pushover of Beam-Column Element with Elastic Shear Calibrated to Yield – Zhang SW7 . . . 573
M.119 Pushover of Beam-Column Element with Elastic Shear Calibrated to Yield – Zhang SW8 . . . 574
M.120 Pushover of Beam-Column Element with Elastic Shear Calibrated to Yield – Zhang SW9 . . . 574
M.121 Pushover of Beam-Column Element with Elastic Shear Calibrated to Maximum Displacement – Lefas SW11 . . . 575
M.122 Pushover of Beam-Column Element with Elastic Shear Calibrated to Maximum Displacement – Lefas SW12 . . . 575
M.123 Pushover of Beam-Column Element with Elastic Shear Calibrated to Maximum Displacement – Lefas SW13 . . . 576
M.124 Pushover of Beam-Column Element with Elastic Shear Calibrated to Maximum Displacement – Lefas SW14 . . . 576
M.125 Pushover of Beam-Column Element with Elastic Shear Calibrated to Maximum Displacement – Lefas SW15 . . . 577
M.126 Pushover of Beam-Column Element with Elastic Shear Calibrated to Maximum Displacement – Lefas SW16 . . . 577
M.127 Pushover of Beam-Column Element with Elastic Shear Calibrated to Maximum Displacement – Lefas SW17 . . . 578
M.128 Pushover of Beam-Column Element with Elastic Shear Calibrated to Maximum Displacement – Lefas SW21 . . . 578
M.129 Pushover of Beam-Column Element with Elastic Shear Calibrated to Maximum Displacement – Lefas SW22 . . . 579
M.130 Pushover of Beam-Column Element with Elastic Shear Calibrated to Maximum Displacement – Lefas SW23 . . . 579
M.131 Pushover of Beam-Column Element with Elastic Shear Calibrated to Maximum Displacement – Lefas SW24 . . . 580
M.132 Pushover of Beam-Column Element with Elastic Shear Calibrated to Maximum Displacement – Lefas SW25 . . . 580

M.133 Pushover of Beam-Column Element with Elastic Shear Calibrated to Maximum Displacement – Lefas SW26 581
M.134 Pushover of Beam-Column Element with Elastic Shear Calibrated to Maximum Displacement – Lefas SW30 581
M.135 Pushover of Beam-Column Element with Elastic Shear Calibrated to Maximum Displacement – Lefas SW31 582
M.136 Pushover of Beam-Column Element with Elastic Shear Calibrated to Maximum Displacement – Lefas SW32 582
M.137 Pushover of Beam-Column Element with Elastic Shear Calibrated to Maximum Displacement – Lefas SW33 583
M.138 Pushover of Beam-Column Element with Elastic Shear Calibrated to Maximum Displacement – Oesterle B1 583
M.139 Pushover of Beam-Column Element with Elastic Shear Calibrated to Maximum Displacement – Oesterle B2 584
M.140 Pushover of Beam-Column Element with Elastic Shear Calibrated to Maximum Displacement – Oesterle B3 584
M.141 Pushover of Beam-Column Element with Elastic Shear Calibrated to Maximum Displacement – Oesterle B4 585
M.142 Pushover of Beam-Column Element with Elastic Shear Calibrated to Maximum Displacement – Oesterle B5 585
M.143 Pushover of Beam-Column Element with Elastic Shear Calibrated to Maximum Displacement – Oesterle B6 586
M.144 Pushover of Beam-Column Element with Elastic Shear Calibrated to Maximum Displacement – Oesterle B7 586
M.145 Pushover of Beam-Column Element with Elastic Shear Calibrated to Maximum Displacement – Oesterle B8 587
M.146 Pushover of Beam-Column Element with Elastic Shear Calibrated to Maximum Displacement – Oesterle B9 587
M.147 Pushover of Beam-Column Element with Elastic Shear Calibrated to Maximum Displacement – Oesterle B10 588
M.148 Pushover of Beam-Column Element with Elastic Shear Calibrated to Maximum Displacement – Oesterle R1 588
M.149 Pushover of Beam-Column Element with Elastic Shear Calibrated to Maximum Displacement – Oesterle R2 589
M.150 Pushover of Beam-Column Element with Elastic Shear Calibrated to Maximum Displacement – Pilakoutas SW4 589
M.151 Pushover of Beam-Column Element with Elastic Shear Calibrated to Maximum Displacement – Pilakoutas SW5 590

M.152 Pushover of Beam-Column Element with Elastic Shear Calibrated to Maximum Displacement – Pilakoutas SW6 590
M.153 Pushover of Beam-Column Element with Elastic Shear Calibrated to Maximum Displacement – Pilakoutas SW7 591
M.154 Pushover of Beam-Column Element with Elastic Shear Calibrated to Maximum Displacement – Pilakoutas SW8 591
M.155 Pushover of Beam-Column Element with Elastic Shear Calibrated to Maximum Displacement – Pilakoutas SW9 592
M.156 Pushover of Beam-Column Element with Elastic Shear Calibrated to Maximum Displacement – Salonikios LSW1 592
M.157 Pushover of Beam-Column Element with Elastic Shear Calibrated to Maximum Displacement – Salonikios LSW2 593
M.158 Pushover of Beam-Column Element with Elastic Shear Calibrated to Maximum Displacement – Salonikios LSW3 593
M.159 Pushover of Beam-Column Element with Elastic Shear Calibrated to Maximum Displacement – Salonikios MSW1 594
M.160 Pushover of Beam-Column Element with Elastic Shear Calibrated to Maximum Displacement – Salonikios MSW2 594
M.161 Pushover of Beam-Column Element with Elastic Shear Calibrated to Maximum Displacement – Salonikios MSW3 595
M.162 Pushover of Beam-Column Element with Elastic Shear Calibrated to Maximum Displacement – Salonikios MSW6 595
M.163 Pushover of Beam-Column Element with Elastic Shear Calibrated to Maximum Displacement – Sittipunt W1 596
M.164 Pushover of Beam-Column Element with Elastic Shear Calibrated to Maximum Displacement – Sittipunt W2 596
M.165 Pushover of Beam-Column Element with Elastic Shear Calibrated to Maximum Displacement – Tasnimi SHW1 597
M.166 Pushover of Beam-Column Element with Elastic Shear Calibrated to Maximum Displacement – Tasnimi SHW2 597
M.167 Pushover of Beam-Column Element with Elastic Shear Calibrated to Maximum Displacement – Tasnimi SHW3 598
M.168 Pushover of Beam-Column Element with Elastic Shear Calibrated to Maximum Displacement – Tasnimi SHW4 598
M.169 Pushover of Beam-Column Element with Elastic Shear Calibrated to Maximum Displacement – Thomsen RW1 599
M.170 Pushover of Beam-Column Element with Elastic Shear Calibrated to Maximum Displacement – Thomsen RW2 599

M.171 Pushover of Beam-Column Element with Elastic Shear Calibrated to Maximum Displacement – Vallenas SW3 600
M.172 Pushover of Beam-Column Element with Elastic Shear Calibrated to Maximum Displacement – Vallenas SW4 600
M.173 Pushover of Beam-Column Element with Elastic Shear Calibrated to Maximum Displacement – Vallenas SW5 601
M.174 Pushover of Beam-Column Element with Elastic Shear Calibrated to Maximum Displacement – Vallenas SW6 601
M.175 Pushover of Beam-Column Element with Elastic Shear Calibrated to Maximum Displacement – Wang SW1 602
M.176 Pushover of Beam-Column Element with Elastic Shear Calibrated to Maximum Displacement – Wang SW2 602
M.177 Pushover of Beam-Column Element with Elastic Shear Calibrated to Maximum Displacement – Yanez S1 603
M.178 Pushover of Beam-Column Element with Elastic Shear Calibrated to Maximum Displacement – Zhang SW7 603
M.179 Pushover of Beam-Column Element with Elastic Shear Calibrated to Maximum Displacement – Zhang SW8 604
M.180 Pushover of Beam-Column Element with Elastic Shear Calibrated to Maximum Displacement – Zhang SW9 604
M.181 Pushover of Beam-Column Element with Bar-Slip and Elastic Shear Calibrated to Yield – Lefas SW11 605
M.182 Pushover of Beam-Column Element with Bar-Slip and Elastic Shear Calibrated to Yield – Lefas SW12 605
M.183 Pushover of Beam-Column Element with Bar-Slip and Elastic Shear Calibrated to Yield – Lefas SW13 606
M.184 Pushover of Beam-Column Element with Bar-Slip and Elastic Shear Calibrated to Yield – Lefas SW14 606
M.185 Pushover of Beam-Column Element with Bar-Slip and Elastic Shear Calibrated to Yield – Lefas SW15 607
M.186 Pushover of Beam-Column Element with Bar-Slip and Elastic Shear Calibrated to Yield – Lefas SW16 607
M.187 Pushover of Beam-Column Element with Bar-Slip and Elastic Shear Calibrated to Yield – Lefas SW17 608
M.188 Pushover of Beam-Column Element with Bar-Slip and Elastic Shear Calibrated to Yield – Lefas SW21 608
M.189 Pushover of Beam-Column Element with Bar-Slip and Elastic Shear Calibrated to Yield – Lefas SW22 609

M.190 Pushover of Beam-Column Element with Bar-Slip and Elastic Shear Calibrated to Yield – Lefas SW23 609
M.191 Pushover of Beam-Column Element with Bar-Slip and Elastic Shear Calibrated to Yield – Lefas SW24 610
M.192 Pushover of Beam-Column Element with Bar-Slip and Elastic Shear Calibrated to Yield – Lefas SW25 610
M.193 Pushover of Beam-Column Element with Bar-Slip and Elastic Shear Calibrated to Yield – Lefas SW26 611
M.194 Pushover of Beam-Column Element with Bar-Slip and Elastic Shear Calibrated to Yield – Lefas SW30 611
M.195 Pushover of Beam-Column Element with Bar-Slip and Elastic Shear Calibrated to Yield – Lefas SW31 612
M.196 Pushover of Beam-Column Element with Bar-Slip and Elastic Shear Calibrated to Yield – Lefas SW32 612
M.197 Pushover of Beam-Column Element with Bar-Slip and Elastic Shear Calibrated to Yield – Lefas SW33 613
M.198 Pushover of Beam-Column Element with Bar-Slip and Elastic Shear Calibrated to Yield – Oesterle B1 613
M.199 Pushover of Beam-Column Element with Bar-Slip and Elastic Shear Calibrated to Yield – Oesterle B2 614
M.200 Pushover of Beam-Column Element with Bar-Slip and Elastic Shear Calibrated to Yield – Oesterle B3 614
M.201 Pushover of Beam-Column Element with Bar-Slip and Elastic Shear Calibrated to Yield – Oesterle B4 615
M.202 Pushover of Beam-Column Element with Bar-Slip and Elastic Shear Calibrated to Yield – Oesterle B5 615
M.203 Pushover of Beam-Column Element with Bar-Slip and Elastic Shear Calibrated to Yield – Oesterle B6 616
M.204 Pushover of Beam-Column Element with Bar-Slip and Elastic Shear Calibrated to Yield – Oesterle B7 616
M.205 Pushover of Beam-Column Element with Bar-Slip and Elastic Shear Calibrated to Yield – Oesterle B8 617
M.206 Pushover of Beam-Column Element with Bar-Slip and Elastic Shear Calibrated to Yield – Oesterle B9 617
M.207 Pushover of Beam-Column Element with Bar-Slip and Elastic Shear Calibrated to Yield – Oesterle B10 618
M.208 Pushover of Beam-Column Element with Bar-Slip and Elastic Shear Calibrated to Yield – Oesterle R1 618

M.209 Pushover of Beam-Column Element with Bar-Slip and Elastic Shear Calibrated to Yield – Oesterle R2 619
M.210 Pushover of Beam-Column Element with Bar-Slip and Elastic Shear Calibrated to Yield – Pilakoutas SW4 619
M.211 Pushover of Beam-Column Element with Bar-Slip and Elastic Shear Calibrated to Yield – Pilakoutas SW5 620
M.212 Pushover of Beam-Column Element with Bar-Slip and Elastic Shear Calibrated to Yield – Pilakoutas SW6 620
M.213 Pushover of Beam-Column Element with Bar-Slip and Elastic Shear Calibrated to Yield – Pilakoutas SW7 621
M.214 Pushover of Beam-Column Element with Bar-Slip and Elastic Shear Calibrated to Yield – Pilakoutas SW8 621
M.215 Pushover of Beam-Column Element with Bar-Slip and Elastic Shear Calibrated to Yield – Pilakoutas SW9 622
M.216 Pushover of Beam-Column Element with Bar-Slip and Elastic Shear Calibrated to Yield – Salonikios LSW1 622
M.217 Pushover of Beam-Column Element with Bar-Slip and Elastic Shear Calibrated to Yield – Salonikios LSW2 623
M.218 Pushover of Beam-Column Element with Bar-Slip and Elastic Shear Calibrated to Yield – Salonikios LSW3 623
M.219 Pushover of Beam-Column Element with Bar-Slip and Elastic Shear Calibrated to Yield – Salonikios MSW1 624
M.220 Pushover of Beam-Column Element with Bar-Slip and Elastic Shear Calibrated to Yield – Salonikios MSW2 624
M.221 Pushover of Beam-Column Element with Bar-Slip and Elastic Shear Calibrated to Yield – Salonikios MSW3 625
M.222 Pushover of Beam-Column Element with Bar-Slip and Elastic Shear Calibrated to Yield – Salonikios MSW6 625
M.223 Pushover of Beam-Column Element with Bar-Slip and Elastic Shear Calibrated to Yield – Sittipunt W1 626
M.224 Pushover of Beam-Column Element with Bar-Slip and Elastic Shear Calibrated to Yield – Sittipunt W2 626
M.225 Pushover of Beam-Column Element with Bar-Slip and Elastic Shear Calibrated to Yield – Tasnimi SHW1 627
M.226 Pushover of Beam-Column Element with Bar-Slip and Elastic Shear Calibrated to Yield – Tasnimi SHW2 627
M.227 Pushover of Beam-Column Element with Bar-Slip and Elastic Shear Calibrated to Yield – Tasnimi SHW3 628

M.228 Pushover of Beam-Column Element with Bar-Slip and Elastic Shear Calibrated to Yield – Tasnimi SHW4 628
M.229 Pushover of Beam-Column Element with Bar-Slip and Elastic Shear Calibrated to Yield – Thomsen RW1 629
M.230 Pushover of Beam-Column Element with Bar-Slip and Elastic Shear Calibrated to Yield – Thomsen RW2 629
M.231 Pushover of Beam-Column Element with Bar-Slip and Elastic Shear Calibrated to Yield – Vallenas SW3 630
M.232 Pushover of Beam-Column Element with Bar-Slip and Elastic Shear Calibrated to Yield – Vallenas SW4 630
M.233 Pushover of Beam-Column Element with Bar-Slip and Elastic Shear Calibrated to Yield – Vallenas SW5 631
M.234 Pushover of Beam-Column Element with Bar-Slip and Elastic Shear Calibrated to Yield – Vallenas SW6 631
M.235 Pushover of Beam-Column Element with Bar-Slip and Elastic Shear Calibrated to Yield – Wang SW1 632
M.236 Pushover of Beam-Column Element with Bar-Slip and Elastic Shear Calibrated to Yield – Wang SW2 632
M.237 Pushover of Beam-Column Element with Bar-Slip and Elastic Shear Calibrated to Yield – Yanez S1 633
M.238 Pushover of Beam-Column Element with Bar-Slip and Elastic Shear Calibrated to Yield – Zhang SW7 633
M.239 Pushover of Beam-Column Element with Bar-Slip and Elastic Shear Calibrated to Yield – Zhang SW8 634
M.240 Pushover of Beam-Column Element with Bar-Slip and Elastic Shear Calibrated to Yield – Zhang SW9 634
M.241 Pushover of Beam-Column Element with Bar-Slip and Elastic Shear Calibrated to Maximum Displacement – Lefas SW11 635
M.242 Pushover of Beam-Column Element with Bar-Slip and Elastic Shear Calibrated to Maximum Displacement – Lefas SW12 635
M.243 Pushover of Beam-Column Element with Bar-Slip and Elastic Shear Calibrated to Maximum Displacement – Lefas SW13 636
M.244 Pushover of Beam-Column Element with Bar-Slip and Elastic Shear Calibrated to Maximum Displacement – Lefas SW14 636
M.245 Pushover of Beam-Column Element with Bar-Slip and Elastic Shear Calibrated to Maximum Displacement – Lefas SW15 637
M.246 Pushover of Beam-Column Element with Bar-Slip and Elastic Shear Calibrated to Maximum Displacement – Lefas SW16 637

M.247 Pushover of Beam-Column Element with Bar-Slip and Elastic Shear Calibrated to Maximum Displacement – Lefas SW17 638
M.248 Pushover of Beam-Column Element with Bar-Slip and Elastic Shear Calibrated to Maximum Displacement – Lefas SW21 638
M.249 Pushover of Beam-Column Element with Bar-Slip and Elastic Shear Calibrated to Maximum Displacement – Lefas SW22 639
M.250 Pushover of Beam-Column Element with Bar-Slip and Elastic Shear Calibrated to Maximum Displacement – Lefas SW23 639
M.251 Pushover of Beam-Column Element with Bar-Slip and Elastic Shear Calibrated to Maximum Displacement – Lefas SW24 640
M.252 Pushover of Beam-Column Element with Bar-Slip and Elastic Shear Calibrated to Maximum Displacement – Lefas SW25 640
M.253 Pushover of Beam-Column Element with Bar-Slip and Elastic Shear Calibrated to Maximum Displacement – Lefas SW26 641
M.254 Pushover of Beam-Column Element with Bar-Slip and Elastic Shear Calibrated to Maximum Displacement – Lefas SW30 641
M.255 Pushover of Beam-Column Element with Bar-Slip and Elastic Shear Calibrated to Maximum Displacement – Lefas SW31 642
M.256 Pushover of Beam-Column Element with Bar-Slip and Elastic Shear Calibrated to Maximum Displacement – Lefas SW32 642
M.257 Pushover of Beam-Column Element with Bar-Slip and Elastic Shear Calibrated to Maximum Displacement – Lefas SW33 643
M.258 Pushover of Beam-Column Element with Bar-Slip and Elastic Shear Calibrated to Maximum Displacement – Oesterle B1 643
M.259 Pushover of Beam-Column Element with Bar-Slip and Elastic Shear Calibrated to Maximum Displacement – Oesterle B2 644
M.260 Pushover of Beam-Column Element with Bar-Slip and Elastic Shear Calibrated to Maximum Displacement – Oesterle B3 644
M.261 Pushover of Beam-Column Element with Bar-Slip and Elastic Shear Calibrated to Maximum Displacement – Oesterle B4 645
M.262 Pushover of Beam-Column Element with Bar-Slip and Elastic Shear Calibrated to Maximum Displacement – Oesterle B5 645
M.263 Pushover of Beam-Column Element with Bar-Slip and Elastic Shear Calibrated to Maximum Displacement – Oesterle B6 646
M.264 Pushover of Beam-Column Element with Bar-Slip and Elastic Shear Calibrated to Maximum Displacement – Oesterle B7 646
M.265 Pushover of Beam-Column Element with Bar-Slip and Elastic Shear Calibrated to Maximum Displacement – Oesterle B8 647

M.266 Pushover of Beam-Column Element with Bar-Slip and Elastic Shear Calibrated to Maximum Displacement – Oesterle B9 647
M.267 Pushover of Beam-Column Element with Bar-Slip and Elastic Shear Calibrated to Maximum Displacement – Oesterle B10 648
M.268 Pushover of Beam-Column Element with Bar-Slip and Elastic Shear Calibrated to Maximum Displacement – Oesterle R1 648
M.269 Pushover of Beam-Column Element with Bar-Slip and Elastic Shear Calibrated to Maximum Displacement – Oesterle R2 649
M.270 Pushover of Beam-Column Element with Bar-Slip and Elastic Shear Calibrated to Maximum Displacement – Pilakoutas SW4 649
M.271 Pushover of Beam-Column Element with Bar-Slip and Elastic Shear Calibrated to Maximum Displacement – Pilakoutas SW5 650
M.272 Pushover of Beam-Column Element with Bar-Slip and Elastic Shear Calibrated to Maximum Displacement – Pilakoutas SW6 650
M.273 Pushover of Beam-Column Element with Bar-Slip and Elastic Shear Calibrated to Maximum Displacement – Pilakoutas SW7 651
M.274 Pushover of Beam-Column Element with Bar-Slip and Elastic Shear Calibrated to Maximum Displacement – Pilakoutas SW8 651
M.275 Pushover of Beam-Column Element with Bar-Slip and Elastic Shear Calibrated to Maximum Displacement – Pilakoutas SW9 652
M.276 Pushover of Beam-Column Element with Bar-Slip and Elastic Shear Calibrated to Maximum Displacement – Salonikios LSW1 652
M.277 Pushover of Beam-Column Element with Bar-Slip and Elastic Shear Calibrated to Maximum Displacement – Salonikios LSW2 653
M.278 Pushover of Beam-Column Element with Bar-Slip and Elastic Shear Calibrated to Maximum Displacement – Salonikios LSW3 653
M.279 Pushover of Beam-Column Element with Bar-Slip and Elastic Shear Calibrated to Maximum Displacement – Salonikios MSW1 654
M.280 Pushover of Beam-Column Element with Bar-Slip and Elastic Shear Calibrated to Maximum Displacement – Salonikios MSW2 654
M.281 Pushover of Beam-Column Element with Bar-Slip and Elastic Shear Calibrated to Maximum Displacement – Salonikios MSW3 655
M.282 Pushover of Beam-Column Element with Bar-Slip and Elastic Shear Calibrated to Maximum Displacement – Salonikios MSW6 655
M.283 Pushover of Beam-Column Element with Bar-Slip and Elastic Shear Calibrated to Maximum Displacement – Sittipunt W1 656
M.284 Pushover of Beam-Column Element with Bar-Slip and Elastic Shear Calibrated to Maximum Displacement – Sittipunt W2 656

M.285 Pushover of Beam-Column Element with Bar-Slip and Elastic Shear Calibrated to Maximum Displacement – Tasnimi SHW1 657
M.286 Pushover of Beam-Column Element with Bar-Slip and Elastic Shear Calibrated to Maximum Displacement – Tasnimi SHW2 657
M.287 Pushover of Beam-Column Element with Bar-Slip and Elastic Shear Calibrated to Maximum Displacement – Tasnimi SHW3 658
M.288 Pushover of Beam-Column Element with Bar-Slip and Elastic Shear Calibrated to Maximum Displacement – Tasnimi SHW4 658
M.289 Pushover of Beam-Column Element with Bar-Slip and Elastic Shear Calibrated to Maximum Displacement – Thomsen RW1 659
M.290 Pushover of Beam-Column Element with Bar-Slip and Elastic Shear Calibrated to Maximum Displacement – Thomsen RW2 659
M.291 Pushover of Beam-Column Element with Bar-Slip and Elastic Shear Calibrated to Maximum Displacement – Vallenas SW3 660
M.292 Pushover of Beam-Column Element with Bar-Slip and Elastic Shear Calibrated to Maximum Displacement – Vallenas SW4 660
M.293 Pushover of Beam-Column Element with Bar-Slip and Elastic Shear Calibrated to Maximum Displacement – Vallenas SW5 661
M.294 Pushover of Beam-Column Element with Bar-Slip and Elastic Shear Calibrated to Maximum Displacement – Vallenas SW6 661
M.295 Pushover of Beam-Column Element with Bar-Slip and Elastic Shear Calibrated to Maximum Displacement – Wang SW1 662
M.296 Pushover of Beam-Column Element with Bar-Slip and Elastic Shear Calibrated to Maximum Displacement – Wang SW2 662
M.297 Pushover of Beam-Column Element with Bar-Slip and Elastic Shear Calibrated to Maximum Displacement – Yanez S1 663
M.298 Pushover of Beam-Column Element with Bar-Slip and Elastic Shear Calibrated to Maximum Displacement – Zhang SW7 663
M.299 Pushover of Beam-Column Element with Bar-Slip and Elastic Shear Calibrated to Maximum Displacement – Zhang SW8 664
M.300 Pushover of Beam-Column Element with Bar-Slip and Elastic Shear Calibrated to Maximum Displacement – Zhang SW9 664

N.1 Elastic Shear Secant Stiffness Absolute Error Change v. Max Shear Stress Ratio 666
N.2 Elastic Shear Secant Stiffness Absolute Error Change v. Max Shear Demand Ratio 666
N.3 Elastic Shear Secant Stiffness Absolute Error Change v. Aspect Ratio . . . 667

N.4 Elastic Shear Secant Stiffness Absolute Error Change v. Normalized Thickness . . . 667
N.5 Elastic Shear Secant Stiffness Absolute Error Change v. Long Reinf Ratio in BE . . . 668
N.6 Elastic Shear Secant Stiffness Absolute Error Change v. Horiz Reinf Ratio . 668
N.7 Elastic Shear Secant Stiffness Absolute Error Change v. Vol Trans Reinf Ratio . . . 669
N.8 Elastic Shear Secant Stiffness Absolute Error Change v. Yield Shear Stress Ratio . . . 669
N.9 Elastic Shear Secant Stiffness Absolute Error Change v. Yield Shear Demand Ratio . . . 670
N.10 Elastic Shear Secant Stiffness Absolute Error Change v. Axial Load Ratio . 670
N.11 Elastic Shear Yield Displacement Absolute Error Change v. Max Shear Stress Ratio . . . 671
N.12 Elastic Shear Yield Displacement Absolute Error Change v. Max Shear Demand Ratio . . . 671
N.13 Elastic Shear Yield Displacement Absolute Error Change v. Aspect Ratio . 672
N.14 Elastic Shear Yield Displacement Absolute Error Change v. Normalized Thickness . . . 672
N.15 Elastic Shear Yield Displacement Absolute Error Change v. Long Reinf Ratio in BE . . . 673
N.16 Elastic Shear Yield Displacement Absolute Error Change v. Horiz Reinf Ratio . . . 673
N.17 Elastic Shear Yield Displacement Absolute Error Change v. Vol Trans Reinf Ratio . . . 674
N.18 Elastic Shear Yield Displacement Absolute Error Change v. Yield Shear Stress Ratio . . . 674
N.19 Elastic Shear Yield Displacement Absolute Error Change v. Yield Shear Demand Ratio . . . 675
N.20 Elastic Shear Yield Displacement Absolute Error Change v. Axial Load Ratio 675
N.21 Elastic Shear Max Displacement Absolute Error Change v. Max Shear Stress Ratio . . . 676
N.22 Elastic Shear Max Displacement Absolute Error Change v. Max Shear Demand Ratio . . . 676
N.23 Elastic Shear Max Displacement Absolute Error Change v. Aspect Ratio . . 677
N.24 Elastic Shear Max Displacement Absolute Error Change v. Normalized Thickness . . . 677

N.25 Elastic Shear Max Displacement Absolute Error Change v. Long Reinf Ratio in BE . . . 678
N.26 Elastic Shear Max Displacement Absolute Error Change v. Horiz Reinf Ratio 678
N.27 Elastic Shear Max Displacement Absolute Error Change v. Vol Trans Reinf Ratio . . . 679
N.28 Elastic Shear Max Displacement Absolute Error Change v. Yield Shear Stress Ratio . . . 679
N.29 Elastic Shear Max Displacement Absolute Error Change v. Yield Shear Demand Ratio . . . 680
N.30 Elastic Shear Max Displacement Absolute Error Change v. Axial Load Ratio 680
N.31 Elastic Shear Secant Stiffness Relative Error Change v. Max Shear Stress Ratio . . . 681
N.32 Elastic Shear Secant Stiffness Relative Error Change v. Max Shear Demand Ratio . . . 681
N.33 Elastic Shear Secant Stiffness Relative Error Change v. Aspect Ratio 682
N.34 Elastic Shear Secant Stiffness Relative Error Change v. Normalized Thickness 682
N.35 Elastic Shear Secant Stiffness Relative Error Change v. Long Reinf Ratio in BE . . . 683
N.36 Elastic Shear Secant Stiffness Relative Error Change v. Horiz Reinf Ratio . 683
N.37 Elastic Shear Secant Stiffness Relative Error Change v. Vol Trans Reinf Ratio . . . 684
N.38 Elastic Shear Secant Stiffness Relative Error Change v. Yield Shear Stress Ratio . . . 684
N.39 Elastic Shear Secant Stiffness Relative Error Change v. Yield Shear Demand Ratio . . . 685
N.40 Elastic Shear Secant Stiffness Relative Error Change v. Axial Load Ratio . 685
N.41 Elastic Shear Yield Displacement Relative Error Change v. Max Shear Stress Ratio . . . 686
N.42 Elastic Shear Yield Displacement Relative Error Change v. Max Shear Demand Ratio . . . 686
N.43 Elastic Shear Yield Displacement Relative Error Change v. Aspect Ratio . 687
N.44 Elastic Shear Yield Displacement Relative Error Change v. Normalized Thickness . . . 687
N.45 Elastic Shear Yield Displacement Relative Error Change v. Long Reinf Ratio in BE . . . 688
N.46 Elastic Shear Yield Displacement Relative Error Change v. Horiz Reinf Ratio 688

N.47 Elastic Shear Yield Displacement Relative Error Change v. Vol Trans Reinf Ratio . . . 689
N.48 Elastic Shear Yield Displacement Relative Error Change v. Yield Shear Stress Ratio . . . 689
N.49 Elastic Shear Yield Displacement Relative Error Change v. Yield Shear Demand Ratio . . . 690
N.50 Elastic Shear Yield Displacement Relative Error Change v. Axial Load Ratio 690
N.51 Elastic Shear Max Displacement Relative Error Change v. Max Shear Stress Ratio . . . 691
N.52 Elastic Shear Max Displacement Relative Error Change v. Max Shear Demand Ratio . . . 691
N.53 Elastic Shear Max Displacement Relative Error Change v. Aspect Ratio . . 692
N.54 Elastic Shear Max Displacement Relative Error Change v. Normalized Thickness . . . 692
N.55 Elastic Shear Max Displacement Relative Error Change v. Long Reinf Ratio in BE . . . 693
N.56 Elastic Shear Max Displacement Relative Error Change v. Horiz Reinf Ratio 693
N.57 Elastic Shear Max Displacement Relative Error Change v. Vol Trans Reinf Ratio . . . 694
N.58 Elastic Shear Max Displacement Relative Error Change v. Yield Shear Stress Ratio . . . 694
N.59 Elastic Shear Max Displacement Relative Error Change v. Yield Shear Demand Ratio . . . 695
N.60 Elastic Shear Max Displacement Relative Error Change v. Axial Load Ratio 695
N.61 Effective Shear Calibrated to Yield Displacement Secant Stiffness Absolute Error Change v. Max Shear Stress Ratio . . . 696
N.62 Effective Shear Calibrated to Yield Displacement Secant Stiffness Absolute Error Change v. Max Shear Demand Ratio . . . 696
N.63 Effective Shear Calibrated to Yield Displacement Secant Stiffness Absolute Error Change v. Aspect Ratio . . . 697
N.64 Effective Shear Calibrated to Yield Displacement Secant Stiffness Absolute Error Change v. Normalized Thickness . . . 697
N.65 Effective Shear Calibrated to Yield Displacement Secant Stiffness Absolute Error Change v. Long Reinf Ratio in BE . . . 698
N.66 Effective Shear Calibrated to Yield Displacement Secant Stiffness Absolute Error Change v. Horiz Reinf Ratio . . . 698
N.67 Effective Shear Calibrated to Yield Displacement Secant Stiffness Absolute Error Change v. Vol Trans Reinf Ratio . . . 699

N.68 Effective Shear Calibrated to Yield Displacement Secant Stiffness Absolute Error Change v. Yield Shear Stress Ratio 699
N.69 Effective Shear Calibrated to Yield Displacement Secant Stiffness Absolute Error Change v. Yield Shear Demand Ratio 700
N.70 Effective Shear Calibrated to Yield Displacement Secant Stiffness Absolute Error Change v. Axial Load Ratio 700
N.71 Effective Shear Calibrated to Yield Displacement Yield Displacement Absolute Error Change v. Max Shear Stress Ratio 701
N.72 Effective Shear Calibrated to Yield Displacement Yield Displacement Absolute Error Change v. Max Shear Demand Ratio 701
N.73 Effective Shear Calibrated to Yield Displacement Yield Displacement Absolute Error Change v. Aspect Ratio 702
N.74 Effective Shear Calibrated to Yield Displacement Yield Displacement Absolute Error Change v. Normalized Thickness 702
N.75 Effective Shear Calibrated to Yield Displacement Yield Displacement Absolute Error Change v. Long Reinf Ratio in BE 703
N.76 Effective Shear Calibrated to Yield Displacement Yield Displacement Absolute Error Change v. Horiz Reinf Ratio 703
N.77 Effective Shear Calibrated to Yield Displacement Yield Displacement Absolute Error Change v. Vol Trans Reinf Ratio 704
N.78 Effective Shear Calibrated to Yield Displacement Yield Displacement Absolute Error Change v. Yield Shear Stress Ratio 704
N.79 Effective Shear Calibrated to Yield Displacement Yield Displacement Absolute Error Change v. Yield Shear Demand Ratio 705
N.80 Effective Shear Calibrated to Yield Displacement Yield Displacement Absolute Error Change v. Axial Load Ratio 705
N.81 Effective Shear Calibrated to Yield Displacement Max Displacement Absolute Error Change v. Max Shear Stress Ratio 706
N.82 Effective Shear Calibrated to Yield Displacement Max Displacement Absolute Error Change v. Max Shear Demand Ratio 706
N.83 Effective Shear Calibrated to Yield Displacement Max Displacement Absolute Error Change v. Aspect Ratio 707
N.84 Effective Shear Calibrated to Yield Displacement Max Displacement Absolute Error Change v. Normalized Thickness 707
N.85 Effective Shear Calibrated to Yield Displacement Max Displacement Absolute Error Change v. Long Reinf Ratio in BE 708
N.86 Effective Shear Calibrated to Yield Displacement Max Displacement Absolute Error Change v. Horiz Reinf Ratio 708

N.87 Effective Shear Calibrated to Yield Displacement Max Displacement Absolute Error Change v. Vol Trans Reinf Ratio 709
N.88 Effective Shear Calibrated to Yield Displacement Max Displacement Absolute Error Change v. Yield Shear Stress Ratio 709
N.89 Effective Shear Calibrated to Yield Displacement Max Displacement Absolute Error Change v. Yield Shear Demand Ratio 710
N.90 Effective Shear Calibrated to Yield Displacement Max Displacement Absolute Error Change v. Axial Load Ratio 710
N.91 Effective Shear Calibrated to Yield Displacement Secant Stiffness Relative Error Change v. Max Shear Stress Ratio 711
N.92 Effective Shear Calibrated to Yield Displacement Secant Stiffness Relative Error Change v. Max Shear Demand Ratio 711
N.93 Effective Shear Calibrated to Yield Displacement Secant Stiffness Relative Error Change v. Aspect Ratio 712
N.94 Effective Shear Calibrated to Yield Displacement Secant Stiffness Relative Error Change v. Normalized Thickness 712
N.95 Effective Shear Calibrated to Yield Displacement Secant Stiffness Relative Error Change v. Long Reinf Ratio in BE 713
N.96 Effective Shear Calibrated to Yield Displacement Secant Stiffness Relative Error Change v. Horiz Reinf Ratio 713
N.97 Effective Shear Calibrated to Yield Displacement Secant Stiffness Relative Error Change v. Vol Trans Reinf Ratio 714
N.98 Effective Shear Calibrated to Yield Displacement Secant Stiffness Relative Error Change v. Yield Shear Stress Ratio 714
N.99 Effective Shear Calibrated to Yield Displacement Secant Stiffness Relative Error Change v. Yield Shear Demand Ratio 715
N.100 Effective Shear Calibrated to Yield Displacement Secant Stiffness Relative Error Change v. Axial Load Ratio 715
N.101 Effective Shear Calibrated to Yield Displacement Yield Displacement Relative Error Change v. Max Shear Stress Ratio 716
N.102 Effective Shear Calibrated to Yield Displacement Yield Displacement Relative Error Change v. Max Shear Demand Ratio 716
N.103 Effective Shear Calibrated to Yield Displacement Yield Displacement Relative Error Change v. Aspect Ratio 717
N.104 Effective Shear Calibrated to Yield Displacement Yield Displacement Relative Error Change v. Normalized Thickness 717
N.105 Effective Shear Calibrated to Yield Displacement Yield Displacement Relative Error Change v. Long Reinf Ratio in BE 718

N.106 Effective Shear Calibrated to Yield Displacement Yield Displacement Relative Error Change v. Horiz Reinf Ratio 718
N.107 Effective Shear Calibrated to Yield Displacement Yield Displacement Relative Error Change v. Vol Trans Reinf Ratio 719
N.108 Effective Shear Calibrated to Yield Displacement Yield Displacement Relative Error Change v. Yield Shear Stress Ratio 719
N.109 Effective Shear Calibrated to Yield Displacement Yield Displacement Relative Error Change v. Yield Shear Demand Ratio 720
N.110 Effective Shear Calibrated to Yield Displacement Yield Displacement Relative Error Change v. Axial Load Ratio 720
N.111 Effective Shear Calibrated to Yield Displacement Max Displacement Relative Error Change v. Max Shear Stress Ratio 721
N.112 Effective Shear Calibrated to Yield Displacement Max Displacement Relative Error Change v. Max Shear Demand Ratio 721
N.113 Effective Shear Calibrated to Yield Displacement Max Displacement Relative Error Change v. Aspect Ratio 722
N.114 Effective Shear Calibrated to Yield Displacement Max Displacement Relative Error Change v. Normalized Thickness 722
N.115 Effective Shear Calibrated to Yield Displacement Max Displacement Relative Error Change v. Long Reinf Ratio in BE 723
N.116 Effective Shear Calibrated to Yield Displacement Max Displacement Relative Error Change v. Horiz Reinf Ratio 723
N.117 Effective Shear Calibrated to Yield Displacement Max Displacement Relative Error Change v. Vol Trans Reinf Ratio 724
N.118 Effective Shear Calibrated to Yield Displacement Max Displacement Relative Error Change v. Yield Shear Stress Ratio 724
N.119 Effective Shear Calibrated to Yield Displacement Max Displacement Relative Error Change v. Yield Shear Demand Ratio 725
N.120 Effective Shear Calibrated to Yield Displacement Max Displacement Relative Error Change v. Axial Load Ratio 725
N.121 Effective Shear Calibrated to Max Displacement Secant Stiffness Absolute Error Change v. Max Shear Stress Ratio 726
N.122 Effective Shear Calibrated to Max Displacement Secant Stiffness Absolute Error Change v. Max Shear Demand Ratio 726
N.123 Effective Shear Calibrated to Max Displacement Secant Stiffness Absolute Error Change v. Aspect Ratio 727
N.124 Effective Shear Calibrated to Max Displacement Secant Stiffness Absolute Error Change v. Normalized Thickness 727

N.125 Effective Shear Calibrated to Max Displacement Secant Stiffness Absolute Error Change v. Long Reinf Ratio in BE 728
N.126 Effective Shear Calibrated to Max Displacement Secant Stiffness Absolute Error Change v. Horiz Reinf Ratio 728
N.127 Effective Shear Calibrated to Max Displacement Secant Stiffness Absolute Error Change v. Vol Trans Reinf Ratio 729
N.128 Effective Shear Calibrated to Max Displacement Secant Stiffness Absolute Error Change v. Yield Shear Stress Ratio 729
N.129 Effective Shear Calibrated to Max Displacement Secant Stiffness Absolute Error Change v. Yield Shear Demand Ratio 730
N.130 Effective Shear Calibrated to Max Displacement Secant Stiffness Absolute Error Change v. Axial Load Ratio 730
N.131 Effective Shear Calibrated to Max Displacement Yield Displacement Absolute Error Change v. Max Shear Stress Ratio 731
N.132 Effective Shear Calibrated to Max Displacement Yield Displacement Absolute Error Change v. Max Shear Demand Ratio 731
N.133 Effective Shear Calibrated to Max Displacement Yield Displacement Absolute Error Change v. Aspect Ratio 732
N.134 Effective Shear Calibrated to Max Displacement Yield Displacement Absolute Error Change v. Normalized Thickness 732
N.135 Effective Shear Calibrated to Max Displacement Yield Displacement Absolute Error Change v. Long Reinf Ratio in BE 733
N.136 Effective Shear Calibrated to Max Displacement Yield Displacement Absolute Error Change v. Horiz Reinf Ratio 733
N.137 Effective Shear Calibrated to Max Displacement Yield Displacement Absolute Error Change v. Vol Trans Reinf Ratio 734
N.138 Effective Shear Calibrated to Max Displacement Yield Displacement Absolute Error Change v. Yield Shear Stress Ratio 734
N.139 Effective Shear Calibrated to Max Displacement Yield Displacement Absolute Error Change v. Yield Shear Demand Ratio 735
N.140 Effective Shear Calibrated to Max Displacement Yield Displacement Absolute Error Change v. Axial Load Ratio 735
N.141 Effective Shear Calibrated to Max Displacement Max Displacement Absolute Error Change v. Max Shear Stress Ratio 736
N.142 Effective Shear Calibrated to Max Displacement Max Displacement Absolute Error Change v. Max Shear Demand Ratio 736
N.143 Effective Shear Calibrated to Max Displacement Max Displacement Absolute Error Change v. Aspect Ratio 737

N.144 Effective Shear Calibrated to Max Displacement Max Displacement Absolute Error Change v. Normalized Thickness 737
N.145 Effective Shear Calibrated to Max Displacement Max Displacement Absolute Error Change v. Long Reinf Ratio in BE 738
N.146 Effective Shear Calibrated to Max Displacement Max Displacement Absolute Error Change v. Horiz Reinf Ratio 738
N.147 Effective Shear Calibrated to Max Displacement Max Displacement Absolute Error Change v. Vol Trans Reinf Ratio 739
N.148 Effective Shear Calibrated to Max Displacement Max Displacement Absolute Error Change v. Yield Shear Stress Ratio 739
N.149 Effective Shear Calibrated to Max Displacement Max Displacement Absolute Error Change v. Yield Shear Demand Ratio 740
N.150 Effective Shear Calibrated to Max Displacement Max Displacement Absolute Error Change v. Axial Load Ratio 740
N.151 Effective Shear Calibrated to Max Displacement Secant Stiffness Relative Error Change v. Max Shear Stress Ratio 741
N.152 Effective Shear Calibrated to Max Displacement Secant Stiffness Relative Error Change v. Max Shear Demand Ratio 741
N.153 Effective Shear Calibrated to Max Displacement Secant Stiffness Relative Error Change v. Aspect Ratio 742
N.154 Effective Shear Calibrated to Max Displacement Secant Stiffness Relative Error Change v. Normalized Thickness 742
N.155 Effective Shear Calibrated to Max Displacement Secant Stiffness Relative Error Change v. Long Reinf Ratio in BE 743
N.156 Effective Shear Calibrated to Max Displacement Secant Stiffness Relative Error Change v. Horiz Reinf Ratio 743
N.157 Effective Shear Calibrated to Max Displacement Secant Stiffness Relative Error Change v. Vol Trans Reinf Ratio 744
N.158 Effective Shear Calibrated to Max Displacement Secant Stiffness Relative Error Change v. Yield Shear Stress Ratio 744
N.159 Effective Shear Calibrated to Max Displacement Secant Stiffness Relative Error Change v. Yield Shear Demand Ratio 745
N.160 Effective Shear Calibrated to Max Displacement Secant Stiffness Relative Error Change v. Axial Load Ratio 745
N.161 Effective Shear Calibrated to Max Displacement Yield Displacement Relative Error Change v. Max Shear Stress Ratio 746
N.162 Effective Shear Calibrated to Max Displacement Yield Displacement Relative Error Change v. Max Shear Demand Ratio 746

N.163 Effective Shear Calibrated to Max Displacement Yield Displacement Relative Error Change v. Aspect Ratio 747
N.164 Effective Shear Calibrated to Max Displacement Yield Displacement Relative Error Change v. Normalized Thickness 747
N.165 Effective Shear Calibrated to Max Displacement Yield Displacement Relative Error Change v. Long Reinf Ratio in BE 748
N.166 Effective Shear Calibrated to Max Displacement Yield Displacement Relative Error Change v. Horiz Reinf Ratio 748
N.167 Effective Shear Calibrated to Max Displacement Yield Displacement Relative Error Change v. Vol Trans Reinf Ratio 749
N.168 Effective Shear Calibrated to Max Displacement Yield Displacement Relative Error Change v. Yield Shear Stress Ratio 749
N.169 Effective Shear Calibrated to Max Displacement Yield Displacement Relative Error Change v. Yield Shear Demand Ratio 750
N.170 Effective Shear Calibrated to Max Displacement Yield Displacement Relative Error Change v. Axial Load Ratio 750
N.171 Effective Shear Calibrated to Max Displacement Max Displacement Relative Error Change v. Max Shear Stress Ratio 751
N.172 Effective Shear Calibrated to Max Displacement Max Displacement Relative Error Change v. Max Shear Demand Ratio 751
N.173 Effective Shear Calibrated to Max Displacement Max Displacement Relative Error Change v. Aspect Ratio 752
N.174 Effective Shear Calibrated to Max Displacement Max Displacement Relative Error Change v. Normalized Thickness 752
N.175 Effective Shear Calibrated to Max Displacement Max Displacement Relative Error Change v. Long Reinf Ratio in BE 753
N.176 Effective Shear Calibrated to Max Displacement Max Displacement Relative Error Change v. Horiz Reinf Ratio 753
N.177 Effective Shear Calibrated to Max Displacement Max Displacement Relative Error Change v. Vol Trans Reinf Ratio 754
N.178 Effective Shear Calibrated to Max Displacement Max Displacement Relative Error Change v. Yield Shear Stress Ratio 754
N.179 Effective Shear Calibrated to Max Displacement Max Displacement Relative Error Change v. Yield Shear Demand Ratio 755
N.180 Effective Shear Calibrated to Max Displacement Max Displacement Relative Error Change v. Axial Load Ratio 755
N.181 Effective Shear Calibrated to Yield Displacement With Slip Secant Stiffness Absolute Error Change v. Max Shear Stress Ratio 756

N.182 Effective Shear Calibrated to Yield Displacement With Slip Secant Stiffness Absolute Error Change v. Max Shear Demand Ratio 756
N.183 Effective Shear Calibrated to Yield Displacement With Slip Secant Stiffness Absolute Error Change v. Aspect Ratio 757
N.184 Effective Shear Calibrated to Yield Displacement With Slip Secant Stiffness Absolute Error Change v. Normalized Thickness 757
N.185 Effective Shear Calibrated to Yield Displacement With Slip Secant Stiffness Absolute Error Change v. Long Reinf Ratio in BE 758
N.186 Effective Shear Calibrated to Yield Displacement With Slip Secant Stiffness Absolute Error Change v. Horiz Reinf Ratio 758
N.187 Effective Shear Calibrated to Yield Displacement With Slip Secant Stiffness Absolute Error Change v. Vol Trans Reinf Ratio 759
N.188 Effective Shear Calibrated to Yield Displacement With Slip Secant Stiffness Absolute Error Change v. Yield Shear Stress Ratio 759
N.189 Effective Shear Calibrated to Yield Displacement With Slip Secant Stiffness Absolute Error Change v. Yield Shear Demand Ratio 760
N.190 Effective Shear Calibrated to Yield Displacement With Slip Secant Stiffness Absolute Error Change v. Axial Load Ratio 760
N.191 Effective Shear Calibrated to Yield Displacement With Slip Yield Displacement Absolute Error Change v. Max Shear Stress Ratio 761
N.192 Effective Shear Calibrated to Yield Displacement With Slip Yield Displacement Absolute Error Change v. Max Shear Demand Ratio 761
N.193 Effective Shear Calibrated to Yield Displacement With Slip Yield Displacement Absolute Error Change v. Aspect Ratio 762
N.194 Effective Shear Calibrated to Yield Displacement With Slip Yield Displacement Absolute Error Change v. Normalized Thickness 762
N.195 Effective Shear Calibrated to Yield Displacement With Slip Yield Displacement Absolute Error Change v. Long Reinf Ratio in BE 763
N.196 Effective Shear Calibrated to Yield Displacement With Slip Yield Displacement Absolute Error Change v. Horiz Reinf Ratio 763
N.197 Effective Shear Calibrated to Yield Displacement With Slip Yield Displacement Absolute Error Change v. Vol Trans Reinf Ratio 764
N.198 Effective Shear Calibrated to Yield Displacement With Slip Yield Displacement Absolute Error Change v. Yield Shear Stress Ratio 764
N.199 Effective Shear Calibrated to Yield Displacement With Slip Yield Displacement Absolute Error Change v. Yield Shear Demand Ratio 765
N.200 Effective Shear Calibrated to Yield Displacement With Slip Yield Displacement Absolute Error Change v. Axial Load Ratio 765

N.201 Effective Shear Calibrated to Yield Displacement With Slip Max Displacement Absolute Error Change v. Max Shear Stress Ratio 766
N.202 Effective Shear Calibrated to Yield Displacement With Slip Max Displacement Absolute Error Change v. Max Shear Demand Ratio 766
N.203 Effective Shear Calibrated to Yield Displacement With Slip Max Displacement Absolute Error Change v. Aspect Ratio 767
N.204 Effective Shear Calibrated to Yield Displacement With Slip Max Displacement Absolute Error Change v. Normalized Thickness 767
N.205 Effective Shear Calibrated to Yield Displacement With Slip Max Displacement Absolute Error Change v. Long Reinf Ratio in BE 768
N.206 Effective Shear Calibrated to Yield Displacement With Slip Max Displacement Absolute Error Change v. Horiz Reinf Ratio 768
N.207 Effective Shear Calibrated to Yield Displacement With Slip Max Displacement Absolute Error Change v. Vol Trans Reinf Ratio 769
N.208 Effective Shear Calibrated to Yield Displacement With Slip Max Displacement Absolute Error Change v. Yield Shear Stress Ratio 769
N.209 Effective Shear Calibrated to Yield Displacement With Slip Max Displacement Absolute Error Change v. Yield Shear Demand Ratio 770
N.210 Effective Shear Calibrated to Yield Displacement With Slip Max Displacement Absolute Error Change v. Axial Load Ratio 770
N.211 Effective Shear Calibrated to Yield Displacement With Slip Secant Stiffness Relative Error Change v. Max Shear Stress Ratio 771
N.212 Effective Shear Calibrated to Yield Displacement With Slip Secant Stiffness Relative Error Change v. Max Shear Demand Ratio 771
N.213 Effective Shear Calibrated to Yield Displacement With Slip Secant Stiffness Relative Error Change v. Aspect Ratio 772
N.214 Effective Shear Calibrated to Yield Displacement With Slip Secant Stiffness Relative Error Change v. Normalized Thickness 772
N.215 Effective Shear Calibrated to Yield Displacement With Slip Secant Stiffness Relative Error Change v. Long Reinf Ratio in BE 773
N.216 Effective Shear Calibrated to Yield Displacement With Slip Secant Stiffness Relative Error Change v. Horiz Reinf Ratio 773
N.217 Effective Shear Calibrated to Yield Displacement With Slip Secant Stiffness Relative Error Change v. Vol Trans Reinf Ratio 774
N.218 Effective Shear Calibrated to Yield Displacement With Slip Secant Stiffness Relative Error Change v. Yield Shear Stress Ratio 774
N.219 Effective Shear Calibrated to Yield Displacement With Slip Secant Stiffness Relative Error Change v. Yield Shear Demand Ratio 775

N.220 Effective Shear Calibrated to Yield Displacement With Slip Secant Stiffness Relative Error Change v. Axial Load Ratio 775
N.221 Effective Shear Calibrated to Yield Displacement With Slip Yield Displacement Relative Error Change v. Max Shear Stress Ratio 776
N.222 Effective Shear Calibrated to Yield Displacement With Slip Yield Displacement Relative Error Change v. Max Shear Demand Ratio 776
N.223 Effective Shear Calibrated to Yield Displacement With Slip Yield Displacement Relative Error Change v. Aspect Ratio 777
N.224 Effective Shear Calibrated to Yield Displacement With Slip Yield Displacement Relative Error Change v. Normalized Thickness 777
N.225 Effective Shear Calibrated to Yield Displacement With Slip Yield Displacement Relative Error Change v. Long Reinf Ratio in BE 778
N.226 Effective Shear Calibrated to Yield Displacement With Slip Yield Displacement Relative Error Change v. Horiz Reinf Ratio 778
N.227 Effective Shear Calibrated to Yield Displacement With Slip Yield Displacement Relative Error Change v. Vol Trans Reinf Ratio 779
N.228 Effective Shear Calibrated to Yield Displacement With Slip Yield Displacement Relative Error Change v. Yield Shear Stress Ratio 779
N.229 Effective Shear Calibrated to Yield Displacement With Slip Yield Displacement Relative Error Change v. Yield Shear Demand Ratio 780
N.230 Effective Shear Calibrated to Yield Displacement With Slip Yield Displacement Relative Error Change v. Axial Load Ratio 780
N.231 Effective Shear Calibrated to Yield Displacement With Slip Max Displacement Relative Error Change v. Max Shear Stress Ratio 781
N.232 Effective Shear Calibrated to Yield Displacement With Slip Max Displacement Relative Error Change v. Max Shear Demand Ratio 781
N.233 Effective Shear Calibrated to Yield Displacement With Slip Max Displacement Relative Error Change v. Aspect Ratio 782
N.234 Effective Shear Calibrated to Yield Displacement With Slip Max Displacement Relative Error Change v. Normalized Thickness 782
N.235 Effective Shear Calibrated to Yield Displacement With Slip Max Displacement Relative Error Change v. Long Reinf Ratio in BE 783
N.236 Effective Shear Calibrated to Yield Displacement With Slip Max Displacement Relative Error Change v. Horiz Reinf Ratio 783
N.237 Effective Shear Calibrated to Yield Displacement With Slip Max Displacement Relative Error Change v. Vol Trans Reinf Ratio 784
N.238 Effective Shear Calibrated to Yield Displacement With Slip Max Displacement Relative Error Change v. Yield Shear Stress Ratio 784

N.239 Effective Shear Calibrated to Yield Displacement With Slip Max Displacement Relative Error Change v. Yield Shear Demand Ratio 785
N.240 Effective Shear Calibrated to Yield Displacement With Slip Max Displacement Relative Error Change v. Axial Load Ratio 785
N.241 Effective Shear Calibrated to Max Displacement With Slip Secant Stiffness Absolute Error Change v. Max Shear Stress Ratio 786
N.242 Effective Shear Calibrated to Max Displacement With Slip Secant Stiffness Absolute Error Change v. Max Shear Demand Ratio 786
N.243 Effective Shear Calibrated to Max Displacement With Slip Secant Stiffness Absolute Error Change v. Aspect Ratio 787
N.244 Effective Shear Calibrated to Max Displacement With Slip Secant Stiffness Absolute Error Change v. Normalized Thickness 787
N.245 Effective Shear Calibrated to Max Displacement With Slip Secant Stiffness Absolute Error Change v. Long Reinf Ratio in BE 788
N.246 Effective Shear Calibrated to Max Displacement With Slip Secant Stiffness Absolute Error Change v. Horiz Reinf Ratio 788
N.247 Effective Shear Calibrated to Max Displacement With Slip Secant Stiffness Absolute Error Change v. Vol Trans Reinf Ratio 789
N.248 Effective Shear Calibrated to Max Displacement With Slip Secant Stiffness Absolute Error Change v. Yield Shear Stress Ratio 789
N.249 Effective Shear Calibrated to Max Displacement With Slip Secant Stiffness Absolute Error Change v. Yield Shear Demand Ratio 790
N.250 Effective Shear Calibrated to Max Displacement With Slip Secant Stiffness Absolute Error Change v. Axial Load Ratio 790
N.251 Effective Shear Calibrated to Max Displacement With Slip Yield Displacement Absolute Error Change v. Max Shear Stress Ratio 791
N.252 Effective Shear Calibrated to Max Displacement With Slip Yield Displacement Absolute Error Change v. Max Shear Demand Ratio 791
N.253 Effective Shear Calibrated to Max Displacement With Slip Yield Displacement Absolute Error Change v. Aspect Ratio 792
N.254 Effective Shear Calibrated to Max Displacement With Slip Yield Displacement Absolute Error Change v. Normalized Thickness 792
N.255 Effective Shear Calibrated to Max Displacement With Slip Yield Displacement Absolute Error Change v. Long Reinf Ratio in BE 793
N.256 Effective Shear Calibrated to Max Displacement With Slip Yield Displacement Absolute Error Change v. Horiz Reinf Ratio 793
N.257 Effective Shear Calibrated to Max Displacement With Slip Yield Displacement Absolute Error Change v. Vol Trans Reinf Ratio 794

N.258 Effective Shear Calibrated to Max Displacement With Slip Yield Displacement Absolute Error Change v. Yield Shear Stress Ratio 794
N.259 Effective Shear Calibrated to Max Displacement With Slip Yield Displacement Absolute Error Change v. Yield Shear Demand Ratio 795
N.260 Effective Shear Calibrated to Max Displacement With Slip Yield Displacement Absolute Error Change v. Axial Load Ratio 795
N.261 Effective Shear Calibrated to Max Displacement With Slip Max Displacement Absolute Error Change v. Max Shear Stress Ratio 796
N.262 Effective Shear Calibrated to Max Displacement With Slip Max Displacement Absolute Error Change v. Max Shear Demand Ratio 796
N.263 Effective Shear Calibrated to Max Displacement With Slip Max Displacement Absolute Error Change v. Aspect Ratio 797
N.264 Effective Shear Calibrated to Max Displacement With Slip Max Displacement Absolute Error Change v. Normalized Thickness 797
N.265 Effective Shear Calibrated to Max Displacement With Slip Max Displacement Absolute Error Change v. Long Reinf Ratio in BE 798
N.266 Effective Shear Calibrated to Max Displacement With Slip Max Displacement Absolute Error Change v. Horiz Reinf Ratio 798
N.267 Effective Shear Calibrated to Max Displacement With Slip Max Displacement Absolute Error Change v. Vol Trans Reinf Ratio 799
N.268 Effective Shear Calibrated to Max Displacement With Slip Max Displacement Absolute Error Change v. Yield Shear Stress Ratio 799
N.269 Effective Shear Calibrated to Max Displacement With Slip Max Displacement Absolute Error Change v. Yield Shear Demand Ratio 800
N.270 Effective Shear Calibrated to Max Displacement With Slip Max Displacement Absolute Error Change v. Axial Load Ratio 800
N.271 Effective Shear Calibrated to Max Displacement With Slip Secant Stiffness Relative Error Change v. Max Shear Stress Ratio 801
N.272 Effective Shear Calibrated to Max Displacement With Slip Secant Stiffness Relative Error Change v. Max Shear Demand Ratio 801
N.273 Effective Shear Calibrated to Max Displacement With Slip Secant Stiffness Relative Error Change v. Aspect Ratio 802
N.274 Effective Shear Calibrated to Max Displacement With Slip Secant Stiffness Relative Error Change v. Normalized Thickness 802
N.275 Effective Shear Calibrated to Max Displacement With Slip Secant Stiffness Relative Error Change v. Long Reinf Ratio in BE 803
N.276 Effective Shear Calibrated to Max Displacement With Slip Secant Stiffness Relative Error Change v. Horiz Reinf Ratio 803

N.277 Effective Shear Calibrated to Max Displacement With Slip Secant Stiffness Relative Error Change v. Vol Trans Reinf Ratio 804
N.278 Effective Shear Calibrated to Max Displacement With Slip Secant Stiffness Relative Error Change v. Yield Shear Stress Ratio 804
N.279 Effective Shear Calibrated to Max Displacement With Slip Secant Stiffness Relative Error Change v. Yield Shear Demand Ratio 805
N.280 Effective Shear Calibrated to Max Displacement With Slip Secant Stiffness Relative Error Change v. Axial Load Ratio 805
N.281 Effective Shear Calibrated to Max Displacement With Slip Yield Displacement Relative Error Change v. Max Shear Stress Ratio 806
N.282 Effective Shear Calibrated to Max Displacement With Slip Yield Displacement Relative Error Change v. Max Shear Demand Ratio 806
N.283 Effective Shear Calibrated to Max Displacement With Slip Yield Displacement Relative Error Change v. Aspect Ratio 807
N.284 Effective Shear Calibrated to Max Displacement With Slip Yield Displacement Relative Error Change v. Normalized Thickness 807
N.285 Effective Shear Calibrated to Max Displacement With Slip Yield Displacement Relative Error Change v. Long Reinf Ratio in BE 808
N.286 Effective Shear Calibrated to Max Displacement With Slip Yield Displacement Relative Error Change v. Horiz Reinf Ratio 808
N.287 Effective Shear Calibrated to Max Displacement With Slip Yield Displacement Relative Error Change v. Vol Trans Reinf Ratio 809
N.288 Effective Shear Calibrated to Max Displacement With Slip Yield Displacement Relative Error Change v. Yield Shear Stress Ratio 809
N.289 Effective Shear Calibrated to Max Displacement With Slip Yield Displacement Relative Error Change v. Yield Shear Demand Ratio 810
N.290 Effective Shear Calibrated to Max Displacement With Slip Yield Displacement Relative Error Change v. Axial Load Ratio 810
N.291 Effective Shear Calibrated to Max Displacement With Slip Max Displacement Relative Error Change v. Max Shear Stress Ratio 811
N.292 Effective Shear Calibrated to Max Displacement With Slip Max Displacement Relative Error Change v. Max Shear Demand Ratio 811
N.293 Effective Shear Calibrated to Max Displacement With Slip Max Displacement Relative Error Change v. Aspect Ratio 812
N.294 Effective Shear Calibrated to Max Displacement With Slip Max Displacement Relative Error Change v. Normalized Thickness 812
N.295 Effective Shear Calibrated to Max Displacement With Slip Max Displacement Relative Error Change v. Long Reinf Ratio in BE 813

N.296 Effective Shear Calibrated to Max Displacement With Slip Max Displacement Relative Error Change v. Horiz Reinf Ratio 813
N.297 Effective Shear Calibrated to Max Displacement With Slip Max Displacement Relative Error Change v. Vol Trans Reinf Ratio 814
N.298 Effective Shear Calibrated to Max Displacement With Slip Max Displacement Relative Error Change v. Yield Shear Stress Ratio 814
N.299 Effective Shear Calibrated to Max Displacement With Slip Max Displacement Relative Error Change v. Yield Shear Demand Ratio 815
N.300 Effective Shear Calibrated to Max Displacement With Slip Max Displacement Relative Error Change v. Axial Load Ratio 815

LIST OF TABLES

Table Number Page

2.1 Compiled Experimental Walls . . . 7
2.2 Experimental Wall Geometry . . . 8
2.3 Experimental Wall Geometry (cont.) . . . 9
2.4 Experimental Wall Reinforcement . . . 10
2.5 Experimental Wall Reinforcement (cont.) . . . 11
2.6 Experimental Wall Material Properties . . . 12
2.7 Experimental Wall Material Properties (cont.) . . . 13
2.8 Experimental Wall Loading . . . 14
2.9 Experimental Wall Loading (cont.) . . . 15
2.10 Experimental Wall Results . . . 16
2.11 Experimental Wall Results (cont.) . . . 17

3.1 Functionality Associated with Data Types . . . 34
3.2 Processed Data Contents for an Example Analysis . . . 39

4.1 Predicted Strength Results Using Beam-Column Element Formulation . . . 60
4.2 Predicted Strength Results Using Beam-Column Element Formulation (cont.) 61
4.3 Predicted Secant Stiffness and Yield Displacement Results Using Two Beam-Column Element Formulations . . . 70
4.4 Predicted Secant Stiffness and Yield Displacement Results Using Two Beam-Column Element Formulations (cont.) . . . 71
4.5 Predicted Maximum Displacement Results Using Two Beam-Column Element Formulations . . . 87
4.6 Predicted Maximum Displacement Results Using Two Beam-Column Element Formulations (cont.) . . . 88

5.1 Response-2000 Prediction Objectives with Default Analysis Parameters . . . 112
5.2 Response-2000 Prediction Objectives with No Bar Slip . . . 113

6.1 VecTor2 Modeling Assumptions . . . 118
6.2 VecTor2 Numerical Decisions . . . 118
6.3 VecTor2: Ratios of Predicted Response Parameters . . . 120

7.1 Bar-Slip Prediction Results 150
7.2 Bar-Slip Prediction Results (cont.) 151
7.3 Difference of Bar-Slip Model Prediction Results to Flexural Model 152
7.4 Difference of Bar-Slip Model Prediction Results to Flexural Model (cont.) . . 153
7.5 Elastic Shear Model Prediction Results 161
7.6 Elastic Shear Model Prediction Results (cont.) 162
7.7 Difference of Elastic Shear Model Prediction Results to Flexural Model . . . 163
7.8 Difference of Elastic Shear Model Prediction Results to Flexural Model (cont.) 164
7.9 Calibrated α's for Elastic Effective Shear Model 168
7.10 Elastic Effective Shear Model Analysis Results 169
7.11 Elastic Effective Shear Model Analysis Results (cont.) 170
7.12 Elastic Effective Shear Model Analysis Results (cont.) 171
7.13 Elastic Effective Shear Model With Bar-Slip Analysis Results 172
7.14 Elastic Effective Shear Model With Bar-Slip Analysis Results (cont.) 173
7.15 Elastic Effective Shear Model With Bar-Slip Analysis Results (cont.) 174
7.16 Difference of Effective Shear Calibrated to Yield Displacement Model Prediction Results to Flexural Model 175
7.17 Difference of Effective Shear Calibrated to Yield Displacement Model Prediction Results to Flexural Model (cont.) 176
7.18 Difference of Effective Shear Calibrated to Maximum Displacement Model Prediction Results to Flexural Model 177
7.19 Difference of Effective Shear Calibrated to Maximum Displacement Model Prediction Results to Flexural Model (cont.) 178
7.20 Difference of Effective Shear Calibrated to Yield Displacement with Bar-Slip Model Prediction Results to Flexural Model 179
7.21 Difference of Effective Shear Calibrated to Yield Displacement with Bar-Slip Model Prediction Results to Flexural Model (cont.) 180
7.22 Difference of Effective Shear Calibrated to Maximum Displacement with Bar-Slip Model Prediction Results to Flexural Model 181
7.23 Difference of Effective Shear Calibrated to Maximum Displacement with Bar-Slip Model Prediction Results to Flexural Model (cont.) 182

ACKNOWLEDGMENTS

This thesis would not have been possible without the tremendous amount of background work conducted by my fellow graduate students Peter Brown and Aaron Sterns. Nor would I have had much to do without the enthusiastic support and encouragement from my two advisors Dawn Lehman and Laura Lowes. Their direction served to help my young mind expand and grow, while keeping it attuned to the zeitgeist of modern structural engineering research. Thanks are greatly in order to Greg Miller for taking time from sabbatical to serve on my committee. He probably ranks as one of my all-time favorite instructors.

Gratitude is in order to the National Science foundation for supporting this research. I am a fan of their role in supporting the public's commitment to scientific research. I also like their method of financing education a lot more than Sallie Mae's.

I have to thank the preceding structural engineering graduate cohort for being a cool group of kids; specifically, I speak of Adam Christopulos, Dave Hieber, Chris White, Jon Wacker, and Angela Kingsley. Also, instrumental in passing the time was the Cheap Beer Friday crew; which included Dylan Freytag, the aforementioned Peter Brown, David Herman, Tyler Sprague, Travis Williams, Colin Kuester, and Mike Rosa. Incidently, Cheap Beer Friday did begin as a celebration of my twenty-sixth birthday. I also have to thank the founders and participants of the More Hall Wiffle-Ball Players Association for giving me my big chance at stardom; the names Peter Carney, Ryan Thody, and Andrew Chronister come to mind.

Lastly, I will take this opportunity to thank my parents and sisters for all of their tolerance and encouragement through the years.

Chapter 1
INTRODUCTION

Reinforced concrete shear walls are commonly used in buildings to sustain lateral loads resulting from earthquakes. At large levels of drift, large forces and nonlinear behavior occur as a result. Significant structural damage to the wall can result. Nonlinear analysis offers methods to predict this behavior. While nonlinear analysis software is being made available to structural designers, limited information exists in the literature to aid the nonlinear analysis of these walls. This study aims to fulfill that need.

1.1 Objectives

Recent advances in computational capabilities, including hardware and software, have made nonlinear finite element analysis a viable tool for structural analysis and design. However, the data management tools and analysis parameter recommendations required for designers to utilize these capabilities, are lacking. Therefore, a study was conducted to evaluate available nonlinear analysis techniques to predict wall response to lateral loading. Evaluation was done by comparing simulated response with experimental data. Experimental data were used also to improve existing models and develop recommendations. These techniques were improved and recommendations for model input parameters are made.

1.2 Methods

The following analytical models for model input parameters represent the current state of engineering practice and are studied in this thesis:

- Flexural beam-column elements with both distributed and lumped plasticity formulations.

- Beam-column element that incorporates shear and flexural effects by the modified compression field theory.

- Two-dimensional continuum modeling considering shear and flexural effects by the modified compression field theory.

For each of these methods, a push-over analysis of previously tested shear wall specimens was conducted. The subsequent output was compared to the measured data to evaluate its "goodness," based on a comparison of strength, stiffness, and displacement limits. The error in prediction objectives for the experimental walls was compared to the wall characteristics (e.g. aspect ratio) to better understand and improve the analysis methods.

This evaluation suggested that additional response effects must be included. In this study, the impact of modeling bar-slip and shear deformation was evaluated by incorporating simulation of these in the distributed-plasticity beam-column element. An elastic shear response model was calibrated to minimize the error of predicted yield displacement and maximum displacement capacity for the experimental wall data set. Finally, the information obtained was used to develop recommended analysis parameters for reinforced concrete shear walls.

1.3 Outline of the Thesis

The following provides a brief description of each chapter in the thesis.

Chapter 2 discusses the experimental data set that was used in this study, previous analytical studies of shear walls, the analytical framework used for the bulk of the analyses, and previous work on data management strategies for structural analysis.

Chapter 3 introduces the preprocessing framework developed to conduct many of the analyses presented in this thesis.

Chapter 4 studies the modeling of the experimental shear walls using the beam-column elements available in OpenSees (McKenna 1997). The analytical results are presented and compared to the engineering design parameters of the walls.

Chapter 5 uses the Response-2000 (Bentz 2000) software to simulate the response of three walls that were tested in the laboratory and exhibited varying response modes. The Response-2000 formulation incorporates the effect of shear in the distributed plasticity beam-column formulation using the modified compression field theory (Vecchio and Collins 1986) (MCFT) constitutive relations.

Chapter 6 uses VecTor2 (Wong and Vecchio 2002), an existing analysis package, to model the three walls considered in Chapter5 using the MCFT with 2D continuum elements.

Chapter 7 extends the distributed-plasticity beam-column formulation, described in Chapter 4, to incorporate the effect of bar slip at the base of the wall and an equivalent (or reduced) elastic shear response at the section level. The elastic shear modulus was calibrated to reduce the average error in displacement capacity prediction of the walls.

Chapter 8 summarizes the thesis, discusses recommendations for the development of future data management frameworks, draws conclusions form the presented data for best practices in conducting analysis of reinforced concrete shear walls with available techniques, and makes recommendations for future development of analysis methods.

Chapter 2
BACKGROUND

2.1 Previous Experiments of Structural Walls

Experimental research has aided the understanding and design of shear walls. Here, the test results were used to evaluate and improve available analytical methods. These data served as the basis for comparison of analytical and experimental results. The following summarizes the data set.

2.1.1 Compiled Experimental Wall Data

The information from tests of planar and barbell walls with typical details and without openings was compiled by Brown (2006). The names, references, and number of walls compiled is shown in Table 2.1. The geometry is summarized in Tables 2.2 & 2.3, reinforcement in Tables 2.4 & 2.5, material properties in Tables 2.6 & 2.7, experimental loading in Tables 2.8 & 2.9, and experimental results in Tables 2.10 & 2.11. The sixty tests were used to evaluate the beam-column elements available in OpenSees.

The values listed in the tables are:

- h_w: height of the wall.
- L_w: length of the wall.
- t_{be}: thickness of the boundary element.
- t_w: thickness of the web.
- L_{be}: length of the boundary element.
- $AspectRatio$: the height of the wall divided by the length of the wall.

- ρ_l: reinforcement ratio of longitudinal steel in the boundary element to the gross cross-sectional area of the boundary element.
- ρ_v: reinforcement ratio of vertical steel in the web to the gross cross-sectional area of the web.
- ρ_h: reinforcement ratio of horizontal steel to the gross area of the web in the plane perpendicular to the horizontal steel.
- ρ_t: volumetric reinforcement ratio of confinement steel to the volume of the boundary element.
- d_{bl}: diameter of the longitudinal bars in the boundary element.
- d_{bv}: diameter of the vertical bars in the web.
- d_{bt}: diameter of the confinement bars in the boundary element.
- f'_c: compressive strength of the concrete.
- f_{yl}: yield strength of the longitudinal steel bars in the boundary element.
- f_{ul}: ultimate strength of the longitudinal steel bars in the boundary element.
- ϵ_u: strain at ultimate strength of the longitudinal steel bars in the boundary element.
- f_{yh}: yield strength of the horizontal steel bars.
- f_{yt}: yield strength of the transverse bars in the boundary element.
- MN: designates monotonic loading.
- PS: designates pseudo-static loading.

- P_{axial}: is the ratio of the applied axial load to the product of the measured compressive strength of the concrete and the gross cross-sectional area of the concrete.

- M_{top}/V_{top}: is the ratio of applied moment at the top of the wall to the applied lateral load at the top of the wall.

Additionally, the terms M_y, k_{sec}, Δ_y, M_{max}, and Δ_{max} are the measured response quantities which are discussed in detail in Section 4.3.2.

Table 2.1: Compiled Experimental Walls

Name of Wall Set	*References*	*Number of Walls*
Lefas	(Lefas and Kostovos 1990; Lefas, Kostovos, and Ambraseys 1990)	17
Oesterle	(Oesterle, Fiorato, Johal, Carpenter, Russell, and Corley 1976; Oesterle, Aristizabal-Ochoa, Fiorato, Russell, and Corley 1979)	12
Pilakoutas	(Pilakoutas and Elnashai 1995; Pilakoutas 1991; Lopes 1991; Elnashai, Pilakoutas, and Ambraseys 1990)	6
Salonikios	(Salonikios, Kappos, Tegos, and Penelis 1999; Salonikios, Kappos, Tegos, and Penelis 2000)	7
Sittipunt	(Sittipunt and Wood 1995; Sittipunt, Wood, Lukkunaprasit, and Pattararattanaku 2001)	2
Tasnimi	(Tasnimi 2000)	4
Thomsen	(Thomsen IV and Wallace 2004)	2
Vallenas	(Vallenas, Bertero, and Popov 1979)	4
Wang	(Wang, Bertero, and Popov 1975)	2
Yanez	(Yanez, Park, and Paulay 1992)	1
Zhang	(Zhang and Wang 2000)	3

Table 2.2: Experimental Wall Geometry

Specimen ID	Shape	h_w (in)	L_w (in)	t_{be} (in)	t_w (in)	L_{be} (in)	$AspectRatio$
Lefas SW30	rectangle	51.18	25.59	2.56	2.56	5.51	2.00
Lefas SW31	rectangle	51.18	25.59	2.56	2.56	5.51	2.00
Lefas SW32	rectangle	51.18	25.59	2.56	2.56	5.51	2.00
Lefas SW33	rectangle	51.18	25.59	2.56	2.56	5.51	2.00
Lefas SW11	rectangle	29.53	29.53	2.76	2.76	5.51	1.00
Lefas SW12	rectangle	29.53	29.53	2.76	2.76	5.51	1.00
Lefas SW13	rectangle	29.53	29.53	2.76	2.76	5.51	1.00
Lefas SW14	rectangle	29.53	29.53	2.76	2.76	5.51	1.00
Lefas SW15	rectangle	29.53	29.53	2.76	2.76	5.51	1.00
Lefas SW16	rectangle	29.53	29.53	2.76	2.76	5.51	1.00
Lefas SW17	rectangle	29.53	29.53	2.76	2.76	5.51	1.00
Lefas SW21	rectangle	51.18	25.59	2.56	2.56	5.51	2.00
Lefas SW22	rectangle	51.18	25.59	2.56	2.56	5.51	2.00
Lefas SW23	rectangle	51.18	25.59	2.56	2.56	5.51	2.00
Lefas SW24	rectangle	51.18	25.59	2.56	2.56	5.51	2.00
Lefas SW25	rectangle	51.18	25.59	2.56	2.56	5.51	2.00
Lefas SW26	rectangle	51.18	25.59	2.56	2.56	5.51	2.00
Oesterle B1	barbell	180.00	75.00	12.00	4.00	12.00	2.40
Oesterle B2	barbell	180.00	75.00	12.00	4.00	12.00	2.40
Oesterle B3	barbell	180.00	75.00	12.00	4.00	12.00	2.40
Oesterle B4	barbell	180.00	75.00	12.00	4.00	12.00	2.40
Oesterle B5	barbell	180.00	75.00	12.00	4.00	12.00	2.40
Oesterle R1	rectangle	180.00	75.00	4.00	4.00	7.50	2.40
Oesterle R2	rectangle	180.00	75.00	4.00	4.00	7.50	2.40
Oesterle B6	barbell	180.00	75.00	12.00	4.00	12.00	2.40
Oesterle B7	barbell	180.00	75.00	12.00	4.00	12.00	2.40
Oesterle B8	barbell	180.00	75.00	12.00	4.00	12.00	2.40
Oesterle B9	barbell	180.00	75.00	12.00	4.00	12.00	2.40
Oesterle B10	barbell	180.00	75.00	12.00	4.00	12.00	2.40
Pilakoutas SW4	rectangle	47.24	23.62	2.36	2.36	4.30	2.00
Pilakoutas SW5	rectangle	47.24	23.62	2.36	2.36	2.40	2.00
Pilakoutas SW6	rectangle	47.24	23.62	2.36	2.36	4.30	2.00
Pilakoutas SW7	rectangle	47.24	23.62	2.36	2.36	2.40	2.00
Pilakoutas SW8	rectangle	47.24	23.62	2.36	2.36	4.30	2.00
Pilakoutas SW9	rectangle	47.24	23.62	2.36	2.36	4.30	2.00
Salonikios LSW1	rectangle	47.24	47.24	3.94	3.94	9.45	1.00
Salonikios LSW2	rectangle	47.24	47.24	3.94	3.94	9.45	1.00
Salonikios LSW3	rectangle	47.24	47.24	3.94	3.94	9.45	1.00
Salonikios MSW1	rectangle	70.87	47.24	3.94	3.94	9.45	1.50
Salonikios MSW2	rectangle	70.87	47.24	3.94	3.94	9.45	1.50
Salonikios MSW3	rectangle	70.87	47.24	3.94	3.94	9.45	1.50
Salonikios MSW6	rectangle	70.87	47.24	3.94	3.94	9.45	1.50
Sittipunt W1	barbell	74.80	59.06	9.84	3.94	9.84	1.27
Sittipunt W2	barbell	74.80	59.06	9.84	3.94	9.84	1.27

Table 2.3: Experimental Wall Geometry (cont.)

Specimen ID	Shape	h_w (in)	L_w (in)	t_{be} (in)	t_w (in)	L_{be} (in)	$AspectRatio$
Tasnimi SHW1	rectangle	59.06	19.69	1.97	1.97	2.20	2.20
Tasnimi SHW2	rectangle	59.06	19.69	1.97	1.97	2.20	2.20
Tasnimi SHW3	rectangle	59.06	19.69	1.97	1.97	2.20	2.20
Tasnimi SHW4	rectangle	59.06	19.69	1.97	1.97	2.20	2.20
Thomsen RW1	rectangle	144.00	48.00	4.00	4.00	7.50	3.13
Thomsen RW2	rectangle	144.00	48.00	4.00	4.00	7.50	3.13
Vallenas SW3	barbell	120.00	94.00	10.00	4.00	10.00	1.85
Vallenas SW4	barbell	120.00	94.00	10.00	4.00	10.00	1.85
Vallenas SW5	rectangle	120.00	95.00	4.50	4.50	11.00	1.59
Vallenas SW6	rectangle	120.00	95.00	4.50	4.50	11.00	1.59
Wang SW1	barbell	132.00	94.00	10.00	4.00	10.00	2.94
Wang SW2	barbell	132.00	94.00	10.00	4.00	10.00	2.94
Yanez S1	rectangle	90.55	78.74	4.72	4.72	0.00	1.15
Zhang SW7	rectangle	68.90	27.56	3.94	3.94	3.94	2.14
Zhang SW8	rectangle	68.90	27.56	3.94	3.94	3.94	2.14
Zhang SW9	rectangle	68.90	27.56	3.94	3.94	3.94	2.14

Table 2.4: Experimental Wall Reinforcement

Specimen ID	ρ_l (%)	ρ_v (%)	ρ_h (%)	ρ_t (%)	d_{bl} (in)	d_{bv} (in)	d_{bt} (in)
Lefas SW30	3.30	1.50	0.35	0.90	0.31	0.31	0.16
Lefas SW31	3.30	1.50	0.35	0.90	0.31	0.31	0.16
Lefas SW32	3.30	1.50	0.35	0.90	0.31	0.31	0.16
Lefas SW33	3.30	1.50	0.35	0.90	0.31	0.31	0.16
Lefas SW11	3.10	2.40	1.10	1.20	0.31	0.31	0.16
Lefas SW12	3.10	2.40	1.10	1.20	0.31	0.31	0.16
Lefas SW13	3.10	2.40	1.10	1.20	0.31	0.31	0.16
Lefas SW14	3.10	2.40	1.10	1.20	0.31	0.31	0.16
Lefas SW15	3.10	2.40	1.10	1.20	0.31	0.31	0.16
Lefas SW16	3.10	2.40	1.10	1.20	0.31	0.31	0.16
Lefas SW17	3.10	2.40	0.37	1.20	0.31	0.31	0.16
Lefas SW21	3.30	2.50	0.80	0.90	0.31	0.31	0.16
Lefas SW22	3.30	2.50	0.80	0.90	0.31	0.31	0.16
Lefas SW23	3.30	2.50	0.80	0.90	0.31	0.31	0.16
Lefas SW24	3.30	2.50	0.80	0.90	0.31	0.31	0.16
Lefas SW25	3.30	2.50	0.80	0.90	0.31	0.31	0.16
Lefas SW26	3.30	2.50	0.40	0.90	0.31	0.31	0.16
Oesterle B1	1.09	0.25	0.31	0.06	0.50	0.24	0.20
Oesterle B2	4.00	0.25	0.31	2.07	0.75	0.24	0.20
Oesterle B3	1.11	0.29	0.31	0.00	0.50	0.24	0.24
Oesterle B4	3.67	0.29	0.31	0.00	0.50	0.24	0.24
Oesterle B5	1.11	0.29	0.31	1.28	0.75	0.24	0.24
Oesterle R1	1.11	0.29	0.31	1.28	0.38	0.24	0.20
Oesterle R2	3.67	0.29	0.63	1.35	0.50	0.24	0.24
Oesterle B6	3.67	0.29	0.63	0.81	0.75	0.24	0.20
Oesterle B7	3.67	0.29	0.63	1.35	0.75	0.24	0.24
Oesterle B8	3.67	0.29	0.63	1.35	0.75	0.24	0.24
Oesterle B9	3.67	0.29	0.63	1.35	0.75	0.24	0.24
Oesterle B10	3.67	0.29	0.63	1.35	0.63	0.24	0.24
Pilakoutas SW4	6.90	0.49	0.39	0.78	0.47	0.24	0.24
Pilakoutas SW5	12.54	0.59	0.31	0.17	0.63	0.24	0.16
Pilakoutas SW6	6.90	0.49	0.31	0.17	0.47	0.24	0.16
Pilakoutas SW7	12.54	0.59	0.39	0.78	0.63	0.24	0.24
Pilakoutas SW8	7.19	0.49	0.31	0.41	0.39	0.24	0.16
Pilakoutas SW9	7.19	0.49	0.31	0.45	0.39	0.24	0.16
Salonikios LSW1	1.68	0.57	0.57	1.70	0.31	0.31	0.17
Salonikios LSW2	1.30	0.28	0.28	1.70	0.31	0.17	0.17
Salonikios LSW3	1.30	0.28	0.28	1.70	0.31	0.17	0.17
Salonikios MSW1	1.70	0.57	0.57	1.70	0.31	0.31	0.17
Salonikios MSW2	1.30	0.28	0.28	1.10	0.31	0.17	0.17
Salonikios MSW3	1.30	0.28	0.28	1.10	0.31	0.17	0.17
Salonikios MSW6	1.70	0.57	0.57	1.70	0.31	0.31	0.17
Sittipunt W1	2.29	0.39	0.52	0.53	0.63	0.39	0.24
Sittipunt W2	2.29	0.52	0.79	0.53	0.63	0.39	0.24

Table 2.5: Experimental Wall Reinforcement (cont.)

Specimen ID	ρ_l (%)	ρ_v (%)	ρ_h (%)	ρ_t (%)	d_{bl} (in)	d_{bv} (in)	d_{bt} (in)
Tasnimi SHW1	4.04	0.22	0.28	0.00	0.24	0.12	0.12
Tasnimi SHW2	4.04	0.22	0.28	0.00	0.24	0.12	0.12
Tasnimi SHW3	4.04	0.22	0.28	0.00	0.24	0.12	0.12
Tasnimi SHW4	4.04	0.22	0.28	0.00	0.24	0.12	0.12
Thomsen RW1	2.93	0.33	0.33	1.35	0.38	0.25	0.19
Thomsen RW2	2.93	0.33	0.33	1.56	0.38	0.25	0.19
Vallenas SW3	3.52	0.82	0.82	1.54	0.75	0.25	0.30
Vallenas SW4	3.52	0.82	0.82	1.54	0.75	0.25	0.30
Vallenas SW5	5.57	0.54	0.54	1.84	0.63	0.25	0.30
Vallenas SW6	5.57	0.54	0.54	1.84	0.63	0.25	0.30
Wang SW1	3.52	0.82	0.82	0.37	0.75	0.25	0.21
Wang SW2	3.52	0.82	0.82	0.37	0.75	0.25	0.21
Yanez S1	0.00	0.50	0.40	0.00	0.33	0.33	0.00
Zhang SW7	6.16	0.67	1.01	2.26	0.55	0.31	0.24
Zhang SW8	4.52	0.67	1.01	2.26	0.55	0.31	0.24
Zhang SW9	12.57	0.67		1.51	0.55	0.31	0.24

Table 2.6: Experimental Wall Material Properties

Specimen ID	f'_c (psi)	f_{yl} (psi)	f_{ul} (psi)	ϵ_u (%)	f_{yh} (psi)	f_{yt} (psi)
Lefas SW30	3635	68150	81925	-	75400	60900
Lefas SW31	4164	68150	81925	-	75400	60900
Lefas SW32	6322	68150	81925	-	75400	60900
Lefas SW33	5684	68150	81925	-	75400	60900
Lefas SW11	6134	68150	81925	-	75400	60900
Lefas SW12	6322	68150	81925	-	75400	60900
Lefas SW13	4676	68150	81925	-	75400	60900
Lefas SW14	4812	68150	81925	-	75400	60900
Lefas SW15	4921	68150	81925	-	75400	60900
Lefas SW16	6047	68150	81925	-	75400	60900
Lefas SW17	5554	68150	81925	-	75400	60900
Lefas SW21	4876	68150	81925	-	75400	60900
Lefas SW22	5887	68150	81925	-	75400	60900
Lefas SW23	5481	68150	81925	-	75400	60900
Lefas SW24	5554	68150	81925	-	75400	60900
Lefas SW25	5075	68150	81925	-	75400	60900
Lefas SW26	3635	68150	81925	-	75400	60900
Oesterle B1	7685	65200	102700	11.7	75500	68700
Oesterle B2	7775	59500	64400	13.3	77200	67100
Oesterle B3	6860	63500	101000	10.9	69400	69400
Oesterle B4	6530	65300	102500	11.8	73200	73200
Oesterle B5	6570	64400	106400	13.2	72800	72800
Oesterle R1	6490	74200	111000	9.8	75700	66000
Oesterle R2	6735	65300	102700	12.3	77600	77600
Oesterle B6	3165	63900	106300	11.3	74200	70700
Oesterle B7	7155	66400	108800	10.8	71000	71000
Oesterle B8	6085	64900	108200	10.8	69900	65800
Oesterle B9	6395	62300	106500	10.9	66900	66900
Oesterle B10	6615	64900	108300	11.4	68900	68900
Pilakoutas SW4	5351	72500	94250	8.25	79750	79750
Pilakoutas SW5	4612	78300	84100	7.5	58000	58000
Pilakoutas SW6	5598	72500	94250	8.25	58000	58000
Pilakoutas SW7	4641	78300	84100	7.5	79750	79750
Pilakoutas SW8	6642	78300	94250	4.25	58000	58000
Pilakoutas SW9	5642	78300	94250	4.25	58000	58000
Salonikios LSW1	3785	84800	-	-	84800	88500
Salonikios LSW2	3132	84800	-	-	88500	88500
Salonikios LSW3	3466	84800	-	-	88500	88500
Salonikios MSW1	3785	84800	-	-	84800	88500
Salonikios MSW2	3799	84800	-	-	88500	88500
Salonikios MSW3	3495	84800	-	-	88500	88500
Salonikios MSW6	3988	84800	-	-	84800	88500
Sittipunt W1	5307	68600	-	-	65250	64400
Sittipunt W2	5191	68600	-	-	65250	64400

Table 2.7: Experimental Wall Material Properties (cont.)

Specimen ID	f'_c (psi)	f_{yl} (psi)	f_{ul} (psi)	ϵ_u (%)	f_{yh} (psi)	f_{yt} (psi)
Tasnimi SHW1	3132	40020	68875	-	31320	-
Tasnimi SHW2	3132	40020	68875	-	31320	-
Tasnimi SHW3	3255	40020	68875	-	31320	-
Tasnimi SHW4	3400	40020	68875	-	31320	-
Thomsen RW1	4580	63000	83000	4.75	65000	63000
Thomsen RW2	4925	63000	83000	4.75	65000	63000
Vallenas SW3	5105	64380	92655	-	73515	63800
Vallenas SW4	5091	64380	92655	-	73515	63800
Vallenas SW5	5020	69890	99615	-	73515	63800
Vallenas SW6	5020	69890	99615	-	73515	63800
Wang SW1	4652.5	72700	106000	-	73000	82800
Wang SW2	4800	72700	106000	-	73000	82800
Yanez S1	4930	68875	100050	16	68875	-
Zhang SW7	4307	58725	-	-	44225	53070
Zhang SW8	4640	62640	-	-	44225	53070
Zhang SW9	5133	54375	-	-	44225	53070

Table 2.8: Experimental Wall Loading

Specimen ID	Loading	P_{axial} (%)	M_{top}/V_{top} (in)	Failure Mode
Lefas SW30	MN	0	0	ductile, failure of compressive zone
Lefas SW31	PS	0	0	ductile, failure of compressive zone
Lefas SW32	PS	0	0	ductile, failure of compressive zone
Lefas SW33	PS	0	0	ductile, failure of compressive zone
Lefas SW11	MN	0	0	crushing of compressive zone
Lefas SW12	MN	10	0	crushing of compressive zone
Lefas SW13	MN	20	0	crushing of compressive zone
Lefas SW14	MN	0	0	crushing of compressive zone
Lefas SW15	MN	10	0	crushing of compressive zone
Lefas SW16	MN	20	0	crushing of compressive zone
Lefas SW17	MN	0	0	crushing of compressive zone
Lefas SW21	MN	0	0	crushing of compressive zone
Lefas SW22	MN	10	0	crushing of compressive zone
Lefas SW23	MN	20	0	crushing of compressive zone
Lefas SW24	MN	0	0	crushing of compressive zone
Lefas SW25	MN	20	0	crushing of compressive zone
Lefas SW26	MN	0	0	crushing of compressive zone
Oesterle B1	PS	0	0	inelastic bar buckling
Oesterle B2	PS	0	0	web crushing
Oesterle B3	PS	0	0	inelastic bar buckling
Oesterle B4	MN	0	0	flexural bar fracture
Oesterle B5	PS	0	0	web crushing
Oesterle R1	PS	0	0	inelastic bar buckling
Oesterle R2	PS	0	0	instablility of compression zone
Oesterle B6	PS	13.4	0	web crushing
Oesterle B7	PS	7.6	0	web crushing
Oesterle B8	PS	9	0	web crushing
Oesterle B9	PS	8.5	0	web crushing
Oesterle B10	PS	8.2	0	boundary elements crushing
Pilakoutas SW4	PS	0	0	crushing in BE
Pilakoutas SW5	PS	0	0	shear failure
Pilakoutas SW6	PS	0	0	crushing in BE
Pilakoutas SW7	PS	0	0	fracture of horiz reinf
Pilakoutas SW8	PS	0	0	load dropped $< 75\%$
Pilakoutas SW9	PS	0	0	lost load capacity

Table 2.9: Experimental Wall Loading (cont.)

Specimen ID	Loading	P_{axial} (%)	M_{top}/V_{top} (in)	Failure Mode
Salonikios LSW1	PS	0	0	predominately flexural mode, concrete crushing and reinf buckling
Salonikios LSW2	PS	0	0	predominately flexural mode, concrete crushing and reinf buckling
Salonikios LSW3	PS	7	0	predominately flexural mode, concrete crushing and reinf buckling
Salonikios MSW1	PS	0	0	predominately flexural mode, concrete crushing and reinf buckling
Salonikios MSW2	PS	0	0	predominately flexural mode, concrete crushing and reinf buckling
Salonikios MSW3	PS	7	0	predominately flexural mode, concrete crushing and reinf buckling
Salonikios MSW6	PS	0	0	predominately flexural mode, concrete crushing and reinf buckling
Sittipunt W1	PS	0	0	web crushing
Sittipunt W2	PS	0	0	web crushing
Tasnimi SHW1	PS	0	0	horizontal cracking near foundation
Tasnimi SHW2	PS	0	0	horizontal cracking near foundation
Tasnimi SHW3	PS	0	0	horizontal cracking near foundation
Tasnimi SHW4	PS	0	0	horizontal cracking near foundation
Thomsen RW1	PS	10	0	long. bar buckling
Thomsen RW2	PS	7	0	long. bar buckling
Vallenas SW3	MN	7.70	54.1	
Vallenas SW4	PS	7.72	54.1	
Vallenas SW5	MN	6	31.5	instability, flexural shear failure
Vallenas SW6	PS	6	31.5	instability
Wang SW1	MN	8.45	144	crushing in base of wall
Wang SW2	PS	8.19	144	crushing in base of wall
Yanez S1	PS	0	0	vert bar fracture and crushing
Zhang SW7	PS	24	0	BE crushing
Zhang SW8	PS	35	0	out of plane buckling
Zhang SW9	PS	24	0	BE crushing

Table 2.10: Experimental Wall Results

Wall	M_y, *in-k*	k_{sec}, k/in	Δ_y, *in*	M_{max}, *in-k*	Δ_{max}, *in*
Lefas SW30				1437	0.82
Lefas SW31				1410	0.87
Lefas SW32				1352	0.96
Lefas SW33				938	0.98
Lefas SW11	1242	270.6	0.14	1827	0.32
Lefas SW12	1535	413.8	0.11	2448	0.35
Lefas SW13	1827	374.0	0.15	2412	0.35
Lefas SW14	1242	249.1	0.15	1937	0.44
Lefas SW15	1535	415.3	0.11	2302	0.32
Lefas SW16	1973	617.2	0.10	2594	0.23
Lefas SW17	1060	212.5	0.15	1805	0.42
Lefas SW21	974	78.7	0.23	1547	0.81
Lefas SW22	1340	128.0	0.19	1827	0.60
Lefas SW23	1462	131.9	0.20	2192	0.52
Lefas SW24	974	73.4	0.25	1462	0.71
Lefas SW25	1583	126.6	0.23	1827	0.37
Lefas SW26	828	70.5	0.22	1498	0.82
Oesterle B1	8298	90.2	0.50	11408	6.00
Oesterle B2	22448	135.6	0.90	28520	5.00
Oesterle B3	8464	92.0	0.50	11776	8.00
Oesterle B4	8464	92.0	0.50	14352	13.00
Oesterle B5	23000	138.9	0.90	31519	5.00
Oesterle R1	4140	50.0	0.45	5060	9.00
Oesterle R2				9292	6.00
Oesterle B6	27048	147.0	1.00	36064	3.00
Oesterle B7	31280	170.0	1.00	40554	6.00
Oesterle B8	30544	166.0	1.00	43424	6.00
Oesterle B9	42504	192.5	1.20	42504	5.30
Oesterle B10	31832	157.3	1.10	31832	5.75
Pilakoutas SW4	877	78.6	0.24	1116	0.94
Pilakoutas SW5				1247	1.02
Pilakoutas SW6	797	71.4	0.24	1137	0.94
Pilakoutas SW7	1131	76.0	0.31	1483	0.87
Pilakoutas SW8	850	76.2	0.24	1184	1.02
Pilakoutas SW9	842	75.4	0.24	1036	1.02
Salonikios LSW1				2761	1.26
Salonikios LSW2				2007	1.26
Salonikios LSW3				2783	1.26
Salonikios MSW1				3107	1.26
Salonikios MSW2				1960	1.26
Salonikios MSW3				2836	1.26
Salonikios MSW6				3186	1.26
Sittipunt W1				9351	1.77
Sittipunt W2				11580	1.34

Table 2.11: Experimental Wall Results (cont.)

Wall	M_y, *in-k*	k_{sec}, k/in	Δ_y, *in*	M_{max}, *in-k*	Δ_{max}, *in*
Tasnimi SHW1				156	0.67
Tasnimi SHW2				195	0.45
Tasnimi SHW3				166	0.61
Tasnimi SHW4				234	0.75
Thomsen RW1	4500	27.8	1.08	4950	3.60
Thomsen RW2	4500	27.8	1.08	5400	3.60
Vallenas SW3	35177	285.1	0.71	42698	6.65
Vallenas SW4	35255	285.8	0.71	35255	3.58
Vallenas SW5	24168	337.7	0.47	31234	3.18
Vallenas SW6	24852	312.1	0.53	28581	1.98
Wang SW1	52716	272.9	0.70	68448	4.25
Wang SW2	55752	288.6	0.70	67620	2.90
Yanez S1				5603	2.76
Zhang SW7	2289	166.6	0.23	2673	1.23
Zhang SW8	2530	195.4	0.22	2976	0.94
Zhang SW9	3395	174.2	0.33	4033	1.24

2.1.2 Reduced Data Set for Evaluation of MCFT-based models

Selected walls were used for evaluation of the capabilities of Response-2000 and VecTor2. The selected walls, exhibited different response modes, one from each of the three following categories:

- Flexural response. The wall chosen is Oesterle B1 (1976).
- Shear-flexure response. The wall chosen is Oesterle B6 (1979).
- Shear response. The wall chosen is Pilakoutas SW7 (1995).

Oesterle B1

Oesterle B1 (1976) is a barbell-shaped wall, constructed at roughly one-third scale, with an aspect ratio of 2.40. A greater percentage of steel is appropriated to the boundary element; 1.09% reinforcement ratio versus 0.25% in the web-zone. Nominal confinement is provided by hoops with cross-ties of 3-mm diameter bars, spaced at 8 inches on center.

The specimen was subjected to a displacement controlled incrementally increasing reversing load history. Lateral load was applied to the top of the wall. No axial load was applied to the specimen during testing.

Oesterle B1 (1976) exhibited flexural cracks that progressed into diagonal shear cracks in the web. At later stages of loading, the cracking pattern was dominated by straight horizontal cracks. Crushing of the boundary element and buckling of flexural bars were first exhibited concurrently at 1.6% drift. Eventually, load carrying capacity was lost due to the fracture of flexural reinforcement. The authors noted that negligible shear degradation was exhibited and that a relatively small component of the deflection corresponded to shear deformation (Oesterle et al. 1976). The specimen's experimental response is represented in Figure 2.1 by shear stress ratio versus drift points taken from the envelope of the reported response history. Figure 2.2 shows the damage that the wall exhibited prior to failure.

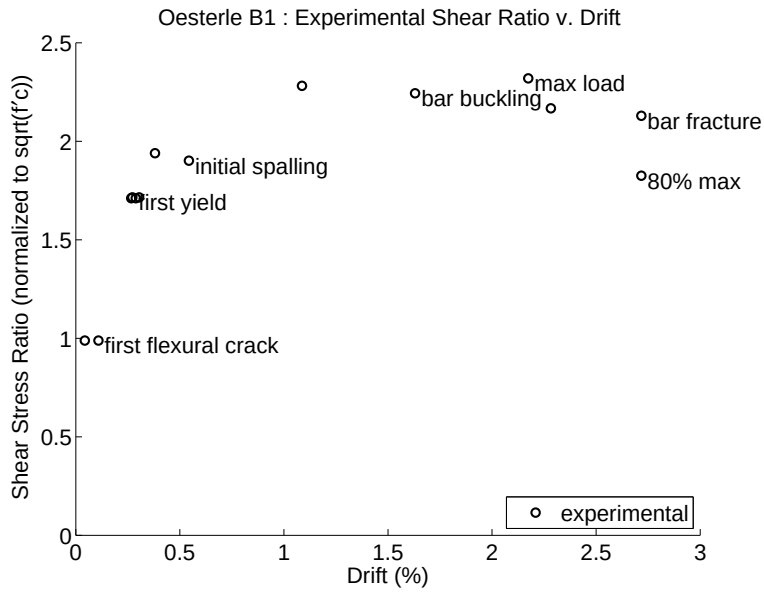

Figure 2.1: Experimental Behavior of Oesterle B1

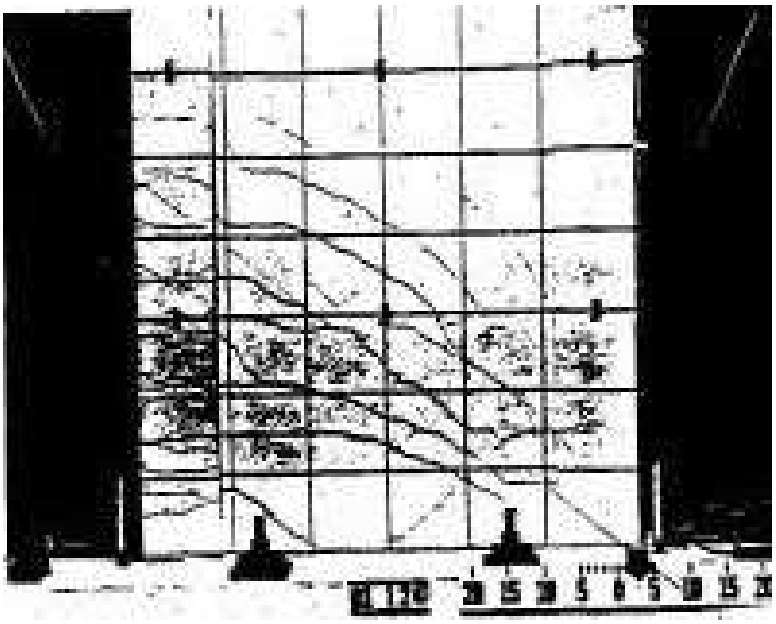

(Oesterle et al. 1976)

Figure 2.2: Experimental Damage of Oesterle B1

Oesterle B6

Oesterle B6 (1979) has similar geometry to Oesterle B1 (1976), but with different quantities of reinforcement and different strength concrete. There is 3.67% longitudinal reinforcement in the boundary element, 0.29% vertical reinforcement in the panel zone, 0.63% horizontal reinforcement, and 0.81% volumetric transverse reinforcement in the boundary element for confinement. The compressive strength of the concrete used is 3.17 ksi versus 7.69 ksi in Oesterle B1 (1976).

A constant axial load of $0.13A_g f'_c$ was applied to the specimen. Then, it was subjected to incrementally increasing reversing displacements at the top.

Oesterle B6 (1979) exhibited prominent diagonal cracking due to the imposed loading. Initial crushing of a diagonal compression strut in the panel zone was noticed before the loss of stiffness. Loss in strength corresponded to significant diagonal crushing of concrete in the panel zone. After completion of the test, the authors note, the boundary elements remained in relatively good condition and were capable of resisting the applied vertical loads (Oesterle et al. 1979). Its experimental response is represented in Figure 2.3 by shear stress ratio versus drift points taken from the envelope of the reported response history. Figure 2.4 shows the damage of the specimen at the end of testing.

Pilakoutas SW7

Pilakoutas SW7 (1995) is a rectangular wall with a 2.40 aspect ratio and a much higher concentration of longitudinal reinforcement in the boundary elements than in the panel zone. Its 2.36-inch thickness indicates that it represents less than one-fifth scale of a lateral force resisting wall in a mid-rise building. The longitudinal reinforcement ratio is 12.5% in the boundary element. The vertical reinforcement ratio is 0.59% in the panel zone. The horizontal reinforcement ratio is 0.39% from five pairs of bars spaced equally along the height. Transverse reinforcement is provided for confinement of the boundary elements with a reinforcement ratio of 0.78%.

The specimen was subjected to a displacement controlled incrementally increasing reversing load history. Lateral load was applied to the top of the wall. No axial load was

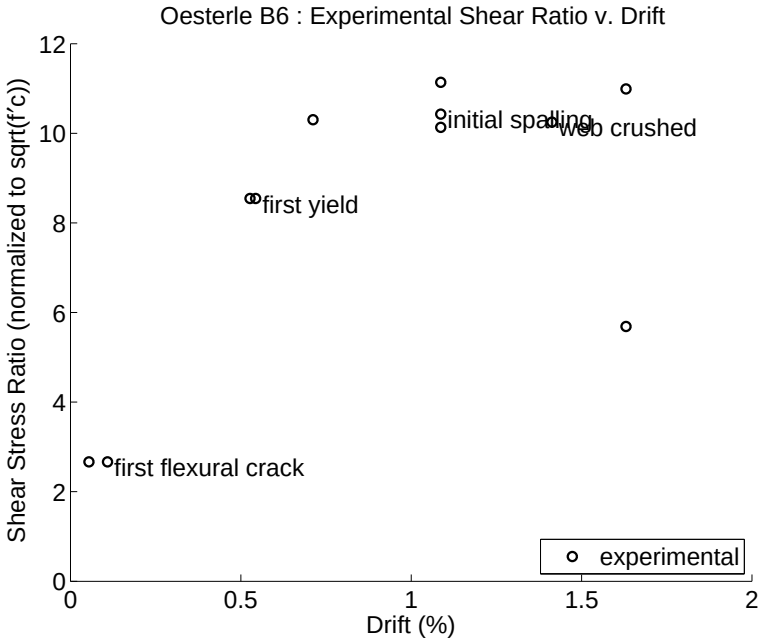

Figure 2.3: Experimental Behavior of Oesterle B6

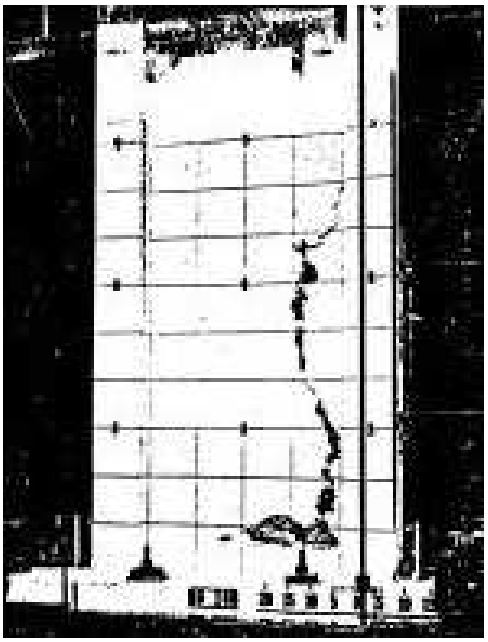

(Oesterle et al. 1979)

Figure 2.4: Experimental Damage of Oesterle B6

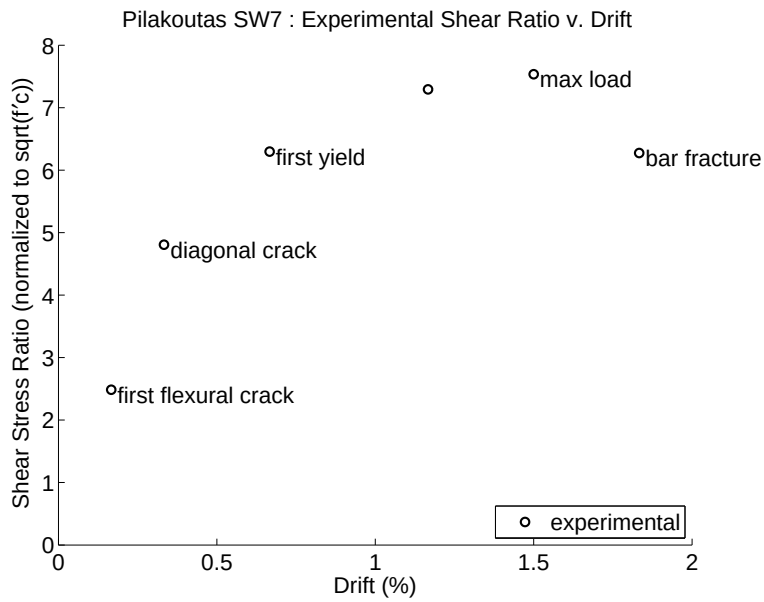

Figure 2.5: Experimental Behavior of Pilakoutas SW7

applied to the specimen during testing.

The cracking due to experimental loading was dominated by diagonal cracks across the panel zone and boundary elements. Ultimate failure resulted from the fracture of a horizontal bar. Its experimental response is represented in Figure 2.5 by shear stress ratio versus drift points taken from the envelope of the reported response history. Figure 2.6 shows the cracking patterns observed after three load steps. The step designated MDL-2 corresponds to a 2-mm imposed displacement. MDL-8 designates an 8-mm imposed displacement.

2.2 Previous Analyses of Structural Walls

Previous research has investigated prediction of wall behavior using the finite element analysis method. A review of studies that compare analytical results with reinforced concrete shear wall experiments for analysis techniques similar to those considered in this study has been conducted. A summary of each study follows.

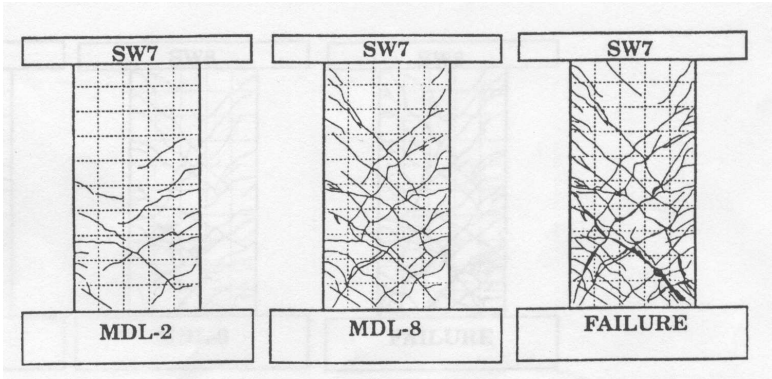

(Pilakoutas and Elnashai 1995)

Figure 2.6: Experimental Damage of Pilakoutas SW7

2.2.1 Martinelli

Martinelli (2001) proposed a beam-column-type fiber element for the analysis of shear-influenced reinforced concrete components. This element formulation is dubbed the Reinforced Concrete Inelastic Zone (RCIZ) element. It is based on a Timoshenko beam formulation, accounting for shear and flexure interaction. In this formulation, the direction of the resultant force of the uniaxial section fibers is allowed to rotate with respect to the longitudinal axis of the beam, which allows the element to simulate the effect of arch action and the formation of compressive struts.

Results generated using this model are compared with data from cyclic tests of three rectangular walls by Dazio et al. (1999). The analytical predictions were found to match well with the experimental results. The model tended towards excessive degradation of strength for subsequent loading cycles. However, the model was able to reproduce the stiffness of loading and reloading very well.

2.2.2 Ile and Reynouard

Ile and Reynouard (2000) proposed a cyclic response model for reinforced concrete continuum based on a fixed, smeared-crack approach. The objective of their study was to determine the applicability and quality of their analytical model with regard to simulation

of reinforced concrete shear wall response. To do this, they compared results from analyses using their model with the experimental results obtained from two reinforced concrete panels with wall-like geometry tested by Cervenka (1970).

The authors found that their model was capable of predicting the monotonic load verse displacement history of the specimen, including the mode of failure. However, the model underestimated the energy dissipation of subsequent load cycles and did not predict residual displacements upon unloading. It was also found that the model exhausted computational resources and refinement of the element mesh was impractical.

2.2.3 Palermo

Palermo (2001) studied cyclic analysis of shear walls using the Modified Compression Field Theory (Vecchio and Collins 1986) (MCFT). See Appendix A for a discussion of the MCFT. The walls studied included four barbell walls tested by Oesterle et al. (1976, 1979), three rectangular walls tested by Pilakoutas and Elnashai (1995), and two I-shaped flange walls he tested. The objective of the analysis was to determine the quality of analytical results obtained from a cyclic implementation of the MCFT and to study the difference in predicted results using a linear versus non-linear loading/reloading concrete model.

It was found that the analytical model accurately predicts the response of walls up to peak load. The choice of loading/reloading rules for the concrete model did not have a large impact, because the walls studied were largely governed by flexural behavior and controlled by the yielding of flexural steel. The model did a poorer job at predicting reloading stiffness and post-peak behavior.

2.2.4 Kwan and He

Kwan and He (2001) proposed a rotating, smeared-crack model that accounts for the effect of confinement and tension stiffening of concrete in a reinforced concrete continuum. They applied this model to six rectangular walls tested by Lefas et al. (1990, 1990) in a series of monotonic push-over analyses to study how the effect of confinement affects strength and ductility of reinforced concrete shear walls.

On average, the maximum load of the specimens was under-predicted. The model over-predicted the initial stiffness and the maximum displacement of each of the specimens. However, it was found that the model predicted cracking patterns well, generally predicted the load-displacement behavior well, and was capable of predicting the post-peak behavior of the specimens. Unfortunately, the specimens were not loaded beyond peak strength, so there is no basis for comparison of the predicted post-peak behavior.

2.3 OpenSees

OpenSees is a computational framework for nonlinear structural mechanics implementations of the finite element method. It was originally introduced by Frank McKenna (1997) and has since remained freely available for open-source development. It takes advantage of object-oriented programming concepts that allow for modularity, encapsulation, and extensibility of code. Additional features added to the framework by the structural engineering community provide users with a wide range of state-of-the-art analysis tools. The OpenSees 1.7.2 release was used in this thesis for the implementation of the beam-column analyses presented in Chapters 4 and 7. Additional information about OpenSees is available from the OpenSees User Manual (Mazzoni et al. 2006).

2.4 Data Management in Finite Element Analysis

In this research, experimentally tested reinforced concrete shear walls were analyzed using a variety of methods. These walls are defined by geometric, material, and test-result data tabulated in a spreadsheet. These data required processing to construct the input for the finite element solver. This processing was very complicated given the varying configurations and varying completeness of the compiled data. Multiple analyses using different modeling assumptions were desired for each wall. Therefore, an adaptable processing framework needed to be implemented. Implicit in this framework is the management of data.

Significant research has been conducted previously on the data management of the solver itself. Lessons from this previous research were applied to the management of user data as it is processed into solver input data.

Daniel (1988) notes that engineering problems are comprised of large amounts of data

that have several different data types and complex relationships. He also states that a system of individual and separate processors offers the most flexibility to process data prior to implementing the solving function.

Likewise, Row and Powell (1978) note the need for modularity in finite element analysis to allow flexibility with the analysis software. Accordingly, they recommend that data management be separated from the analysis functions.

In Daniel's (1988) implementation, the preprocessing phase consisted of reorganizing data into tabular database format using a rule-based procedure. Prior to processing of data and arranging the database, the analysis was initialized by determining all of the processors that will be used and the order that they will be used. (The preprocessor proposed in Chapter 3 does not do this. See the recommendations in Section 8.2.)

VanLuchene et al. (1986) demonstrated that the ordering of data for a finite element analysis is important to allow the program to efficiently step sequentially through the data. A tree structured database was proposed.

While the aforementioned studies are primarily concerned with the data management of the solver, Lowes and Miller (2006) look at the model-building (preprocessing) part of finite element analysis. They state that the current approach to model building leaves much to be desired for the following reasons:

- *The traditional approach to model building becomes increasingly time consuming, tedious and error prone as the complexity and nature of the modeling data changes.*

- *The traditional approach to model building forces the engineer to spend an inordinate amount of time focusing on specifying individual input parameters rather than on over-reaching modeling assumptions.*

- *The traditional approach to model building assumes that the end result is a single model; however, for nonlinear analysis it is often desirable to create multiple versions of the model that include variable levels of model complexity.*

- *The data required to build a nonlinear model define different types of model features*

including material response, component design, material response models, element formulation, and solution algorithms. These data have a structure that cannot be captured adequately using traditional model-building techniques.

- *It is typical that intermediate models, such as confined concrete models or component shear-strength models, are required to assemble the nonlinear model of the global structure. The use of intermediate models is not easily supported using a traditional approach to model building.*

- *The traditional approach to model-building introduces a high penalty for changing the model to accommodate an improved understanding, investigate the impact of modeling decisions, or conduct parameter studies.* (Lowes and Miller 2006)

All of the problems stated above are likely to arise given the proposed set of analyses for this research. So, it is evident that a formal model building strategy is needed to address these issues. Accordingly, Lowes and Miller state that a model building framework should meet the following objectives. It should:

1. *be sufficiently efficient as to make nonlinear analysis viable and practical for consulting and research engineers,*

2. *allow the engineer to focus on high-level modeling decisions,*

3. *support parameterized analysis and investigation of the impact of aleatory (i.e., modeling decision) and epistemic (i.e., random input variables) uncertainty of predicted response,*

4. *support a multi-step approach to completing the nonlinear analysis of the full structural system, in which increasingly sophisticated models are employed to simulate response,*

5. *enable the engineer to check the model by evaluating predicted response at the material, section, element and sub-structure level, and*

6. *facilitate model management by enabling systematic and rapid comparison of multiple versions of the models.* (Lowes and Miller 2006)

To facilitate the ability to meet these objectives, Lowes and Miller propose separating raw data from processed data. With this is in mind, they recommend the following eight steps to create a framework that meets the stated objectives and alleviates the problems associated with traditional model building techniques:

1. *Identify the models that potentially will be used to simulate structural response.*

2. *Identify the super-set of processed structural data required to build all versions of the model as well as the raw structural data and methods required to generate processed data.*

3. *Identify the numerical algorithms that will be complete the analyses.*

4. *Define a structure for storing the raw and processed data, the methods employed to process the data, and the structural response models and simulation algorithms used to simulate behavior.*

5. *Develop methods for populating the data structure.*

6. *Determine methods for verifying that the data are consistent and correct.*

7. *Develop methods for creating a specific version of the structural model for use in a full system analysis.*

8. *Establish a protocol for characterizing a specific version of the structural model to enable rapid comparison of different versions of the model.* (Lowes and Miller 2006)

Once this is formulated, one instance of a model is constructed. Creating a model with a different structural assemblage or set of modeling decisions consists of merely supplying a different set of raw data, provided that the processing functions for those modeling decisions exist. If they do not, the framework can be extended by creating the functions needed.

Chapter 3
PREPROCESSOR

In this chapter, a preprocessor that facilitates the model-building process for nonlinear finite element analysis is introduced. The preprocessor is intended to:

- enable users to focus on high-level modeling decisions and automate the implementation of these decisions in the creation of input files for finite element analysis.
- facilitate the creation of models for evaluation studies in which the same set of modeling decisions is applied to analyze multiple similar samples withe different basic material and geometric analysis parameters.
- facilitate the creation of models for parameter studies in which modeling decisions are changed to investigate the impact of modeling decisions on predicted response.
- automate the process of handling incomplete or incorrect basic data used in model creation.
- facilitate model management including developing a framework for characterizing models that reflects high-level modeling decisions and relationships with other versions of the model.

For the current project, the preprocessor was implemented in MATLAB using object-oriented coding methods and used to facilitate nonlinear analysis of the experimental wall specimens introduced in Section 2.1 using OpenSees. This implementation of the preprocessor also serves as a case study in using the model building strategies proposed by Lowes and Miller (2006).

3.1 Preprocessor Overview

The preprocessor is implemented in MATLAB because of the ease of code development. Object-oriented programming principals are used to facilitate development and the modification/expansion of the code. Use of objects also allows users to create analysis specifications by combining modular components.

The basic functionality of the preprocessor is to take basic data from multiple sources, manage and process this data to create output. It supports parameter studies by looping through different modeling cases of the same specimen. It also supports evaluation studies by looping through multiple material and geometric configurations of specimens. The end product of the preprocessor is a series of input files for the OpenSees solver. Additionally, the preprocessor is capable of documenting and describing the models in terms that focus on high-level modeling decisions that can be understood by the user.

To meet the functionality requirements and facilitate the code development process, the results of previous research in this area were used. It follow's Daniel's (1988) suggestion to use a system of individual processors. Individual processors range in functionality from defining all of the nodes for an analysis to determining the measured strength of concrete of a test specimen. The individual processors are implemented as objects. More complex processors have sub-processors, creating a tree-like structure of processing objects.

Row and Powell's (1978) notion of separation of data management from data processors is also incorporated. Objects that store data are kept separate from objects that process the data.

VanLuchene's (1986) recommendation to store data in an advantageous order is incorporated too. Data processors are stored in tree structures. This allows the preprocessor to step through the branches of the tree, in the correct order, and allow the sub-branches to conduct their processing functions efficiently.

Lowes and Miller's (2006) separation of processed data from raw data is implemented by creating separate classes for raw data and processed data. Neither of these classes is responsible for processing the data. Rather, the processing is performed by a separate set of objects. To ensure that raw data is not lost, no functionality to overwrite raw data is

provided to external objects.

Additionally, Lowes and Miller's (2006) eight steps to formulating an extensible model building framework are followed. However, departing slightly from Lowes and Miller, the modeling decisions are not stored in the raw data, but rather within the construction and arrangement of the data processors.

3.2 General Formulation

In this section, the preprocessor formulation is introduced in general terms. This includes presentation of the data types employed and the functionality encapsulated with each data type, as well as a general overview of the data flow and transformation of the preprocessor and the basic "parts" of the preprocessor, which include both data and functional code to transform data. Its parts and their interaction are outlined in a manner that is irrespective of the specifics of the data being modeled or the specifics of the solver.

3.2.1 Data Types

Six data types are used to manage data as it is processed. These types are data sources, raw data, modeling decisions, processed data, solver input, and solver output. Below, each of these data types are discussed briefly, examples of each data type are given, and possible formats of each are provided.

Data Sources include any collection of data that the user has that may be needed for the analysis. An example would be the geometric dimensions of an experimental structural assemblage or the compressive strength of concrete and yield strength of steel. The data sources can take on any form or combination of forms. It is expected that different formats may be used for different types of data within a single model-building activity. Such forms may include a collection of XML files, MATLAB scripts, or Excel spreadsheets.

Raw Data are the data collected from the data sources. They are not processed. The data can be stored as a 'struct' or as the member values of an object.

Modeling Decisions are the set of data that represent the user's decisions about what information, representational models, and analytical procedures to use when constructing the analytical model. An example is the decision to use the design compressive strength , without adjusting to account for age and over-strength at casting of concrete. Modeling decisions are typically in the form of a script; although other forms are possible. The preprocessor is also capable of assembling these modeling decisions into an output form that can be read by the user.

Processed Data are the data that constitute the mathematical model that is sent to the solver. It has been processed per the user's instructions. However, it may not be in a format that is understood by the solver.

Solver Input are the processed data translated into the format that the solver understands. In the case where OpenSees is the solver, this is a Tcl script.

Solver Output are the data that are generated by the solver. Typically, this will be displacements, stresses, and strains or any other applicable output data that are desired.

3.2.2 Transformation of Data

As data are transformed through the preprocessing and analysis, they take on the forms described in Section 3.2.1. This is a linear, unidirectional flow of data. The data begin as data sources and modeling decisions. The data sources are used to create the raw data. The raw data and the modeling decisions are combined to create the processed data. The processed data are converted into solver input. When the solver is called to run, it creates solver output. This process is shown in Figure 3.1.

3.2.3 Functionality Associated with Data Types

Functionality is associated with many of the previously discussed data types. Thus these data types are implemented as objects within the context of an object-oriented framework. The extent of functionality varies from the ability to 'set & get' data values to 'processing' of

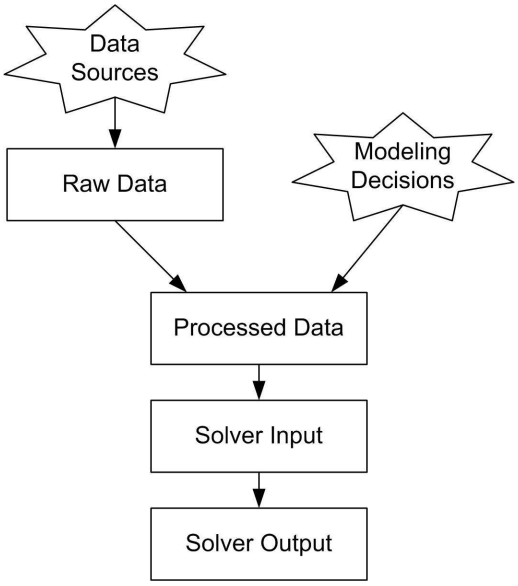

Figure 3.1: Transformation of Data in the Preprocessor

data. 'Set & get' implies that, beyond storing data, the object sets data values and provides data values to other entities that request the values. 'Processing' functionality implies that, in addition to data storage and set & get functionality, the object also processes data.

Table 3.1 summarizes the level of functionality associated with each data type. As shown, the processed data is the only data type that has processing functionality associated with it. The processed data object is capable of creating the solver input. This will be discussed further in Section 3.2.4 along with how the other types of data are transformed from one type to another.

3.2.4 Parts of the Preprocessor

The preprocessor is separated into distinct parts to facilitate the interaction and development of its objects. To understand the preprocessor, it is necessary to understand the individual parts of the preprocessor. Some of these parts are data classes with associated functionality. Others are functional classes. The preprocessor consists of the following parts:

Data Sources is as described in Section 3.2.1.

Table 3.1: Functionality Associated with Data Types

Data Type	*Functionality*
Data Sources	none
Raw Data	set & get
Modeling Decisions	none
Processed Data	processing
Solver Input	none
Solver Output	none

The Raw Data is as described in Section 3.2.1 with the addition of set & get functionality as described in Section 3.2.3.

The Raw Data Generator creates raw data objects from the data sources. It returns a raw data object when requested to do so by the global driver.

The Data Processor is the object that processes the raw data into the processed data. The data processor implements modeling decisions input by the user.

The Data Processor Generator creates data processors that reflect the modeling decisions. It returns a data processor object when requested by the global driver.

The Processed Data is as described in Section 3.2.1. In addition, it has set & get functionality and may be capable of creating the solver input as described in Section 3.2.3.

The Global Driver is the heart of pre-processor. It manages the analytical models sent to the solver. An analytical model comprises one set of raw data and one set of modeling decisions. In the event of a parameter study or an evaluation study, there will be multiple analytical models.

The run function of the global driver, shown in Figure 3.2, illustrates the purpose and the processes of the driver. The global driver has a raw data generator and it

```
RawDataGenerator = reset(RawDataGenerator);

while true
{
    RawData = getNext(RawDataGenerator);
    DataProcessorGenerator = reset(AnaSpecGen);

    if isnan(RawData) %---raw data object is ‘NaN’
    {
        break; %---break from loop over raw data
    }

    while true
    {
        DataProcessor = getNext(DataProcessorGenerator);

        if isnan(DataProcessor) %---data processor is ‘NaN’
        {
            break; %---break loop over data processors
        }

        run(DataProcessor, RawData);
    }
}
```

Figure 3.2: The Global Processor Run Command

has a data processor generator. It loops through sets of raw data until the raw data returns ‘NaN’, which indicates that the end of a raw data set has been reached. For each set of raw data, it loops through sets of data processors until the data processor generator returns ‘NaN’. Within this loop, it executes the current data processor’s run command, giving the current set of raw data to the data processor.

Figure 3.3 illustrates the organization and associations of the parts of the preprocessor within the global driver.

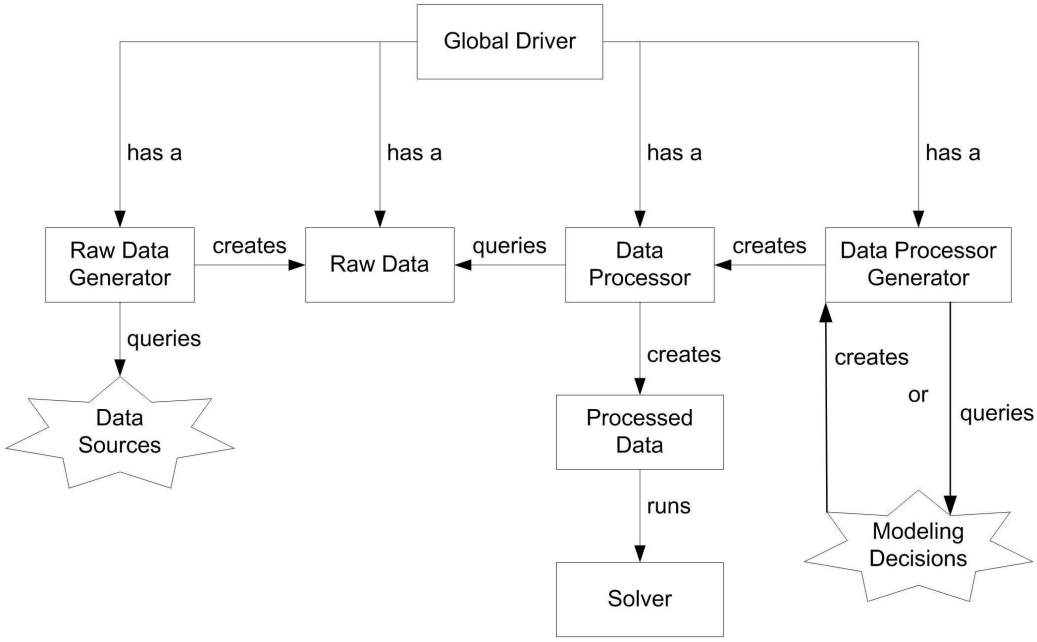

Figure 3.3: Preprocessor Top Level Classes and Associations

3.3 Specific Implementation

This section discusses the specific implementation of the preprocessor developed for the current project. The preprocessor is implemented in MATLAB, using the raw data described in Section 2.1. The solver is OpenSees and the goals of the analyses are described in Chapter 1. The parts of the MATLAB-based OpenSees preprocessor are discussed in reverse chronological order of their occurrence in the execution of the preprocessor.

Note that due to the lack of pointers in MATLAB's object oriented programming capabilities, objects have to be passed around from function to function as their data structure is being populated by other objects. Special attention to detail has to be maintained to prevent multiple copies of one object from being instantiated. If this occurs, it is possible that loss of data may result in the object being populated.

3.3.1 Solver – OpenSees

The solver used is OpenSees. See Section 2.3 for a discussion of the solver.

3.3.2 OpenSees Tcl Script Writing Classes

To run OpenSees commands from the MATLAB implementation of the preprocessor, additional utilities are required. The format for OpenSees input is the Tcl scripting language. Therefore, a series of OpenSees Tcl script writing classes were created. The OpenSees functions provided in the current set of writing classes are those required to accomplish the research activities specific to this project. However, this framework closely follows the organization of the OpenSees commands themselves and are easily extended to meet additional needs.

3.3.3 Processed Data – Processed_OpenSees

The contents of Processed_OpenSees follows that of OpenSees as closely as possible. However, since the intent of Processed_OpenSees is to write a script, not conduct an analysis, it's class associations and functionality are organized very differently from OpenSees.

What does Processed_OpenSees comprise?

The Processed_OpenSees portion of the preprocessor consists of a top level class and subclasses. The top level class holds the subclasses, manages the order of data, and manages the functions to write the input script. There are two types of subclasses: OpenSees command classes and OpenSees scheme classes.

OpenSees command classes are classes that represents OpenSees commands. The data stored in these classes are those required to write OpenSees input commands in Tcl. The functions included in these classes are a constructor; set, get, and add functions, as well as a function to write the OpenSees command in the script. See Mazzoni et al. (2006) for more information on OpenSees commands.

OpenSees scheme classes serve as organizers of OpenSees the command classes that are frequently associated with each other practically and conceptually. They have no parallel in the OpenSees framework. However, grouping these command classes

mirrors the human process of writing an input script and makes the process of script writing more efficient.

An example of the objects that would be included in the processed data for a simple pushover analysis script are shown in Table 3.2.

How is Processed_OpenSees organized?

The organization of the processed data is shown in Figure 3.4. Many of the objects shown in the figure represent vectors of objects. For instance, in most cases, there will be several instances of a concrete material used in the analysis. Therefore, the material value in Processed_OpenSees will be a vector of material objects. In MATLAB, this is implemented as a cell array.

Note that the AnalysisSchemes OpenSees scheme class is used to organize the details of the analysis portion of the script. It associates an appropriate convergence scheme with each set of load patterns applied to the model. The convergence scheme is a series of convergence steps. Each convergence step has an integrator, an algorithm, and a test object.

There are two OpenSees command classes that have subclasses associated with them. These are the section class and the pattern class. These are organized this way because these OpenSees commands have associated OpenSees sub-commands.

How is Processed_OpenSees populated?

The Processed_OpenSees object is populated using the set and add functions. For single data points (e.g., the model command), the set function is used. For multiple data points (e.g., material commands), the add function is used.

The functionality to alter, reorder, or delete Processed_OpenSees' contents are not provided. This functionality could be added if deemed necessary. However, the intent of this preprocessor is that all manipulation of data should be conducted in the data processing part of the framework.

Table 3.2: Processed Data Contents for an Example Analysis

Object Type	*Object Name*
Top Level Object	Processed_OpenSees
OpenSees Commands	Algorithm_Newtown
	Analysis
	Constraints_Plain
	Convergence_Displacement
	Element_NonlinearBeamColumn
	Fix
	GeomTransf_Linear2D
	Integrator_DisplacementControl
	Layer_Straight
	Load
	Material_Concrete01
	Material_Steel02
	Material_MinMax
	Model
	Node
	Numberer_Plain
	Recorder_Node
	Section_Fiber
	System_BandGeneral
	Test_NormDispIncr
	TimeSeries_Linear
OpenSees Schemes	AnalysisGeneral
	AnalysisScheme
	ConvergenceScheme
	ConvergenceStep
	LoadingScheme
	LoadingStage

Note: object names have been abbreviated.

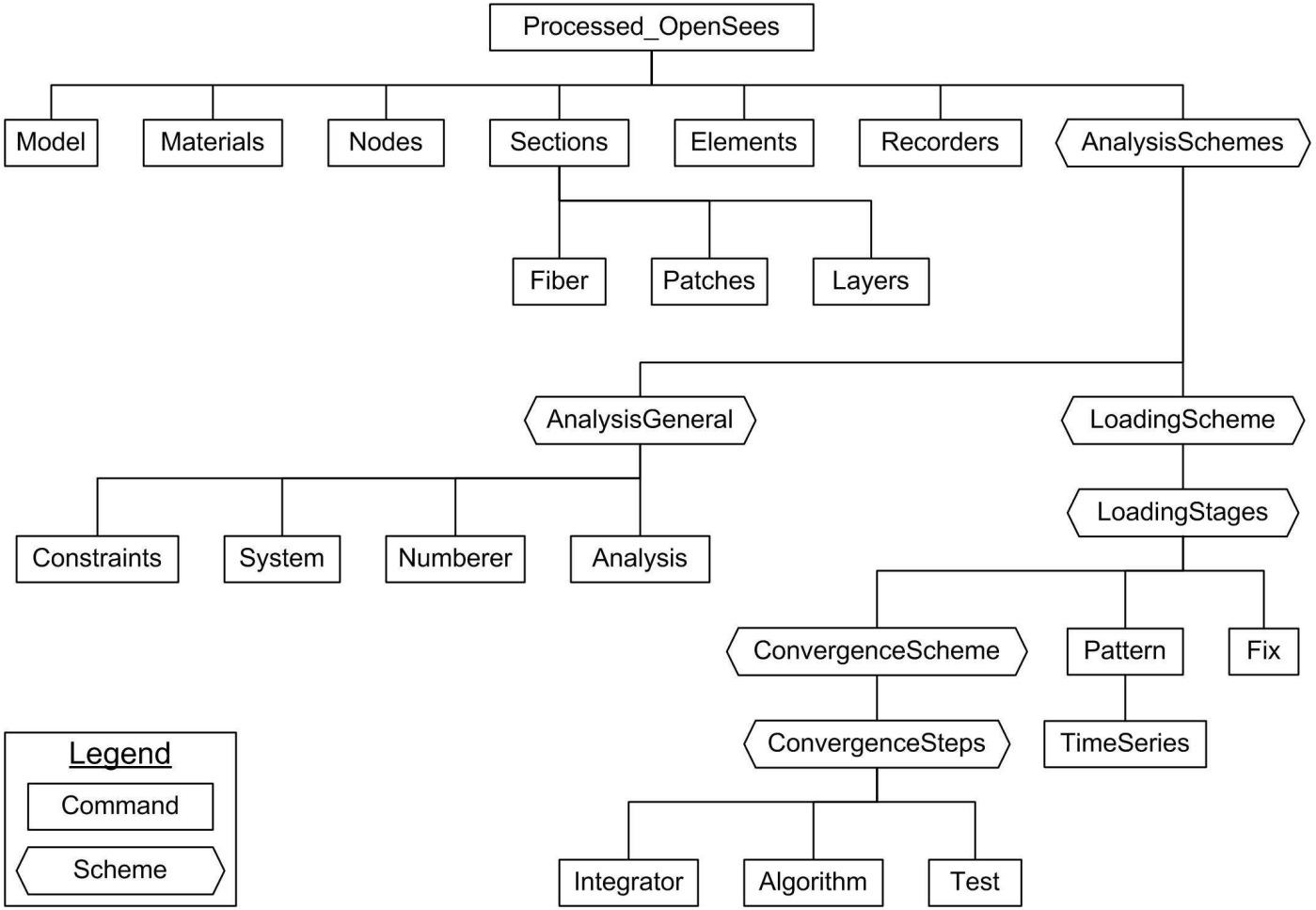

Figure 3.4: Processed Data Organization and Associations

How does Processed_OpenSees write an input file?

When the write function is executed, the Processed_OpenSees object takes the following steps (illustrated in Figure 3.4):

1. Instantiates an OpenSees Tcl Script.
2. Tells the model object to write its command to the script.
3. Goes through the materials vector and tells each material object to write itself to the script.
4. Goes through the nodes and tells each node object to write itself to the script.
5. Goes through the sections and tells each section object to write itself to the script.
6. Goes through the elements and tells each element object to write itself to the script.
7. Goes through the recorders and tells each recorder object to write itself to the script.
8. Goes through the analysis schemes and tells each analysis scheme object to write itself to the script.

In turn, each object will tell each of its sub-objects to write themselves to the script as necessary.

Visualization and error checking

An important aspect of constructing a model is to check if the model specified is in fact the model desired by the user. After the processed data is populated, it is possible to execute routines that will check for possible errors and help the user visualize the model.

An example of this is the drawSections function that is a member of the Processed_OpenSees object. This function will create a figure in MATLAB of each of the sections in the section vector.

3.3.4 Data Processor – DataProcessor_SW

Unlike Processed_OpenSees, the data processor is specific to the raw data structure and format. The formulation of DataProcessor_SW and some of its classes can be generalized; however, many of the details are specific to the shear wall analyses done as part of this study.

What does DataProcessor_SW comprise?

DataProcessor_SW consists of the following parts:

The Model Object processes the number of dimensions and the number of degrees of freedom of the model. It creates the model object and places it in the processed data.

The Materials Object processes all of the materials that are to be used in the model. It creates each of the material objects and places them in the processed data.

The Elements Object processes all of the sections, elements, nodes, and connectivity. These pieces of information are interconnected by the decision of which type(s) of element(s) and the mesh formulation to use in the model. The elements object creates all of the node, section, and element objects and places them in the processed data.

The Output Object processes all of the data recorders to use during the analysis. It creates all of the recorder objects and places them in the processed data.

The Analysis Object processes all of the data needed to apply boundary conditions and loading to the model. It also processes all of the data needed to create all of the inputs needed for the numerical side of the analysis. The analysis object creates the analysis scheme, analysis general, loading scheme, loading scheme, loading stage, convergence scheme, and convergence step OpenSees scheme objects. It also creates all of the constraint, system, numberer, analysis, integrator, algorithm, test, fix, pattern, and time series OpenSees command objects. It places these all in the correct order and adds them to the processed data.

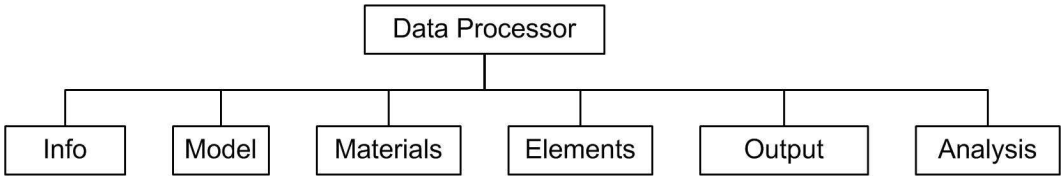

Figure 3.5: General Data Processor Organization and Associations

The Info Struct serves as a means to pass data from one of the processor objects mentioned above to subsequent processor objects. For example, when the elements object is creating sections, it needs to know the material indexes that were determined by the materials object.

How is DataProcessor_SW organized?

Figure 3.5 shows the top level class associations of a general data processor object. This level of structure and organization remains constant for most implementations of the data processor. However, with exception to the model class, the subclasses and the info struct will vary greatly from one implementation to the next as raw data and modeling decisions change.

How is DataProcessor_SW populated?

DataProcessor_SW is created and populated by the data processor generator. See Section 3.3.5 for more discussion.

How does DataProcessor_SW populate Processed_OpenSees?

The DataProcessor_SW begins to process the raw data when the process function is executed. The inputs of this function include the raw data object. First the model processor is executed, then the materials processor, then the elements processor, then the output processor, and finally the analysis processor. This follows the tree-like structure of the data processor. All of the sub-objects of a processor are executed before the next processor is executed.

How does DataProcessor_SW populate Processed_OpenSees?

While processing, the sub-objects of DataProcessor_SW each add their processed data to Processed_OpenSees. A processing function first determines if the data necessary to complete its processing function are present. If they are, it will process the data and add it to Processed_OpenSees. If not, the processing function will not add anything to the processed data and will indicate that the processing failed. This prevents data from being added to Processed_OpenSees that is not complete.

How does DataProcessor_SW account for missing information in WallData?

The structure and functions of the data processor classes allow for multiple methods of processing data to be specified in preferential order. For example, a user may want to use actual concrete strengths for a concrete material. If the actual strength is not available, then it may be acceptable to use the design strength of the concrete. If the design strength is not available, it may be acceptable to use the average strength of concrete produced by the batch plant over the past thirty years, and so on and so forth. These functions will be placed in a vector. The final in the vector may for use of a default value or model.

The processor will execute the first processing function in the vector. The processing function returns a flag, indicating success or failure. If the processor returns a true value for success, then the output is valid. However, if the processor returns a false value for success, then the next processor in the vector will be attempted. This is continued until success is true or the end of the vector is reached.

In many cases, a default value may be acceptable. If a default is specified, the processing will always succeed.

How does DataProcessor_SW report processing errors?

If the end of the vector is reached without achieving success, then the processing has failed. In some cases, this may be the desired result. Why conduct an analysis if the strength of the concrete is unknown? In other cases, this may indicate an error in the formulation of the processor, the raw data, or the data sources. Regardless, it is important to have the

ability to determine why and where a processor failed.

The error reporting process is intended to address this need. If a processor fails, the processor's name and the reason for failure are placed in a character string that is a part of the status struct. If this failure propagates back to the failure of the entire instance of DataProcessor_SW, then a file is placed in the output folder that contains this message.

3.3.5 Data Processor Generator

Several data generators were created. One for each type of OpenSees analysis to be done as part of this study: moment-curvature, push-over using a lumped-plasticity beam-column element, and push-over using a distributed-plasticity element. None of these are implemented as parameter studies. Therefore, these data processor generators will create one data processor and return it the first time that getNext is called by the global driver. Subsequent executions of getNext will return a 'NaN' value until the reset command is executed.

Resetting the data processor generator does not discard the data processor that it has created. Rather, this is saved so that the data processor does not have to be regenerated for subsequent sets of raw data.

3.3.6 Raw Data – WallData

WallData is a simple class that holds the raw material and geometric data compiled for one wall from the Excel spreadsheet that holds the raw data for all wall specimens. It is populated by WallDataGenerator_WallInfo050922.

*3.3.7 Raw Data Generator – WallDataGenerator_WallInfo*050922

WallDataGenerator_WallInfo050922 generates WallData objects for the global driver. When instantiated, it loads the Excel spreadsheet that, for the current application holds the raw material and geometric data for all walls, into MATLAB. When its getNext function is called in the global driver, it assembles a WallData object from one row of data (i.e. one wall) in the Excel spreadsheet and returns this object. Subsequent executions of its getNext function cause the generator to increment the number of the row from which it draws data.

After the last row is reached, it returns 'NaN' until the reset function is executed.

3.3.8 Global Driver

The global driver is a general function and does not require any modification for specific cases.

3.4 Using the Preprocessor

The following steps must be taken by the user to conduct a series of analyses, either a parametric or evaluation study, using the pre-processor as implemented:

1. Instantiate the preprocessor (global driver).
2. Instantiate a raw data generator.
3. Populate the raw data generator with the necessary information.
4. Register the raw data generator with the preprocessor.
5. Instantiate a data processor generator.
6. Populate the data processor generator with the necessary data to reflect the modeling decisions desired for the analyses.
7. Register the data processor generator with the preprocessor.
8. Run the preprocessor.

3.5 Summary

In this chapter, a preprocessor for the analysis of shear walls was introduced. A general formulation applicable to any type of analysis was proposed. Then, this general formulation was extended to the specific implementation of analyzing experimental walls whose data is compiled in Excel with the intention of satisfying the goals of the proposed research. Chapter 4 gives examples of analyses conducted using this framework.

Chapter 4

EVALUATION OF BEAM-COLUMN ELEMENTS FOR SIMULATION OF STRUCTURAL WALLS

4.1 Introduction/Overview

4.1.1 Research Impetus

The primary objective of this study was to provide information and tools to support the analysis of structural walls. A study of nonlinear analysis techniques available in design offices was conducted to determine the benefits and limitations of each. This study also served as a test case for the structural model building framework discussed in Chapter 3.

Discussions with an external advisory board (Lepage and Taylor 2005; Hooper, Klemencic, Lepage, and Taylor 2005) indicate that practicing engineers are typically using moment-curvature analyses to determine the cross-sectional strength of walls and elastic dynamic models with effective stiffness values to determine drifts. Nonlinear pushover analyses are performed for more rigorous analysis. Beyond this in complexity, there are nonlinear continuum models, which are currently being made available in new commercial software packages.

4.1.2 Approach

Each of the experimental walls in the database described in Section 2.1 was modeled using the lumped-plasticity and the distributed-plasticity beam-column fiber elements in OpenSees. This database of wall parameters served as a source of information to construct the analysis models. The corresponding database of test results for each of these walls served as a reference to judge the quality of the analyses. One set of "reasonable" analysis assumptions (in terms of material model parameters, number of integration points, etc.) was used for each of the analysis techniques explored.

4.1.3 Organization of Chapter

The following provides a brief outline of this chapter.

Section 4.2 describes the beam-column modeling techniques.

Section 4.3 discusses how the analysis results were compared to the experimental data to evaluate the goodness of each analysis technique.

Section 4.4 discusses the strength predictions obtained from the beam-column analysis.

Section 4.5 discusses the yield displacement and secant stiffness prediction results.

Section 4.6 discusses the displacement predictions at maximum moment.

Section 4.7 compares the overall findings of the two integration methods discussed in this chapter.

4.2 Description of Simulation Elements and Constitutive Models

The models were built using the actual specimen geometry, reinforcement, and measured material properties where available. The walls were modeled by one element, fixed at the base, with a monotonic horizontal load applied at the top node. In some cases, a moment was also applied to the top node in accordance with the experimental test. A constant axial load was also applied at the top, if applicable.

The bending response of the model elements was considered using a fiber model of the cross-section, described further in Section 4.2.1. The two types of elements used, lumped-plasticity and distributed-plasticity, integrate this cross-sectional response along the length of the element to determine the displacement response of the wall. Therefore, the strength predictions of both elements were the same.

The lumped-plasticity model assumes that all nonlinear behavior of the wall is lumped at the base. Therefore, it only has one nonlinear integration point. The response of the remainder of the wall is determined from elastic mechanics. A schematic of the lumped-plasticity element is shown in Figure 4.1 and a further description is provided in Section 4.2.2.

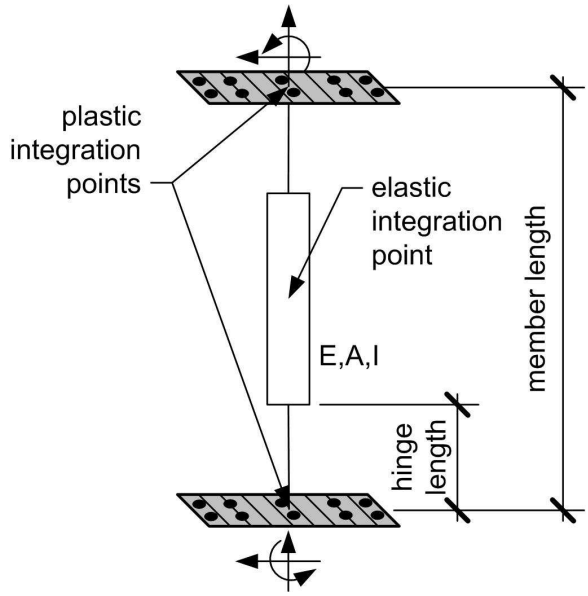

Figure 4.1: Lumped Plasticity Force Based Element

The distributed-plasticity does not make assumptions about the location and extent of nonlinear behavior in the element. Rather, it has multiple nonlinear integration points distributed along the length of the element. A schematic of the distributed-plasticity element is shown in Figure 4.2 and it is discussed further in Section 4.2.3.

4.2.1 Cross Section Analysis

At the cross-section level, the axial strain and curvature response of the wall due to applied loading is determined by strain compatibility and force equilibrium using uniaxial material models. It assumes that plane sections remain plane and perpendicular to the neutral axis. The characteristics that define the cross-sectional response are the fiber discretization, the uniaxial concrete constitutive model, and the uniaxial steel constitutive model.

The geometry of the wall is defined by the following parameters (further explanation of parameters is given by Figure 4.3):

- L_w is the length of the wall.

- t_w is the thickness of the wall in the panel zone.

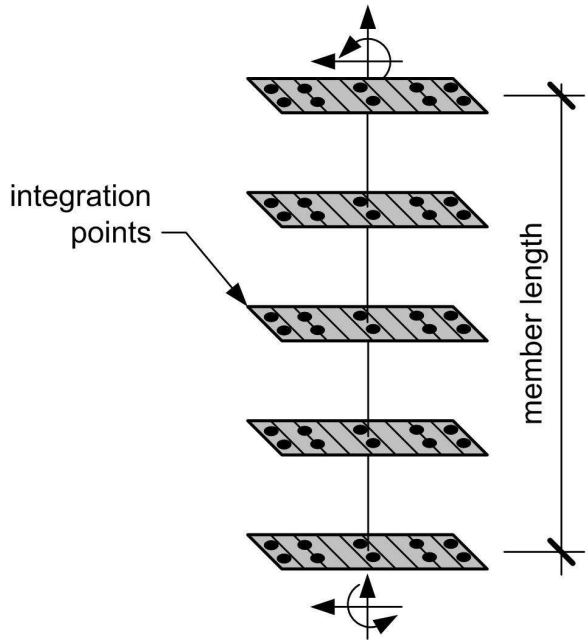

Figure 4.2: Force Based Distributed Plasticity Element

- t_{be} is the thickness of the boundary element.
- L_{be} is the length of the boundary element.
- $clrcvr$ is the clear cover distance provided.
- $numRowPZ$ is the number of rows of longitudinal steel provided in the panel zone.
- ρ_v is the ratio of the total area of longitudinal bars in the panel zone to the gross area of panel zone concrete perpendicular to these bars.
- d_{bv} is the diameter of the longitudinal bars in the panel zone.
- d_{bt} is the diameter of the transverse reinforcement bars in the boundary element.
- $numRowBE$ is the number of rows of longitudinal steel provided in the boundary element.

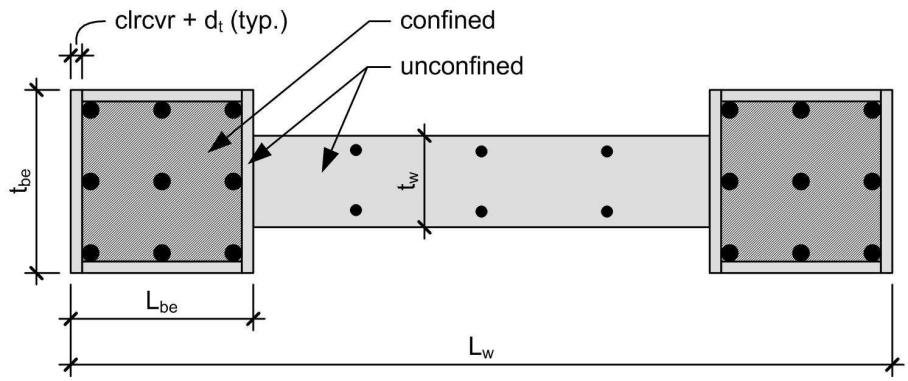

Figure 4.3: Wall Cross Section Definitions for Sectional Analysis

- ρ_l is the ratio of the total area of longitudinal bars in the boundary element to the gross area of boundary element concrete perpendicular to these bars.

- d_{bl} is the diameter of the longitudinal bars in the boundary element.

The constitutive relationship of the concrete was given by the Modified Kent and Park Model (Park, Priestley, and Gill 1982). This model was developed for columns with rectangular hoops. It accounts for the increased strength and ductility that concrete gets from confinement. In OpenSees, this was implemented using the concrete01 uniaxial material model (Mazzoni et al. 2006).

The Giuffré Menegotto Pinto Model is used to represent the constitutive behavior of the longitudinal steel. The model can simulate cycling and accounts for post-yield strain hardening. Figure 4.4 shows the cyclic behavior of this model. The Giuffré Menegotto Pinto Model has infinite strain and stress capacities. To limit these capacities, OpenSees' MinMax material wrapper is employed. The maximum tensile strain allowed is 0.08 in/in. Strains exceeding this value return zero stress. This limit accounts for the loss in strength of bars due to fracture. The minimum compressive strain limit is -0.08 in/in. Strains less than this value return zero stress. This limit accounts for the loss of strength observed in bars due to buckling.

The primary numerical decision at the cross-section level of the analysis is the level of mesh refinement in the construction of the fiber section. The mesh resolution method

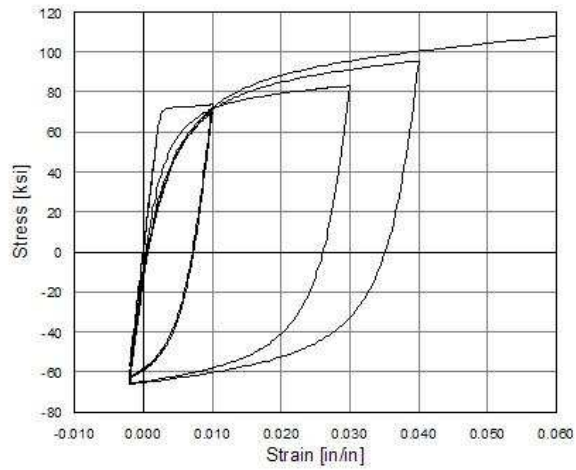

(Mazzoni et al.)

Figure 4.4: Cyclic Example of Giuffré Menegotto Pinto Model

employed seeks to divide the concrete patches into 1-inch thick strips in the boundary element and 3-inch strips in the panel zone. The higher resolution specified in the boundary element was intended to capture the more nonlinear stress behavior in the concrete caused by higher strains.

4.2.2 Lumped Plasticity Beam-Column Element

The lumped-plasticity model takes advantage of an a priori knowledge of how frame elements behave when subjected to loading. When a wall is fixed at its base and subjected to a lateral load at the top, plastic hinge formation occurs at the base. Accordingly, the lumped plasticity model only accounts for nonlinear behavior at the base of the element and the remainder of the element remains elastic. The effect of the plastic deformation on the displacement is weighted by adjusting the plastic hinge length. This simplifies the numerical model and reduces computational effort.

Controlling the length of the plastic hinge can be used to account for causes of deformation that cannot be modeled with the distributed plasticity force based element alone. These causes of deformation include shear deformations at the base and fixed-end rotation resulting from strain penetration of the wall longitudinal reinforcement in the foundation.

The elastic properties of the wall can also be adjusted to achieve a better match between predicted and observed behavior.

The lumped-plasticity element was implemented as a force-based element in OpenSees as the beamWithHinges3 element (Mazzoni et al. 2006). The plastic hinge located at the top is set to zero, to force all plastic behavior to occur in the base of the wall.

The numerical modeling decisions involved in using this element include the elastic section properties and the length of the plastic hinge L_p. The elastic section properties are the elastic modulus E, the cross sectional area for axial stiffness A, and the moment of inertia for bending stiffness I.

The value used for E was $57,000\sqrt{f'_c}$, where f'_c is in *psi* units, using the recommendations in ACI 318–02 (ACI Committee 318 2002). The value used for EI is 50% EI_{gross}, as commonly used in practice to model cracked concrete. The value used for L_p is $\frac{1}{2}L_w$. This value has been cited as a reasonable approximation (Paulay and Priestley 1992; Wallace and Moehle 1992) and is commonly used by practitioners.

4.2.3 Distributed Plasticity Beam-Column Element

The distributed-plasticity method makes no assumptions about the location and extent of nonlinear behavior in the beam-column element. Rather, multiple integration points are distributed along the length of the element according to the Gauss-Lobatto quadrature rule. The model was implemented using the force-based nonlinearBeamColumn element in OpenSees. Five integration points were used, following Berry's (2006) recommendations, which were based on similar analyses of columns.

4.2.4 Typical Predicted Force-Displacement Response Curves

Figures 4.5–4.7 show the predicted and experimental force-displacement response curves of the three experimental walls for further study discussed in Section 2.1.1. The results of the lumped-plasticity analysis are denoted in the legends as BwH3 (beamWithHinges3 abbreviated) and the results of the distributed-plasticity analysis are denoted as NLBC (nonlinearBeamColumn abbreviated). The applied lateral load was normalized by the cross-

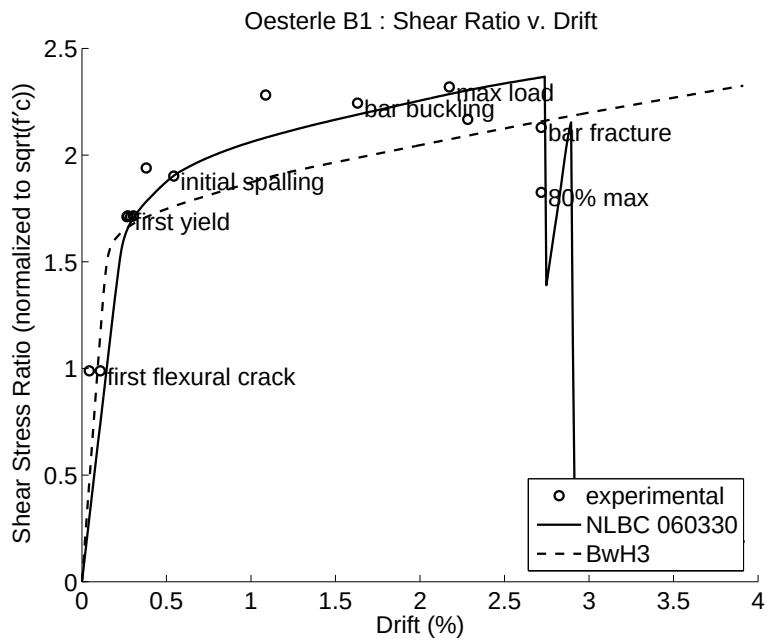

Figure 4.5: Comparison of Experimental and Analytical Force-Displacement Curves - Oesterle B1

sectional area of the wall and the square-root of the concrete compressive strength. The displacement at the top of the wall was normalized by the height to obtain drift.

4.3 Description of Evaluation Method

4.3.1 Description of Wall Characteristics

The quality of the predicted results are corroborated against design parameters to make predictions about cases where the analysis techniques are reliable and what improvements can be made to these analysis techniques when they are not reliable. The design parameters used in this study are:

Aspect ratio, h_w/L_w, is the ratio of the height of the wall to the length of the wall. If a moment is applied to the top of the wall, h_w is taken as the theoretical height of the wall. This is the distance from the base of the wall to the point that a single point load would be applied to, to obtain an identical moment distribution along the height

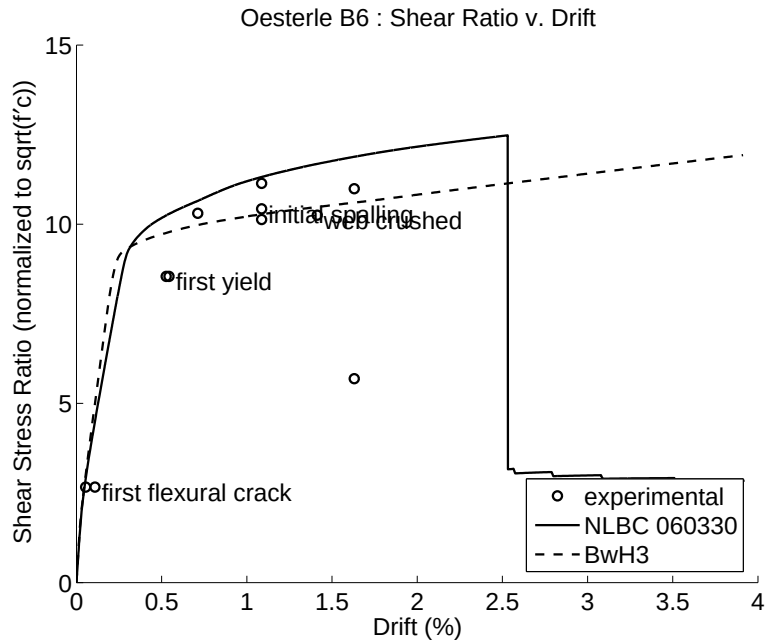

Figure 4.6: Comparison of Experimental and Analytical Force-Displacement Curves - Oesterle B6

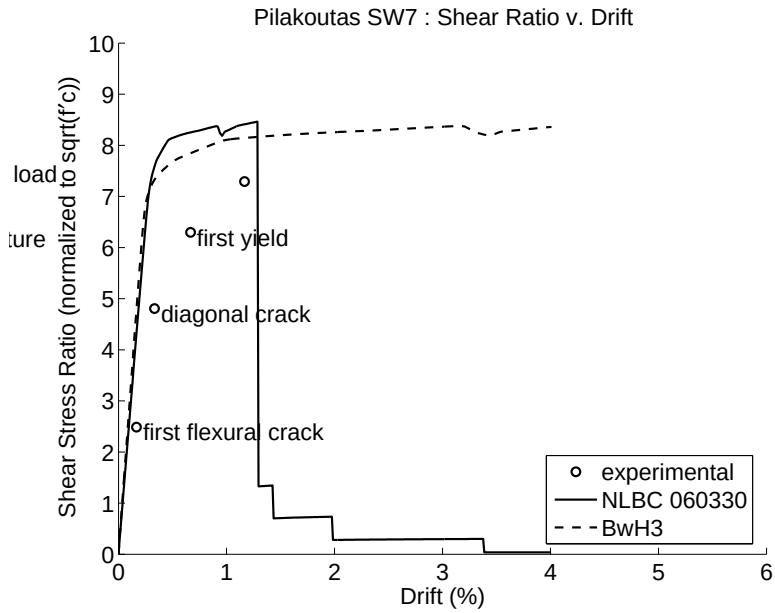

Figure 4.7: Comparison of Experimental and Analytical Force-Displacement Curves - Pilakoutas SW7

of the wall.

Axial load ratio, $P_{axial}/(A_g f'_c)$, is the percent of the axial force divided by the product of the cross-sectional area and the measured compressive strength of the concrete. Where, P_{axial} is the applied axial load, A_g is the gross cross-sectional area of the wall, f'_c is the measured compressive strength of the concrete. Compression is positive.

Horizontal reinforcement ratio, ρ_h, is the ratio of the area of horizontal reinforcement to the gross concrete area perpendicular to that reinforcement.

Longitudinal reinforcement ratio, ρ_l, is the ratio of area of vertical reinforcement in the boundary element to the area of the boundary element. If the wall does not have boundary elements, then the ratio of all vertical reinforcement to the area of the wall cross-section is used.

Maximum shear stress ratio, $V_{max}/(A_{cv}\sqrt{f'_c})$, is the maximum recorded shear applied to the wall divided by the product of the shear area of the wall, as defined by Chapter 21 of ACI 318 (2002), and the square root of the measured compressive strength of the concrete.

Maximum shear demand ratio, V_{max}/V_n, is the maximum recorded shear applied to the wall divided by the nominal shear strength of the wall, as defined by Chapter 21 of ACI 318 (2002):

$$V_n = A_{cv}(\alpha_c\sqrt{f'_c} + \rho_h f_y) \tag{4.1}$$

where α_c is a coefficient given by the code based on the aspect ratio and f_y is the yield strength of the horizontal steel.

Normalized thickness is the thickness of the wall divided by 12 inches. This is an indicator of the scale of the experimental wall. The minimum wall thickness of actual walls in buildings was 12 inches, based on an inventory review of shear walls built in the western United States.

Shear stress ratio at yield, $V_y/(A_{cv}\sqrt{f'_c})$, is the recorded shear applied to the wall at yield divided by the product of the shear area of the wall, as defined by Chapter 21 of ACI 318 (2002) and the square root of the measured compressive strength of the concrete.

Shear demand ratio at yield, V_y/V_n, is the recorded shear applied to the wall at yield divided by the nominal shear strength of the wall, as defined by Chapter 21 of ACI 318 (2002).

Volumetric transverse reinforcement ratio, ρ_t, is the ratio of the volume of hoop steel in the boundary element to the volume of the boundary element.

4.3.2 Description of Measured Response Quantities

The following measured response quantities from the experimental wall tests are used to determine the quality of each analyses:

Yield moment strength, $M_{y,obs}$, is the moment at the base of the wall when first yielding in the longitudinal steel is reported by the experimental researcher.

Yield displacement, $\Delta_{y,obs}$, is the displacement of the wall measured at the application of the lateral load when first yield in the longitudinal reinforcement is reported.

Stiffness up to yield, $k_{sec,obs}$, is a secant stiffness, defined by the shear force at yield (corresponding to the above stated measured yield moment) divided by the measured yield displacement.

Maximum moment strength, $M_{max,obs}$, is the moment at the base of the wall when the maximum recorded lateral load is applied to the top of the wall.

Maximum displacement, $\Delta_{max,obs}$, is the maximum top displacement of the wall reported by the experimental researcher.

4.3.3 Description of Simulated Response Quantities

The following simulated response quantities from the analyses of the experimental walls are compared against the correlating measured quantities to determine the quality of each analysis:

Yield moment strength, $M_{y,pred}$, is the moment at the base of the wall when the extreme tensile longitudinal reinforcement first exceeds the yield strain.

Yield displacement, $\Delta_{y,pred}$, is the displacement of the top node of the wall model predicted when the extreme tensile longitudinal reinforcement bar first exceeds the yield strain.

Stiffness up to yield, $k_{sec,pred}$, is a secant stiffness, defined by the predicted lateral load at yield divided by the predicted displacement of the top node at yield.

Maximum moment strength, $M_{max,pred}$, is the moment at the base of the wall when a strain of -0.003 in/in at the extreme compression fiber is predicted. This is also known as the nominal strength, M_n, in ACI 318 (2002).

Maximum displacement, $\Delta_{max,pred}$, is the displacement at the first occurrence of one of the following events: (1.) the tensile steel exceeds the fracture strain, (2.) the strength decreases to 80% of the maximum strength, or (3.) the concrete exceeds a compressive strain larger than Sasani et al.'s (2001) maximum usable concrete strain for walls, ϵ_c^{max}, given by:

$$\epsilon_c^{max} = 0.00355 + 0.822\frac{f_{yt}\rho_t}{60ksi} \tag{4.2}$$

where f_{yt} is the yield strength of the hoop steel and ρ_t is the volumetric ratio of hoop steel in the compressive boundary element.

4.3.4 Method of Determining Quality of Results

The quality of the individual analysis results were determined by comparing the ratio of the simulated response quantities described in Section 4.3.3 to the corresponding measured response quantities described in Section 4.3.2. A ratio value of one indicates that the analysis precisely predicted the response quantity. A ratio value less than one indicates that the response quantity was under-predicted. A ratio value greater than one indicates that the analysis over-predicted the response quantity. Additionally, the shape of the predicted load-displacement curves were compared against the backbone of the experimental load-displacement curves.

The overall quality of each analysis method was evaluated by examining the average, standard deviation, and coefficient of variation of the predicted to observed response quantity ratios of all of the experimental walls for the method. The trends of prediction quality ratios were compared to the design parameters discussed in Section 4.3.1 by visual inspection of data scatter plots.

4.4 Flexural Strength Analysis

4.4.1 Comparison of Experimental and Analytical Results

For the sixty experimental walls specified, the average $M_{max,pred}/M_{max,obs}$ ratio is 0.94. The standard deviation is 0.16. This corresponds to a coefficient of variation of 17%. The average $M_{y,pred}/M_{y,obs}$ ratio is 0.88. The standard deviation is 0.15. This corresponds to a coefficient of variation of 17%. Tables 4.1 & 4.2 show the ability to meet these prediction objectives for each wall.

Appendix B includes plots of all of the moment curvature relationships determined by the analyses. Appendix C includes plots of all of the moment curvature relationships determined by the the moment curvature analyses to those of a similar implementation of the moment curvature method in MATLAB. Appendix D includes plots of the ability to predict the maximum strength of individual walls versus each of the design parameters examined.

Table 4.1: Predicted Strength Results Using Beam-Column Element Formulation

Objective	*Maximum Strength (in-k)*		*Yield Strength (in-k)*	
Name	$M_{max,obs}$	$M_{max,pred}/M_{max,obs}$	$M_{y,obs}$	$M_{y,pred}/M_{y,obs}$
Lefas SW30	1437	0.74		
Lefas SW31	1410	0.77		
Lefas SW32	1352	0.86		
Lefas SW33	938	1.22		
Lefas SW11	1827	0.97	1242	0.89
Lefas SW12	2448	0.88	1535	1.02
Lefas SW13	2412	0.86	1827	0.92
Lefas SW14	1937	0.87	1242	0.86
Lefas SW15	2302	0.85	1535	0.92
Lefas SW16	2594	0.91	1973	0.98
Lefas SW17	1805	0.97	1060	1.03
Lefas SW21	1547	0.81	974	0.83
Lefas SW22	1827	0.83	1340	0.83
Lefas SW23	2192	0.74	1462	0.90
Lefas SW24	1462	0.88	974	0.84
Lefas SW25	1827	0.85	1583	0.80
Lefas SW26	1498	0.78	828	0.94
Oesterle B1	11408	0.98	8298	0.82
Oesterle B2	28520	0.84	22448	0.84
Oesterle B3	11776	0.95	8464	0.79
Oesterle B4	14352	0.77	8464	0.81
Oesterle B5	31519	0.90	23000	0.89
Oesterle R1	5060	0.97	4140	0.73
Oesterle R2	9292	0.87		
Oesterle B6	36064	0.88	27048	0.95
Oesterle B7	40554	0.91	31280	0.93
Oesterle B8	43424	0.83	30544	0.93
Oesterle B9	42504	0.83	42504	0.65
Oesterle B10	31832	0.78	31832	0.62
Pilakoutas SW4	1116	1.08	877	1.05
Pilakoutas SW5	1247	1.17		
Pilakoutas SW6	1137	1.06	797	1.15
Pilakoutas SW7	1483	0.98	1131	1.06
Pilakoutas SW8	1184	1.15	850	1.22
Pilakoutas SW9	1036	1.29	842	1.22
Salonikios LSW1	2761	1.26		
Salonikios LSW2	2007	1.16		
Salonikios LSW3	2783	1.12		
Salonikios MSW1	3107	1.12		
Salonikios MSW2	1960	1.20		
Salonikios MSW3	2836	1.09		
Salonikios MSW6	3186	1.09		
Sittipunt W1	9351	1.12		
Sittipunt W2	11580	0.94		

Table 4.2: Predicted Strength Results Using Beam-Column Element Formulation (cont.)

Objective	*Maximum Strength (in-k)*		*Yield Strength (in-k)*	
Name	$M_{max,obs}$	$M_{max,pred}/M_{max,obs}$	$M_{y,obs}$	$M_{y,pred}/M_{y,obs}$
Tasnimi SHW1	156	1.14		
Tasnimi SHW2	195	0.91		
Tasnimi SHW3	166	1.08		
Tasnimi SHW4	234	0.77		
Thomsen RW1	4950	0.96	4500	0.84
Thomsen RW2	5400	0.82	4500	0.77
Vallenas SW3	42698	0.86	35177	0.80
Vallenas SW4	35255	1.04	35255	0.80
Vallenas SW5	31234	0.83	24168	0.82
Vallenas SW6	28581	0.91	24852	0.80
Wang SW1	68448	0.56	52716	0.58
Wang SW2	67620	0.57	55752	0.55
Yanez S1	5603	0.89		
Zhang SW7	2673	1.00	2289	1.00
Zhang SW8	2976	0.80	2530	0.90
Zhang SW9	4033	1.00	3395	1.02
Average	–	0.94	–	0.88
St. Dev.	–	0.16	–	0.15
COV	–	0.17	–	0.17

4.4.2 Influence of Wall Parameters on Strength Prediction

Normalized Thickness: The strength prediction ratios were compared to the normalized thickness to determine the effect of scale in experimental testing affected the ability of the flexural beam-column analysis method to predict the strength of walls. It was anticipated that walls of smaller scales would have less reliable test results resulting in an increased trend of poor strength prediction. Figure 4.8 demonstrates that the prediction results have consistent prediction ratio averages and variability at all tested normalized thicknesses. Therefore, it was concluded that the effect of size was not an issue.

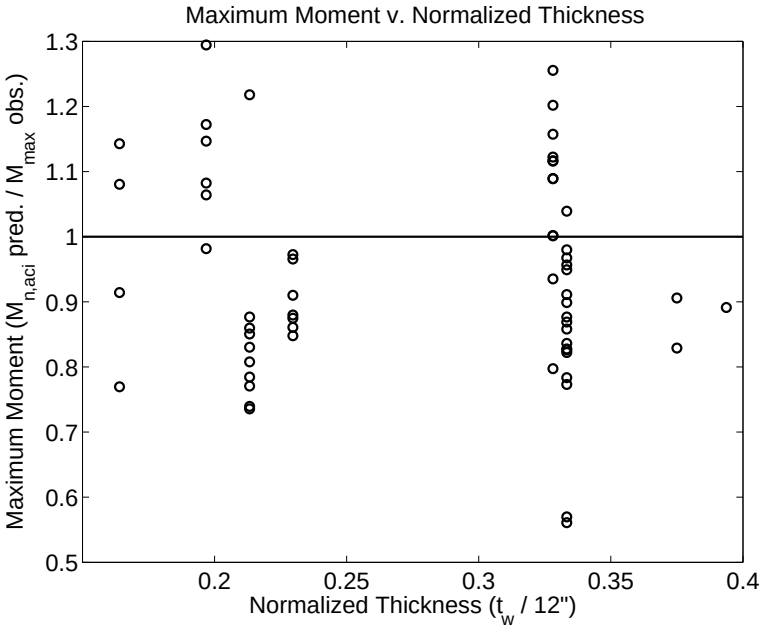

Figure 4.8: Maximum Moment Prediction Ratio v. Normalized Thickness

Aspect ratio: As aspect ratio increases, a wall's behavior was anticipated to become less shear critical and more likely to lose strength prior to the development of flexural the wall's flexural strength capacity. This would result in less strength over-prediction in walls with higher aspect ratios. Figure 4.9 shows that walls with higher aspect ratios were indeed less likely to have their strength's over-predicted.

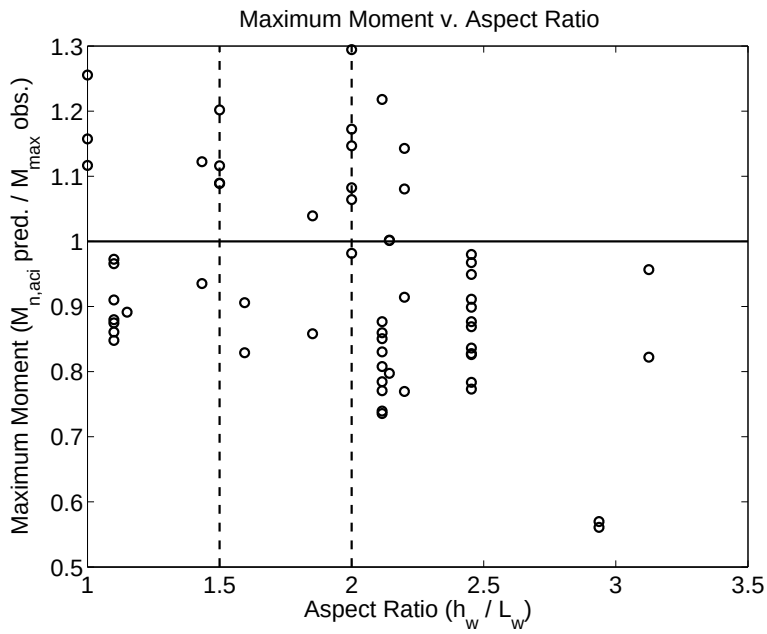

Figure 4.9: Maximum Moment Prediction Ratio v. Aspect Ratio

Axial load ratio: Actual walls in buildings are likely to carry gravity loads through axial compression. Axial load both increases shear and flexural strength of walls. The introduction of axial load was observed to greatly decrease the likelihood that wall strength would be over-predicted, as shown in Figure 4.10. Only 12% of walls with axial load had their strength over-predicted. Of those, no walls with axial load ratios of 10% or greater had their strengths over-predicted.

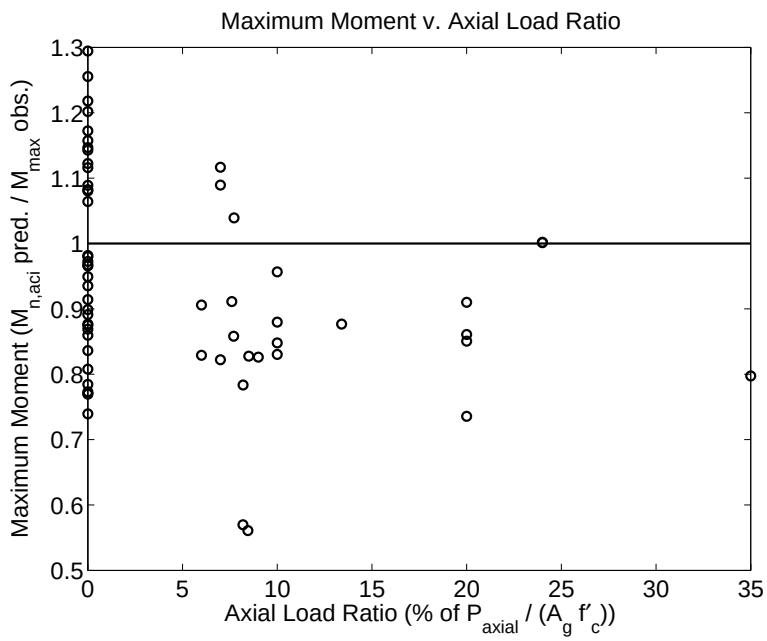

Figure 4.10: Maximum Moment Prediction Ratio v. Axial Load Ratio

Horizontal reinforcement ratio: It was anticipated that a higher horizontal reinforcement ratio would decrease the likelihood of over-predicted strength, because walls would be less likely to lose strength due to shear prior to the development of the flexural strength capacity. This expected behavior is indeed demonstrated in Figure 4.11. Walls with higher horizontal reinforcement ratios were less likely to have their strengths' over-predicted.

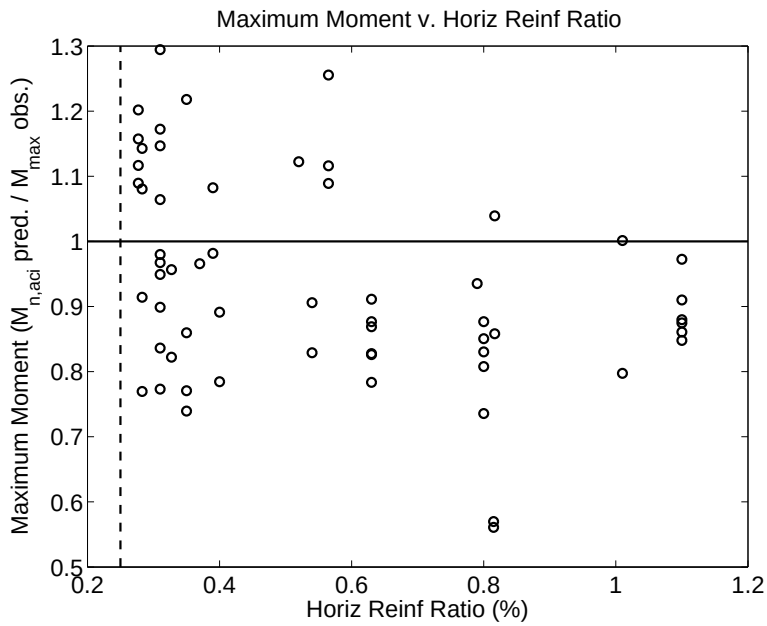

Figure 4.11: Maximum Moment Prediction Ratio v. Horizontal Reinforcement Ratio

Longitudinal reinforcement ratio: Walls with excessive amounts of reinforcement in the boundary elements were anticipated to be incapable of developing the strength of the bars through bond. Larger concentrations of reinforcement in the boundary element also make a wall more susceptible to localized damage in the panel zone. These effects were not accounted for in the beam-column element formulation. Therefore, walls with higher longitudinal reinforcement ratios were anticipated to be more likely to have their strengths over-predicted. The analysis results in Figure 4.12 support verify this hypothesis. Strength capacities of walls with reinforcement ratios greater than 5% were more likely to over-predicted. At ratios less than 5%, there was no discernable trend.

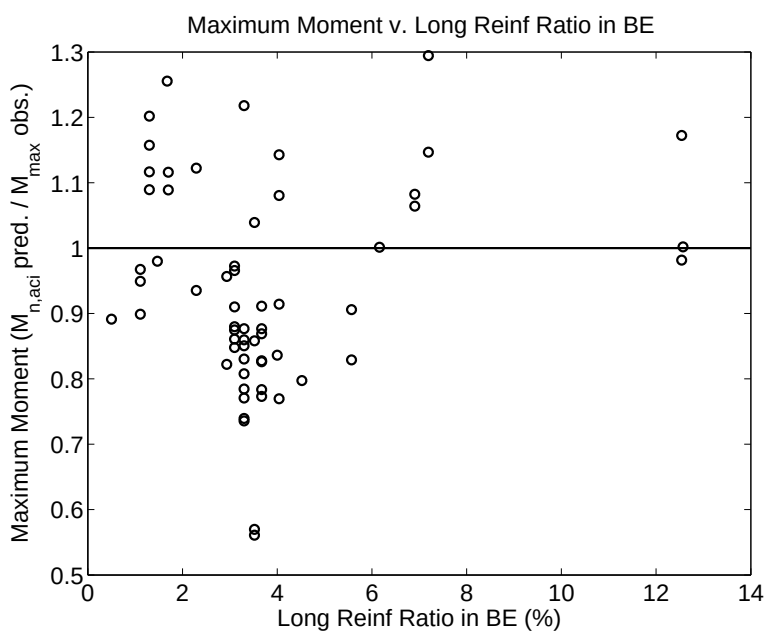

Figure 4.12: Maximum Moment Prediction Ratio v. Longitudinal Reinforcement Ratio in the Boundary Element

Maximum shear stress ratio: It was anticipated that a wall is only capable of resisting a certain amount of applied shear stress. So, walls whose flexural strengths exceeded such a limit would fail due to shear prior to the development of the flexural capacity. Therefore, the strengths would be over-predicted by the flexural beam-column method. Contrarily, the opposite was observed, as shown in Figure 4.13. Walls with lower shear stress ratios were more likely to have their strengths over-predicted. Design parameters like higher axial load and more horizontal reinforcement appeared to increase the capacity of the wall to achieve higher shear stress ratios, thus reducing the likelihood of maximum strength over-prediction.

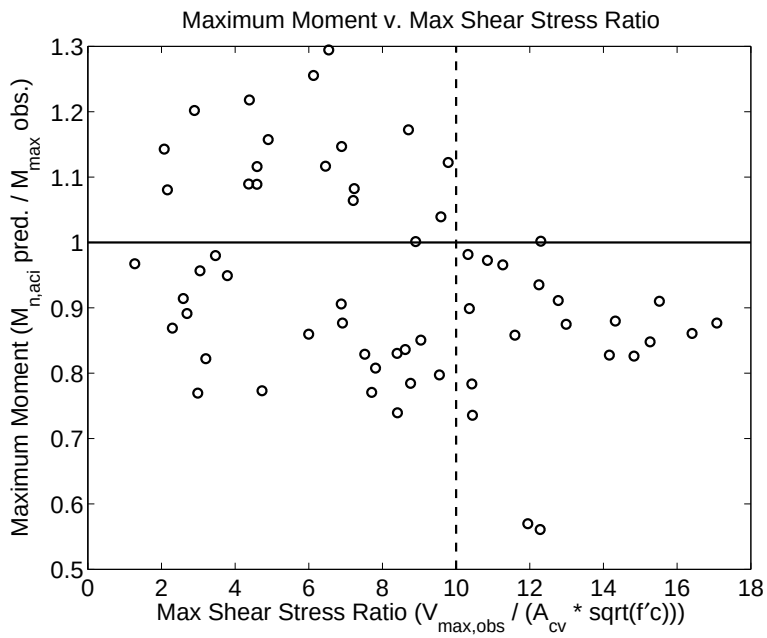

Figure 4.13: Maximum Moment Prediction Ratio v. Maximum Shear Stress Ratio

Maximum shear demand/capacity ratio: Again, it was anticipated that walls with higher shear demand-capacity ratios would be more prone to loss of strength prior to the development of flexural capacity. However, Figure 4.14 shows no discernable trend in the results.

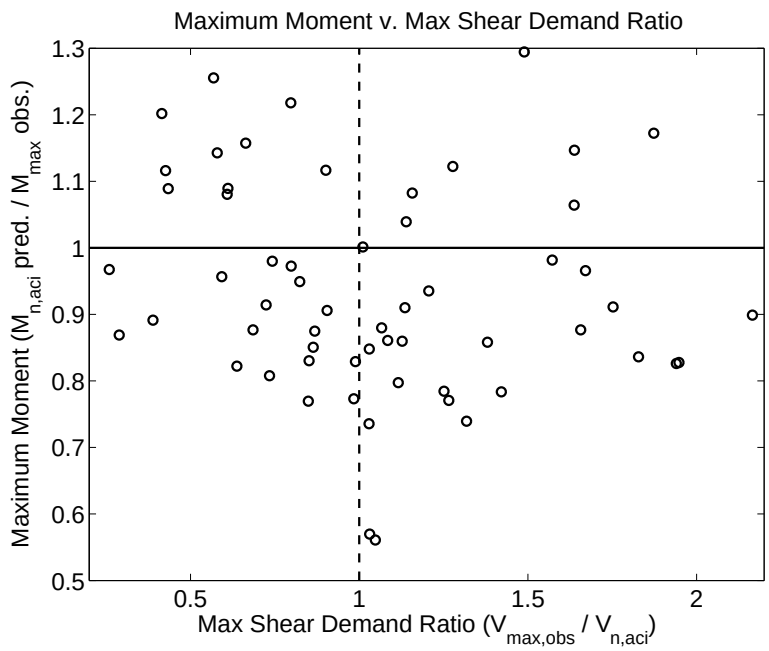

Figure 4.14: Maximum Moment Prediction Ratio v. Maximum Shear Demand Ratio

4.4.3 Summary

Below is a list of the more significant findings resulting from the examination of the strength capacity predictions using the beam-column element formulations.

- A trend related to shear demand-capacity ratio was not observable in the results.
- No negative impact on strength capacity was observed in walls whose loading exceeded the ACI 318 (2002) shear stress limit of $10\sqrt{f'_c}$.
- For walls with an applied axial load, the measured strength exceeds the predicted

nominal strength in 88% of the cases, indicating a better ability to predict the flexural response of actual walls (since they indeed will have an axial load).

- For slender walls (aspect ratio of 2.5 or more), the actual strength exceeds the nominal strength.

4.5 Initial Stiffness and Yield Displacement Capacity

4.5.1 Comparison of Experimental and Predicted Results

The individual yield displacement and secant stiffness predictions for the sixty experimental walls are shown in Tables 4.3 & 4.4. BwH3 denotes the lumped-plasticity element and NLBC denotes distributed-plasticity element. The averages of the wall predictions are listed at the bottom of Table 4.4.

Appendix E includes plots that compare the lumped-plasticity and distributed-plasticity analyses for each of the beam-column analyses of the sixty experimental walls. Appendix F has scatter plots that compare the performance objective quantity prediction ratios of the lumped-plasticity analyses to the engineering design parameters discussed in Section 4.3.1. Appendix G has similar plots for the distributed-plasticity analyses.

The predicted secant stiffness up to yield is linked is directly proportionate to the predicted yield displacement with respect to the predicted yield strength. Provided that the yield strength prediction is reasonably accurate, it would be redundant to discuss both the secant stiffness up to yield and the yield displacement. The results discussed in Section 4.4 suggest that this is the case. The secant stiffness and yield displacement results confirm this. Therefore, the displacement predictions up to yield are only discussed in terms of the secant stiffness in the remainder of this section.

Table 4.3: Predicted Secant Stiffness and Yield Displacement Results Using Two Beam-Column Element Formulations

Objective	*Secant Stiffness, k_{sec} (k/in)*			*Yield Displacement, Δ_y (in)*		
Element		*NLBC*	*BwH3*		*NLBC*	*BwH3*
Name	*Obs.*	*Pred./Obs.*	*Pred./Obs.*	*Obs.*	*Pred./Obs.*	*Pred./Obs.*
Lefas SW30						
Lefas SW31						
Lefas SW32						
Lefas SW33						
Lefas SW11	270.6	3.30	2.54	0.14	0.27	0.35
Lefas SW12	413.8	3.14	2.13	0.11	0.33	0.48
Lefas SW13	374.0	3.40	2.25	0.15	0.27	0.41
Lefas SW14	249.1	3.38	2.61	0.15	0.26	0.33
Lefas SW15	415.3	2.69	1.88	0.11	0.34	0.49
Lefas SW16	617.2	2.50	1.59	0.10	0.39	0.62
Lefas SW17	212.5	4.10	3.16	0.15	0.25	0.33
Lefas SW21	78.7	1.48	1.86	0.23	0.56	0.44
Lefas SW22	128.0	1.31	1.43	0.19	0.64	0.58
Lefas SW23	131.9	1.44	1.46	0.20	0.63	0.62
Lefas SW24	73.4	1.64	2.07	0.25	0.51	0.41
Lefas SW25	126.6	1.42	1.46	0.23	0.56	0.55
Lefas SW26	70.5	1.54	1.91	0.22	0.61	0.49
Oesterle B1	90.2	1.08	1.66	0.50	0.76	0.49
Oesterle B2	135.6	2.02	2.90	0.90	0.42	0.29
Oesterle B3	92.0	1.06	1.63	0.50	0.75	0.48
Oesterle B4	92.0	1.05	1.62	0.50	0.77	0.50
Oesterle B5	138.9	1.94	2.76	0.90	0.46	0.32
Oesterle R1	50.0	0.74	1.12	0.45	0.99	0.65
Oesterle R2						
Oesterle B6	147.0	2.04	2.54	1.00	0.47	0.37
Oesterle B7	170.0	2.29	2.80	1.00	0.41	0.33
Oesterle B8	166.0	2.28	2.77	1.00	0.41	0.34
Oesterle B9	192.5	2.01	2.44	1.20	0.32	0.27
Oesterle B10	157.3	1.96	2.23	1.10	0.32	0.28
Pilakoutas SW4	78.6	2.24	2.62	0.24	0.47	0.40
Pilakoutas SW5						
Pilakoutas SW6	71.4	2.49	2.91	0.24	0.46	0.40
Pilakoutas SW7	76.0	2.71	2.95	0.31	0.39	0.36
Pilakoutas SW8	76.2	2.46	2.89	0.24	0.49	0.42
Pilakoutas SW9	75.4	2.42	2.82	0.24	0.50	0.43
Salonikios LSW1						
Salonikios LSW2						
Salonikios LSW3						

Table 4.4: Predicted Secant Stiffness and Yield Displacement Results Using Two Beam-Column Element Formulations (cont.)

Objective	*Secant Stiffness, k_{sec} (k/in)*			*Yield Displacement, Δ_y (in)*		
Element		*NLBC*	*BwH3*		*NLBC*	*BwH3*
Name	*Obs.*	*Pred./Obs.*	*Pred./Obs.*	*Obs.*	*Pred./Obs.*	*Pred./Obs.*
Salonikios MSW1						
Salonikios MSW2						
Salonikios MSW3						
Salonikios MSW6						
Sittipunt W1						
Sittipunt W2						
Tasnimi SHW1						
Tasnimi SHW2						
Tasnimi SHW3						
Tasnimi SHW4						
Thomsen RW1	27.8	2.18	2.88	1.08	0.39	0.29
Thomsen RW2	27.8	2.02	2.80	1.08	0.38	0.27
Vallenas SW3	285.1	3.38	3.05	0.71	0.24	0.26
Vallenas SW4	285.8	3.37	3.04	0.71	0.24	0.26
Vallenas SW5	337.7	2.21	1.93	0.47	0.37	0.43
Vallenas SW6	312.1	2.40	2.09	0.53	0.33	0.38
Wang SW1	272.9	1.54	1.64	0.70	0.38	0.35
Wang SW2	288.6	1.47	1.57	0.70	0.37	0.35
Yanez S1						
Zhang SW7	166.6	1.74	1.74	0.23	0.57	0.57
Zhang SW8	195.4	1.36	1.21	0.22	0.66	0.74
Zhang SW9	174.2	2.50	2.47	0.33	0.41	0.41
Average	–	2.16	2.24	–	0.46	0.42
St. Dev.	–	0.78	0.59	–	0.17	0.12
COV	–	0.36	0.27	–	0.37	0.28

4.5.2 Influence of Wall Parameters

Normalized Thickness: The effect of normalized thickness is investigated to determine if the test specimen scale affects the prediction results, as discussed in Section 4.3.1. Figures 4.15 & 4.16 demonstrate that their is not correlation between scale and secant stiffness prediction.

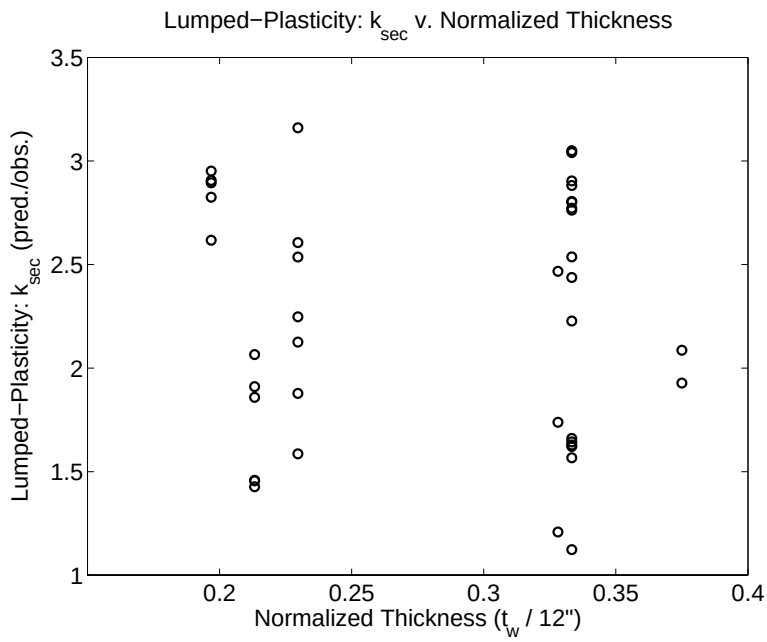

Figure 4.15: Lumped-Plasticity Secant Stiffness Up To Yield v. Normalized Thickness

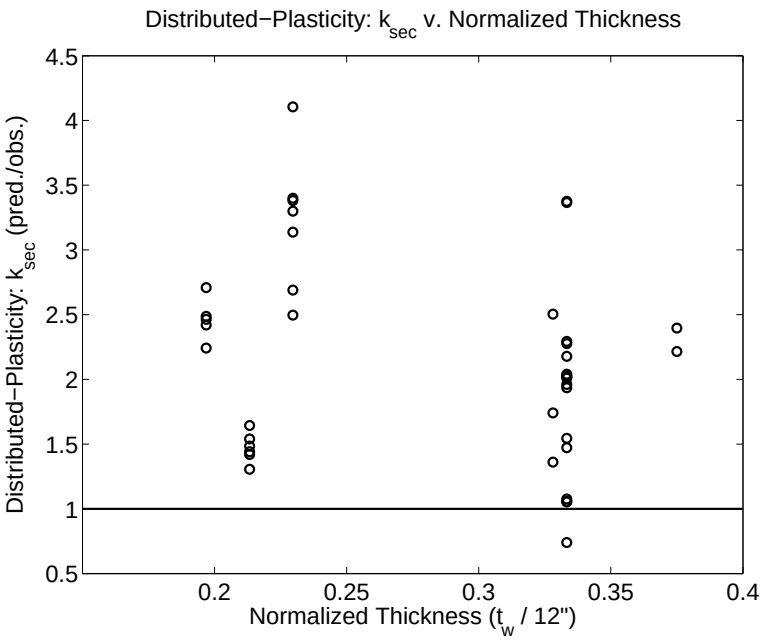

Figure 4.16: Distributed-Plasticity Secant Stiffness Up To Yield v. Normalized Thickness

Aspect ratio: Walls with higher aspect ratios were expected to exhibit more influence of shear behavior that would be overlooked by the beam-column formulations causing the secant stiffness predictions to be over-predicted for walls with lower aspect ratios. The lumped-plasticity analyses did not demonstrate such a trend, as shown in Figure 4.17. However, Figure 4.18, shows that the distributed-plasticity formulation did exhibit the anticipated trend.

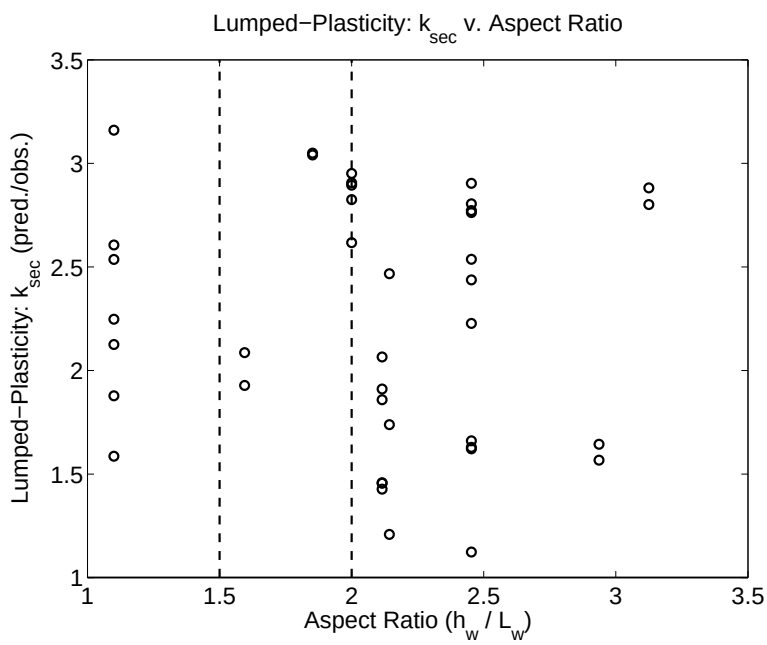

Figure 4.17: Lumped-Plasticity Secant Stiffness Up To Yield v. Aspect Ratio

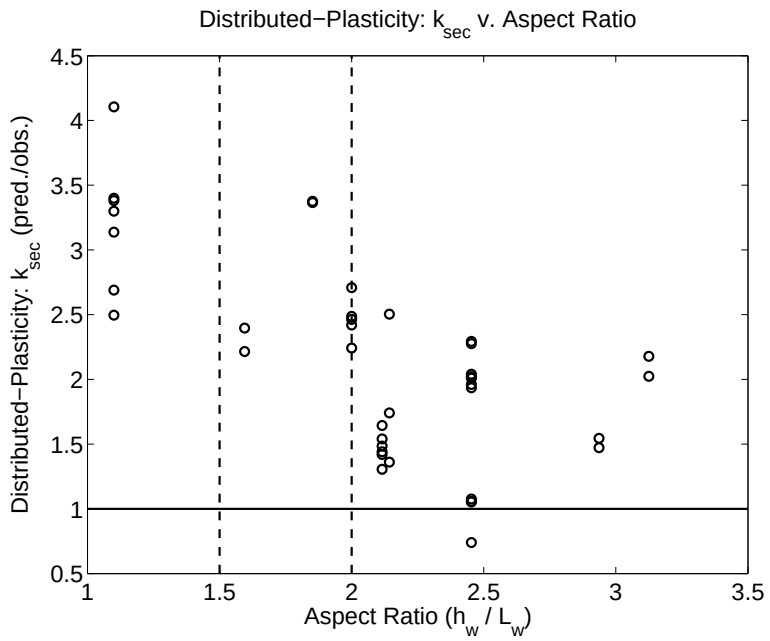

Figure 4.18: Distributed-Plasticity Secant Stiffness Up To Yield v. Aspect Ratio

Axial load ratio: The presence of axial load in the experimental walls was not anticipated to have a significant impact on the prediction of initial stiffness. Accordingly, Figures 4.19 &4.20 demonstrate that no strong correlation between secant stiffness up to yield and axial load was exhibited.

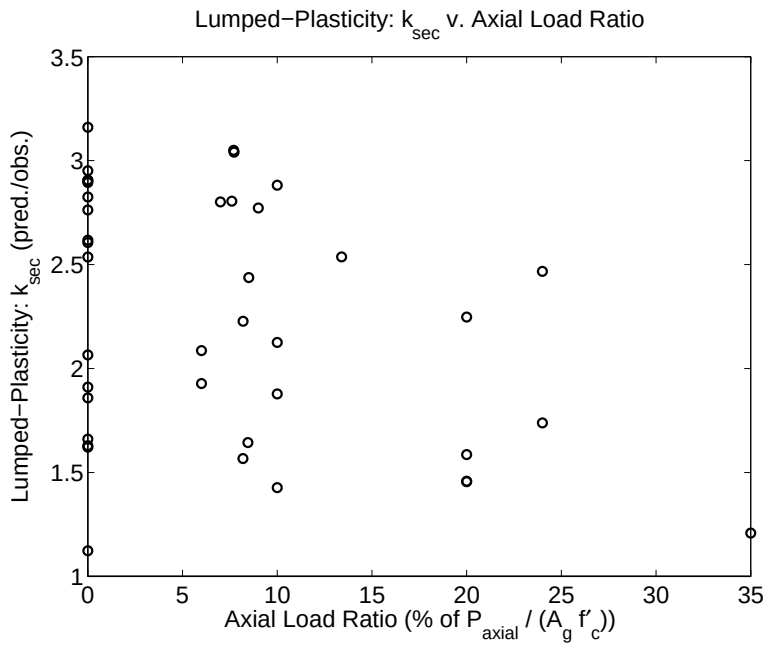

Figure 4.19: Lumped-Plasticity Secant Stiffness Up To Yield v. Axial Load Ratio

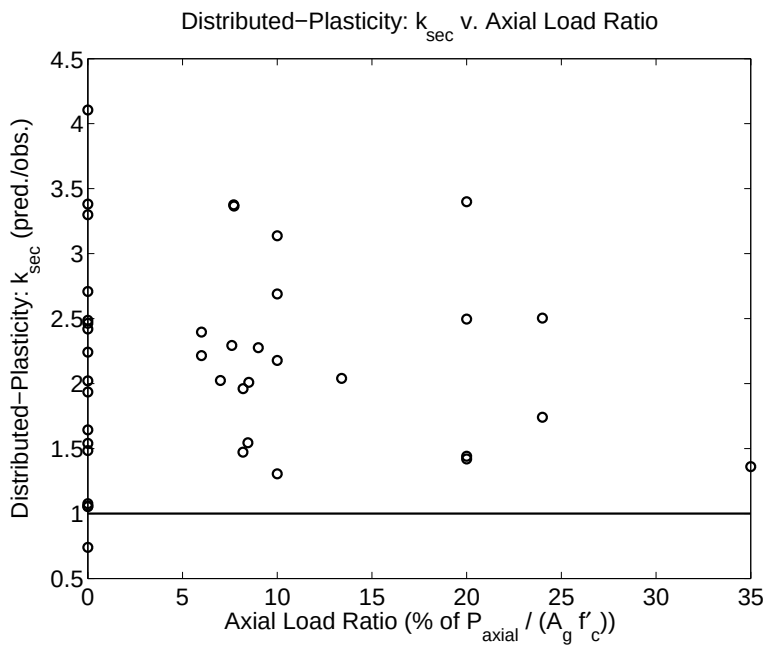

Figure 4.20: Distributed-Plasticity Secant Stiffness Up To Yield v. Axial Load Ratio

Horizontal reinforcement ratio: Horizontal reinforcement does not affect wall behavior until after the onset of diagonal cracking. Walls will not typically experience significant diagonal cracking prior to flexural yielding. Therefore, the horizontal reinforcement ratio was not expected to have an impact on the secant stiffness prediction. No trend was exhibited in the results. See Figures 4.21 & 4.22.

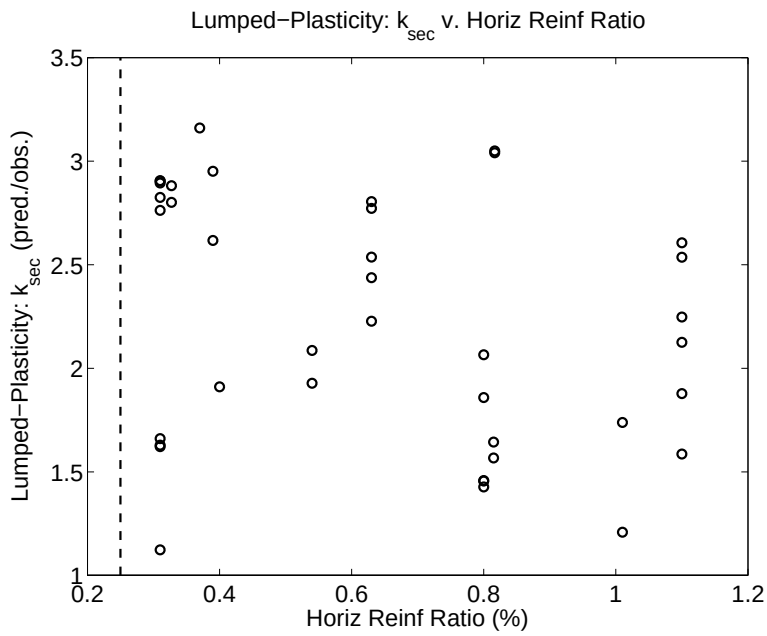

Figure 4.21: Lumped-Plasticity Secant Stiffness Up To Yield v. Horizontal Reinforcement Ratio

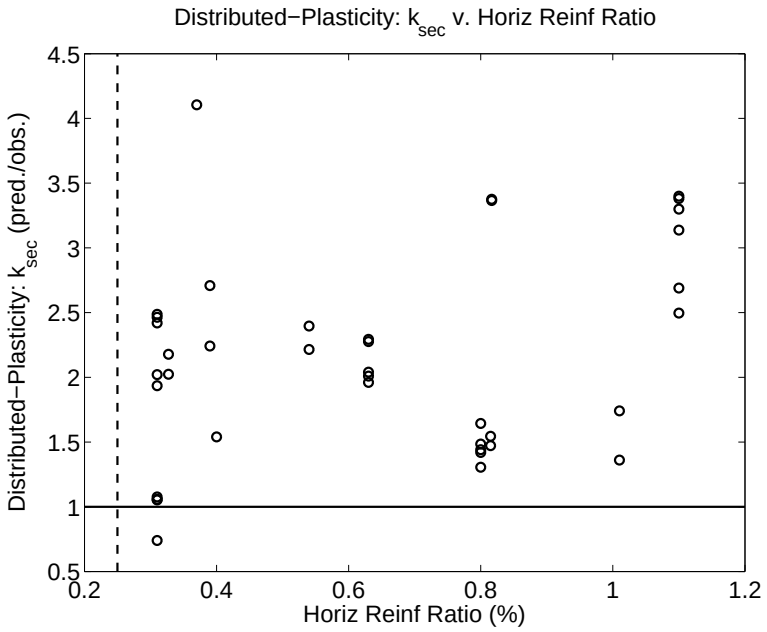

Figure 4.22: Distributed-Plasticity Secant Stiffness Up To Yield v. Horizontal Reinforcement Ratio

Longitudinal reinforcement ratio: The longitudinal reinforcement ratio was not anticipated to have an effect on the prediction of secant stiffness. The analytical results confirm this prediction. See Figures 4.23 & 4.24.

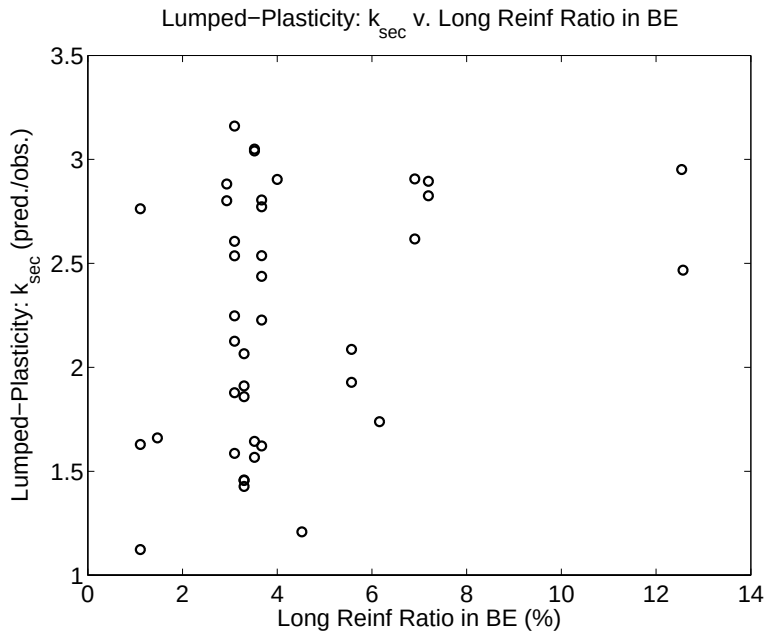

Figure 4.23: Lumped-Plasticity Secant Stiffness Up To Yield v. Longitudinal Reinforcement Ratio in the Boundary Element

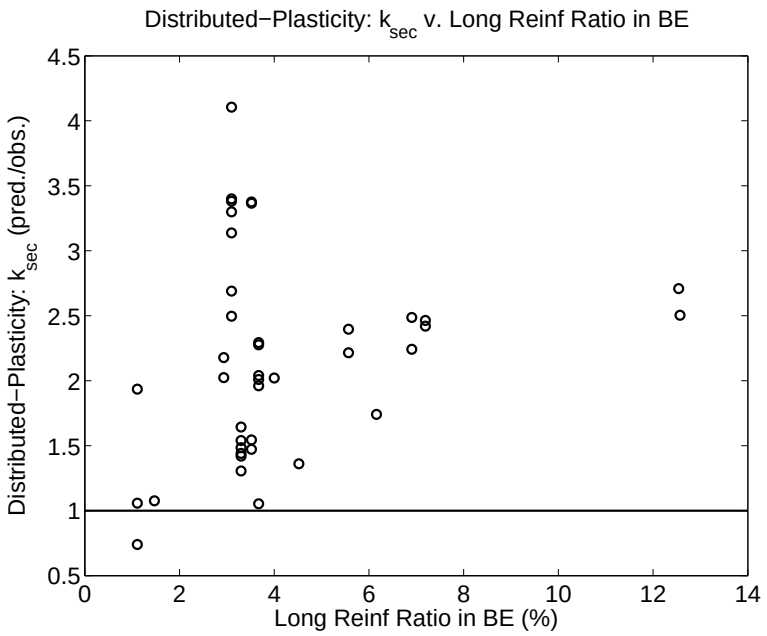

Figure 4.24: Distributed-Plasticity Secant Stiffness Up To Yield v. Longitudinal Reinforcement Ratio in the Boundary Element

Shear stress ratio at yield: It was anticipated that as the shear stress ratio at yield increased, the effect of shear on secant stiffness would increase. Therefore, the beam-column formulations would over-predict secant stiffness as the shear stress ratio increased. The lumped-plasticity formulation did not exhibit a trend between the two parameters, as seen in Figure 4.25, and the distributed-plasticity formulation did exhibit the anticipated trend in prediction (see Figure 4.26).

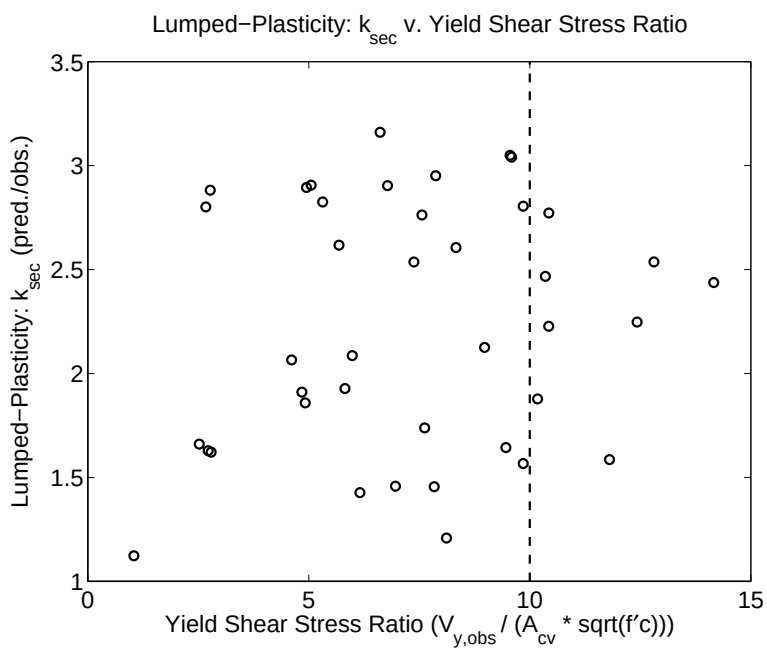

Figure 4.25: Lumped-Plasticity Secant Stiffness Up To Yield v. Shear Stress Ratio at Yield

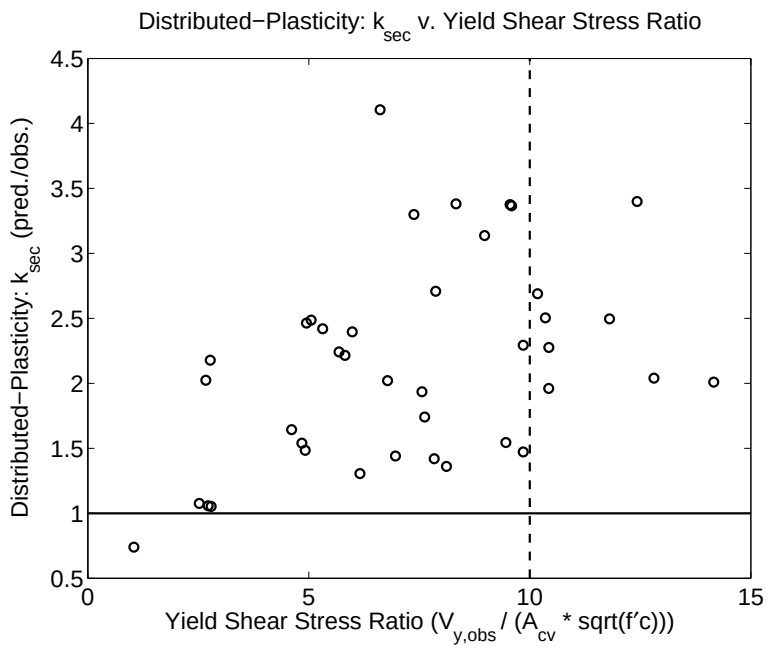

Figure 4.26: Distributed-Plasticity Secant Stiffness Up To Yield v. Shear Stress Ratio at Yield

Shear demand ratio at yield: It was expected that as the shear demand-capacity ratio increased, the beam-column element formulations would increasingly over-predict the secant stiffness up to yield. Both element formulations did indeed exhibit this prediction response, as shown in Figures 4.27 & 4.28.

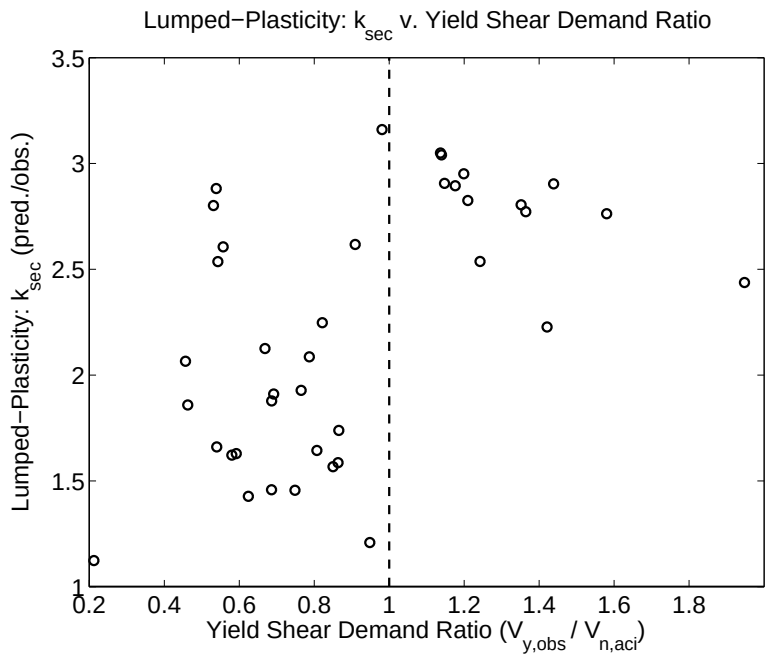

Figure 4.27: Lumped-Plasticity Secant Stiffness Up To Yield v. Shear Demand Ratio at Yield

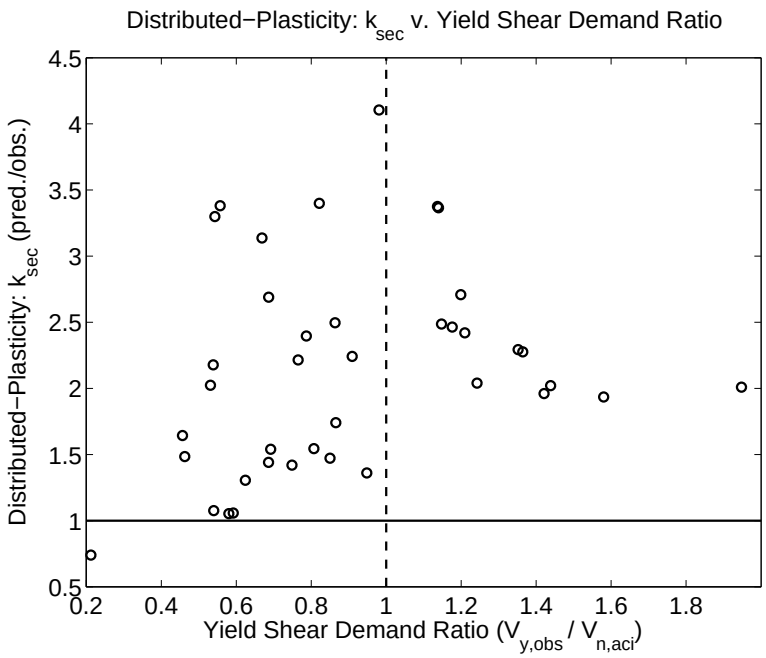

Figure 4.28: Distributed-Plasticity Secant Stiffness Up To Yield v. Shear Demand Ratio at Yield

4.5.3 Summary

In the examination of the displacement predictions at yield, using both the lumped-plasticity and distributed-plasticity formulations, a systemic over-prediction of secant stiffness was observed. The average prediction by the lumped-plasticity method was better than that of the distributed-plasticity method. However, the lumped-plasticity results exhibited fewer discernable trends with respect to the design parameters investigated than the distributed-plasticity method.

4.6 Maximum Displacement Capacity

4.6.1 Comparison of Experimental and Predicted Results

The individual maximum displacement predictions for the sixty experimental walls are shown in Tables 4.5 & 4.6. BwH3 denotes the lumped-plasticity element and NLBC denotes distributed-plasticity element. The averages of the wall predictions are listed at the bottom of Table 4.6.

Appendix E includes plots that compare the lumped-plasticity and distributed-plasticity analyses for each of the beam-column analyses of the sixty experimental walls. Appendix F has scatter plots that compare the performance objective quantity prediction ratios of the lumped-plasticity analyses to the engineering design parameters discussed in Section 4.3.1. Appendix G has similar plots for the distributed-plasticity analyses.

Table 4.5: Predicted Maximum Displacement Results Using Two Beam-Column Element Formulations

Objective	*Maximum Displacement, Δ_{max} (in)*		
Element		*NLBC*	*BwH3*
Name	*Obs.*	*Pred./Obs.*	*Pred./Obs.*
Lefas SW30	0.82	0.48	1.26
Lefas SW31	0.87	0.46	1.21
Lefas SW32	0.96	0.42	1.19
Lefas SW33	0.98	0.41	1.13
Lefas SW11	0.32	0.46	2.60
Lefas SW12	0.35	0.28	1.57
Lefas SW13	0.35	0.23	1.10
Lefas SW14	0.44	0.30	1.57
Lefas SW15	0.32	0.31	1.64
Lefas SW16	0.23	0.31	1.56
Lefas SW17	0.42	0.33	1.83
Lefas SW21	0.81	0.49	1.26
Lefas SW22	0.60	0.48	1.23
Lefas SW23	0.52	0.44	1.11
Lefas SW24	0.71	0.56	1.47
Lefas SW25	0.37	0.62	1.58
Lefas SW26	0.82	0.46	1.14
Oesterle B1	6.00	0.84	
Oesterle B2	5.00	0.48	
Oesterle B3	8.00	0.67	
Oesterle B4	13.00	0.38	
Oesterle B5	5.00	1.03	
Oesterle R1	9.00	0.50	
Oesterle R2	6.00	0.79	
Oesterle B6	3.00	0.99	2.33
Oesterle B7	6.00	0.76	
Oesterle B8	6.00	0.77	
Oesterle B9	5.30	0.91	
Oesterle B10	5.75	0.64	
Pilakoutas SW4	0.94	0.57	1.90
Pilakoutas SW5	1.02	0.31	0.93
Pilakoutas SW6	0.94	0.29	0.79
Pilakoutas SW7	0.87	0.58	2.15
Pilakoutas SW8	1.02	0.36	1.02
Pilakoutas SW9	1.02	0.37	1.03
Salonikios LSW1	1.26	0.30	
Salonikios LSW2	1.26	0.31	
Salonikios LSW3	1.26	0.26	

Table 4.6: Predicted Maximum Displacement Results Using Two Beam-Column Element Formulations (cont.)

Objective	*Maximum Displacement,* Δ_{max} *(in)*		
Element		*NLBC*	*BwH3*
Name	*Obs.*	*Pred./Obs.*	*Pred./Obs.*
Salonikios MSW1	1.26	0.66	
Salonikios MSW2	1.26	0.66	
Salonikios MSW3	1.26	0.54	
Salonikios MSW6	1.26	0.64	
Sittipunt W1	1.77	0.57	
Sittipunt W2	1.34	0.69	
Tasnimi SHW1	0.67	1.61	3.23
Tasnimi SHW2	0.45	2.38	4.77
Tasnimi SHW3	0.61	1.76	3.54
Tasnimi SHW4	0.75	1.50	2.89
Thomsen RW1	3.60	0.60	1.42
Thomsen RW2	3.60	0.87	
Vallenas SW3	6.65	0.28	
Vallenas SW4	3.58	0.50	
Vallenas SW5	3.18	0.45	
Vallenas SW6	1.98	0.73	
Wang SW1	4.25	0.15	0.48
Wang SW2	2.90	0.23	0.73
Yanez S1	2.76	0.24	
Zhang SW7	1.23	0.28	0.77
Zhang SW8	0.94	0.19	0.46
Zhang SW9	1.24	0.25	0.75
Average	–	0.58	1.58
St. Dev.	–	0.40	0.93
COV	–	0.69	0.59

4.6.2 Influence of Wall Parameters

Normalized Thickness: The effect of normalized thickness is investigated to determine if the test specimen scale affects the prediction results, as discussed in Section 4.3.1. For both the lumped-plasticity and distributed-plasticity methods, one set of four significantly smaller scale walls exhibited a more dramatic over-prediction of the maximum displacement (see Figures 4.29 & 4.30. In the case of the distributed-plasticity analyses, these are the only walls that exhibited a significant over-prediction of maximum displacement. These walls will be negated in the remainder of the discussion of this section.

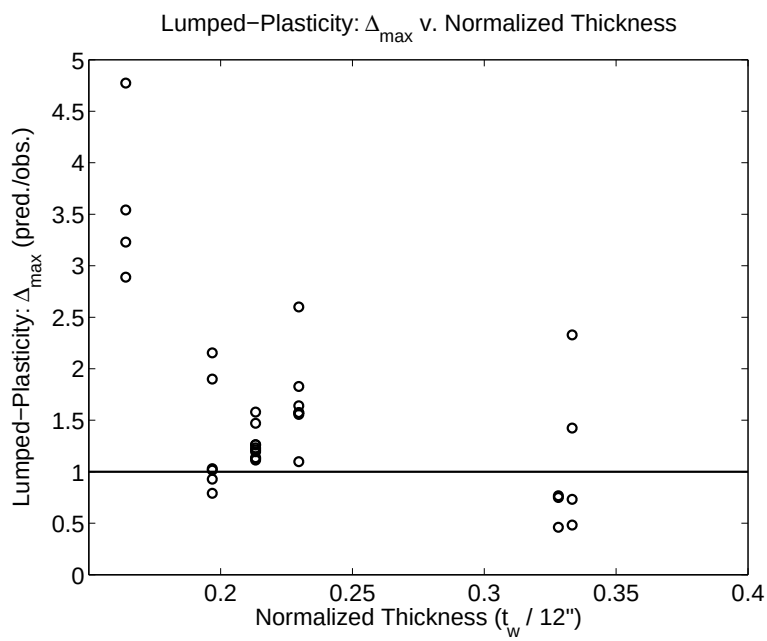

Figure 4.29: Lumped-Plasticity Maximum Displacement Prediction Ratio v. Normalized Thickness

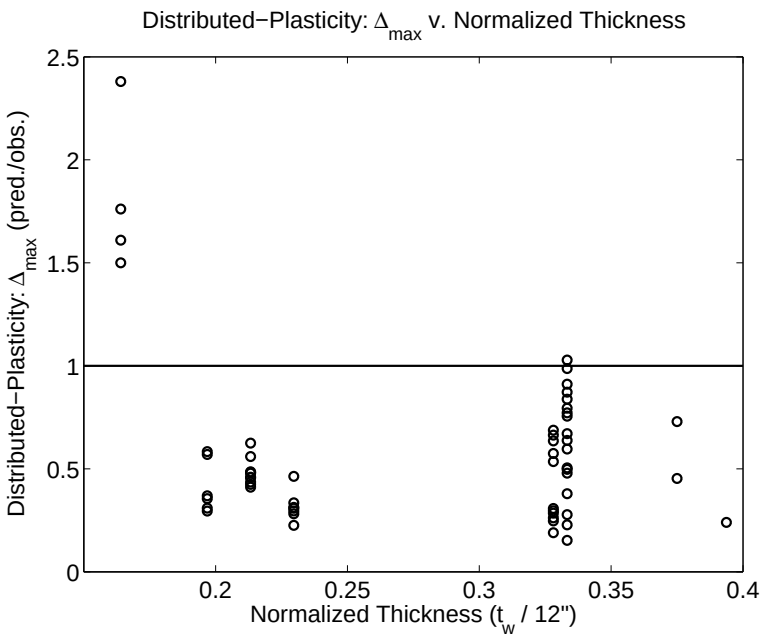

Figure 4.30: Distributed-Plasticity Maximum Displacement Prediction Ratio v. Normalized Thickness

Aspect ratio: Lower values of aspect ratio were expected to cause under-prediction of the maximum displacement, because shear deformations were not considered by the beam-column element formulations. However, no strong correlation was demonstrated in either formulation (see Figures 4.31 & 4.32).

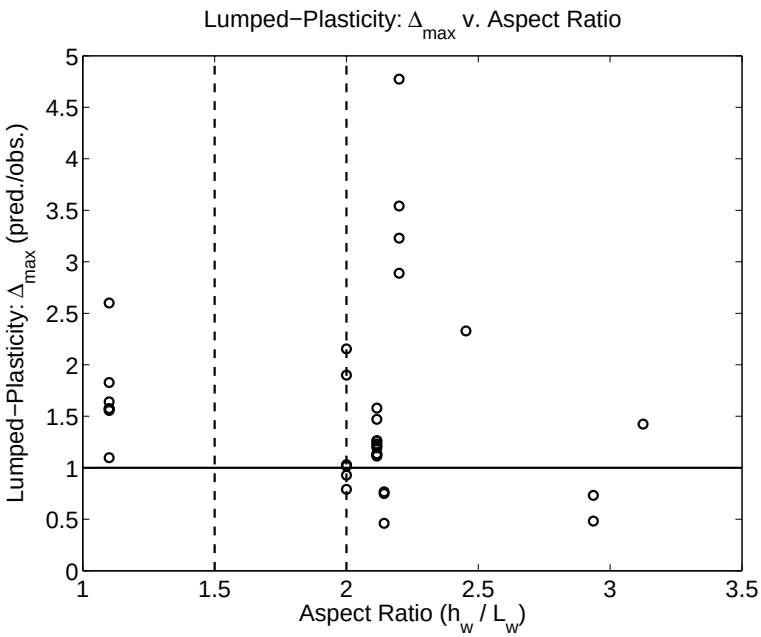

Figure 4.31: Lumped-Plasticity Maximum Displacement Prediction Ratio v. Aspect Ratio

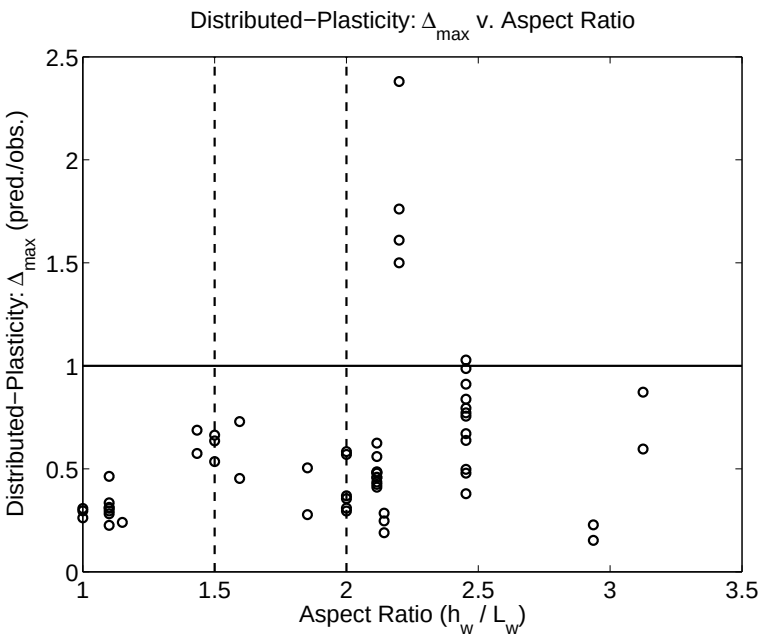

Figure 4.32: Distributed-Plasticity Maximum Displacement Prediction Ratio v. Aspect Ratio

Axial load ratio: The presence of axial load is expected to increase the maximum displacement capacity of walls. However, no prediction was made regarding the effect it would have on the ability to predict the maximum displacement. With the lumped-plasticity formulation, the walls' maximum displacements were better predicted when axial load was present, as demonstrated in Figure 4.33. No trend was evident in the results using the distributed-plasticity formulation (Figure 4.34).

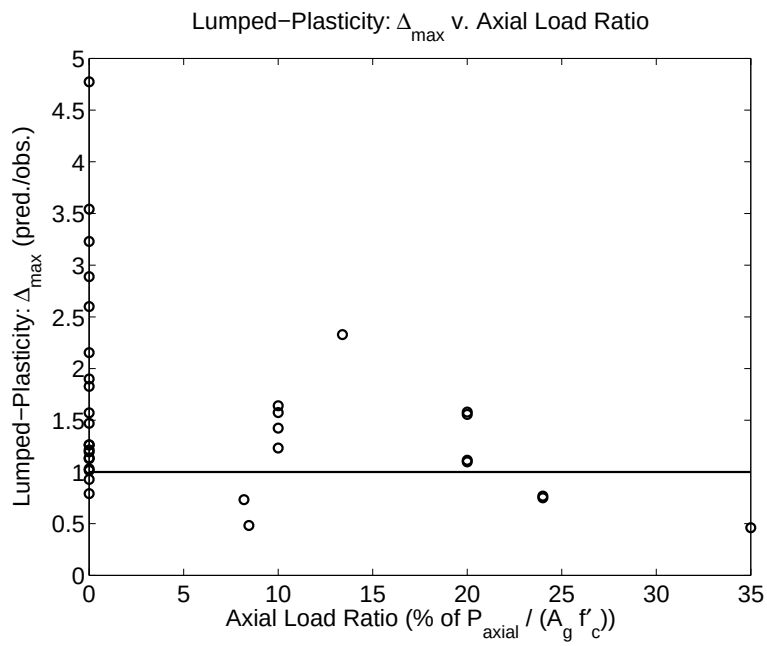

Figure 4.33: Lumped-Plasticity Maximum Displacement Prediction Ratio v. Axial Load Ratio

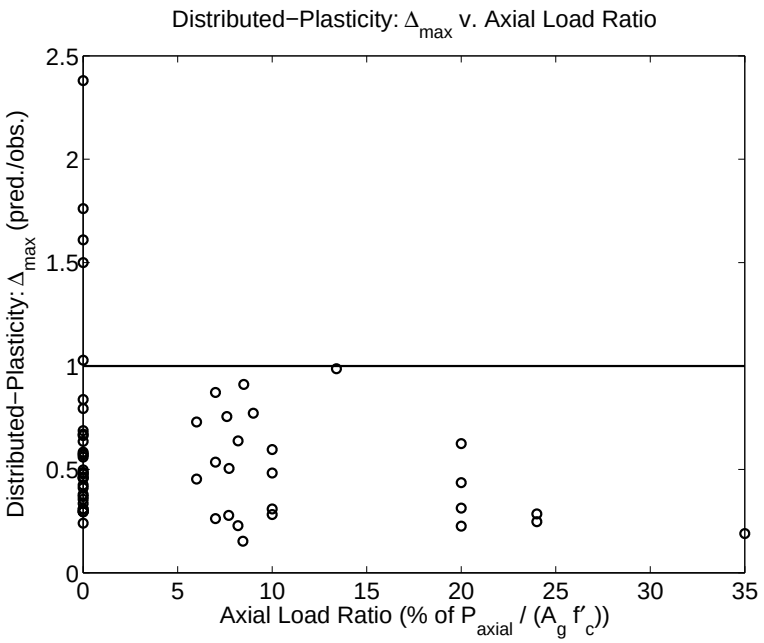

Figure 4.34: Distributed-Plasticity Maximum Displacement Prediction Ratio v. Axial Load Ratio

Horizontal reinforcement ratio: The effect of horizontal reinforcement ratio on the prediction of maximum displacement was not known prior the analyses. Neither analysis method exhibited much correlation between the maximum displacement prediction ratio and the horizontal reinforcement ratio, as shown in Figures 4.35 & 4.36.

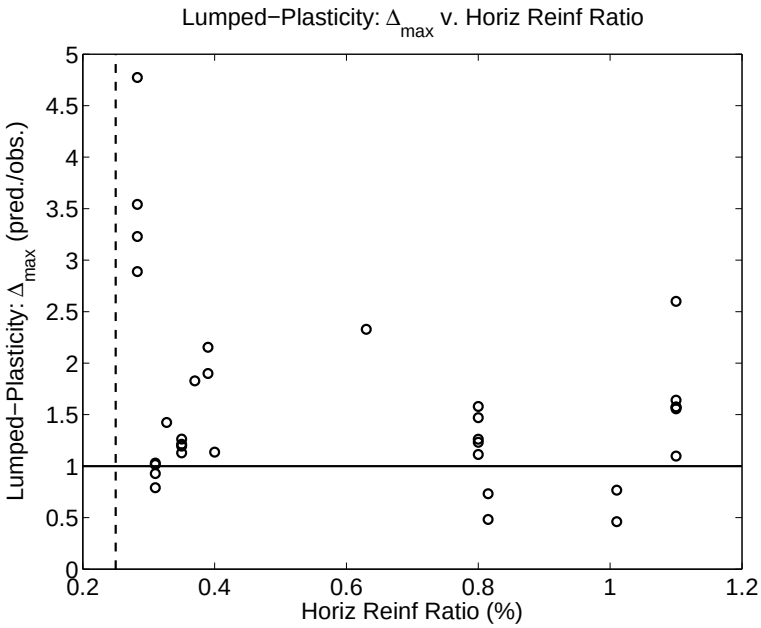

Figure 4.35: Lumped-Plasticity Maximum Displacement Prediction Ratio v. Horizontal Reinforcement Ratio

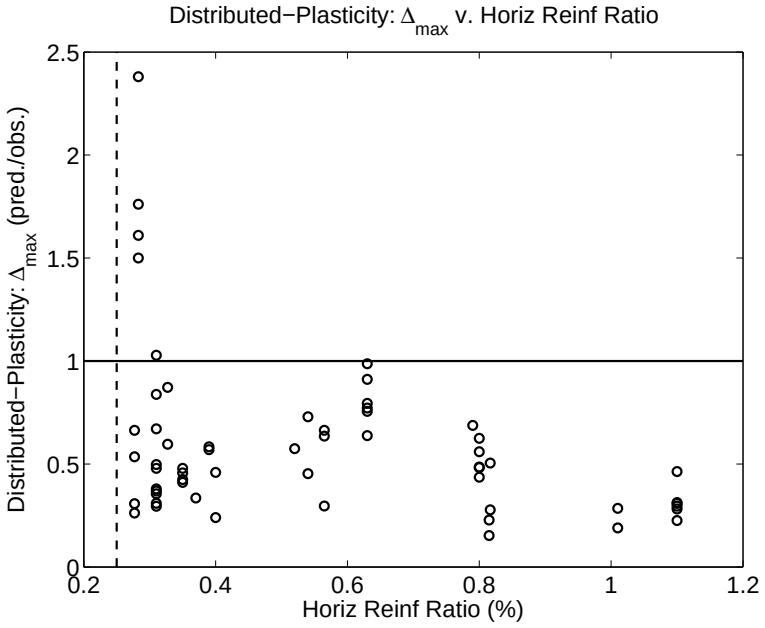

Figure 4.36: Distributed-Plasticity Maximum Displacement Prediction Ratio v. Horizontal Reinforcement Ratio

Longitudinal reinforcement ratio: The effect of longitudinal reinforcement ratio on the prediction of maximum displacement was not known prior the analyses. Neither analysis method exhibited much correlation between the maximum displacement prediction ratio and the longitudinal reinforcement ratio, as shown in Figures 4.37 & 4.38.

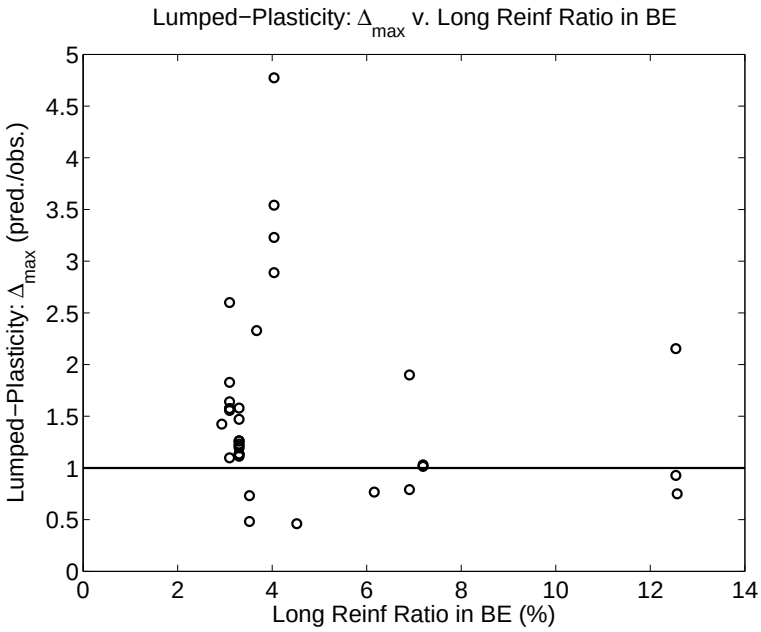

Figure 4.37: Lumped-Plasticity Maximum Displacement Prediction Ratio v. Longitudinal Reinforcement Ratio in the Boundary Element

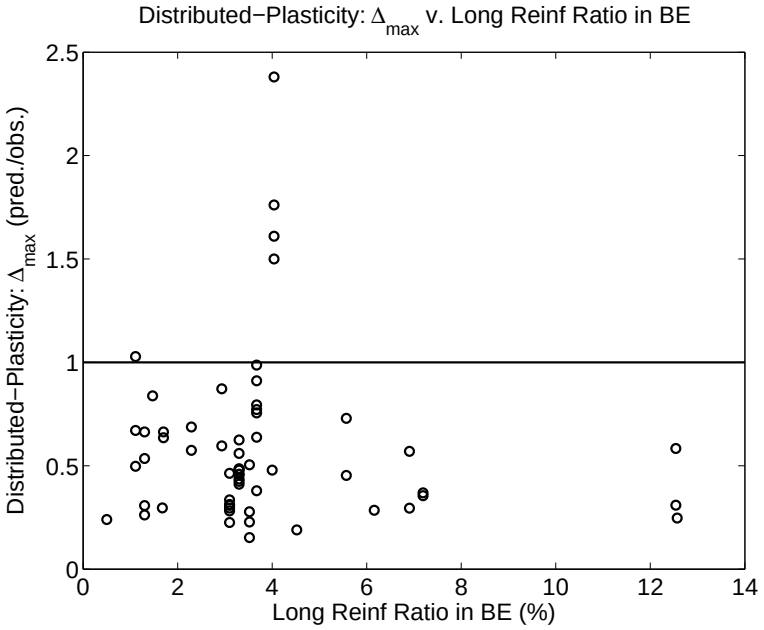

Figure 4.38: Distributed-Plasticity Maximum Displacement Prediction Ratio v. Longitudinal Reinforcement Ratio in the Boundary Element

Maximum shear stress ratio: On one hand, a higher maximum shear stress ratio would limit development of flexural strength capacity and decrease ductility that would not be accounted for by the beam-column element formulations. On the other, it would contribute additional shear deformations that would not be accounted for either. These two tendencies seemed to cancel each other out in the ability to predict the maximum displacement of the experimental walls using both methods. Figures 4.39 & 4.40 do not demonstrated a relationship between maximum displacement prediction and maximum shear stress ratio.

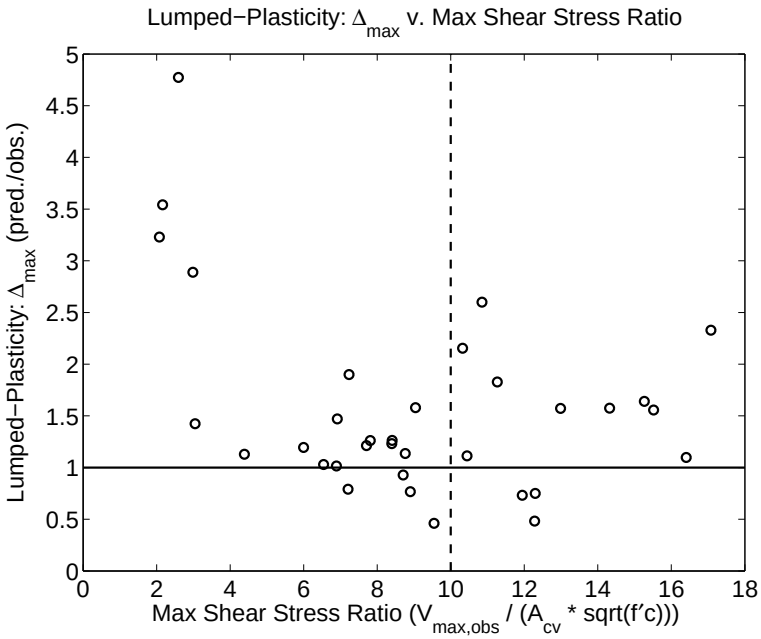

Figure 4.39: Lumped-Plasticity Maximum Displacement Prediction Ratio v. Maximum Shear Stress Ratio

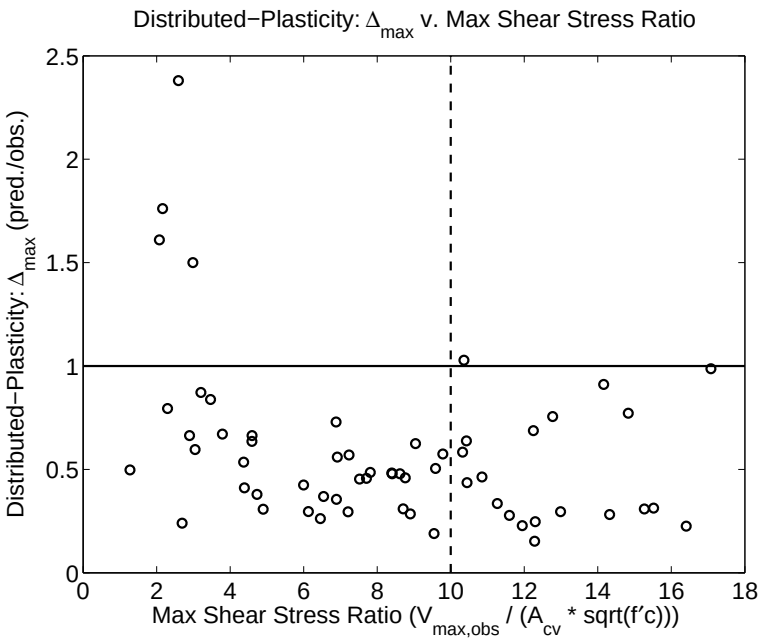

Figure 4.40: Distributed-Plasticity Maximum Displacement Prediction Ratio v. Maximum Shear Stress Ratio

Maximum shear demand-capacity ratio: Unlike the shear stress ratio, the shear demand-capacity ratio accounts for the presence of horizontal reinforcement to resist higher shear forces. Therefore, the maximum displacement prediction ratio should decrease as the shear demand-capacity ratio increases. The lumped-plasticity analyses exhibited the anticipated behavior as demonstrated in Figure 4.41. The distributed-plasticity analyses exhibited no trend (Figure 4.42).

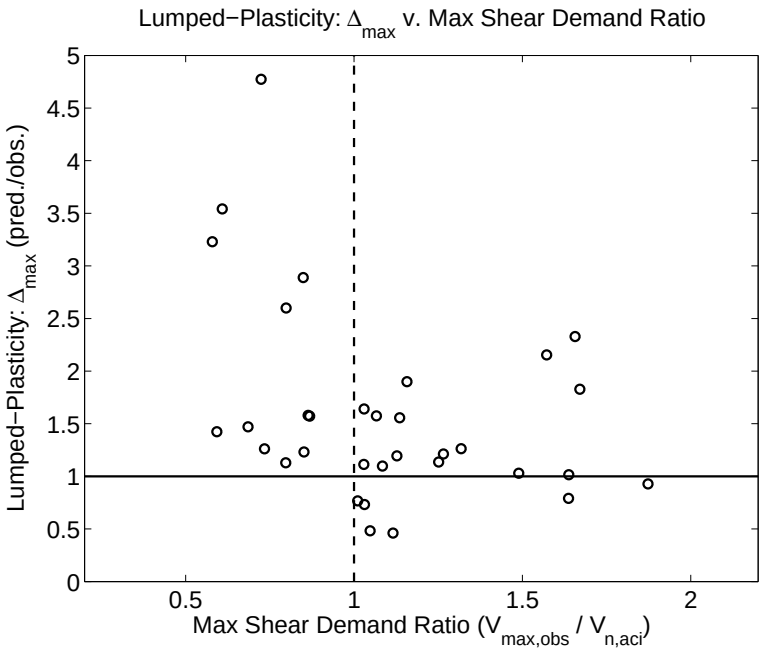

Figure 4.41: Lumped-Plasticity Maximum Displacement Prediction Ratio v. Maximum Shear Demand Ratio

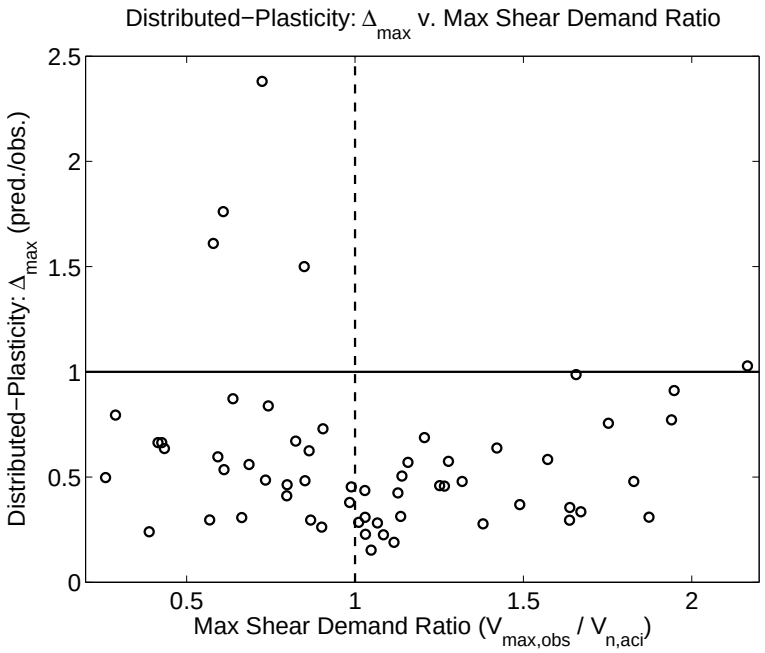

Figure 4.42: Distributed-Plasticity Maximum Displacement Prediction Ratio v. Maximum Shear Demand Ratio

4.6.3 Summary

The examination of the maximum displacement predictions of the lumped-plasticity and distributed-plasticity beam-column analyses discussed in this section provided the following insights:

- The lumped-plasticity formulation tended to over-predict maximum displacement, while the distributed-plasticity formulation tended to under-predict the maximum displacement.

- The lumped-plasticity analyses did not show a strong correlation between the ability to predict maximum displacement and aspect ratio, horizontal reinforcement ratio, longitudinal reinforcement ratio, or maximum shear stress. The expected trend between increasing over-prediction of maximum displacement with increased shear demand-capacity ratio was observed.

- The distributed-plasticity analysis maximum displacement prediction ratios did not exhibit a correlation to any of the examined design parameters.

4.7 Comparison of Lumped-Plasticity and Distributed-Plasticity Analytical Results

In this chapter, the beam-column analysis method was employed using both the lumped-plasticity and distributed-plasticity element integration schemes to predict the behavior of the sixty experimental walls' behavior. The analysis results were compared to performance objective quantities. The ratios of predicted to observed performance objectives were compared against wall design parameters to determine which wall characteristics affect the ability to predict structural wall behavior.

The ability to predict the strength of walls was found be affected by wall characteristics that would indicate a greater influence of shear effects. These characteristics include lower aspect ratios and lower horizontal reinforcement ratios.

Both element formulations investigated systemically over-predicted the secant stiffness up to yield of the wall specimens. Both formulations demonstrated that increased shear

demand-capacity ratios negatively affected the secant stiffness prediction. While the distributed-plasticity formulation showed a strong trend between secant stiffness prediction and aspect ratio, as expected, the lumped-plasticity formulations did not exhibit the same trend.

It was found that the shear stress ratio was typically not a good indicator of an analysis formulation's ability to predict wall displacements. Whereas, the shear demand-capacity ratio was.

The lumped-plasticity analyses typically over-predicted the maximum displacements of the wall specimens. Combined with the systemic under-prediction of yield displacement cause an over-estimation in displacement ductility. The distributed-plasticity element typically under-predicted the maximum displacements of the experimental walls, yet it did not exhibit any corresponding trends with any of the investigated design parameters.

Chapter 5

RESPONSE-2000

Following the beam-column analyses, further investigation of the effect of shear, shear-flexure interaction, and bar-slip at the base of the wall was warranted. Response-2000 was chosen for the next stage of analysis because it accounts for the effect of shear and shear-flexure interaction on strength and displacement using the Modified Compression Field Theory (MCFT). A further discussion of the MCFT is in Appendix A. Response-2000 also can account for the effect of bar-slip on fixed-end rotation at the base of the wall (albeit in perhaps an overly simplistic formulation).

Response-2000 is essentially a sectional analysis program, but it is capable of integrating the sectional response of a prismatic line element for a variety of loading and boundary conditions to obtain displacement response. Thus, Response-2000 serves as a pseudo-distributed-plasticity analysis method for frame members.

The three walls for further study discussed in Sections 2.1.2–2.1.2 were investigated rather than all sixty experimental walls, because of the time of manual labor required to input data, manage files, and assemble useful output. The quality of the output was investigated in terms of the response quantity objectives discussed in Sections 4.3.2 & 4.3.3, with the exception that the predicted maximum strength and displacement were simply the maximum values reported by Response-2000.

5.1 Sectional Analysis in Response-2000

The key features and analytical modeling decisions of Response-2000 are discussed here. Additional information, is available in Bentz (2000).

Finding the sectional response at any point along the length of the member is an iterative process. The three unknowns at the section are the shear strain profile, the curvature, and the strain at the top fiber of the section. Compatibility is enforced by maintaining that

plane sections remain plane (note that this ignores the constraint that strain compatibility does not permit a non-constant shear strain profile when plane sections remain plane). Equilibrium is enforced for axial and shear forces, while maintaining a user-specified shear to moment ratio. Constitutive relations are governed by the MCFT.

The model allows shear stress and strain to vary over the length of the section, despite assumption that plane sections remain plane. Therefore, a method to determine the shear stress along the length of the wall section is needed. In the general case of a prismatic beam-column member, the shear stress can be found by examining the free body diagram of a differential element. This is demonstrated in Figure 5.1 and yields the following equation:

$$\begin{aligned} F_v(y) = \quad & \int_0^y \left(f_{c,x}(x,y) - f_{c,x}(x+\Delta x, y)\right) b(y) dy \\ & + \int_0^y \left(f_{s,x}(x,y) - f_{s,x}(x+\Delta x, y)\right) A_s(y) dy \end{aligned} \tag{5.1}$$

where $b(y)$ is the width of the section at depth y, $A_s(y)$ is the area of steel at depth y, and the remainder of the variables are explained in Figure 5.1. Thus, the average shear stress, $\tau(x, y)$, is:

$$\tau(x,y) = \frac{F_v(y)}{b(y)\Delta x} \tag{5.2}$$

The closed form solution would be found for specific cases by taking the limit as $\Delta\ x \rightarrow\ 0$ of Equations 5.1 & 5.2. However, Vecchio and Collins (1988) propose a sectional analysis model that calculates this shear stress on a finite layer from longitudinal forces calculated at two sections a distance, S, apart from each other. This is depicted in Figure 5.2.

In this method, the longitudinal force at layer i is given by:

$$C_i = f_{cxi} b_i h_i + C_{si} \tag{5.3}$$

where, f_{cxi} is the x-component of stress in the concrete of layer i, b_i is the width of layer i, h_i is the height of layer i, and C_{si} is the force in the steel that runs through layer i.

Similar to Equation 5.1, the force at the top of the concrete layer is the cumulative summation of the difference of forces acting on the layers above. Using the finite layer, the force at the bottom of the layer is also needed. This is found by adding the difference of

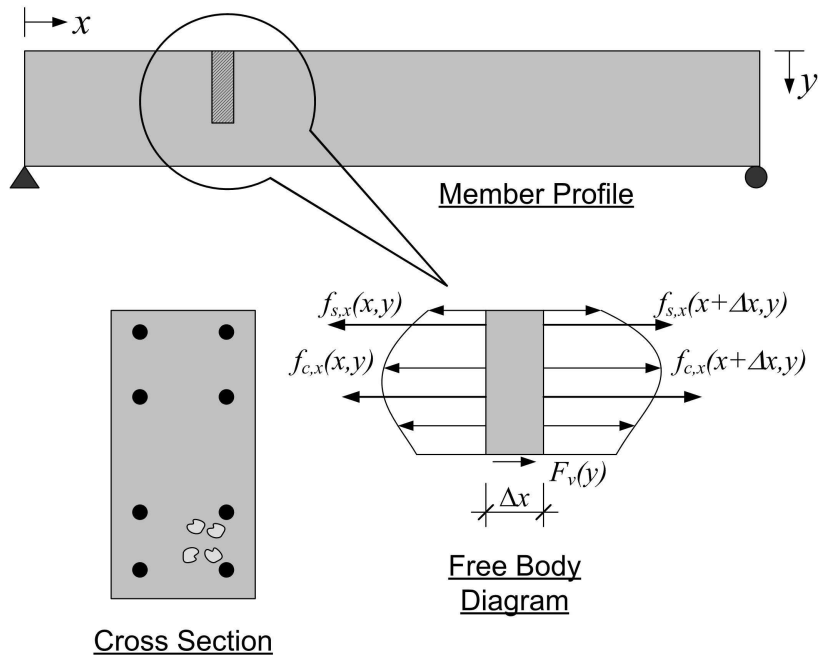

Figure 5.1: Differential Element for Determination of Shear at Cross Section

force between section 1 and 2 at the layer of interest and adding it to the shear force at the top of the layer. Therefore, the horizontal forces at the top and bottom of a layer are:

$$F_{k-1} = \sum_{i=1}^{k-1} (C_{i1} - C_{i2}) \tag{5.4}$$

$$F_k = F_{k-1} + C_{k1} - C_{k2} \tag{5.5}$$

See Figure 5.2 for definition of variables. Examining the free body diagram shown in Figure 5.2 and enforcing rotational equilibrium yields the shear force on the layer:

$$V_k = \frac{(F_k + F_{k-1})}{2} \frac{h_k}{S} \tag{5.6}$$

Thus, the shear stress on the layer is:

$$v_k = \frac{V_k}{b_k h_k} \tag{5.7}$$

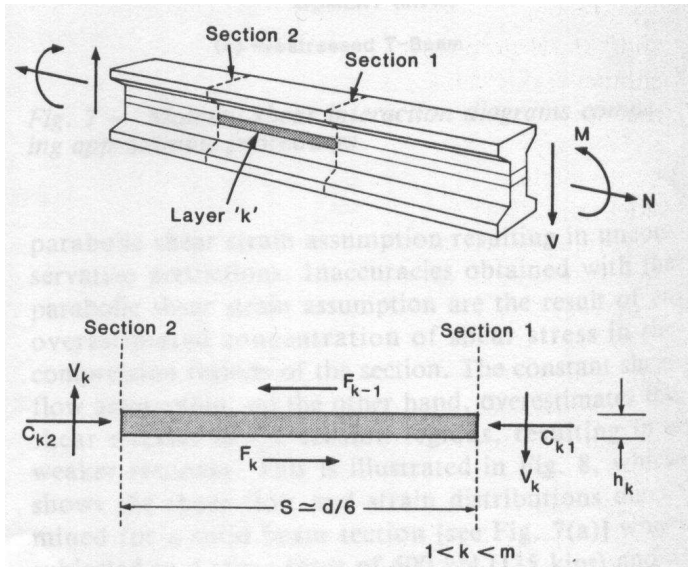

Figure 5.2: Free Body Diagram for Concrete Layer k (Vecchio and Collins 1988)

Based on this approach, Bentz (2000) formulated the Longitudinal Stiffness Method; this method is implemented in Response-2000. A great improvement over the previous method, it effectively takes the limit of the shear stress as the distance between the two sections approaches zero, while only requiring analysis at one section.

While calculating the axial response of the fibers at one section, the section stiffness is determined from the derivatives of the stress-strain relationship of the fibers. Rather than conducting a second sectional analysis, the axial response of the layers is extrapolated a distance M/V away using the calculated section stiffness. These axial load values are used to calculate the shear stress between each fiber.

The Longitudinal Stiffness Method increases the numeric stability and reduces computational effort over the previous two-section analysis method. However, this improvement comes at the expense of being able to predict response at curvatures exceeding that at which the maximum moment occurs. This is because the longitudinal stiffness method requires a positive definite stiffness matrix to project the longitudinal response a distance away from the section of interest.

Once the shear stress profile is determined, the shear strain profile can be calculated.

The shear strain profile is determined by an iterative secant stiffness method. Response-2000 loops through these methods to solve for strain fields and determine corresponding internal forces.

The sectional analysis provides a variety of output. Notable output data include the moment-curvature relationship, moment-shear interaction envelope, longitudinal stress-strain data at fiber nodes, shear stress-strain data at fiber nodes, and cracking information. While the format of the output is not particularly convenient (e.g. strain data is not provided for a given point throughout the analysis), this information can be pieced together to gain an understanding of the section's behavior under loading. Additionally, the program uses this information to determine the load-displacement behavior of a full member.

5.2 Full Member Analysis in Response-2000

Response-2000 calculates the load versus deflection behavior of a single prismatic member subjected to a variety of possible load and support conditions. However, the limitations of the longitudinal stiffness method prevent calculation of load-deformation response beyond the maximum load. Load-Deformation response is determined by the following steps.

1. The full moment-shear (M-V) interaction response is determined for the cross-section.

2. The member is divided into 20 segments (integration points).

3. The internal moment and shear at each segment is determined for each load step.

4. The resultant shear strain and curvature are determined at each segment by interpolating the data points from the moment-shear interaction diagram.

5. The displacements are calculated by the moment-area method, using the resultant shear strains and curvature values.

In performing these tasks, Response-2000 makes some additional assumptions. First, it is assumed that shear is transferred from the member to fixed supports, bearing supports, and point loads by direct compression struts. Therefore, the effect of shear is reduced in

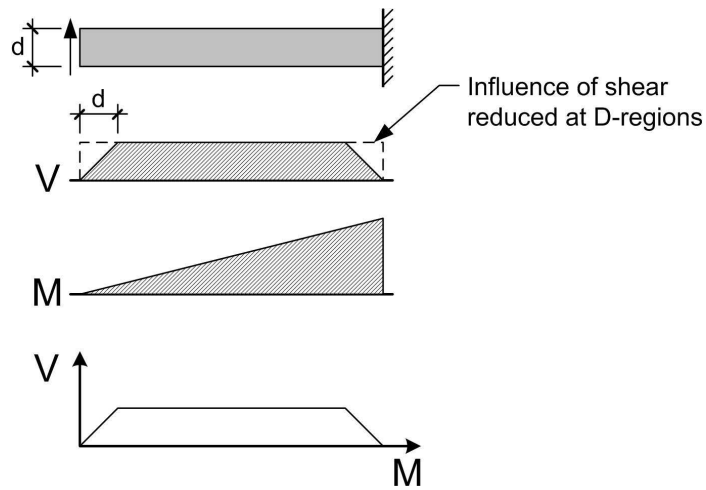

Figure 5.3: Shear and Moment in Wall Assumed by Response-2000

these locations up to a distance, d (the depth of the section), away. The internal shear force is reduced to zero at the location of the load or support and increased linearly to the calculated value d away. The internal shear and moment diagrams for a wall, as determined by Response-2000, are shown in Figure 5.3.

Additionally, Response-2000 accounts for rotation caused by bar-slip and strain penetration at fixed supports. This is implemented as an additional flexural element at the support. The curvature of the element is approximated as:

$$\phi = \frac{\epsilon_{bar}}{y_{bar}} \tag{5.8}$$

where, ϵ_{bar} is the strain in the maximum stressed bar and y_{bar} is the distance of the maximum stressed bar to the compression face of the element. This may not be an accurate approach. Rather than using the distance of the bar to the extreme compression fiber for y_{bar}, it would be more accurate to use the distance of the bar to the neutral axis to obtain the actual curvature. The length of the element is:

$$D_\phi = 0.022\sigma_m d_b \tag{5.9}$$

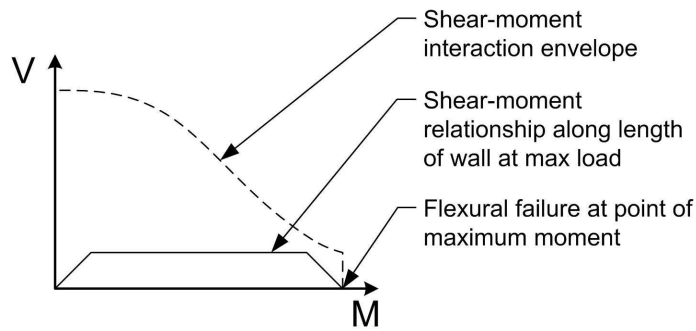

Figure 5.4: Flexural Failure in Response-2000

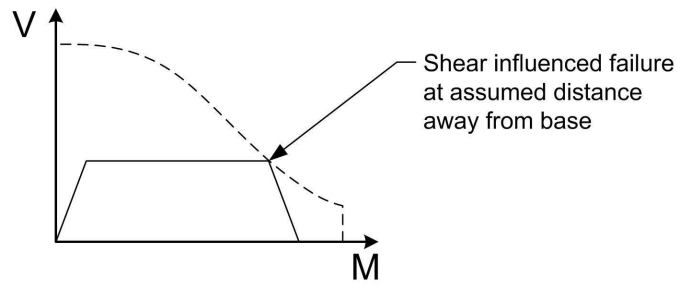

Figure 5.5: Shear Influenced Failure in Response-2000

where, σ_m is the stress in the maximum stressed steel bar, d_b is the diameter of the maximum stressed bar, and 0.022 is a default multiplier subject to change by the user to account for the effective bond stress on the bar and to account for the depth of the neutral axis when approximating the curvature.

The failure mode predicted by Response-2000 can be determined by comparing the assumed moment to shear values of the member to the M-V interaction failure envelope. If the member's curve intersects the failure envelope where moment is maximum and shear is 0, then the member failed in flexure. Otherwise, if the curves intersect anywhere else, then the member's failure is influenced by shear effects. These two cases are shown in Figures 5.4 & 5.5.

Table 5.1: Response-2000 Prediction Objectives with Default Analysis Parameters

	Oesterle B1		*Oesterle B6*		*Pilakoutas SW7*	
Objective	*Obs.*	*Pred./Obs.*	*Obs.*	*Pred./Obs.*	*Obs.*	*Pred./Obs.*
M_y, *in-k*	8298	0.962	27048	0.989	1131	1.072
Δ_y, *in*	0.50	0.951	1.00	0.859	0.31	0.791
K_{ini}, *k/in*	90.2	1.012	147.0	1.151	76.0	1.356
M_{max}, *in-k*	11408	1.046	36064	0.893	1483	0.977
Δ_{max}, *in*	6.00	0.621	3.00	0.619	0.87	0.441

5.3 Response-2000 Results

The three experimental walls were modeled in Response-2000 using measured values for material parameters where possible. Default values for the strain at the end of the elastic plateau in the reinforcing bars. One set of analyses was conducted with all default analysis parameters. A second set of analyses was conducted neglecting the effect of bond slip and strain penetration at the base of the wall.

The results of the analyses using default analysis parameters are summarized in Table 5.1. The results of the analyses neglecting the effect of bar slip are summarized in Table 5.2. Figures 5.6–5.8 show the shear stress ratio versus drift for the Response-2000 analyses using default analysis parameters and without bar slip compared to experimental results and the distributed-plasticity analyses discussed in Chapter 4.

5.4 Response-2000 Discussion

In general, the strength predictions given by Response-2000 show a marked improvement over those given by the moment-curvature analyses that neglect the effects of shear. The yield strength prediction is vastly improved for Oesterle B1 (Pred./Obs. strength is 0.96 with Response-2000 compared to 0.82). A slight improvement in yield strength prediction is demonstrated for Oesterle B6, while Pilakoutas SW7 is slightly more over-predicted.

Similarly, very good predictions of maximum strength are provided by Response-2000.

Table 5.2: Response-2000 Prediction Objectives with No Bar Slip

	Oesterle B1		*Oesterle B6*		*Pilakoutas SW7*	
Objective	*Obs.*	*Pred./Obs.*	*Obs.*	*Pred./Obs.*	*Obs.*	*Pred./Obs.*
M_y, *in-k*	8298	0.962	27048	0.989	1131	1.072
Δ_y, *in*	0.50	0.909	1.00	0.833	0.31	0.674
K_{ini}, k/in	90.2	1.059	147.0	1.188	76.0	1.590
M_{max}, *in-k*	11408	1.046	36064	0.893	1483	0.977
Δ_{max}, *in*	6.00	0.560	3.00	0.576	0.87	0.370

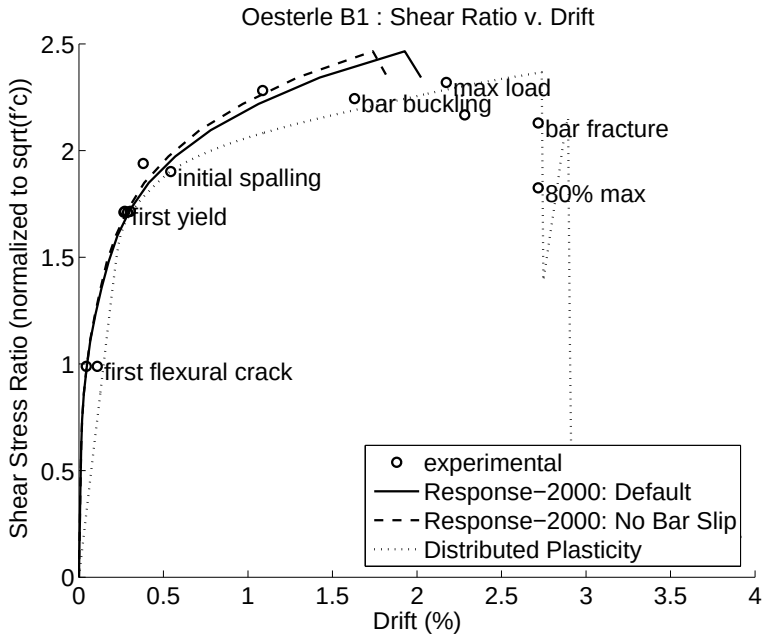

Figure 5.6: Oesterle B1 - Shear Stress Ratio v. Drift from Response-2000

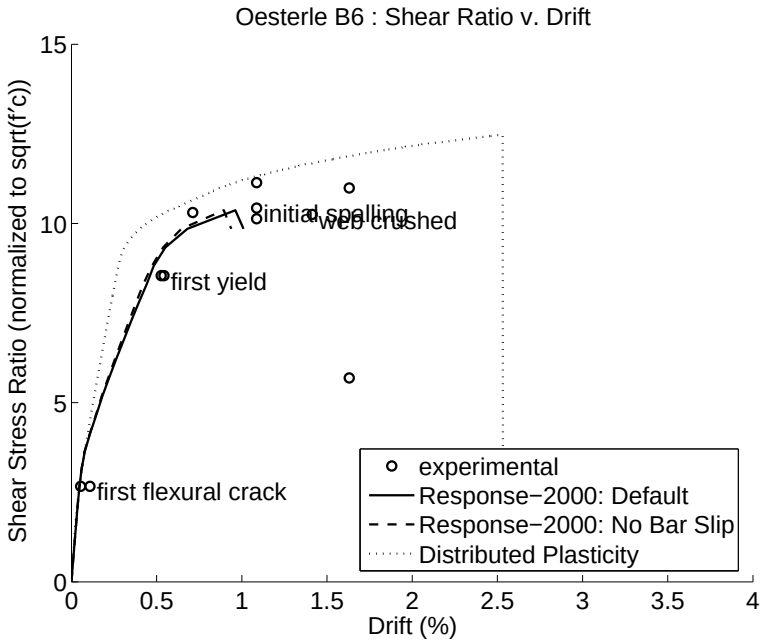

Figure 5.7: Oesterle B6 - Shear Stress Ratio v. Drift from Response-2000

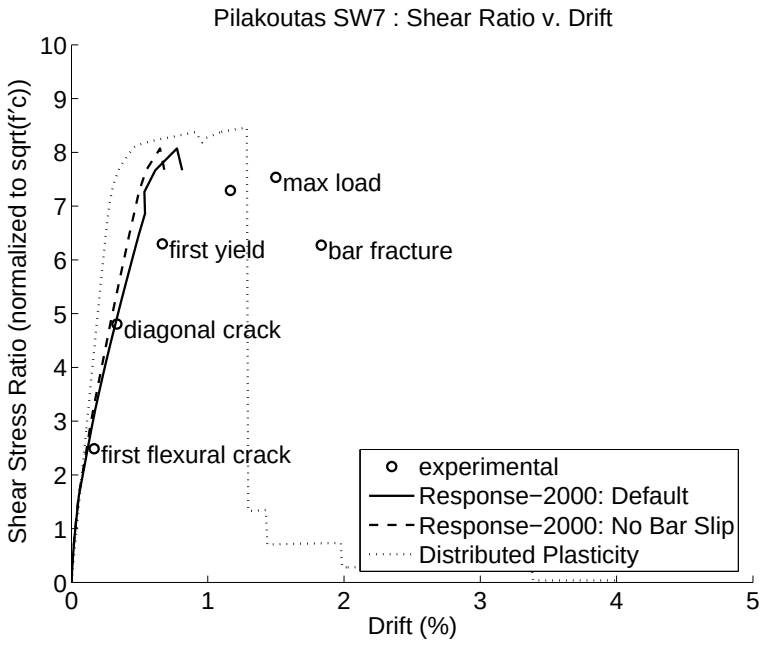

Figure 5.8: Pilakoutas SW7 - Shear Stress Ratio v. Drift from Response-2000

The two Oesterle specimens are under-predicted by less than 5%, while Pilakoutas is over-predicted by 7%.

The displacement and stiffness predictions are also generally improved in Response-2000 over the methods that only consider flexural bending. All three walls exhibit very good stiffness predictions up to cracking and yield. While the initial stiffness predicted for Pilakoutas SW7 is still too high, there is a significant improvement over the previous analysis methods.

However, predicting displacements at higher load demands is restricted by the limitation of not being able to determine load-displacement behavior beyond the maximum load capacity. The maximum displacements calculated by Response-2000 do not correspond well with the experimental results. Nor do they correspond, theoretically, with the maximum displacements based on strain limits used for the flexural analyses. Rather, they can be compared with the displacement at maximum load observed in the experimental tests. Figures 5.6 & 5.7 show that, while a little low, these displacements are reasonably well predicted for the three walls. However, Figure 5.8 shows that the displacement at maximum load for the shear-critical Pilakoutas SW7 is still significantly lower than observed.

The limitation of not being able to predict displacement beyond the maximum load also affects the examination of failure modes. Using the failure criteria shown in Figures 5.4 & 5.5, Response-2000 predicts that both Oesterle walls fail due to shear effects and that Pilakoutas SW7 fails due to flexure. However, Oesterle B1 failed due to inelastic bar buckling, which could be considered a flexural failure mode. Pilakoutas SW7 failed due to fracture of a horizontal bar, which could be considered a shear failure. The failure modes predicted by Response-2000 correspond to the cause of strength loss, rather than the cause of the loss of load carrying capacity. Therefore, a full understanding of ductility is not provided by Response-2000.

The results of this study show the impact of longitudinal bar-slip at the base of the wall on response. The difference in results shown in Tables 5.1 & 5.2 demonstrates that the inclusion of bar-slip effects at the base of the wall improves the displacement and stiffness predictions for each wall's prediction objectives. The improvement is most notable for the more squat wall, Pilakoutas SW7.

The data in Figures 5.6–5.8 show that the inclusion of bar-slip effects is not the sole reason for the improved displacement predictions. The inclusion of shear effects played a larger role than the addition of bar-slip in the improvement of the prediction results over those using the beam-column element formulations. Therefore, the inclusion of shear effects play a large role in the improved prediction values and should be accounted for in reinforced concrete shear wall analysis.

5.5 Response-2000 Summary

Analyses of three experimental shear walls demonstrates that sectional analysis using the modified compression field theory greatly improves the ability to predict wall behavior over methods that are based solely on flexural behavior. Therefore, shear effects are deemed a significant influence on behavior prediction. The effect of bar slip at the base of walls is also found to affect displacement and stiffness prediction, but to a lesser extent.

Chapter 6
VECTOR2

Nonlinear continuum analysis could be expected to yield the most accurate simulation of wall response. This type of analysis does not restrict section deformations; as does both Response-2000 and OpenSees, and allows for a high level of discretization both along and up the height of the wall. For this study, the VecTor2 software (Wong and Vecchio 2002), which employs the MCFT (Appendix A), was used to simulate the response of the three reference walls discussed in Sections 2.1.2–2.1.2. Modeling characteristics, modeling decisions, results, and comparison between simulated and observed response quantities are presented.

6.1 Modeling Decisions

The three walls were modeled using VecTor2's default analysis parameters with 4-node plane-stress elements. Reported values were used for material properties. Specification of a model in VecTor2 requires specification of the element mesh, material models, model parameters, and boundary conditions.

The walls were meshed using 4-node plane-stress elements. Along the length of the wall, enough elements were used so that the length of the boundary element comprised three rectangular elements for the Oesterle walls and two elements for Pilakoutas SW7. The height of the elements were chosen to make their aspect ratio roughly square. Similar by size elements were used in the panel zone. This resulted in a 19 by 30 element mesh for the two Oesterle walls and a 15 by 40 element mesh for Pilakoutas SW7. Preliminary analyses demonstrated that the inclusion of the cap beam, typically provided in laboratory specimens to ensure uniform load distribution was necessary to prevent premature vertical shear failure at the top of the wall.

In specifying material models and parameters, the default analysis parameters specified by VecTor2 were used. These are shown in Tables 6.1 & 6.2.

Table 6.1: VecTor2 Modeling Assumptions

Analysis Parameter	*Model*
Compression Base Curve	Hognestad Parabola
Compression Post-Peak	Modified Park-Kent
Compression Softening	Vecchio 1992-A
Tension Stiffening	Modified Bentz
Tension Softening	Linear
Tension Splitting	Not Considered
Confinement Strength	Kupfer / Richart
Concrete Dilation	Variable - Kupfer
Cracking Criterion	Mohr-Coulomb (Stress)
Crack Shear Check	Not Considered
Crack Width Check	Crack Limit (Agg/5)
Concrete Hysteresis	Linear w/ Offsets
Steel Hysteresis	Seckin Model
Rebar Dowel Action	Tassios (Crack Slip)
Rebar Buckling	Asatsu Model
Slip Distortion	Vecchio-Lai

Table 6.2: VecTor2 Numerical Decisions

Analysis Parameter	*Model*
Convergence Criteria	Displacements - Weighted
Previous Load History	Considered
Geometric Nonlinearity	Not Considered
Crack Allocation	Uniform Spacing

Reported material properties were used. To represent the load conditions in the laboratory, the nodes at the base of the wall were restrained against displacement. The wall is monotonically pushed over by incrementally increasing the displacement of the nodes at the height where load was applied in experimental testing.

6.2 Analysis Output Evaluation Method

The analysis output for each of the three walls was examined to study the mechanisms of deformation, loss of stiffness, and loss of strength. The studied response parameters included:

- first flexural cracking determined as the point where stiffness initially decreases in the load-displacement plot,
- onset of diagonal cracking,
- initial yielding of longitudinal reinforcement, and
- mode of failure (including associated behavior).

Additionally, the quality of the analytical results was evaluated using the same criteria used to evaluate the OpenSees and Response-2000 analyses; namely strength, stiffness, and displacement capacity. These results are shown in Table 6.3 and compared with the experimental values.

6.3 Description of Results

6.3.1 Oesterle B1

Figure 6.1 shows the simulated load-displacement response and points from the experimental response history. Figures 6.2–6.6 show crack patterns at various drift levels in the simulated response history. Initial flexural cracking is predicted at a drift of 0.026%, corresponding to a 27.3-kip applied load. The predicted displacement and cracking at this load step is shown in Figure 6.2. The reported drift for initially observed cracking was 0.107%, with a 26 k

Table 6.3: VecTor2: Ratios of Predicted Response Parameters

	Oesterle B1		*Oesterle B6*		*Pilakoutas SW7*	
Objective	*Obs.*	*Pred./Obs.*	*Obs.*	*Pred./Obs.*	*Obs.*	*Pred./Obs.*
M_y, *k-in*	8298	1.049	27048	1.034	1131	1.200
Δ_y, *in*	0.50	0.752	1.00	0.882	0.31	0.831
k_{sec}, *k/in*	90.2	1.395	147.0	1.172	76.0	1.445
M_{max}, *k-in*	11408	1.153	36064	0.886	1483	0.984
Δ_{max}, *in*	6.00	1.867	3.00	0.646	0.87	0.475

applied load. Thus, the analysis greatly over-predicts the stiffness up to initial cracking; the ratio of predicted to observed secant stiffness is 4.44.

After initial cracking, the predicted stiffness of the wall decreases. Similar response is observed in the lab (Figure 6.1). The predicted applied load and drift at initial yielding of the longitudinal reinforcement is 47.2 kips and 0.20% drift. Thus, the analysis over-predicted stiffness to yield. The ratio of predicted-to-observed yield secant stiffness values is 1.42 (Table 6.3). The predicted displacement and cracking at initial yielding is shown in Figure 6.3. These data show that diagonal cracks occur in the fourth column of elements from the left. This is the first column of elements beyond the tensile boundary element. The crack pattern suggests that the abrupt change in stiffness between the boundary element and the panel zone causes a significant concentration of shear at the edge of the panel zone.

As displacement is increased beyond initial yielding, the predicted stiffness decreases considerably and continues to do so as yielding spreads up the height of the wall and along the base. At a drift of 77%, the load-displacement curve becomes coarse indicating difficulties in convergence. Figure 6.4 shows that cracking has spread to 60% of wall height. Flexural cracks have widened in the bottom row of elements and penetrated into the compressive boundary element at this point.

At the observed maximum drift (3.26%), cracking spreads further and existing cracks grow wider (Figure 6.5). Nearly vertical cracks initiated in the toe of the wall at the base caused by the large vertical compression force from bending in the elements. The predicted

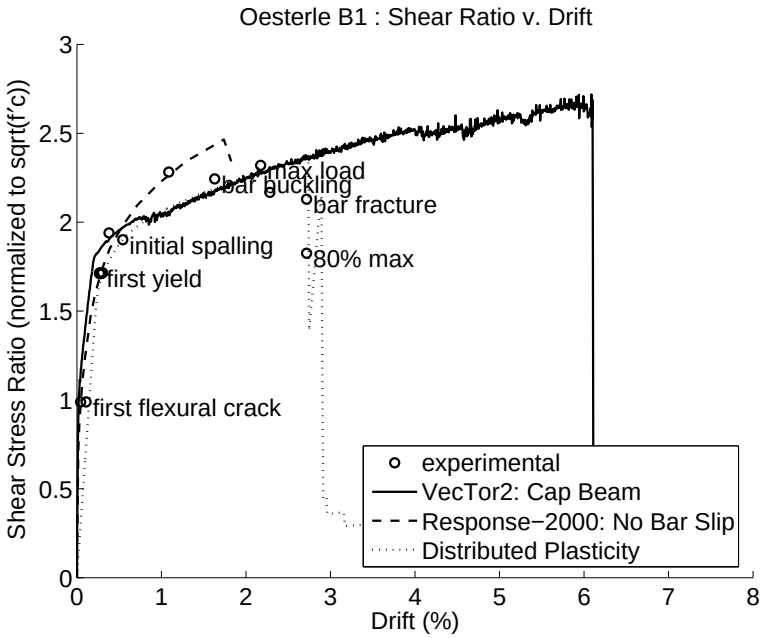

Figure 6.1: VecTor2 Predicted Response of Oesterle B1

load at this drift is 63.9 kips (compared to the reported 62 kips). However, strength loss is not predicted at this drift level.

Using the VecTor2 model, strength continues to increase to the point of the maximum predicted of 71.5 k load and 11.2% drift. At this point, the element at the toe of the wall crushes and loses strength. The maximum displacement is over-predicted by 87% and the maximum load is over-predicted by 15%. The deformation and cracking at this load step is shown in Figure 6.6. It shows that wide flexural cracks occured nearly halfway up the height of the wall and at the base penetrate most of the length. Wide diagonal cracks were concentrated at the interface of the tensile boundary element and the panel zone in conjunction with significantly skewed elements, indicating large concentration of shear strain and stress at this location.

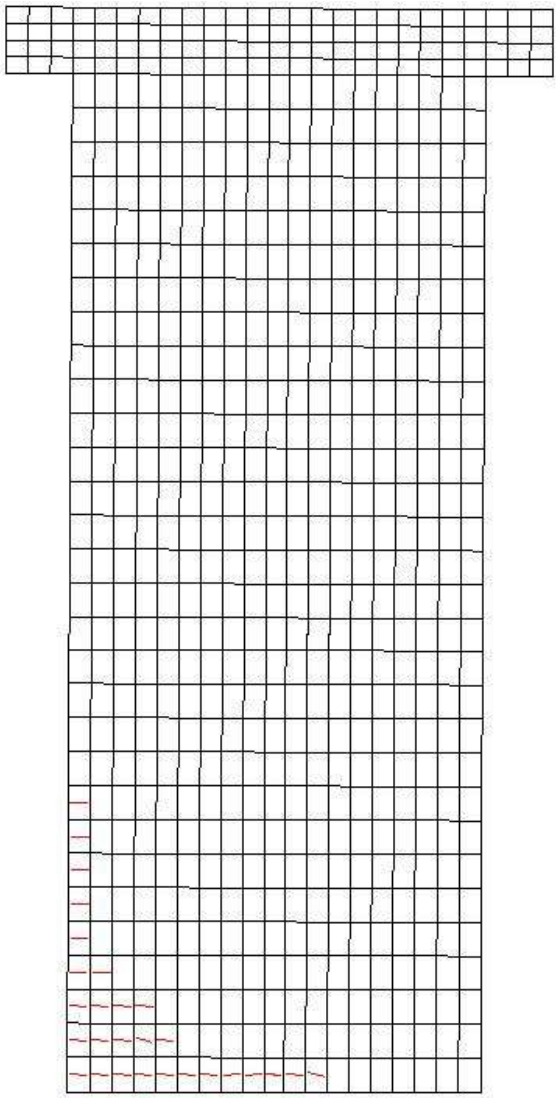

Displacement Magnification: 20.00 x

Crack Widths: thin < 1.00 mm, mid, thick > 2.00 mm

Figure 6.2: Initial Cracking of Oesterle B1 by VecTor2

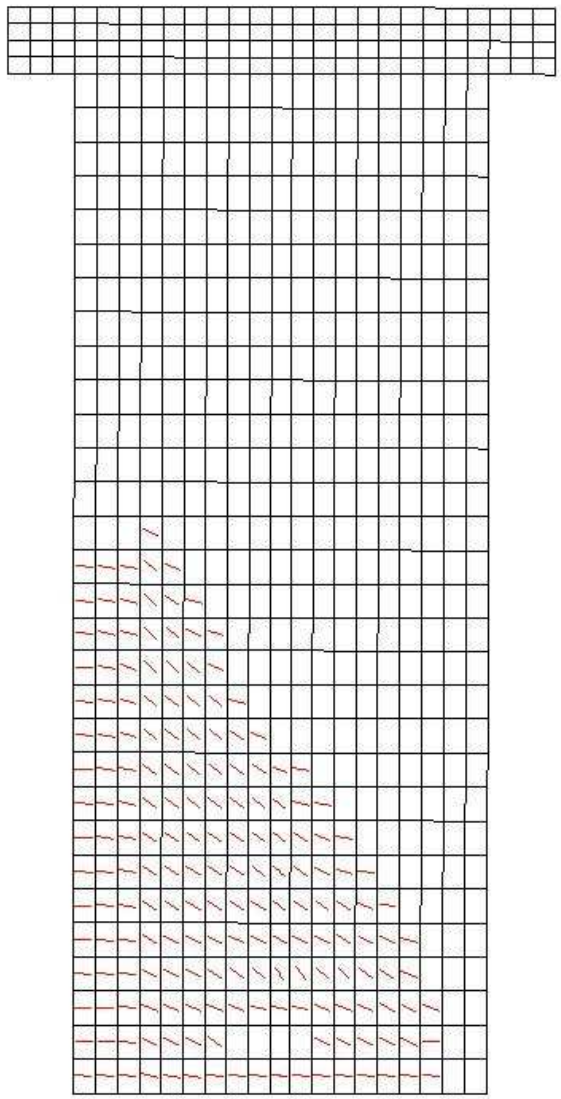

Displacement Magnification: 1.00 x

Crack Widths: thin < 5.00 mm, mid, thick > 10.00 mm

Figure 6.3: First Yield of Oesterle B1 by VecTor2

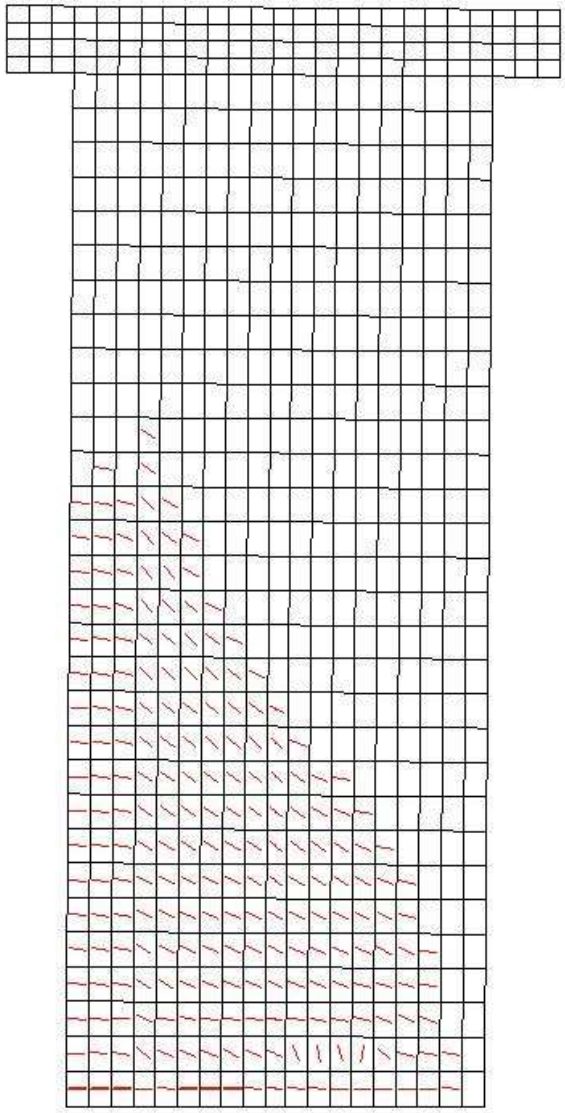

Displacement Magnification: 1.00 x

Crack Widths: thin < 5.00 mm, mid, thick > 10.00 mm

Figure 6.4: Onset of Reduced Convergence of Oesterle B1 by VecTor2

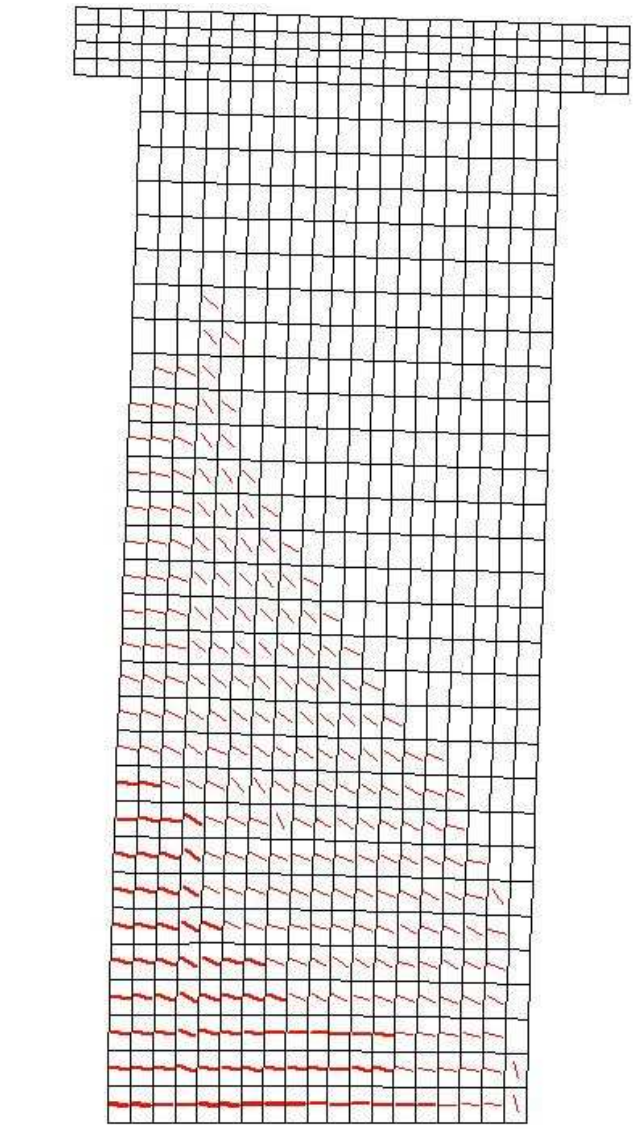

Displacement Magnification: 1.00 x
Crack Widths: thin < 5.00 mm, mid, thick > 10.00 mm

Figure 6.5: Oesterle B1 at Observed Maximum Displacement by VecTor2

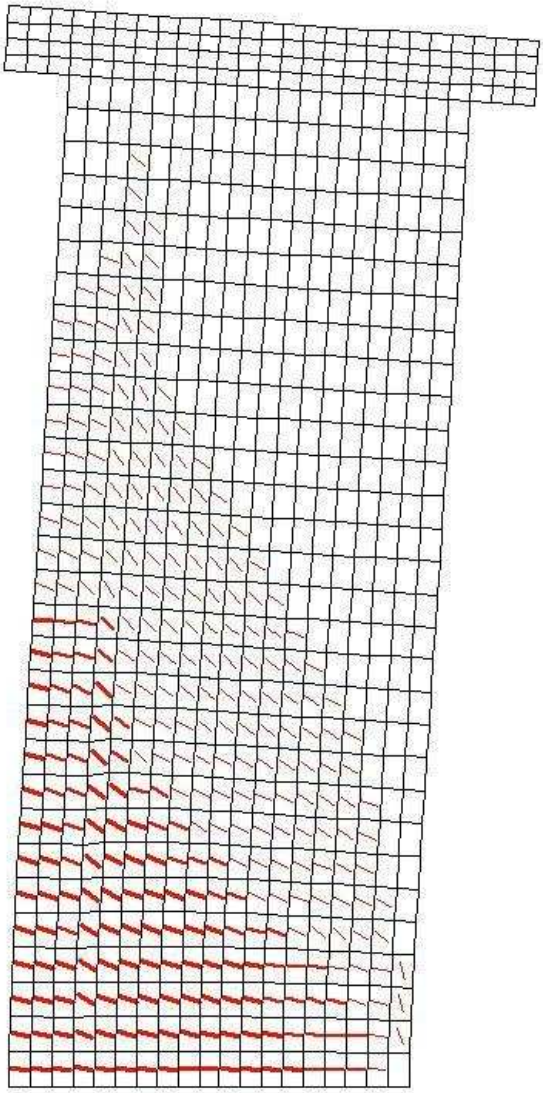

Displacement Magnification: 1.00 x

Crack Widths: thin < 5.00 mm, mid, thick > 10.00 mm

Figure 6.6: Predicted Maximum Drift of Oesterle B1 by VecTor2

6.3.2 Oesterle B6

The wall B6 tested by Oesterle exhibited a flexure-shear response. The VecTor2 simulation model was developed to model the planar wall using 670 elements and a monotonic displacement controlled load history. Figure 6.7 shows the measured and predicted load-displacement response curves. Figures 6.8–6.11 show the predicted crack patterns at various load levels.

The predicted load-displacement relationship is primarily linear to the predicted cracking load of 43.4 kips (0.047% drift). The predicted flexural cracking is primarily located in the tensile boundary element (Figure 6.8). The predicted-to-observed ratio of secant stiffness up to initial cracking is 1.11, which is an improvement over that predicted for the flexural specimen Oesterle B1 (ratio of 4.44).

The simulated stiffness decreases after cracking and the response remains linear until first yielding (0.48% drift). (Predicted yield load is 152 kips. The predicted-to-observed yield stiffness ratio is 1.45 (similar to the flexural wall). Figure 6.9 shows that cracking is distributed throughout the height of the wall at initial yielding. Horizontal cracks are limited primarily to the base of the wall. Diagonal cracking dominates the wall region between the boundary elements. These cracks are all less than 1/16 inches. The literature does not report the onset of diagonal cracking for comparison.

Once yielding occurs, there is an abrupt decrease in simulated stiffness. However, the load increases steadily with increasing displacement. Figure 6.10 shows that the width of the flexural cracks at the base are increasing, but the cracking pattern remains relatively unchanged during this portion of the load regime.

In contrast to the flexural wall (Oesterle B1), this analysis predicts maximum drift and load that are less than that measured in the laboratory. The predicted maximum drift is 65% of the observed and the predicted maximum load is 89% of the observed. However, the mode of failure predicted, web crushing, is the observed mode of failure. The loss of load carrying capacity is attributed to the loss of compressive strength in the second principal direction in the panel zone elements immediately adjacent to the compressive boundary element near the base of the wall. The direction of principal stress and strain was approximately 45° in

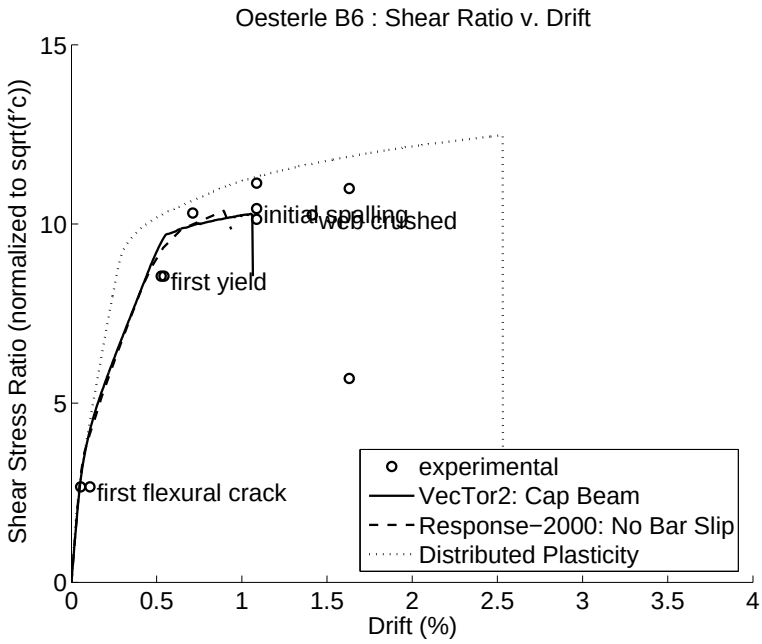

Figure 6.7: VecTor2 Predicted Response of Oesterle B6

these elements. The final deformation and cracking patterns are shown in Figure 6.11.

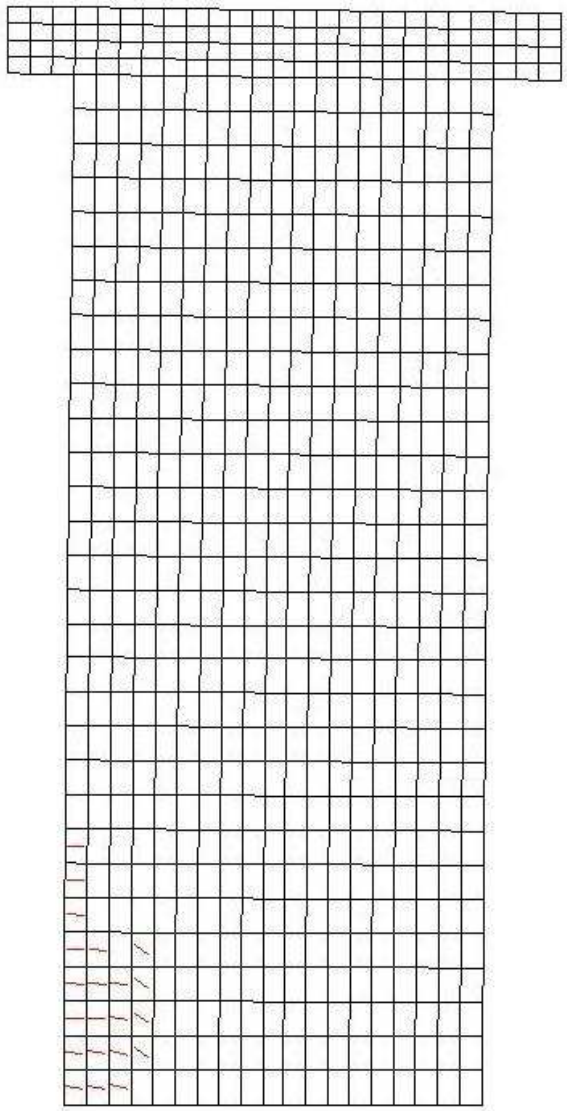

Displacement Magnification: 20.00 x
Crack Widths: thin < 1.00 mm, mid, thick > 2.00 mm

Figure 6.8: Initial Cracking of Oesterle B6 by VecTor2

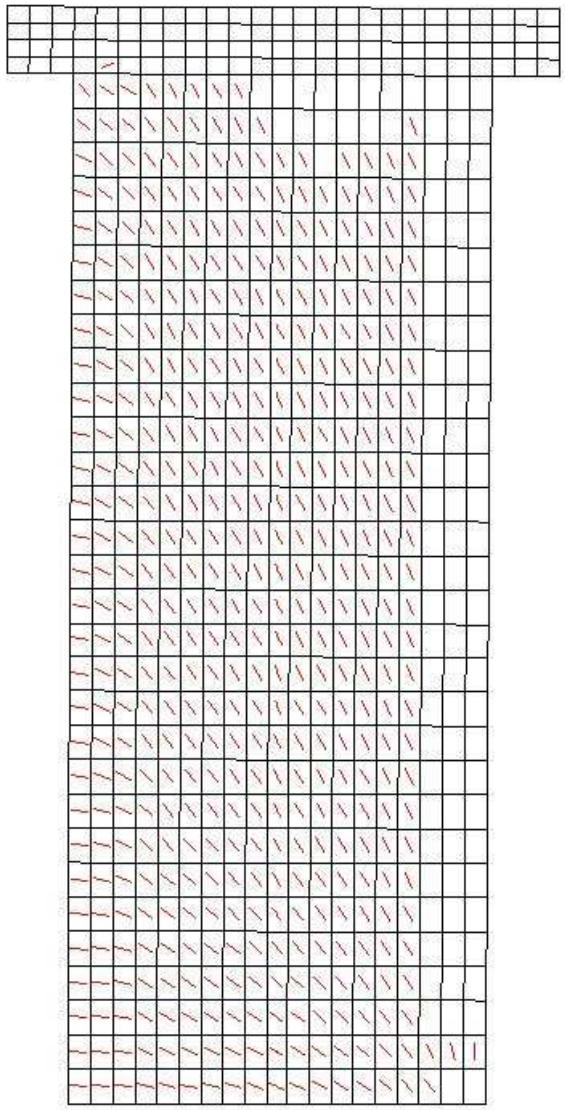

Displacement Magnification: 1.00 x
Crack Widths: thin < 1.00 mm, mid, thick > 2.00 mm

Figure 6.9: First Yield of Oesterle B6 by VecTor2

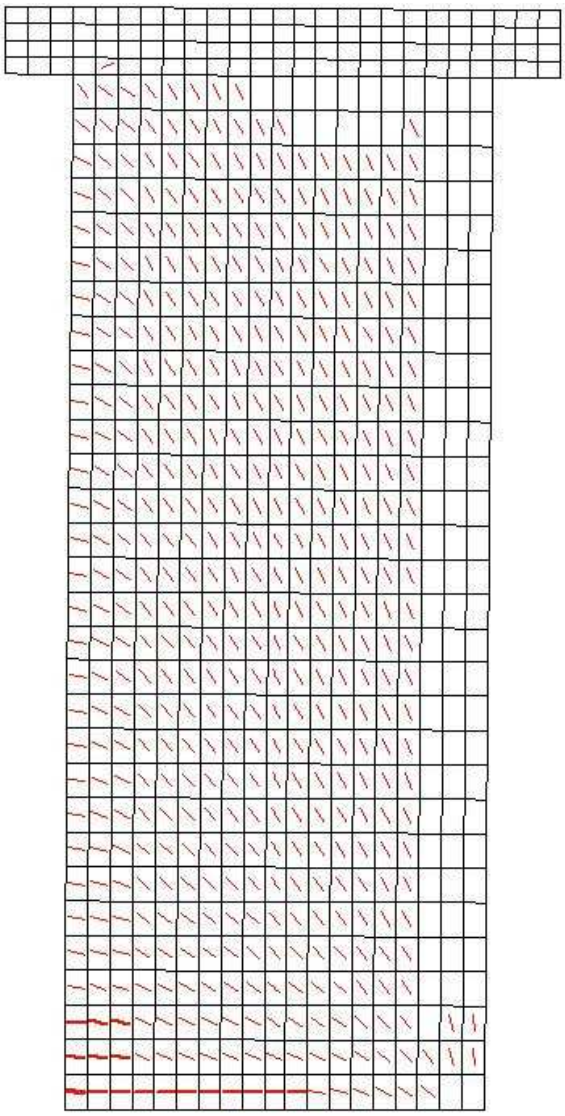

Displacement Magnification: 1.00 x
Crack Widths: thin < 1.00 mm, mid, thick > 2.00 mm

Figure 6.10: Oesterle B6 Halfway Between Yield and Max Drift by VecTor2

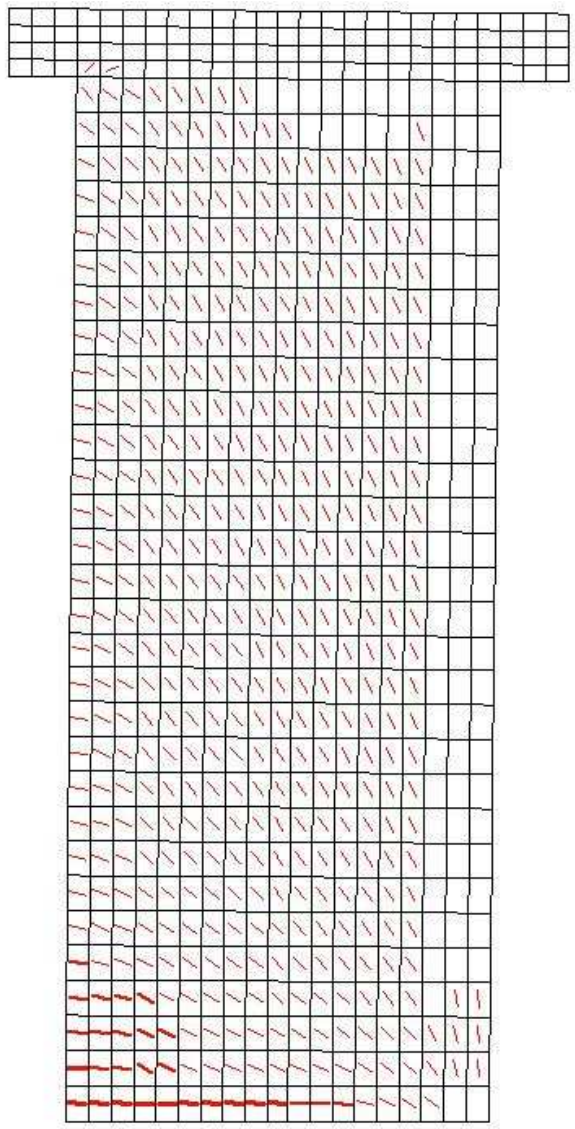

Displacement Magnification: 1.00 x
Crack Widths: thin < 1.00 mm, mid, thick > 2.00 mm

Figure 6.11: Predicted Maximum Drift of Oesterle B6 by VecTor2

6.3.3 Pilakoutas SW7

The initial flexural crack was predicted at 0.03% drift and 4.4 kips load. This is at a significantly smaller drift and load than was measured in the laboratory, 0.17% and 9.5 kips, respectively. This difference may be due to difficulties in identifying cracks immediately during testing which are often only recorded at the peak of a load cycle. The predicted cracking pattern at initial cracking is shown in Figure 6.13.

Measured diagonal cracking was reported at 0.34% drift, after which the measured stiffness decreased significantly. In the simulation, however, diagonal cracking initiated at a larger level of drift. The predicted response does not exhibit a significant stiffness loss, as shown in Figure 6.12. Additionally, the predicted cracking pattern shown in Figure 6.14 consist of evenly distributed cracks at fairly steep diagonals throughout the panel zone; this is in contrast to the observed diagonal cracking patterns (Figure 6.15).

The drift at which diagonal cracking is reported falls between the two walls on the left in Figure 6.15. This wall has five pairs of horizontal bars spaced at $9\frac{1}{2}$ inches apart. In the simulation, the reinforcement is evenly distributed in each element. Many of the diagonal cracks intersect with one bar or less. The discrepancy between the predicted stiffness and the observed stiffness likely has to do with the lack of validity in the assumptions about smeared properties in the MCFT formulation for this wall.

The model's over-predicted stiffness after diagonal cracking under-predicts yield displacement. Figure 6.16 shows the deformation and crack patterns at the predicted yield drift. This shows little difference from the crack pattern reported at the initiation of diagonal cracking, other than the development of vertical cracks in the compressive boundary element.

Similar to the other specimens, simulated and observed stiffness decreases when yielding initiates (Figure 6.12). Figure 6.17 shows that as drift is increased beyond yield, the flexural cracks in the base of the panel zone widen. Cracks in the panel zone widen substantially more than boundary element cracks.

Little changes in the simulated cracking patterns at maximum drift and load (Figure 6.18). However, at this drift level, the extreme compressive element at the base of the

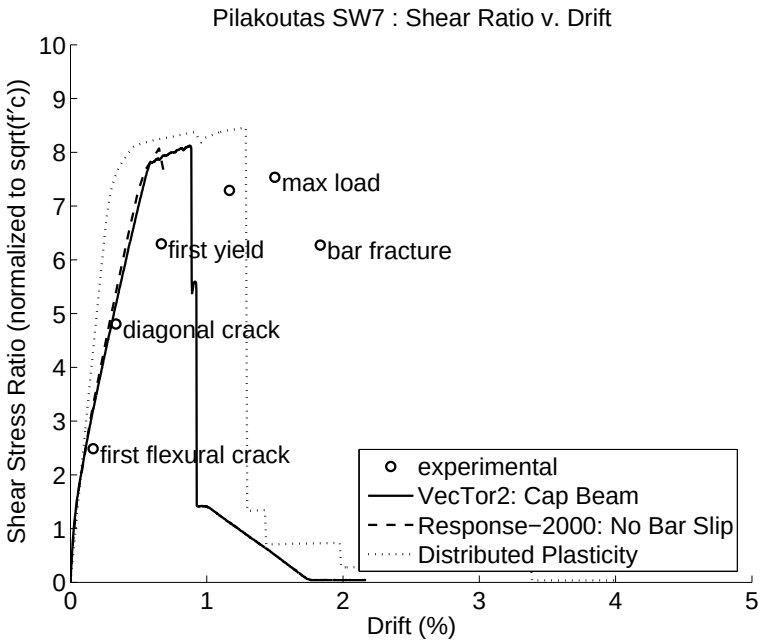

Figure 6.12: VecTor2 Predicted Response of Pilakoutas SW7

wall exhibits strength loss due to crushing; this causes strength loss for the entire wall. This could be considered a flexural failure mode. The observed failure mode was fracture of a horizontal bar, which could be considered a shear-type failure mode. The predicted maximum strength is approximately equal to (98%) the measured strength, but the predicted maximum displacement is low (48% of the observed value).

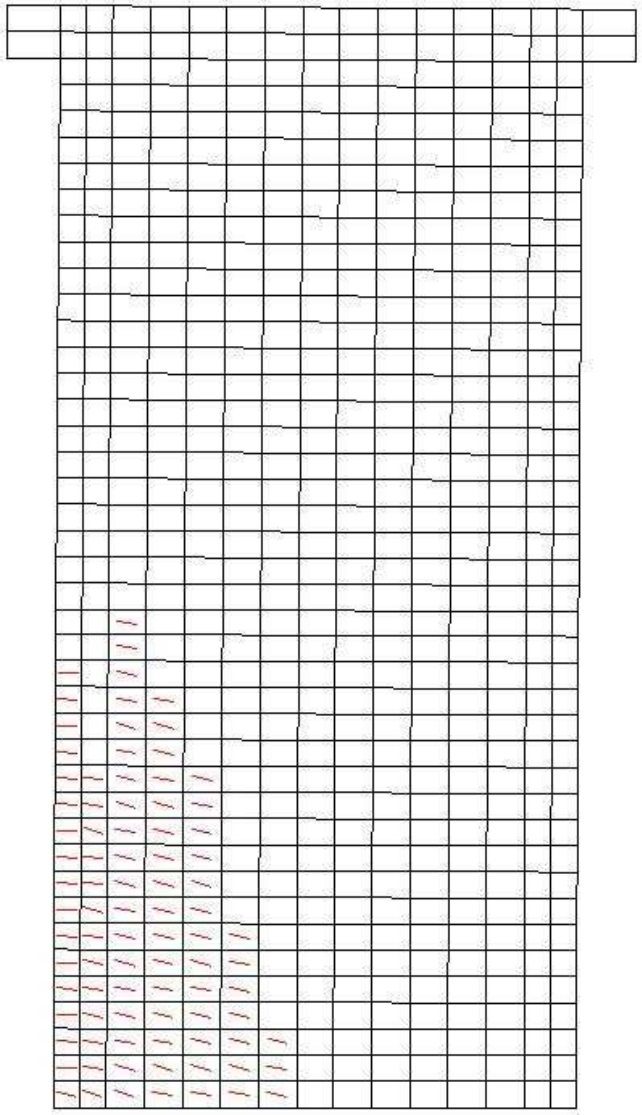

Displacement Magnification: 20.00 x
Crack Widths: thin < 1.00 mm, mid, thick > 2.00 mm

Figure 6.13: Initial Cracking of Pilakoutas SW7 by VecTor2

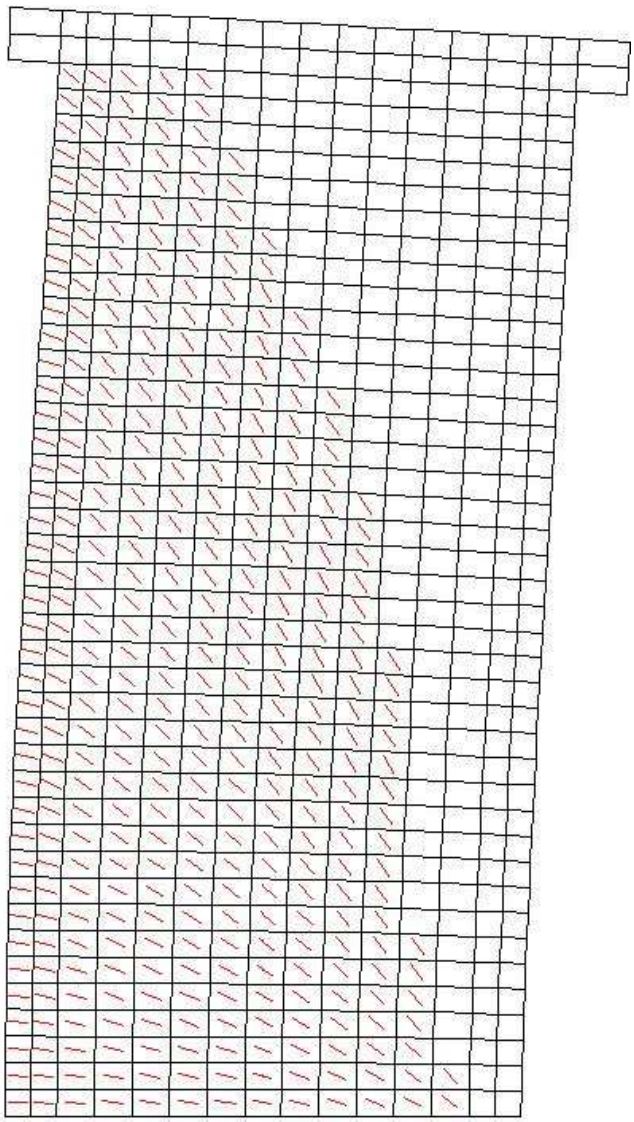

Displacement Magnification: 20.00 x
Crack Widths: thin < 1.00 mm, mid, thick > 2.00 mm

Figure 6.14: Pilakoutas SW7 at Observed Diagonal Cracking Displacement by VecTor2

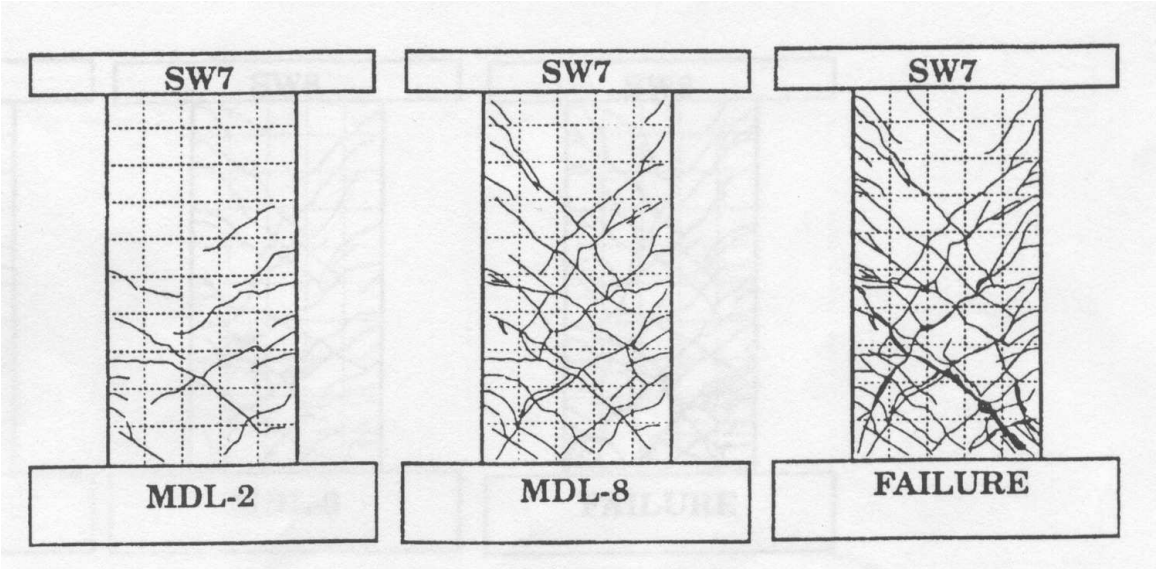

Figure 6.15: Pilakoutas SW7 Experimental Crack Patterns at Three Levels of Drift

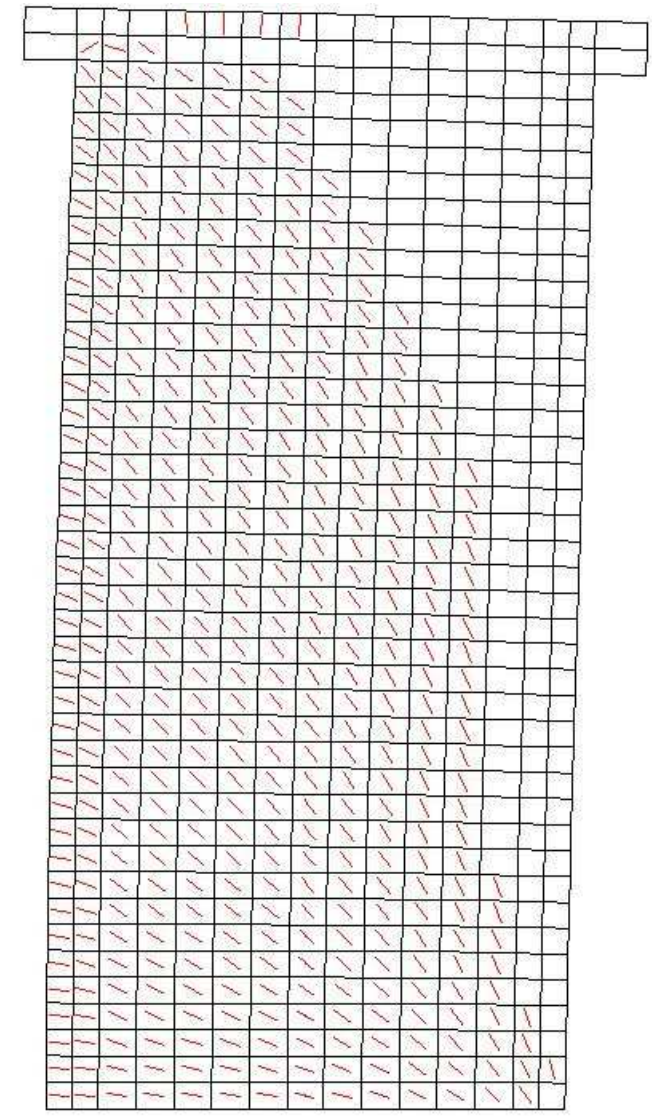

Displacement Magnification: 5.00 x
Crack Widths: thin < 1.00 mm, mid, thick > 2.00 mm

Figure 6.16: First Yield of Pilakoutas SW7 by VecTor2

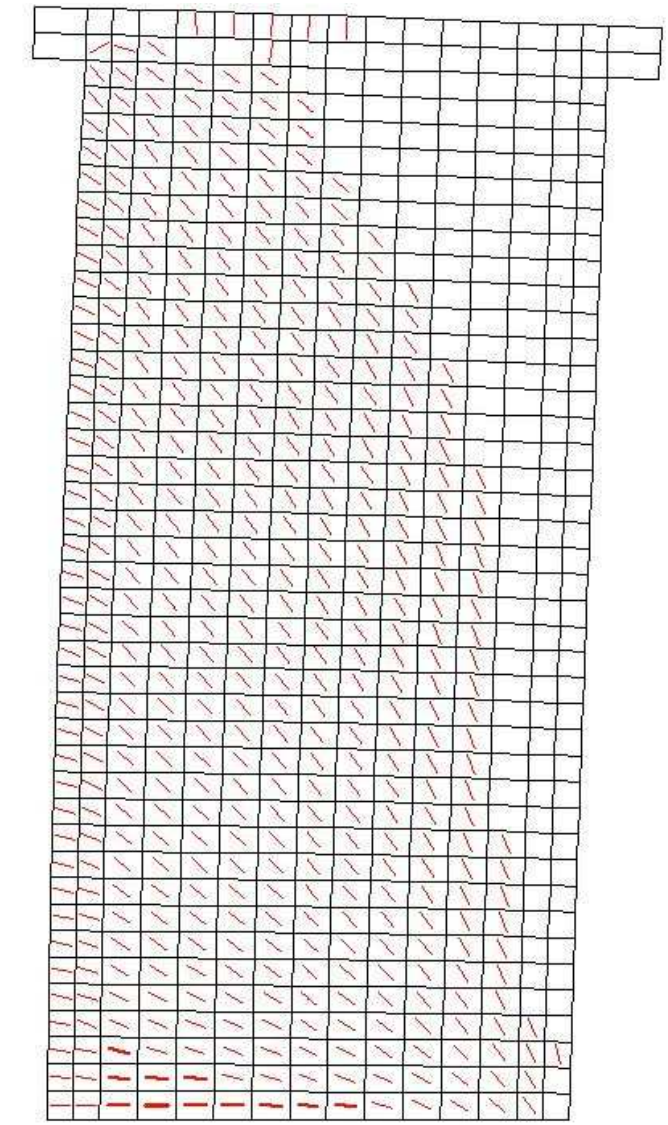

Displacement Magnification: 5.00 x
Crack Widths: thin < 1.00 mm, mid, thick > 2.00 mm

Figure 6.17: Pilakoutas SW7 Halfway Between Yield and Max Drift by VecTor2

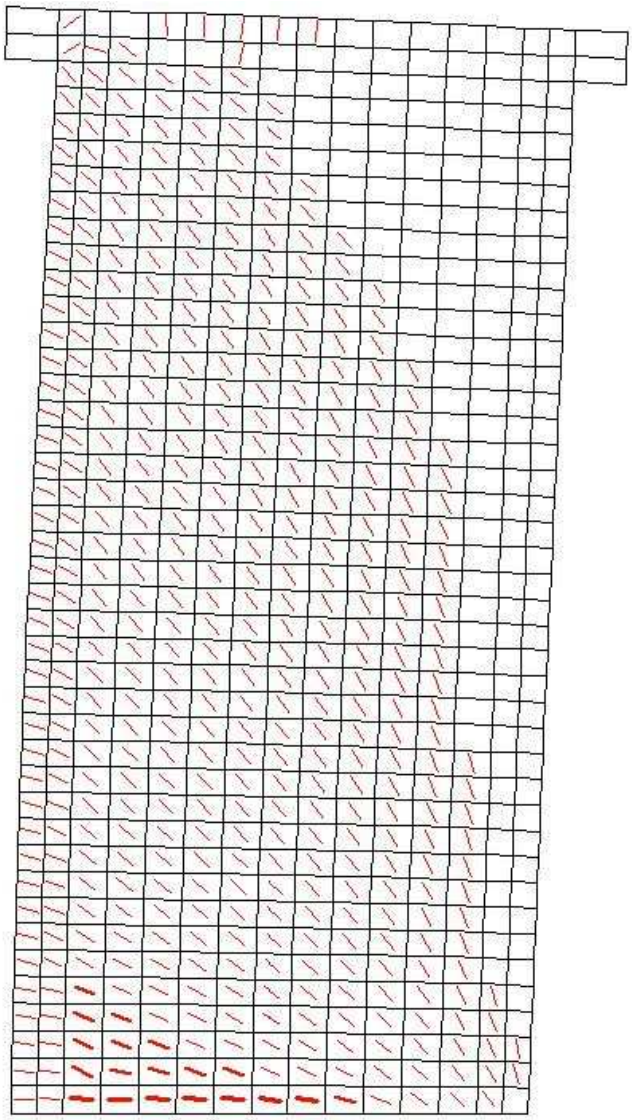

Displacement Magnification: 5.00 x
Crack Widths: thin < 1.00 mm, mid, thick > 2.00 mm

Figure 6.18: Predicted Maximum Drift of Pilakoutas SW7 by VecTor2

6.4 Discussion and Comparison of Results

Evaluation of the VecTor2 analysis results supports the following observations and conclusions:

- The analyses under monotonic loading do not predict the gradual loss in strength beyond maximum predicted strength observed in the laboratory for cyclic loading.

- The distinct yield point with an abrupt change in stiffness exhibited in the VecTor2 analyses do not correlate to the behavior observed in experiments. Stiffness should gradually decrease as bar yielding propagates up the height and along the length of the wall.

- Concentration of shear at the edges of the panel zone suggests that plane sections do not remain plane as is assumed in Response-2000 analysis. This is partially responsible for the greater decrease in stiffness after yield predicted by VecTor2.

- An additional reason that Response-2000 is stiffer after yield than VecTor2 is that it reduces the influence of shear at the base of the wall to better predict the strength. Reducing the effect of shear both decreases the effect that shear strain has on the displacement as well as the effect that it has on softening the flexural stiffness by reducing the normal stress in the section fibers.

- Finally, the mode of failure observed in Oesterle B6 sheds light on the mechanism causing web crushing in reinforced concrete walls. Two logical possibilities exist. First, web crushing could be caused by the formation of a diagonal compressive strut and subsequent loss in strength of that strut. Alternatively, if the neutral axis is located in the panel zone, the mechanism could be due to vertical compressive stress causing the unconfined panel zone to fail prior to the confined boundary element. Since the analytical data shows that the angle of principal compressive stress and strain is nearly 45° approaching failure, it is suggested that the diagonal strut mechanism is correct.

Chapter 7
ENHANCED BEAM-COLUMN ELEMENT

Analyses presented in Chapters 5 & 6 indicate that the MCFT resulted in an improved prediction of the wall stiffness, indicating the importance of shearing deformation. However, this model is not readily available to practitioners for use in analysis of structural systems. Thus, the distributed-plasticity element was modified to include the effects of bar-slip and shear deformation. This chapter described the development and evaluation of this model. First, the evaluation method is discussed. Next, the bar-slip model is described and the results of its implementation discussed. Then, the development and implementation of an equivalent (reduced) elastic shear model, which was calibrated to minimize error in the prediction of yield displacement and maximum displacement for use with or without the bar-slip model is discussed. Finally, the recommended parameters are summarized.

7.1 Description of Evaluation Method

The evaluation method was similar to that used for the flexural beam-column analyses described in Section 4.3. Evaluation is based on the same wall characteristics, measured response quantities, and predicted response. However, strengths were not studied, because the applied enhancements do not affect strength prediction.

The new models are evaluated on the basis of the improved prediction of specific response quantities. The improvements were quantified by the difference between the normalized error of the flexural and enhanced beam column elements respectively. For a given response quantity, A:

$$\delta_{abs,error,enhancement,A} = \left|\frac{A_{pred,flexural} - A_{obs}}{A_{obs}}\right| - \left|\frac{A_{pred,enhancement} - A_{obs}}{A_{obs}}\right| \tag{7.1}$$

where A indicates a response quantity (e.g. k_{sec}, Δ_y, or Δ_{max}). $\delta_{error,abs,A}$ is the absolute change in error of the response quantity A. The subscript *pred* indicates a predicted value,

the subscript *obs* indicates an observed value, the subscript $flexural$ indicates a result using the flexural beam-column analysis, and the subscript *enhancement* indicates a result using the enhanced element with a particular modification (e.g. $slip$, $shear$, $\alpha_{\Delta y}$, $\alpha_{\Delta max}$, $\alpha_{\Delta y,slip}$, $\alpha_{\Delta max,slip}$). Positive values indicate an improved prediction using bar-slip. Negative values indicate a worse prediction for using the enhanced model.

The relative difference in error is the difference of the error from the enhanced beam-column analysis and the error of the flexural beam-column analyses. The observed response quantity value drops out of the numerator. So it can be thought of more as a normalized change in predicted response than a measurement of error. The relative difference in error is given by:

$$\delta_{rel,error,enhancement,A} = \frac{A_{pred,enhancement} - A_{pred,flexural}}{A_{obs}} \tag{7.2}$$

A positive value indicates that the prediction of the response quantity increased using the enhancement. A negative value indicates that the response quantity predicted decreased using the enhanced model.

7.2 The Bar-Slip Model

The bar-slip model intends to capture the fixed end rotation at the base of the wall due to strain penetration into the foundation. First, the theoretical model is explained. Then, the implementation of the model is described. The results are discussed by observing the effect on the three walls for in depth study and the prediction objectives are examined for all of the walls.

7.2.1 Implementation with Distributed Plasticity Model

In OpenSees (McKenna 1997), the effect of strain penetration at the base of the wall was modeled by introducing a zero-length fiber-section element between the bottom of the distributed plasticity element and the fixed node at the base of the wall (Figure 7.1). The zero-length element has the same geometry as the fiber section used to model the wall. The material properties are expressed in terms of stress versus displacement relationship. Thus, the zero-length section element results in a moment versus rotation relationship, rather

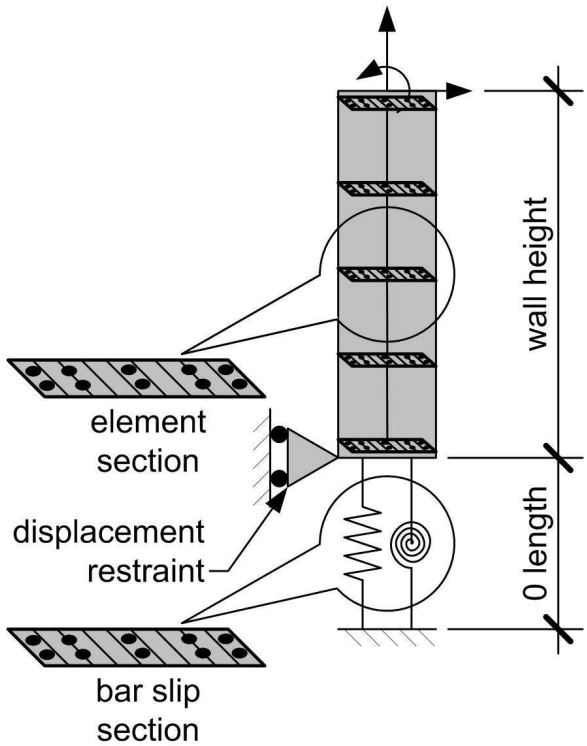

Figure 7.1: Implementation of Bar Slip Model with Distributed Plasticity Element

than force versus curvature relationship. The stress-displacement relationships, discussed in Section 7.2.2, were used for the steel reinforcement and the concrete.

An additional node was added for the connection of the zero-length element to the distributed plasticity element. This node requires an imposed restraint against displacement in the transverse direction to maintain structural stability, since the zero-length fiber section element does not carry shear force.

Figure 7.2 shows how the parameters for the steel stress-displacement model differ from those of the stress-strain model. The three parameters required for the stress-strain model are the elastic modulus, E_s, the yield stress, f_y, and the hardening ratio, b. The three parameters needed for the stress-displacement relationship become E_{slip}, f_y, and b_{slip}. These

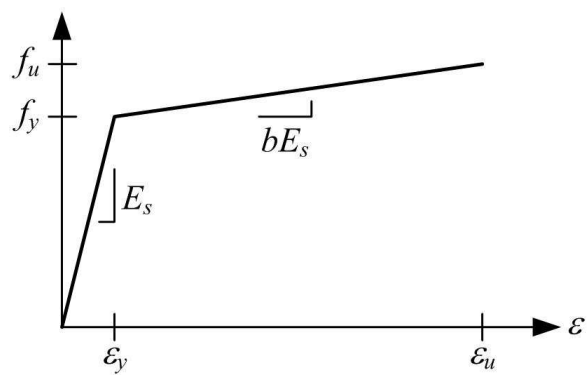

(a) Reinforcement Stress Versus Strain Relationship

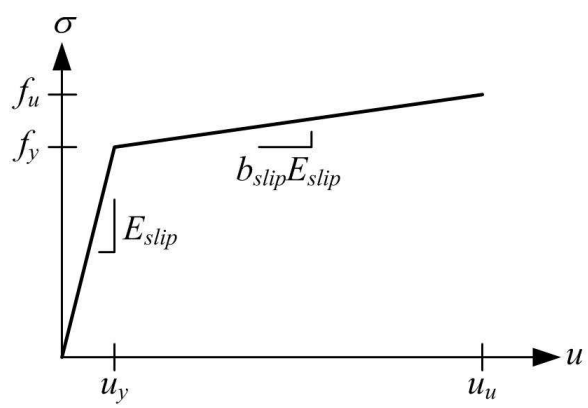

(b) Reinforcement Stress Versus Displacement Relationship

Figure 7.2: Definition of Bar Slip Material Model

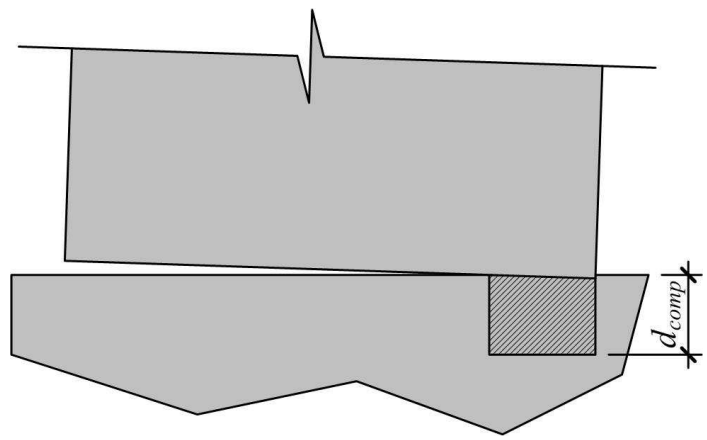

Figure 7.3: Assumed Compressive Depth

are illustrated in Figure 7.2 and given by:

$$E_{slip} = \frac{f_y}{u_y} \tag{7.3}$$

$$f_y = f_y \tag{7.4}$$

$$b_{slip} = \frac{f_u - f_y}{E_{slip}(u_u - u_y)} \tag{7.5}$$

where u_y is the slip displacement given by Equation 7.9 with $\epsilon = \epsilon_y$ and u_u is the displacement of the bar at ultimate stress given by Equation 7.9 with $\epsilon = \epsilon_u$, where the strain at ultimate is defined as:

$$\epsilon_u = \epsilon_y + \frac{f_u - f_y}{bE_s} \tag{7.6}$$

Similarly, a stress-displacement relationship is required for the concrete. To accomplish this, Berry (2006) suggests multiplying the concrete strains by an effective compressive depth, d_{comp} in Figure 7.3. This method was adopted. Berry recommends using the depth of the neutral axis for the section when the extreme compressive fiber is at a strain of 0.002.

7.2.2 Theoretical Bar-Slip Model

Integration of the strain diagrams shown in Figure 7.4 result in the following equations for the displacement due to slip along the elastic region of the bar, u_e, and the displacement

due to slip along the inelastic region of the bar, u_i:

$$u_e = \begin{cases} \frac{1}{2}\epsilon L_d & \text{if } \epsilon \leq \epsilon_y \\ \frac{1}{2}\epsilon_y \left(L_d - L_{di}\right) & \text{if } \epsilon > \epsilon_y \end{cases} \tag{7.7}$$

$$u_i = \begin{cases} 0 & \text{if } \epsilon \leq \epsilon_y \\ \frac{1}{2}L_{di}\left(\epsilon + \epsilon_y\right) & \text{if } \epsilon > \epsilon_y \end{cases} \tag{7.8}$$

where ϵ is the strain in the bar at the base of the wall, ϵ_y is the yield strain of the bar, L_d is the development length, and L_{di} is the length of the inelastic region of the bar. Summation of u_e and u_i gives the total displacement of the bar at the base of the wall, u_t:

$$u_t = \begin{cases} \frac{1}{2}\epsilon L_d & \text{if } \epsilon \leq \epsilon_y \\ \frac{1}{2}\left(\epsilon_y L_d + \epsilon L_{di}\right) & \text{if } \epsilon > \epsilon_y \end{cases} \tag{7.9}$$

Assuming a uniform bond strength, the development length an elastic bar, L_d is:

$$L_d = \frac{f_s d_b}{4\tau_{be}} \tag{7.10}$$

where:

$$f_s = \frac{\epsilon_y}{E_s} \tag{7.11}$$

where f_s is the elastic stress in the bar, d_b is the diameter of the bar, and τ_{be} is the uniform bond strength of an elastic bar. Equation 7.12 defines the bond strength:

$$\tau_{be} = \lambda\sqrt{f'_c} \tag{7.12}$$

where λ is a calibrated parameter and f'_c is the measured compressive strength of the concrete. Lehman and Moehle (2000) propose that $\lambda = 1.0$ for f'_c in MPa ($\lambda = 0.381$ for f'_c in ksi).

For a yielded bar, the length of the inelastic region, L_{di}, is calculated:

$$L_{di} = \frac{bE_s(\epsilon - \epsilon_y)d_b}{4\tau_{bi}} \tag{7.13}$$

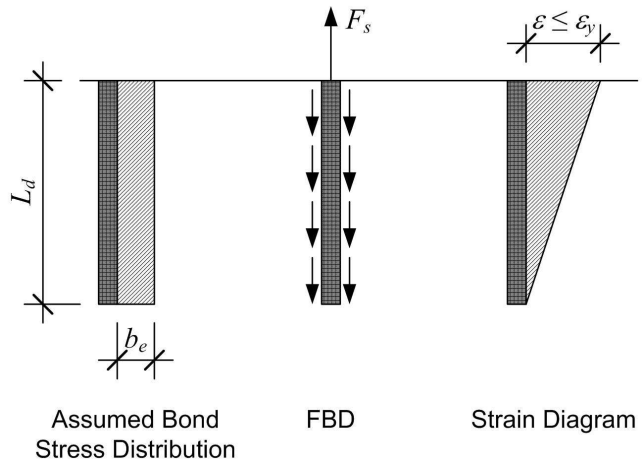

(a) Prior to Yield

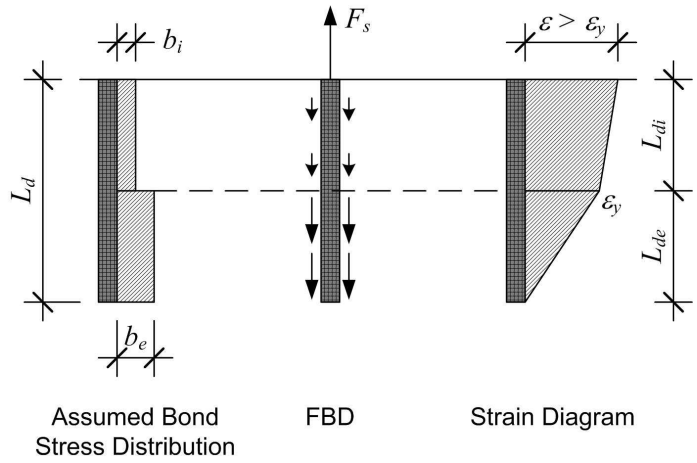

(b) Beyond Elasticity

Figure 7.4: Stress and Strain Distribution of an Anchored Bar

where b is the strain hardening ratio of the steel (typically 0.01), E is the elastic modulus of the steel, and τ_{bi} is the bond stress in the inelastic portion of the bar, defined by:

$$\tau_{bi} = \frac{\tau_{be}}{2} \tag{7.14}$$

7.2.3 Results Using Bar-Slip Model

The response quantity prediction values of all of the walls for the bar-slip analyses are summarized in Tables 7.1 & 7.2. The change in error from the analyses without bar-slip to those with bar-slip is presented in Tables 7.3 & 7.4.

The shear stress ratio versus drift plots for each of the bar-slip analyses of the walls are in Appendix I. Plots of the each of the response quantities of predicted to observed ratio compared to each of the design parameters are located in Appendix J. Plots of each of the absolute and relative changes in prediction error of each of the response quantities compared to each of the engineering design parameters are in Appendix K.

Table 7.1: Bar-Slip Prediction Results

Objective	k_{sec}, k/in		Δ_y, in		Δ_{max}, in	
Name	*Obs.*	*Pred./Obs.*	*Obs.*	*Pred./Obs.*	*Obs.*	*Pred./Obs.*
Lefas SW30					0.82	0.60
Lefas SW31					0.87	0.56
Lefas SW32					0.96	0.51
Lefas SW33					0.98	0.50
Lefas SW11	270.6	2.44	0.14	0.36	0.32	0.62
Lefas SW12	413.8	2.11	0.11	0.48	0.35	0.42
Lefas SW13	374.0	2.06	0.15	0.45	0.35	0.36
Lefas SW14	249.1	2.42	0.15	0.36	0.44	0.41
Lefas SW15	415.3	1.78	0.11	0.52	0.32	0.47
Lefas SW16	617.2	1.50	0.10	0.65	0.23	0.52
Lefas SW17	212.5	3.00	0.15	0.34	0.42	0.46
Lefas SW21	78.7	1.21	0.23	0.68	0.81	0.59
Lefas SW22	128.0	1.02	0.19	0.81	0.60	0.62
Lefas SW23	131.9	1.06	0.20	0.85	0.52	0.60
Lefas SW24	73.4	1.35	0.25	0.62	0.71	0.67
Lefas SW25	126.6	1.05	0.23	0.76	0.37	0.84
Lefas SW26	70.5	1.22	0.22	0.77	0.82	0.58
Oesterle B1	90.2	1.01	0.50	0.81	6.00	0.98
Oesterle B2	135.6	1.84	0.90	0.46	5.00	0.53
Oesterle B3	92.0	0.99	0.50	0.80	8.00	0.78
Oesterle B4	92.0	0.98	0.50	0.82	13.00	0.45
Oesterle B5	138.9	1.74	0.90	0.51	5.00	1.34
Oesterle R1	50.0	0.70	0.45	1.05	9.00	0.56
Oesterle R2					6.00	0.93
Oesterle B6	147.0	1.71	1.00	0.56	3.00	1.61
Oesterle B7	170.0	2.02	1.00	0.46	6.00	1.01
Oesterle B8	166.0	1.98	1.00	0.47	6.00	1.06
Oesterle B9	192.5	1.76	1.20	0.37	5.30	1.23
Oesterle B10	157.3	1.73	1.10	0.36	5.75	0.86
Pilakoutas SW4	78.6	1.69	0.24	0.62	0.94	0.93
Pilakoutas SW5					1.02	0.50
Pilakoutas SW6	71.4	1.88	0.24	0.61	0.94	0.47
Pilakoutas SW7	76.0	1.83	0.31	0.58	0.87	0.79
Pilakoutas SW8	76.2	1.93	0.24	0.63	1.02	0.50
Pilakoutas SW9	75.4	1.86	0.24	0.66	1.02	0.53
Salonikios LSW1					1.26	0.54
Salonikios LSW2					1.26	0.52
Salonikios LSW3					1.26	0.43
Salonikios MSW1					1.26	1.04
Salonikios MSW2					1.26	0.94
Salonikios MSW3					1.26	0.72
Salonikios MSW6					1.26	0.91

Table 7.2: Bar-Slip Prediction Results (cont.)

Objective	k_{sec}, k/in		Δ_y, in		Δ_{max}, in	
Name	*Obs.*	*Pred./Obs.*	*Obs.*	*Pred./Obs.*	*Obs.*	*Pred./Obs.*
Sittipunt W1					1.77	0.85
Sittipunt W2					1.34	1.03
Tasnimi SHW1					0.67	2.12
Tasnimi SHW2					0.45	3.14
Tasnimi SHW3					0.61	2.39
Tasnimi SHW4					0.75	1.95
Thomsen RW1	27.8	1.92	1.08	0.44	3.60	0.68
Thomsen RW2	27.8	1.82	1.08	0.42	3.60	0.99
Vallenas SW3	285.1	2.84	0.71	0.28	6.65	0.35
Vallenas SW4	285.8	2.83	0.71	0.28	3.58	0.65
Vallenas SW5	337.7	1.84	0.47	0.45	3.18	0.61
Vallenas SW6	312.1	2.00	0.53	0.40	1.98	0.98
Wang SW1	272.9	1.31	0.70	0.44	4.25	0.20
Wang SW2	288.6	1.25	0.70	0.44	2.90	0.29
Yanez S1					2.76	0.48
Zhang SW7	166.6	1.22	0.23	0.82	1.23	0.37
Zhang SW8	195.4	0.82	0.22	1.10	0.94	0.31
Zhang SW9	174.2	1.85	0.33	0.55	1.24	0.33
Average	–	1.69	–	0.58	–	0.79
St. Dev.	–	0.55	–	0.20	–	0.53
COV	–	0.33	–	0.35	–	0.67

Table 7.3: Difference of Bar-Slip Model Prediction Results to Flexural Model

Objective	k_{sec}, k/in		Δ_y, in		Δ_{max}, in	
Name	*Absolute*	*Relative*	*Absolute*	*Relative*	*Absolute*	*Relative*
Lefas SW30					0.12	0.12
Lefas SW31					0.11	0.11
Lefas SW32					0.09	0.09
Lefas SW33					0.09	0.09
Lefas SW11	0.86	-0.86	0.09	0.09	0.16	0.16
Lefas SW12	1.02	-1.02	0.16	0.16	0.14	0.14
Lefas SW13	1.34	-1.34	0.18	0.18	0.13	0.13
Lefas SW14	0.96	-0.96	0.10	0.10	0.12	0.12
Lefas SW15	0.91	-0.91	0.17	0.17	0.16	0.16
Lefas SW16	1.00	-1.00	0.26	0.26	0.21	0.21
Lefas SW17	1.11	-1.11	0.09	0.09	0.13	0.13
Lefas SW21	0.28	-0.28	0.13	0.13	0.11	0.11
Lefas SW22	0.28	-0.28	0.18	0.18	0.14	0.14
Lefas SW23	0.38	-0.38	0.22	0.22	0.16	0.16
Lefas SW24	0.29	-0.29	0.11	0.11	0.11	0.11
Lefas SW25	0.37	-0.37	0.20	0.20	0.22	0.22
Lefas SW26	0.32	-0.32	0.16	0.16	0.12	0.12
Oesterle B1	0.07	-0.07	0.05	0.05	0.14	0.14
Oesterle B2	0.18	-0.18	0.04	0.04	0.05	0.05
Oesterle B3	0.05	-0.07	0.05	0.05	0.11	0.11
Oesterle B4	0.04	-0.07	0.05	0.05	0.07	0.07
Oesterle B5	0.20	-0.20	0.05	0.05	-0.31	0.31
Oesterle R1	-0.04	-0.04	-0.03	0.06	0.07	0.07
Oesterle R2					0.14	0.14
Oesterle B6	0.33	-0.33	0.09	0.09	-0.59	0.62
Oesterle B7	0.28	-0.28	0.06	0.06	0.23	0.26
Oesterle B8	0.29	-0.29	0.06	0.06	0.17	0.29
Oesterle B9	0.25	-0.25	0.05	0.05	-0.14	0.32
Oesterle B10	0.23	-0.23	0.04	0.04	0.22	0.22
Pilakoutas SW4	0.55	-0.55	0.15	0.15	0.36	0.36
Pilakoutas SW5					0.19	0.19
Pilakoutas SW6	0.61	-0.61	0.15	0.15	0.17	0.17
Pilakoutas SW7	0.88	-0.88	0.19	0.19	0.20	0.20
Pilakoutas SW8	0.54	-0.54	0.14	0.14	0.15	0.15
Pilakoutas SW9	0.56	-0.56	0.15	0.15	0.16	0.16
Salonikios LSW1					0.24	0.24
Salonikios LSW2					0.21	0.21
Salonikios LSW3					0.17	0.17
Salonikios MSW1					0.30	0.38
Salonikios MSW2					0.27	0.27
Salonikios MSW3					0.19	0.19
Salonikios MSW6					0.28	0.28

Table 7.4: Difference of Bar-Slip Model Prediction Results to Flexural Model (cont.)

Objective	k_{sec}, k/in		Δ_y, in		Δ_{max}, in	
Name	*Absolute*	*Relative*	*Absolute*	*Relative*	*Absolute*	*Relative*
Sittipunt W1					0.28	0.28
Sittipunt W2					0.28	0.35
Tasnimi SHW1					-0.51	0.51
Tasnimi SHW2					-0.76	0.76
Tasnimi SHW3					-0.63	0.63
Tasnimi SHW4					-0.45	0.45
Thomsen RW1	0.25	-0.25	0.05	0.05	0.08	0.08
Thomsen RW2	0.21	-0.21	0.04	0.04	0.12	0.12
Vallenas SW3	0.54	-0.54	0.04	0.04	0.07	0.07
Vallenas SW4	0.54	-0.54	0.04	0.04	0.15	0.15
Vallenas SW5	0.37	-0.37	0.07	0.07	0.16	0.16
Vallenas SW6	0.40	-0.40	0.07	0.07	0.25	0.25
Wang SW1	0.24	-0.24	0.07	0.07	0.05	0.05
Wang SW2	0.22	-0.22	0.07	0.07	0.06	0.06
Yanez S1					0.24	0.24
Zhang SW7	0.52	-0.52	0.24	0.24	0.09	0.09
Zhang SW8	0.18	-0.54	0.24	0.44	0.12	0.12
Zhang SW9	0.66	-0.66	0.15	0.15	0.09	0.09
Average	0.46	-0.47	0.11	0.12	0.08	0.21
St. Dev.	0.33	0.32	0.07	0.08	0.23	0.15
COV	0.72	-0.68	0.62	0.69	2.74	0.71

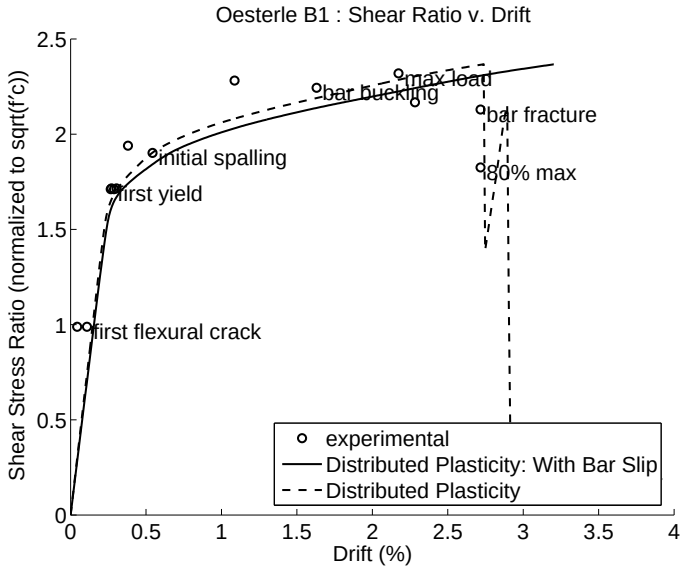

Figure 7.5: Pushover of Beam-Column Element with Bar-Slip – Oesterle B1

7.2.4 Typical Response Curves of Bar-Slip Model

Figure 7.5 shows that for the flexurally responding specimen, Oesterle B1, the addition of the bar-slip model has little impact on the response up to yield. After yield, however, the analysis gains additional flexibility, resulting in the increased maximum displacement predicted. While not seen in the figure, the concrete strain limit is exceeded just prior to the maximum drift level observed experimentally, resulting in a maximum displacement prediction ratio of 0.98.

Similarly, the addition of bar-slip to the beam-column element does not alter the results significantly for the wall exhibiting shear-flexure behavior, Oesterle B6. This is illustrated in Figure 7.6. The maximum displacement is over-predicted significantly.

The example wall chosen to illustrate shear behavior, Pilakoutas SW7, demonstrates more added flexibility prior to yield than Oesterle B1 and Oesterle B6. Its response curve is shown in Figure 7.7. The predicted maximum displacement is significantly increased compared to the element without bar-slip.

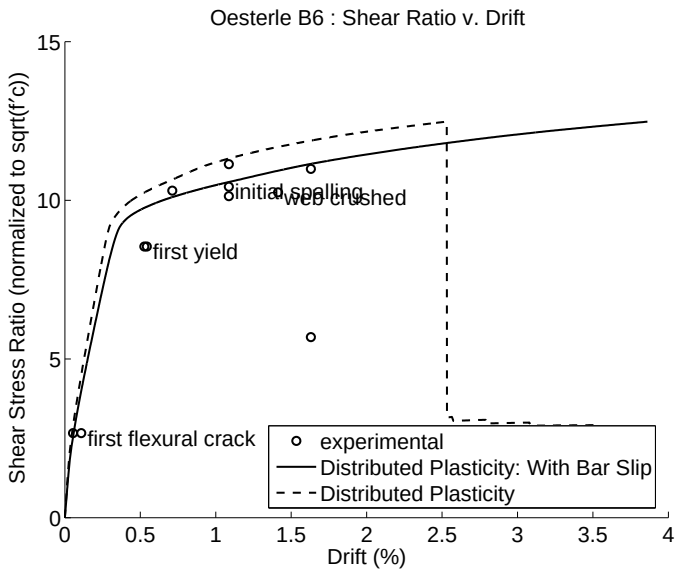

Figure 7.6: Pushover of Beam-Column Element with Bar-Slip – Oesterle B6

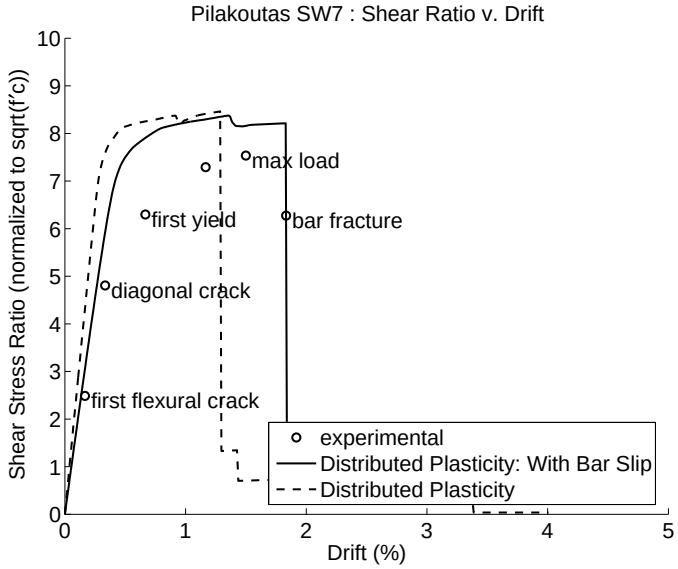

Figure 7.7: Pushover of Beam-Column Element with Bar-Slip – Pilakoutas SW7

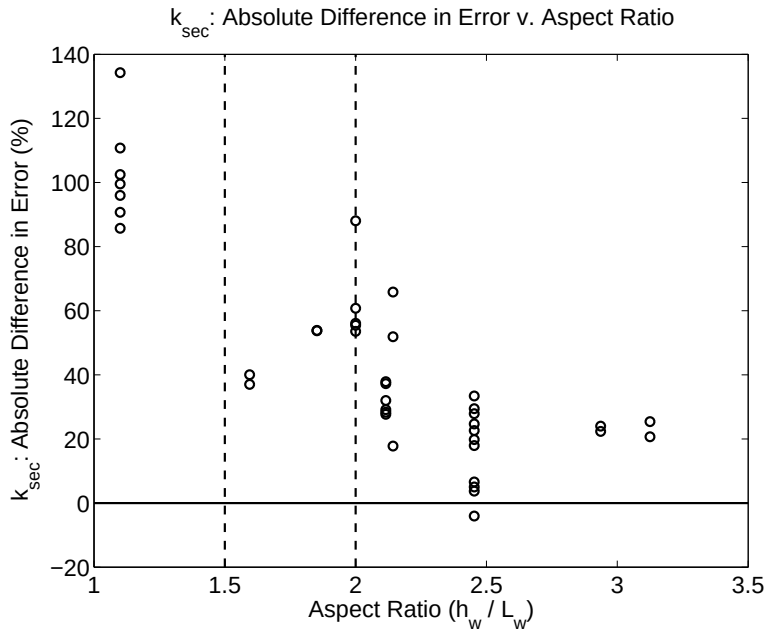

Figure 7.8: Initial Stiffness Absolute Difference in Error v. Aspect Ratio Using Beam-Column Element with Bar-Slip Enhancement

7.2.5 Effect of Bar-Slip on Secant Stiffness and Yield Displacement Prediction

The average error for the prediction of secant stiffness is improved by 46%. For all but one of the walls, the secant stiffness values were over-predicted by the basic flexural beam-column element. The average ratio of predicted to observed secant stiffness is 1.69 with the inclusion of the bar-slip model. This indicates that the quality of the model's prediction is improved, but that it is stiffer than the measured response.

Comparison plots of the absolute difference in error prediction versus engineering design parameters reveal that inclusion of bar-slip in the model improves the prediction of secant stiffness the most in walls with low aspect ratios (Figure 7.8) and walls with larger reinforcement ratios (Figure 7.9). Seven data points do not follow this trend in the longitudinal reinforcement ratio plot, but they can be correlated to the seven walls with an aspect ratio approaching 1 in the aspect ratio plot. Other engineering design parameters do not reveal a strong trend regarding the improvement of secant stiffness.

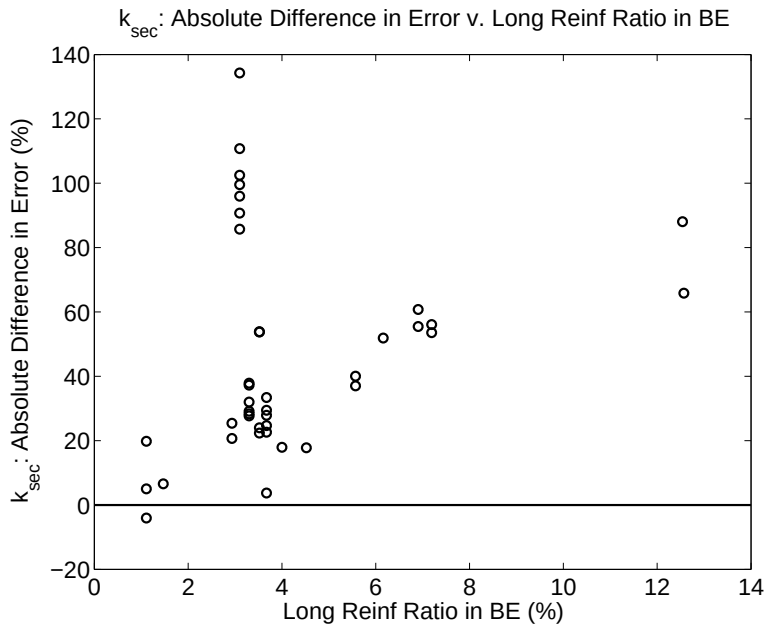

Figure 7.9: Initial Stiffness Absolute Difference in Error v. Longitudinal Reinforcement Ratio in BE Using Beam-Column Element with Bar-Slip Enhancement

The improved prediction of secant stiffness corresponds with improved predictions of yield displacement. The same trends are relevant for yield displacement with regard to the engineering design parameters, with the exception that the magnitudes of prediction improvement are not as high. The average improvement of prediction error is 11% for yield displacement.

7.2.6 Effect of Bar-Slip on Maximum Displacement Prediction

The addition of bar-slip to the flexural model increased the average maximum displacement predicted by 22%. This corresponds to an 8% improvement of the average prediction. Trends between the increase in ability to predict maximum displacement and engineering design parameters, like aspect ratio and longitudinal reinforcement ratio,Figures 7.10 & 7.11, are less identifiable than in the response quantities measured at yield.

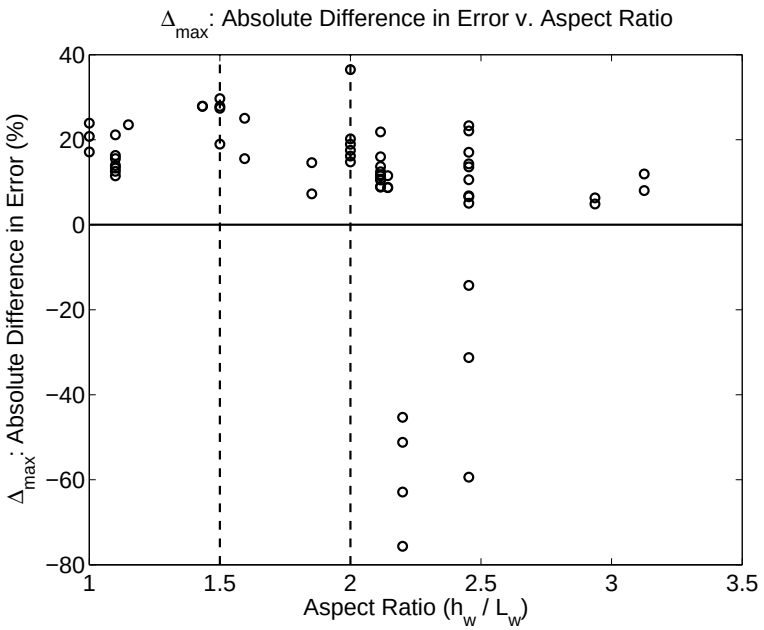

Figure 7.10: Maximum Displacement Absolute Difference in Error v. Aspect Ratio Using Beam-Column Element with Bar-Slip Enhancement

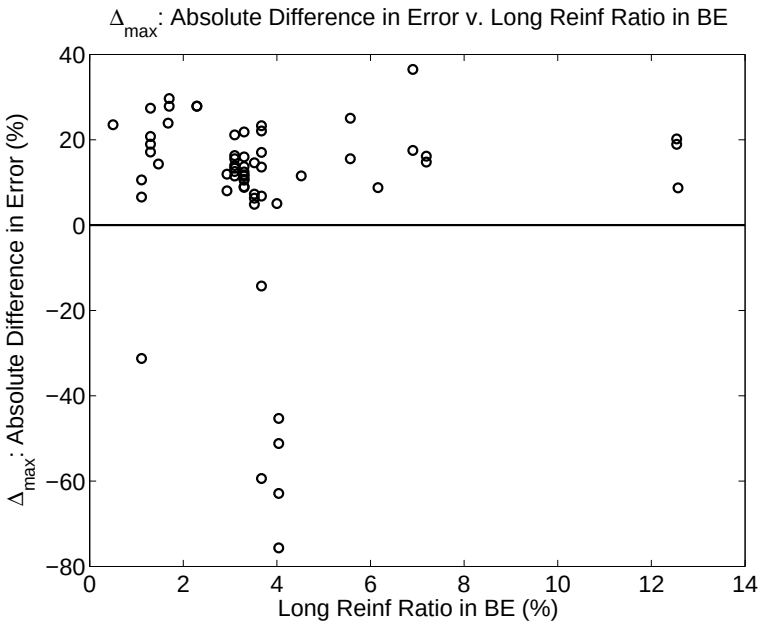

Figure 7.11: Maximum Displacement Absolute Difference in Error v. Longitudinal Reinforcement Ratio in BE Using Beam-Column Element with Bar-Slip Enhancement

7.3 Elastic Shear Model

The elastic shear model accounts for wall flexibility resulting from shear deformations. This model does not account for degradation of strength or stiffness of the wall that can result from inadequate shear strength. First, the theoretical model is explained. Then, the implementation of the model is described. The results are evaluated in depth by comparing the three walls that differ in their shear stress demand. Finally, the tabulated results for all of the compiled experimental walls are discussed.

7.3.1 Theoretical Model and Implementation

Elastic theory states that the contribution of shear to displacement, Δ_v, for a cantilevered, prismatic element subjected to a point load is

$$\Delta_v = \frac{f_s V L}{G A_g} \tag{7.15}$$

where f_s is the form factor for shear ($f_s = 6/5$ for rectangular sections), V is the applied shear force, L is the length of the cantilever, G is the elastic shear modulus, and A_g is the gross cross-sectional area of the member.

For reinforced concrete, the elastic shear modulus, G, is assumed to be proportional to the elastic modulus of the plain concrete,

$$G = \alpha E_c \tag{7.16}$$

where α is a proportional constant for elastic shear response and E_c is the elastic modulus of concrete, assumed to be

$$E_c = 57000\sqrt{f'_c} \quad (psi \text{ units}) \tag{7.17}$$

as recommended by ACI 318 (2002). Using elastic theory, assuming isotropy, and approximating the Poisson's ratio of concrete as 0.25, Park and Paulay (1975) recommend $\alpha = 0.4$.

This effect is added to the flexural beam-column model using the aggregator function in OpenSees (Mazzoni et al. 2006). The results are shown in Tables 7.5 & 7.6. The differences

in results from the flexural model are summarized in Tables 7.7 & 7.8.

Table 7.5: Elastic Shear Model Prediction Results

Objective	k_{sec}, k/in		Δ_y, in		Δ_{max}, in	
Name	*Obs.*	*Pred./Obs.*	*Obs.*	*Pred./Obs.*	*Obs.*	*Pred./Obs.*
Lefas SW30					0.82	0.50
Lefas SW31					0.87	0.47
Lefas SW32					0.96	0.44
Lefas SW33					0.98	0.42
Lefas SW11	270.6	2.66	0.14	0.33	0.32	0.51
Lefas SW12	413.8	2.34	0.11	0.44	0.35	0.33
Lefas SW13	374.0	2.44	0.15	0.38	0.35	0.27
Lefas SW14	249.1	2.69	0.15	0.32	0.44	0.33
Lefas SW15	415.3	2.02	0.11	0.46	0.32	0.37
Lefas SW16	617.2	1.76	0.10	0.55	0.23	0.39
Lefas SW17	212.5	3.29	0.15	0.31	0.42	0.37
Lefas SW21	78.7	1.38	0.23	0.60	0.81	0.50
Lefas SW22	128.0	1.19	0.19	0.70	0.60	0.50
Lefas SW23	131.9	1.30	0.20	0.70	0.52	0.47
Lefas SW24	73.4	1.54	0.25	0.55	0.71	0.57
Lefas SW25	126.6	1.28	0.23	0.62	0.37	0.67
Lefas SW26	70.5	1.43	0.22	0.66	0.82	0.47
Oesterle B1	90.2	1.04	0.50	0.79	6.00	0.84
Oesterle B2	135.6	1.84	0.90	0.46	5.00	0.49
Oesterle B3	92.0	1.02	0.50	0.78	8.00	0.67
Oesterle B4	92.0	1.01	0.50	0.80	13.00	0.38
Oesterle B5	138.9	1.75	0.90	0.51	5.00	1.04
Oesterle R1	50.0	0.73	0.45	1.00	9.00	0.50
Oesterle R2					6.00	0.80
Oesterle B6	147.0	1.74	1.00	0.55	3.00	1.02
Oesterle B7	170.0	2.00	1.00	0.47	6.00	0.77
Oesterle B8	166.0	1.97	1.00	0.47	6.00	0.79
Oesterle B9	192.5	1.74	1.20	0.38	5.30	0.93
Oesterle B10	157.3	1.75	1.10	0.35	5.75	0.65
Pilakoutas SW4	78.6	2.02	0.24	0.52	0.94	0.59
Pilakoutas SW5					1.02	0.33
Pilakoutas SW6	71.4	2.25	0.24	0.51	0.94	0.31
Pilakoutas SW7	76.0	2.39	0.31	0.44	0.87	0.61
Pilakoutas SW8	76.2	2.23	0.24	0.55	1.02	0.37
Pilakoutas SW9	75.4	2.18	0.24	0.56	1.02	0.38
Salonikios LSW1					1.26	0.31
Salonikios LSW2					1.26	0.32
Salonikios LSW3					1.26	0.27
Salonikios MSW1					1.26	0.68
Salonikios MSW2					1.26	0.68
Salonikios MSW3					1.26	0.55
Salonikios MSW6					1.26	0.65

Table 7.6: Elastic Shear Model Prediction Results (cont.)

Objective	k_{sec}, k/in		Δ_y, in		Δ_{max}, in	
Name	*Obs.*	*Pred./Obs.*	*Obs.*	*Pred./Obs.*	*Obs.*	*Pred./Obs.*
Sittipunt W1					1.77	0.60
Sittipunt W2					1.34	0.72
Tasnimi SHW1					0.67	1.62
Tasnimi SHW2					0.45	2.39
Tasnimi SHW3					0.61	1.77
Tasnimi SHW4					0.75	1.53
Thomsen RW1	27.8	2.10	1.08	0.40	3.60	0.60
Thomsen RW2	27.8	1.96	1.08	0.39	3.60	0.84
Vallenas SW3	285.1	2.75	0.71	0.29	6.65	0.28
Vallenas SW4	285.8	2.74	0.71	0.29	3.58	0.52
Vallenas SW5	337.7	1.92	0.47	0.43	3.18	0.47
Vallenas SW6	312.1	2.07	0.53	0.39	1.98	0.75
Wang SW1	272.9	1.39	0.70	0.42	4.25	0.16
Wang SW2	288.6	1.32	0.70	0.42	2.90	0.24
Yanez S1					2.76	0.24
Zhang SW7	166.6	1.54	0.23	0.65	1.23	0.26
Zhang SW8	195.4	1.22	0.22	0.74	0.94	0.21
Zhang SW9	174.2	2.13	0.33	0.48	1.24	0.26
Average	–	1.85	–	0.52	–	0.60
St. Dev.	–	0.57	–	0.16	–	0.40
COV	–	0.31	–	0.31	–	0.66

Table 7.7: Difference of Elastic Shear Model Prediction Results to Flexural Model

Objective	k_{sec}, k/in		Δ_y, in		Δ_{max}, in	
Name	*Absolute*	*Relative*	*Absolute*	*Relative*	*Absolute*	*Relative*
Lefas SW30					0.02	0.02
Lefas SW31					0.01	0.01
Lefas SW32					0.01	0.01
Lefas SW33					0.01	0.01
Lefas SW11	0.64	-0.64	0.06	0.06	0.05	0.05
Lefas SW12	0.80	-0.80	0.11	0.11	0.05	0.05
Lefas SW13	0.96	-0.96	0.11	0.11	0.04	0.04
Lefas SW14	0.69	-0.69	0.07	0.07	0.03	0.03
Lefas SW15	0.67	-0.67	0.11	0.11	0.06	0.06
Lefas SW16	0.73	-0.73	0.16	0.16	0.08	0.08
Lefas SW17	0.81	-0.81	0.06	0.06	0.03	0.03
Lefas SW21	0.10	-0.10	0.04	0.04	0.01	0.01
Lefas SW22	0.11	-0.11	0.06	0.06	0.02	0.02
Lefas SW23	0.14	-0.14	0.07	0.07	0.03	0.03
Lefas SW24	0.11	-0.11	0.04	0.04	0.01	0.01
Lefas SW25	0.14	-0.14	0.06	0.06	0.04	0.04
Lefas SW26	0.11	-0.11	0.05	0.05	0.01	0.01
Oesterle B1	0.04	-0.04	0.03	0.03	0.00	0.00
Oesterle B2	0.18	-0.18	0.04	0.04	0.01	0.01
Oesterle B3	0.04	-0.04	0.03	0.03	0.00	0.00
Oesterle B4	0.04	-0.04	0.03	0.03	0.00	0.00
Oesterle B5	0.19	-0.19	0.05	0.05	-0.01	0.01
Oesterle R1	-0.01	-0.01	0.01	0.01	0.00	0.00
Oesterle R2					0.00	0.00
Oesterle B6	0.30	-0.30	0.08	0.08	-0.01	0.04
Oesterle B7	0.30	-0.30	0.06	0.06	0.01	0.01
Oesterle B8	0.31	-0.31	0.06	0.06	0.02	0.02
Oesterle B9	0.27	-0.27	0.05	0.05	0.02	0.02
Oesterle B10	0.21	-0.21	0.04	0.04	0.01	0.01
Pilakoutas SW4	0.22	-0.22	0.05	0.05	0.02	0.02
Pilakoutas SW5					0.02	0.02
Pilakoutas SW6	0.24	-0.24	0.05	0.05	0.01	0.01
Pilakoutas SW7	0.32	-0.32	0.05	0.05	0.02	0.02
Pilakoutas SW8	0.23	-0.23	0.05	0.05	0.02	0.02
Pilakoutas SW9	0.24	-0.24	0.05	0.05	0.01	0.01
Salonikios LSW1					0.02	0.02
Salonikios LSW2					0.01	0.01
Salonikios LSW3					0.01	0.01
Salonikios MSW1					0.02	0.02
Salonikios MSW2					0.01	0.01
Salonikios MSW3					0.01	0.01
Salonikios MSW6					0.02	0.02

Table 7.8: Difference of Elastic Shear Model Prediction Results to Flexural Model (cont.)

Objective	k_{sec}, k/in		Δ_y, in		Δ_{max}, in	
Name	*Absolute*	*Relative*	*Absolute*	*Relative*	*Absolute*	*Relative*
Sittipunt W1					0.02	0.02
Sittipunt W2					0.03	0.03
Tasnimi SHW1					-0.01	0.01
Tasnimi SHW2					-0.01	0.01
Tasnimi SHW3					-0.01	0.01
Tasnimi SHW4					-0.03	0.03
Thomsen RW1	0.08	-0.08	0.01	0.01	0.00	0.00
Thomsen RW2	0.06	-0.06	0.01	0.01	-0.03	-0.03
Vallenas SW3	0.62	-0.62	0.05	0.05	0.00	0.00
Vallenas SW4	0.62	-0.62	0.05	0.05	0.02	0.02
Vallenas SW5	0.30	-0.30	0.06	0.06	0.02	0.02
Vallenas SW6	0.32	-0.32	0.05	0.05	0.02	0.02
Wang SW1	0.16	-0.16	0.04	0.04	0.01	0.01
Wang SW2	0.15	-0.15	0.04	0.04	0.01	0.01
Yanez S1					0.00	0.00
Zhang SW7	0.20	-0.20	0.07	0.07	-0.02	-0.02
Zhang SW8	0.14	-0.14	0.07	0.07	0.02	0.02
Zhang SW9	0.37	-0.37	0.07	0.07	0.02	0.02
Average	0.30	-0.30	0.06	0.06	0.01	0.02
St. Dev.	0.25	0.25	0.03	0.03	0.02	0.02
COV	0.83	-0.83	0.50	0.50	1.36	0.97

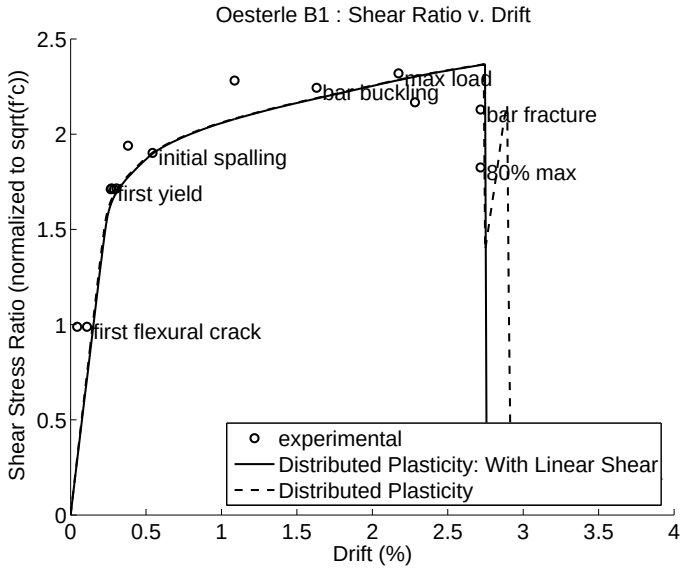

Figure 7.12: Pushover of Beam-Column Element with Elastic Shear – Oesterle B1

7.3.2 Typical Response Curves of Elastic Shear Model

There is relatively no change in the load-displacement response of Oesterle B1, as shown in Figure 7.12. Oesterle B6 exhibits slightly more flexibility with the added shear deformation. In Figure 7.13, the elastic component of shear is shown to add a small amount of displacement for a given load. The same is seen in Figure 7.14 for Pilakoutas SW7. The addition of elastic shear has little effect.

7.3.3 Effect of Elastic Shear on Prediction of Displacements

The inclusion of elastic shear effects does not improve the displacement prediction results greatly. The absolute change in error is 6% for yield displacement and 1% for maximum displacement.

7.4 Calibration of the Elastic Effective Shear Modulus Model

Previous research indicates that shearing deformation can contribute significantly to the response of structural walls. To better approximate this effect, the elastic shear modulus

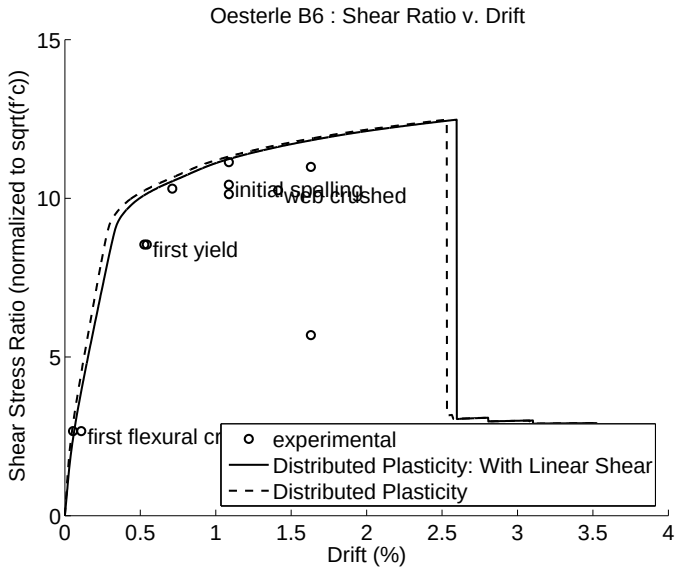

Figure 7.13: Pushover of Beam-Column Element with Elastic Shear – Oesterle B6

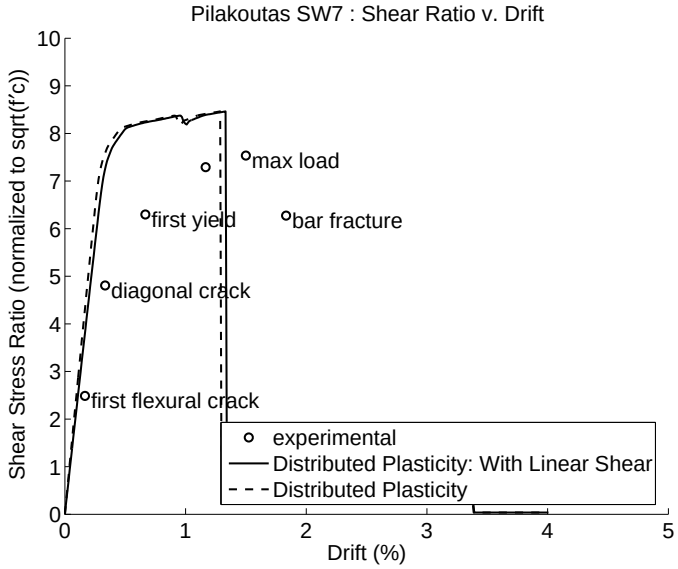

Figure 7.14: Pushover of Beam-Column Element with Elastic Shear – Pilakoutas SW7

was reduced to better approximate this flexibility.

7.4.1 Method

The elastic effective modulus model was calibrated for prediction of yield and maximum displacements for the beam-column element with and without the bar-slip component. For each case, a value for α, in Equation 7.16, was determined to minimize the average prediction error for the specified displacement response quantity. The sixty walls described in Section 2.1, for which reported values of the response quantities were under-predicted using the basic flexural beam-column model were used to calibrate the model.

A search routine was employed to determine the value of α such that the sum of the displacement errors was zero. To do this, the preprocessor described in Chapter 3 was altered to run in conjunction with the MATLAB Optimization Toolbox (2005).

7.4.2 Calibrated Parameters

The calibrated parameters for the elastic effective shear model are shown in Table 7.9. The four calibrated α parameters were defined as:

- α_{Δ_y} was calibrated for prediction of yield displacement without the bar-slip component,
- $\alpha_{\Delta_{max}}$ was calibrated for prediction of maximum displacement without the bar-slip component,
- $\alpha_{\Delta_y,slip}$ was calibrated for prediction of yield displacement with the bar-slip component, and
- $\alpha_{\Delta_{max},slip}$ was calibrated for prediction of maximum displacement with the bar-slip component.

The results of the analyses using the calibrated parameters for each of the walls are shown in Tables 7.10–7.15. Shear stress ratio versus drift plots of each of the experimental

Table 7.9: Calibrated α's for Elastic Effective Shear Model

Calibrated To	*No Bar-Slip*	*With Bar-Slip*
Δ_y	0.0423	0.0541
Δ_{max}	0.0180	0.0223

walls analyzed using each of the calibrated parameters are in Appendix M. The change in the error of the prediction objective quantities from the flexural beam-column analysis method for each of the experimental walls using each of the calibrated parameters is shown in Tables 7.16– 7.23. Plots comparing the change in error of the predicted objective quantities compared to design parameters are in Appendix N.

Table 7.10: Elastic Effective Shear Model Analysis Results

Objective	k_{sec}, k/in			Δ_y, in			Δ_{max}, in		
Shear Coefficient Name	*Obs.*	α_{Δ_y} *Pred./Obs.*	$\alpha_{\Delta_{max}}$ *Pred./Obs.*	*Obs.*	α_{Δ_y} *Pred./Obs.*	$\alpha_{\Delta_{max}}$ *Pred./Obs.*	*Obs.*	α_{Δ_y} *Pred./Obs.*	$\alpha_{\Delta_{max}}$ *Pred./Obs.*
Lefas SW30							0.82	0.63	0.85
Lefas SW31							0.87	0.59	0.78
Lefas SW32							0.96	0.53	0.67
Lefas SW33							0.98	0.52	0.66
Lefas SW11	270.6	1.01	0.52	0.14	0.88	1.71	0.32	0.87	1.42
Lefas SW12	413.8	0.74	0.36	0.11	1.38	2.81	0.35	0.71	1.34
Lefas SW13	374.0	0.72	0.35	0.15	1.27	2.62	0.35	0.73	1.45
Lefas SW14	249.1	0.99	0.51	0.15	0.87	1.71	0.44	0.62	1.07
Lefas SW15	415.3	0.65	0.32	0.11	1.43	2.89	0.32	0.80	1.51
Lefas SW16	617.2	0.51	0.24	0.10	1.93	4.01	0.23	1.11	2.21
Lefas SW17	212.5	1.23	0.64	0.15	0.84	1.63	0.42	0.66	1.09
Lefas SW21	78.7	0.88	0.57	0.23	0.94	1.46	0.81	0.64	0.85
Lefas SW22	128.0	0.69	0.42	0.19	1.21	1.97	0.60	0.70	1.02
Lefas SW23	131.9	0.70	0.41	0.20	1.29	2.18	0.52	0.73	1.15
Lefas SW24	73.4	0.99	0.64	0.25	0.85	1.31	0.71	0.72	0.95
Lefas SW25	126.6	0.70	0.41	0.23	1.15	1.94	0.37	1.05	1.61
Lefas SW26	70.5	0.88	0.56	0.22	1.06	1.67	0.82	0.63	0.86
Oesterle B1	90.2	0.80	0.60	0.50	1.02	1.36	6.00	0.87	0.93
Oesterle B2	135.6	1.04	0.63	0.90	0.81	1.35	5.00	0.57	0.69
Oesterle B3	92.0	0.78	0.57	0.50	1.02	1.38	8.00	0.70	0.75
Oesterle B4	92.0	0.77	0.57	0.50	1.05	1.43	13.00	0.40	0.43

Table 7.11: Elastic Effective Shear Model Analysis Results (cont.)

Objective	k_{sec}, k/in			Δ_y, in			Δ_{max}, in		
Shear Coefficient Name	*Obs.*	α_{Δ_y} *Pred./Obs.*	$\alpha_{\Delta_{max}}$ *Pred./Obs.*	*Obs.*	α_{Δ_y} *Pred./Obs.*	$\alpha_{\Delta_{max}}$ *Pred./Obs.*	*Obs.*	α_{Δ_y} *Pred./Obs.*	$\alpha_{\Delta_{max}}$ *Pred./Obs.*
Oesterle B5	138.9	0.96	0.57	0.90	0.93	1.56	5.00	1.16	1.35
Oesterle R1	50.0	0.65	0.56	0.45	1.13	1.31	9.00	0.51	0.53
Oesterle R2							6.00	0.83	0.87
Oesterle B6	147.0	0.78	0.42	1.00	1.22	2.25	3.00	1.35	1.84
Oesterle B7	170.0	0.95	0.53	1.00	0.98	1.75	6.00	0.90	1.09
Oesterle B8	166.0	0.92	0.51	1.00	1.02	1.84	6.00	0.93	1.13
Oesterle B9	192.5	0.81	0.45	1.20	0.80	1.45	5.30	1.07	1.30
Oesterle B10	157.3	0.91	0.53	1.10	0.68	1.17	5.75	0.74	0.87
Pilakoutas SW4	78.6	1.11	0.66	0.24	0.94	1.59	0.94	0.74	0.98
Pilakoutas SW5							1.02	0.50	0.76
Pilakoutas SW6	71.4	1.24	0.74	0.24	0.93	1.56	0.94	0.45	0.66
Pilakoutas SW7	76.0	1.19	0.68	0.31	0.89	1.56	0.87	0.81	1.12
Pilakoutas SW8	76.2	1.25	0.75	0.24	0.97	1.62	1.02	0.51	0.72
Pilakoutas SW9	75.4	1.20	0.71	0.24	1.02	1.72	1.02	0.54	0.76
Salonikios LSW1							1.26	0.43	0.61
Salonikios LSW2							1.26	0.41	0.54
Salonikios LSW3							1.26	0.38	0.55
Salonikios MSW1							1.26	0.80	0.99
Salonikios MSW2							1.26	0.75	0.88
Salonikios MSW3							1.26	0.65	0.81
Salonikios MSW6							1.26	0.77	0.94

Table 7.12: Elastic Effective Shear Model Analysis Results (cont.)

Objective	k_{sec}, k/in			Δ_y, in			Δ_{max}, in		
Shear Coefficient Name	*Obs.*	α_{Δ_y} *Pred./Obs.*	$\alpha_{\Delta_{max}}$ *Pred./Obs.*	*Obs.*	α_{Δ_y} *Pred./Obs.*	$\alpha_{\Delta_{max}}$ *Pred./Obs.*	*Obs.*	α_{Δ_y} *Pred./Obs.*	$\alpha_{\Delta_{max}}$ *Pred./Obs.*
Sittipunt W1							1.77	0.77	1.03
Sittipunt W2							1.34	0.96	1.31
Tasnimi SHW1							0.67	1.71	2.09
Tasnimi SHW2							0.45	2.53	3.09
Tasnimi SHW3							0.61	1.84	1.94
Tasnimi SHW4							0.75	1.61	1.64
Thomsen RW1	27.8	1.62	1.20	1.08	0.52	0.70	3.60	0.65	0.72
Thomsen RW2	27.8	1.54	1.17	1.08	0.50	0.66	3.60	0.92	0.99
Vallenas SW3	285.1	1.08	0.56	0.71	0.75	1.43	6.65	0.35	0.46
Vallenas SW4	285.8	1.07	0.56	0.71	0.75	1.43	3.58	0.65	0.86
Vallenas SW5	337.7	0.89	0.50	0.47	0.92	1.66	3.18	0.58	0.74
Vallenas SW6	312.1	0.97	0.54	0.53	0.83	1.49	1.98	0.93	1.20
Wang SW1	272.9	0.74	0.44	0.70	0.78	1.33	4.25	0.24	0.35
Wang SW2	288.6	0.71	0.42	0.70	0.77	1.31	2.90	0.35	0.51
Yanez S1							2.76	0.28	0.32
Zhang SW7	166.6	0.79	0.46	0.23	1.26	2.18	1.23	0.41	0.57
Zhang SW8	195.4	0.66	0.39	0.22	1.36	2.30	0.94	0.35	0.58
Zhang SW9	174.2	0.94	0.51	0.33	1.08	1.98	1.24	0.45	0.69
Average	–	0.93	0.55	–	1.00	1.73	–	0.76	1.01
St. Dev.	–	0.24	0.19	–	0.26	0.60	–	0.40	0.50
COV	–	0.26	0.33	–	0.26	0.34	–	0.52	0.49

Table 7.13: Elastic Effective Shear Model With Bar-Slip Analysis Results

Objective	k_{sec}, k/in			Δ_y, in			Δ_{max}, in		
Shear Coefficient Name	*Obs.*	$\alpha_{\Delta_y,slip}$ *Pred./Obs.*	$\alpha_{\Delta_{max},slip}$ *Pred./Obs.*	*Obs.*	$\alpha_{\Delta_y,slip}$ *Pred./Obs.*	$\alpha_{\Delta_{max},slip}$ *Pred./Obs.*	*Obs.*	$\alpha_{\Delta_y,slip}$ *Pred./Obs.*	$\alpha_{\Delta_{max},slip}$ *Pred./Obs.*
Lefas SW30							0.82	0.72	0.90
Lefas SW31							0.87	0.67	0.83
Lefas SW32							0.96	0.59	0.72
Lefas SW33							0.98	0.58	0.70
Lefas SW11	270.6	1.06	0.58	0.14	0.84	1.52	0.32	0.94	1.38
Lefas SW12	413.8	0.78	0.41	0.11	1.31	2.49	0.35	0.76	1.27
Lefas SW13	374.0	0.75	0.39	0.15	1.23	2.34	0.35	0.76	1.36
Lefas SW14	249.1	1.03	0.57	0.15	0.84	1.53	0.44	0.67	1.04
Lefas SW15	415.3	0.68	0.36	0.11	1.37	2.57	0.32	0.85	1.44
Lefas SW16	617.2	0.53	0.27	0.10	1.85	3.57	0.23	1.15	2.07
Lefas SW17	212.5	1.29	0.71	0.15	0.80	1.45	0.42	0.71	1.06
Lefas SW21	78.7	0.84	0.59	0.23	0.98	1.41	0.81	0.71	0.89
Lefas SW22	128.0	0.66	0.44	0.19	1.26	1.89	0.60	0.80	1.05
Lefas SW23	131.9	0.66	0.43	0.20	1.37	2.10	0.52	0.83	1.17
Lefas SW24	73.4	0.95	0.66	0.25	0.89	1.27	0.71	0.81	1.00
Lefas SW25	126.6	0.66	0.43	0.23	1.22	1.87	0.37	1.17	1.65
Lefas SW26	70.5	0.84	0.58	0.22	1.12	1.62	0.82	0.71	0.90
Oesterle B1	90.2	0.81	0.63	0.50	1.01	1.30	6.00	1.01	1.05
Oesterle B2	135.6	1.10	0.70	0.90	0.77	1.21	5.00	0.60	0.70
Oesterle B3	92.0	0.79	0.61	0.50	1.01	1.31	8.00	0.80	0.84
Oesterle B4	92.0	0.78	0.60	0.50	1.05	1.36	13.00	0.47	0.48

Table 7.14: Elastic Effective Shear Model With Bar-Slip Analysis Results (cont.)

Objective	k_{sec}, k/in			Δ_y, in			Δ_{max}, in		
Shear Coefficient Name	*Obs.*	$\alpha_{\Delta_y,slip}$ *Pred./Obs.*	$\alpha_{\Delta_{max},slip}$ *Pred./Obs.*	*Obs.*	$\alpha_{\Delta_y,slip}$ *Pred./Obs.*	$\alpha_{\Delta_{max},slip}$ *Pred./Obs.*	*Obs.*	$\alpha_{\Delta_y,slip}$ *Pred./Obs.*	$\alpha_{\Delta_{max},slip}$ *Pred./Obs.*
Oesterle B5	138.9	1.02	0.64	0.90	0.88	1.40	5.00	1.44	1.44
Oesterle R1	50.0	0.63	0.56	0.45	1.15	1.31	9.00	0.57	0.59
Oesterle R2							6.00	0.95	0.99
Oesterle B6	147.0	0.83	0.48	1.00	1.15	1.99	3.00	1.89	2.30
Oesterle B7	170.0	1.02	0.60	1.00	0.91	1.55	6.00	1.12	1.20
Oesterle B8	166.0	0.99	0.58	1.00	0.95	1.62	6.00	1.18	1.20
Oesterle B9	192.5	0.88	0.51	1.20	0.74	1.28	5.30	1.36	1.36
Oesterle B10	157.3	0.96	0.59	1.10	0.64	1.05	5.75	0.94	1.05
Pilakoutas SW4	78.6	1.06	0.69	0.24	0.99	1.53	0.94	1.07	1.27
Pilakoutas SW5							1.02	0.65	0.86
Pilakoutas SW6	71.4	1.18	0.77	0.24	0.98	1.50	0.94	0.60	0.77
Pilakoutas SW7	76.0	1.09	0.70	0.31	0.97	1.52	0.87	1.00	1.26
Pilakoutas SW8	76.2	1.21	0.79	0.24	1.01	1.54	1.02	0.62	0.79
Pilakoutas SW9	75.4	1.15	0.75	0.24	1.06	1.64	1.02	0.66	0.85
Salonikios LSW1							1.26	0.64	0.80
Salonikios LSW2							1.26	0.59	0.71
Salonikios LSW3							1.26	0.53	0.67
Salonikios MSW1							1.26	1.15	1.30
Salonikios MSW2							1.26	1.01	1.11
Salonikios MSW3							1.26	0.82	0.95
Salonikios MSW6							1.26	1.02	1.16

Table 7.15: Elastic Effective Shear Model With Bar-Slip Analysis Results (cont.)

Objective	k_{sec}, k/in			Δ_y, in			Δ_{max}, in		
Shear Coefficient Name	*Obs.*	$\alpha_{\Delta_y,slip}$ *Pred./Obs.*	$\alpha_{\Delta_{max},slip}$ *Pred./Obs.*	*Obs.*	$\alpha_{\Delta_y,slip}$ *Pred./Obs.*	$\alpha_{\Delta_{max},slip}$ *Pred./Obs.*	*Obs.*	$\alpha_{\Delta_y,slip}$ *Pred./Obs.*	$\alpha_{\Delta_{max},slip}$ *Pred./Obs.*
Sittipunt W1							1.77	1.00	1.22
Sittipunt W2							1.34	1.24	1.54
Tasnimi SHW1							0.67	2.18	2.26
Tasnimi SHW2							0.45	3.22	3.34
Tasnimi SHW3							0.61	2.38	2.46
Tasnimi SHW4							0.75	1.92	2.07
Thomsen RW1	27.8	1.55	1.22	1.08	0.54	0.69	3.60	0.72	0.78
Thomsen RW2	27.8	1.49	1.19	1.08	0.51	0.65	3.60	1.03	1.09
Vallenas SW3	285.1	1.18	0.64	0.71	0.68	1.25	6.65	0.41	0.50
Vallenas SW4	285.8	1.18	0.64	0.71	0.68	1.25	3.58	0.77	0.94
Vallenas SW5	337.7	0.94	0.55	0.47	0.87	1.48	3.18	0.70	0.84
Vallenas SW6	312.1	1.02	0.60	0.53	0.79	1.33	1.98	1.13	1.35
Wang SW1	272.9	0.76	0.48	0.70	0.76	1.21	4.25	0.26	0.36
Wang SW2	288.6	0.73	0.46	0.70	0.75	1.20	2.90	0.39	0.53
Yanez S1							2.76	0.60	0.18
Zhang SW7	166.6	0.74	0.47	0.23	1.35	2.12	1.23	0.47	0.60
Zhang SW8	195.4	0.55	0.37	0.22	1.65	2.43	0.94	0.44	0.63
Zhang SW9	174.2	0.95	0.56	0.33	1.08	1.82	1.24	0.48	0.69
Average	–	0.93	0.59	–	1.00	1.60	–	0.92	1.11
St. Dev.	–	0.24	0.18	–	0.28	0.54	–	0.51	0.55
COV	–	0.25	0.31	–	0.28	0.33	–	0.55	0.50

Table 7.16: Difference of Effective Shear Calibrated to Yield Displacement Model Prediction Results to Flexural Model

Objective	k_{sec}, k/in		Δ_y, in		Δ_{max}, in	
Name	*Absolute*	*Relative*	*Absolute*	*Relative*	*Absolute*	*Relative*
Lefas SW30					0.16	0.16
Lefas SW31					0.13	0.13
Lefas SW32					0.11	0.11
Lefas SW33					0.10	0.10
Lefas SW11	2.29	-2.29	0.61	0.61	0.41	0.41
Lefas SW12	1.88	-2.40	0.29	1.06	0.43	0.43
Lefas SW13	2.12	-2.68	0.46	1.00	0.51	0.51
Lefas SW14	2.37	-2.39	0.62	0.62	0.33	0.33
Lefas SW15	1.34	-2.04	0.23	1.08	0.49	0.49
Lefas SW16	1.00	-1.99	-0.32	1.54	0.58	0.80
Lefas SW17	2.87	-2.87	0.58	0.58	0.32	0.32
Lefas SW21	0.36	-0.61	0.38	0.38	0.15	0.15
Lefas SW22	-0.01	-0.62	0.16	0.57	0.22	0.22
Lefas SW23	0.14	-0.74	0.09	0.66	0.29	0.29
Lefas SW24	0.63	-0.66	0.34	0.34	0.16	0.16
Lefas SW25	0.12	-0.72	0.29	0.58	0.32	0.43
Lefas SW26	0.42	-0.66	0.33	0.45	0.17	0.17
Oesterle B1	-0.12	-0.27	0.22	0.26	0.04	0.04
Oesterle B2	0.98	-0.98	0.40	0.40	0.09	0.09
Oesterle B3	-0.16	-0.28	0.24	0.27	0.03	0.03
Oesterle B4	-0.18	-0.28	0.18	0.28	0.02	0.02
Oesterle B5	0.90	-0.97	0.47	0.47	-0.14	0.14
Oesterle R1	-0.09	-0.09	-0.11	0.14	0.01	0.01
Oesterle R2					0.03	0.03
Oesterle B6	0.82	-1.26	0.31	0.76	-0.34	0.36
Oesterle B7	1.25	-1.34	0.57	0.57	0.14	0.14
Oesterle B8	1.19	-1.36	0.57	0.61	0.15	0.15
Oesterle B9	0.82	-1.20	0.48	0.48	0.02	0.16
Oesterle B10	0.87	-1.05	0.37	0.37	0.10	0.10
Pilakoutas SW4	1.13	-1.13	0.48	0.48	0.17	0.17
Pilakoutas SW5					0.19	0.19
Pilakoutas SW6	1.24	-1.24	0.46	0.46	0.16	0.16
Pilakoutas SW7	1.52	-1.52	0.50	0.50	0.23	0.23
Pilakoutas SW8	1.21	-1.21	0.48	0.48	0.16	0.16
Pilakoutas SW9	1.22	-1.22	0.47	0.52	0.17	0.17
Salonikios LSW1					0.14	0.14
Salonikios LSW2					0.10	0.10
Salonikios LSW3					0.12	0.12
Salonikios MSW1					0.14	0.14
Salonikios MSW2					0.09	0.09
Salonikios MSW3					0.12	0.12
Salonikios MSW6					0.13	0.13

Table 7.17: Difference of Effective Shear Calibrated to Yield Displacement Model Prediction Results to Flexural Model (cont.)

Objective	k_{sec}, k/in		Δ_y, in		Δ_{max}, in	
Name	*Absolute*	*Relative*	*Absolute*	*Relative*	*Absolute*	*Relative*
Sittipunt W1					0.19	0.19
Sittipunt W2					0.27	0.27
Tasnimi SHW1					-0.10	0.10
Tasnimi SHW2					-0.15	0.15
Tasnimi SHW3					-0.08	0.08
Tasnimi SHW4					-0.11	0.11
Thomsen RW1	0.56	-0.56	0.13	0.13	0.05	0.05
Thomsen RW2	0.48	-0.48	0.12	0.12	0.05	0.05
Vallenas SW3	2.30	-2.30	0.51	0.51	0.07	0.07
Vallenas SW4	2.29	-2.29	0.51	0.51	0.15	0.15
Vallenas SW5	1.11	-1.32	0.55	0.55	0.13	0.13
Vallenas SW6	1.36	-1.43	0.49	0.49	0.20	0.20
Wang SW1	0.29	-0.80	0.41	0.41	0.08	0.08
Wang SW2	0.18	-0.76	0.40	0.40	0.12	0.12
Yanez S1					0.04	0.04
Zhang SW7	0.53	-0.95	0.17	0.69	0.12	0.12
Zhang SW8	0.02	-0.70	-0.02	0.70	0.16	0.16
Zhang SW9	1.45	-1.56	0.52	0.67	0.21	0.21
Average	0.97	-1.23	0.35	0.54	0.14	0.18
St. Dev.	0.80	0.72	0.21	0.27	0.16	0.14
COV	0.82	-0.59	0.60	0.50	1.13	0.79

Table 7.18: Difference of Effective Shear Calibrated to Maximum Displacement Model Prediction Results to Flexural Model

Objective	k_{sec}, k/in		Δ_y, in		Δ_{max}, in	
Name	*Absolute*	*Relative*	*Absolute*	*Relative*	*Absolute*	*Relative*
Lefas SW30					0.37	0.37
Lefas SW31					0.32	0.32
Lefas SW32					0.25	0.25
Lefas SW33					0.25	0.25
Lefas SW11	1.82	-2.78	0.02	1.44	0.12	0.96
Lefas SW12	1.50	-2.77	-1.13	2.48	0.37	1.06
Lefas SW13	1.75	-3.05	-0.89	2.35	0.32	1.23
Lefas SW14	1.89	-2.87	0.04	1.45	0.64	0.77
Lefas SW15	1.01	-2.37	-1.23	2.55	0.18	1.20
Lefas SW16	0.74	-2.25	-2.40	3.62	-0.52	1.90
Lefas SW17	2.74	-3.47	0.12	1.37	0.58	0.75
Lefas SW21	0.05	-0.92	-0.01	0.90	0.36	0.36
Lefas SW22	-0.27	-0.89	-0.61	1.34	0.50	0.54
Lefas SW23	-0.15	-1.03	-0.80	1.55	0.42	0.71
Lefas SW24	0.28	-1.00	0.18	0.80	0.39	0.39
Lefas SW25	-0.17	-1.01	-0.50	1.37	-0.24	0.99
Lefas SW26	0.10	-0.98	-0.27	1.06	0.40	0.40
Oesterle B1	-0.32	-0.48	-0.13	0.60	0.09	0.09
Oesterle B2	0.65	-1.40	0.24	0.93	0.21	0.21
Oesterle B3	-0.37	-0.48	-0.12	0.63	0.08	0.08
Oesterle B4	-0.38	-0.49	-0.20	0.66	0.05	0.05
Oesterle B5	0.51	-1.36	-0.02	1.10	-0.32	0.32
Oesterle R1	-0.18	-0.18	-0.30	0.33	0.03	0.03
Oesterle R2					0.07	0.07
Oesterle B6	0.46	-1.62	-0.71	1.78	-0.83	0.85
Oesterle B7	0.83	-1.76	-0.16	1.34	0.15	0.34
Oesterle B8	0.78	-1.77	-0.25	1.43	0.10	0.36
Oesterle B9	0.46	-1.56	0.22	1.13	-0.21	0.39
Oesterle B10	0.49	-1.43	0.51	0.86	0.23	0.23
Pilakoutas SW4	0.90	-1.58	-0.06	1.12	0.40	0.40
Pilakoutas SW5					0.45	0.45
Pilakoutas SW6	1.23	-1.74	-0.02	1.09	0.37	0.37
Pilakoutas SW7	1.39	-2.03	0.05	1.17	0.30	0.53
Pilakoutas SW8	1.21	-1.71	-0.12	1.13	0.36	0.36
Pilakoutas SW9	1.13	-1.71	-0.22	1.21	0.39	0.39
Salonikios LSW1					0.32	0.32
Salonikios LSW2					0.24	0.24
Salonikios LSW3					0.29	0.29
Salonikios MSW1					0.33	0.33
Salonikios MSW2					0.21	0.21
Salonikios MSW3					0.28	0.28
Salonikios MSW6					0.31	0.31

Table 7.19: Difference of Effective Shear Calibrated to Maximum Displacement Model Prediction Results to Flexural Model (cont.)

Objective	k_{sec}, k/in		Δ_y, in		Δ_{max}, in	
Name	*Absolute*	*Relative*	*Absolute*	*Relative*	*Absolute*	*Relative*
Sittipunt W1					0.40	0.46
Sittipunt W2					0.00	0.63
Tasnimi SHW1					-0.48	0.48
Tasnimi SHW2					-0.71	0.71
Tasnimi SHW3					-0.18	0.18
Tasnimi SHW4					-0.14	0.14
Thomsen RW1	0.98	-0.98	0.32	0.32	0.12	0.12
Thomsen RW2	0.86	-0.86	0.28	0.28	0.12	0.12
Vallenas SW3	1.94	-2.82	0.33	1.19	0.18	0.18
Vallenas SW4	1.92	-2.81	0.33	1.19	0.35	0.35
Vallenas SW5	0.71	-1.72	-0.03	1.29	0.29	0.29
Vallenas SW6	0.93	-1.86	0.18	1.16	0.07	0.47
Wang SW1	-0.02	-1.11	0.30	0.95	0.20	0.20
Wang SW2	-0.11	-1.05	0.31	0.94	0.28	0.28
Yanez S1					0.08	0.08
Zhang SW7	0.20	-1.28	-0.76	1.61	0.29	0.29
Zhang SW8	-0.25	-0.97	-0.96	1.64	0.39	0.39
Zhang SW9	1.02	-1.99	-0.39	1.58	0.44	0.44
Average	0.71	-1.60	-0.22	1.27	0.17	0.43
St. Dev.	0.77	0.80	0.56	0.63	0.29	0.34
COV	1.09	-0.50	-2.53	0.50	1.70	0.78

Table 7.20: Difference of Effective Shear Calibrated to Yield Displacement with Bar-Slip Model Prediction Results to Flexural Model

Objective	k_{sec}, k/in		Δ_y, in		Δ_{max}, in	
Name	*Absolute*	*Relative*	*Absolute*	*Relative*	*Absolute*	*Relative*
Lefas SW30					0.24	0.24
Lefas SW31					0.22	0.22
Lefas SW32					0.17	0.17
Lefas SW33					0.17	0.17
Lefas SW11	2.24	-2.24	0.57	0.57	0.47	0.47
Lefas SW12	1.92	-2.36	0.37	0.98	0.47	0.47
Lefas SW13	2.15	-2.65	0.50	0.96	0.54	0.54
Lefas SW14	2.35	-2.35	0.58	0.58	0.37	0.37
Lefas SW15	1.36	-2.01	0.29	1.02	0.54	0.54
Lefas SW16	1.02	-1.97	-0.25	1.46	0.54	0.84
Lefas SW17	2.82	-2.82	0.55	0.55	0.37	0.37
Lefas SW21	0.32	-0.64	0.43	0.43	0.23	0.23
Lefas SW22	-0.03	-0.65	0.11	0.62	0.31	0.31
Lefas SW23	0.10	-0.78	0.01	0.74	0.39	0.39
Lefas SW24	0.59	-0.70	0.38	0.38	0.25	0.25
Lefas SW25	0.08	-0.76	0.22	0.66	0.21	0.54
Lefas SW26	0.38	-0.70	0.27	0.51	0.25	0.25
Oesterle B1	-0.12	-0.27	0.23	0.25	0.15	0.17
Oesterle B2	0.92	-0.92	0.35	0.35	0.12	0.12
Oesterle B3	-0.16	-0.27	0.25	0.26	0.13	0.13
Oesterle B4	-0.17	-0.28	0.18	0.27	0.09	0.09
Oesterle B5	0.92	-0.92	0.42	0.42	-0.41	0.41
Oesterle R1	-0.11	-0.11	-0.14	0.17	0.08	0.08
Oesterle R2					0.16	0.16
Oesterle B6	0.87	-1.21	0.39	0.68	-0.88	0.90
Oesterle B7	1.27	-1.27	0.50	0.50	0.12	0.37
Oesterle B8	1.26	-1.29	0.54	0.54	0.05	0.41
Oesterle B9	0.89	-1.13	0.42	0.42	-0.27	0.45
Oesterle B10	0.92	-1.00	0.33	0.33	0.30	0.30
Pilakoutas SW4	1.19	-1.19	0.53	0.53	0.36	0.50
Pilakoutas SW5					0.34	0.34
Pilakoutas SW6	1.31	-1.31	0.51	0.51	0.30	0.30
Pilakoutas SW7	1.62	-1.62	0.58	0.58	0.41	0.42
Pilakoutas SW8	1.25	-1.25	0.50	0.51	0.27	0.27
Pilakoutas SW9	1.27	-1.27	0.44	0.56	0.29	0.29
Salonikios LSW1					0.35	0.35
Salonikios LSW2					0.29	0.29
Salonikios LSW3					0.27	0.27
Salonikios MSW1					0.19	0.48
Salonikios MSW2					0.33	0.35
Salonikios MSW3					0.28	0.28
Salonikios MSW6					0.35	0.38

Table 7.21: Difference of Effective Shear Calibrated to Yield Displacement with Bar-Slip Model Prediction Results to Flexural Model (cont.)

Objective	k_{sec}, k/in		Δ_y, in		Δ_{max}, in	
Name	*Absolute*	*Relative*	*Absolute*	*Relative*	*Absolute*	*Relative*
Sittipunt W1					0.42	0.43
Sittipunt W2					0.07	0.55
Tasnimi SHW1					-0.57	0.57
Tasnimi SHW2					-0.84	0.84
Tasnimi SHW3					-0.62	0.62
Tasnimi SHW4					-0.42	0.42
Thomsen RW1	0.63	-0.63	0.16	0.16	0.13	0.13
Thomsen RW2	0.53	-0.53	0.14	0.14	0.10	0.16
Vallenas SW3	2.20	-2.20	0.44	0.44	0.13	0.13
Vallenas SW4	2.19	-2.19	0.44	0.44	0.26	0.26
Vallenas SW5	1.16	-1.27	0.50	0.50	0.25	0.25
Vallenas SW6	1.38	-1.38	0.45	0.45	0.14	0.40
Wang SW1	0.31	-0.78	0.39	0.39	0.11	0.11
Wang SW2	0.20	-0.74	0.38	0.38	0.16	0.16
Yanez S1					0.36	0.36
Zhang SW7	0.48	-1.00	0.07	0.78	0.18	0.18
Zhang SW8	-0.09	-0.81	-0.31	0.99	0.25	0.25
Zhang SW9	1.45	-1.56	0.52	0.67	0.23	0.23
Average	0.97	-1.23	0.33	0.54	0.16	0.34
St. Dev.	0.80	0.70	0.22	0.26	0.30	0.18
COV	0.82	-0.57	0.67	0.49	1.86	0.53

Table 7.22: Difference of Effective Shear Calibrated to Maximum Displacement with Bar-Slip Model Prediction Results to Flexural Model

Objective	k_{sec}, k/in		Δ_y, in		Δ_{max}, in	
Name	*Absolute*	*Relative*	*Absolute*	*Relative*	*Absolute*	*Relative*
Lefas SW30					0.42	0.42
Lefas SW31					0.37	0.37
Lefas SW32					0.29	0.29
Lefas SW33					0.29	0.29
Lefas SW11	1.88	-2.71	0.21	1.25	0.15	0.92
Lefas SW12	1.55	-2.73	-0.81	2.16	0.45	0.99
Lefas SW13	1.79	-3.01	-0.61	2.07	0.41	1.14
Lefas SW14	1.95	-2.82	0.22	1.27	0.67	0.74
Lefas SW15	1.05	-2.33	-0.92	2.23	0.25	1.13
Lefas SW16	0.77	-2.22	-1.96	3.18	-0.38	1.75
Lefas SW17	2.81	-3.39	0.30	1.20	0.60	0.73
Lefas SW21	0.07	-0.90	0.03	0.85	0.40	0.40
Lefas SW22	-0.26	-0.87	-0.53	1.26	0.47	0.57
Lefas SW23	-0.13	-1.01	-0.73	1.48	0.40	0.73
Lefas SW24	0.31	-0.98	0.22	0.76	0.44	0.44
Lefas SW25	-0.15	-0.99	-0.43	1.31	-0.27	1.03
Lefas SW26	0.12	-0.96	-0.23	1.01	0.44	0.44
Oesterle B1	-0.29	-0.44	-0.06	0.54	0.11	0.21
Oesterle B2	0.72	-1.32	0.37	0.79	0.22	0.22
Oesterle B3	-0.34	-0.45	-0.05	0.56	0.17	0.17
Oesterle B4	-0.35	-0.46	-0.13	0.59	0.10	0.10
Oesterle B5	0.57	-1.30	0.14	0.94	-0.41	0.41
Oesterle R1	-0.18	-0.18	-0.30	0.32	0.09	0.09
Oesterle R2					0.19	0.19
Oesterle B6	0.52	-1.56	-0.46	1.53	-1.28	1.31
Oesterle B7	0.90	-1.69	0.04	1.14	0.04	0.44
Oesterle B8	0.85	-1.70	-0.03	1.21	0.03	0.43
Oesterle B9	0.52	-1.50	0.40	0.95	-0.27	0.45
Oesterle B10	0.55	-1.37	0.63	0.73	0.31	0.41
Pilakoutas SW4	0.93	-1.55	0.01	1.06	0.16	0.70
Pilakoutas SW5					0.55	0.55
Pilakoutas SW6	1.26	-1.71	0.04	1.03	0.47	0.47
Pilakoutas SW7	1.40	-2.01	0.09	1.13	0.16	0.67
Pilakoutas SW8	1.25	-1.67	-0.04	1.05	0.44	0.44
Pilakoutas SW9	1.17	-1.67	-0.14	1.13	0.48	0.48
Salonikios LSW1					0.50	0.50
Salonikios LSW2					0.40	0.40
Salonikios LSW3					0.41	0.41
Salonikios MSW1					0.03	0.64
Salonikios MSW2					0.23	0.45
Salonikios MSW3					0.41	0.41
Salonikios MSW6					0.20	0.53

Table 7.23: Difference of Effective Shear Calibrated to Maximum Displacement with Bar-Slip Model Prediction Results to Flexural Model (cont.)

Objective	k_{sec}, k/in		Δ_y, in		Δ_{max}, in	
Name	*Absolute*	*Relative*	*Absolute*	*Relative*	*Absolute*	*Relative*
Sittipunt W1					0.21	0.65
Sittipunt W2					-0.22	0.85
Tasnimi SHW1					-0.65	0.65
Tasnimi SHW2					-0.96	0.96
Tasnimi SHW3					-0.70	0.70
Tasnimi SHW4					-0.57	0.57
Thomsen RW1	0.96	-0.96	0.31	0.31	0.18	0.18
Thomsen RW2	0.84	-0.84	0.27	0.27	0.04	0.22
Vallenas SW3	2.02	-2.73	0.52	1.01	0.23	0.23
Vallenas SW4	2.01	-2.72	0.52	1.01	0.44	0.44
Vallenas SW5	0.77	-1.66	0.14	1.11	0.39	0.39
Vallenas SW6	1.00	-1.80	0.33	1.00	-0.08	0.63
Wang SW1	0.02	-1.07	0.41	0.84	0.20	0.20
Wang SW2	-0.07	-1.01	0.43	0.83	0.30	0.30
Yanez S1					-0.06	-0.06
Zhang SW7	0.21	-1.27	-0.69	1.54	0.32	0.32
Zhang SW8	-0.27	-0.99	-1.09	1.77	0.44	0.44
Zhang SW9	1.06	-1.95	-0.23	1.42	0.44	0.44
Average	0.74	-1.56	-0.10	1.15	0.15	0.53
St. Dev.	0.79	0.78	0.52	0.56	0.39	0.32
COV	1.06	-0.50	-5.47	0.49	2.55	0.61

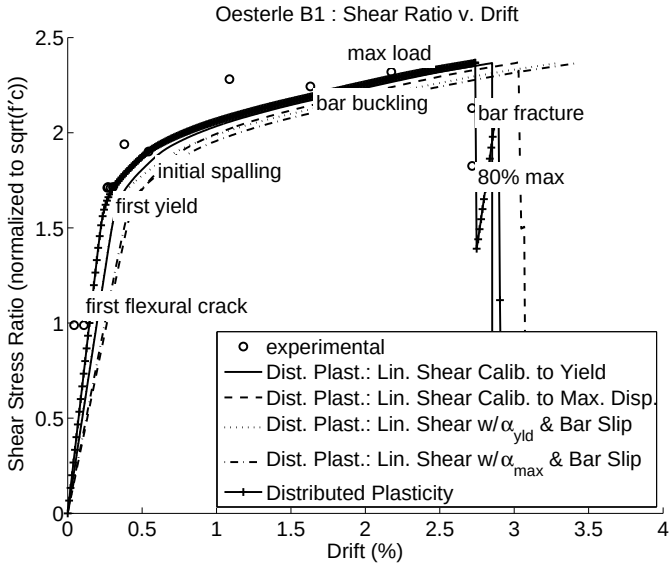

Figure 7.15: Comparison of predicted behavior of Oesterle B1 using each calibrated parameter

7.4.3 Results of Example Walls

Figure 7.15 shows the shear stress ratio to drift relationship predicted using each of the four calibrated parameters compared to the experimental results and the flexural beam column prediction for Oesterle B1. There is a slight increase in predicted flexibility both prior to yield and after. The increase in flexibility is more pronounced using the parameters calibrated to maximum displacement.

The predicted responses for Oesterle B6 and Pilakoutas SW7 are shown in Figures 7.16 & 7.17. A greater increase in the predicted flexibility compared to that of Oesterle B1 is apparent for each of the enhanced beam-column analyses. This results in a better prediction of the displacements of these walls whose behavior is more affected by shear.

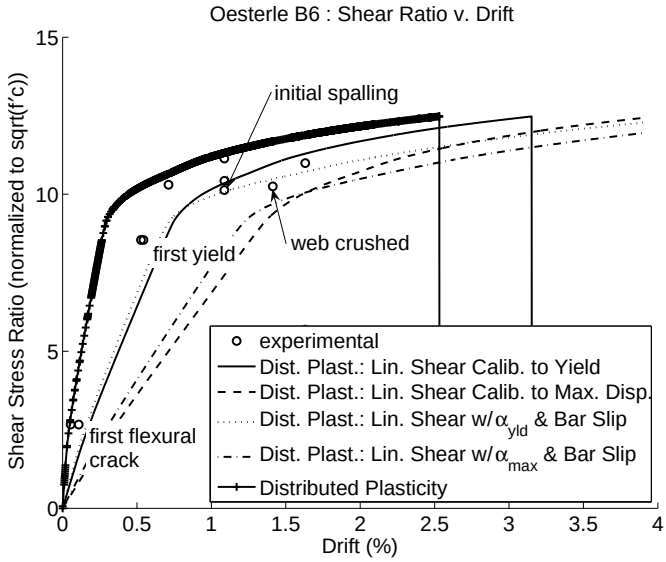

Figure 7.16: Comparison of predicted behavior of Oesterle B6 using each calibrated parameter

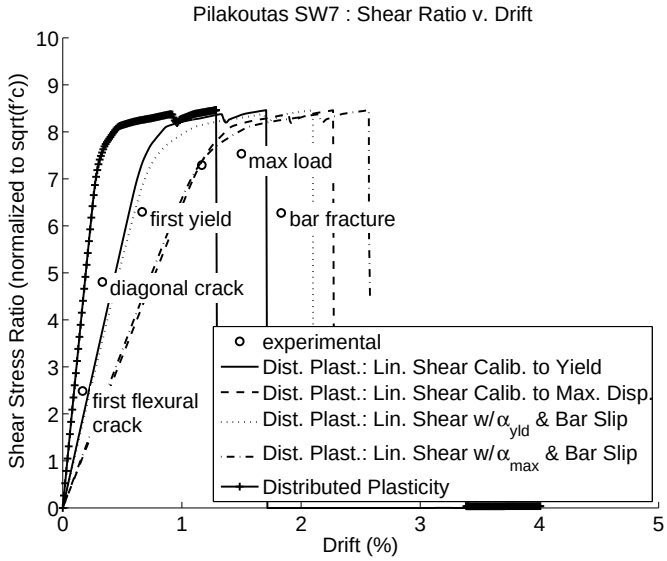

Figure 7.17: Comparison of predicted behavior of Pilakoutas SW7 using each calibrated parameter

7.4.4 Displacement Prediction Using Shear Models Calibrated to Yield Displacement

Secant Stiffness and Yield Displacement Prediction

The average error in the predicted yield displacement using these two models is zero. This leads to a 35% change in the absolute error in the model without bar-slip and 33% in the model with bar-slip. For both models, this corresponds to a 97% average improvement of the secant stiffness prediction.

The coefficient of variation for the yield displacement predicted to observed ratio is 26% using the calibrated model without bar-slip. The ratio is 28% using the calibrated model with bar-slip. Since the same improvement is attained using both models with little difference in the variability of results, it can be concluded that the inclusion of bar-slip has little benefit for the prediction yield displacement and secant stiffness up to yield.

Maximum Displacement Prediction

The improvement in the prediction of maximum displacement is less profound, yet still significant. The absolute change in error for the prediction of maximum displacement neglecting bar-slip is 14%. It is 16% with bar-slip. This corresponds to an average maximum displacement predicted to observed ratio of 0.76 neglecting bar-slip, with a 52% coefficient of variation. Including bar-slip, the average ratio is 0.92, with a 55% coefficient of variation. While the variation is large in both cases, the average maximum displacement predicted values are better using the bar-slip model.

7.4.5 Displacement Prediction Using Shear Models Calibrated to Maximum Displacement

Secant Stiffness and Yield Displacement Prediction

On average, the predicted yield displacements are worse using shear models calibrated to maximum displacement than the values predicted by the flexural model. The flexural model significantly under-predicts the yield displacement and the models with shear calibrated to maximum displacement significantly over-predict the yield displacement. The maximum displacement predicted to observed ratio is 1.73 using neglecting bar-slip, with a 34% coef-

ficient of variation. This ratio is 1.60 with bar-slip. The coefficient of variation is 33%.

Maximum Displacement Prediction

The average ratio of predicted to observed maximum displacement is 1.01 neglecting bar-slip with a 49% coefficient of variation and 1.11 including bar-slip with a 50% coefficient of variation. These ratios are not exactly unity, because the shear coefficients were calibrated using only walls for which the basic flexural beam-column model under-predicted maximum displacement.

7.5 Conclusions

Evaluation of the enhanced beam-column element implementations lead to the following conclusions:

- Inclusion of bar-slip in the beam-column model resulted in the limited improvement of displacement predictions.

- Inclusion of elastic shear in the beam-column element model had an insignificant improvement on displacement prediction.

- The proposed effective reduced shear beam-column enhancements provided improved displacement prediction results. Granted, the model was calibrated to reduce the average error to zero. However, use of the calibrated shear modulus did not cause a significant increase in the displacement prediction error for walls whose behavior was well simulated by the basic flexural beam-column element model.

- The range of error in improvement of the maximum displacement was found to be fairly significant. Investigation into the improvement of maximum usable strain criteria is warranted. Development of drift criteria for maximum displacement may be a feasible approach to addressing this problem.

Chapter 8
DISCUSSION AND CONCLUSIONS

The objectives of the study were to:

- Evaluate the ability of existing nonlinear analysis methods to predict shear wall behavior.
- Develop enhancements for these methods to enable improved prediction of critical response quantities.

To achieve these goals, a study of previous experimental shear wall research was conducted. A preprocessor was developed to facilitate the analysis of these walls using several nonlinear analysis techniques. Then, analyses were conducted using methods that represent the state of engineering practice to determine the quality of the prediction results. This information was used to improve these methods and recommend best practices for analysis of shear walls.

8.1 Summary of Research Program

The experimental walls were first modeled using the force-based beam-column. The model over-predicted the strength o walls with high shear demand. Additionally, for all but one wall in sixty, this model simulated secant stiffness up to yield that was substantially larger than measured in the laboratory. Similarly, maximum displacement was under-predicted for 92% of the walls. Evaluation of simulated results and wall design parameters indicated that (1.) additional flexibility is needed to improve this analysis method and (2.) the effect of shear deformation plays a significant role in the systemic under-prediction of displacement capacities.

Three walls, which were considered to have exhibited flexural, shear-flexure, and shear response, were then modeled using Response-2000. The Response-2000 model comprises

a distributed plasticity beam-column element in which the MCFT (Vecchio and Collins 1986) is used to define the constitutive relationship for reinforced concrete. This model was used to investigate the effect of shear on predicted strength and displacement. The results demonstrated a significant improvement, over the flexural beam-column element model, in prediction of strength and secant stiffness up to yield. However, the Response-2000 model had limited ability to predict maximum displacement capacity; with displacement capacity under-predicted by more than 20% for the walls considered. Response-2000's simplistic bar-slip model was also examined to determine the impact on simulated displacement capacity. While it did improve the results, displacement capacity was still under-predicted. This is likely due to the fact that the model does not account for the depth of the neutral axis when determining curvature at the base and uses a conservative assumption of bond stress.

The same three walls were then modeled using VecTor2 (Wong and Vecchio 2002), which employs 2D continuum elements with constitutive relationships defined by the MCFT. The goal of these analyses was to gain a better understanding of the failure and deformation mechanisms. VecTor2 provided results similar to Response-2000 for strength and secant stiffness up to yield. The VecTor2 analyses provided improved simulation of maximum displacement for the two walls that exhibit shear-affected behavior. These analyses show that shear deformation near the base contributes significantly to the overall displacement of the wall. This explains some of the error in the simulated displacement capacity.

While the MCFT based models offer the potential for accurate simulation response, including interaction of flexure and shear mechanisms, an immediate improvement can be made to the flexural beam-column analyses typically used in practice by including the effects of bar slip and shear deformation. Thus, a bar-slip model was added to the distributed plasticity model. Evaluating the model using the experimental wall data set showed that this enhancement greatly improved simulation of displacement capacity. However, the enhanced model still under-predicted displacement capacity on average. Linear elastic shear deformation was added to the model. Thus, evaluation of the model showed that use of the concrete elastic shear modulus model resulted in little additional deformation due to shear. An effective shear model was introduced to simulate the impact of flexural cracking on shear stiffness. This effective modulus was calibrated to minimize the error in prediction

of yield and maximum displacement for both the case where bar slip is included and when it is neglected.

8.2 Recommendations for Future Preprocessor Implementations

The preprocessor introduced in Chapter 3 served as an initial attempt at implementing a novel framework for finite element model building proposed by Lowes and Miller (2006). Many lessons were learned. Future development of the preprocessor introduced in this thesis or implementations of similar processors should follow these suggestions:

1. **Eliminate multiple processing of the same data value.** Implementation of the rule-based processing and database techniques described by Daniel (1988) would reduce redundant calculations and specification of processors. Thereby, allowing the engineer to focus on higher level modeling issues as stated in Lowes and Miller (2006) model-building framework objectives. For example, only one value for clear cover distance should be used throughout the analysis of a single wall. However, in the current implementation, clear cover must be specified for each processor that uses the value. Thus, it is calculated multiple times. However, there does need to be a way to allow different values to be used for some values within the analysis, if that is what the user desires. For example, multiple concrete confinement models may be needed for multiple reinforcement configurations within one wall.

2. **Increase modularity of processing classes.** By virtue of making the raw data, data processors, processed data, and the solver dependent on each other, the objects are not fully modular. Future research should attempt to make the following objects independent:

    - raw data & data processors
    - data processors & processed data
    - processed data & solver

The processed data could be made independent from the solver by using a standardized format for storing the processed data. Then, a separate solver-specific parser would construct the solver input. For instance, the femML (Michopoulos et al. 2001) format could be used to store the data.

3. **Implement the 'info' struct as an object.** The 'info' struct is used to pass processed data from one processor to subsequent processors. For instance, the processor that creates elements needs the ID tags assigned to materials by the processor that creates the materials. In the current implementation, the data values are added to the struct throughout the processing by a variety of processors. This does not allow the programmer to easily see what information is in 'info' and to know how to access it. Definition of an 'info' class would state the information that belongs there and give commands to set and get these values. This would also have the benefit of incorporating the benefits of object oriented programming (encapsulation, modularity, and extensibility) to the system.

8.3 Recommendations for Nonlinear Analysis of Shear Walls

The results of this study support these recommendations:

1. **Adequate determination of peak strength requires modeling the effect of shear.** Evaluation of the analytical results showed that strength was over-predicted in walls with high shear demand-capacity ratios when shear was not accounted for.

2. **Adequate simulation of displacement response requires modeling the effect of bar-slip.** The comparison of analytical and experimental results demonstrate that inclusion of bar slip is necessary for accurate prediction of shear wall displacement. It is needed to account for rotation at the interface of the wall to the footing due to slip of reinforcing steel out of the foundation. Without this, analyses will typically under-predict displacements.

3. **Accurate simulation of displacement response requires modeling of shear deformation.** The inclusion of shear deformation is necessary for the accurate prediction of displacement in shear walls. Shear contributes significant flexibility both before and after yielding of longitudinal steel. This is even evident in walls that are considered to be dominated by flexural behavior.

8.4 Recommendations for Future Development of Analysis Methods

The results of this study support the following recommendations for future research:

1. **Develop inelastic shear model for enhanced flexural beam-column element.** The calibrated elastic shear models indicate that more shear flexibility is needed to predict maximum displacement accurately than to predict yield displacement. This indicates that shear stiffness decreases as displacement demand increases, as expected. Therefore, a shear model that simulates decreasing stiffness with increasing shear strain would be appropriate. A bilinear shear stress-strain model with a stress or strain base failure criteria would likely result in accurate simulation of both yield and maximum displacement.

2. **Implement the Response-2000 model within a finite element framework.** Response-2000 showed significant promise for accurate simulation of shear walls. The strength predictions for the three walls were very good, as were the secant stiffness up to yield predictions. However, maximum displacement was not accurately simulated. This is likely due to the fact that the current implementation is unable to predict displacement beyond the maximum strength of the wall, but could be a result of the reduction of shear effects near the base of the wall. It is recommended tat future research focus on improving prediction of displacement capacity.

   Additionally, in its current form, the Response-2000 model can not represent a wall loaded at multiple points. Nor can it be used in conjunction with other elements. These conditions are common in real structures. Thus, it is recommended that the Response-2000 formulation be generalized and implemented as a force-based element.

3. **Conduct similar analysis of shear walls with more complex geometry.** All of the walls analyzed in this study are rectangular or barbell shaped. In practice, walls often have openings, are coupled, have complex cross-sections, or are a part of a core-wall system. By nature, rectangular walls are less susceptible to shear failure, multidimensional loading, and torsional effect than these other types of walls. For comprehensive understanding of the applicability of nonlinear analysis methods to typical shear walls, extension of the current study to walls with non-planar and non-regular configurations is recommended.

BIBLIOGRAPHY

ACI Committee 318 (2002). *Building Code Requirements for Structural Concrete and Commentary*. American Concrete Institute.

Archer, G. C., G. Fenves, and C. Thewalt (1999). A new object–oriented finite element analysis program architecture. *Computers and Structures 70*(1), 63–75.

Belarbi, A. and T. T. C. Hsu (1994). Constitutive laws of concrete in tension and reinforcing bars stiffened by concrete. *ACI Structural Journal 91*(4), 465–474.

Belarbi, A. and T. T. C. Hsu (1995). Constitutive laws of softened concrete in biaxial tension-compression. *ACI Structural Journal 92*(5), 562–573.

Bentz, E. C. (2000). *Sectional Analysis of Reinforced Concrete Members*. Ph. D. thesis, University of Toronto.

Bentz, E. C. (2005). Explaining the riddle of tension stiffening models for shear panel experiments. *Journal of Structural Engineering 131*(9), 1422–1425.

Berry, M. P. (2006). *Performance Modeling Strategies for Modern Reinforced Concrete Bridge Columns*. Ph. D. thesis, University of Washington.

Brown, P. (2006). No title. Master's thesis, University of Washington, Seattle, Washington.

Cervenka, V. (1970). *Inelastic Finite Element Analysis of Reinforced Concrete Panels Under In-plane Loads*. Ph. D. thesis, University of Colorado.

Cocchi, G. M. and P. Tiriaca (2004). Nonlinear analysis of reinforced concrete beam elements subject to cyclical combined actions of torsion, biaxial flexure and axial forces. *Structural Engineering and Mechanics 17*(6), 829–862.

Collins, M. P. (1978). Toward a rational theory for RC members in shear. *Journal of the Structural Division, ASCE 104*(4), 649–666.

Daniel, W. J. T. (1988). Integration of rule-based and procedural code to obtain flexible engineering software. *Advanced Engineering Software 10*(2), 72–76.

Dazio, A., T. Wenk, and H. Bachmann (1999). Versuche an stahlbetontragwanden unter zyklisch-statischer einwirkung. Technical report, Institut fur Baustatik und Konstruktion ETH, Zurich.

Elnashai, A., K. Pilakoutas, and N. N. Ambraseys (1990). Experimental behaviour of reinforced concrete walls under earthquake loading. *Earthquake Engineering and Structural Dynamics 19*, 389–407.

Hooper, J., R. Klemencic, A. Lepage, and A. Taylor (2005, June). Meeting with external advisory committee. unpublished data.

Hsu, T. T. C. (1993). *Unified Theory of Reinforced Concrete*. Boca Raton: CRC Press.

Ile, N. and J. M. Reynouard (2000). Nonlinear analysis of reinforced concrete shear wall under earthquake loading. *Journal of Earthquake Engineering 4*(2), 183–213.

Kwan, A. K. H. and X. G. He (2001). Finite element analysis of effect of concrete confinement on behavior of shear walls. *Computers and Structures 79*(19), 1799–1810.

Lefas, I. D. and M. D. Kostovos (1990). Strength and deformation characteristics of reinforced concrete walls under load reversals. *ACI Structural Journal 87*(6), 716–726.

Lefas, I. D., M. D. Kostovos, and N. N. Ambraseys (1990). Behavior of reinforced concrete structural walls: Strength, deformation characteristics, and failure mechanism. *ACI Structural Journal 87*(1), 23–31.

Lehman, D. E. and J. P. Moehle (2000). *Seismic Performance of Well-Confined Concrete Bridge Columns*. PEER 1998/01, Pacific Earthquake Engineering Research Center, Berkeley, CA.

Lepage, A. and A. Taylor (2005, February). Meeting with external advisory committee. unpublished data.

Lopes, M. S. (1991). *Seismic Behaviour of RC Walls with Low Shear Ratio*. Ph. D. thesis, Imperial College of Science Technology and Medicine.

Lowes, L. N. and G. R. Miller (2006). Model building for simulation of nonlinear structural response.

Martinelli, L. (2001). Numerical simulation of cyclic tests of R/C shear walls. In *The Twelfth European Conference on Earthquake Engineering*. Elsevier Science Ltd.

MATLAB (2005). Version 7.1. http://www.mathworks.com/.

Mazzoni, S., F. McKenna, G. L. Fenves, and et al. (2006). *Open System for Earthquake Engineering Simulation User Manual*. http://opensees.berkeley.edu: Pacific Earthquake Engineering Research Center.

McKenna, F. T. (1997). *Object Oriented Finite Element Programming: Frameworks for Analysis, Algorithms and Parallel Computing*. Ph. D. thesis, University of California, Berkeley.

Michopoulos, J., P. Mast, T. Chwastyk, L. Gause, and R. Badaliance (2001, October). FemML for data exchange between FEA codes. In *ANSYS Users' Group Conference*, University of Maryland.

Oesterle, R. G., J. D. Aristizabal-Ochoa, A. E. Fiorato, H. G. Russell, and W. G. Corley (1979, October). Earthquake resistant structural walls – tests of isolated walls – phase II. Technical report, National Science Foundation, Washington, D. C.

Oesterle, R. G., A. E. Fiorato, L. S. Johal, J. E. Carpenter, H. G. Russell, and W. G. Corley (1976, November). Earthquake resistant structural walls – tests of isolated walls. Technical report, National Science Foundation, Washington, D. C.

Palermo, D. (2001). *Behaviour and Analysis of Reinforced Concrete Walls Subjected to Reversed Cyclic Loading*. Ph. D. thesis, University of Toronto.

Palermo, D. and F. J. Vecchio (2003). Compression field modeling of reinforced concrete subjected to reversed loading: Formulation. *ACI Structural Journal 100*(5), 616–625.

Palermo, D. and F. J. Vecchio (2004). Compression field modeling of reinforced concrete subjected to reversed loading: Verification. *ACI Structural Journal 101*(2), 155–164.

Pang, X. B. and T. T. C. Hsu (1995). Behavior of reinforced concrete membrane elements in shear. *ACI Structural Journal 92*(6), 665–679.

Park, R. and T. Paulay (1975). *Reinforced Concrete Structures*. New York: John Wiley & Sons, Inc.

Park, R., M. J. N. Priestley, and W. D. Gill (1982). Ductility of square-confined concrete columns. *Journal of the Structural Division, ASCE 108*(4), 929–950.

Paulay, T. and M. J. N. Priestley (1992). *Seismic Design of Reinforced Concrete and Masonry Buildings*. New York: John Wiley & Sons, Inc.

Pilakoutas, K. (1991). *Earthquake Resistant Design of Reinforced Concrete Walls*. Ph. D. thesis, Imperial College of Science Technology and Medicine.

Pilakoutas, K. and A. Elnashai (1995). Cyclic behavior of reinforced concrete cantilever walls, part i: Experimental results. *ACI Structural Journal 92*(3), 272–281.

Row, D. G. and G. H. Powell (1978, August). A substructure technique for nonlinear static and dynamic analysis. Technical report, Earthquake Engineering Research Center, University of California, Berkeley.

Salonikios, T. N., A. J. Kappos, I. A. Tegos, and G. G. Penelis (1999). Cyclic load behavior of low–slenderness reinforced concrete walls: Design basis and test results. *ACI Structural Journal 96*(4), 649–660.

Salonikios, T. N., A. J. Kappos, I. A. Tegos, and G. G. Penelis (2000). Cyclic load behavior of low–slenderness reinforced concrete walls: Failure modes, strength and deformation analysis, and design implications. *ACI Structural Journal 97*(1), 132–141.

Sasani, M. and A. Der Kiureghian (2001). Seismic fragility of RC structural walls: Displacement approach. *Journal of Structural Engineering 127*(2), 219–228.

Sengupta, A. K. and A. Belarbi (2001). Modeling effect of biaxial stresses on average stress-strain relationship of reinforcing bar in reinforced concrete panels. *ACI Structural Journal 98*(5), 629–637.

Sittipunt, C. and S. L. Wood (1995). Influence of web reinforcement on the cyclic response of structural walls. *ACI Structural Journal 92*(6), 745–756.

Sittipunt, C., S. L. Wood, P. Lukkunaprasit, and P. Pattararattanaku (2001). Cyclic behavior of reinforced concrete structural walls with diagonal web reinforcement. *ACI Structural Journal 98*(4), 554–562.

Stevens, N. J., S. M. Uzumeri, and M. P. Collins (1991). Reinforced concrete subjected to reversed cyclic shear – experiments and constitutive model. *ACI Structural Journal 88*(2), 135–146.

Stevens, N. J., S. M. Uzumeri, M. P. Collins, and G. T. Will (1991). Constitutive model for reinforced concrete finite element analysis. *ACI Structural Journal 88*(1), 49–59.

Tasnimi, A. A. (2000). Strength and deformation of mid-rise shear walls under load reversal. *Engineering Structures 22*(4), 311–322.

Thomsen IV, J. H. and J. W. Wallace (2004). Displacement-based design of slender reinforced concrete structural walls – experimental verification. *Journal of Structural Engineering 130*(4), 618–630.

Vallenas, J. M., V. V. Bertero, and E. P. Popov (1979, August). Hysteretic behavior of reinforced concrete structural walls. Technical report, Earthquake Engineering Research Center, University of California, Berkeley.

VanLuchene, R. D., R. H. Lee, and V. J. Meyers (1986). Large scale finite element analyses on a vector processor. *Computers and Structures 24*(4), 625–635.

Vecchio, F. J. (1990). Reinforced concrete membrane element formulations. *Journal of Structural Engineering 116*(3), 730–750.

Vecchio, F. J. (1992). Finite element modeling of concrete expansion and confinement. *Journal of Structural Engineering 118*(9), 2390–2406.

Vecchio, F. J. (1999). Towards cyclic load modeling of reinforced concrete. *ACI Structural Journal 96*(2), 193–202.

Vecchio, F. J. (2000). Disturbed stress field model for reinforced concrete: Formulation. *Journal of Structural Engineering 126*(9), 1070–1077.

Vecchio, F. J. (2001). Disturbed stress field model for reinforced concrete: Implementation. *Journal of Structural Engineering 127*(1), 12–20.

Vecchio, F. J. and M. P. Collins (1986). The modified compression-field theory for reinforced concrete elements subjected to shear. *Journal of the American Concrete Institute 83*(2), 219–231.

Vecchio, F. J. and M. P. Collins (1988). Predicting the response of reinforced concrete beams subjected to shear using modified compression field theory. *ACI Structural Journal 85*(3), 258–268.

Vecchio, F. J. and M. P. Collins (1993). Compression response of cracked reinforced concrete. *Journal of Structural Engineering 119*(12), 3590–3611.

Vecchio, F. J., D. Lai, W. Shim, and J. Ng (2001). Disturbed stress field model for reinforced concrete: Validation. *Journal of Structural Engineering 127*(4), 350–358.

Wagner, H. (1929). Ebene blechwandträger mit sehr dünnem stegblech. *Zeitschrift für Flugtechnik und Motorluftschiffahrt 20*(8–12).

Wallace, J. W. and J. P. Moehle (1992). Ductility and detailing requirements of bearing wall buildings. *Journal of Structural Engineering 118*(6), 1625–1644.

Wang, T. Y., V. V. Bertero, and E. P. Popov (1975, December). Hysteretic behavior of reinforced concrete framed walls. Technical report, Earthquake Engineering Research Center, University of California, Berkeley.

Wong, P. S. and F. J. Vecchio (2002, August). *VecTor2 & Formworks Users Manual*.

Yanez, F. V., R. Park, and T. Paulay (1992). Seismic behaviour of walls with irregular openings. In *Proceedings of the Tenth World Conference on Earthquake Engineering*, Rotterdam, pp. 3303–3308. A. A. Balkema.

Zhang, Y. and Z. Wang (2000). Seismic behavior of reinforced concrete shear walls subjected to high axial loading. *ACI Structural Journal 97*(5), 739–750.

Appendix A
THE MODIFIED COMPRESSION FIELD THEORY

The MCFT (Vecchio and Collins 1986) derives from compression field theory (Collins 1978), which in turn derives from tension field theory (Wagner 1929). Each of these are rational theories that satisfy equilibrium of stress, compatibility, and uniaxial stress-strain relationships.

Tension field theory was developed for analysis of metallic membranes. The theory postulates that after buckling occurs in a membrane loaded in shear, the stress is transferred across by a diagonal tension strut. Additional stress transfer methods, like bending of the buckling plate, are neglected.

Similarly, compression field theory states that after a reinforced concrete element has cracked, tension in the concrete can be neglected. Stress is transferred by axial stress in the reinforcement and compressive stress in the concrete parallel to the direction of cracking. The MCFT generalizes the compression field theory and also accounts for the stress that concrete carries between cracks, a phenomenon called tension stiffening.

A.1 MCFT Assumptions

The MCFT makes the following assumptions:

- Cracks are free to rotate over time and their direction coincides with the second principal direction of stress at the given load step.
- Steel is perfectly bonded to concrete at the boundaries of the element.
- Reinforcement is uniformly distributed and can be represented as being smeared across the element.
- Stresses can be represented as average values across multiple cracks.

- The direction of principal stress in concrete coincides with the direction of principal strain of the element.

A.2 MCFT Steps

The following steps are taken in the implementation of the modified compression field theory:

1. Given a two-dimensional strain field, find the direction of principal strain. This direction is also assumed to be the direction of principal stress.

2. Determine the average tensile stress in the concrete from a uniaxial material model. If this stress does not exceed the cracking stress, determine stresses from elastic theory. Otherwise, continue with the MCFT.

3. Determine the compressive stress in the concrete from the uniaxial material model.

4. Determine the average stresses in each of the steel layers.

5. Check the stresses at the crack. If the reinforcement is unable to transfer forces across the crack, reduce the average tensile stress in the concrete.

6. Transform all stresses to basis coordinates and sum.

A.3 Material Model for Average Tensile Stress in Concrete

While concrete is not able to transfer tension across cracks, it does carry some tension between cracks. This has the effect of making the reinforcement appear to be stiffer than it would if the concrete carried no tension. This effect is called tension stiffening.

Experimental tests have shown that as the strain above cracking increases, the average tensile stress in the concrete decreases. This is called tension softening and is shown in Figure A.1. The equation recommended by Vecchio and Collins (1986) is,

$$f_{c1} = \begin{cases} E_c \epsilon_1 & \text{if } \epsilon_1 \leq \epsilon_{cr} \\ \frac{f_{cr}}{1+\sqrt{200\epsilon_1}} & \text{if } \epsilon_1 > \epsilon_{cr} \end{cases} \tag{A.1}$$

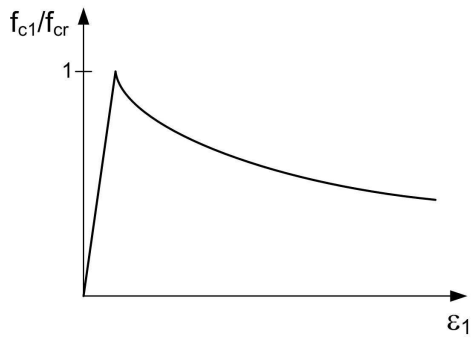

Figure A.1: Average Concrete Tensile Stress Strain Relationship

Where f_{c1} is the concrete stress in the first principal direction, E_c is the initial modulus of the concrete, ϵ_1 is the strain in the first principal direction, ϵ_{cr} is the concrete cracking strain, and f_{cr} is the concrete cracking stress.

Bentz (2005) modified the Vecchio and Collins tension stiffening model to account for differing abilities of bars to transfer stress to concrete. As the bond area of the bars decrease relative to the area of concrete in tension, the effect of tension stiffening decreases. This model was used for tension stiffening for analyses in VecTor2 and Response-2000. It is given by the following equations:

$$f_{c1} = \frac{f_{cr}}{1 + \sqrt{0.15 M \epsilon_1}} \tag{A.2}$$

$$M = \frac{A_c}{\Sigma d_b \pi} \tag{A.3}$$

Where M is the bond parameter given in in, A_c is the area of concrete whose stress is being considered, and d_b is the diameter of the reinforcing bars.

A.4 Material Model for Concrete in Compression

The uniaxial model proposed by Vecchio and Collins (1986) follows the Hognestad parabola up to the maximum compressive strength of the concrete. However, the maximum compressive strength is reduced by the strain in the principal tensile direction to account for the

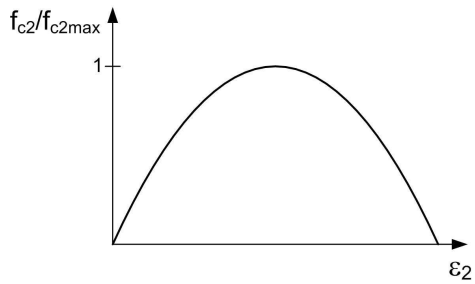

Figure A.2: Concrete Compressive Stress Strain Relationship

effect of biaxial loading. The stress strain relationship is shown in Figure A.2. The model is defined by the following equations:

$$f_{c2} = f_{c2max}\left[2\left(\frac{\epsilon_2}{\epsilon'_c}\right) - \left(\frac{\epsilon_2}{\epsilon'_c}\right)^2\right] \tag{A.4}$$

$$\frac{f_{c2max}}{f'_c} = \frac{1}{0.8 - 0.34\epsilon_1/\epsilon'_c} \quad \leq 1.0 \tag{A.5}$$

Where f_{c2} is concrete stress in the second principal direction, f_{c2max} is the maximum concrete compressive stress for the strain state, ϵ_2 is the strain in the second principal direction, and ϵ'_c is the strain where maximum stress occurs in the concrete cylinder test.

The model used in Response-2000 assumes that $\epsilon'_c = 0.002$. This reduces Equation A.5 to:

$$\frac{f_{c2max}}{f'_c} = \frac{1}{0.8 - 170\epsilon_1} \quad \leq 1.0 \tag{A.6}$$

The VecTor2 analyses conducted implement a more complicated model, Model-A proposed by Vecchio and Collins (1993).

A.5 Material Model for Average Stress in Reinforcement

The MCFT assumes that the stress-strain response of a bare bar can be used to adequately predict the average stress-strain response of a bar embedded in concrete. Originally, the model proposed by Vecchio and Collins (1986) is the elastic perfectly plastic model. How-

ever, this can be extended to other models that include a yield plateau and strain hardening.

A.6 The Crack Check

The crack check is a result of the use of average stresses and strains for the material models. Essentially, the concrete and steel combined cannot carry more tensile stress than the steel itself can transfer across the cracks. Therefore, the stresses at the crack location have to be checked. If the steel is not able to transfer the stress across the crack, the average tensile stress in the concrete is reduced. Failure to conduct the crack check in the implementation of the MCFT produces unconservative results. Bentz (2000) provides a thorough explanation of the crack check and procedures for its implementation.

A.7 Applicability of the MCFT

Studies have shown that the MCFT gives generally acceptable predictions of strength and load-deformation results for a variety of structural assemblages. However, panel tests have demonstrated that the method typically underestimates the shear strength and stiffness when the concrete is heavily reinforced in both directions and subjected to biaxial compression with shear. Underestimation of shear strength and stiffness also occurs when panels are loaded such that the direction of principal strain and stress remains relatively constant. On the other hand, overestimation of shear strength and stiffness tends to occur in panels with little or no reinforcement in one direction. Furthermore, applications of the MCFT to shear-critical beams with little or no transverse reinforcement ($\rho_t < 0.05\%$) tend to over-predict ductility and either over or under-predict the strength, depending on the structural and loading properties of the element (Vecchio 2000).

Typically, shear walls will not be subjected to biaxial compression and should have at least the code minimum reinforcement in both directions. Therefore, the stated limitations should not be a problem for the analysis of shear walls. However, the savvy analyst will not overlook these limitations, possible unstated limitations, and other general limitations of the finite element method when conducting any study of shear wall behavior.

Appendix B

MOMENT CURVATURE ANALYSIS FIGURES

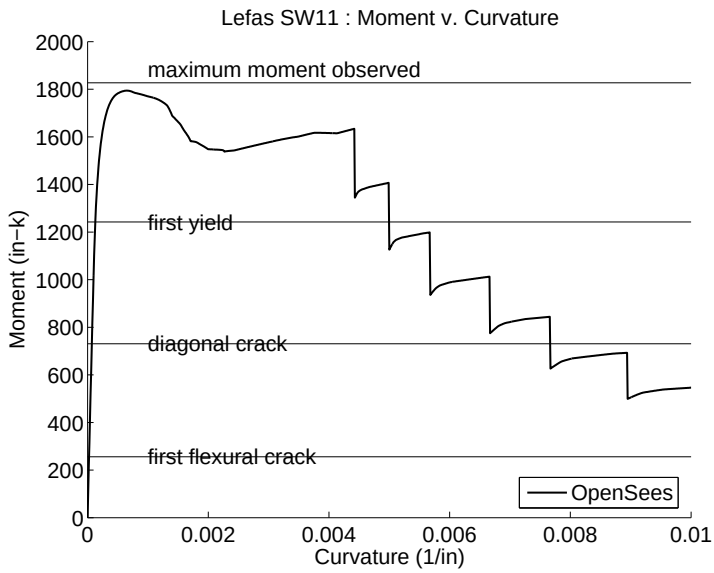

Figure B.1: Moment Curvature Analysis – Lefas SW11

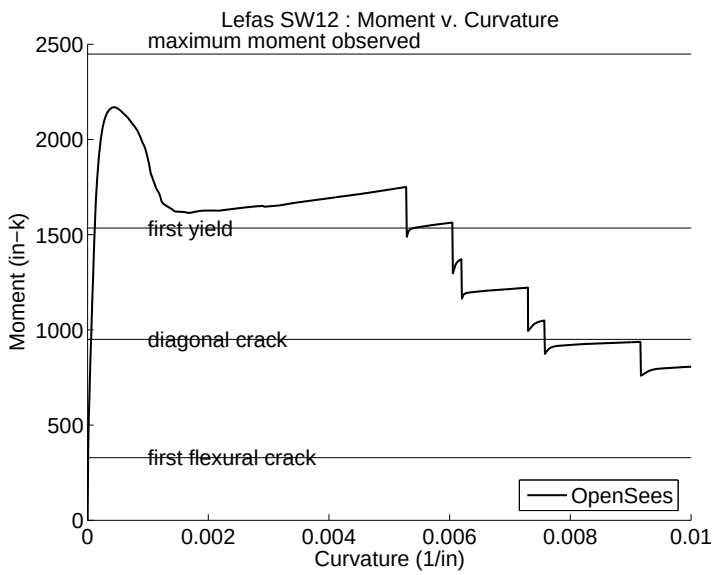

Figure B.2: Moment Curvature Analysis – Lefas SW12

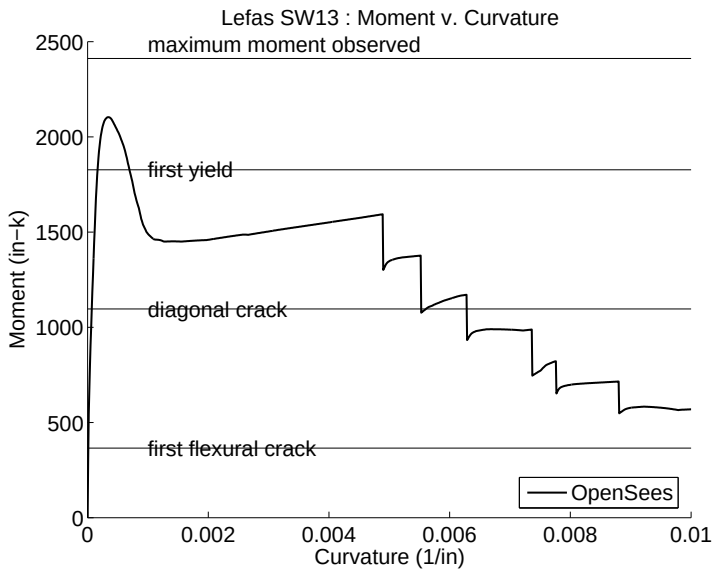

Figure B.3: Moment Curvature Analysis – Lefas SW13

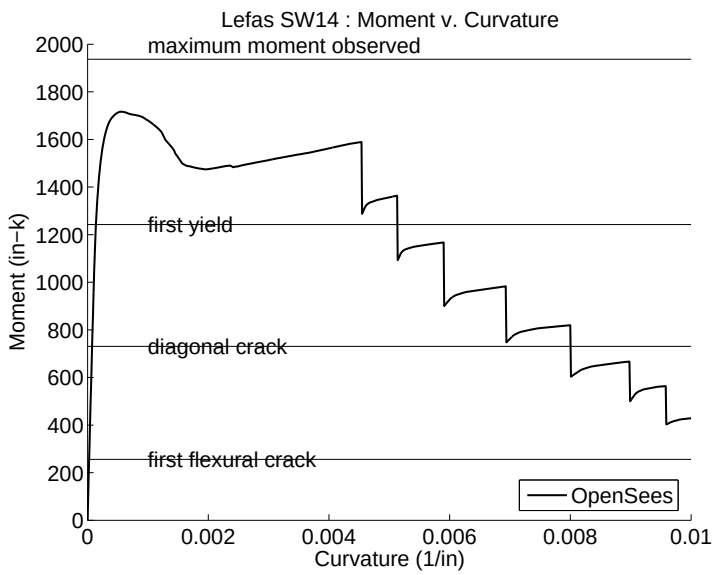

Figure B.4: Moment Curvature Analysis – Lefas SW14

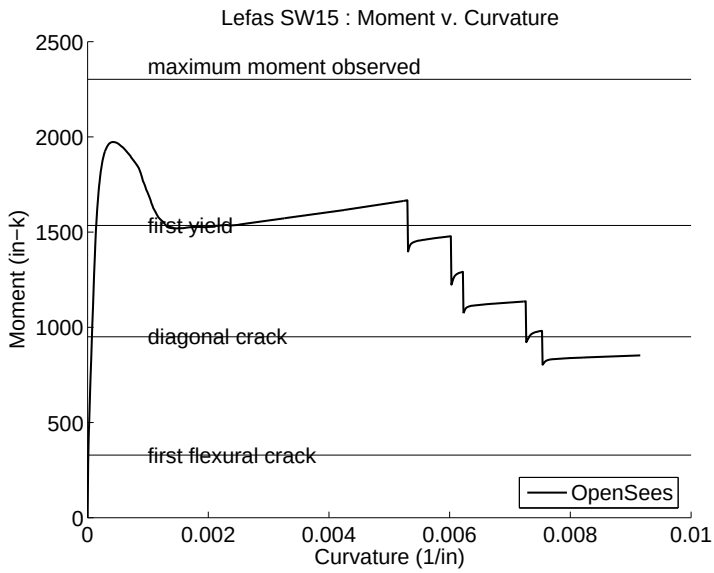

Figure B.5: Moment Curvature Analysis – Lefas SW15

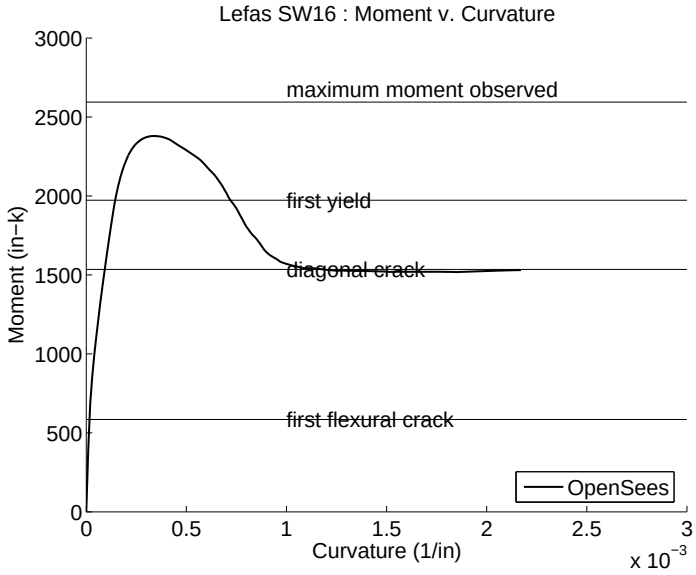

Figure B.6: Moment Curvature Analysis – Lefas SW16

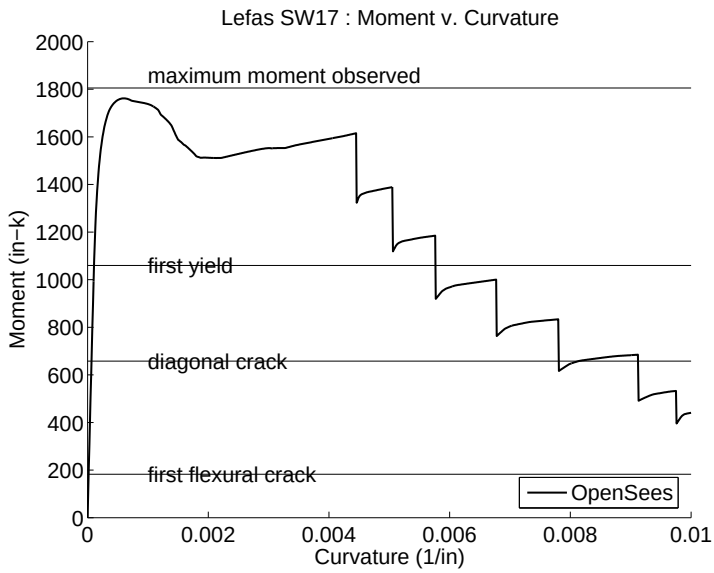

Figure B.7: Moment Curvature Analysis – Lefas SW17

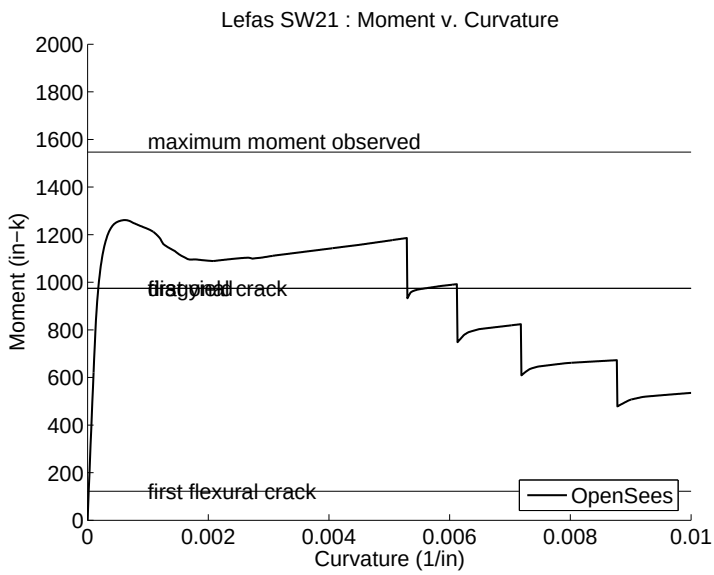

Figure B.8: Moment Curvature Analysis – Lefas SW21

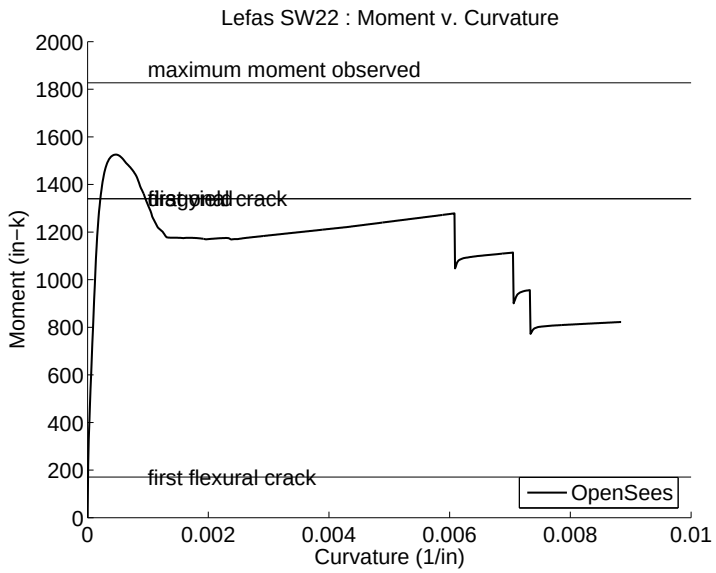

Figure B.9: Moment Curvature Analysis – Lefas SW22

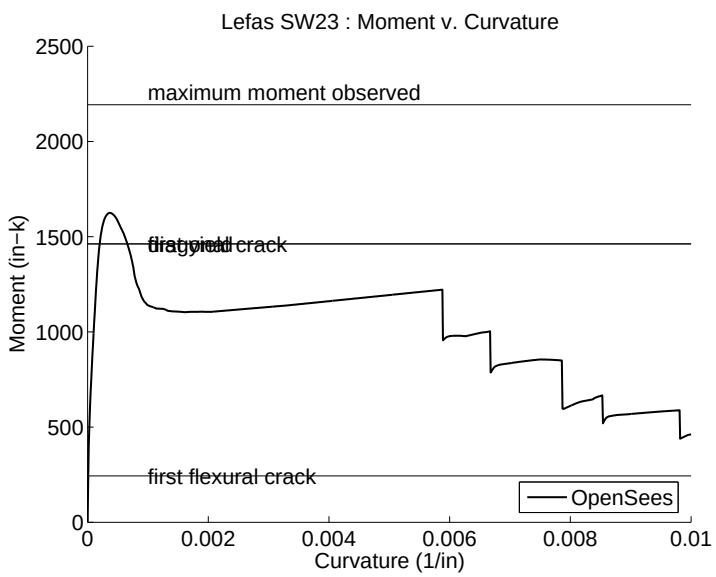

Figure B.10: Moment Curvature Analysis – Lefas SW23

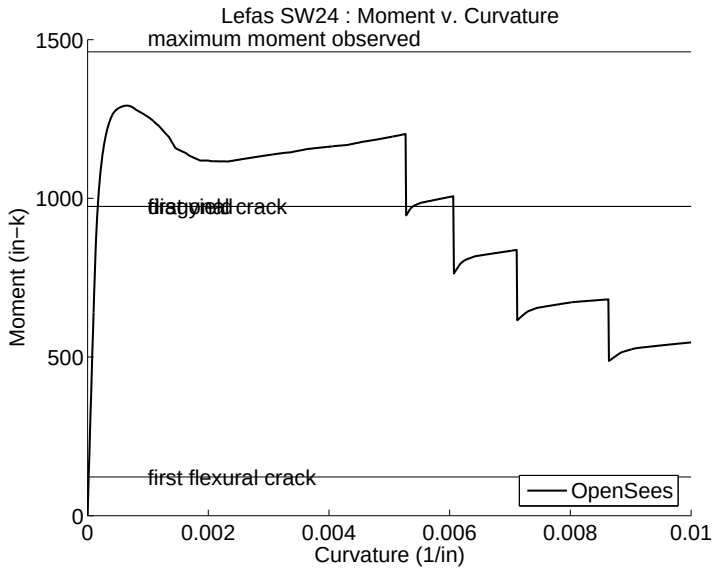

Figure B.11: Moment Curvature Analysis – Lefas SW24

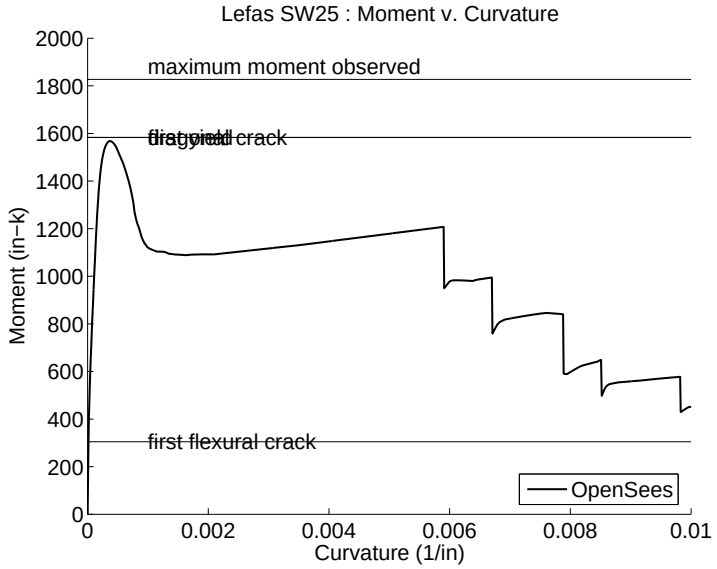

Figure B.12: Moment Curvature Analysis – Lefas SW25

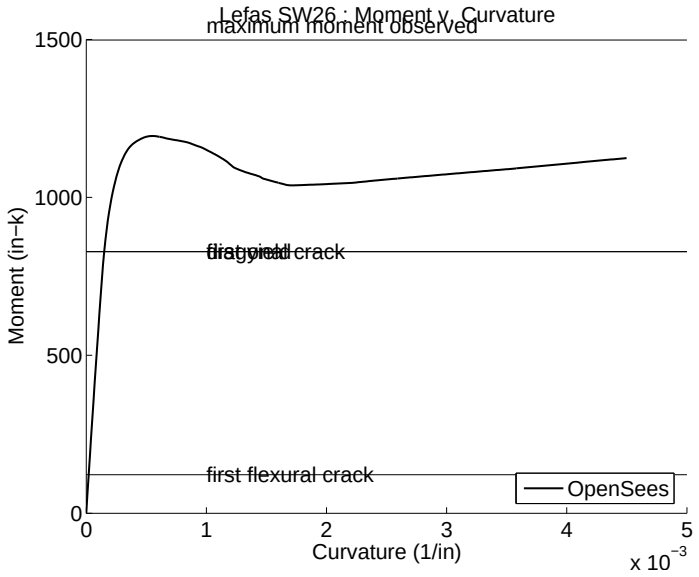

Figure B.13: Moment Curvature Analysis – Lefas SW26

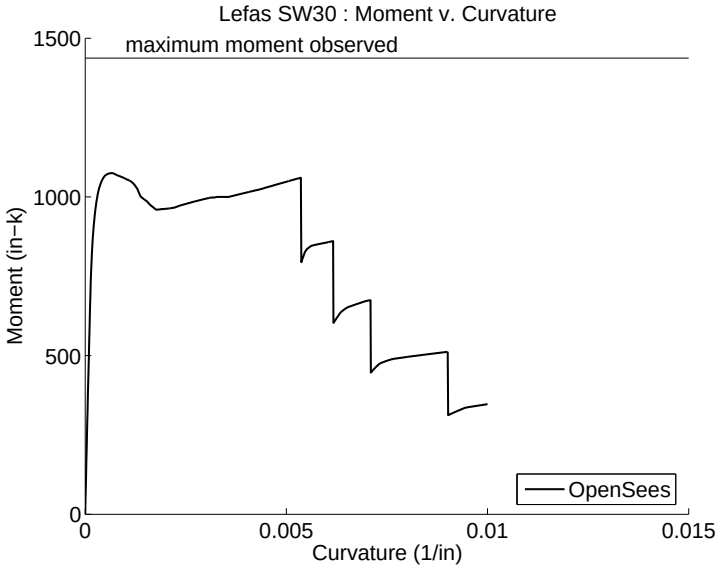

Figure B.14: Moment Curvature Analysis – Lefas SW30

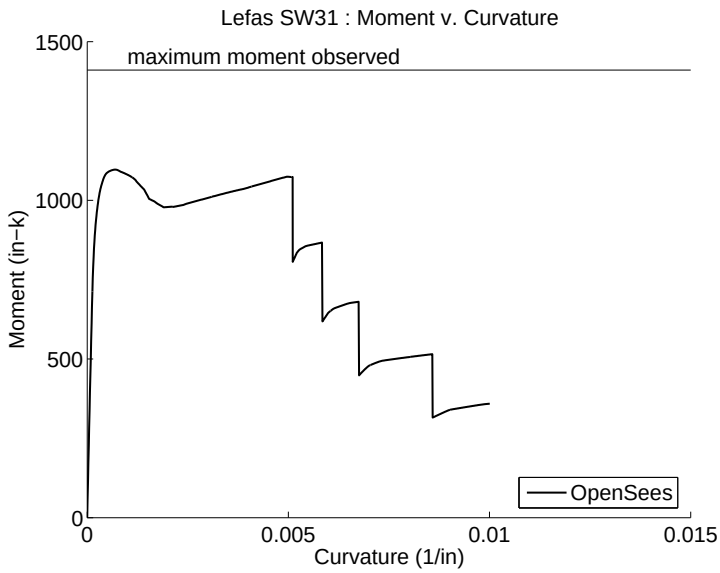

Figure B.15: Moment Curvature Analysis – Lefas SW31

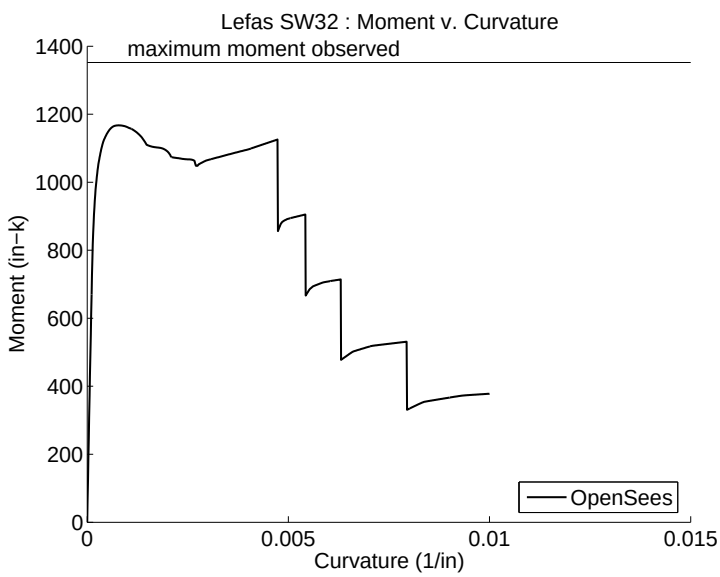

Figure B.16: Moment Curvature Analysis – Lefas SW32

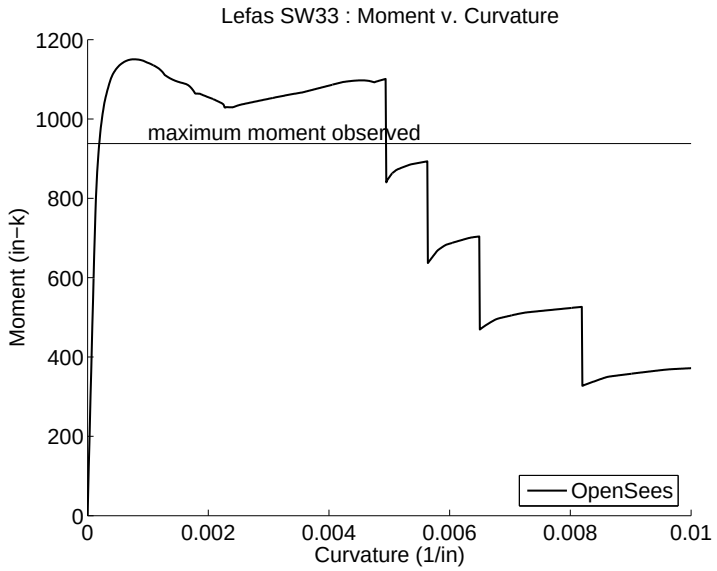

Figure B.17: Moment Curvature Analysis – Lefas SW33

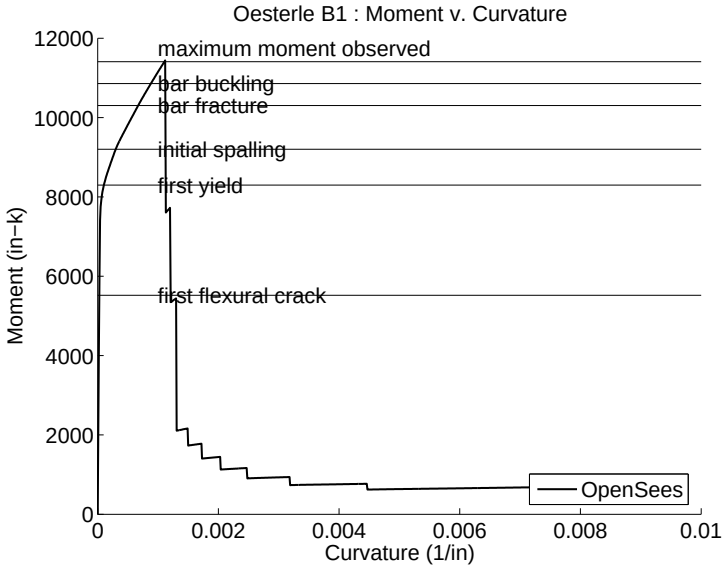

Figure B.18: Moment Curvature Analysis – Oesterle B1

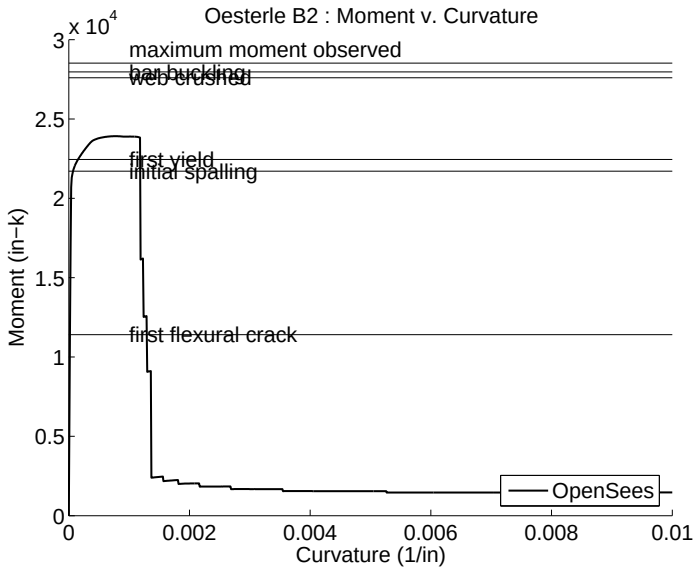

Figure B.19: Moment Curvature Analysis – Oesterle B2

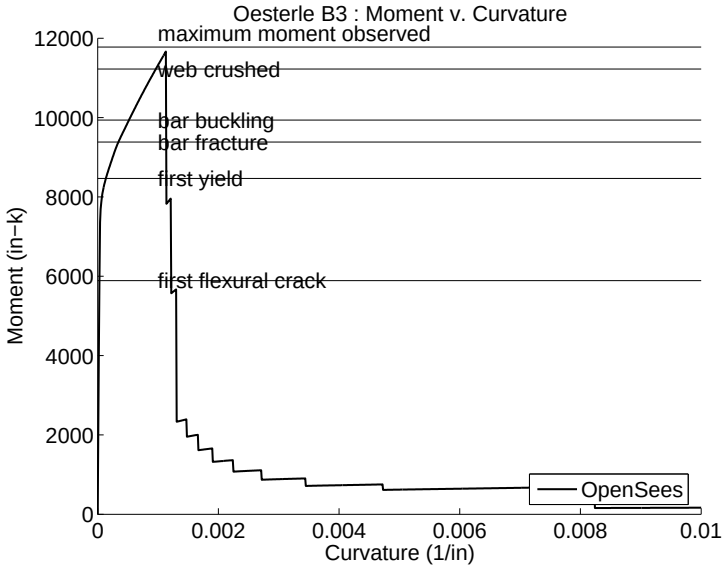

Figure B.20: Moment Curvature Analysis – Oesterle B3

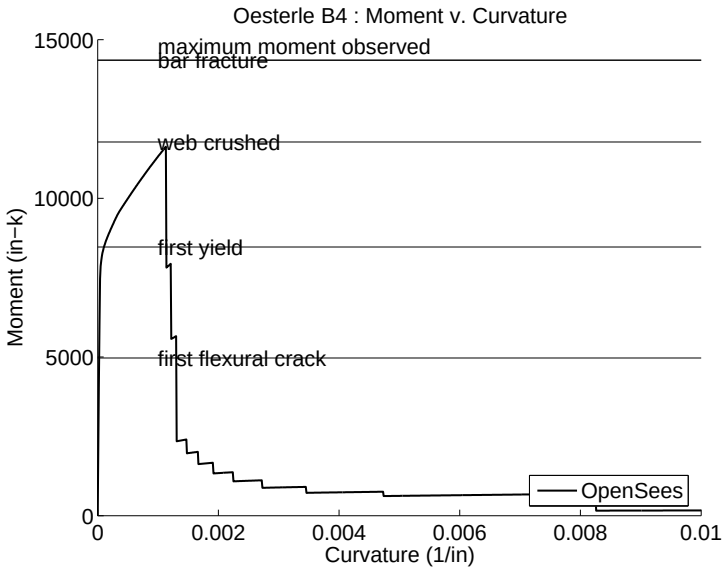

Figure B.21: Moment Curvature Analysis – Oesterle B4

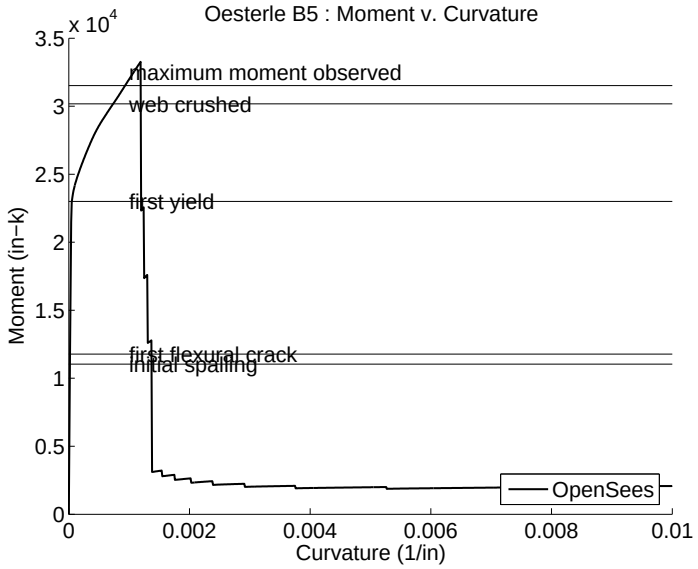

Figure B.22: Moment Curvature Analysis – Oesterle B5

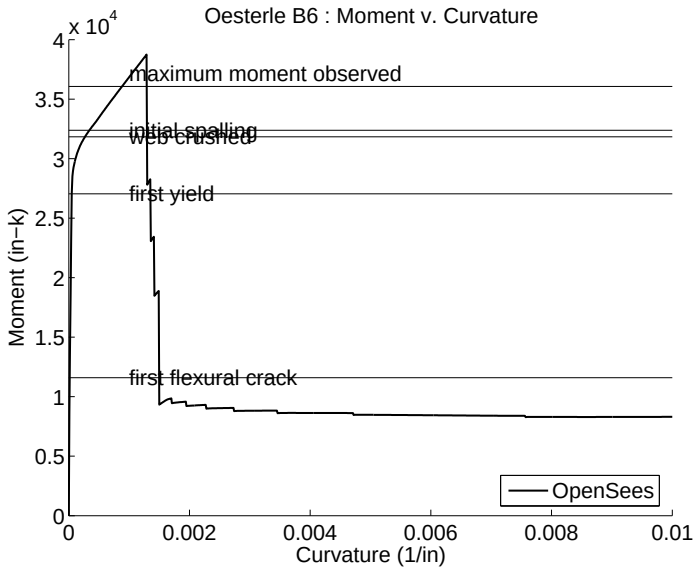

Figure B.23: Moment Curvature Analysis – Oesterle B6

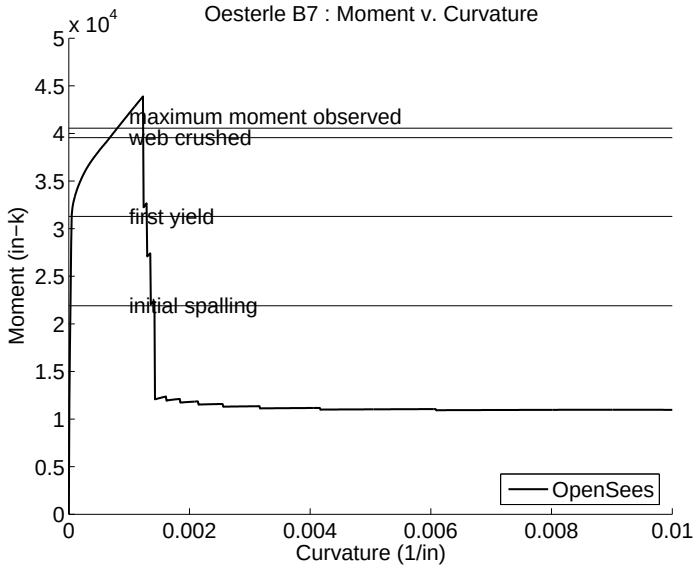

Figure B.24: Moment Curvature Analysis – Oesterle B7

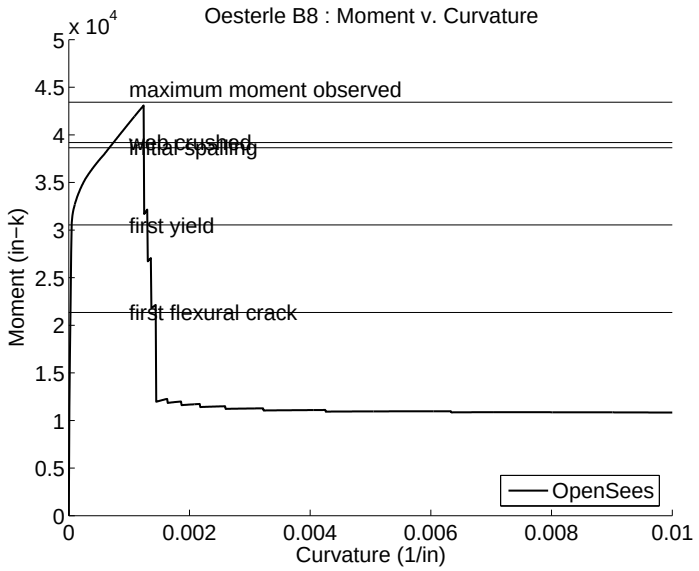

Figure B.25: Moment Curvature Analysis – Oesterle B8

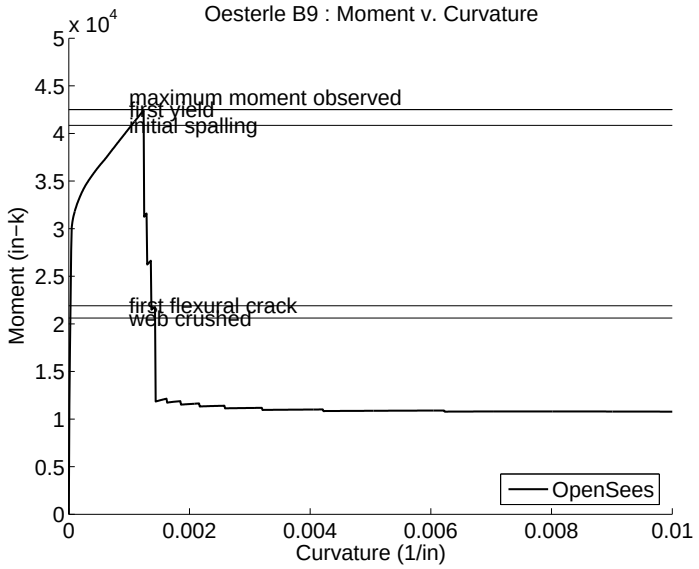

Figure B.26: Moment Curvature Analysis – Oesterle B9

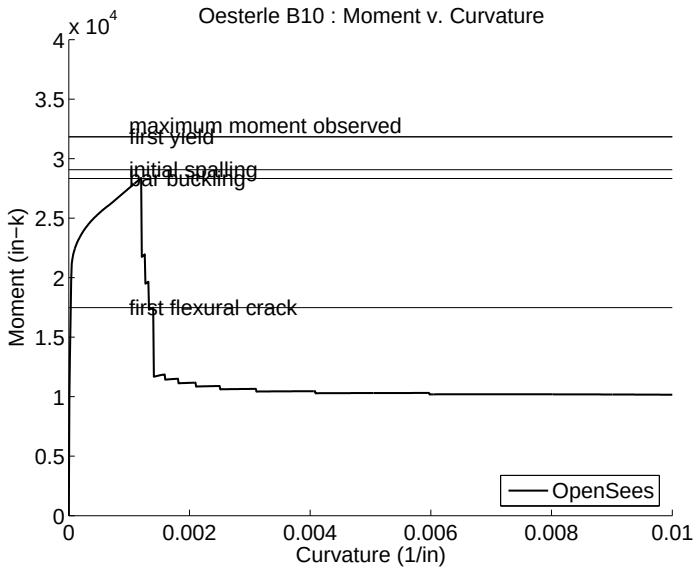

Figure B.27: Moment Curvature Analysis – Oesterle B10

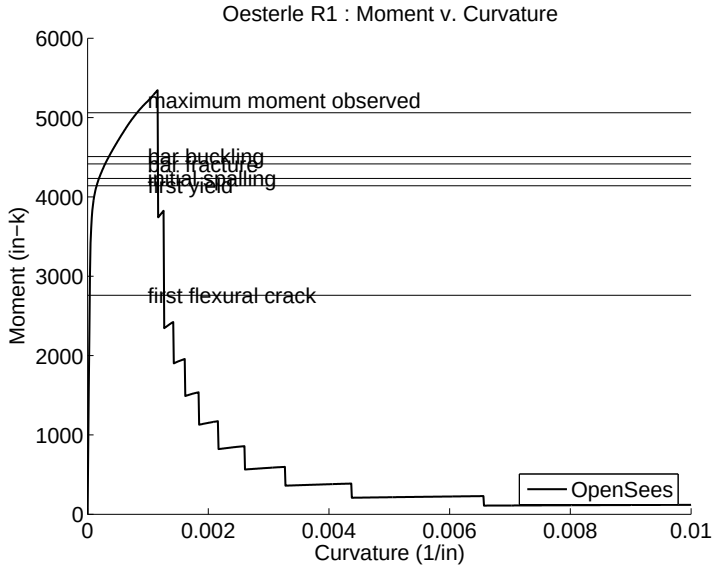

Figure B.28: Moment Curvature Analysis – Oesterle R1

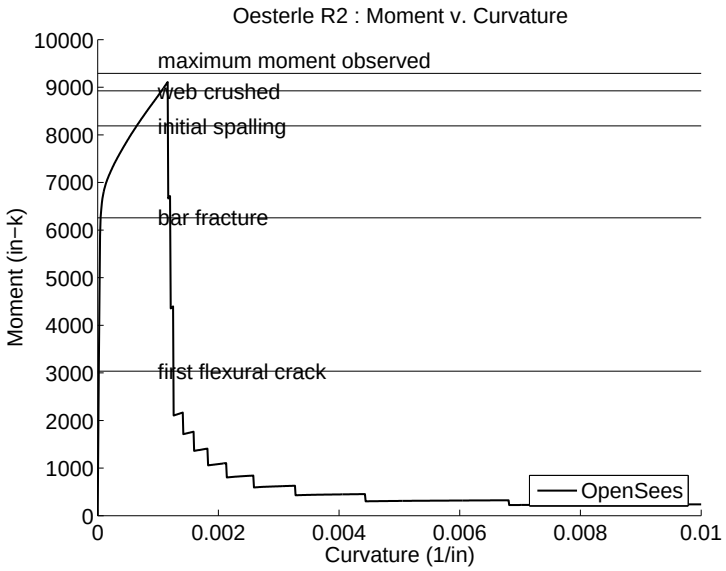

Figure B.29: Moment Curvature Analysis – Oesterle R2

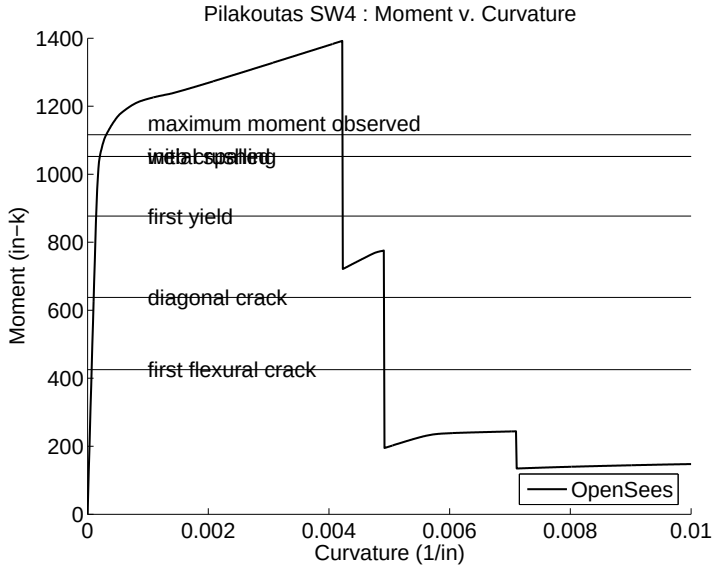

Figure B.30: Moment Curvature Analysis – Pilakoutas SW4

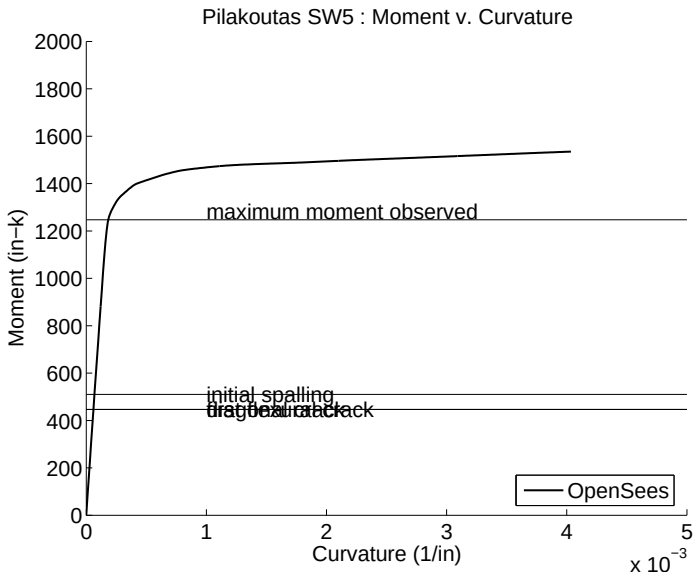

Figure B.31: Moment Curvature Analysis – Pilakoutas SW5

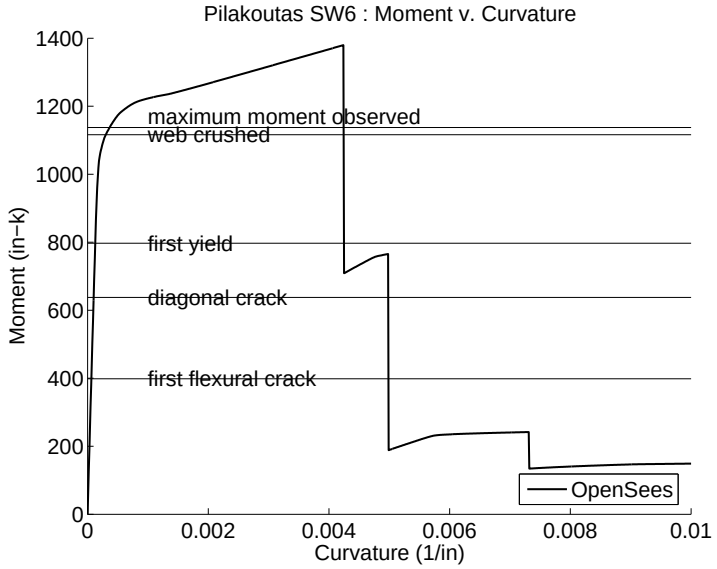

Figure B.32: Moment Curvature Analysis – Pilakoutas SW6

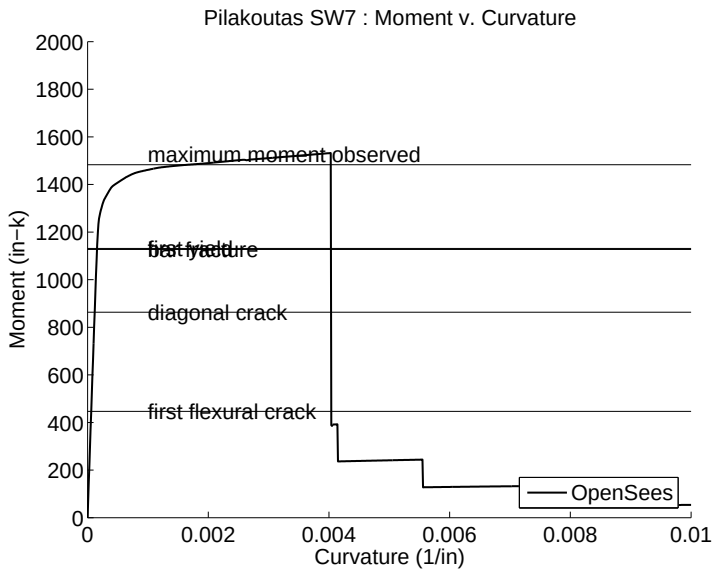

Figure B.33: Moment Curvature Analysis – Pilakoutas SW7

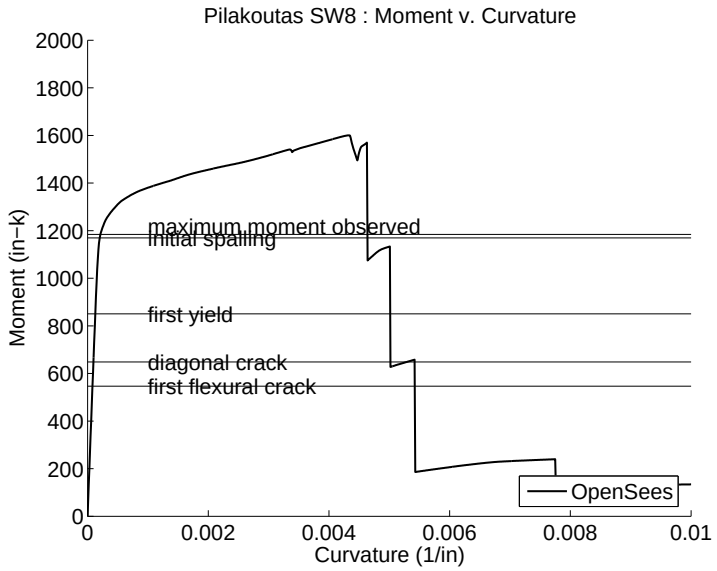

Figure B.34: Moment Curvature Analysis – Pilakoutas SW8

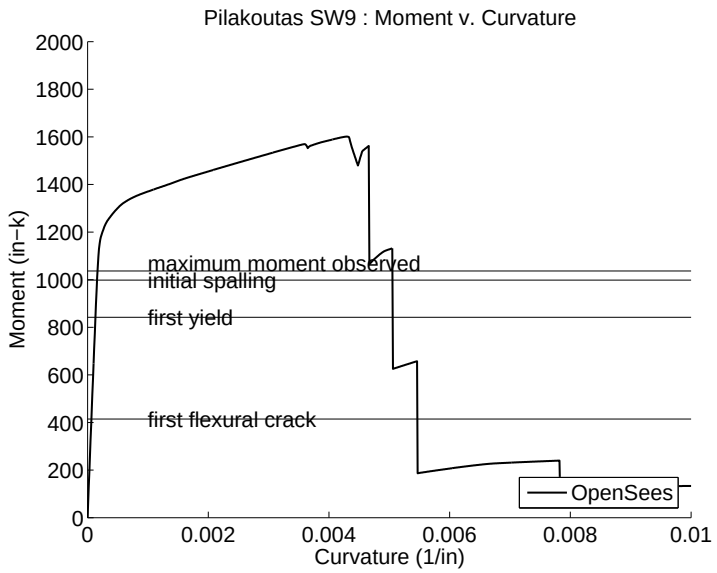

Figure B.35: Moment Curvature Analysis – Pilakoutas SW9

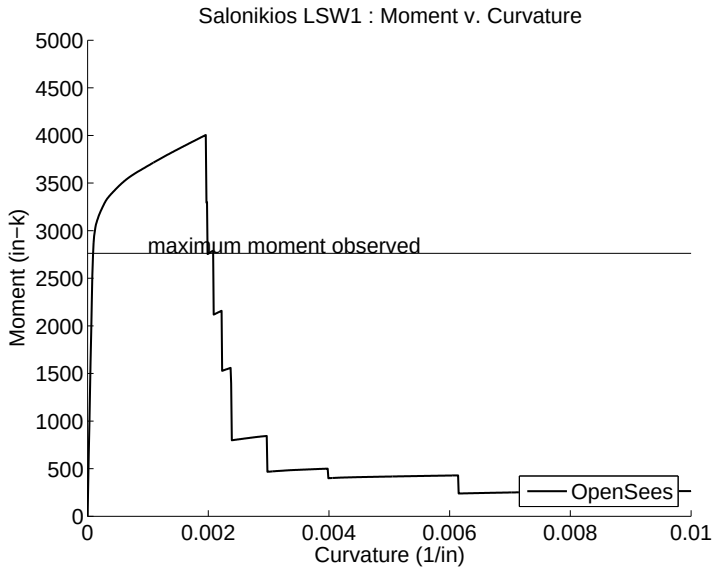

Figure B.36: Moment Curvature Analysis – Salonikios LSW1

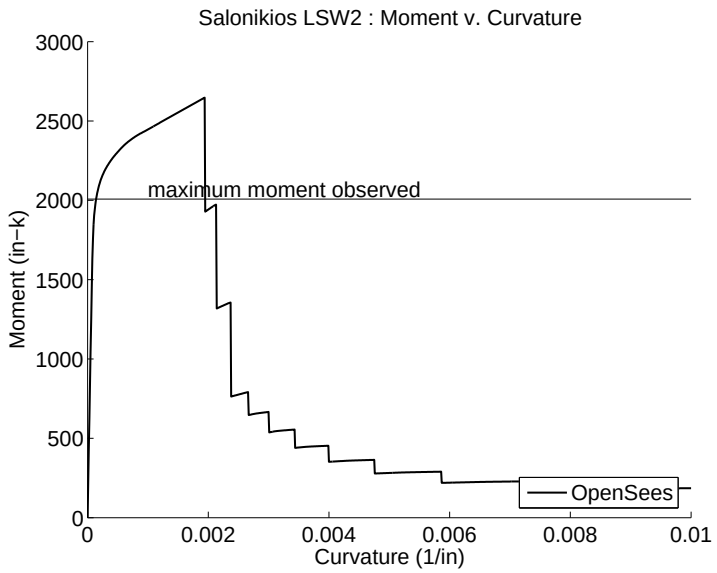

Figure B.37: Moment Curvature Analysis – Salonikios LSW2

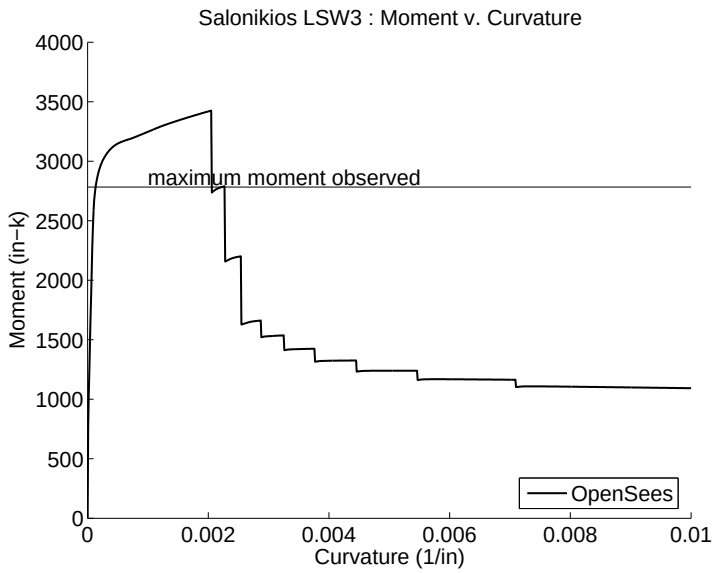

Figure B.38: Moment Curvature Analysis – Salonikios LSW3

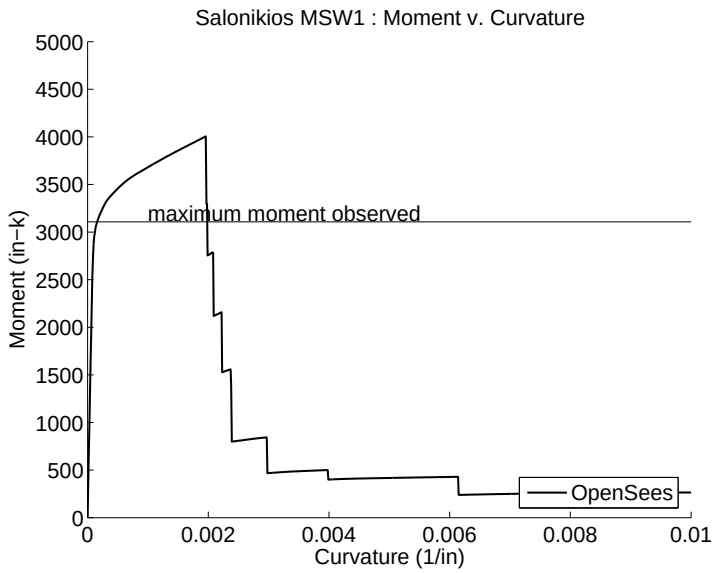

Figure B.39: Moment Curvature Analysis – Salonikios MSW1

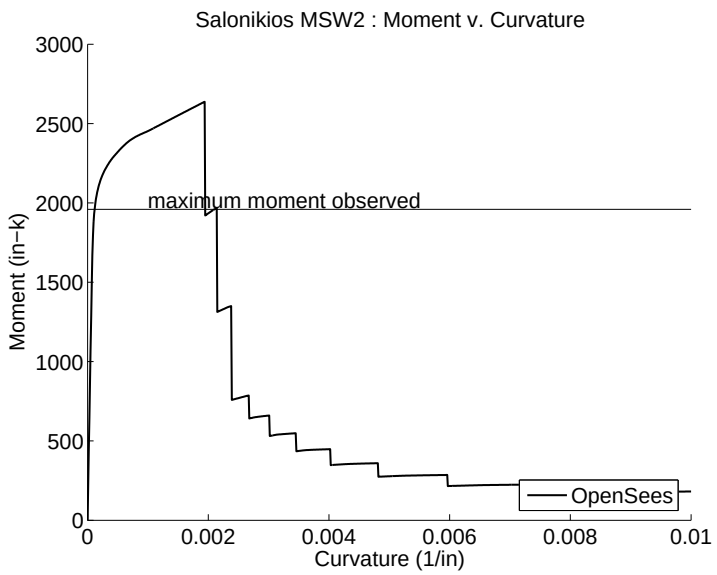

Figure B.40: Moment Curvature Analysis – Salonikios MSW2

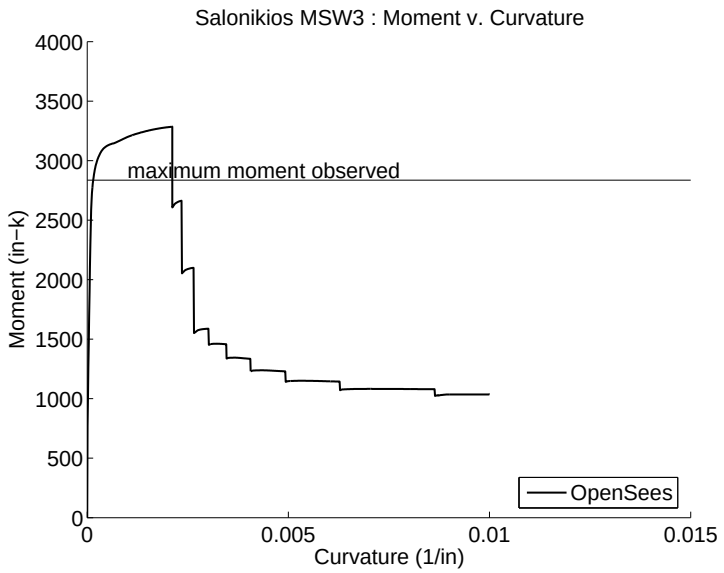

Figure B.41: Moment Curvature Analysis – Salonikios MSW3

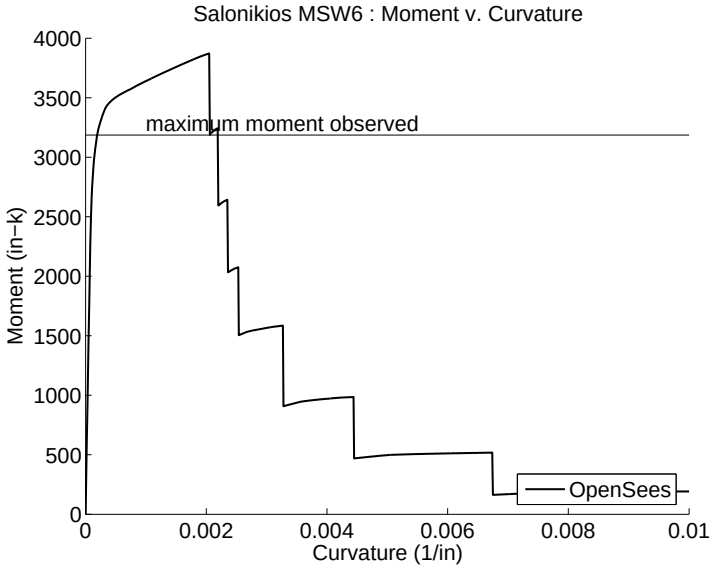

Figure B.42: Moment Curvature Analysis – Salonikios MSW6

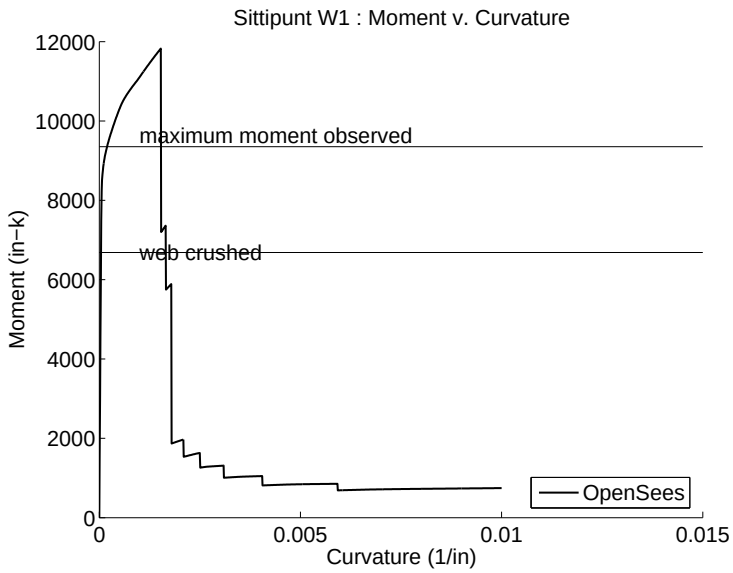

Figure B.43: Moment Curvature Analysis – Sittipunt W1

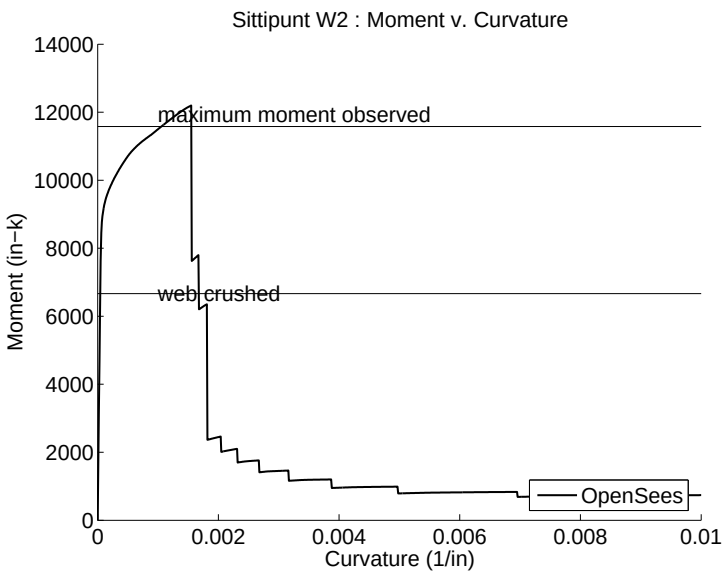

Figure B.44: Moment Curvature Analysis – Sittipunt W2

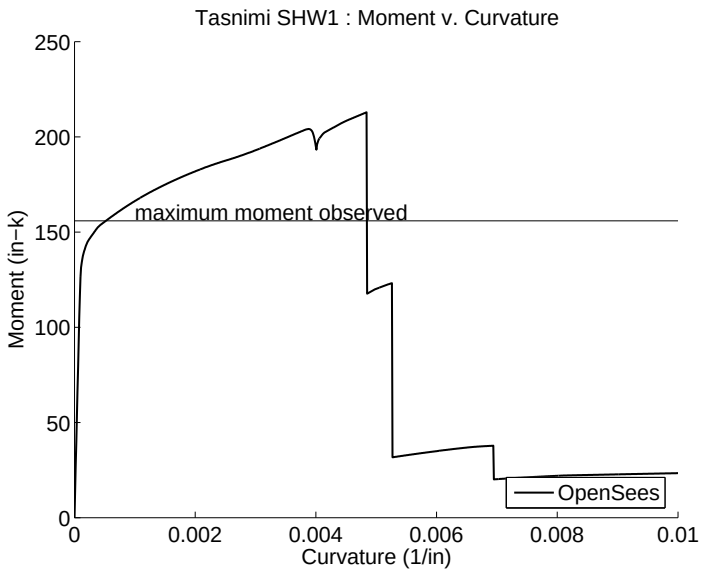

Figure B.45: Moment Curvature Analysis – Tasnimi SHW1

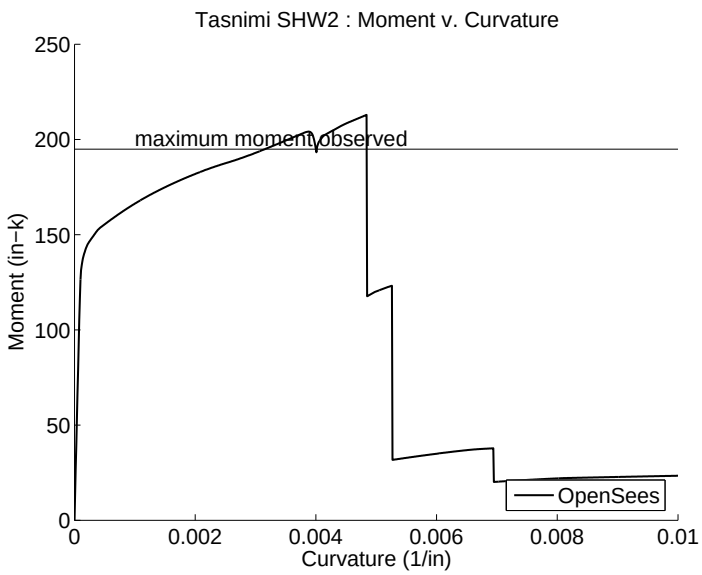

Figure B.46: Moment Curvature Analysis – Tasnimi SHW2

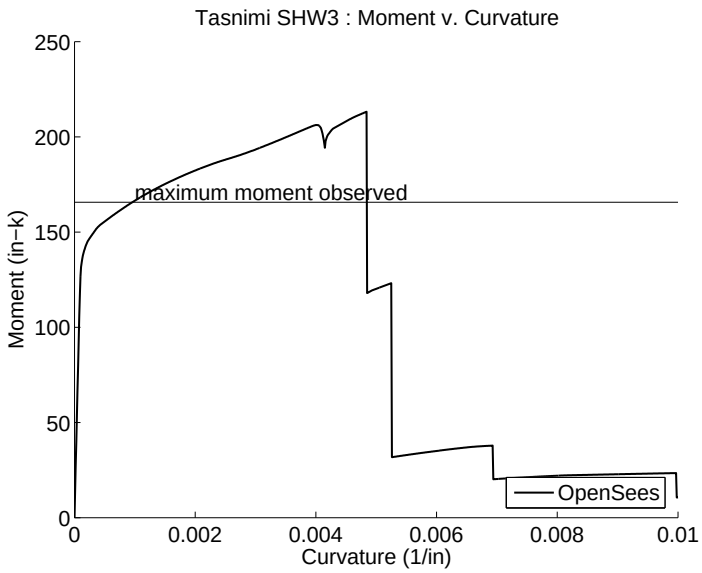

Figure B.47: Moment Curvature Analysis – Tasnimi SHW3

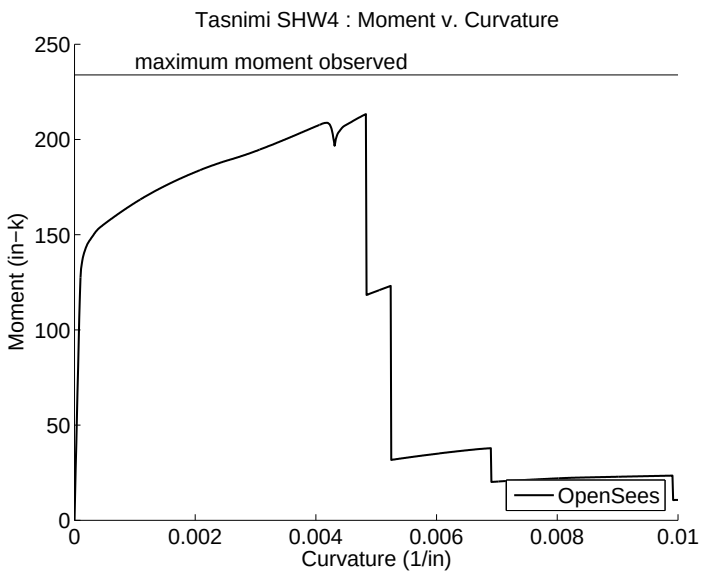

Figure B.48: Moment Curvature Analysis – Tasnimi SHW4

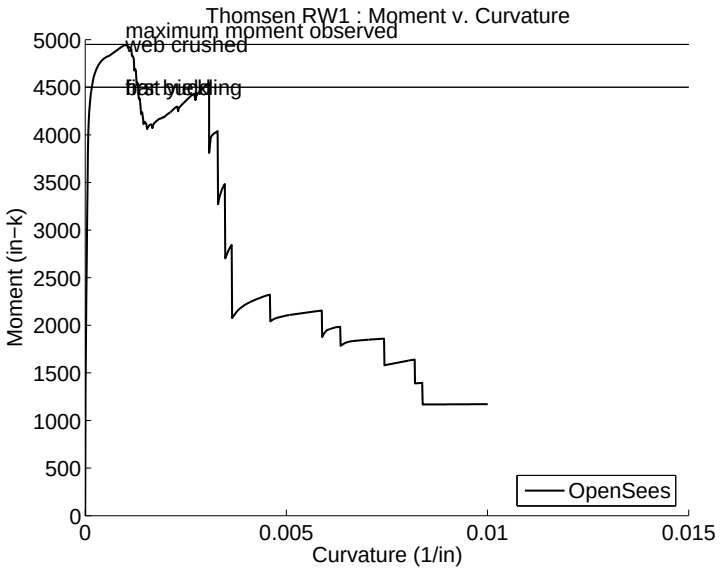

Figure B.49: Moment Curvature Analysis – Thomsen RW1

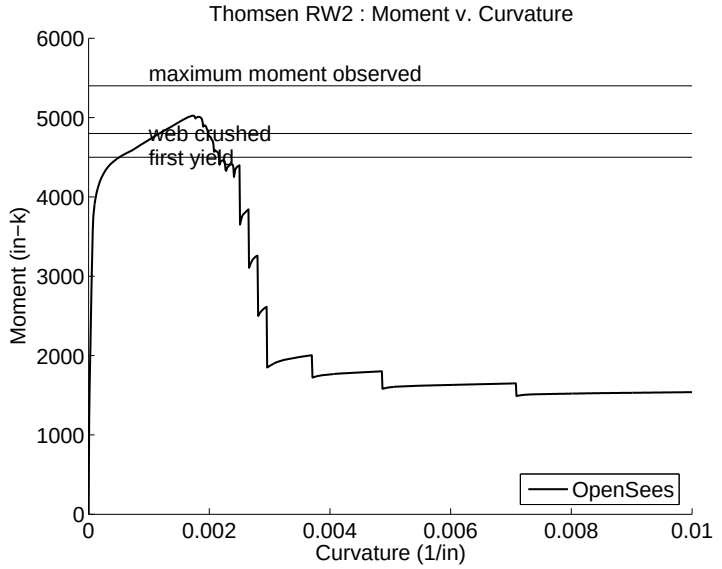

Figure B.50: Moment Curvature Analysis – Thomsen RW2

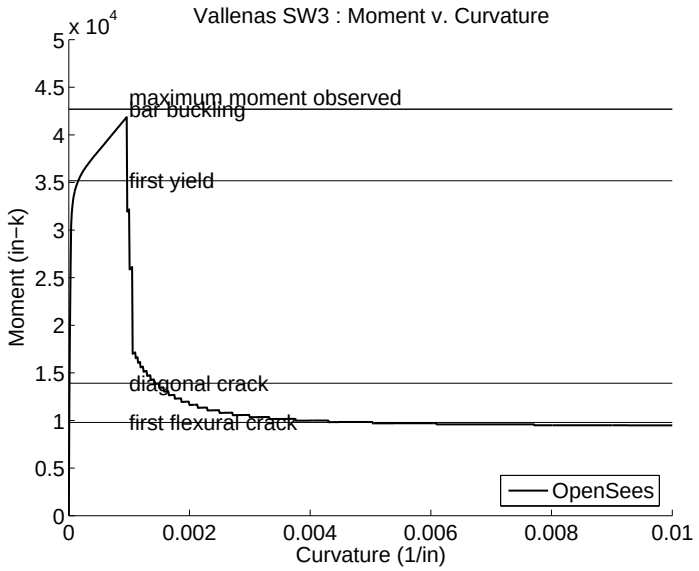

Figure B.51: Moment Curvature Analysis – Vallenas SW3

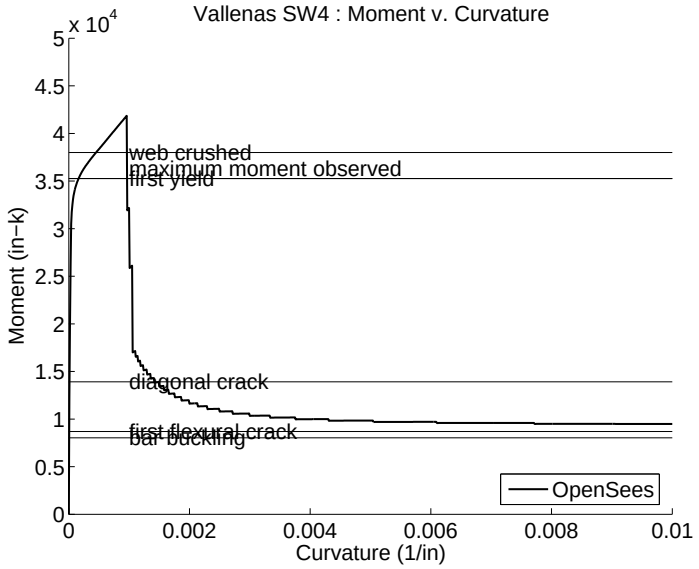

Figure B.52: Moment Curvature Analysis – Vallenas SW4

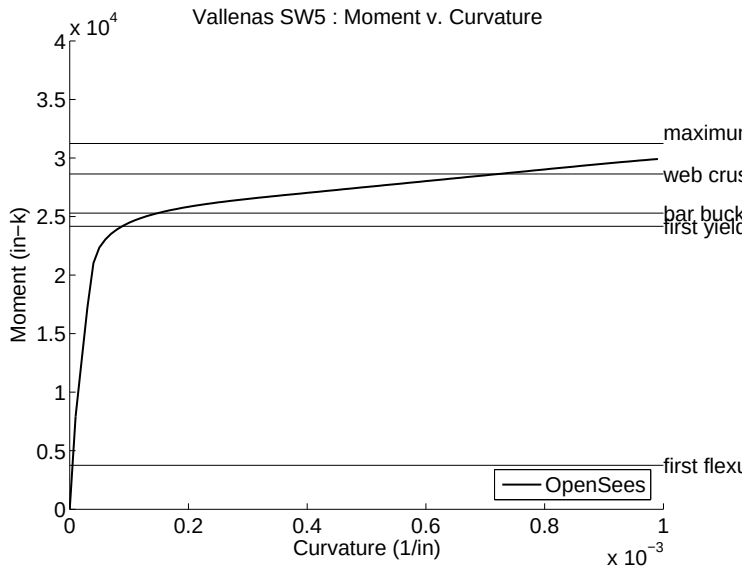

Figure B.53: Moment Curvature Analysis – Vallenas SW5

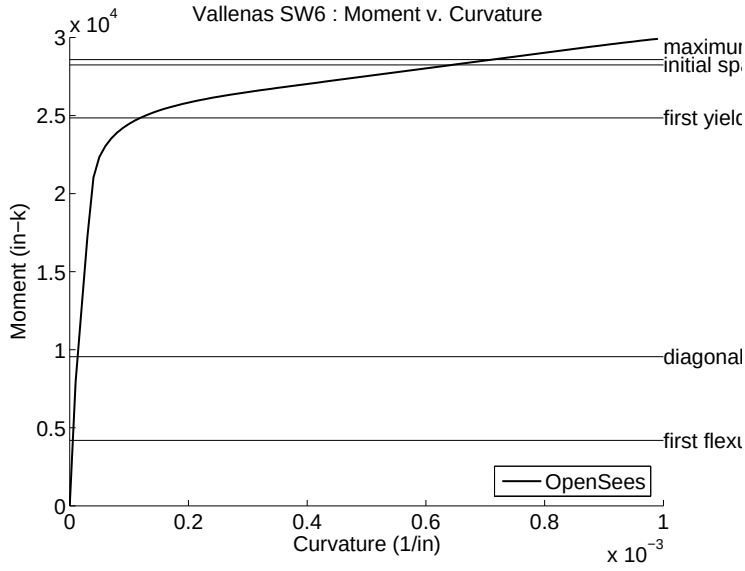

Figure B.54: Moment Curvature Analysis – Vallenas SW6

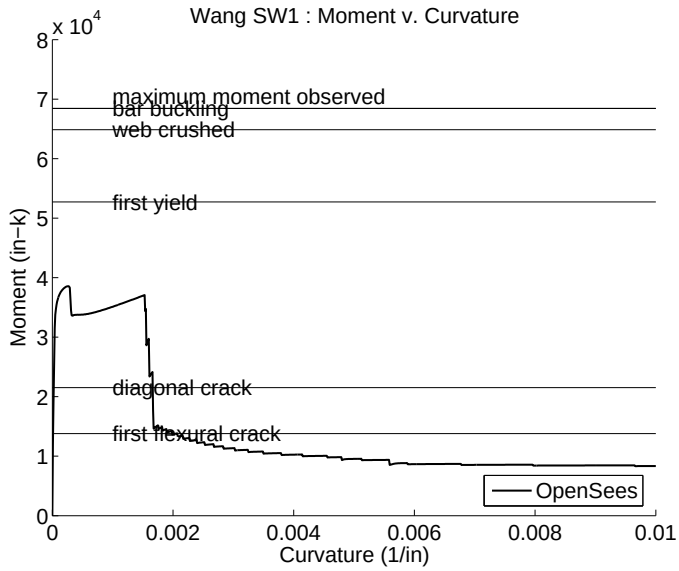

Figure B.55: Moment Curvature Analysis – Wang SW1

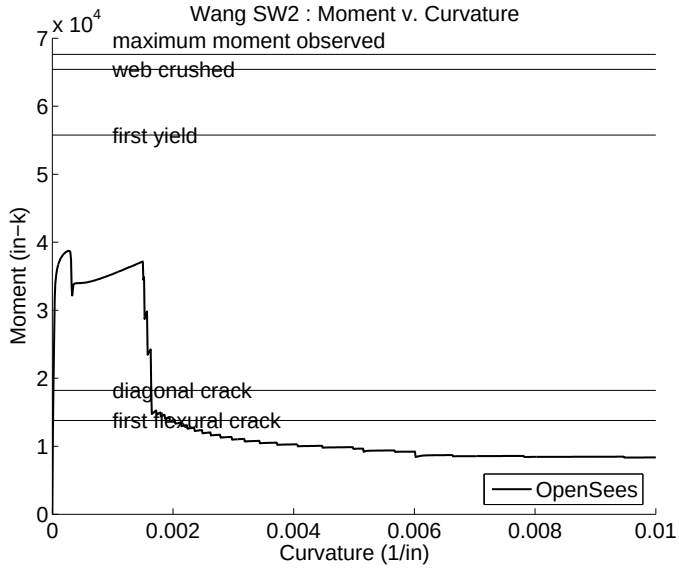

Figure B.56: Moment Curvature Analysis – Wang SW2

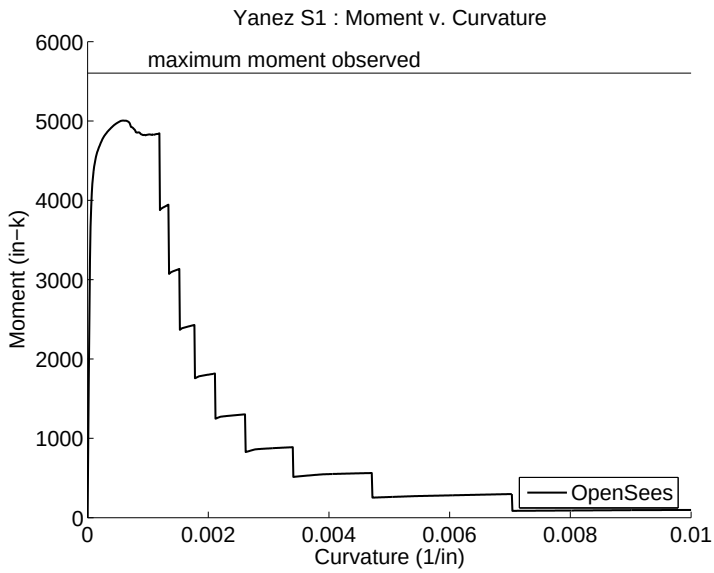

Figure B.57: Moment Curvature Analysis – Yanez S1

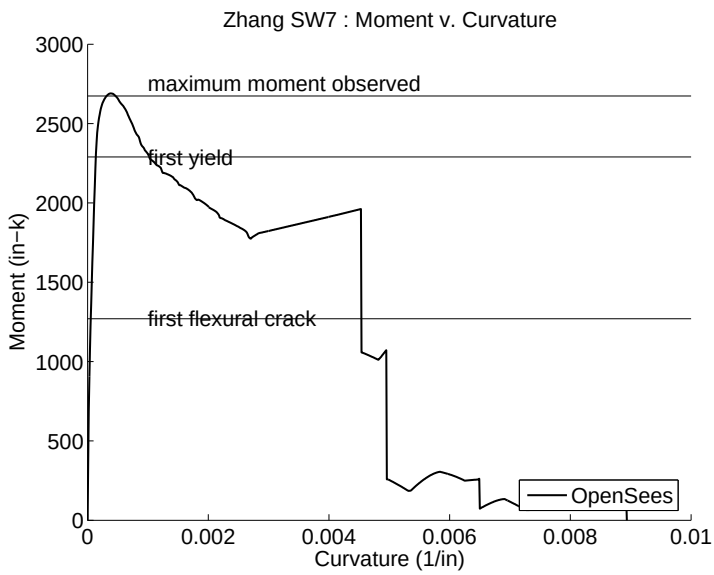

Figure B.58: Moment Curvature Analysis – Zhang SW7

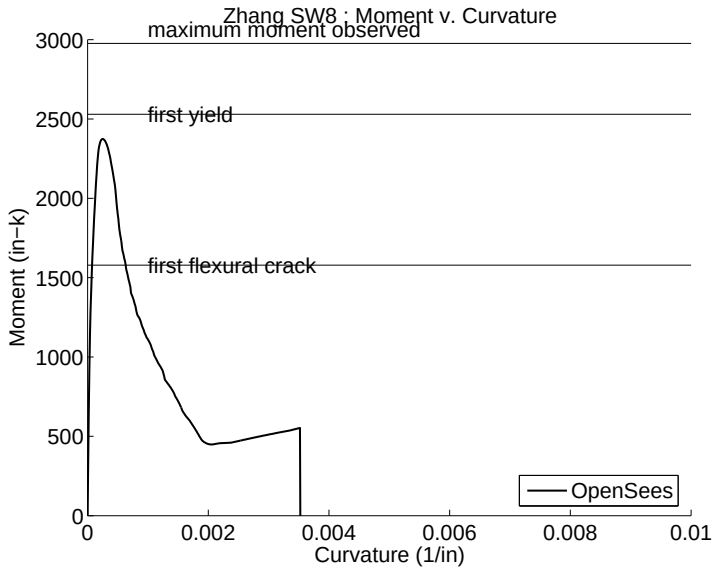

Figure B.59: Moment Curvature Analysis – Zhang SW8

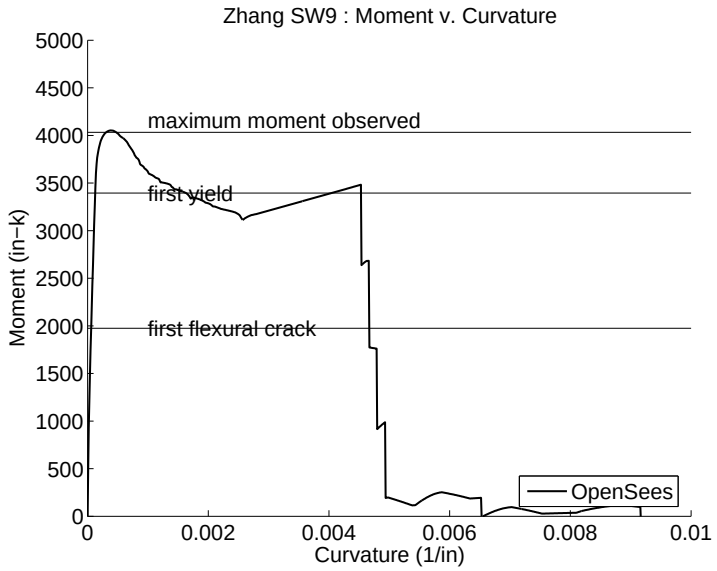

Figure B.60: Moment Curvature Analysis – Zhang SW9

Appendix C

MOMENT CURVATURE ANALYSIS FIGURES – COMPARE PROGRAMS

The moment curvature results were compared to those provided by a similar moment curvature program implemented in Matlab. The Matlab model uses a different integration scheme for the concrete and a different material model for the reinforcement. Despite these differences, good agreement was found between the two implementations. These comparisons were performed to debug and validate the model construction techniques of the preprocessor. Figures C.1 – C.60 show these relationships.

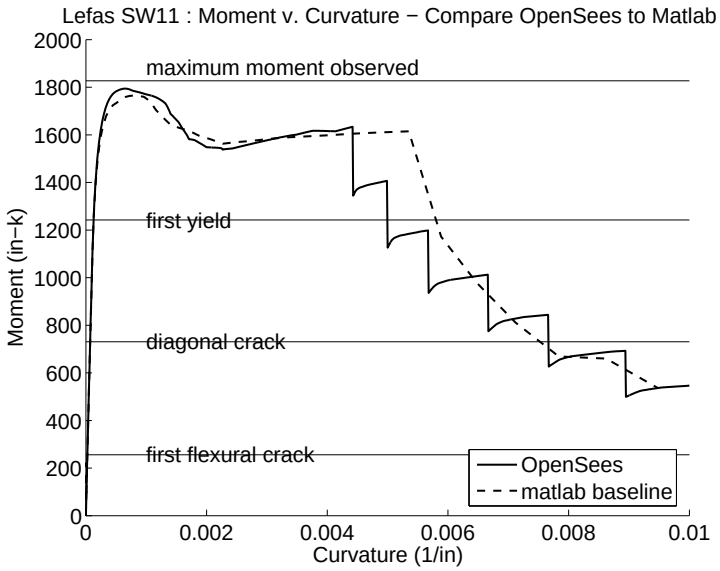

Figure C.1: Moment Curvature Analysis Comparison – Lefas SW11

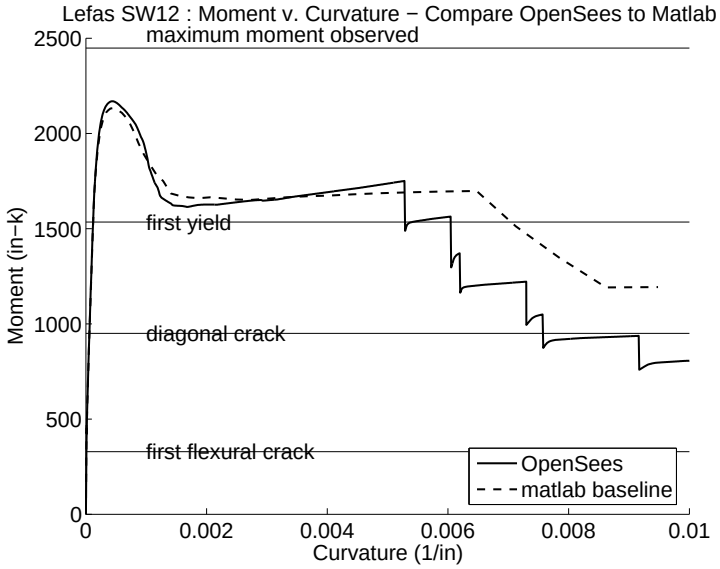

Figure C.2: Moment Curvature Analysis Comparison – Lefas SW12

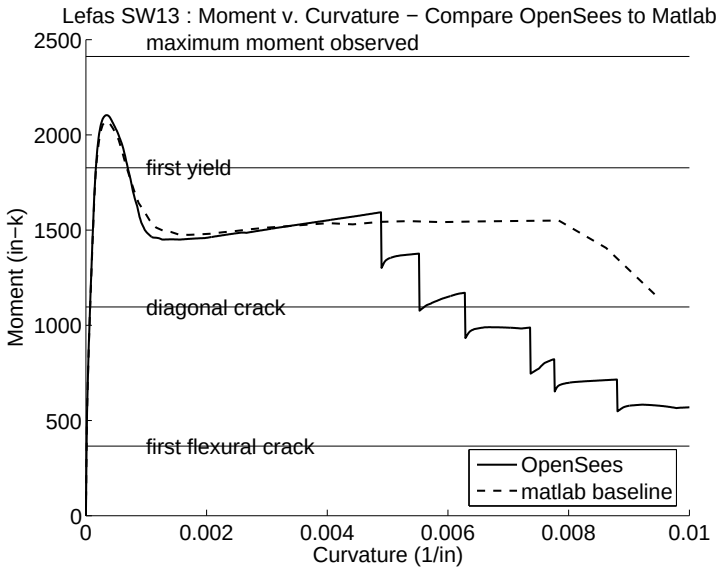

Figure C.3: Moment Curvature Analysis Comparison – Lefas SW13

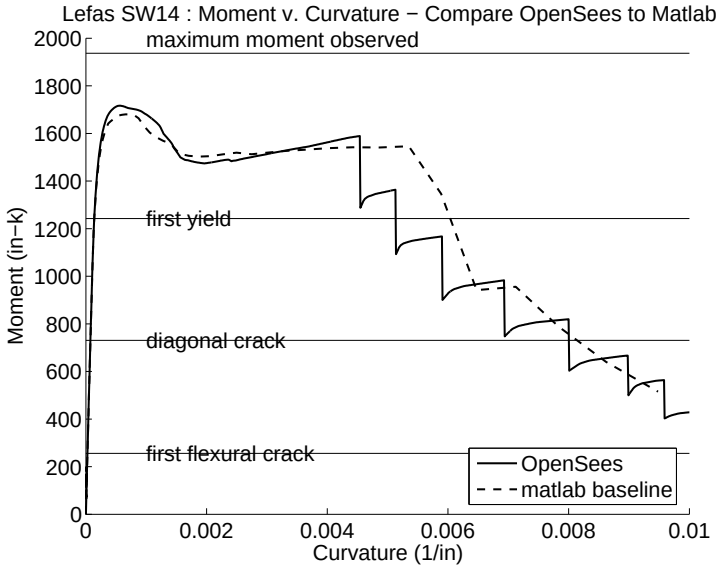

Figure C.4: Moment Curvature Analysis Comparison – Lefas SW14

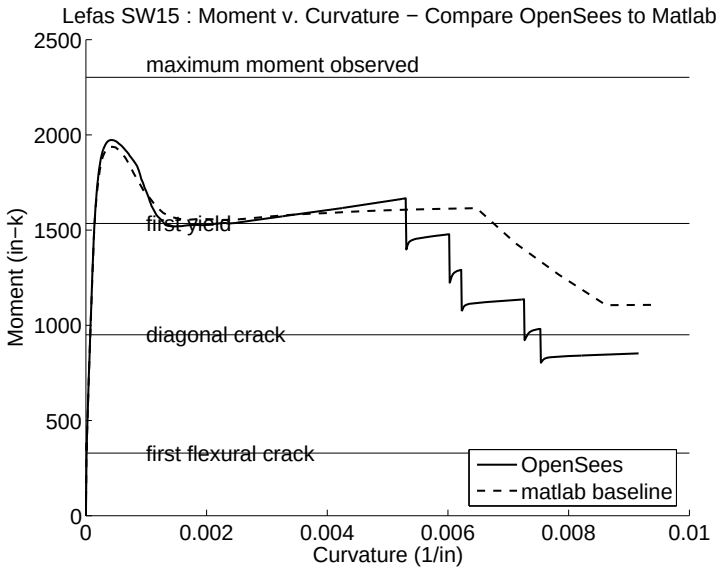

Figure C.5: Moment Curvature Analysis Comparison – Lefas SW15

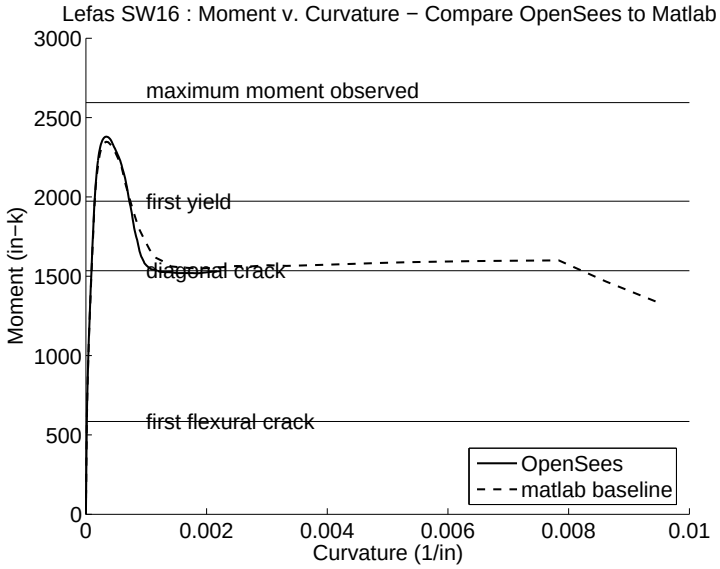

Figure C.6: Moment Curvature Analysis Comparison – Lefas SW16

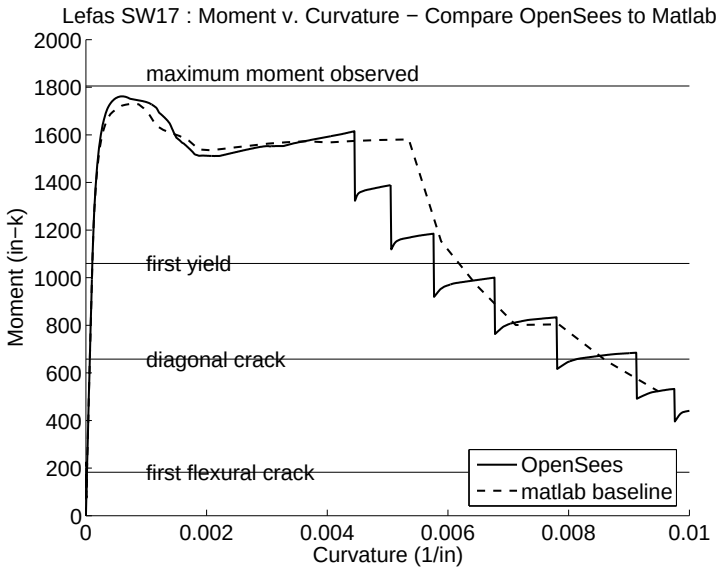

Figure C.7: Moment Curvature Analysis Comparison – Lefas SW17

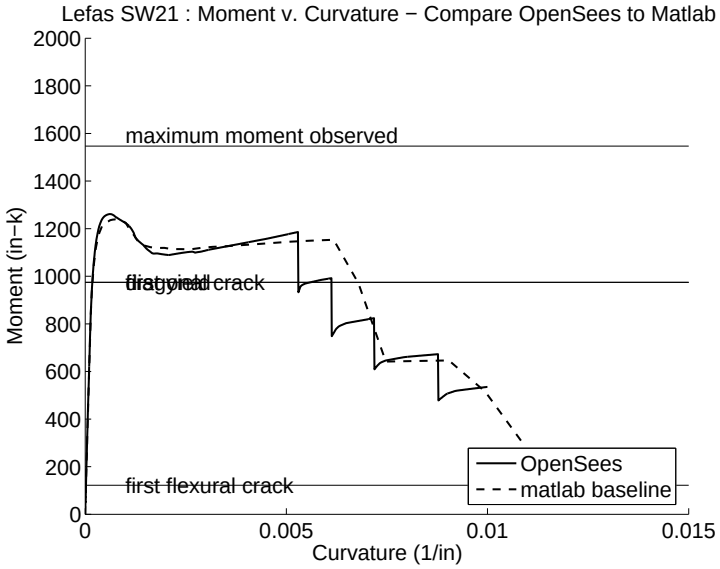

Figure C.8: Moment Curvature Analysis Comparison – Lefas SW21

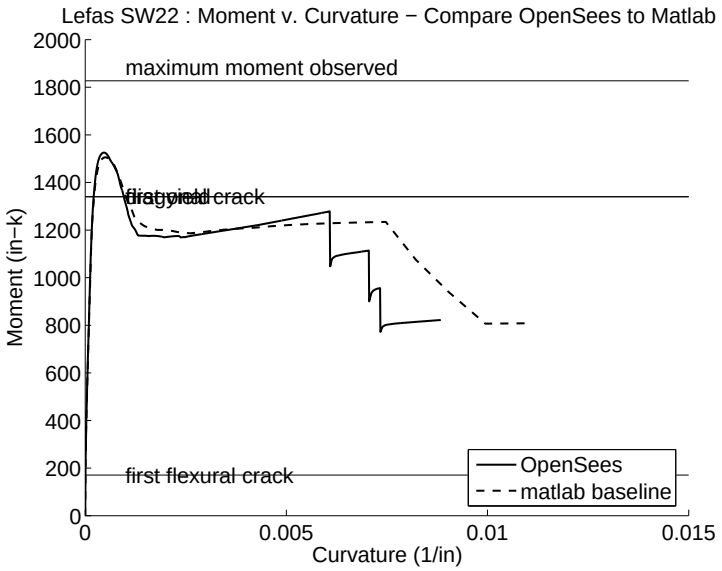

Figure C.9: Moment Curvature Analysis Comparison – Lefas SW22

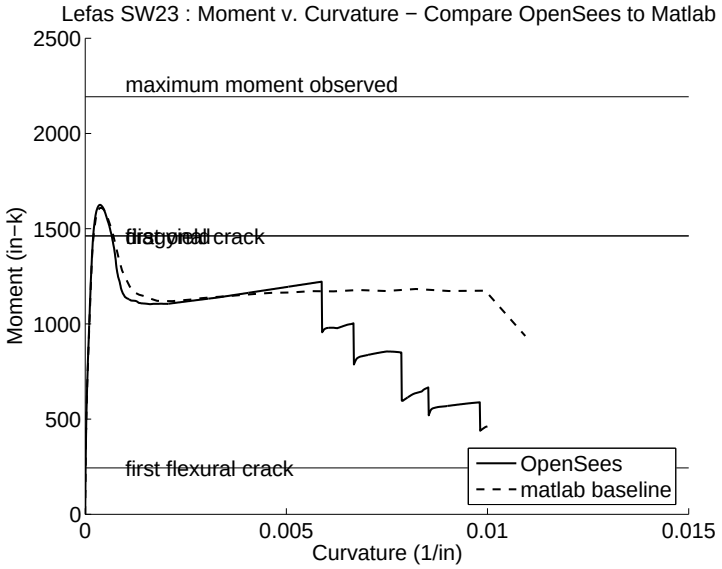

Figure C.10: Moment Curvature Analysis Comparison – Lefas SW23

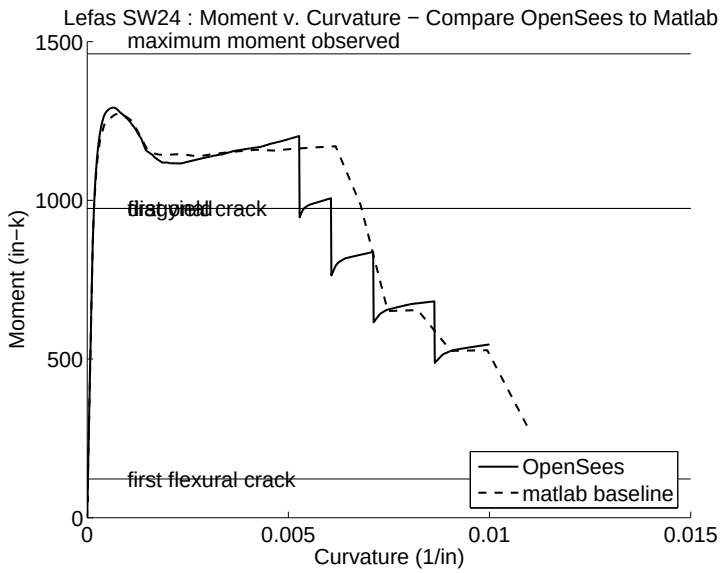

Figure C.11: Moment Curvature Analysis Comparison – Lefas SW24

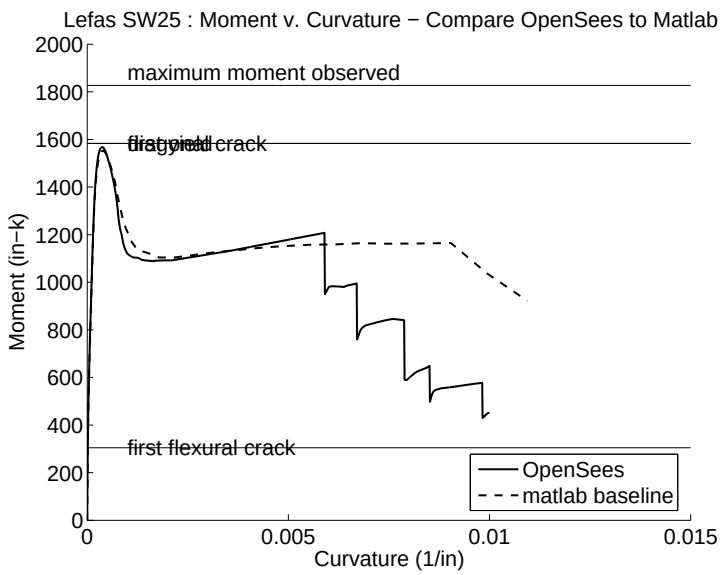

Figure C.12: Moment Curvature Analysis Comparison – Lefas SW25

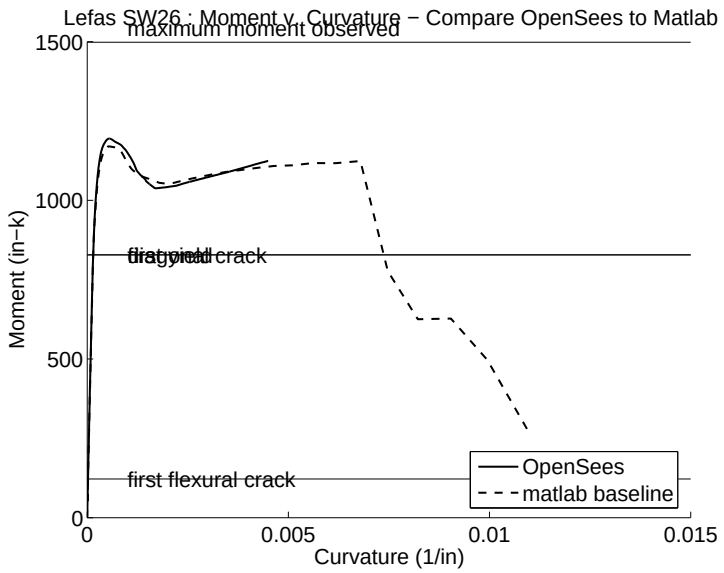

Figure C.13: Moment Curvature Analysis Comparison – Lefas SW26

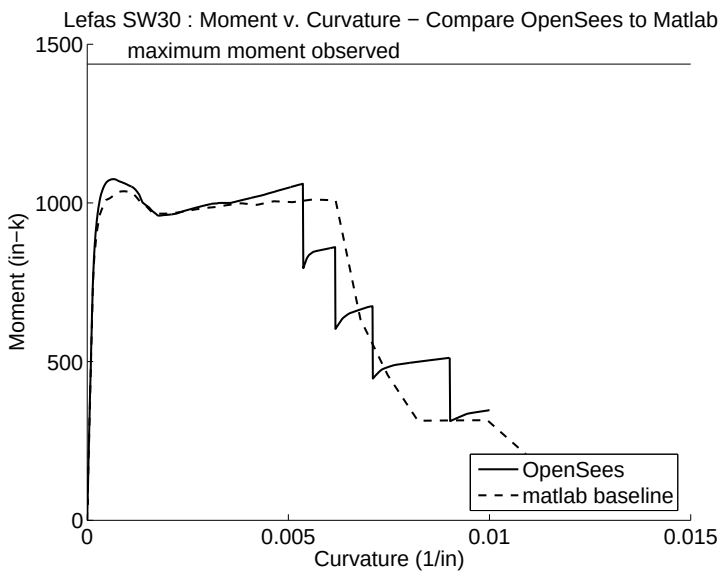

Figure C.14: Moment Curvature Analysis Comparison – Lefas SW30

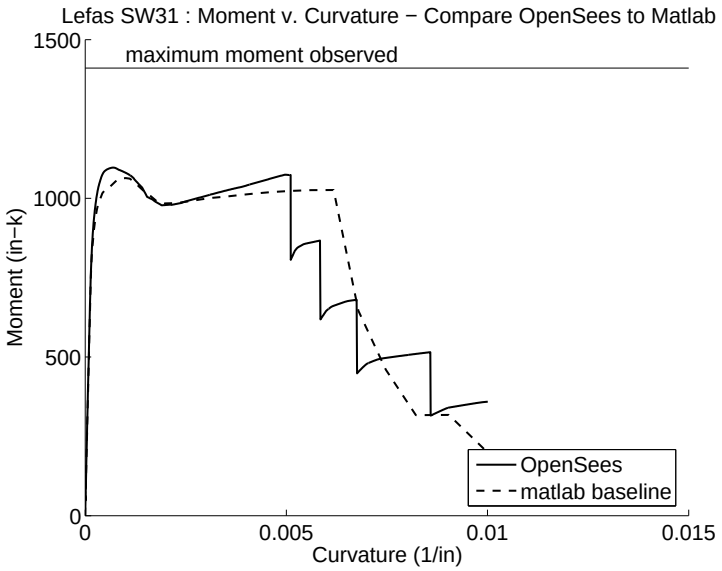

Figure C.15: Moment Curvature Analysis Comparison – Lefas SW31

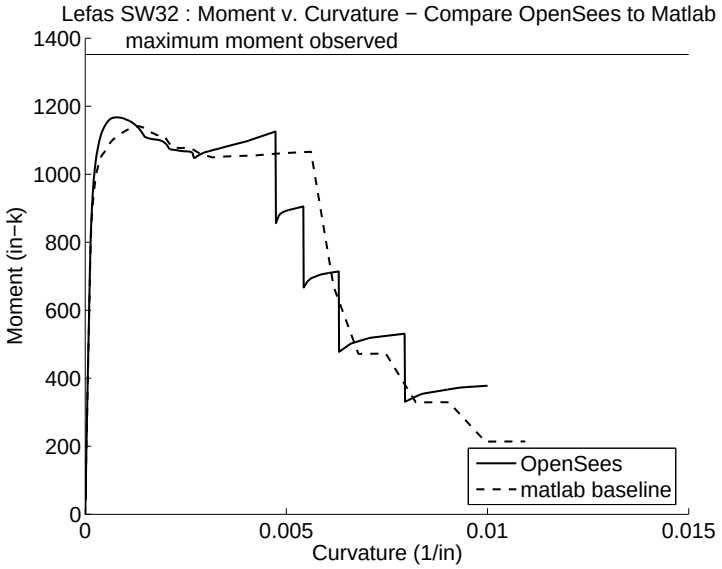

Figure C.16: Moment Curvature Analysis Comparison – Lefas SW32

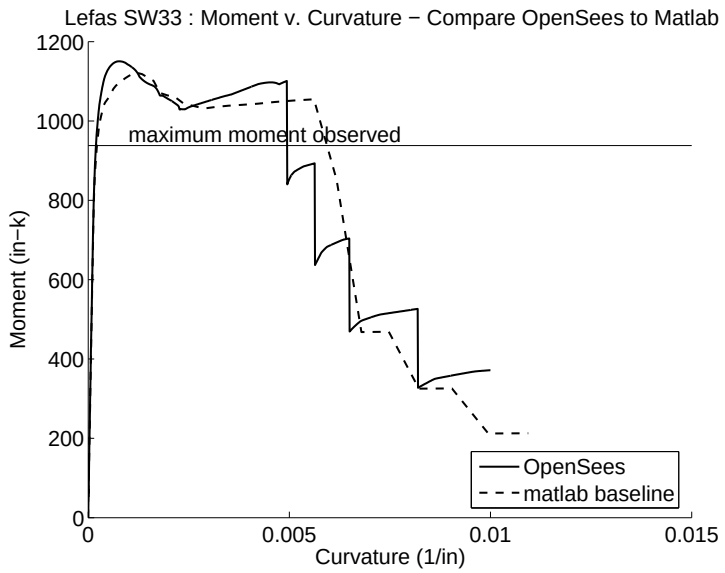

Figure C.17: Moment Curvature Analysis Comparison – Lefas SW33

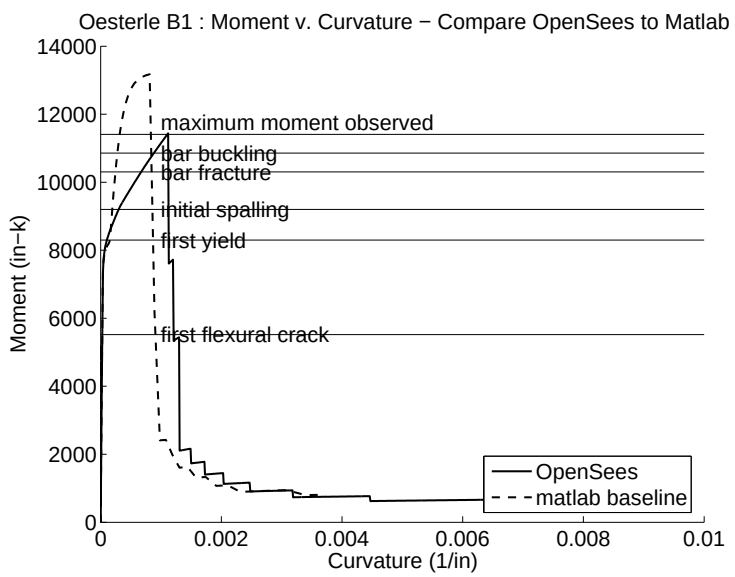

Figure C.18: Moment Curvature Analysis Comparison – Oesterle B1

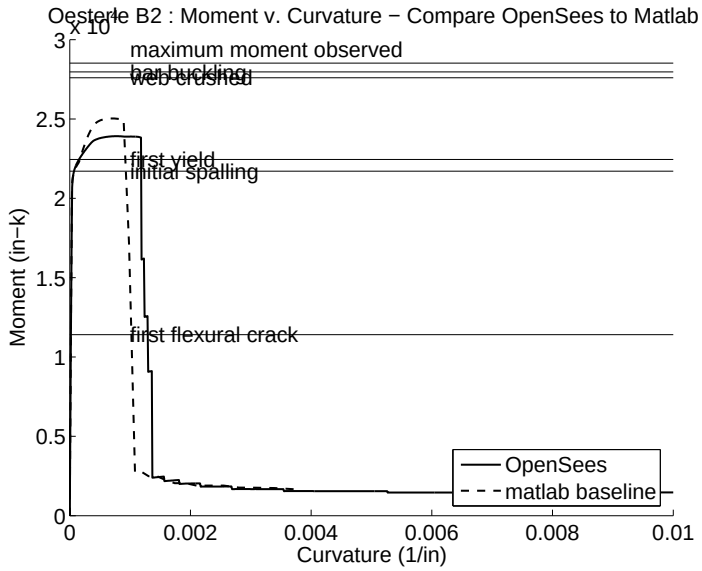

Figure C.19: Moment Curvature Analysis Comparison – Oesterle B2

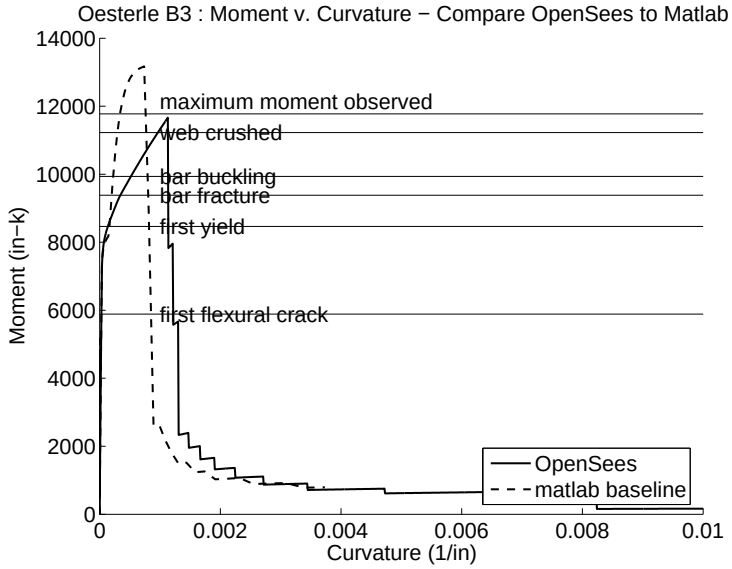

Figure C.20: Moment Curvature Analysis Comparison – Oesterle B3

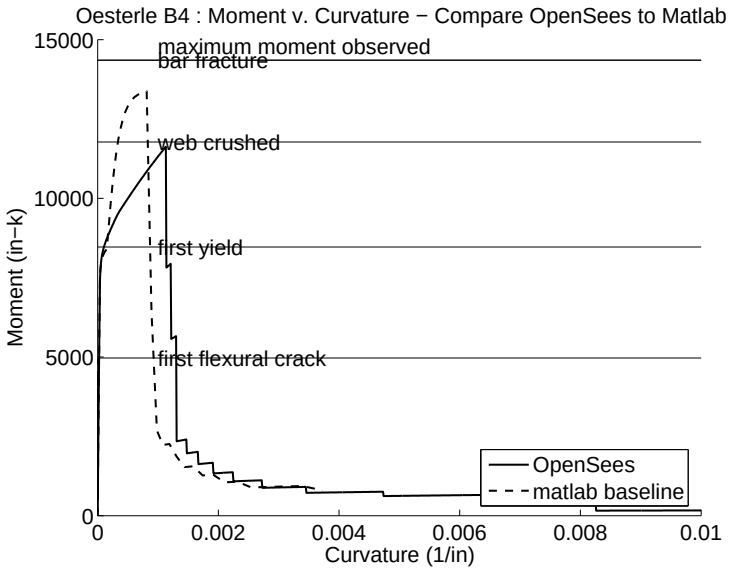

Figure C.21: Moment Curvature Analysis Comparison – Oesterle B4

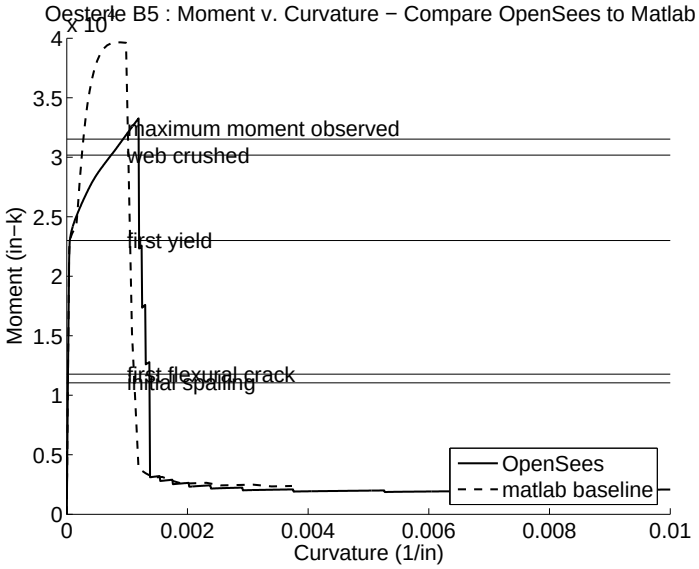

Figure C.22: Moment Curvature Analysis Comparison – Oesterle B5

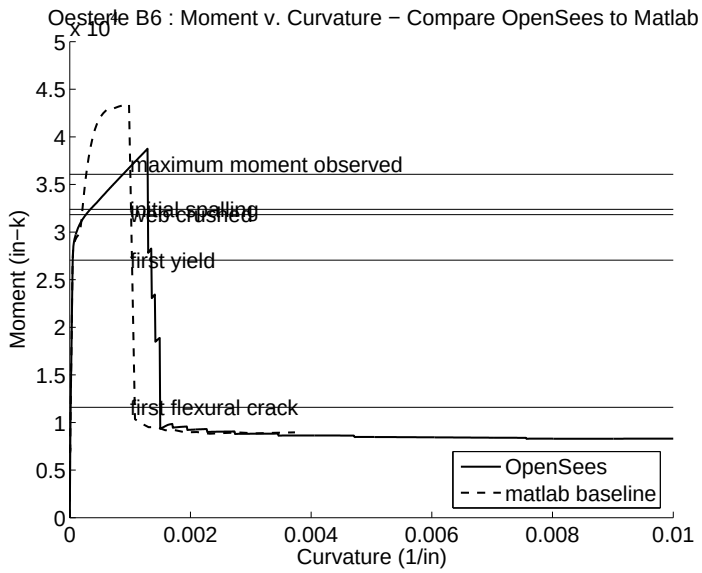

Figure C.23: Moment Curvature Analysis Comparison – Oesterle B6

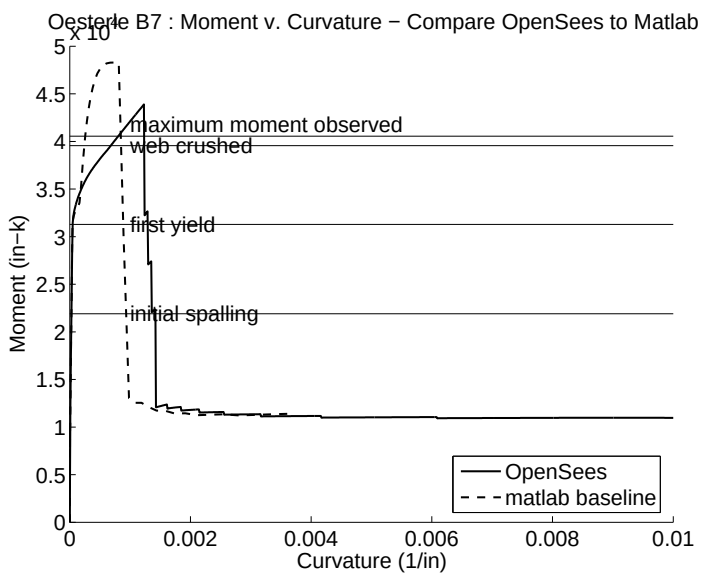

Figure C.24: Moment Curvature Analysis Comparison – Oesterle B7

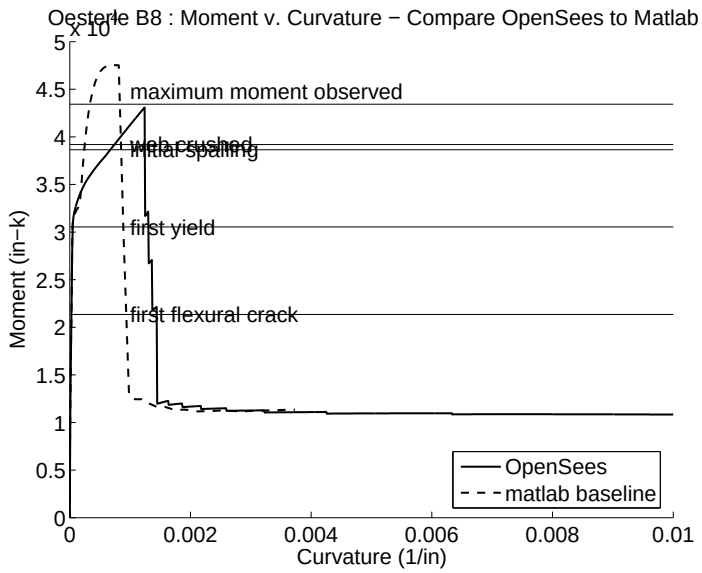

Figure C.25: Moment Curvature Analysis Comparison – Oesterle B8

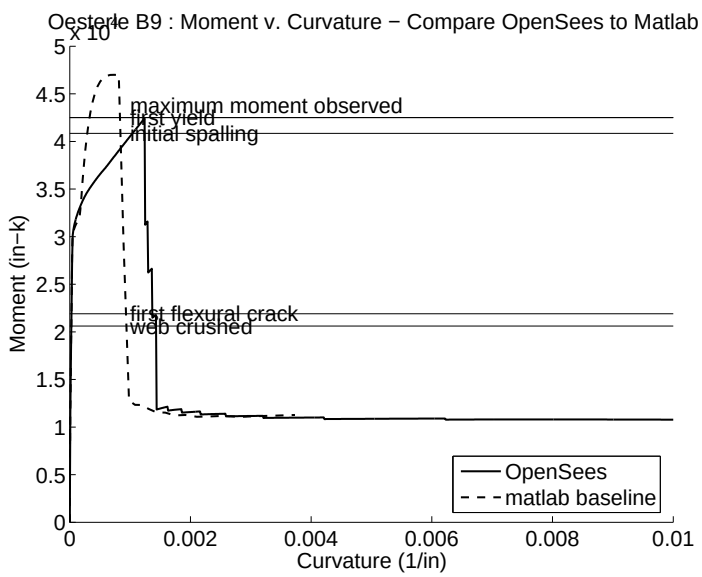

Figure C.26: Moment Curvature Analysis Comparison – Oesterle B9

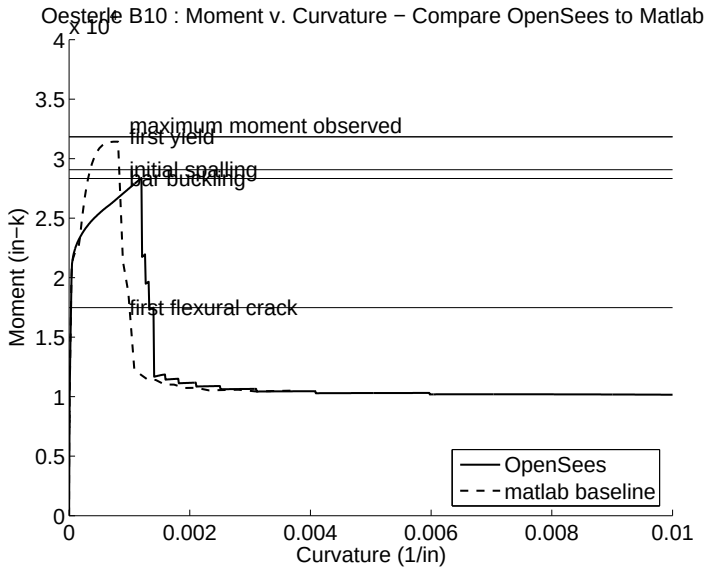

Figure C.27: Moment Curvature Analysis Comparison – Oesterle B10

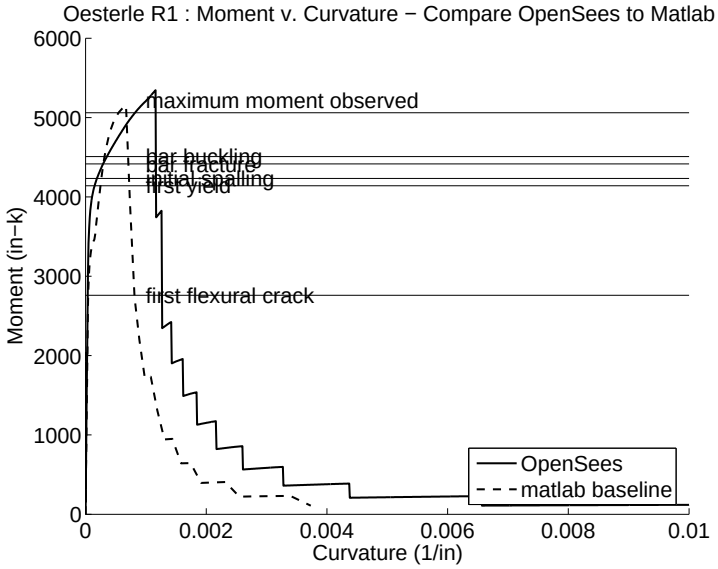

Figure C.28: Moment Curvature Analysis Comparison – Oesterle R1

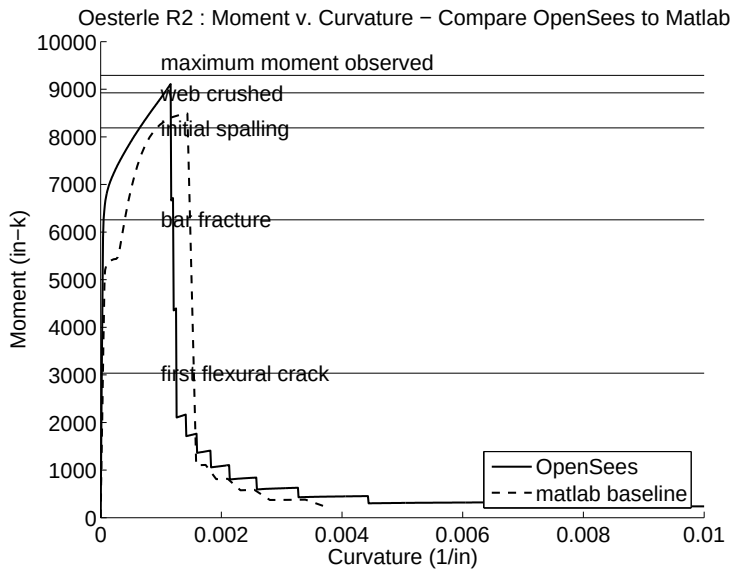

Figure C.29: Moment Curvature Analysis Comparison – Oesterle R2

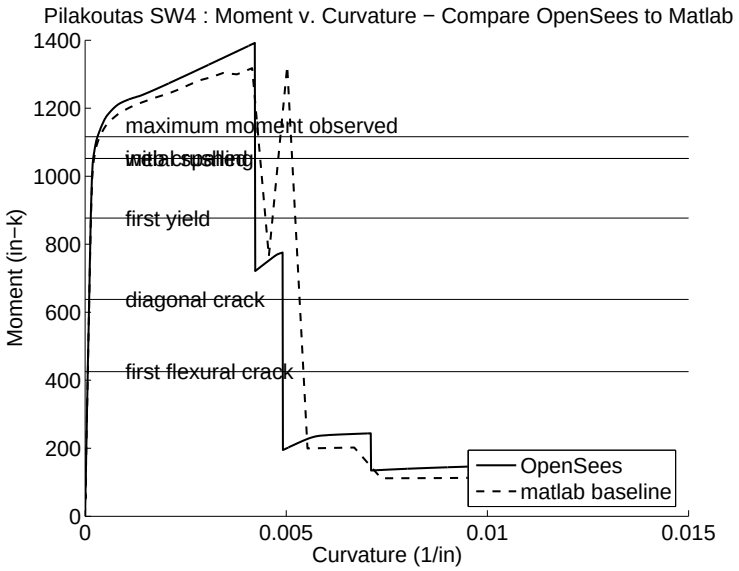

Figure C.30: Moment Curvature Analysis Comparison – Pilakoutas SW4

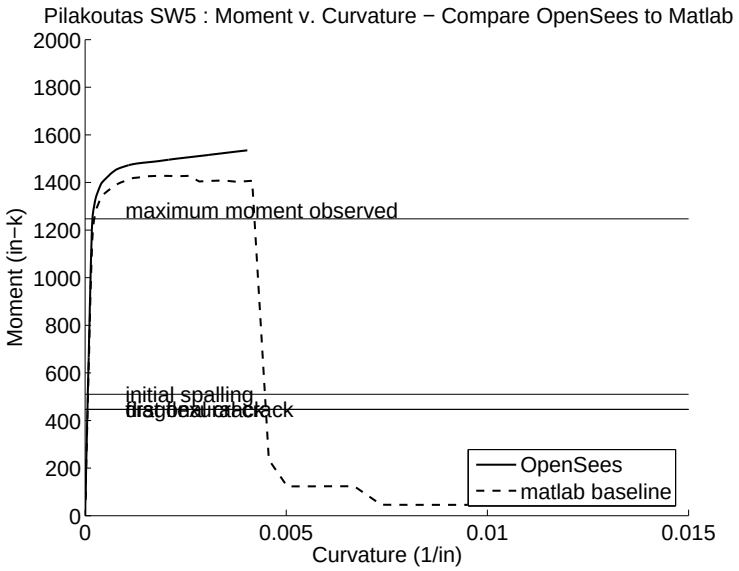

Figure C.31: Moment Curvature Analysis Comparison – Pilakoutas SW5

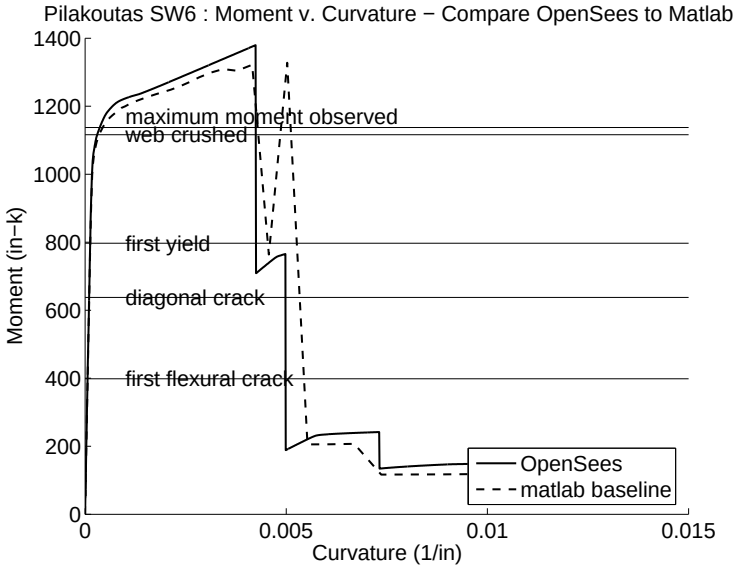

Figure C.32: Moment Curvature Analysis Comparison – Pilakoutas SW6

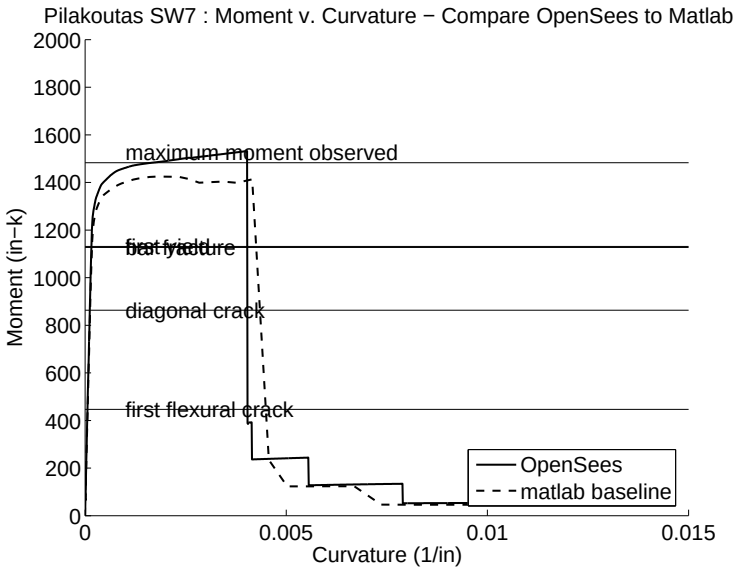

Figure C.33: Moment Curvature Analysis Comparison – Pilakoutas SW7

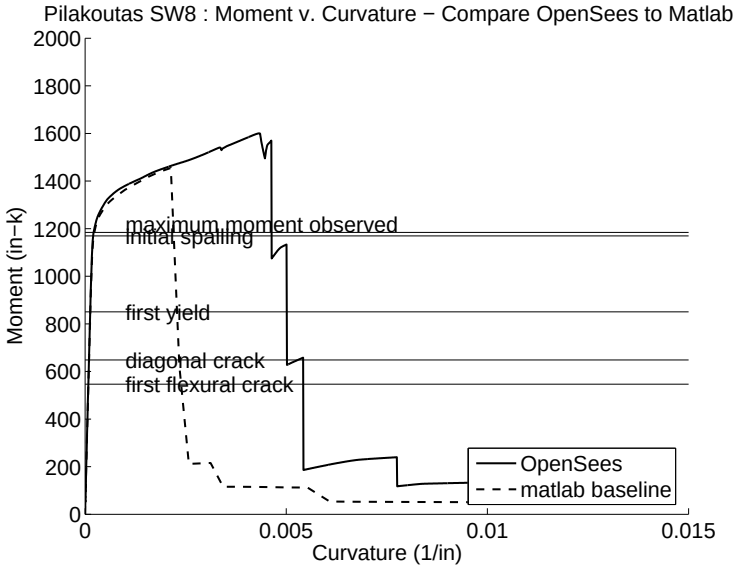

Figure C.34: Moment Curvature Analysis Comparison – Pilakoutas SW8

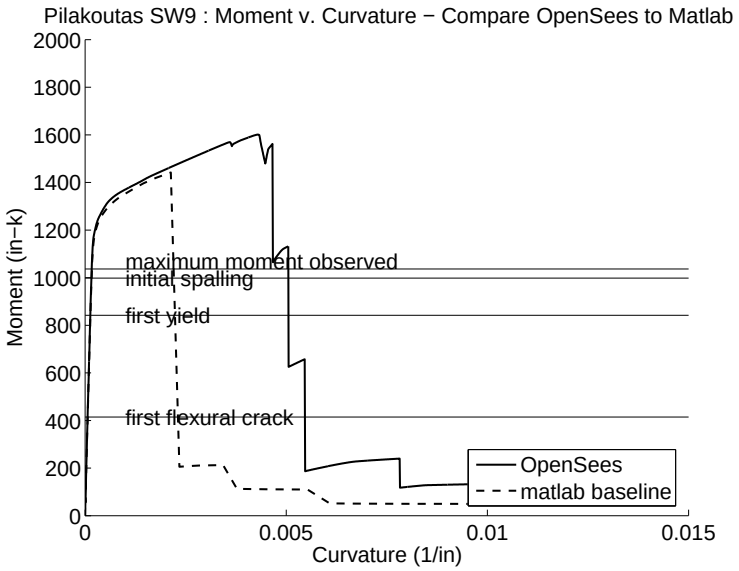

Figure C.35: Moment Curvature Analysis Comparison – Pilakoutas SW9

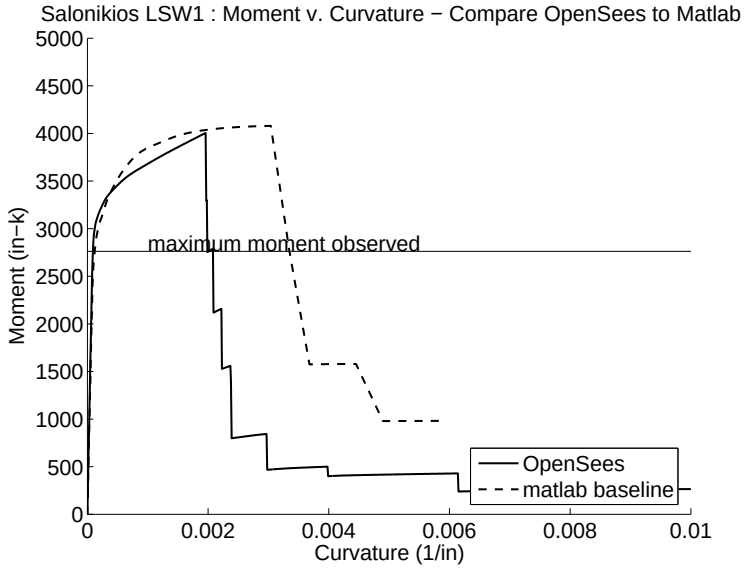

Figure C.36: Moment Curvature Analysis Comparison – Salonikios LSW1

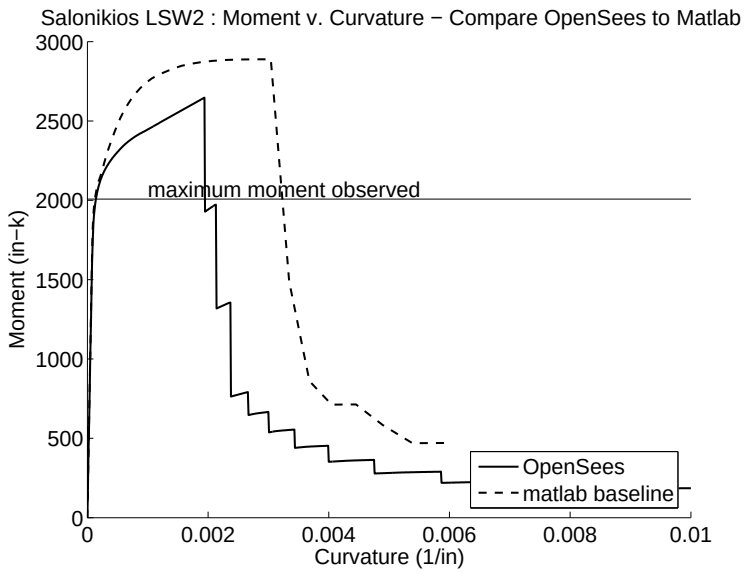

Figure C.37: Moment Curvature Analysis Comparison – Salonikios LSW2

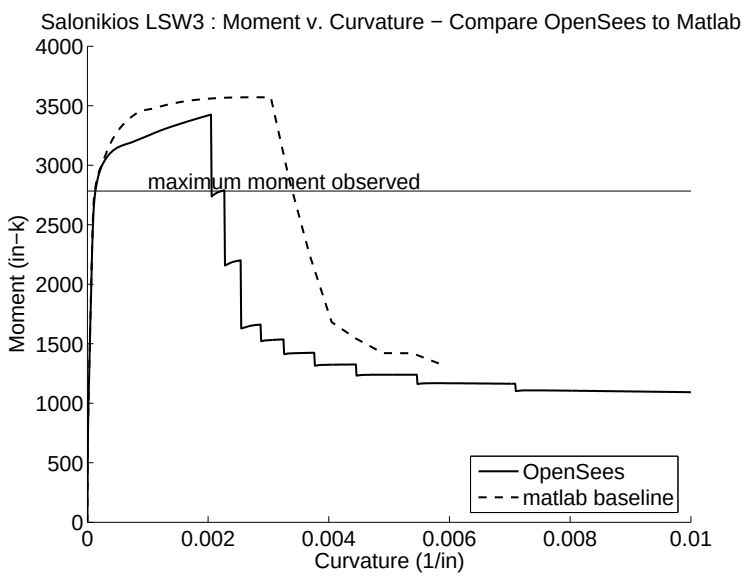

Figure C.38: Moment Curvature Analysis Comparison – Salonikios LSW3

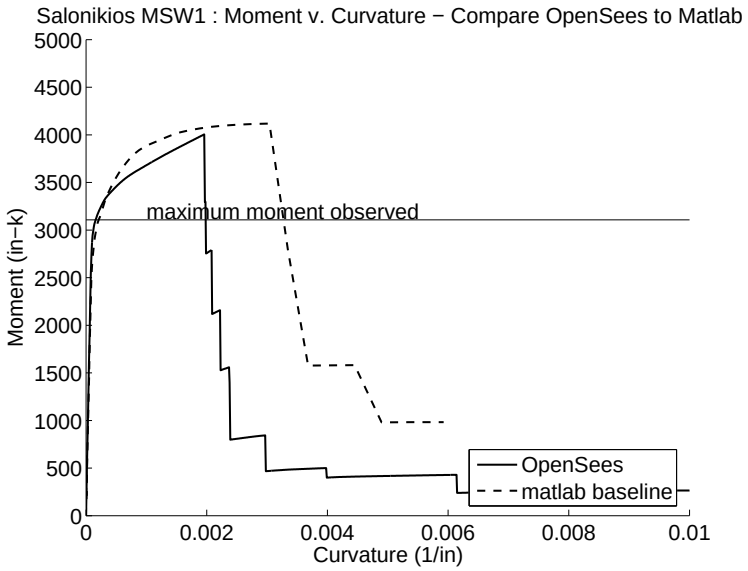

Figure C.39: Moment Curvature Analysis Comparison – Salonikios MSW1

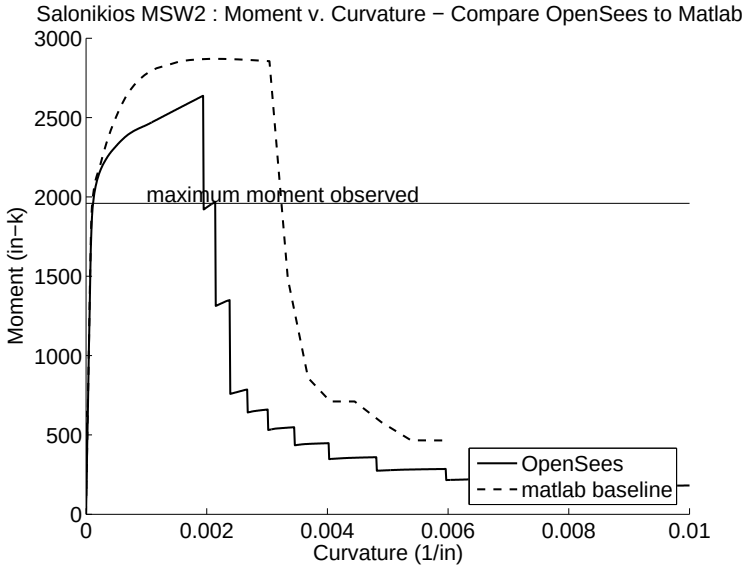

Figure C.40: Moment Curvature Analysis Comparison – Salonikios MSW2

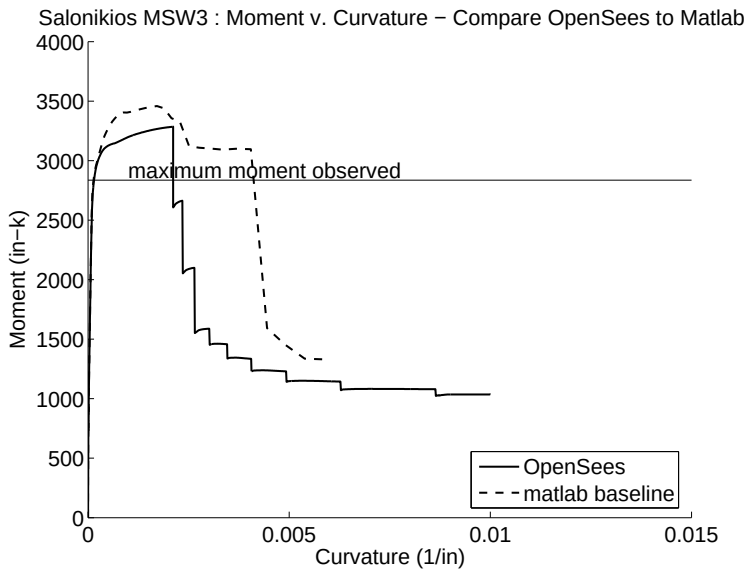

Figure C.41: Moment Curvature Analysis Comparison – Salonikios MSW3

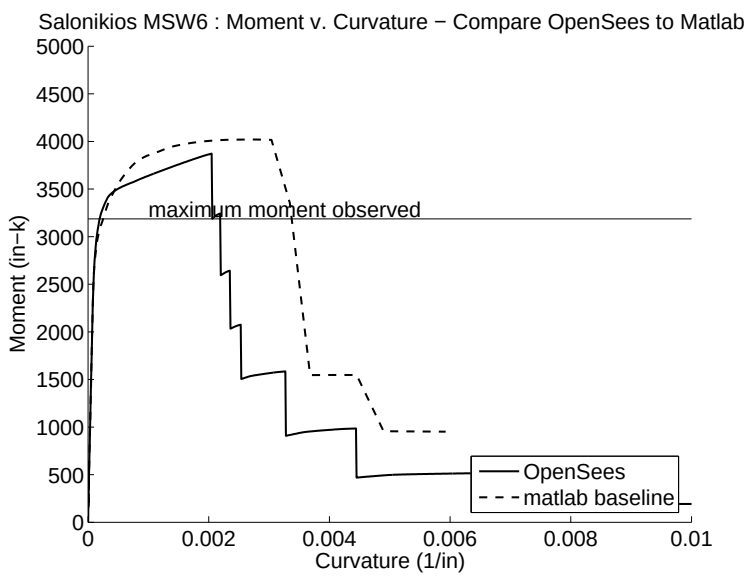

Figure C.42: Moment Curvature Analysis Comparison – Salonikios MSW6

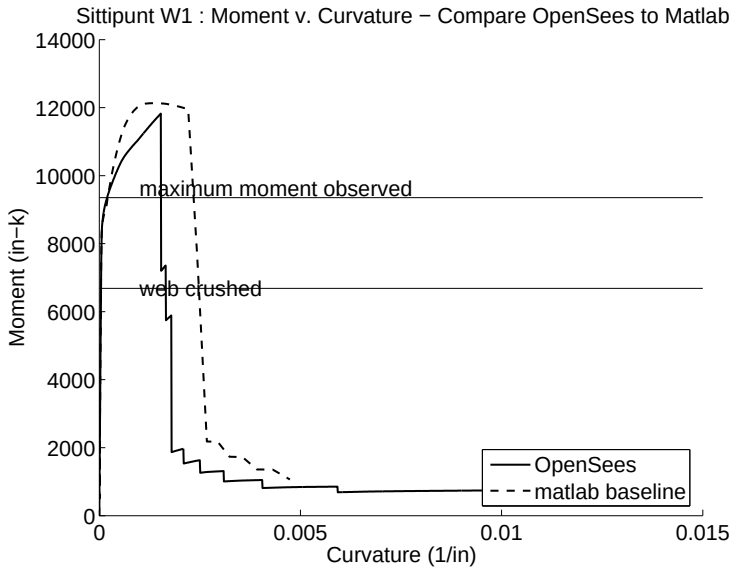

Figure C.43: Moment Curvature Analysis Comparison – Sittipunt W1

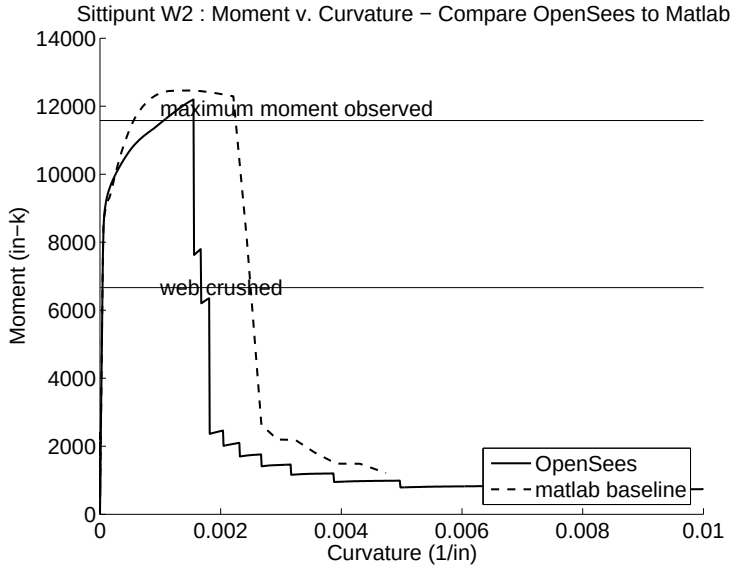

Figure C.44: Moment Curvature Analysis Comparison – Sittipunt W2

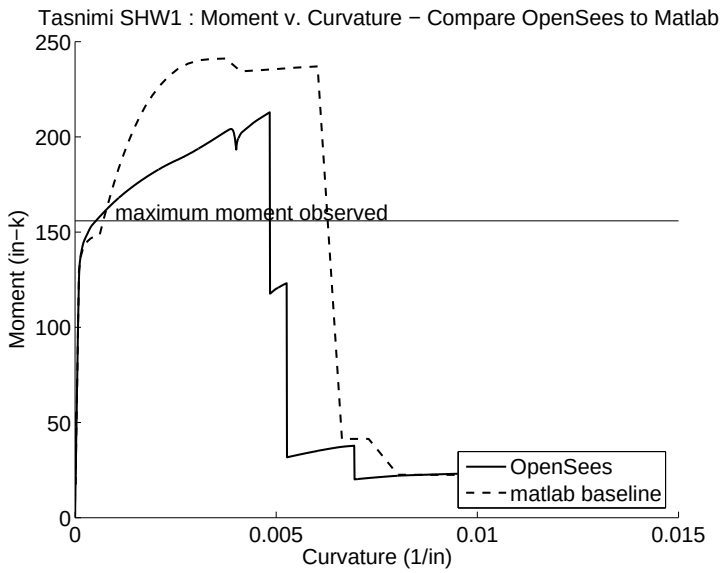

Figure C.45: Moment Curvature Analysis Comparison – Tasnimi SHW1

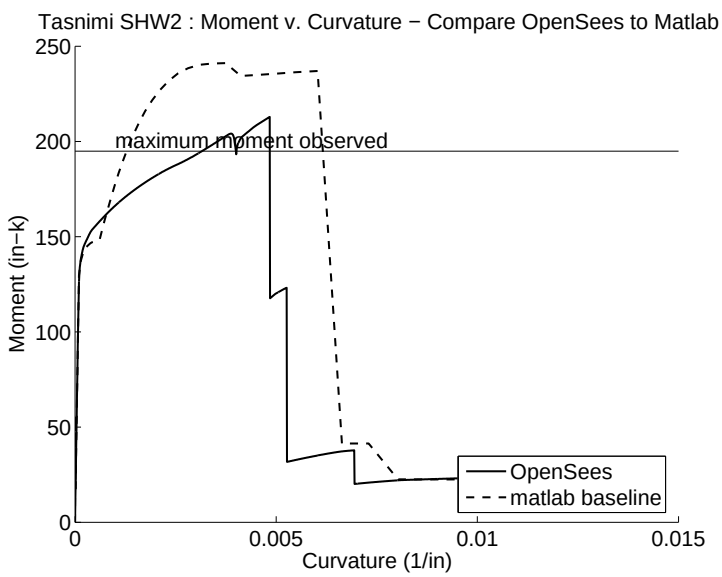

Figure C.46: Moment Curvature Analysis Comparison – Tasnimi SHW2

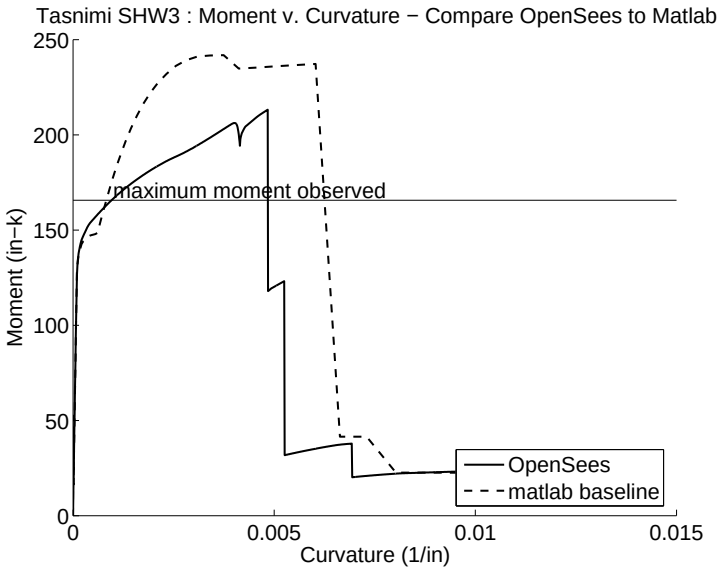

Figure C.47: Moment Curvature Analysis Comparison – Tasnimi SHW3

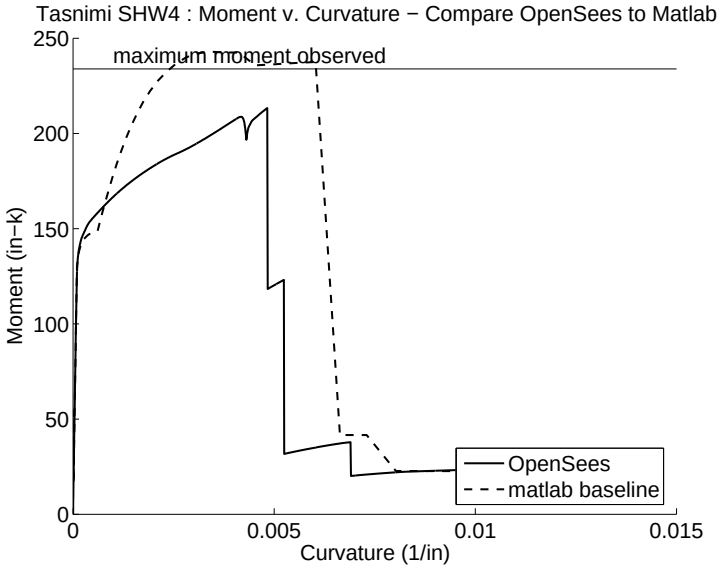

Figure C.48: Moment Curvature Analysis Comparison – Tasnimi SHW4

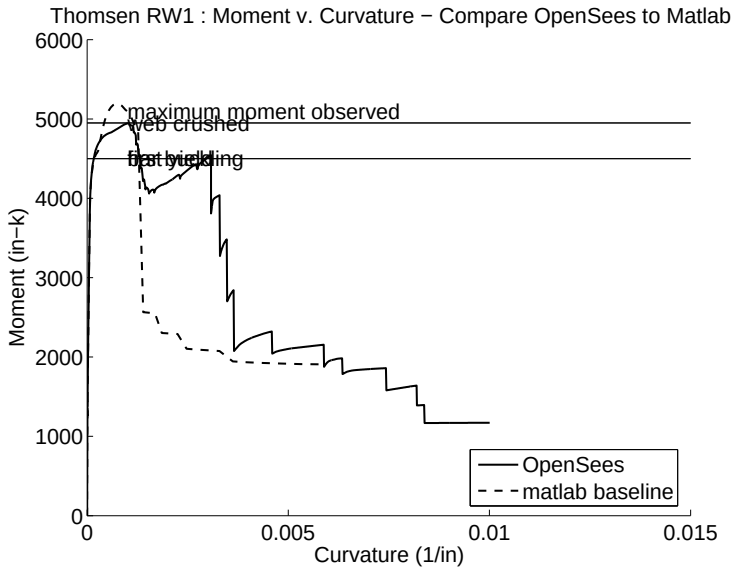

Figure C.49: Moment Curvature Analysis Comparison – Thomsen RW1

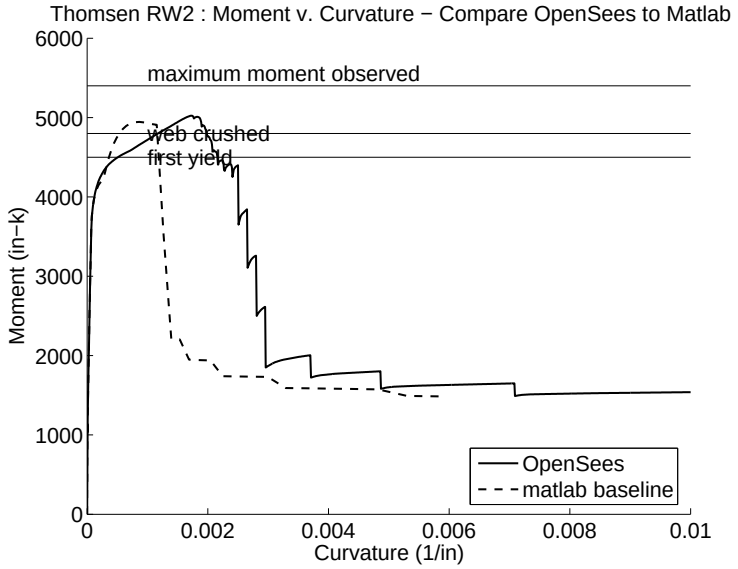

Figure C.50: Moment Curvature Analysis Comparison – Thomsen RW2

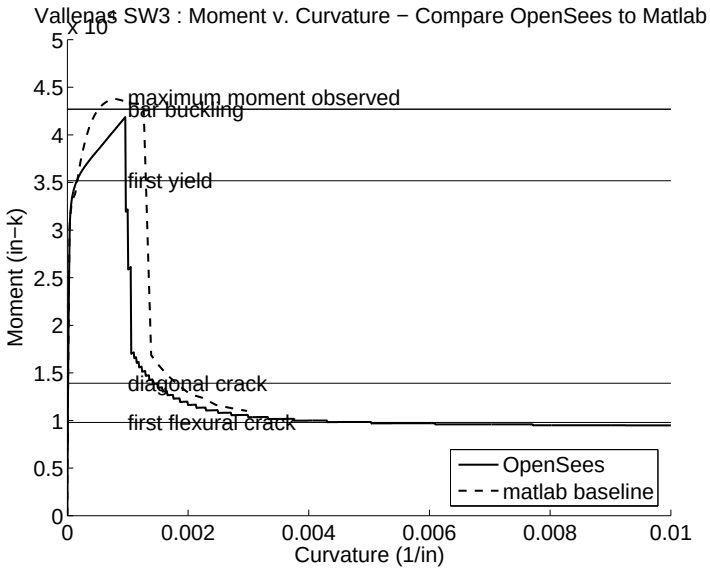

Figure C.51: Moment Curvature Analysis Comparison – Vallenas SW3

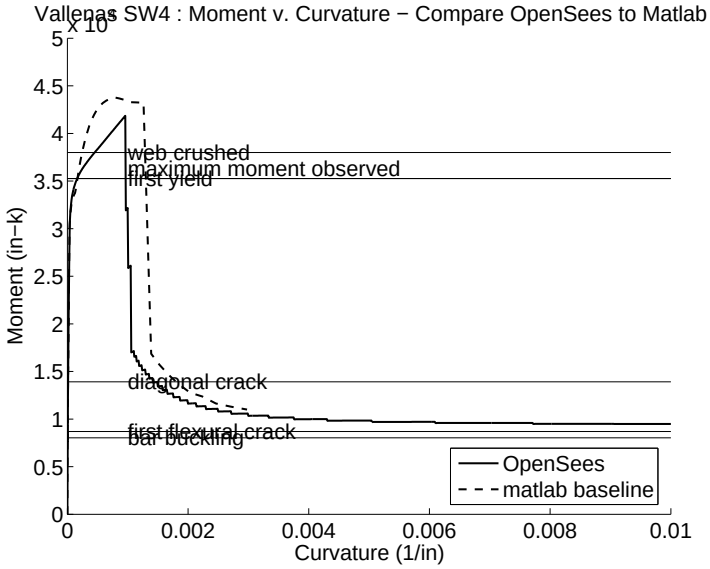

Figure C.52: Moment Curvature Analysis Comparison – Vallenas SW4

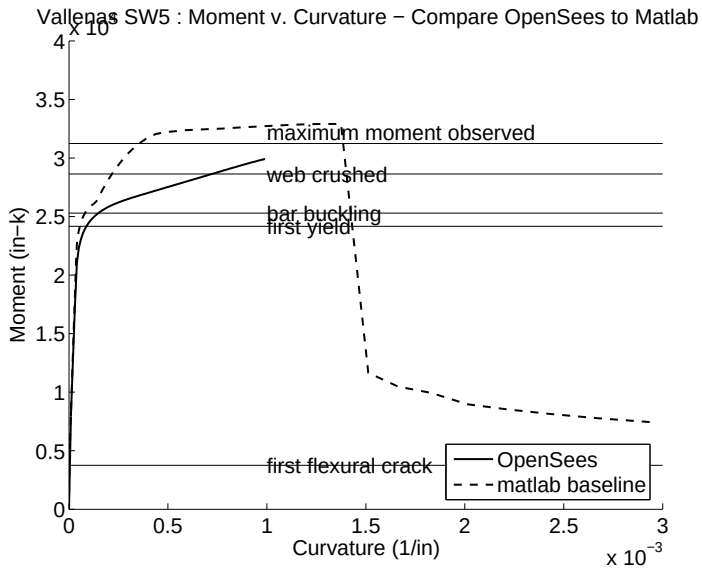

Figure C.53: Moment Curvature Analysis Comparison – Vallenas SW5

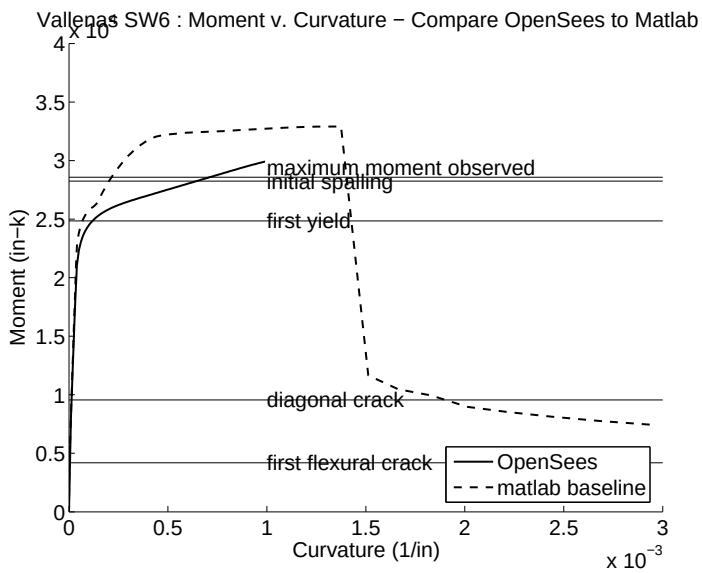

Figure C.54: Moment Curvature Analysis Comparison – Vallenas SW6

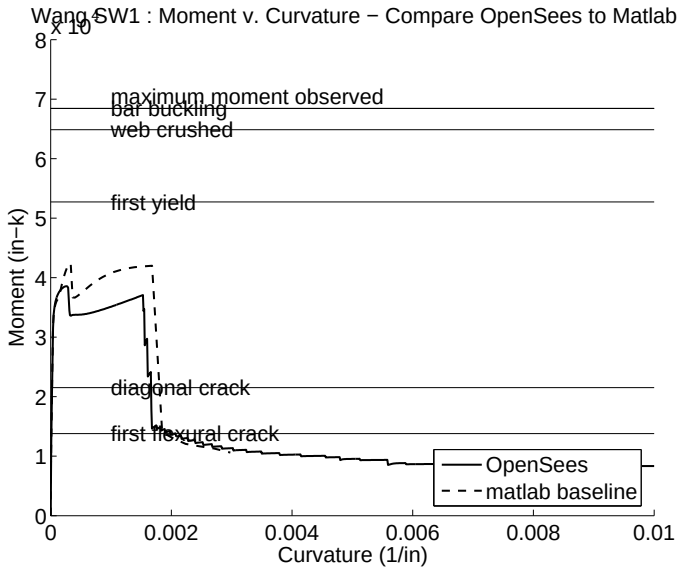

Figure C.55: Moment Curvature Analysis Comparison – Wang SW1

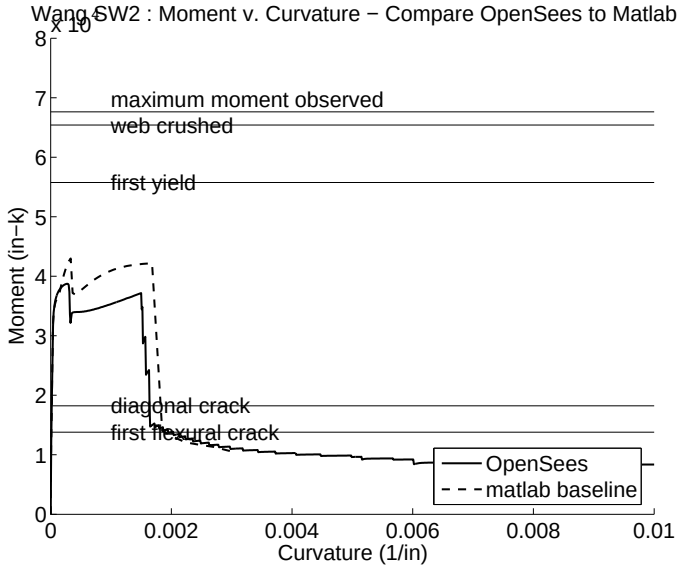

Figure C.56: Moment Curvature Analysis Comparison – Wang SW2

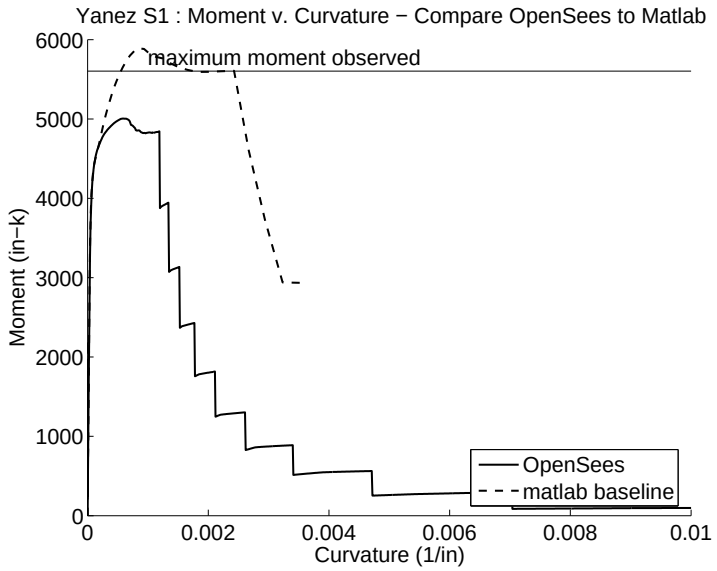

Figure C.57: Moment Curvature Analysis Comparison – Yanez S1

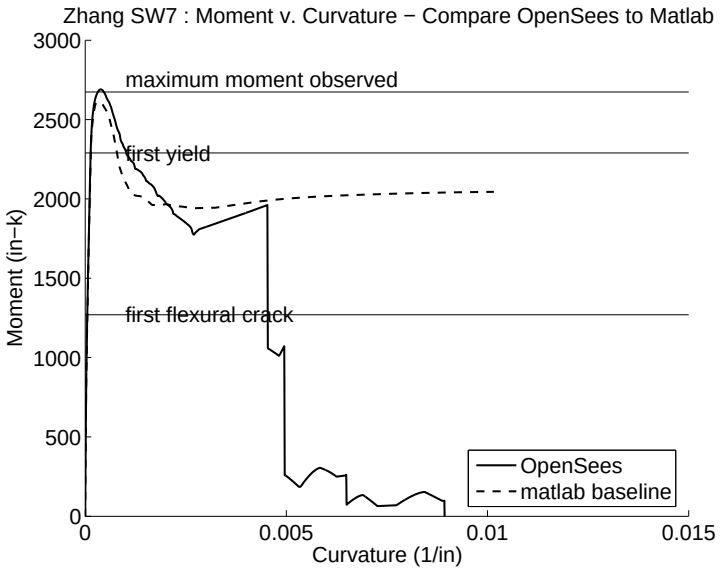

Figure C.58: Moment Curvature Analysis Comparison – Zhang SW7

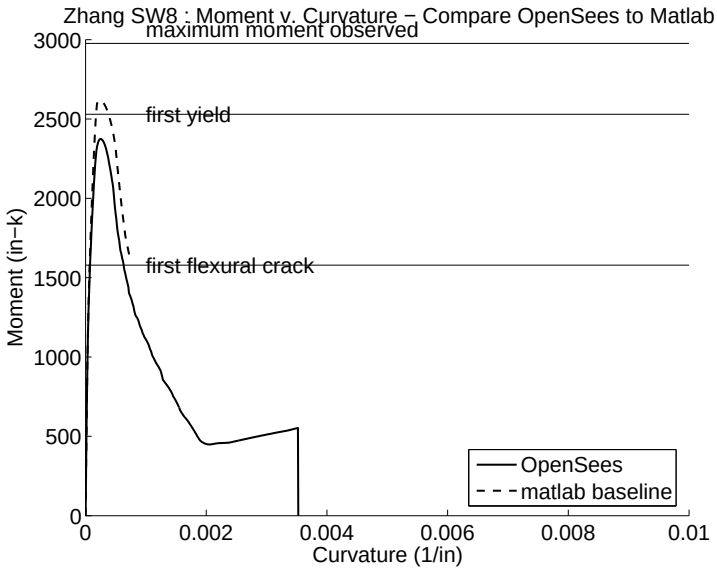

Figure C.59: Moment Curvature Analysis Comparison – Zhang SW8

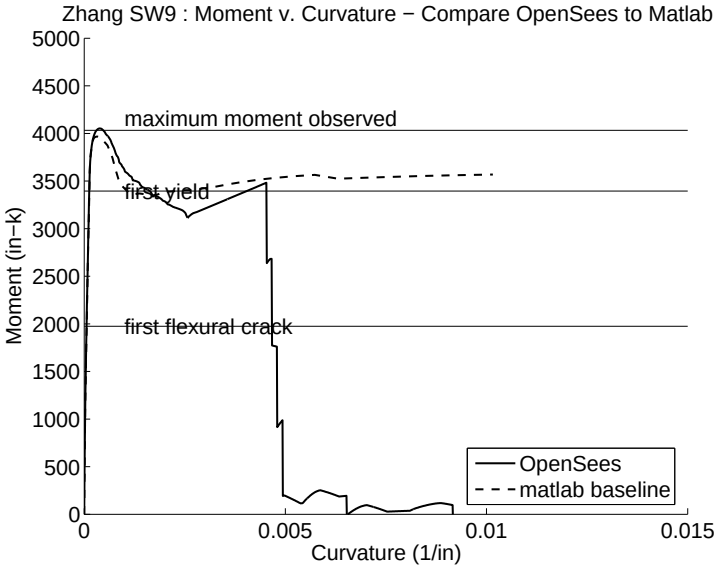

Figure C.60: Moment Curvature Analysis Comparison – Zhang SW9

Appendix D

STRENGTH PREDICTION VERSUS DESIGN PARAMETER FIGURES

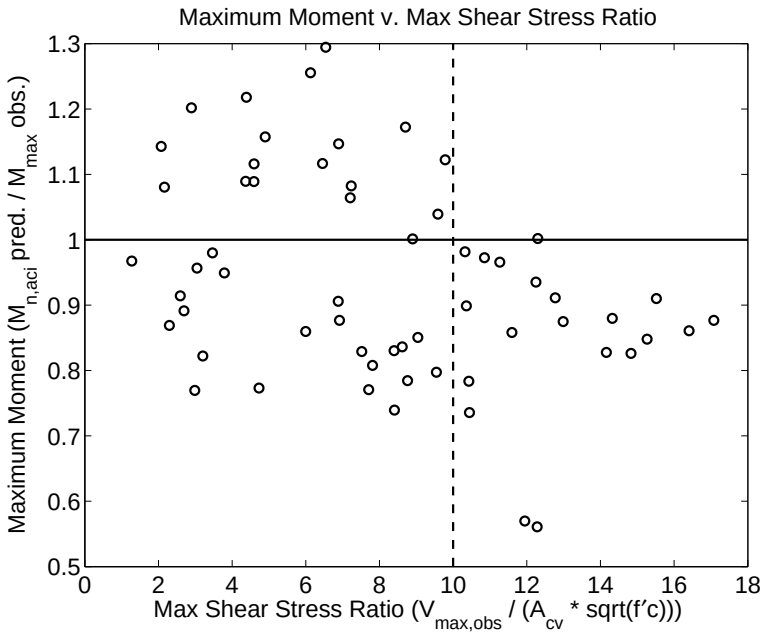

Figure D.1: Maximum Moment Prediction Ratio v. Maximum Shear Stress Ratio

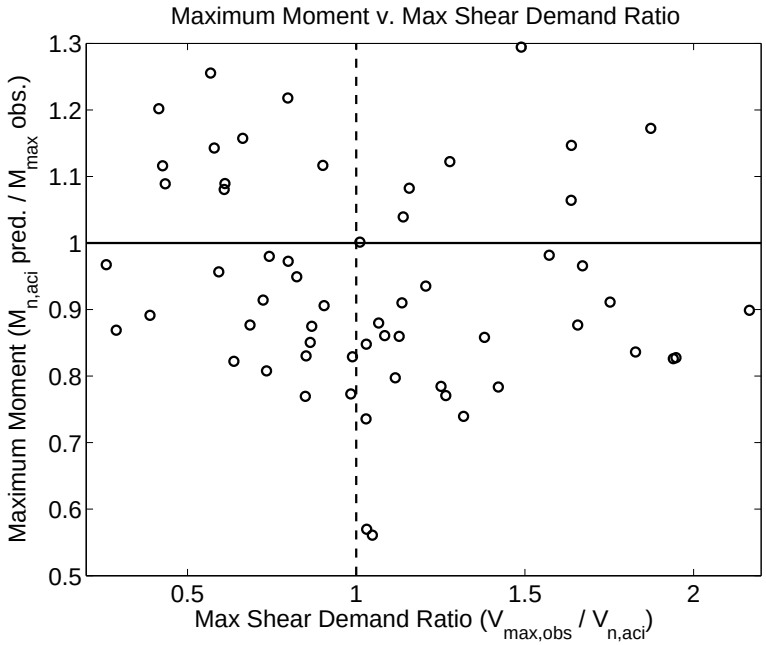

Figure D.2: Maximum Moment Prediction Ratio v. Maximum Shear Demand Ratio

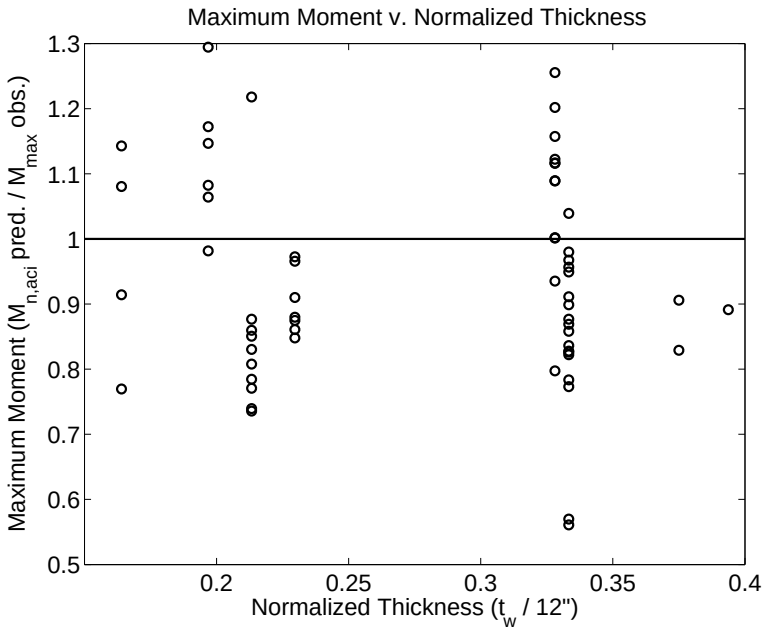

Figure D.3: Maximum Moment Prediction Ratio v. Normalized Thickness

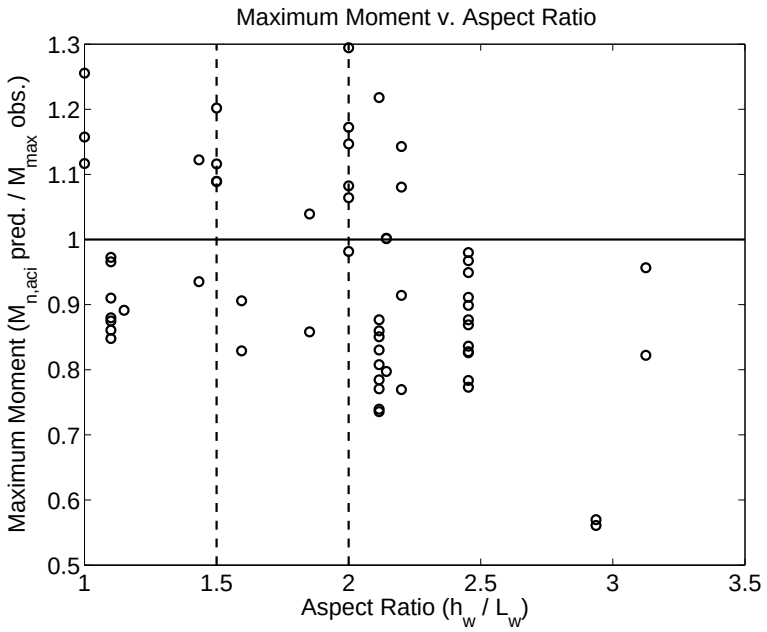

Figure D.4: Maximum Moment Prediction Ratio v. Aspect Ratio

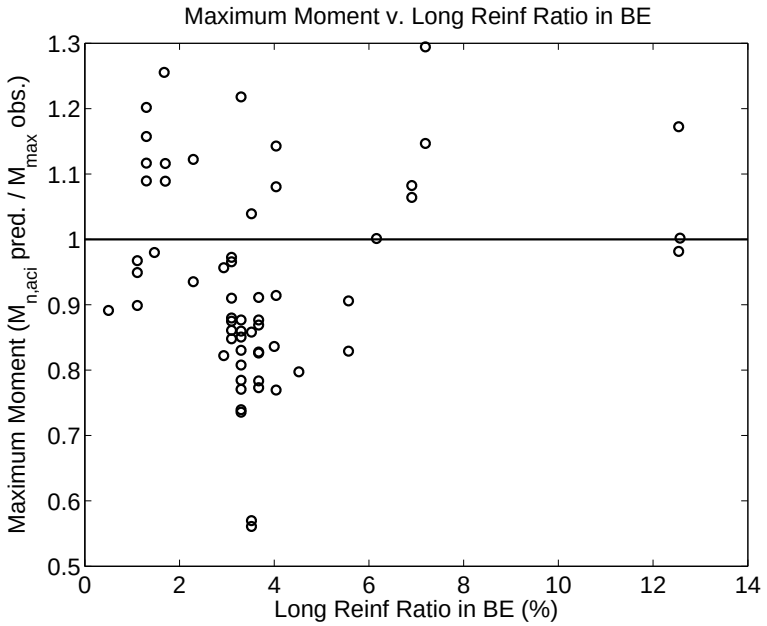

Figure D.5: Maximum Moment Prediction Ratio v. Longitudinal Reinforcement Ratio in the Boundary Element

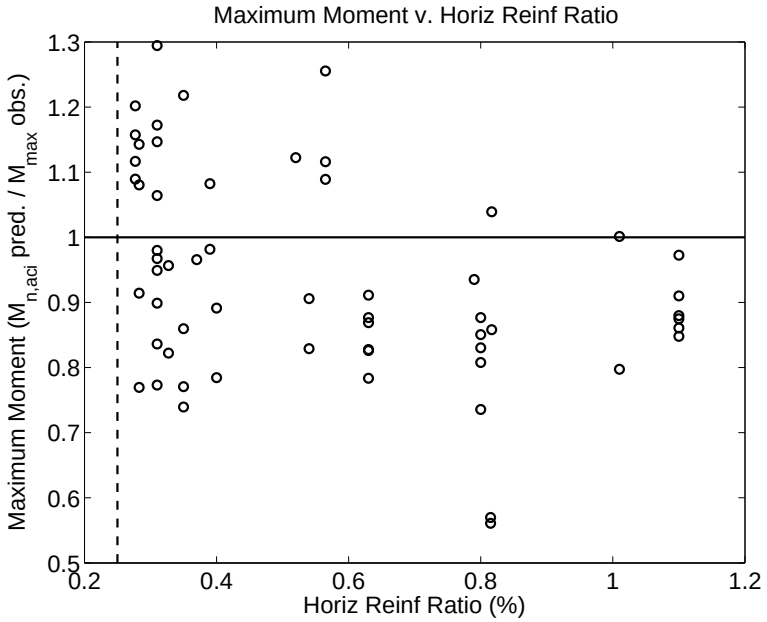

Figure D.6: Maximum Moment Prediction Ratio v. Horizontal Reinforcement Ratio

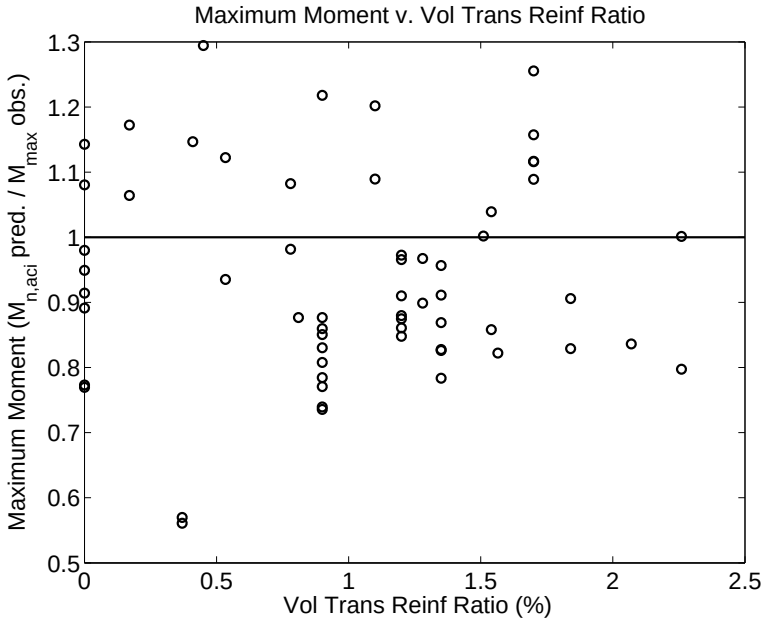

Figure D.7: Maximum Moment Prediction Ratio v. Volumetric Transverse Reinforcement Ratio

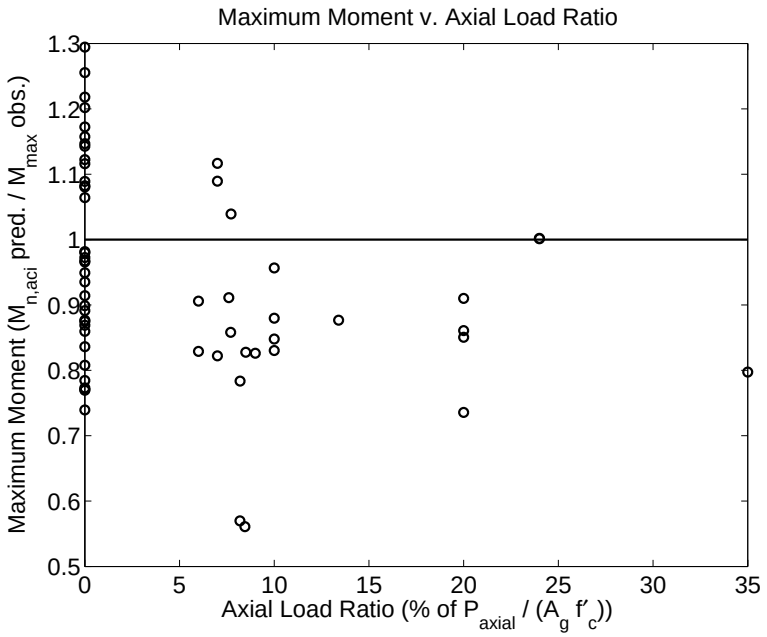

Figure D.8: Maximum Moment Prediction Ratio v. Axial Load Ratio

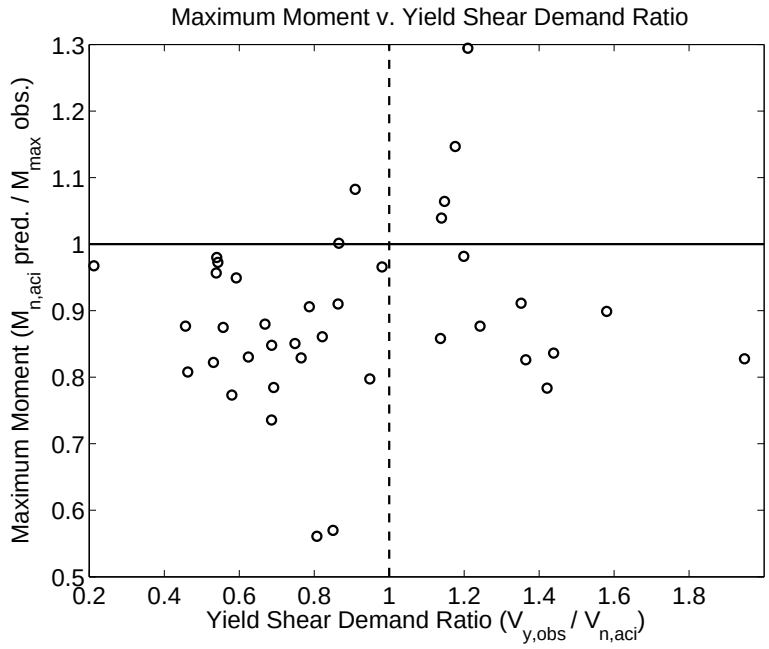

Figure D.9: Maximum Moment Prediction Ratio v. Yield Shear Demand Ratio

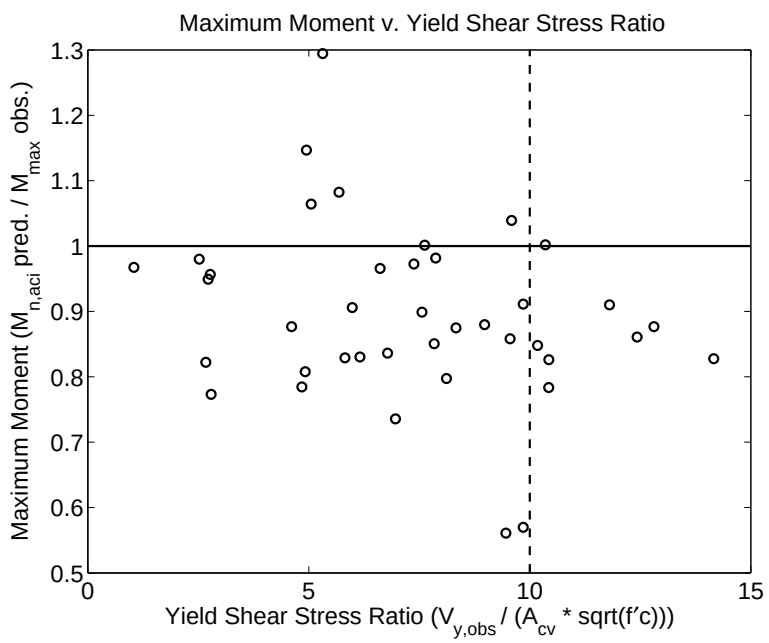

Figure D.10: Maximum Moment Prediction Ratio v. Yield Shear Stress Ratio

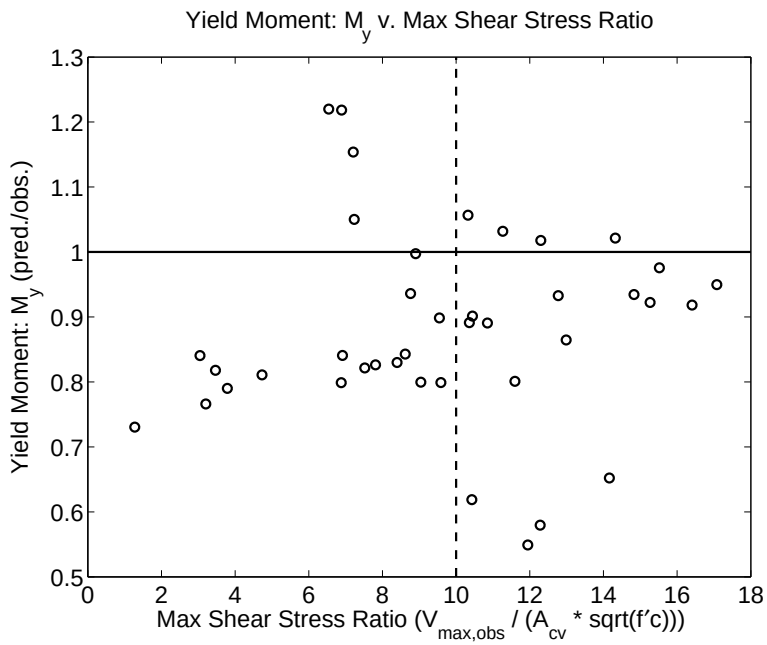

Figure D.11: Yield Moment Prediction Ratio v. Maximum Shear Stress Ratio

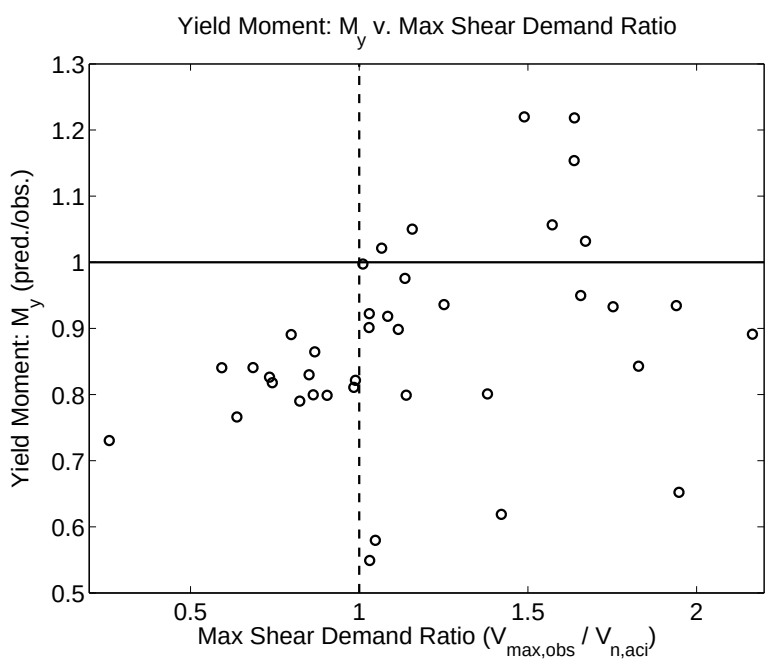

Figure D.12: Yield Moment Prediction Ratio v. Maximum Shear Demand Ratio

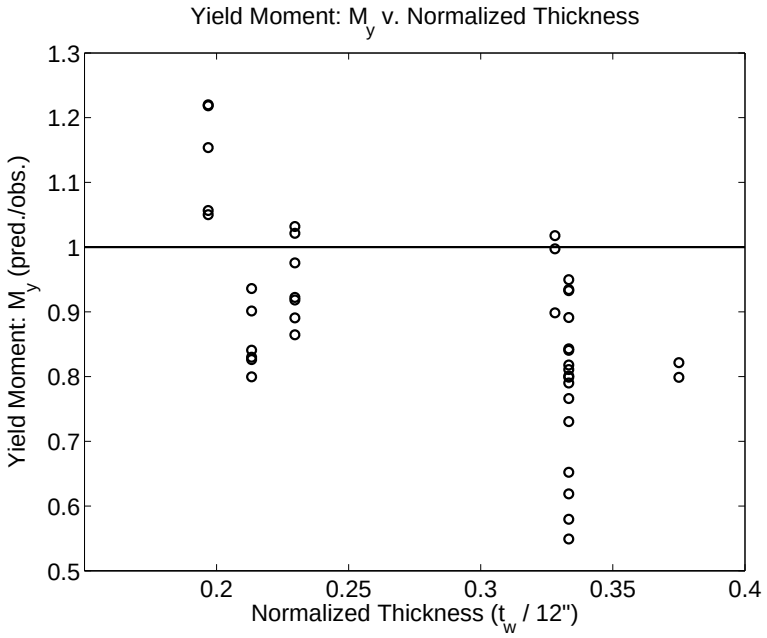

Figure D.13: Yield Moment Prediction Ratio v. Normalized Thickness

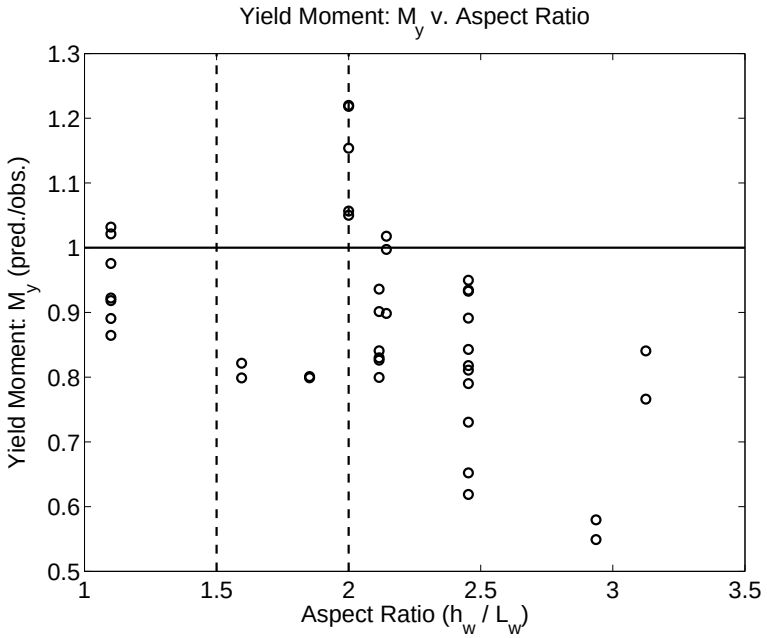

Figure D.14: Yield Moment Prediction Ratio v. Aspect Ratio

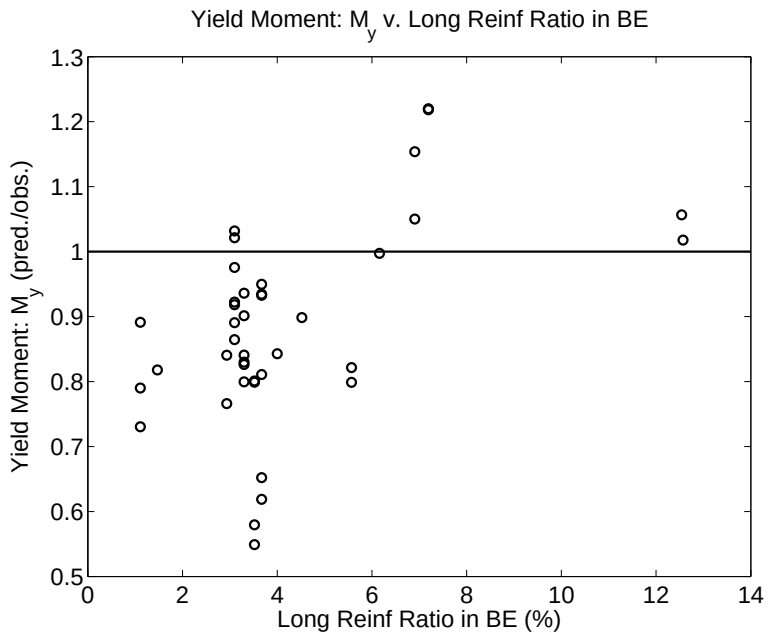

Figure D.15: Yield Moment Prediction Ratio v. Longitudinal Reinforcement Ratio in the Boundary Element

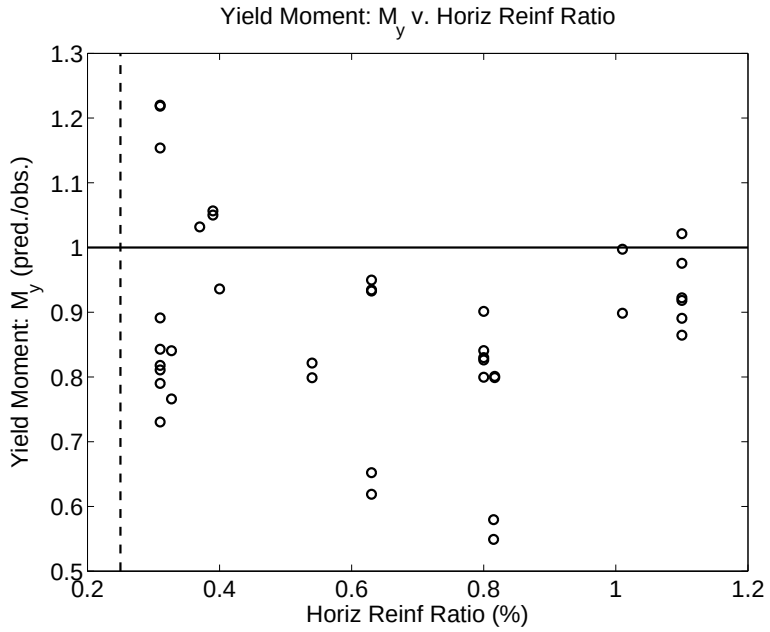

Figure D.16: Yield Moment Prediction Ratio v. Horizontal Reinforcement Ratio

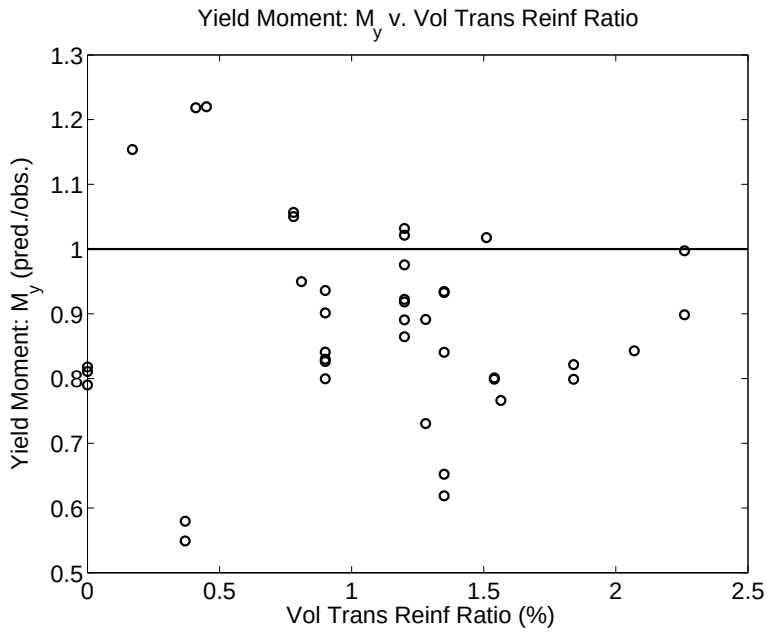

Figure D.17: Yield Moment Prediction Ratio v. Volumetric Transverse Reinforcement Ratio

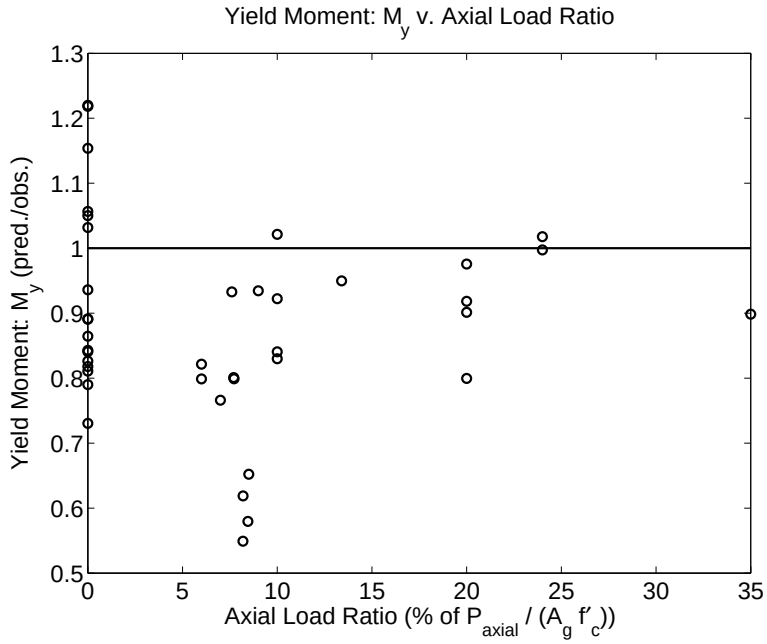

Figure D.18: Yield Moment Prediction Ratio v. Axial Load Ratio

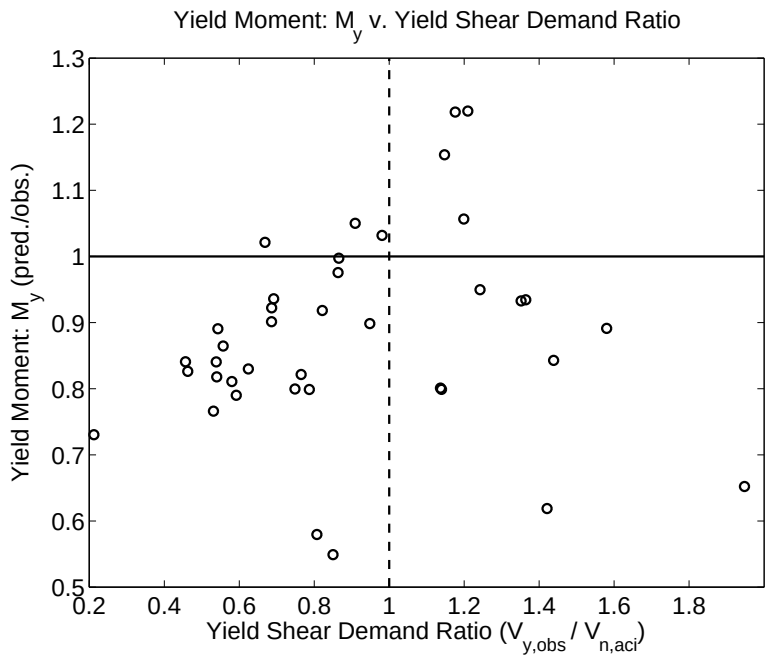

Figure D.19: Yield Moment Prediction Ratio v. Yield Shear Demand Ratio

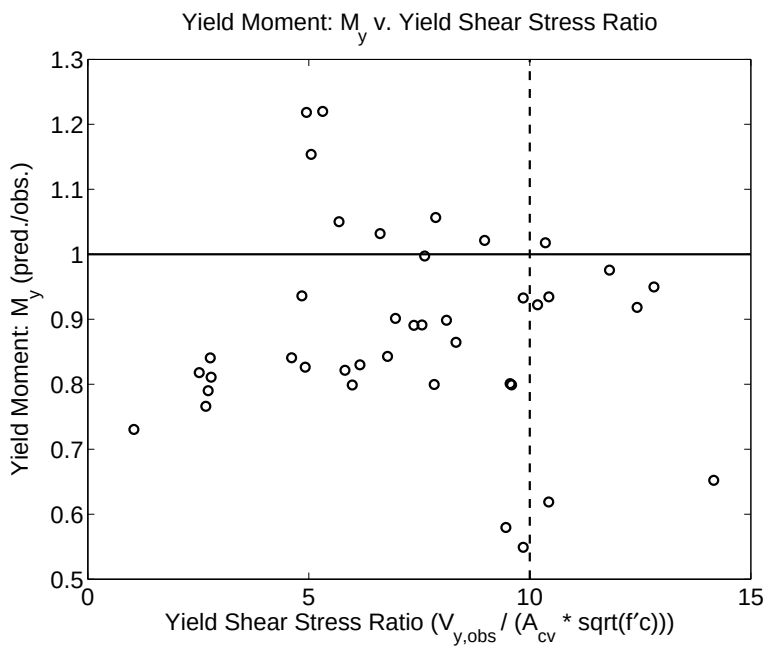

Figure D.20: Yield Moment Prediction Ratio v. Yield Shear Stress Ratio

Appendix E

BEAM-COLUMN ELEMENT PUSH OVER ANALYSIS FIGURES

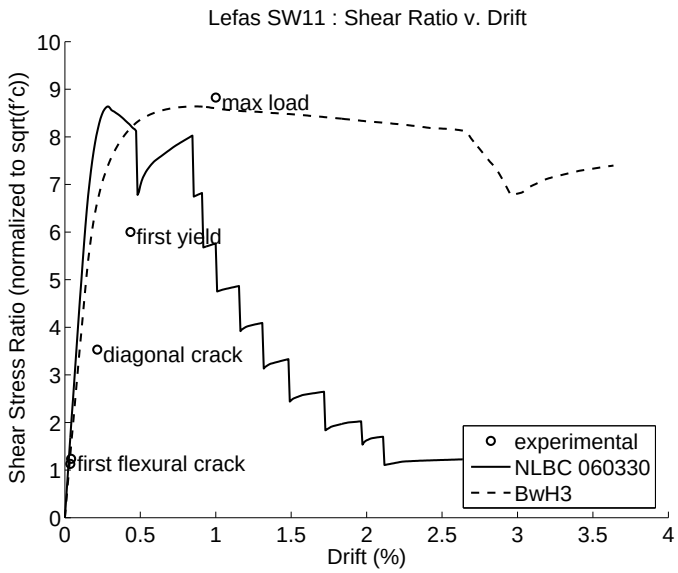

Figure E.1: Push Over Analysis – Lefas SW11

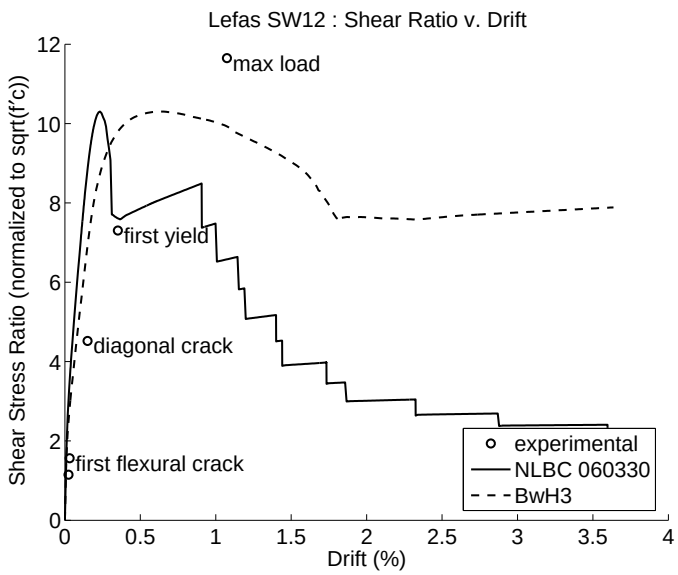

Figure E.2: Push Over Analysis – Lefas SW12

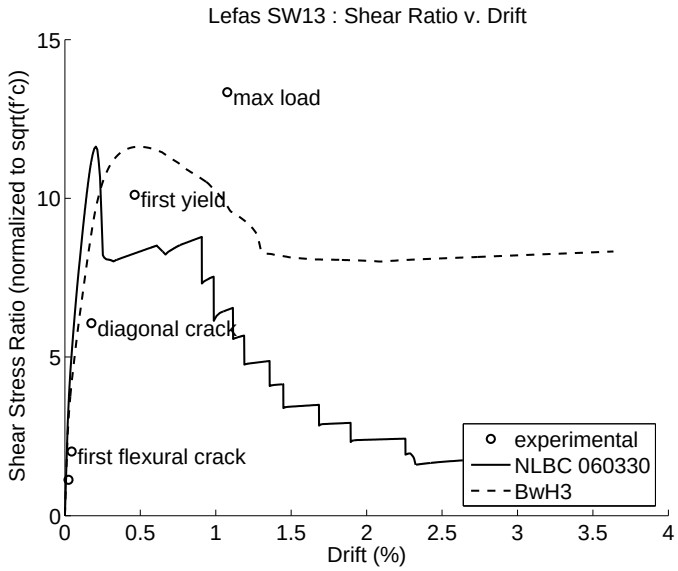

Figure E.3: Push Over Analysis – Lefas SW13

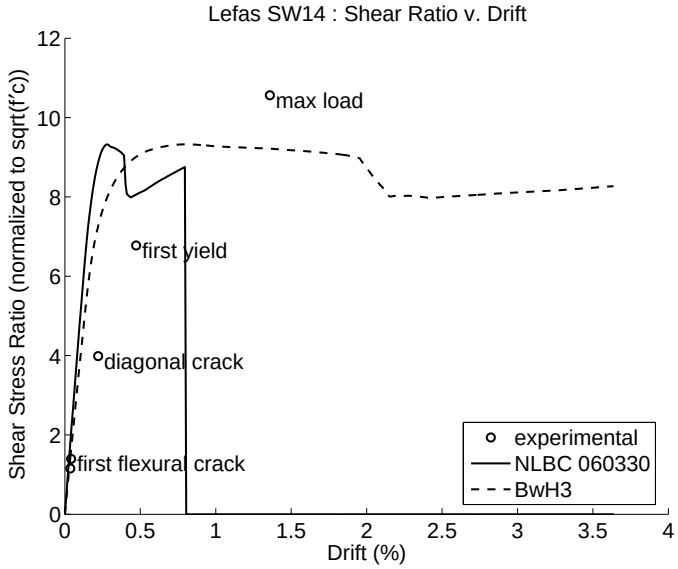

Figure E.4: Push Over Analysis – Lefas SW14

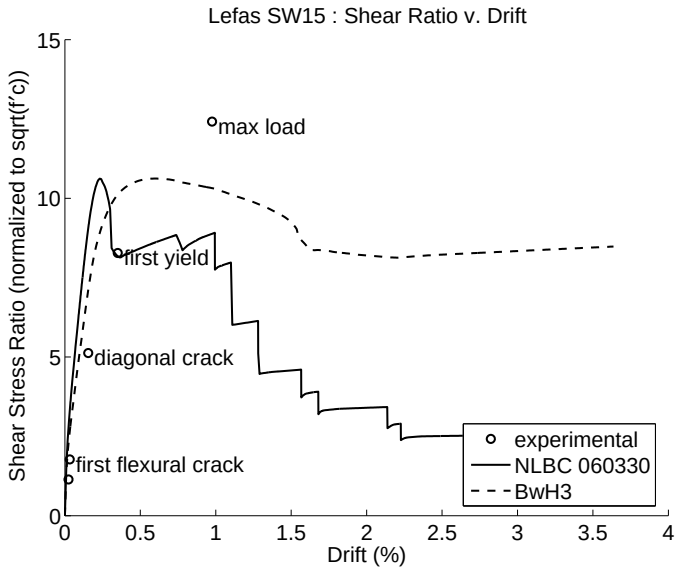

Figure E.5: Push Over Analysis – Lefas SW15

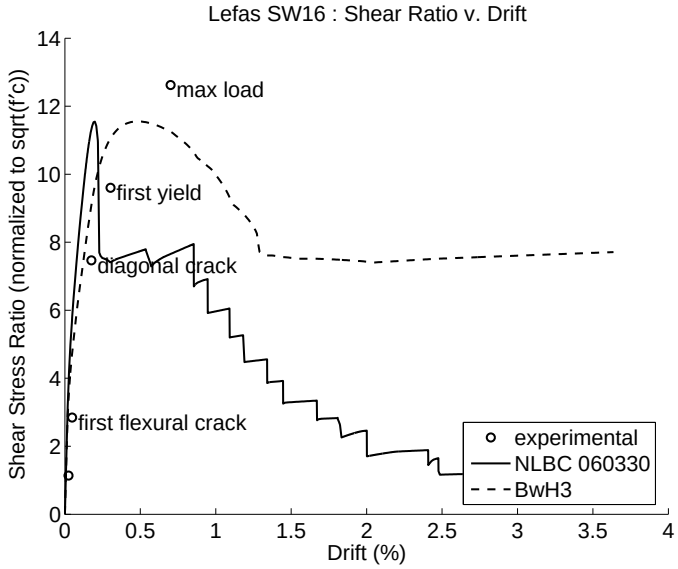

Figure E.6: Push Over Analysis – Lefas SW16

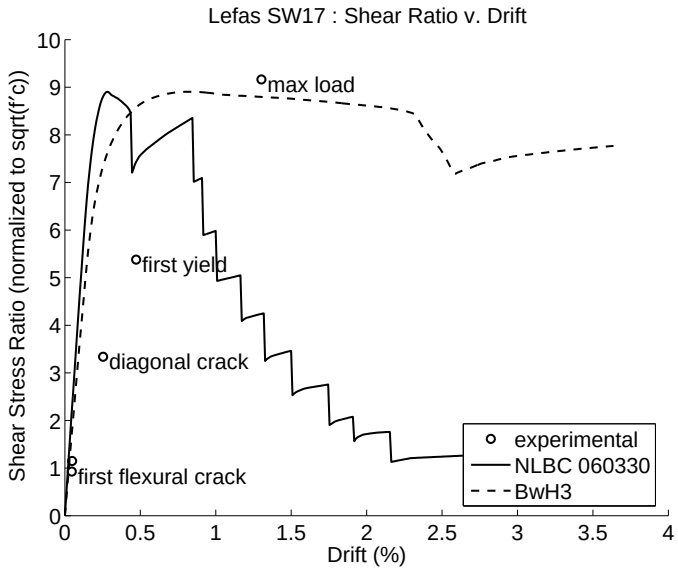

Figure E.7: Push Over Analysis – Lefas SW17

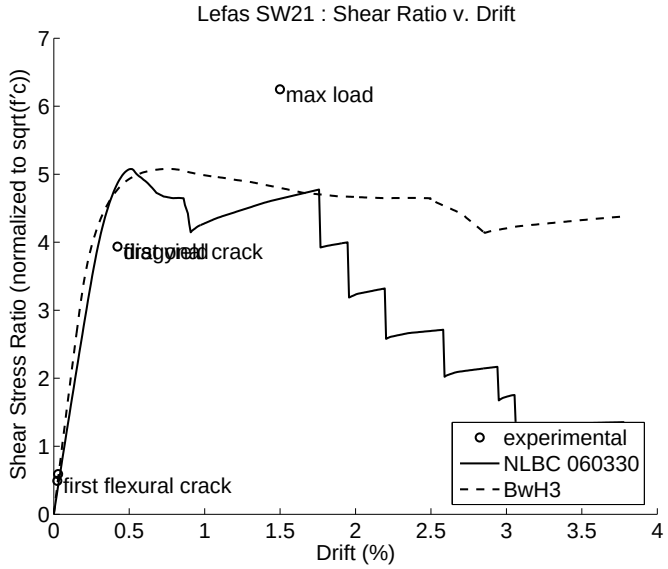

Figure E.8: Push Over Analysis – Lefas SW21

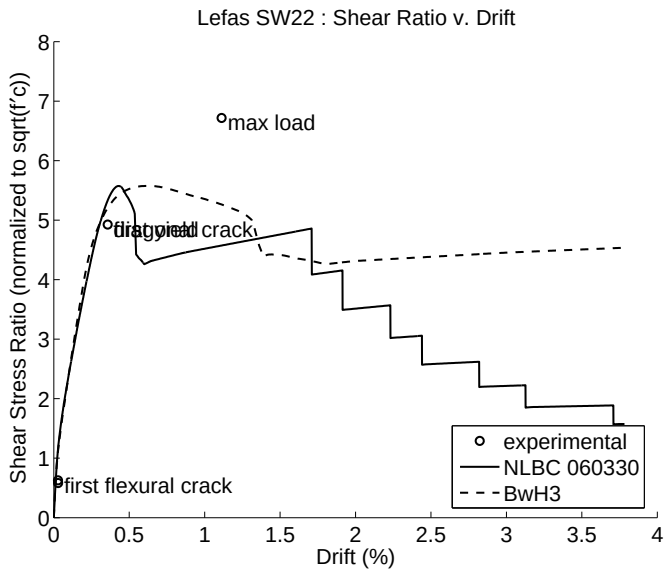

Figure E.9: Push Over Analysis – Lefas SW22

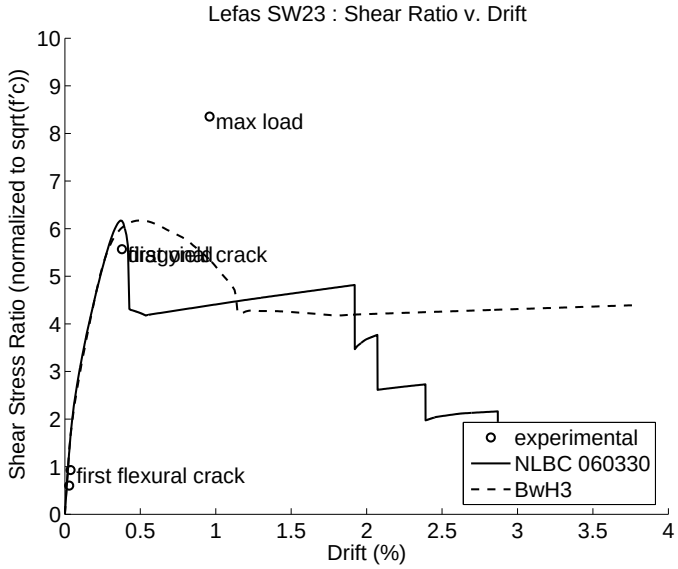

Figure E.10: Push Over Analysis – Lefas SW23

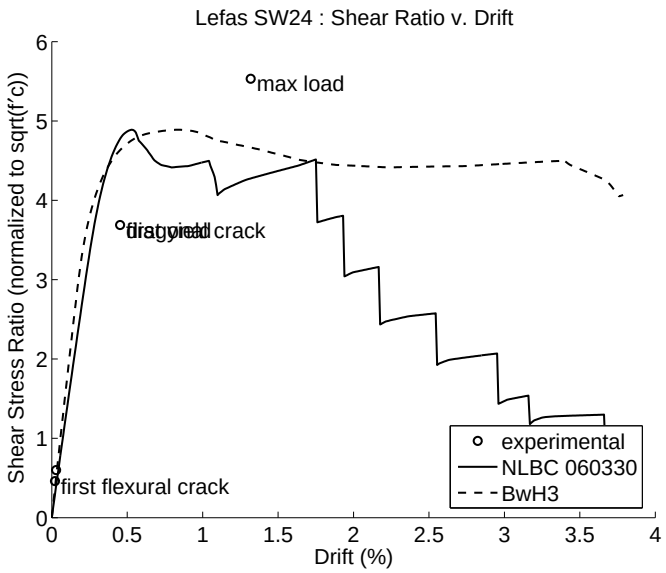

Figure E.11: Push Over Analysis – Lefas SW24

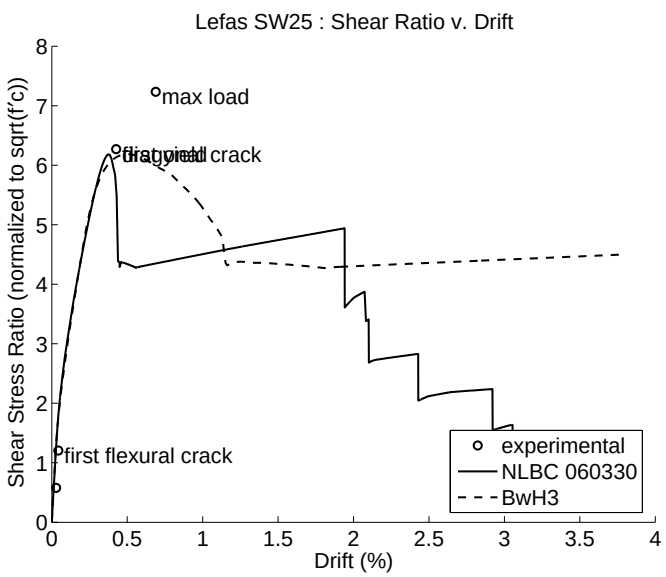

Figure E.12: Push Over Analysis – Lefas SW25

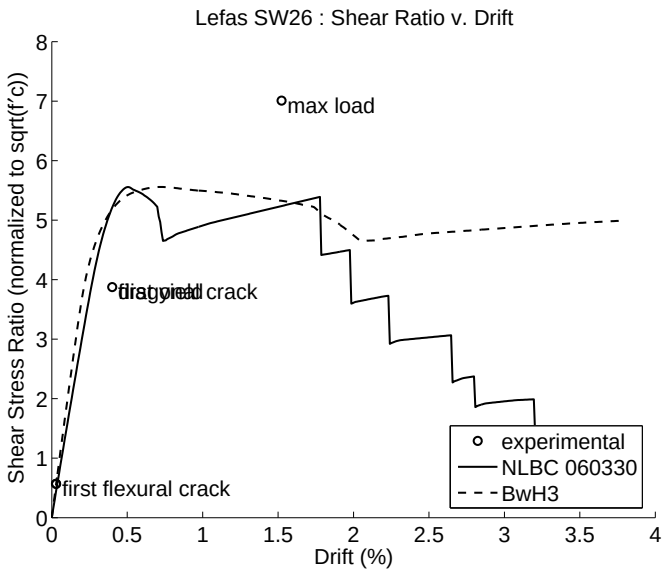

Figure E.13: Push Over Analysis – Lefas SW26

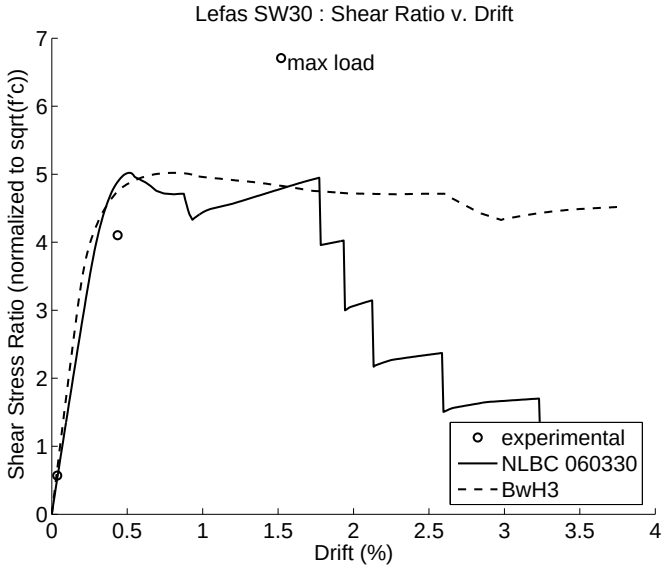

Figure E.14: Push Over Analysis – Lefas SW30

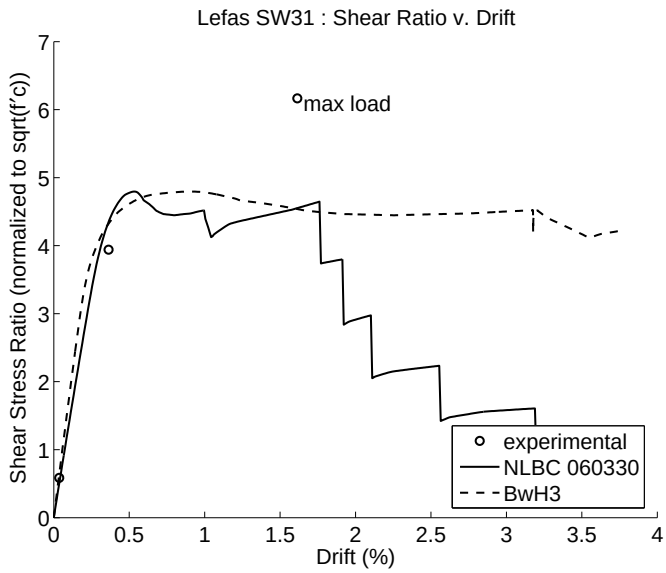

Figure E.15: Push Over Analysis – Lefas SW31

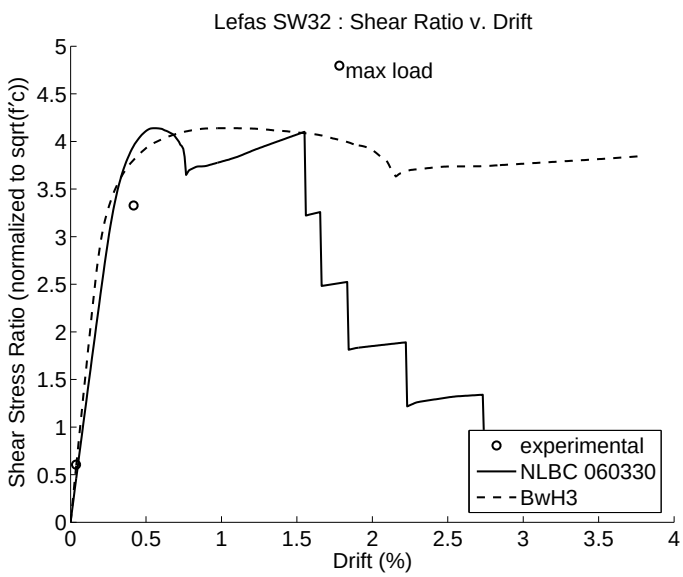

Figure E.16: Push Over Analysis – Lefas SW32

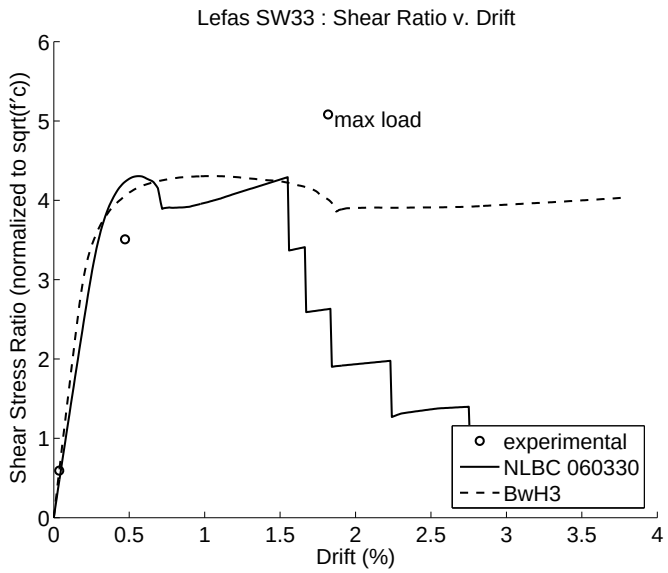

Figure E.17: Push Over Analysis – Lefas SW33

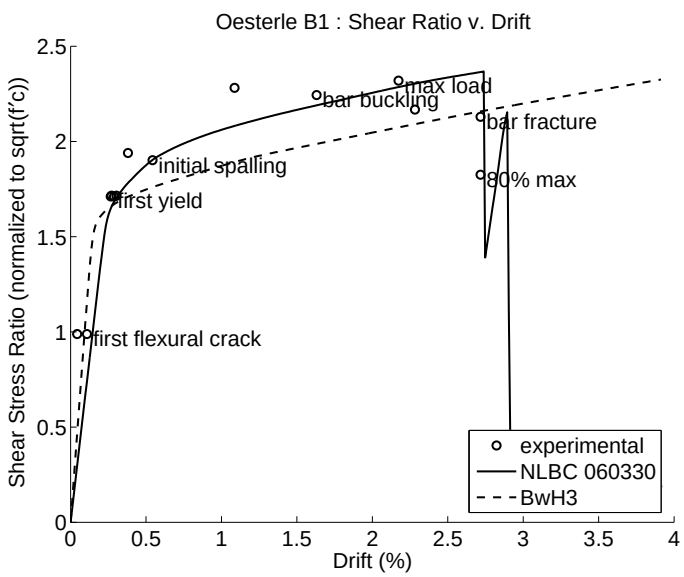

Figure E.18: Push Over Analysis – Oesterle B1

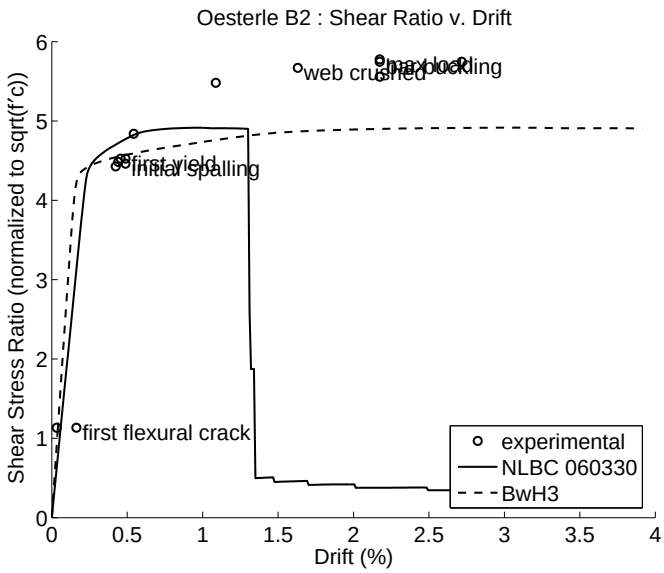

Figure E.19: Push Over Analysis – Oesterle B2

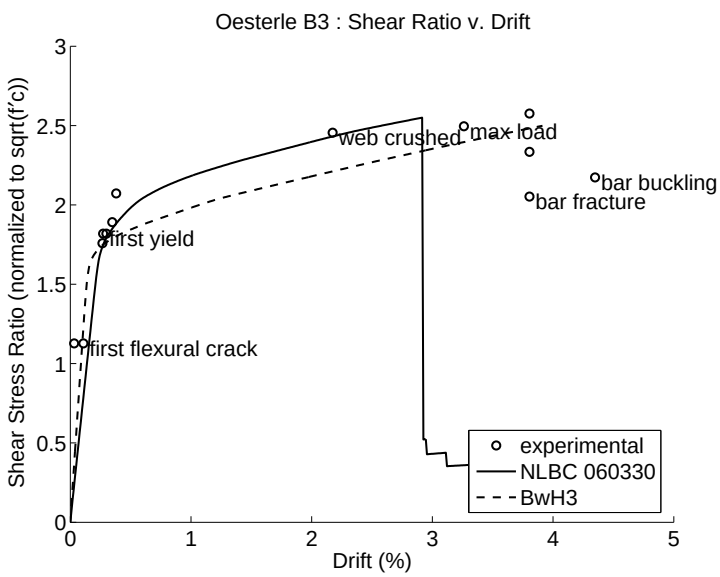

Figure E.20: Push Over Analysis – Oesterle B3

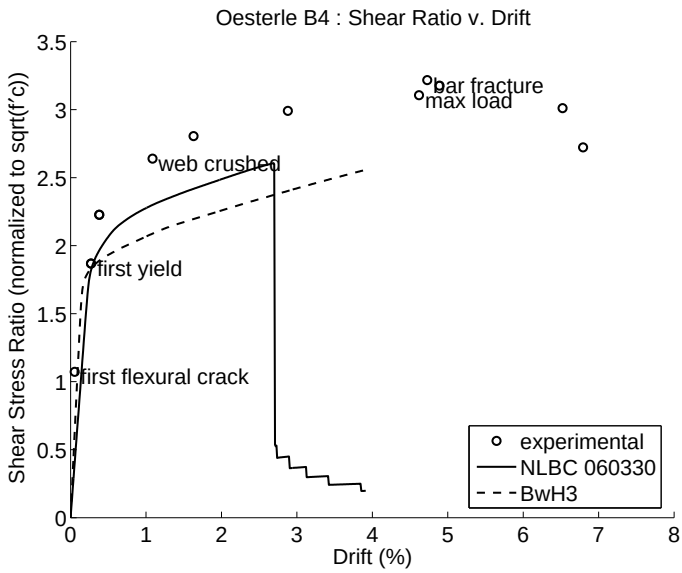

Figure E.21: Push Over Analysis – Oesterle B4

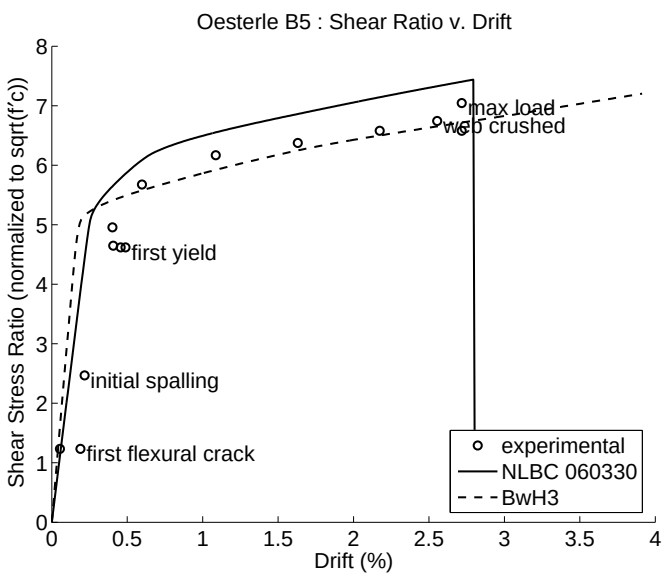

Figure E.22: Push Over Analysis – Oesterle B5

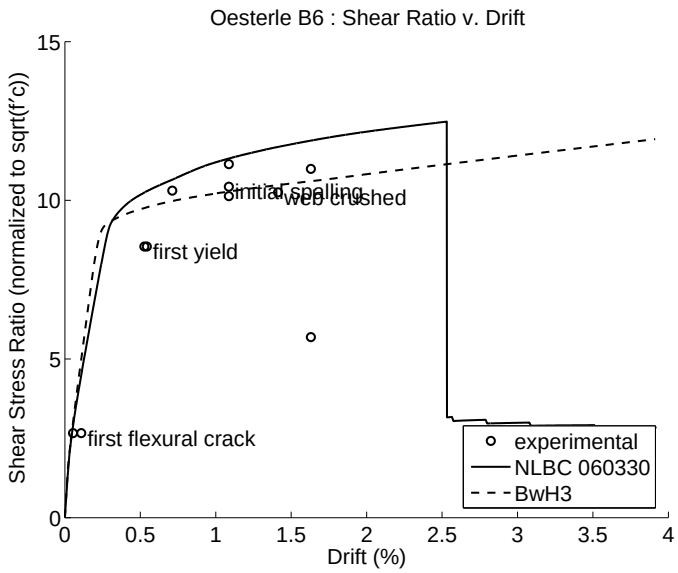

Figure E.23: Push Over Analysis – Oesterle B6

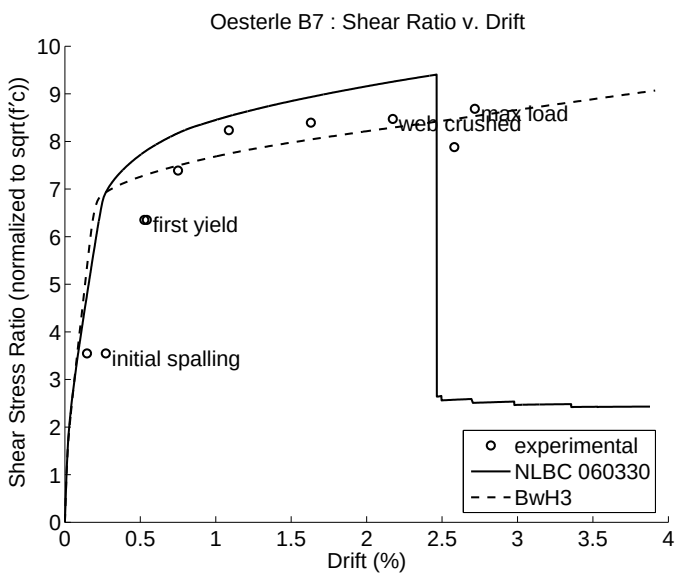

Figure E.24: Push Over Analysis – Oesterle B7

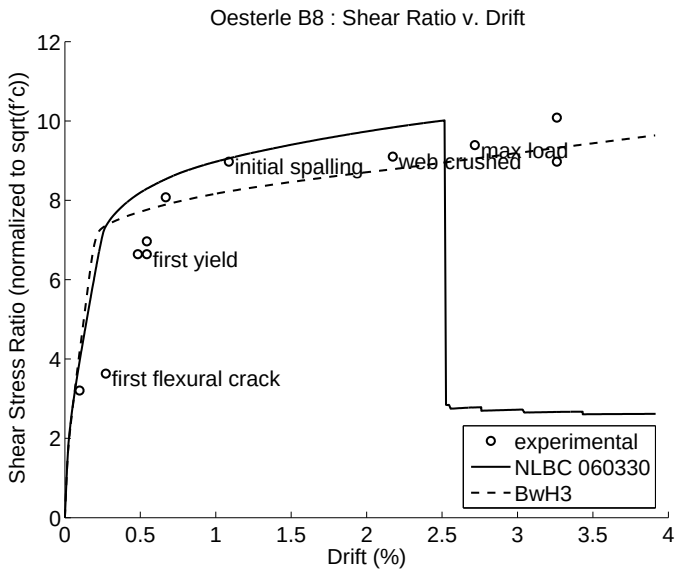

Figure E.25: Push Over Analysis – Oesterle B8

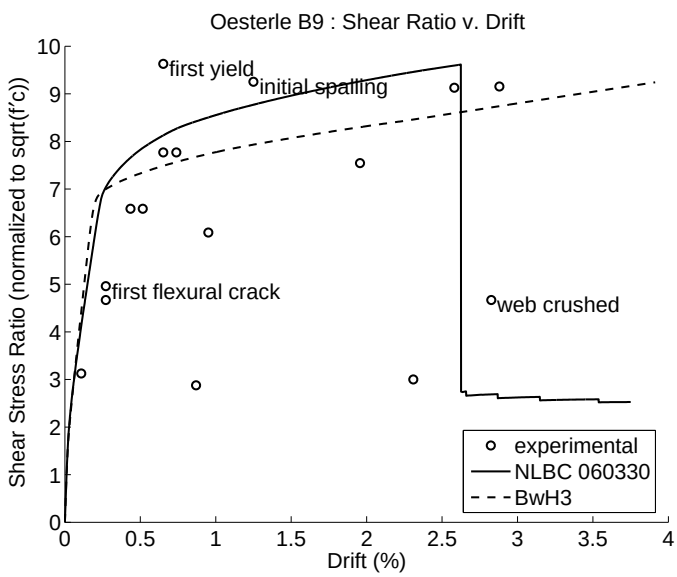

Figure E.26: Push Over Analysis – Oesterle B9

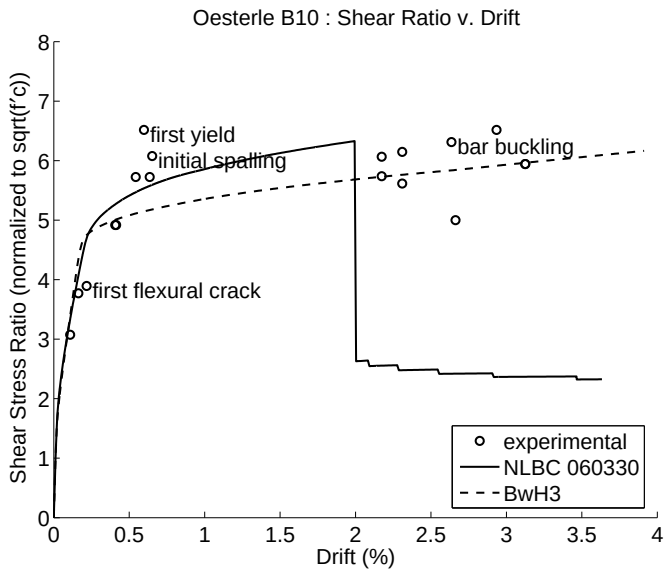

Figure E.27: Push Over Analysis – Oesterle B10

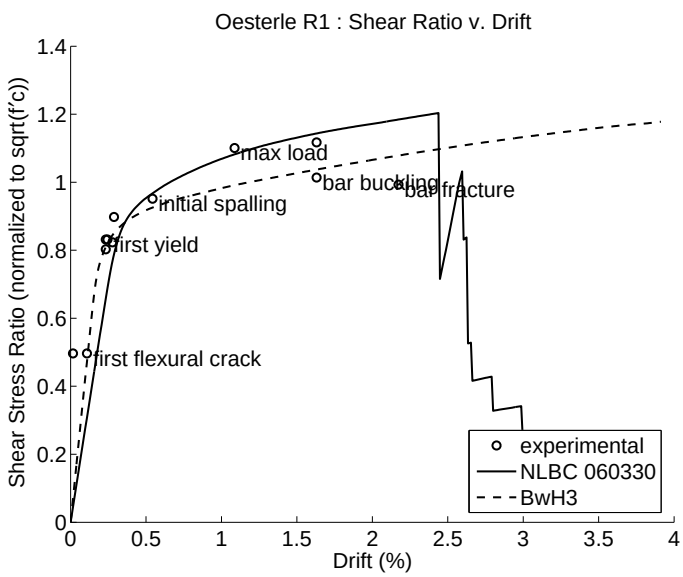

Figure E.28: Push Over Analysis – Oesterle R1

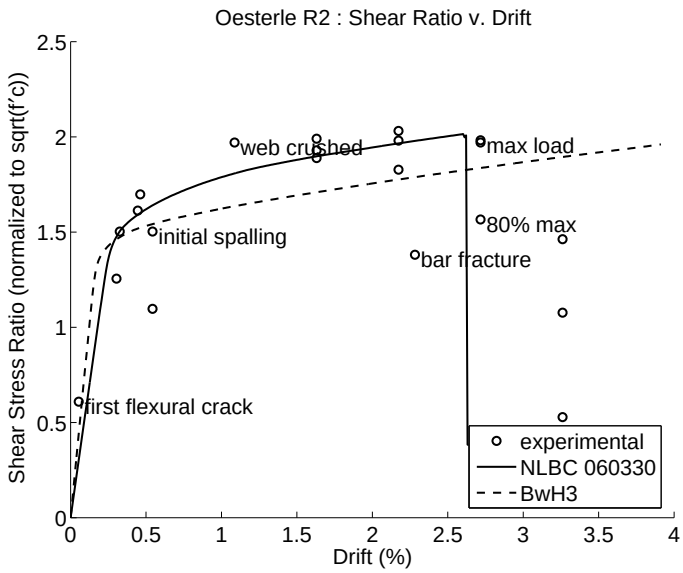

Figure E.29: Push Over Analysis – Oesterle R2

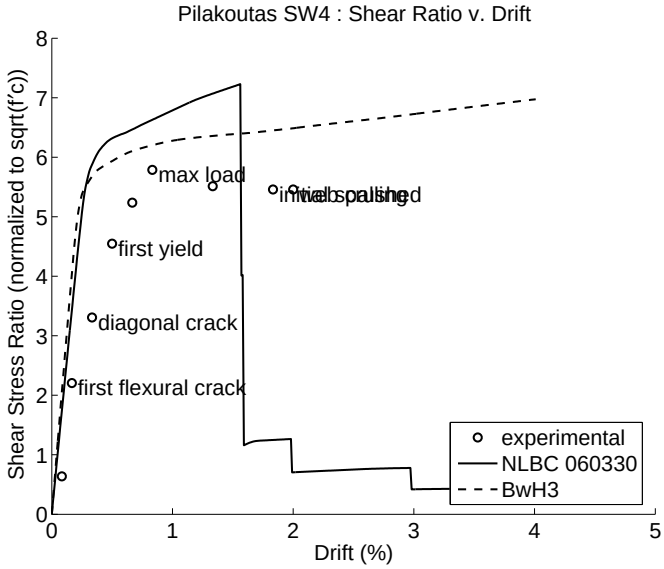

Figure E.30: Push Over Analysis – Pilakoutas SW4

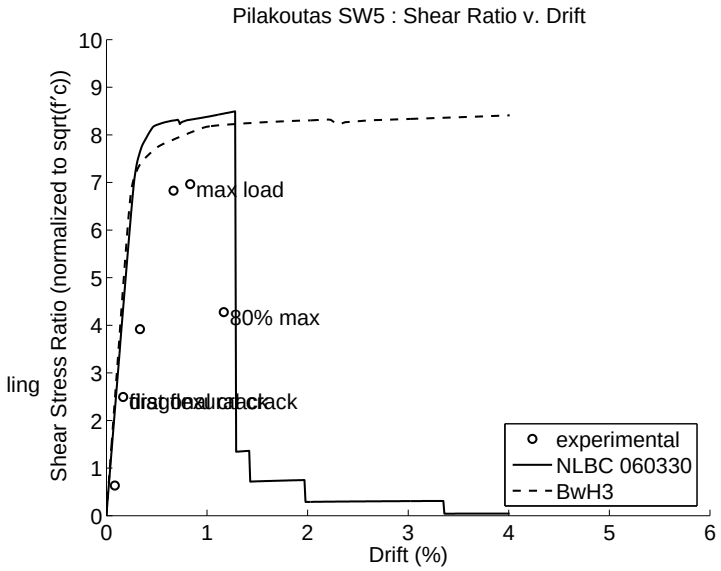

Figure E.31: Push Over Analysis – Pilakoutas SW5

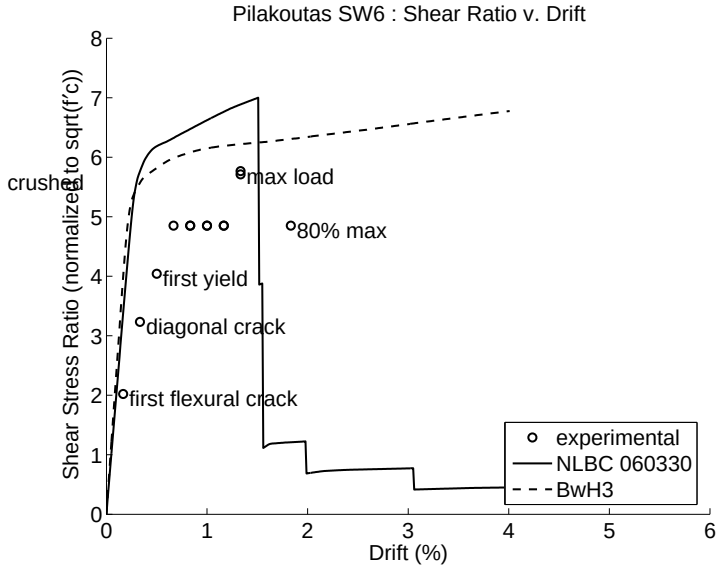

Figure E.32: Push Over Analysis – Pilakoutas SW6

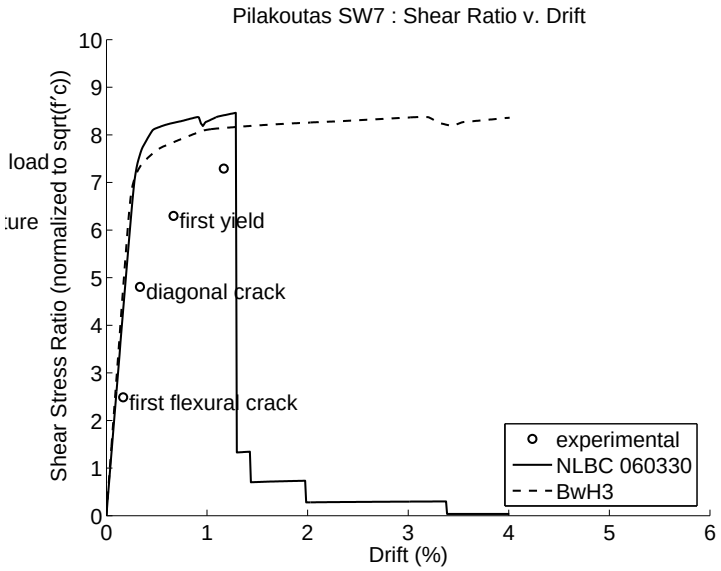

Figure E.33: Push Over Analysis – Pilakoutas SW7

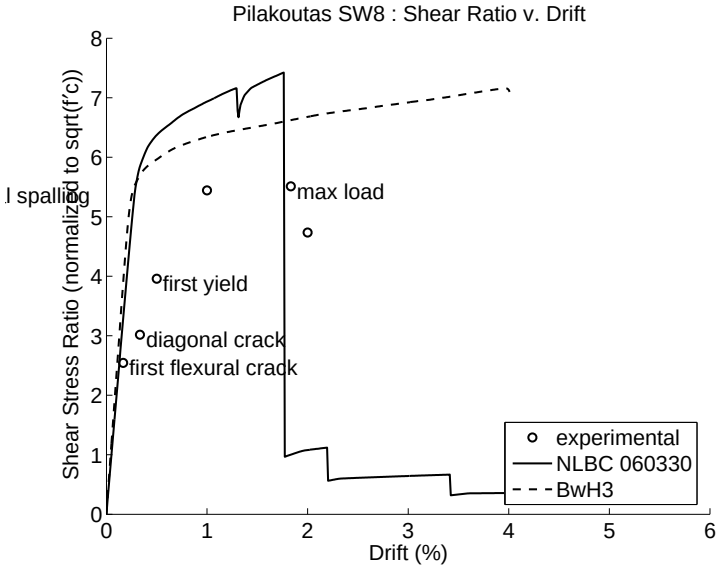

Figure E.34: Push Over Analysis – Pilakoutas SW8

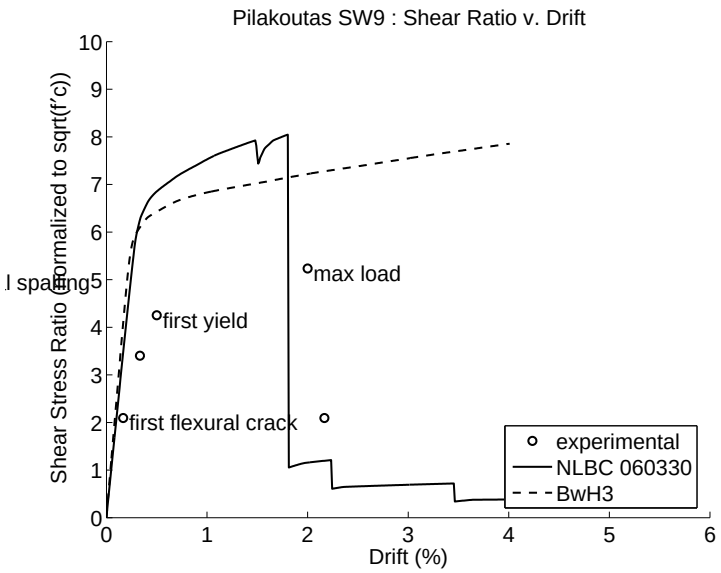

Figure E.35: Push Over Analysis – Pilakoutas SW9

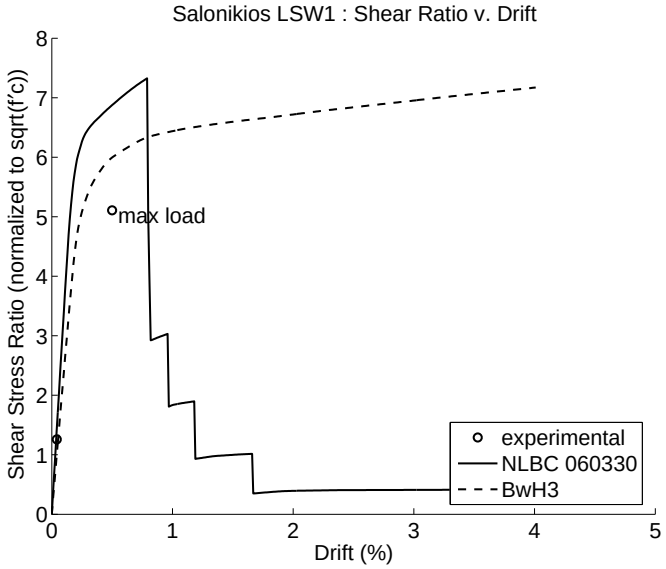

Figure E.36: Push Over Analysis – Salonikios LSW1

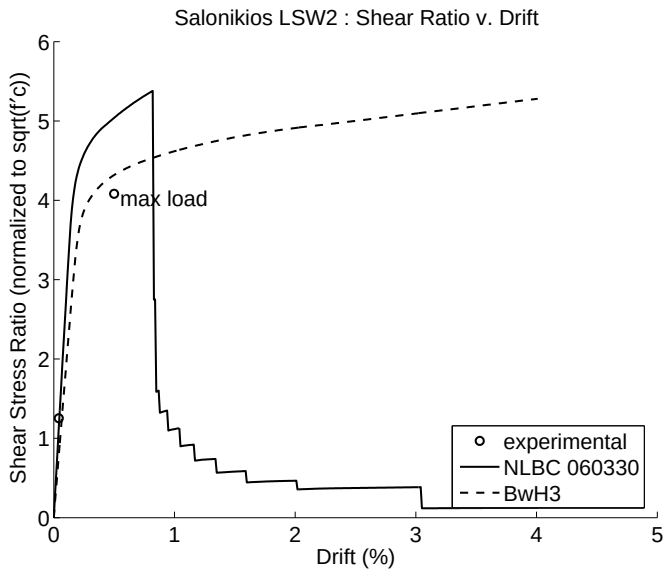

Figure E.37: Push Over Analysis – Salonikios LSW2

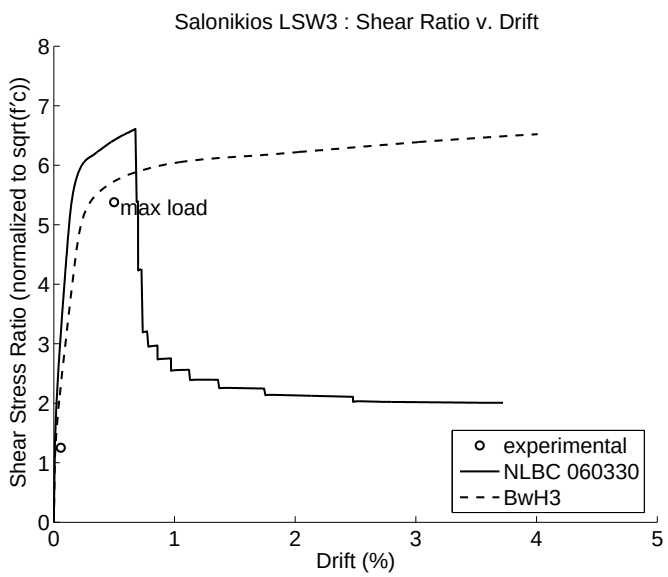

Figure E.38: Push Over Analysis – Salonikios LSW3

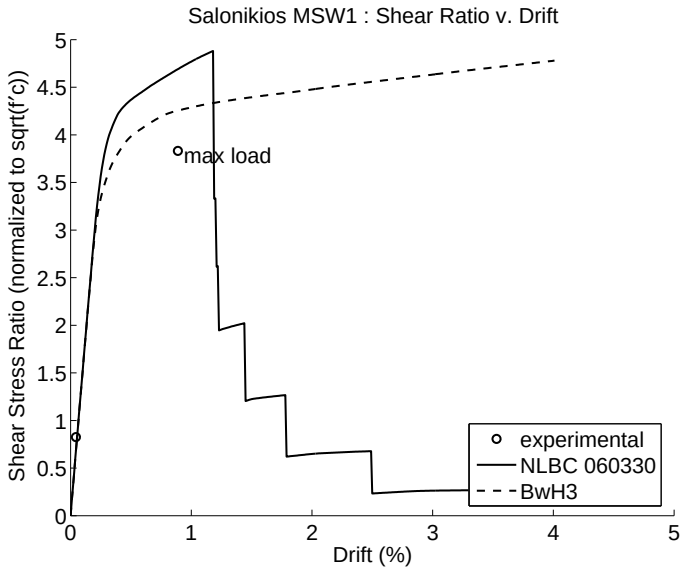

Figure E.39: Push Over Analysis – Salonikios MSW1

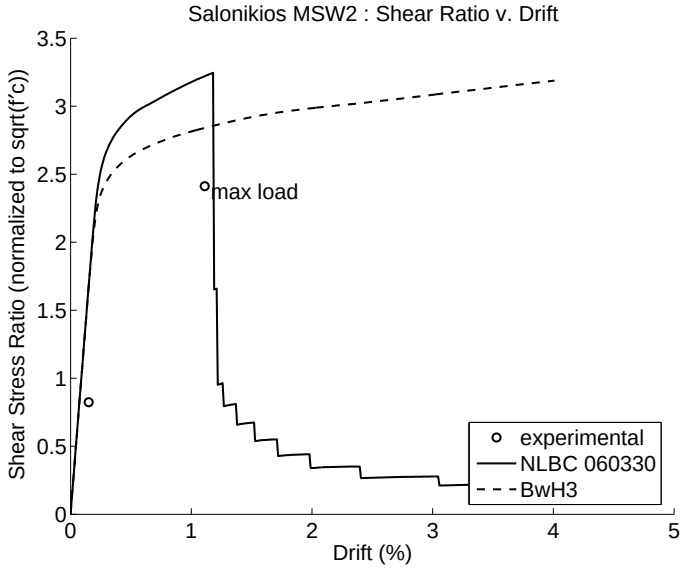

Figure E.40: Push Over Analysis – Salonikios MSW2

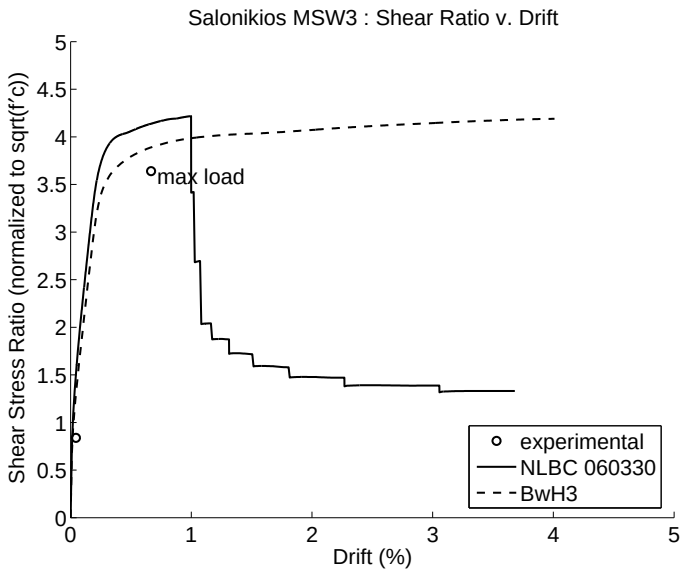

Figure E.41: Push Over Analysis – Salonikios MSW3

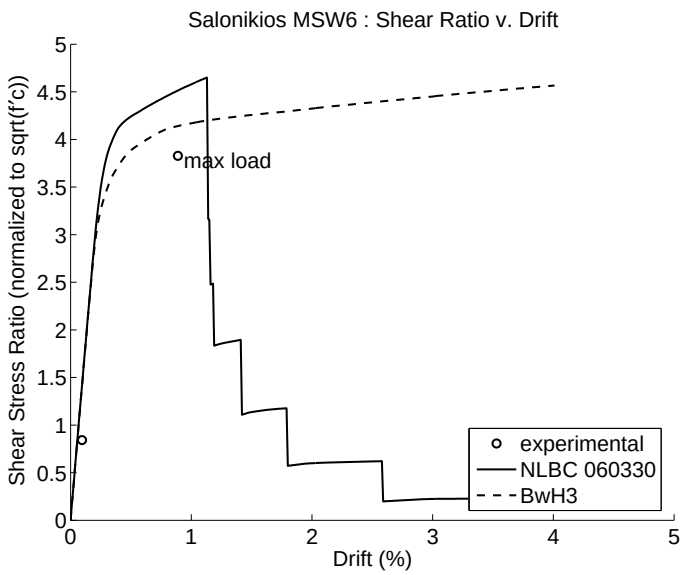

Figure E.42: Push Over Analysis – Salonikios MSW6

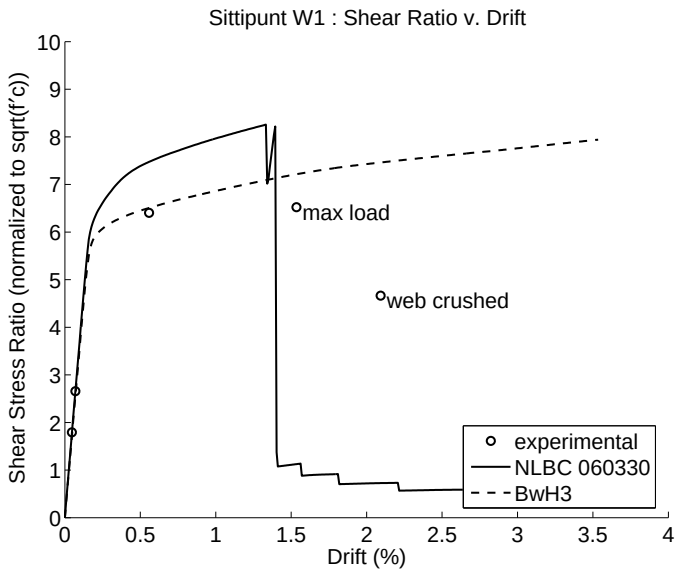

Figure E.43: Push Over Analysis – Sittipunt W1

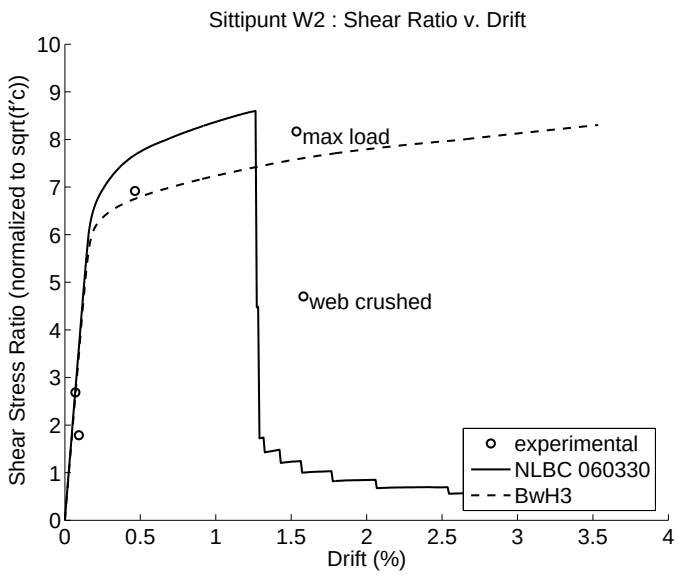

Figure E.44: Push Over Analysis – Sittipunt W2

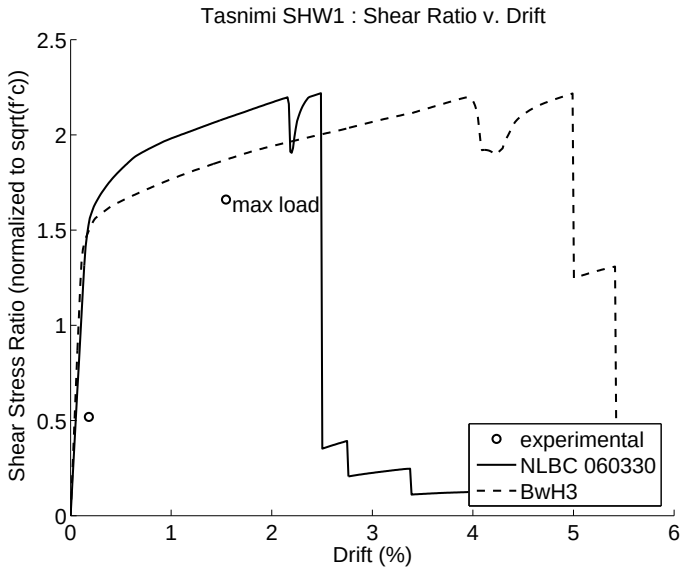

Figure E.45: Push Over Analysis – Tasnimi SHW1

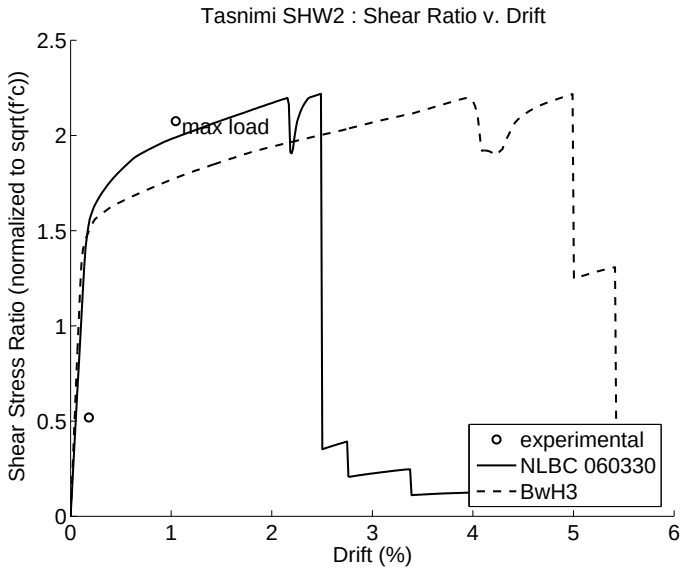

Figure E.46: Push Over Analysis – Tasnimi SHW2

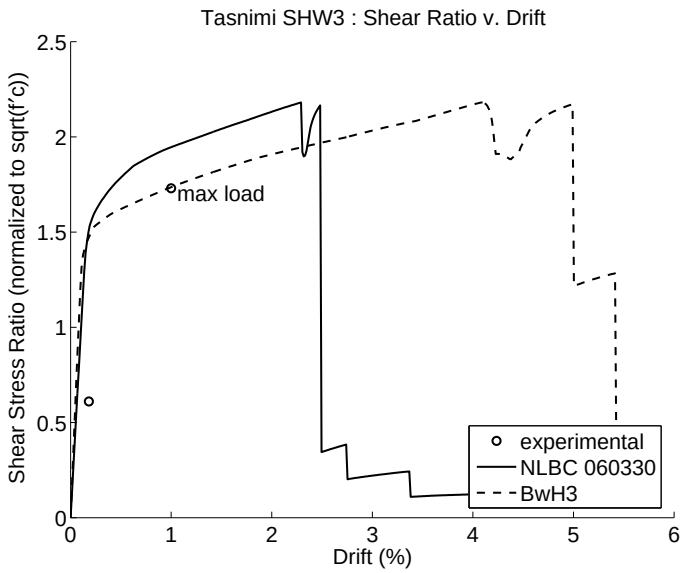

Figure E.47: Push Over Analysis – Tasnimi SHW3

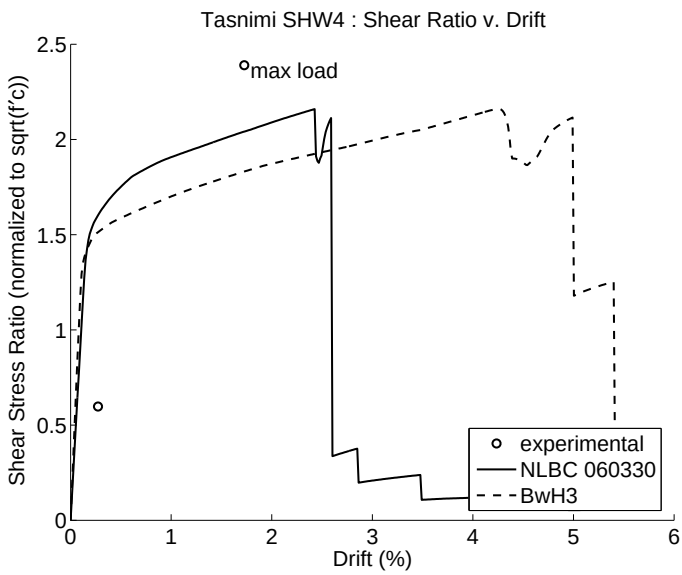

Figure E.48: Push Over Analysis – Tasnimi SHW4

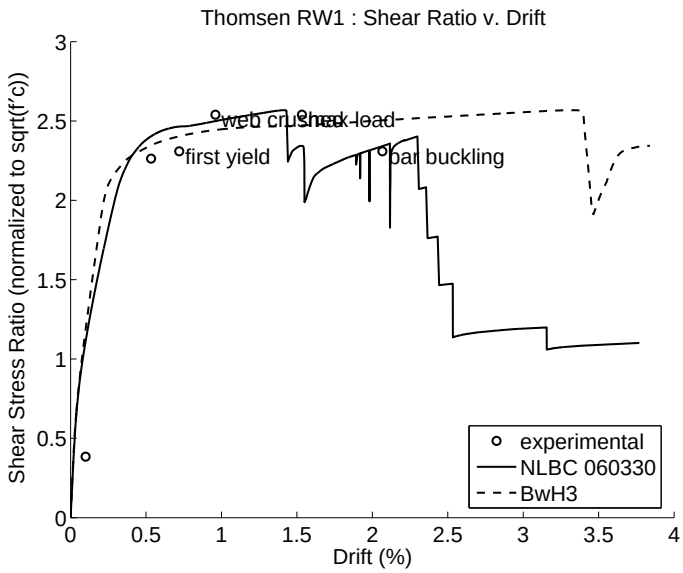

Figure E.49: Push Over Analysis – Thomsen RW1

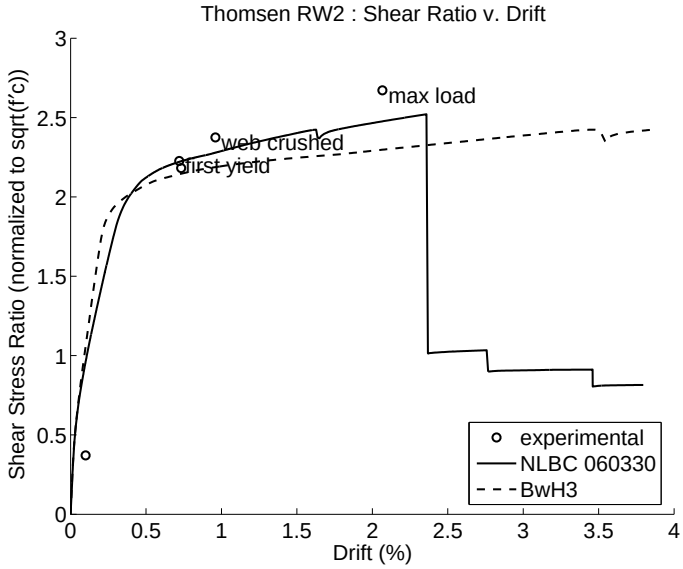

Figure E.50: Push Over Analysis – Thomsen RW2

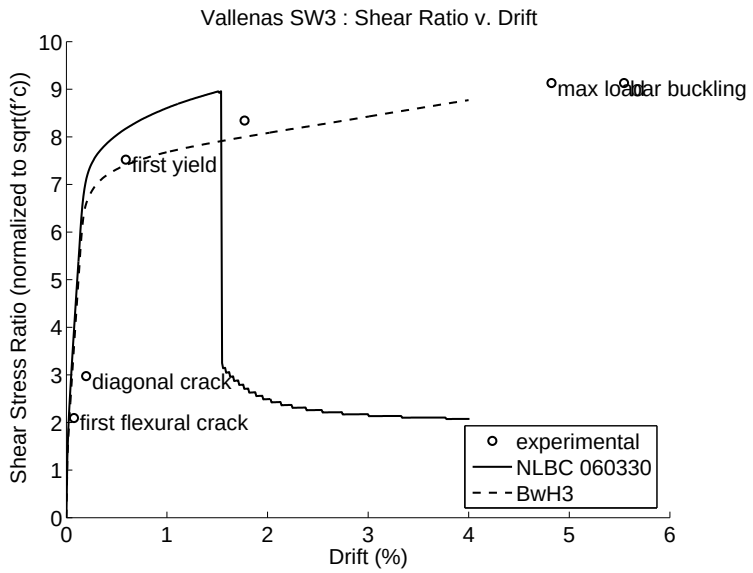

Figure E.51: Push Over Analysis – Vallenas SW3

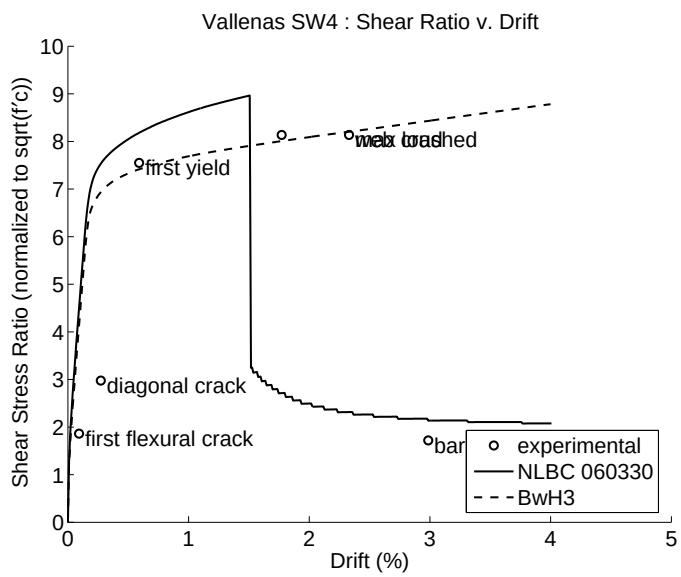

Figure E.52: Push Over Analysis – Vallenas SW4

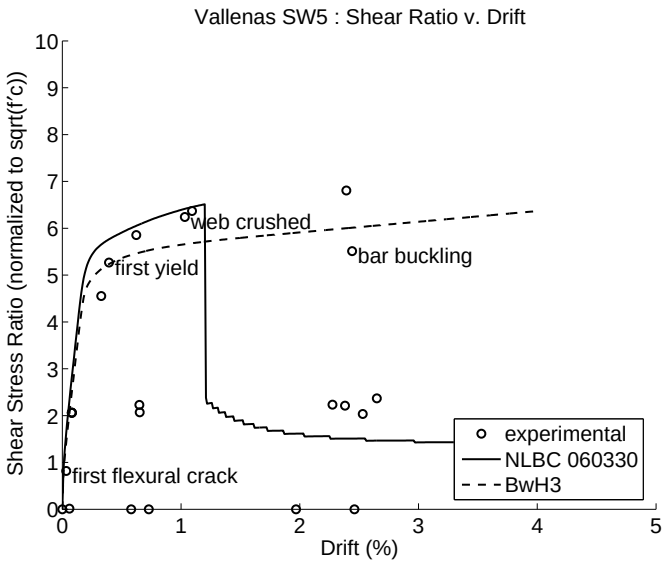

Figure E.53: Push Over Analysis – Vallenas SW5

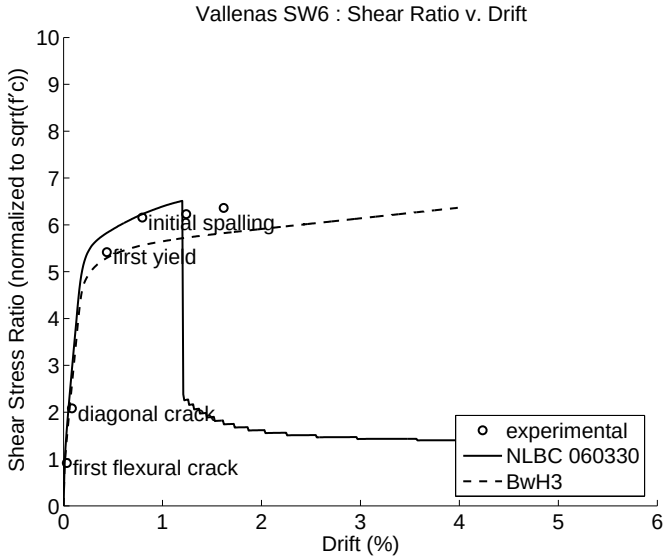

Figure E.54: Push Over Analysis – Vallenas SW6

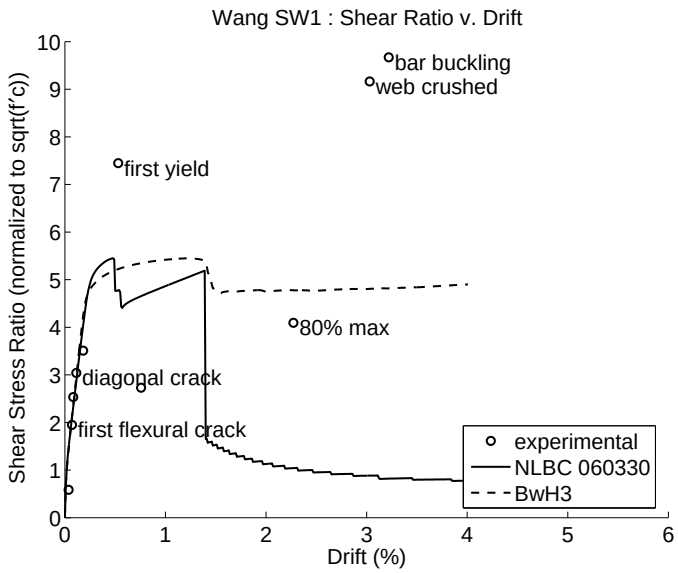

Figure E.55: Push Over Analysis – Wang SW1

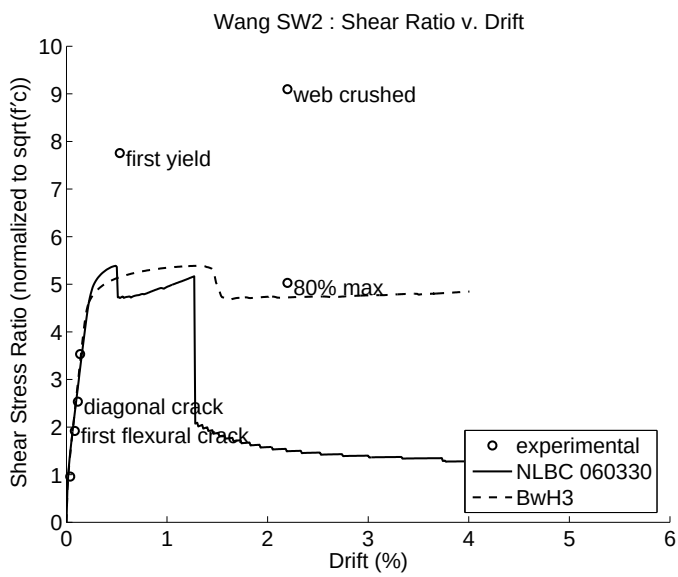

Figure E.56: Push Over Analysis – Wang SW2

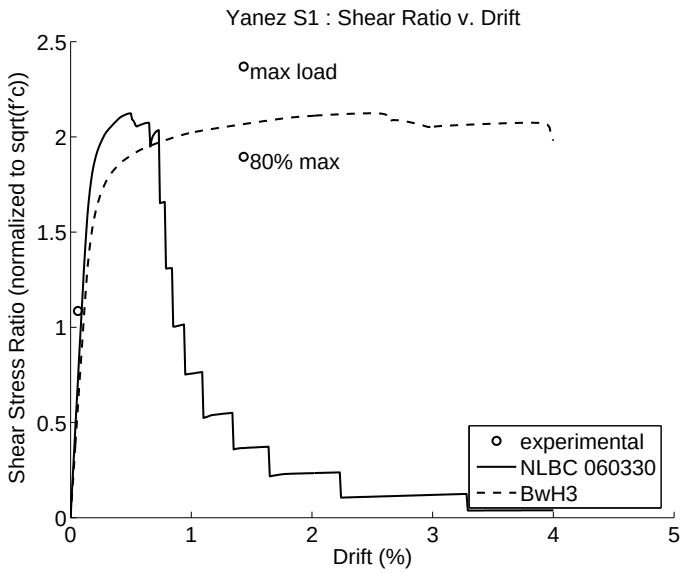

Figure E.57: Push Over Analysis – Yanez S1

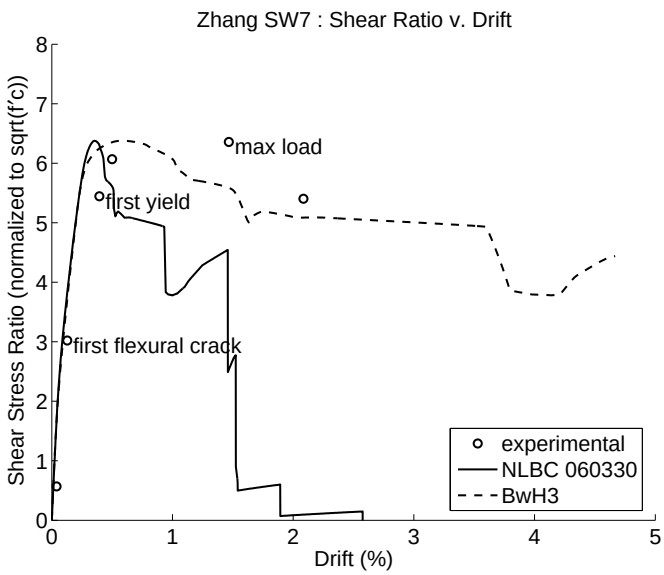

Figure E.58: Push Over Analysis – Zhang SW7

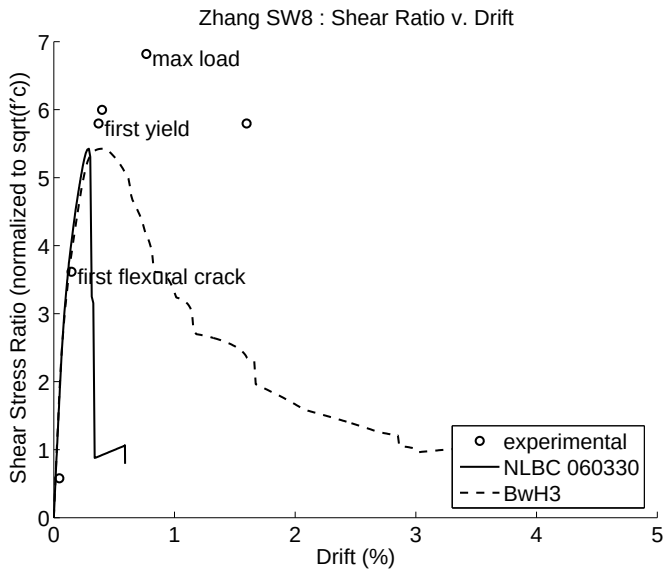

Figure E.59: Push Over Analysis – Zhang SW8

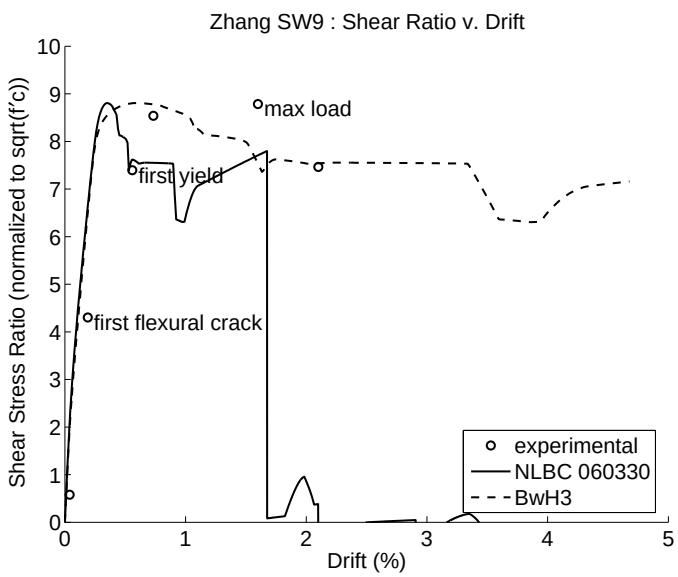

Figure E.60: Push Over Analysis – Zhang SW9

Appendix F

LUMPED PLASTICITY PREDICTIONS VERSUS DESIGN PARAMETER FIGURES

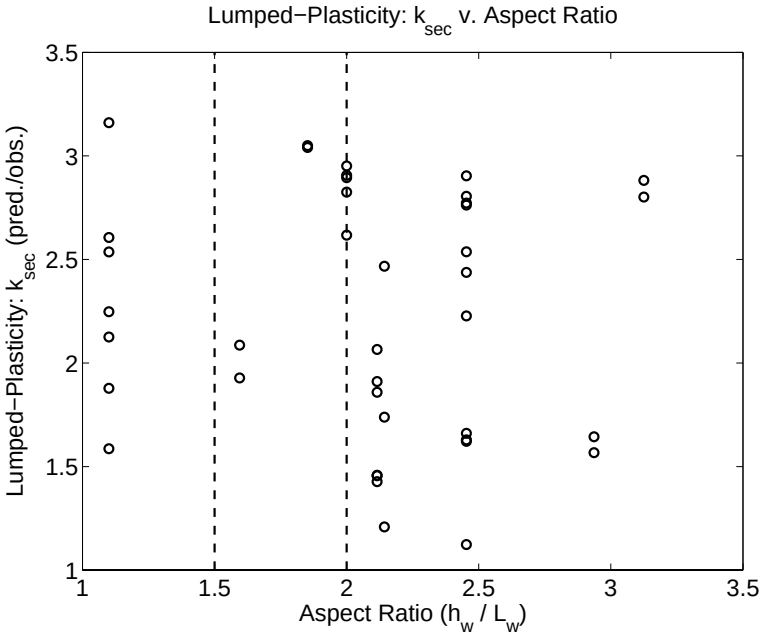

Figure F.1: Initial Stiffness Prediction v. Aspect Ratio

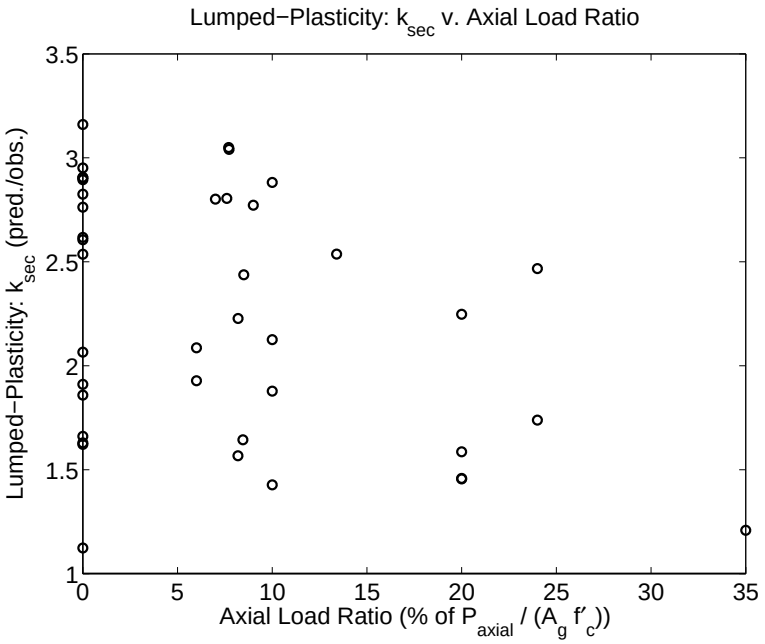

Figure F.2: Initial Stiffness Prediction v. Axial Load

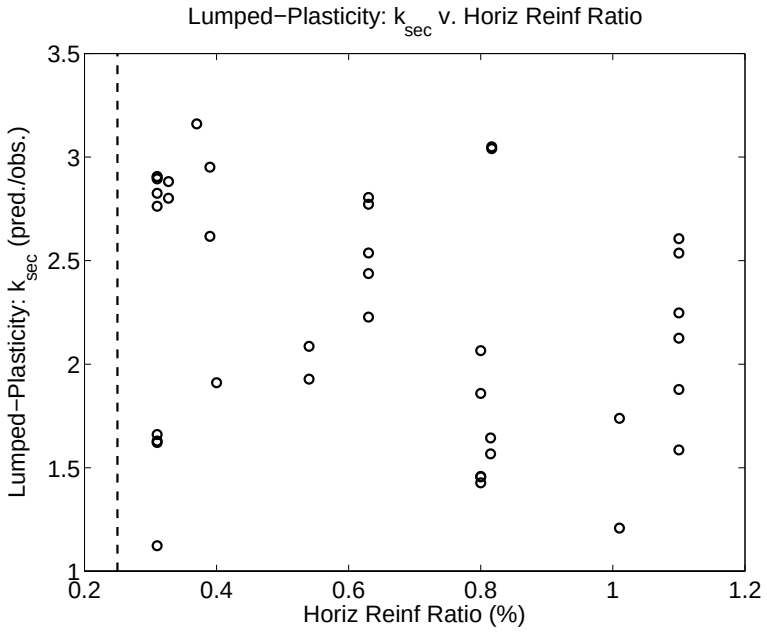

Figure F.3: Initial Stiffness Prediction v. Horizontal Reinforcement Ratio

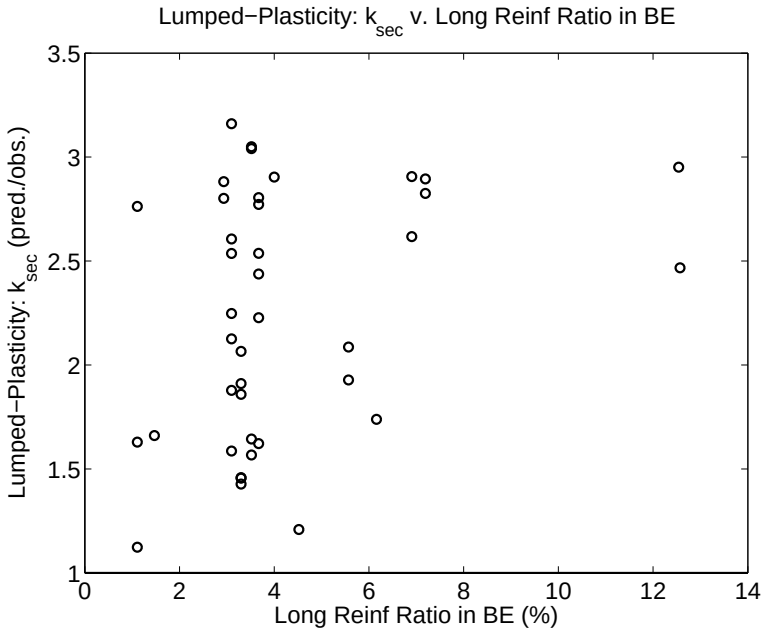

Figure F.4: Initial Stiffness Prediction v. Longitudinal Reinforcement Ratio

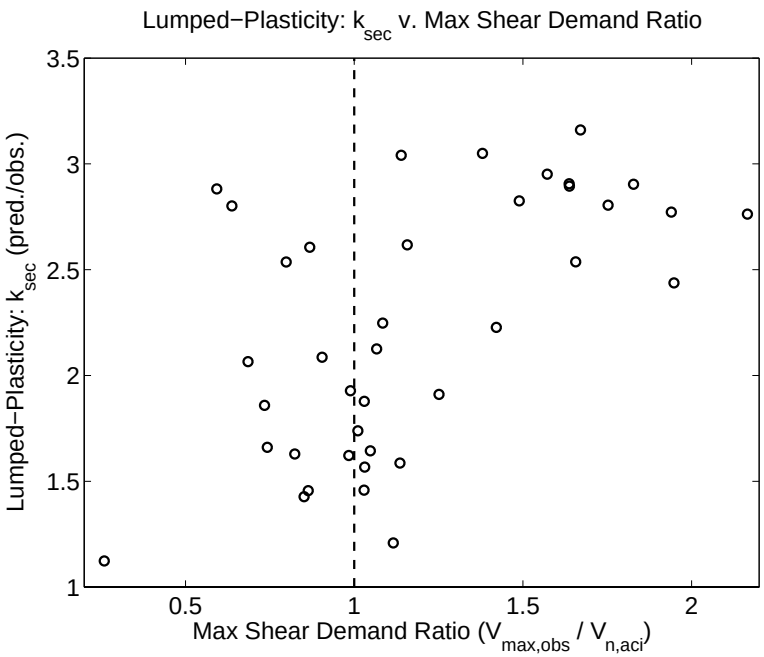

Figure F.5: Initial Stiffness Prediction v. Maximum Shear Demand Ratio

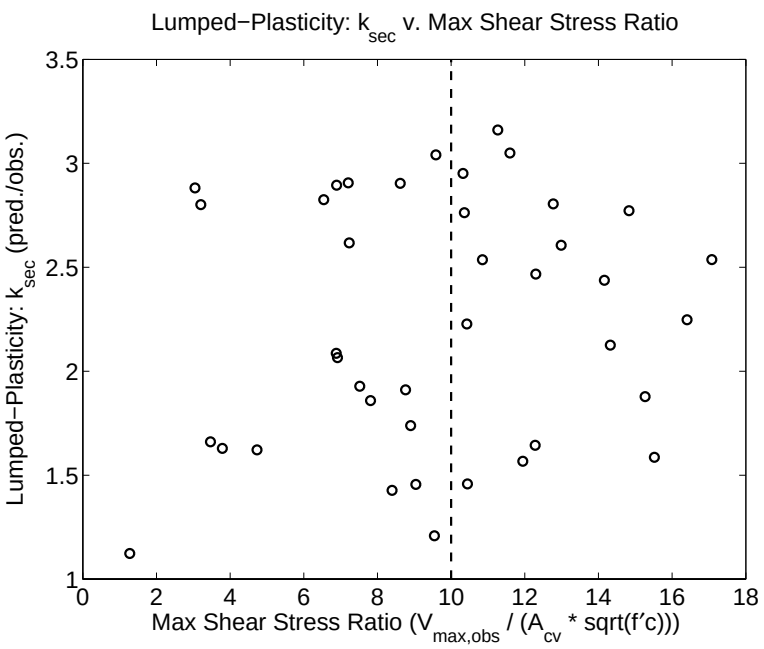

Figure F.6: Initial Stiffness Prediction v. Maximum Shear Stress Ratio

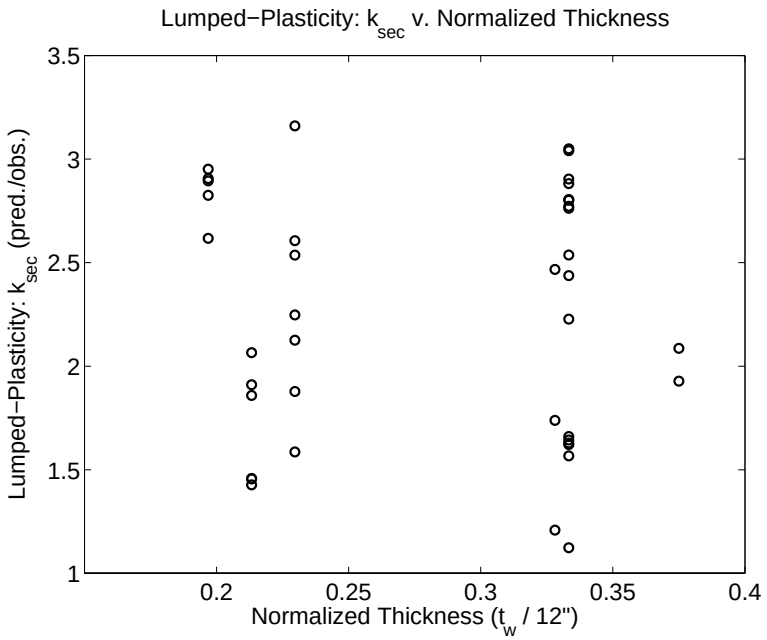

Figure F.7: Initial Stiffness Prediction v. Normalized Thickness

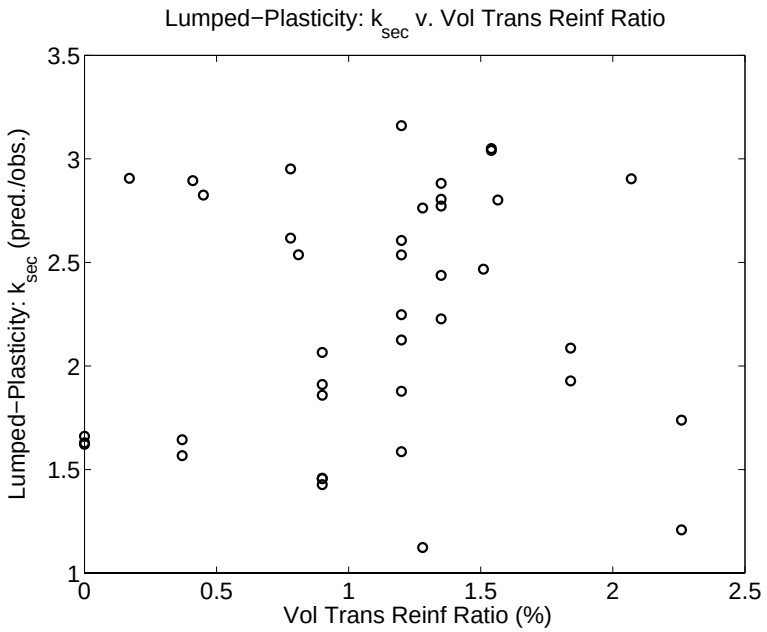

Figure F.8: Initial Stiffness Prediction v. Volumetric Transverse Reinforcement Ratio

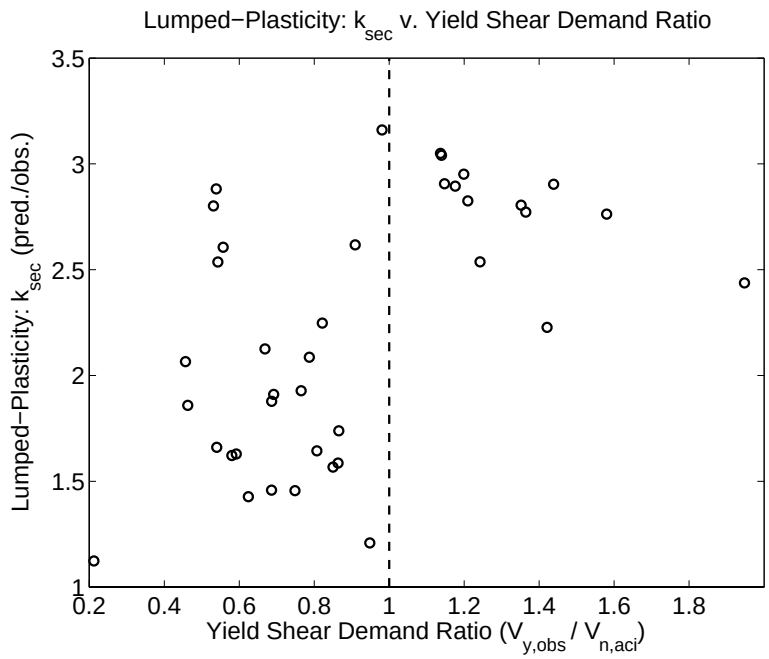

Figure F.9: Initial Stiffness Prediction v. Yield Shear Demand Ratio

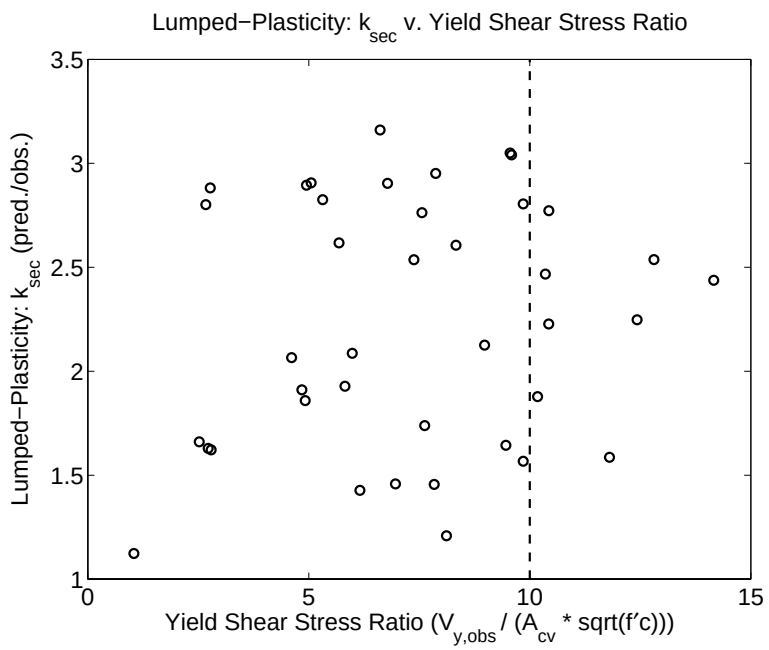

Figure F.10: Initial Stiffness Prediction v. Yield Shear Stress Ratio

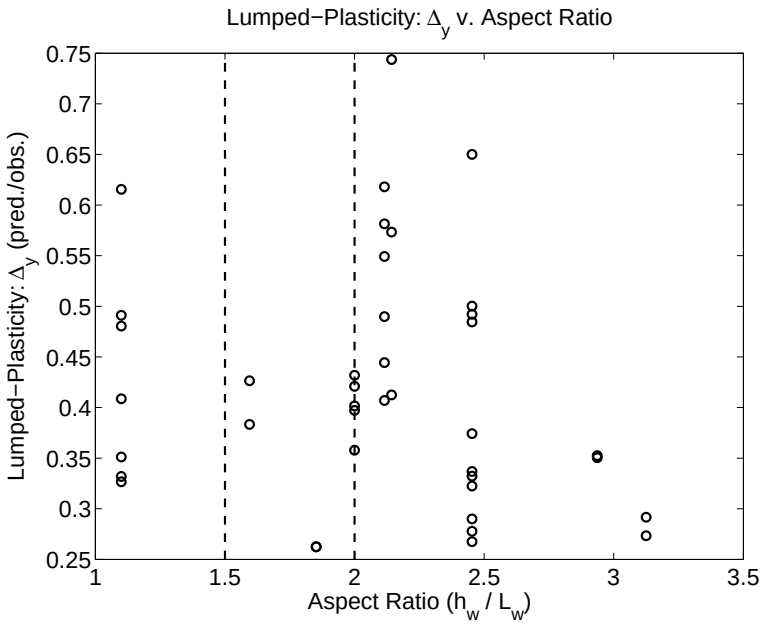

Figure F.11: Yield Displacement Prediction v. Aspect Ratio

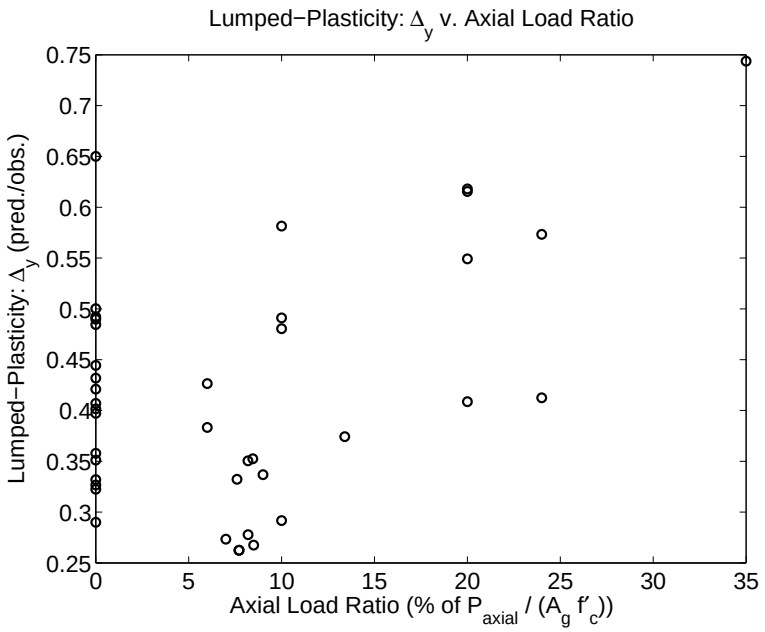

Figure F.12: Yield Displacement Prediction v. Axial Load

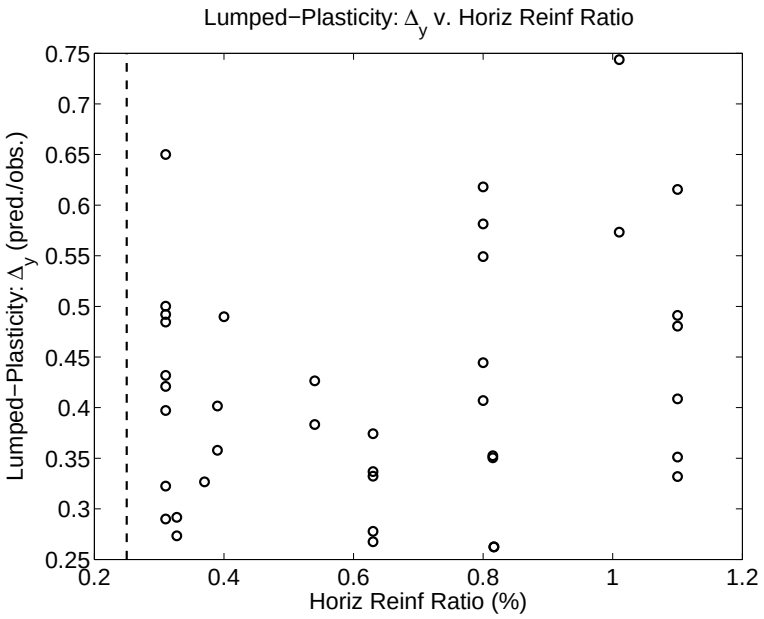

Figure F.13: Yield Displacement Prediction v. Horizontal Reinforcement Ratio

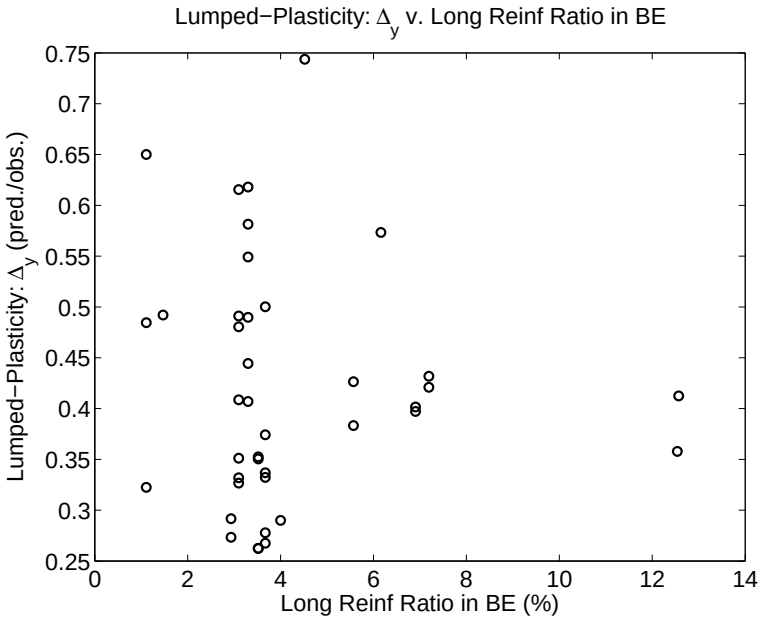

Figure F.14: Yield Displacement Prediction v. Longitudinal Reinforcement Ratio

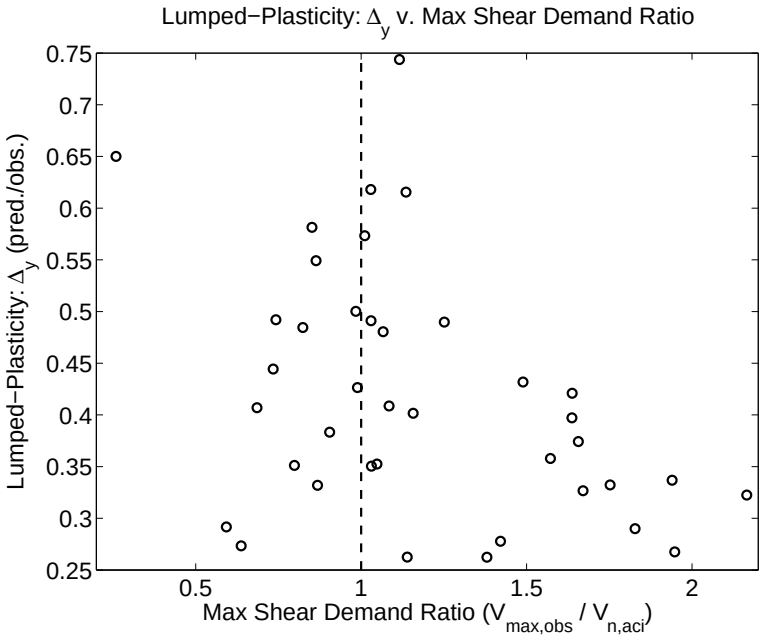

Figure F.15: Yield Displacement Prediction v. Maximum Shear Demand Ratio

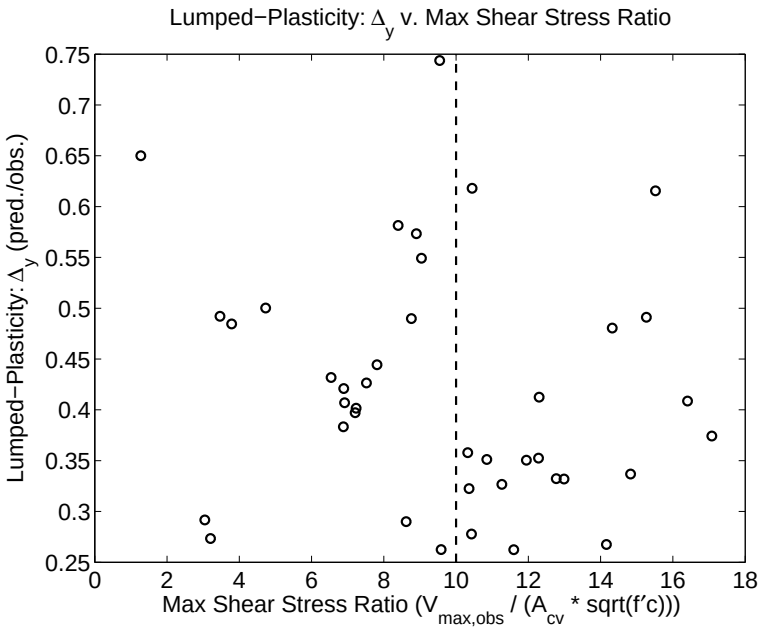

Figure F.16: Yield Displacement Prediction v. Maximum Shear Stress Ratio

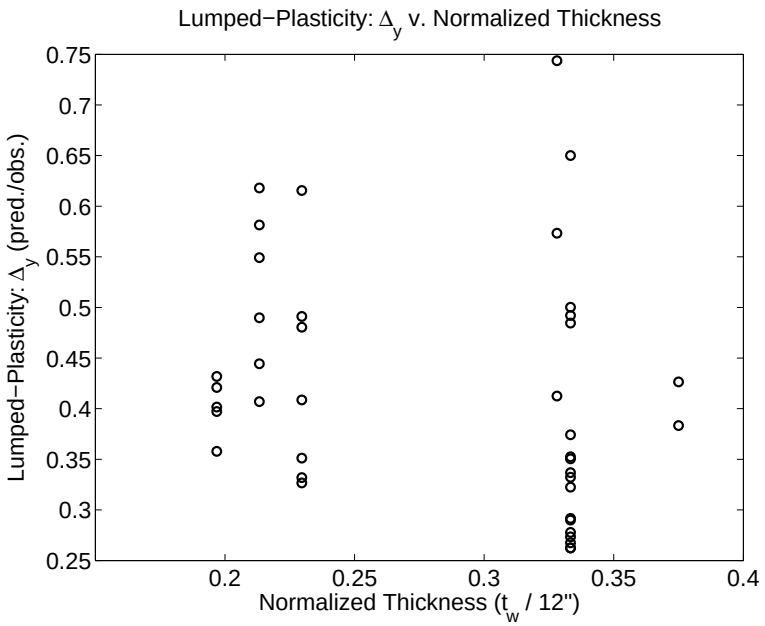

Figure F.17: Yield Displacement Prediction v. Normalized Thickness

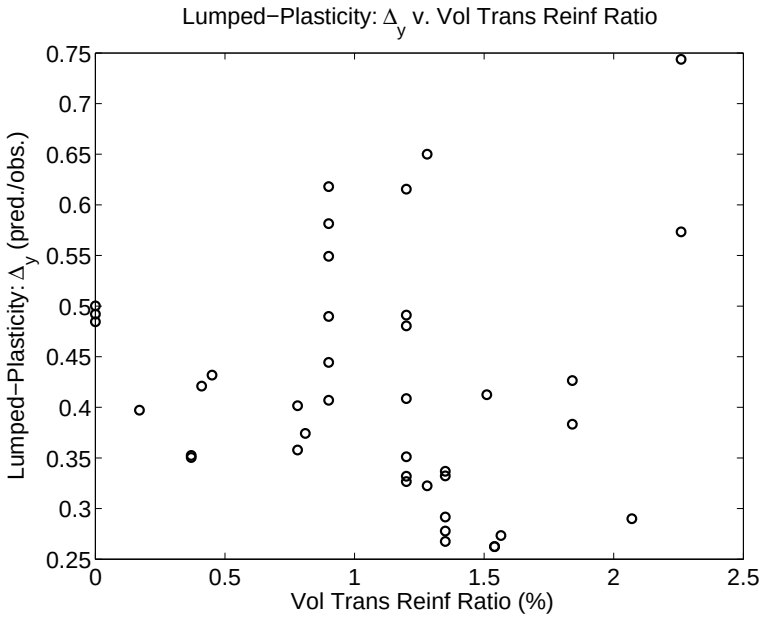

Figure F.18: Yield Displacement Prediction v. Volumetric Transverse Reinforcement Ratio

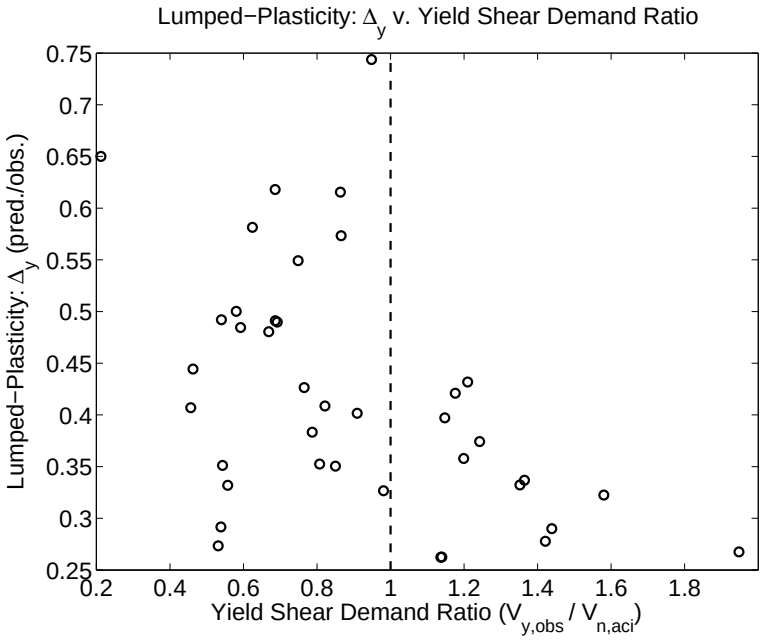

Figure F.19: Yield Displacement Prediction v. Yield Shear Demand Ratio

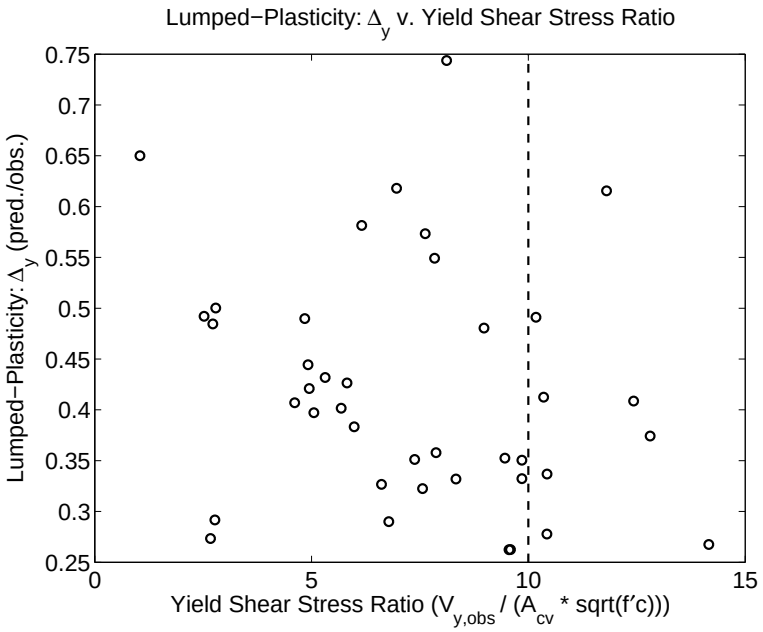

Figure F.20: Yield Displacement Prediction v. Yield Shear Stress Ratio

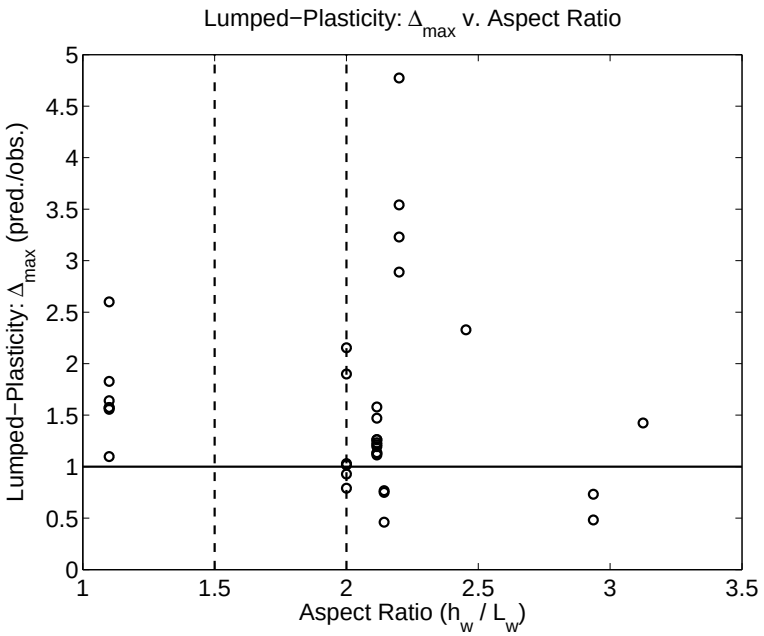

Figure F.21: Maximum Displacement Prediction v. Aspect Ratio

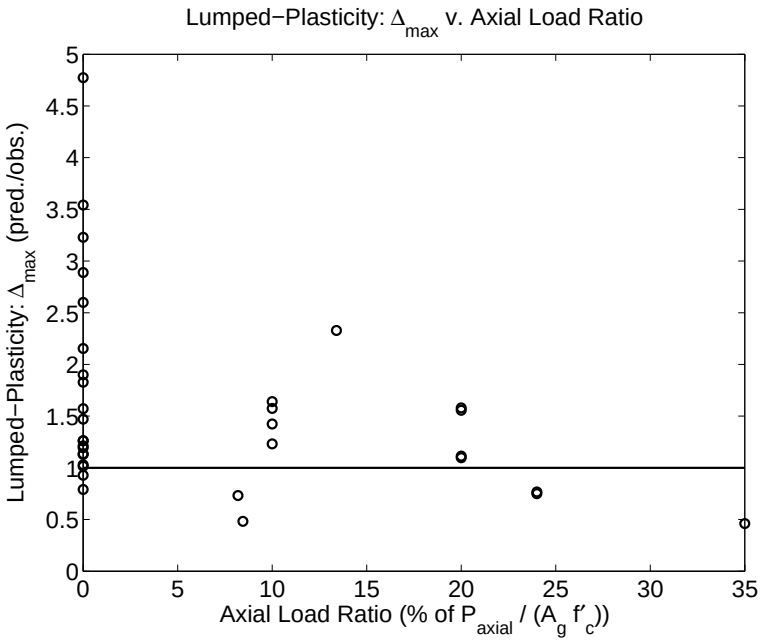

Figure F.22: Maximum Displacement Prediction v. Axial Load

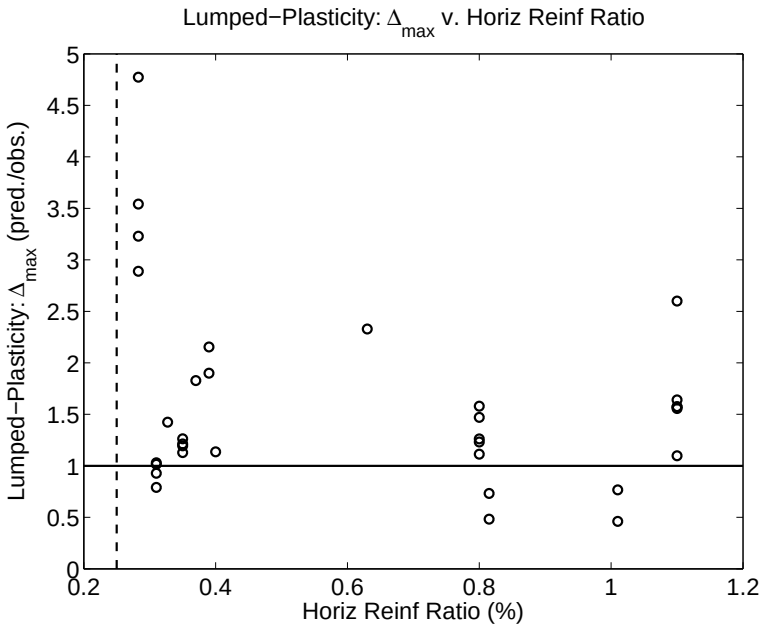

Figure F.23: Maximum Displacement Prediction v. Horizontal Reinforcement Ratio

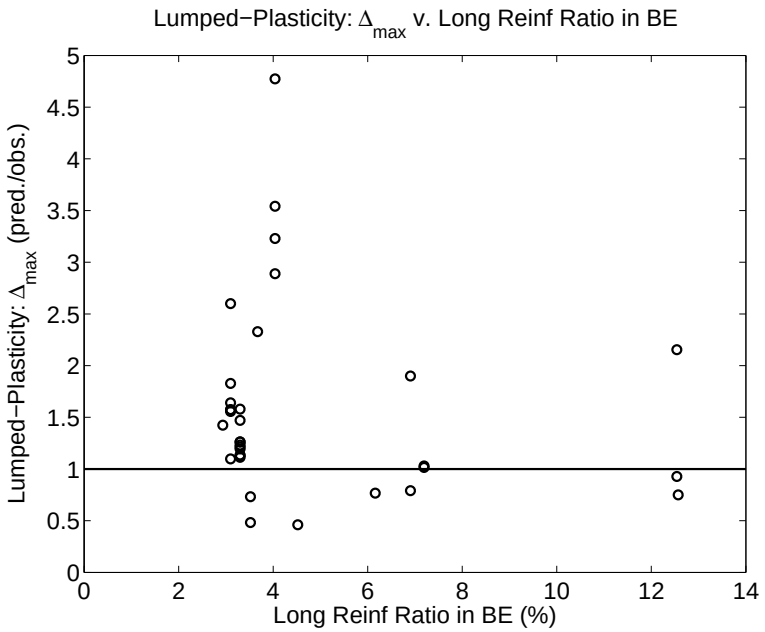

Figure F.24: Maximum Displacement Prediction v. Longitudinal Reinforcement Ratio

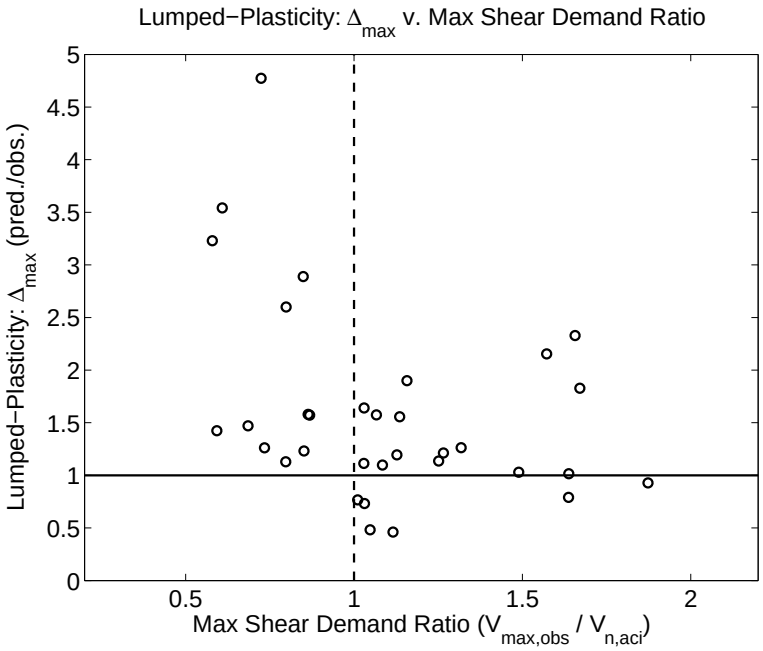

Figure F.25: Maximum Displacement Prediction v. Maximum Shear Demand Ratio

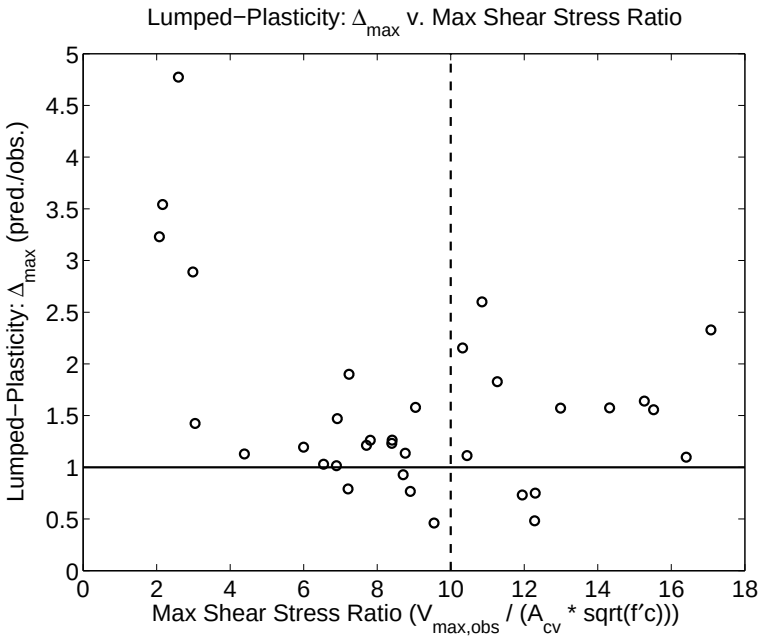

Figure F.26: Maximum Displacement Prediction v. Maximum Shear Stress Ratio

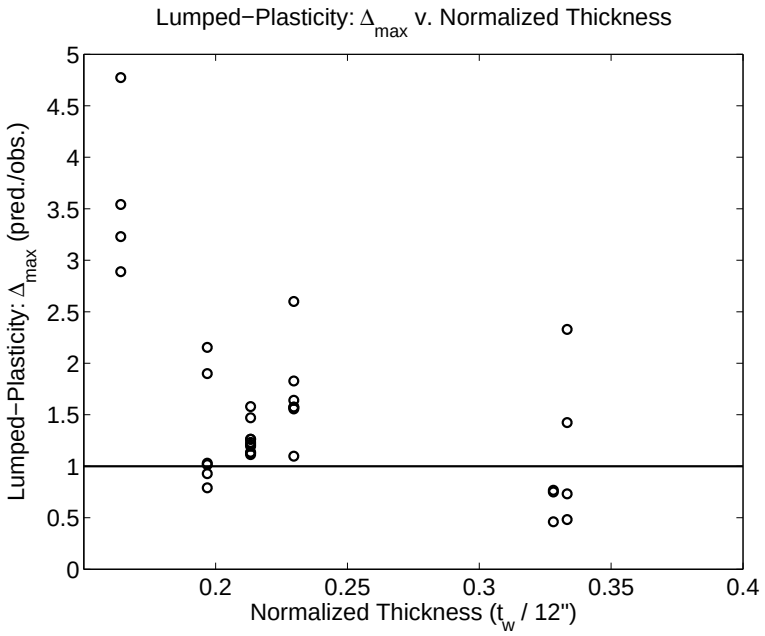

Figure F.27: Maximum Displacement Prediction v. Normalized Thickness

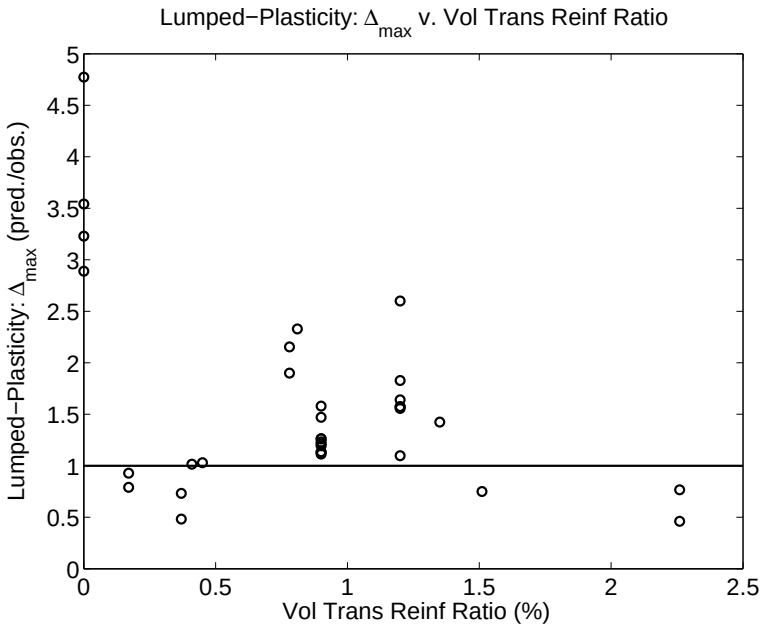

Figure F.28: Maximum Displacement Prediction v. Volumetric Transverse Reinforcement Ratio

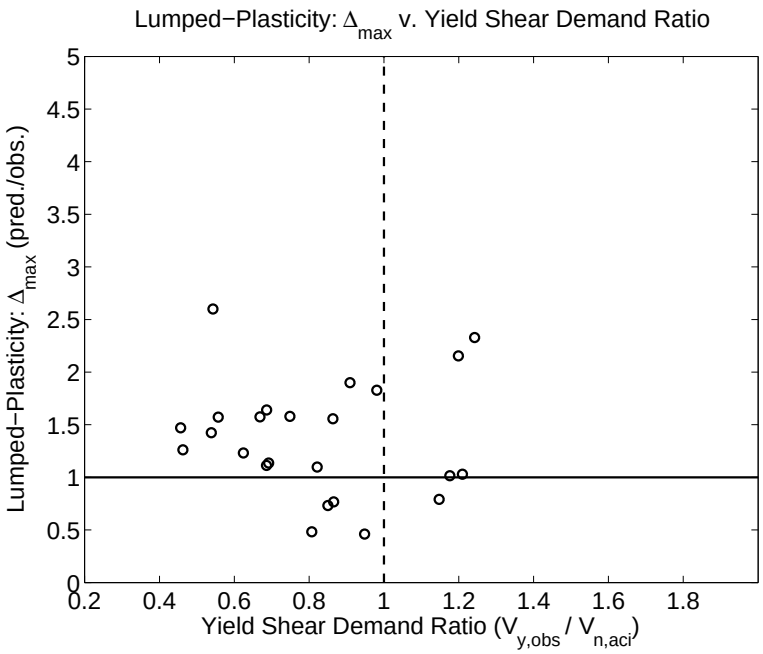

Figure F.29: Maximum Displacement Prediction v. Yield Shear Demand Ratio

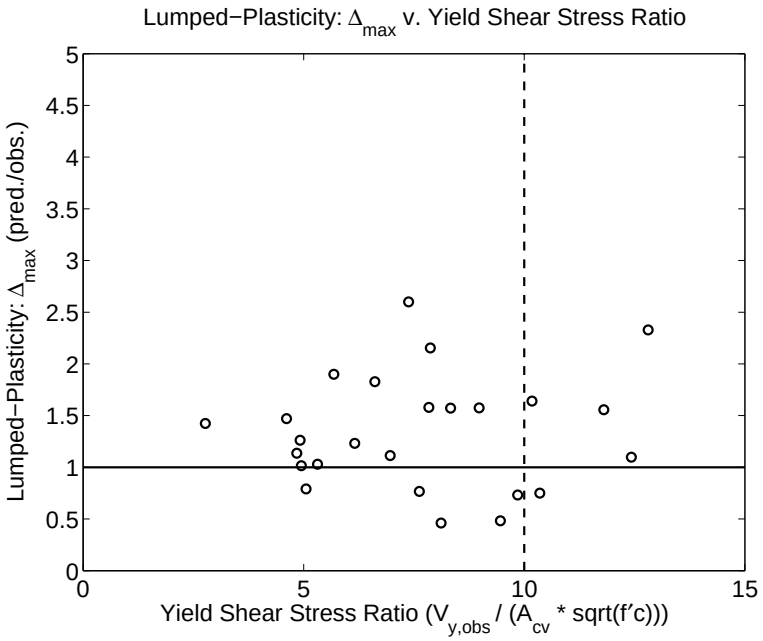

Figure F.30: Maximum Displacement Prediction v. Yield Shear Stress Ratio

Appendix G

DISTRIBUTED PLASTICITY PREDICTIONS VERSUS DESIGN PARAMETER FIGURES

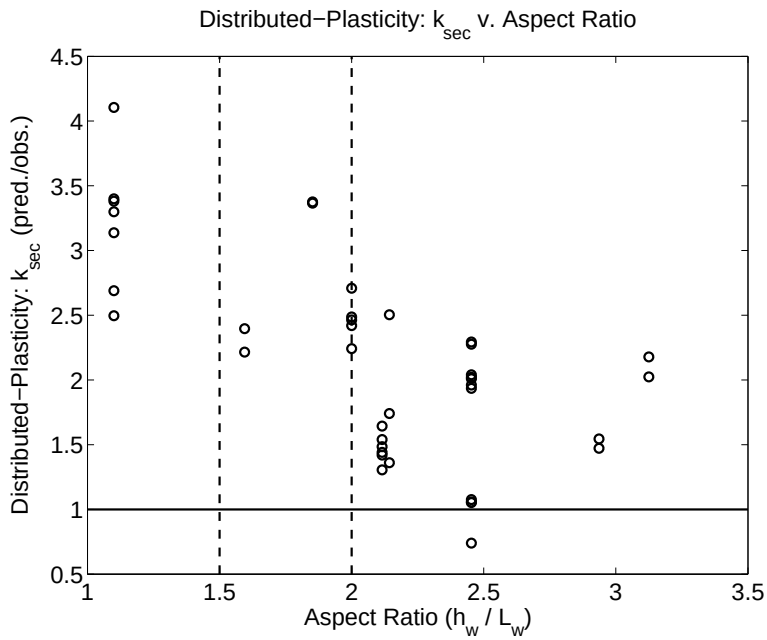

Figure G.1: Initial Stiffness Prediction v. Aspect Ratio

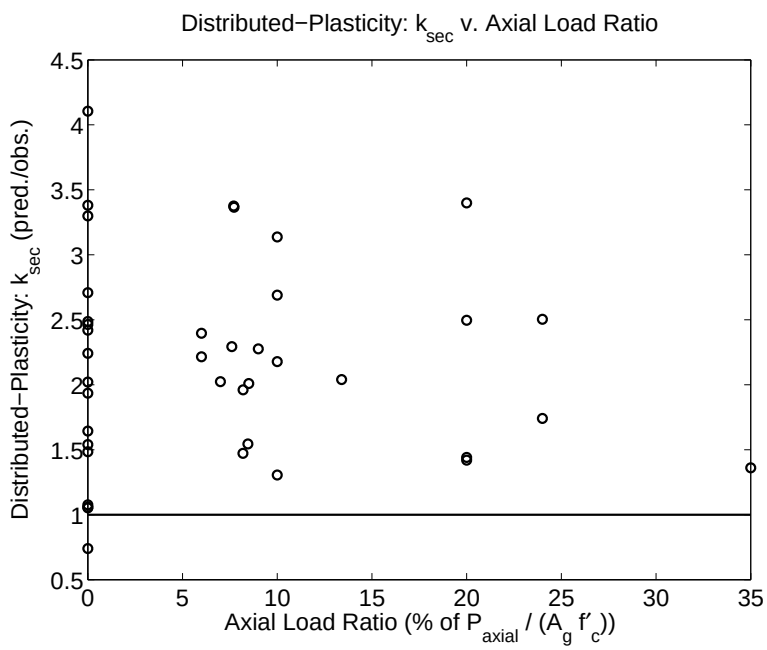

Figure G.2: Initial Stiffness Prediction v. Axial Load

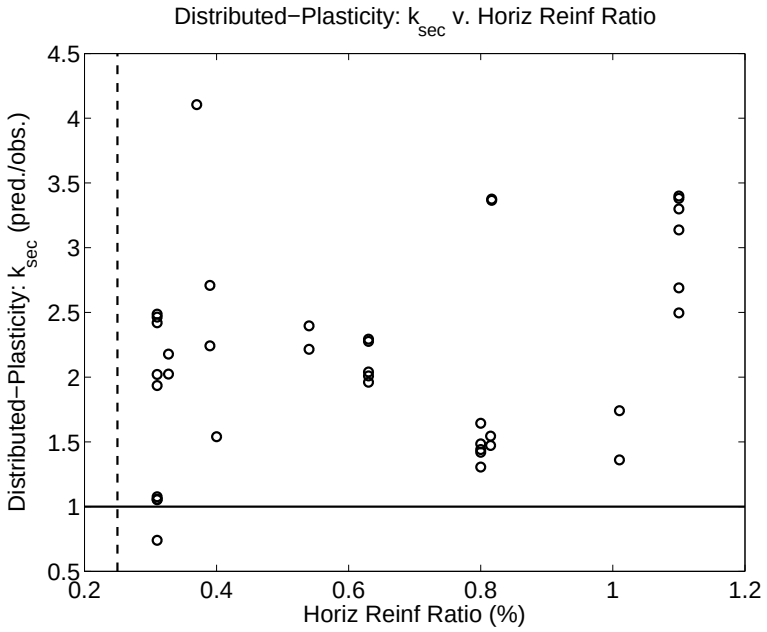

Figure G.3: Initial Stiffness Prediction v. Horizontal Reinforcement Ratio

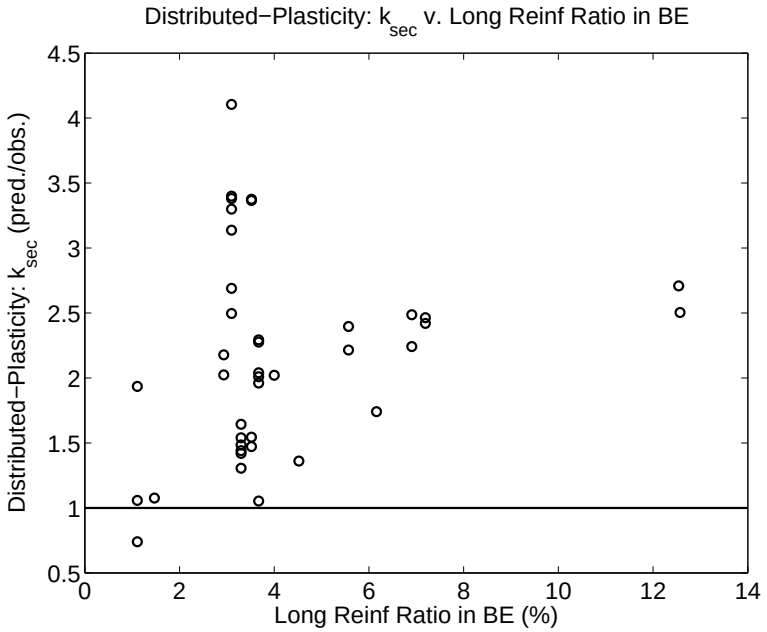

Figure G.4: Initial Stiffness Prediction v. Longitudinal Reinforcement Ratio

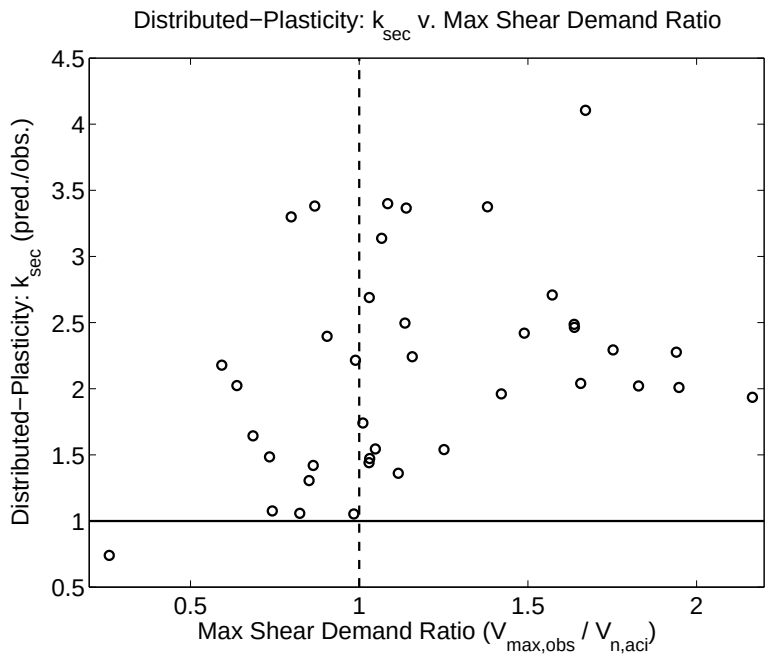

Figure G.5: Initial Stiffness Prediction v. Maximum Shear Demand Ratio

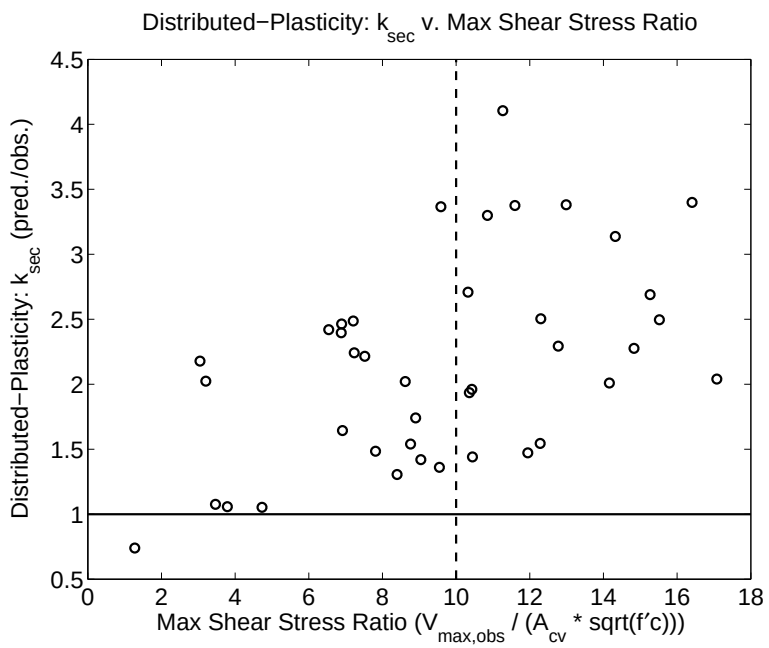

Figure G.6: Initial Stiffness Prediction v. Maximum Shear Stress Ratio

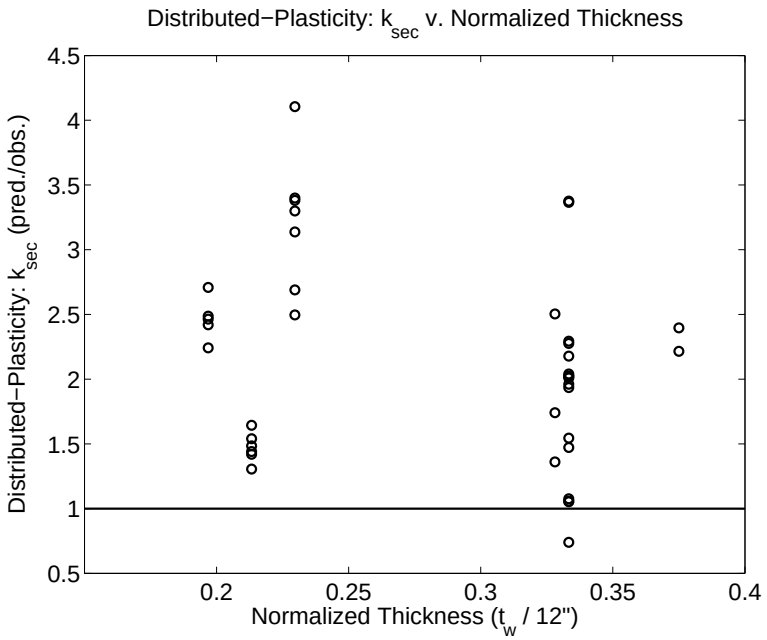

Figure G.7: Initial Stiffness Prediction v. Normalized Thickness

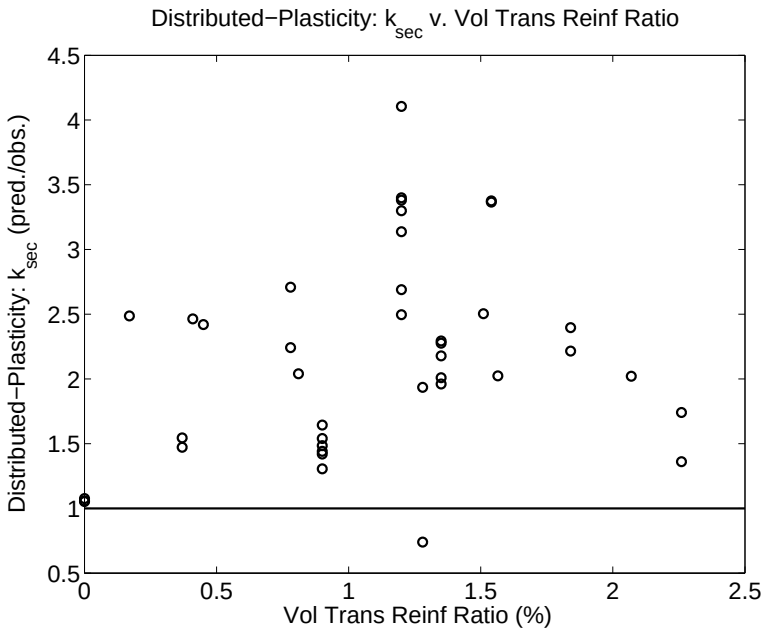

Figure G.8: Initial Stiffness Prediction v. Volumetric Transverse Reinforcement Ratio

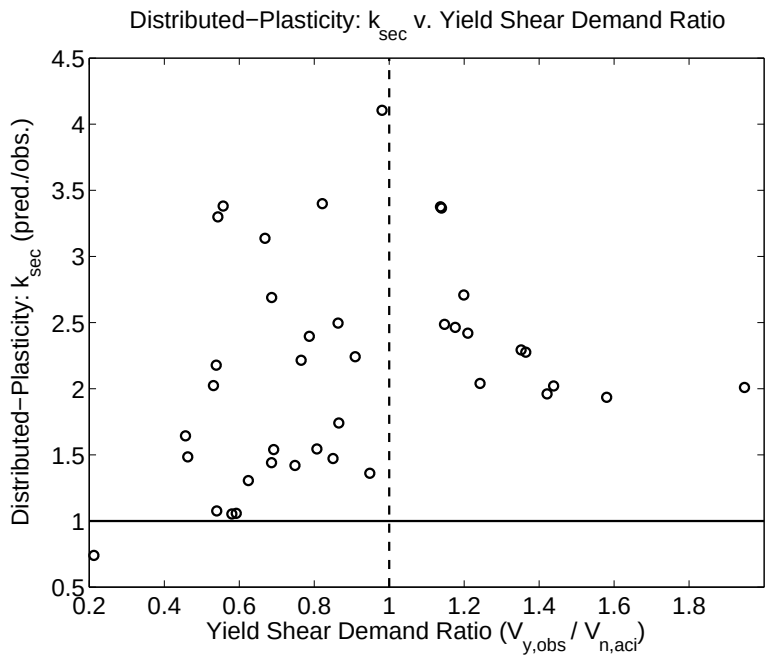

Figure G.9: Initial Stiffness Prediction v. Yield Shear Demand Ratio

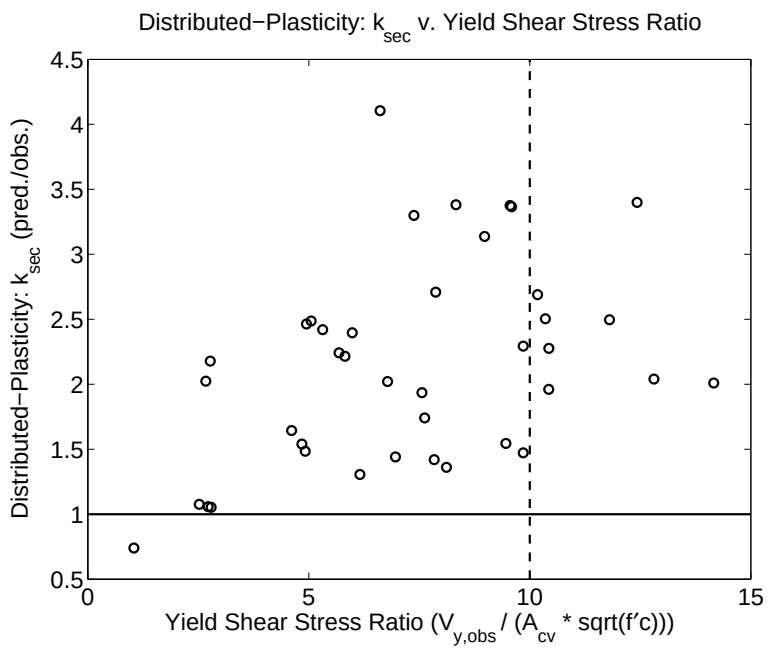

Figure G.10: Initial Stiffness Prediction v. Yield Shear Stress Ratio

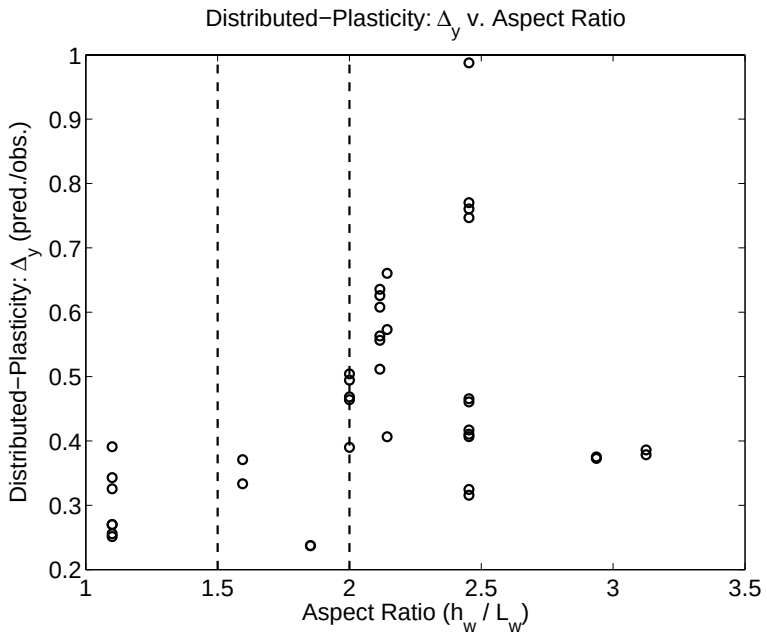

Figure G.11: Yield Displacement Prediction v. Aspect Ratio

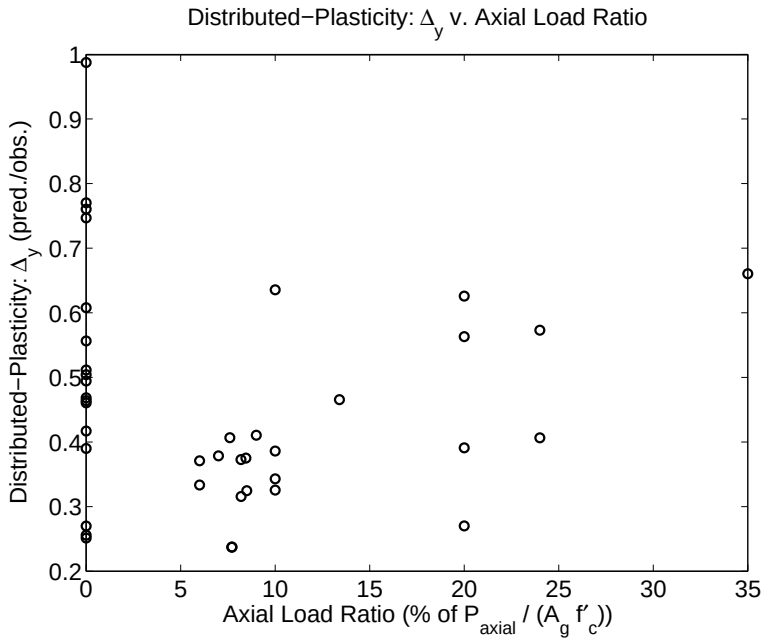

Figure G.12: Yield Displacement Prediction v. Axial Load

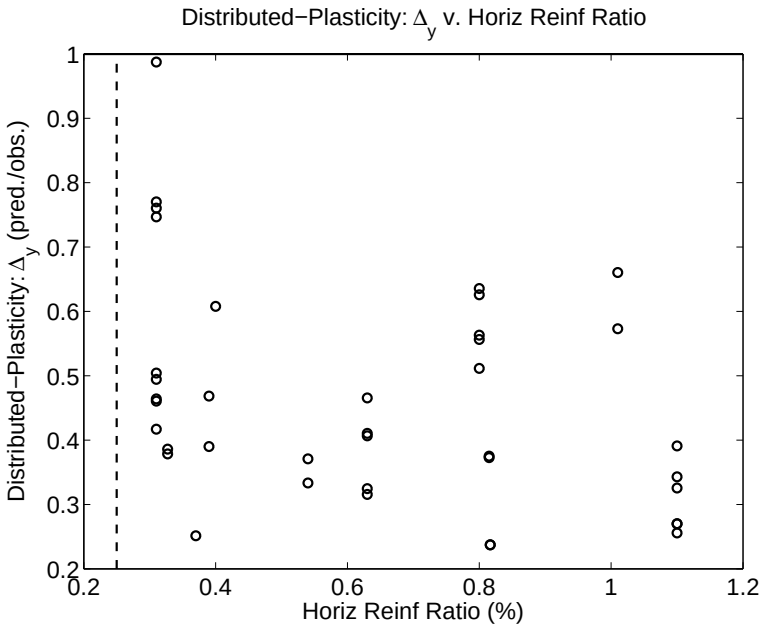

Figure G.13: Yield Displacement Prediction v. Horizontal Reinforcement Ratio

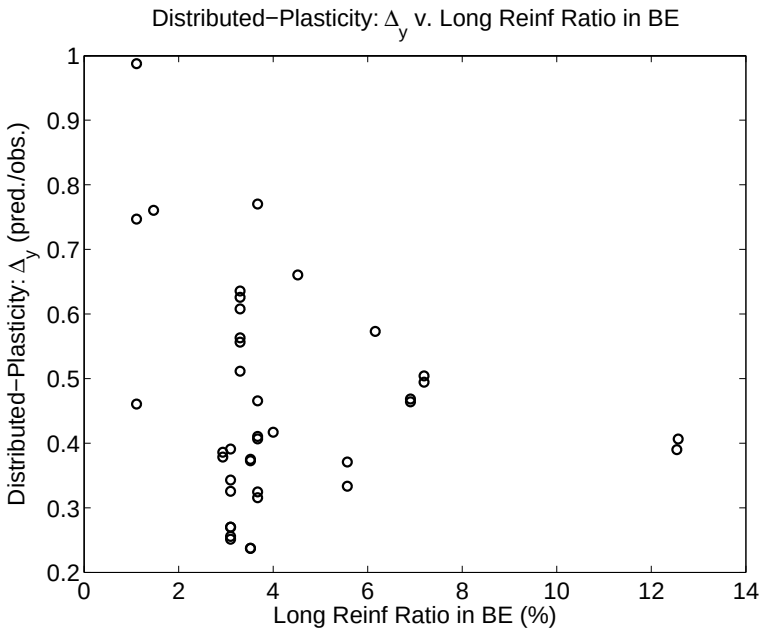

Figure G.14: Yield Displacement Prediction v. Longitudinal Reinforcement Ratio

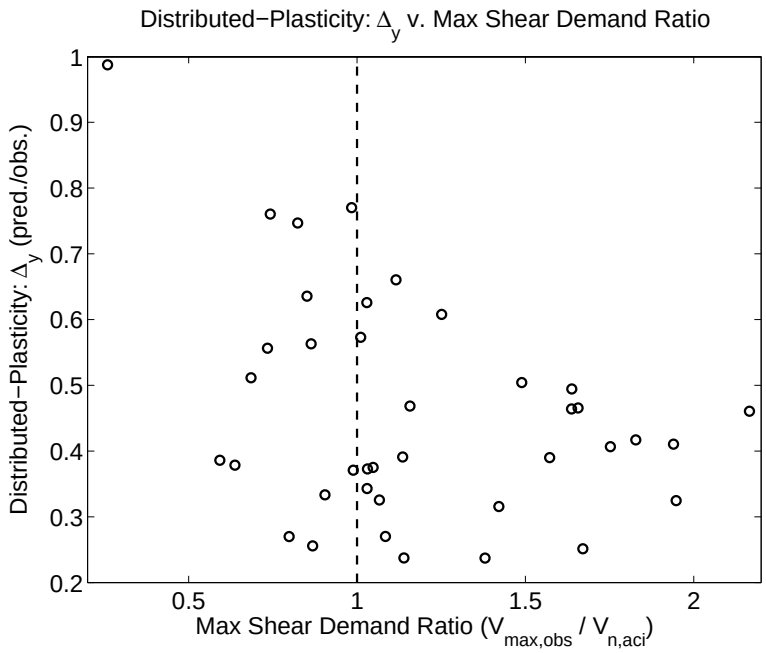

Figure G.15: Yield Displacement Prediction v. Maximum Shear Demand Ratio

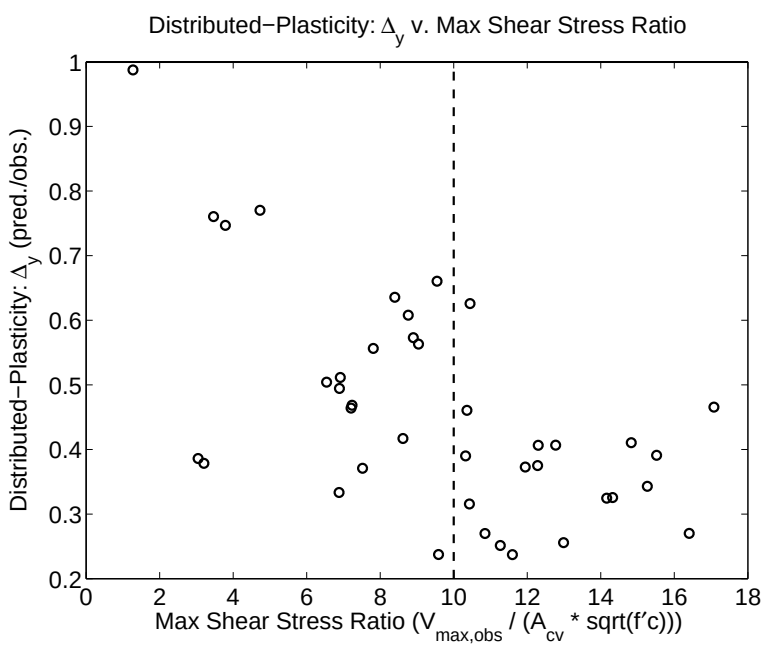

Figure G.16: Yield Displacement Prediction v. Maximum Shear Stress Ratio

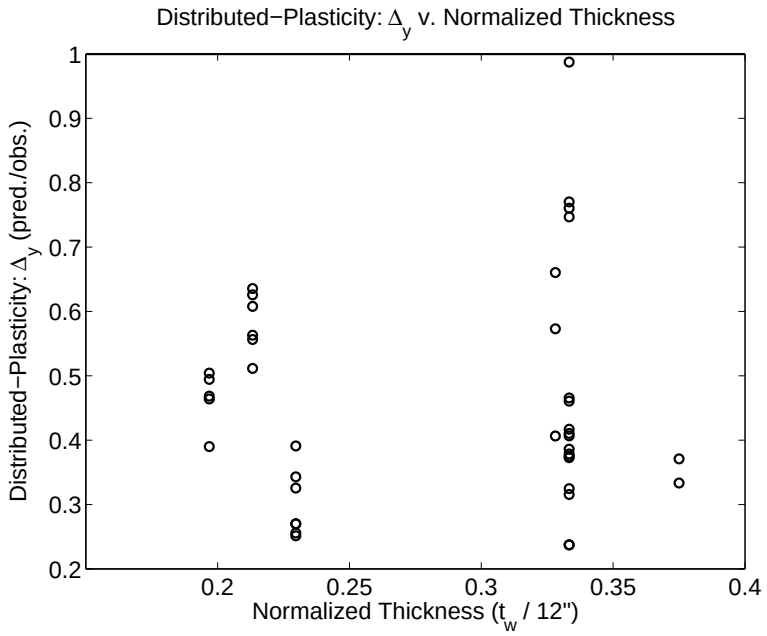

Figure G.17: Yield Displacement Prediction v. Normalized Thickness

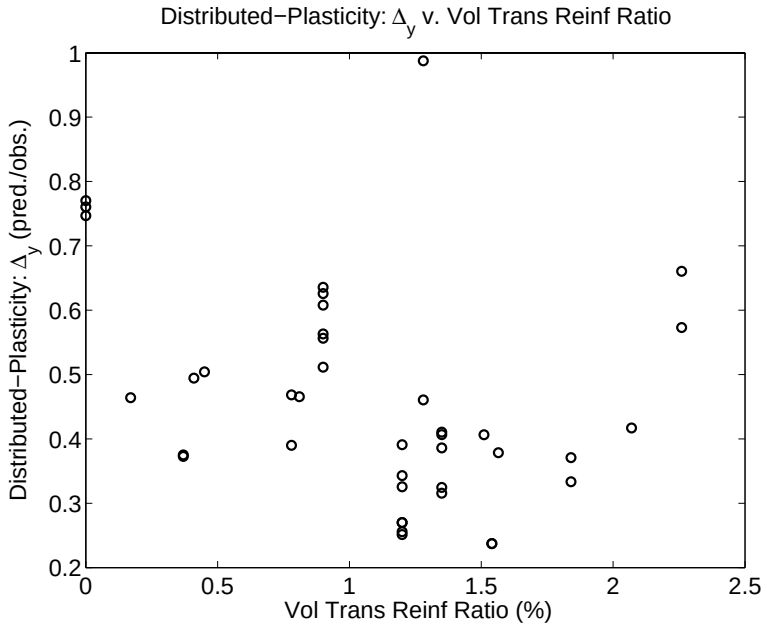

Figure G.18: Yield Displacement Prediction v. Volumetric Transverse Reinforcement Ratio

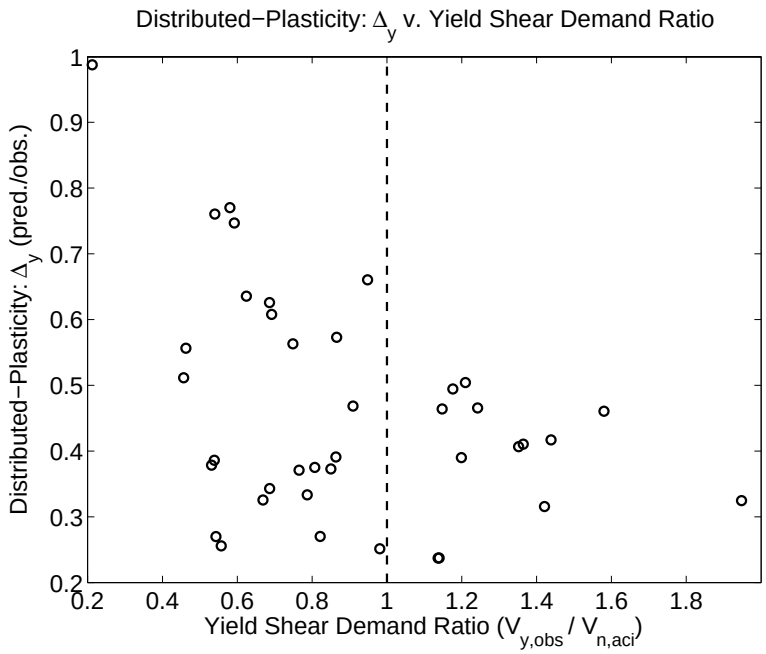

Figure G.19: Yield Displacement Prediction v. Yield Shear Demand Ratio

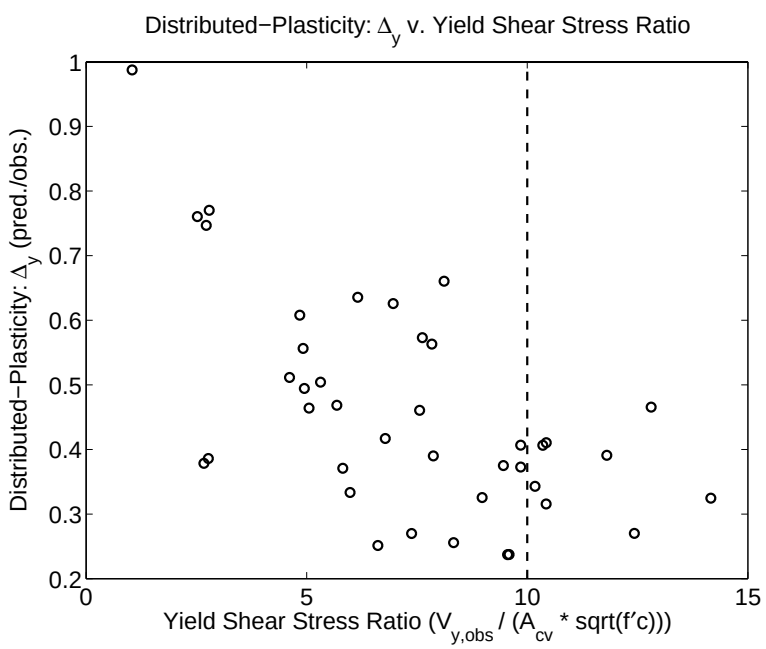

Figure G.20: Yield Displacement Prediction v. Yield Shear Stress Ratio

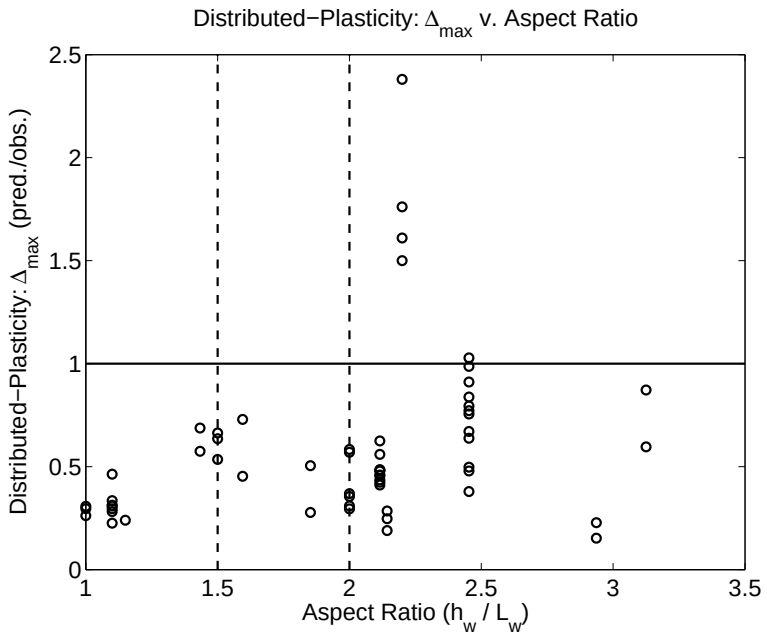

Figure G.21: Maximum Displacement Prediction v. Aspect Ratio

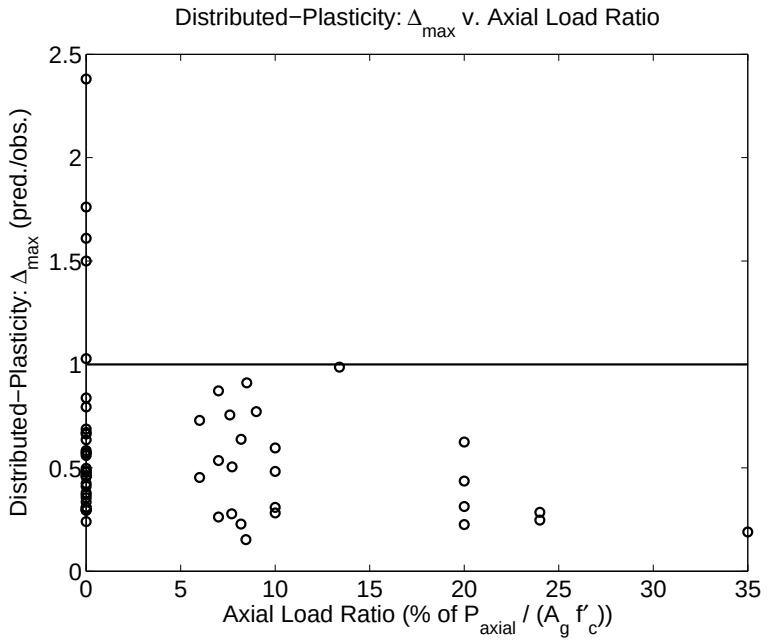

Figure G.22: Maximum Displacement Prediction v. Axial Load

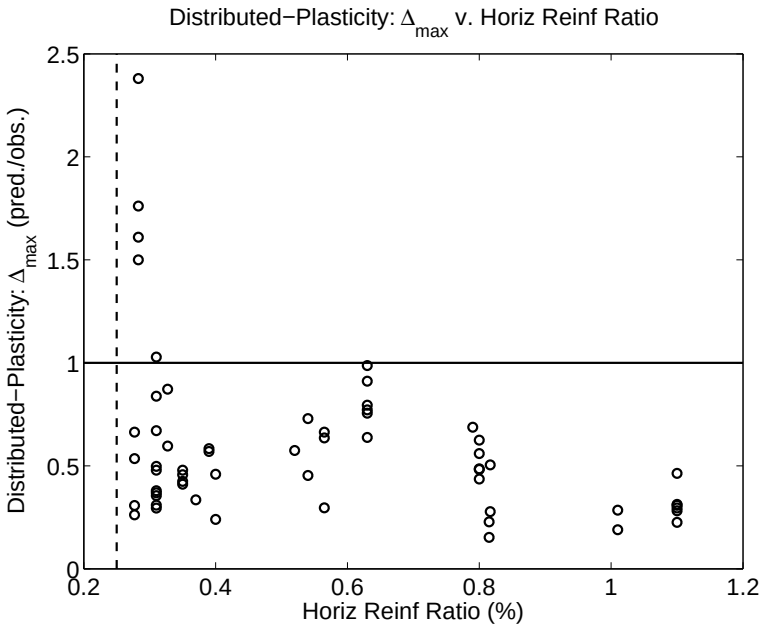

Figure G.23: Maximum Displacement Prediction v. Horizontal Reinforcement Ratio

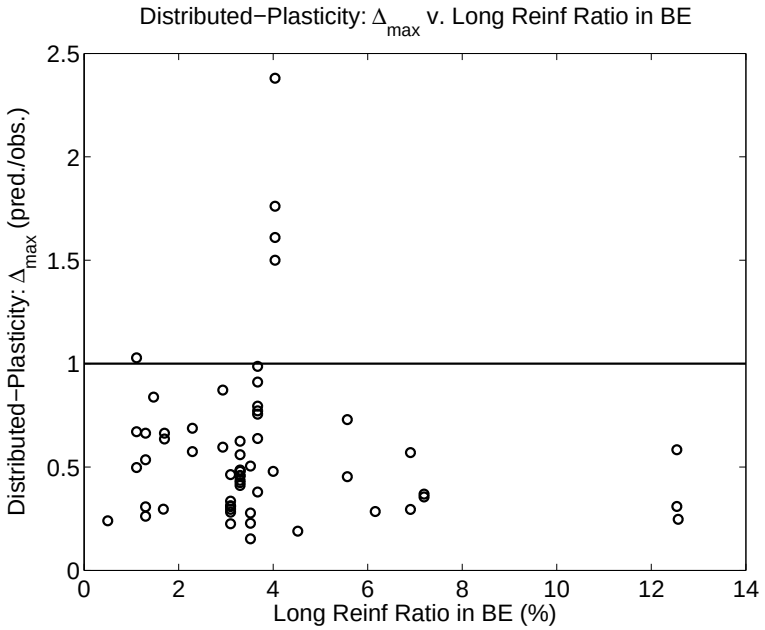

Figure G.24: Maximum Displacement Prediction v. Longitudinal Reinforcement Ratio

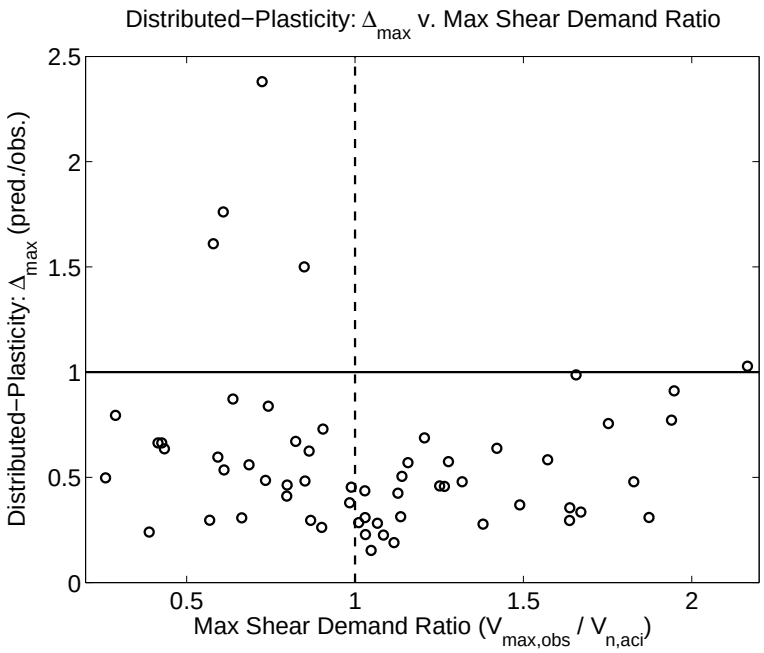

Figure G.25: Maximum Displacement Prediction v. Maximum Shear Demand Ratio

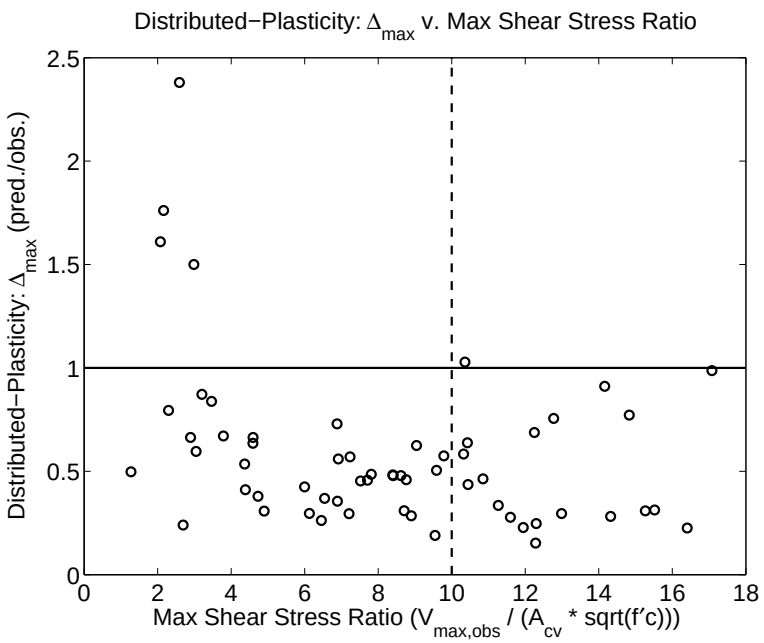

Figure G.26: Maximum Displacement Prediction v. Maximum Shear Stress Ratio

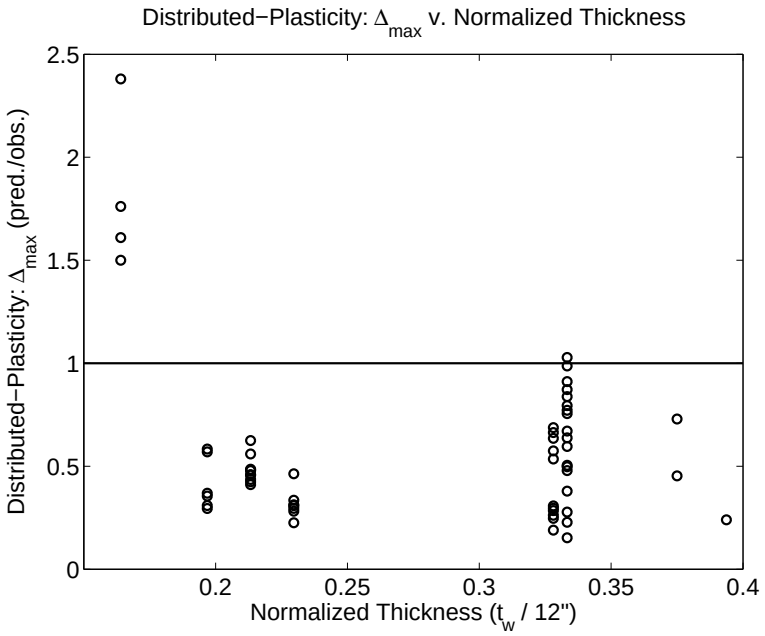

Figure G.27: Maximum Displacement Prediction v. Normalized Thickness

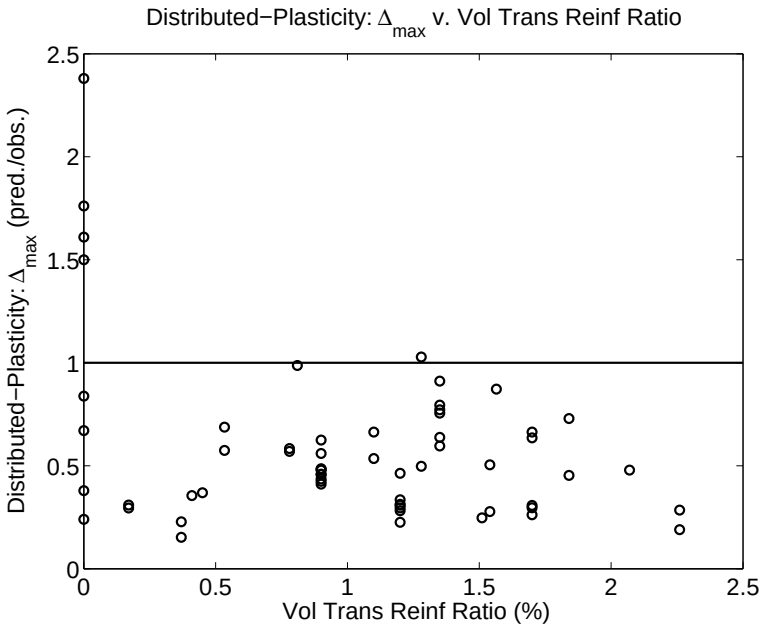

Figure G.28: Maximum Displacement Prediction v. Volumetric Transverse Reinforcement Ratio

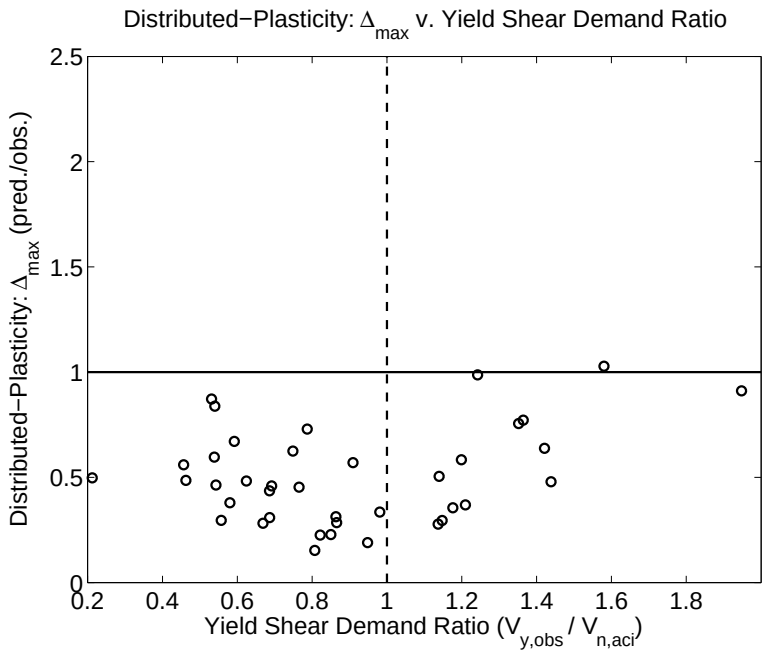

Figure G.29: Maximum Displacement Prediction v. Yield Shear Demand Ratio

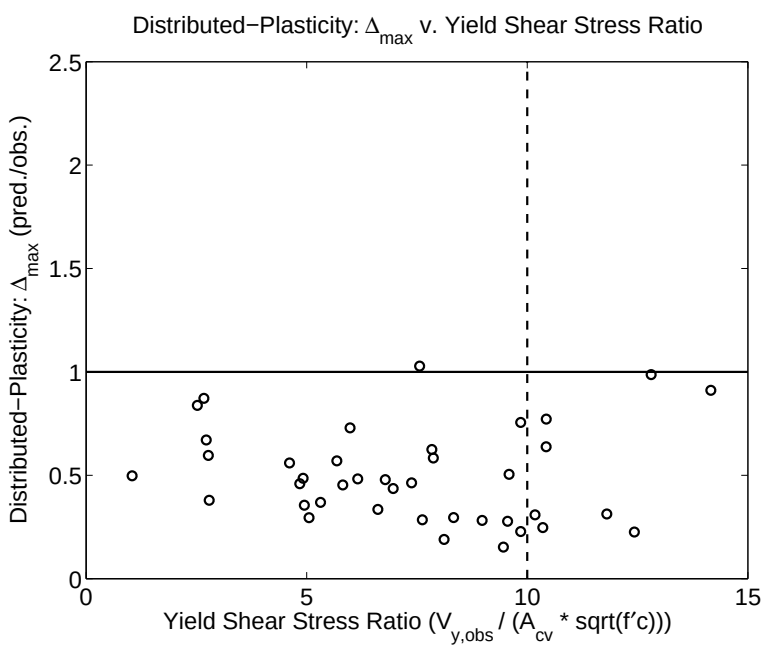

Figure G.30: Maximum Displacement Prediction v. Yield Shear Stress Ratio

Appendix H

CALIBRATED LINEAR SHEAR COEFFICIENTS VERSUS DESIGN PARAMETER FIGURES

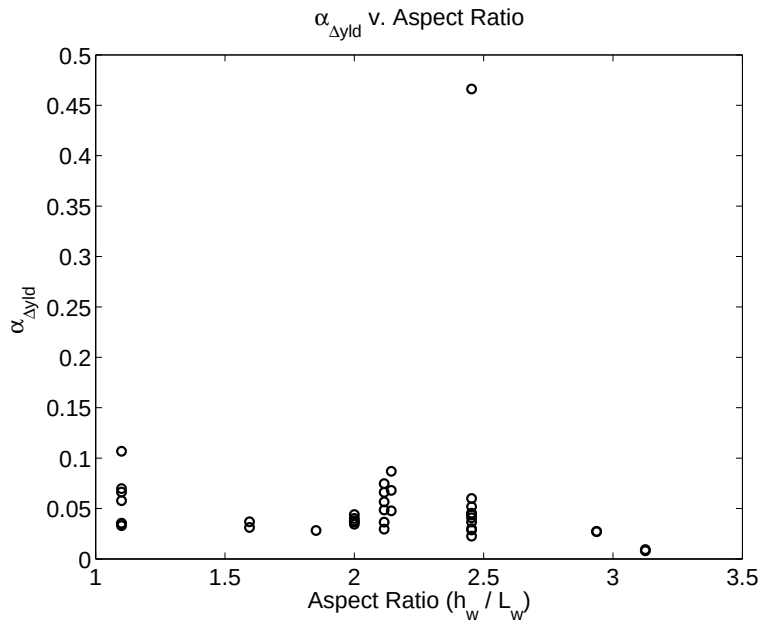

Figure H.1: Alpha Calibrated to Yield v. Aspect Ratio

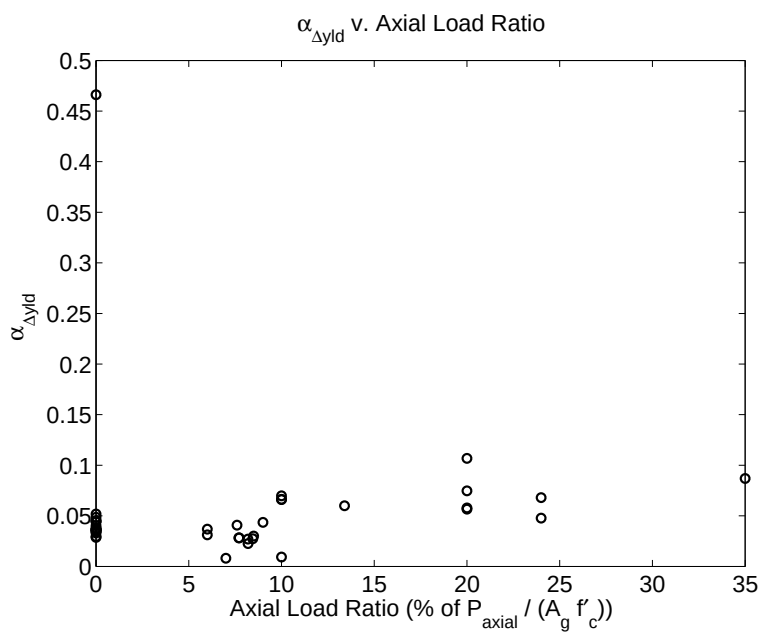

Figure H.2: Alpha Calibrated to Yield v. Axial Load Ratio

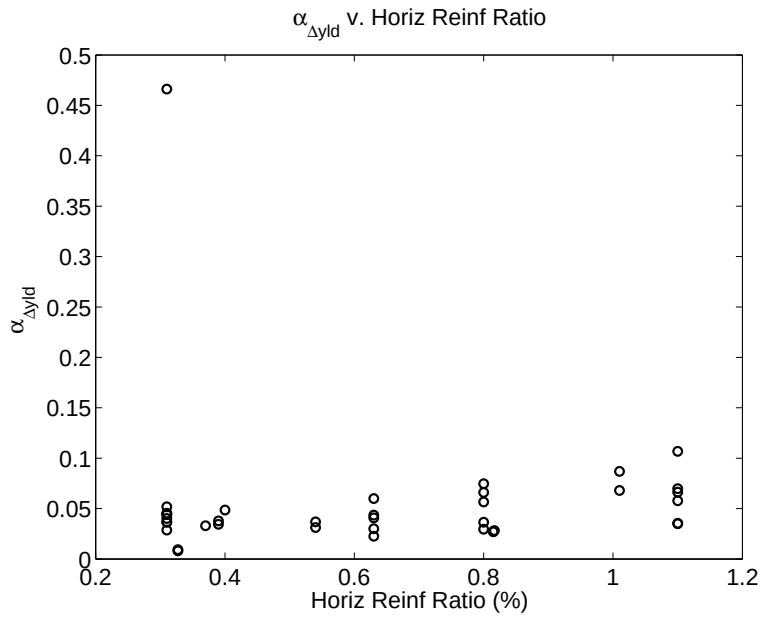

Figure H.3: Alpha Calibrated to Yield v. Horizontal Reinforcement Ratio

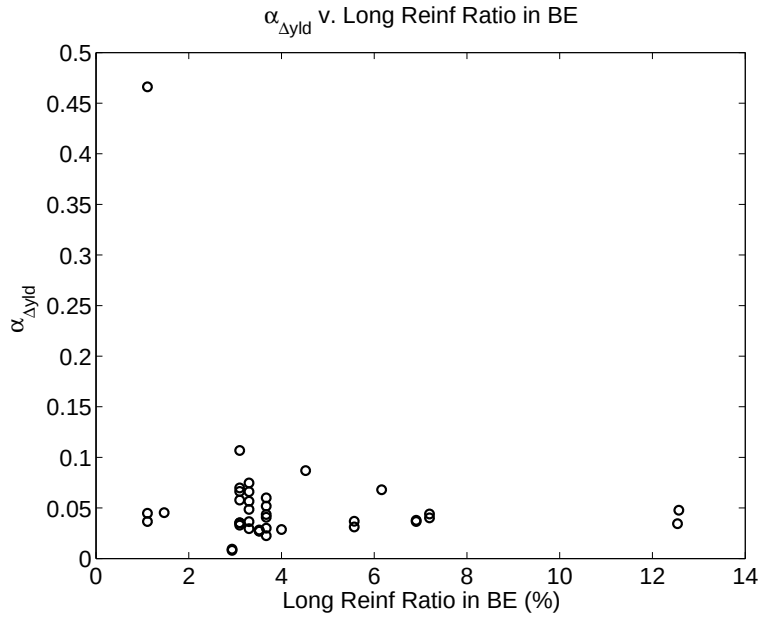

Figure H.4: Alpha Calibrated to Yield v. Longitudinal Reinforcement Ratio

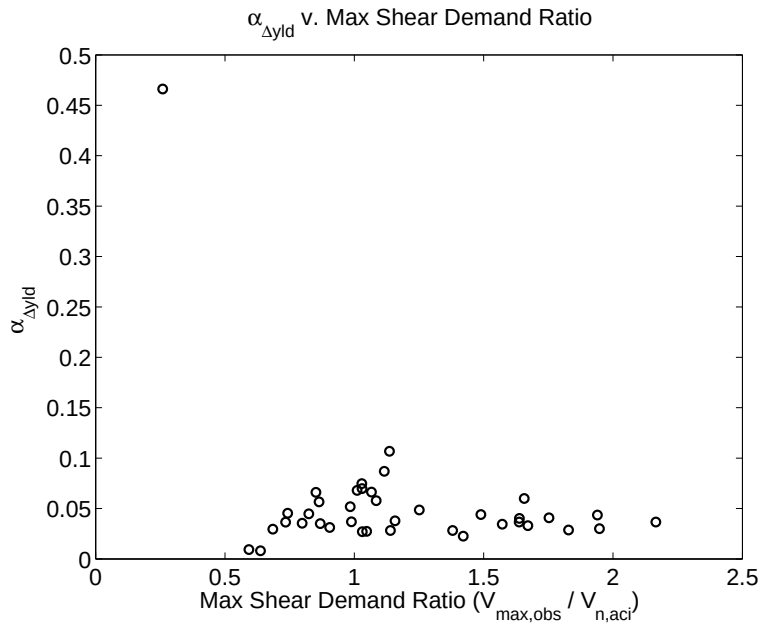

Figure H.5: Alpha Calibrated to Yield v. Max Shear Demand Ratio

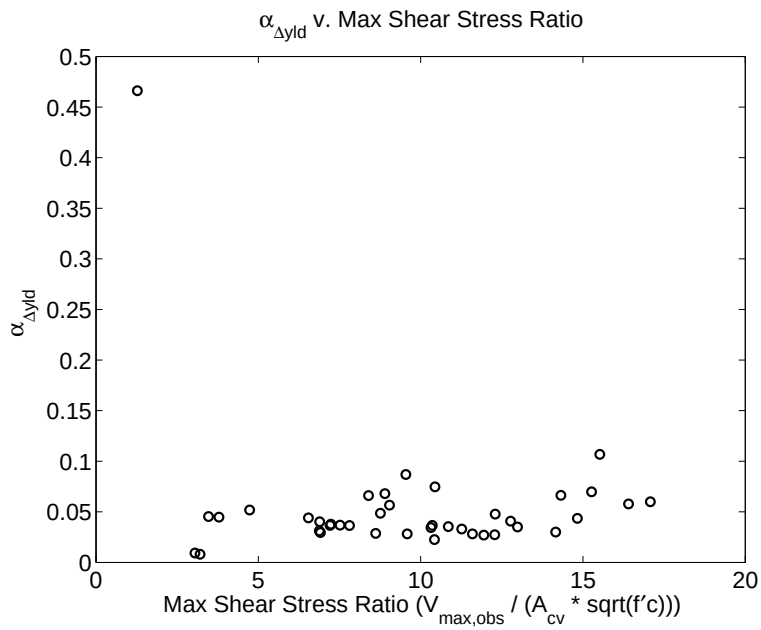

Figure H.6: Alpha Calibrated to Yield v. Max Shear Stress Ratio

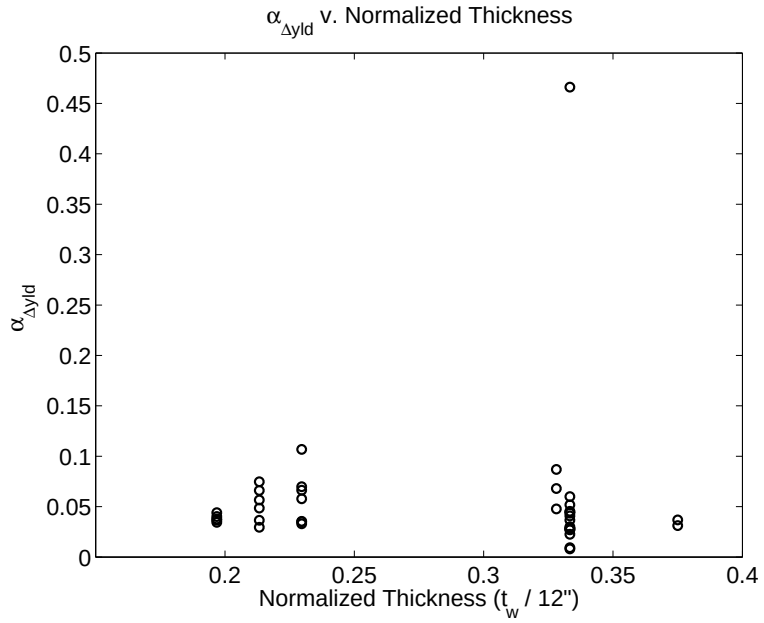

Figure H.7: Alpha Calibrated to Yield v. Aspect Ratio

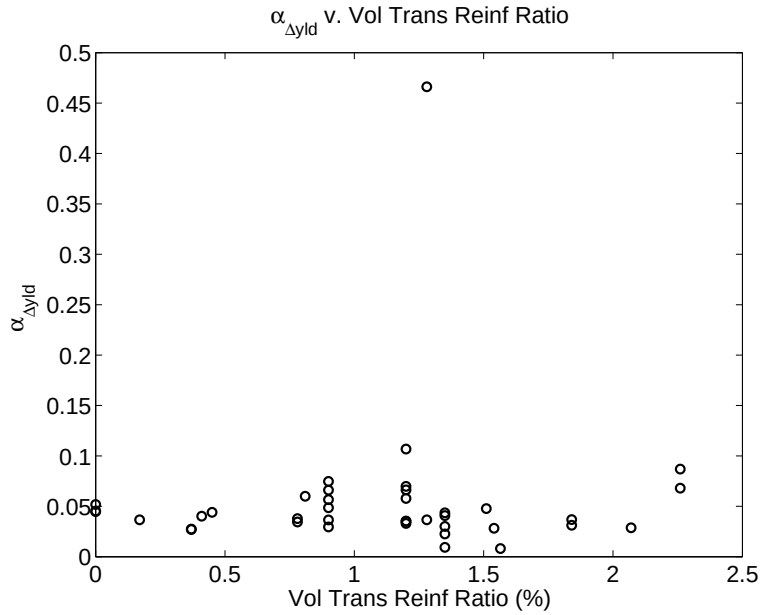

Figure H.8: Alpha Calibrated to Yield v. Volumetric Transverse Reinforcement Ratio

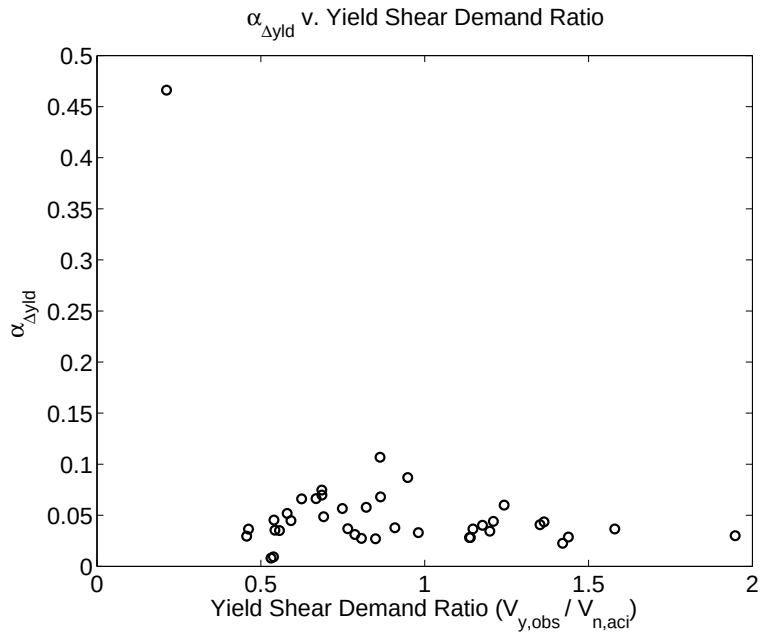

Figure H.9: Alpha Calibrated to Yield v. Shear Demand Ratio at Yield

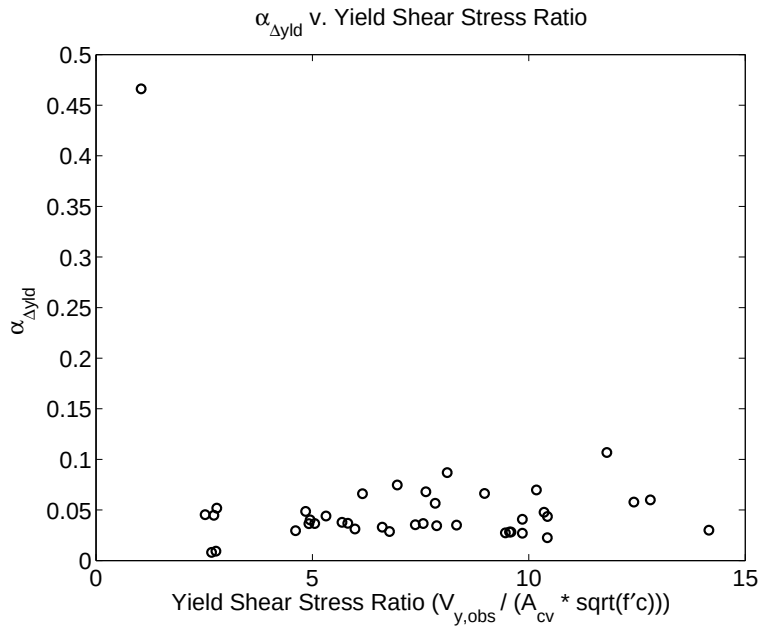

Figure H.10: Alpha Calibrated to Yield v. Shear Stress Ratio at Yield

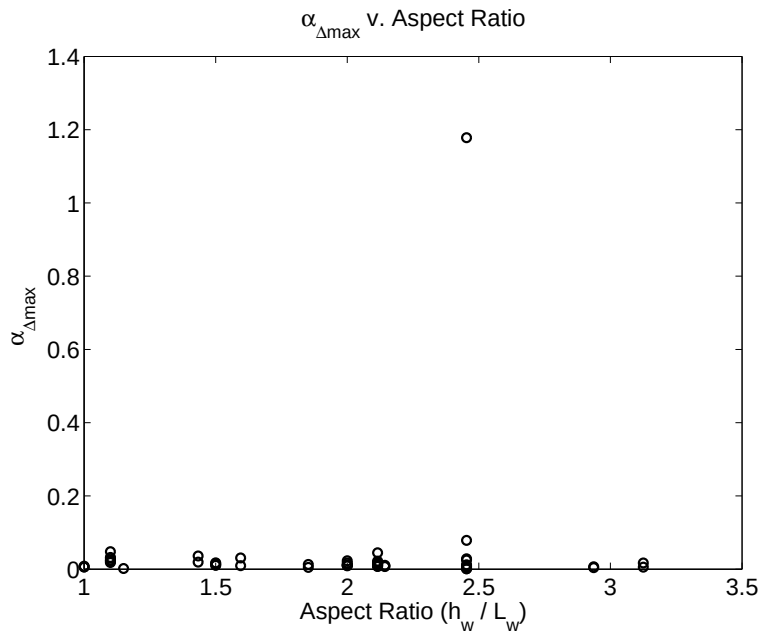

Figure H.11: Alpha Calibrated to Max Displacement v. Aspect Ratio

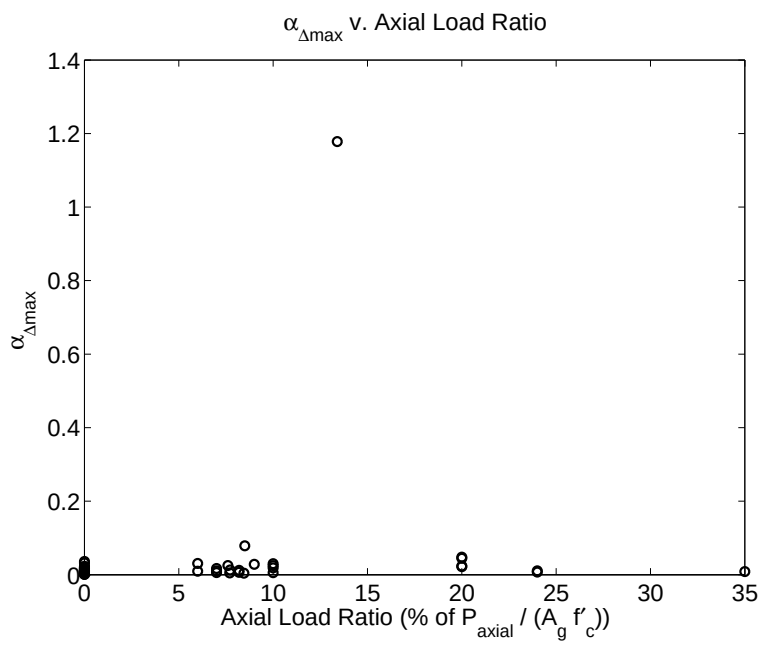

Figure H.12: Alpha Calibrated to Max Displacement v. Axial Load Ratio

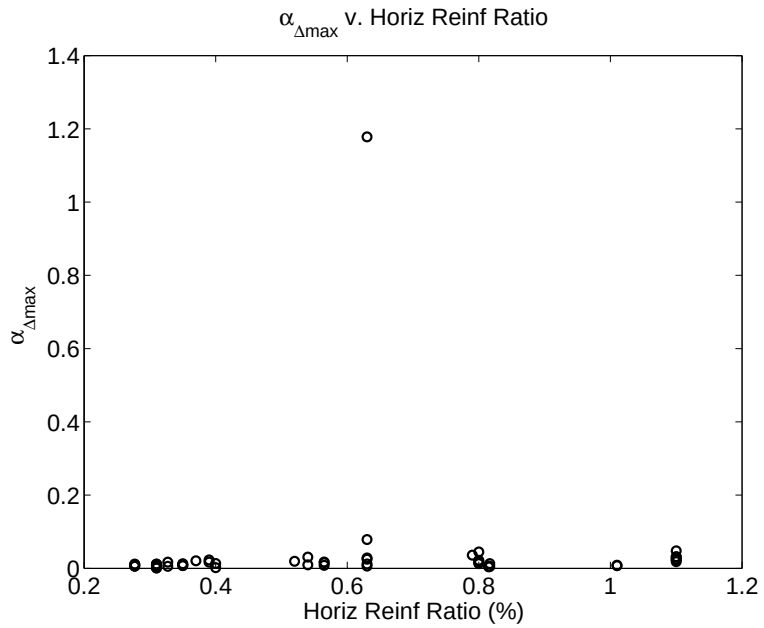

Figure H.13: Alpha Calibrated to Max Displacement v. Horizontal Reinforcement Ratio

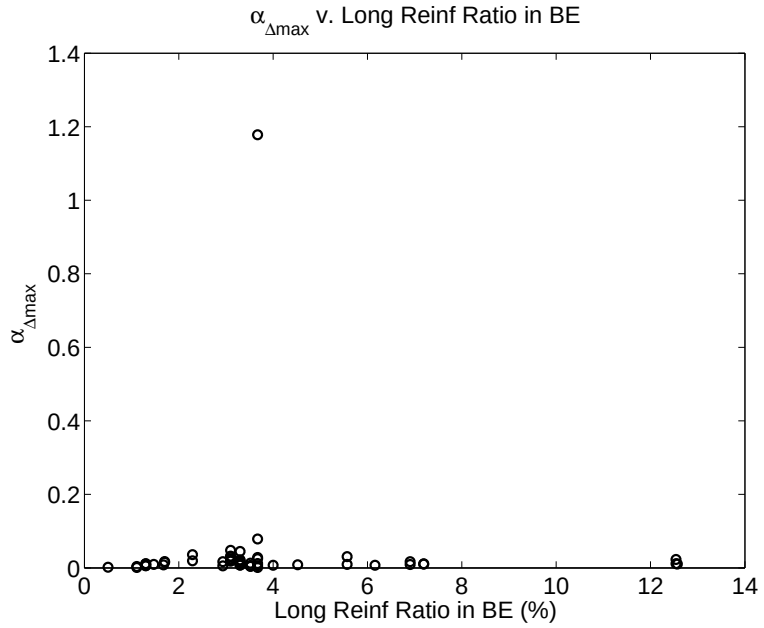

Figure H.14: Alpha Calibrated to Max Displacement v. Longitudinal Reinforcement Ratio

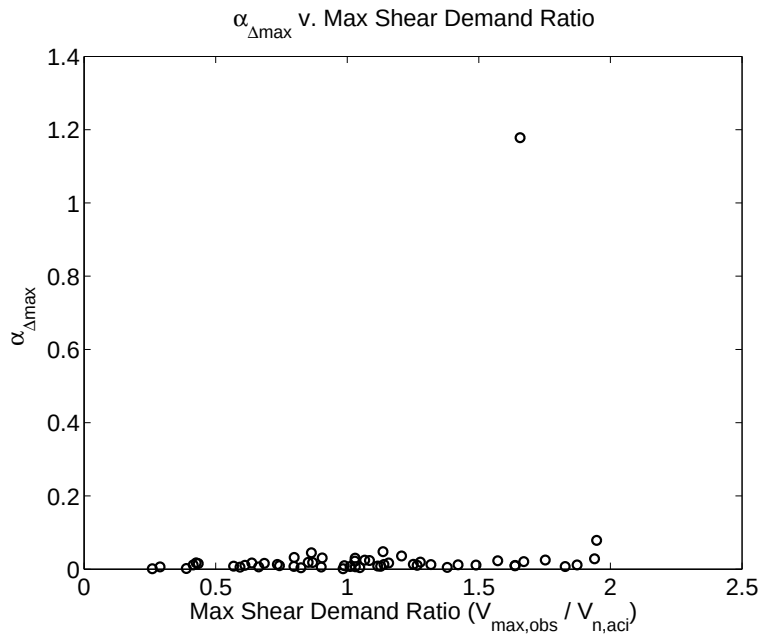

Figure H.15: Alpha Calibrated to Max Displacement v. Max Shear Demand Ratio

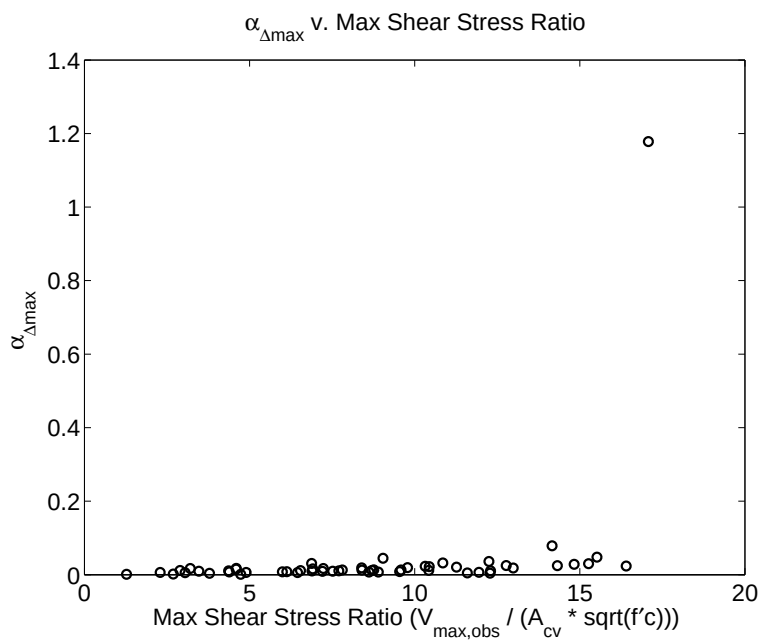

Figure H.16: Alpha Calibrated to Max Displacement v. Max Shear Stress Ratio

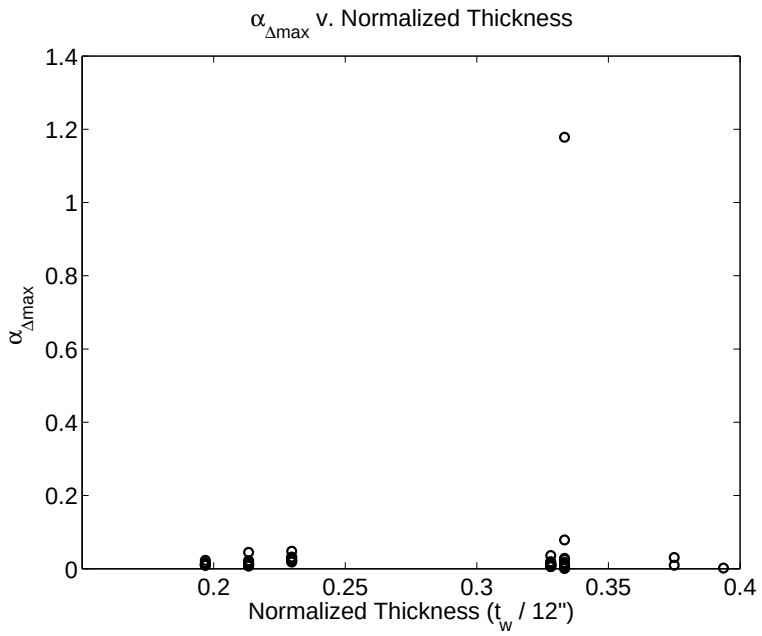

Figure H.17: Alpha Calibrated to Max Displacement v. Aspect Ratio

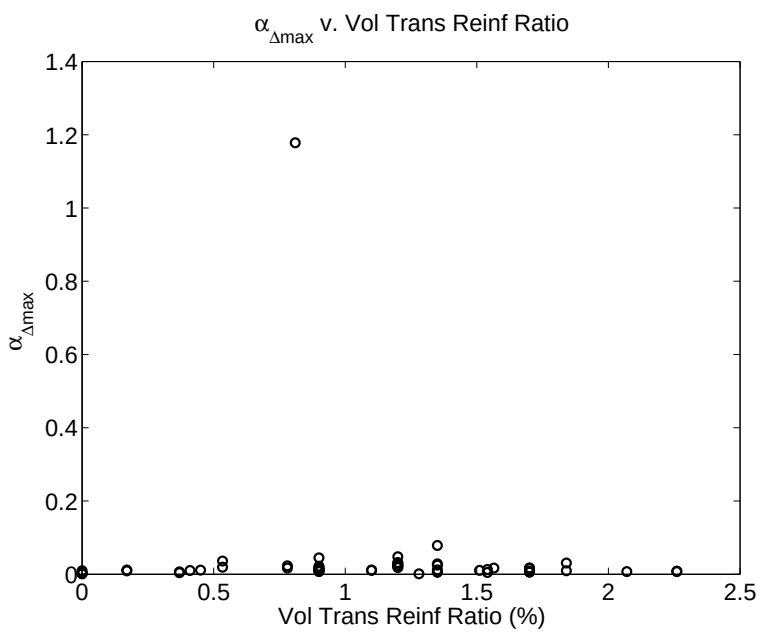

Figure H.18: Alpha Calibrated to Max Displacement v. Volumetric Transverse Reinforcement Ratio

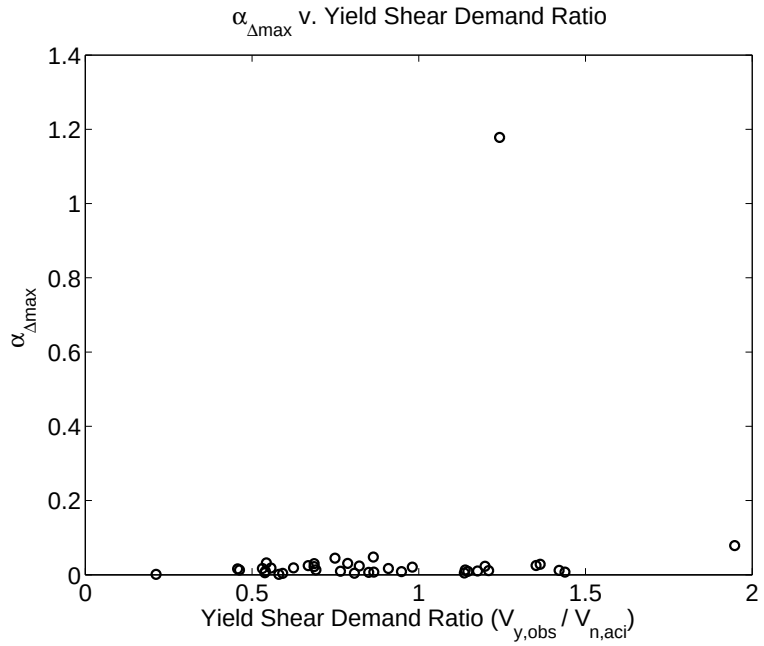

Figure H.19: Alpha Calibrated to Max Displacement v. Shear Demand Ratio at Yield

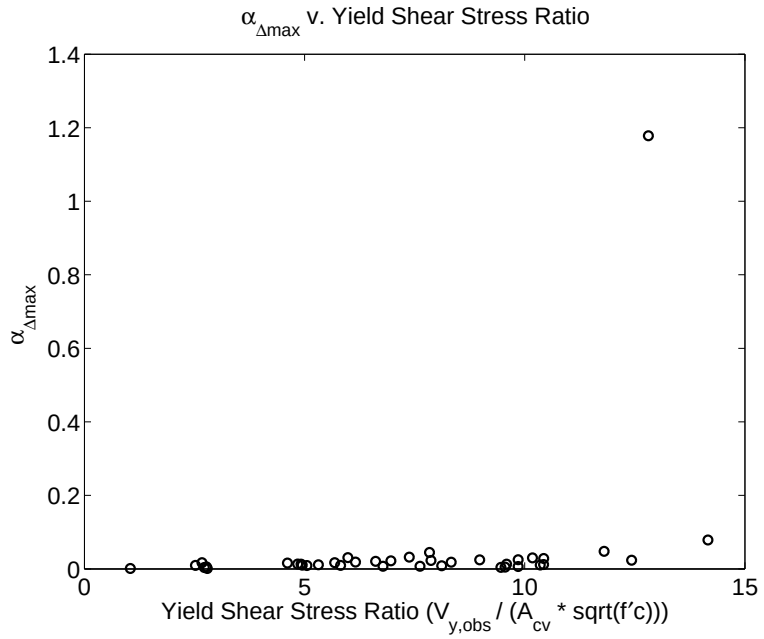

Figure H.20: Alpha Calibrated to Max Displacement v. Shear Stress Ratio at Yield

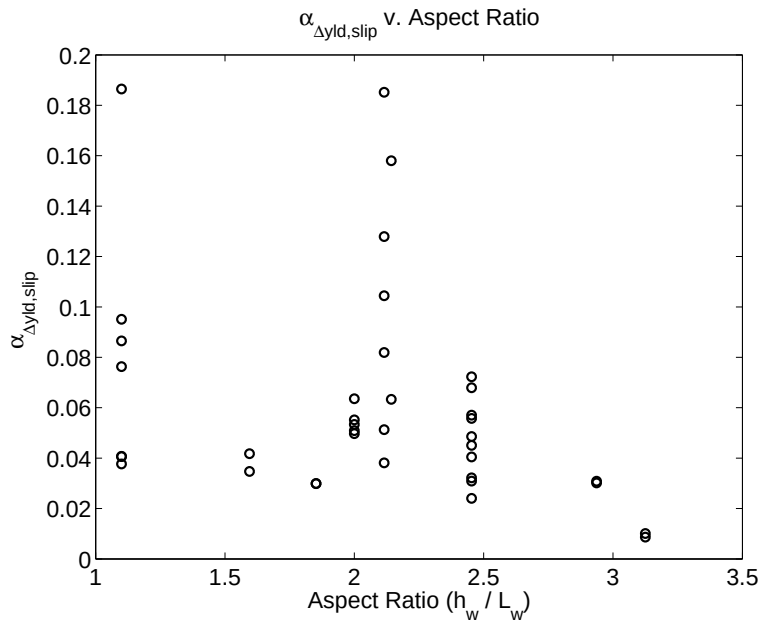

Figure H.21: Alpha Calibrated to Yield with Bar Slip v. Aspect Ratio

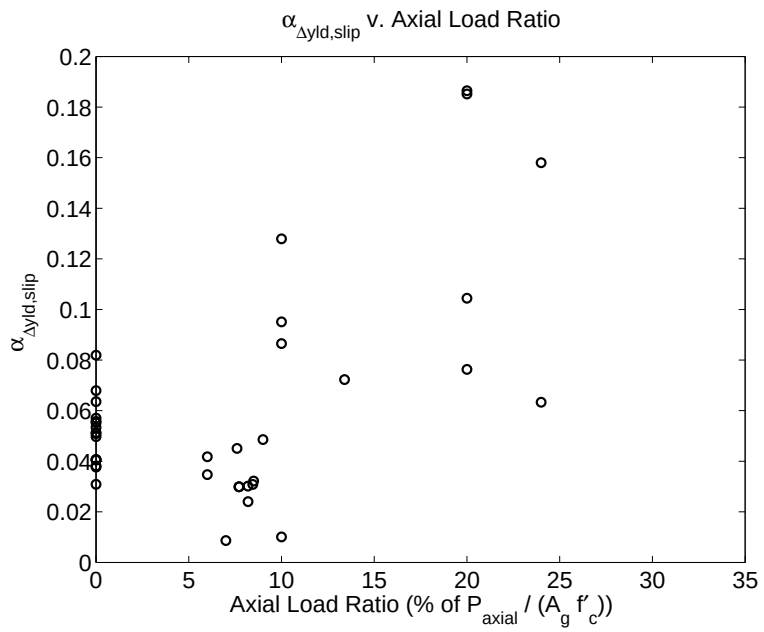

Figure H.22: Alpha Calibrated to Yield with Bar Slip v. Axial Load Ratio

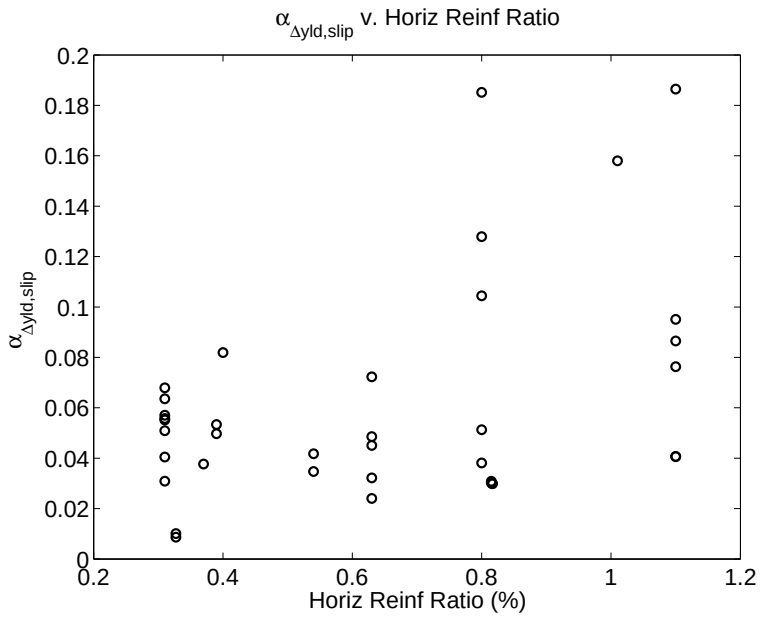

Figure H.23: Alpha Calibrated to Yield with Bar Slip v. Horizontal Reinforcement Ratio

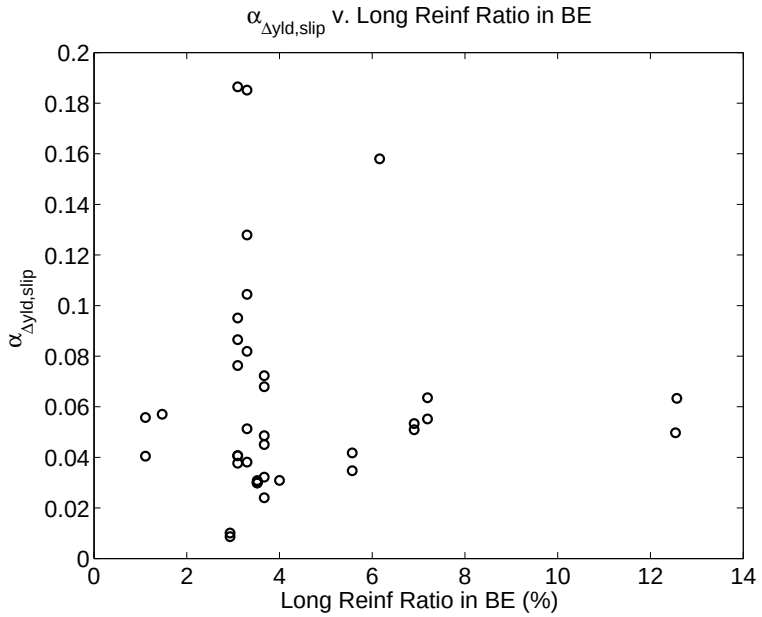

Figure H.24: Alpha Calibrated to Yield with Bar Slip v. Longitudinal Reinforcement Ratio

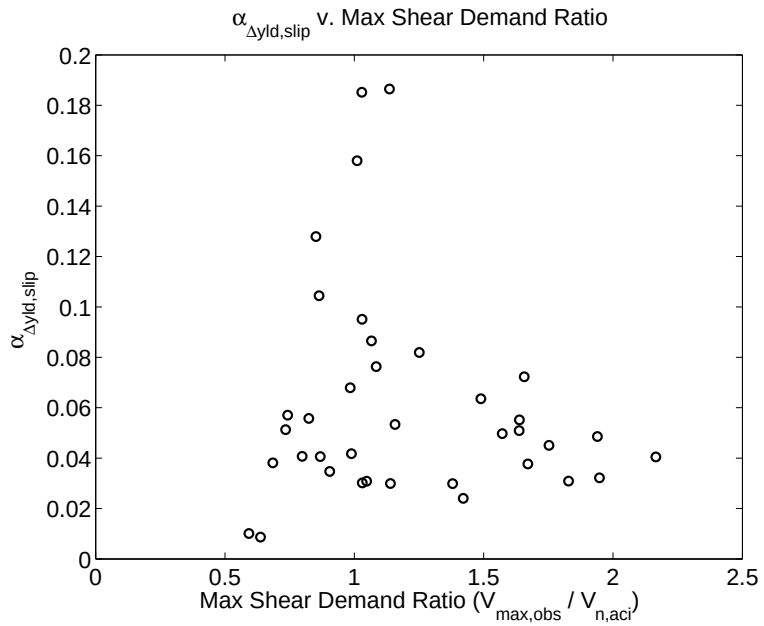

Figure H.25: Alpha Calibrated to Yield with Bar Slip v. Max Shear Demand Ratio

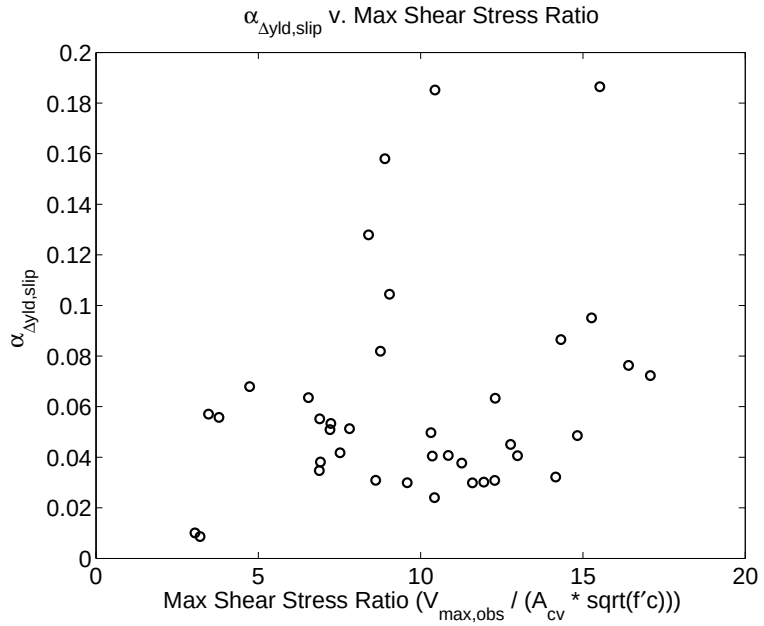

Figure H.26: Alpha Calibrated to Yield with Bar Slip v. Max Shear Stress Ratio

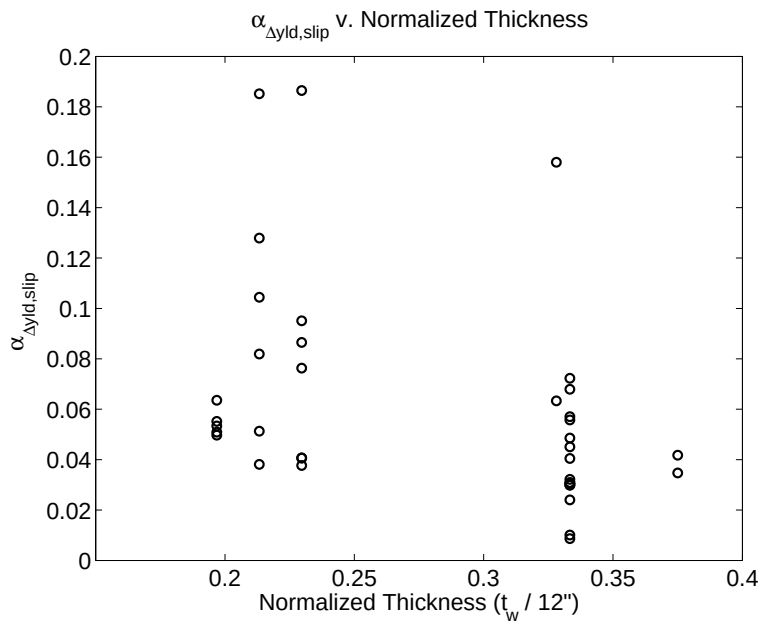

Figure H.27: Alpha Calibrated to Yield with Bar Slip v. Aspect Ratio

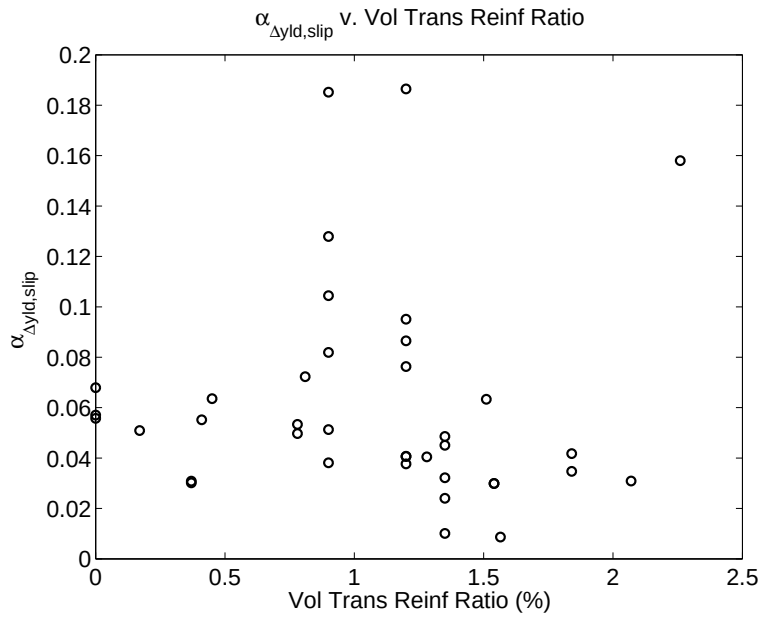

Figure H.28: Alpha Calibrated to Yield with Bar Slip v. Volumetric Transverse Reinforcement Ratio

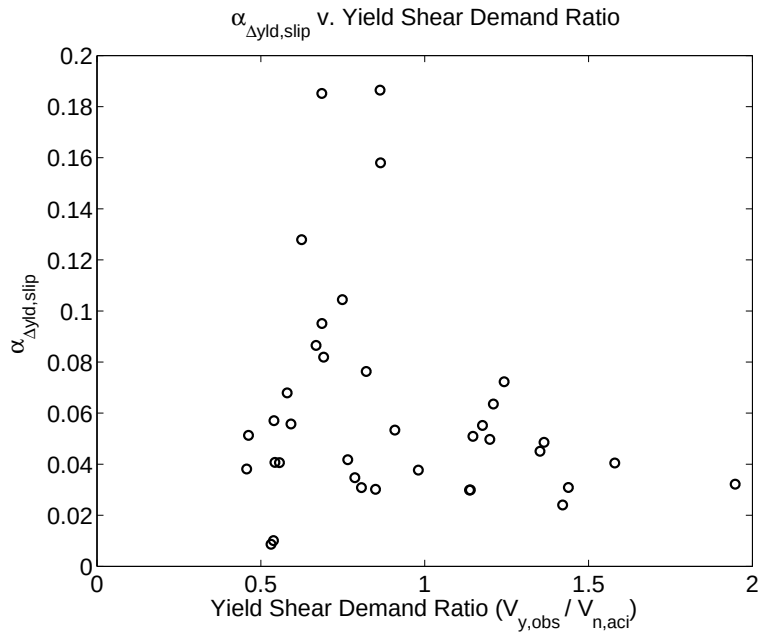

Figure H.29: Alpha Calibrated to Yield with Bar Slip v. Shear Demand Ratio at Yield

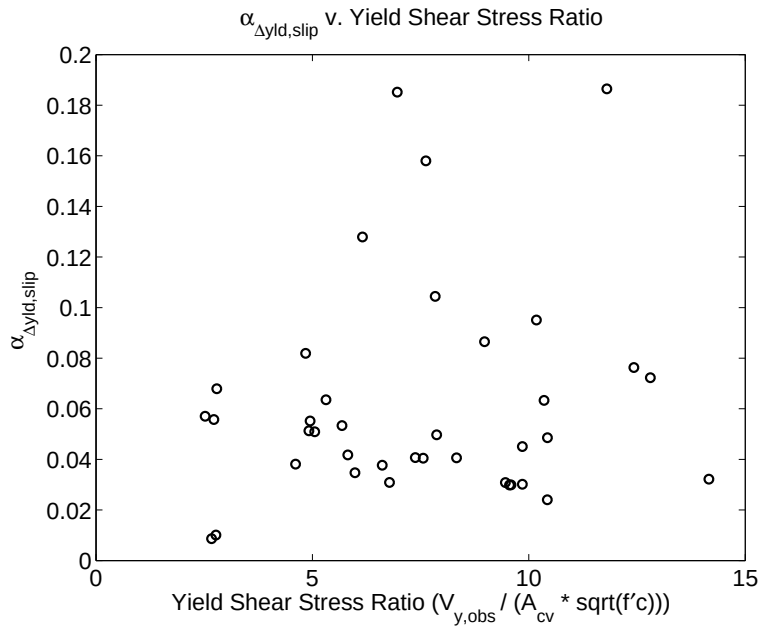

Figure H.30: Alpha Calibrated to Yield with Bar Slip v. Shear Stress Ratio at Yield

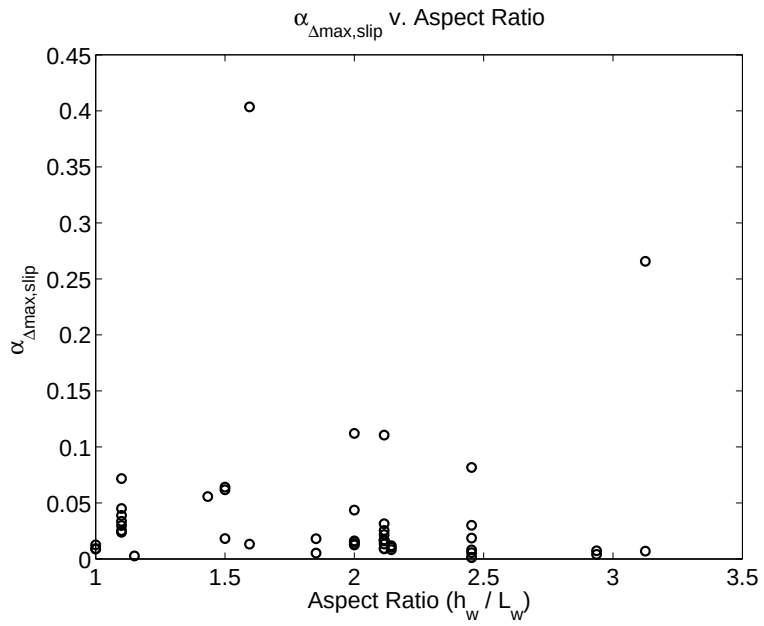

Figure H.31: Alpha Calibrated to Max Displacement with Bar Slip v. Aspect Ratio

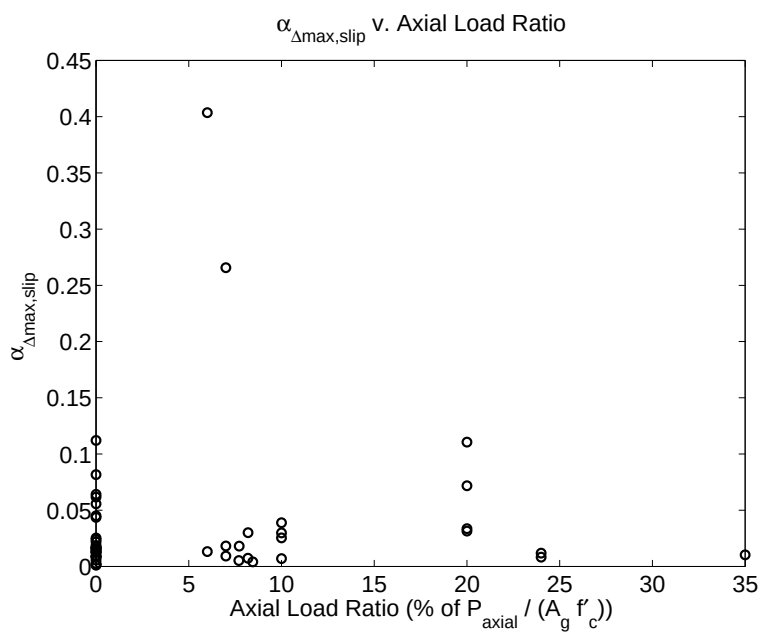

Figure H.32: Alpha Calibrated to Max Displacement with Bar Slip v. Axial Load Ratio

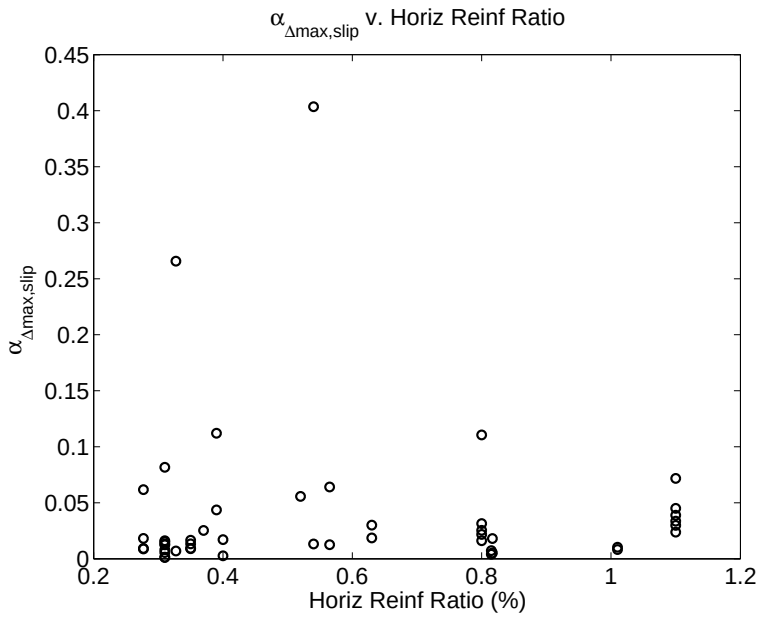

Figure H.33: Alpha Calibrated to Max Displacement with Bar Slip v. Horizontal Reinforcement Ratio

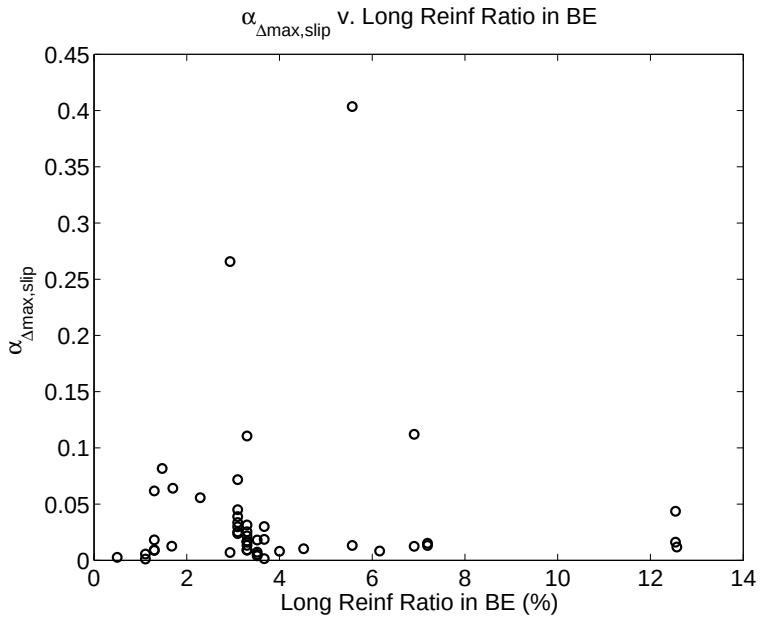

Figure H.34: Alpha Calibrated to Max Displacement with Bar Slip v. Longitudinal Reinforcement Ratio

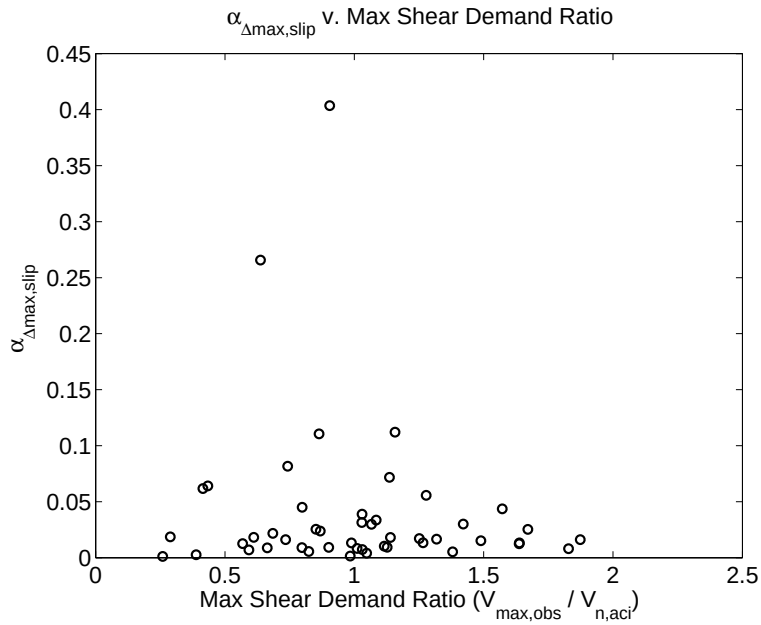

Figure H.35: Alpha Calibrated to Max Displacement with Bar Slip v. Max Shear Demand Ratio

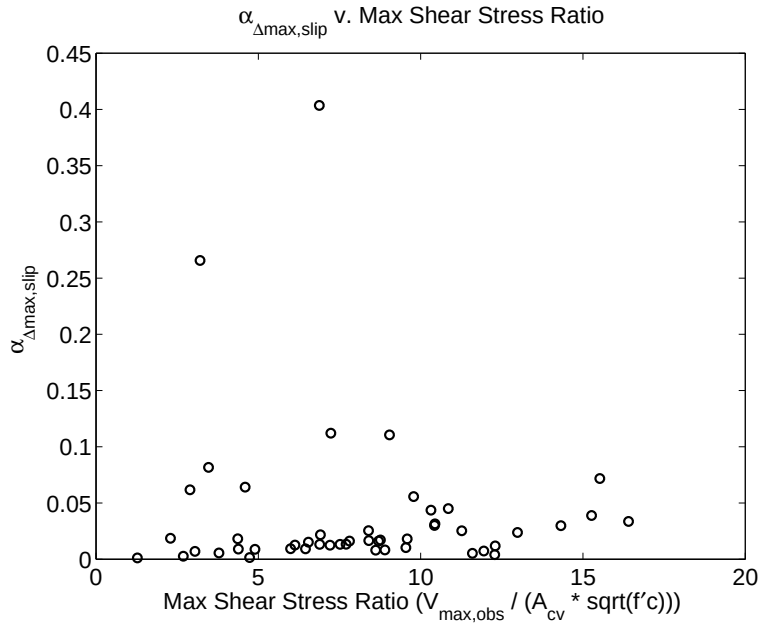

Figure H.36: Alpha Calibrated to Max Displacement with Bar Slip v. Max Shear Stress Ratio

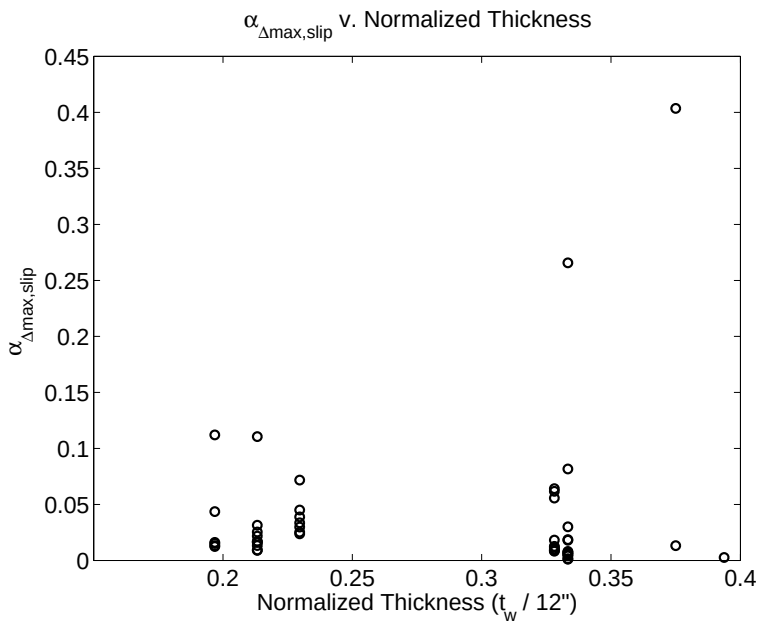

Figure H.37: Alpha Calibrated to Max Displacement with Bar Slip v. Aspect Ratio

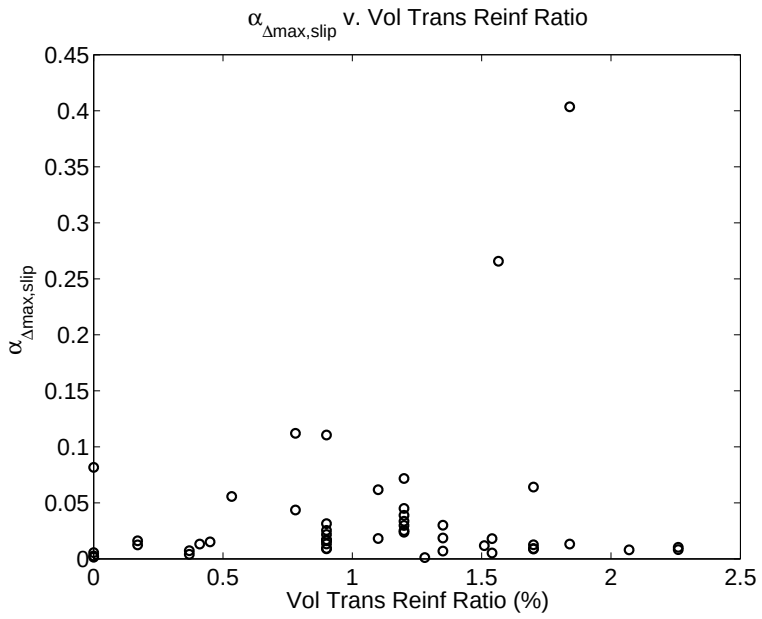

Figure H.38: Alpha Calibrated to Max Displacement with Bar Slip v. Volumetric Transverse Reinforcement Ratio

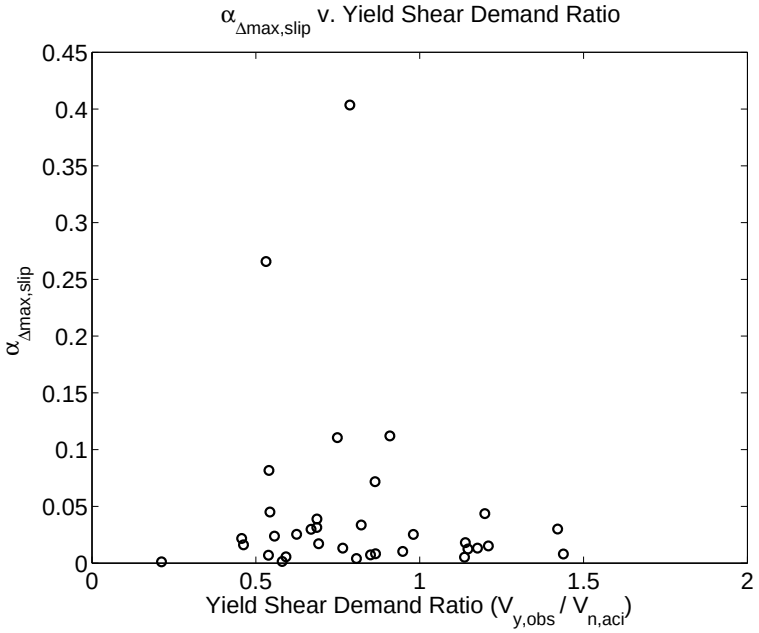

Figure H.39: Alpha Calibrated to Max Displacement with Bar Slip v. Shear Demand Ratio at Yield

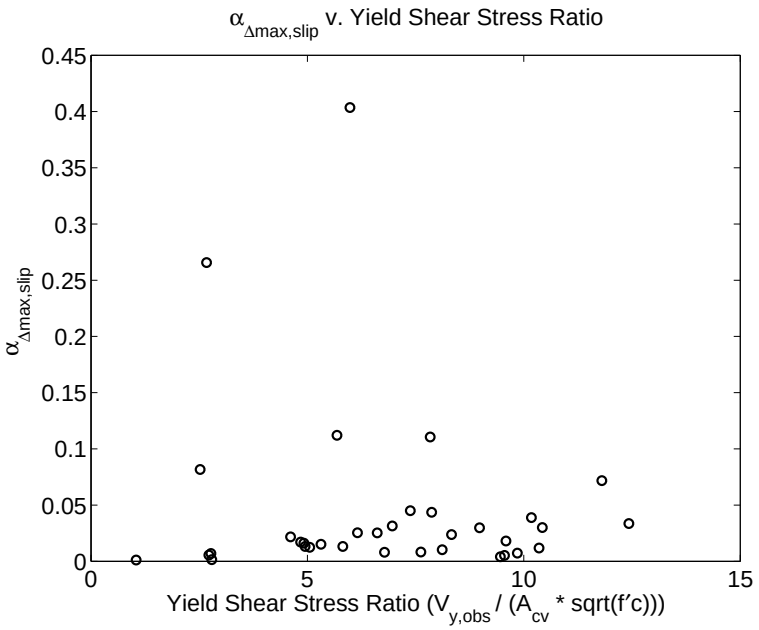

Figure H.40: Alpha Calibrated to Max Displacement with Bar Slip v. Shear Stress Ratio at Yield

Appendix I

BAR-SLIP PUSH OVER ANALYSIS FIGURES

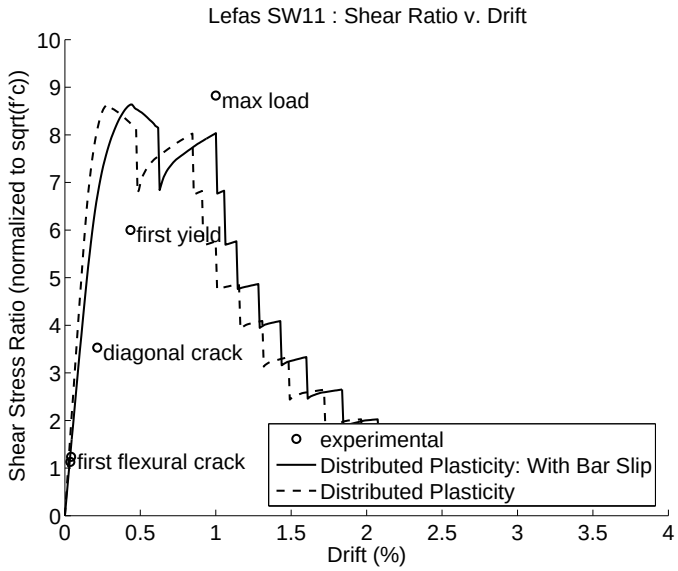

Figure I.1: Pushover of Beam-Column Element with Bar-Slip – Lefas SW11

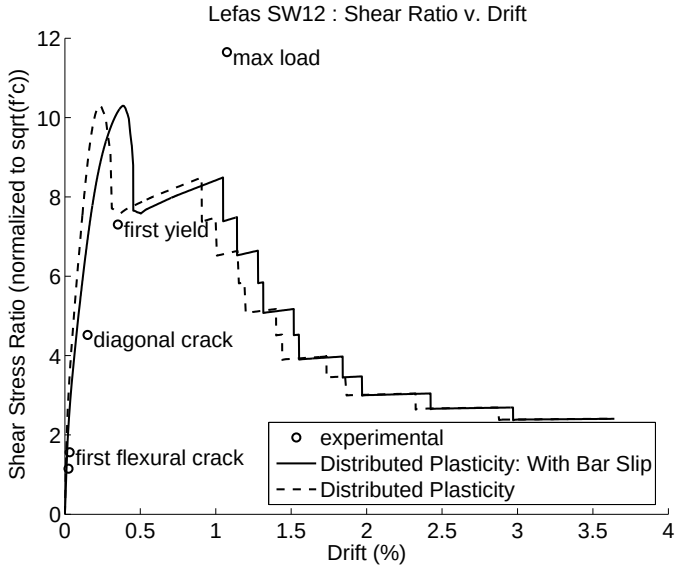

Figure I.2: Pushover of Beam-Column Element with Bar-Slip – Lefas SW12

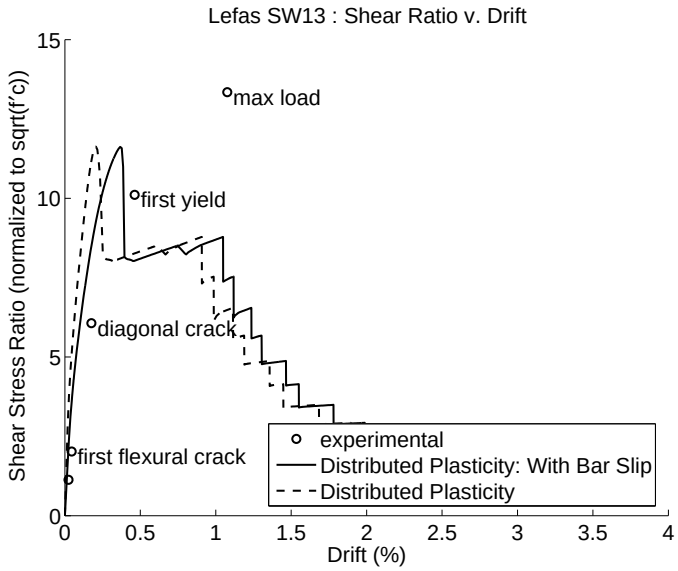

Figure I.3: Pushover of Beam-Column Element with Bar-Slip – Lefas SW13

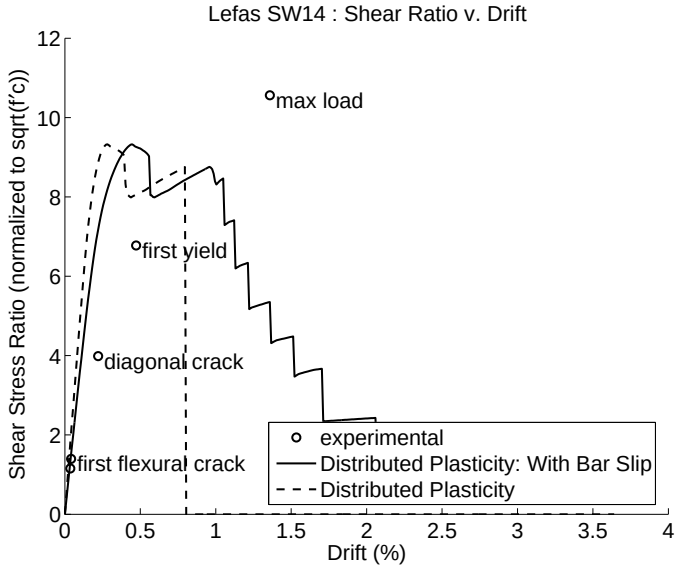

Figure I.4: Pushover of Beam-Column Element with Bar-Slip – Lefas SW14

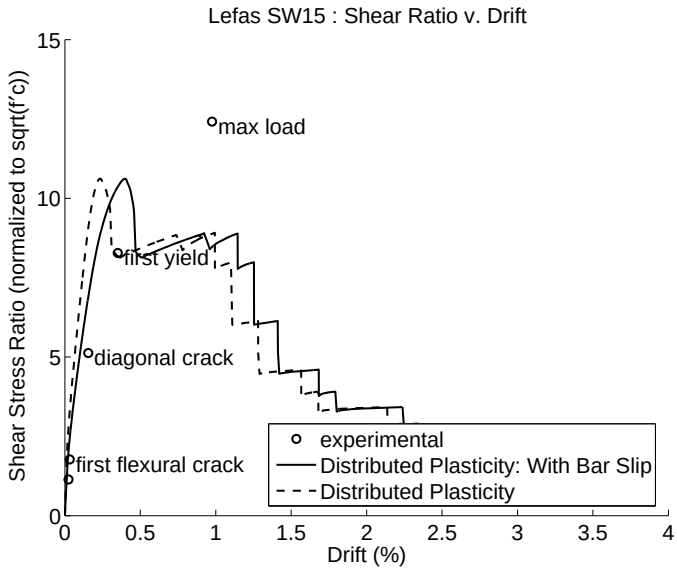

Figure I.5: Pushover of Beam-Column Element with Bar-Slip – Lefas SW15

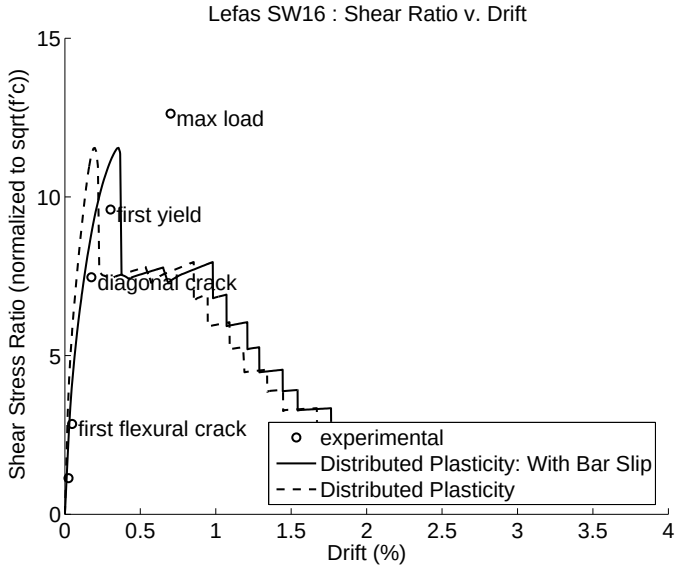

Figure I.6: Pushover of Beam-Column Element with Bar-Slip – Lefas SW16

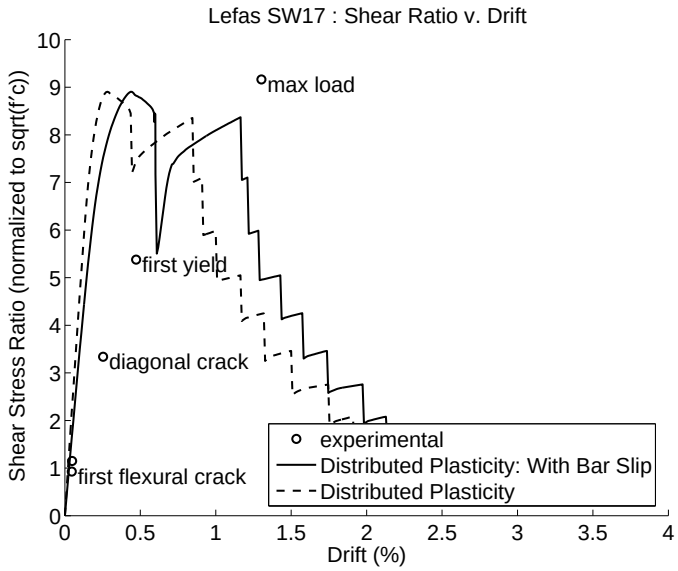

Figure I.7: Pushover of Beam-Column Element with Bar-Slip – Lefas SW17

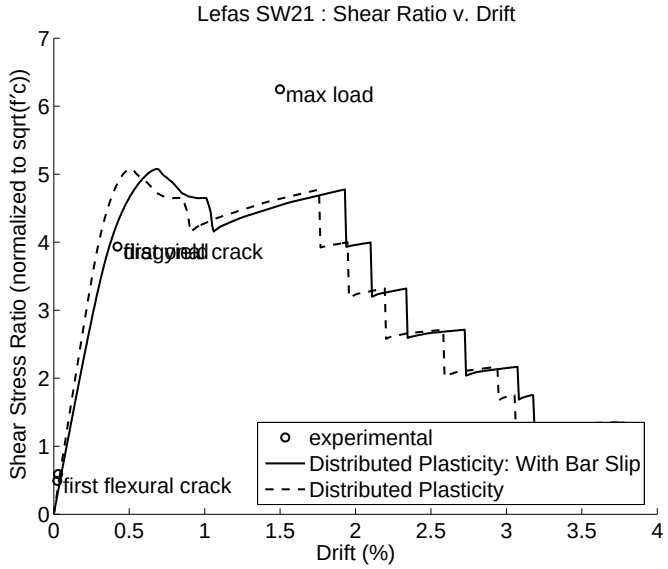

Figure I.8: Pushover of Beam-Column Element with Bar-Slip – Lefas SW21

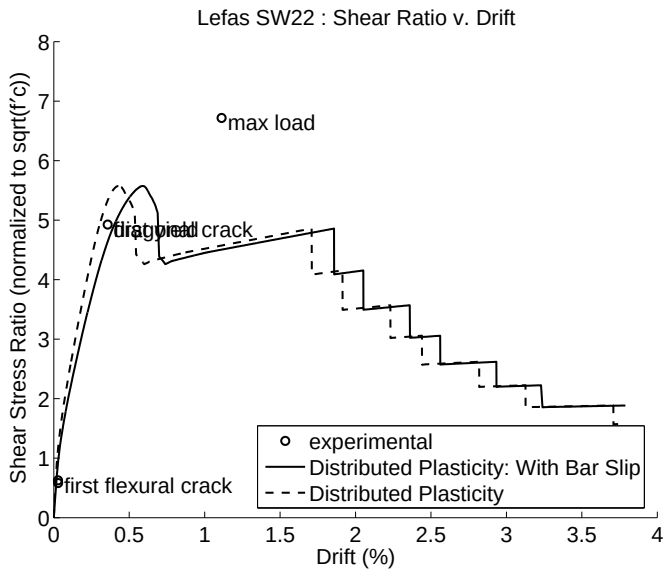

Figure I.9: Pushover of Beam-Column Element with Bar-Slip – Lefas SW22

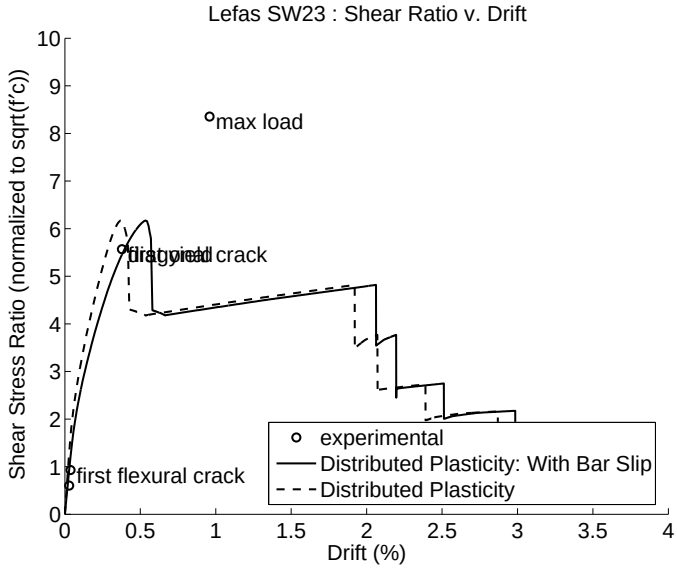

Figure I.10: Pushover of Beam-Column Element with Bar-Slip – Lefas SW23

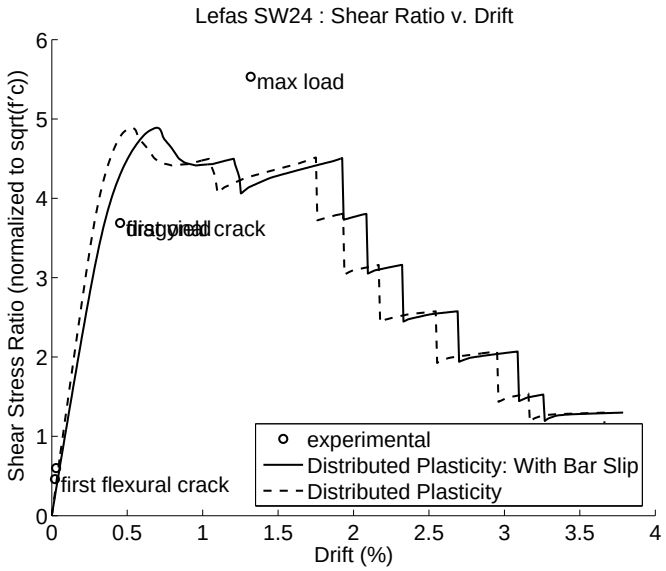

Figure I.11: Pushover of Beam-Column Element with Bar-Slip – Lefas SW24

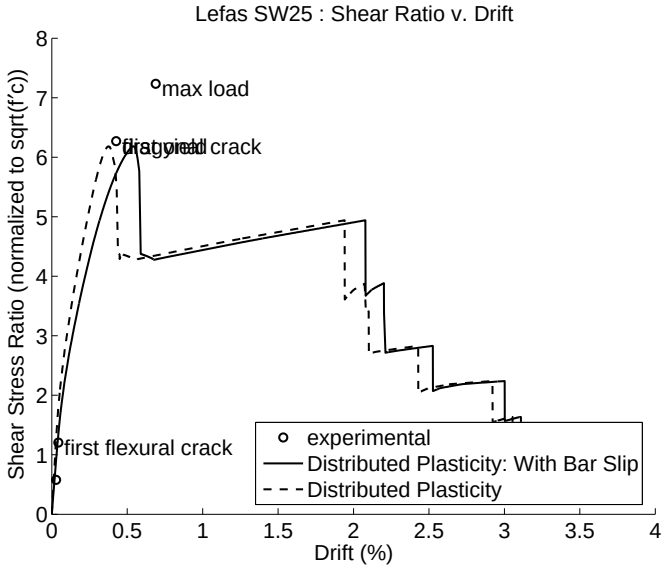

Figure I.12: Pushover of Beam-Column Element with Bar-Slip – Lefas SW25

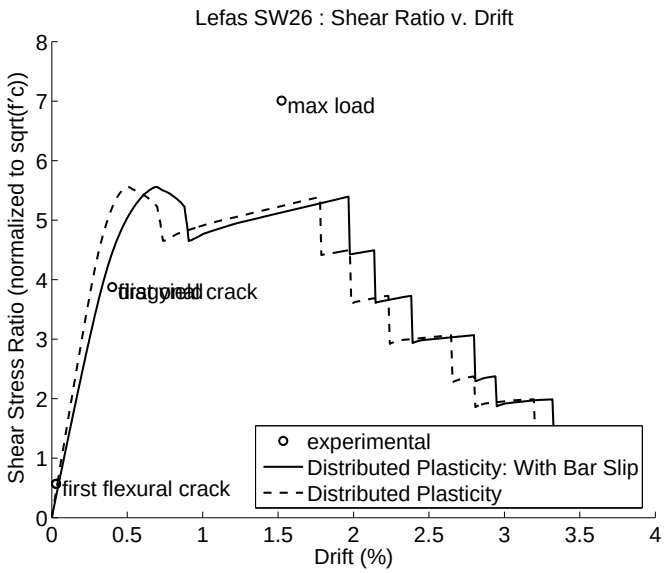

Figure I.13: Pushover of Beam-Column Element with Bar-Slip – Lefas SW26

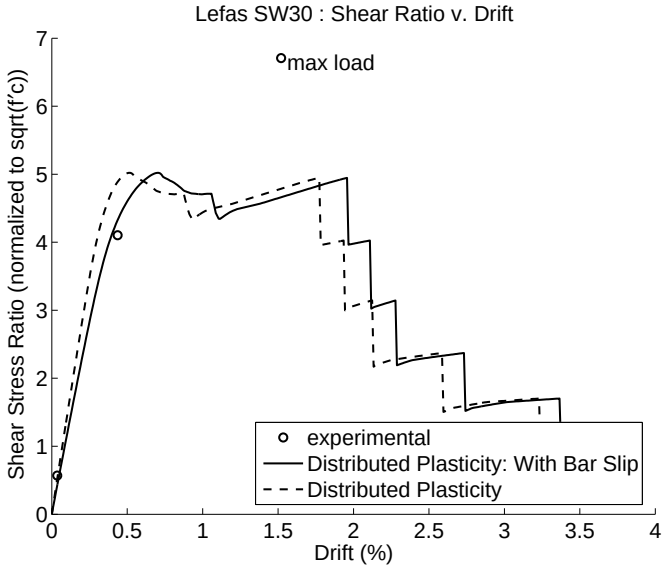

Figure I.14: Pushover of Beam-Column Element with Bar-Slip – Lefas SW30

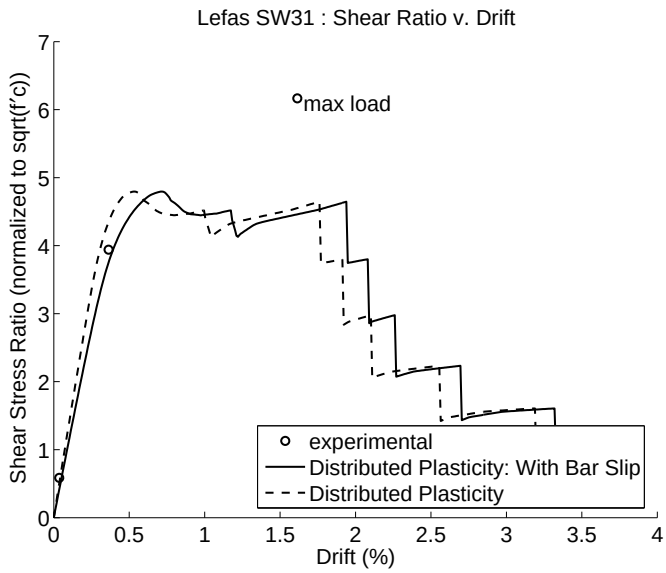

Figure I.15: Pushover of Beam-Column Element with Bar-Slip – Lefas SW31

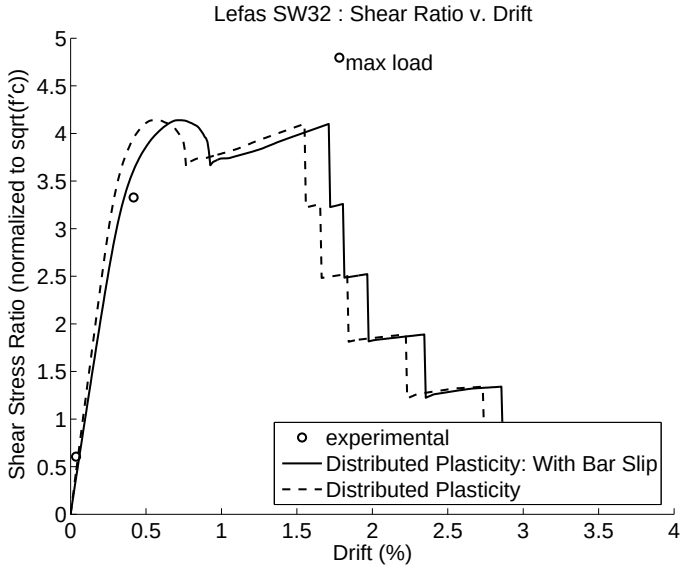

Figure I.16: Pushover of Beam-Column Element with Bar-Slip – Lefas SW32

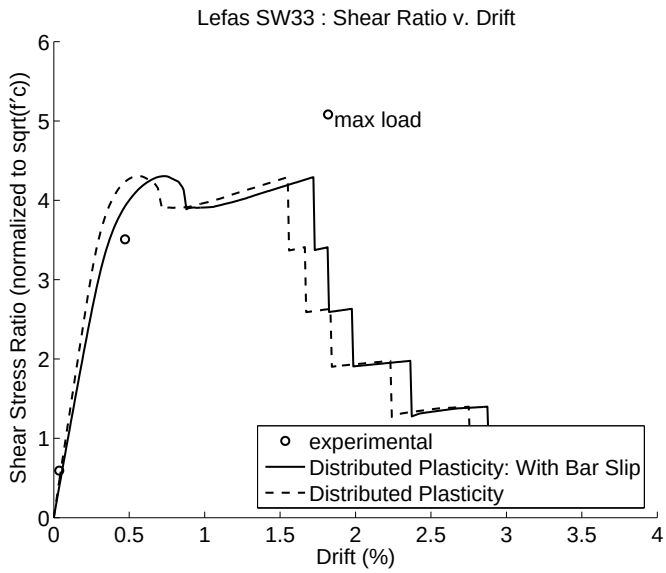

Figure I.17: Pushover of Beam-Column Element with Bar-Slip – Lefas SW33

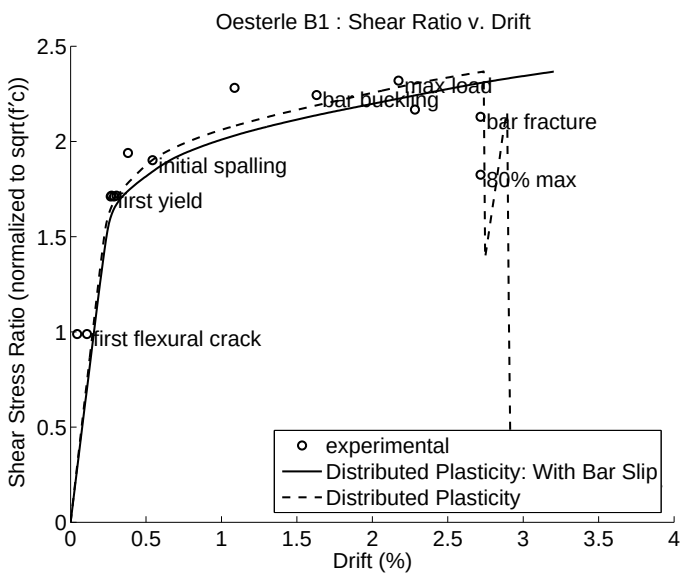

Figure I.18: Pushover of Beam-Column Element with Bar-Slip – Oesterle B1

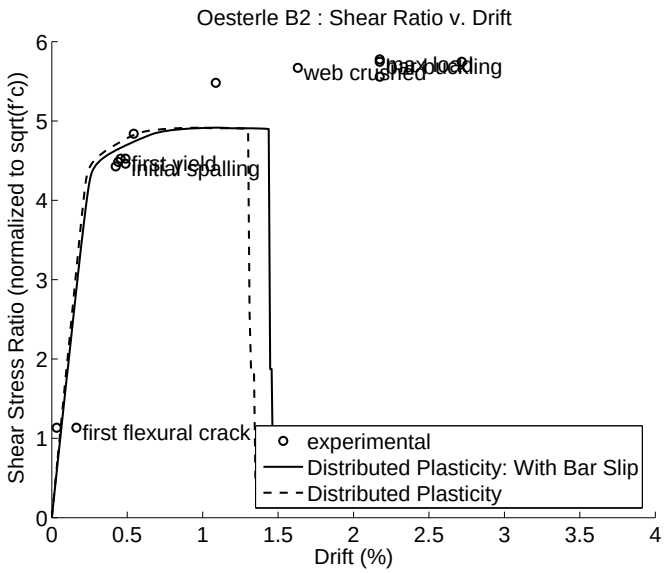

Figure I.19: Pushover of Beam-Column Element with Bar-Slip – Oesterle B2

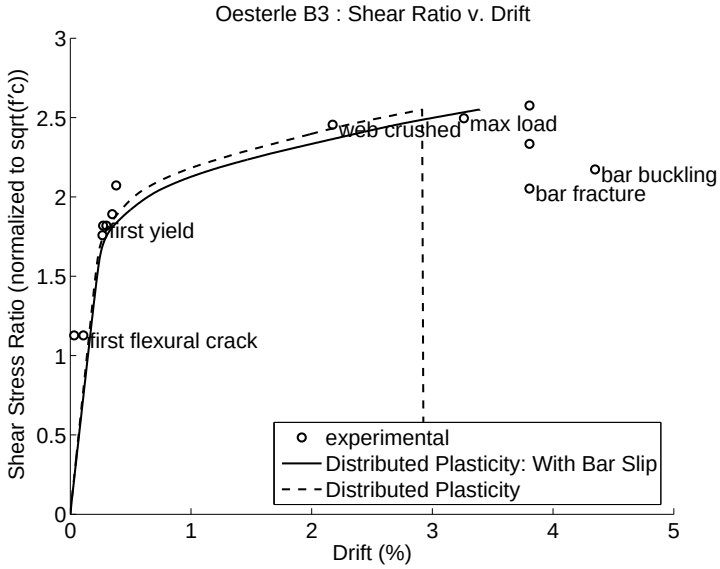

Figure I.20: Pushover of Beam-Column Element with Bar-Slip – Oesterle B3

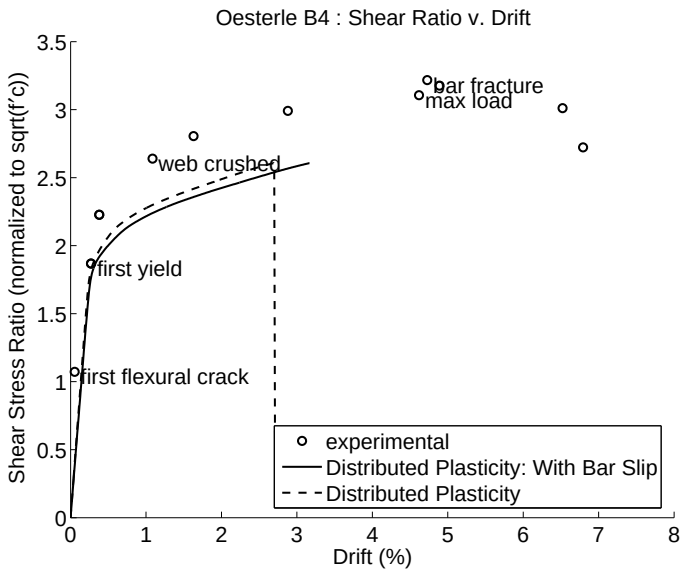

Figure I.21: Pushover of Beam-Column Element with Bar-Slip – Oesterle B4

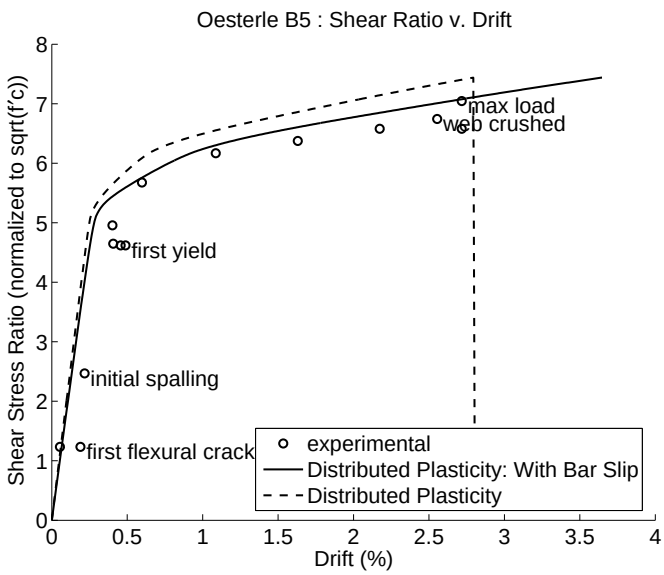

Figure I.22: Pushover of Beam-Column Element with Bar-Slip – Oesterle B5

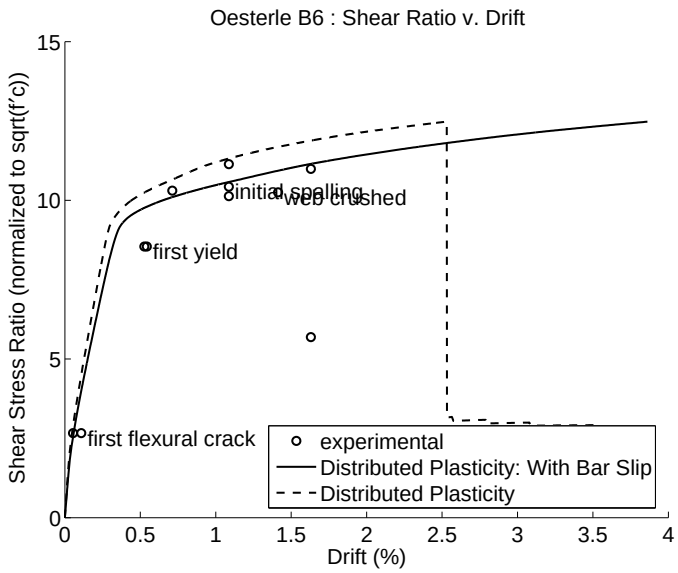

Figure I.23: Pushover of Beam-Column Element with Bar-Slip – Oesterle B6

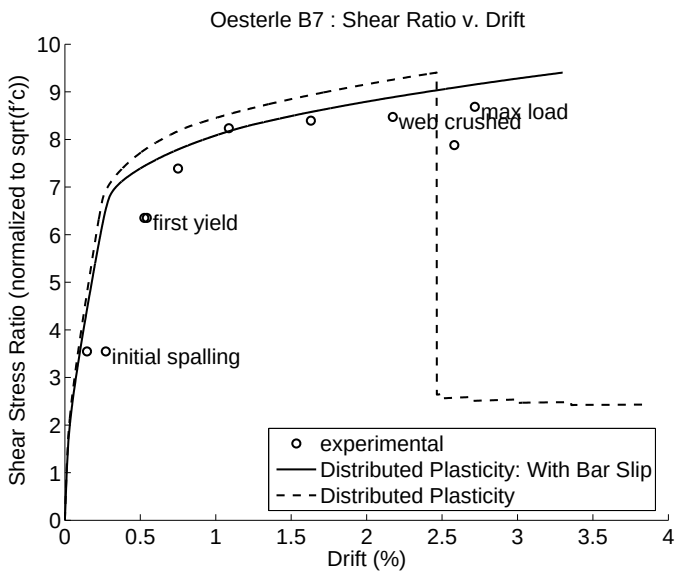

Figure I.24: Pushover of Beam-Column Element with Bar-Slip – Oesterle B7

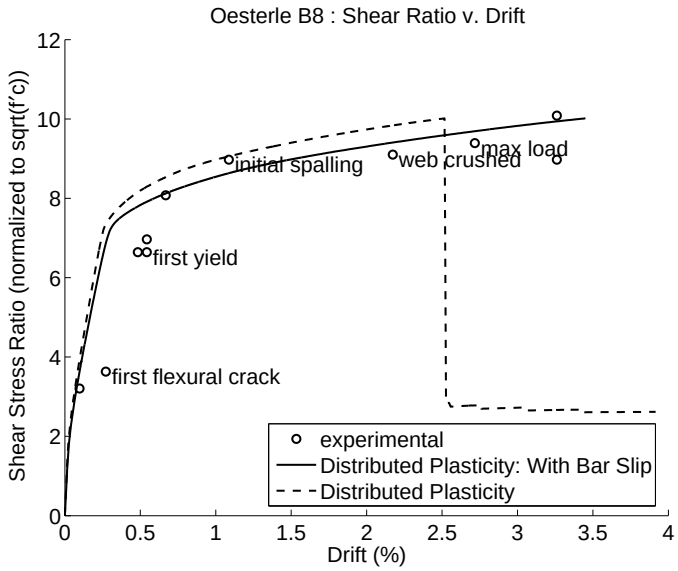

Figure I.25: Pushover of Beam-Column Element with Bar-Slip – Oesterle B8

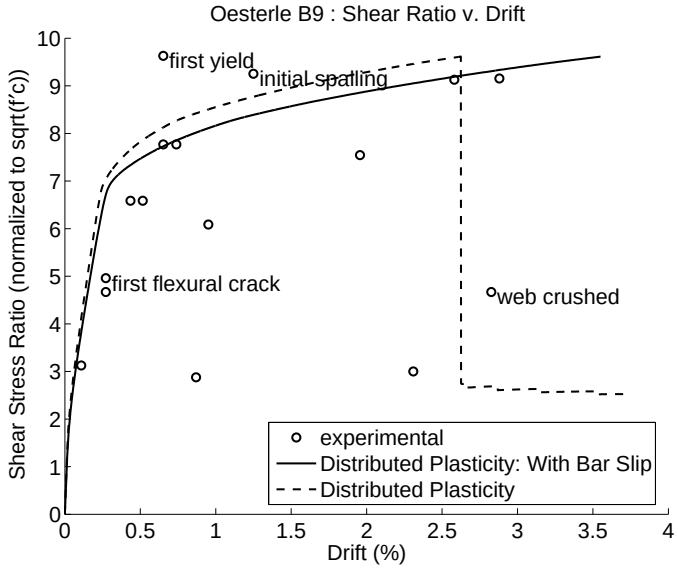

Figure I.26: Pushover of Beam-Column Element with Bar-Slip – Oesterle B9

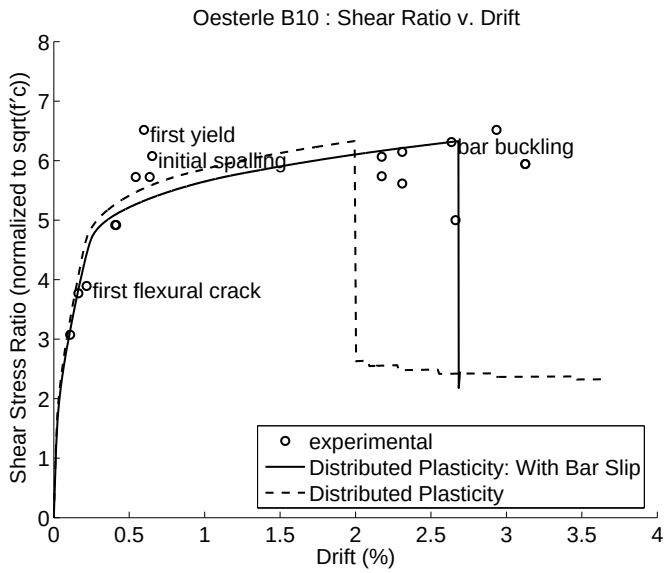

Figure I.27: Pushover of Beam-Column Element with Bar-Slip – Oesterle B10

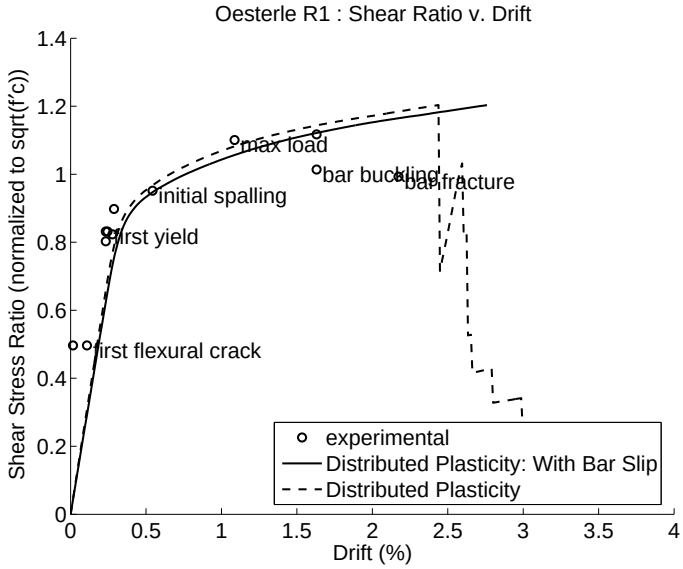

Figure I.28: Pushover of Beam-Column Element with Bar-Slip – Oesterle R1

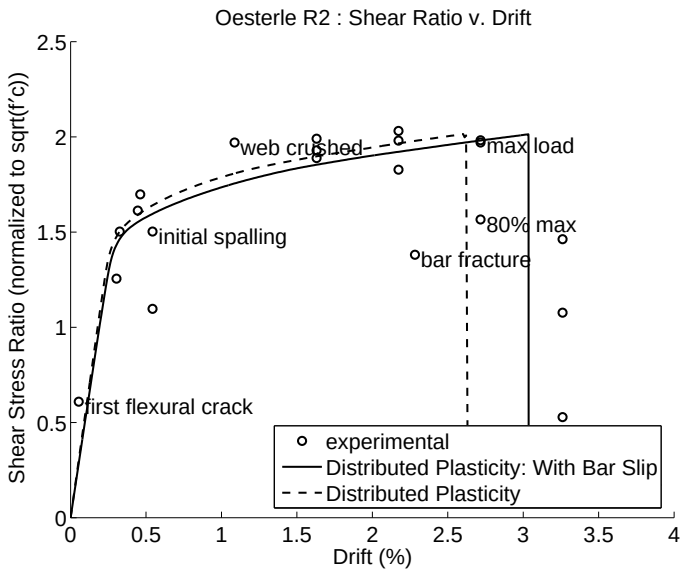

Figure I.29: Pushover of Beam-Column Element with Bar-Slip – Oesterle R2

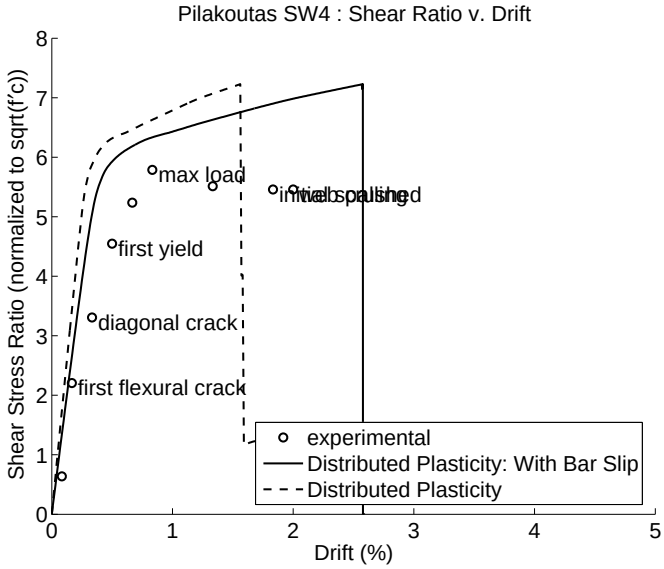

Figure I.30: Pushover of Beam-Column Element with Bar-Slip – Pilakoutas SW4

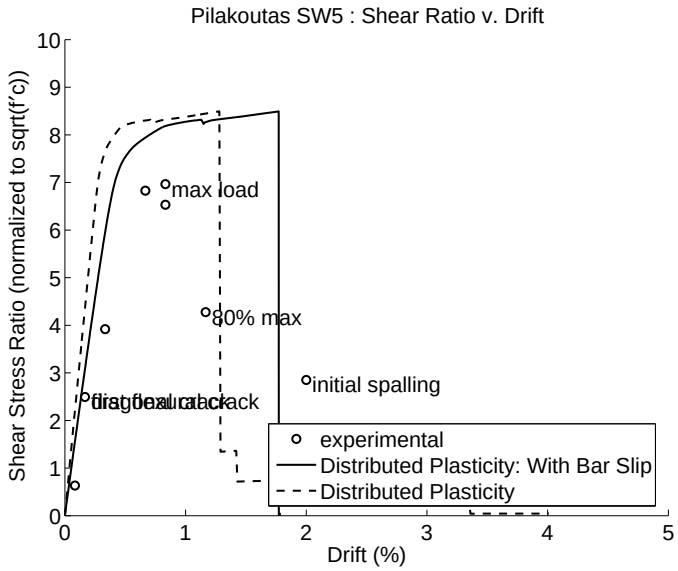

Figure I.31: Pushover of Beam-Column Element with Bar-Slip – Pilakoutas SW5

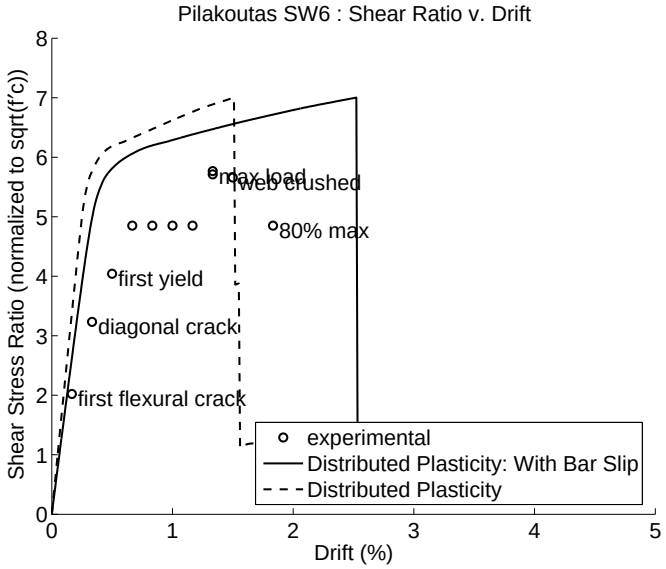

Figure I.32: Pushover of Beam-Column Element with Bar-Slip – Pilakoutas SW6

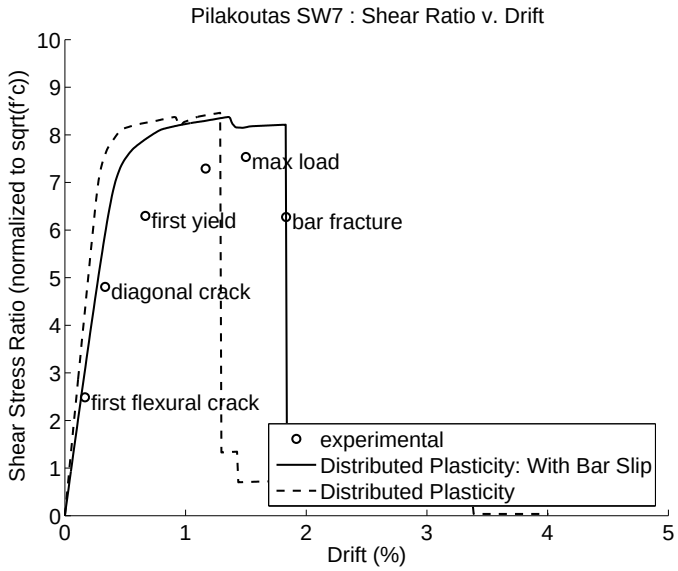

Figure I.33: Pushover of Beam-Column Element with Bar-Slip – Pilakoutas SW7

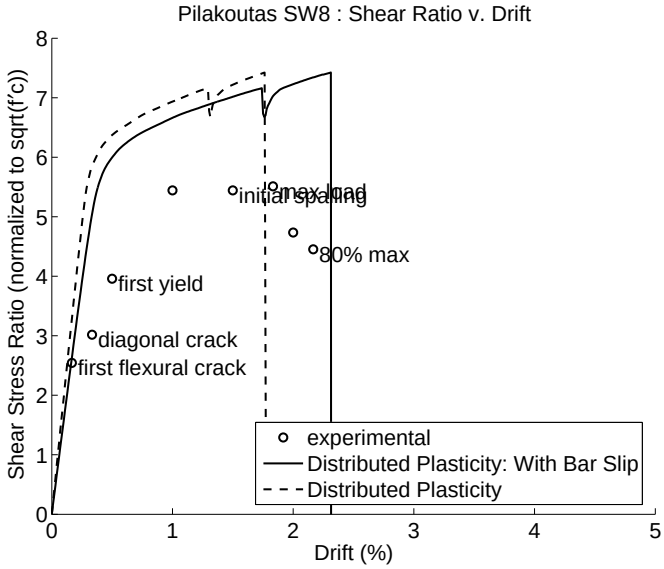

Figure I.34: Pushover of Beam-Column Element with Bar-Slip – Pilakoutas SW8

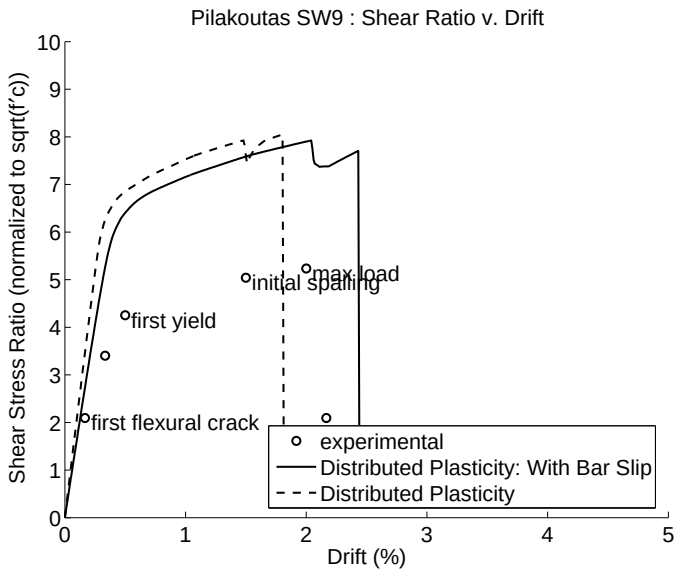

Figure I.35: Pushover of Beam-Column Element with Bar-Slip – Pilakoutas SW9

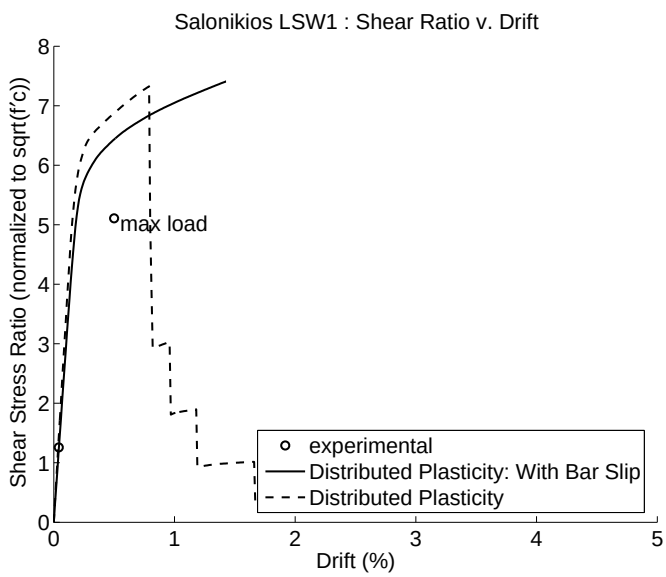

Figure I.36: Pushover of Beam-Column Element with Bar-Slip – Salonikios LSW1

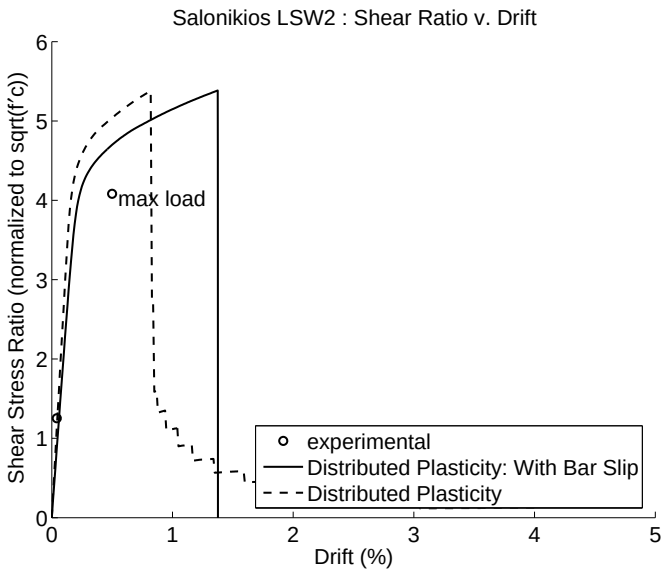

Figure I.37: Pushover of Beam-Column Element with Bar-Slip – Salonikios LSW2

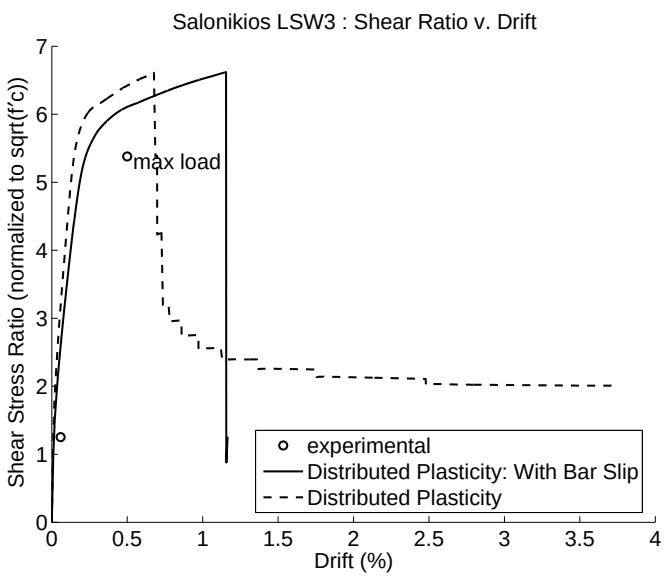

Figure I.38: Pushover of Beam-Column Element with Bar-Slip – Salonikios LSW3

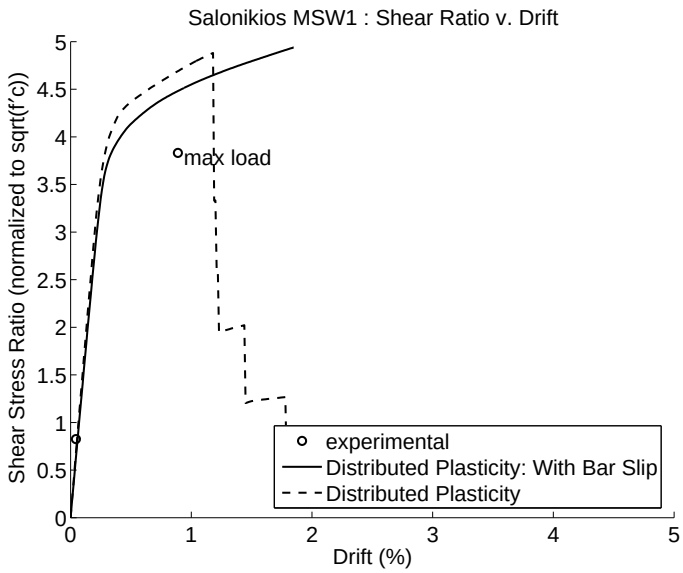

Figure I.39: Pushover of Beam-Column Element with Bar-Slip – Salonikios MSW1

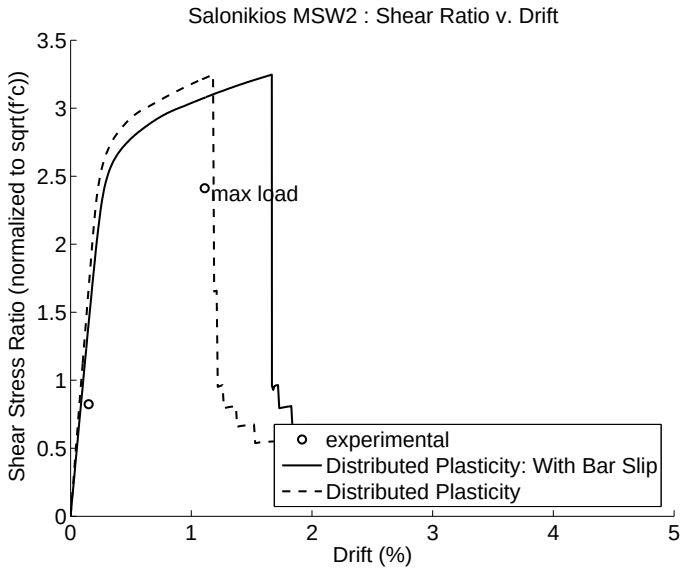

Figure I.40: Pushover of Beam-Column Element with Bar-Slip – Salonikios MSW2

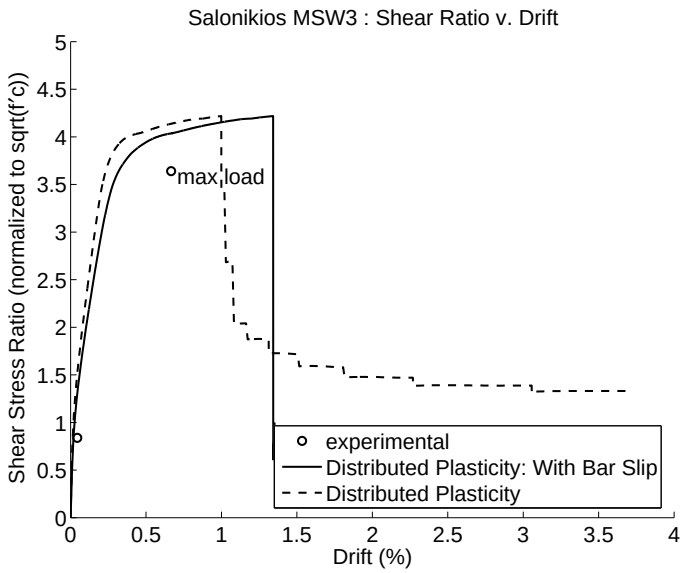

Figure I.41: Pushover of Beam-Column Element with Bar-Slip – Salonikios MSW3

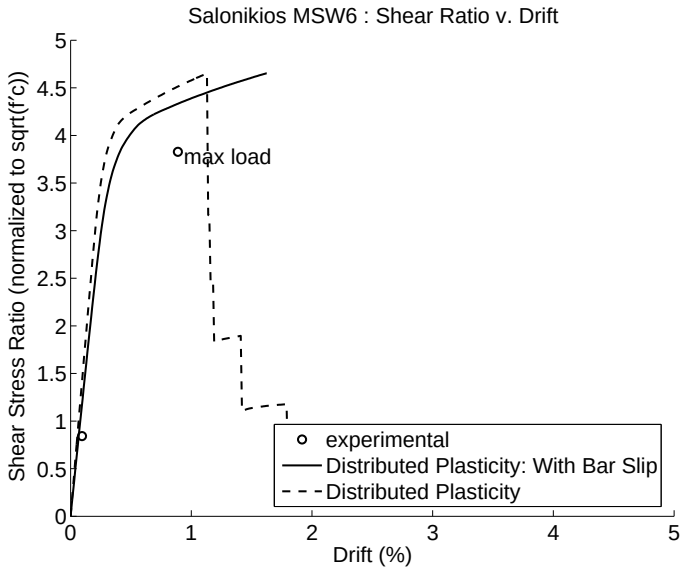

Figure I.42: Pushover of Beam-Column Element with Bar-Slip – Salonikios MSW6

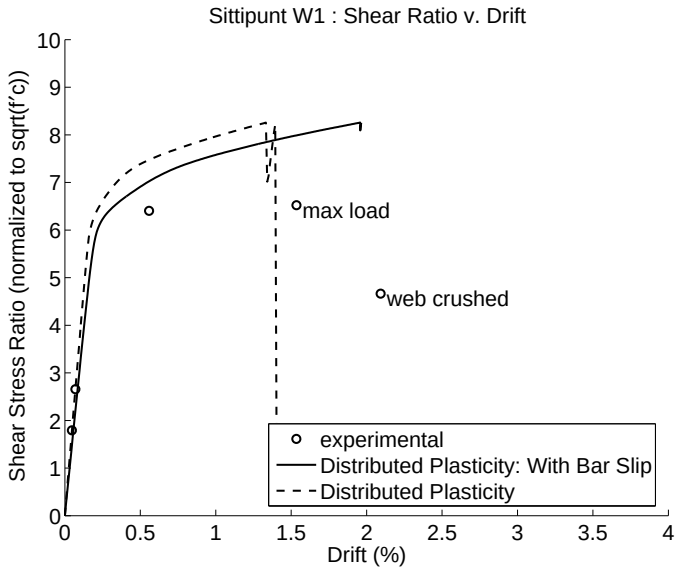

Figure I.43: Pushover of Beam-Column Element with Bar-Slip – Sittipunt W1

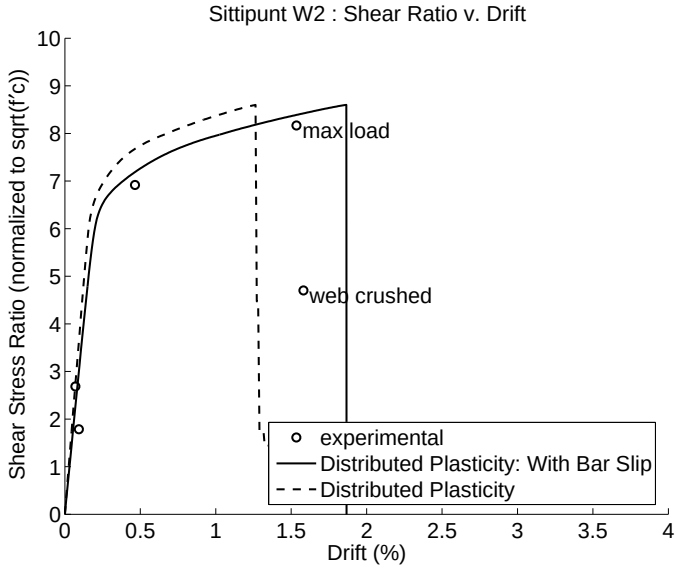

Figure I.44: Pushover of Beam-Column Element with Bar-Slip – Sittipunt W2

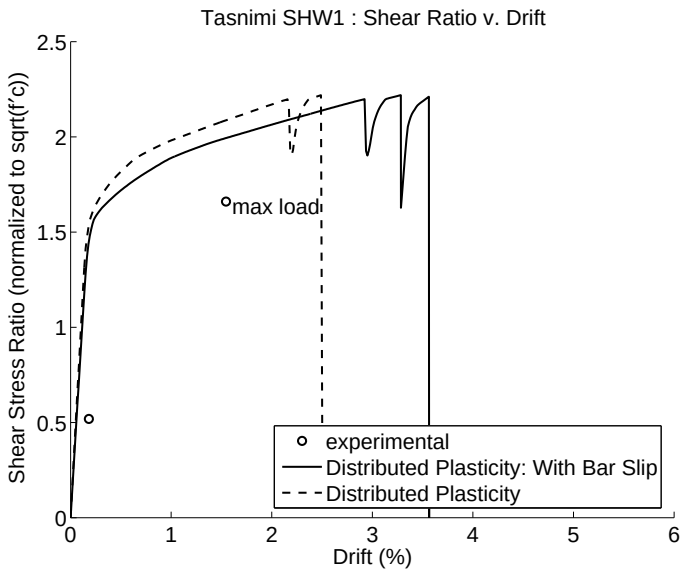

Figure I.45: Pushover of Beam-Column Element with Bar-Slip – Tasnimi SHW1

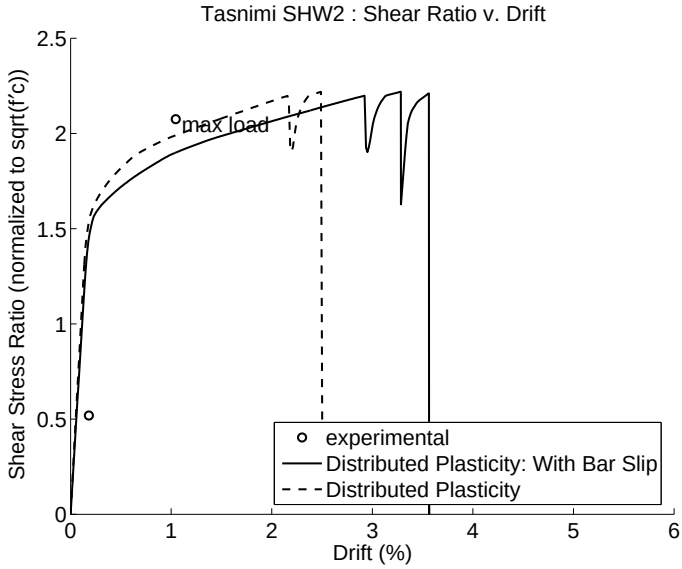

Figure I.46: Pushover of Beam-Column Element with Bar-Slip – Tasnimi SHW2

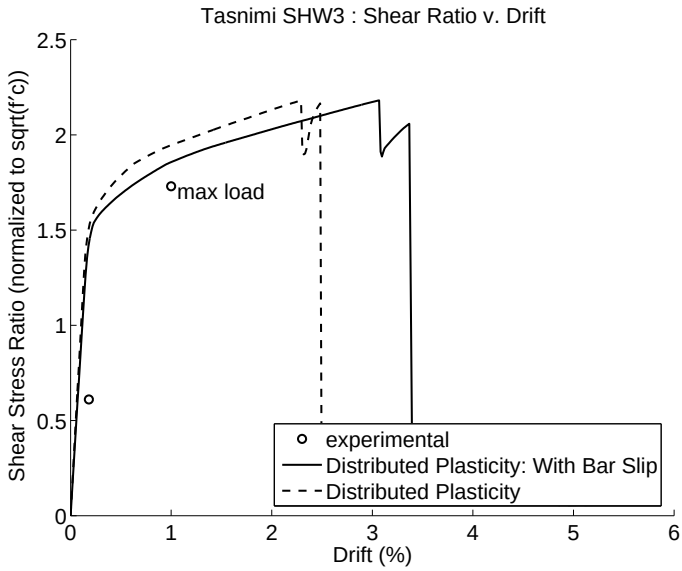

Figure I.47: Pushover of Beam-Column Element with Bar-Slip – Tasnimi SHW3

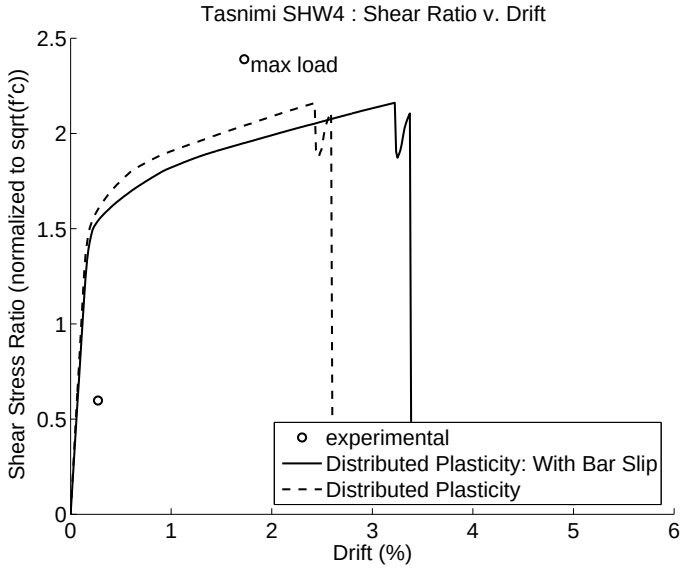

Figure I.48: Pushover of Beam-Column Element with Bar-Slip – Tasnimi SHW4

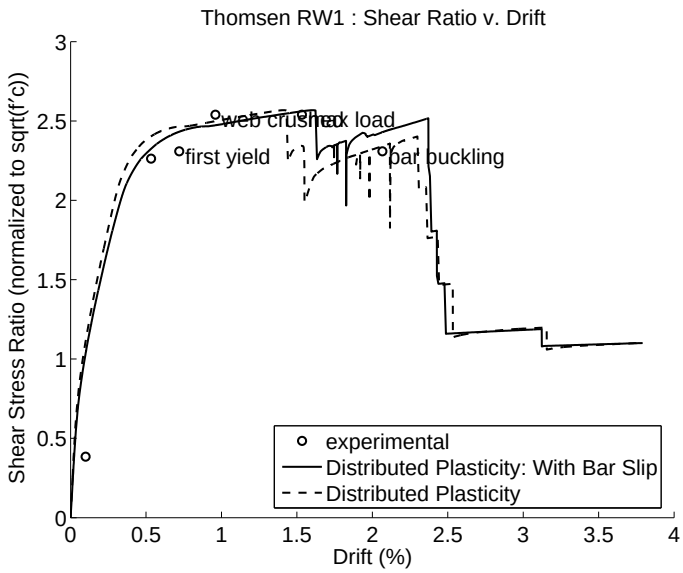

Figure I.49: Pushover of Beam-Column Element with Bar-Slip – Thomsen RW1

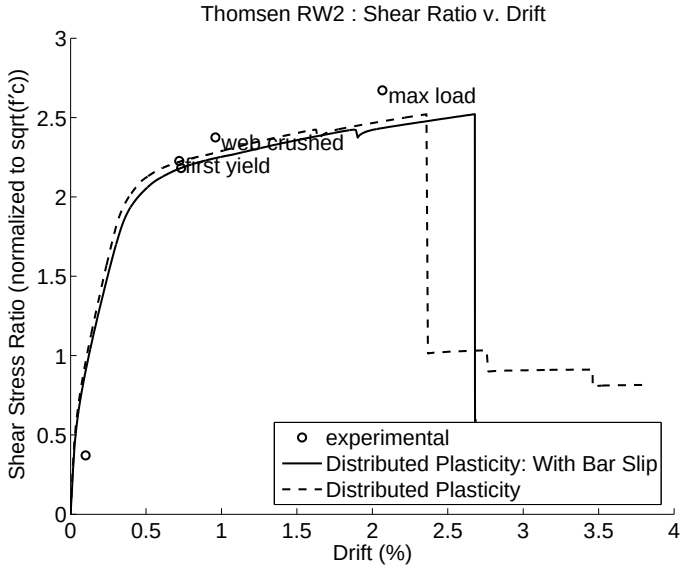

Figure I.50: Pushover of Beam-Column Element with Bar-Slip – Thomsen RW2

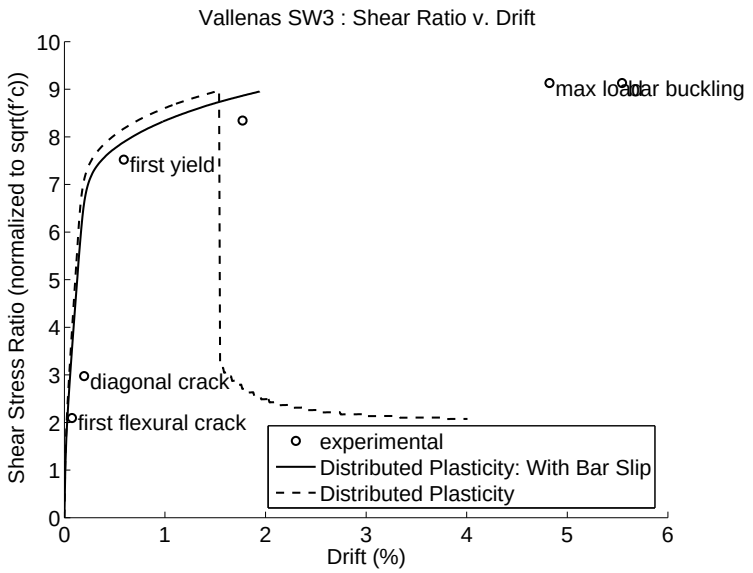

Figure I.51: Pushover of Beam-Column Element with Bar-Slip – Vallenas SW3

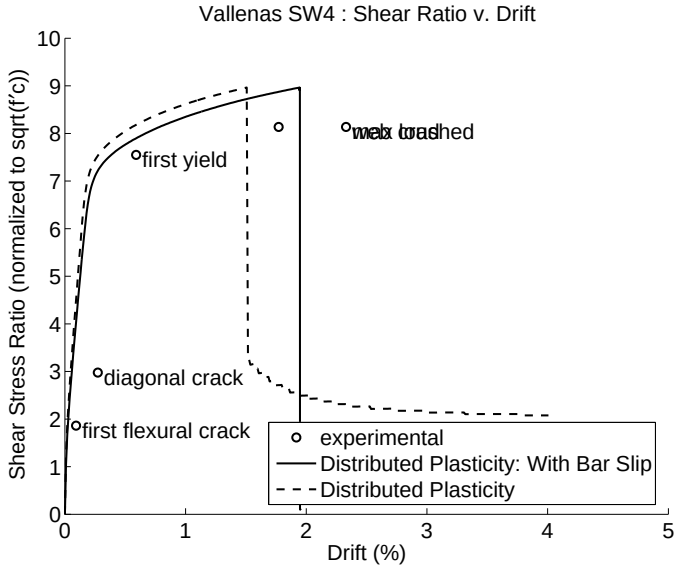

Figure I.52: Pushover of Beam-Column Element with Bar-Slip – Vallenas SW4

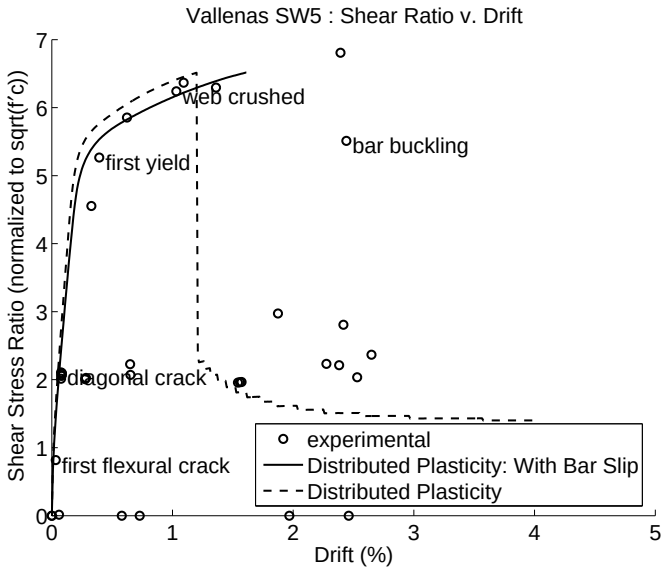

Figure I.53: Pushover of Beam-Column Element with Bar-Slip – Vallenas SW5

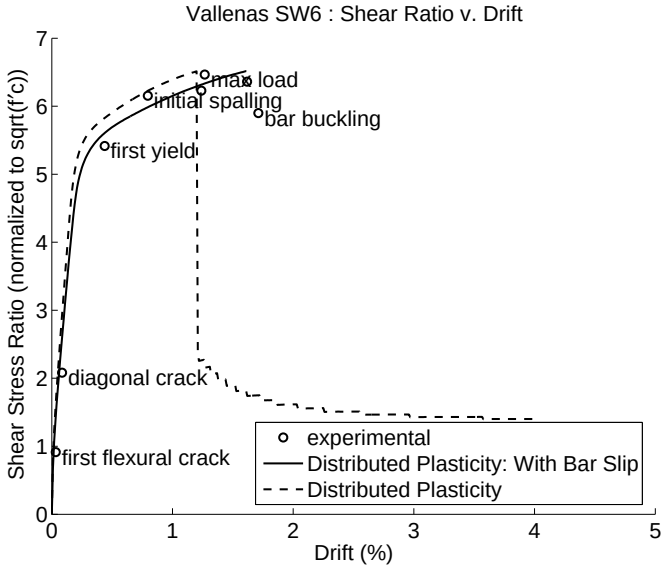

Figure I.54: Pushover of Beam-Column Element with Bar-Slip – Vallenas SW6

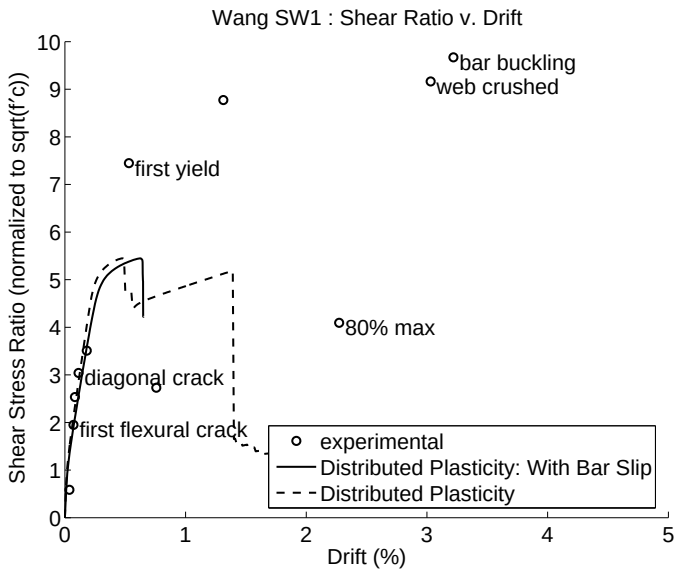

Figure I.55: Pushover of Beam-Column Element with Bar-Slip – Wang SW1

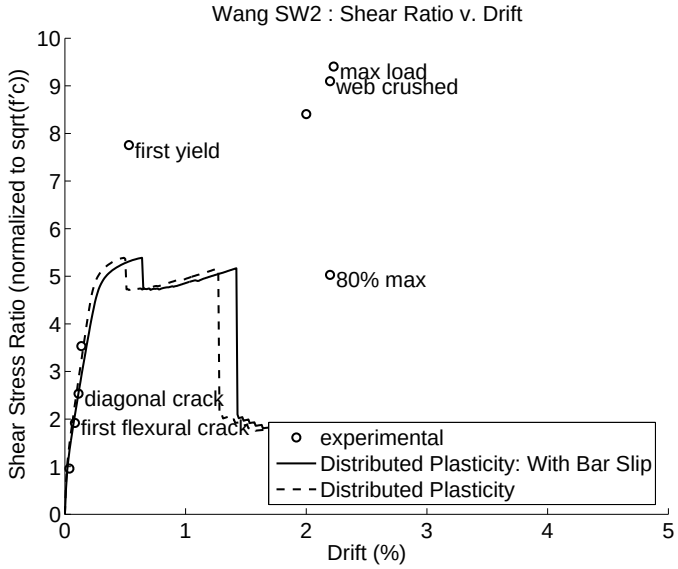

Figure I.56: Pushover of Beam-Column Element with Bar-Slip – Wang SW2

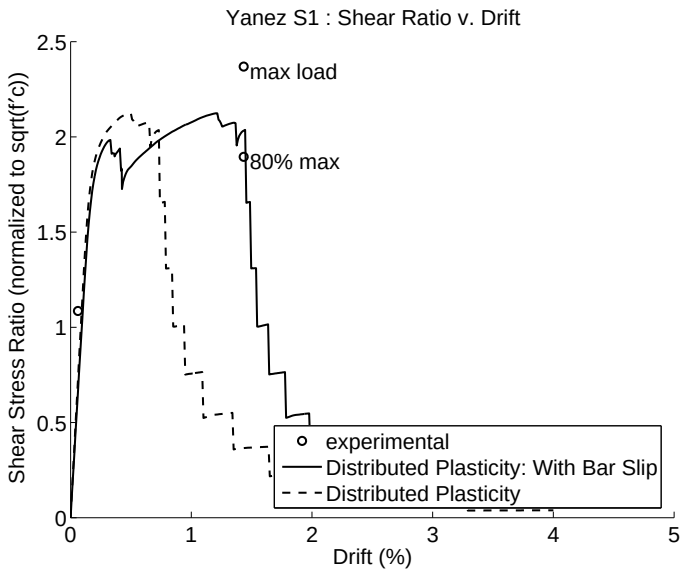

Figure I.57: Pushover of Beam-Column Element with Bar-Slip – Yanez S1

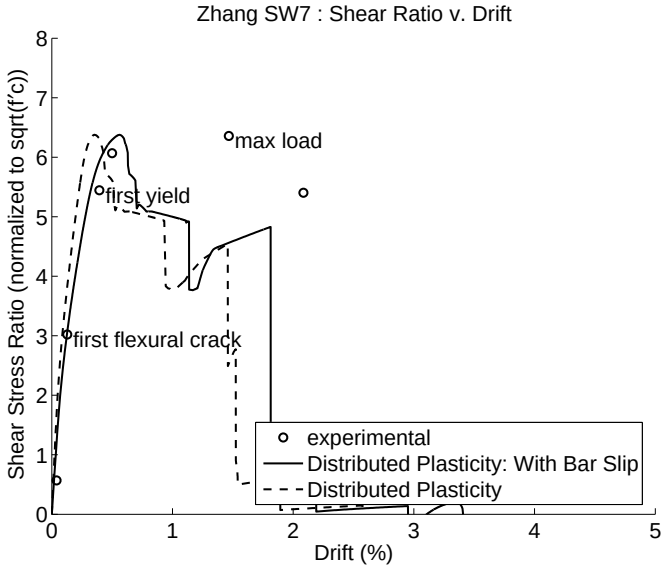

Figure I.58: Pushover of Beam-Column Element with Bar-Slip – Zhang SW7

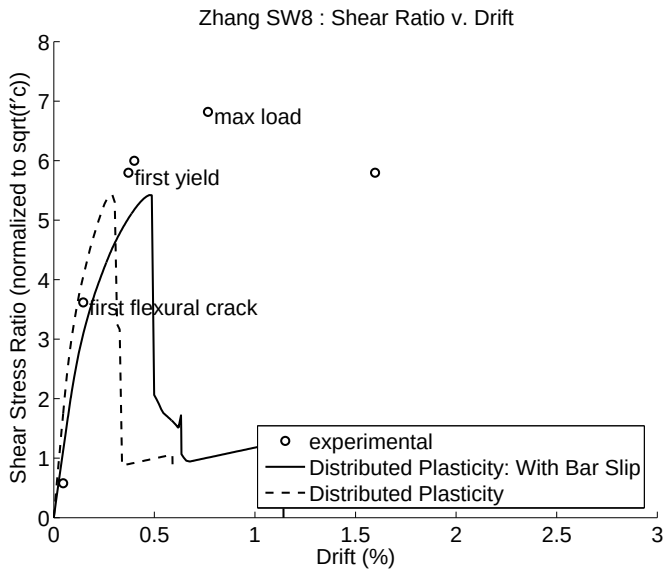

Figure I.59: Pushover of Beam-Column Element with Bar-Slip – Zhang SW8

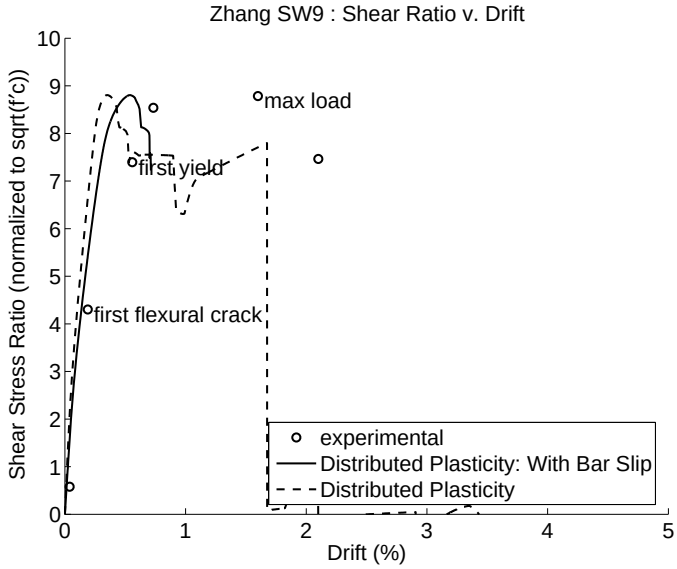

Figure I.60: Pushover of Beam-Column Element with Bar-Slip – Zhang SW9

Appendix J

BAR-SLIP PREDICTIONS COMPARED TO DESIGN PARAMETER FIGURES

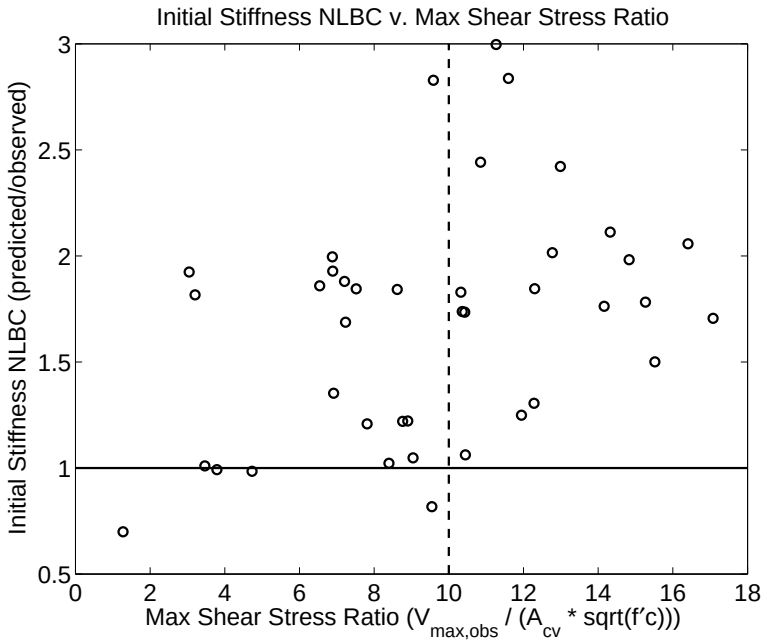

Figure J.1: Initial Stiffness NLBC v Max Shear Stress Ratio

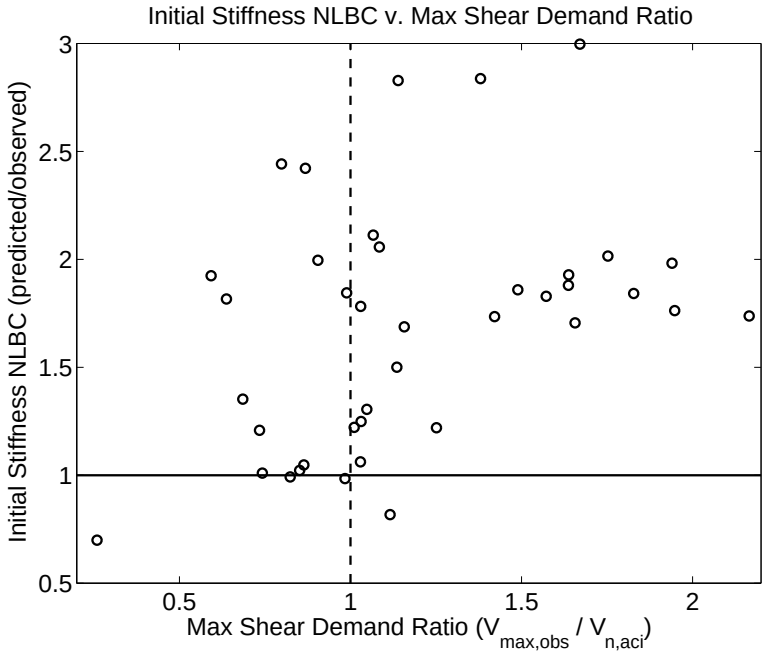

Figure J.2: Initial Stiffness NLBC v Max Shear Demand Ratio

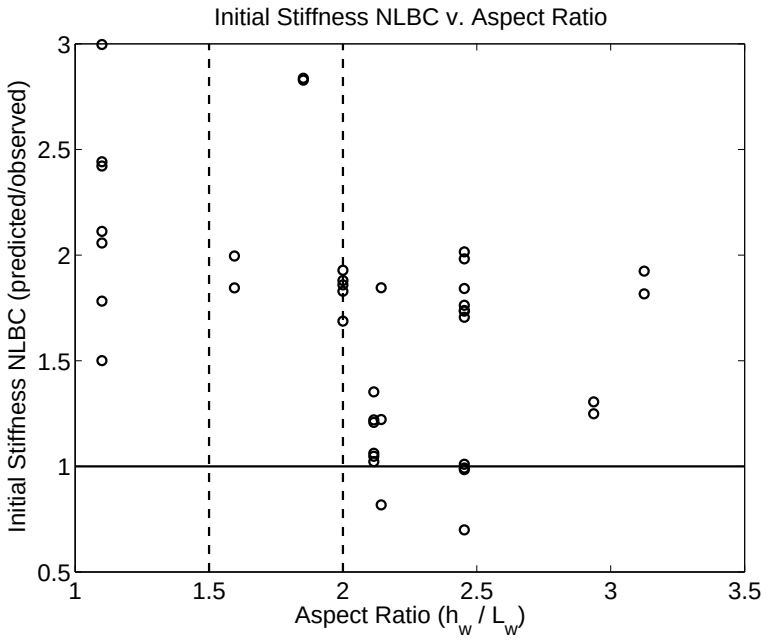

Figure J.3: Initial Stiffness NLBC v Aspect Ratio

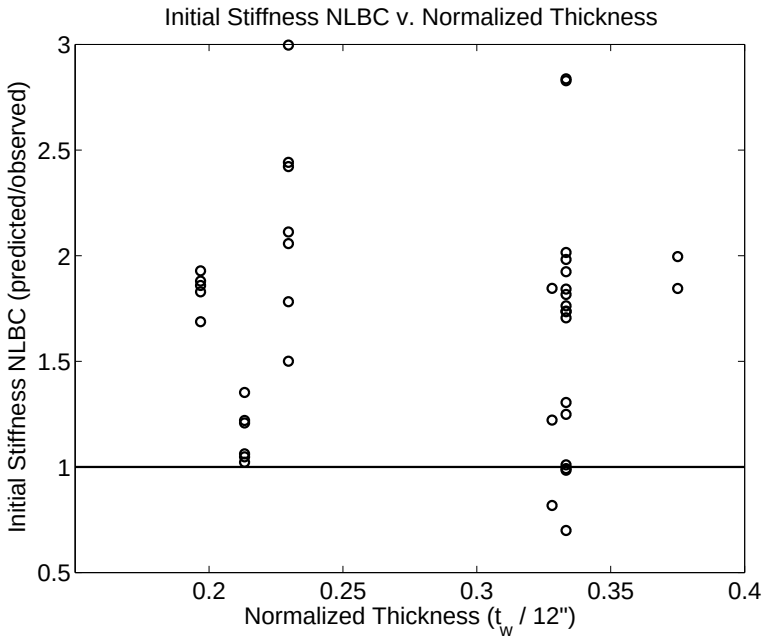

Figure J.4: Initial Stiffness NLBC v Normalized Thickness

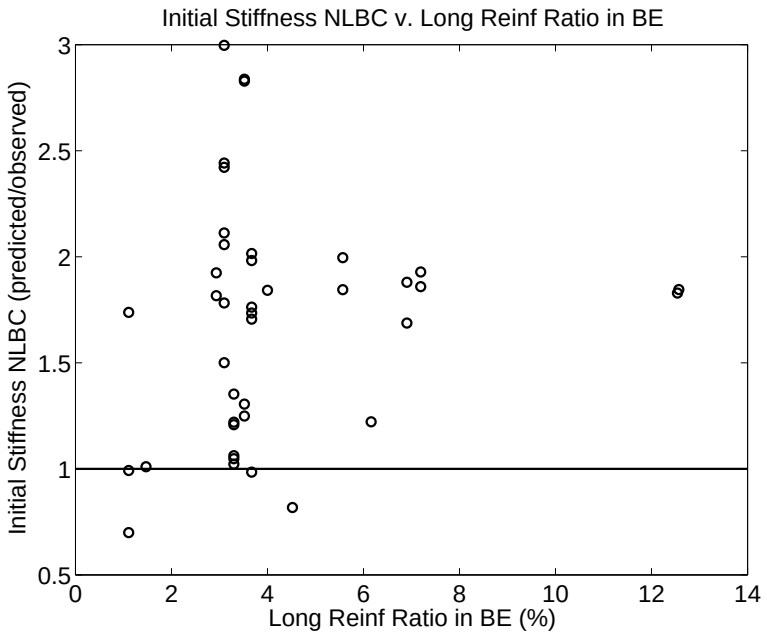

Figure J.5: Initial Stiffness NLBC v Long Reinf Ratio in BE

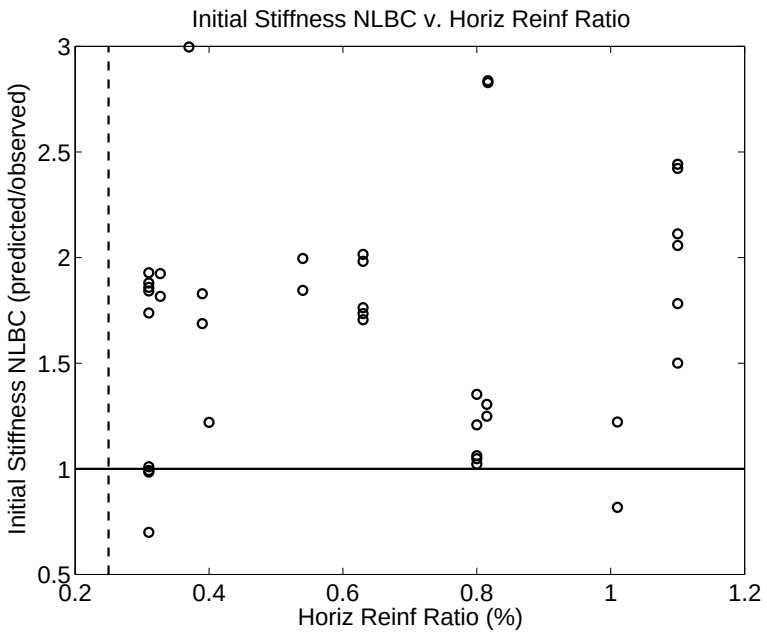

Figure J.6: Initial Stiffness NLBC v Horiz Reinf Ratio

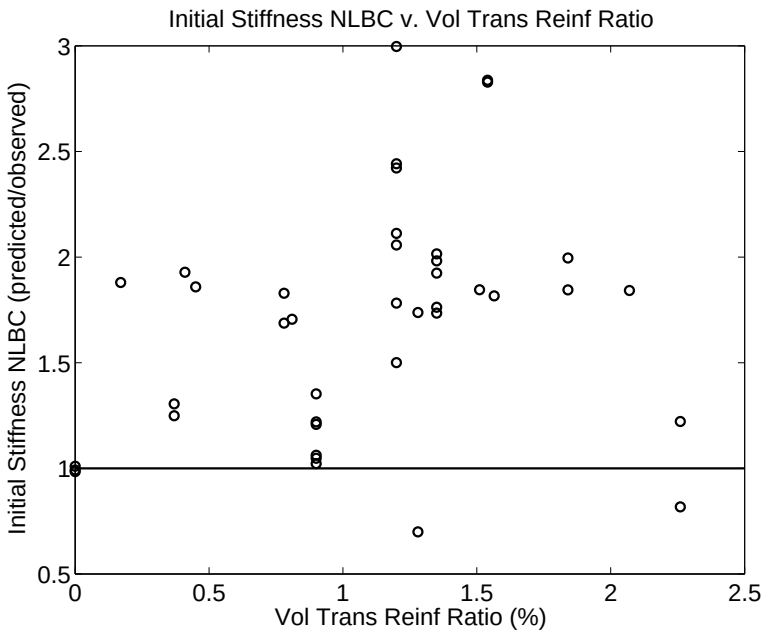

Figure J.7: Initial Stiffness NLBC v Vol Trans Reinf Ratio

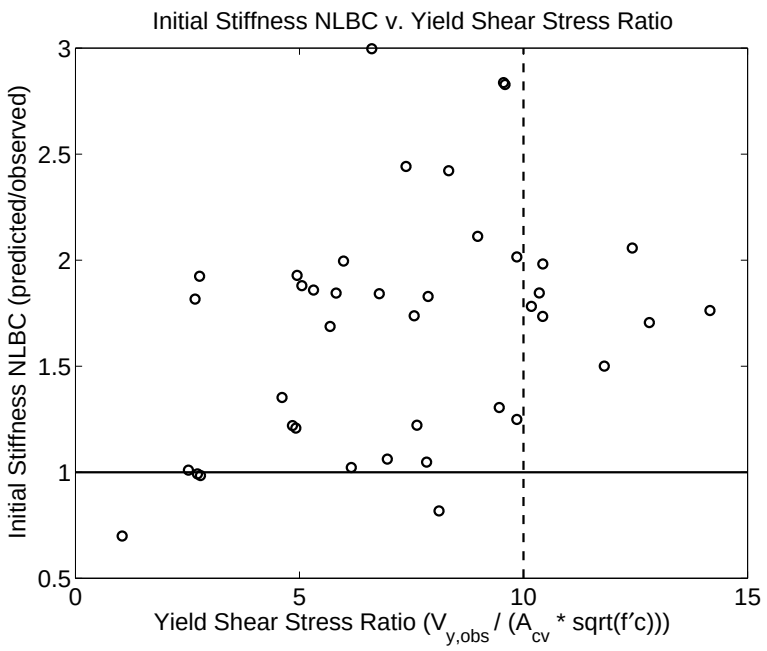

Figure J.8: Initial Stiffness NLBC v Yield Shear Stress Ratio

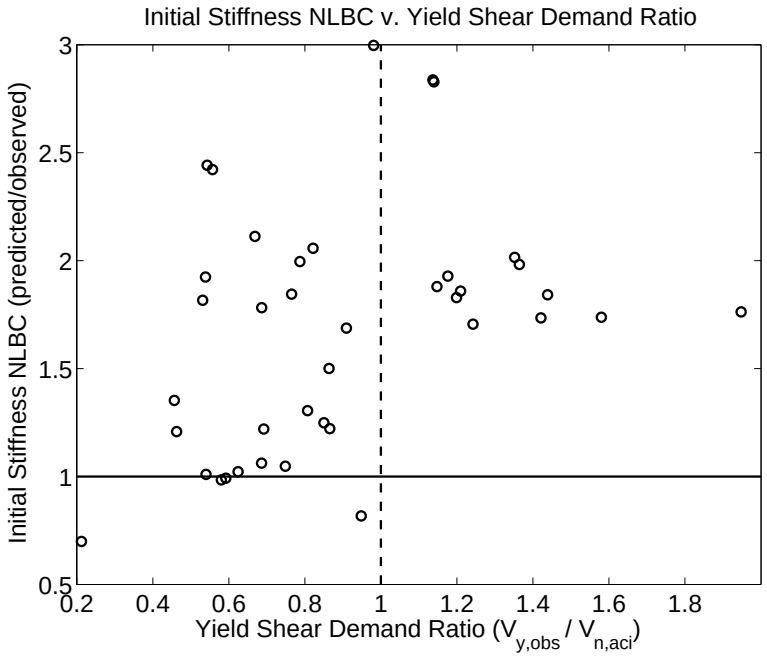

Figure J.9: Initial Stiffness NLBC v Yield Shear Demand Ratio

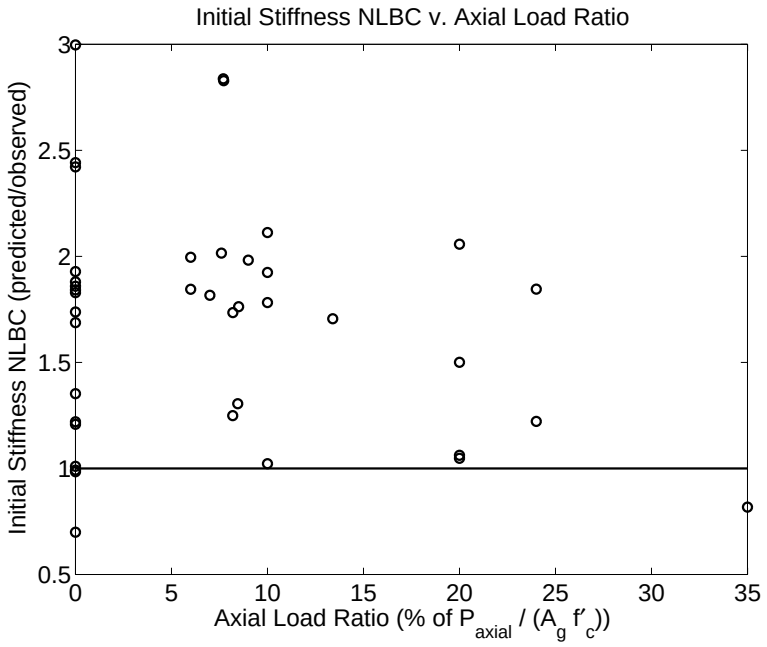

Figure J.10: Initial Stiffness NLBC v Axial Load Ratio

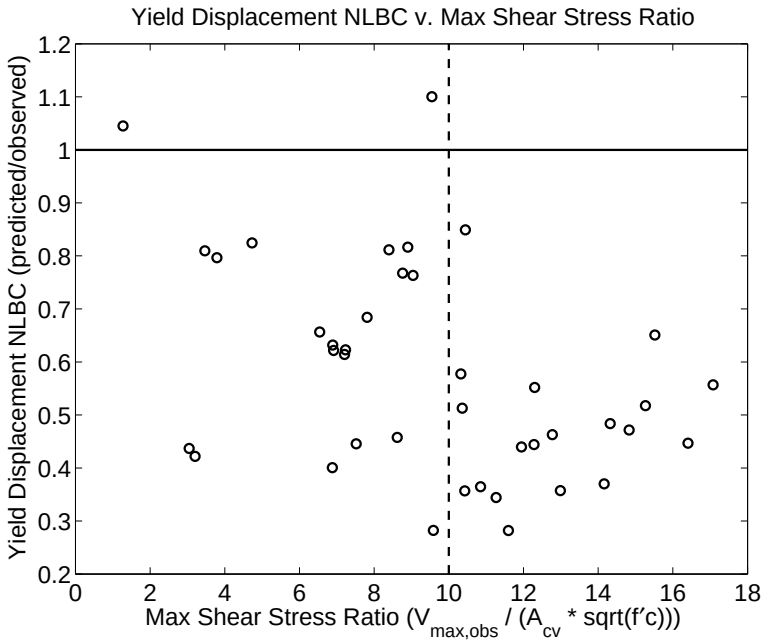

Figure J.11: Yield Displacement NLBC v Max Shear Stress Ratio

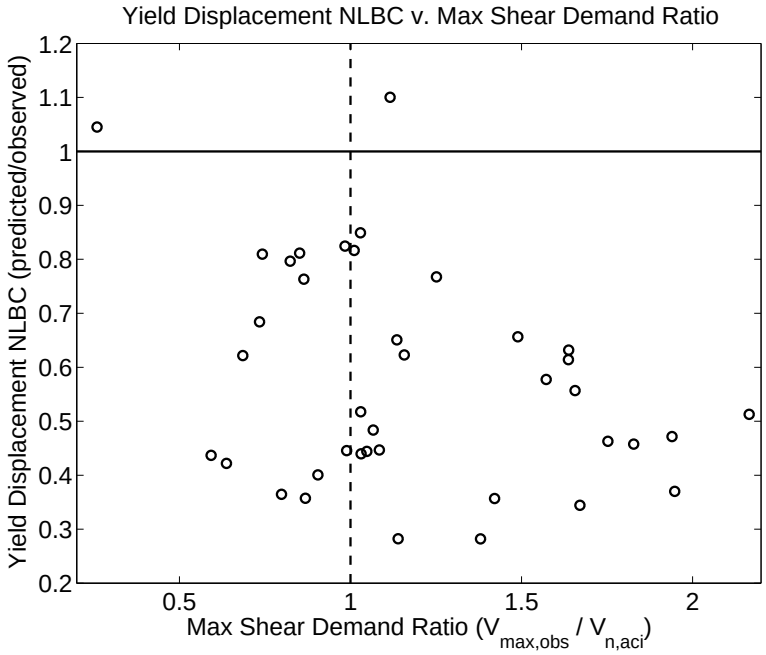

Figure J.12: Yield Displacement NLBC v Max Shear Demand Ratio

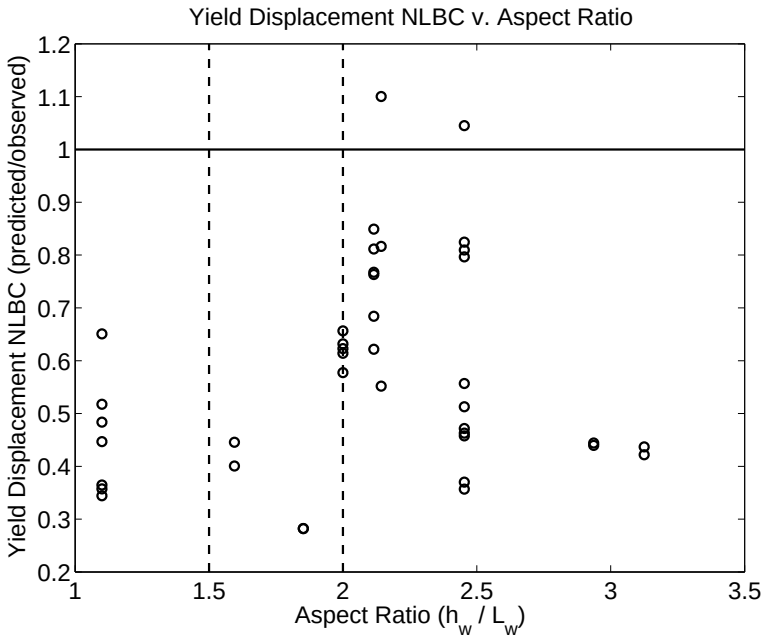

Figure J.13: Yield Displacement NLBC v Aspect Ratio

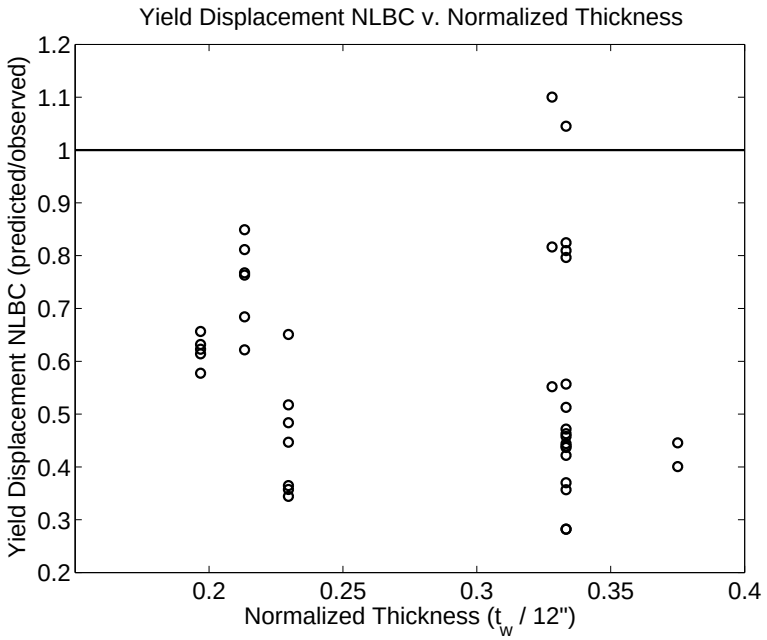

Figure J.14: Yield Displacement NLBC v Normalized Thickness

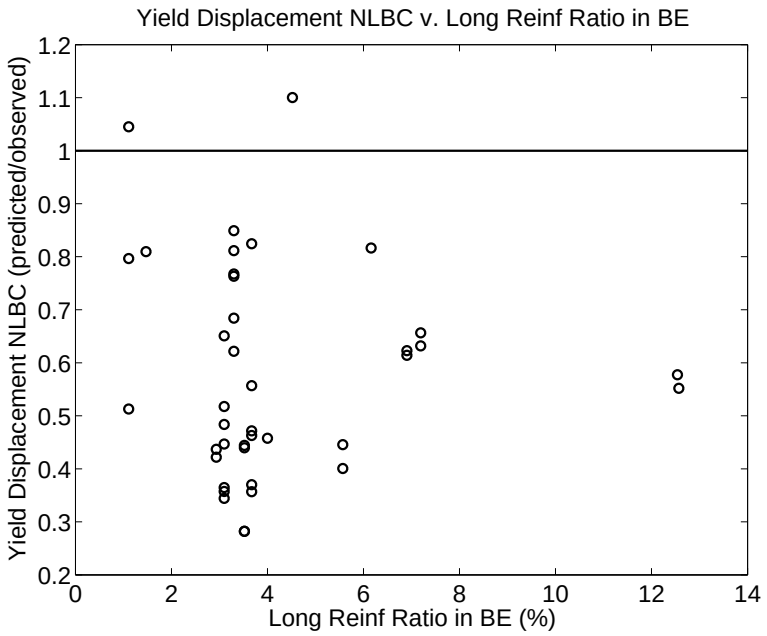

Figure J.15: Yield Displacement NLBC v Long Reinf Ratio in BE

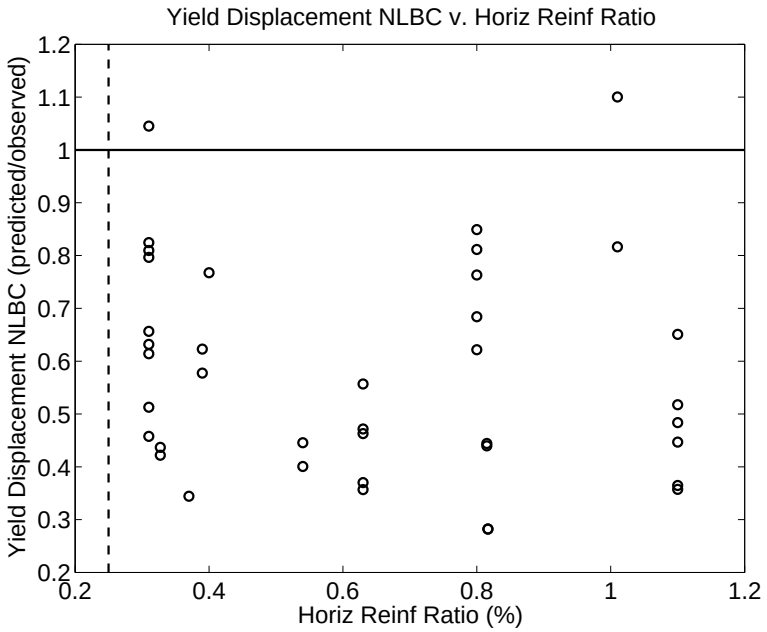

Figure J.16: Yield Displacement NLBC v Horiz Reinf Ratio

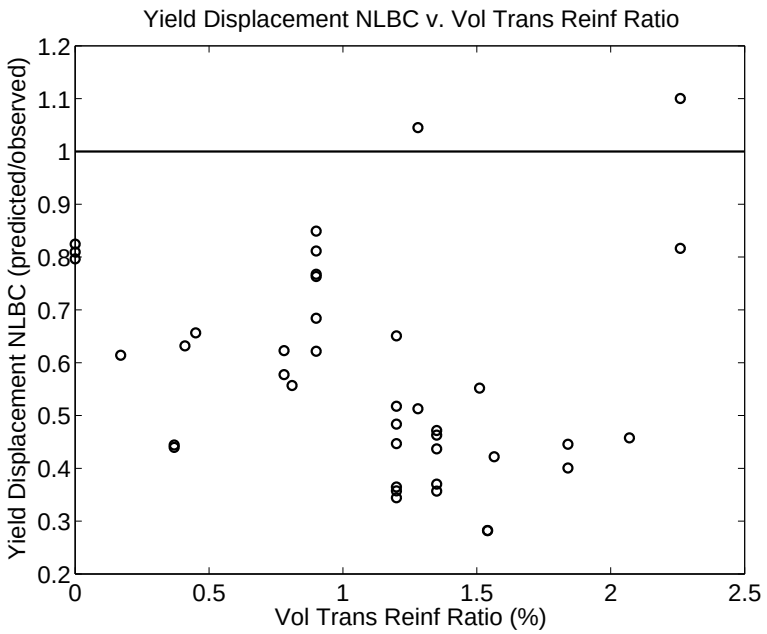

Figure J.17: Yield Displacement NLBC v Vol Trans Reinf Ratio

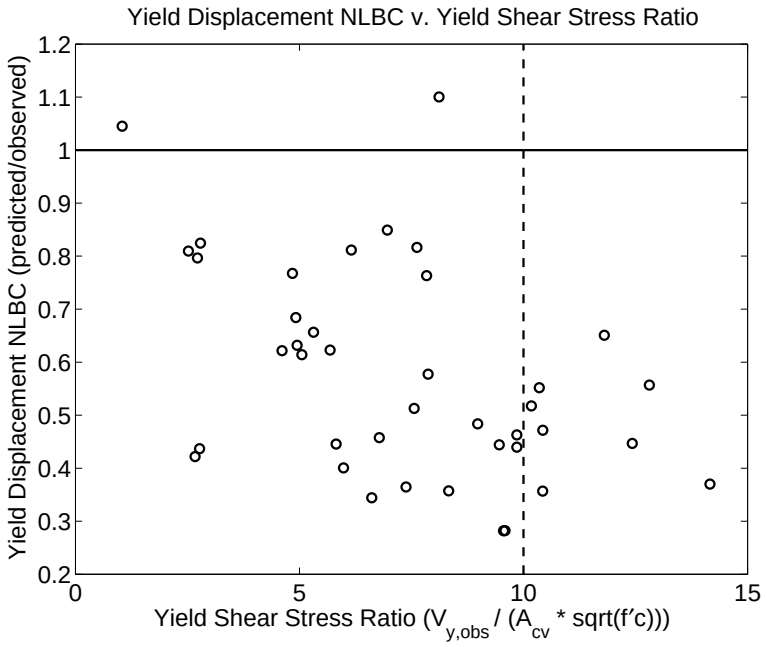

Figure J.18: Yield Displacement NLBC v Yield Shear Stress Ratio

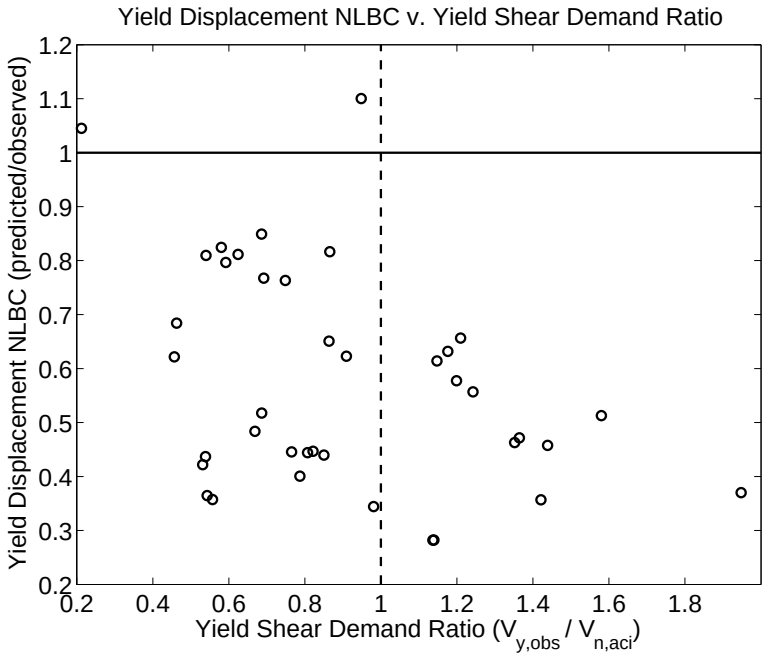

Figure J.19: Yield Displacement NLBC v Yield Shear Demand Ratio

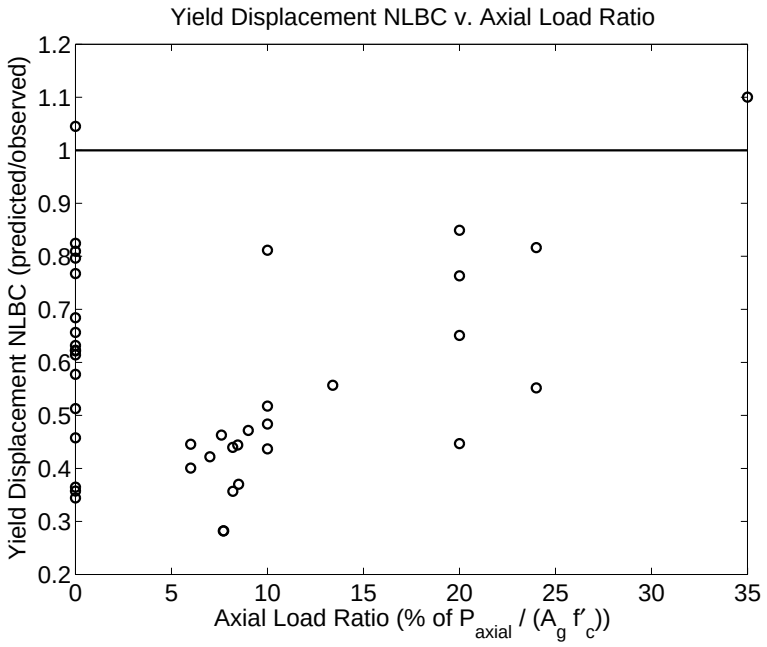

Figure J.20: Yield Displacement NLBC v Axial Load Ratio

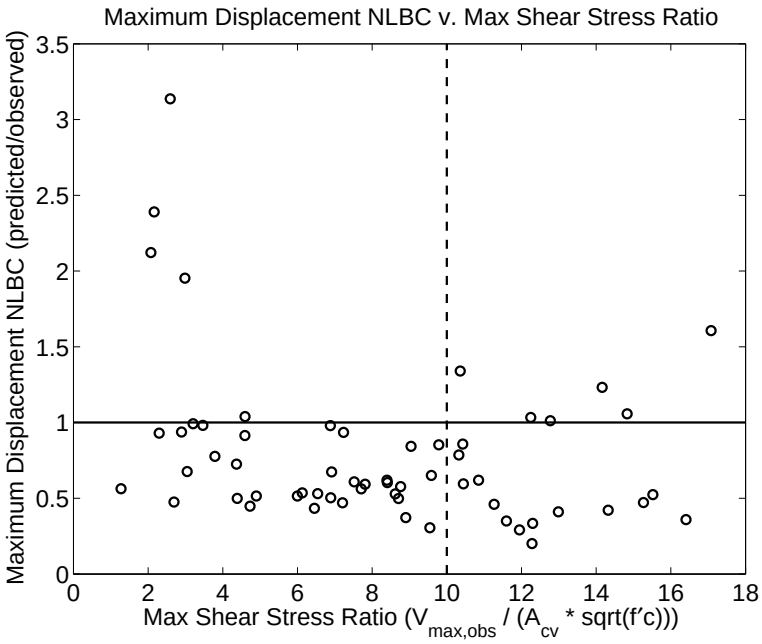

Figure J.21: Maximum Displacement NLBC v Max Shear Stress Ratio

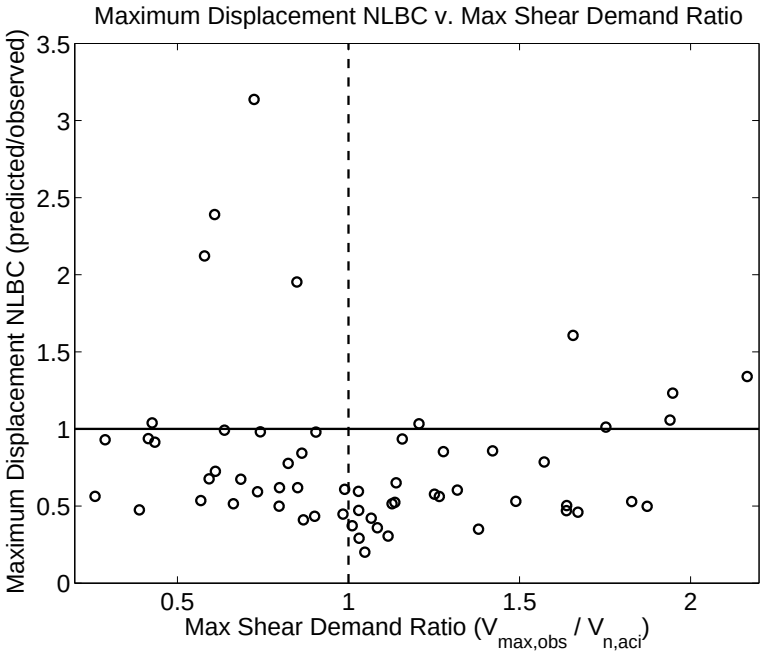

Figure J.22: Maximum Displacement NLBC v Max Shear Demand Ratio

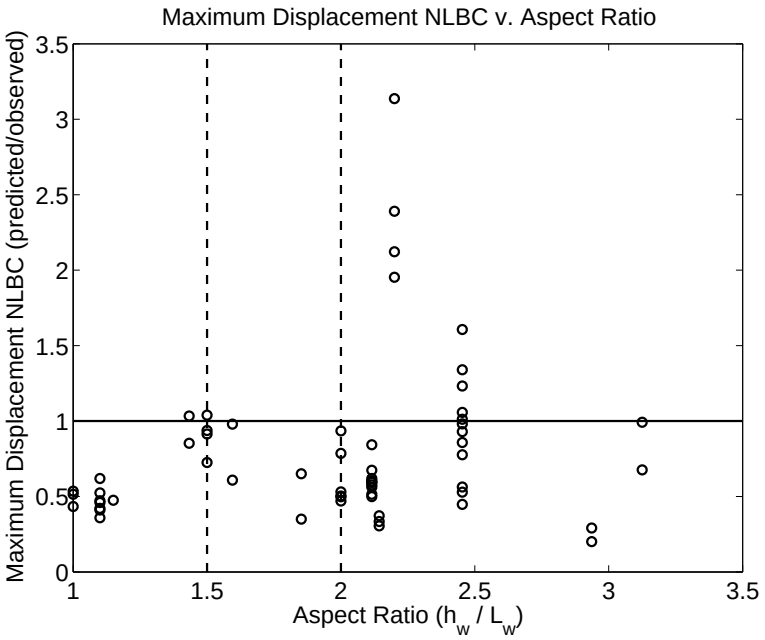

Figure J.23: Maximum Displacement NLBC v Aspect Ratio

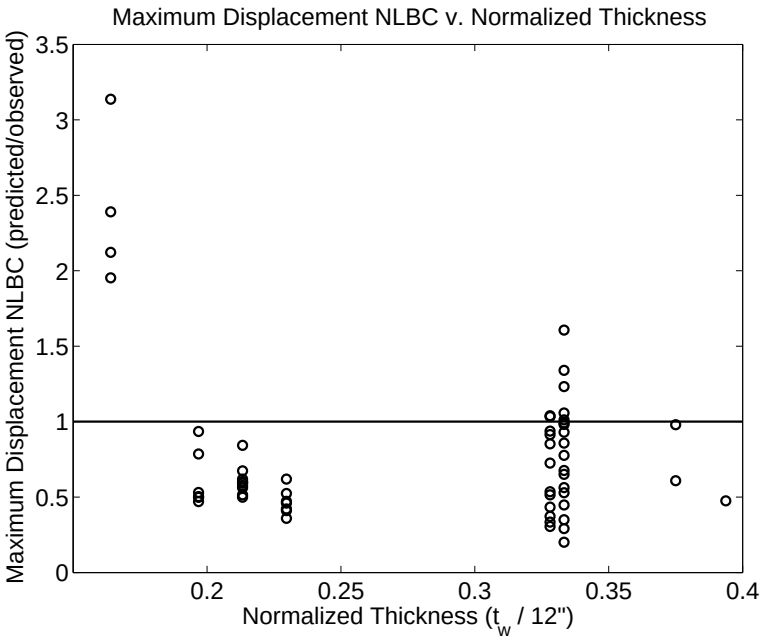

Figure J.24: Maximum Displacement NLBC v Normalized Thickness

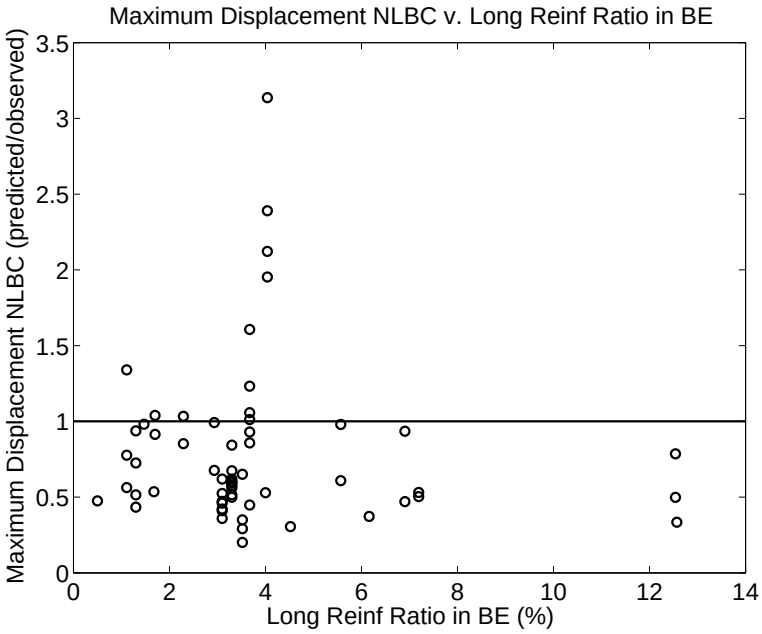

Figure J.25: Maximum Displacement NLBC v Long Reinf Ratio in BE

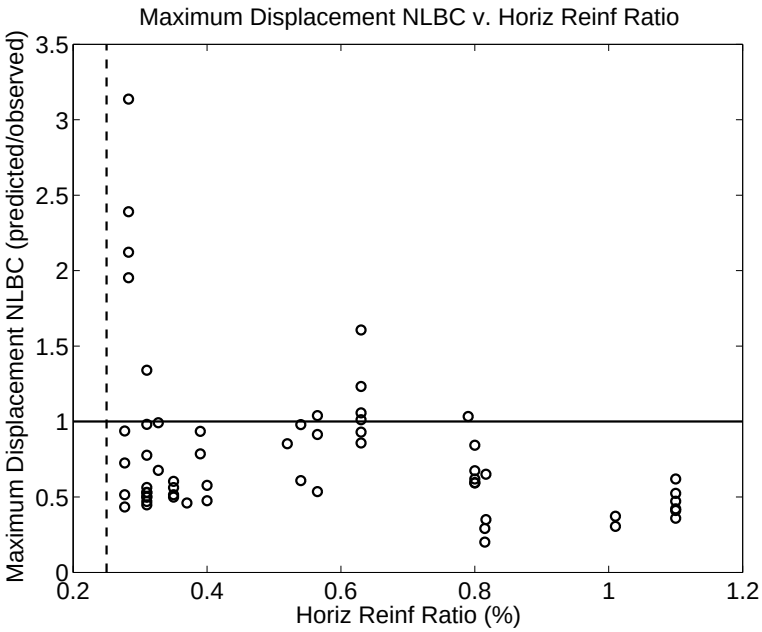

Figure J.26: Maximum Displacement NLBC v Horiz Reinf Ratio

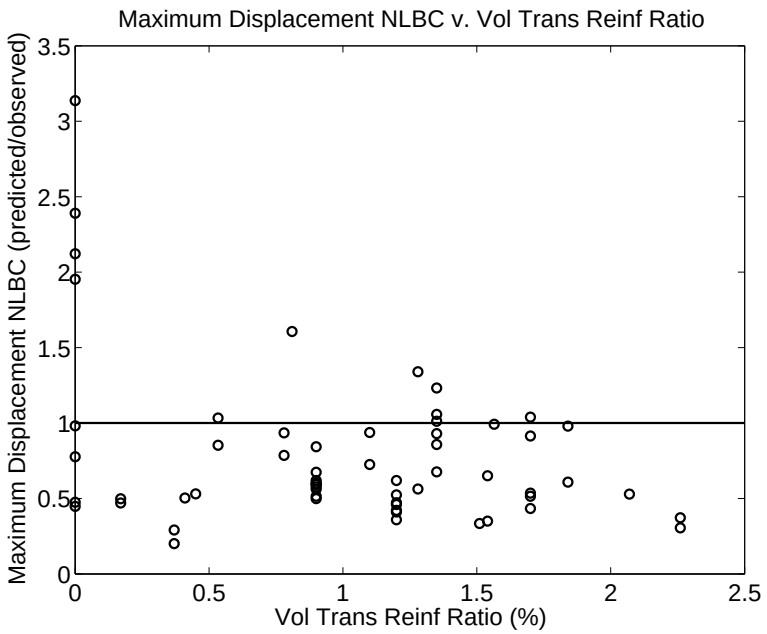

Figure J.27: Maximum Displacement NLBC v Vol Trans Reinf Ratio

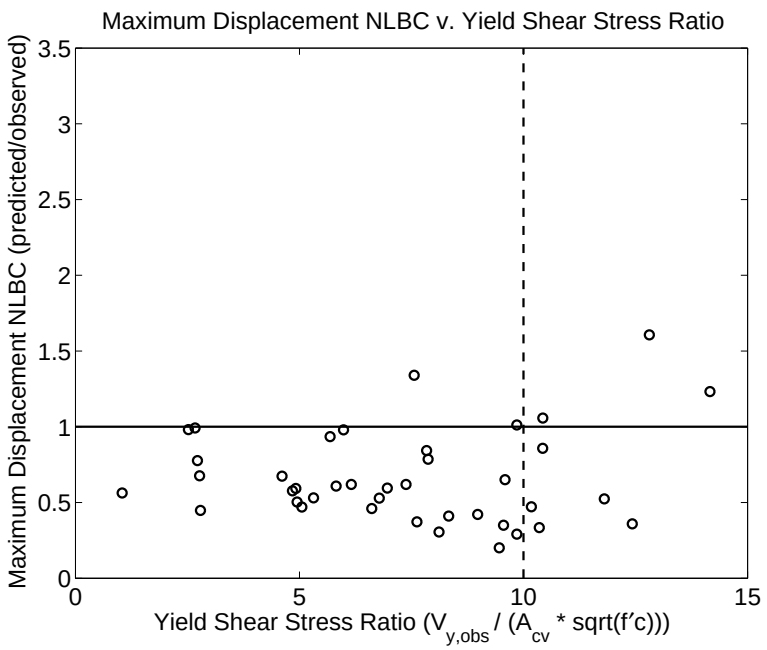

Figure J.28: Maximum Displacement NLBC v Yield Shear Stress Ratio

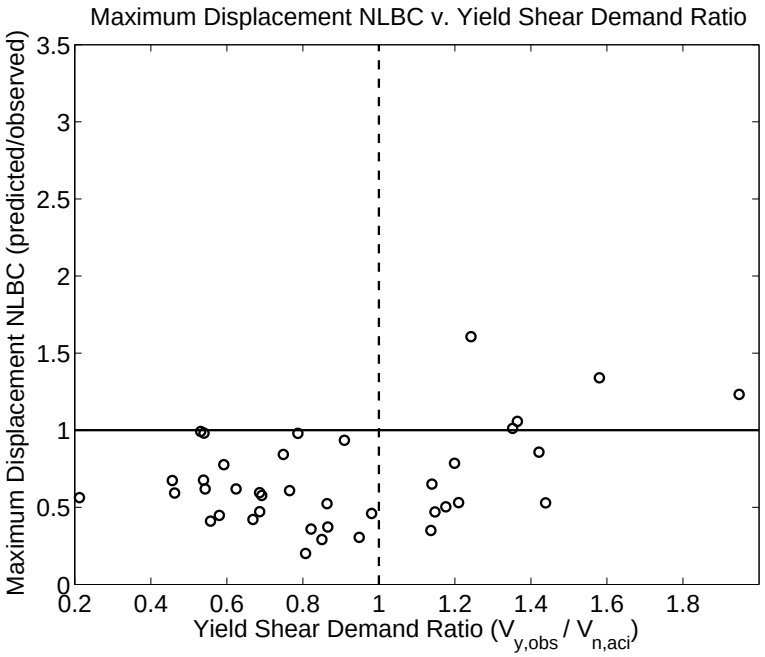

Figure J.29: Maximum Displacement NLBC v Yield Shear Demand Ratio

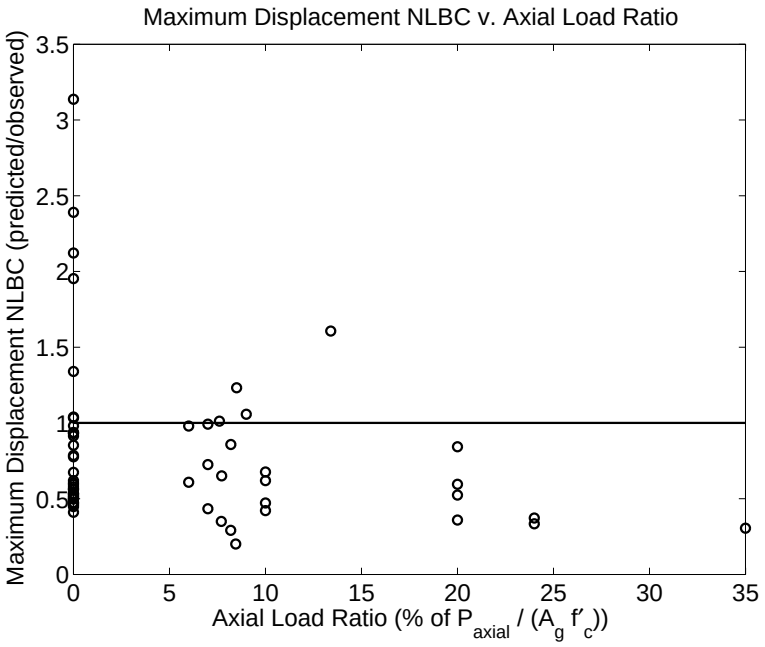

Figure J.30: Maximum Displacement NLBC v Axial Load Ratio

Appendix K

BAR-SLIP CHANGE IN ERROR COMPARED TO DESIGN PARAMETER FIGURES

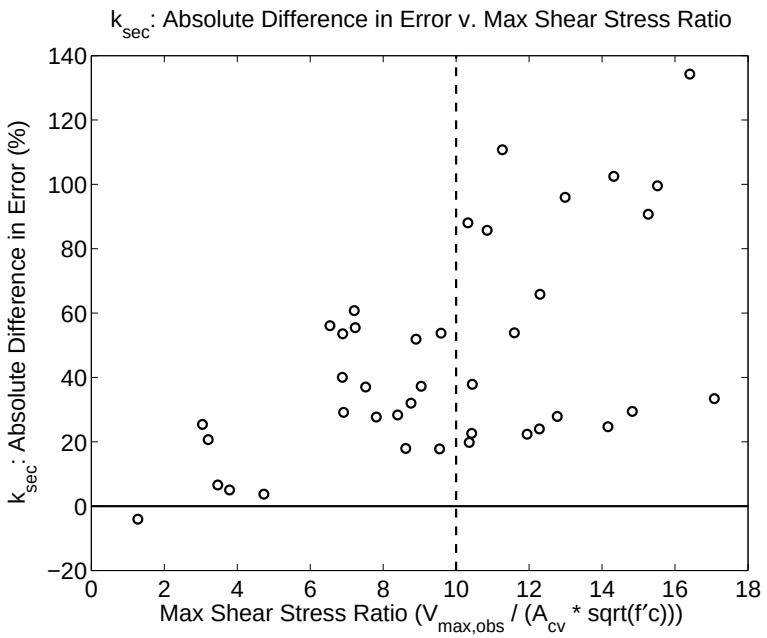

Figure K.1: Initial Stiffness Absolute Error v Max Shear Stress Ratio

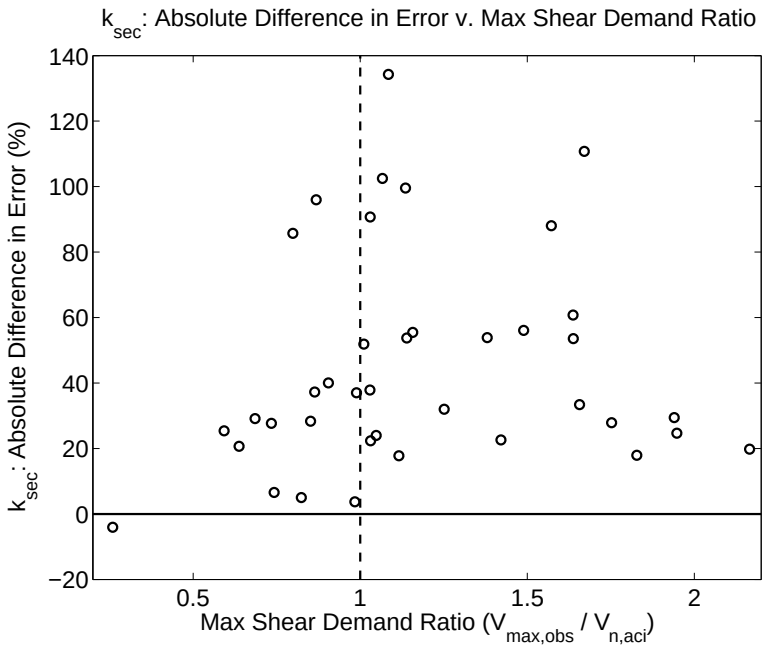

Figure K.2: Initial Stiffness Absolute Error v Max Shear Demand Ratio

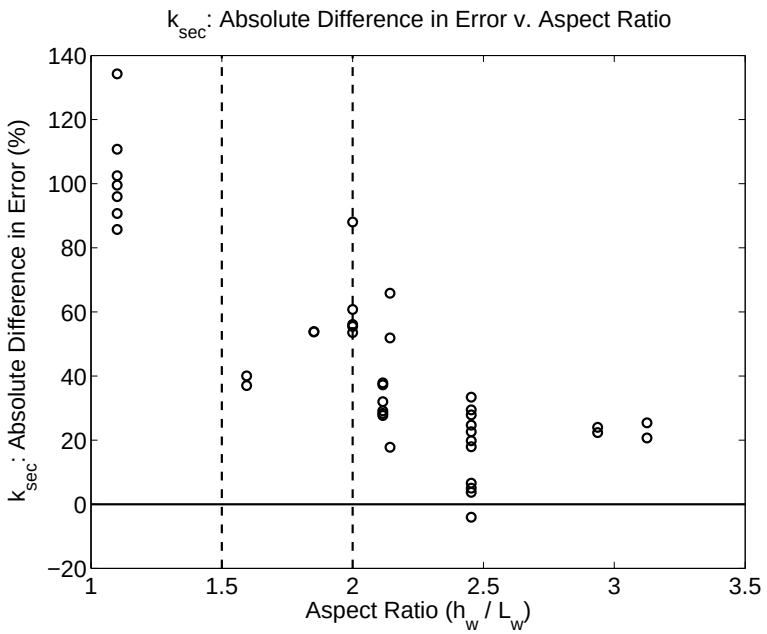

Figure K.3: Initial Stiffness Absolute Error v Aspect Ratio

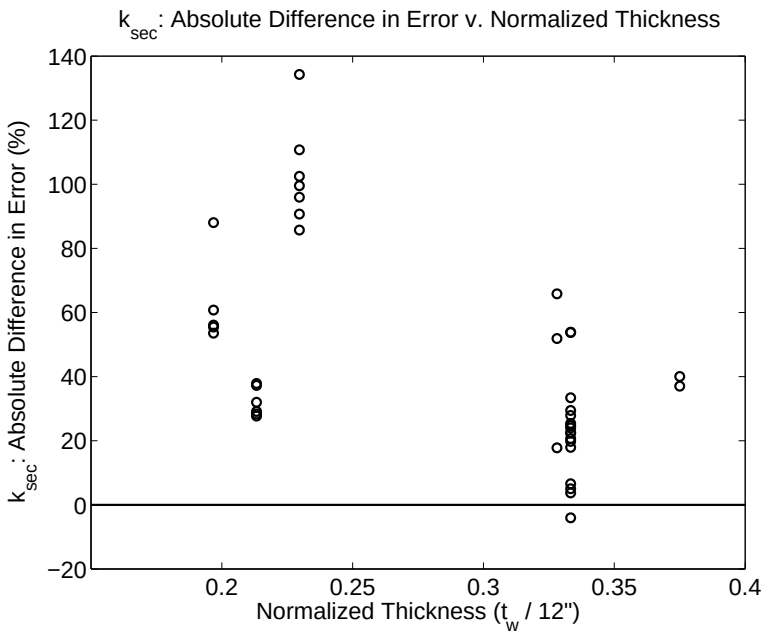

Figure K.4: Initial Stiffness Absolute Error v Normalized Thickness

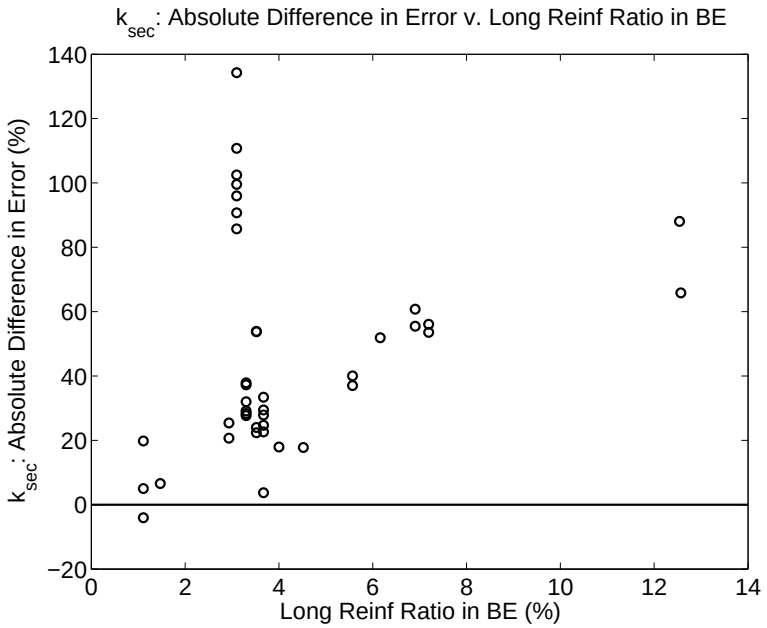

Figure K.5: Initial Stiffness Absolute Error v Long Reinf Ratio in BE

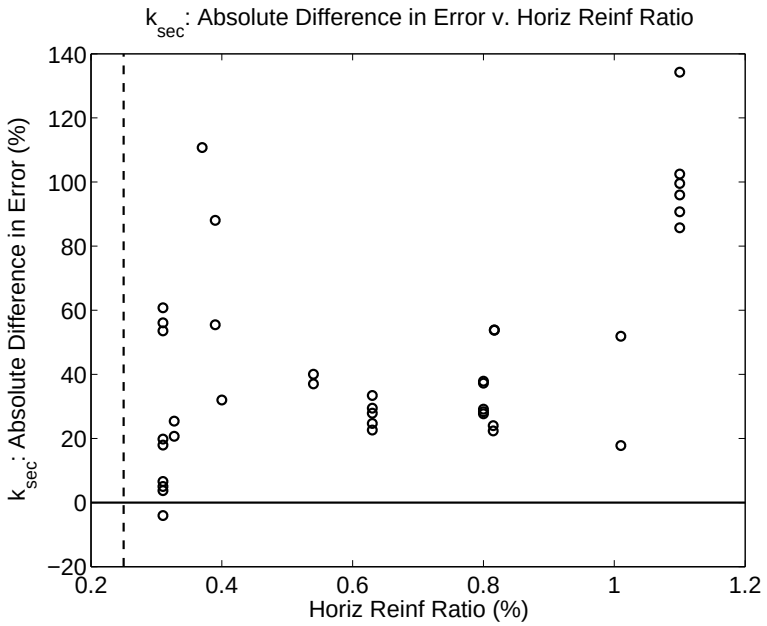

Figure K.6: Initial Stiffness Absolute Error v Horiz Reinf Ratio

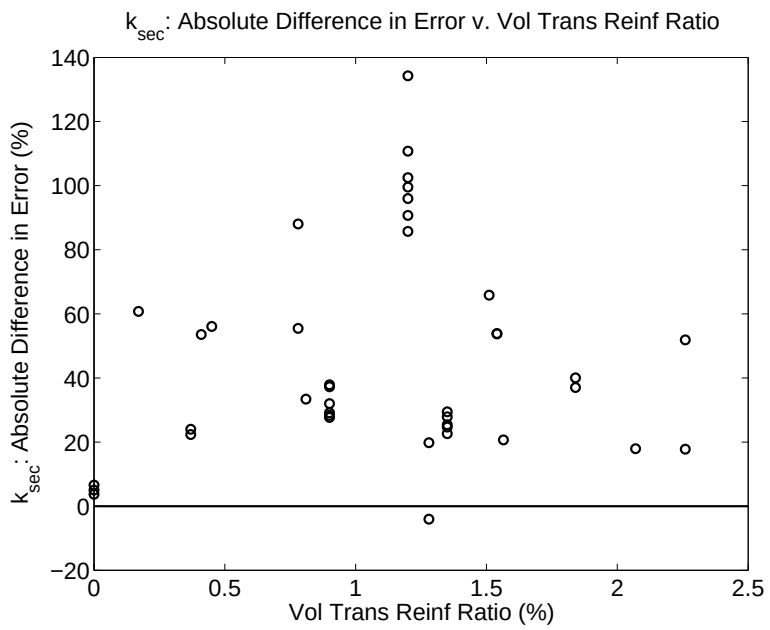

Figure K.7: Initial Stiffness Absolute Error v Vol Trans Reinf Ratio

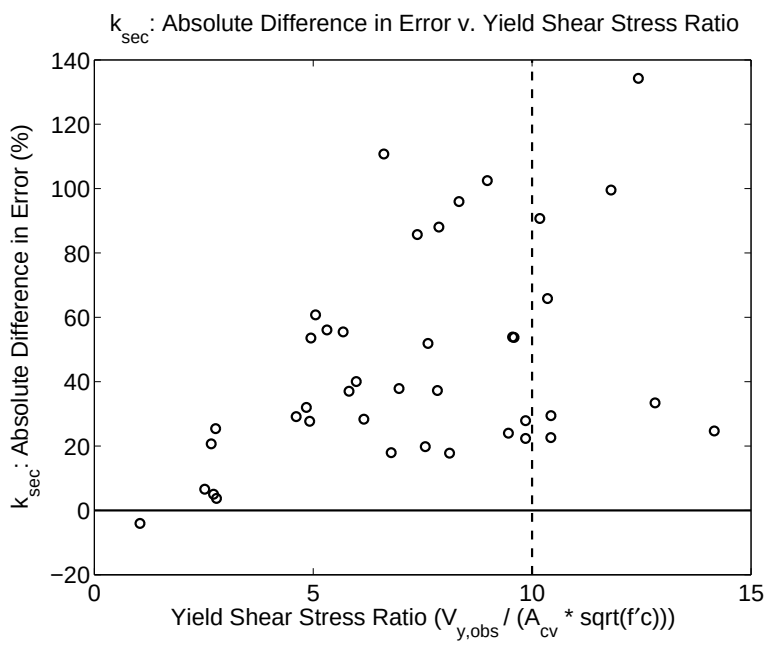

Figure K.8: Initial Stiffness Absolute Error v Yield Shear Stress Ratio

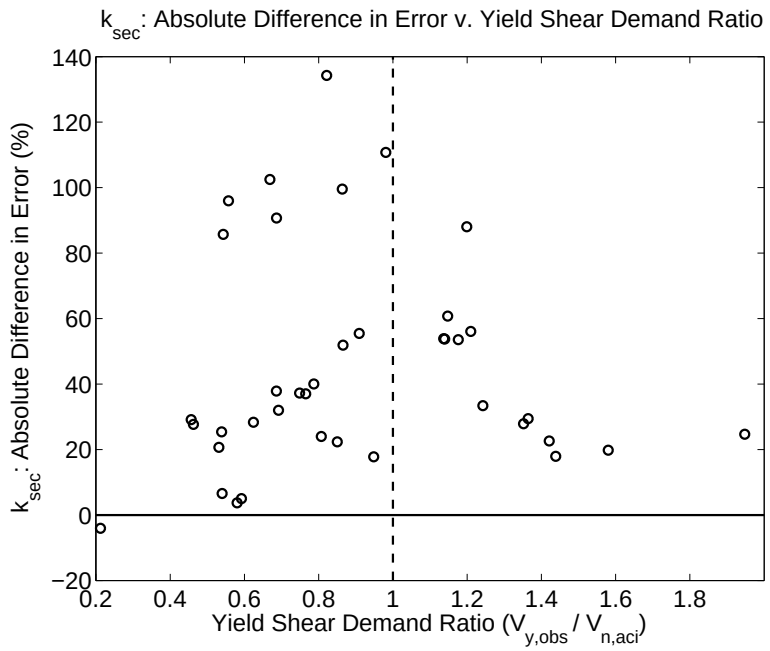

Figure K.9: Initial Stiffness Absolute Error v Yield Shear Demand Ratio

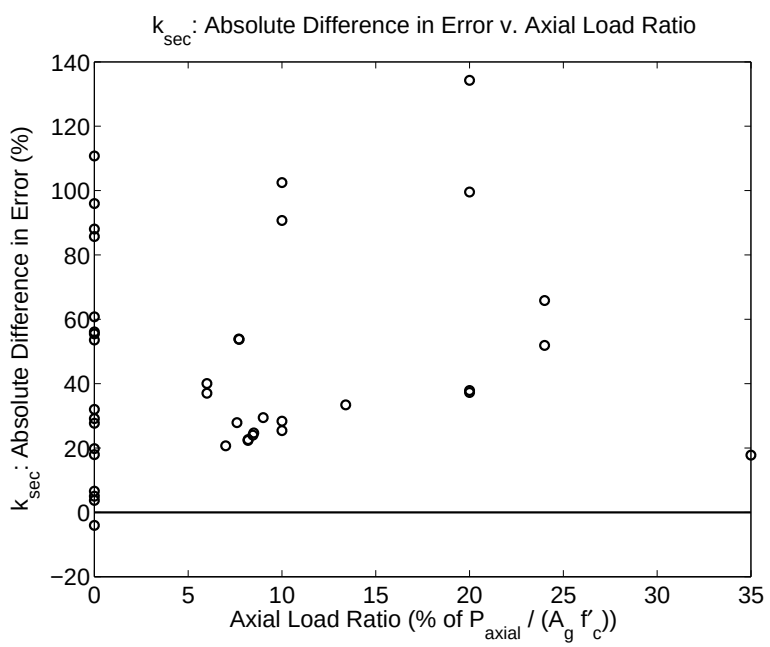

Figure K.10: Initial Stiffness Absolute Error v Axial Load Ratio

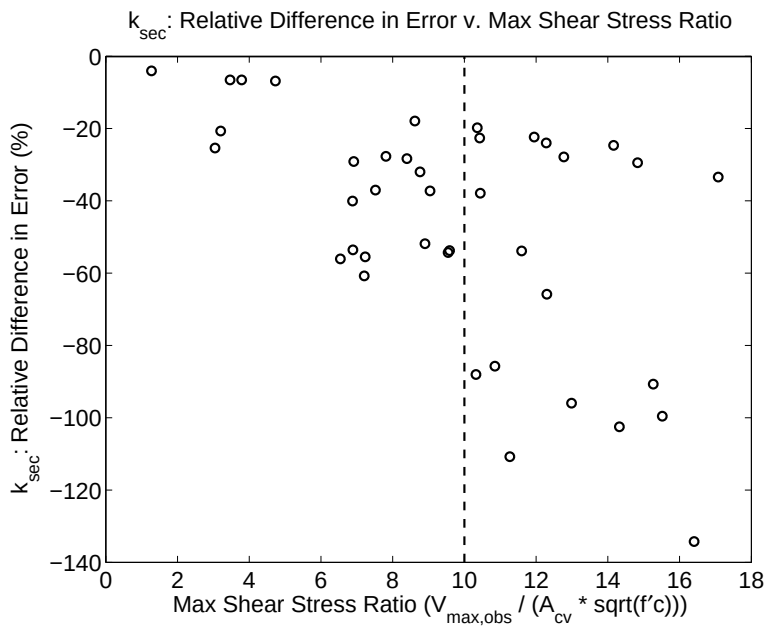

Figure K.11: Initial Stiffness Relative Error v Max Shear Stress Ratio

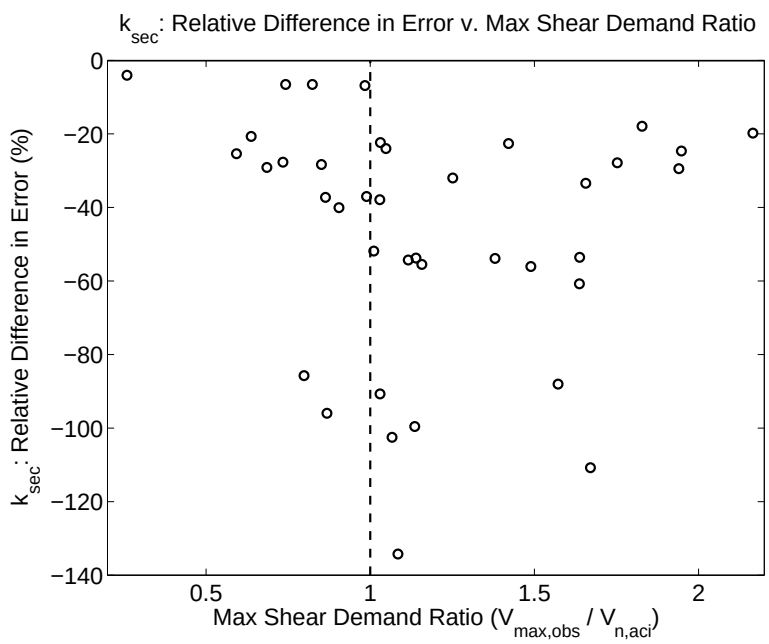

Figure K.12: Initial Stiffness Relative Error v Max Shear Demand Ratio

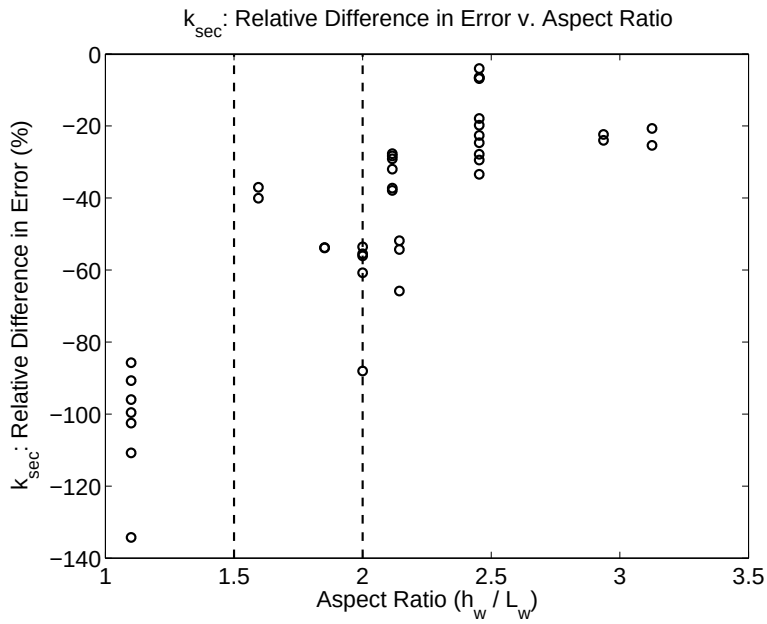

Figure K.13: Initial Stiffness Relative Error v Aspect Ratio

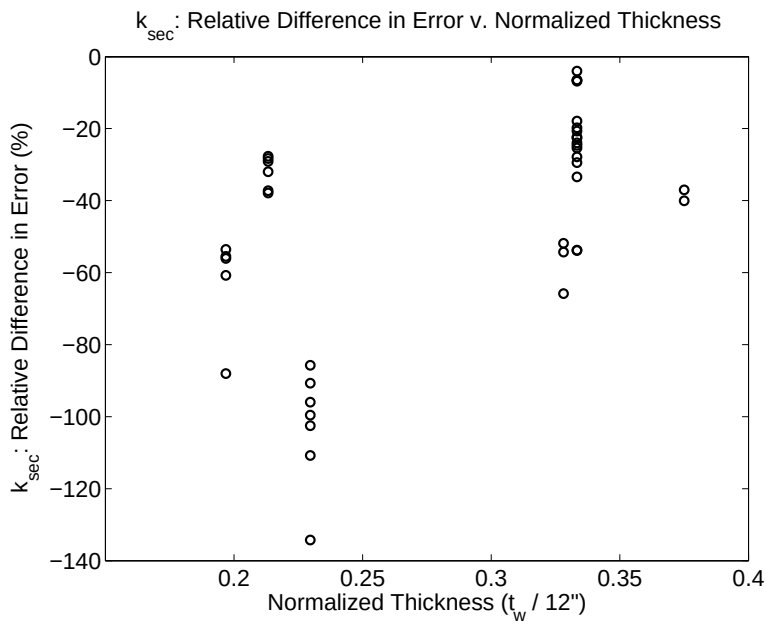

Figure K.14: Initial Stiffness Relative Error v Normalized Thickness

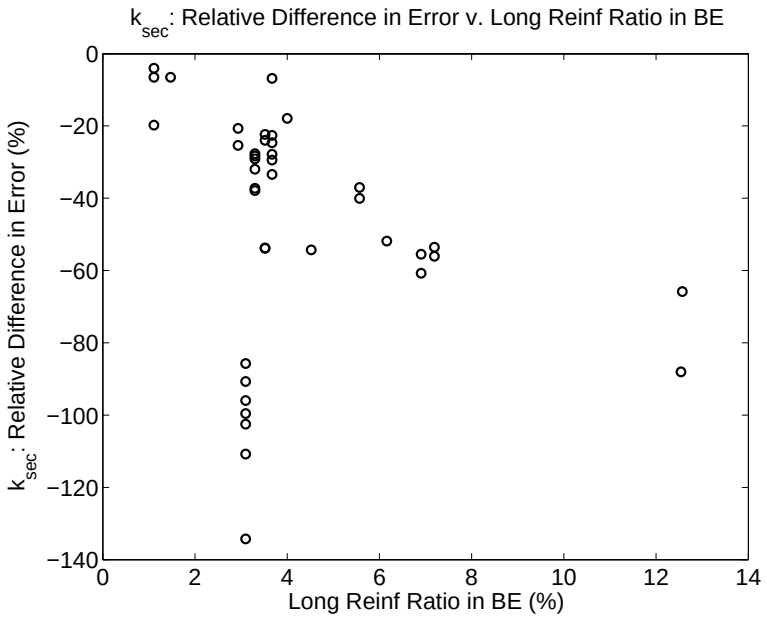

Figure K.15: Initial Stiffness Relative Error v Long Reinf Ratio in BE

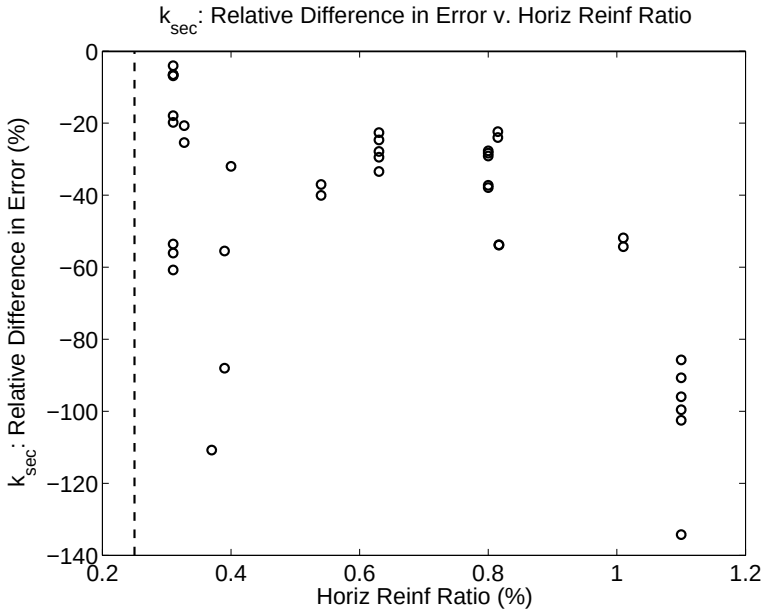

Figure K.16: Initial Stiffness Relative Error v Horiz Reinf Ratio

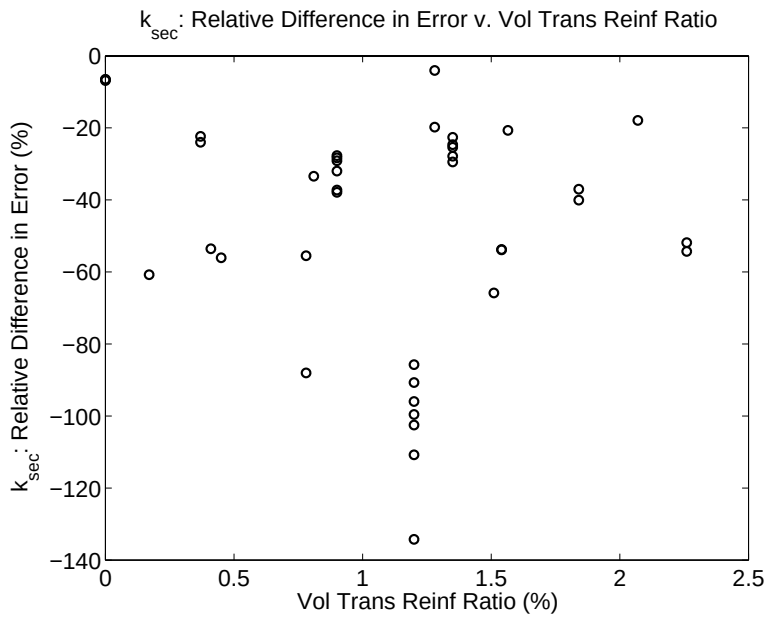

Figure K.17: Initial Stiffness Relative Error v Vol Trans Reinf Ratio

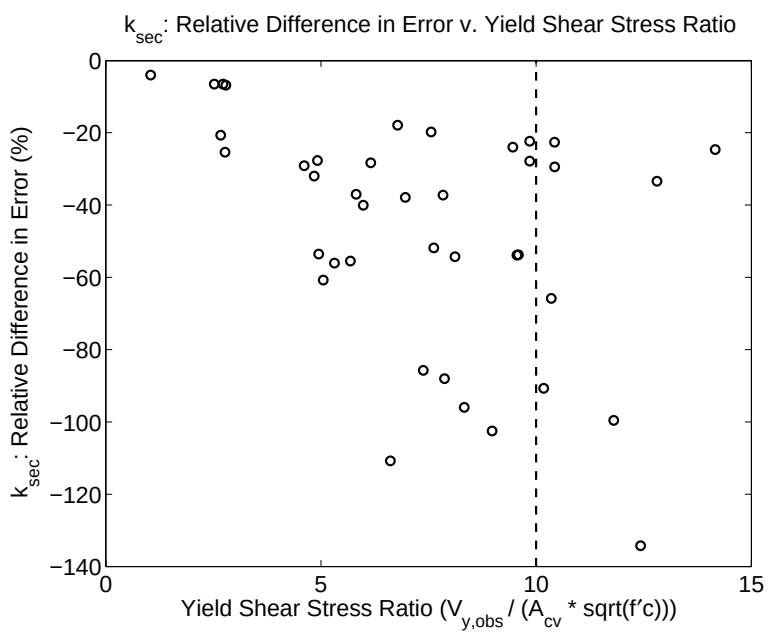

Figure K.18: Initial Stiffness Relative Error v Yield Shear Stress Ratio

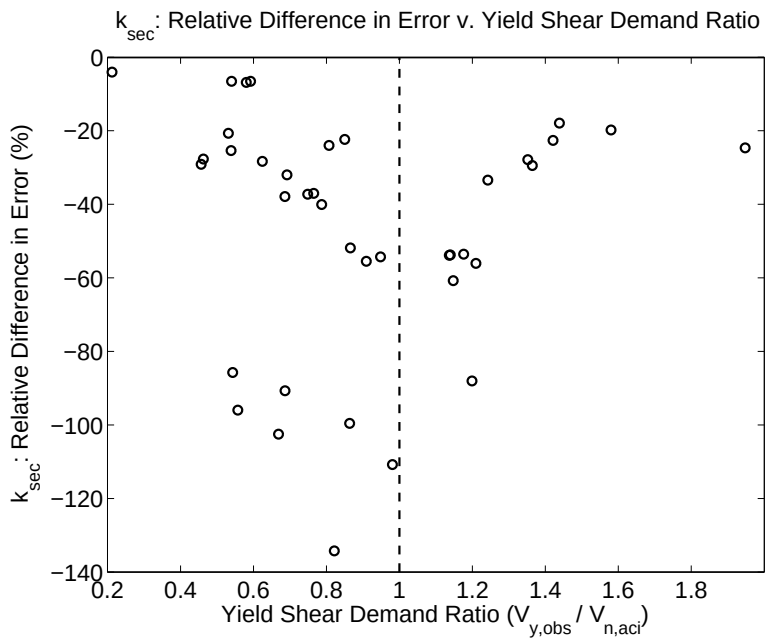

Figure K.19: Initial Stiffness Relative Error v Yield Shear Demand Ratio

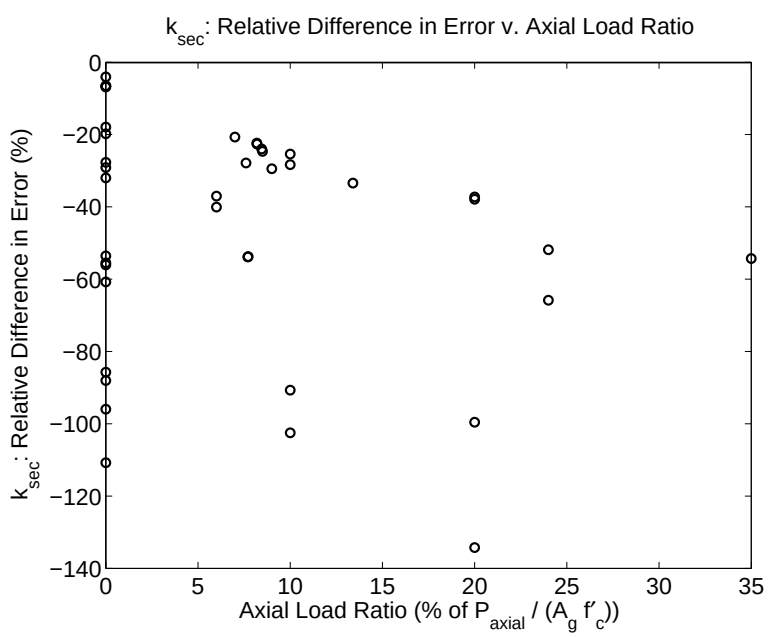

Figure K.20: Initial Stiffness Relative Error v Axial Load Ratio

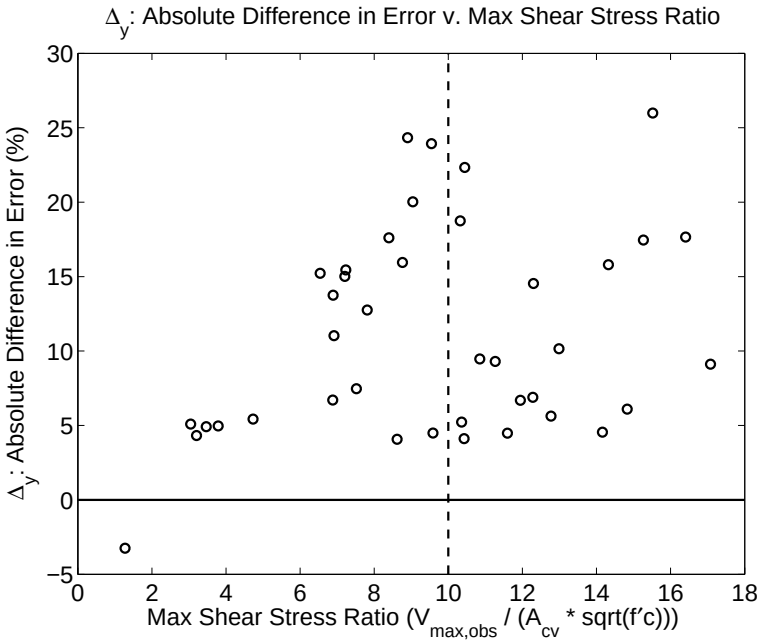

Figure K.21: Yield Displacement Absolute Error v Max Shear Stress Ratio

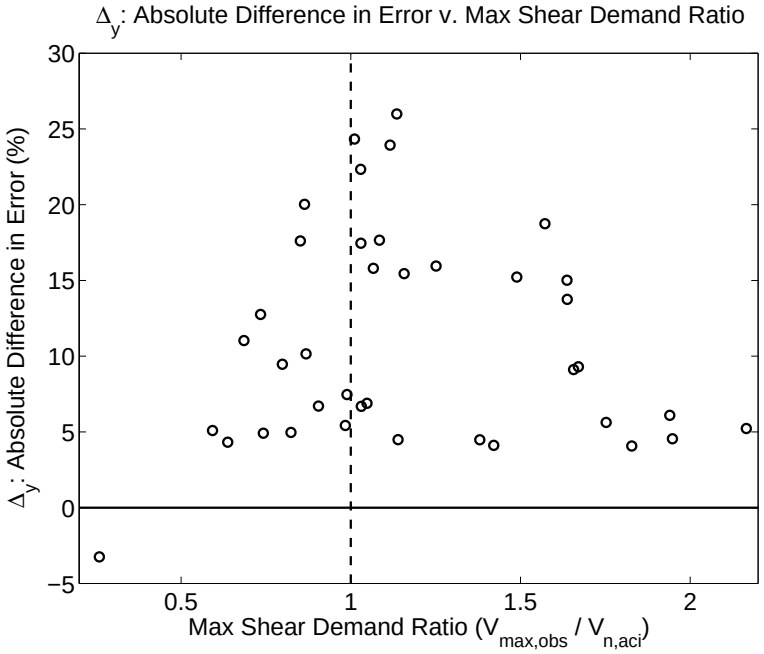

Figure K.22: Yield Displacement Absolute Error v Max Shear Demand Ratio

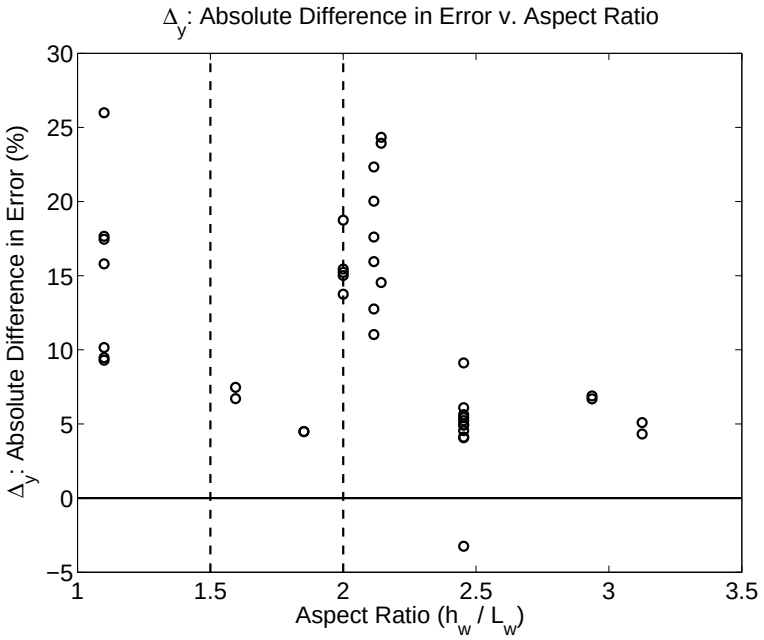

Figure K.23: Yield Displacement Absolute Error v Aspect Ratio

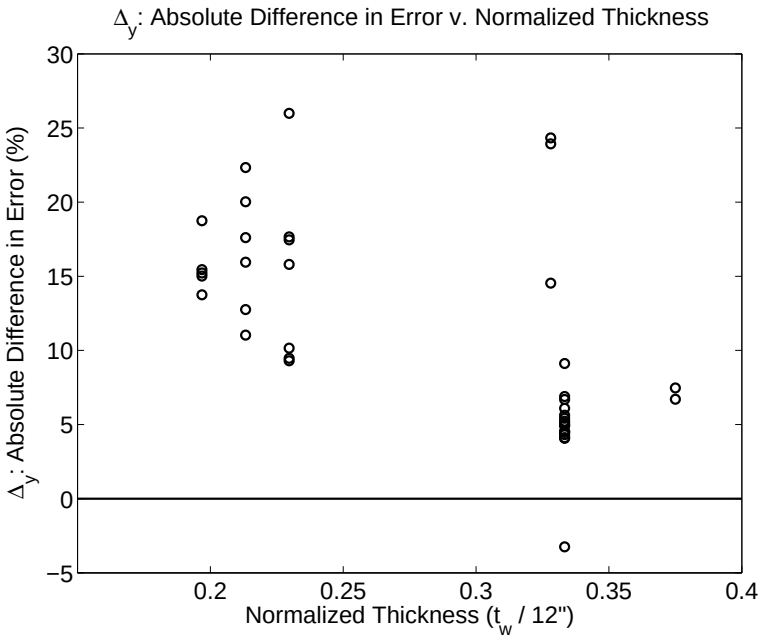

Figure K.24: Yield Displacement Absolute Error v Normalized Thickness

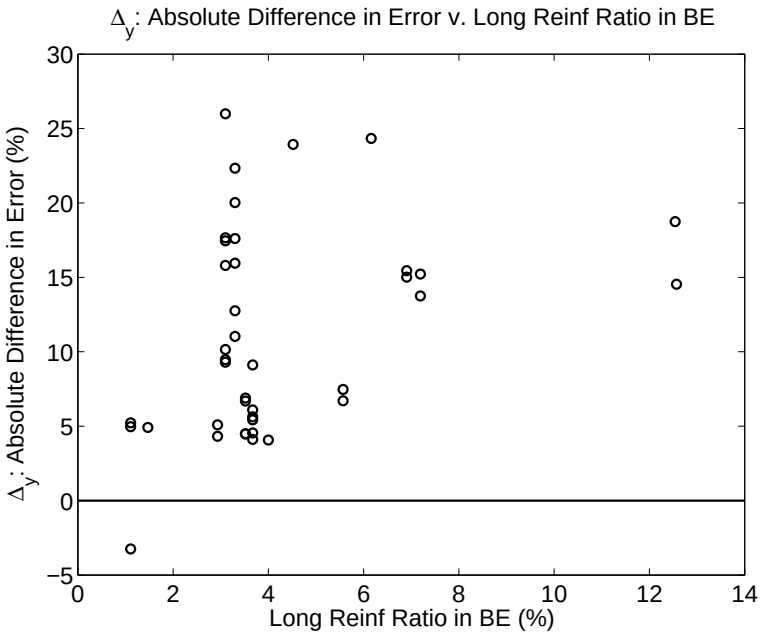

Figure K.25: Yield Displacement Absolute Error v Long Reinf Ratio in BE

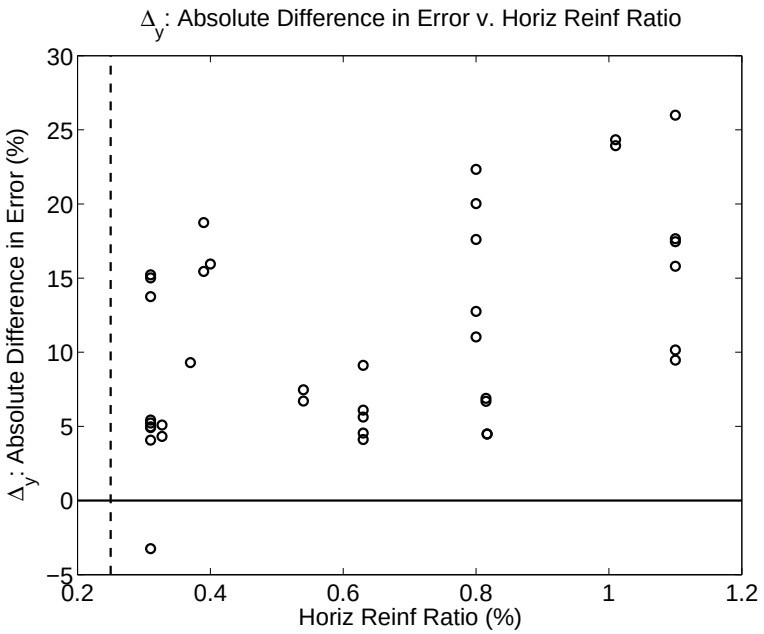

Figure K.26: Yield Displacement Absolute Error v Horiz Reinf Ratio

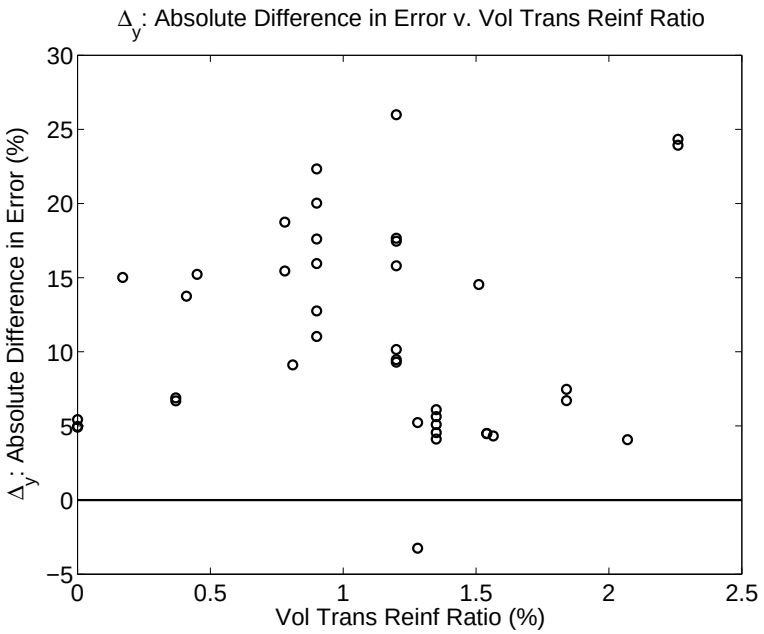

Figure K.27: Yield Displacement Absolute Error v Vol Trans Reinf Ratio

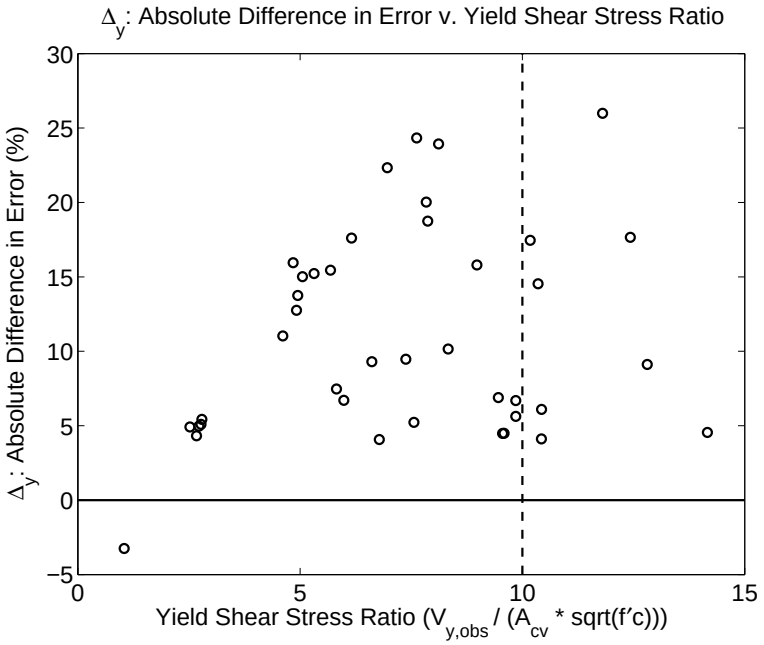

Figure K.28: Yield Displacement Absolute Error v Yield Shear Stress Ratio

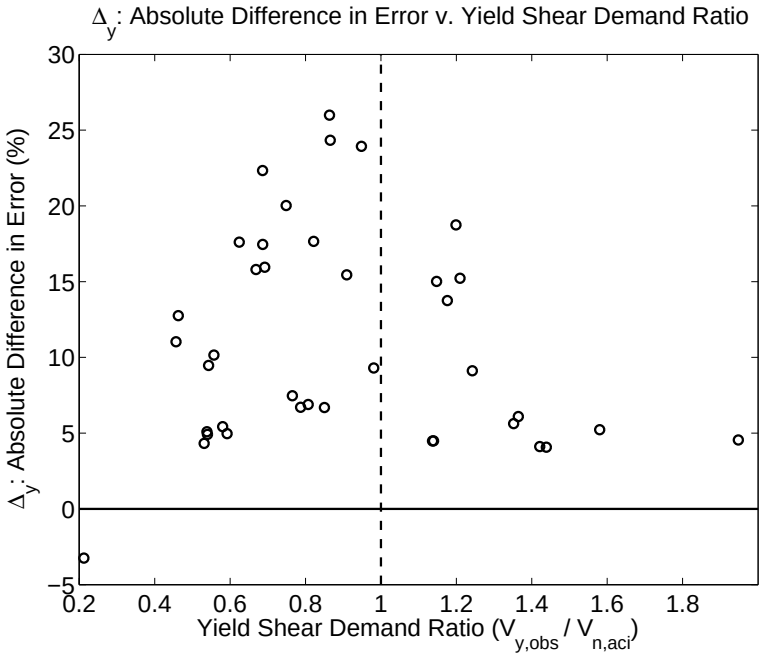

Figure K.29: Yield Displacement Absolute Error v Yield Shear Demand Ratio

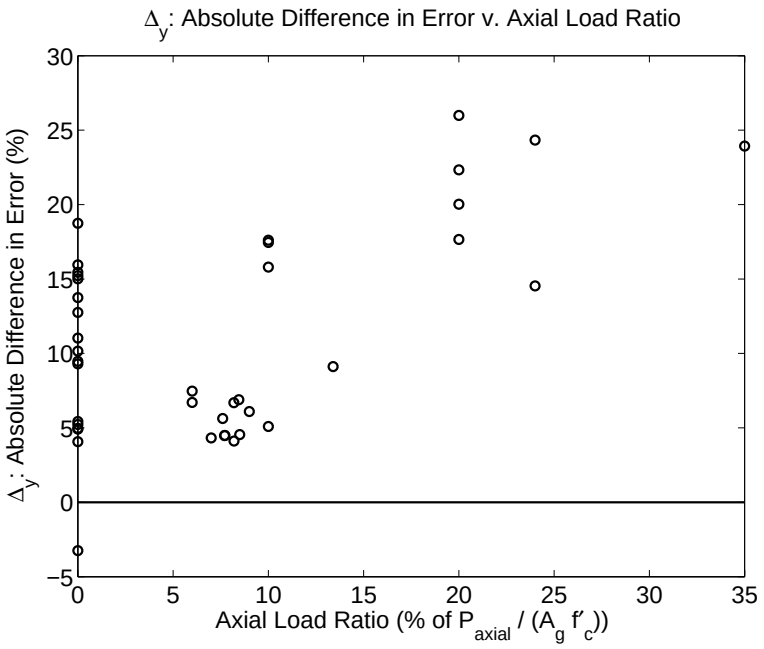

Figure K.30: Yield Displacement Absolute Error v Axial Load Ratio

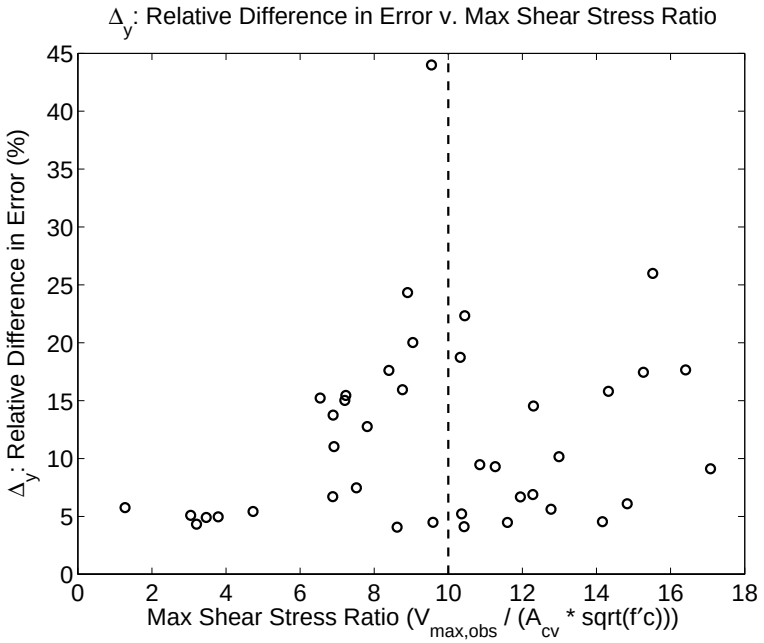

Figure K.31: Yield Displacement Relative Error v Max Shear Stress Ratio

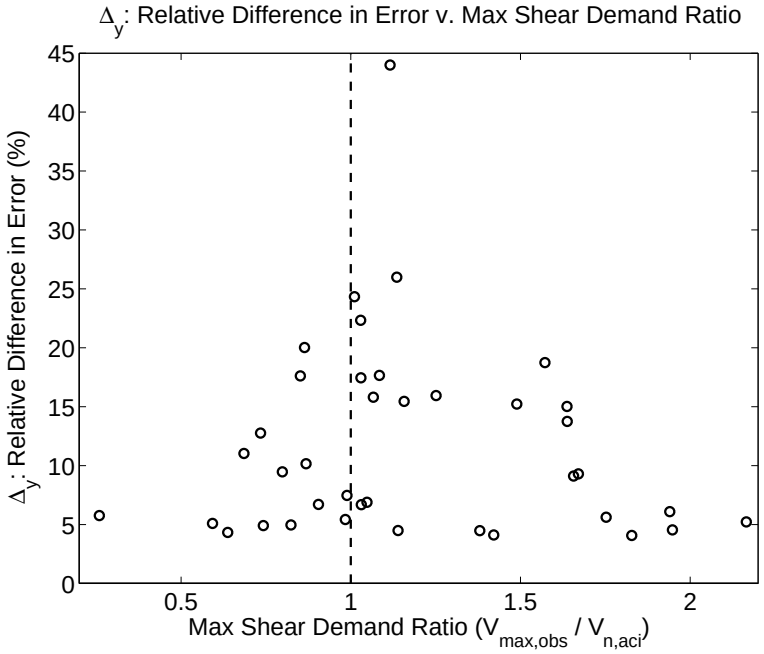

Figure K.32: Yield Displacement Relative Error v Max Shear Demand Ratio

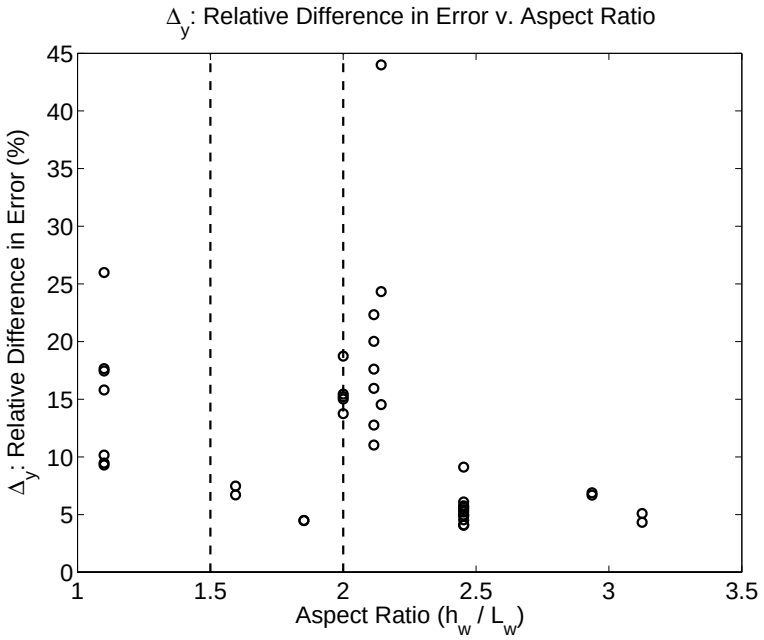

Figure K.33: Yield Displacement Relative Error v Aspect Ratio

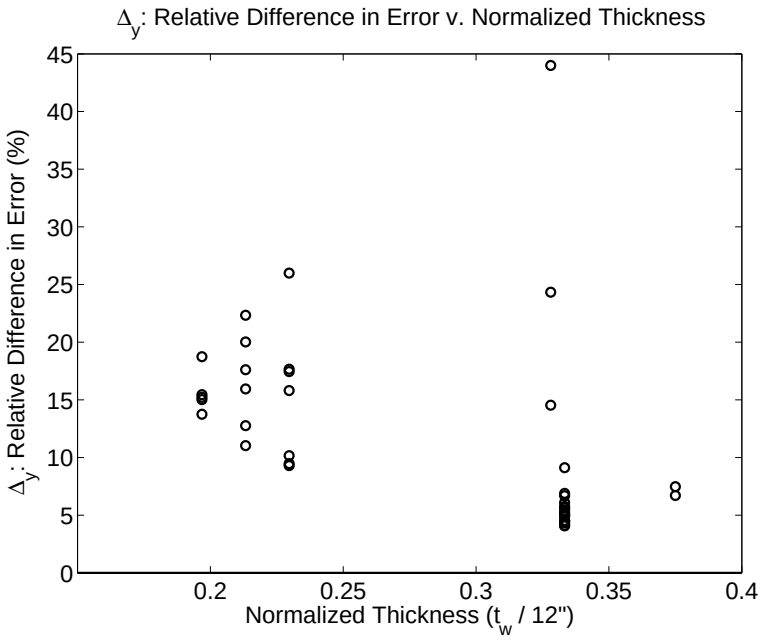

Figure K.34: Yield Displacement Relative Error v Normalized Thickness

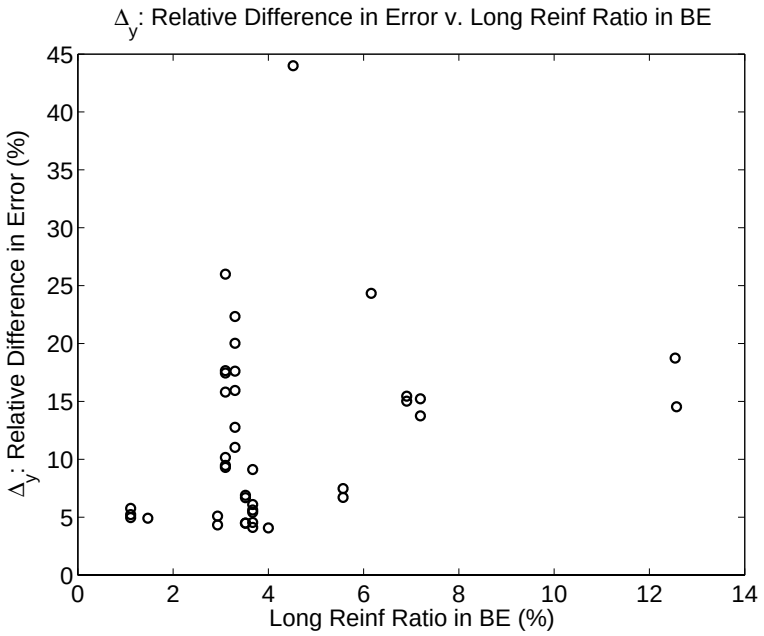

Figure K.35: Yield Displacement Relative Error v Long Reinf Ratio in BE

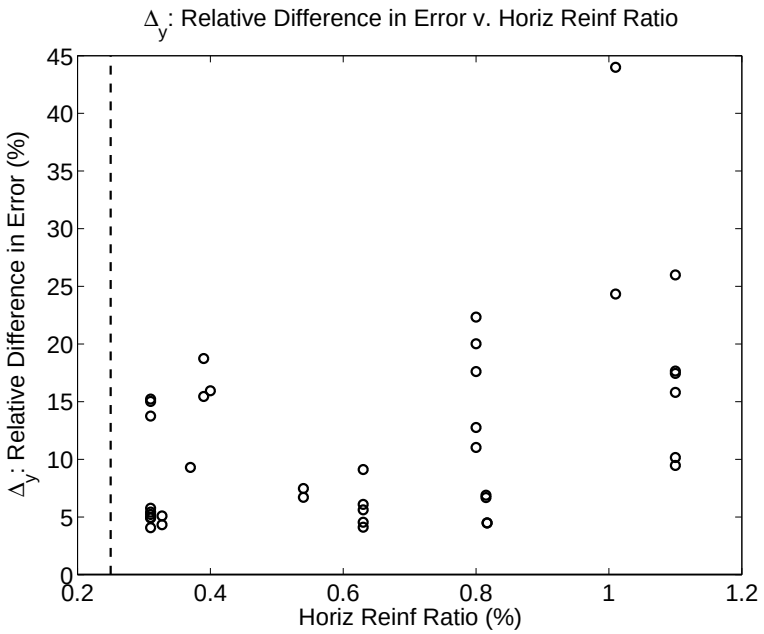

Figure K.36: Yield Displacement Relative Error v Horiz Reinf Ratio

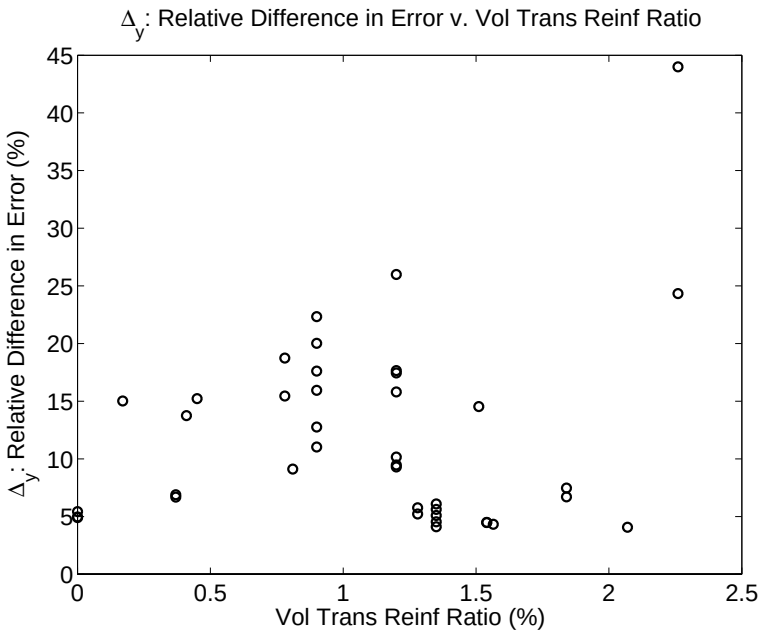

Figure K.37: Yield Displacement Relative Error v Vol Trans Reinf Ratio

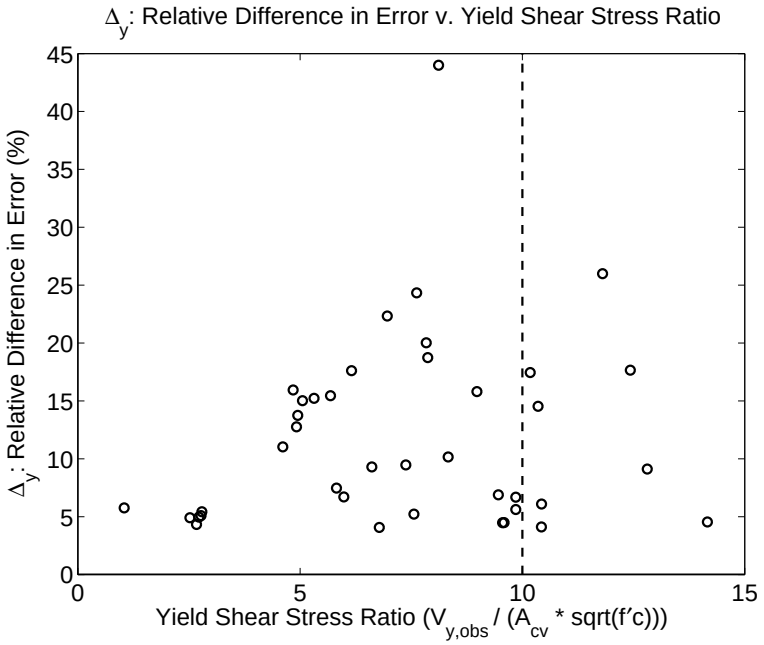

Figure K.38: Yield Displacement Relative Error v Yield Shear Stress Ratio

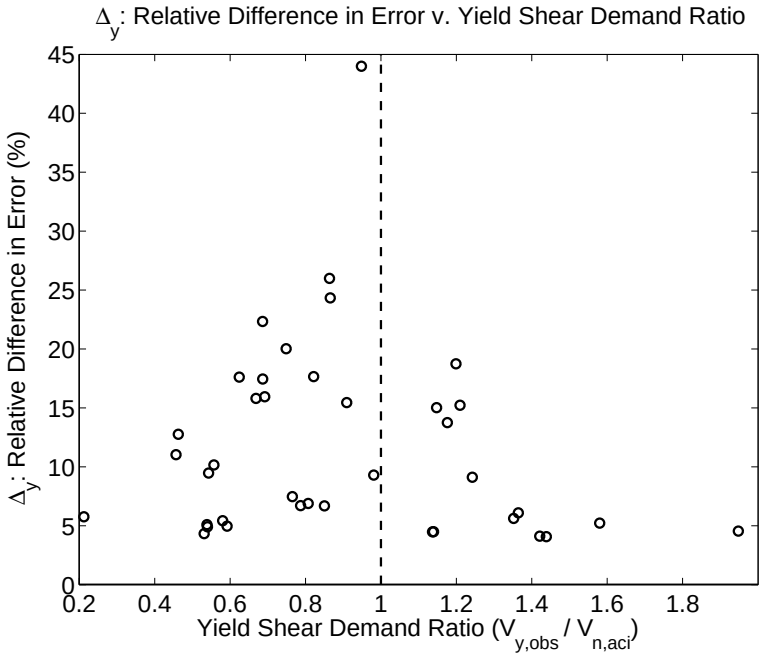

Figure K.39: Yield Displacement Relative Error v Yield Shear Demand Ratio

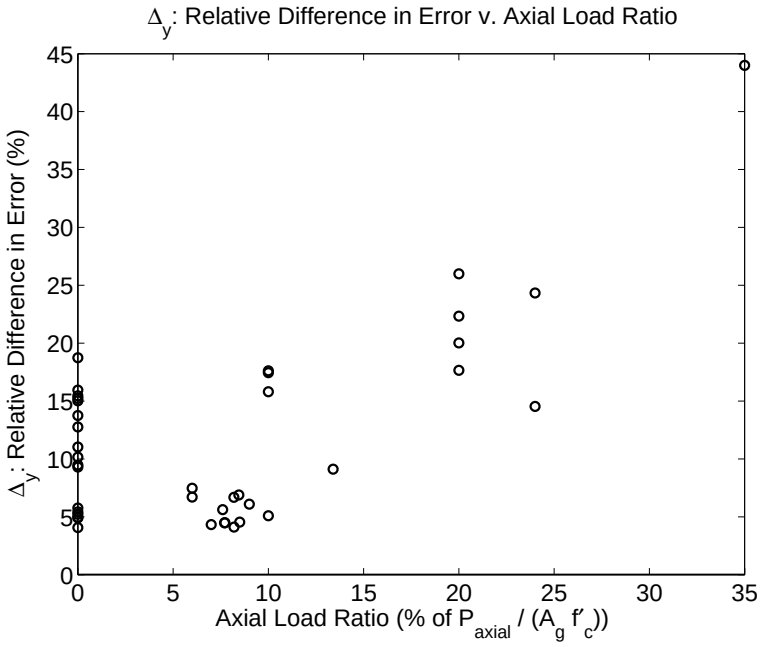

Figure K.40: Yield Displacement Relative Error v Axial Load Ratio

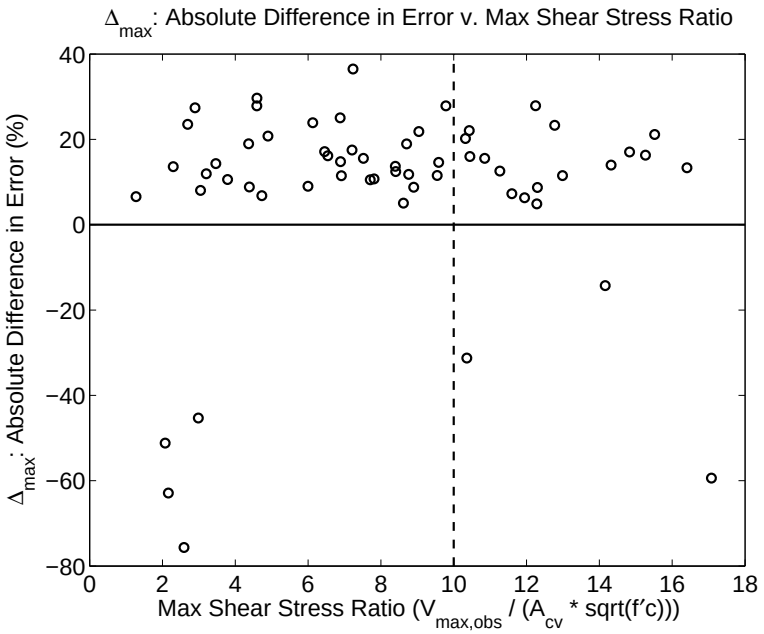

Figure K.41: Max Displacement Absolute Error v Max Shear Stress Ratio

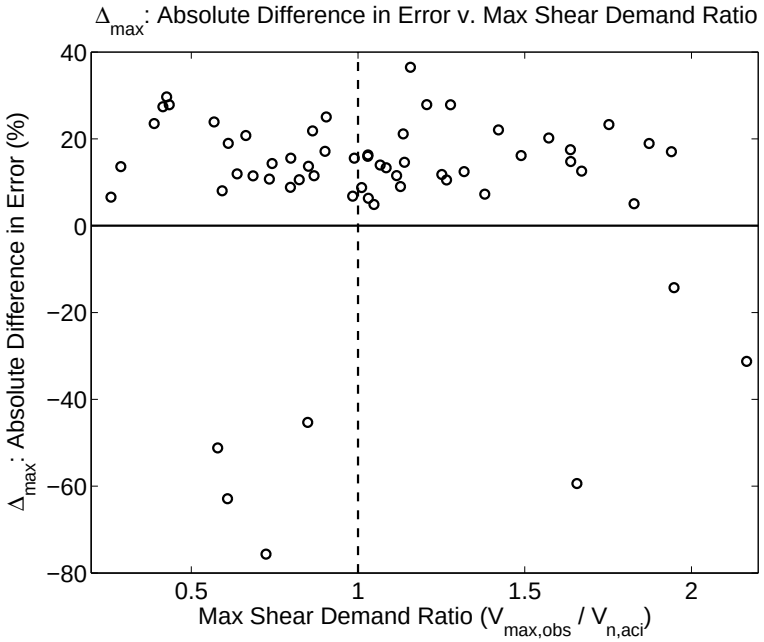

Figure K.42: Max Displacement Absolute Error v Max Shear Demand Ratio

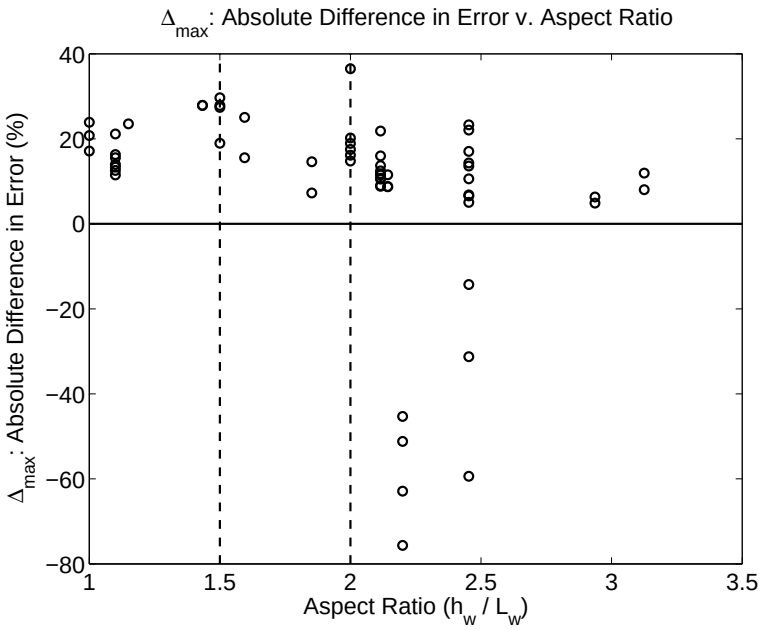

Figure K.43: Max Displacement Absolute Error v Aspect Ratio

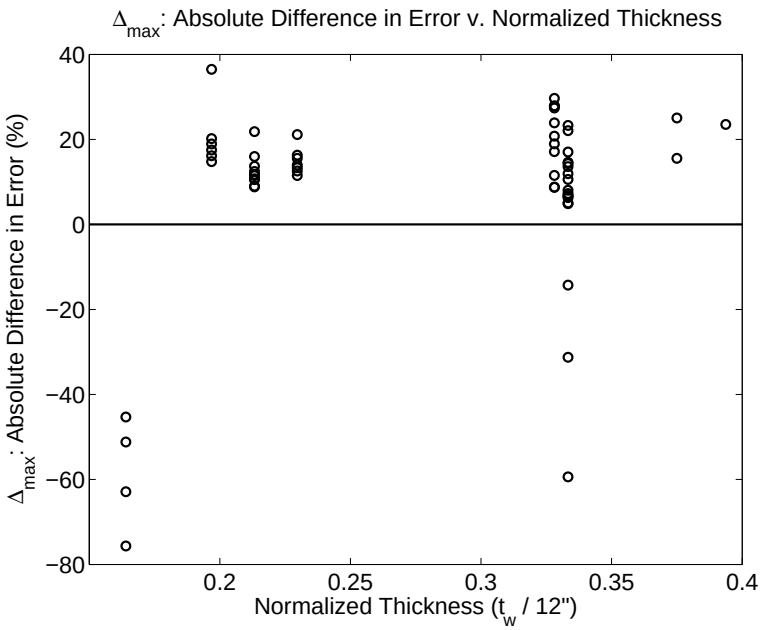

Figure K.44: Max Displacement Absolute Error v Normalized Thickness

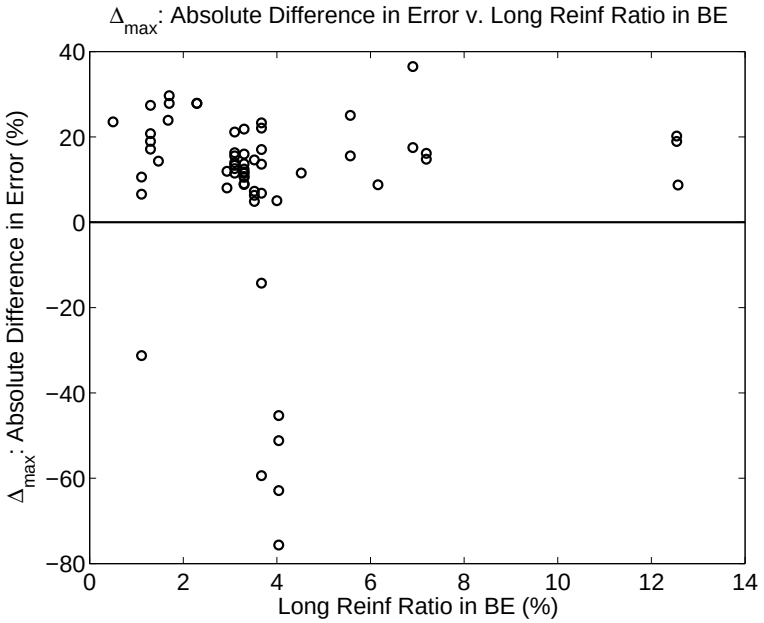

Figure K.45: Max Displacement Absolute Error v Long Reinf Ratio in BE

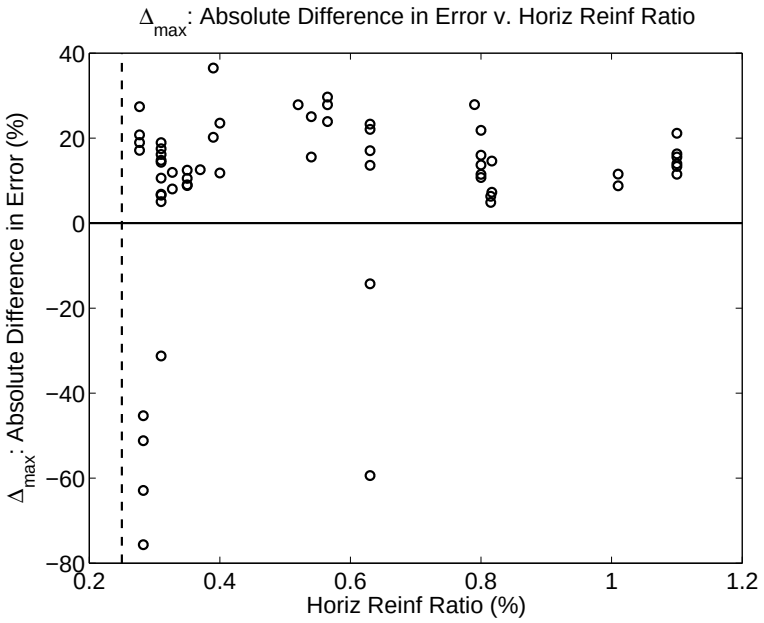

Figure K.46: Max Displacement Absolute Error v Horiz Reinf Ratio

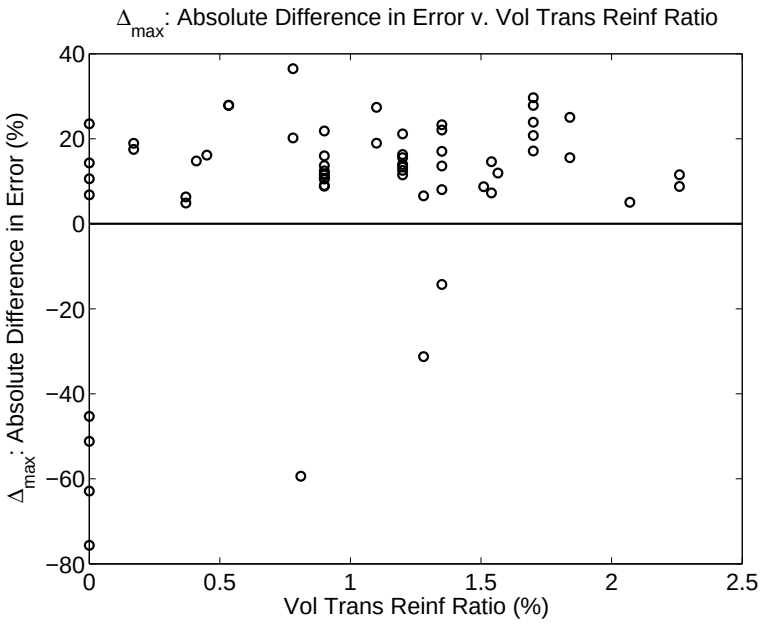

Figure K.47: Max Displacement Absolute Error v Vol Trans Reinf Ratio

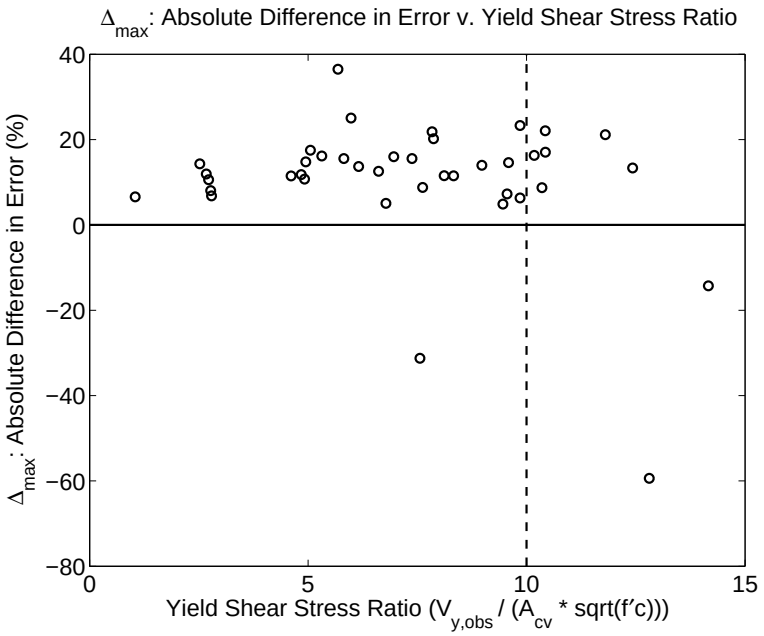

Figure K.48: Max Displacement Absolute Error v Yield Shear Stress Ratio

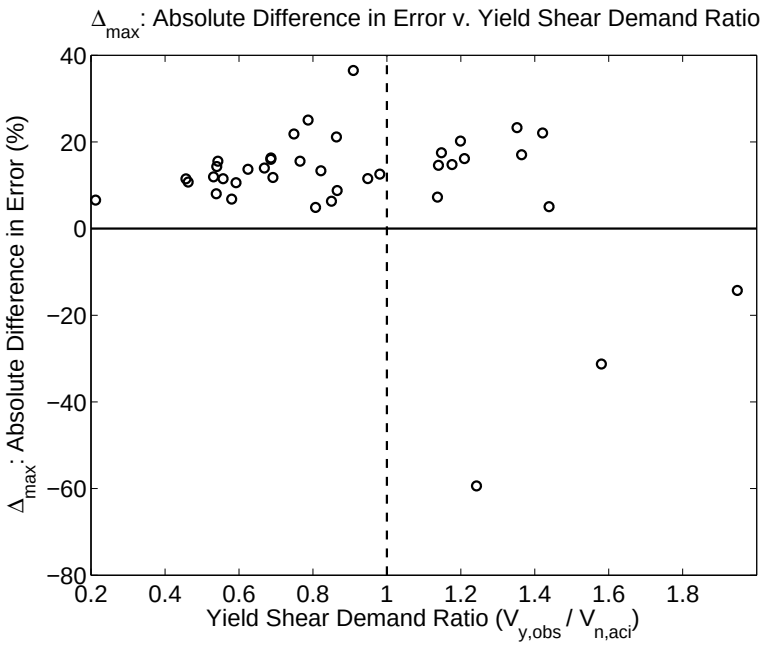

Figure K.49: Max Displacement Absolute Error v Yield Shear Demand Ratio

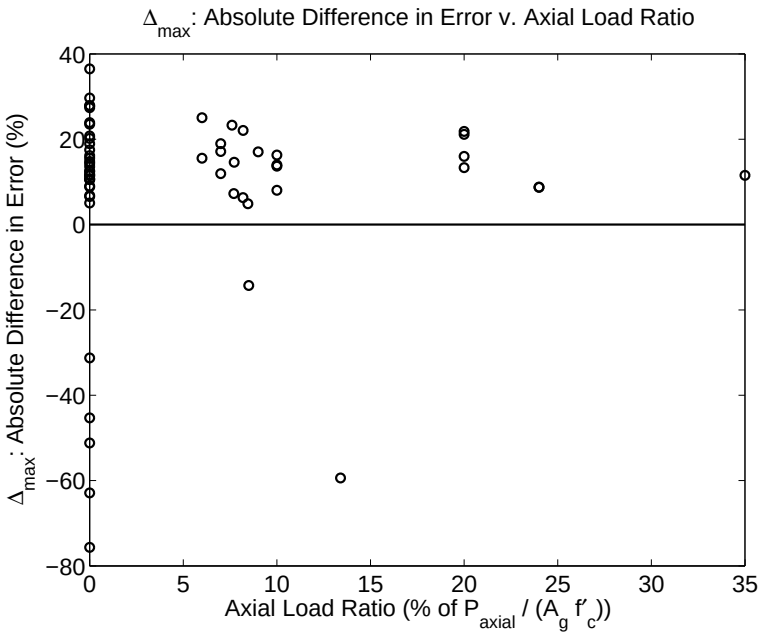

Figure K.50: Max Displacement Absolute Error v Axial Load Ratio

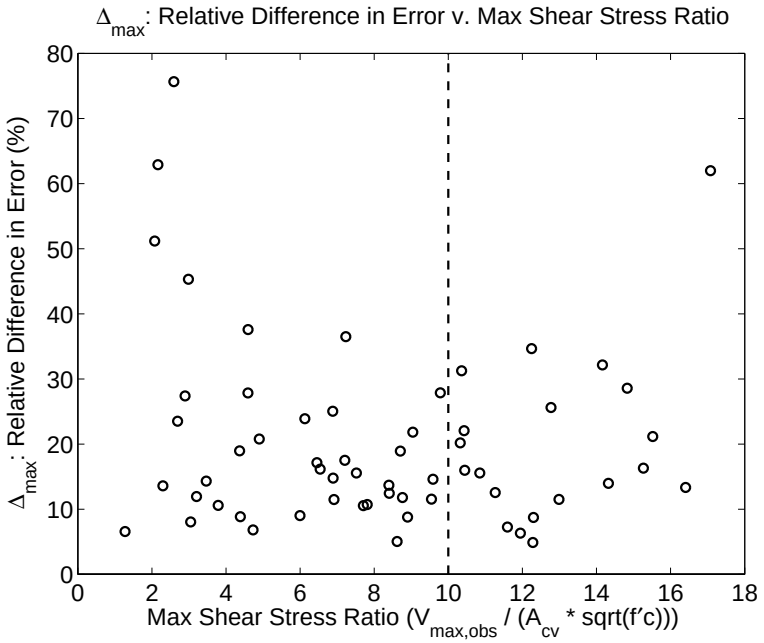

Figure K.51: Max Displacement Relative Error v Max Shear Stress Ratio

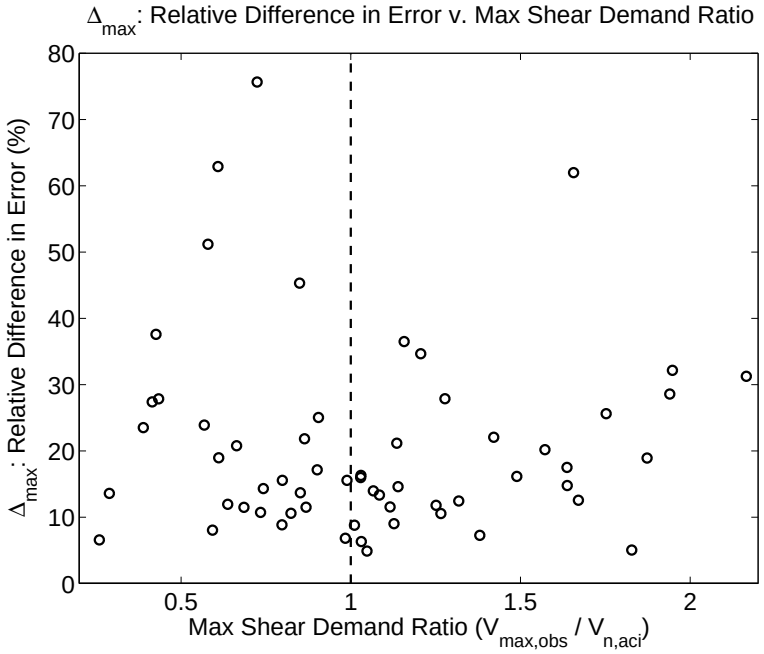

Figure K.52: Max Displacement Relative Error v Max Shear Demand Ratio

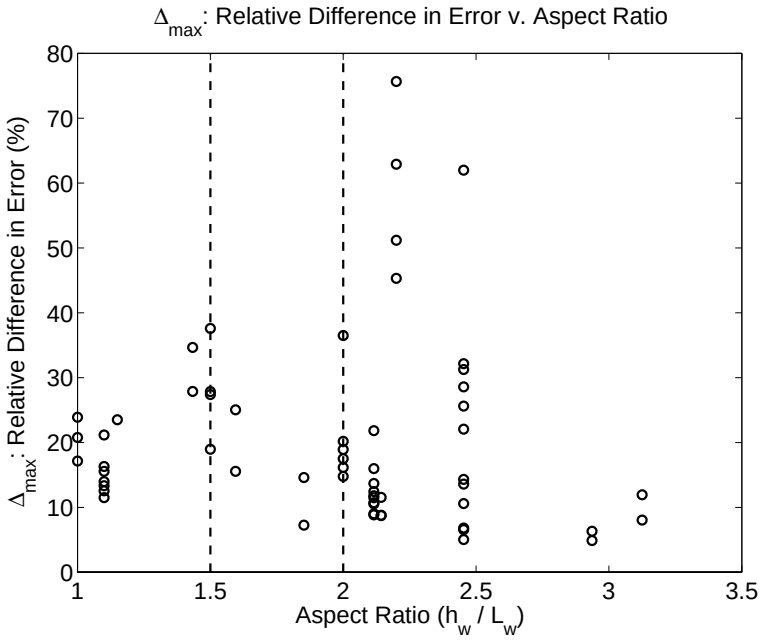

Figure K.53: Max Displacement Relative Error v Aspect Ratio

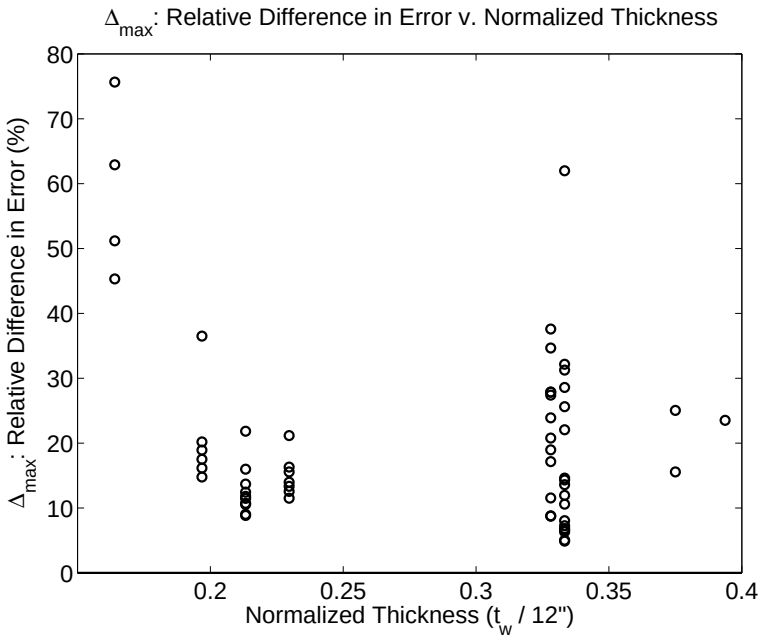

Figure K.54: Max Displacement Relative Error v Normalized Thickness

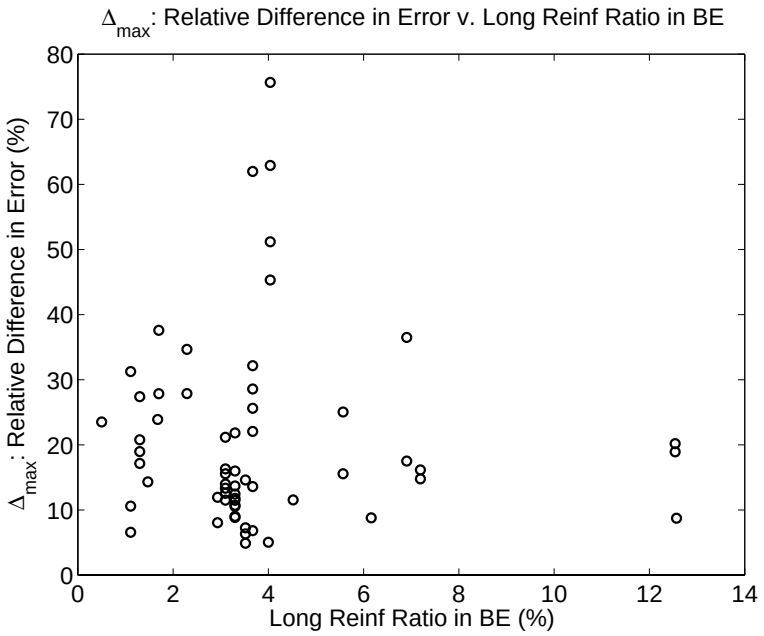

Figure K.55: Max Displacement Relative Error v Long Reinf Ratio in BE

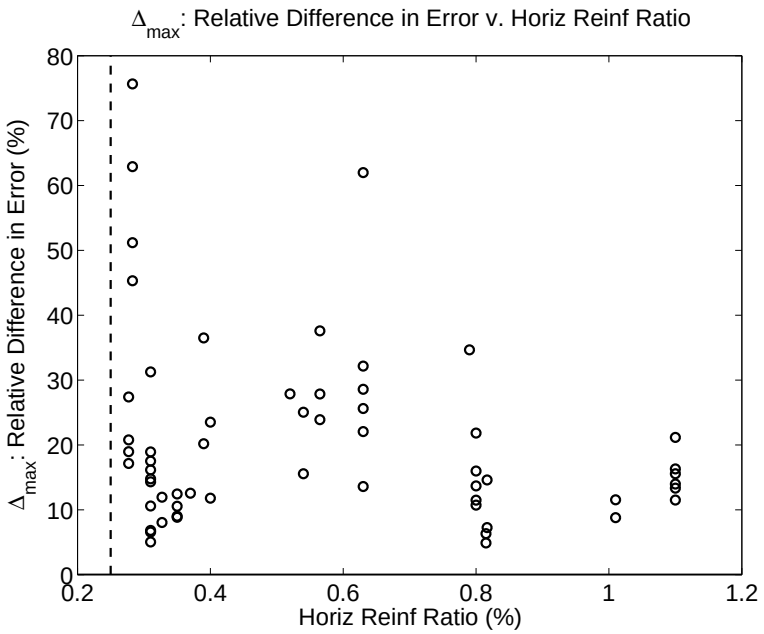

Figure K.56: Max Displacement Relative Error v Horiz Reinf Ratio

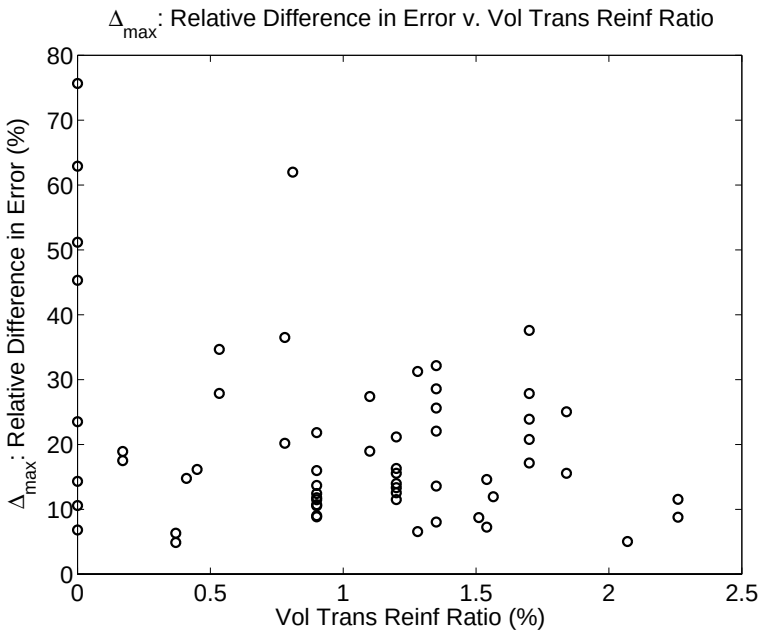

Figure K.57: Max Displacement Relative Error v Vol Trans Reinf Ratio

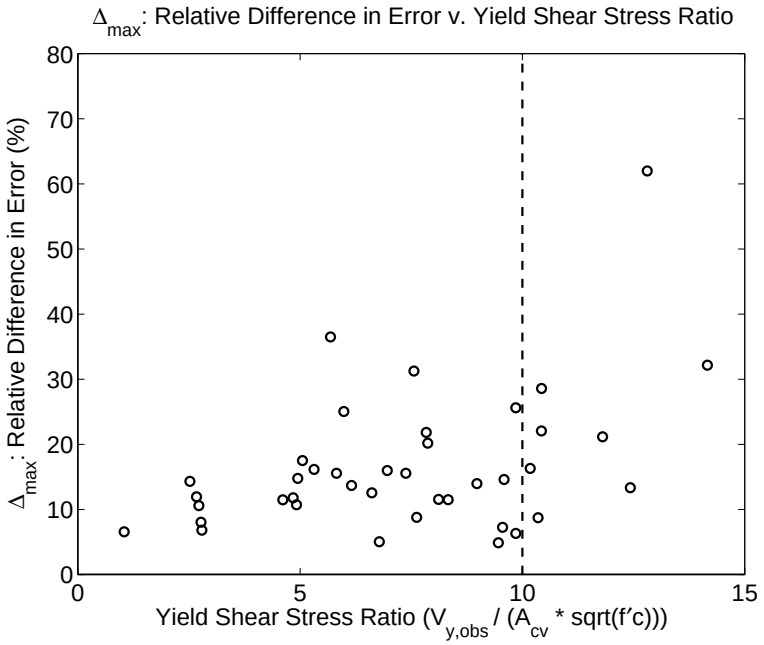

Figure K.58: Max Displacement Relative Error v Yield Shear Stress Ratio

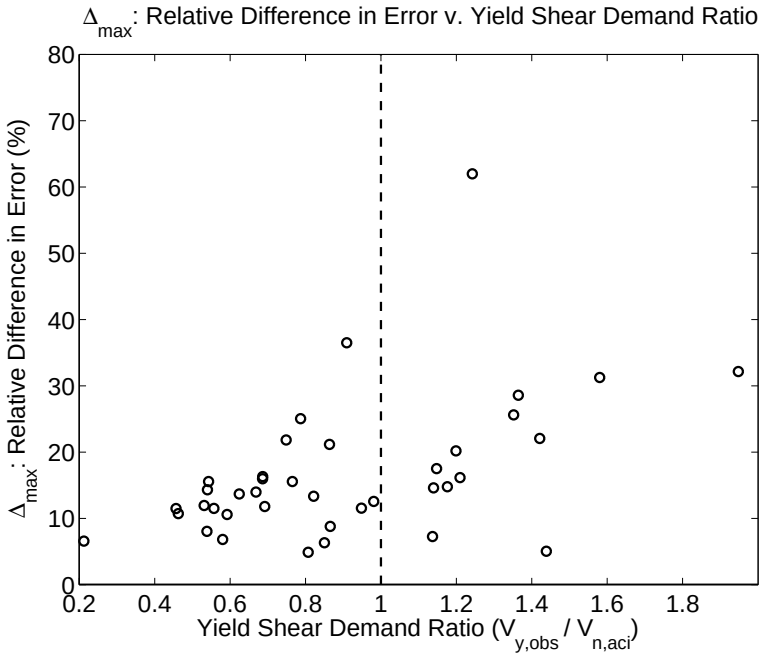

Figure K.59: Max Displacement Relative Error v Yield Shear Demand Ratio

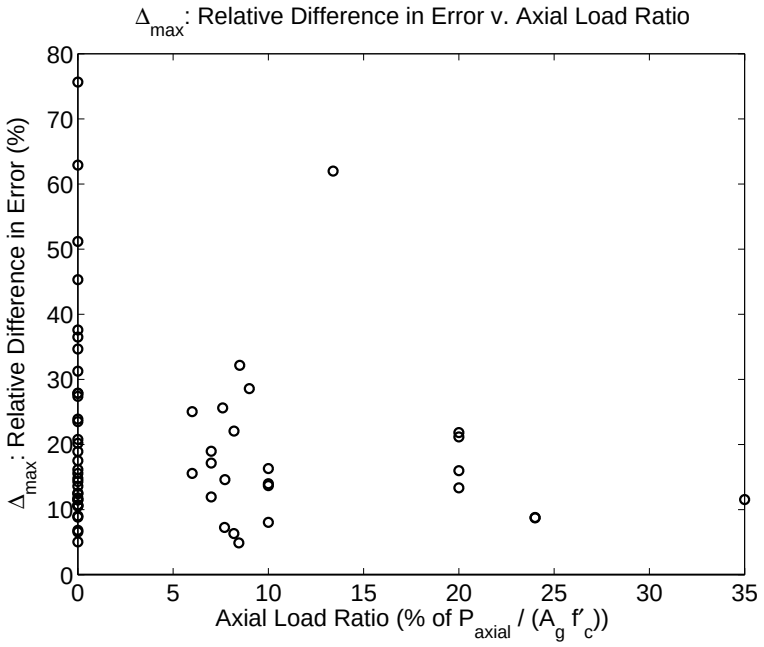

Figure K.60: Max Displacement Relative Error v Axial Load Ratio

Appendix L

EFFECTIVE SHEAR MODEL PREDICTIONS COMPARED TO DESIGN PARAMETER FIGURES

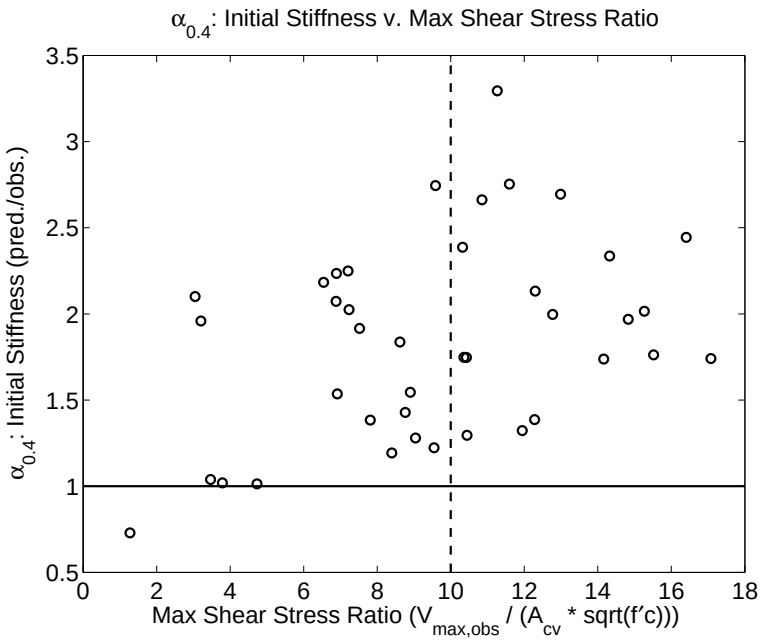

Figure L.1: Beam-Column With Shear Initial Stiffness v Max Shear Stress Ratio

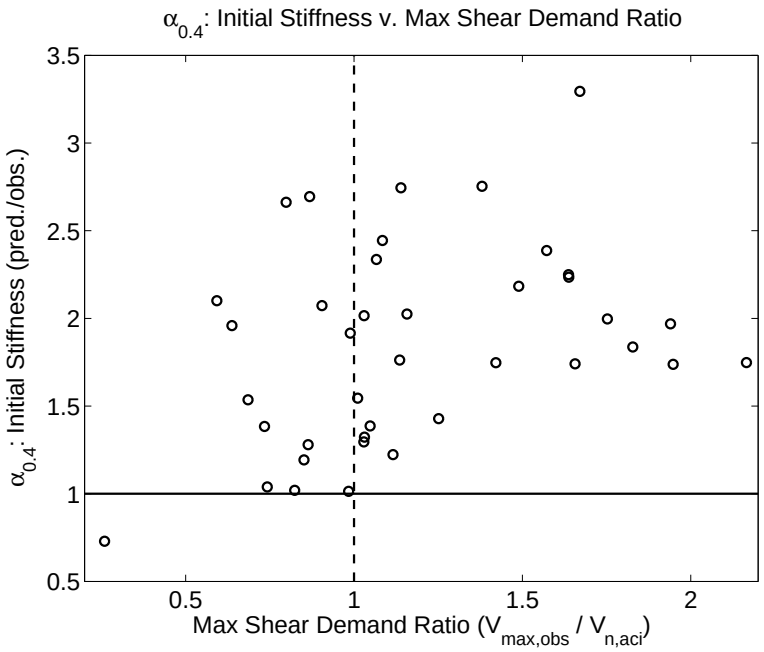

Figure L.2: Beam-Column With Shear Initial Stiffness v Max Shear Demand Ratio

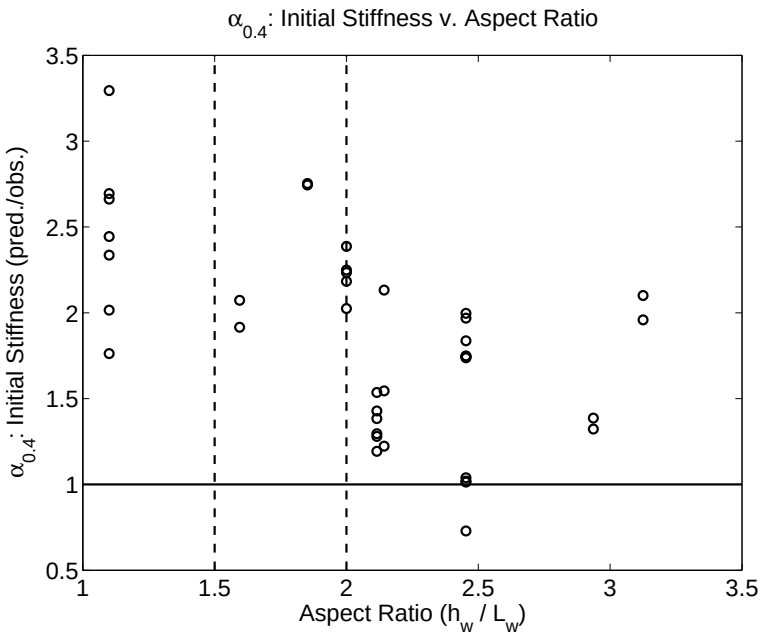

Figure L.3: Beam-Column With Shear Initial Stiffness v Aspect Ratio

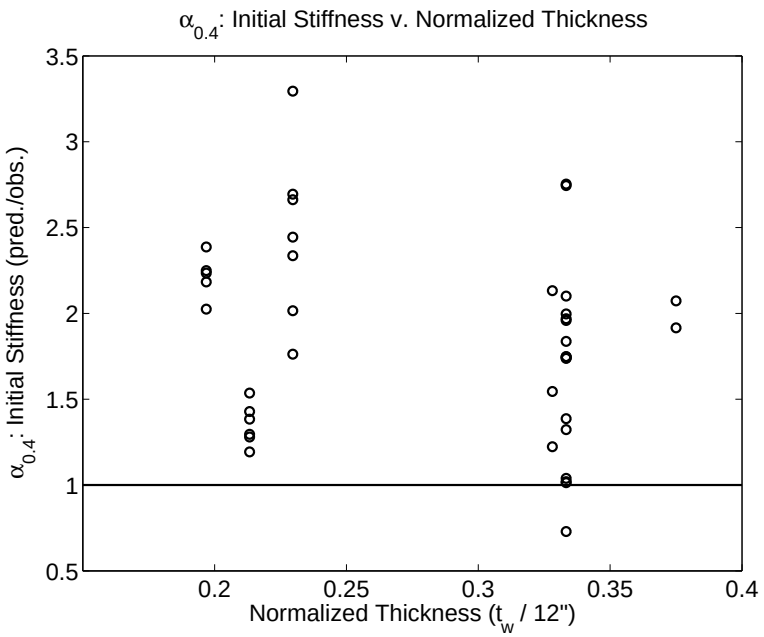

Figure L.4: Beam-Column With Shear Initial Stiffness v Normalized Thickness

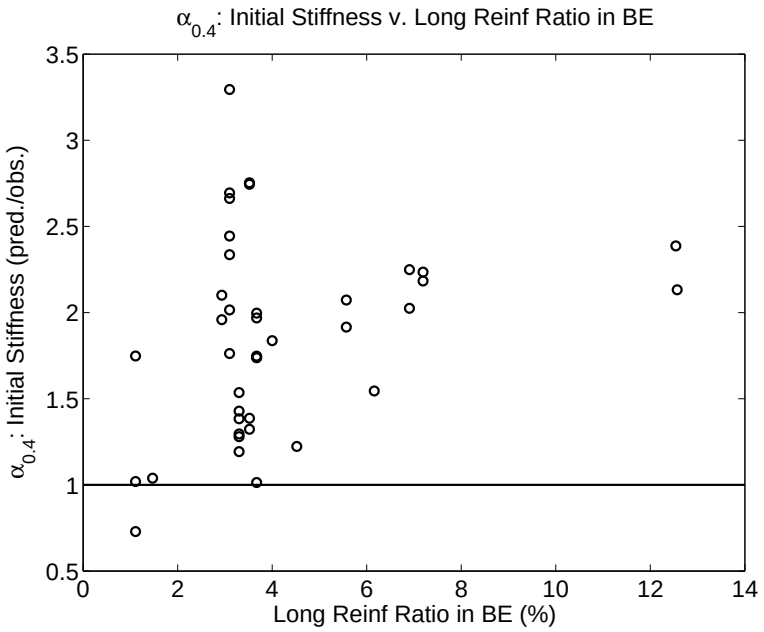

Figure L.5: Beam-Column With Shear Initial Stiffness v Long Reinf Ratio in BE

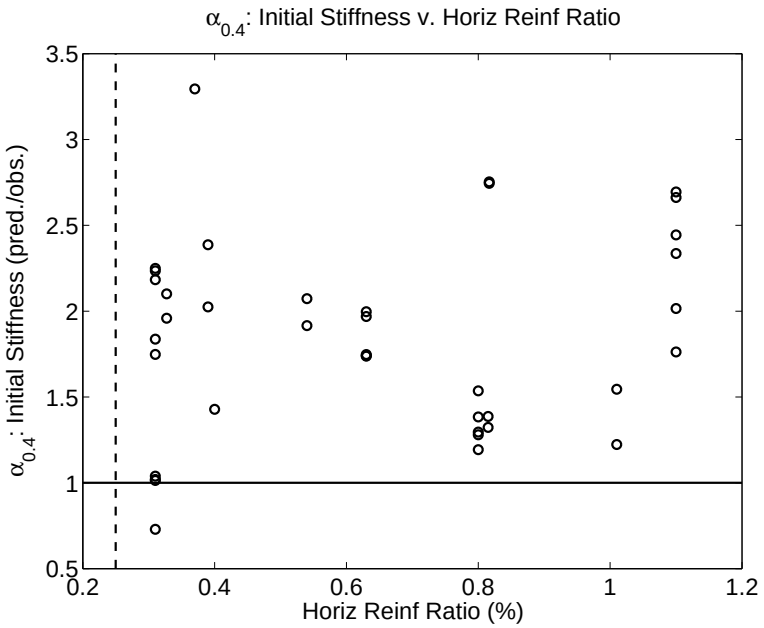

Figure L.6: Beam-Column With Shear Initial Stiffness v Horiz Reinf Ratio

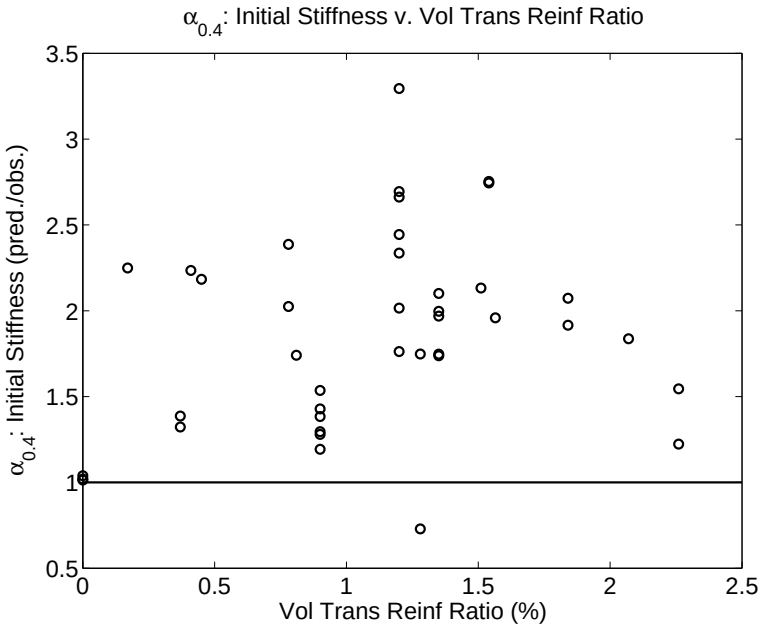

Figure L.7: Beam-Column With Shear Initial Stiffness v Vol Trans Reinf Ratio

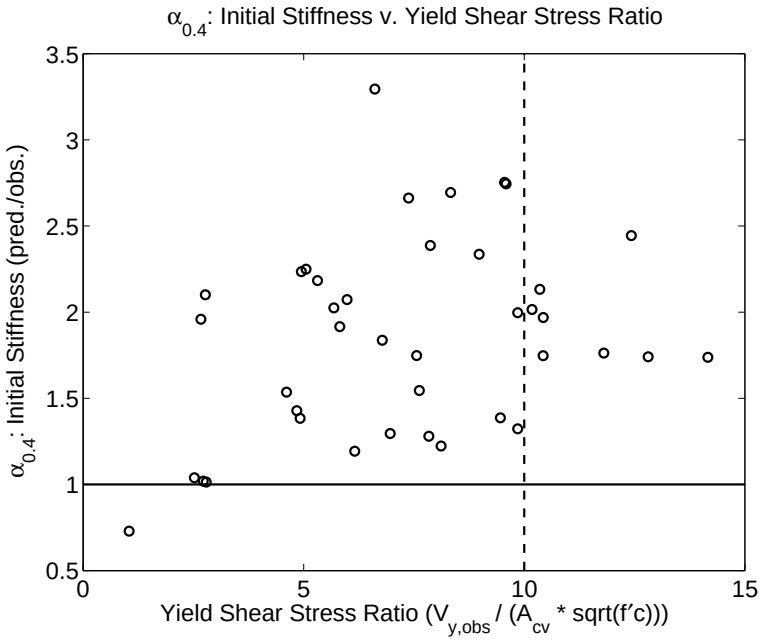

Figure L.8: Beam-Column With Shear Initial Stiffness v Yield Shear Stress Ratio

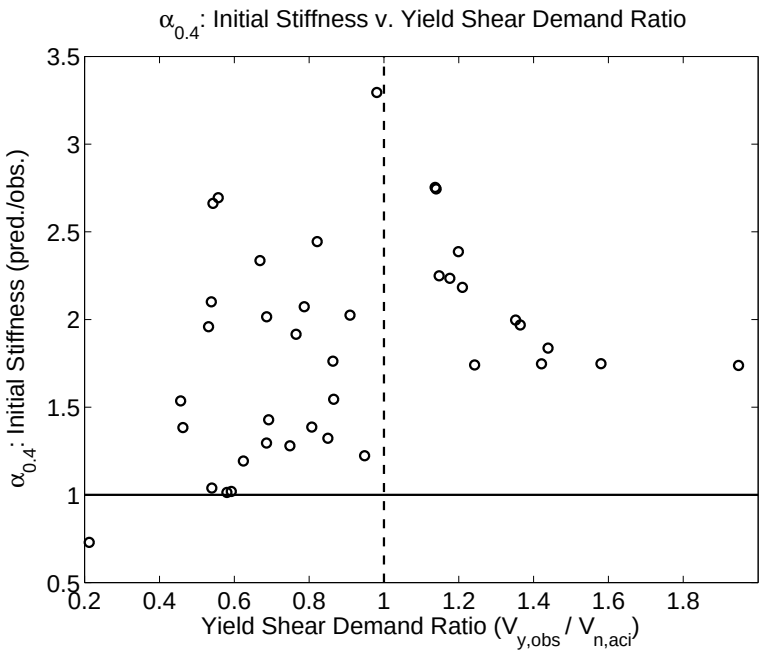

Figure L.9: Beam-Column With Shear Initial Stiffness v Yield Shear Demand Ratio

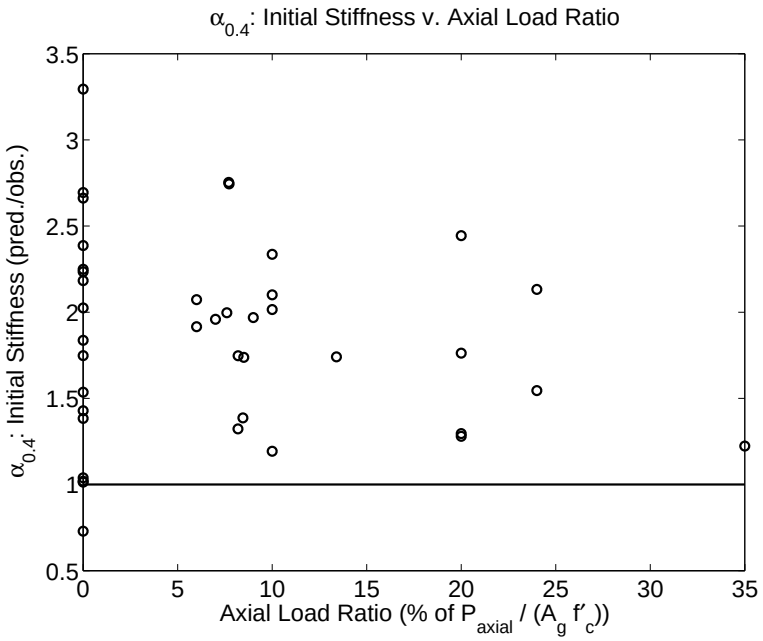

Figure L.10: Beam-Column With Shear Initial Stiffness v Axial Load Ratio

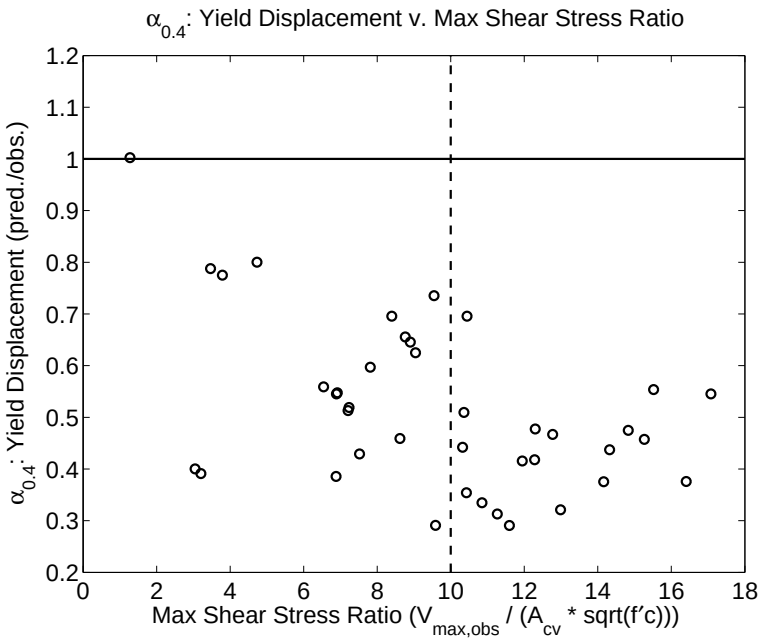

Figure L.11: Beam-Column With Shear Yield Displacement v Max Shear Stress Ratio

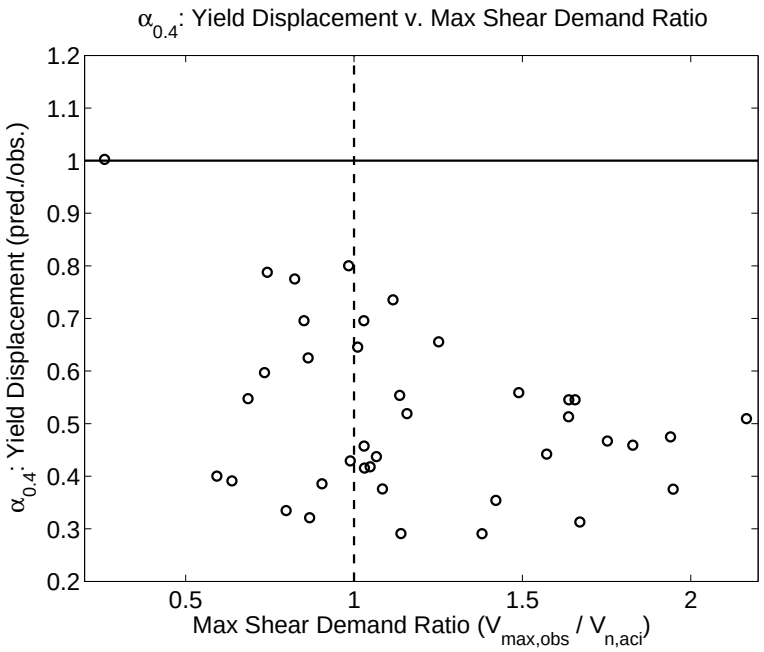

Figure L.12: Beam-Column With Shear Yield Displacement v Max Shear Demand Ratio

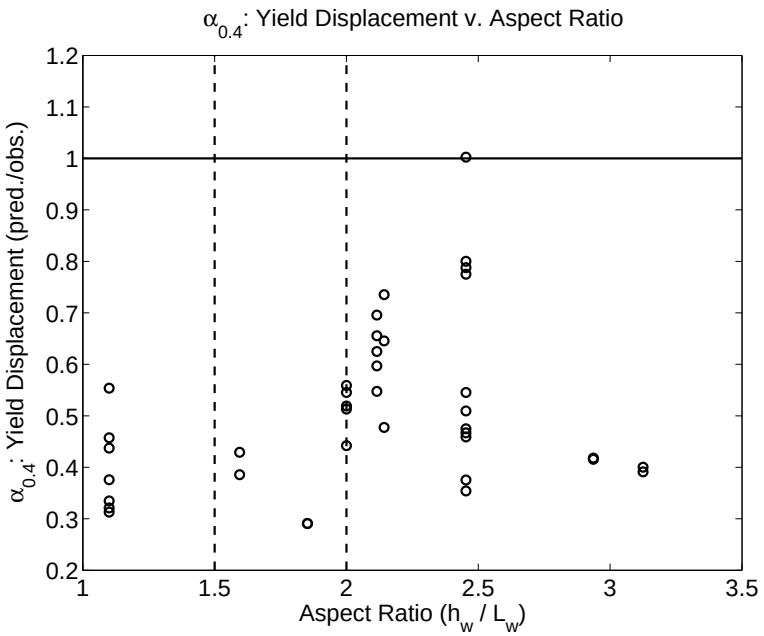

Figure L.13: Beam-Column With Shear Yield Displacement v Aspect Ratio

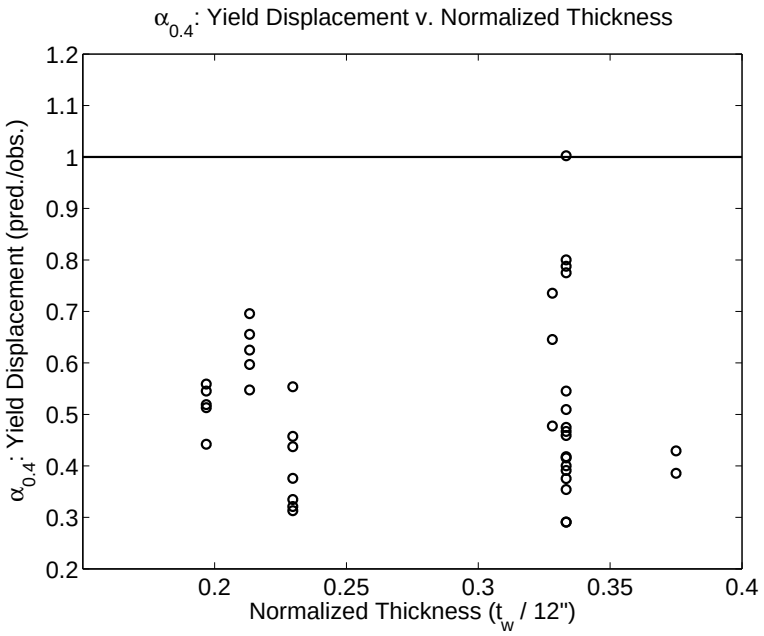

Figure L.14: Beam-Column With Shear Yield Displacement v Normalized Thickness

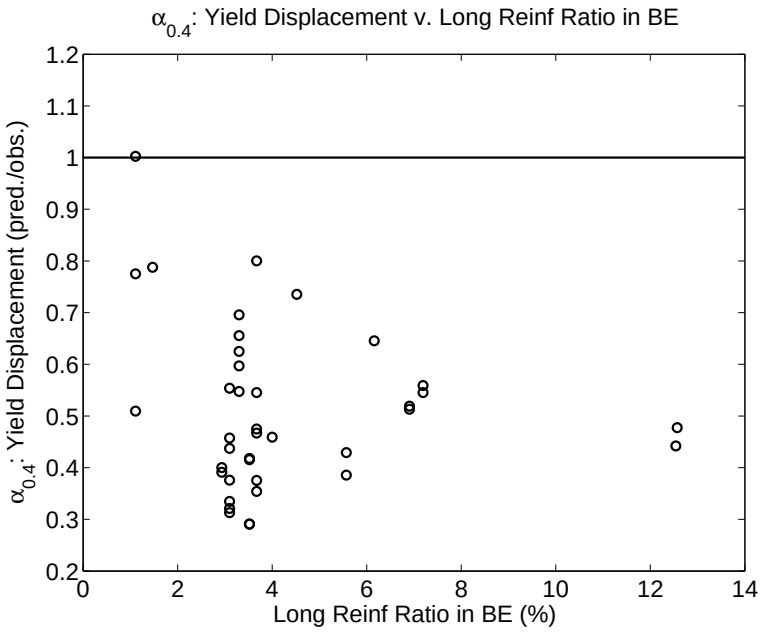

Figure L.15: Beam-Column With Shear Yield Displacement v Long Reinf Ratio in BE

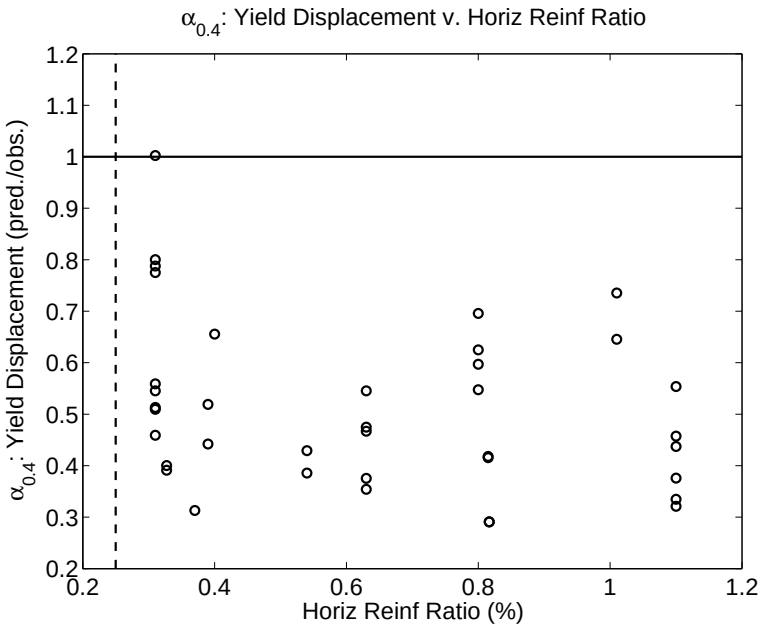

Figure L.16: Beam-Column With Shear Yield Displacement v Horiz Reinf Ratio

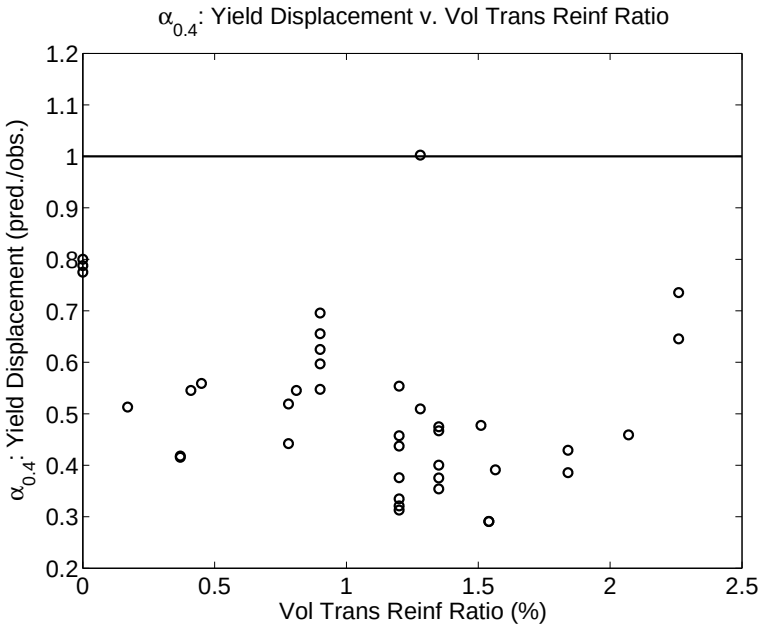

Figure L.17: Beam-Column With Shear Yield Displacement v Vol Trans Reinf Ratio

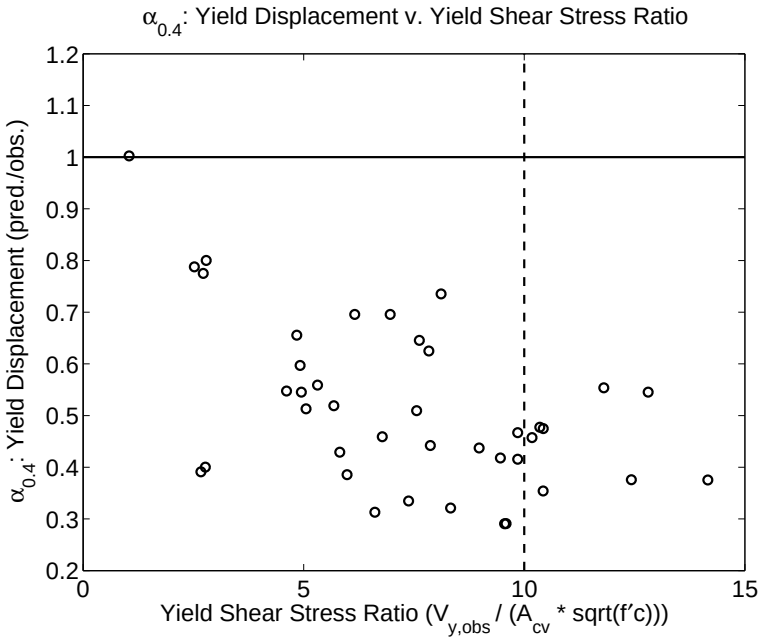

Figure L.18: Beam-Column With Shear Yield Displacement v Yield Shear Stress Ratio

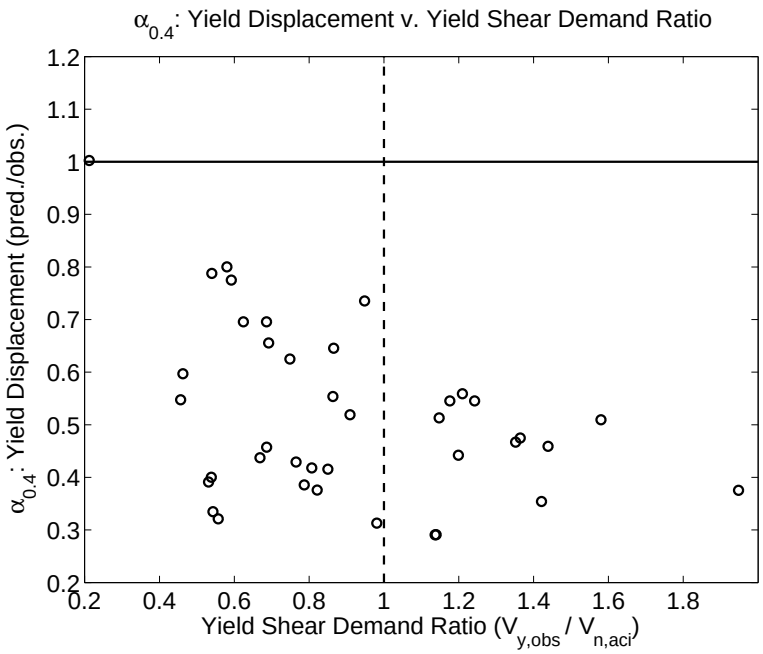

Figure L.19: Beam-Column With Shear Yield Displacement v Yield Shear Demand Ratio

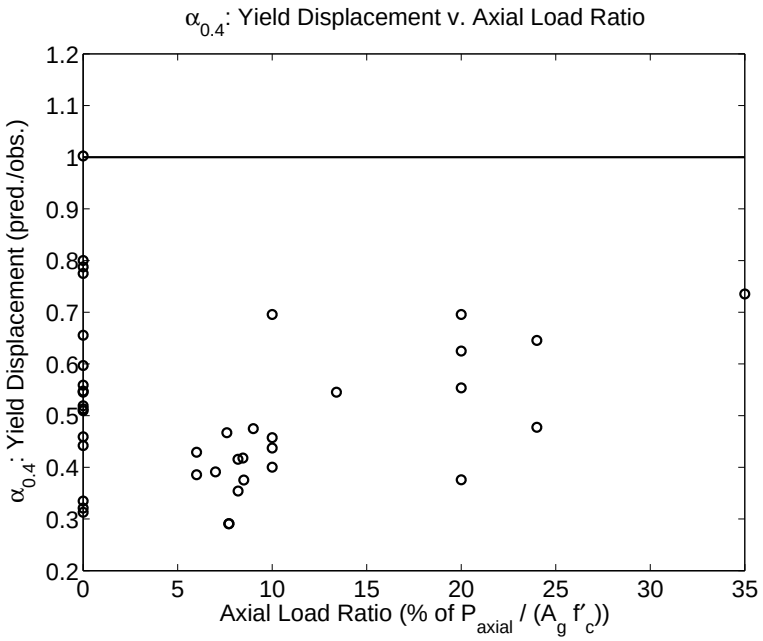

Figure L.20: Beam-Column With Shear Yield Displacement v Axial Load Ratio

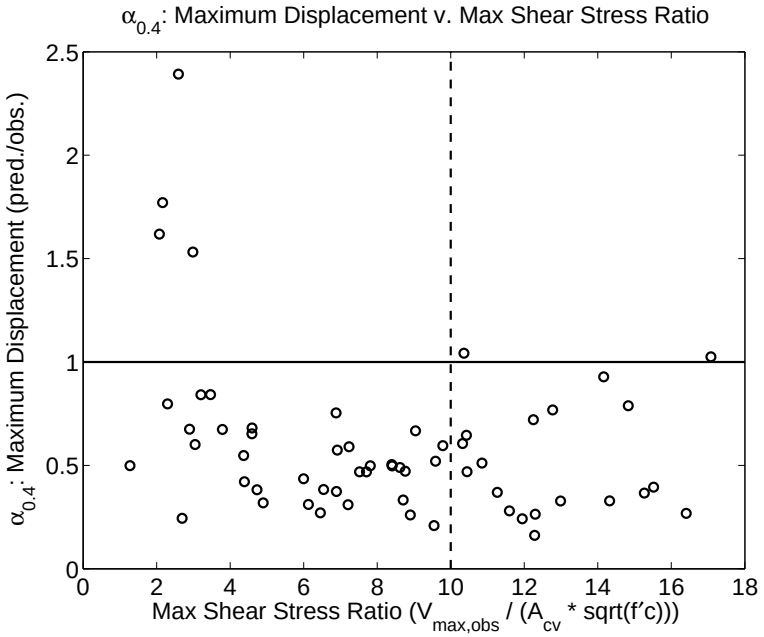

Figure L.21: Beam-Column With Shear Maximum Displacement v Max Shear Stress Ratio

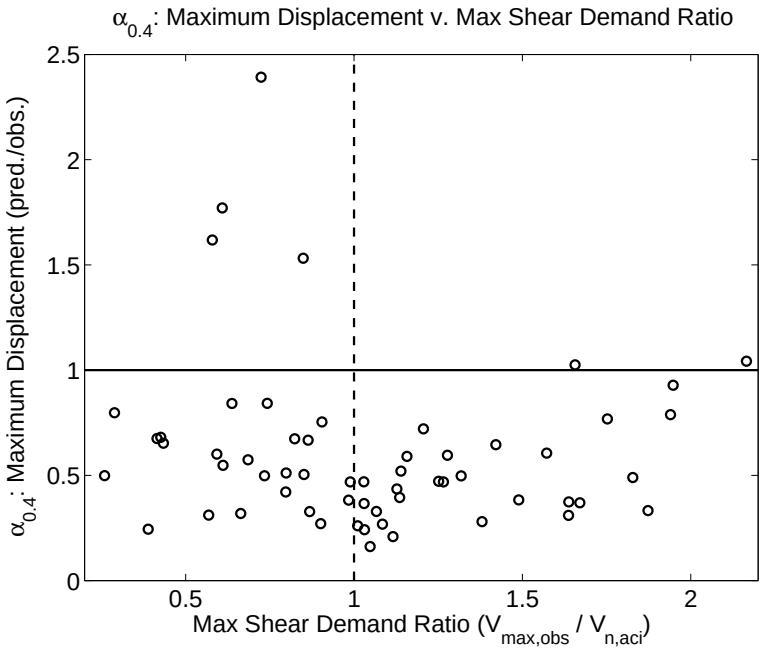

Figure L.22: Beam-Column With Shear Maximum Displacement v Max Shear Demand Ratio

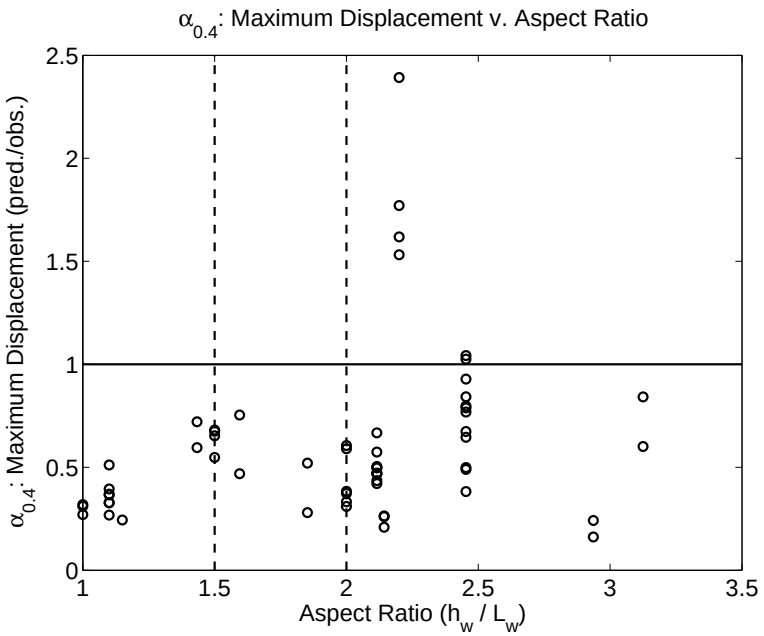

Figure L.23: Beam-Column With Shear Maximum Displacement v Aspect Ratio

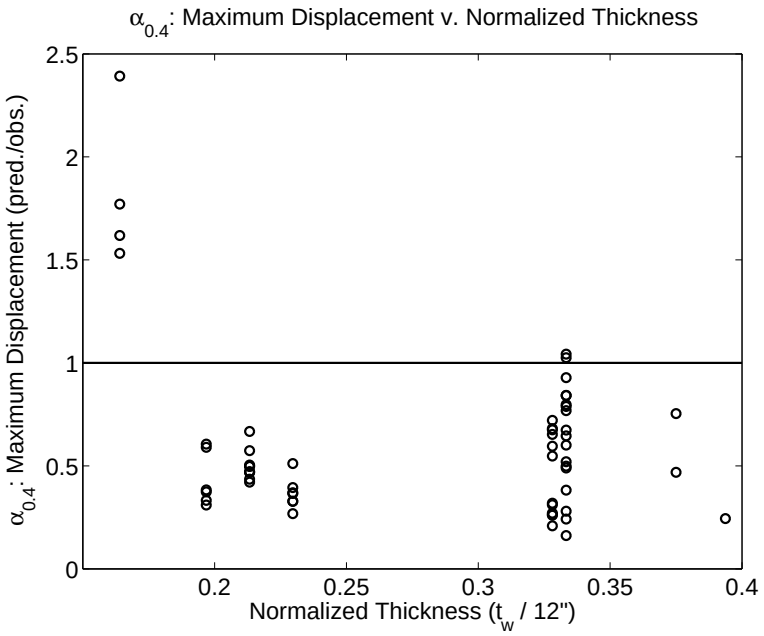

Figure L.24: Beam-Column With Shear Maximum Displacement v Normalized Thickness

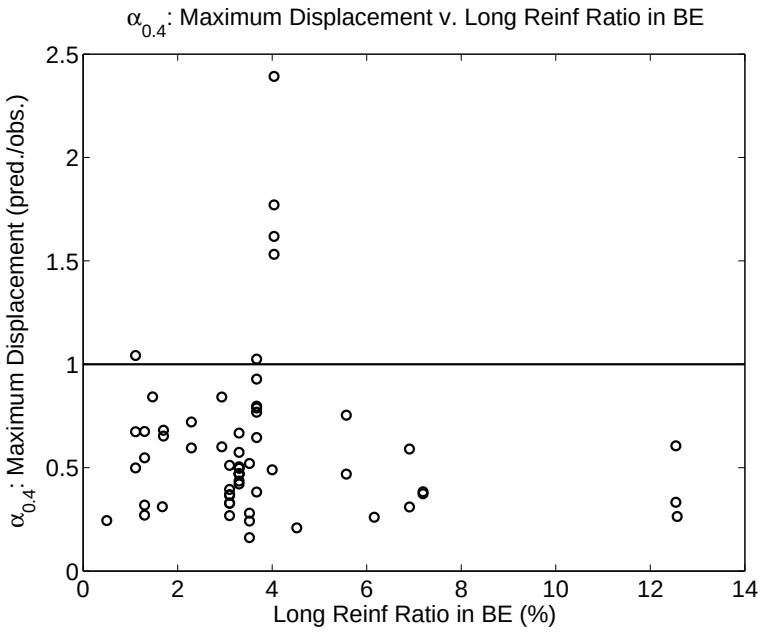

Figure L.25: Beam-Column With Shear Maximum Displacement v Long Reinf Ratio in BE

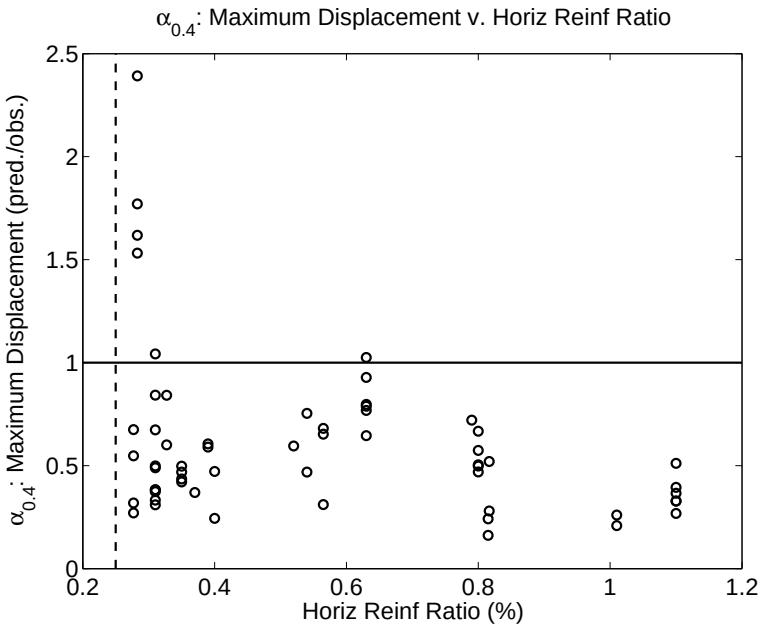

Figure L.26: Beam-Column With Shear Maximum Displacement v Horiz Reinf Ratio

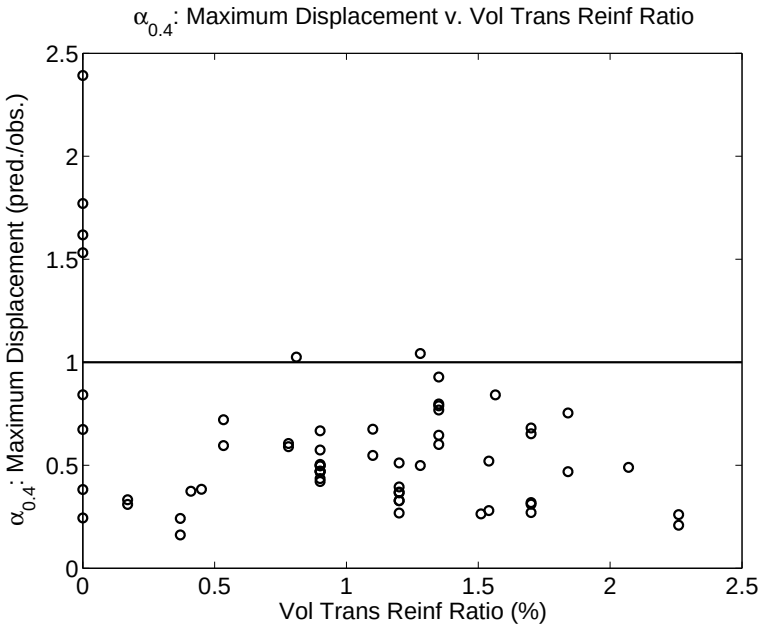

Figure L.27: Beam-Column With Shear Maximum Displacement v Vol Trans Reinf Ratio

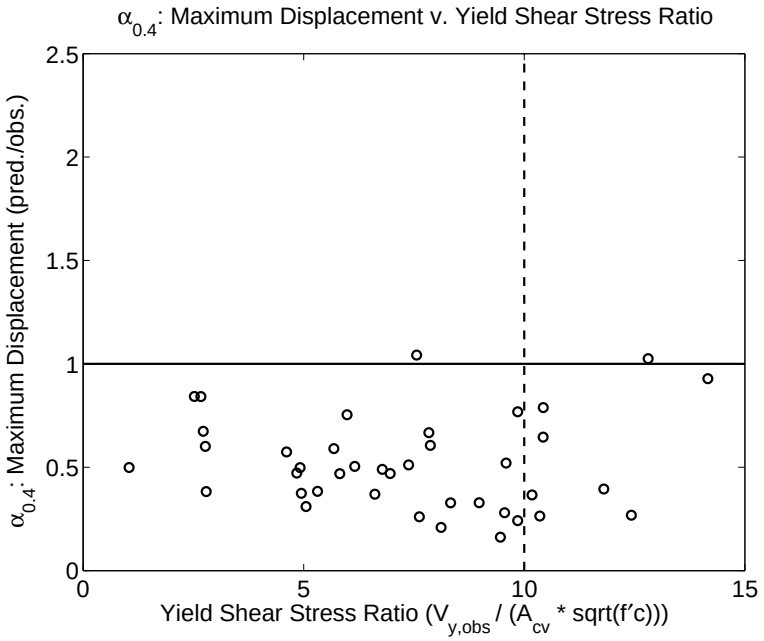

Figure L.28: Beam-Column With Shear Maximum Displacement v Yield Shear Stress Ratio

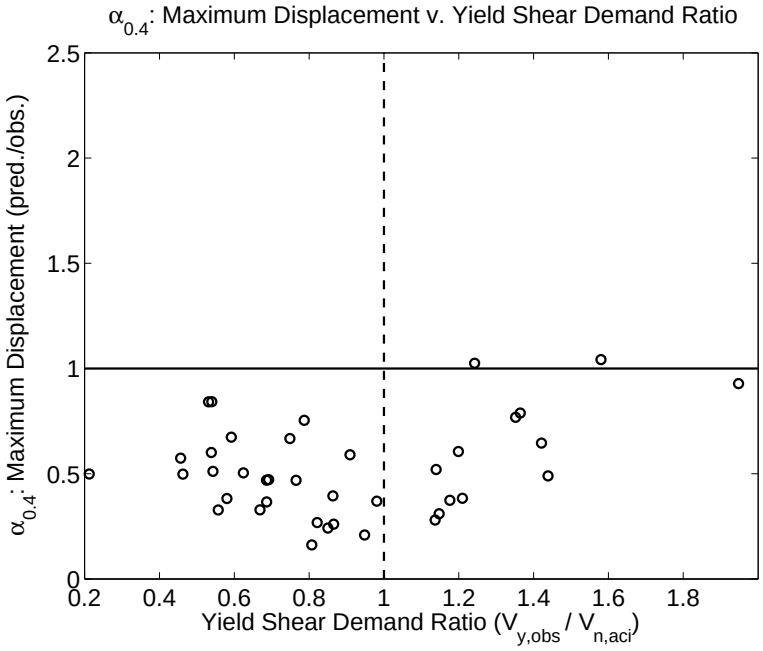

Figure L.29: Beam-Column With Shear Maximum Displacement v Yield Shear Demand Ratio

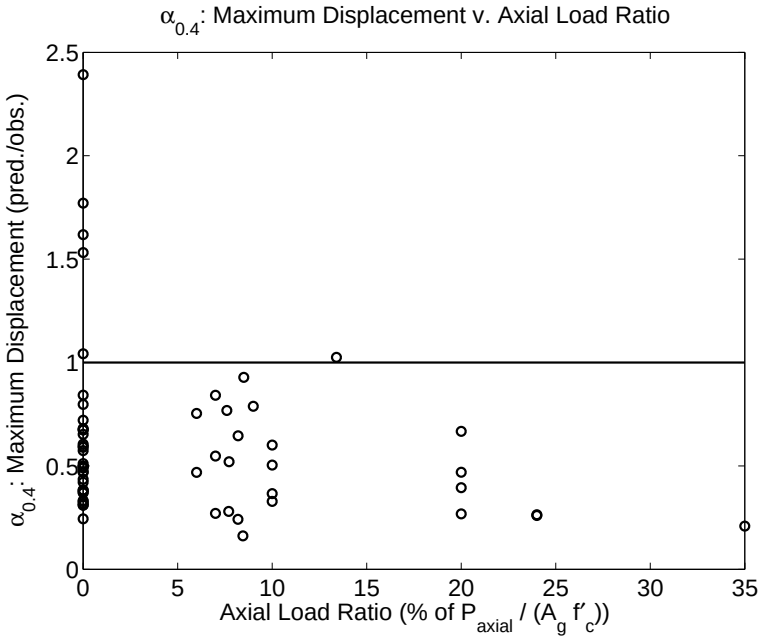

Figure L.30: Beam-Column With Shear Maximum Displacement v Axial Load Ratio

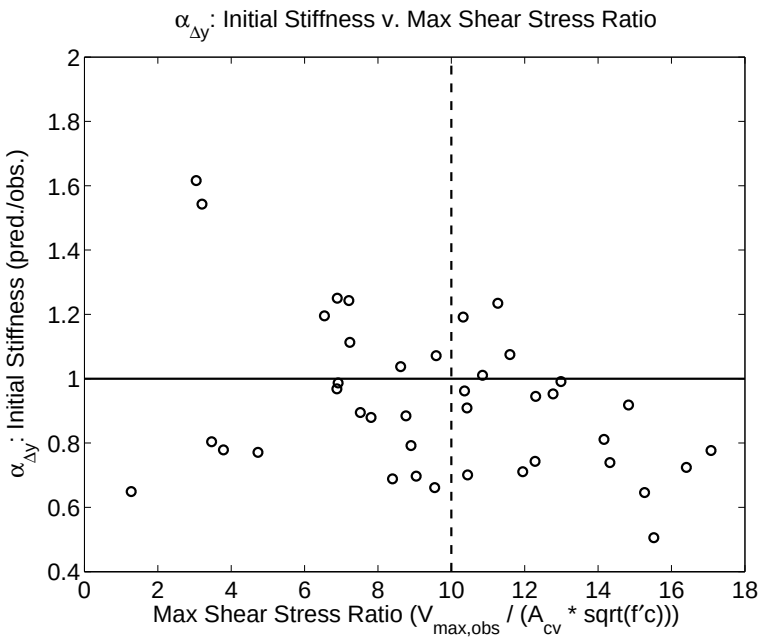

Figure L.31: Beam-Column With Shear Modulus Calibrated to Yield Displacment - Initial Stiffness v Max Shear Stress Ratio

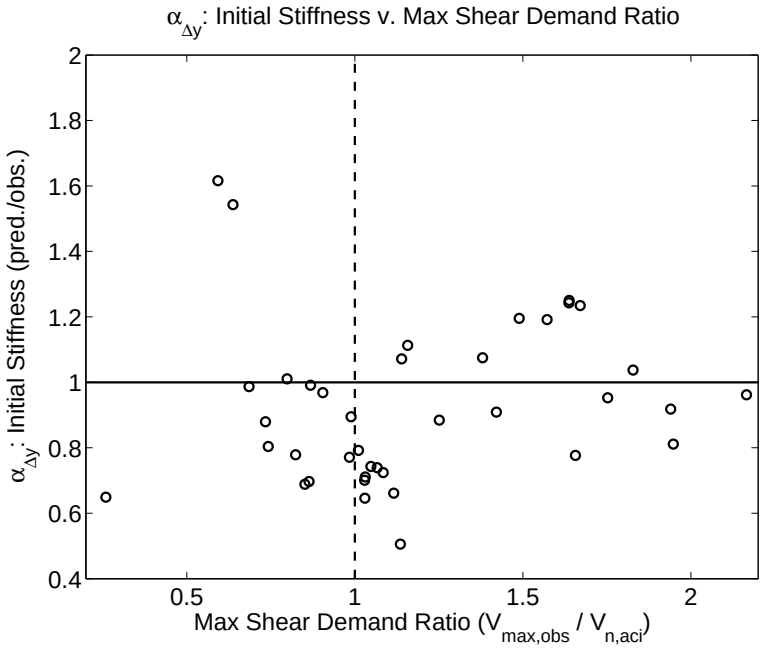

Figure L.32: Beam-Column With Shear Modulus Calibrated to Yield Displacment - Initial Stiffness v Max Shear Demand Ratio

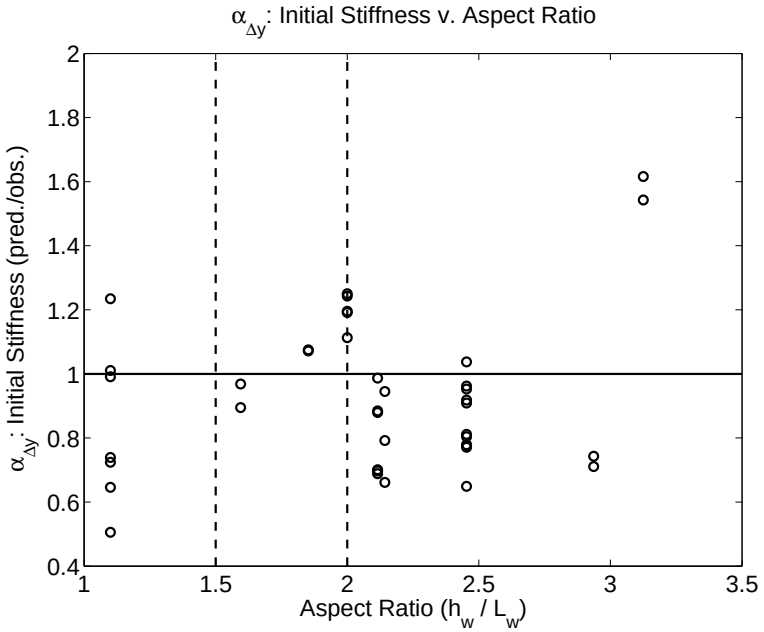

Figure L.33: Beam-Column With Shear Modulus Calibrated to Yield Displacment - Initial Stiffness v Aspect Ratio

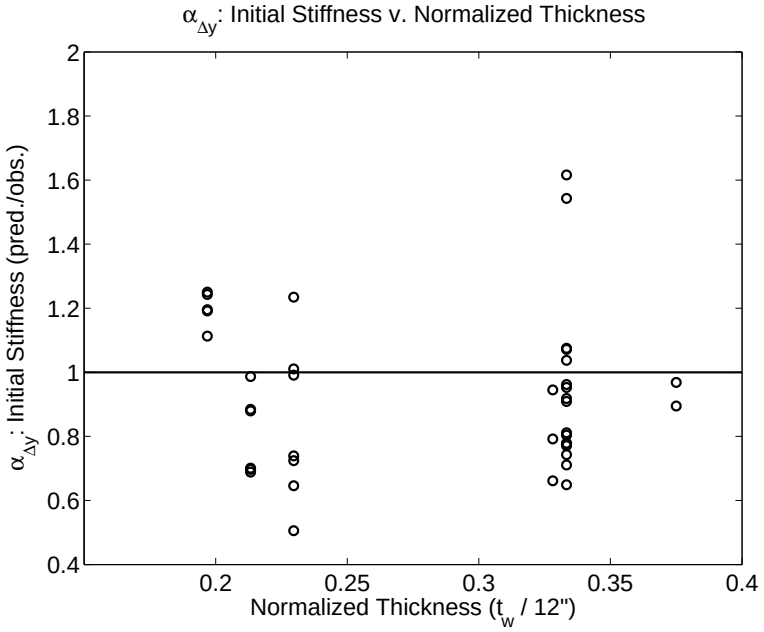

Figure L.34: Beam-Column With Shear Modulus Calibrated to Yield Displacment - Initial Stiffness v Normalized Thickness

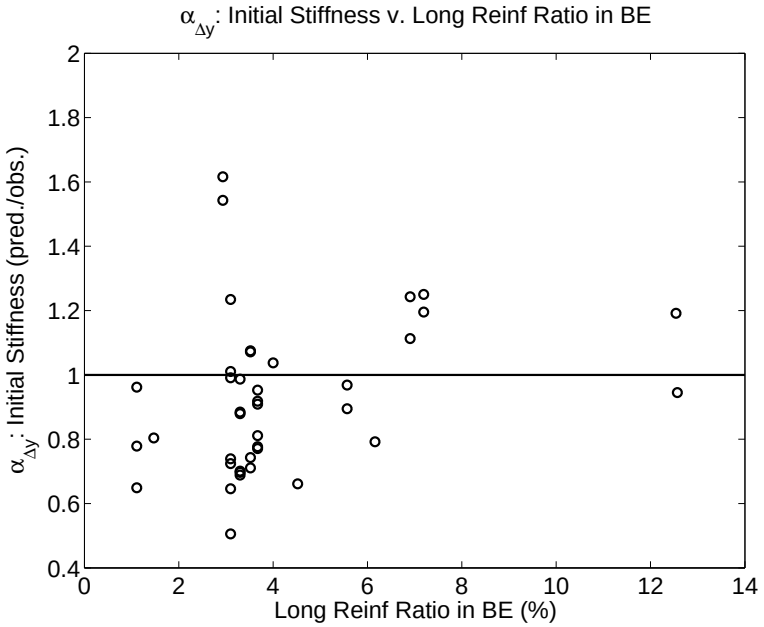

Figure L.35: Beam-Column With Shear Modulus Calibrated to Yield Displacment - Initial Stiffness v Long Reinf Ratio in BE

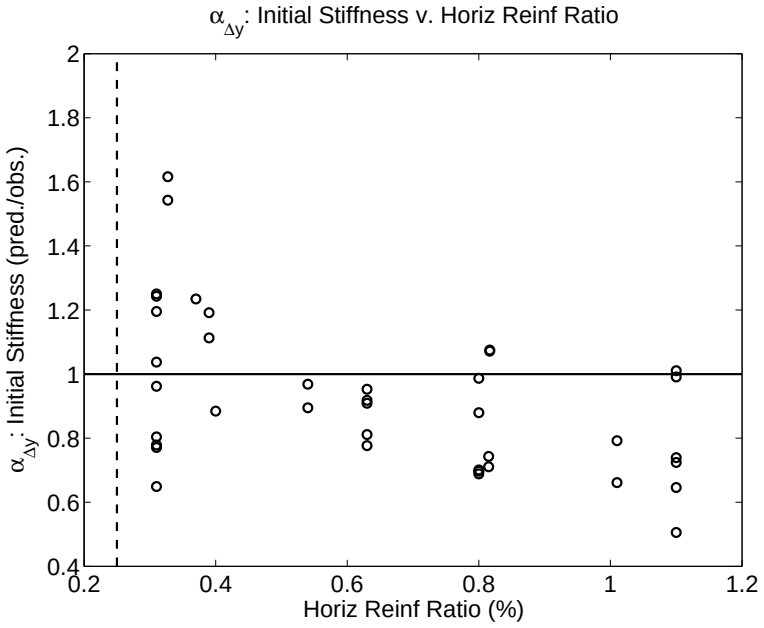

Figure L.36: Beam-Column With Shear Modulus Calibrated to Yield Displacment - Initial Stiffness v Horiz Reinf Ratio

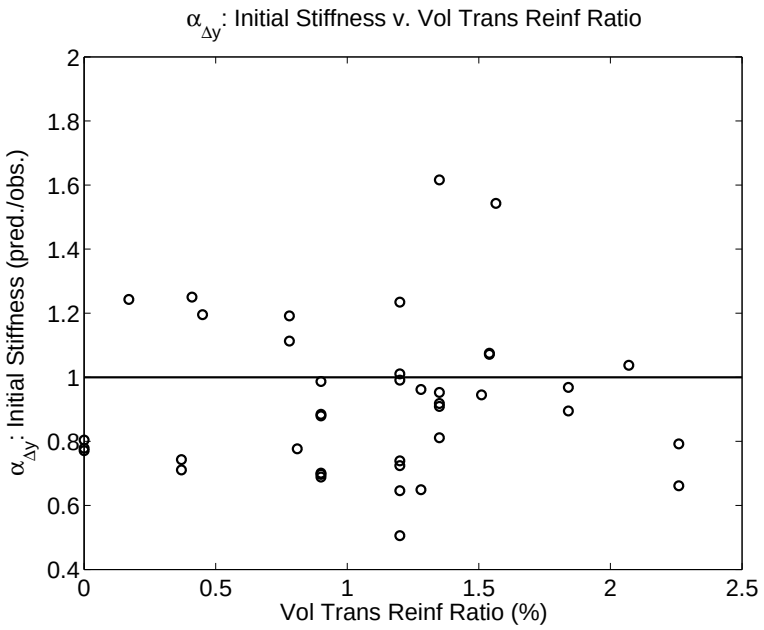

Figure L.37: Beam-Column With Shear Modulus Calibrated to Yield Displacment - Initial Stiffness v Vol Trans Reinf Ratio

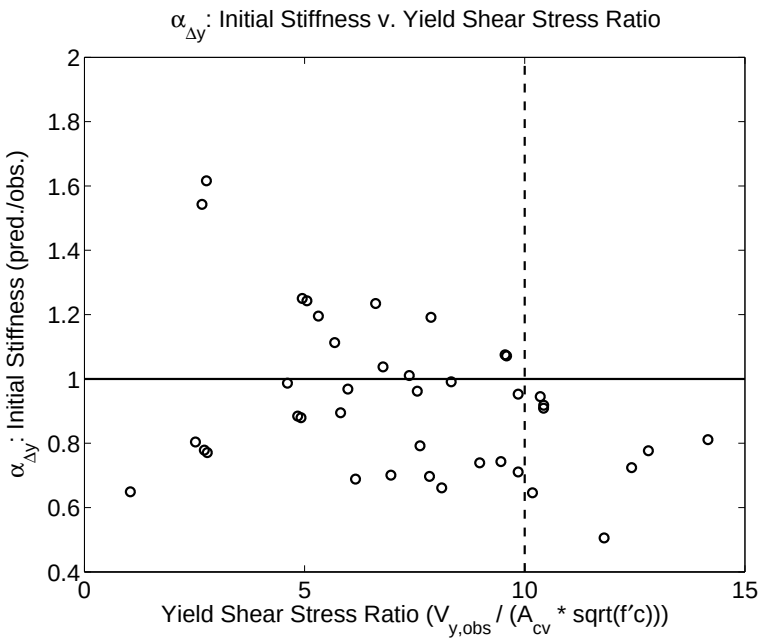

Figure L.38: Beam-Column With Shear Modulus Calibrated to Yield Displacment - Initial Stiffness v Yield Shear Stress Ratio

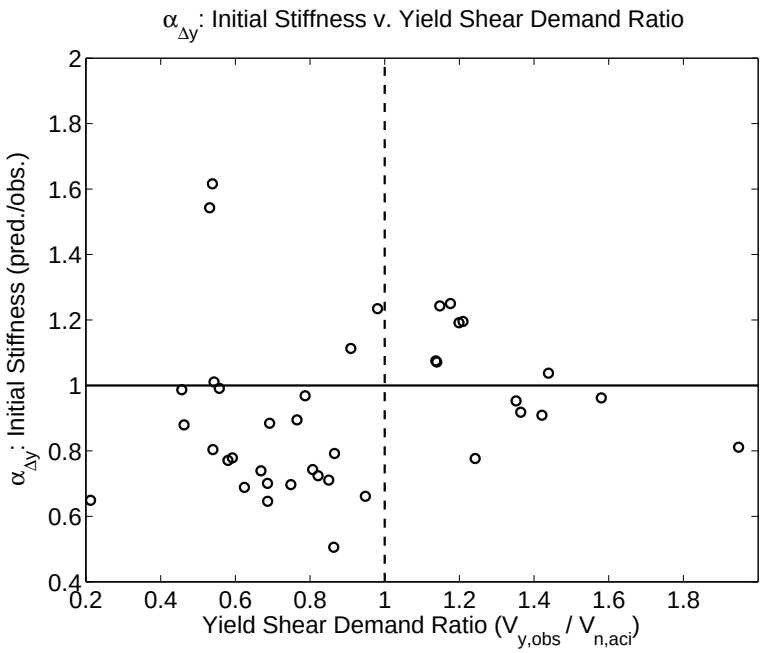

Figure L.39: Beam-Column With Shear Modulus Calibrated to Yield Displacment - Initial Stiffness v Yield Shear Demand Ratio

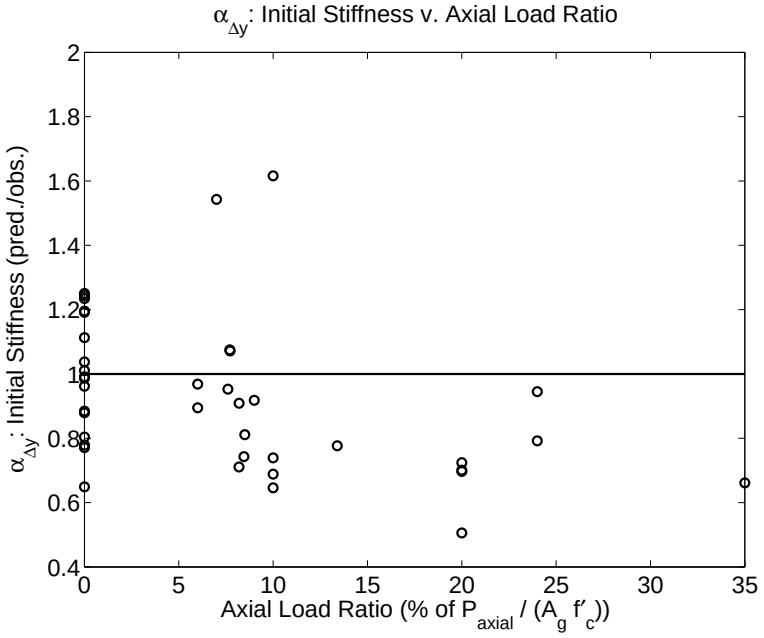

Figure L.40: Beam-Column With Shear Modulus Calibrated to Yield Displacment - Initial Stiffness v Axial Load Ratio

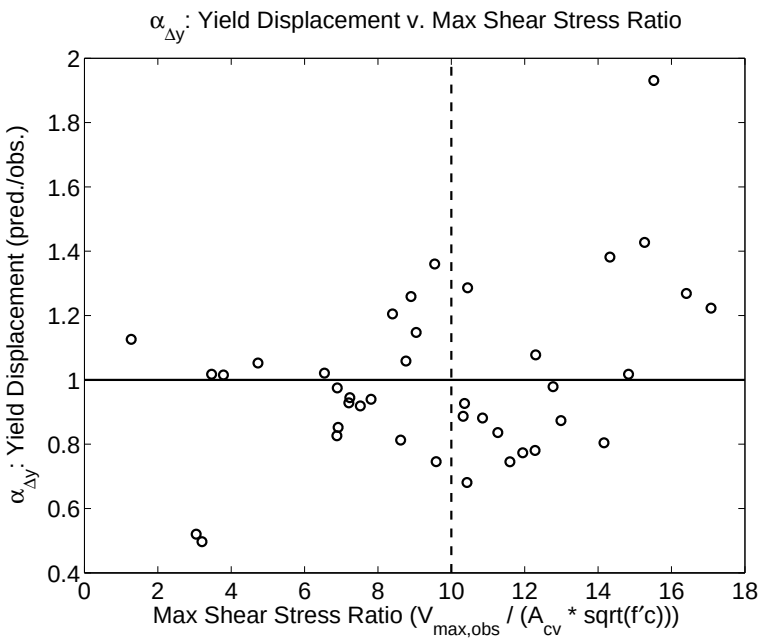

Figure L.41: Beam-Column With Shear Modulus Calibrated to Yield Displacment - Yield Displacement v Max Shear Stress Ratio

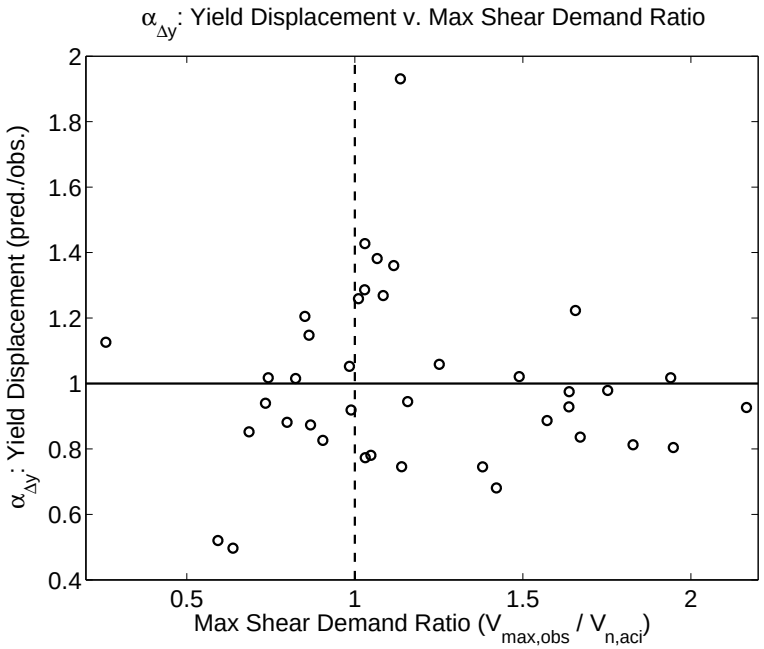

Figure L.42: Beam-Column With Shear Modulus Calibrated to Yield Displacment - Yield Displacement v Max Shear Demand Ratio

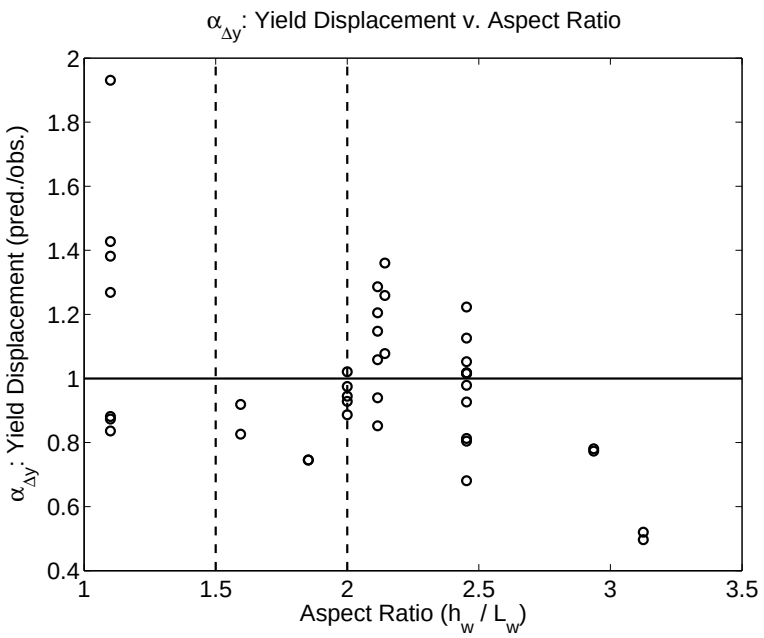

Figure L.43: Beam-Column With Shear Modulus Calibrated to Yield Displacment - Yield Displacement v Aspect Ratio

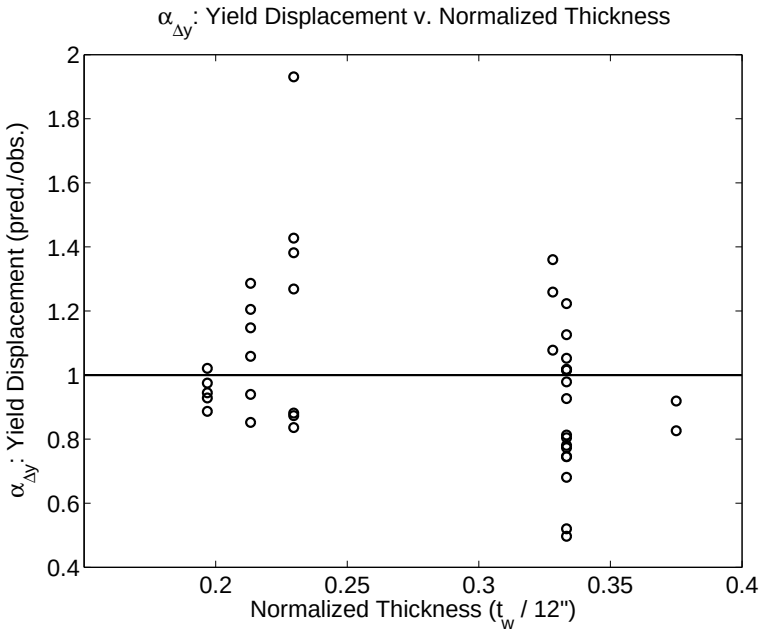

Figure L.44: Beam-Column With Shear Modulus Calibrated to Yield Displacment - Yield Displacement v Normalized Thickness

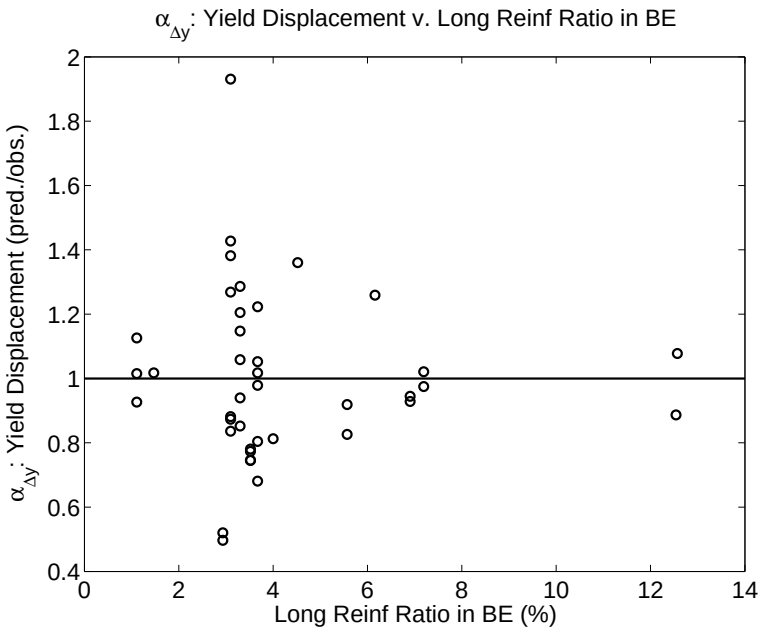

Figure L.45: Beam-Column With Shear Modulus Calibrated to Yield Displacment - Yield Displacement v Long Reinf Ratio in BE

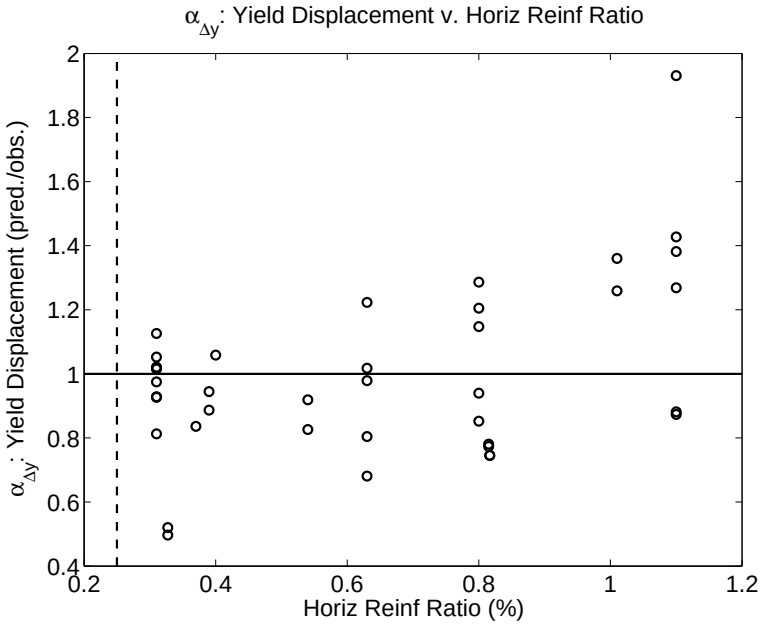

Figure L.46: Beam-Column With Shear Modulus Calibrated to Yield Displacment - Yield Displacement v Horiz Reinf Ratio

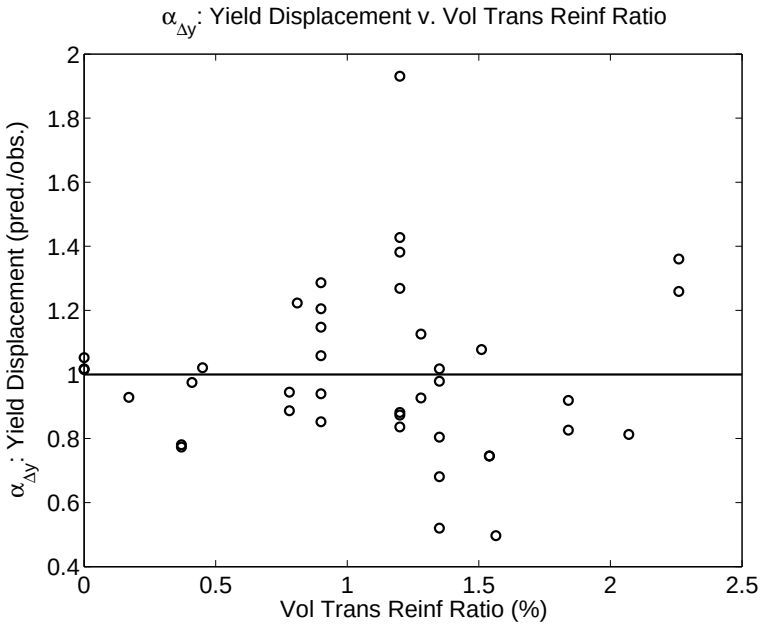

Figure L.47: Beam-Column With Shear Modulus Calibrated to Yield Displacment - Yield Displacement v Vol Trans Reinf Ratio

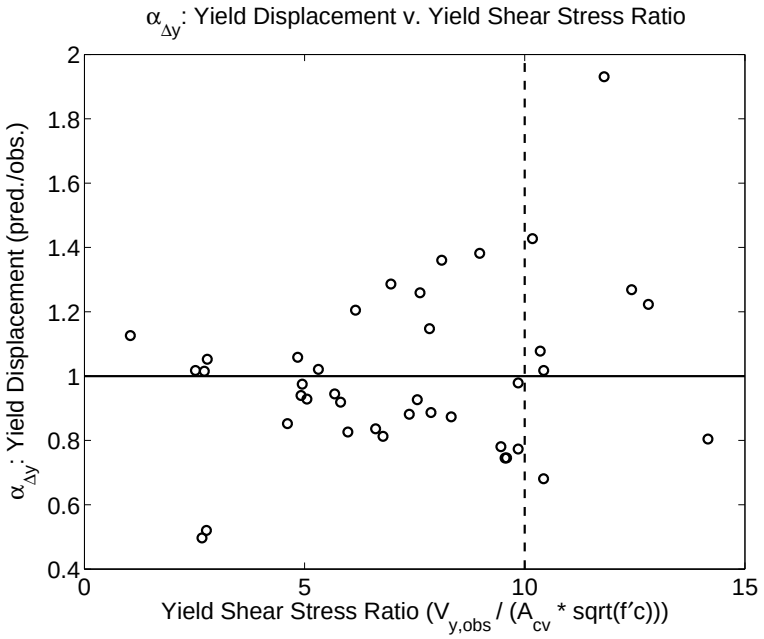

Figure L.48: Beam-Column With Shear Modulus Calibrated to Yield Displacment - Yield Displacement v Yield Shear Stress Ratio

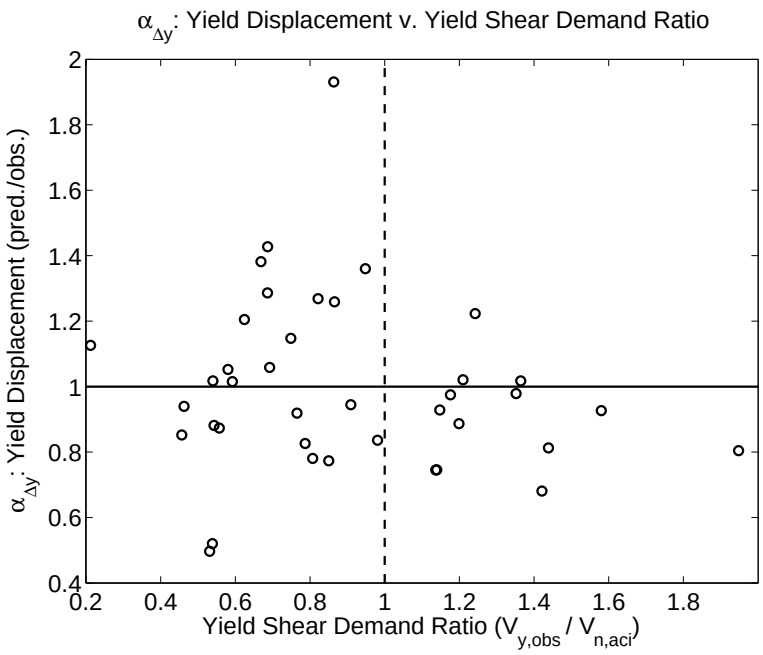

Figure L.49: Beam-Column With Shear Modulus Calibrated to Yield Displacment - Yield Displacement v Yield Shear Demand Ratio

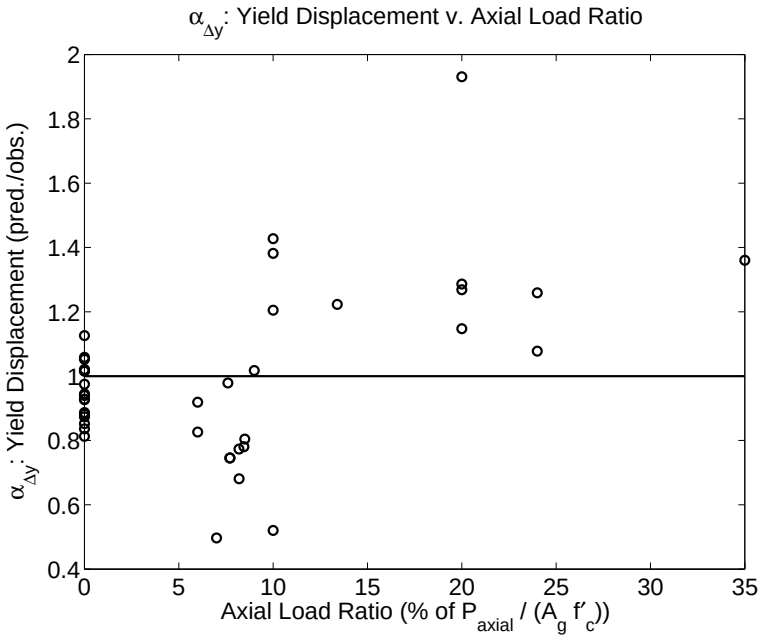

Figure L.50: Beam-Column With Shear Modulus Calibrated to Yield Displacment - Yield Displacement v Axial Load Ratio

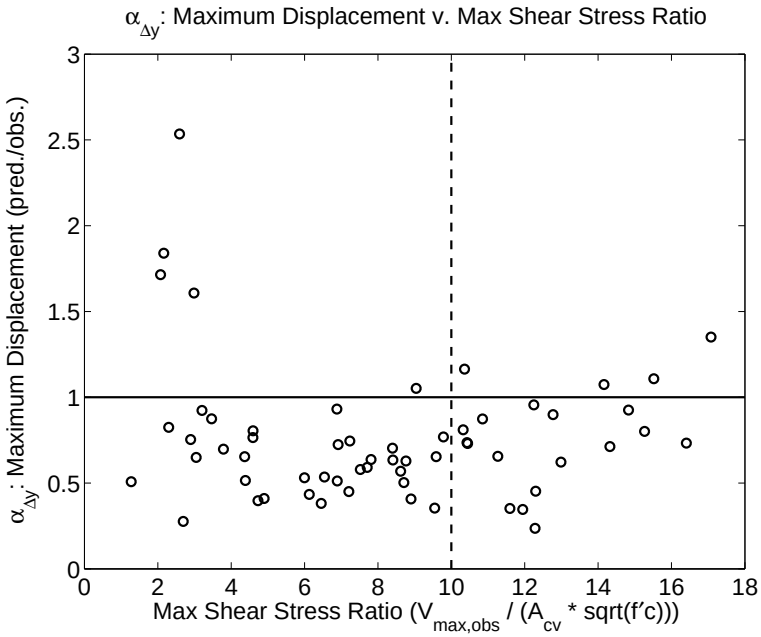

Figure L.51: Beam-Column With Shear Modulus Calibrated to Yield Displacment - Maximum Displacement v Max Shear Stress Ratio

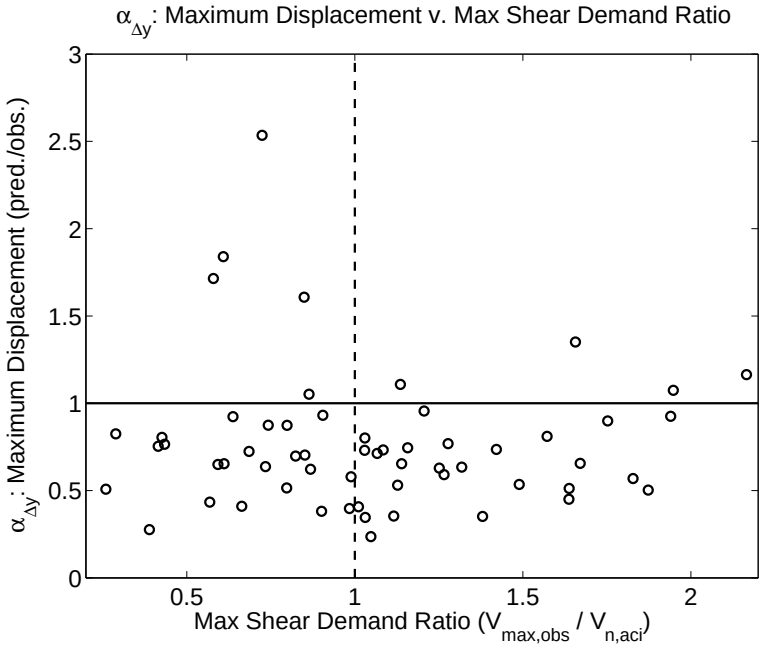

Figure L.52: Beam-Column With Shear Modulus Calibrated to Yield Displacment - Maximum Displacement v Max Shear Demand Ratio

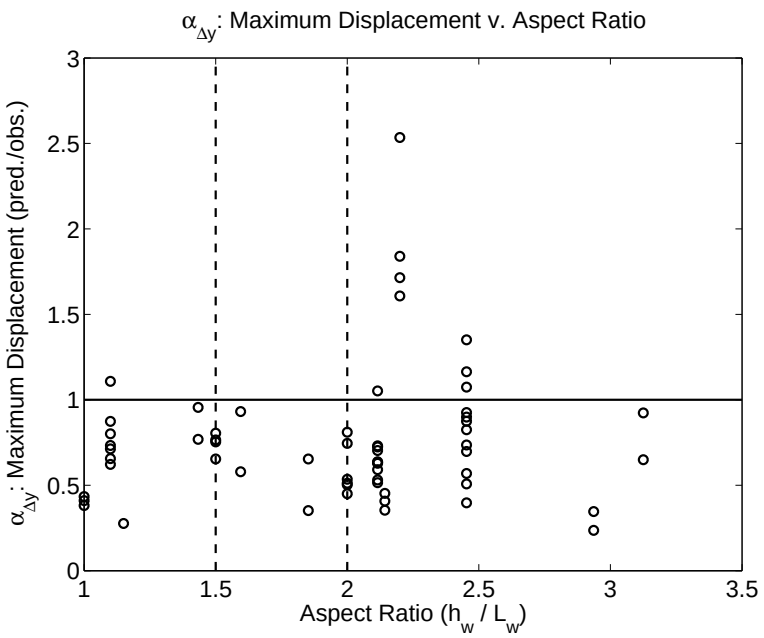

Figure L.53: Beam-Column With Shear Modulus Calibrated to Yield Displacment - Maximum Displacement v Aspect Ratio

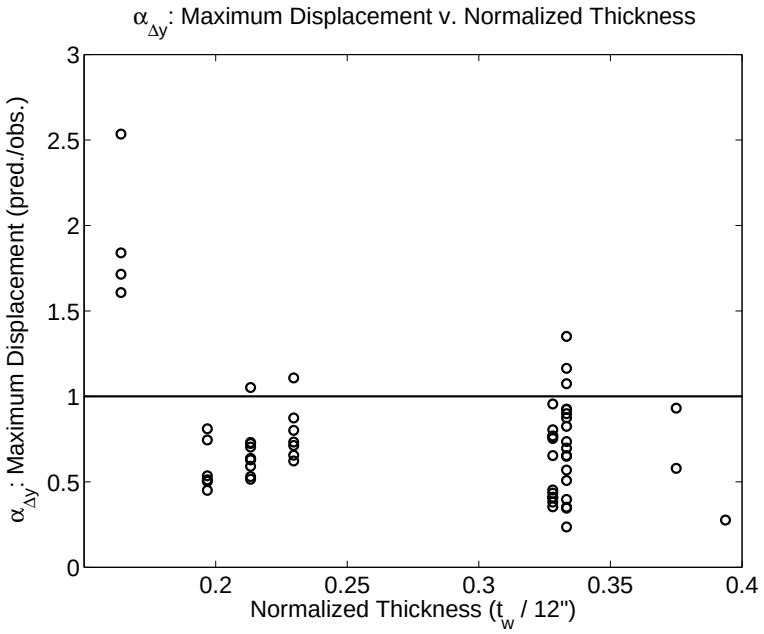

Figure L.54: Beam-Column With Shear Modulus Calibrated to Yield Displacment - Maximum Displacement v Normalized Thickness

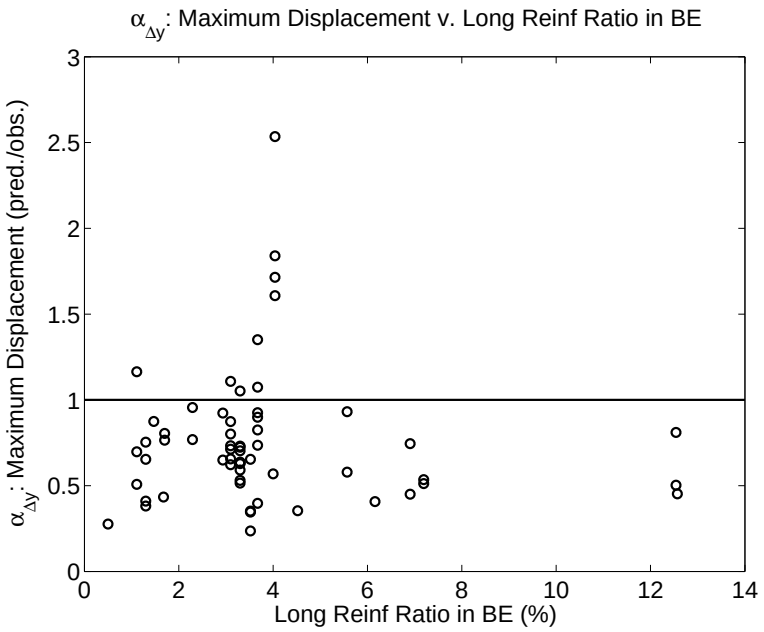

Figure L.55: Beam-Column With Shear Modulus Calibrated to Yield Displacment - Maximum Displacement v Long Reinf Ratio in BE

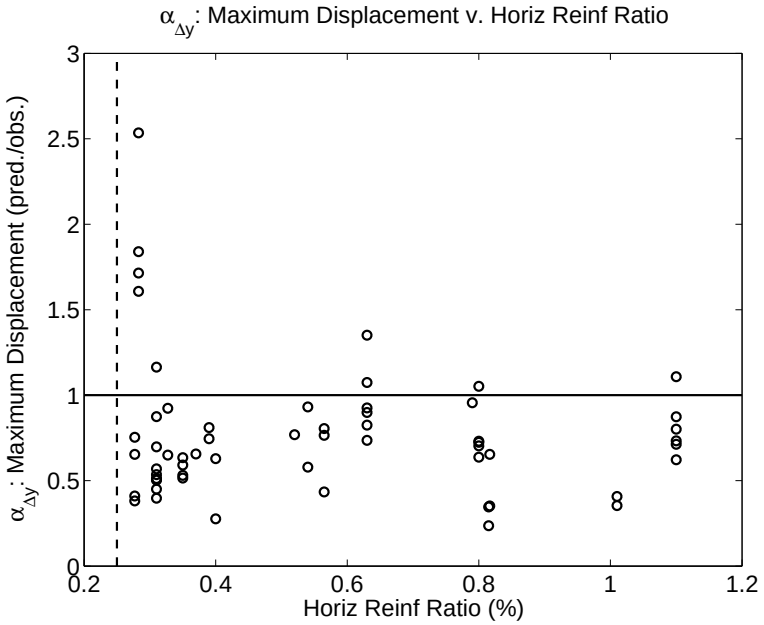

Figure L.56: Beam-Column With Shear Modulus Calibrated to Yield Displacment - Maximum Displacement v Horiz Reinf Ratio

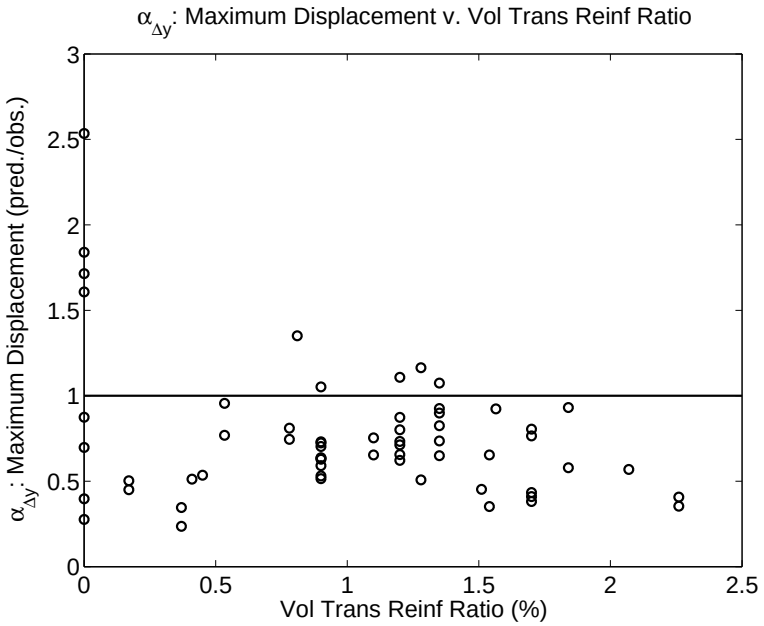

Figure L.57: Beam-Column With Shear Modulus Calibrated to Yield Displacment - Maximum Displacement v Vol Trans Reinf Ratio

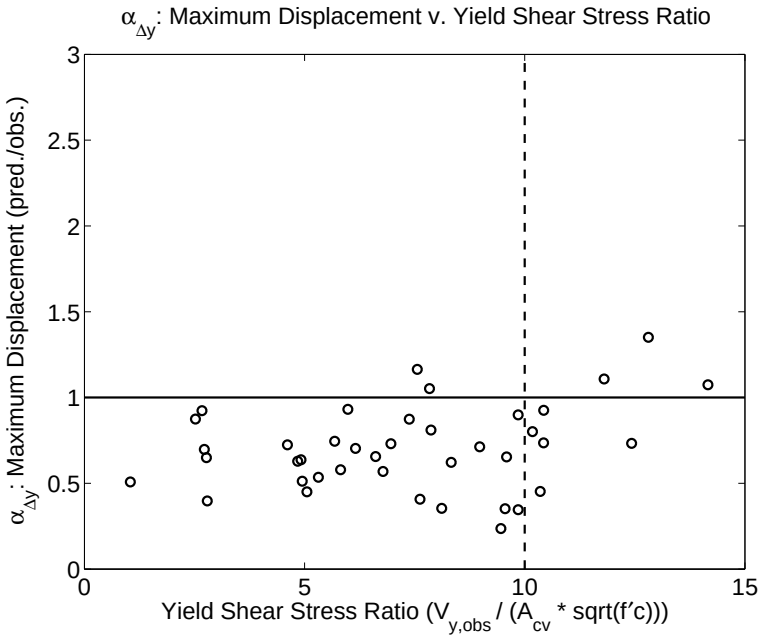

Figure L.58: Beam-Column With Shear Modulus Calibrated to Yield Displacment - Maximum Displacement v Yield Shear Stress Ratio

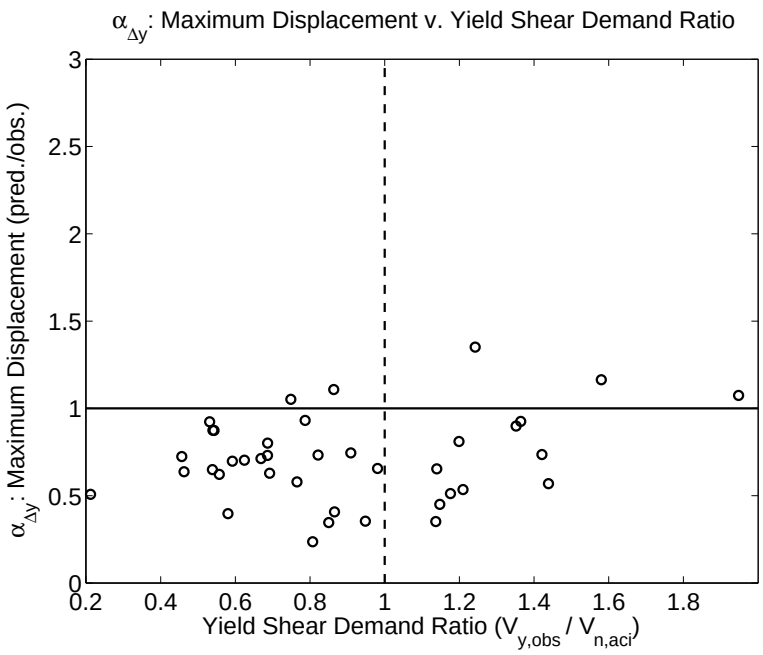

Figure L.59: Beam-Column With Shear Modulus Calibrated to Yield Displacment - Maximum Displacement v Yield Shear Demand Ratio

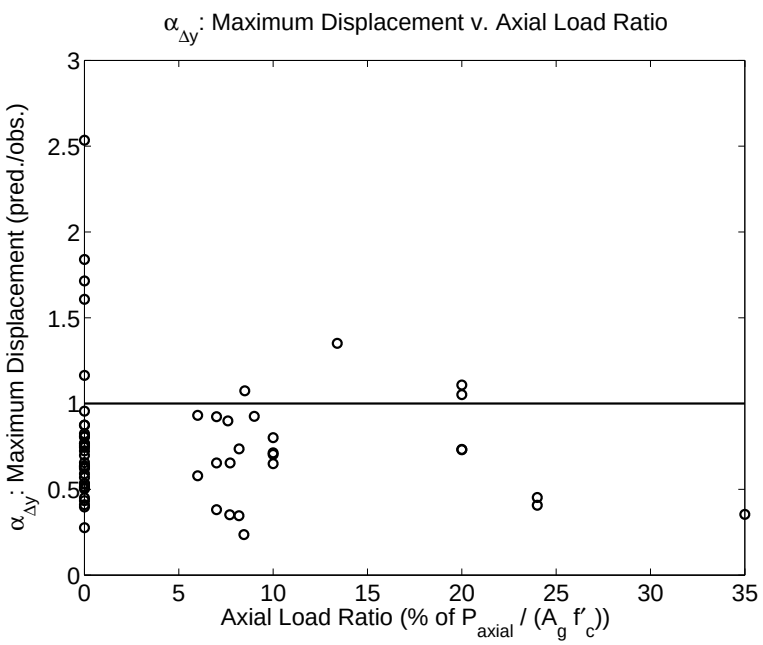

Figure L.60: Beam-Column With Shear Modulus Calibrated to Yield Displacment - Maximum Displacement v Axial Load Ratio

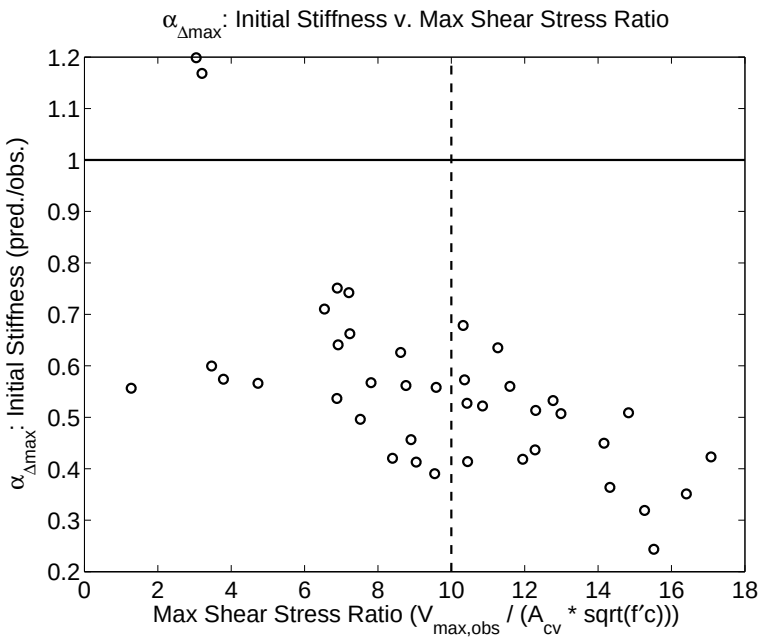

Figure L.61: Beam-Column With Shear Modulus Calibrated to Maximum Displacment - Initial Stiffness v Max Shear Stress Ratio

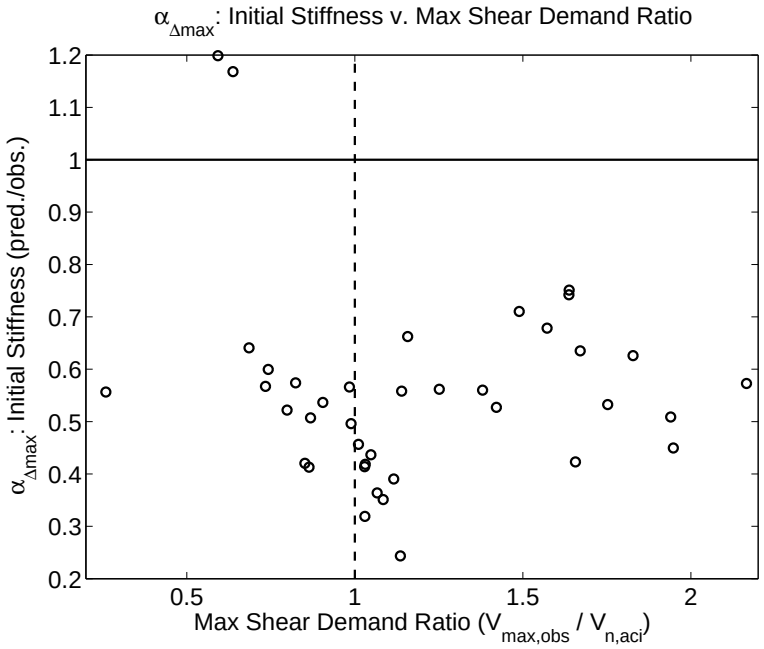

Figure L.62: Beam-Column With Shear Modulus Calibrated to Maximum Displacment - Initial Stiffness v Max Shear Demand Ratio

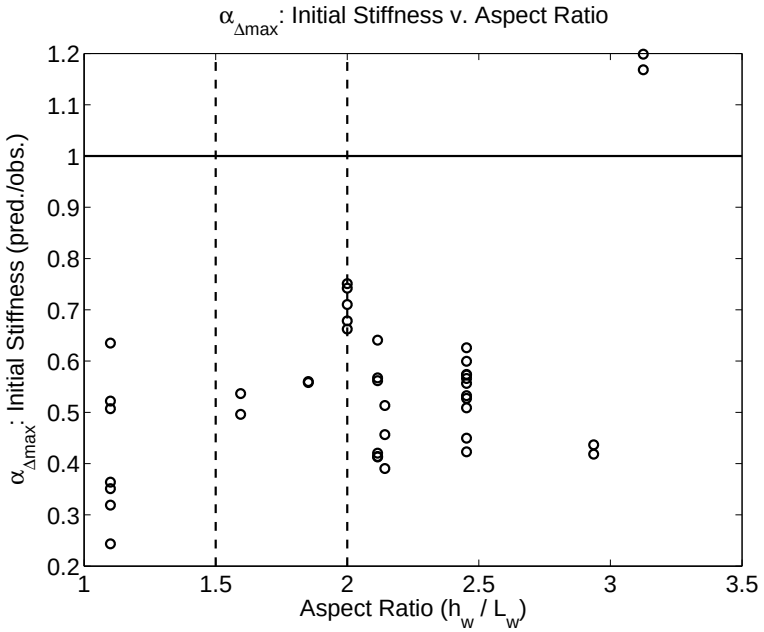

Figure L.63: Beam-Column With Shear Modulus Calibrated to Maximum Displacment - Initial Stiffness v Aspect Ratio

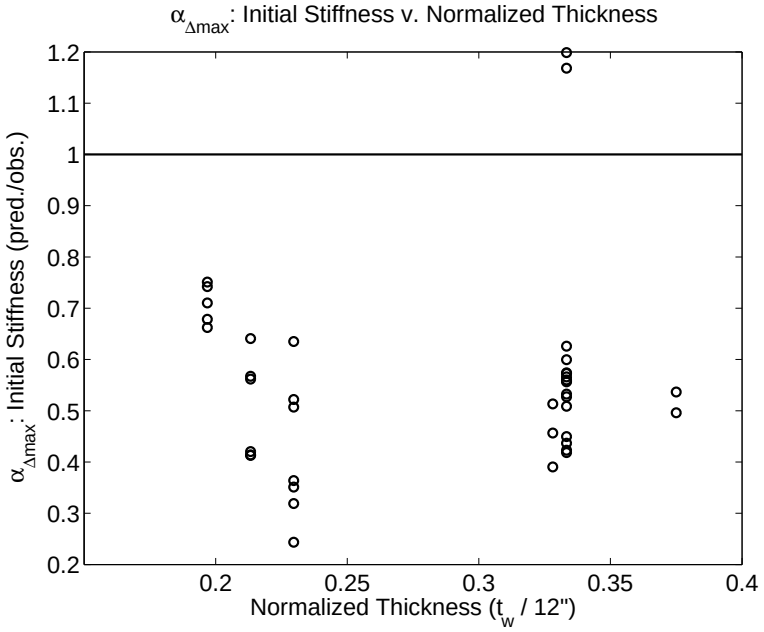

Figure L.64: Beam-Column With Shear Modulus Calibrated to Maximum Displacment - Initial Stiffness v Normalized Thickness

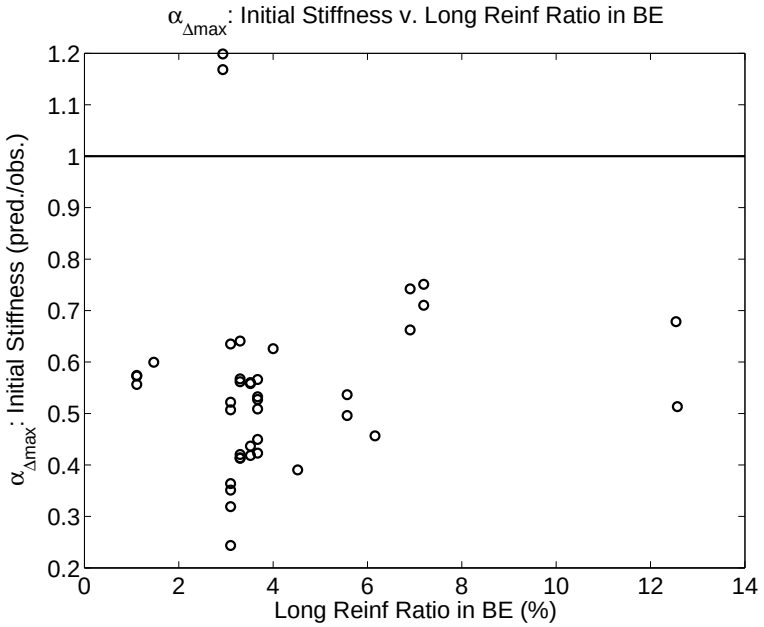

Figure L.65: Beam-Column With Shear Modulus Calibrated to Maximum Displacment - Initial Stiffness v Long Reinf Ratio in BE

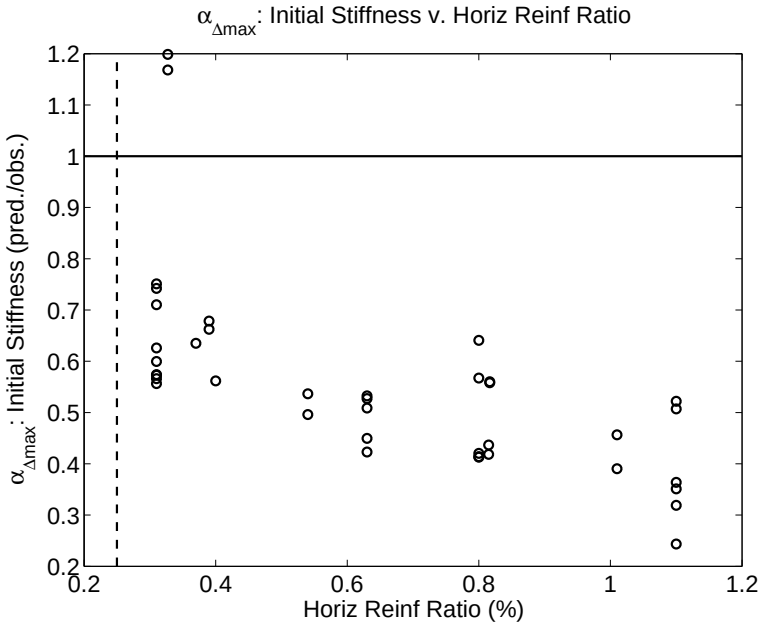

Figure L.66: Beam-Column With Shear Modulus Calibrated to Maximum Displacment - Initial Stiffness v Horiz Reinf Ratio

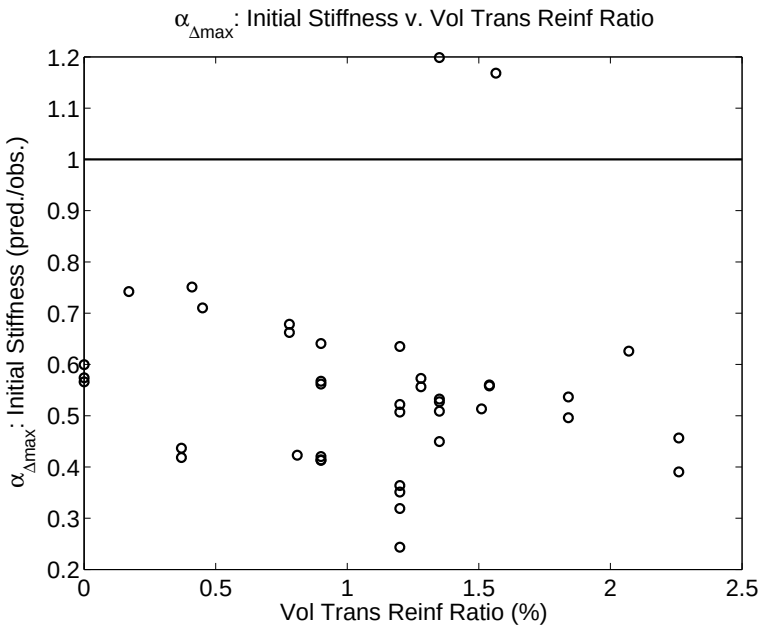

Figure L.67: Beam-Column With Shear Modulus Calibrated to Maximum Displacment - Initial Stiffness v Vol Trans Reinf Ratio

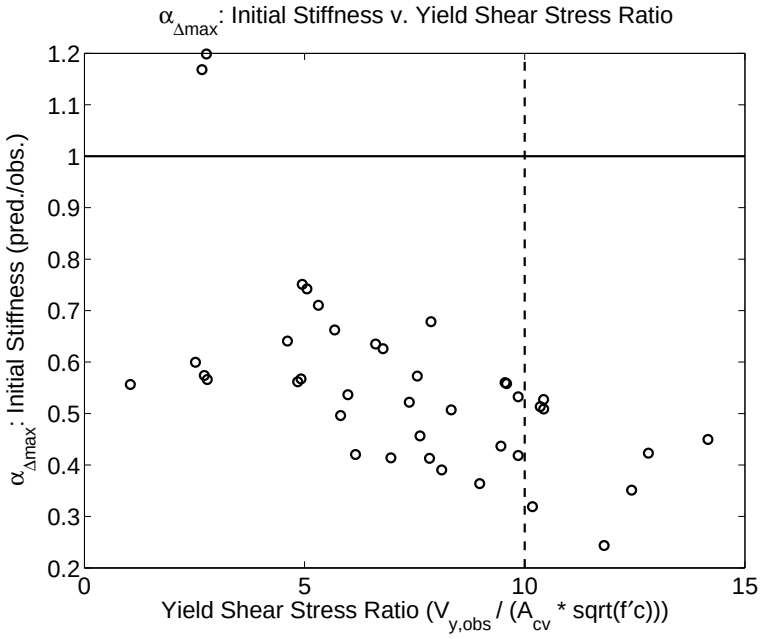

Figure L.68: Beam-Column With Shear Modulus Calibrated to Maximum Displacment - Initial Stiffness v Yield Shear Stress Ratio

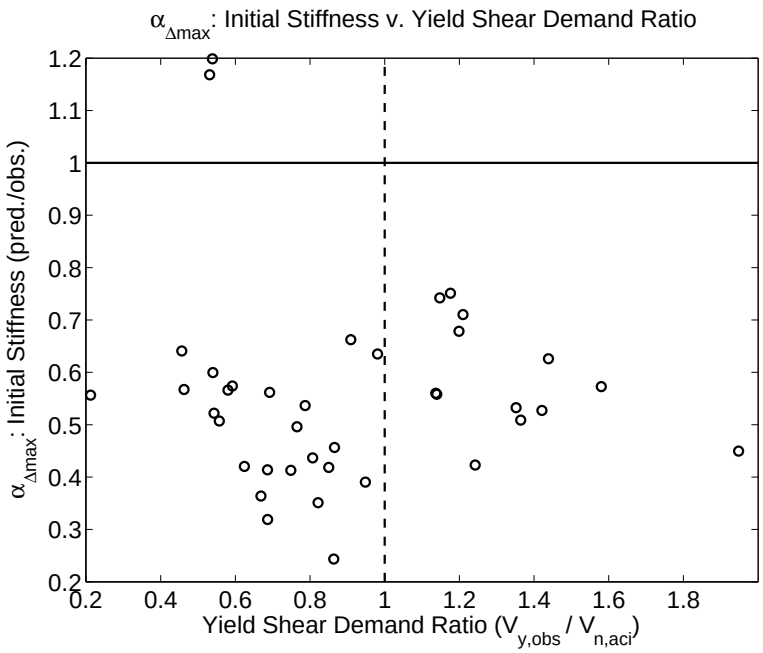

Figure L.69: Beam-Column With Shear Modulus Calibrated to Maximum Displacment - Initial Stiffness v Yield Shear Demand Ratio

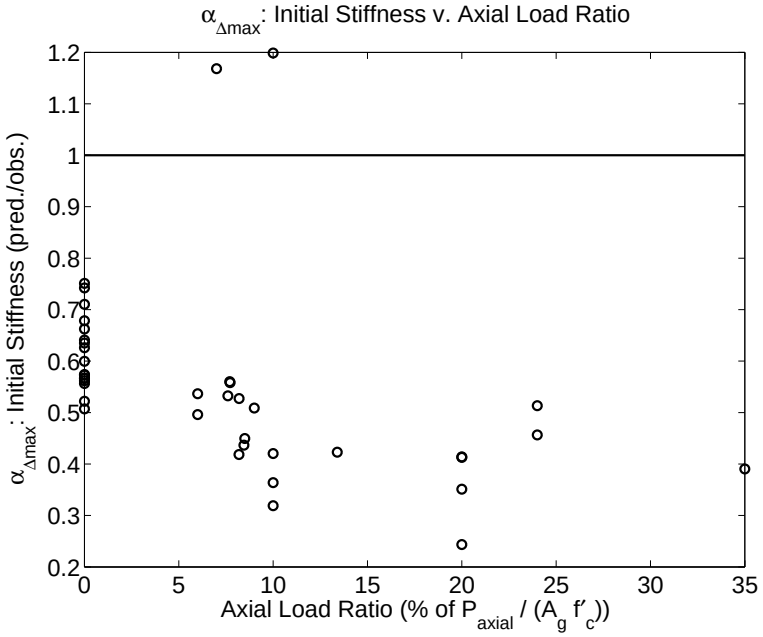

Figure L.70: Beam-Column With Shear Modulus Calibrated to Maximum Displacment - Initial Stiffness v Axial Load Ratio

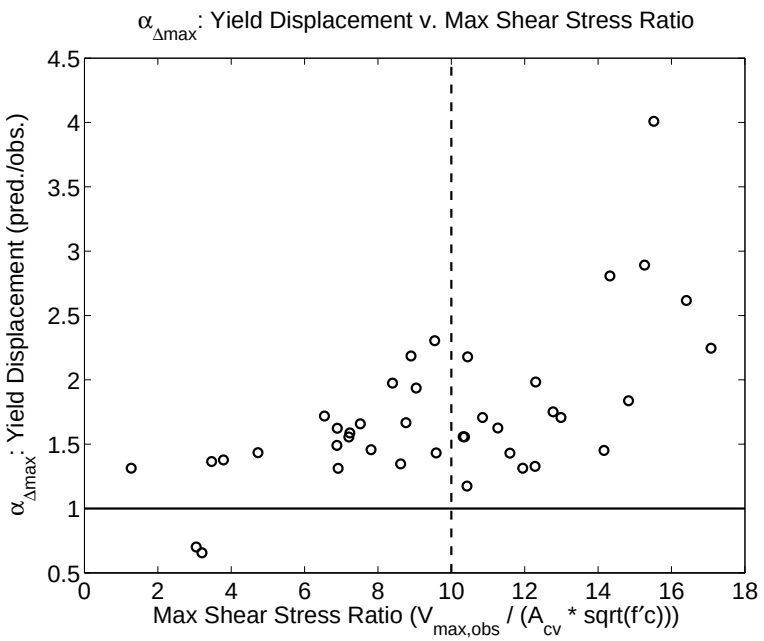

Figure L.71: Beam-Column With Shear Modulus Calibrated to Maximum Displacment - Yield Displacement v Max Shear Stress Ratio

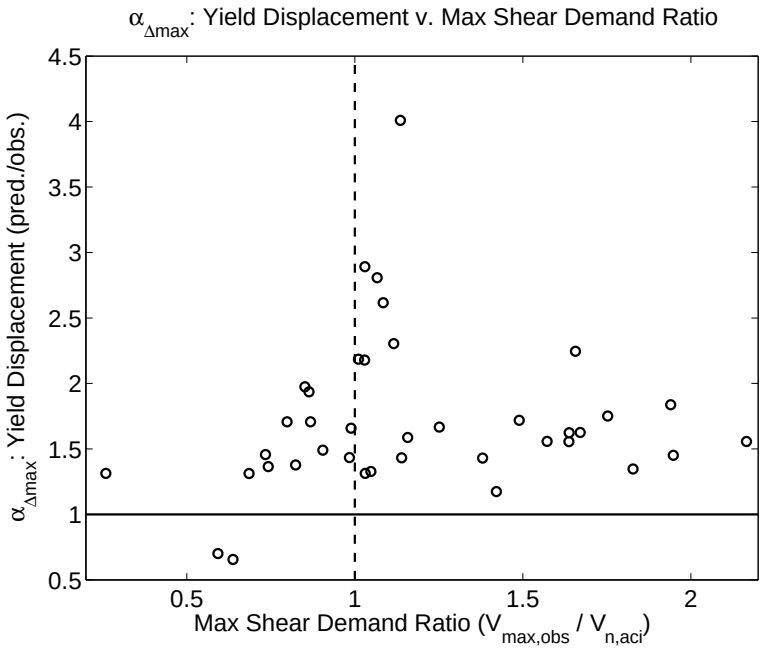

Figure L.72: Beam-Column With Shear Modulus Calibrated to Maximum Displacment - Yield Displacement v Max Shear Demand Ratio

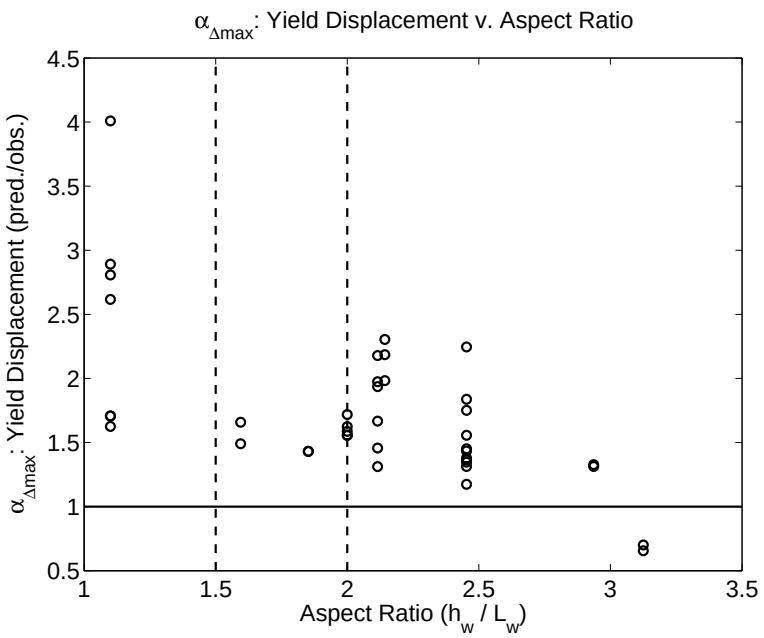

Figure L.73: Beam-Column With Shear Modulus Calibrated to Maximum Displacment - Yield Displacement v Aspect Ratio

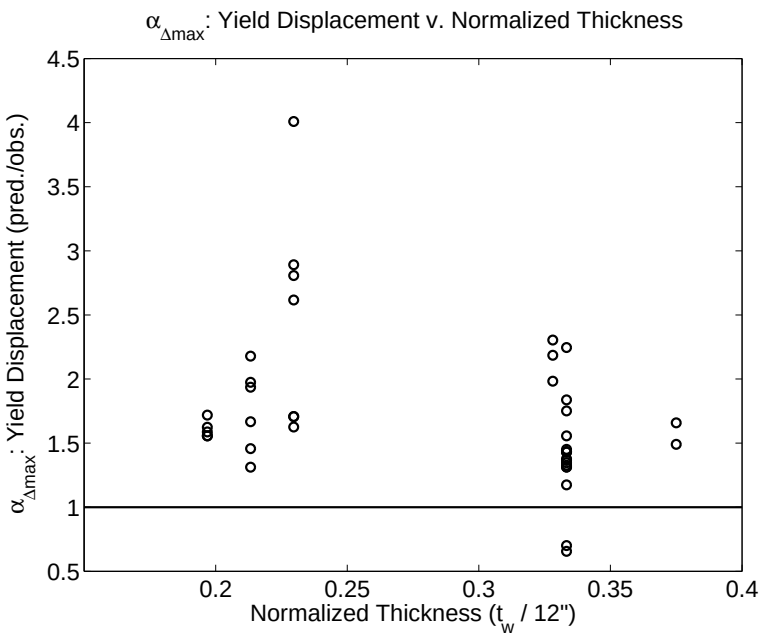

Figure L.74: Beam-Column With Shear Modulus Calibrated to Maximum Displacment - Yield Displacement v Normalized Thickness

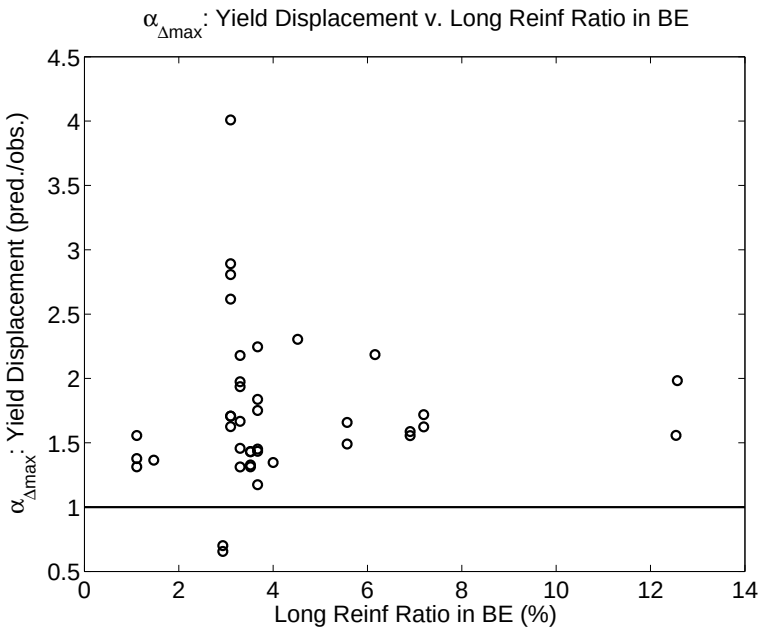

Figure L.75: Beam-Column With Shear Modulus Calibrated to Maximum Displacment - Yield Displacement v Long Reinf Ratio in BE

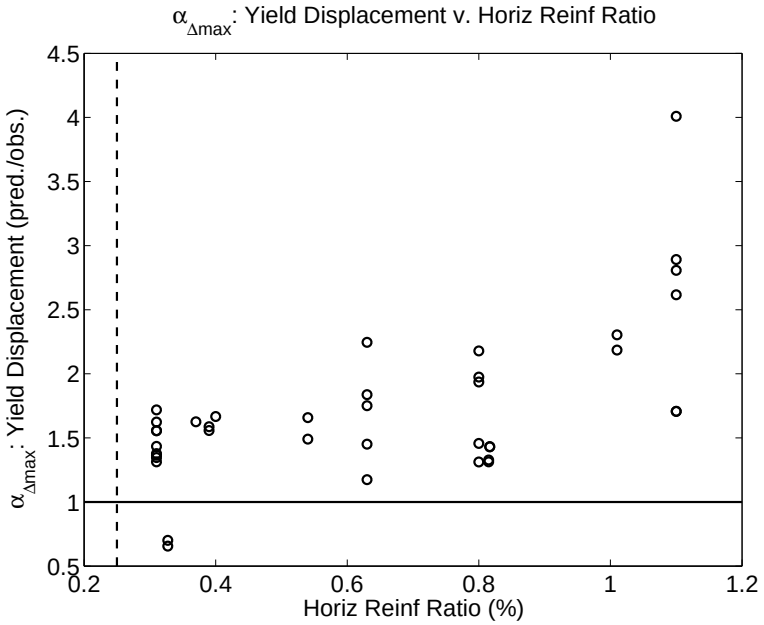

Figure L.76: Beam-Column With Shear Modulus Calibrated to Maximum Displacment - Yield Displacement v Horiz Reinf Ratio

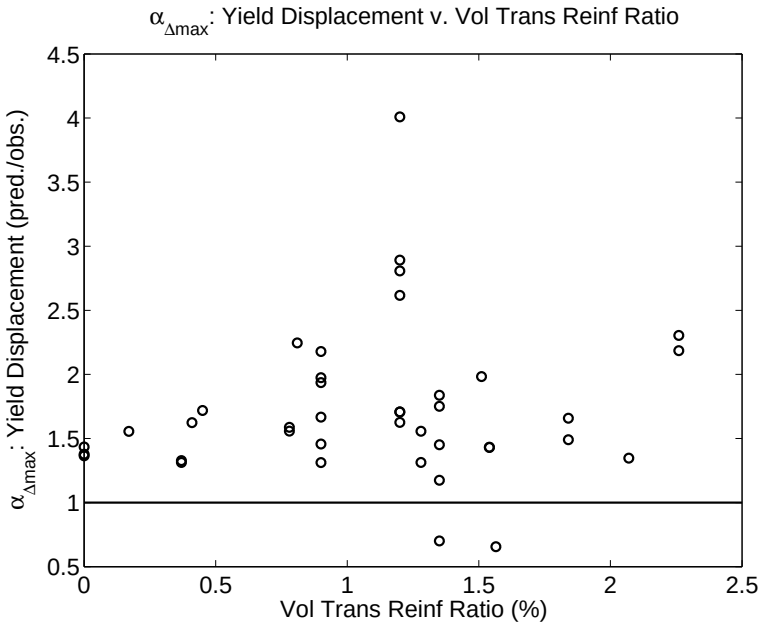

Figure L.77: Beam-Column With Shear Modulus Calibrated to Maximum Displacment - Yield Displacement v Vol Trans Reinf Ratio

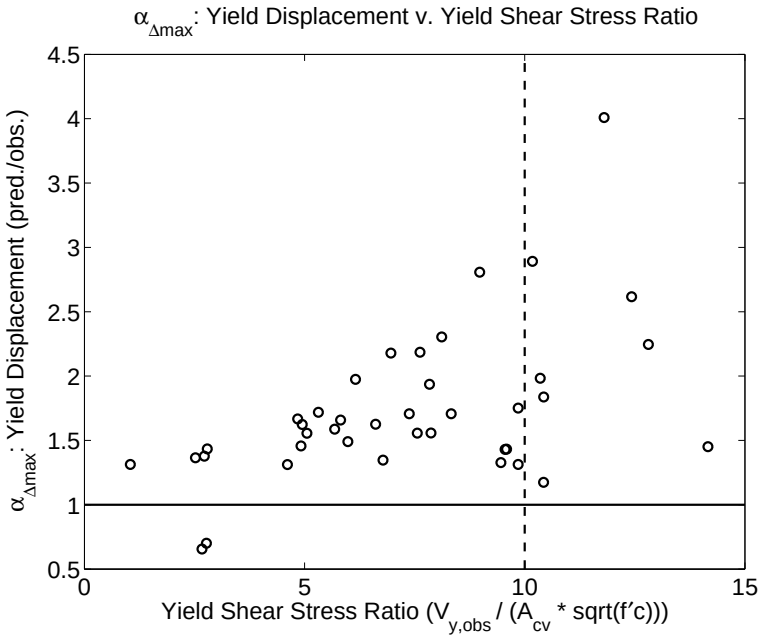

Figure L.78: Beam-Column With Shear Modulus Calibrated to Maximum Displacment - Yield Displacement v Yield Shear Stress Ratio

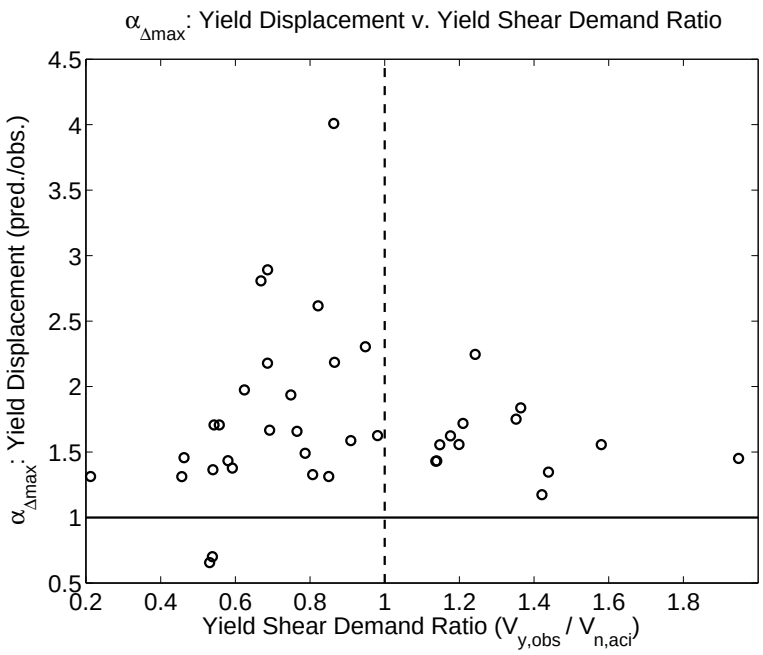

Figure L.79: Beam-Column With Shear Modulus Calibrated to Maximum Displacment - Yield Displacement v Yield Shear Demand Ratio

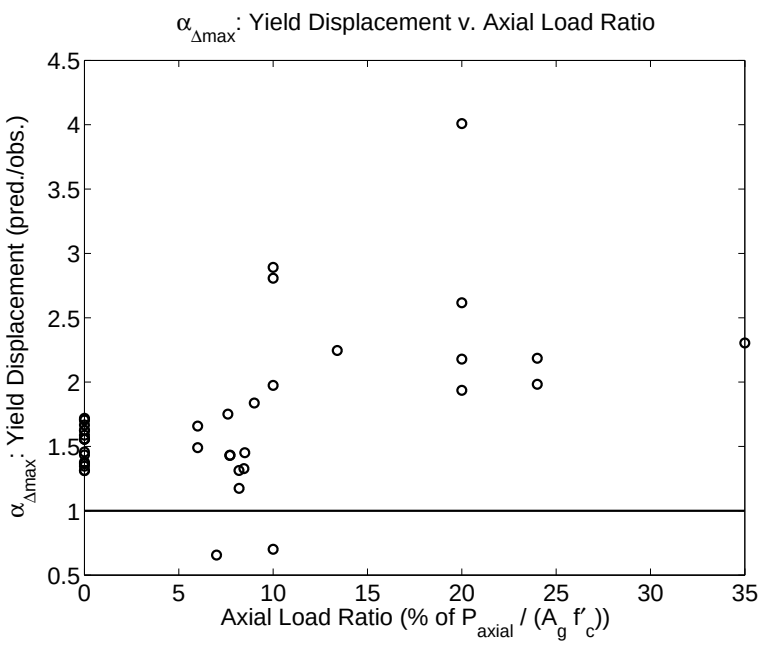

Figure L.80: Beam-Column With Shear Modulus Calibrated to Maximum Displacment - Yield Displacement v Axial Load Ratio

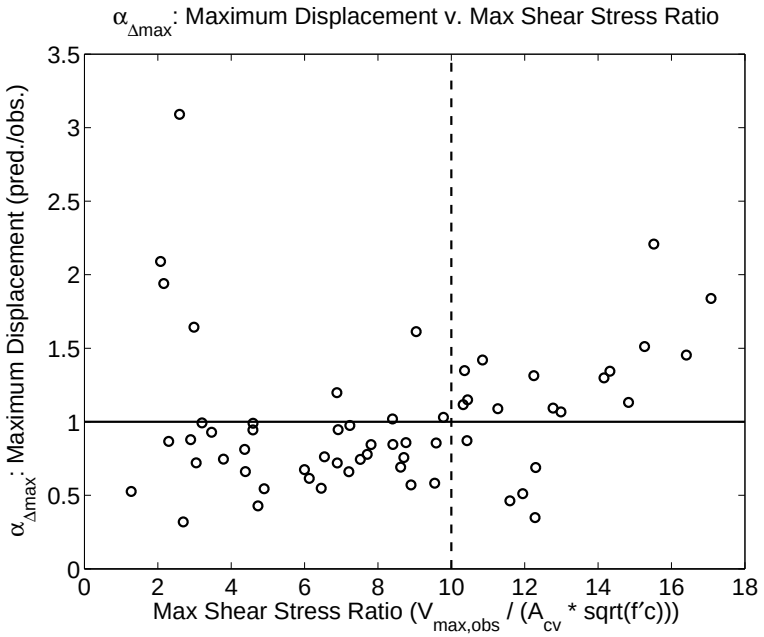

Figure L.81: Beam-Column With Shear Modulus Calibrated to Maximum Displacment - Maximum Displacement v Max Shear Stress Ratio

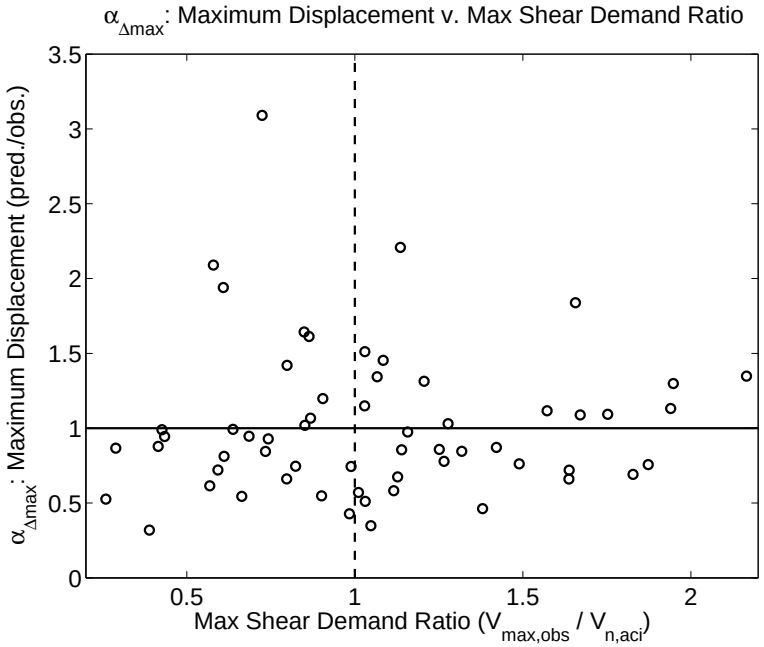

Figure L.82: Beam-Column With Shear Modulus Calibrated to Maximum Displacment - Maximum Displacement v Max Shear Demand Ratio

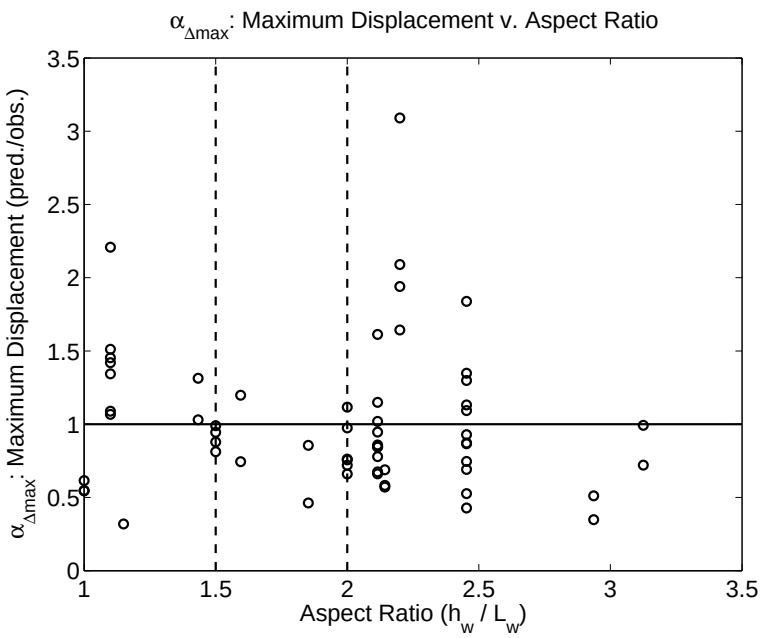

Figure L.83: Beam-Column With Shear Modulus Calibrated to Maximum Displacment - Maximum Displacement v Aspect Ratio

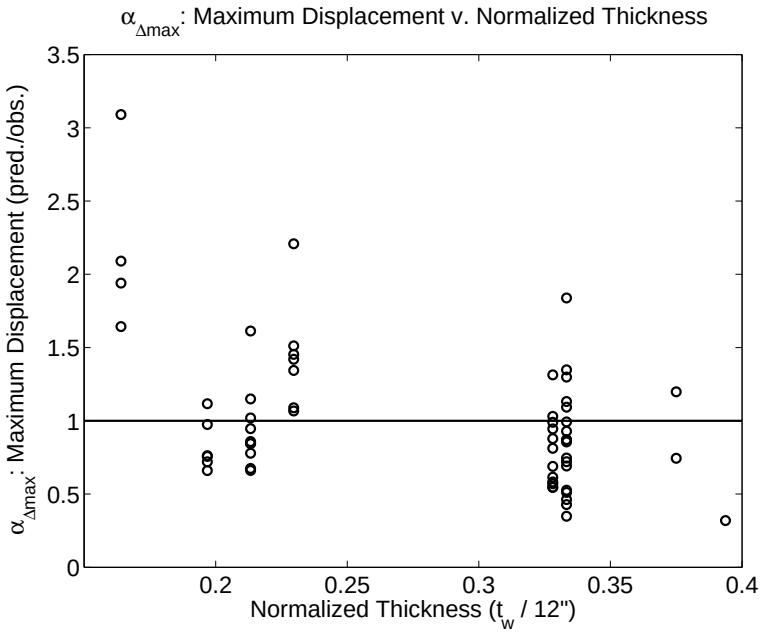

Figure L.84: Beam-Column With Shear Modulus Calibrated to Maximum Displacment - Maximum Displacement v Normalized Thickness

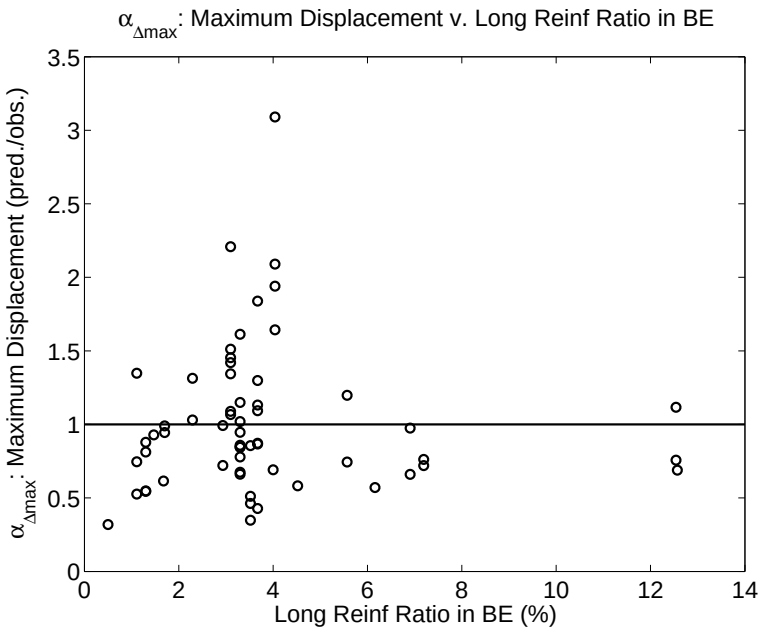

Figure L.85: Beam-Column With Shear Modulus Calibrated to Maximum Displacment - Maximum Displacement v Long Reinf Ratio in BE

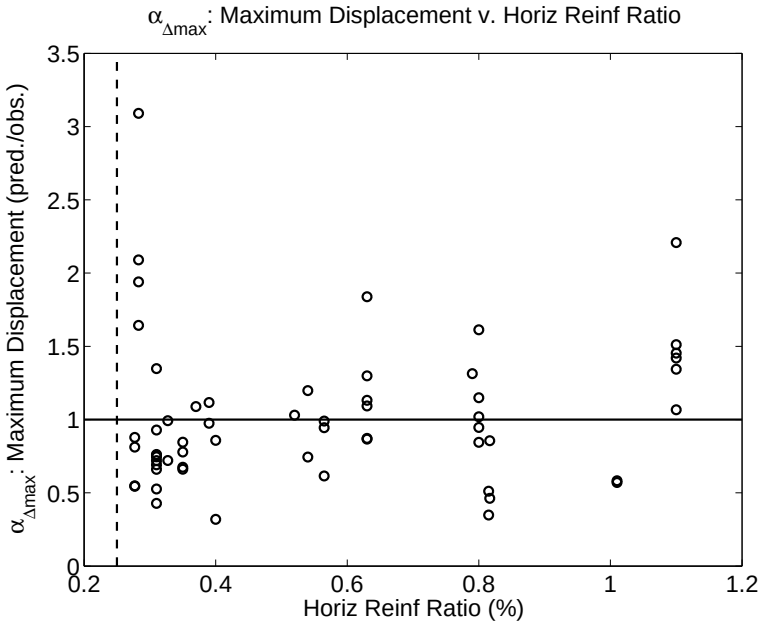

Figure L.86: Beam-Column With Shear Modulus Calibrated to Maximum Displacment - Maximum Displacement v Horiz Reinf Ratio

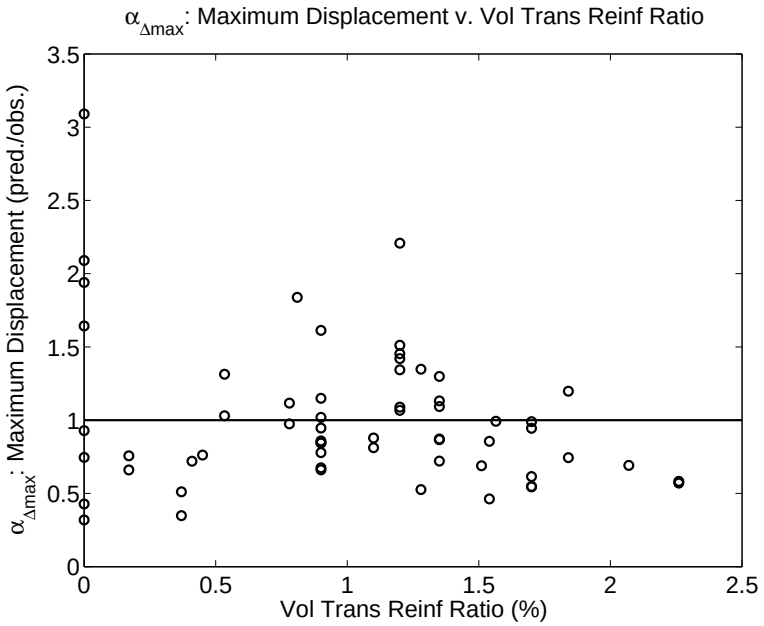

Figure L.87: Beam-Column With Shear Modulus Calibrated to Maximum Displacment - Maximum Displacement v Vol Trans Reinf Ratio

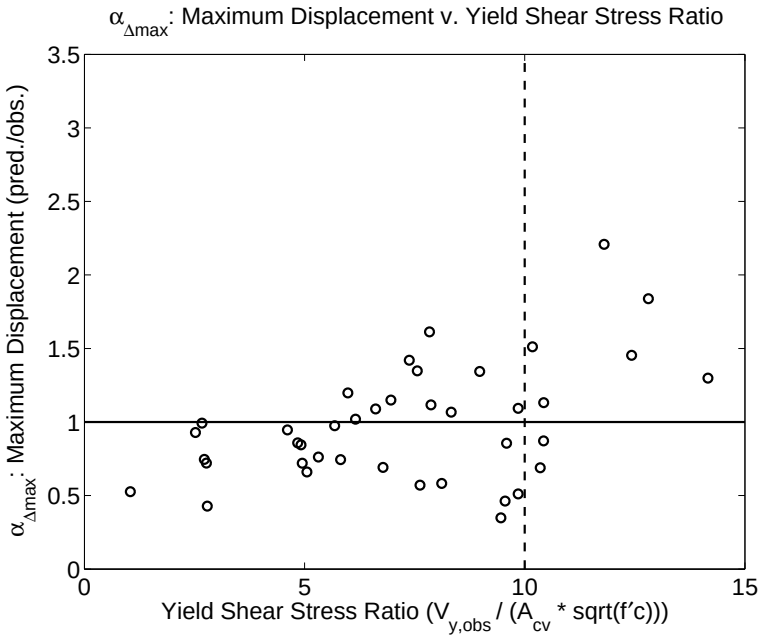

Figure L.88: Beam-Column With Shear Modulus Calibrated to Maximum Displacment - Maximum Displacement v Yield Shear Stress Ratio

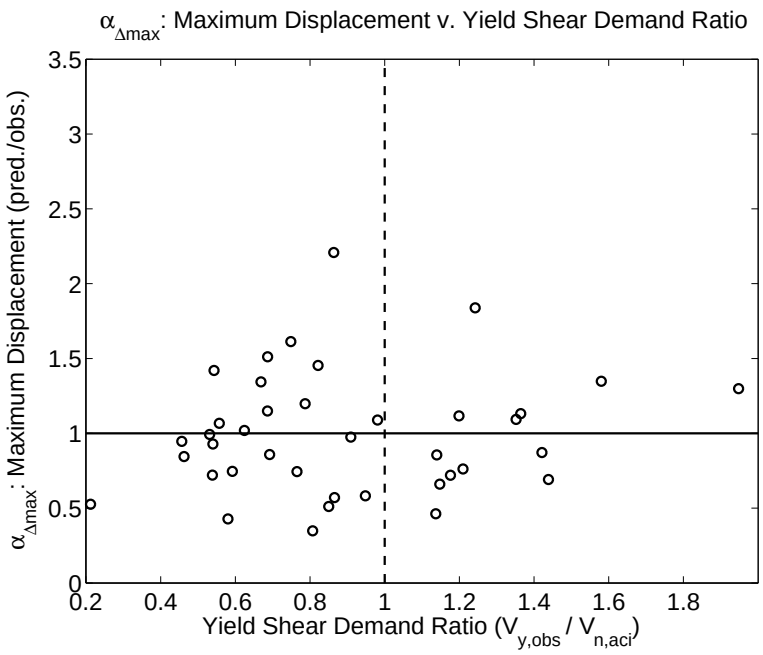

Figure L.89: Beam-Column With Shear Modulus Calibrated to Maximum Displacment - Maximum Displacement v Yield Shear Demand Ratio

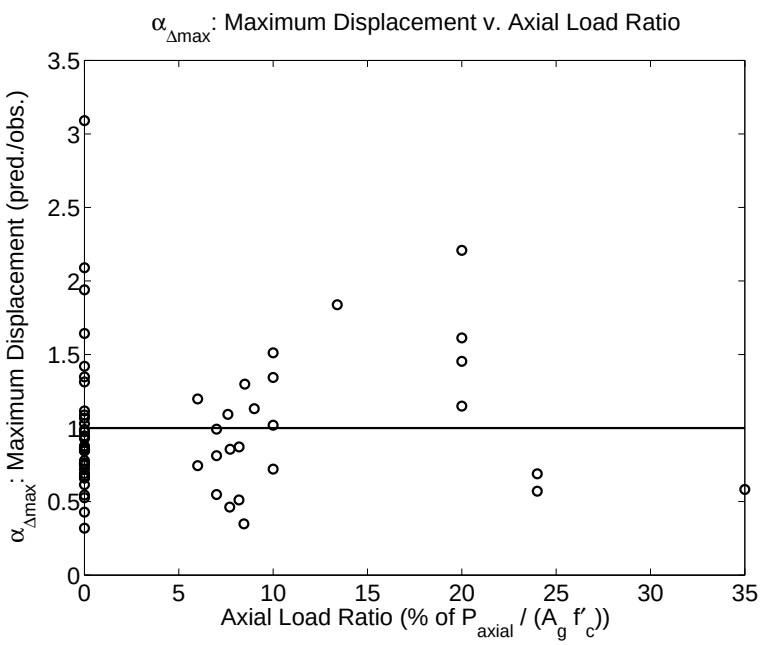

Figure L.90: Beam-Column With Shear Modulus Calibrated to Maximum Displacment - Maximum Displacement v Axial Load Ratio

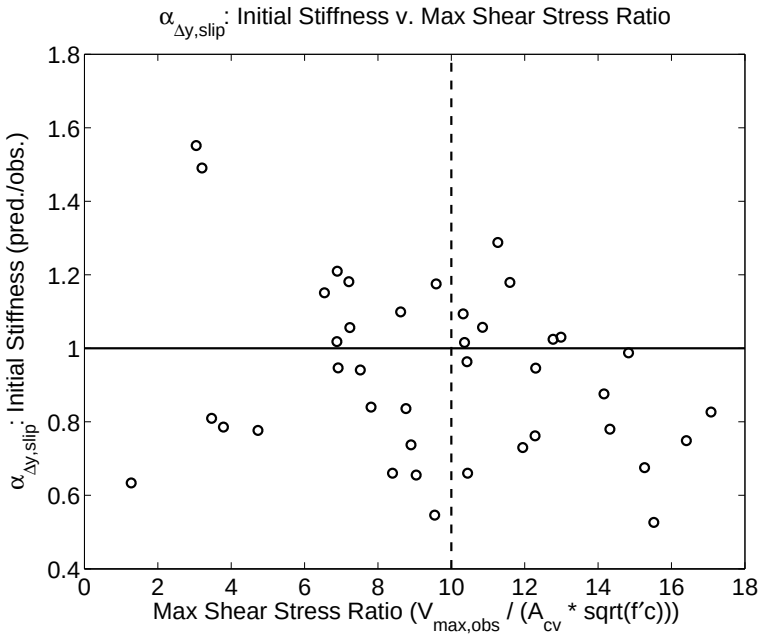

Figure L.91: Beam-Column With Shear Modulus Calibrated to Yield Displacment With Slip - Initial Stiffness v Max Shear Stress Ratio

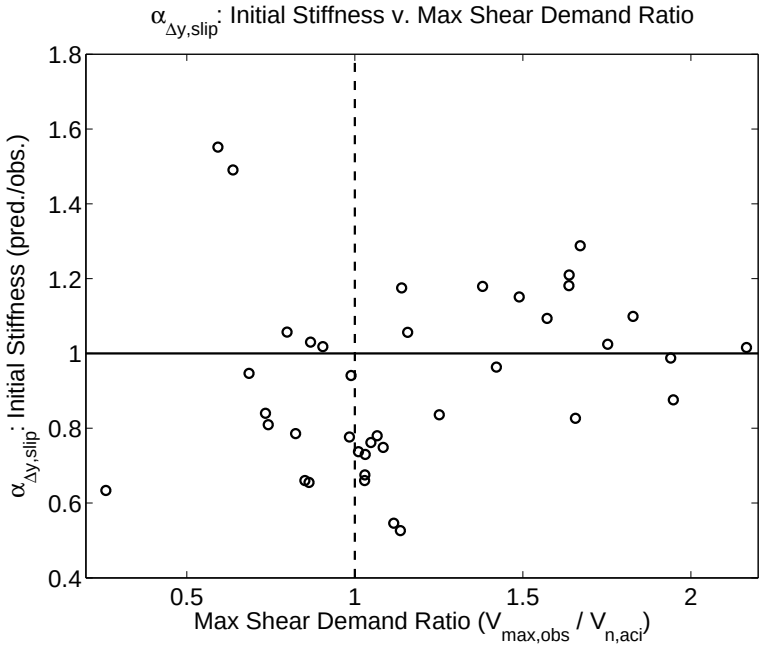

Figure L.92: Beam-Column With Shear Modulus Calibrated to Yield Displacment With Slip - Initial Stiffness v Max Shear Demand Ratio

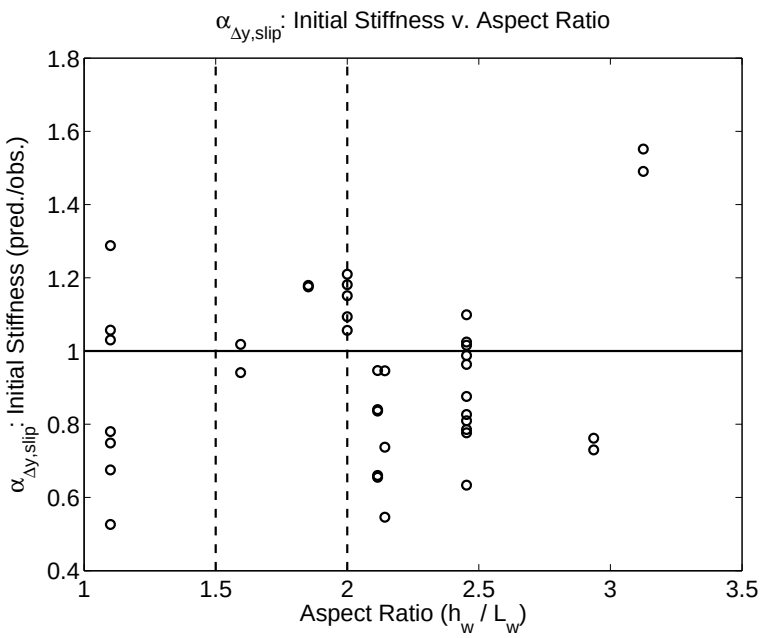

Figure L.93: Beam-Column With Shear Modulus Calibrated to Yield Displacment With Slip - Initial Stiffness v Aspect Ratio

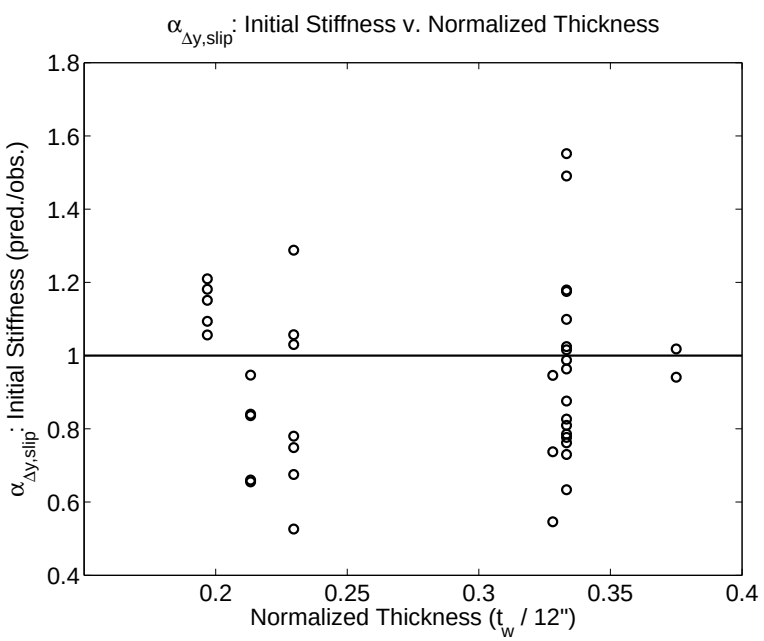

Figure L.94: Beam-Column With Shear Modulus Calibrated to Yield Displacment With Slip - Initial Stiffness v Normalized Thickness

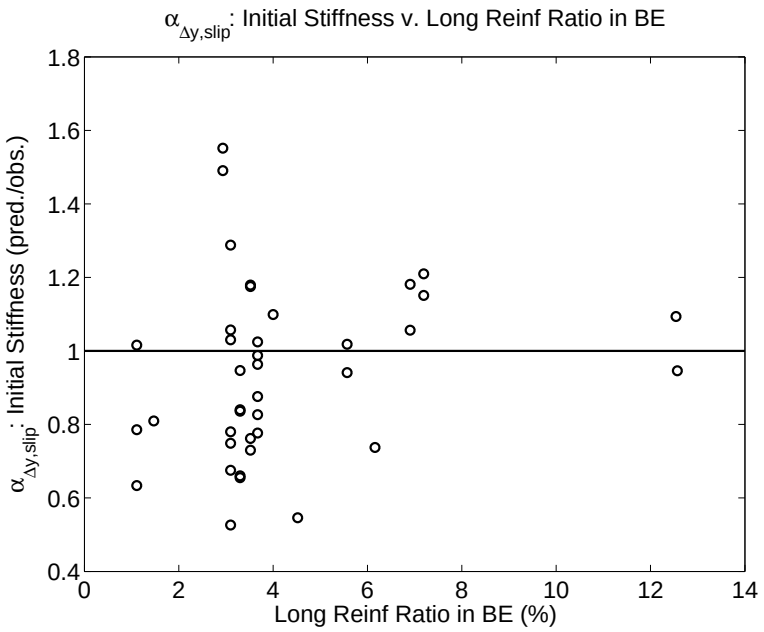

Figure L.95: Beam-Column With Shear Modulus Calibrated to Yield Displacment With Slip - Initial Stiffness v Long Reinf Ratio in BE

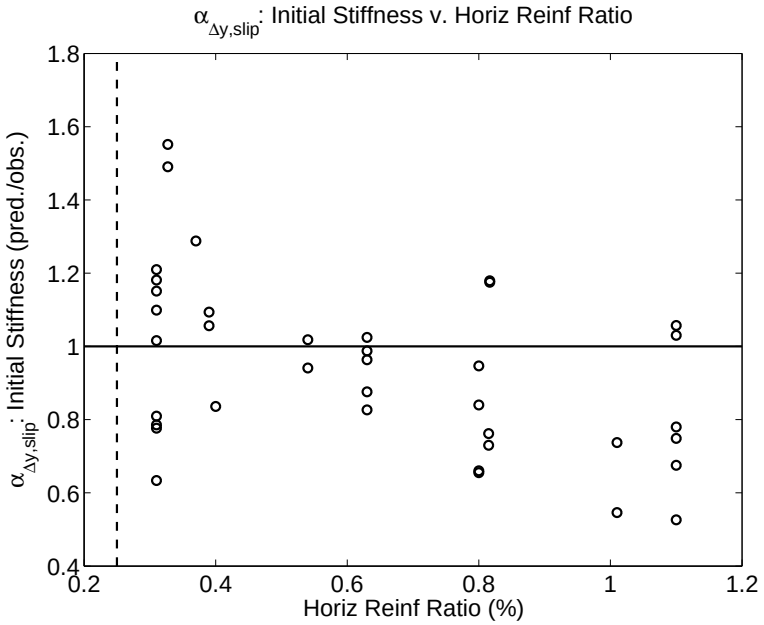

Figure L.96: Beam-Column With Shear Modulus Calibrated to Yield Displacment With Slip - Initial Stiffness v Horiz Reinf Ratio

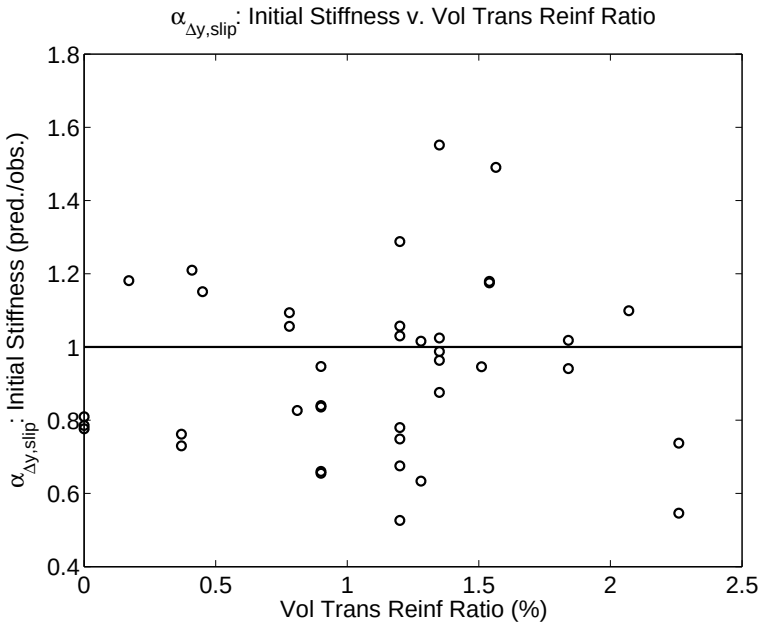

Figure L.97: Beam-Column With Shear Modulus Calibrated to Yield Displacment With Slip - Initial Stiffness v Vol Trans Reinf Ratio

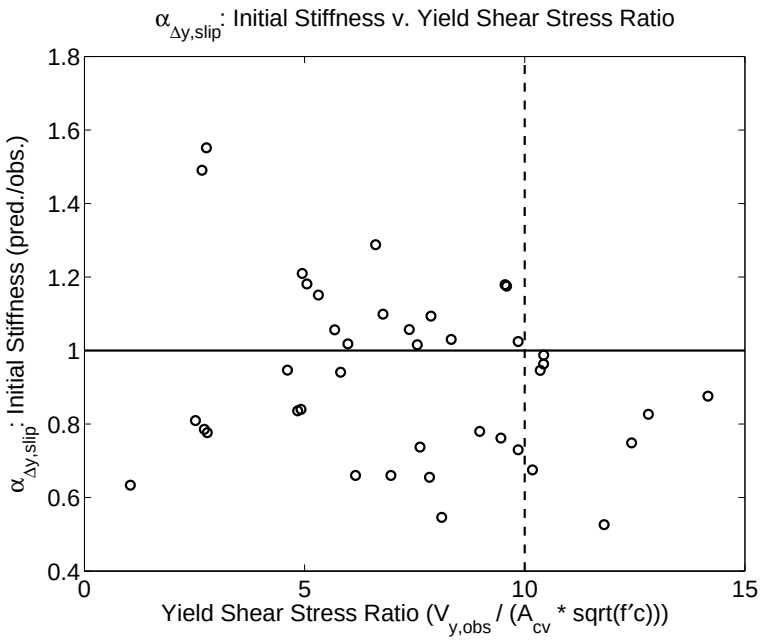

Figure L.98: Beam-Column With Shear Modulus Calibrated to Yield Displacment With Slip - Initial Stiffness v Yield Shear Stress Ratio

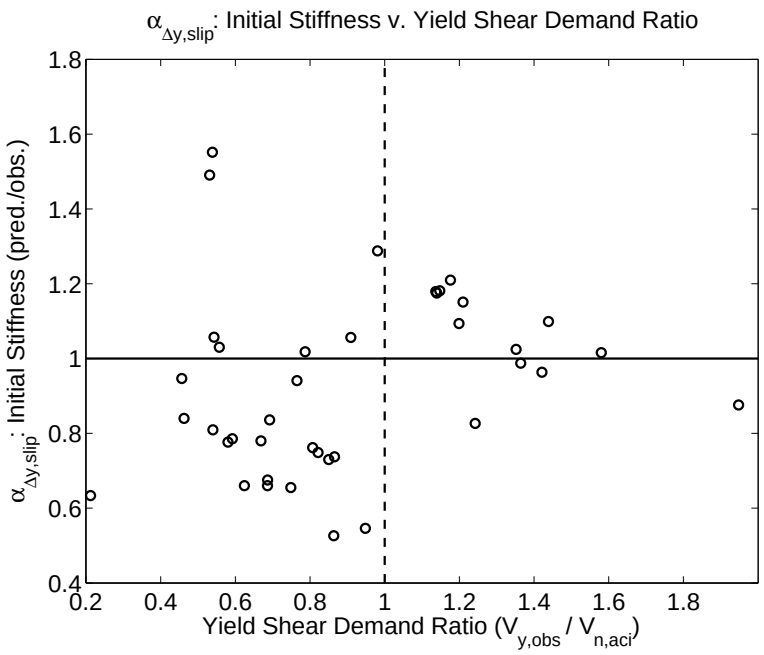

Figure L.99: Beam-Column With Shear Modulus Calibrated to Yield Displacment With Slip - Initial Stiffness v Yield Shear Demand Ratio

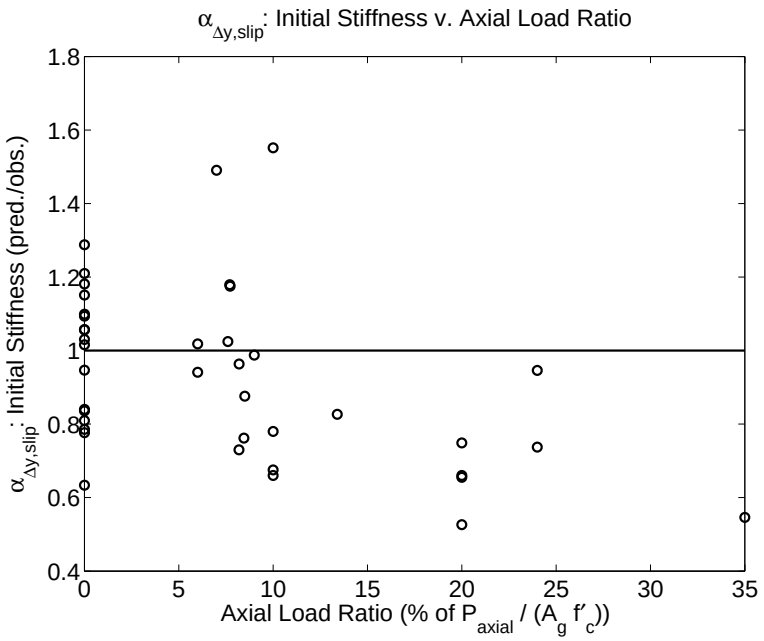

Figure L.100: Beam-Column With Shear Modulus Calibrated to Yield Displacment With Slip - Initial Stiffness v Axial Load Ratio

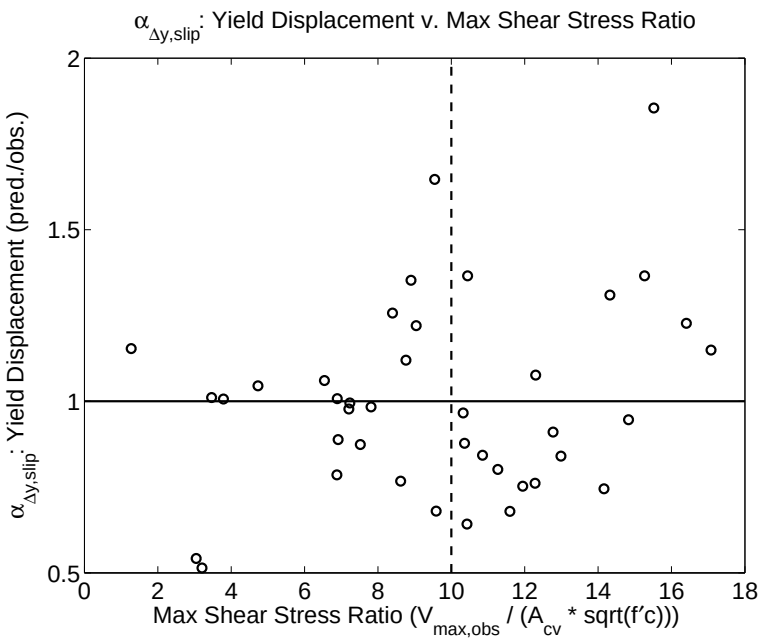

Figure L.101: Beam-Column With Shear Modulus Calibrated to Yield Displacment With Slip - Yield Displacement v Max Shear Stress Ratio

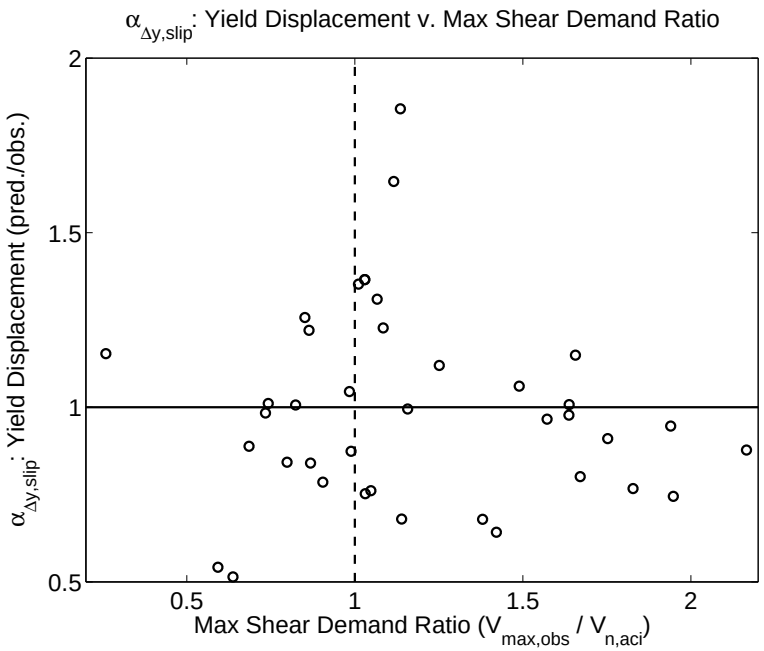

Figure L.102: Beam-Column With Shear Modulus Calibrated to Yield Displacment With Slip - Yield Displacement v Max Shear Demand Ratio

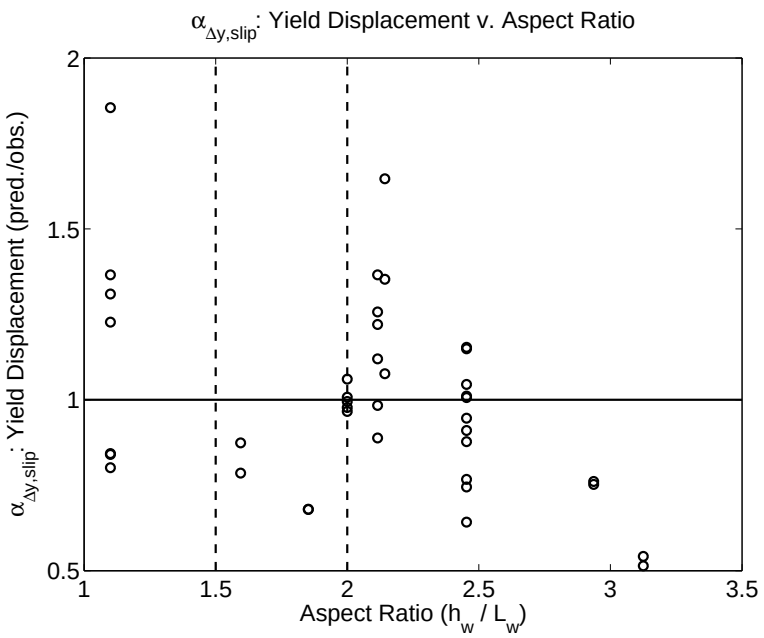

Figure L.103: Beam-Column With Shear Modulus Calibrated to Yield Displacment With Slip - Yield Displacement v Aspect Ratio

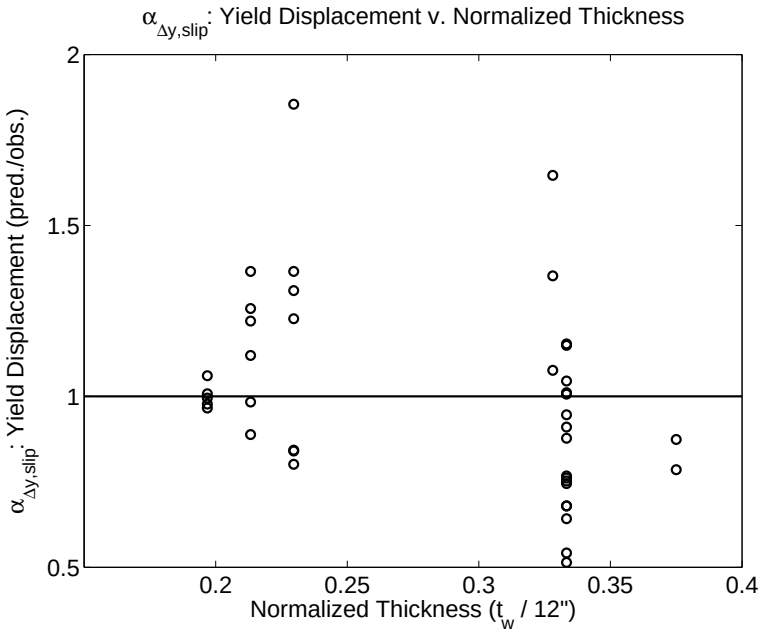

Figure L.104: Beam-Column With Shear Modulus Calibrated to Yield Displacment With Slip - Yield Displacement v Normalized Thickness

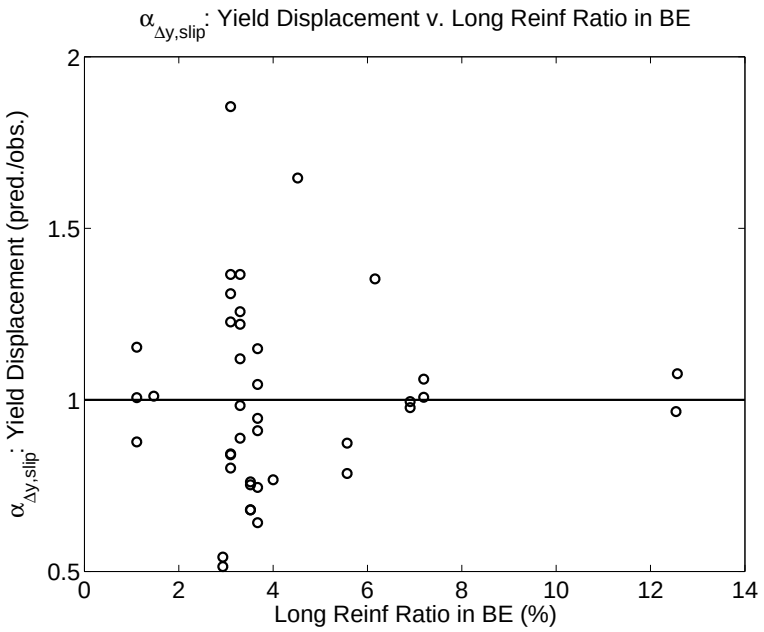

Figure L.105: Beam-Column With Shear Modulus Calibrated to Yield Displacment With Slip - Yield Displacement v Long Reinf Ratio in BE

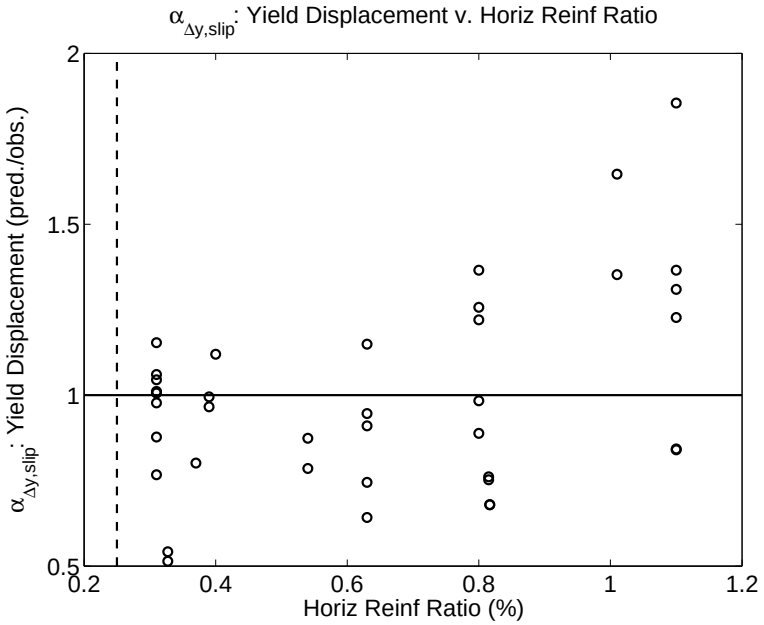

Figure L.106: Beam-Column With Shear Modulus Calibrated to Yield Displacment With Slip - Yield Displacement v Horiz Reinf Ratio

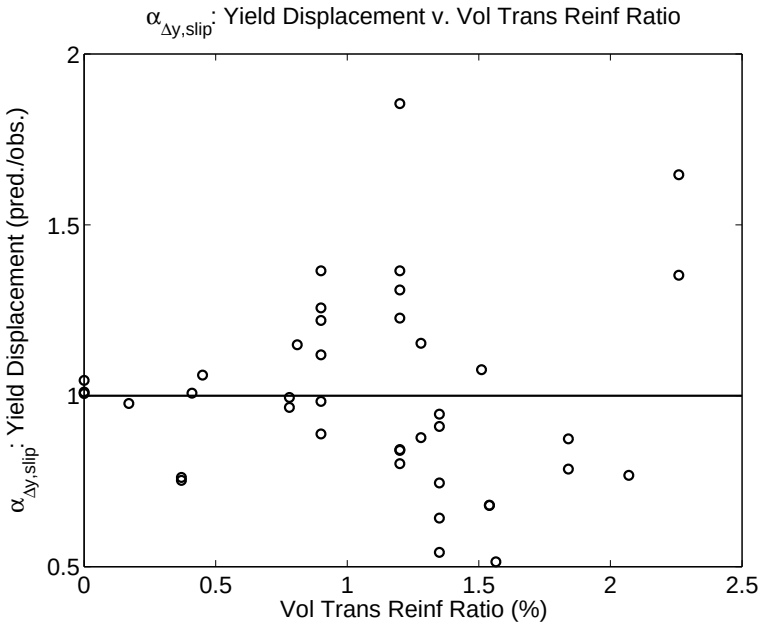

Figure L.107: Beam-Column With Shear Modulus Calibrated to Yield Displacment With Slip - Yield Displacement v Vol Trans Reinf Ratio

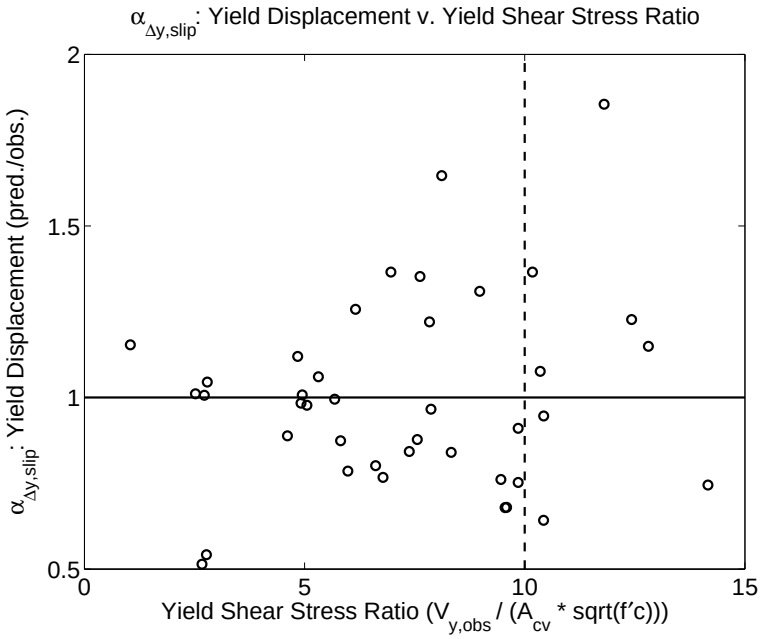

Figure L.108: Beam-Column With Shear Modulus Calibrated to Yield Displacment With Slip - Yield Displacement v Yield Shear Stress Ratio

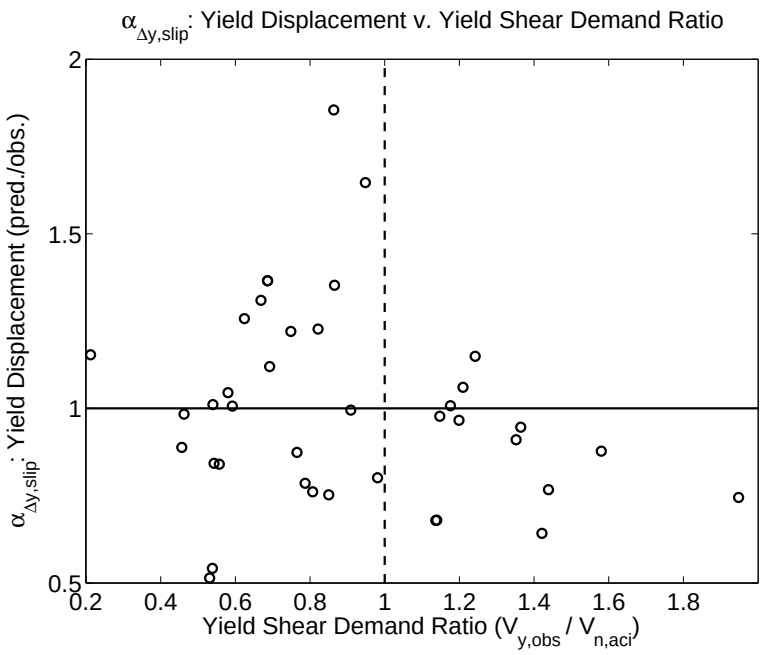

Figure L.109: Beam-Column With Shear Modulus Calibrated to Yield Displacment With Slip - Yield Displacement v Yield Shear Demand Ratio

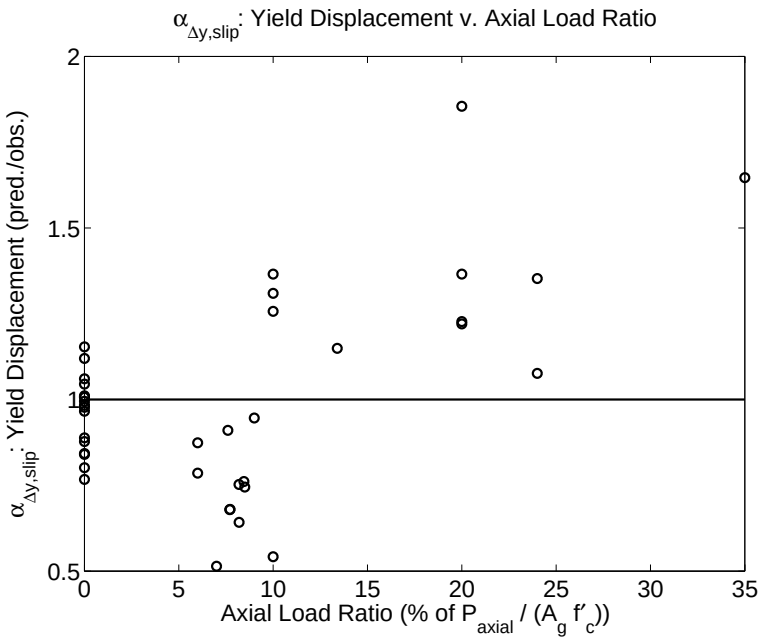

Figure L.110: Beam-Column With Shear Modulus Calibrated to Yield Displacment With Slip - Yield Displacement v Axial Load Ratio

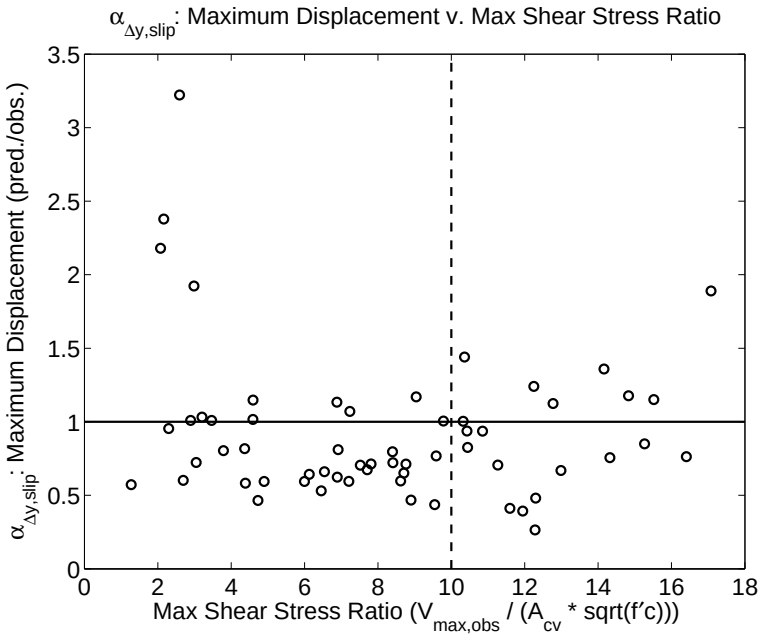

Figure L.111: Beam-Column With Shear Modulus Calibrated to Yield Displacment With Slip - Maximum Displacement v Max Shear Stress Ratio

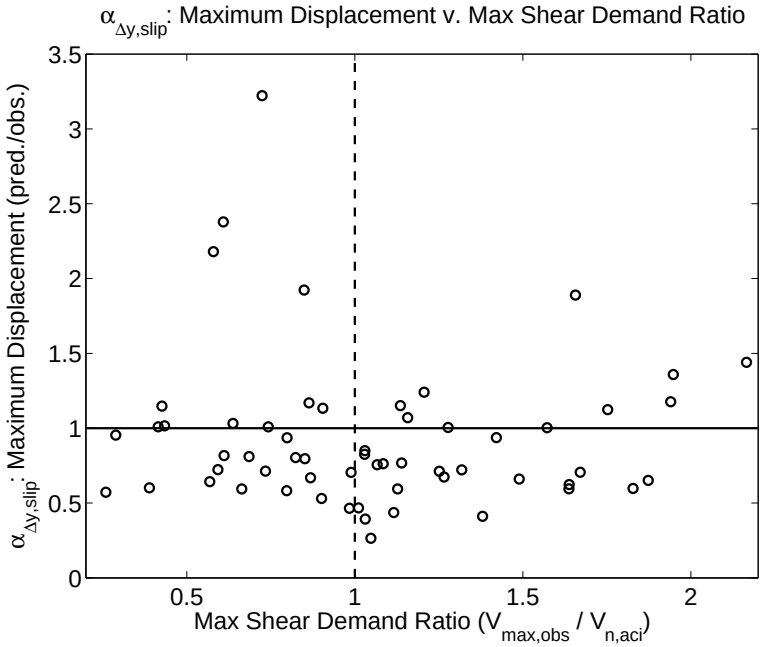

Figure L.112: Beam-Column With Shear Modulus Calibrated to Yield Displacment With Slip - Maximum Displacement v Max Shear Demand Ratio

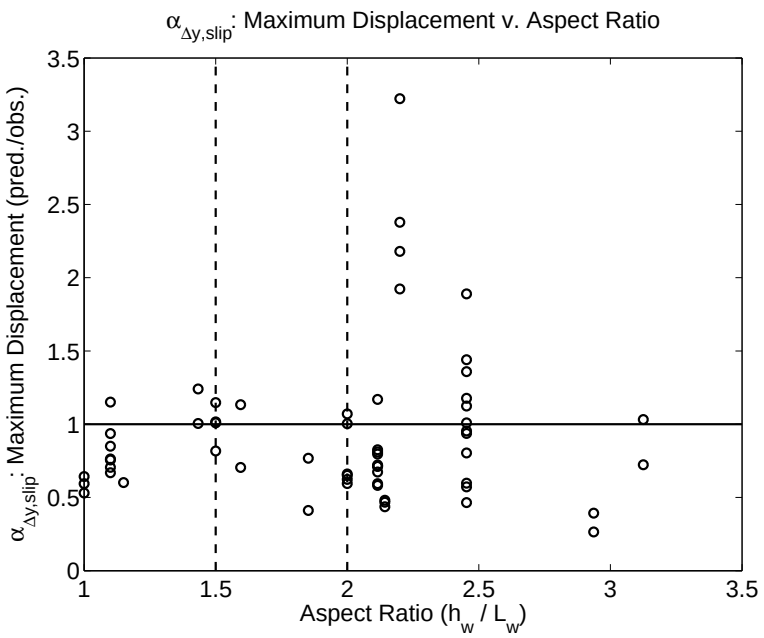

Figure L.113: Beam-Column With Shear Modulus Calibrated to Yield Displacment With Slip - Maximum Displacement v Aspect Ratio

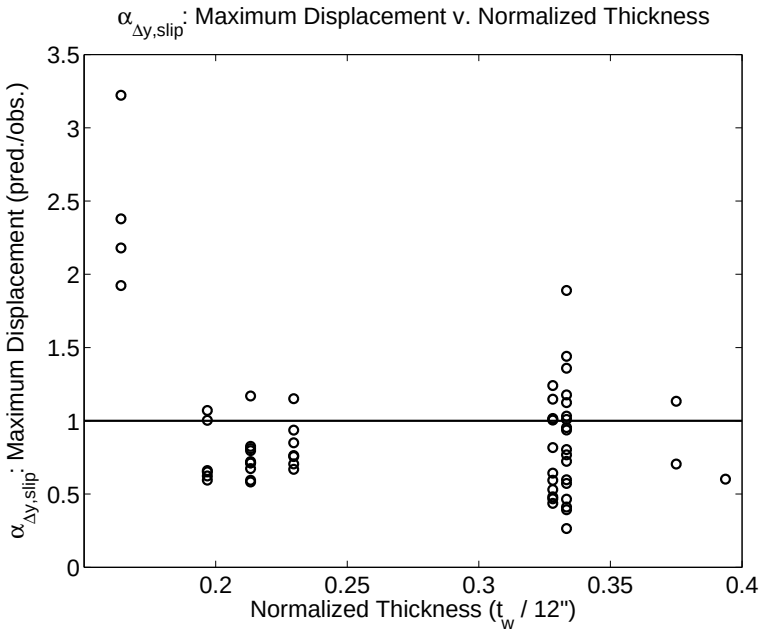

Figure L.114: Beam-Column With Shear Modulus Calibrated to Yield Displacment With Slip - Maximum Displacement v Normalized Thickness

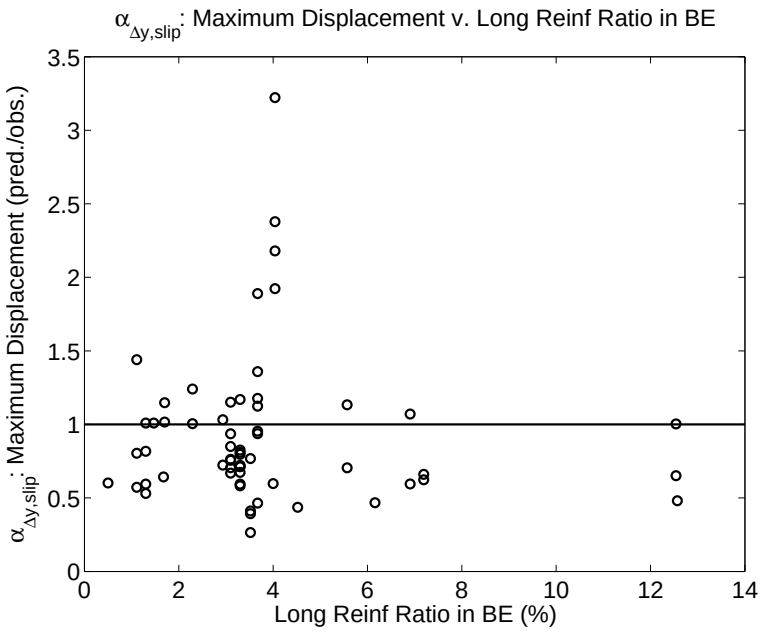

Figure L.115: Beam-Column With Shear Modulus Calibrated to Yield Displacment With Slip - Maximum Displacement v Long Reinf Ratio in BE

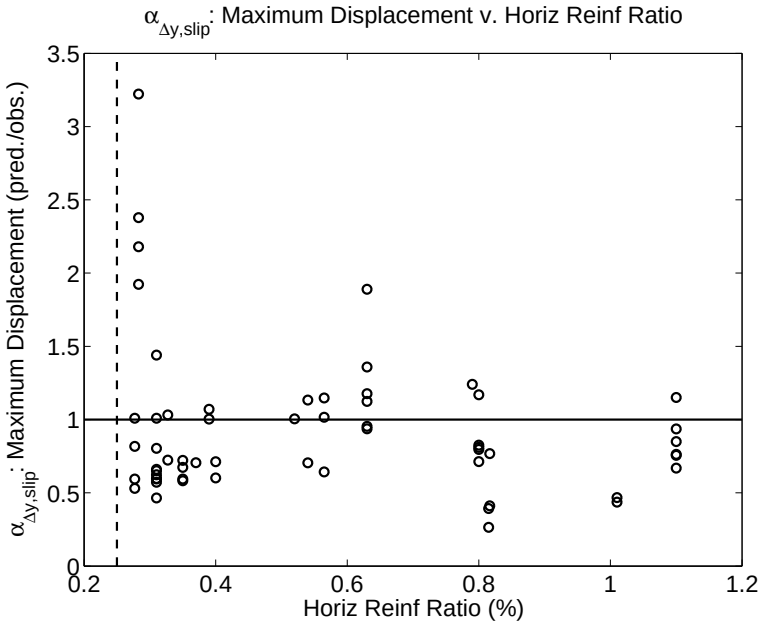

Figure L.116: Beam-Column With Shear Modulus Calibrated to Yield Displacment With Slip - Maximum Displacement v Horiz Reinf Ratio

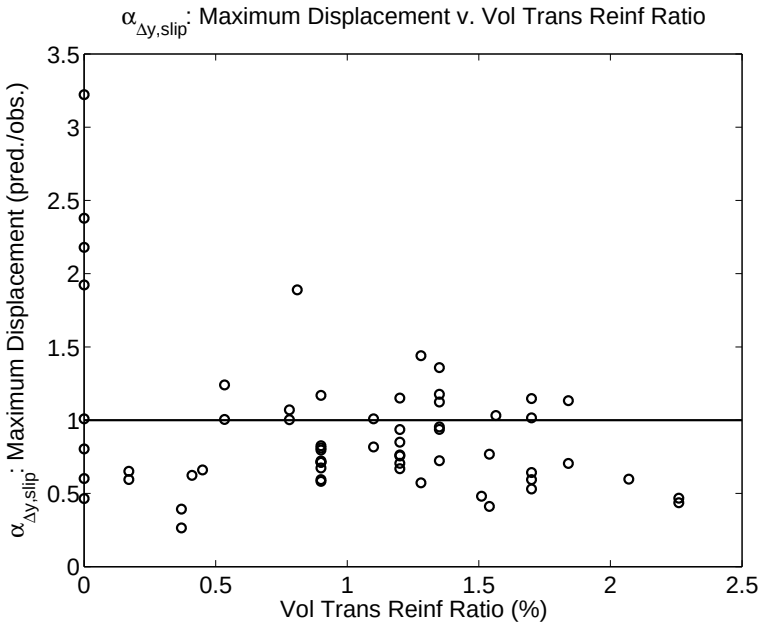

Figure L.117: Beam-Column With Shear Modulus Calibrated to Yield Displacment With Slip - Maximum Displacement v Vol Trans Reinf Ratio

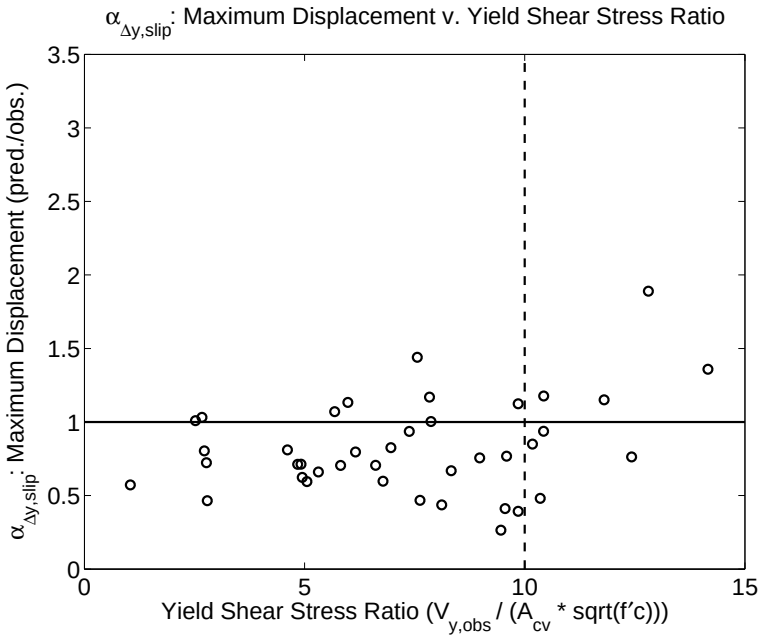

Figure L.118: Beam-Column With Shear Modulus Calibrated to Yield Displacment With Slip - Maximum Displacement v Yield Shear Stress Ratio

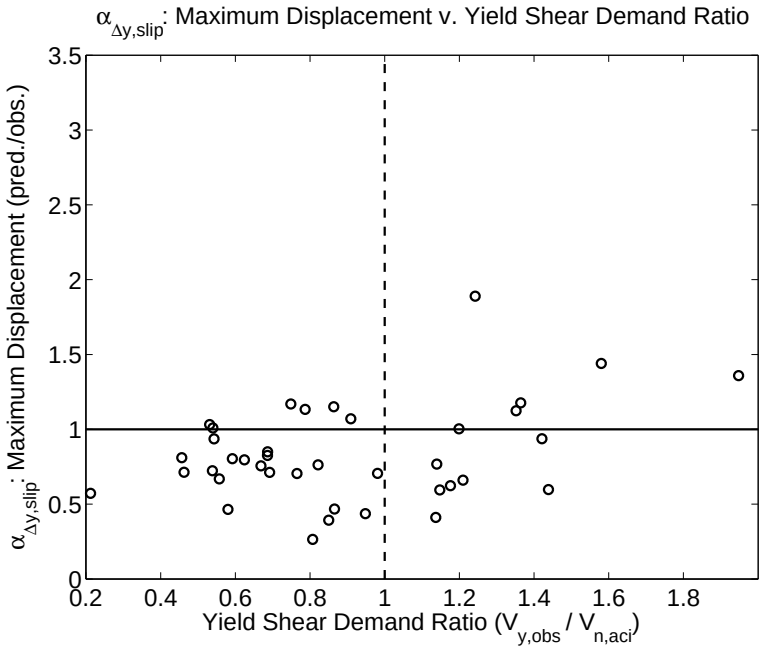

Figure L.119: Beam-Column With Shear Modulus Calibrated to Yield Displacment With Slip - Maximum Displacement v Yield Shear Demand Ratio

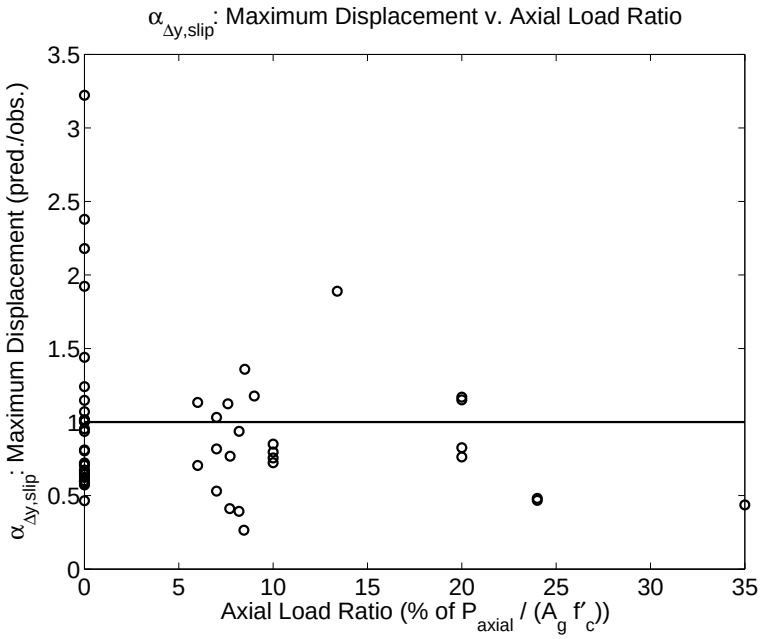

Figure L.120: Beam-Column With Shear Modulus Calibrated to Yield Displacment With Slip - Maximum Displacement v Axial Load Ratio

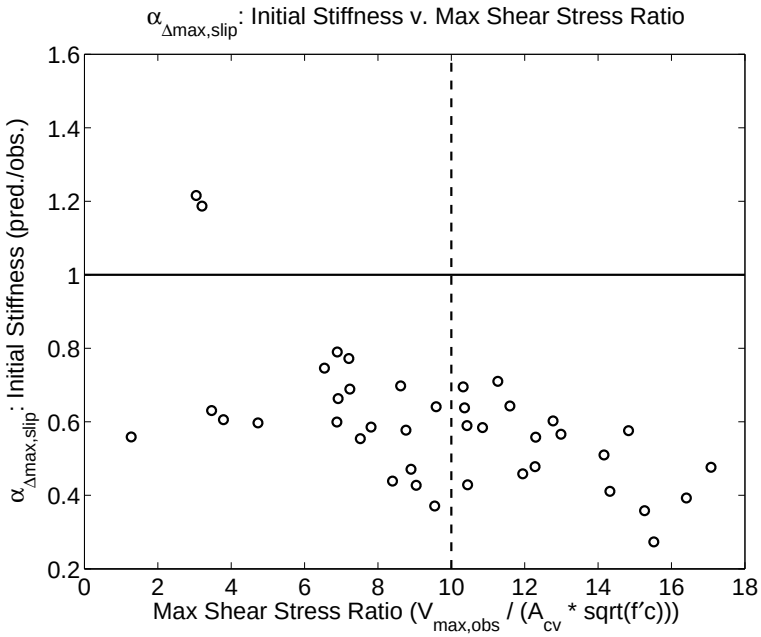

Figure L.121: Beam-Column With Shear Modulus Calibrated to Maximum Displacment With Slip - Initial Stiffness v Max Shear Stress Ratio

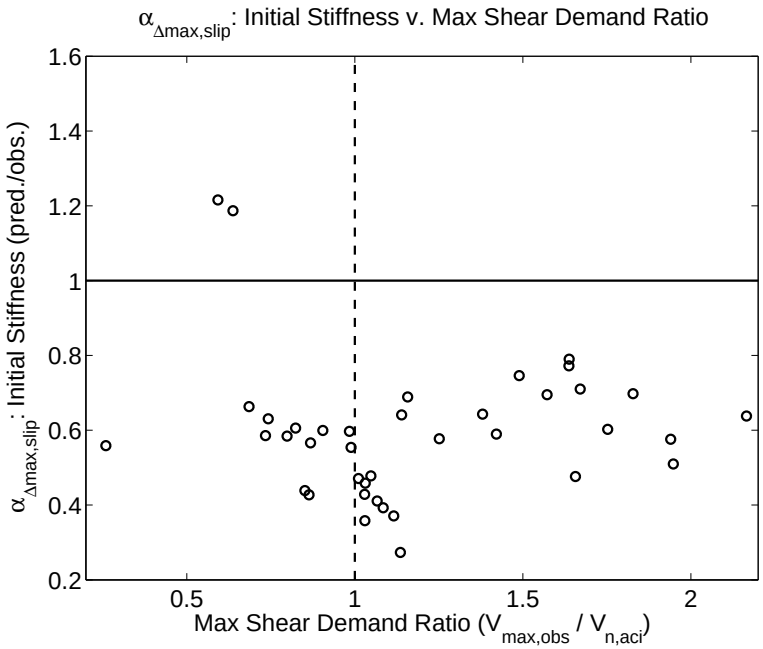

Figure L.122: Beam-Column With Shear Modulus Calibrated to Maximum Displacment With Slip - Initial Stiffness v Max Shear Demand Ratio

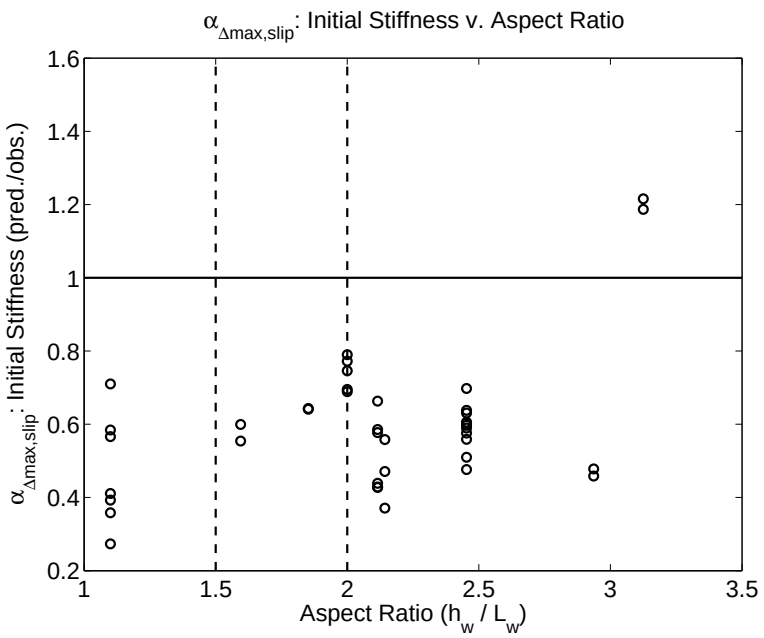

Figure L.123: Beam-Column With Shear Modulus Calibrated to Maximum Displacment With Slip - Initial Stiffness v Aspect Ratio

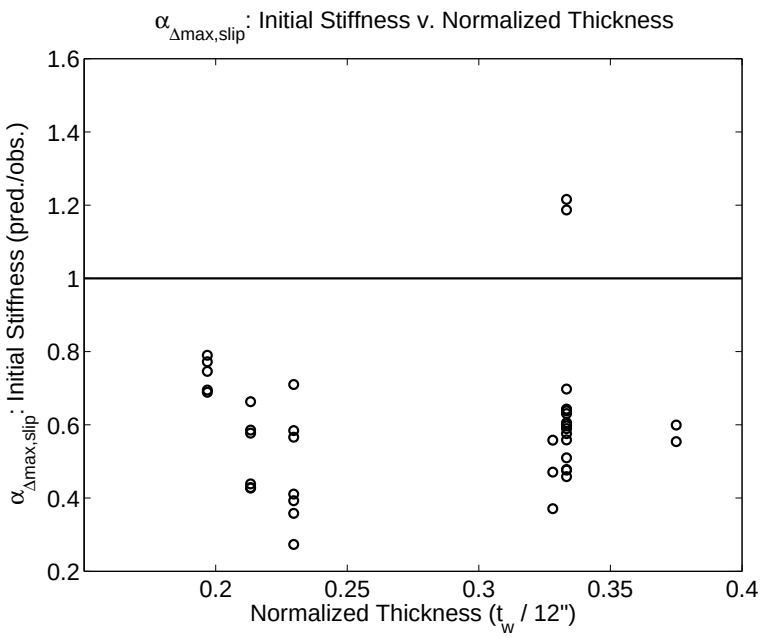

Figure L.124: Beam-Column With Shear Modulus Calibrated to Maximum Displacment With Slip - Initial Stiffness v Normalized Thickness

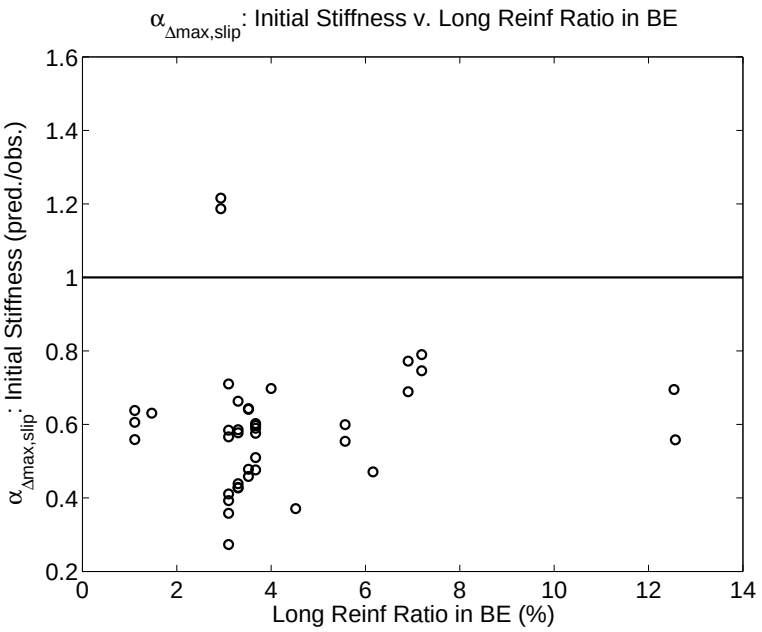

Figure L.125: Beam-Column With Shear Modulus Calibrated to Maximum Displacment With Slip - Initial Stiffness v Long Reinf Ratio in BE

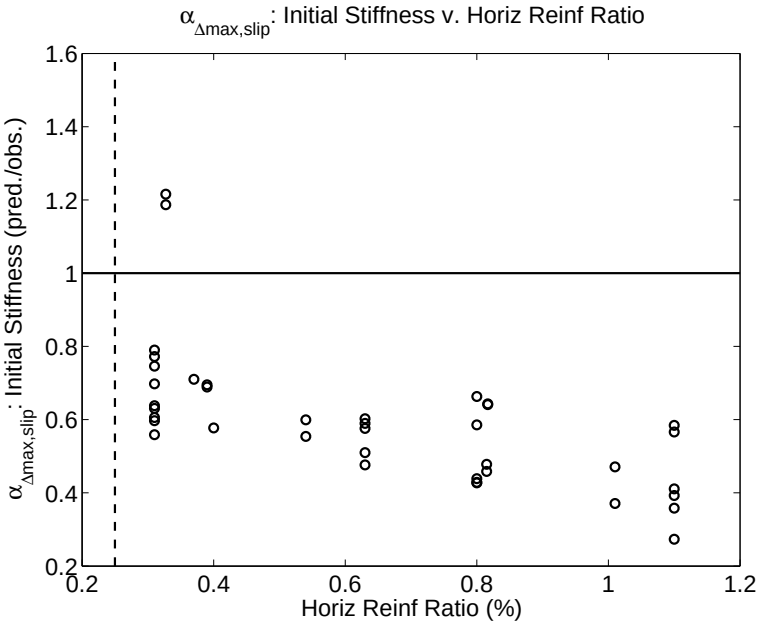

Figure L.126: Beam-Column With Shear Modulus Calibrated to Maximum Displacment With Slip - Initial Stiffness v Horiz Reinf Ratio

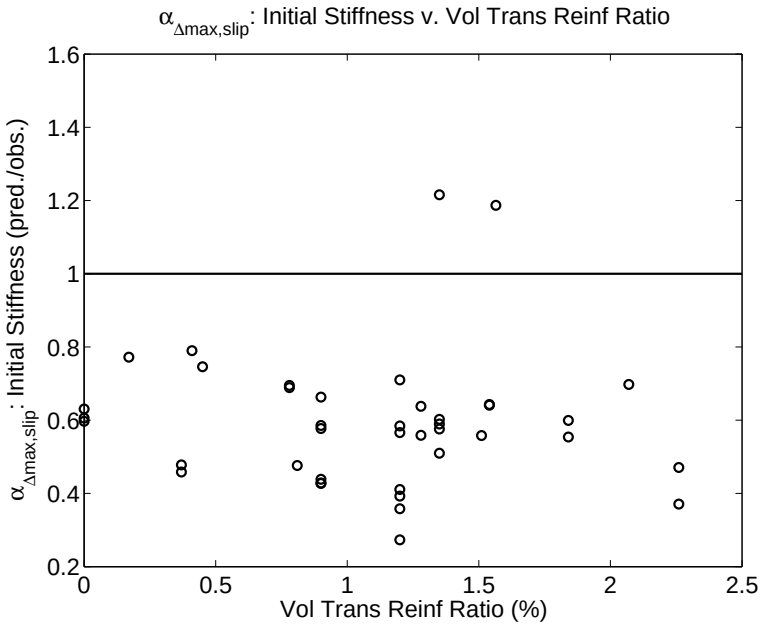

Figure L.127: Beam-Column With Shear Modulus Calibrated to Maximum Displacment With Slip - Initial Stiffness v Vol Trans Reinf Ratio

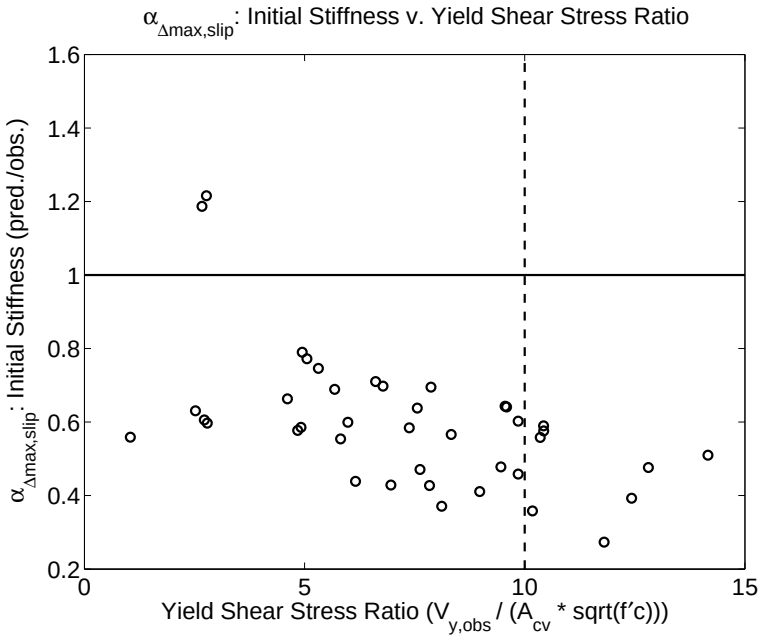

Figure L.128: Beam-Column With Shear Modulus Calibrated to Maximum Displacment With Slip - Initial Stiffness v Yield Shear Stress Ratio

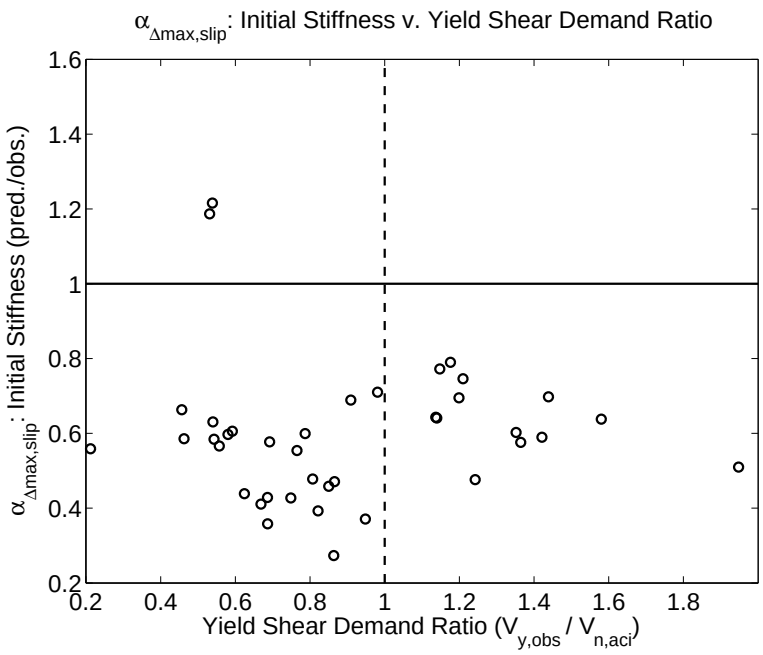

Figure L.129: Beam-Column With Shear Modulus Calibrated to Maximum Displacment With Slip - Initial Stiffness v Yield Shear Demand Ratio

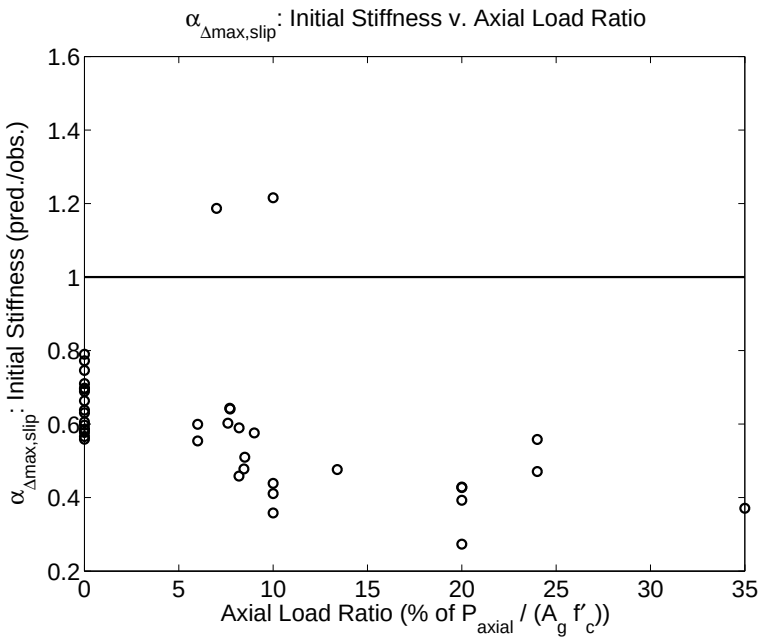

Figure L.130: Beam-Column With Shear Modulus Calibrated to Maximum Displacment With Slip - Initial Stiffness v Axial Load Ratio

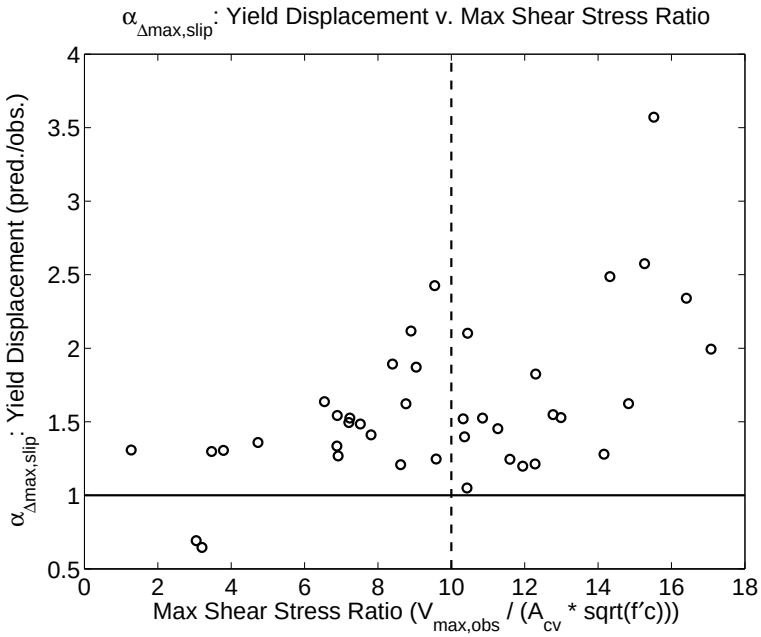

Figure L.131: Beam-Column With Shear Modulus Calibrated to Maximum Displacment With Slip - Yield Displacement v Max Shear Stress Ratio

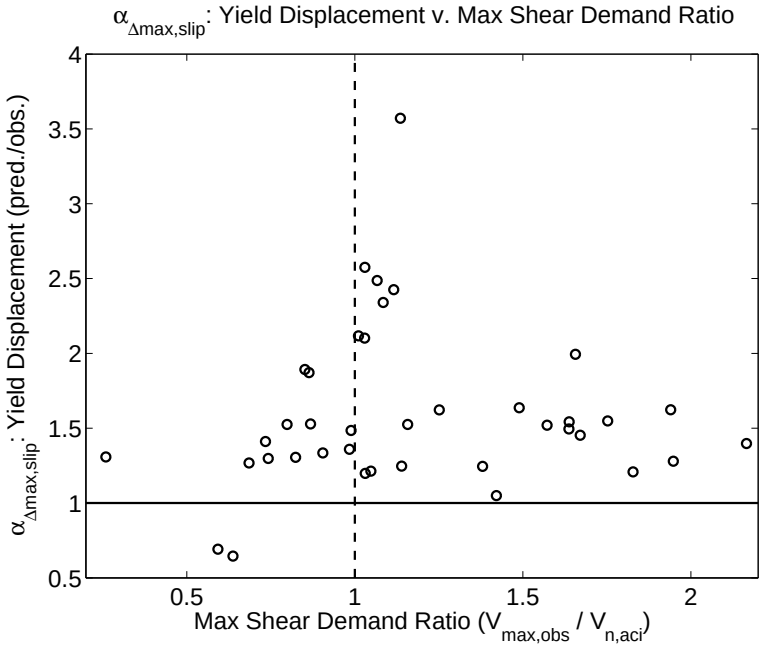

Figure L.132: Beam-Column With Shear Modulus Calibrated to Maximum Displacment With Slip - Yield Displacement v Max Shear Demand Ratio

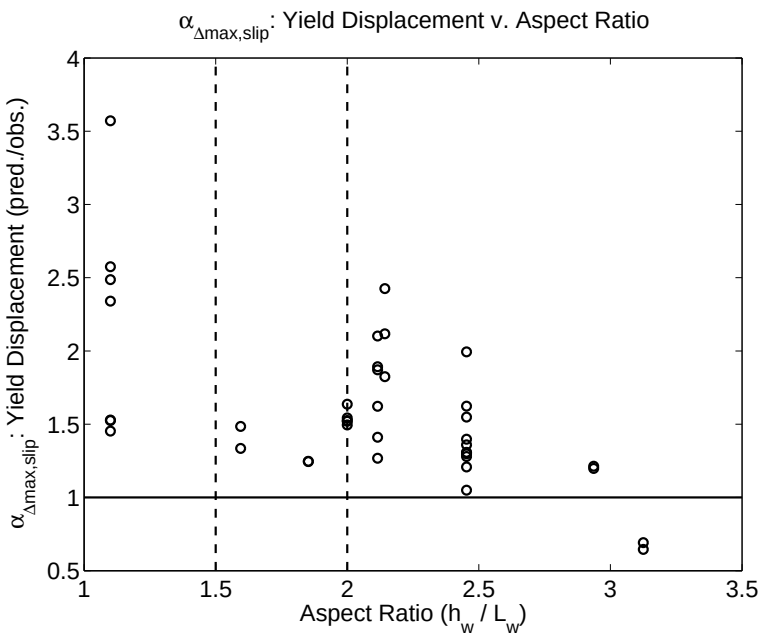

Figure L.133: Beam-Column With Shear Modulus Calibrated to Maximum Displacment With Slip - Yield Displacement v Aspect Ratio

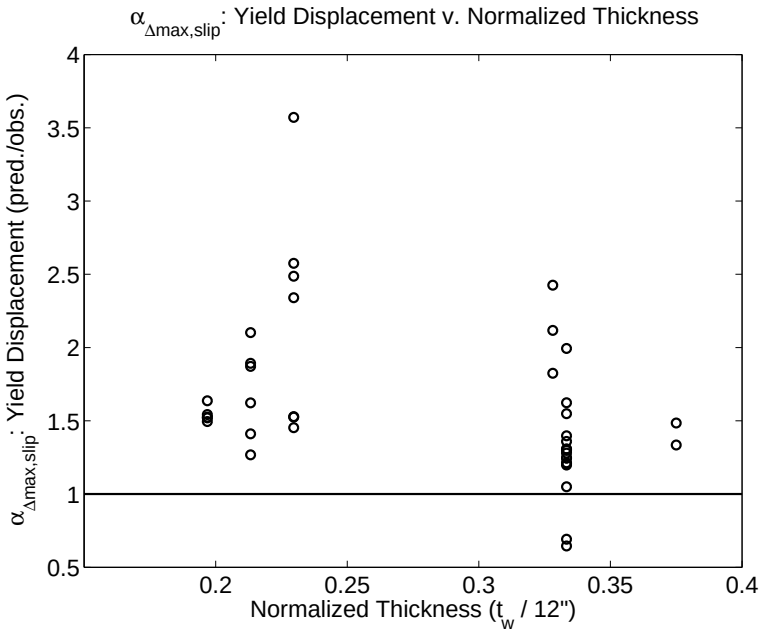

Figure L.134: Beam-Column With Shear Modulus Calibrated to Maximum Displacment With Slip - Yield Displacement v Normalized Thickness

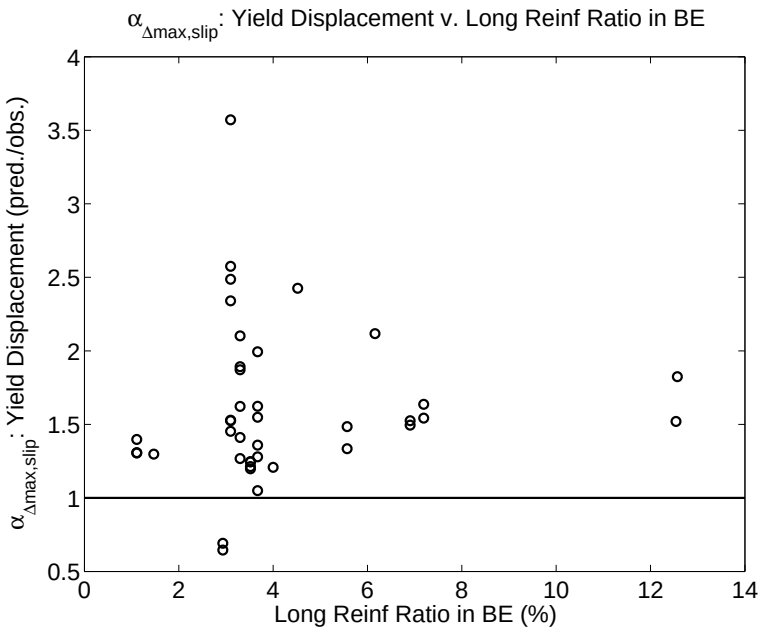

Figure L.135: Beam-Column With Shear Modulus Calibrated to Maximum Displacment With Slip - Yield Displacement v Long Reinf Ratio in BE

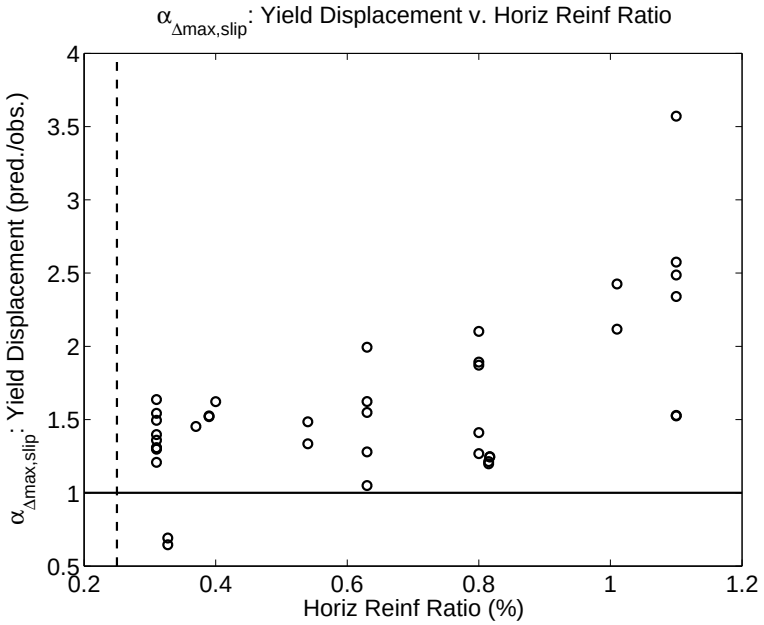

Figure L.136: Beam-Column With Shear Modulus Calibrated to Maximum Displacment With Slip - Yield Displacement v Horiz Reinf Ratio

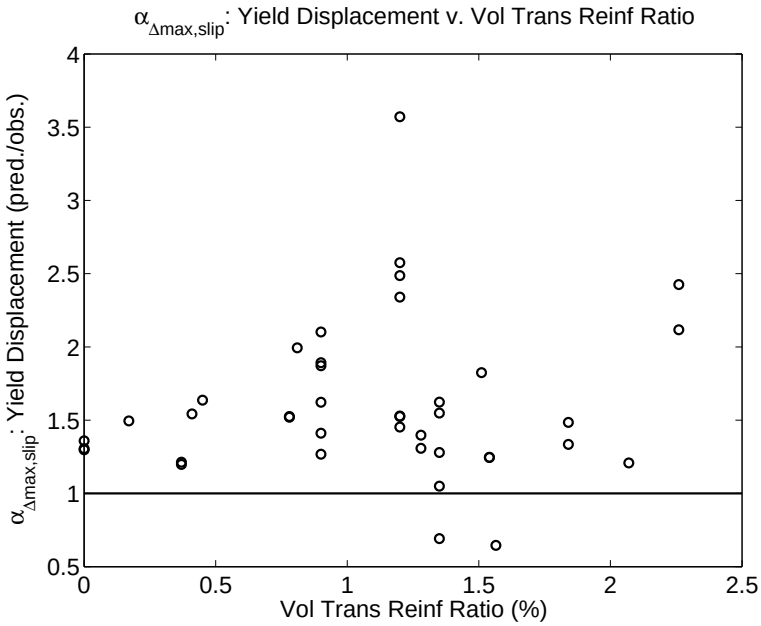

Figure L.137: Beam-Column With Shear Modulus Calibrated to Maximum Displacment With Slip - Yield Displacement v Vol Trans Reinf Ratio

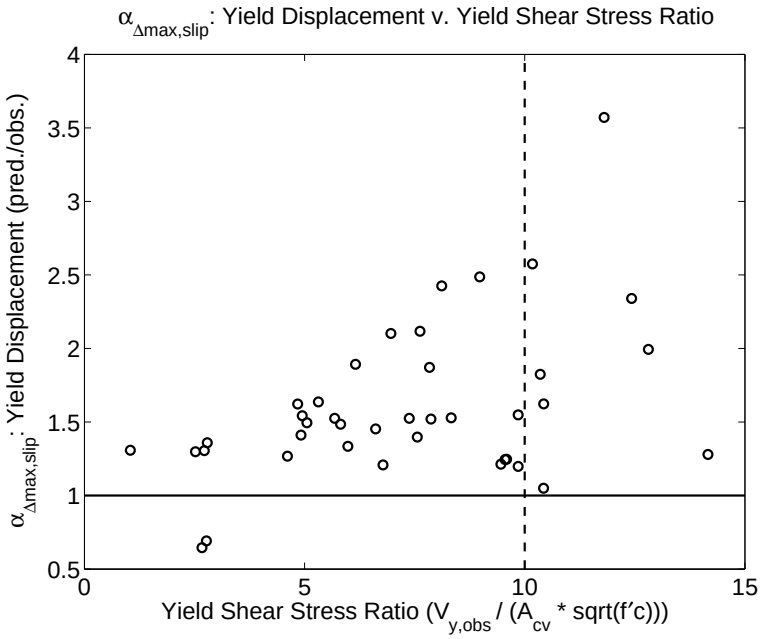

Figure L.138: Beam-Column With Shear Modulus Calibrated to Maximum Displacment With Slip - Yield Displacement v Yield Shear Stress Ratio

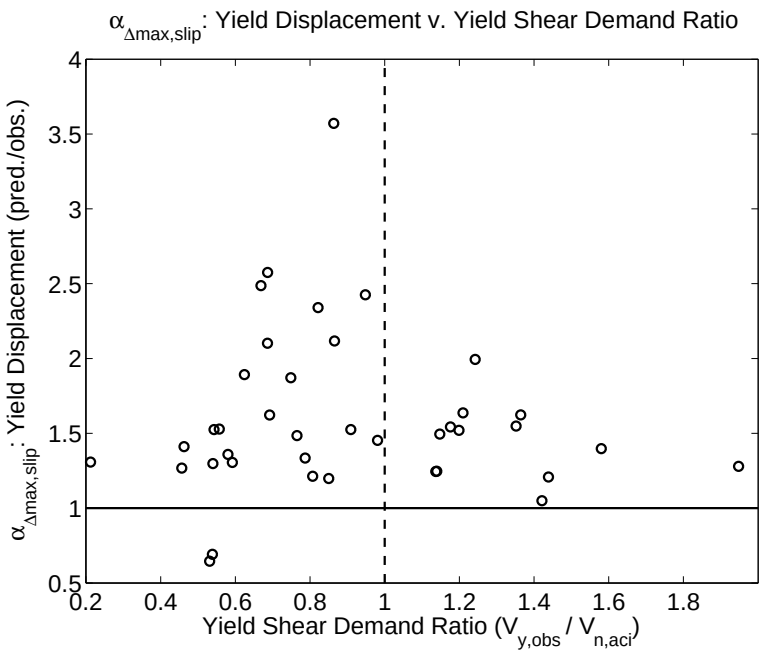

Figure L.139: Beam-Column With Shear Modulus Calibrated to Maximum Displacment With Slip - Yield Displacement v Yield Shear Demand Ratio

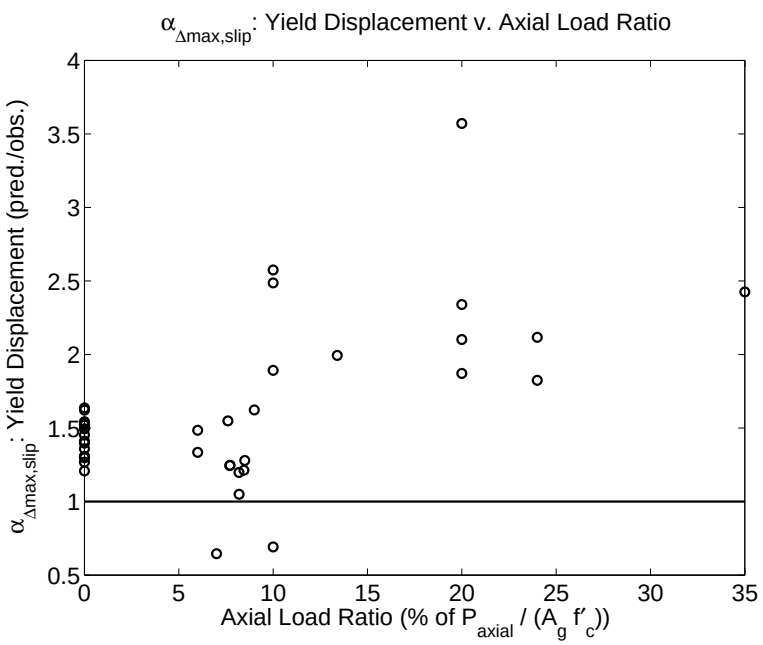

Figure L.140: Beam-Column With Shear Modulus Calibrated to Maximum Displacment With Slip - Yield Displacement v Axial Load Ratio

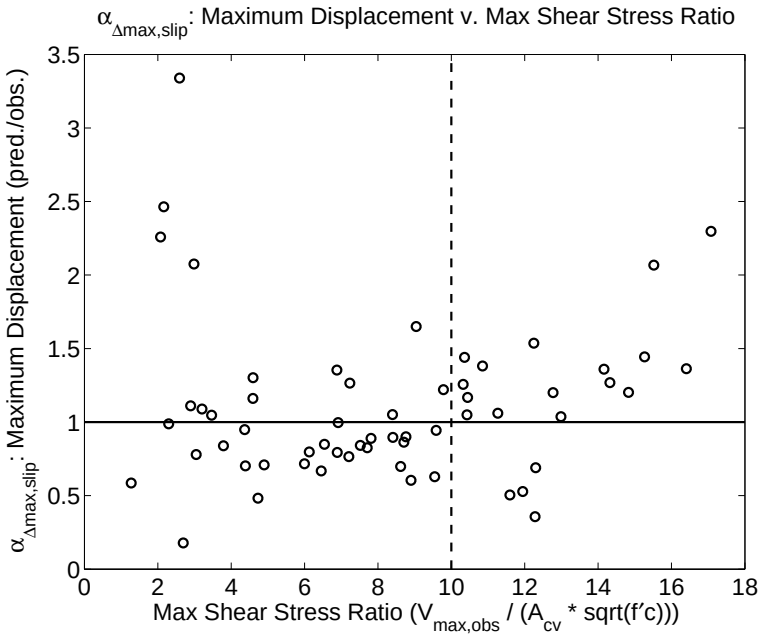

Figure L.141: Beam-Column With Shear Modulus Calibrated to Maximum Displacment With Slip - Maximum Displacement v Max Shear Stress Ratio

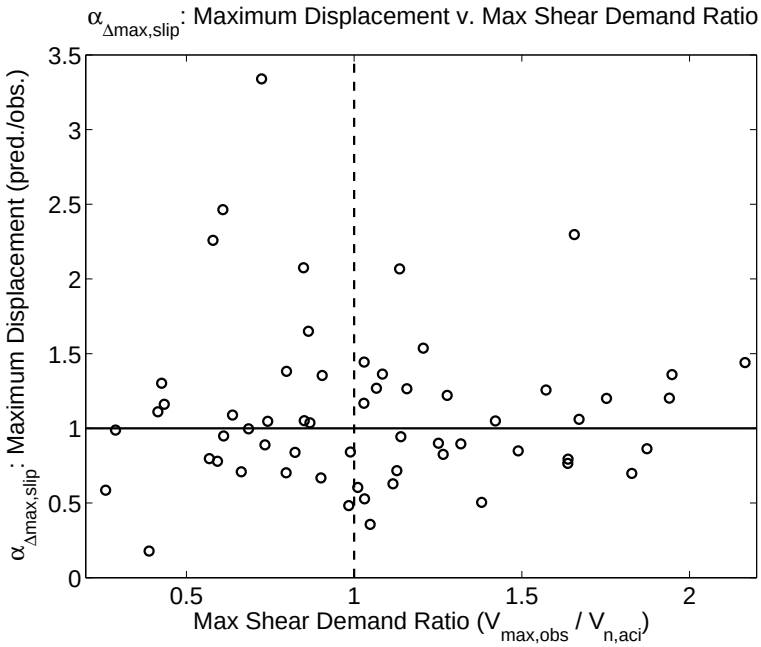

Figure L.142: Beam-Column With Shear Modulus Calibrated to Maximum Displacment With Slip - Maximum Displacement v Max Shear Demand Ratio

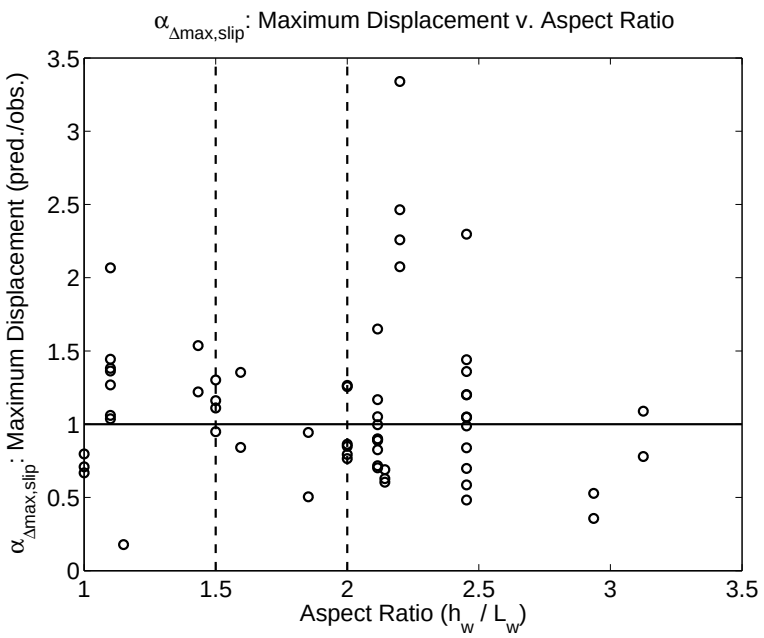

Figure L.143: Beam-Column With Shear Modulus Calibrated to Maximum Displacment With Slip - Maximum Displacement v Aspect Ratio

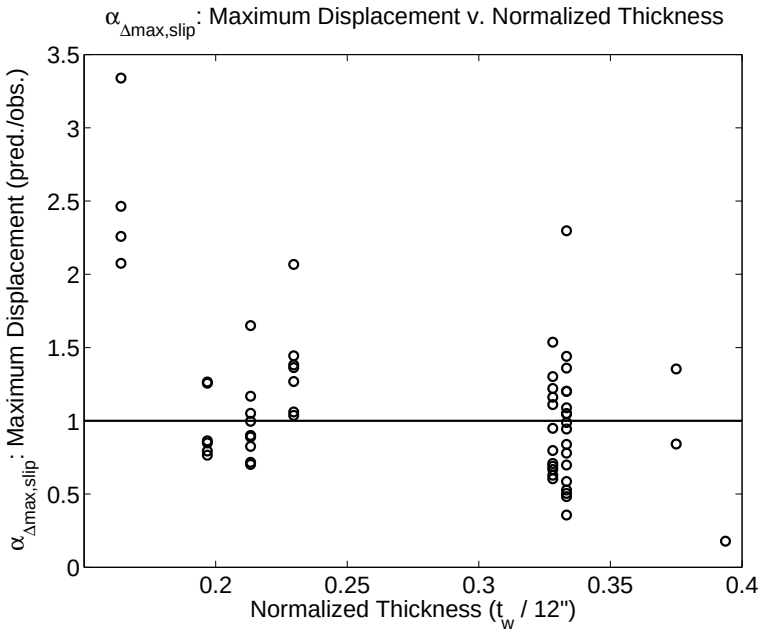

Figure L.144: Beam-Column With Shear Modulus Calibrated to Maximum Displacment With Slip - Maximum Displacement v Normalized Thickness

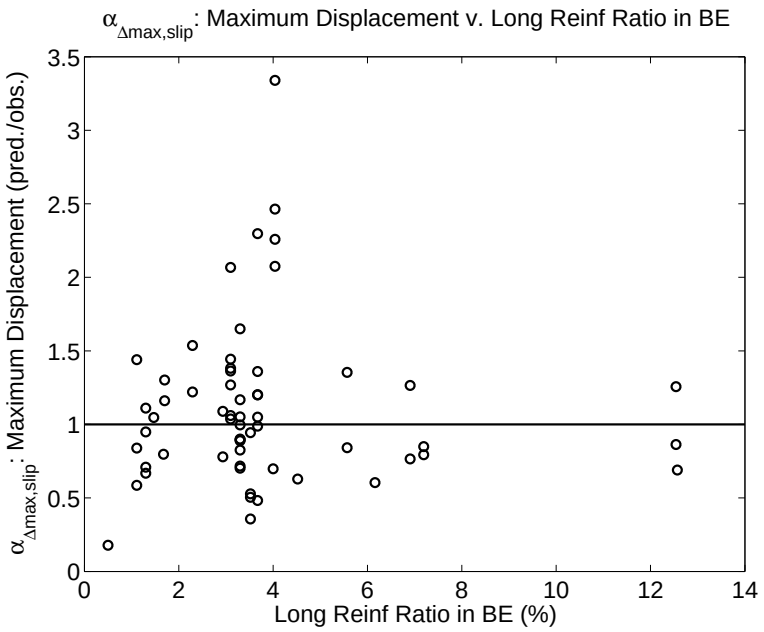

Figure L.145: Beam-Column With Shear Modulus Calibrated to Maximum Displacment With Slip - Maximum Displacement v Long Reinf Ratio in BE

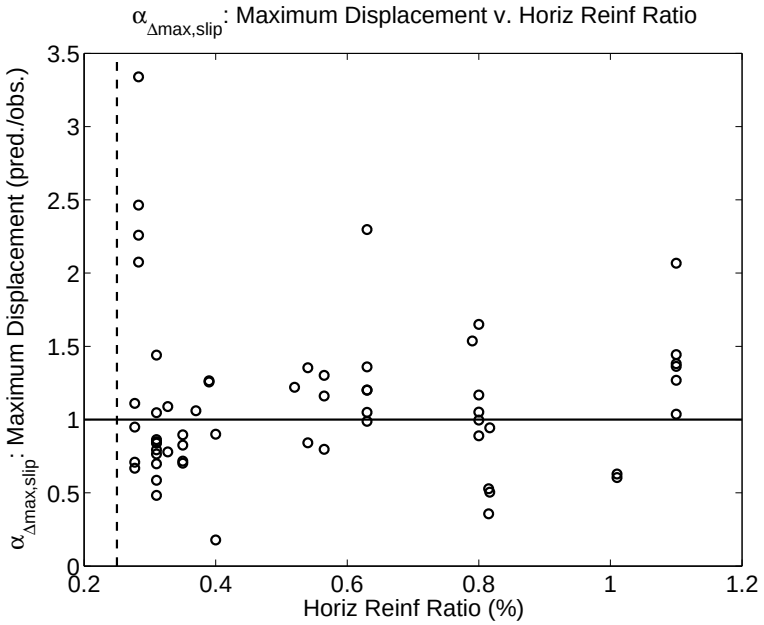

Figure L.146: Beam-Column With Shear Modulus Calibrated to Maximum Displacment With Slip - Maximum Displacement v Horiz Reinf Ratio

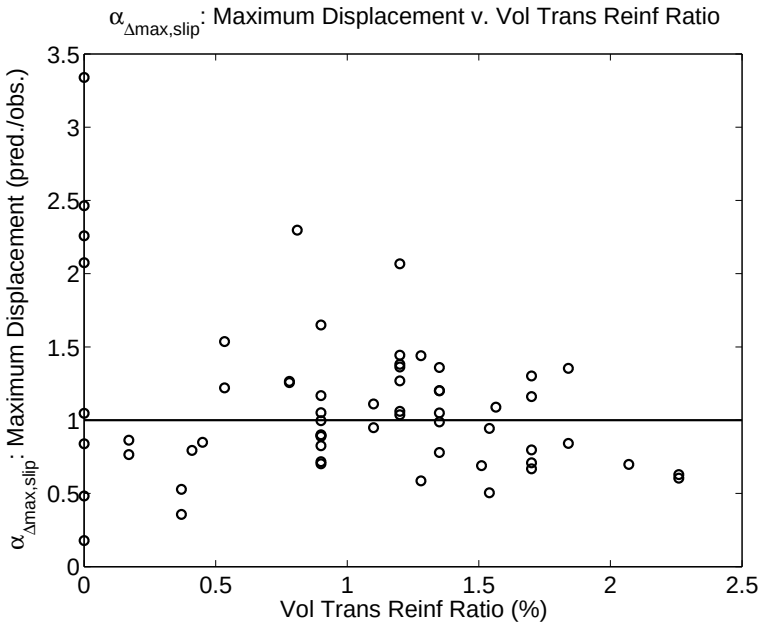

Figure L.147: Beam-Column With Shear Modulus Calibrated to Maximum Displacment With Slip - Maximum Displacement v Vol Trans Reinf Ratio

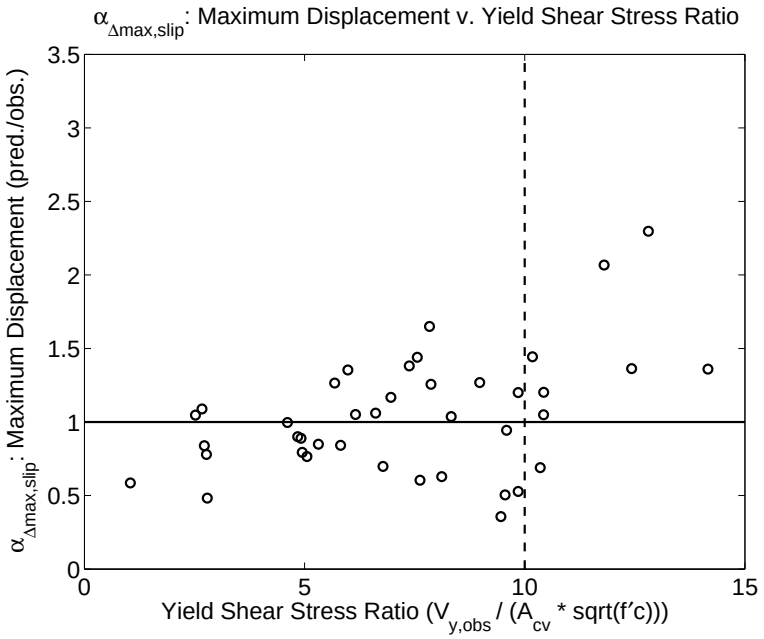

Figure L.148: Beam-Column With Shear Modulus Calibrated to Maximum Displacment With Slip - Maximum Displacement v Yield Shear Stress Ratio

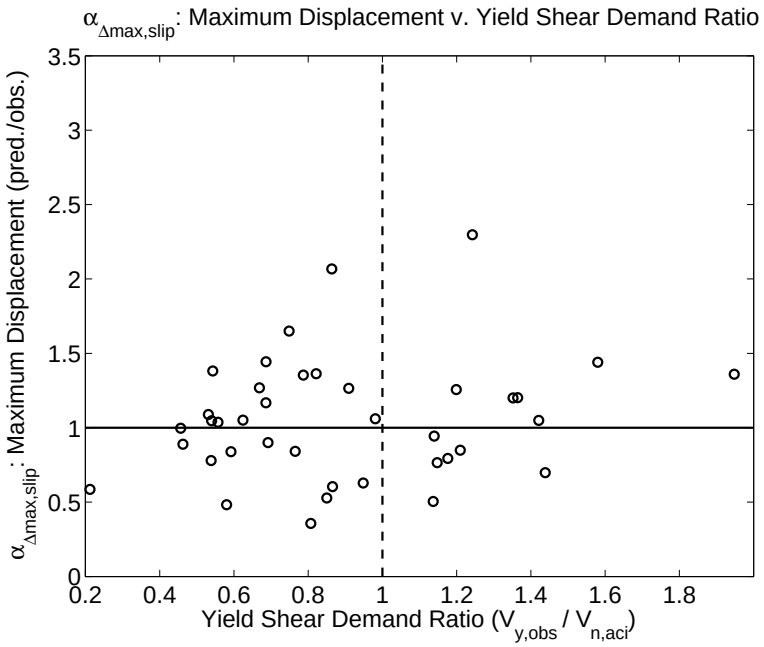

Figure L.149: Beam-Column With Shear Modulus Calibrated to Maximum Displacment With Slip - Maximum Displacement v Yield Shear Demand Ratio

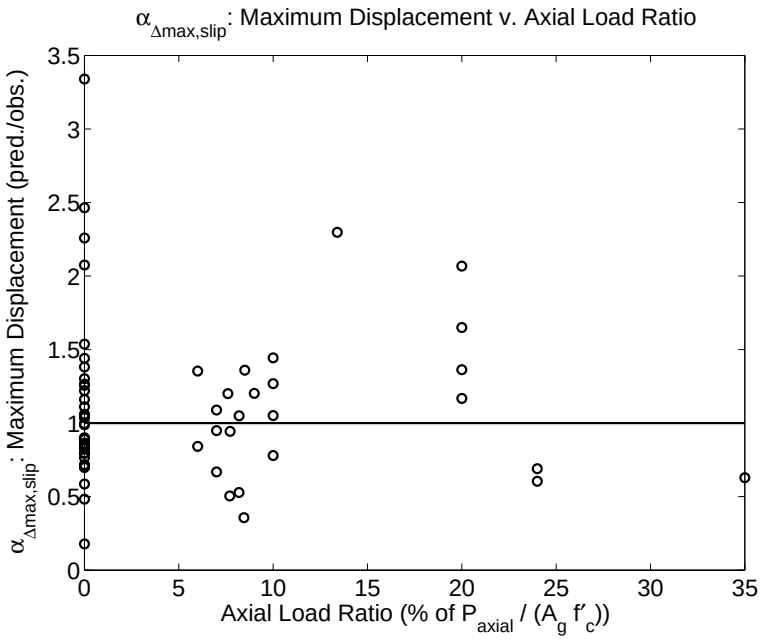

Figure L.150: Beam-Column With Shear Modulus Calibrated to Maximum Displacment With Slip - Maximum Displacement v Axial Load Ratio

Appendix M

ELASTIC EFFECTIVE SHEAR PUSH OVER ANALYSIS FIGURES

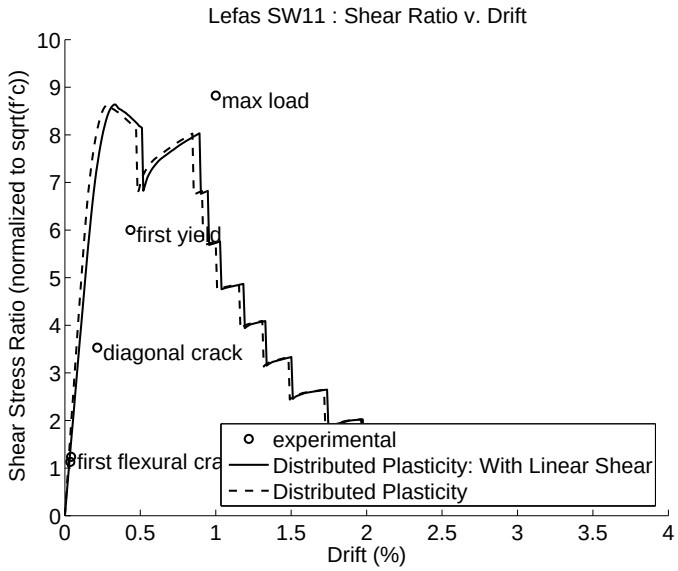

Figure M.1: Pushover of Beam-Column Element with Elastic Shear – Lefas SW11

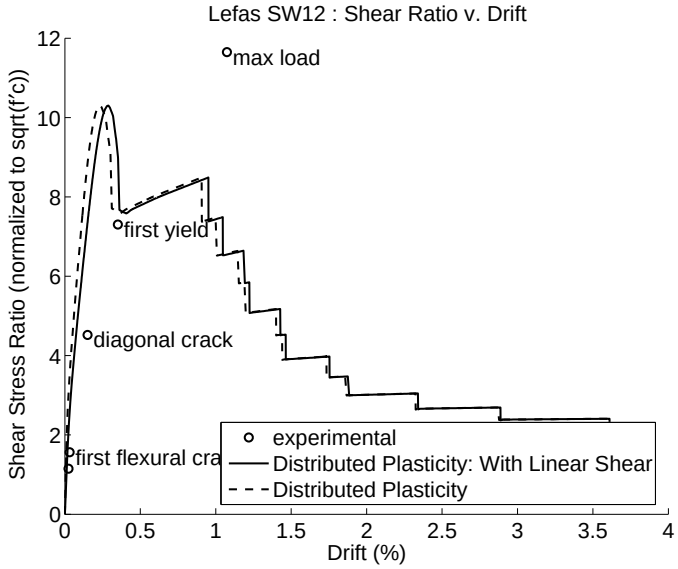

Figure M.2: Pushover of Beam-Column Element with Elastic Shear – Lefas SW12

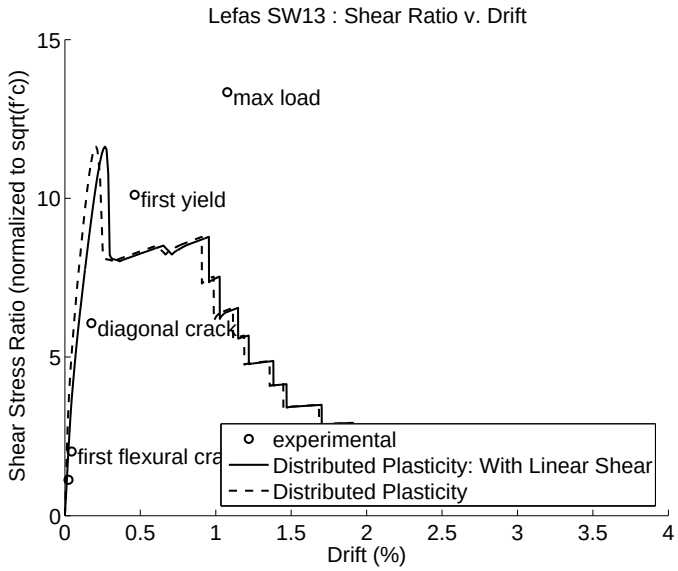

Figure M.3: Pushover of Beam-Column Element with Elastic Shear – Lefas SW13

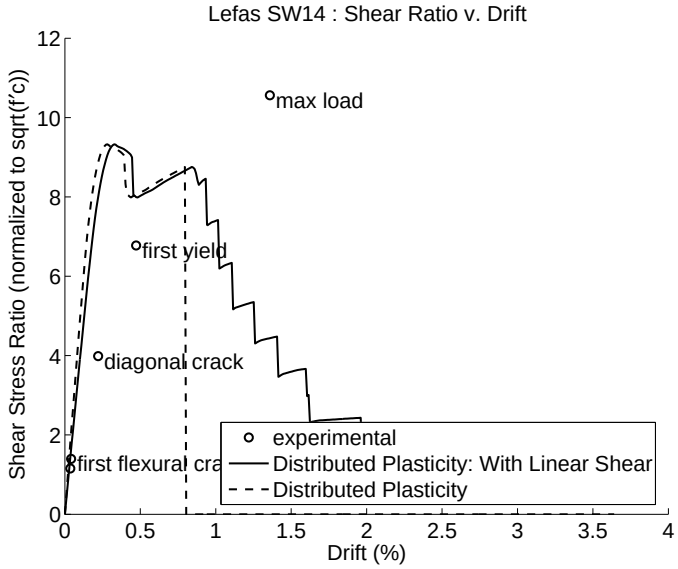

Figure M.4: Pushover of Beam-Column Element with Elastic Shear – Lefas SW14

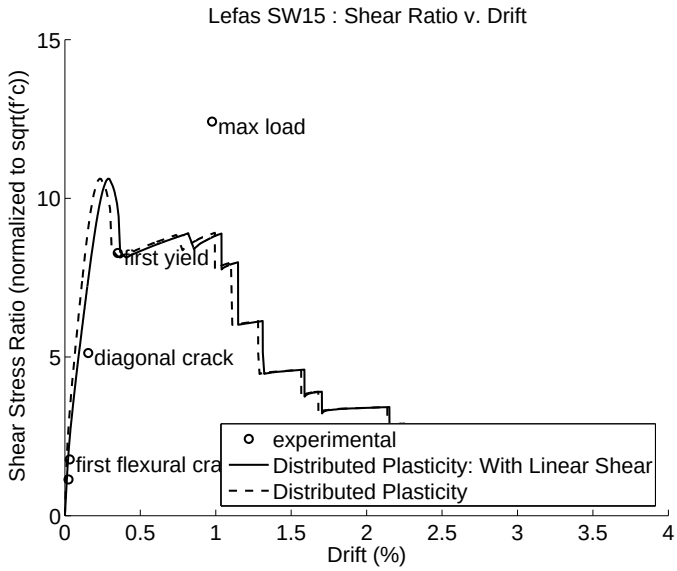

Figure M.5: Pushover of Beam-Column Element with Elastic Shear – Lefas SW15

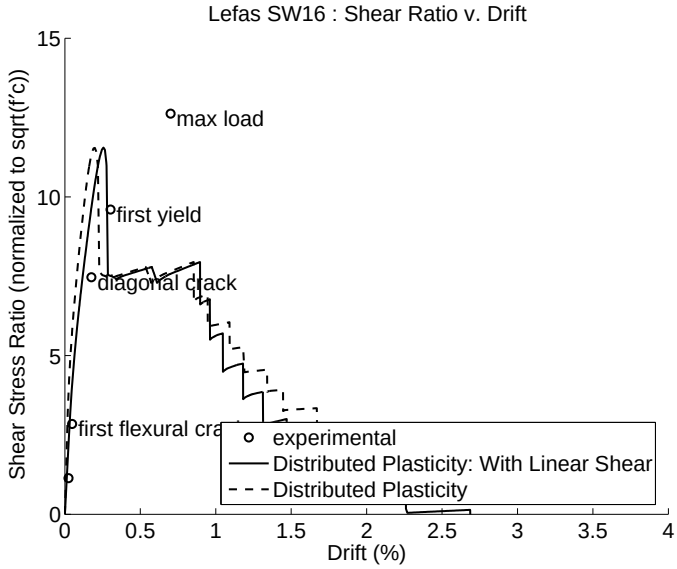

Figure M.6: Pushover of Beam-Column Element with Elastic Shear – Lefas SW16

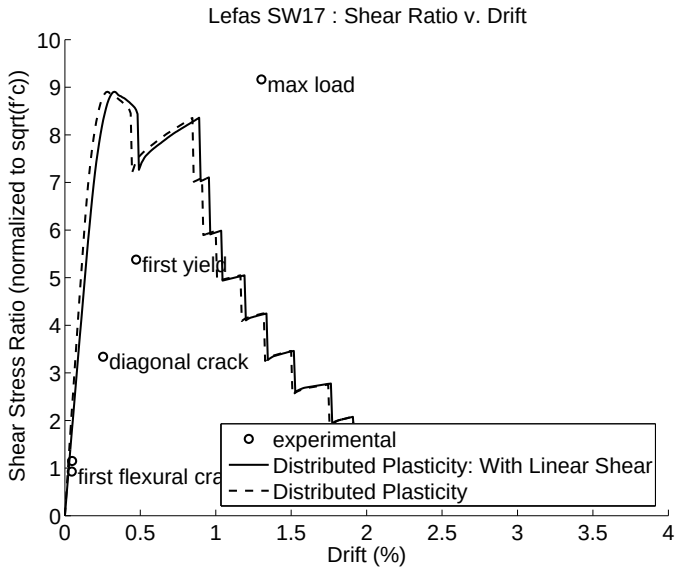

Figure M.7: Pushover of Beam-Column Element with Elastic Shear – Lefas SW17

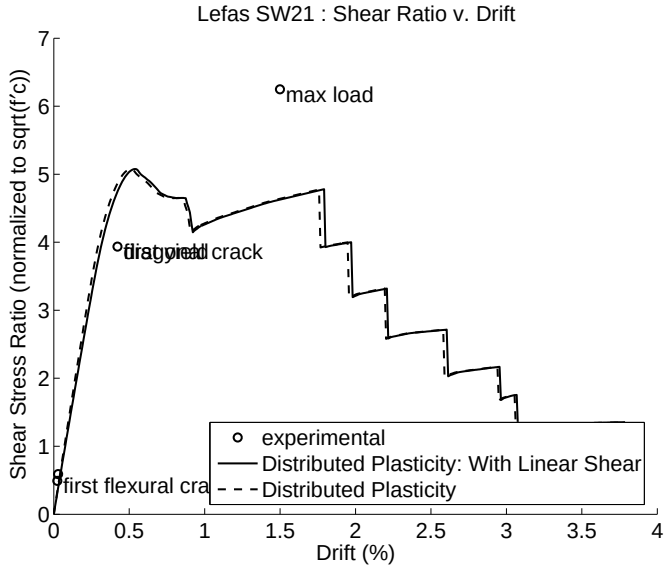

Figure M.8: Pushover of Beam-Column Element with Elastic Shear – Lefas SW21

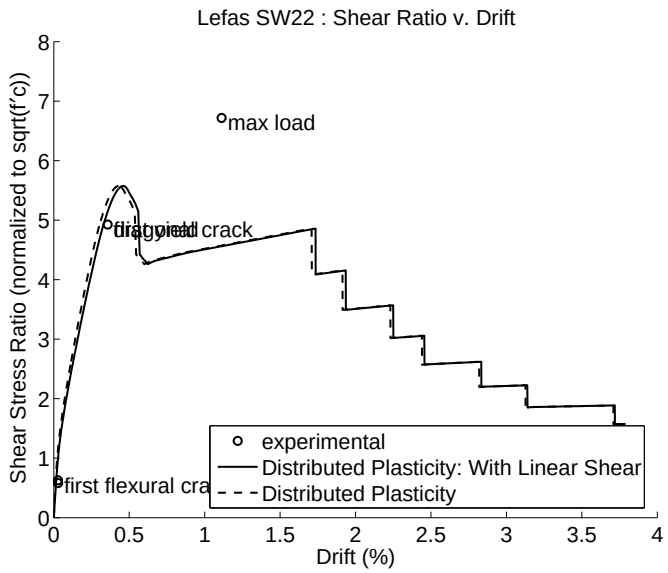

Figure M.9: Pushover of Beam-Column Element with Elastic Shear – Lefas SW22

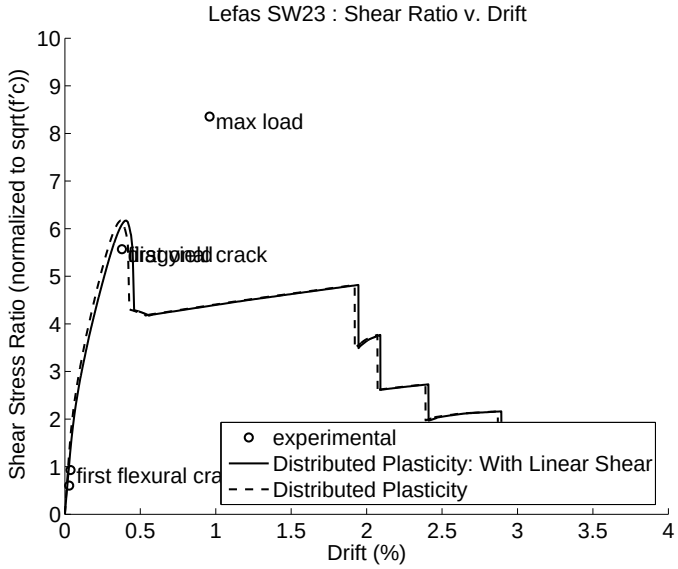

Figure M.10: Pushover of Beam-Column Element with Elastic Shear – Lefas SW23

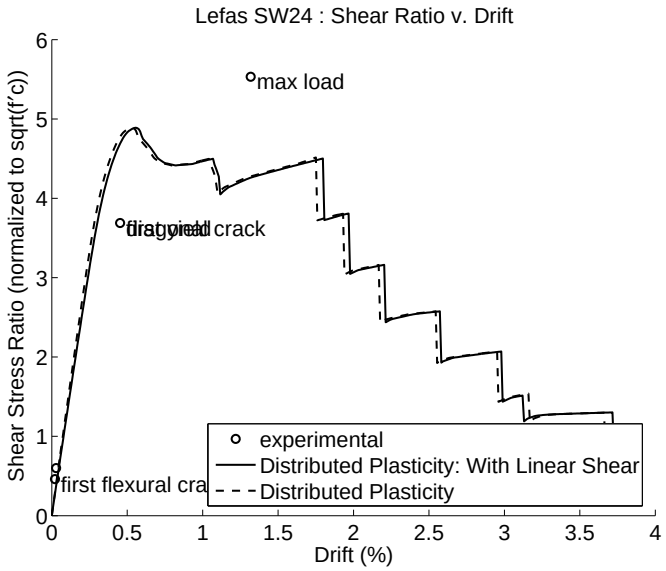

Figure M.11: Pushover of Beam-Column Element with Elastic Shear – Lefas SW24

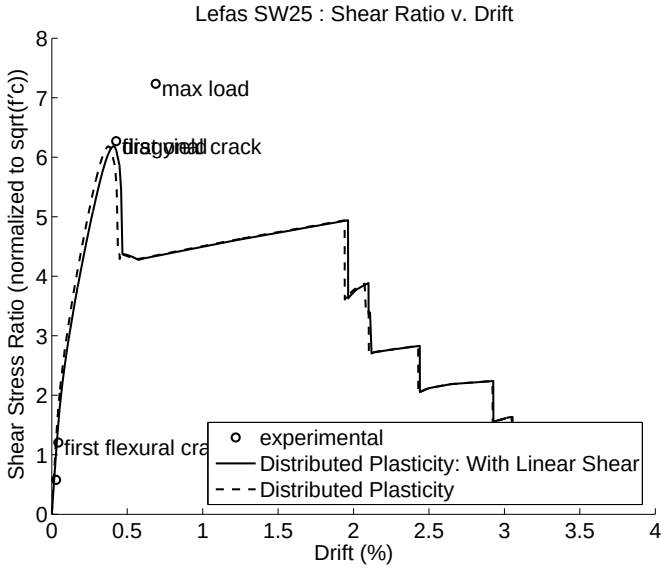

Figure M.12: Pushover of Beam-Column Element with Elastic Shear – Lefas SW25

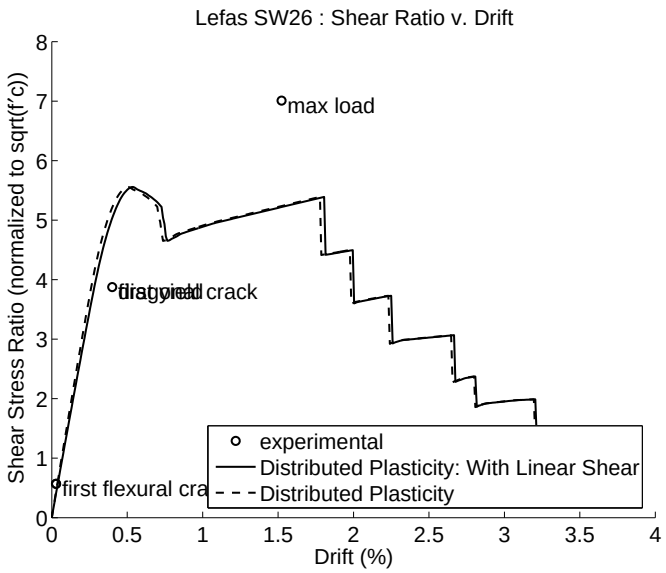

Figure M.13: Pushover of Beam-Column Element with Elastic Shear – Lefas SW26

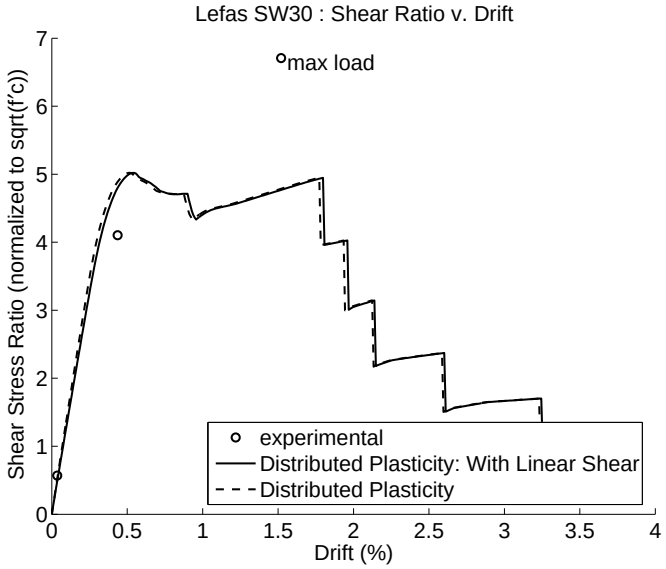

Figure M.14: Pushover of Beam-Column Element with Elastic Shear – Lefas SW30

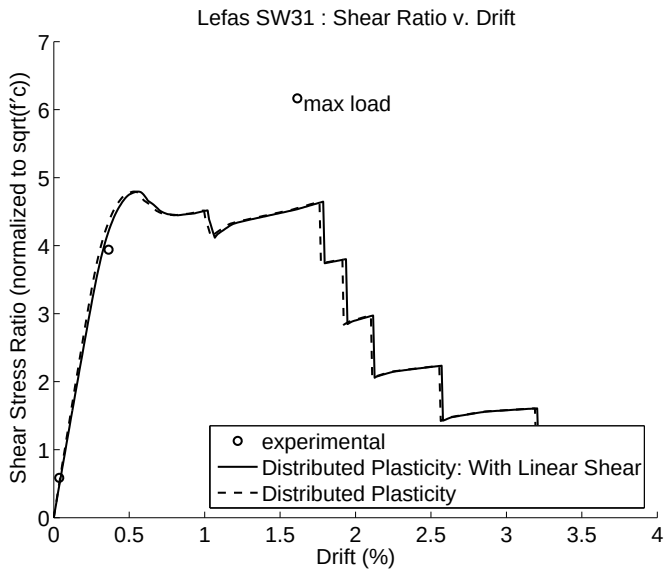

Figure M.15: Pushover of Beam-Column Element with Elastic Shear – Lefas SW31

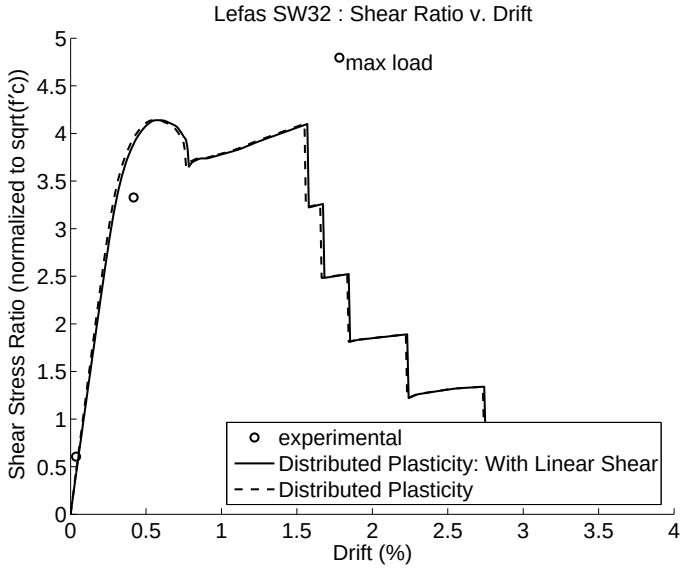

Figure M.16: Pushover of Beam-Column Element with Elastic Shear – Lefas SW32

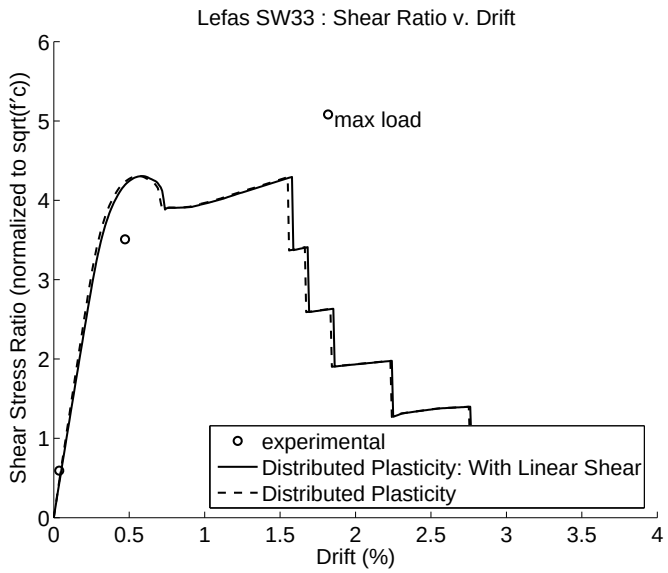

Figure M.17: Pushover of Beam-Column Element with Elastic Shear – Lefas SW33

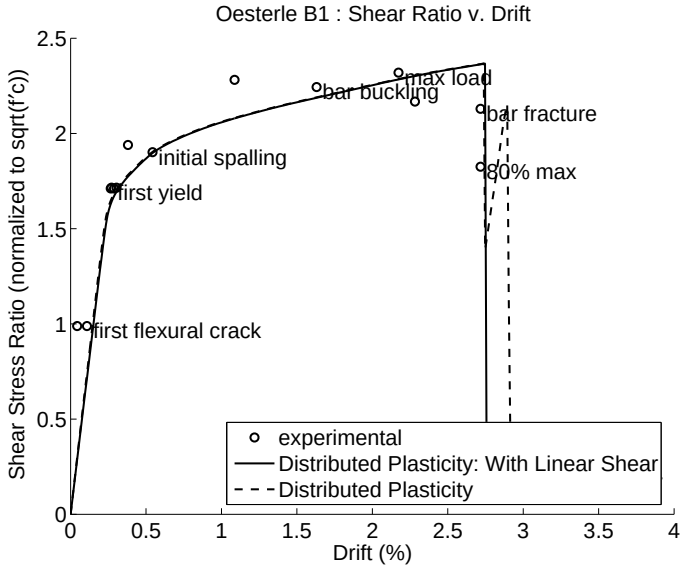

Figure M.18: Pushover of Beam-Column Element with Elastic Shear – Oesterle B1

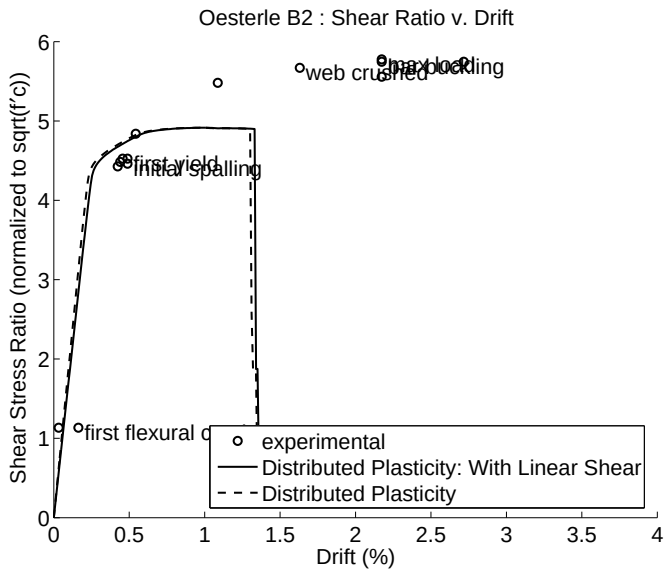

Figure M.19: Pushover of Beam-Column Element with Elastic Shear – Oesterle B2

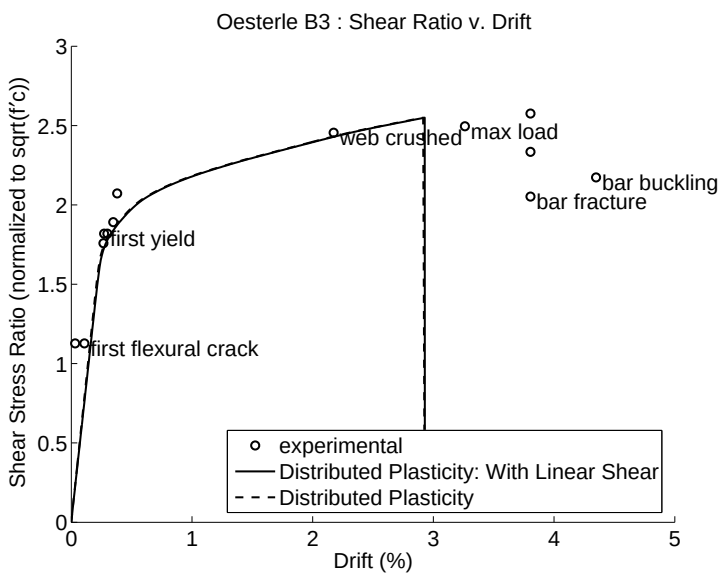

Figure M.20: Pushover of Beam-Column Element with Elastic Shear – Oesterle B3

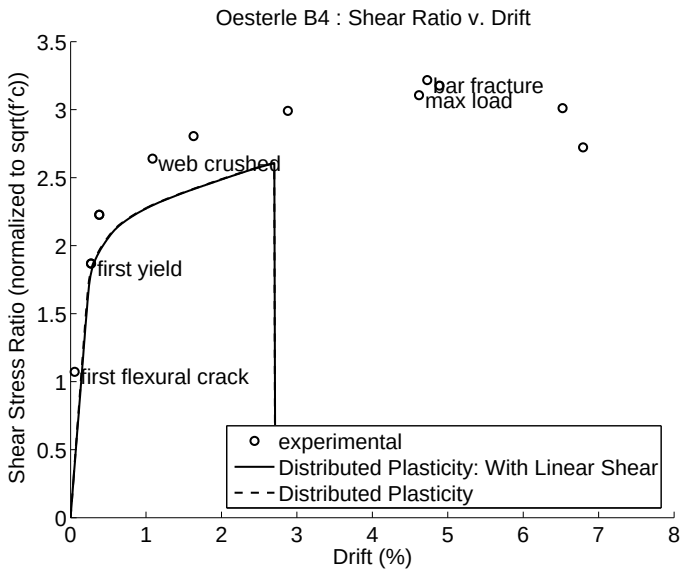

Figure M.21: Pushover of Beam-Column Element with Elastic Shear – Oesterle B4

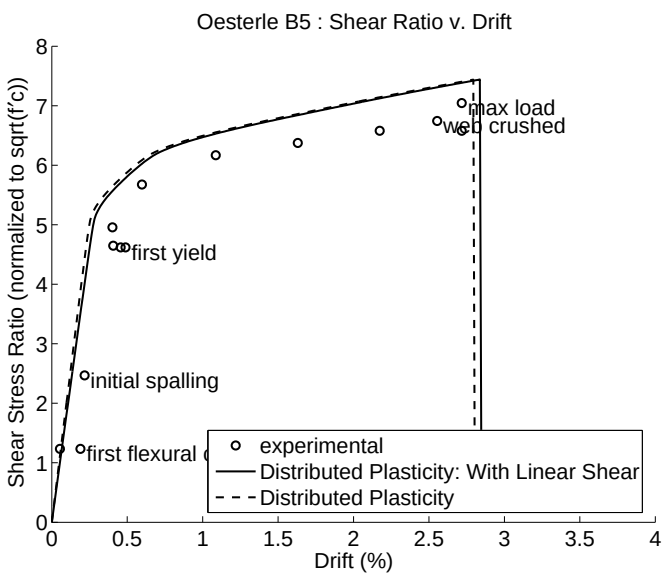

Figure M.22: Pushover of Beam-Column Element with Elastic Shear – Oesterle B5

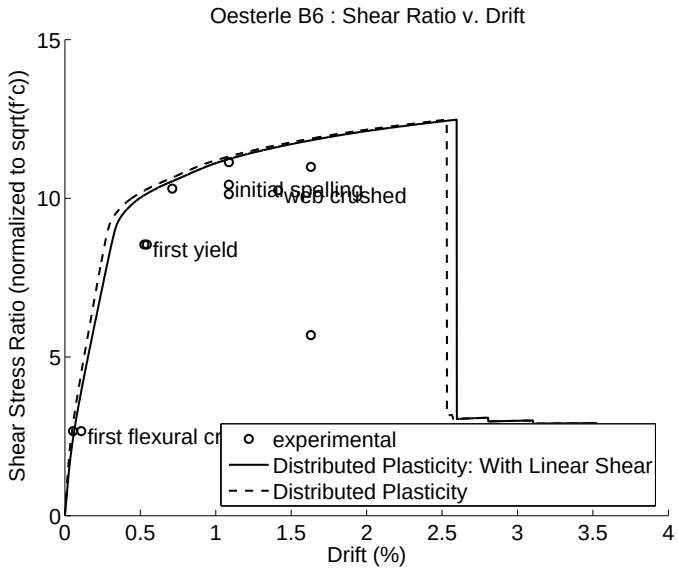

Figure M.23: Pushover of Beam-Column Element with Elastic Shear – Oesterle B6

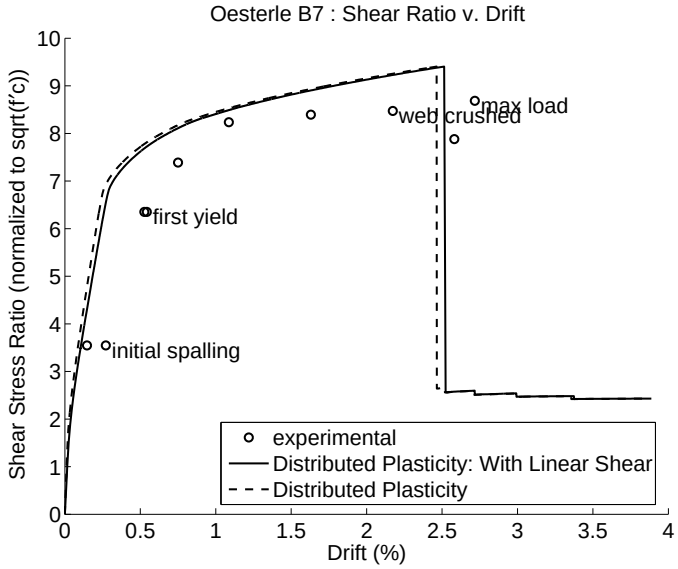

Figure M.24: Pushover of Beam-Column Element with Elastic Shear – Oesterle B7

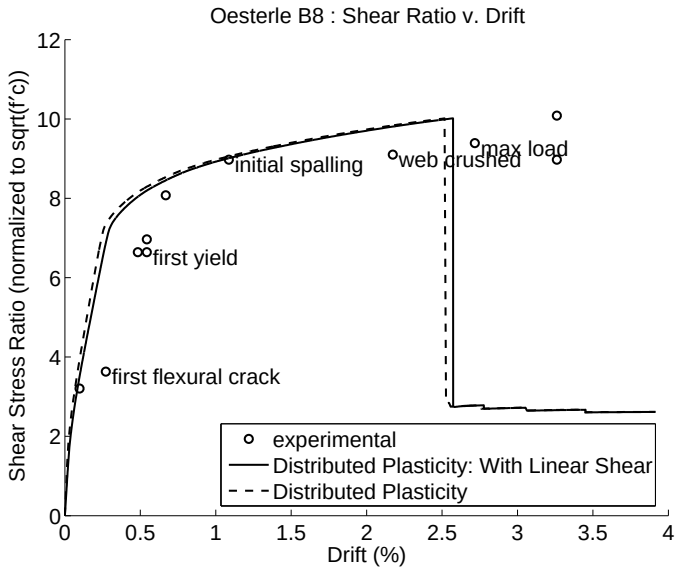

Figure M.25: Pushover of Beam-Column Element with Elastic Shear – Oesterle B8

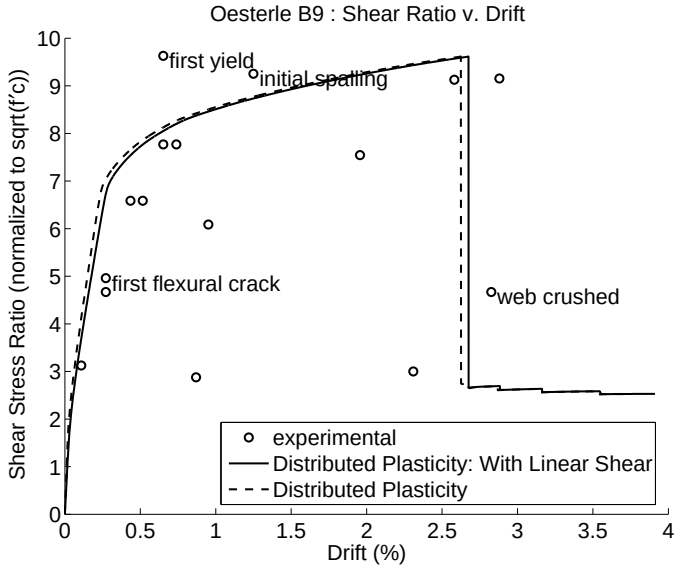

Figure M.26: Pushover of Beam-Column Element with Elastic Shear – Oesterle B9

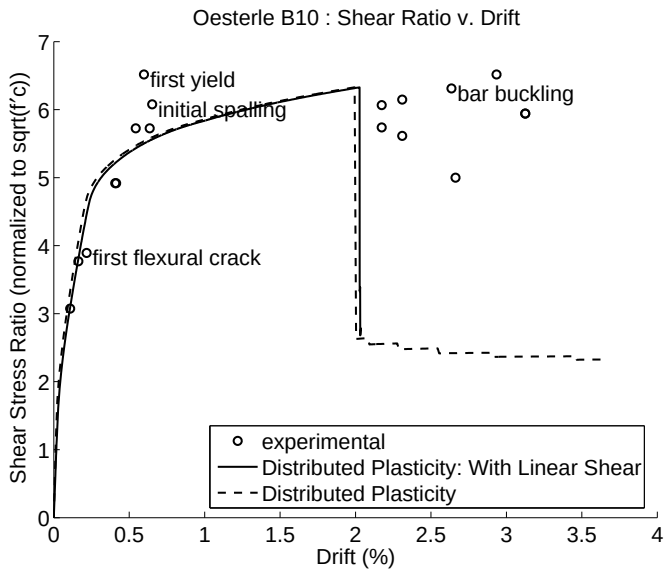

Figure M.27: Pushover of Beam-Column Element with Elastic Shear – Oesterle B10

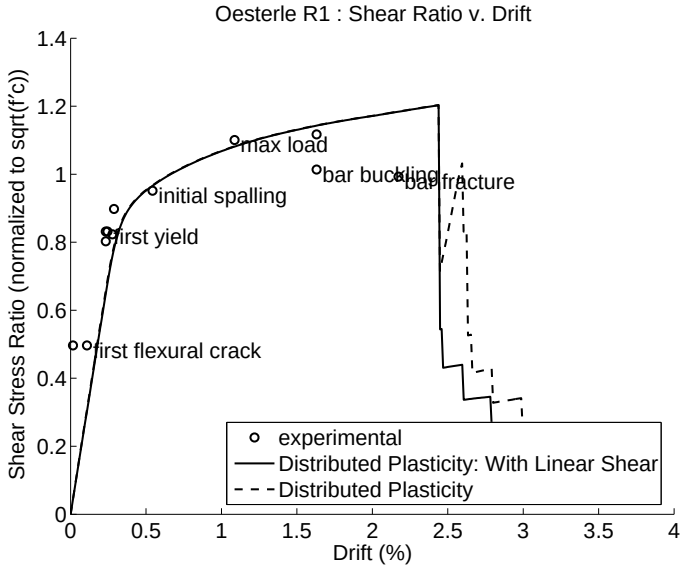

Figure M.28: Pushover of Beam-Column Element with Elastic Shear – Oesterle R1

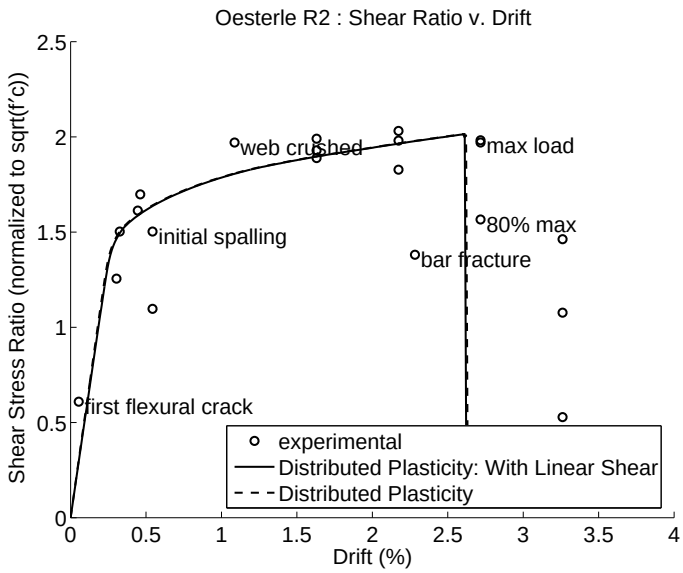

Figure M.29: Pushover of Beam-Column Element with Elastic Shear – Oesterle R2

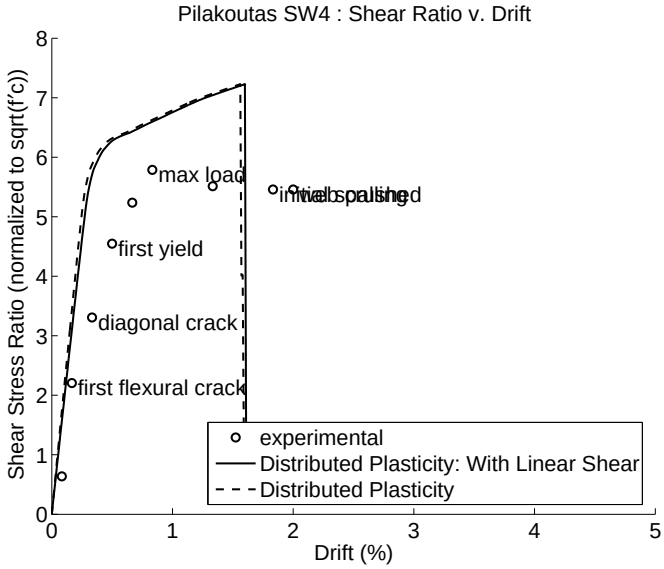

Figure M.30: Pushover of Beam-Column Element with Elastic Shear – Pilakoutas SW4

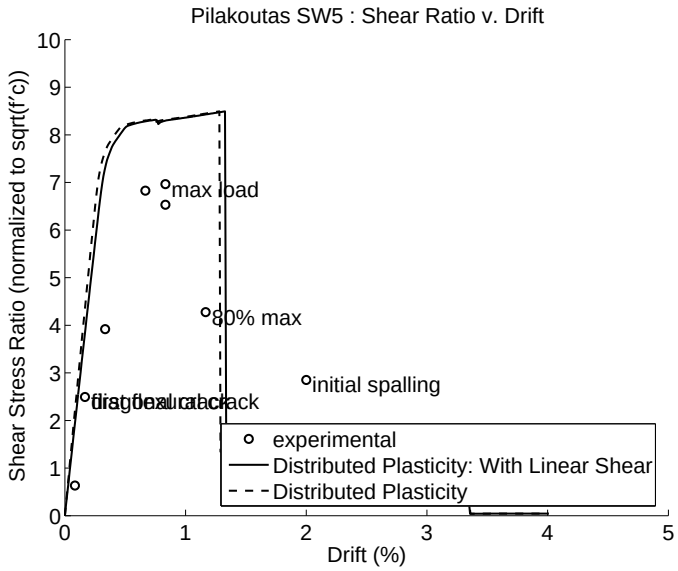

Figure M.31: Pushover of Beam-Column Element with Elastic Shear – Pilakoutas SW5

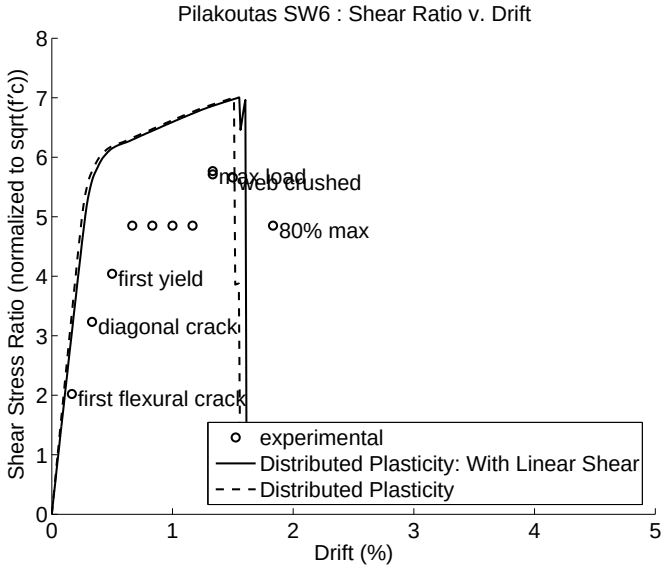

Figure M.32: Pushover of Beam-Column Element with Elastic Shear – Pilakoutas SW6

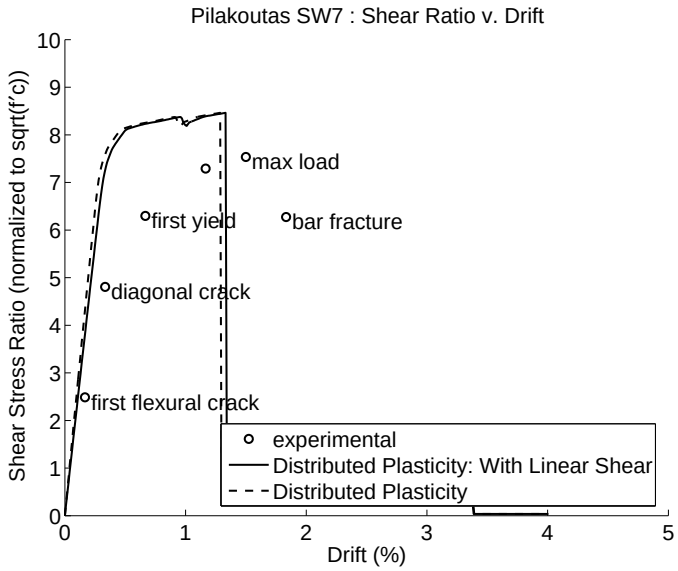

Figure M.33: Pushover of Beam-Column Element with Elastic Shear – Pilakoutas SW7

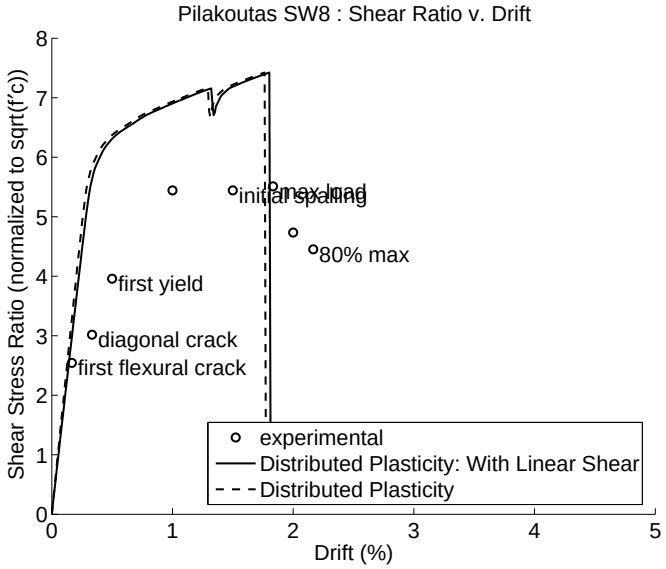

Figure M.34: Pushover of Beam-Column Element with Elastic Shear – Pilakoutas SW8

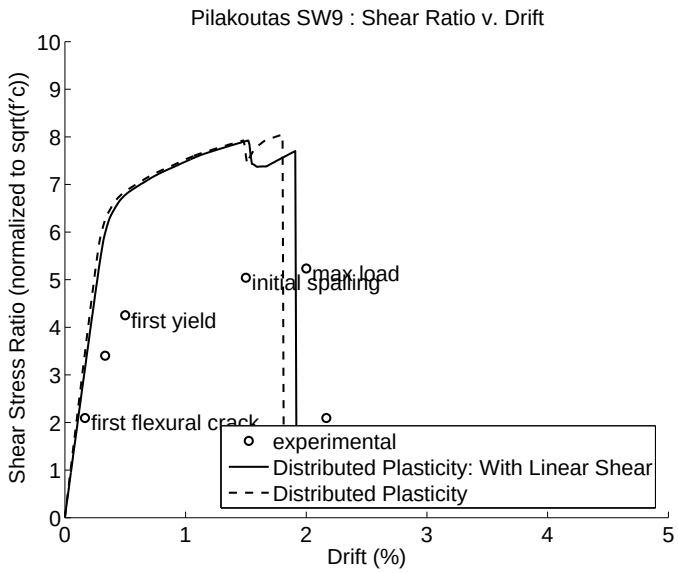

Figure M.35: Pushover of Beam-Column Element with Elastic Shear – Pilakoutas SW9

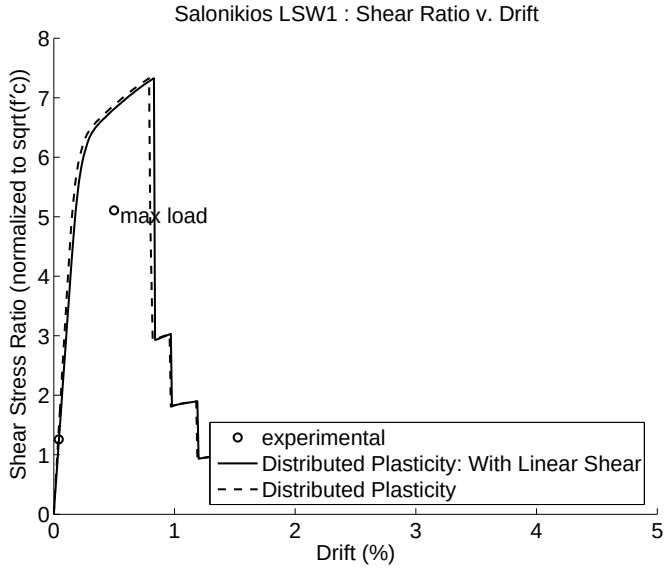

Figure M.36: Pushover of Beam-Column Element with Elastic Shear – Salonikios LSW1

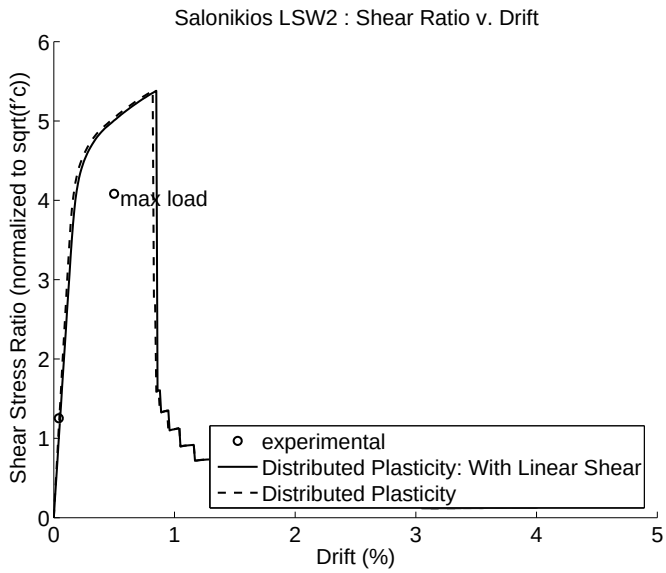

Figure M.37: Pushover of Beam-Column Element with Elastic Shear – Salonikios LSW2

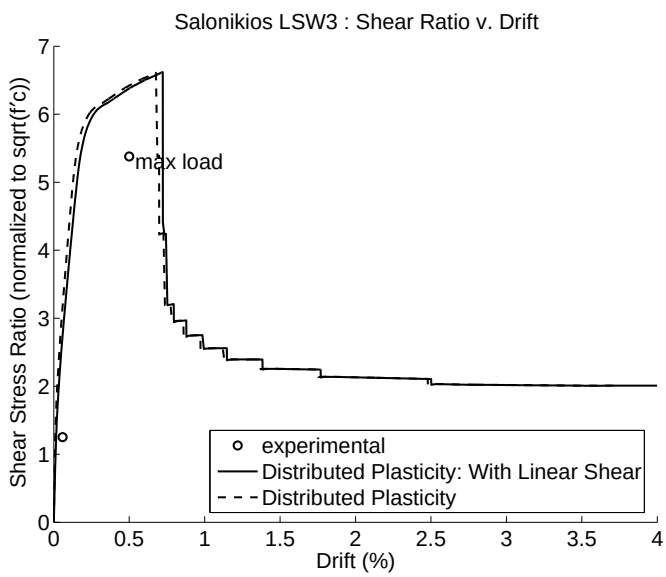

Figure M.38: Pushover of Beam-Column Element with Elastic Shear – Salonikios LSW3

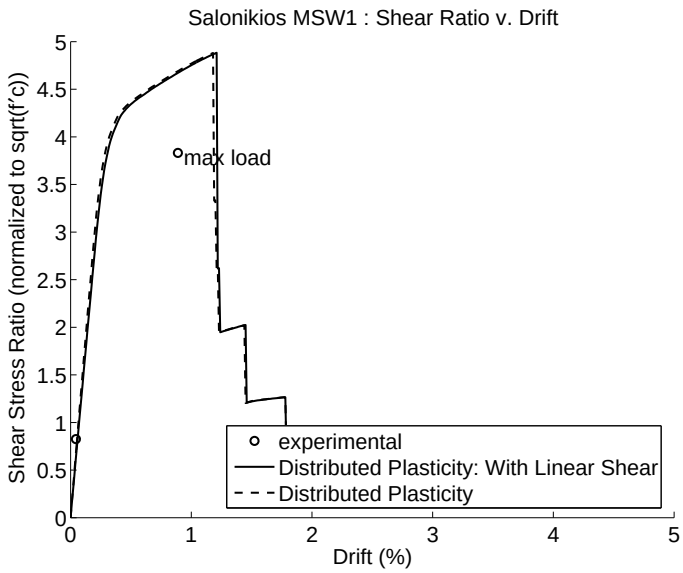

Figure M.39: Pushover of Beam-Column Element with Elastic Shear – Salonikios MSW1

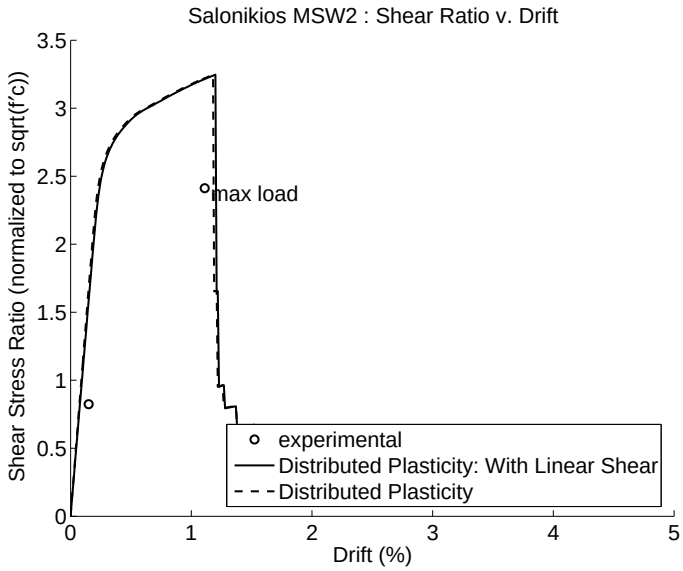

Figure M.40: Pushover of Beam-Column Element with Elastic Shear – Salonikios MSW2

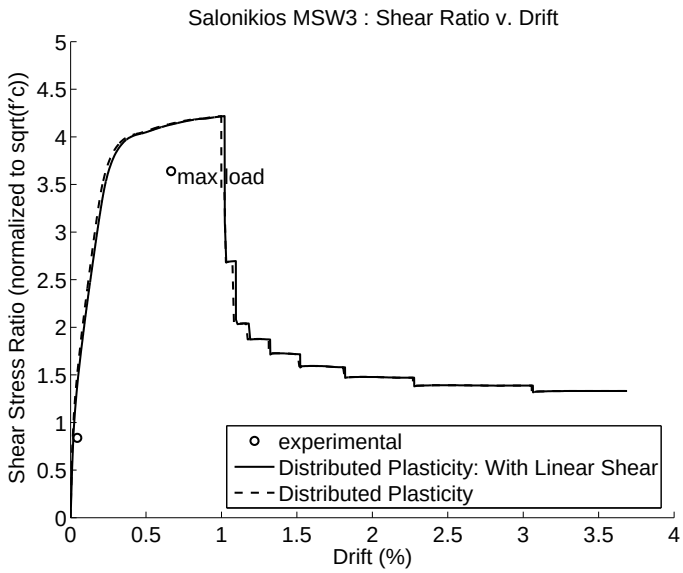

Figure M.41: Pushover of Beam-Column Element with Elastic Shear – Salonikios MSW3

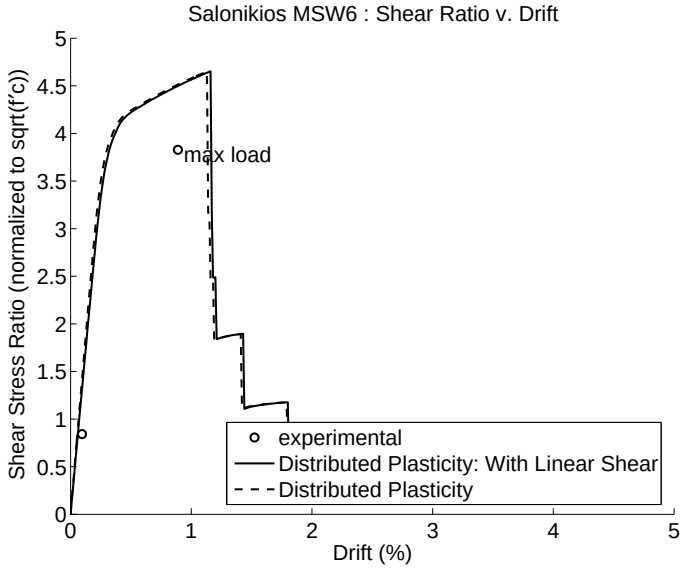

Figure M.42: Pushover of Beam-Column Element with Elastic Shear – Salonikios MSW6

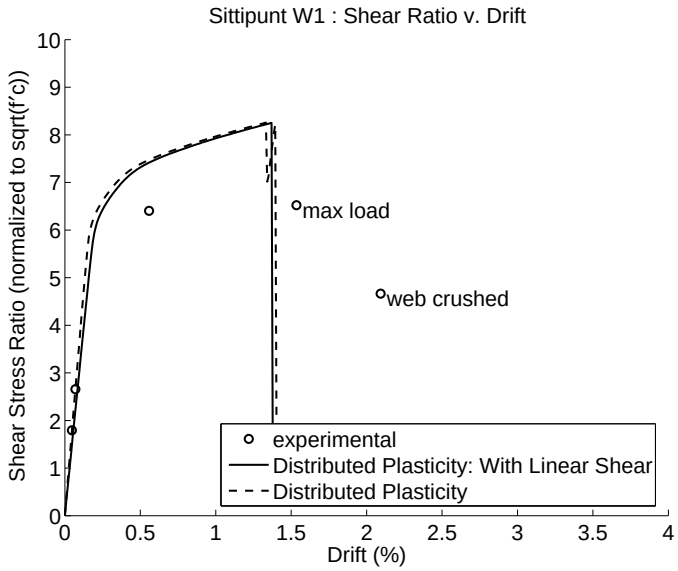

Figure M.43: Pushover of Beam-Column Element with Elastic Shear – Sittipunt W1

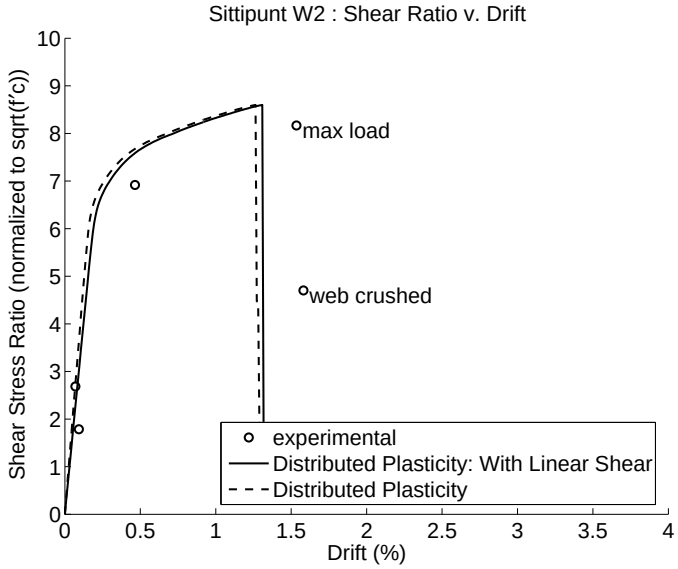

Figure M.44: Pushover of Beam-Column Element with Elastic Shear – Sittipunt W2

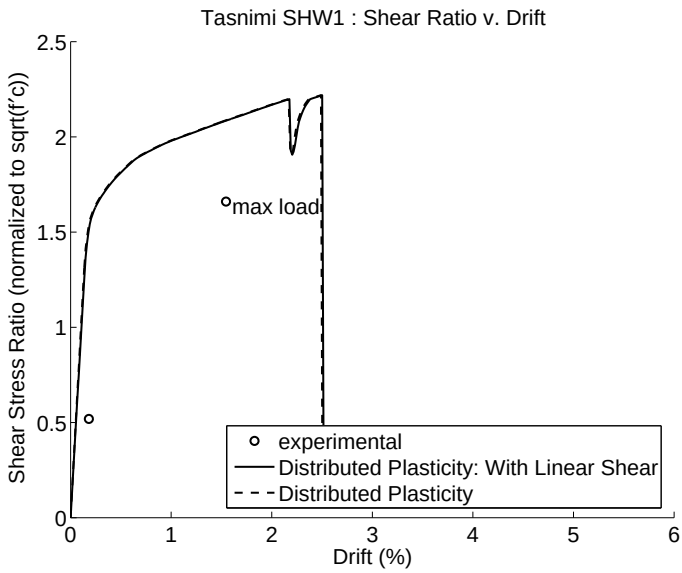

Figure M.45: Pushover of Beam-Column Element with Elastic Shear – Tasnimi SHW1

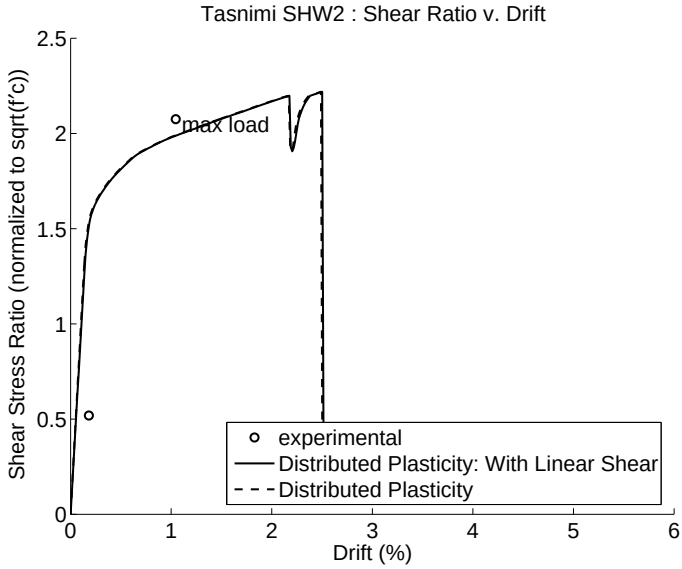

Figure M.46: Pushover of Beam-Column Element with Elastic Shear – Tasnimi SHW2

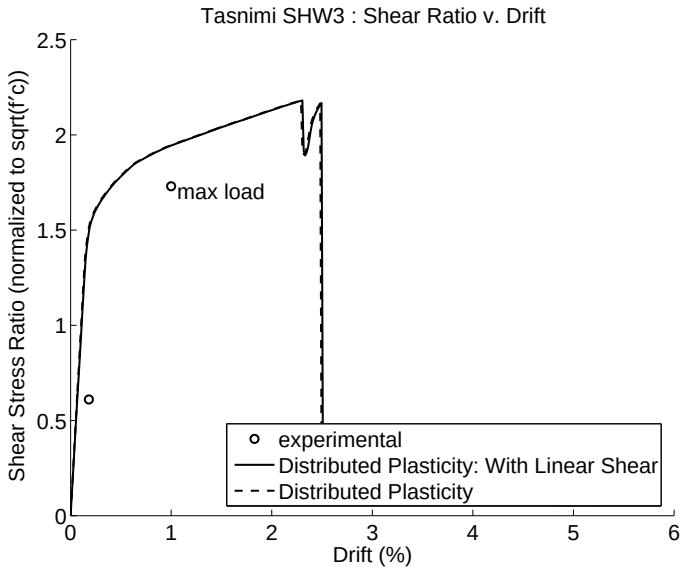

Figure M.47: Pushover of Beam-Column Element with Elastic Shear – Tasnimi SHW3

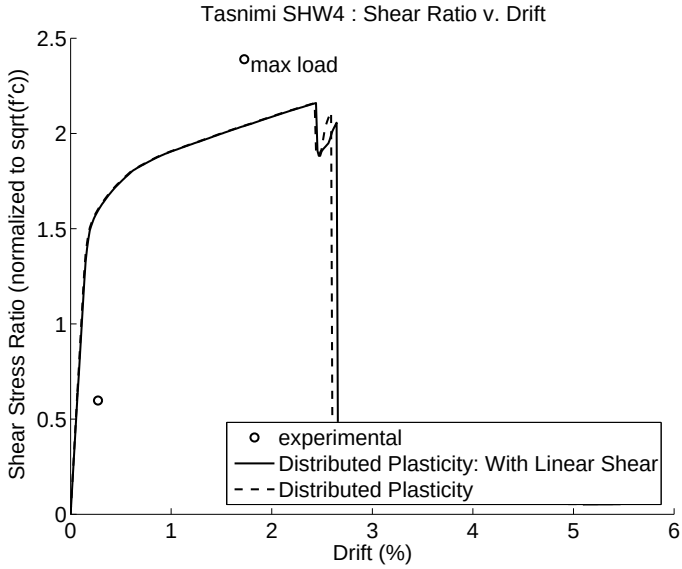

Figure M.48: Pushover of Beam-Column Element with Elastic Shear – Tasnimi SHW4

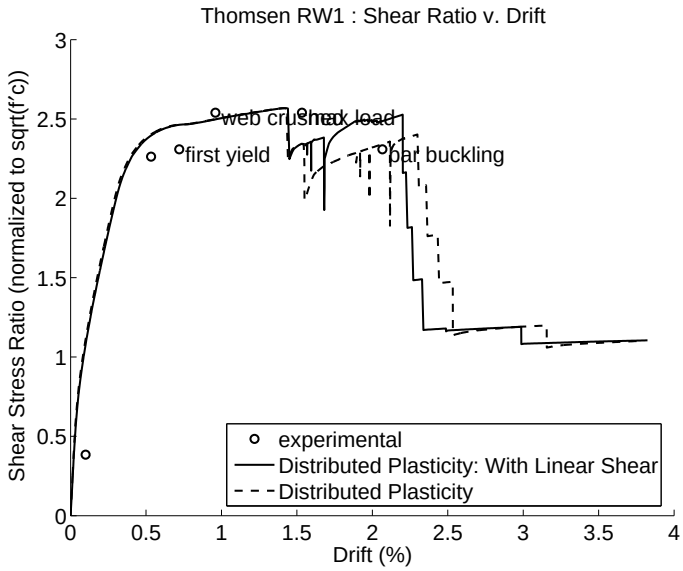

Figure M.49: Pushover of Beam-Column Element with Elastic Shear – Thomsen RW1

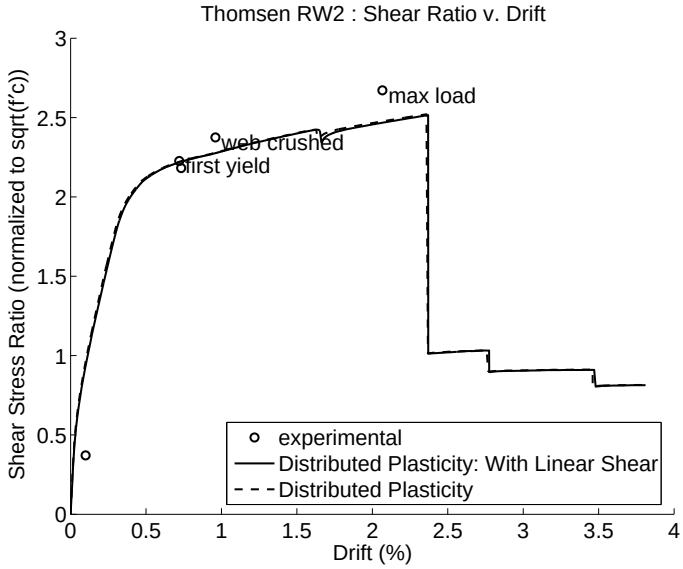

Figure M.50: Pushover of Beam-Column Element with Elastic Shear – Thomsen RW2

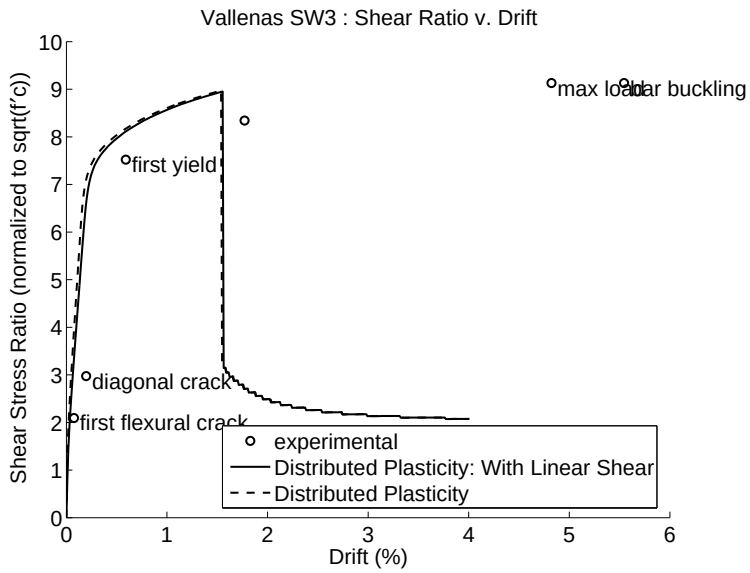

Figure M.51: Pushover of Beam-Column Element with Elastic Shear – Vallenas SW3

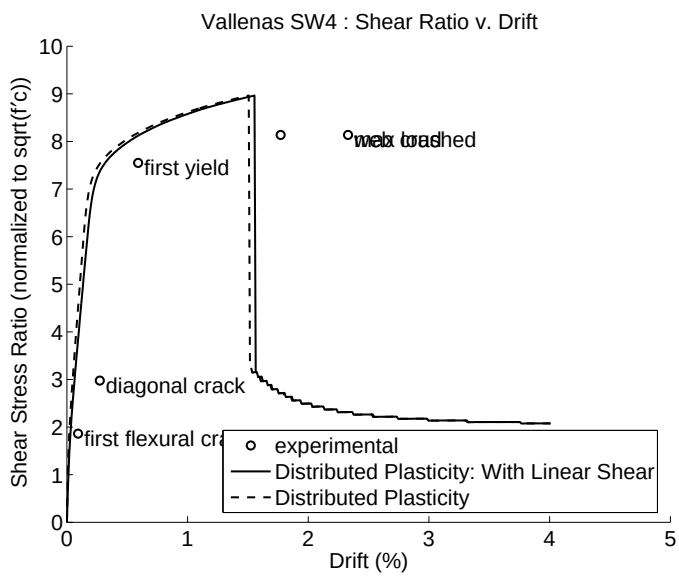

Figure M.52: Pushover of Beam-Column Element with Elastic Shear – Vallenas SW4

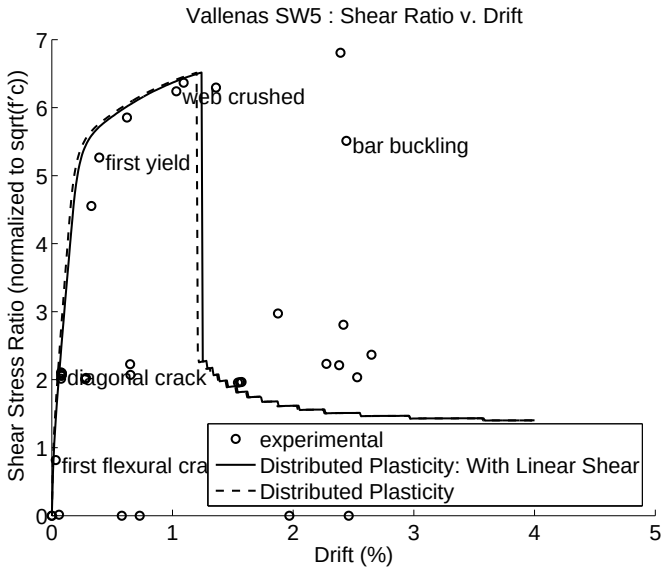

Figure M.53: Pushover of Beam-Column Element with Elastic Shear – Vallenas SW5

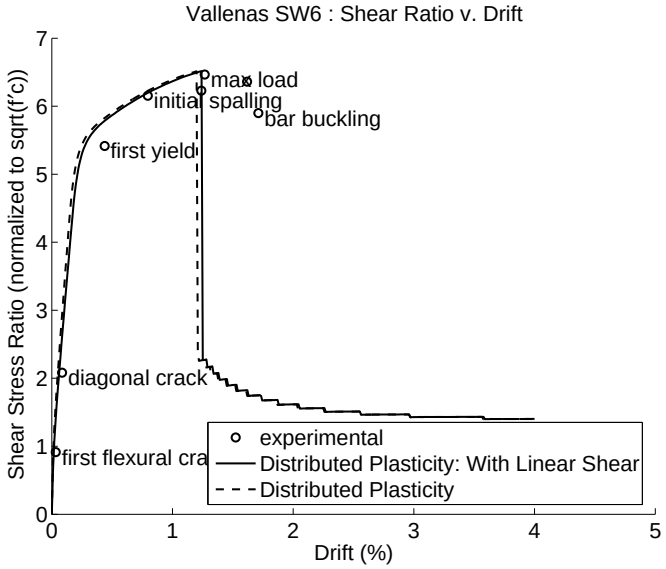

Figure M.54: Pushover of Beam-Column Element with Elastic Shear – Vallenas SW6

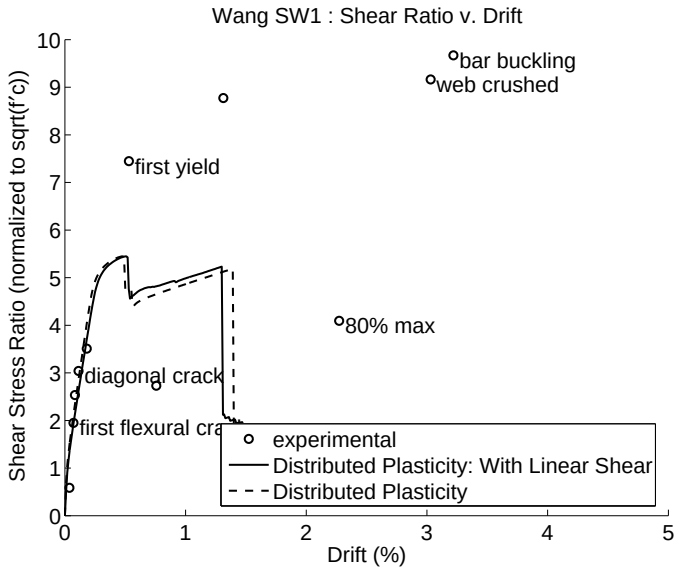

Figure M.55: Pushover of Beam-Column Element with Elastic Shear – Wang SW1

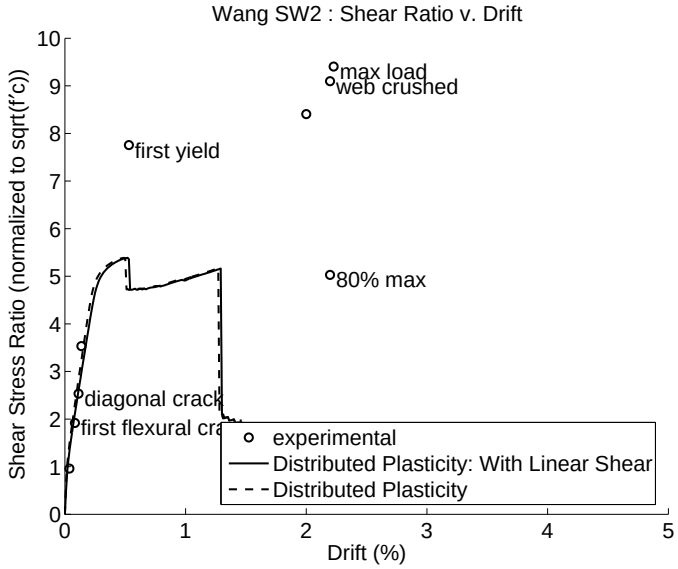

Figure M.56: Pushover of Beam-Column Element with Elastic Shear – Wang SW2

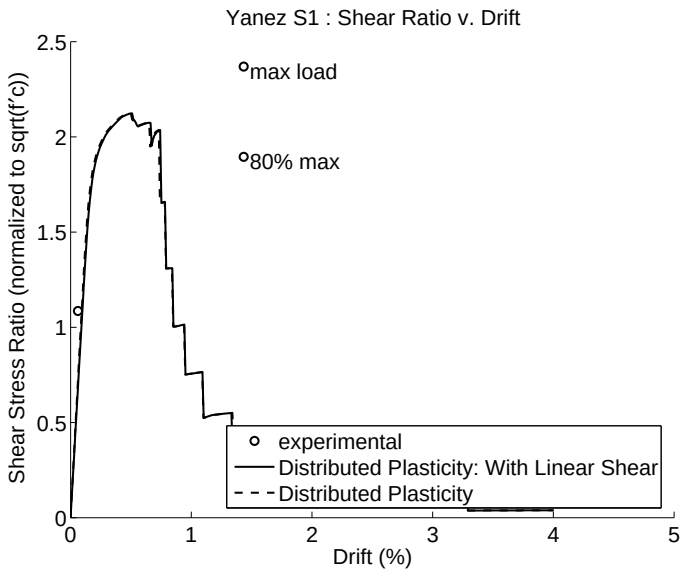

Figure M.57: Pushover of Beam-Column Element with Elastic Shear – Yanez S1

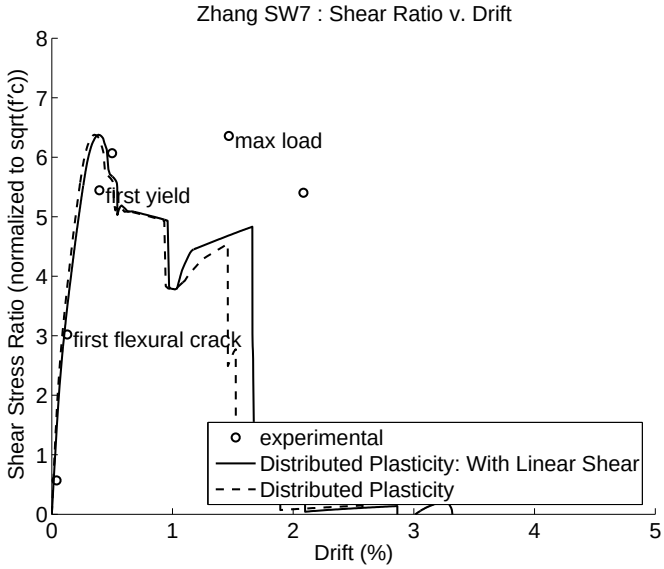

Figure M.58: Pushover of Beam-Column Element with Elastic Shear – Zhang SW7

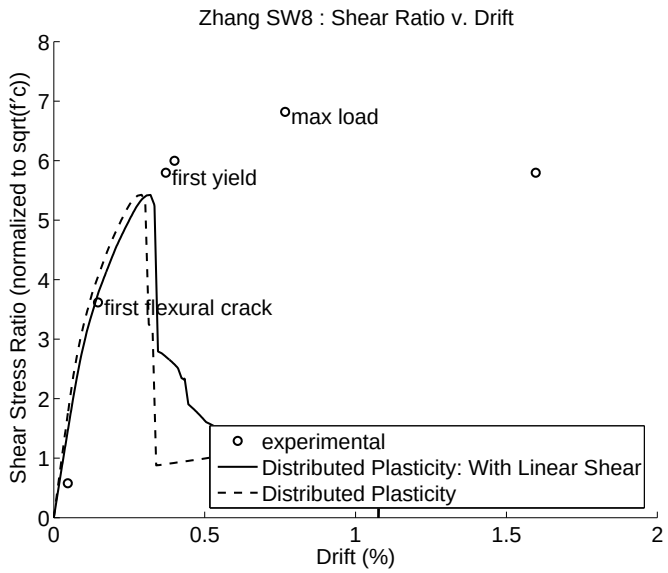

Figure M.59: Pushover of Beam-Column Element with Elastic Shear – Zhang SW8

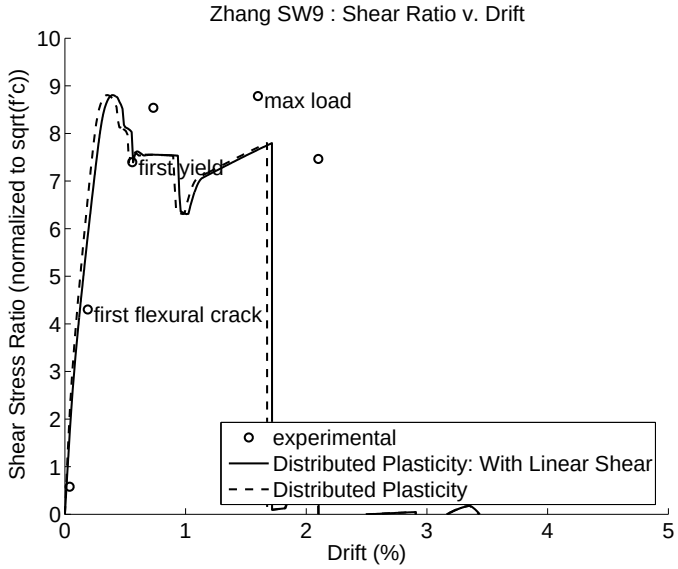

Figure M.60: Pushover of Beam-Column Element with Elastic Shear – Zhang SW9

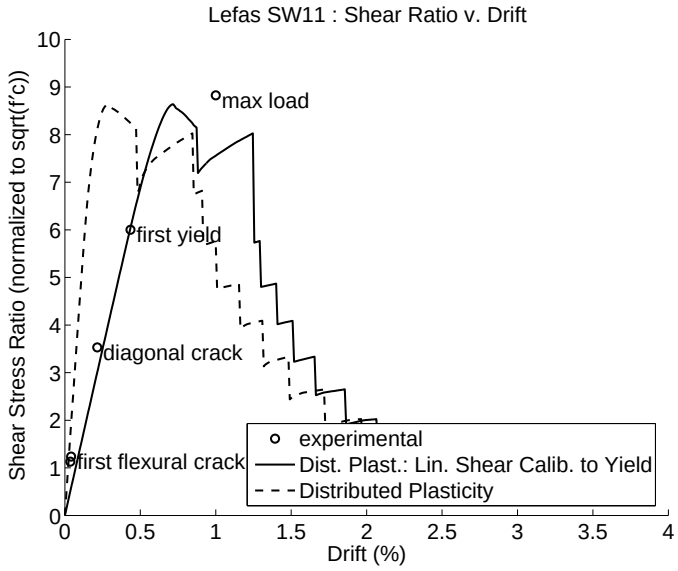

Figure M.61: Pushover of Beam-Column Element with Elastic Shear Calibrated to Yield – Lefas SW11

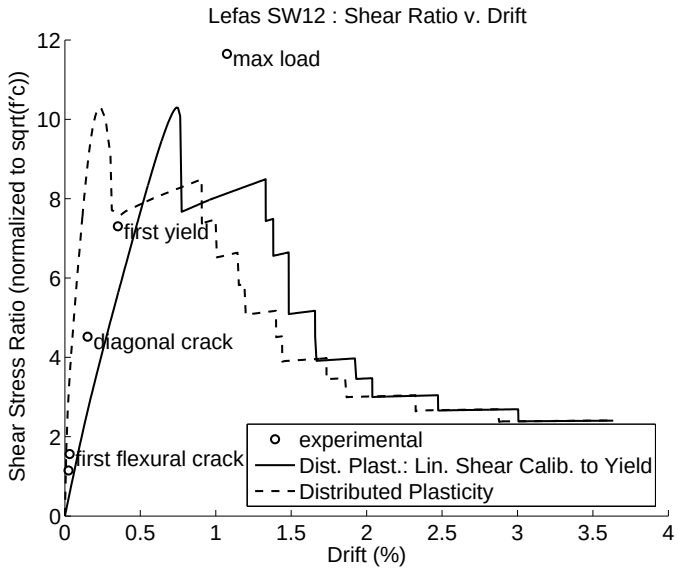

Figure M.62: Pushover of Beam-Column Element with Elastic Shear Calibrated to Yield – Lefas SW12

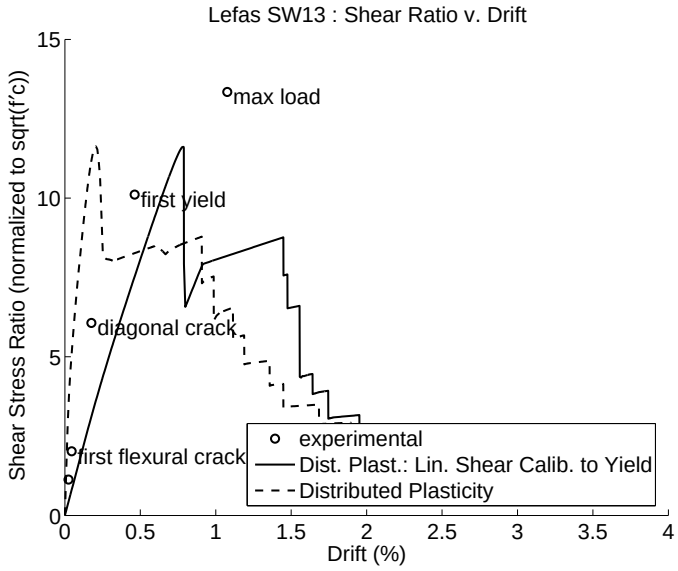

Figure M.63: Pushover of Beam-Column Element with Elastic Shear Calibrated to Yield – Lefas SW13

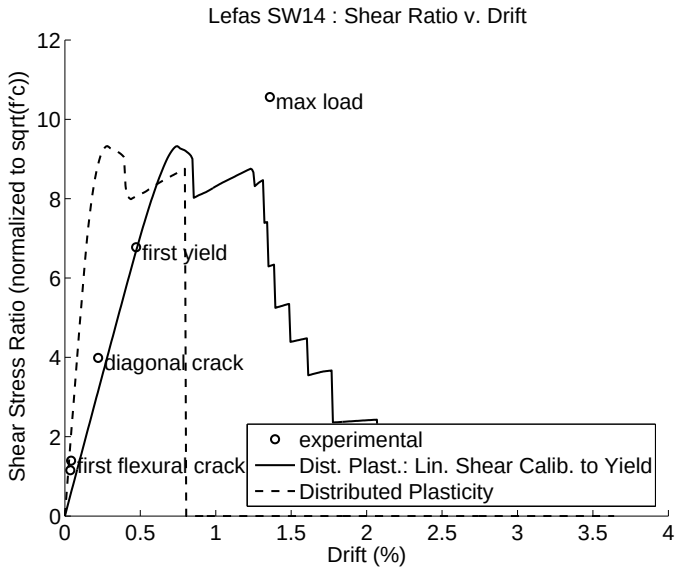

Figure M.64: Pushover of Beam-Column Element with Elastic Shear Calibrated to Yield – Lefas SW14

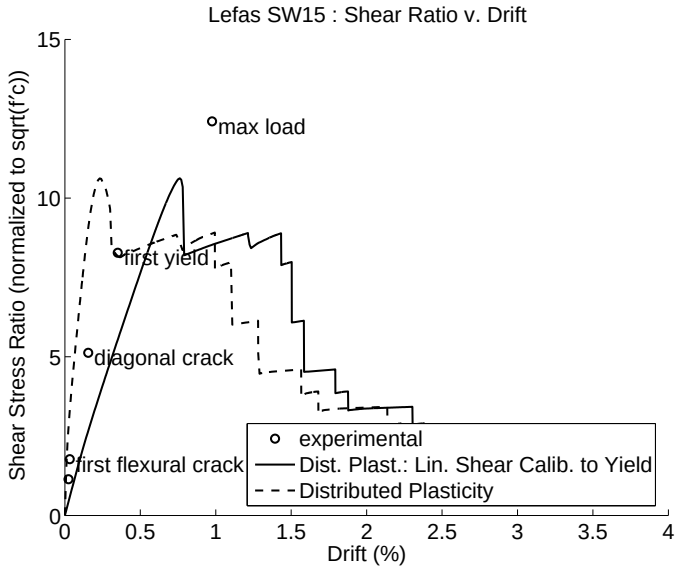

Figure M.65: Pushover of Beam-Column Element with Elastic Shear Calibrated to Yield – Lefas SW15

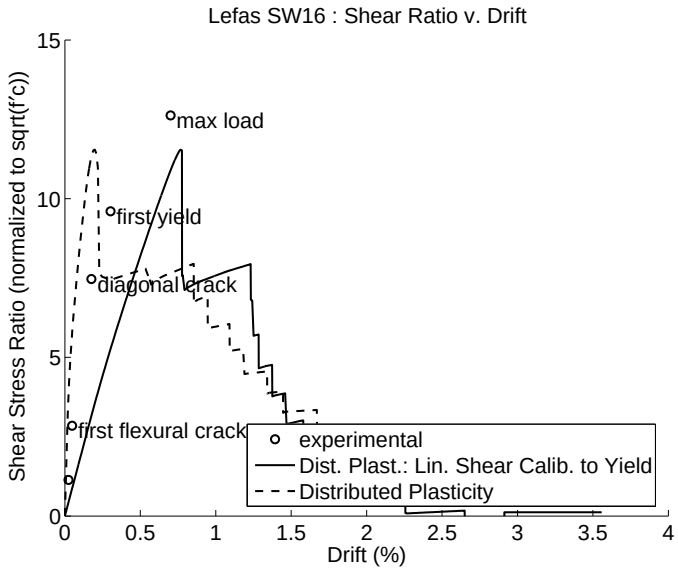

Figure M.66: Pushover of Beam-Column Element with Elastic Shear Calibrated to Yield – Lefas SW16

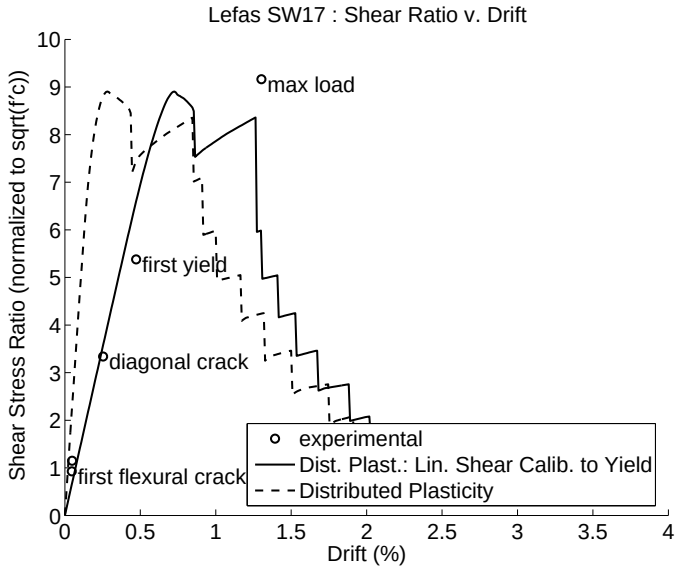

Figure M.67: Pushover of Beam-Column Element with Elastic Shear Calibrated to Yield – Lefas SW17

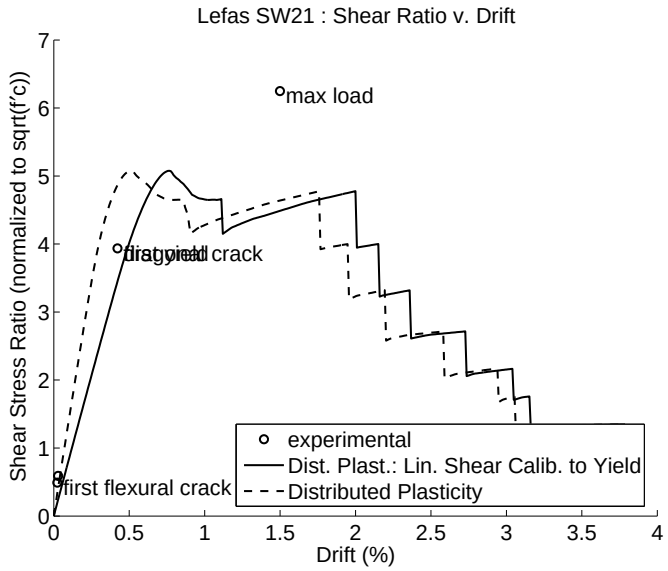

Figure M.68: Pushover of Beam-Column Element with Elastic Shear Calibrated to Yield – Lefas SW21

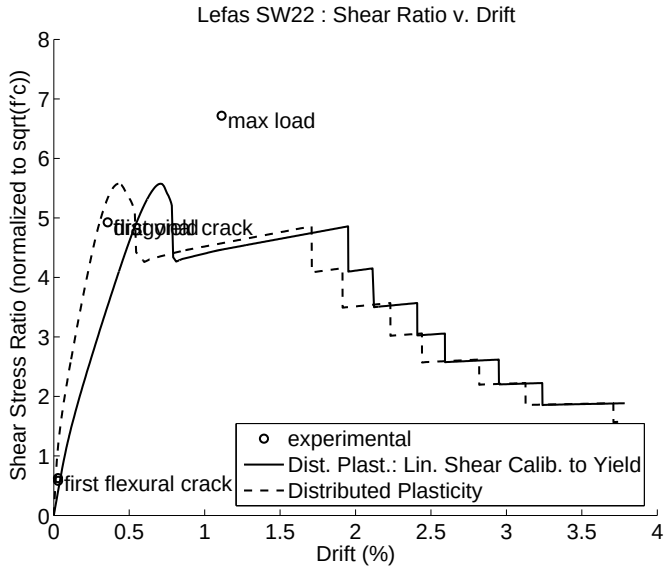

Figure M.69: Pushover of Beam-Column Element with Elastic Shear Calibrated to Yield – Lefas SW22

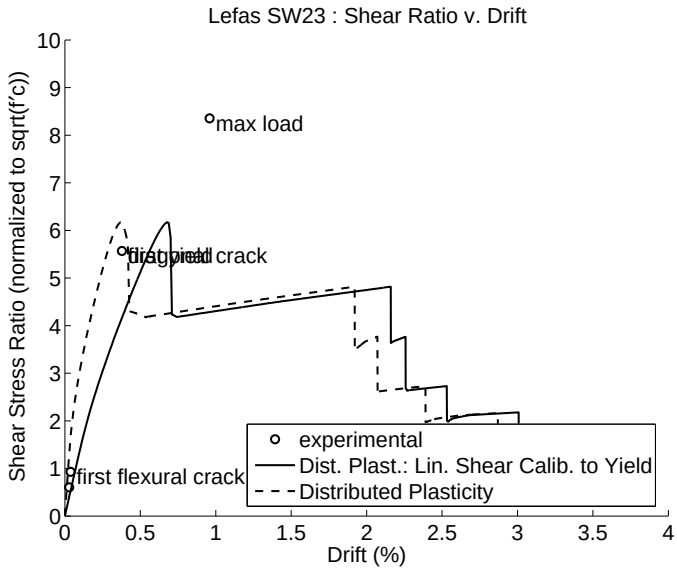

Figure M.70: Pushover of Beam-Column Element with Elastic Shear Calibrated to Yield – Lefas SW23

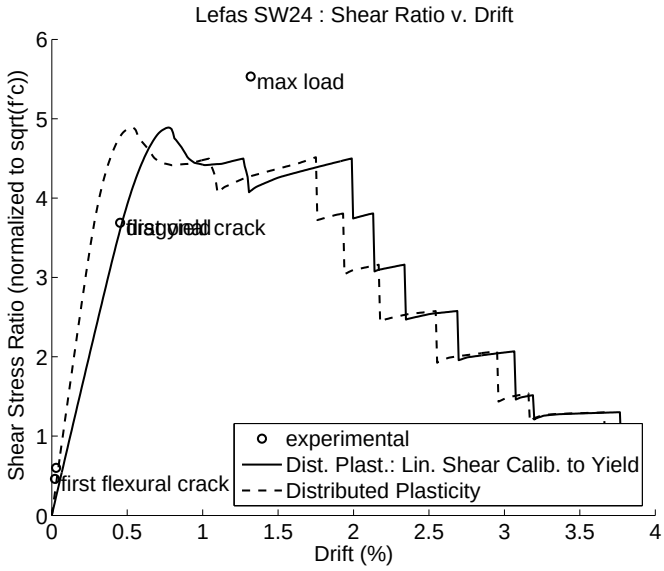

Figure M.71: Pushover of Beam-Column Element with Elastic Shear Calibrated to Yield – Lefas SW24

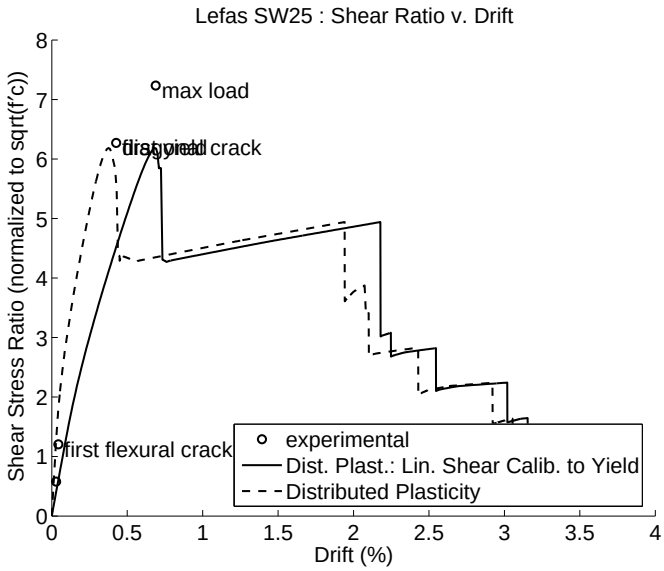

Figure M.72: Pushover of Beam-Column Element with Elastic Shear Calibrated to Yield – Lefas SW25

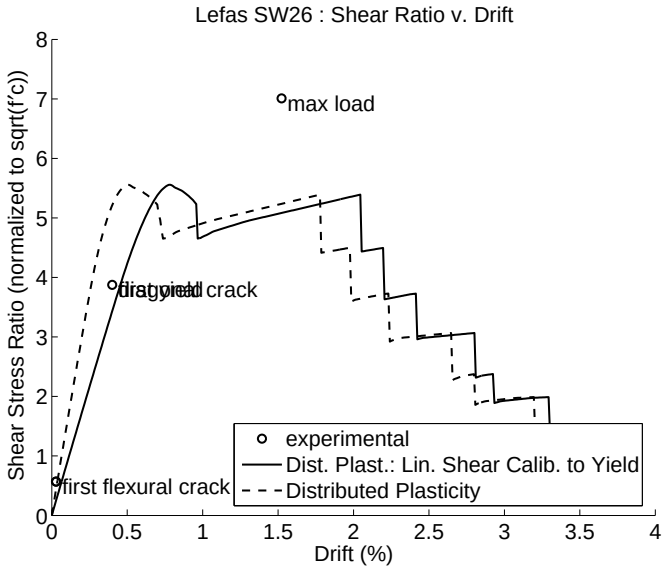

Figure M.73: Pushover of Beam-Column Element with Elastic Shear Calibrated to Yield – Lefas SW26

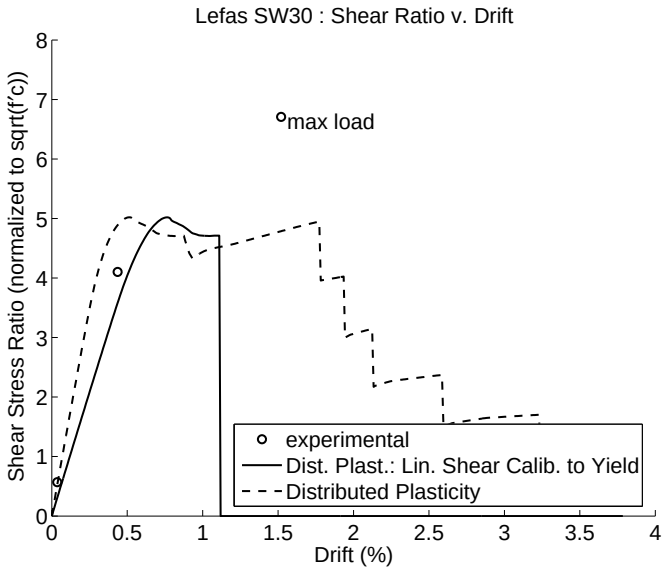

Figure M.74: Pushover of Beam-Column Element with Elastic Shear Calibrated to Yield – Lefas SW30

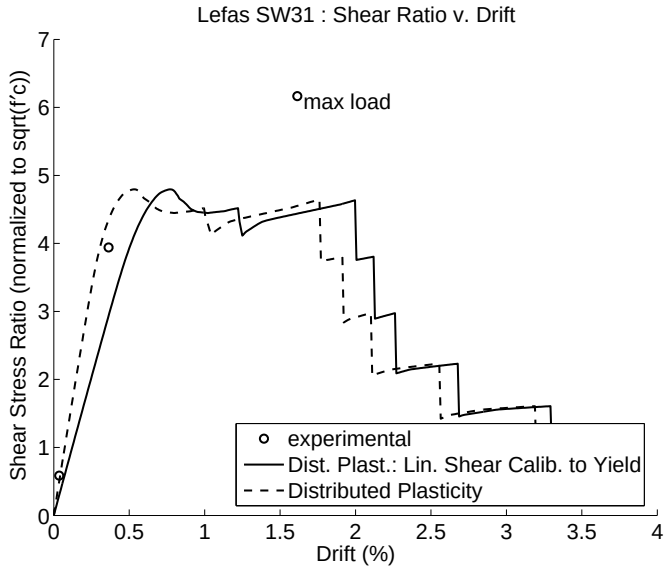

Figure M.75: Pushover of Beam-Column Element with Elastic Shear Calibrated to Yield – Lefas SW31

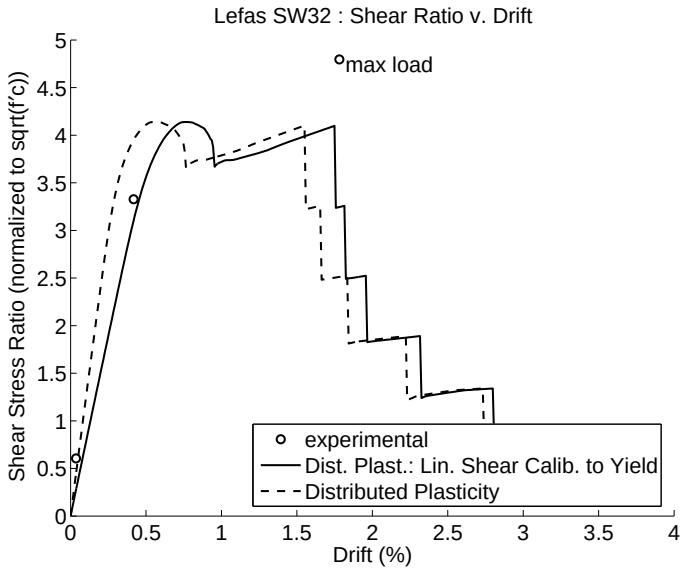

Figure M.76: Pushover of Beam-Column Element with Elastic Shear Calibrated to Yield – Lefas SW32

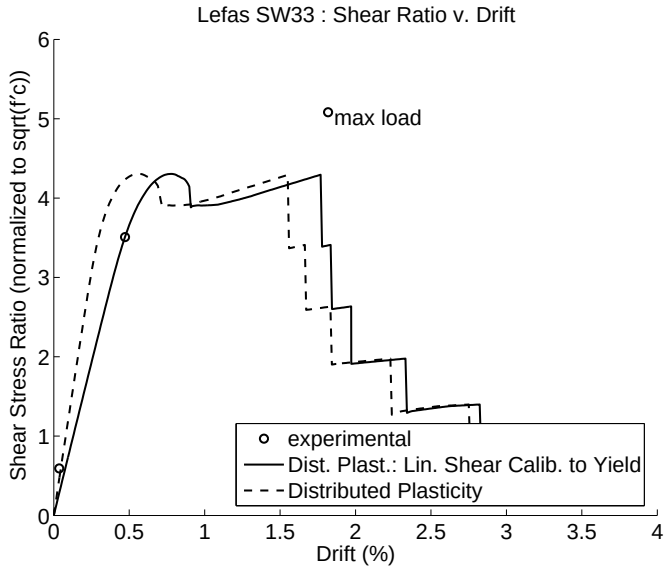

Figure M.77: Pushover of Beam-Column Element with Elastic Shear Calibrated to Yield – Lefas SW33

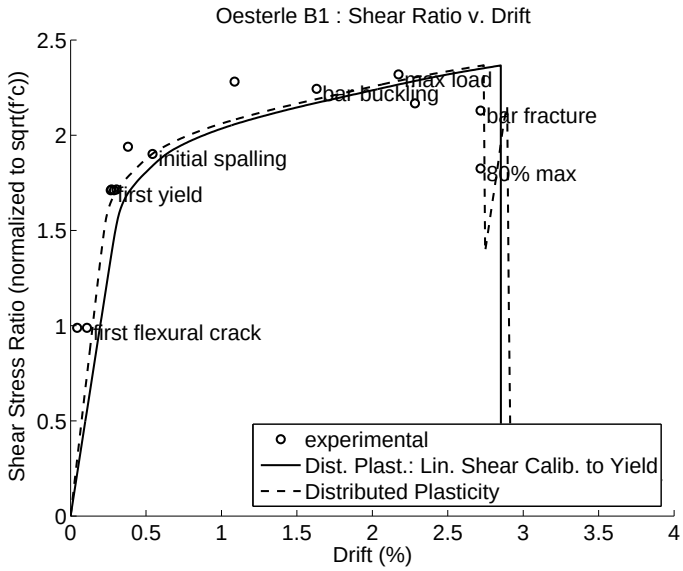

Figure M.78: Pushover of Beam-Column Element with Elastic Shear Calibrated to Yield – Oesterle B1

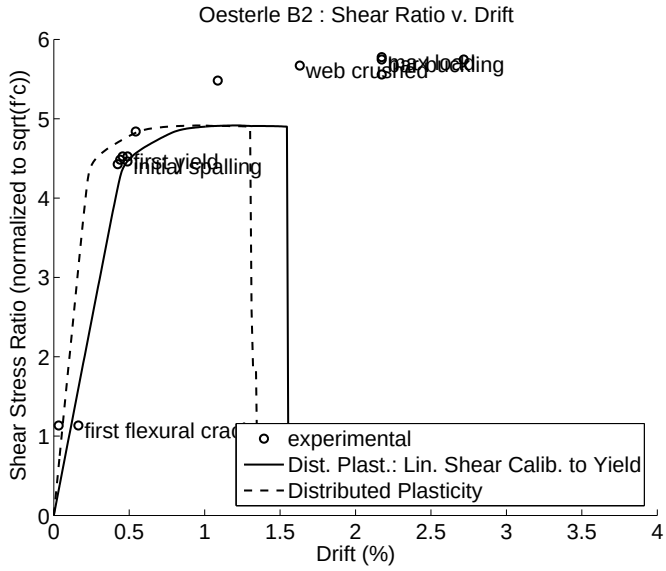

Figure M.79: Pushover of Beam-Column Element with Elastic Shear Calibrated to Yield – Oesterle B2

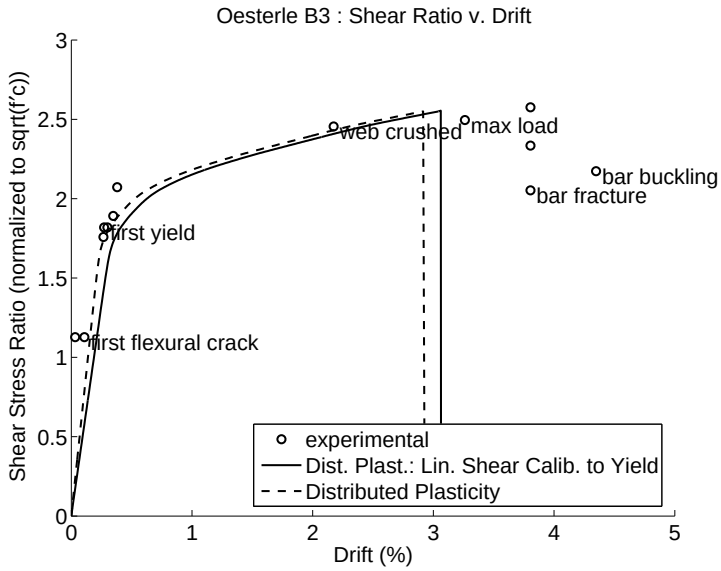

Figure M.80: Pushover of Beam-Column Element with Elastic Shear Calibrated to Yield – Oesterle B3

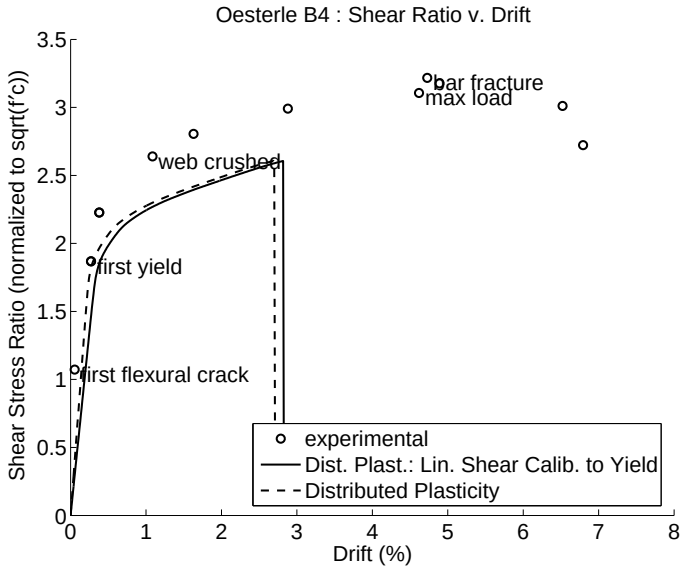

Figure M.81: Pushover of Beam-Column Element with Elastic Shear Calibrated to Yield – Oesterle B4

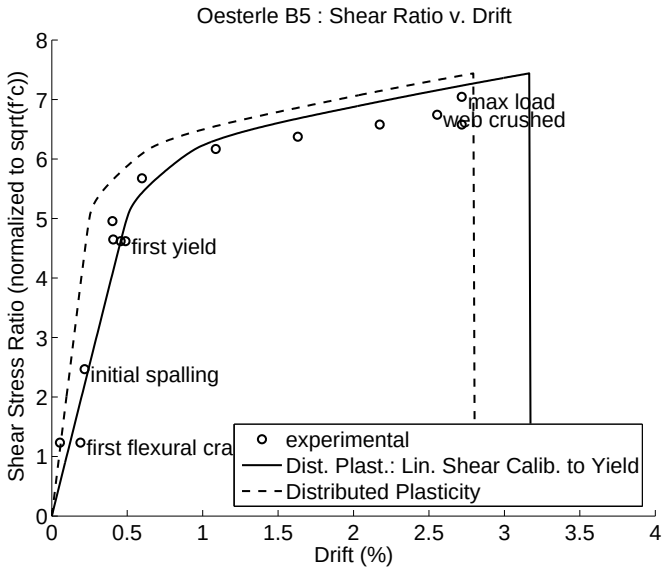

Figure M.82: Pushover of Beam-Column Element with Elastic Shear Calibrated to Yield – Oesterle B5

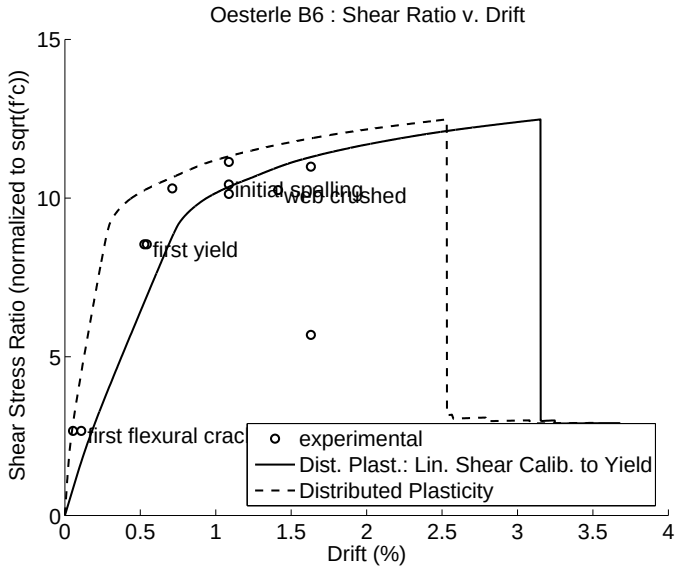

Figure M.83: Pushover of Beam-Column Element with Elastic Shear Calibrated to Yield – Oesterle B6

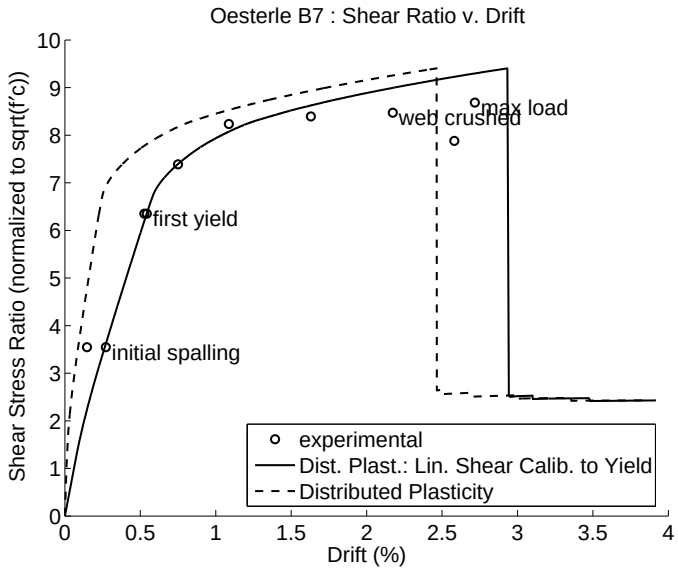

Figure M.84: Pushover of Beam-Column Element with Elastic Shear Calibrated to Yield – Oesterle B7

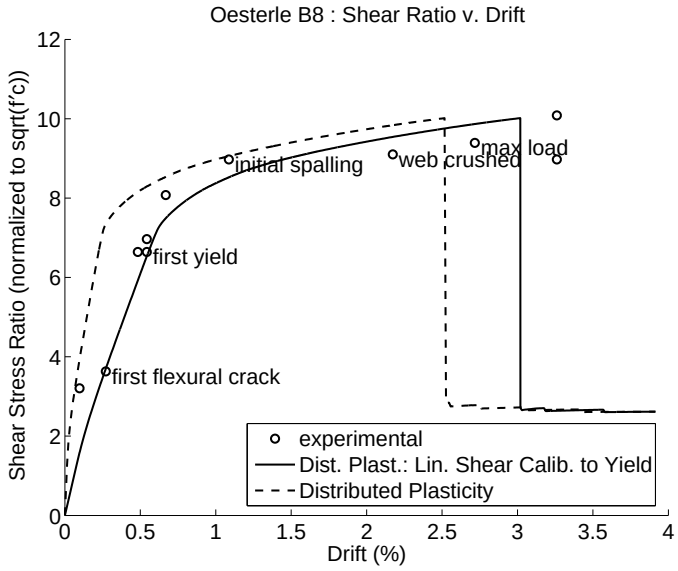

Figure M.85: Pushover of Beam-Column Element with Elastic Shear Calibrated to Yield – Oesterle B8

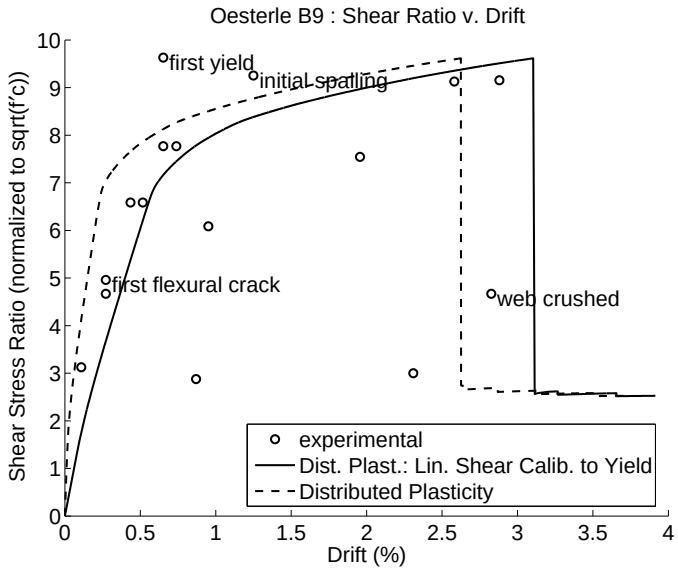

Figure M.86: Pushover of Beam-Column Element with Elastic Shear Calibrated to Yield – Oesterle B9

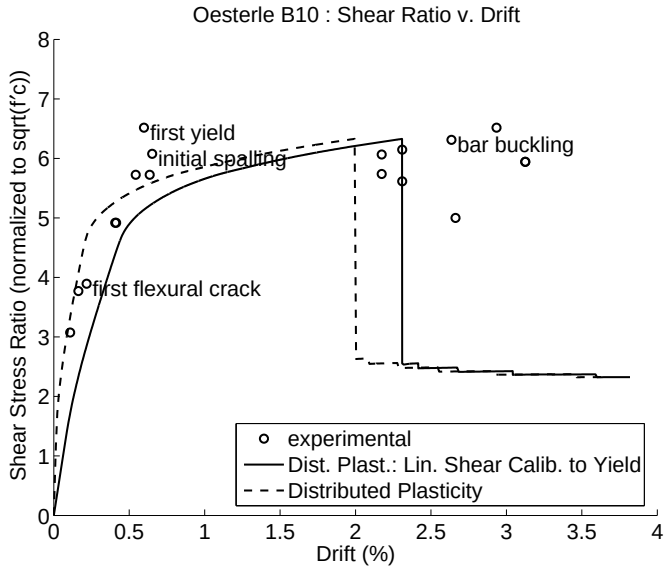

Figure M.87: Pushover of Beam-Column Element with Elastic Shear Calibrated to Yield – Oesterle B10

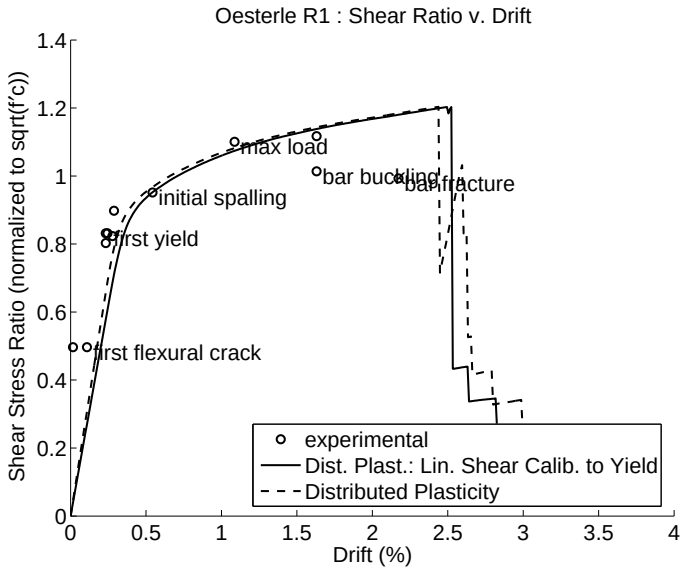

Figure M.88: Pushover of Beam-Column Element with Elastic Shear Calibrated to Yield – Oesterle R1

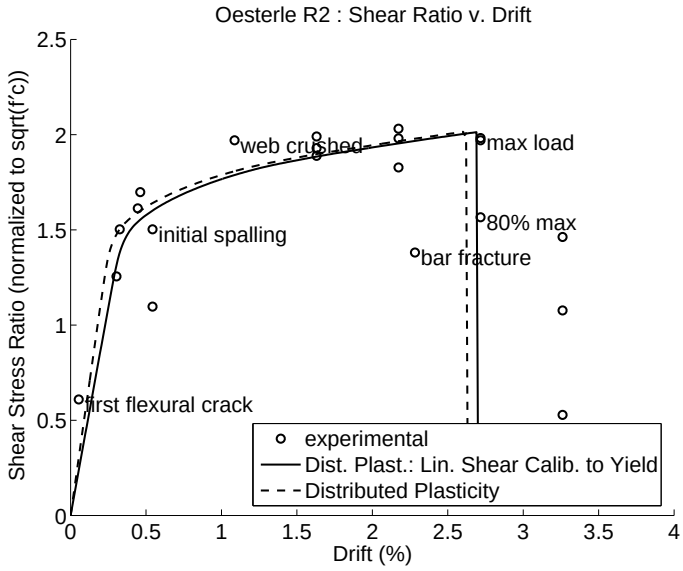

Figure M.89: Pushover of Beam-Column Element with Elastic Shear Calibrated to Yield – Oesterle R2

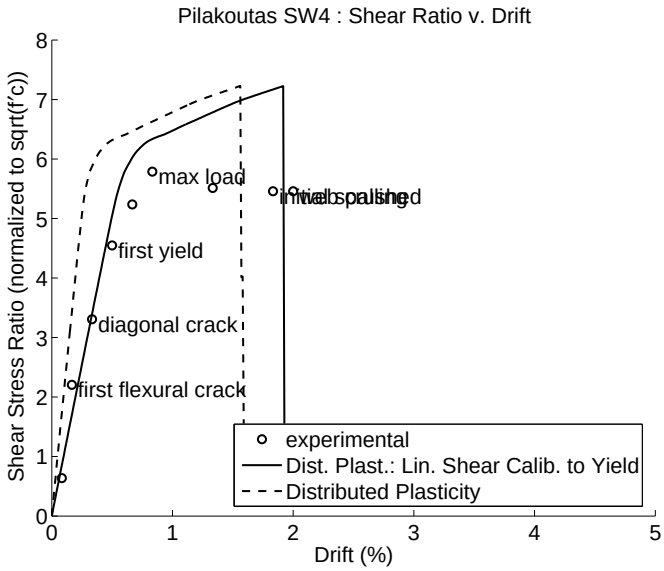

Figure M.90: Pushover of Beam-Column Element with Elastic Shear Calibrated to Yield – Pilakoutas SW4

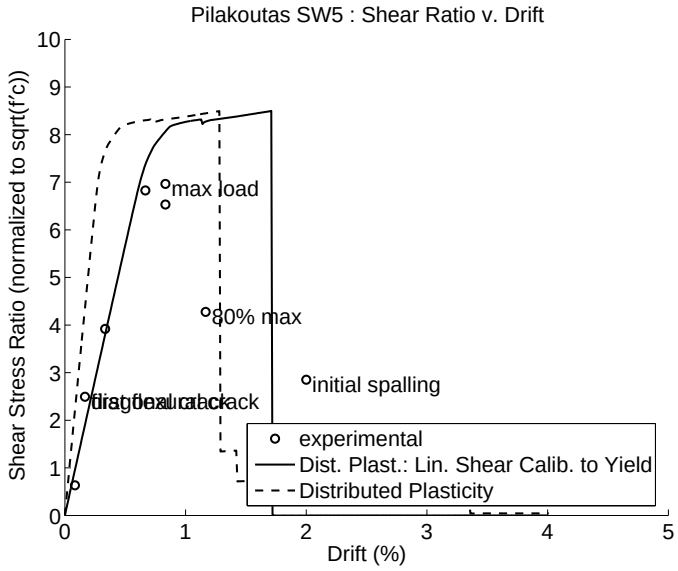

Figure M.91: Pushover of Beam-Column Element with Elastic Shear Calibrated to Yield – Pilakoutas SW5

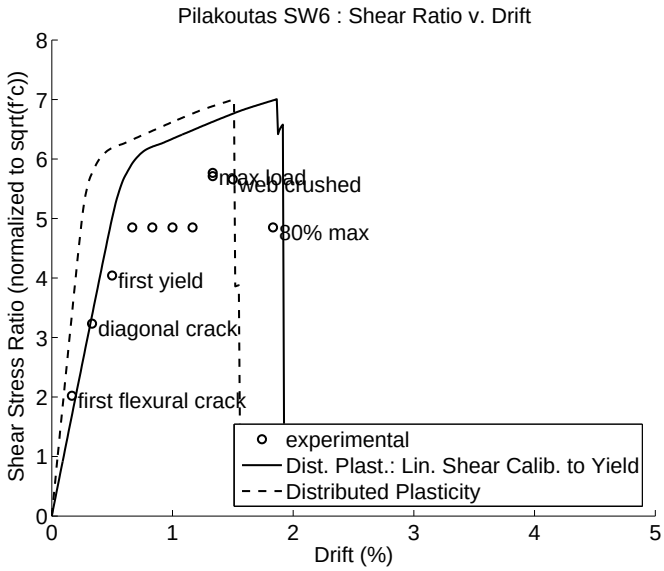

Figure M.92: Pushover of Beam-Column Element with Elastic Shear Calibrated to Yield – Pilakoutas SW6

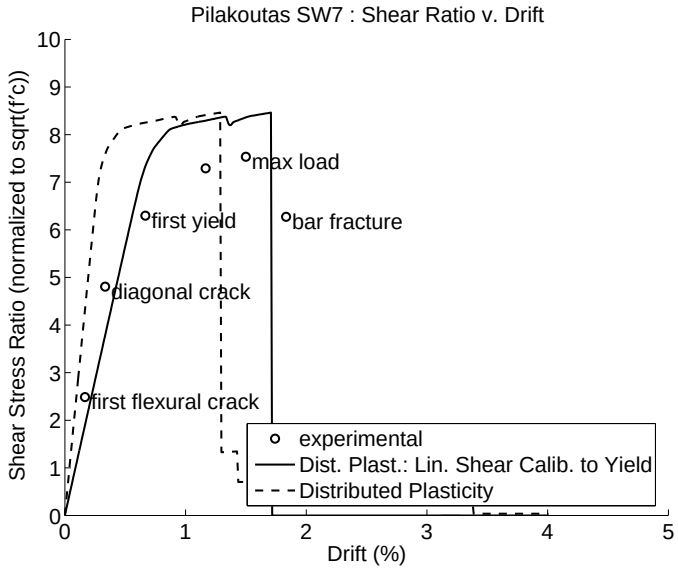

Figure M.93: Pushover of Beam-Column Element with Elastic Shear Calibrated to Yield – Pilakoutas SW7

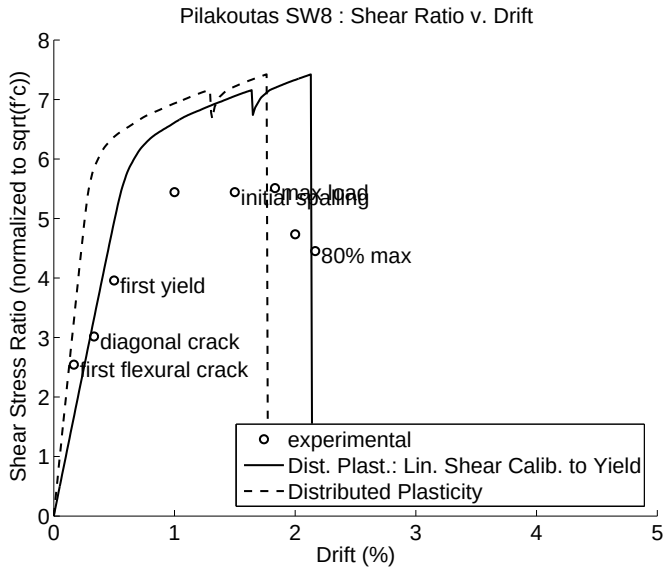

Figure M.94: Pushover of Beam-Column Element with Elastic Shear Calibrated to Yield – Pilakoutas SW8

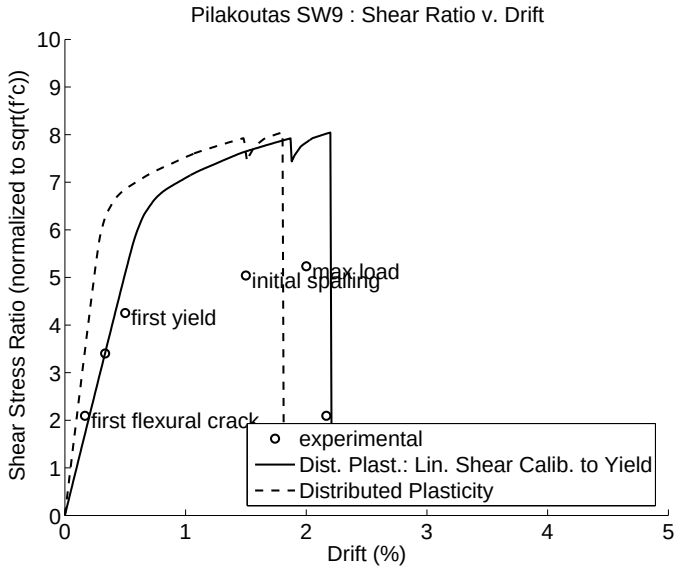

Figure M.95: Pushover of Beam-Column Element with Elastic Shear Calibrated to Yield – Pilakoutas SW9

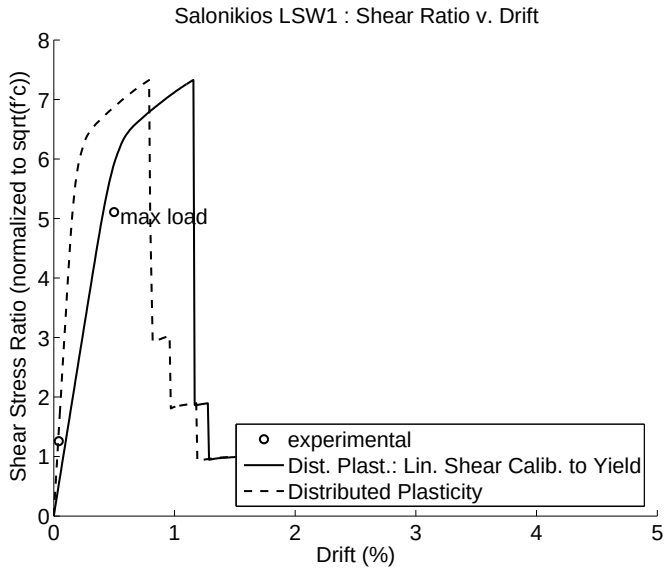

Figure M.96: Pushover of Beam-Column Element with Elastic Shear Calibrated to Yield – Salonikios LSW1

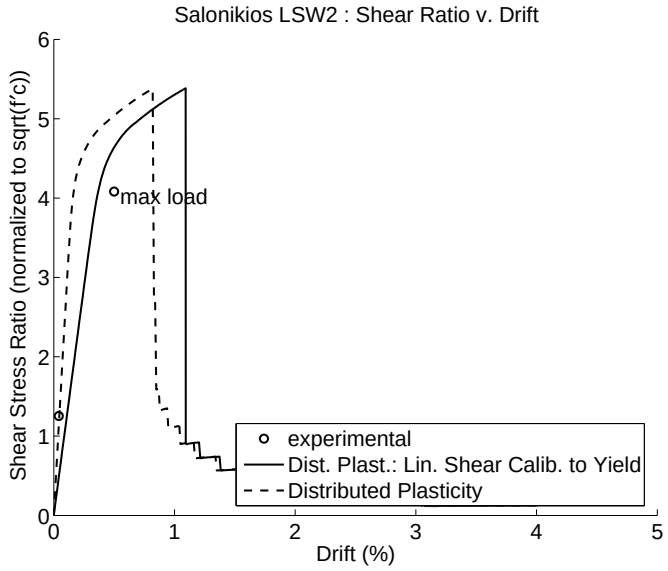

Figure M.97: Pushover of Beam-Column Element with Elastic Shear Calibrated to Yield – Salonikios LSW2

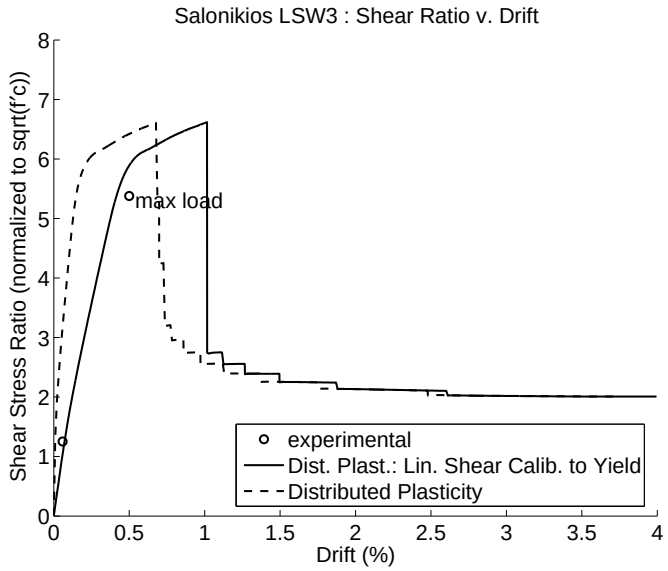

Figure M.98: Pushover of Beam-Column Element with Elastic Shear Calibrated to Yield – Salonikios LSW3

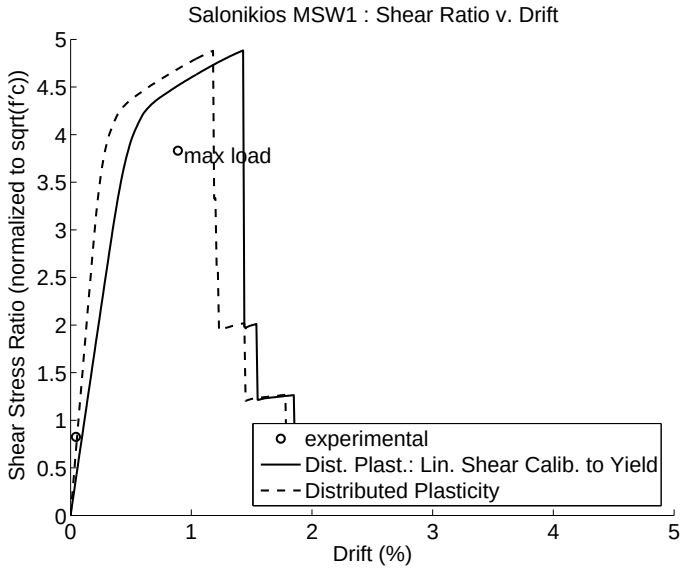

Figure M.99: Pushover of Beam-Column Element with Elastic Shear Calibrated to Yield – Salonikios MSW1

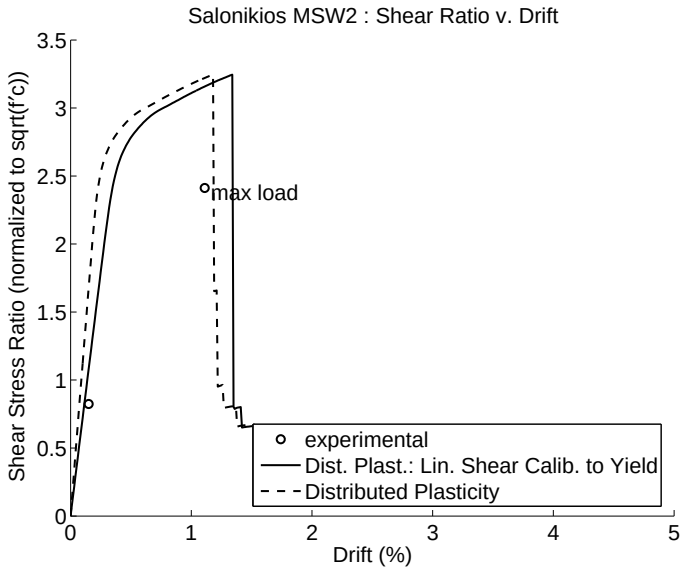

Figure M.100: Pushover of Beam-Column Element with Elastic Shear Calibrated to Yield – Salonikios MSW2

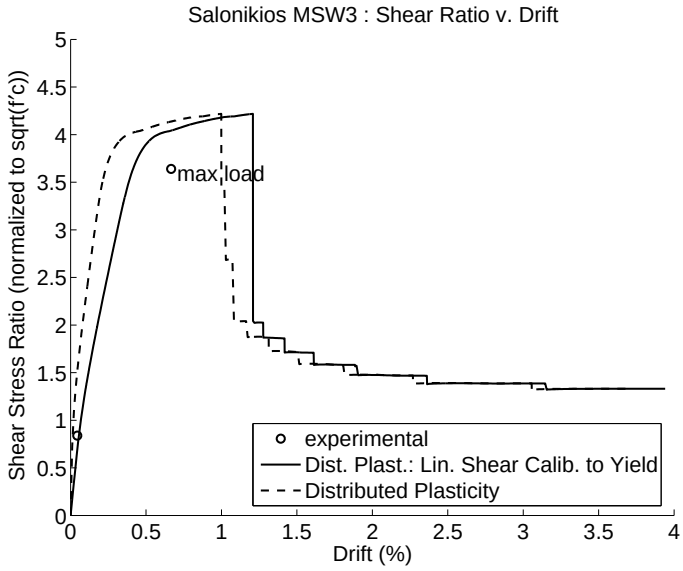

Figure M.101: Pushover of Beam-Column Element with Elastic Shear Calibrated to Yield – Salonikios MSW3

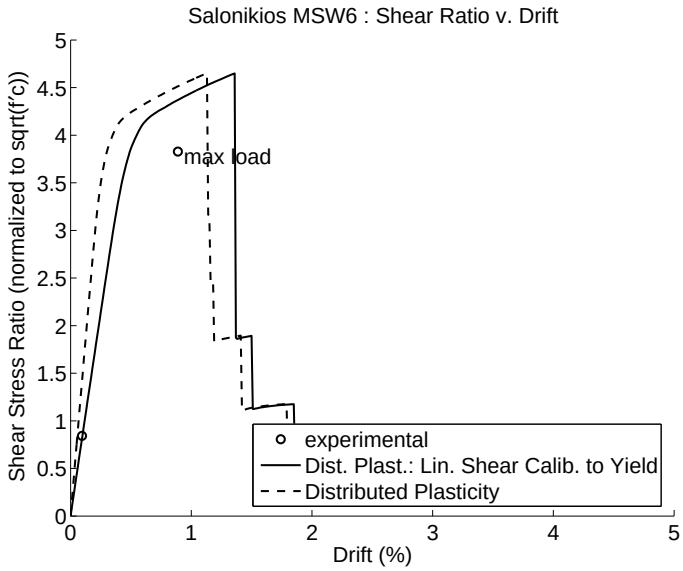

Figure M.102: Pushover of Beam-Column Element with Elastic Shear Calibrated to Yield – Salonikios MSW6

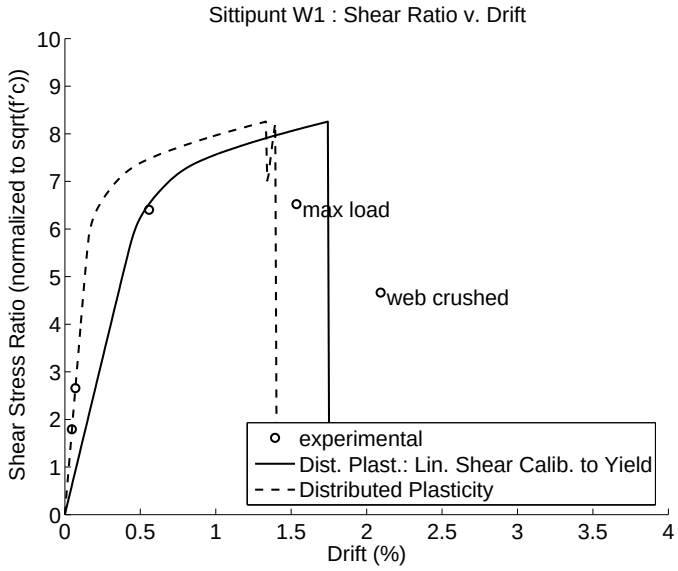

Figure M.103: Pushover of Beam-Column Element with Elastic Shear Calibrated to Yield – Sittipunt W1

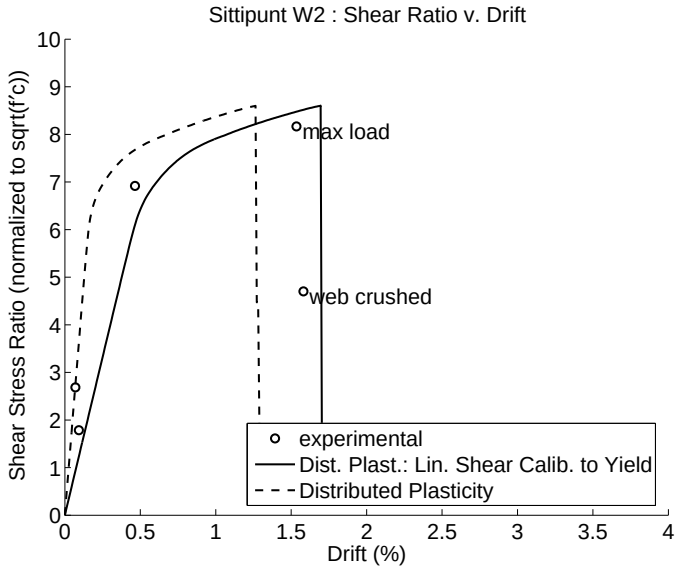

Figure M.104: Pushover of Beam-Column Element with Elastic Shear Calibrated to Yield – Sittipunt W2

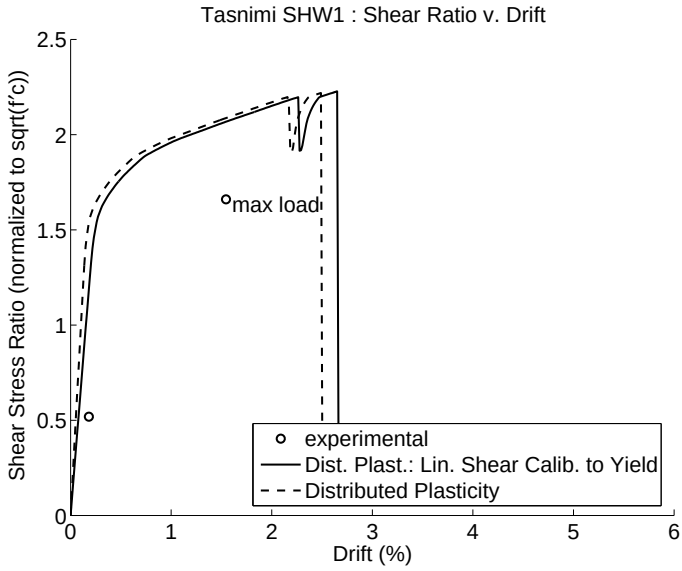

Figure M.105: Pushover of Beam-Column Element with Elastic Shear Calibrated to Yield – Tasnimi SHW1

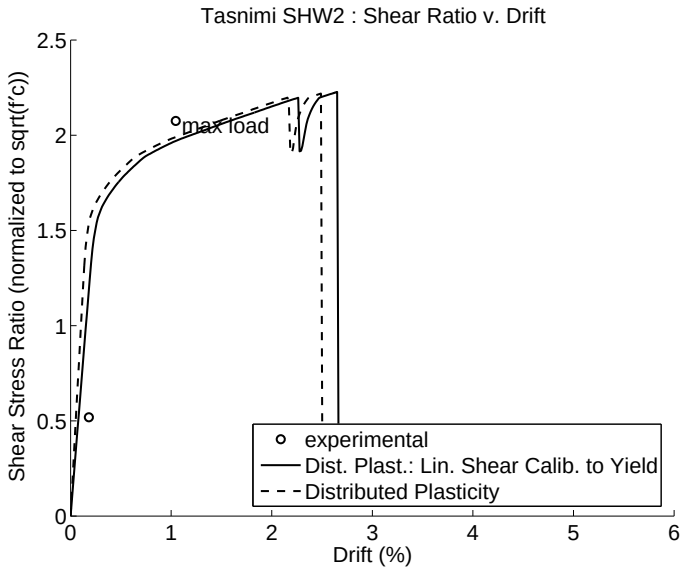

Figure M.106: Pushover of Beam-Column Element with Elastic Shear Calibrated to Yield – Tasnimi SHW2

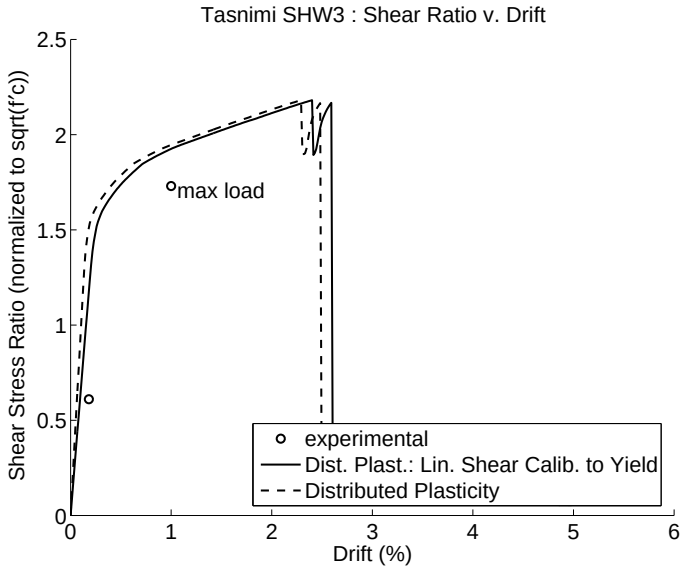

Figure M.107: Pushover of Beam-Column Element with Elastic Shear Calibrated to Yield – Tasnimi SHW3

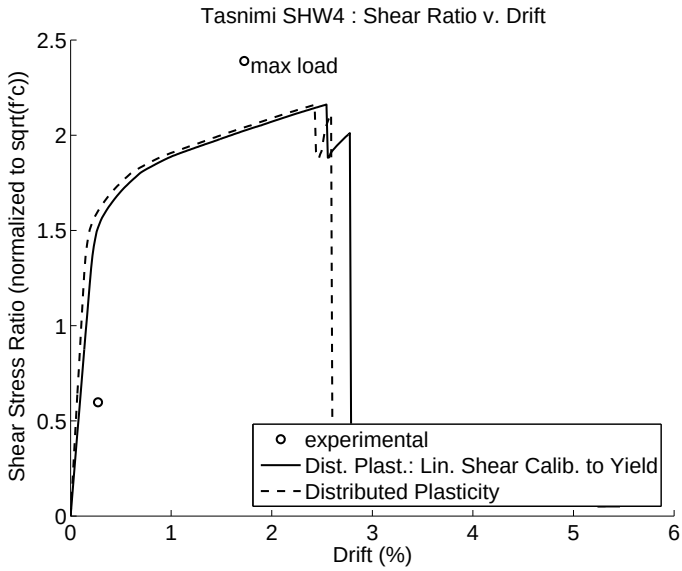

Figure M.108: Pushover of Beam-Column Element with Elastic Shear Calibrated to Yield – Tasnimi SHW4

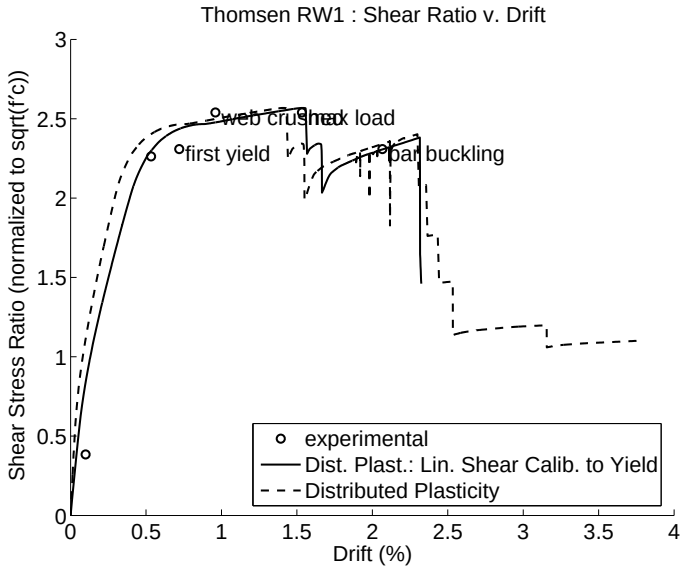

Figure M.109: Pushover of Beam-Column Element with Elastic Shear Calibrated to Yield – Thomsen RW1

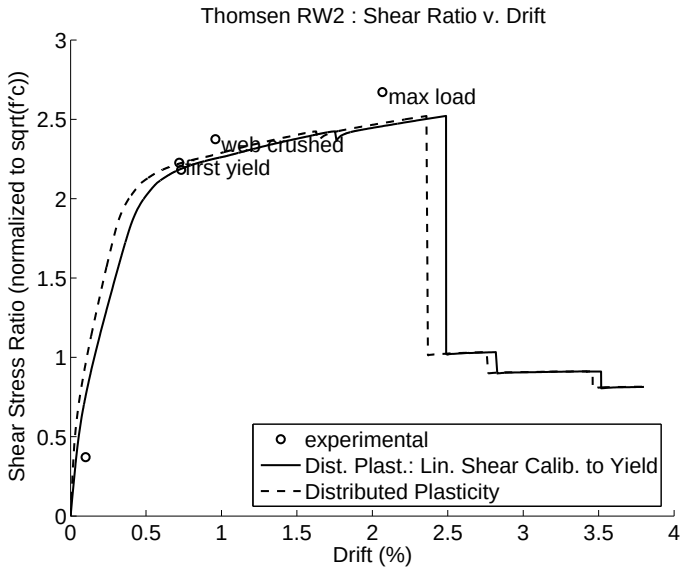

Figure M.110: Pushover of Beam-Column Element with Elastic Shear Calibrated to Yield – Thomsen RW2

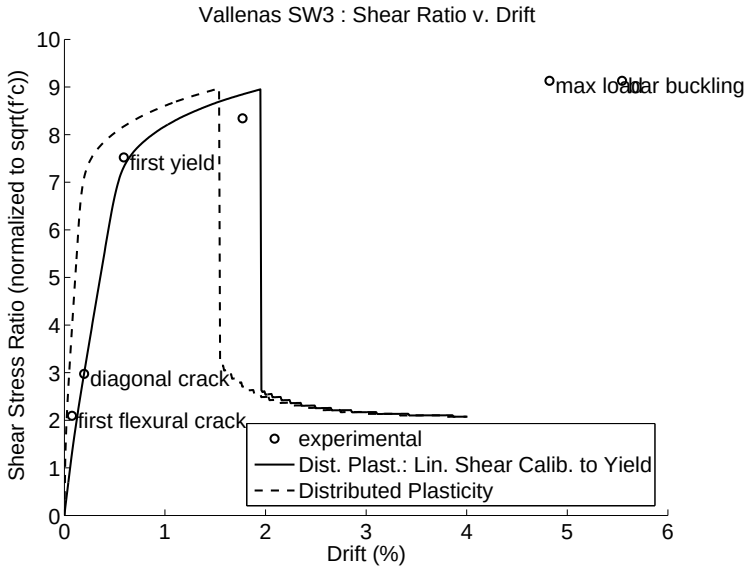

Figure M.111: Pushover of Beam-Column Element with Elastic Shear Calibrated to Yield – Vallenas SW3

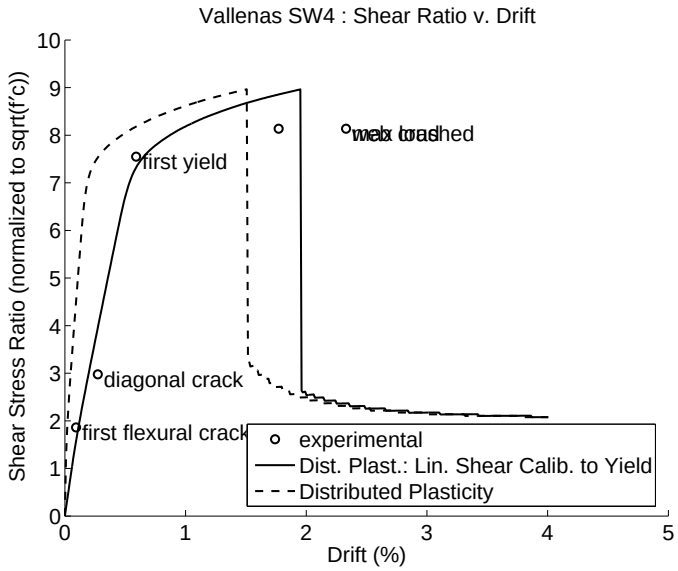

Figure M.112: Pushover of Beam-Column Element with Elastic Shear Calibrated to Yield – Vallenas SW4

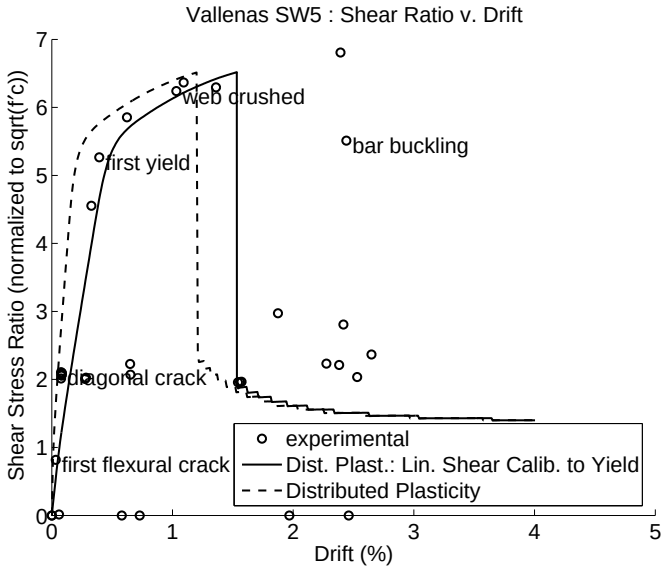

Figure M.113: Pushover of Beam-Column Element with Elastic Shear Calibrated to Yield – Vallenas SW5

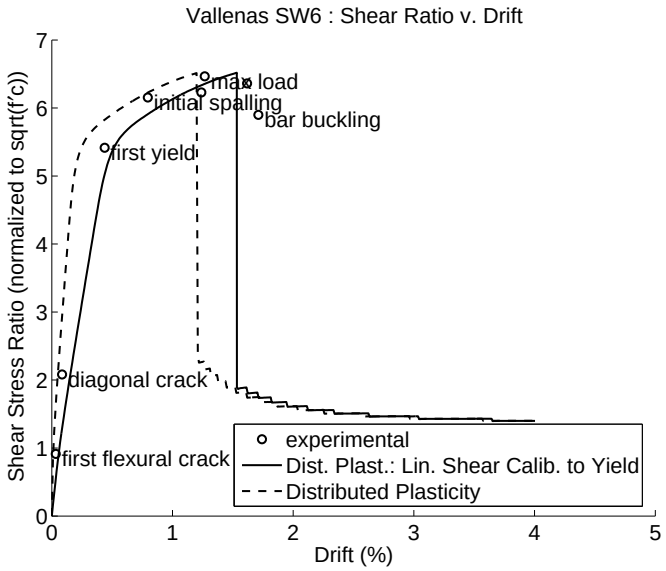

Figure M.114: Pushover of Beam-Column Element with Elastic Shear Calibrated to Yield – Vallenas SW6

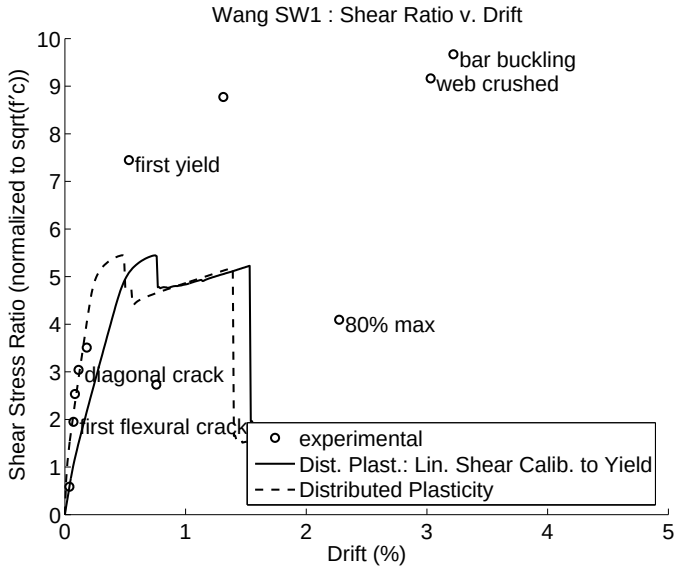

Figure M.115: Pushover of Beam-Column Element with Elastic Shear Calibrated to Yield – Wang SW1

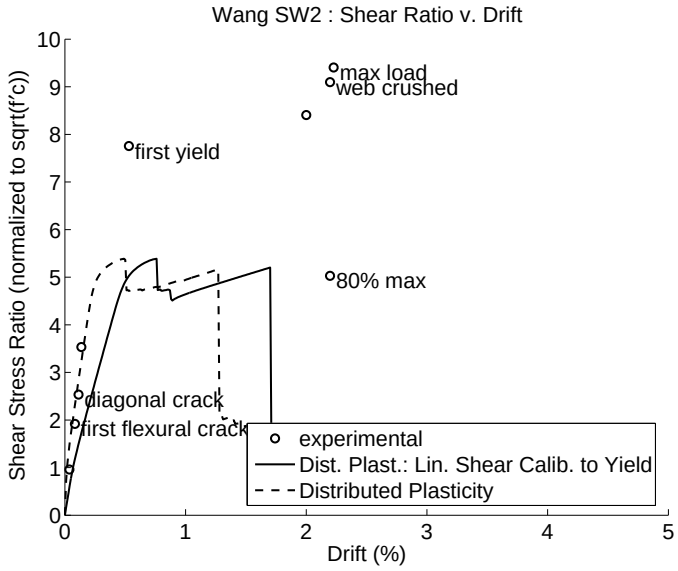

Figure M.116: Pushover of Beam-Column Element with Elastic Shear Calibrated to Yield – Wang SW2

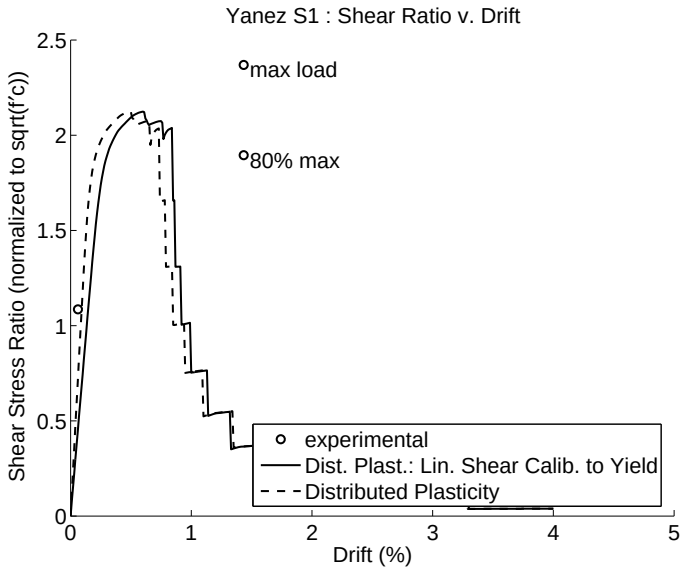

Figure M.117: Pushover of Beam-Column Element with Elastic Shear Calibrated to Yield – Yanez S1

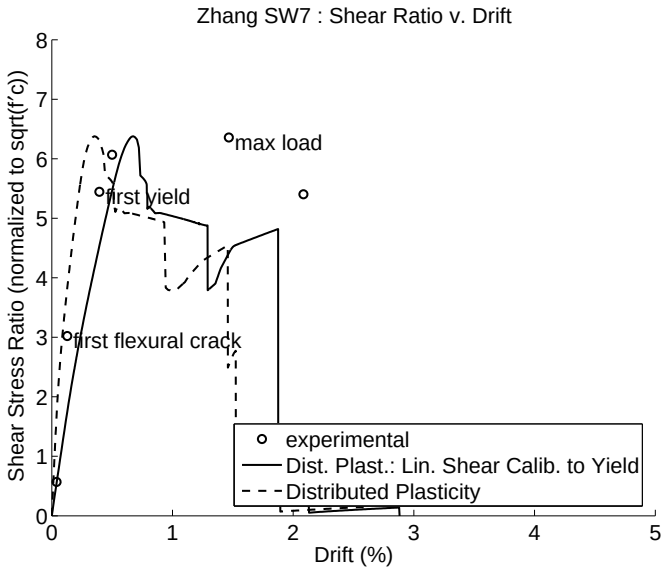

Figure M.118: Pushover of Beam-Column Element with Elastic Shear Calibrated to Yield – Zhang SW7

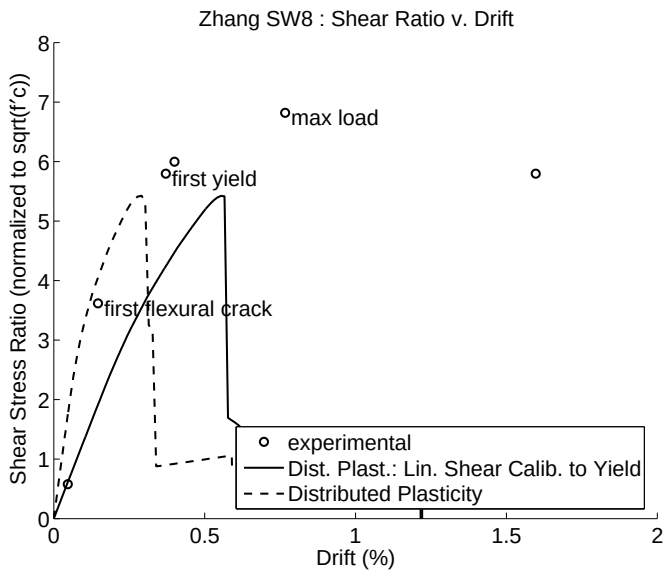

Figure M.119: Pushover of Beam-Column Element with Elastic Shear Calibrated to Yield – Zhang SW8

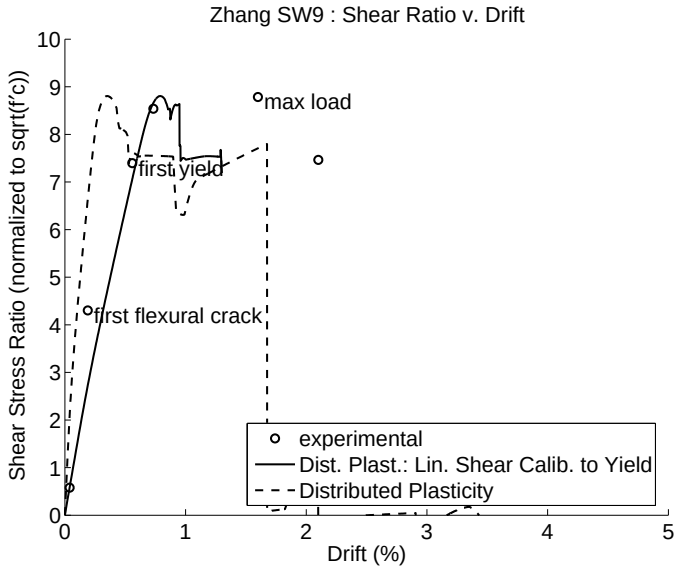

Figure M.120: Pushover of Beam-Column Element with Elastic Shear Calibrated to Yield – Zhang SW9

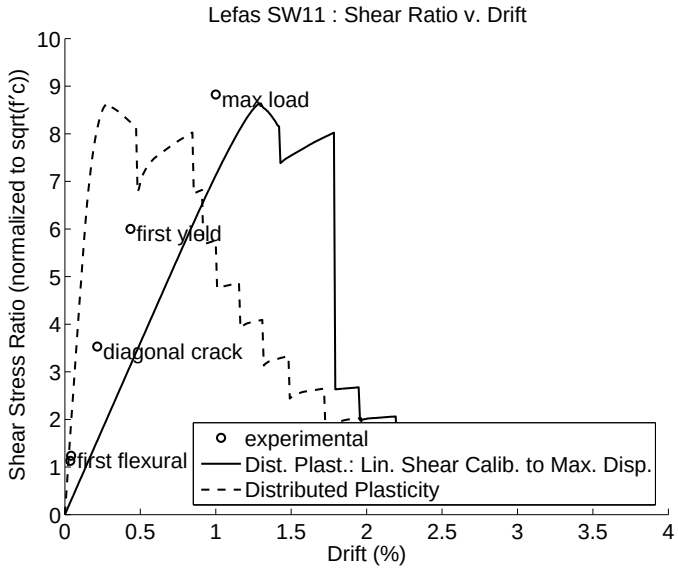

Figure M.121: Pushover of Beam-Column Element with Elastic Shear Calibrated to Maximum Displacement – Lefas SW11

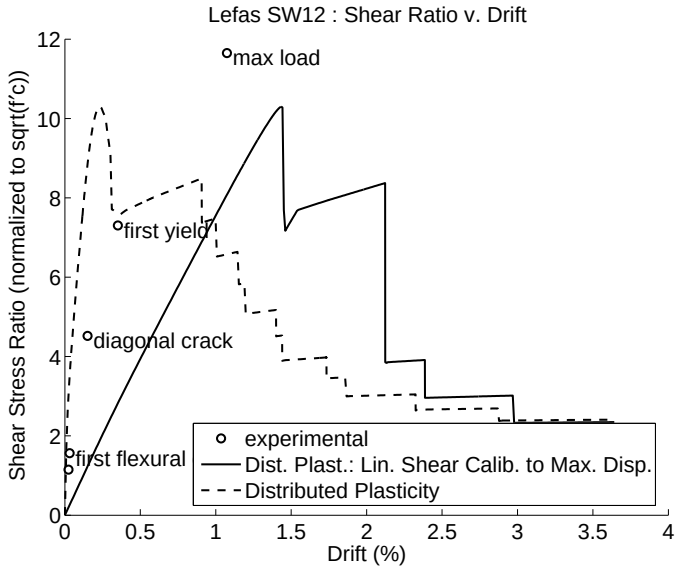

Figure M.122: Pushover of Beam-Column Element with Elastic Shear Calibrated to Maximum Displacement – Lefas SW12

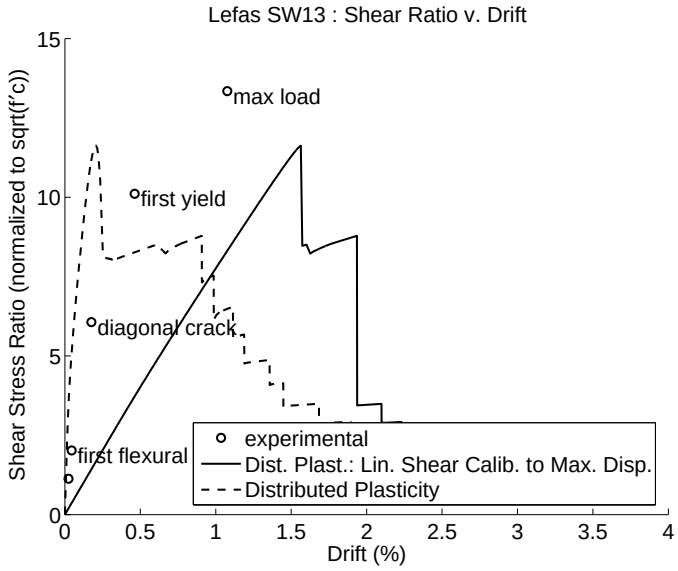

Figure M.123: Pushover of Beam-Column Element with Elastic Shear Calibrated to Maximum Displacement – Lefas SW13

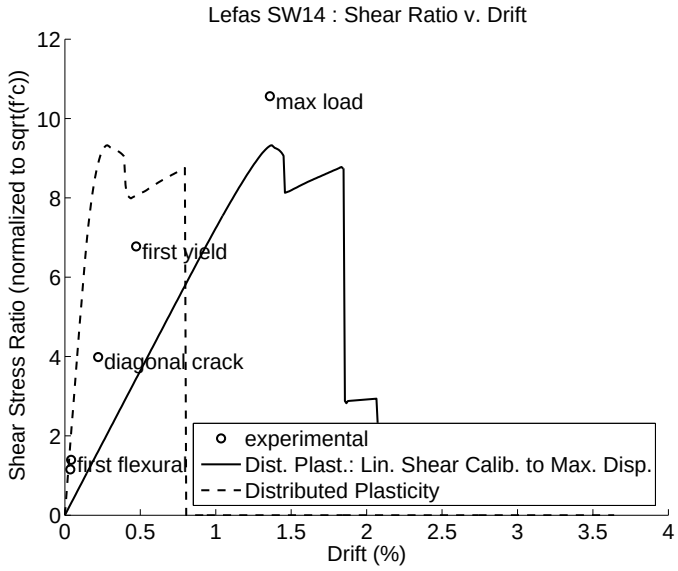

Figure M.124: Pushover of Beam-Column Element with Elastic Shear Calibrated to Maximum Displacement – Lefas SW14

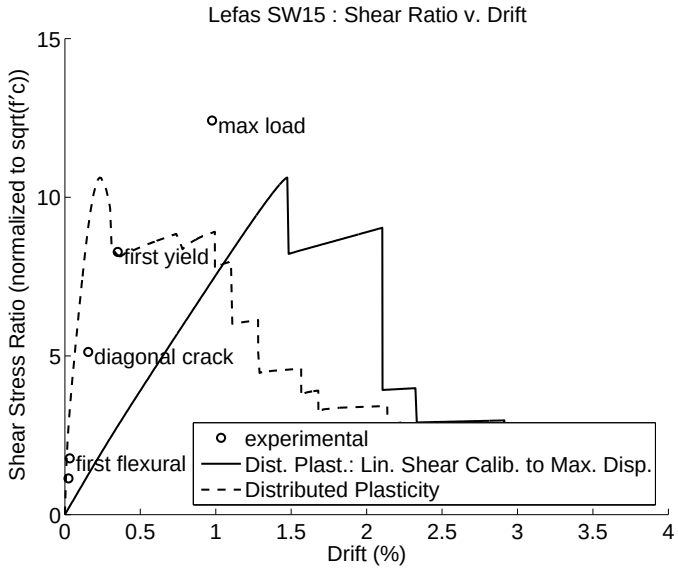

Figure M.125: Pushover of Beam-Column Element with Elastic Shear Calibrated to Maximum Displacement – Lefas SW15

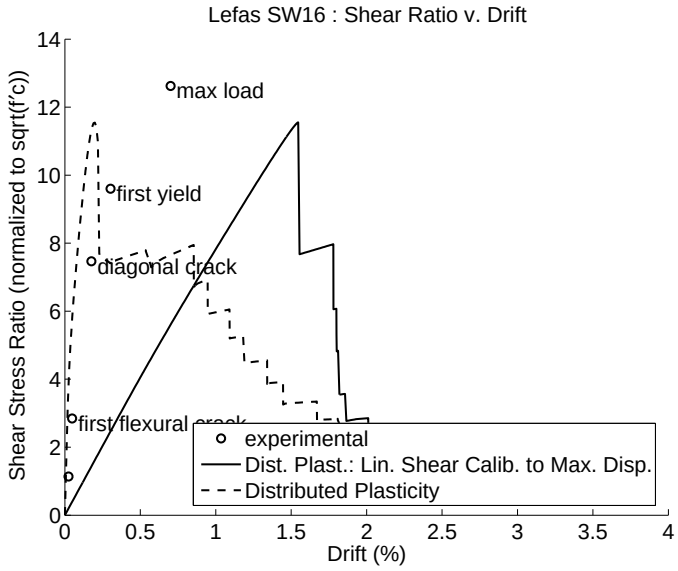

Figure M.126: Pushover of Beam-Column Element with Elastic Shear Calibrated to Maximum Displacement – Lefas SW16

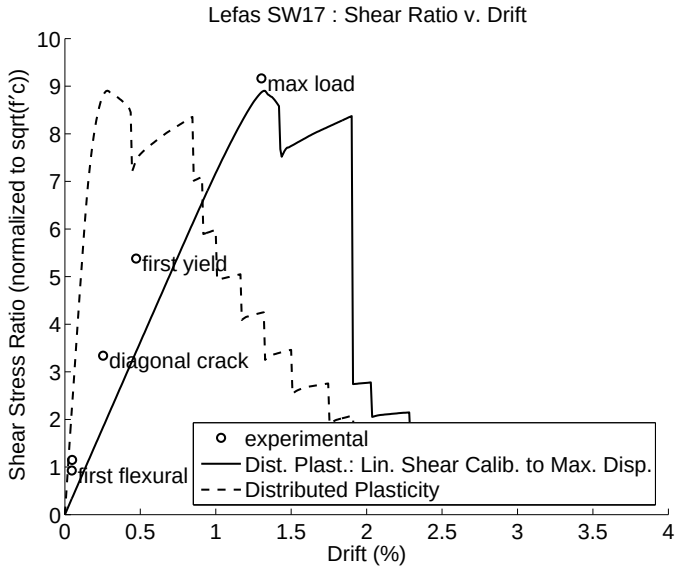

Figure M.127: Pushover of Beam-Column Element with Elastic Shear Calibrated to Maximum Displacement – Lefas SW17

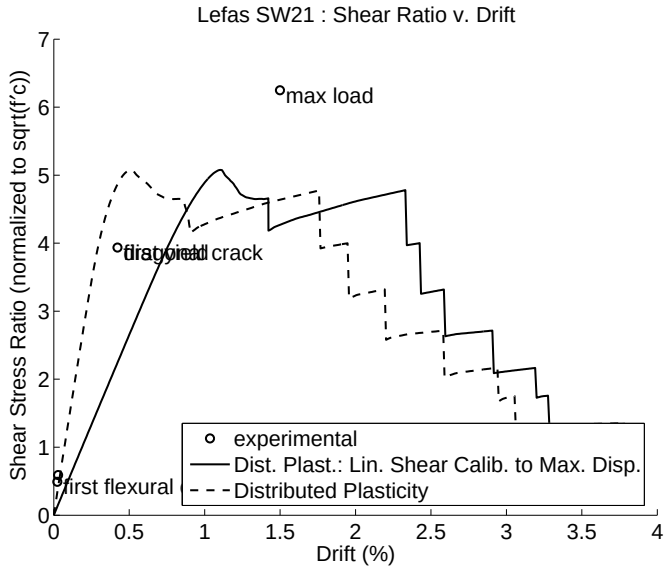

Figure M.128: Pushover of Beam-Column Element with Elastic Shear Calibrated to Maximum Displacement – Lefas SW21

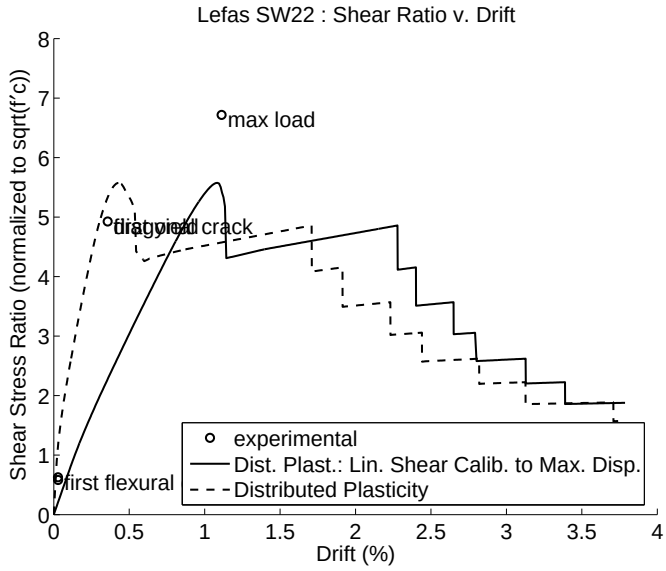

Figure M.129: Pushover of Beam-Column Element with Elastic Shear Calibrated to Maximum Displacement – Lefas SW22

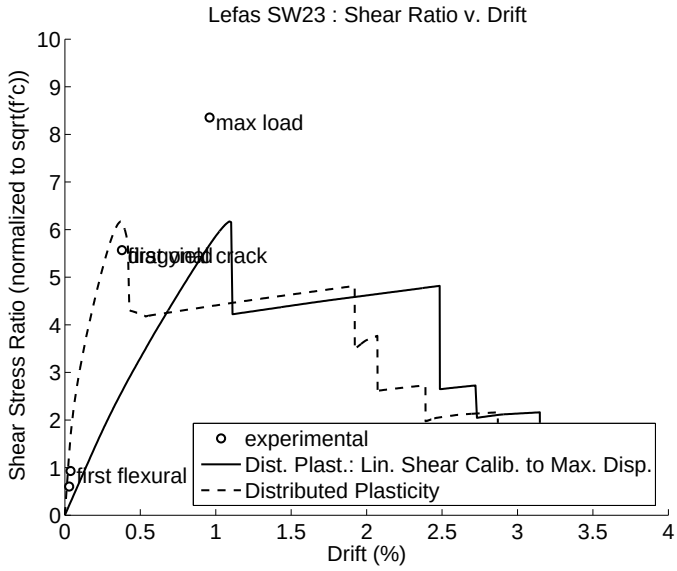

Figure M.130: Pushover of Beam-Column Element with Elastic Shear Calibrated to Maximum Displacement – Lefas SW23

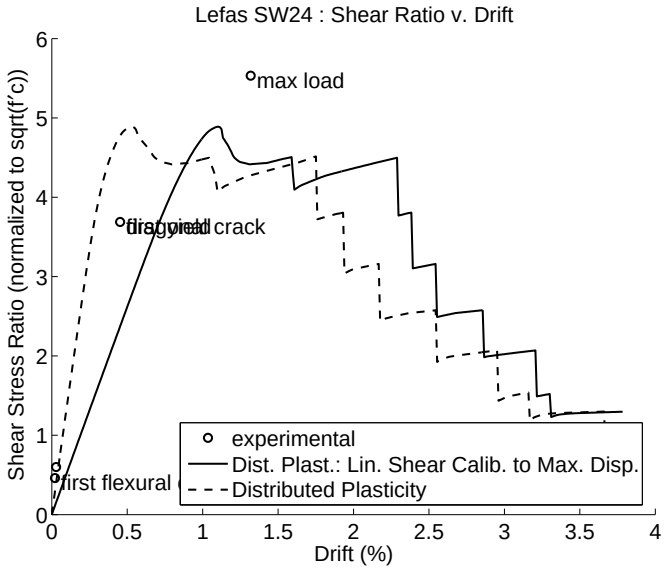

Figure M.131: Pushover of Beam-Column Element with Elastic Shear Calibrated to Maximum Displacement – Lefas SW24

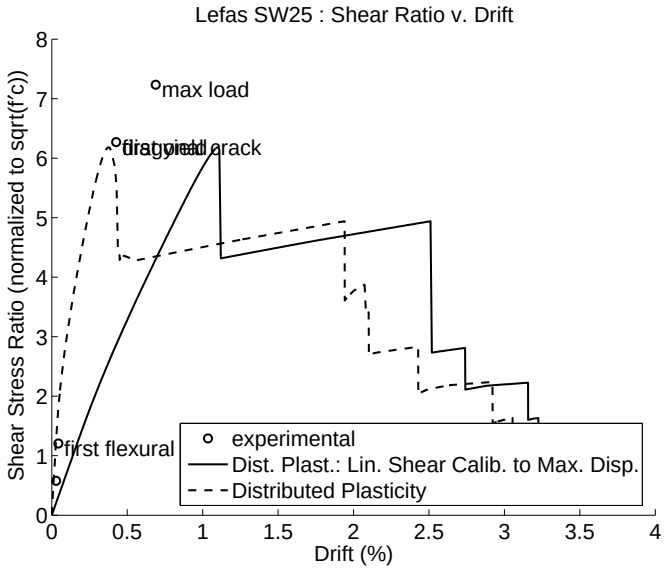

Figure M.132: Pushover of Beam-Column Element with Elastic Shear Calibrated to Maximum Displacement – Lefas SW25

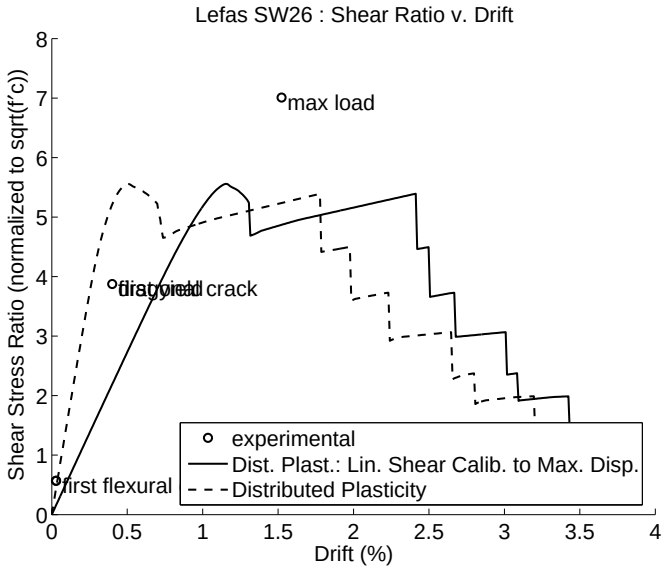

Figure M.133: Pushover of Beam-Column Element with Elastic Shear Calibrated to Maximum Displacement – Lefas SW26

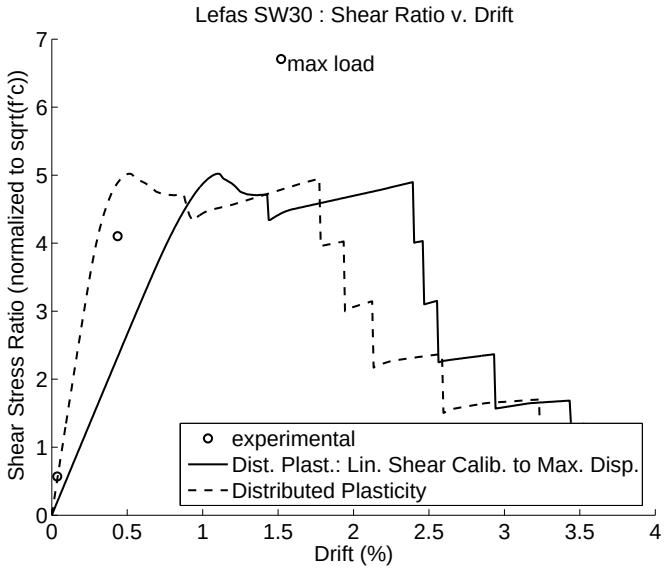

Figure M.134: Pushover of Beam-Column Element with Elastic Shear Calibrated to Maximum Displacement – Lefas SW30

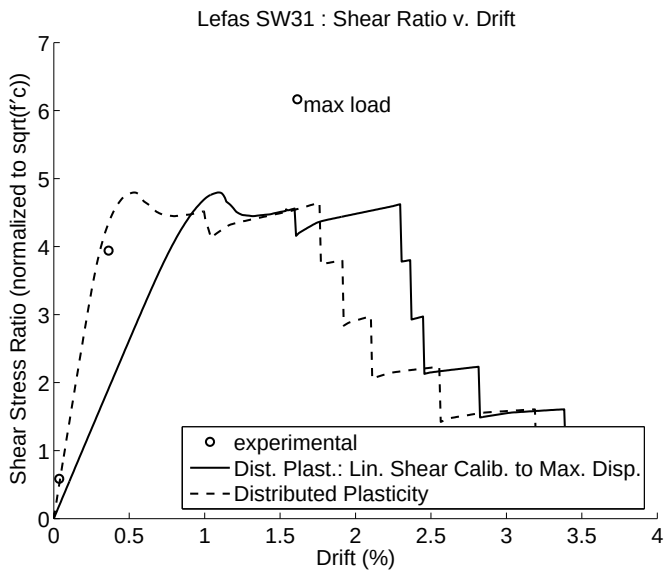

Figure M.135: Pushover of Beam-Column Element with Elastic Shear Calibrated to Maximum Displacement – Lefas SW31

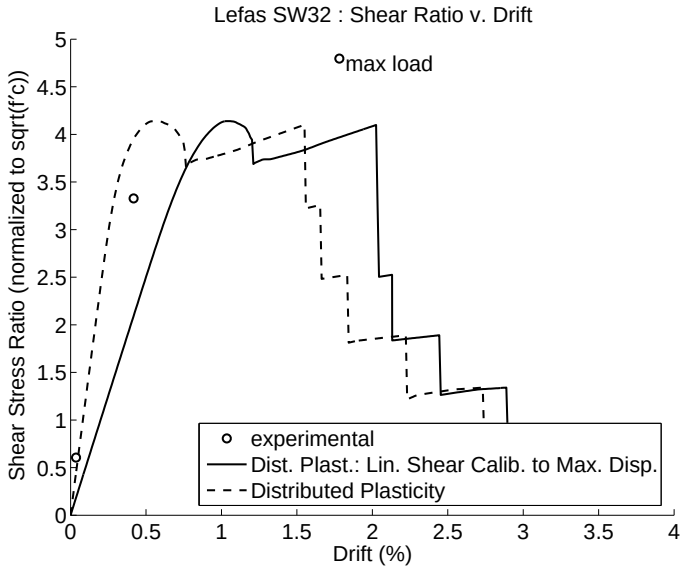

Figure M.136: Pushover of Beam-Column Element with Elastic Shear Calibrated to Maximum Displacement – Lefas SW32

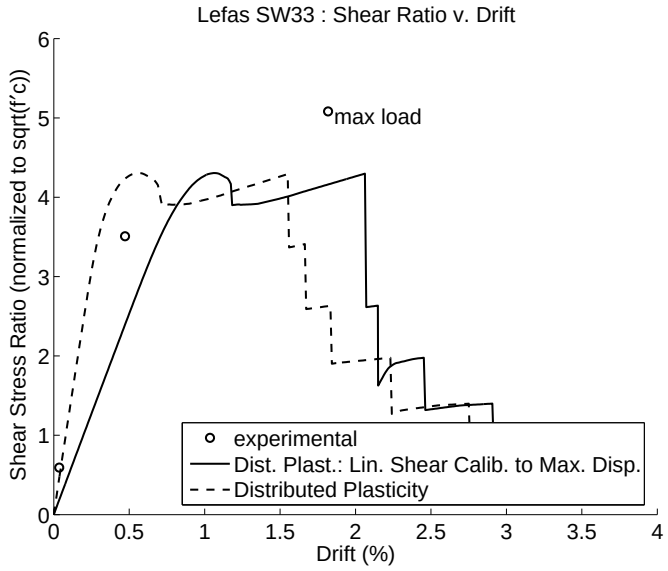

Figure M.137: Pushover of Beam-Column Element with Elastic Shear Calibrated to Maximum Displacement – Lefas SW33

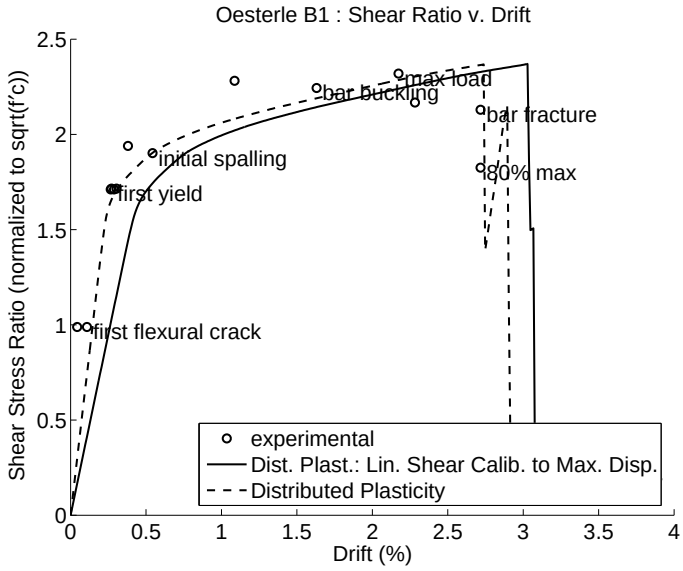

Figure M.138: Pushover of Beam-Column Element with Elastic Shear Calibrated to Maximum Displacement – Oesterle B1

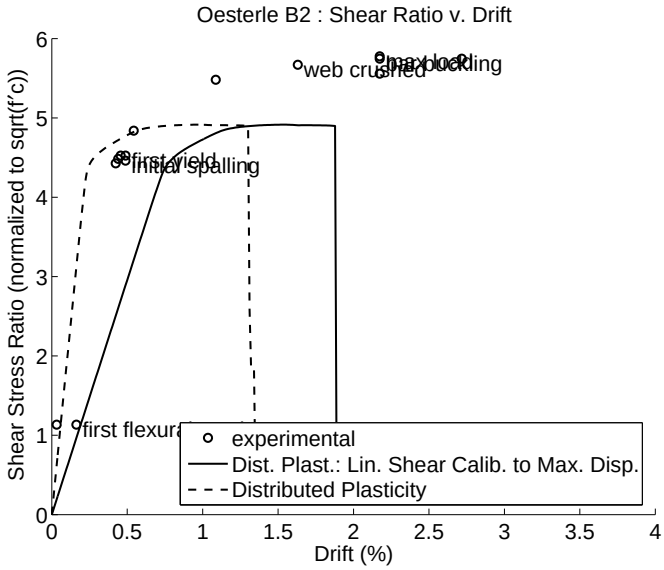

Figure M.139: Pushover of Beam-Column Element with Elastic Shear Calibrated to Maximum Displacement – Oesterle B2

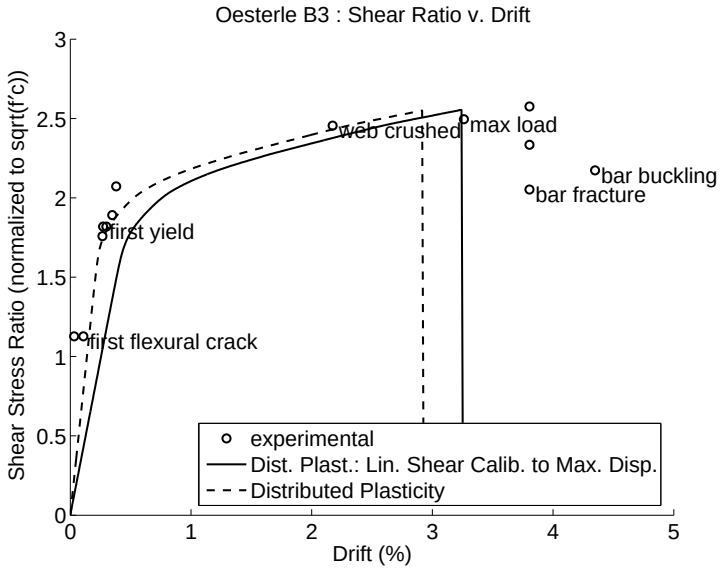

Figure M.140: Pushover of Beam-Column Element with Elastic Shear Calibrated to Maximum Displacement – Oesterle B3

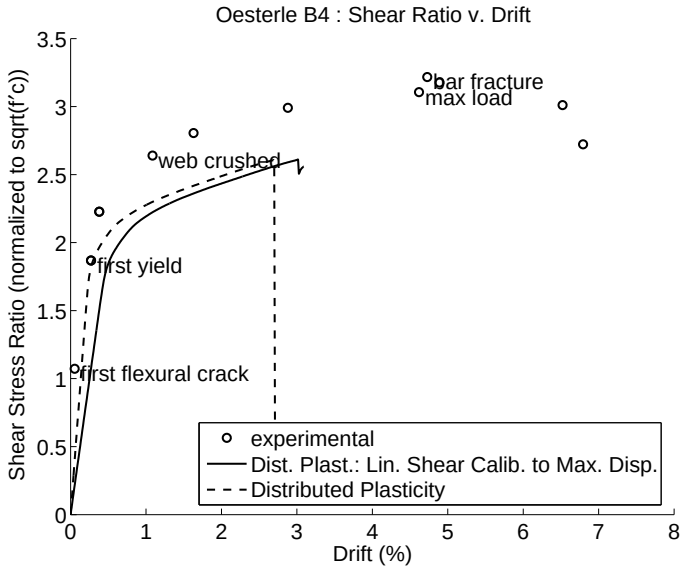

Figure M.141: Pushover of Beam-Column Element with Elastic Shear Calibrated to Maximum Displacement – Oesterle B4

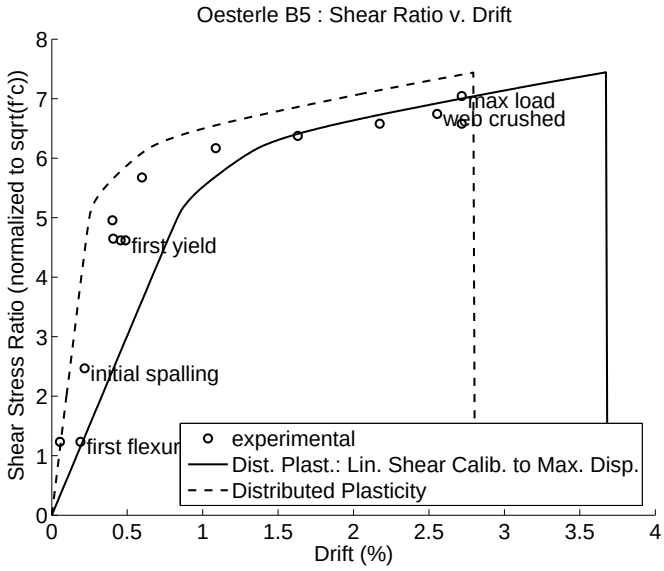

Figure M.142: Pushover of Beam-Column Element with Elastic Shear Calibrated to Maximum Displacement – Oesterle B5

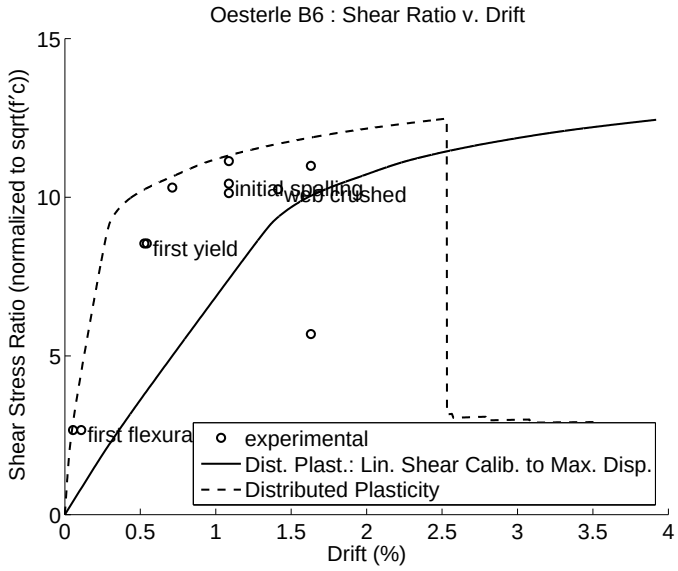

Figure M.143: Pushover of Beam-Column Element with Elastic Shear Calibrated to Maximum Displacement – Oesterle B6

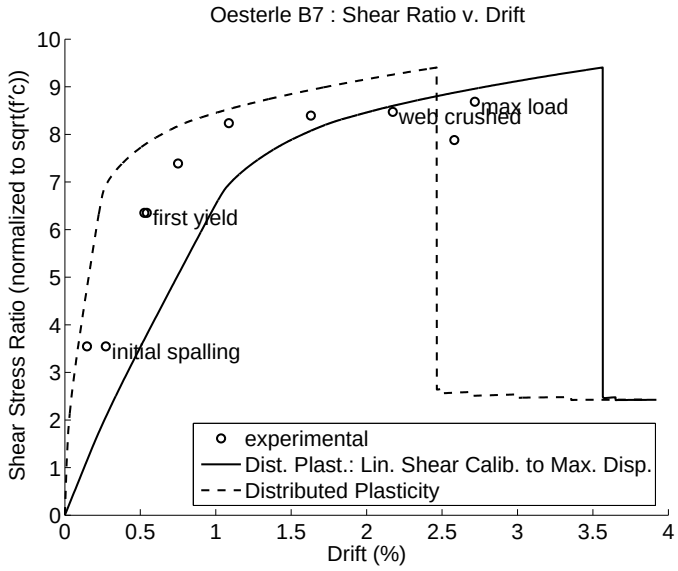

Figure M.144: Pushover of Beam-Column Element with Elastic Shear Calibrated to Maximum Displacement – Oesterle B7

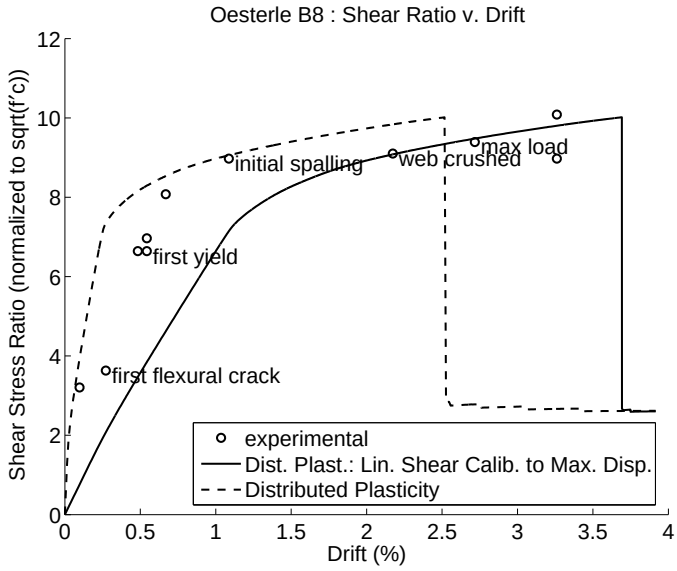

Figure M.145: Pushover of Beam-Column Element with Elastic Shear Calibrated to Maximum Displacement – Oesterle B8

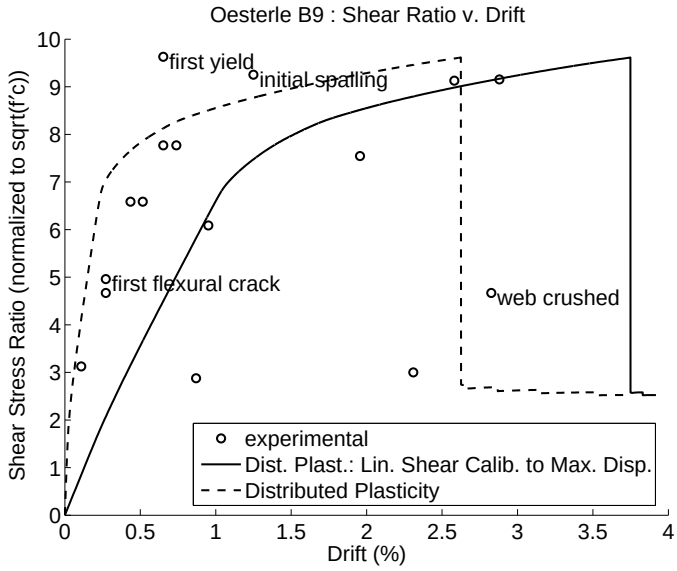

Figure M.146: Pushover of Beam-Column Element with Elastic Shear Calibrated to Maximum Displacement – Oesterle B9

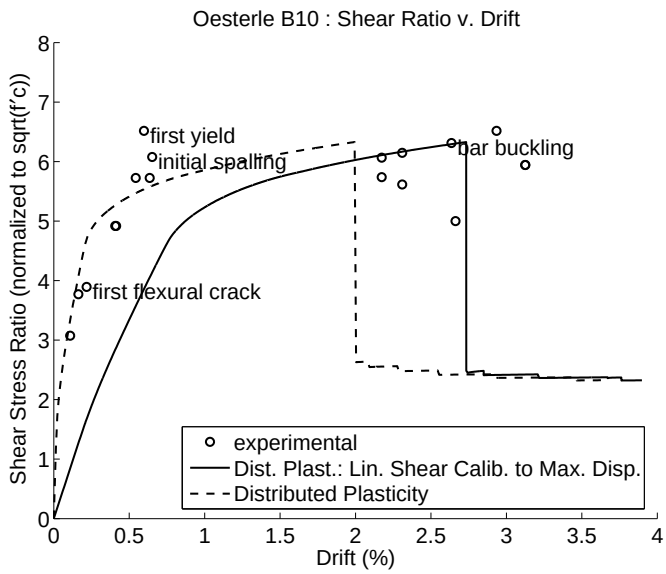

Figure M.147: Pushover of Beam-Column Element with Elastic Shear Calibrated to Maximum Displacement – Oesterle B10

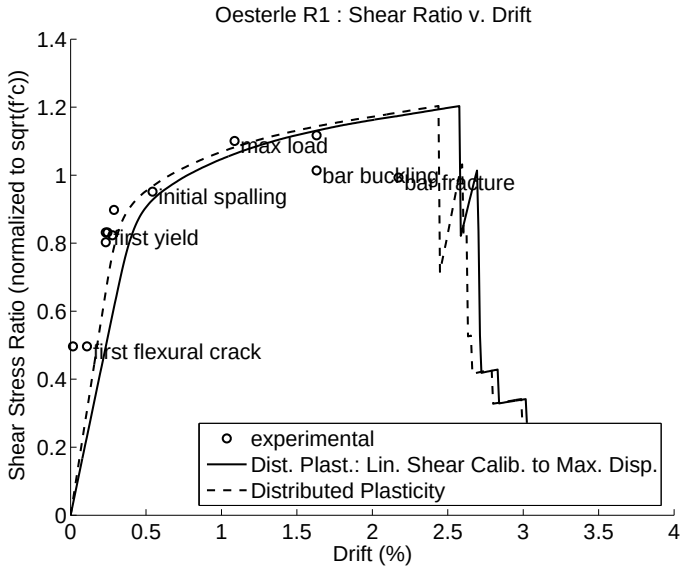

Figure M.148: Pushover of Beam-Column Element with Elastic Shear Calibrated to Maximum Displacement – Oesterle R1

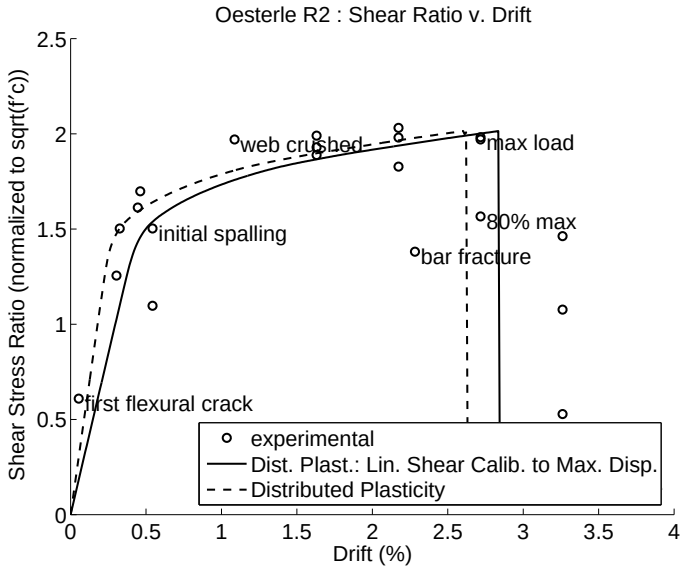

Figure M.149: Pushover of Beam-Column Element with Elastic Shear Calibrated to Maximum Displacement – Oesterle R2

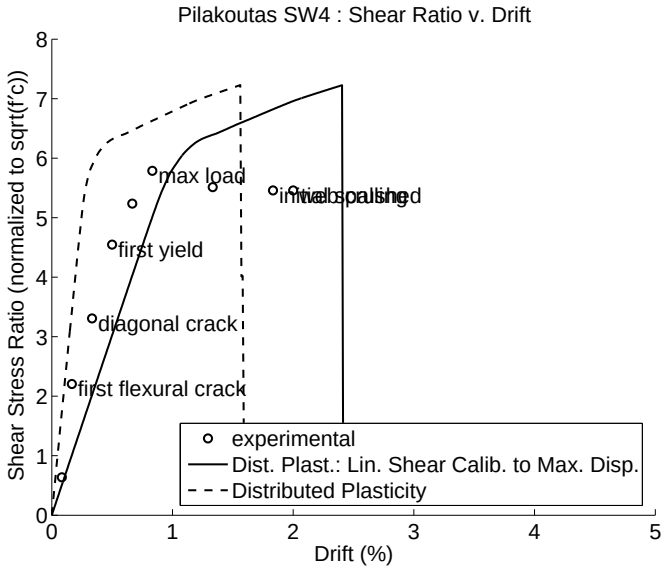

Figure M.150: Pushover of Beam-Column Element with Elastic Shear Calibrated to Maximum Displacement – Pilakoutas SW4

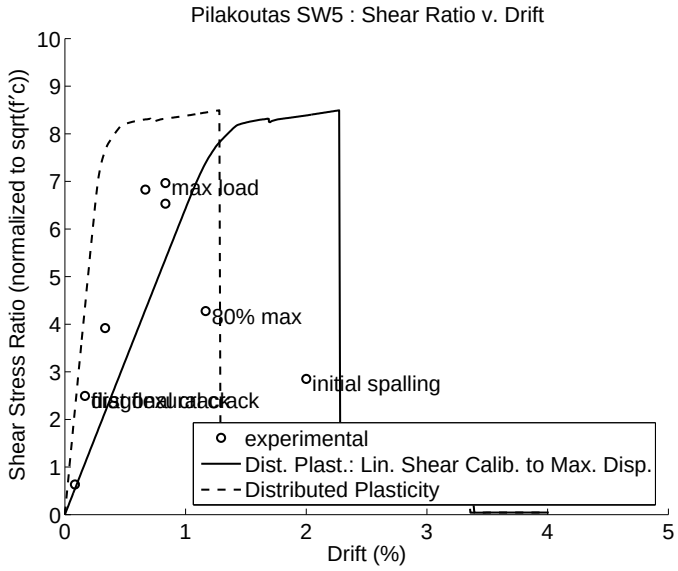

Figure M.151: Pushover of Beam-Column Element with Elastic Shear Calibrated to Maximum Displacement – Pilakoutas SW5

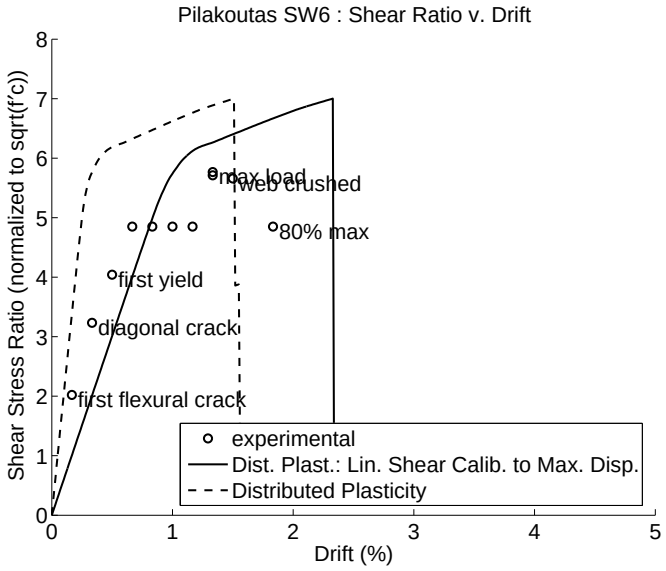

Figure M.152: Pushover of Beam-Column Element with Elastic Shear Calibrated to Maximum Displacement – Pilakoutas SW6

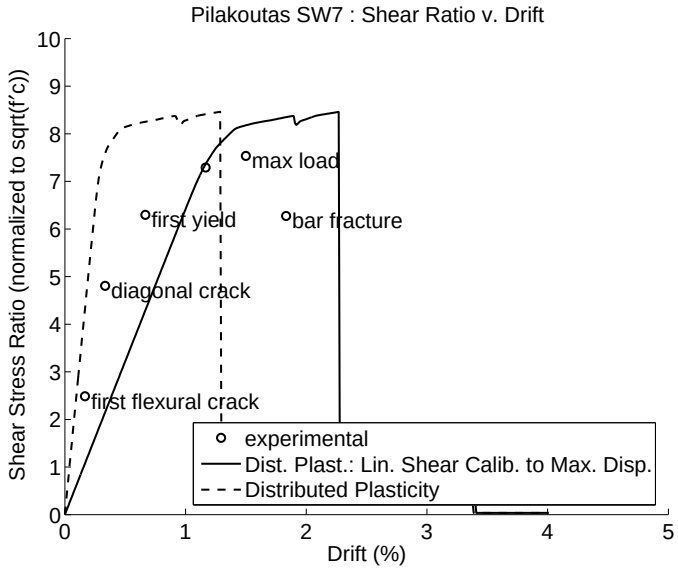

Figure M.153: Pushover of Beam-Column Element with Elastic Shear Calibrated to Maximum Displacement – Pilakoutas SW7

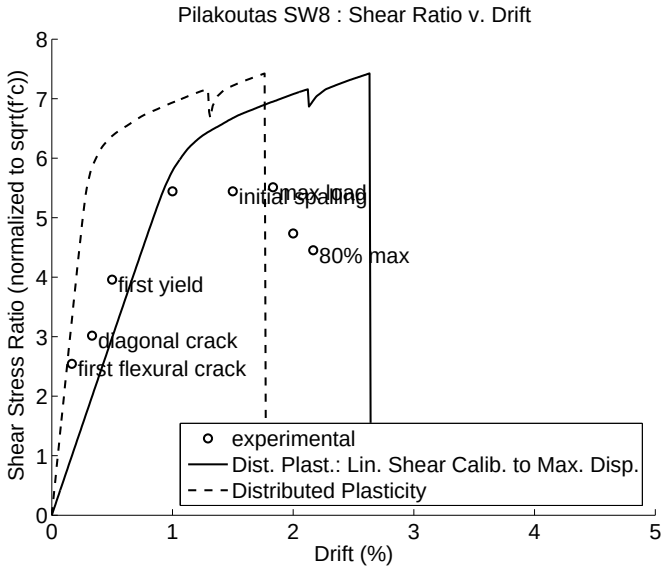

Figure M.154: Pushover of Beam-Column Element with Elastic Shear Calibrated to Maximum Displacement – Pilakoutas SW8

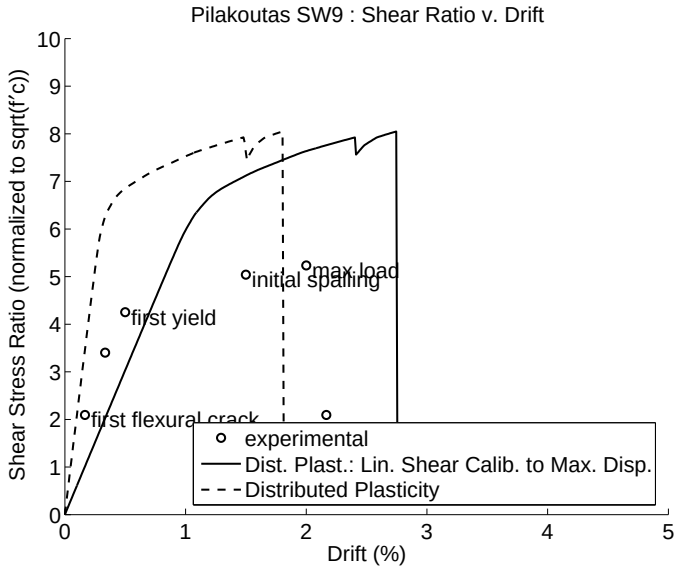

Figure M.155: Pushover of Beam-Column Element with Elastic Shear Calibrated to Maximum Displacement – Pilakoutas SW9

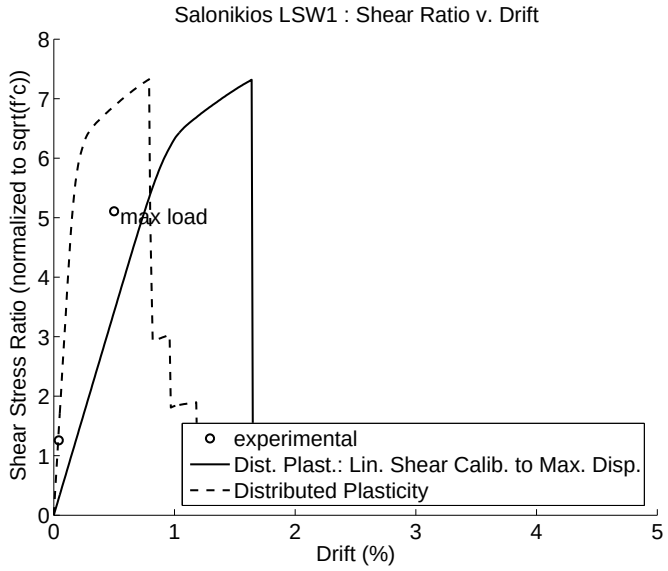

Figure M.156: Pushover of Beam-Column Element with Elastic Shear Calibrated to Maximum Displacement – Salonikios LSW1

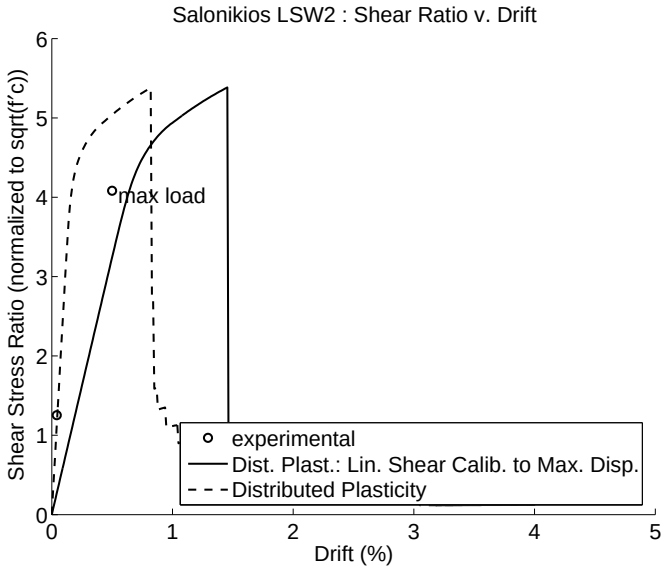

Figure M.157: Pushover of Beam-Column Element with Elastic Shear Calibrated to Maximum Displacement – Salonikios LSW2

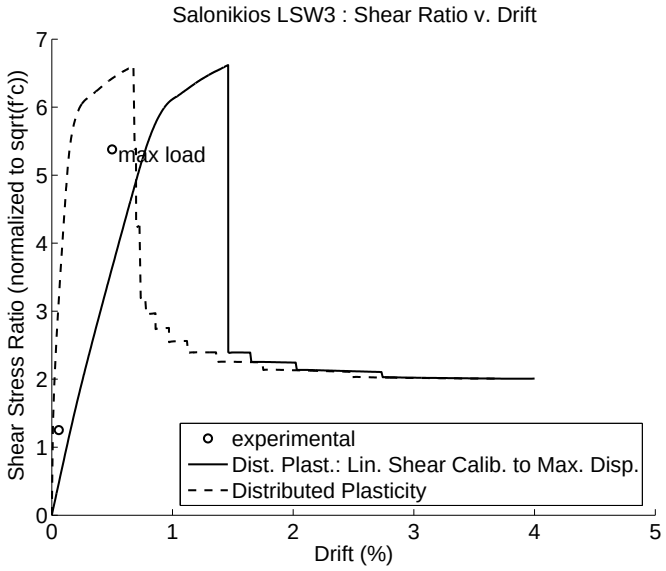

Figure M.158: Pushover of Beam-Column Element with Elastic Shear Calibrated to Maximum Displacement – Salonikios LSW3

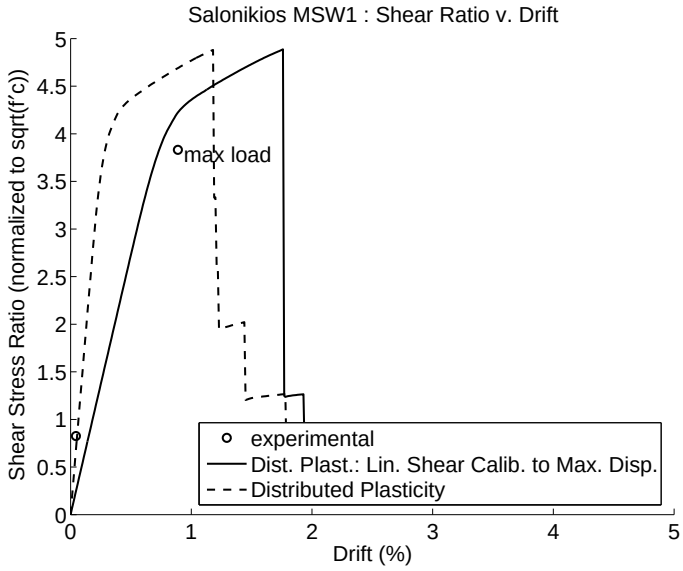

Figure M.159: Pushover of Beam-Column Element with Elastic Shear Calibrated to Maximum Displacement – Salonikios MSW1

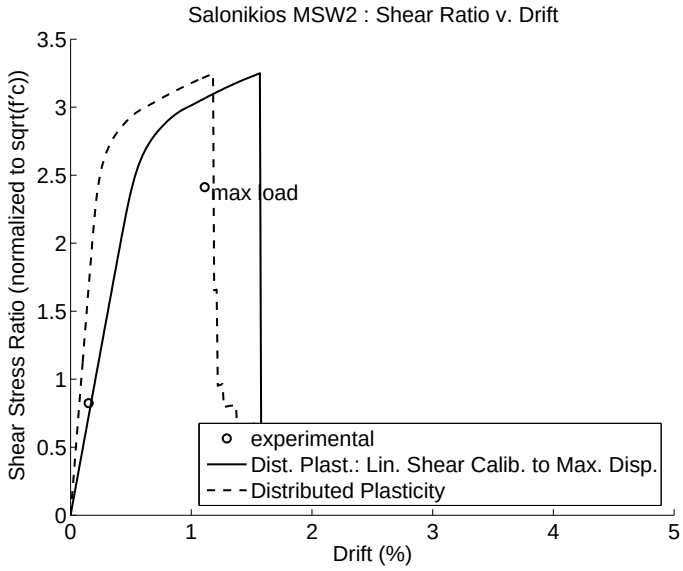

Figure M.160: Pushover of Beam-Column Element with Elastic Shear Calibrated to Maximum Displacement – Salonikios MSW2

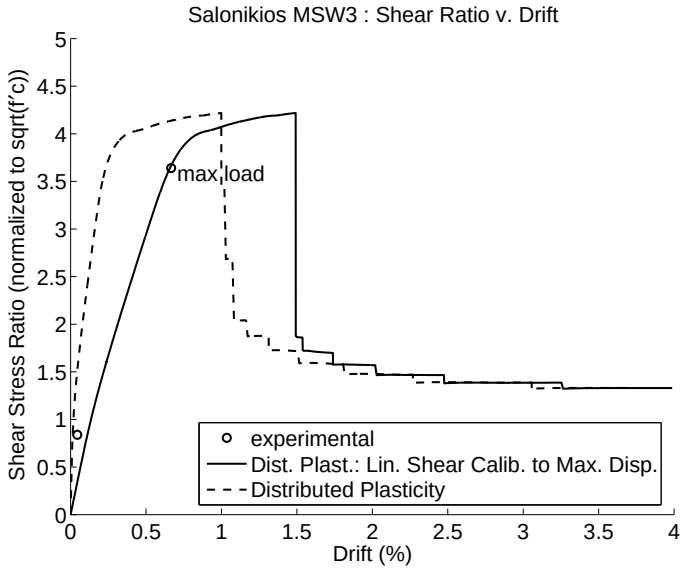

Figure M.161: Pushover of Beam-Column Element with Elastic Shear Calibrated to Maximum Displacement – Salonikios MSW3

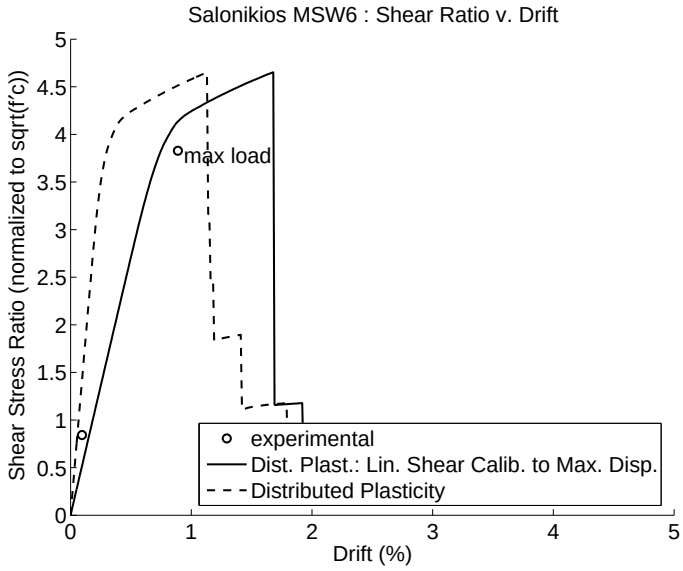

Figure M.162: Pushover of Beam-Column Element with Elastic Shear Calibrated to Maximum Displacement – Salonikios MSW6

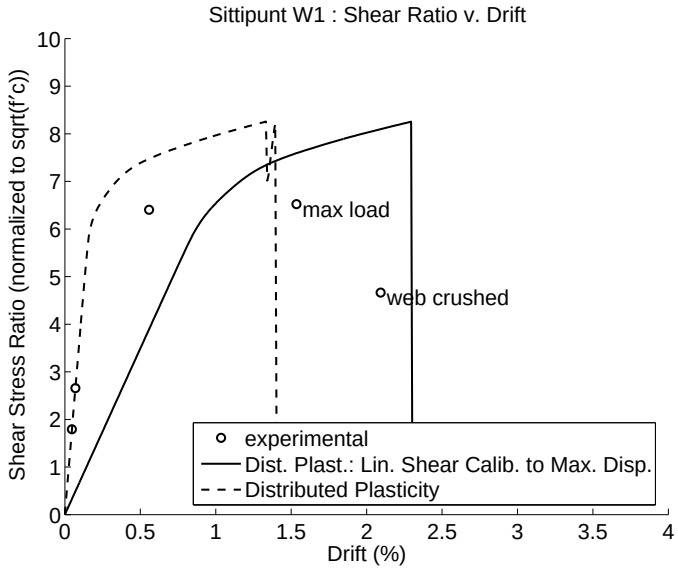

Figure M.163: Pushover of Beam-Column Element with Elastic Shear Calibrated to Maximum Displacement – Sittipunt W1

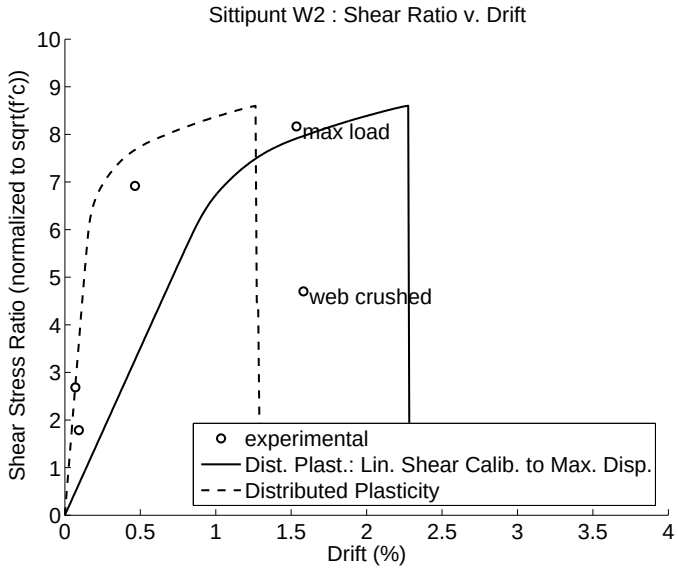

Figure M.164: Pushover of Beam-Column Element with Elastic Shear Calibrated to Maximum Displacement – Sittipunt W2

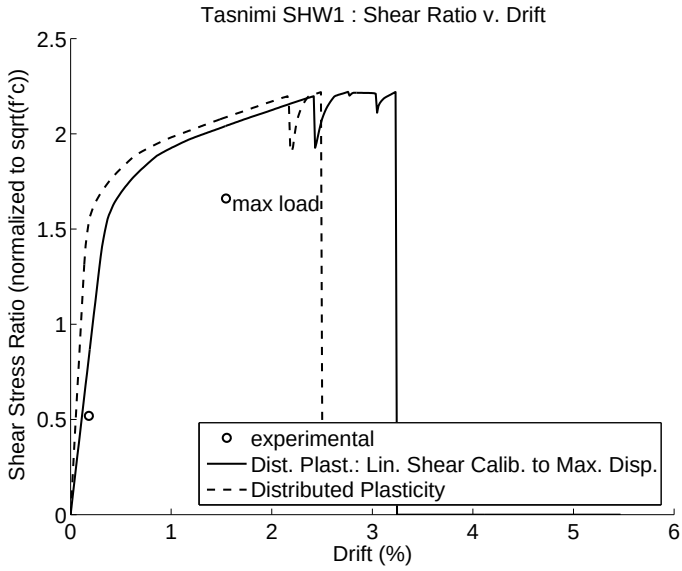

Figure M.165: Pushover of Beam-Column Element with Elastic Shear Calibrated to Maximum Displacement – Tasnimi SHW1

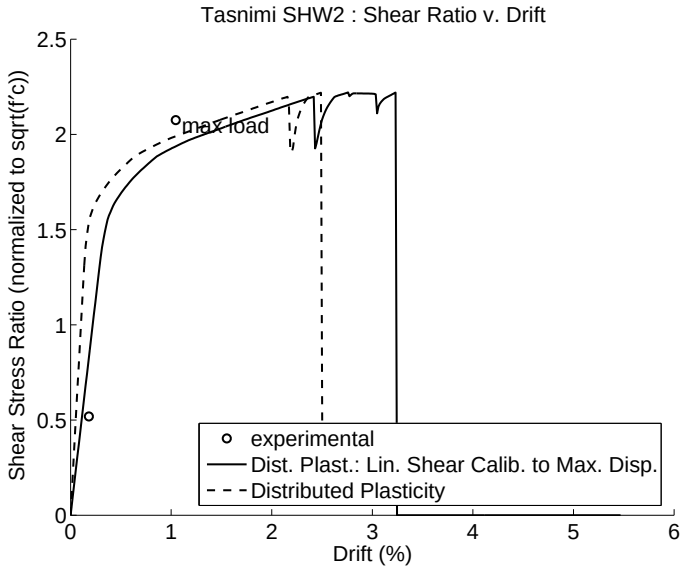

Figure M.166: Pushover of Beam-Column Element with Elastic Shear Calibrated to Maximum Displacement – Tasnimi SHW2

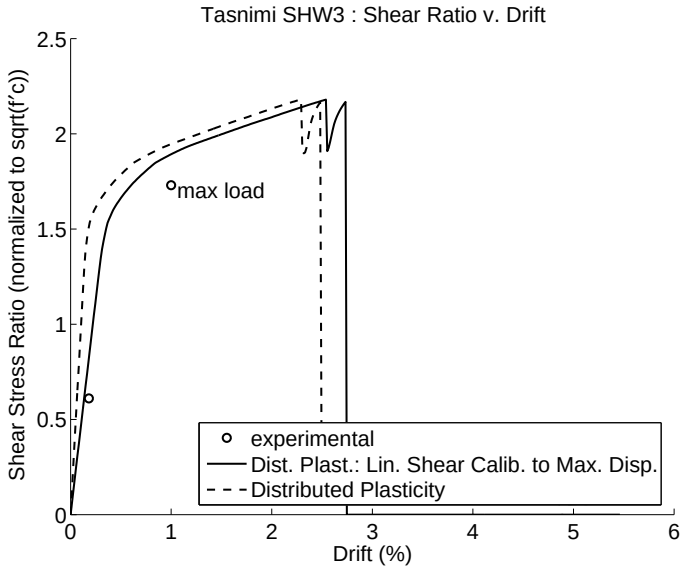

Figure M.167: Pushover of Beam-Column Element with Elastic Shear Calibrated to Maximum Displacement – Tasnimi SHW3

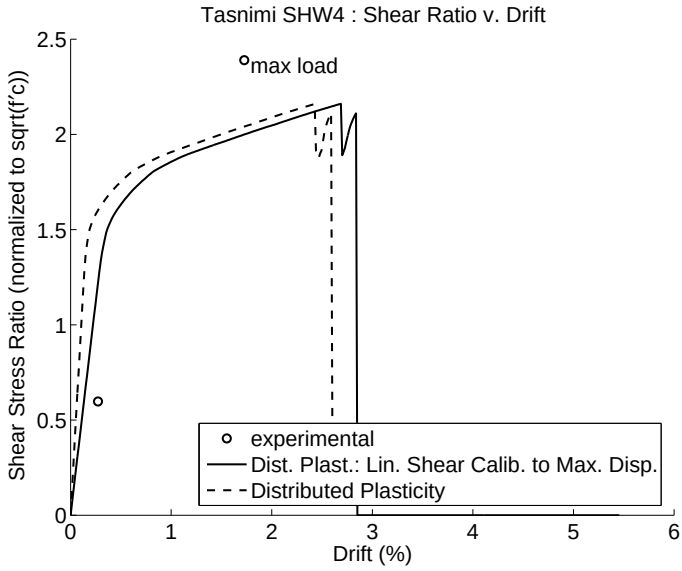

Figure M.168: Pushover of Beam-Column Element with Elastic Shear Calibrated to Maximum Displacement – Tasnimi SHW4

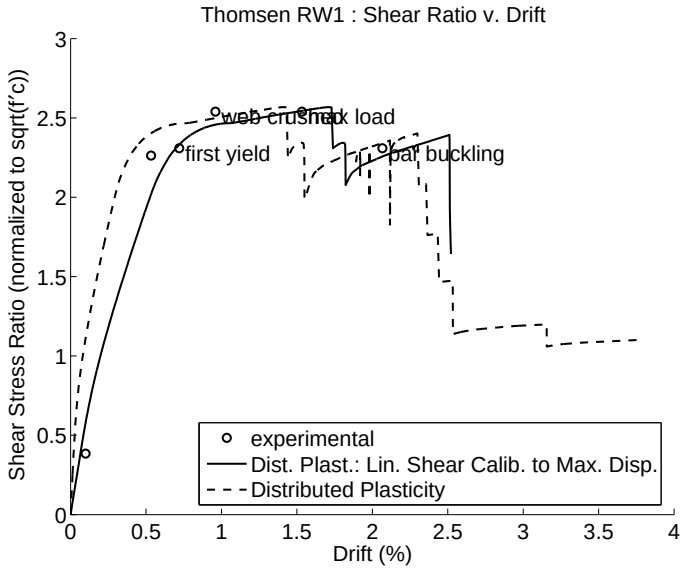

Figure M.169: Pushover of Beam-Column Element with Elastic Shear Calibrated to Maximum Displacement – Thomsen RW1

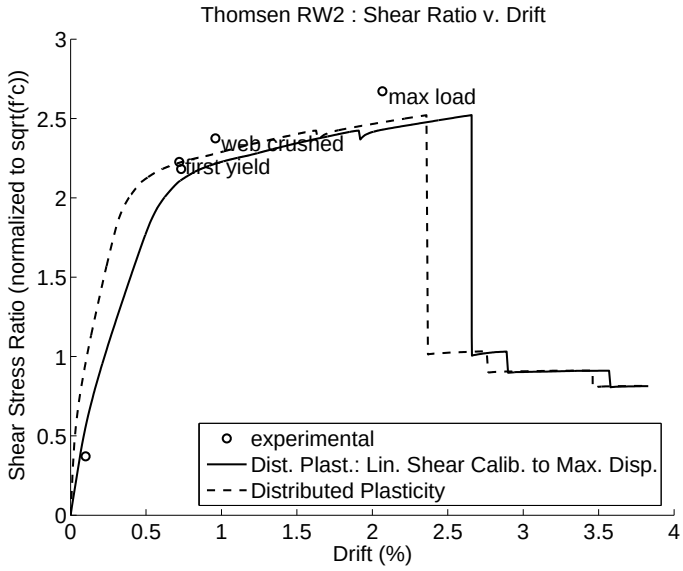

Figure M.170: Pushover of Beam-Column Element with Elastic Shear Calibrated to Maximum Displacement – Thomsen RW2

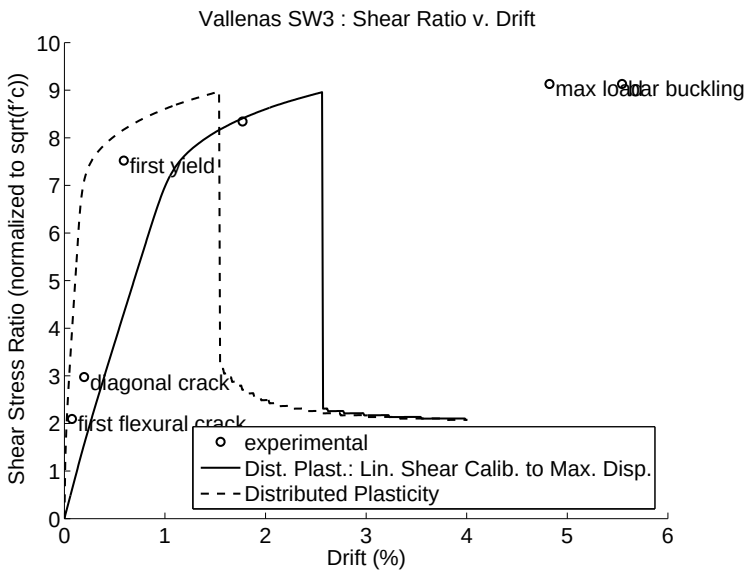

Figure M.171: Pushover of Beam-Column Element with Elastic Shear Calibrated to Maximum Displacement – Vallenas SW3

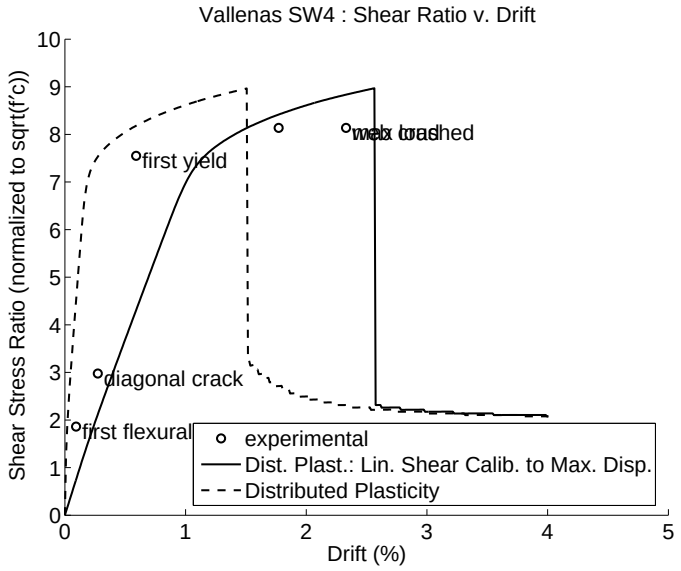

Figure M.172: Pushover of Beam-Column Element with Elastic Shear Calibrated to Maximum Displacement – Vallenas SW4

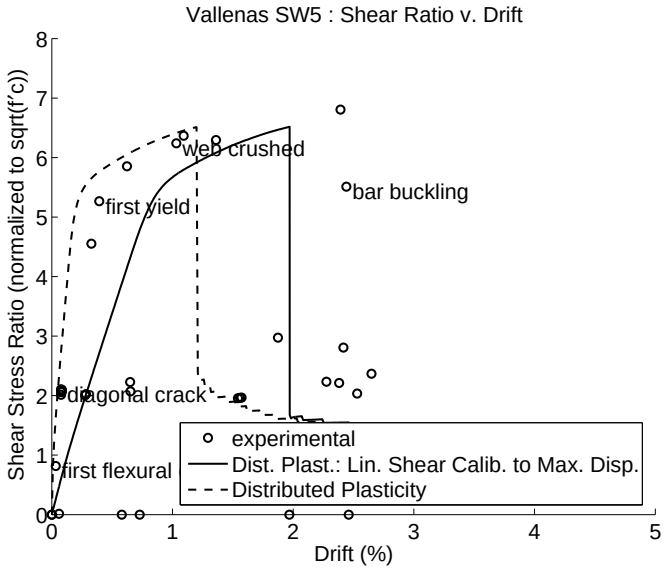

Figure M.173: Pushover of Beam-Column Element with Elastic Shear Calibrated to Maximum Displacement – Vallenas SW5

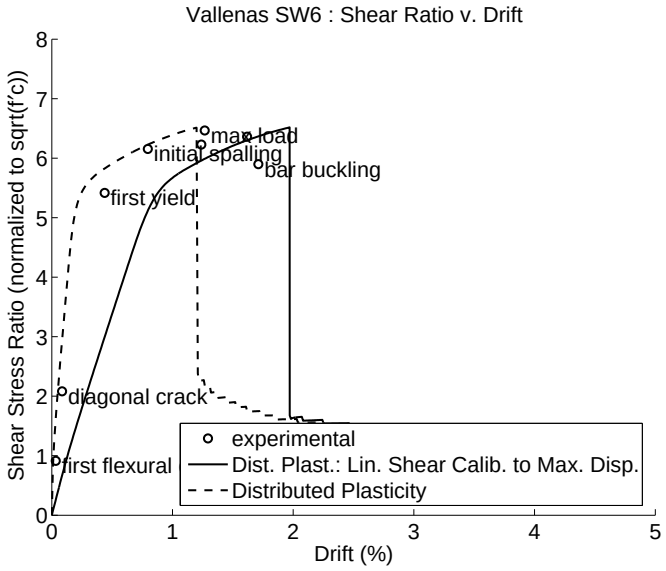

Figure M.174: Pushover of Beam-Column Element with Elastic Shear Calibrated to Maximum Displacement – Vallenas SW6

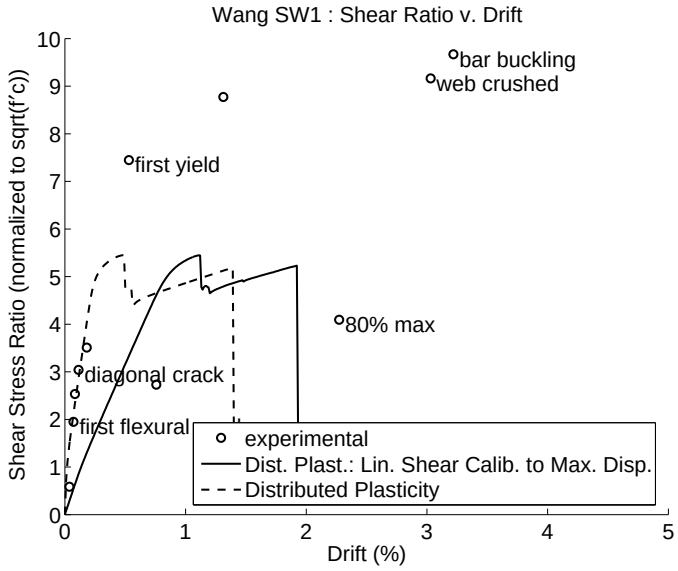

Figure M.175: Pushover of Beam-Column Element with Elastic Shear Calibrated to Maximum Displacement – Wang SW1

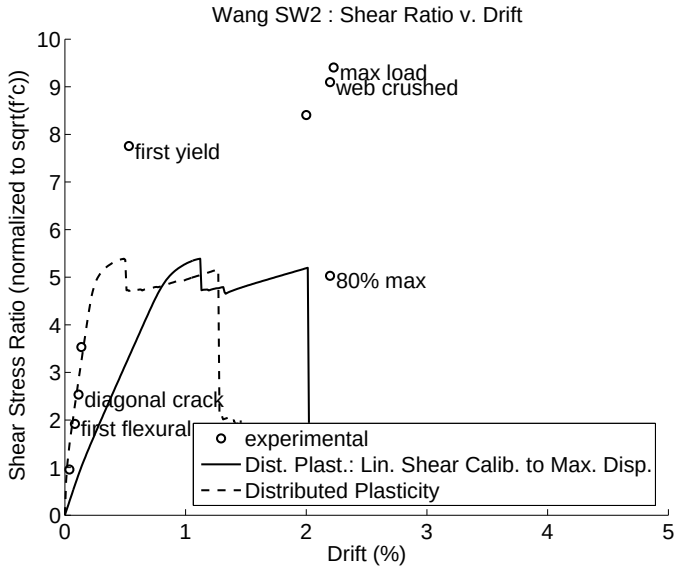

Figure M.176: Pushover of Beam-Column Element with Elastic Shear Calibrated to Maximum Displacement – Wang SW2

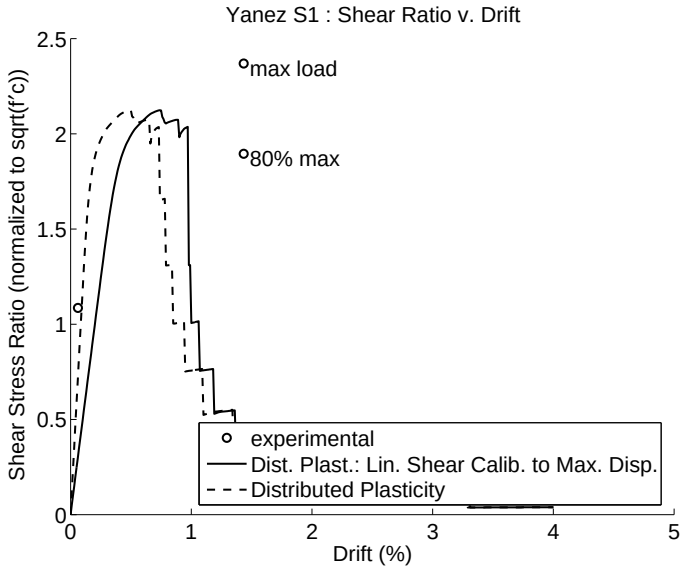

Figure M.177: Pushover of Beam-Column Element with Elastic Shear Calibrated to Maximum Displacement – Yanez S1

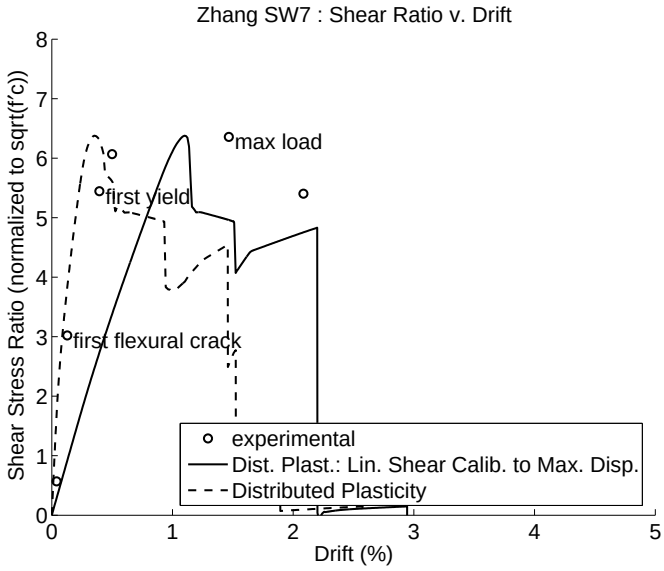

Figure M.178: Pushover of Beam-Column Element with Elastic Shear Calibrated to Maximum Displacement – Zhang SW7

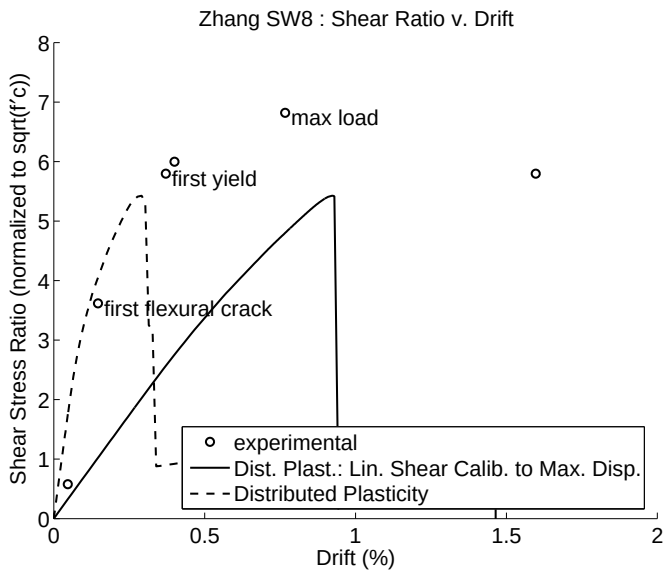

Figure M.179: Pushover of Beam-Column Element with Elastic Shear Calibrated to Maximum Displacement – Zhang SW8

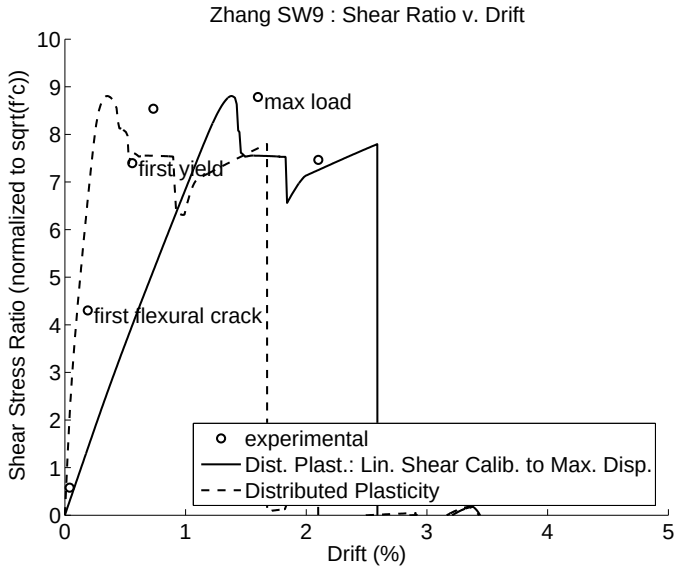

Figure M.180: Pushover of Beam-Column Element with Elastic Shear Calibrated to Maximum Displacement – Zhang SW9

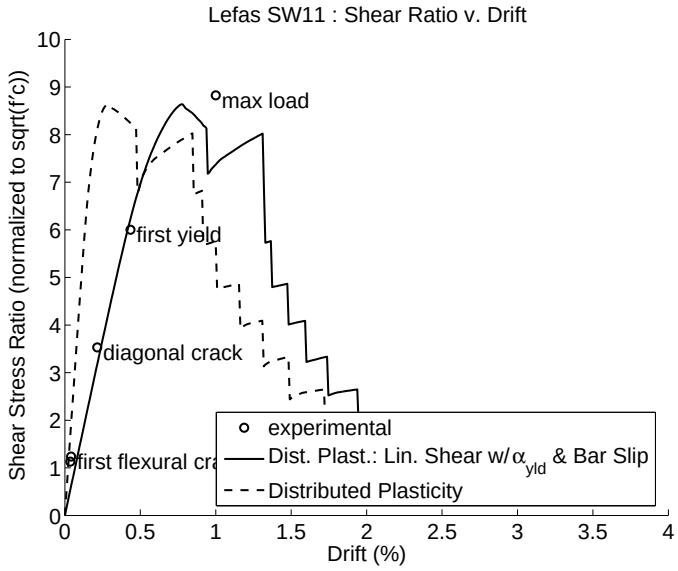

Figure M.181: Pushover of Beam-Column Element with Bar-Slip and Elastic Shear Calibrated to Yield – Lefas SW11

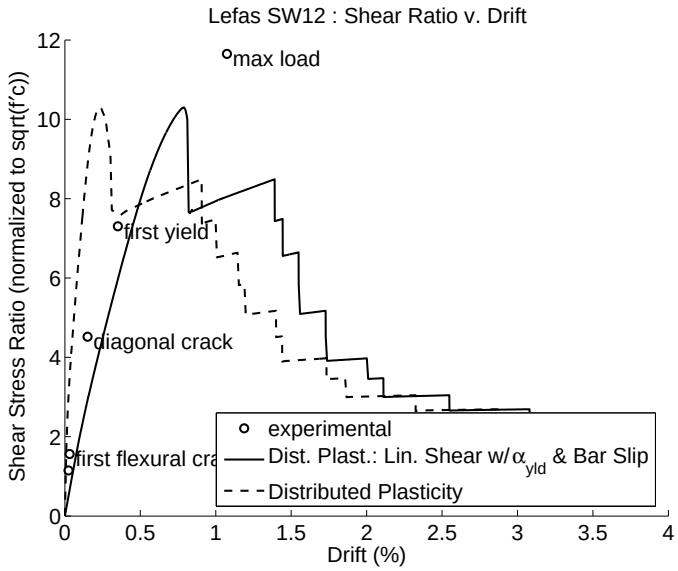

Figure M.182: Pushover of Beam-Column Element with Bar-Slip and Elastic Shear Calibrated to Yield – Lefas SW12

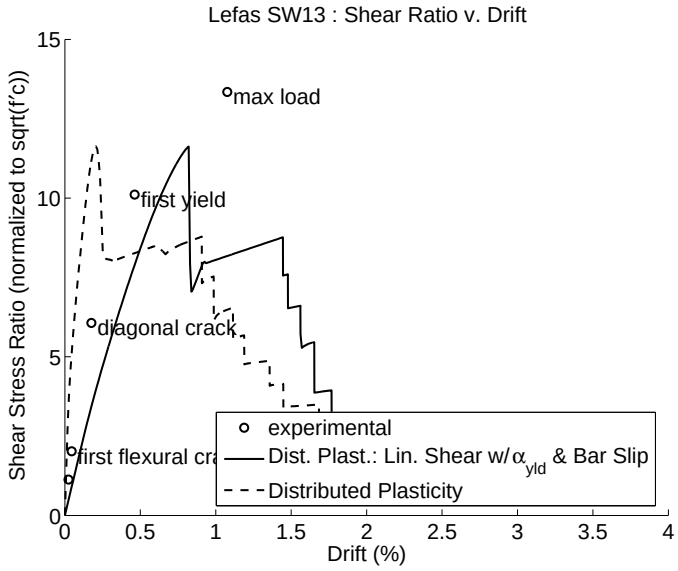

Figure M.183: Pushover of Beam-Column Element with Bar-Slip and Elastic Shear Calibrated to Yield – Lefas SW13

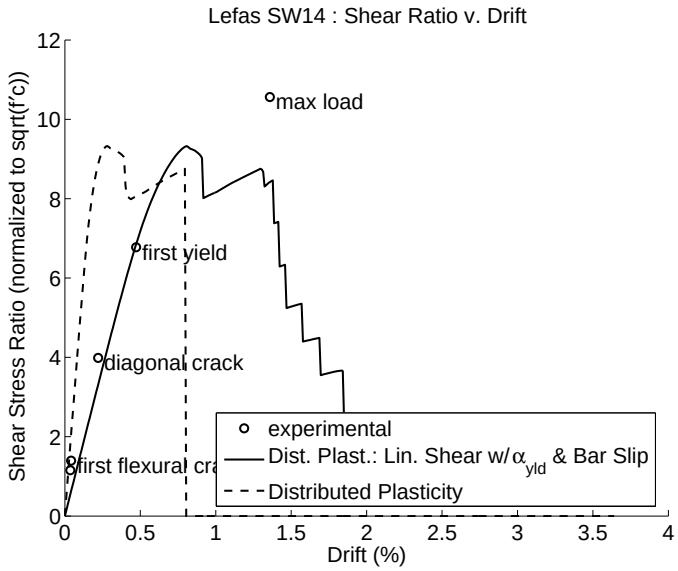

Figure M.184: Pushover of Beam-Column Element with Bar-Slip and Elastic Shear Calibrated to Yield – Lefas SW14

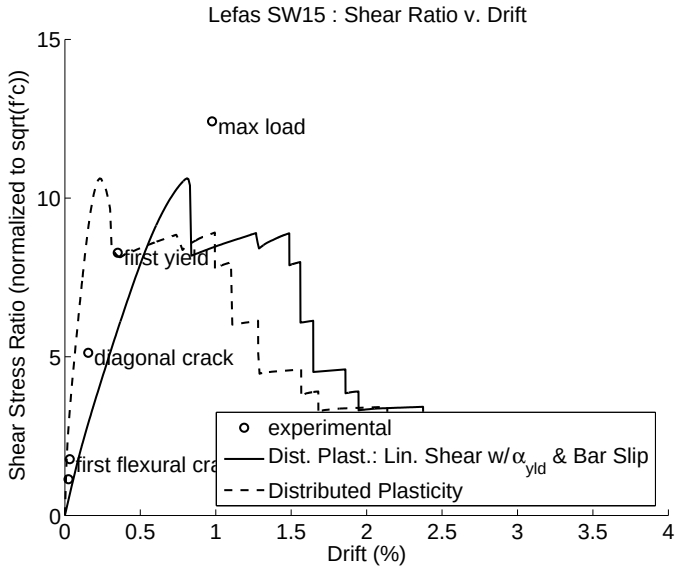

Figure M.185: Pushover of Beam-Column Element with Bar-Slip and Elastic Shear Calibrated to Yield – Lefas SW15

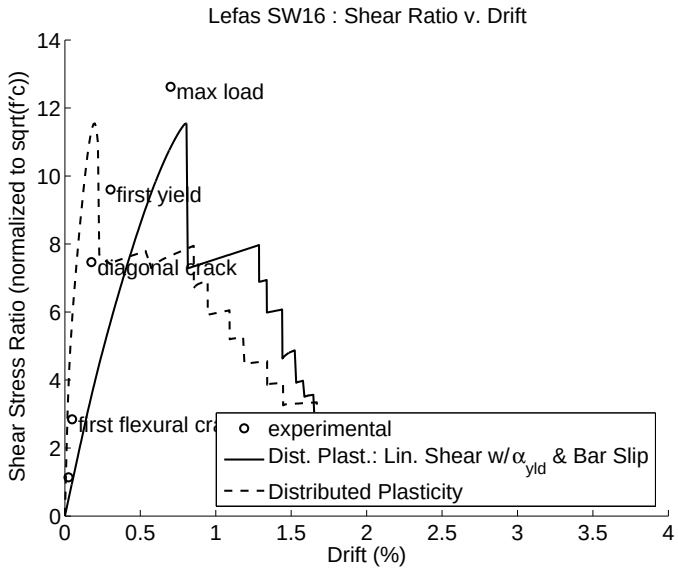

Figure M.186: Pushover of Beam-Column Element with Bar-Slip and Elastic Shear Calibrated to Yield – Lefas SW16

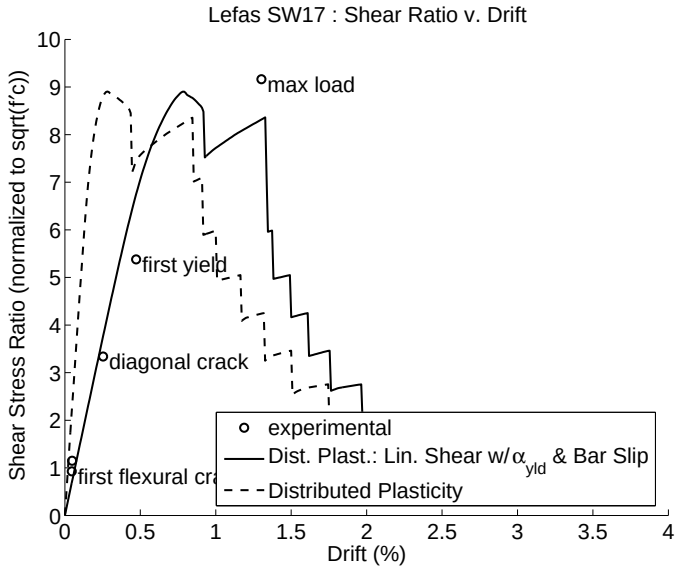

Figure M.187: Pushover of Beam-Column Element with Bar-Slip and Elastic Shear Calibrated to Yield – Lefas SW17

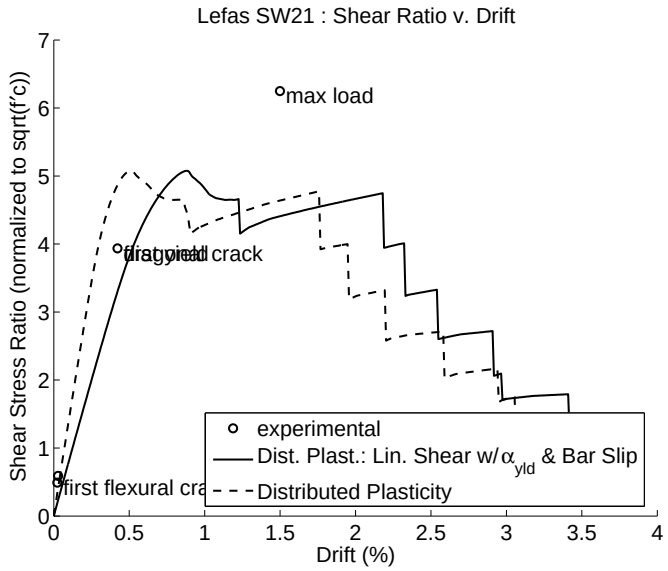

Figure M.188: Pushover of Beam-Column Element with Bar-Slip and Elastic Shear Calibrated to Yield – Lefas SW21

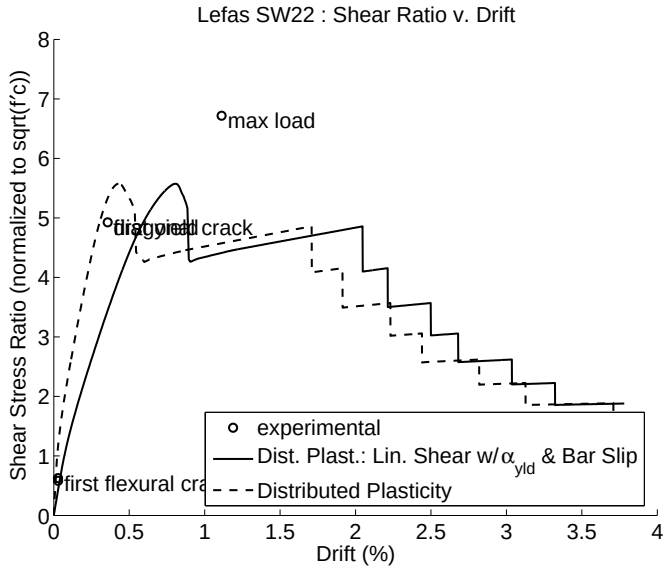

Figure M.189: Pushover of Beam-Column Element with Bar-Slip and Elastic Shear Calibrated to Yield – Lefas SW22

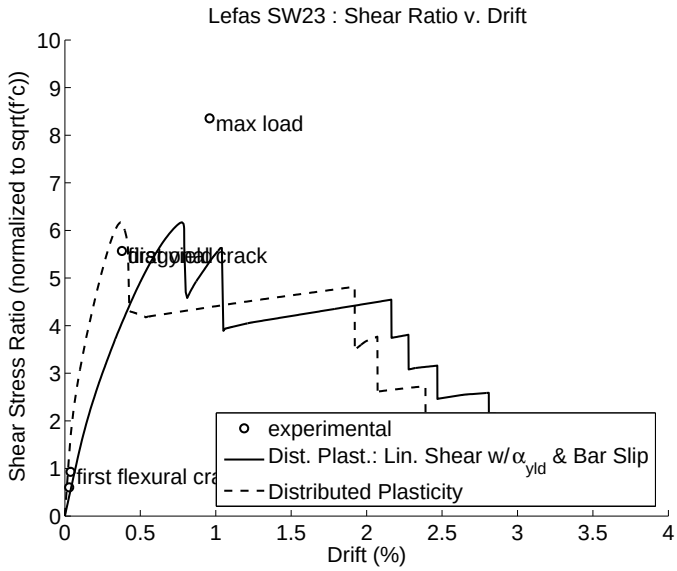

Figure M.190: Pushover of Beam-Column Element with Bar-Slip and Elastic Shear Calibrated to Yield – Lefas SW23

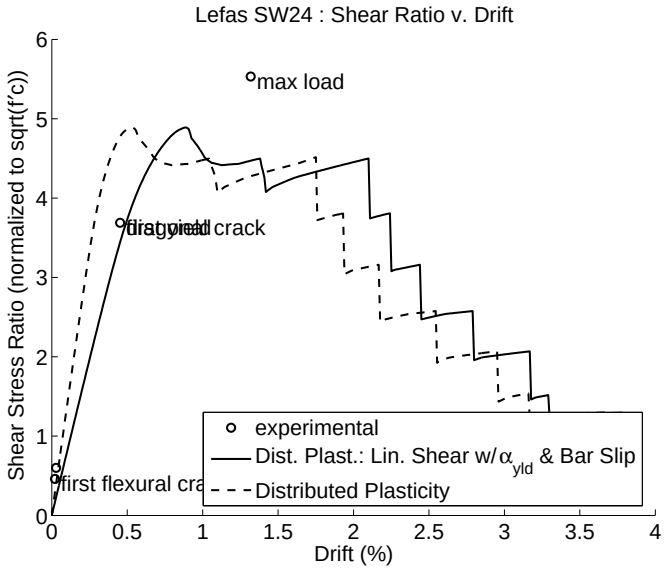

Figure M.191: Pushover of Beam-Column Element with Bar-Slip and Elastic Shear Calibrated to Yield – Lefas SW24

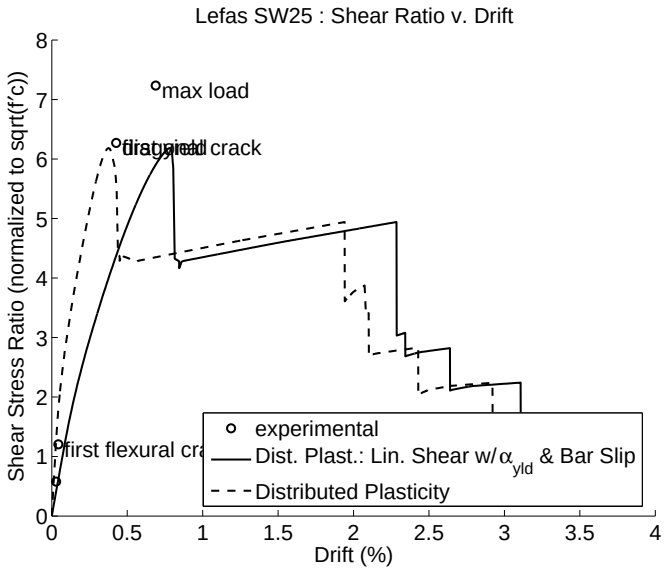

Figure M.192: Pushover of Beam-Column Element with Bar-Slip and Elastic Shear Calibrated to Yield – Lefas SW25

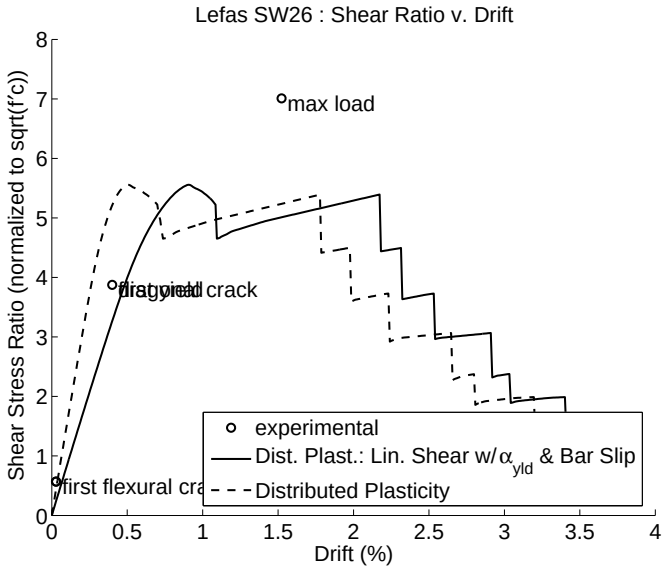

Figure M.193: Pushover of Beam-Column Element with Bar-Slip and Elastic Shear Calibrated to Yield – Lefas SW26

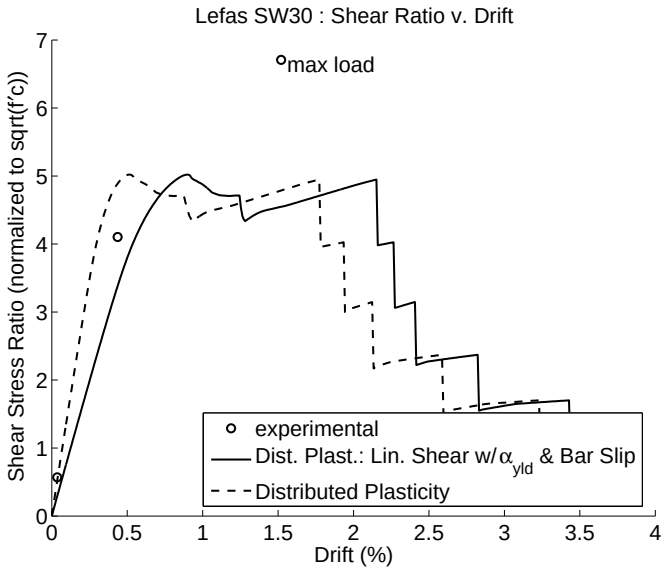

Figure M.194: Pushover of Beam-Column Element with Bar-Slip and Elastic Shear Calibrated to Yield – Lefas SW30

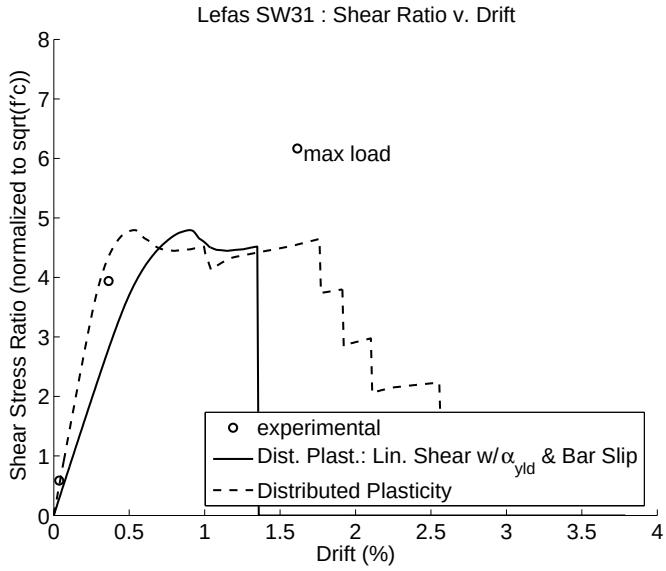

Figure M.195: Pushover of Beam-Column Element with Bar-Slip and Elastic Shear Calibrated to Yield – Lefas SW31

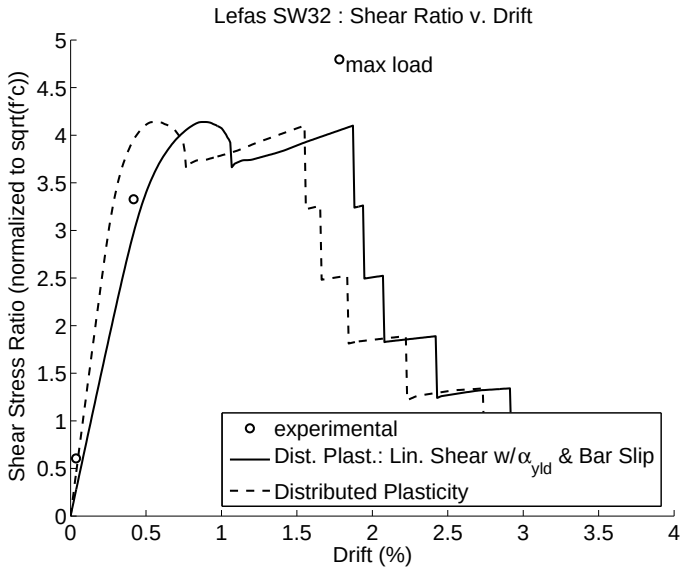

Figure M.196: Pushover of Beam-Column Element with Bar-Slip and Elastic Shear Calibrated to Yield – Lefas SW32

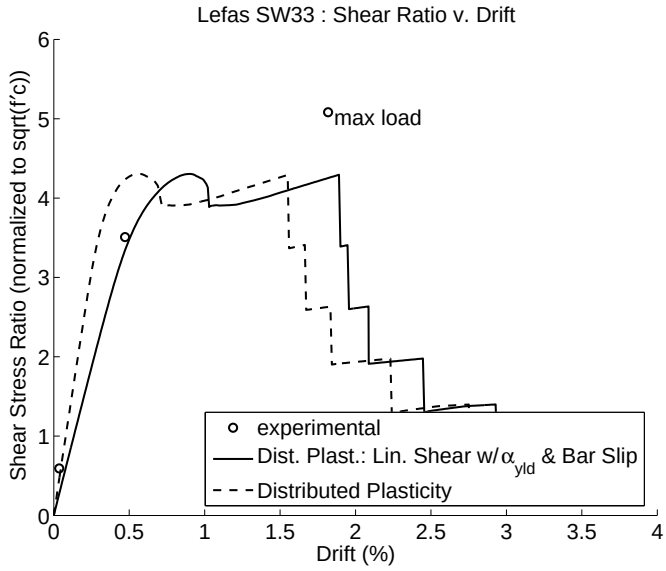

Figure M.197: Pushover of Beam-Column Element with Bar-Slip and Elastic Shear Calibrated to Yield – Lefas SW33

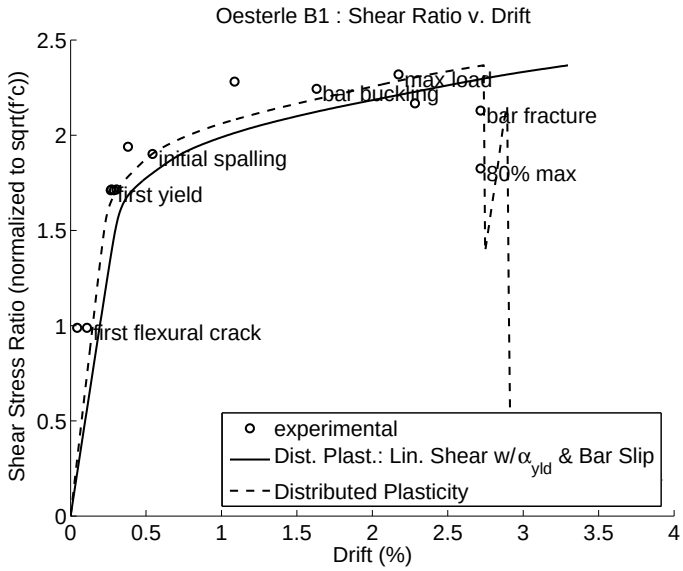

Figure M.198: Pushover of Beam-Column Element with Bar-Slip and Elastic Shear Calibrated to Yield – Oesterle B1

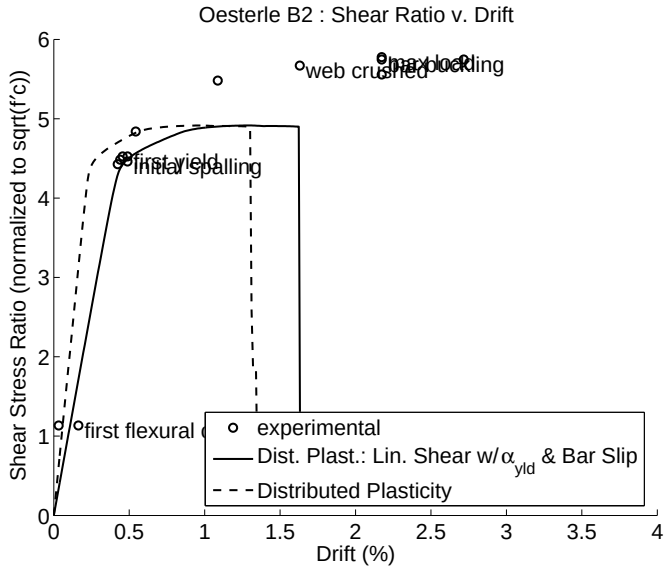

Figure M.199: Pushover of Beam-Column Element with Bar-Slip and Elastic Shear Calibrated to Yield – Oesterle B2

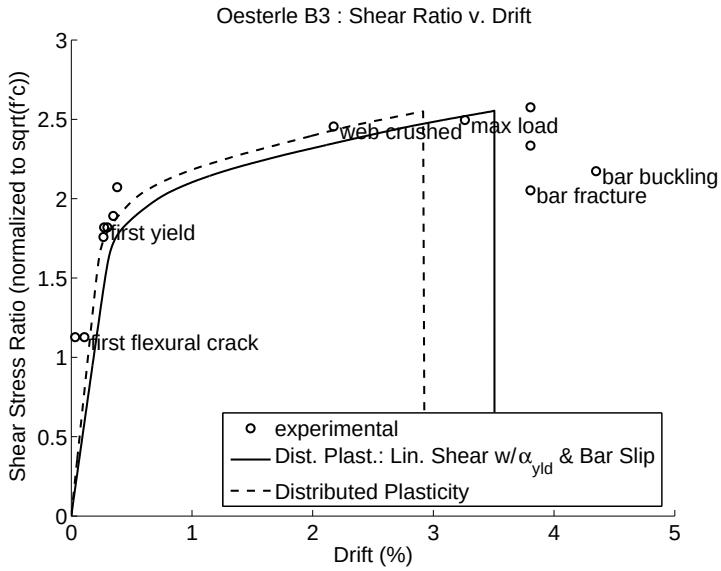

Figure M.200: Pushover of Beam-Column Element with Bar-Slip and Elastic Shear Calibrated to Yield – Oesterle B3

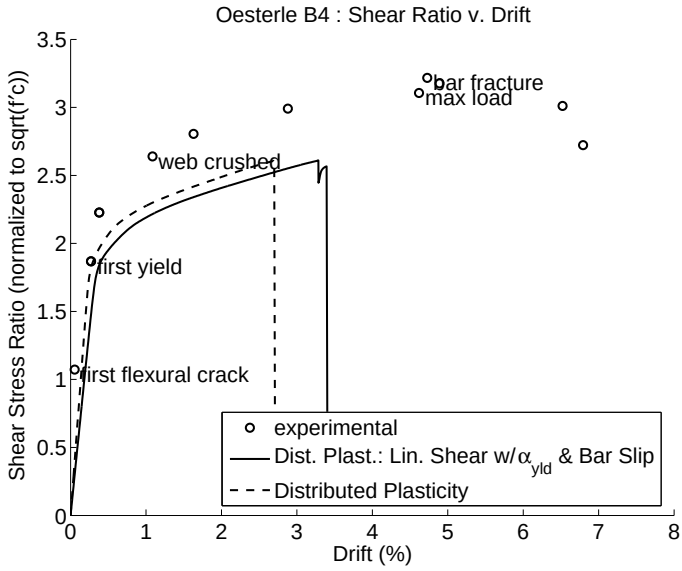

Figure M.201: Pushover of Beam-Column Element with Bar-Slip and Elastic Shear Calibrated to Yield – Oesterle B4

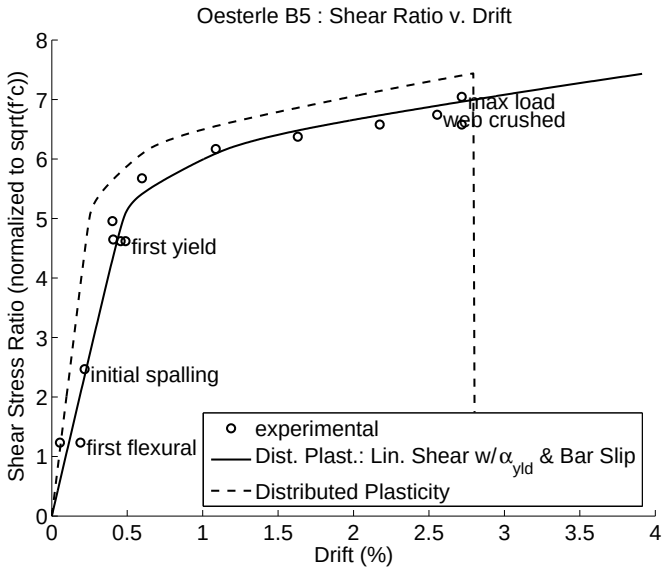

Figure M.202: Pushover of Beam-Column Element with Bar-Slip and Elastic Shear Calibrated to Yield – Oesterle B5

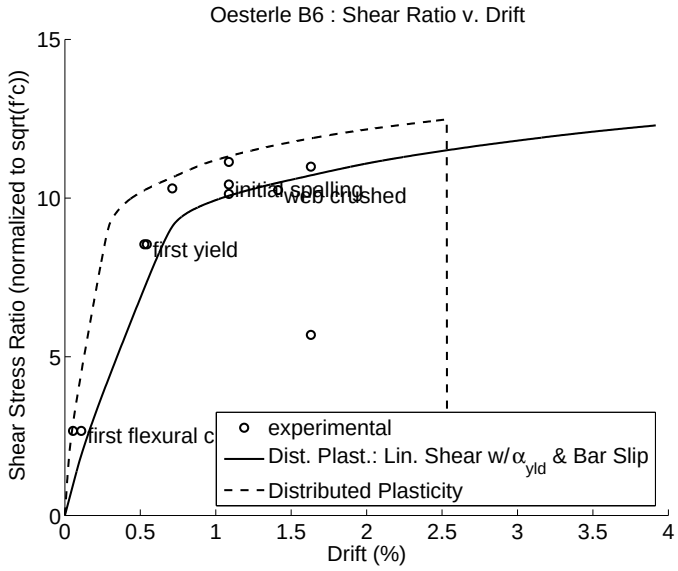

Figure M.203: Pushover of Beam-Column Element with Bar-Slip and Elastic Shear Calibrated to Yield – Oesterle B6

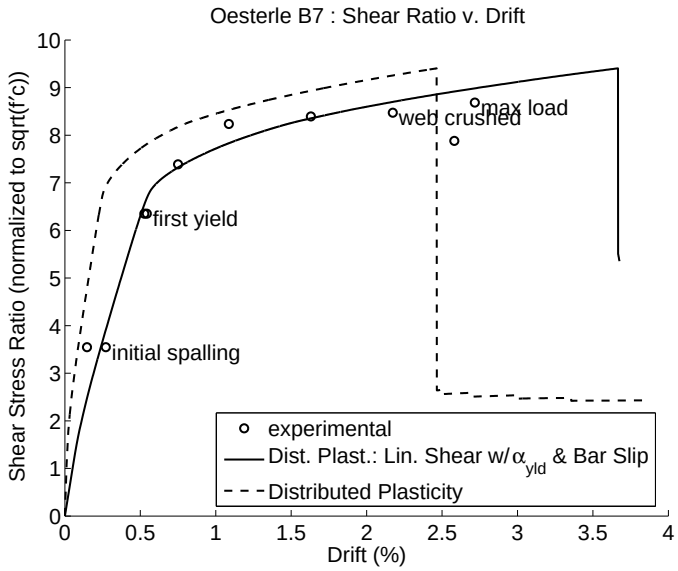

Figure M.204: Pushover of Beam-Column Element with Bar-Slip and Elastic Shear Calibrated to Yield – Oesterle B7

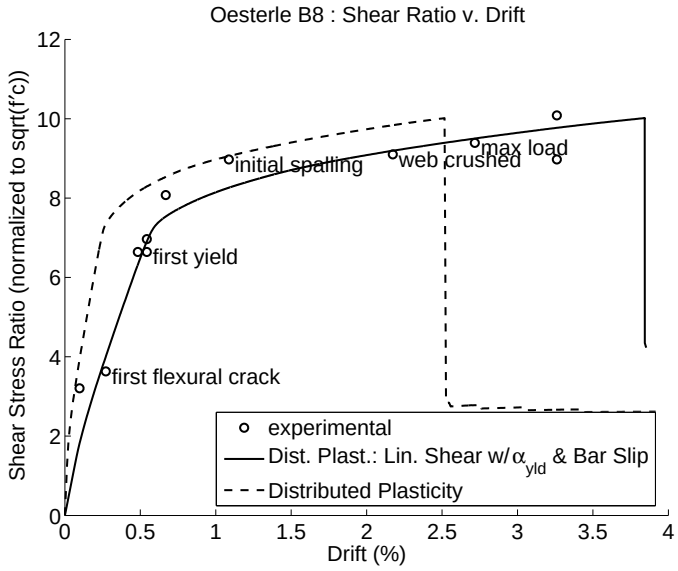

Figure M.205: Pushover of Beam-Column Element with Bar-Slip and Elastic Shear Calibrated to Yield – Oesterle B8

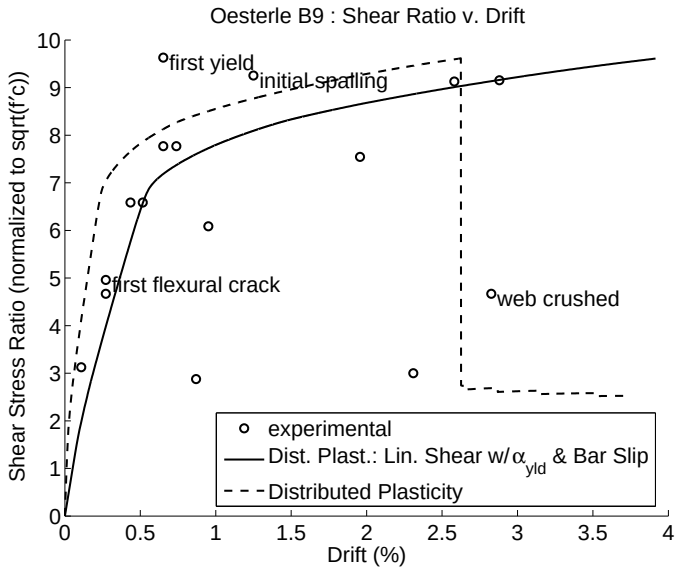

Figure M.206: Pushover of Beam-Column Element with Bar-Slip and Elastic Shear Calibrated to Yield – Oesterle B9

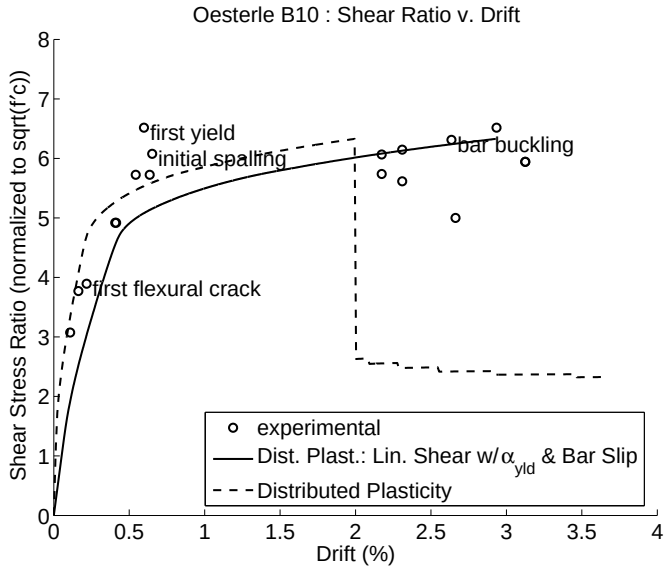

Figure M.207: Pushover of Beam-Column Element with Bar-Slip and Elastic Shear Calibrated to Yield – Oesterle B10

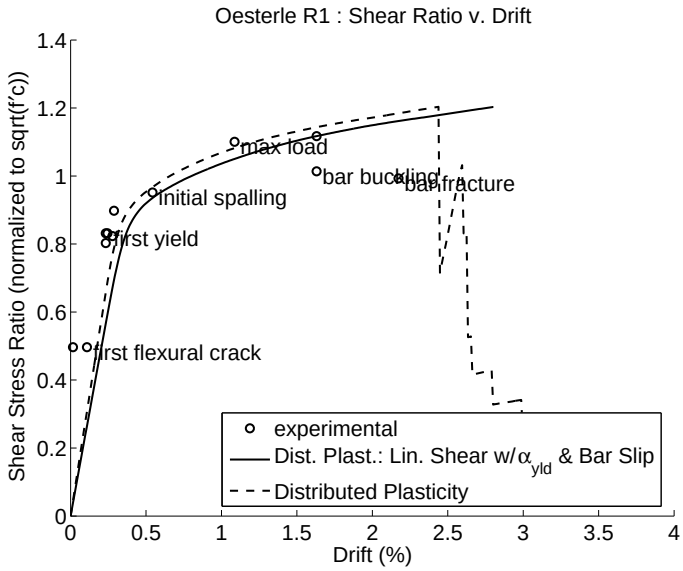

Figure M.208: Pushover of Beam-Column Element with Bar-Slip and Elastic Shear Calibrated to Yield – Oesterle R1

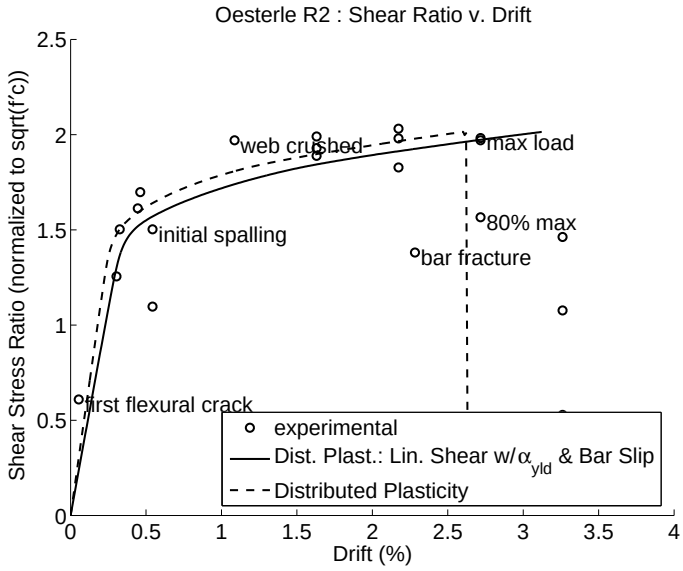

Figure M.209: Pushover of Beam-Column Element with Bar-Slip and Elastic Shear Calibrated to Yield – Oesterle R2

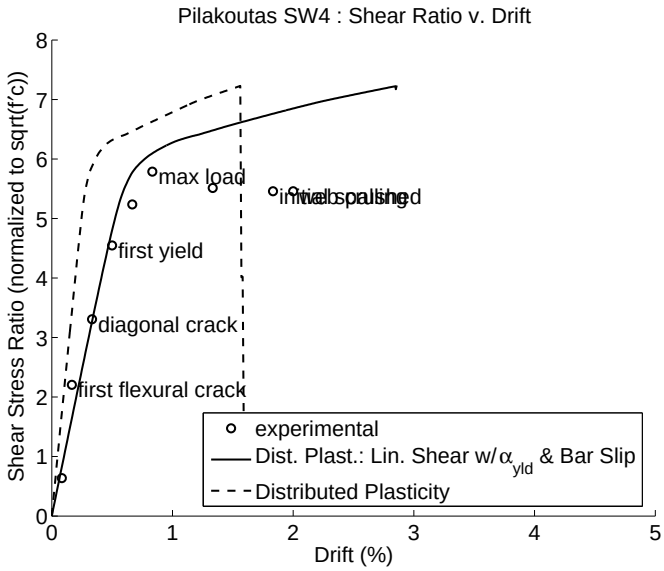

Figure M.210: Pushover of Beam-Column Element with Bar-Slip and Elastic Shear Calibrated to Yield – Pilakoutas SW4

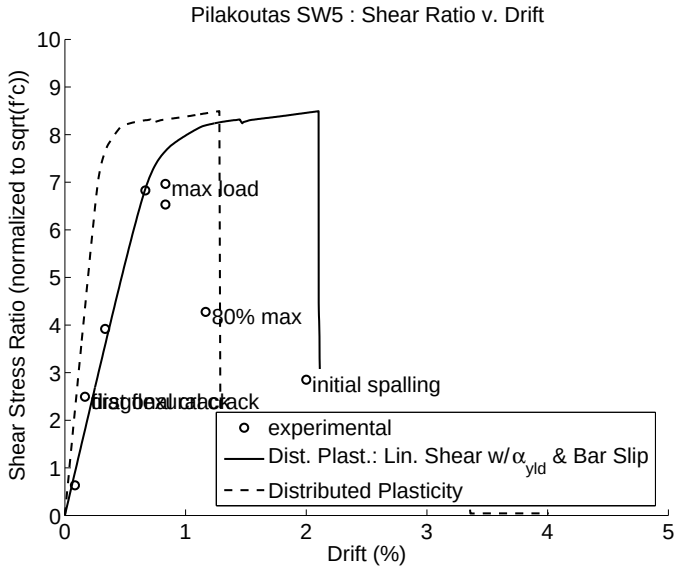

Figure M.211: Pushover of Beam-Column Element with Bar-Slip and Elastic Shear Calibrated to Yield – Pilakoutas SW5

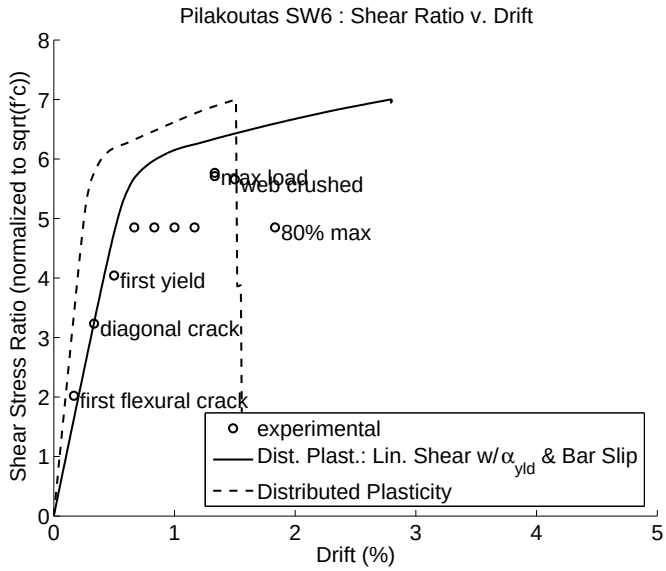

Figure M.212: Pushover of Beam-Column Element with Bar-Slip and Elastic Shear Calibrated to Yield – Pilakoutas SW6

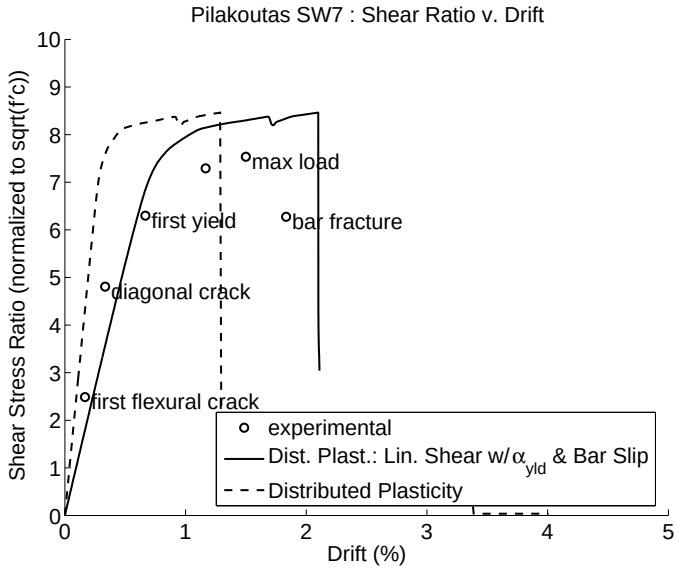

Figure M.213: Pushover of Beam-Column Element with Bar-Slip and Elastic Shear Calibrated to Yield – Pilakoutas SW7

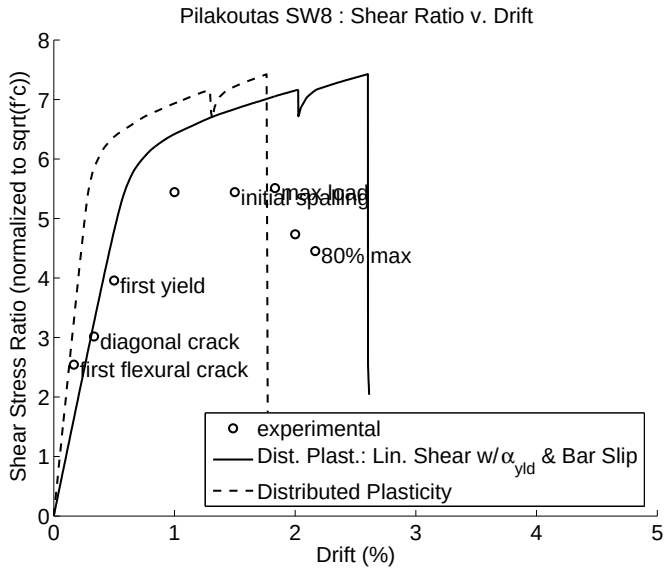

Figure M.214: Pushover of Beam-Column Element with Bar-Slip and Elastic Shear Calibrated to Yield – Pilakoutas SW8

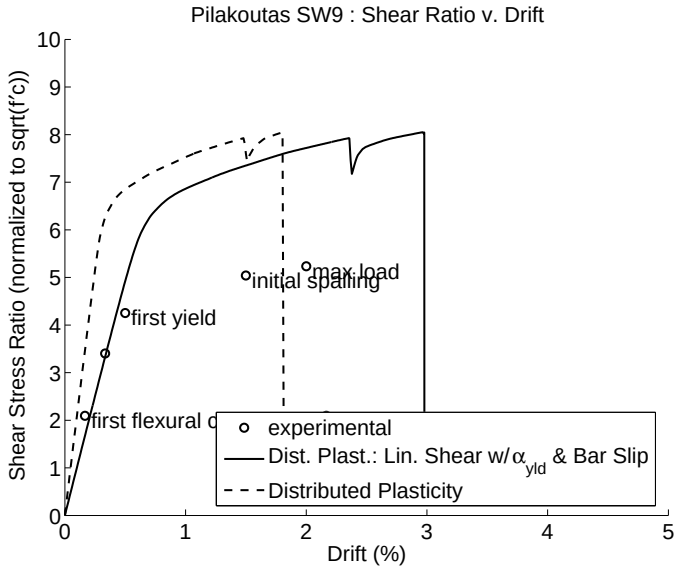

Figure M.215: Pushover of Beam-Column Element with Bar-Slip and Elastic Shear Calibrated to Yield – Pilakoutas SW9

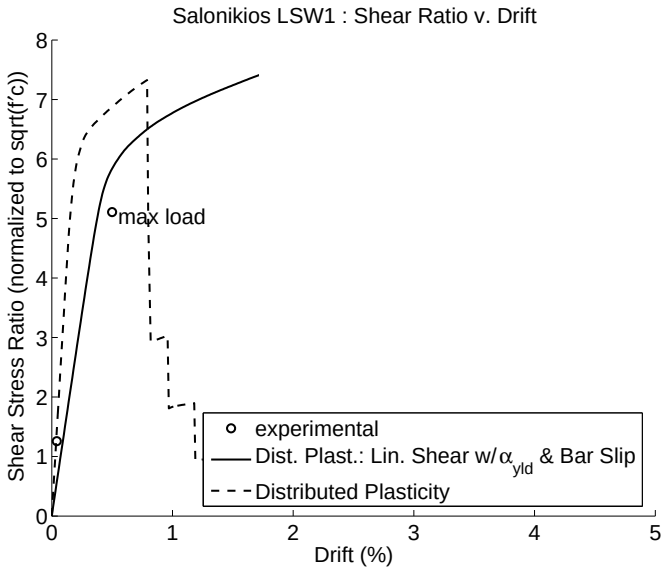

Figure M.216: Pushover of Beam-Column Element with Bar-Slip and Elastic Shear Calibrated to Yield – Salonikios LSW1

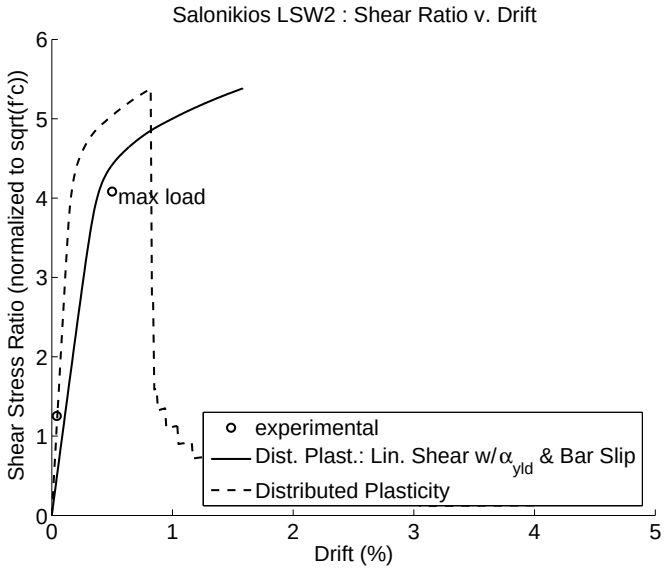

Figure M.217: Pushover of Beam-Column Element with Bar-Slip and Elastic Shear Calibrated to Yield – Salonikios LSW2

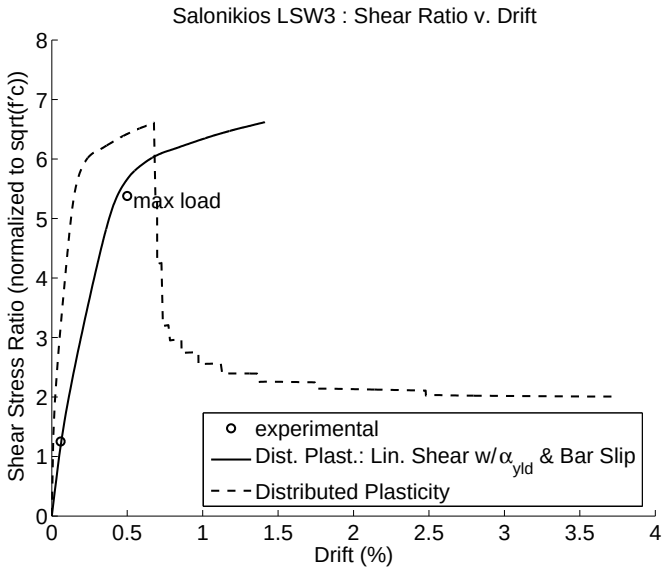

Figure M.218: Pushover of Beam-Column Element with Bar-Slip and Elastic Shear Calibrated to Yield – Salonikios LSW3

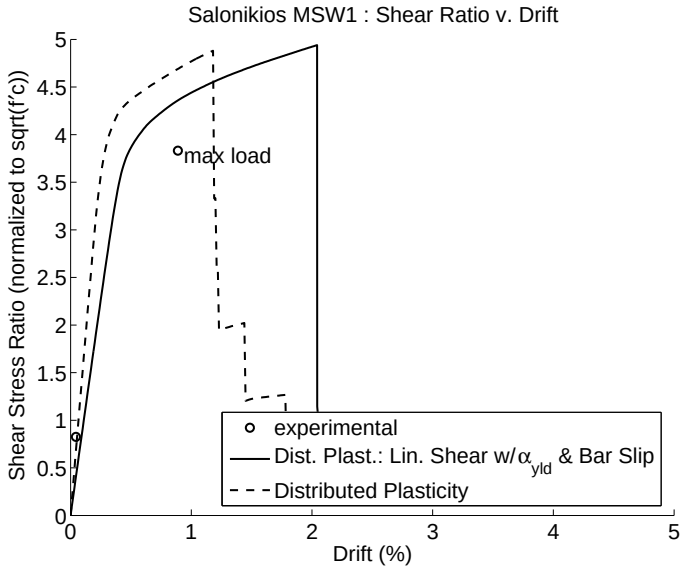

Figure M.219: Pushover of Beam-Column Element with Bar-Slip and Elastic Shear Calibrated to Yield – Salonikios MSW1

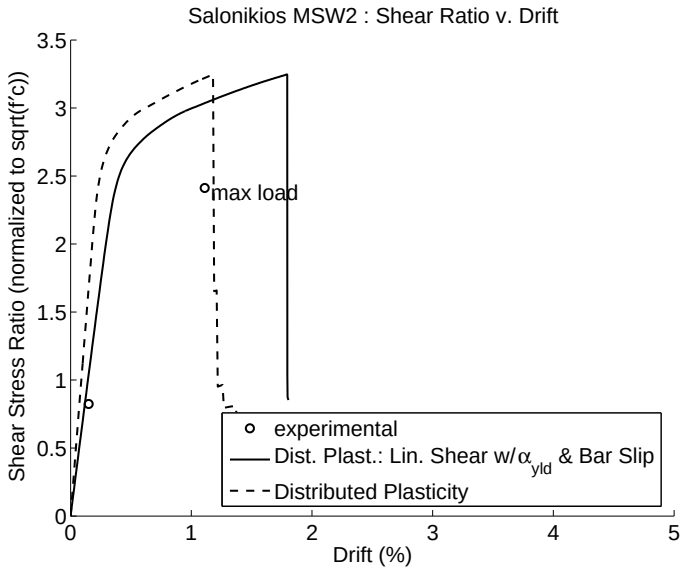

Figure M.220: Pushover of Beam-Column Element with Bar-Slip and Elastic Shear Calibrated to Yield – Salonikios MSW2

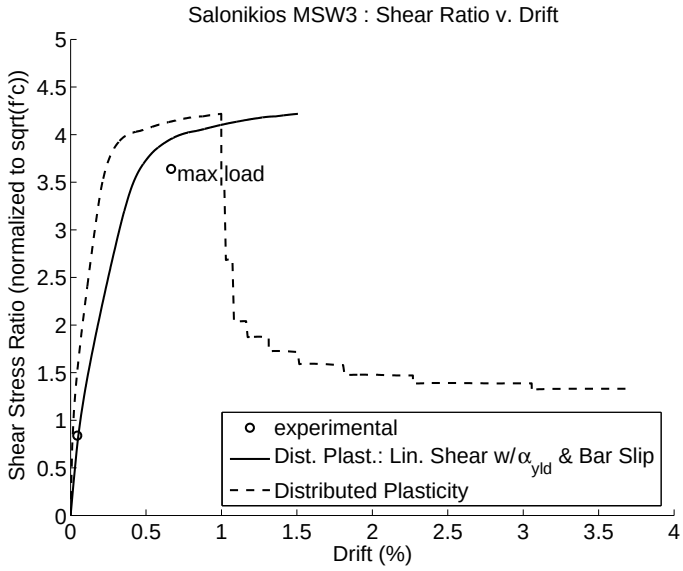

Figure M.221: Pushover of Beam-Column Element with Bar-Slip and Elastic Shear Calibrated to Yield – Salonikios MSW3

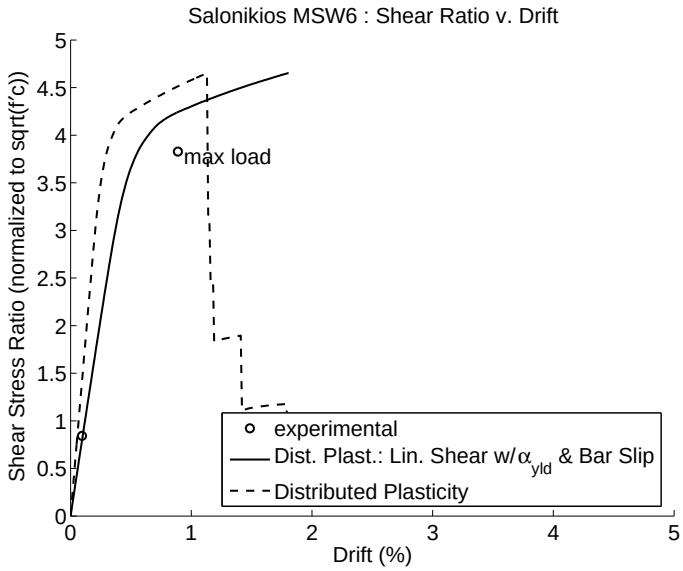

Figure M.222: Pushover of Beam-Column Element with Bar-Slip and Elastic Shear Calibrated to Yield – Salonikios MSW6

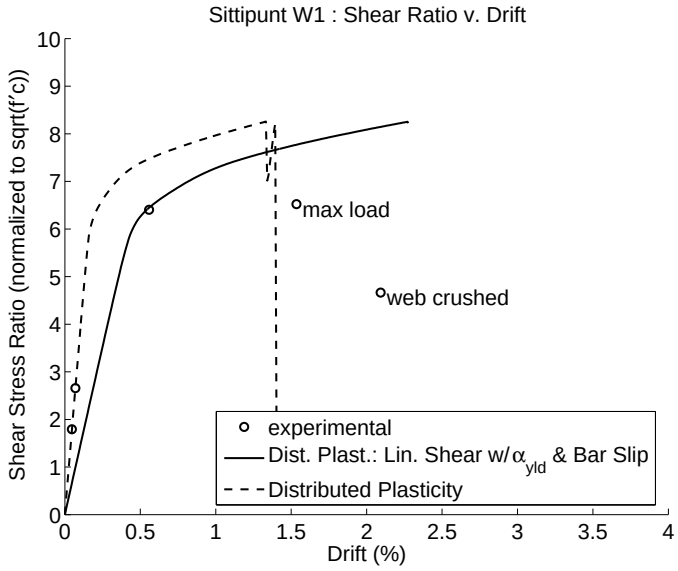

Figure M.223: Pushover of Beam-Column Element with Bar-Slip and Elastic Shear Calibrated to Yield – Sittipunt W1

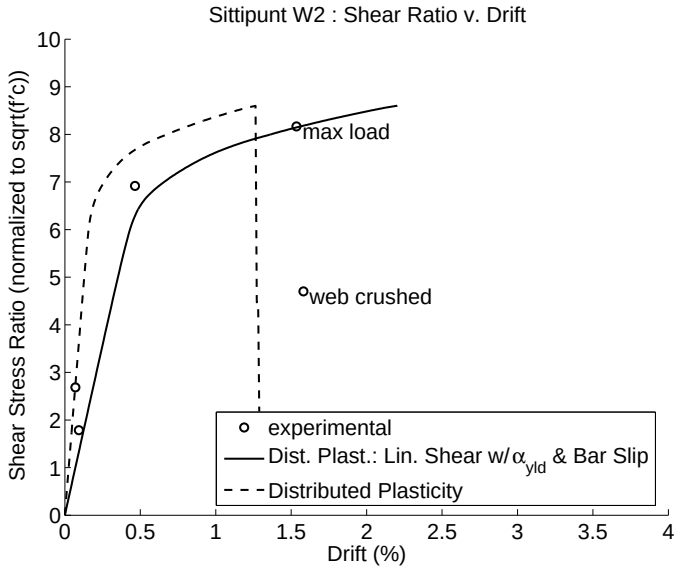

Figure M.224: Pushover of Beam-Column Element with Bar-Slip and Elastic Shear Calibrated to Yield – Sittipunt W2

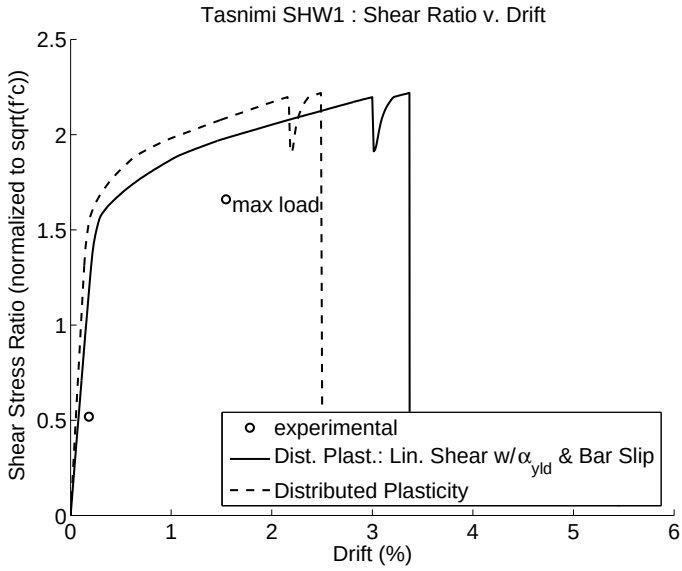

Figure M.225: Pushover of Beam-Column Element with Bar-Slip and Elastic Shear Calibrated to Yield – Tasnimi SHW1

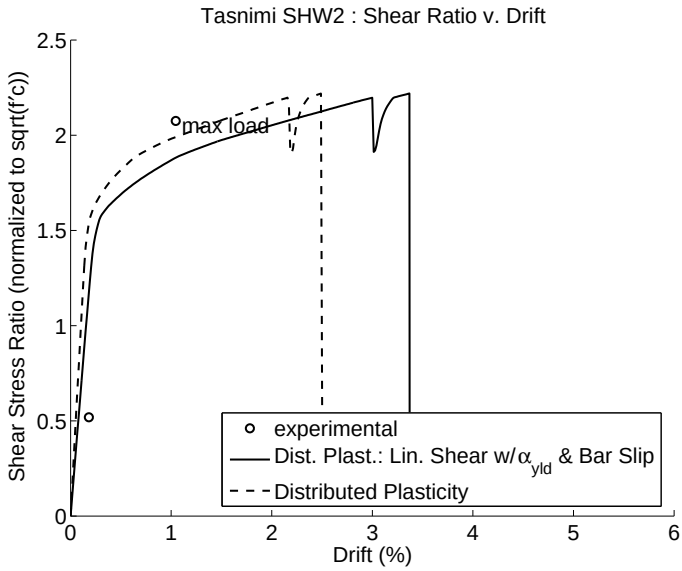

Figure M.226: Pushover of Beam-Column Element with Bar-Slip and Elastic Shear Calibrated to Yield – Tasnimi SHW2

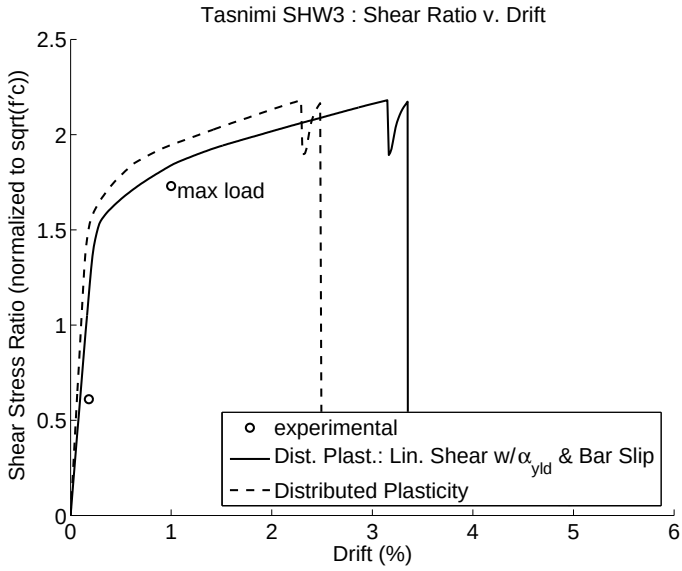

Figure M.227: Pushover of Beam-Column Element with Bar-Slip and Elastic Shear Calibrated to Yield – Tasnimi SHW3

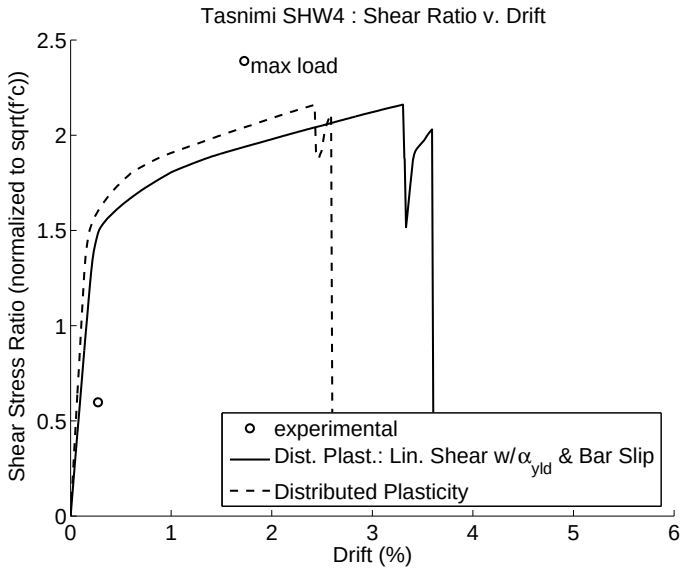

Figure M.228: Pushover of Beam-Column Element with Bar-Slip and Elastic Shear Calibrated to Yield – Tasnimi SHW4

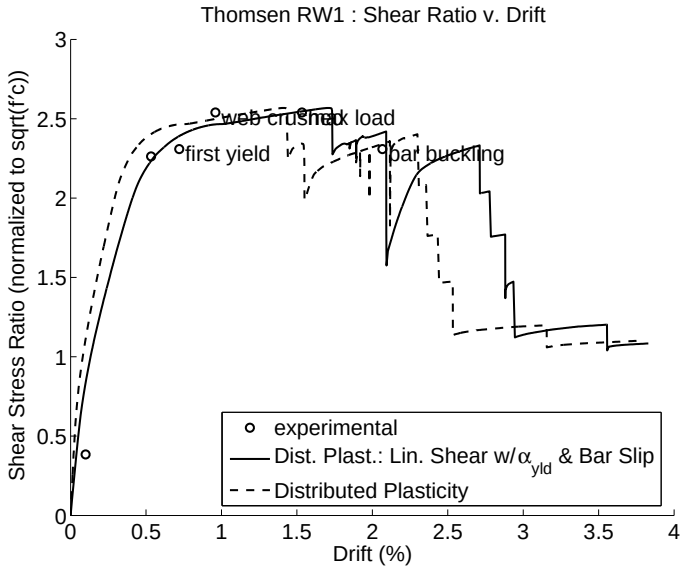

Figure M.229: Pushover of Beam-Column Element with Bar-Slip and Elastic Shear Calibrated to Yield – Thomsen RW1

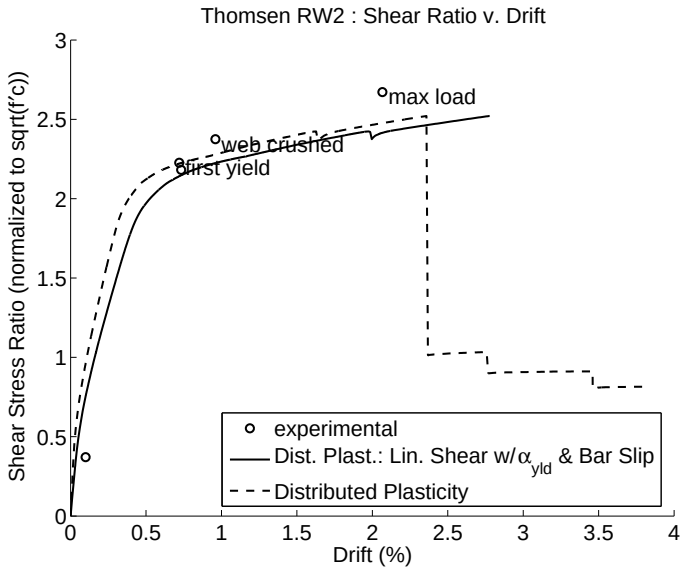

Figure M.230: Pushover of Beam-Column Element with Bar-Slip and Elastic Shear Calibrated to Yield – Thomsen RW2

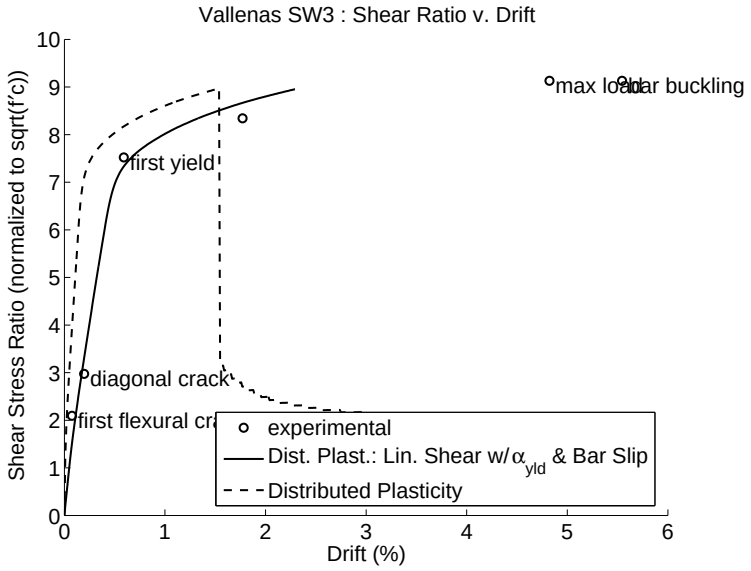

Figure M.231: Pushover of Beam-Column Element with Bar-Slip and Elastic Shear Calibrated to Yield – Vallenas SW3

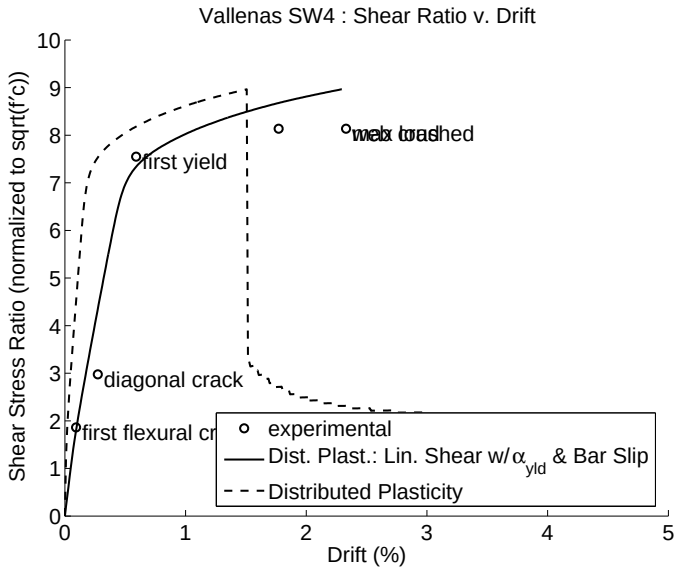

Figure M.232: Pushover of Beam-Column Element with Bar-Slip and Elastic Shear Calibrated to Yield – Vallenas SW4

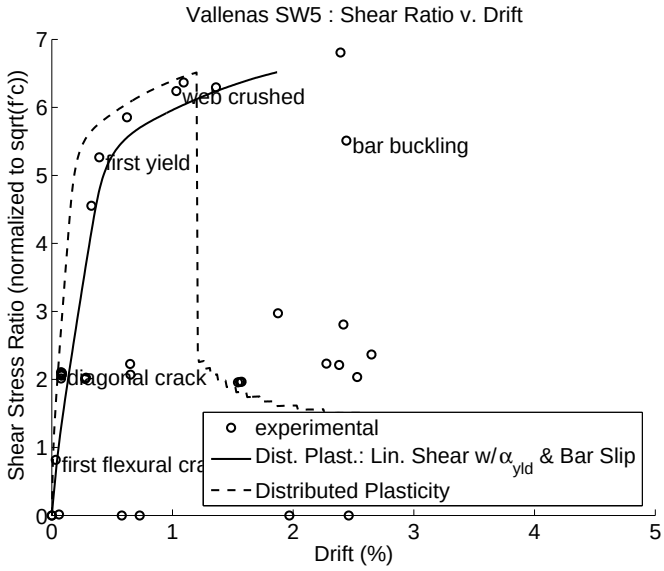

Figure M.233: Pushover of Beam-Column Element with Bar-Slip and Elastic Shear Calibrated to Yield – Vallenas SW5

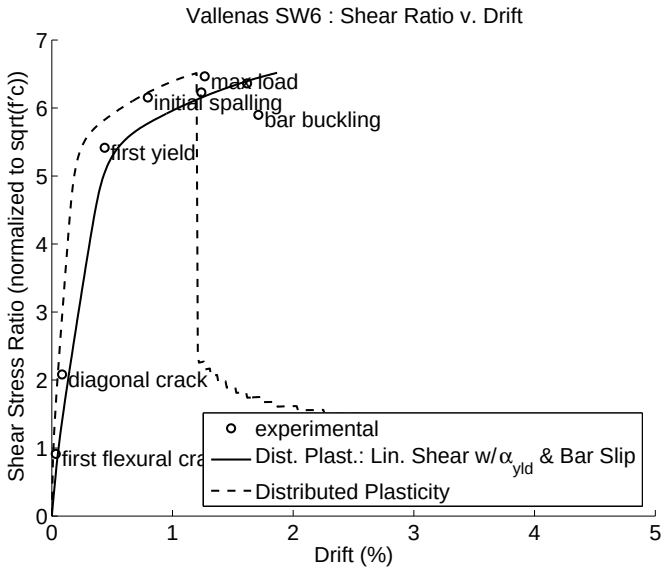

Figure M.234: Pushover of Beam-Column Element with Bar-Slip and Elastic Shear Calibrated to Yield – Vallenas SW6

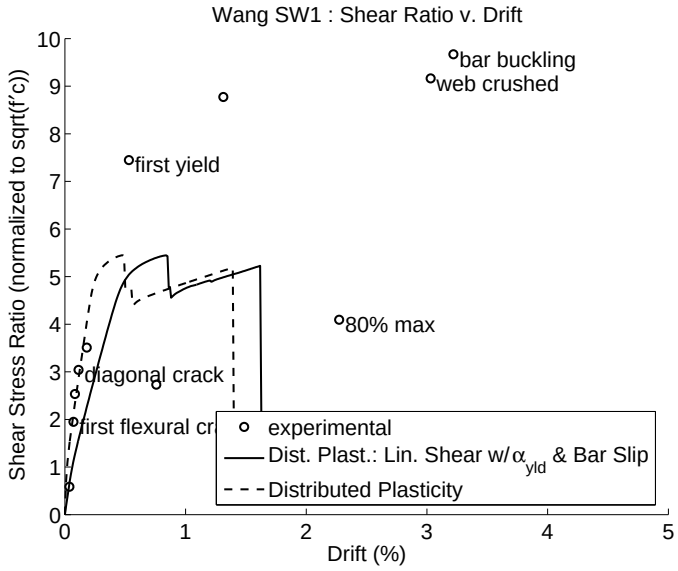

Figure M.235: Pushover of Beam-Column Element with Bar-Slip and Elastic Shear Calibrated to Yield – Wang SW1

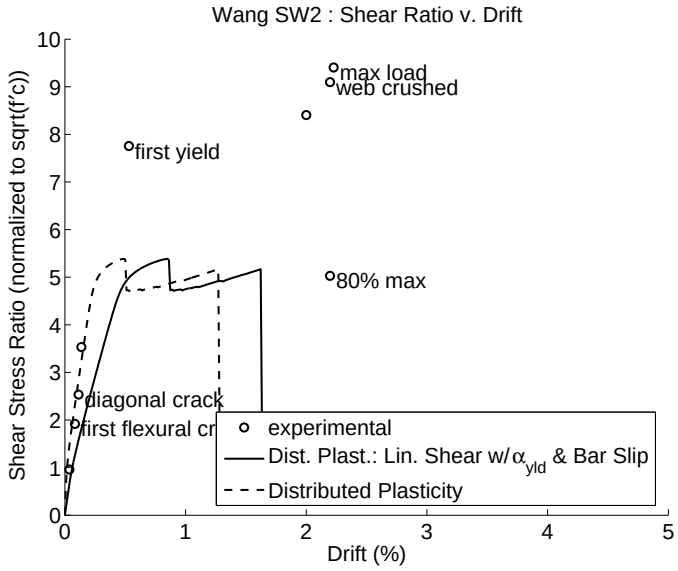

Figure M.236: Pushover of Beam-Column Element with Bar-Slip and Elastic Shear Calibrated to Yield – Wang SW2

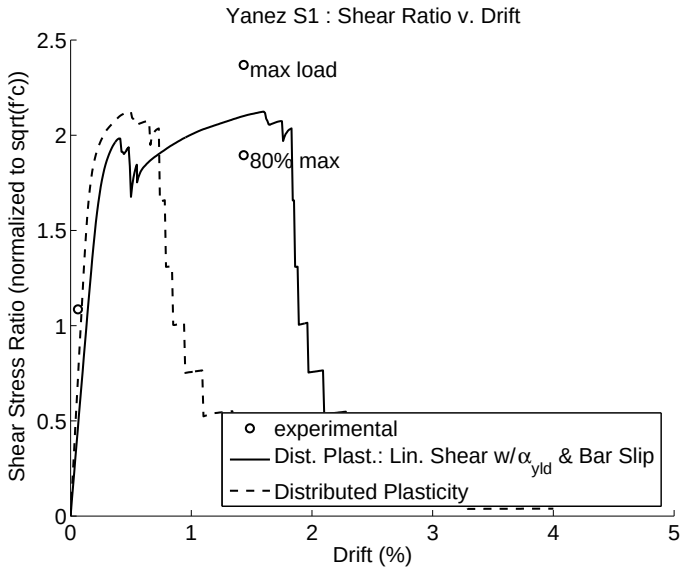

Figure M.237: Pushover of Beam-Column Element with Bar-Slip and Elastic Shear Calibrated to Yield – Yanez S1

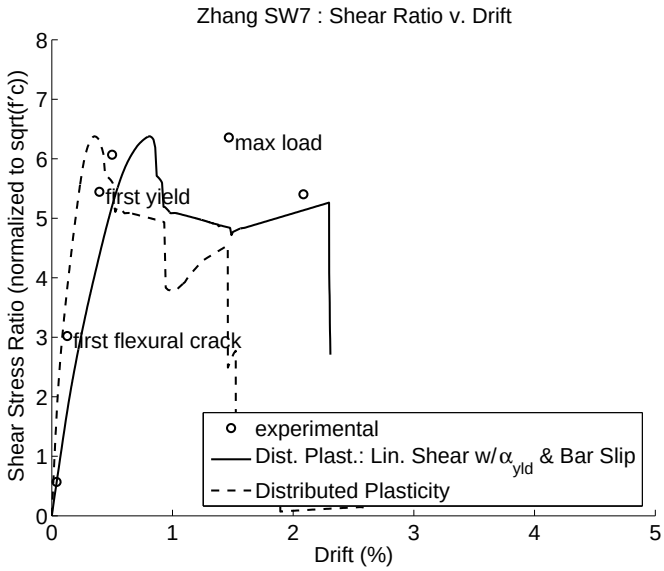

Figure M.238: Pushover of Beam-Column Element with Bar-Slip and Elastic Shear Calibrated to Yield – Zhang SW7

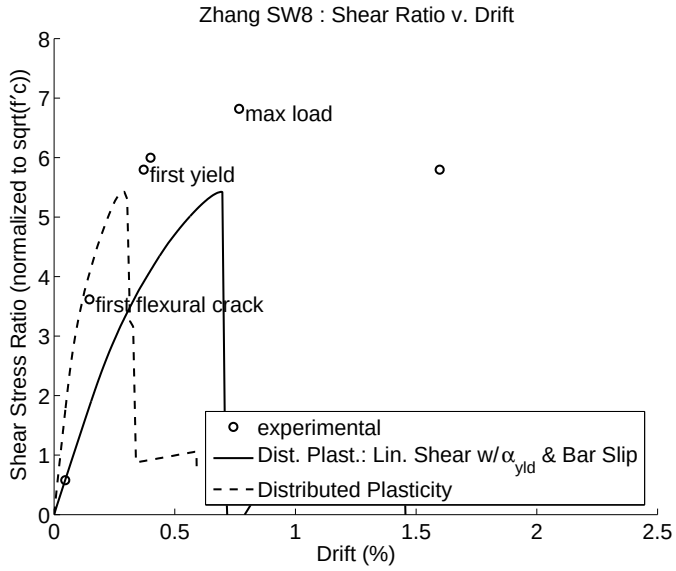

Figure M.239: Pushover of Beam-Column Element with Bar-Slip and Elastic Shear Calibrated to Yield – Zhang SW8

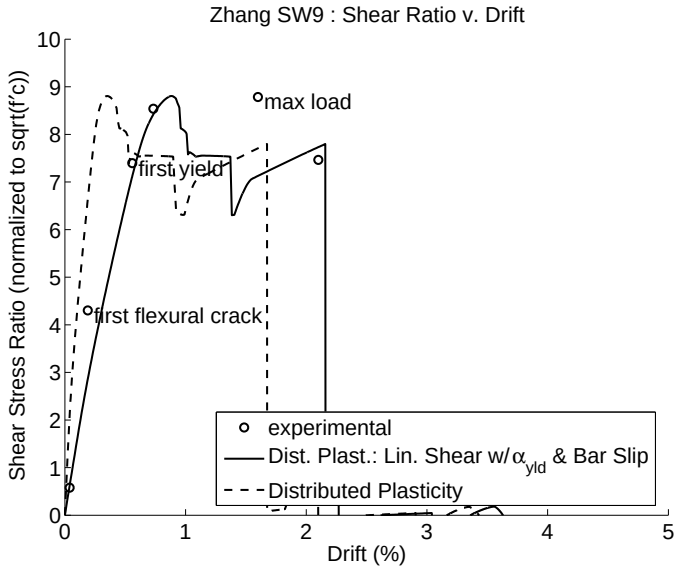

Figure M.240: Pushover of Beam-Column Element with Bar-Slip and Elastic Shear Calibrated to Yield – Zhang SW9

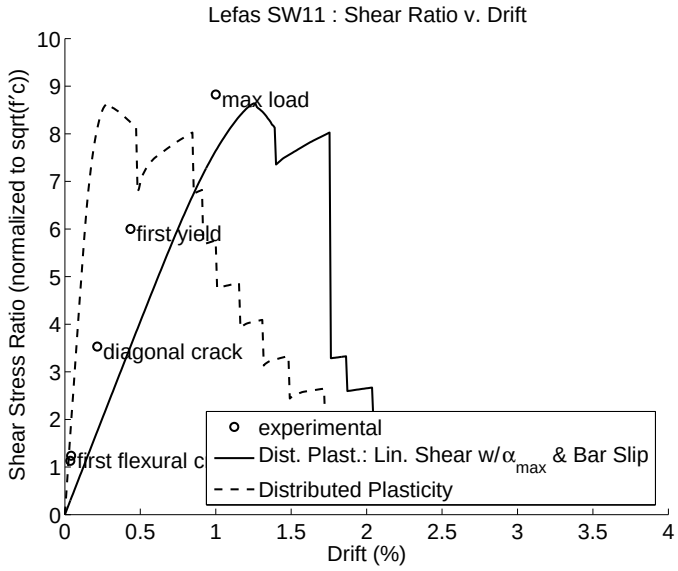

Figure M.241: Pushover of Beam-Column Element with Bar-Slip and Elastic Shear Calibrated to Maximum Displacement – Lefas SW11

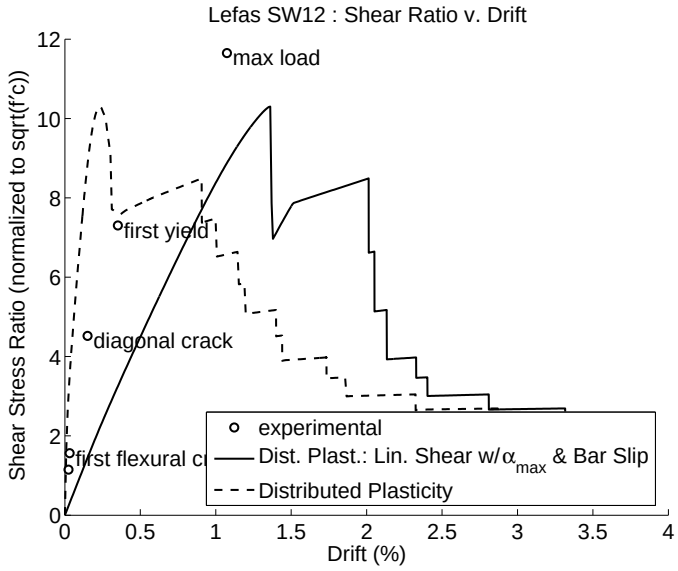

Figure M.242: Pushover of Beam-Column Element with Bar-Slip and Elastic Shear Calibrated to Maximum Displacement – Lefas SW12

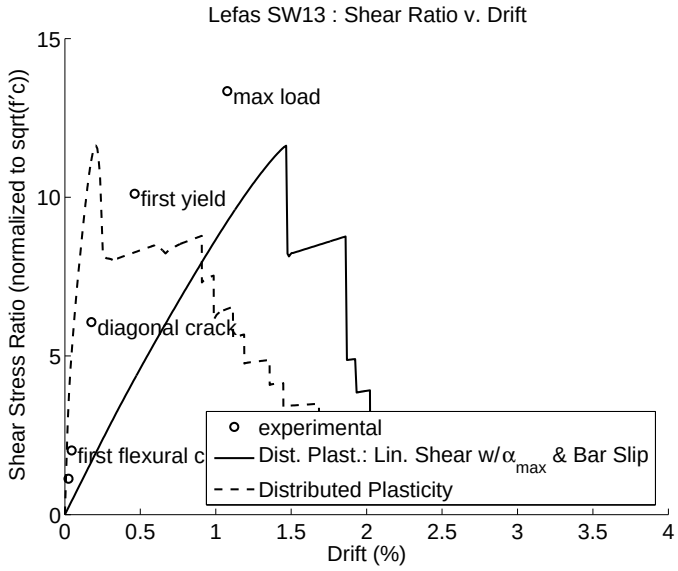

Figure M.243: Pushover of Beam-Column Element with Bar-Slip and Elastic Shear Calibrated to Maximum Displacement – Lefas SW13

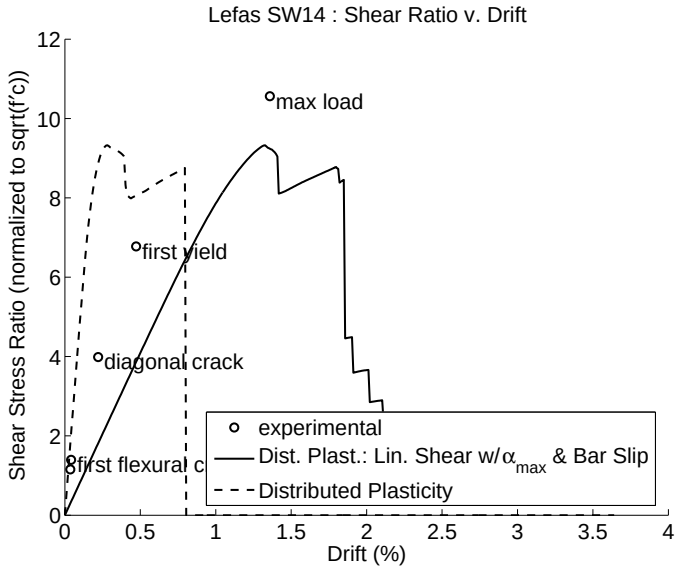

Figure M.244: Pushover of Beam-Column Element with Bar-Slip and Elastic Shear Calibrated to Maximum Displacement – Lefas SW14

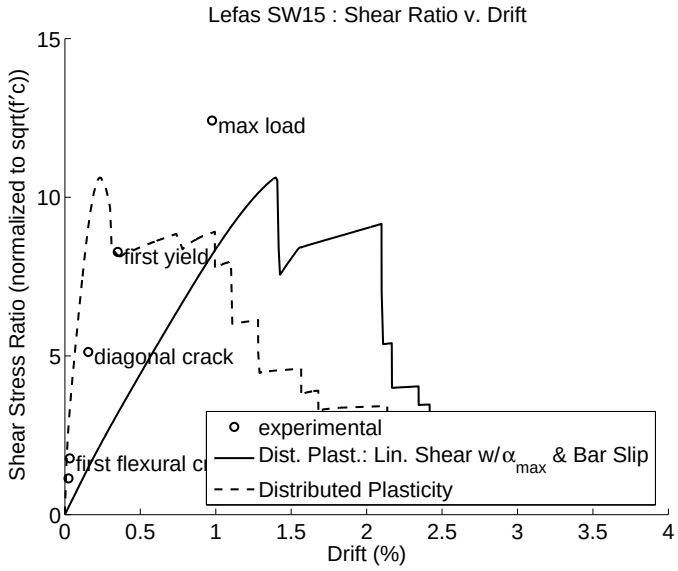

Figure M.245: Pushover of Beam-Column Element with Bar-Slip and Elastic Shear Calibrated to Maximum Displacement – Lefas SW15

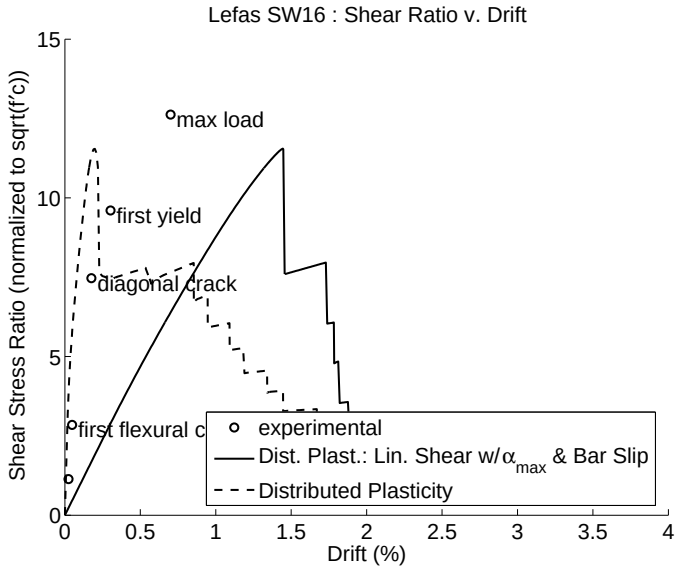

Figure M.246: Pushover of Beam-Column Element with Bar-Slip and Elastic Shear Calibrated to Maximum Displacement – Lefas SW16

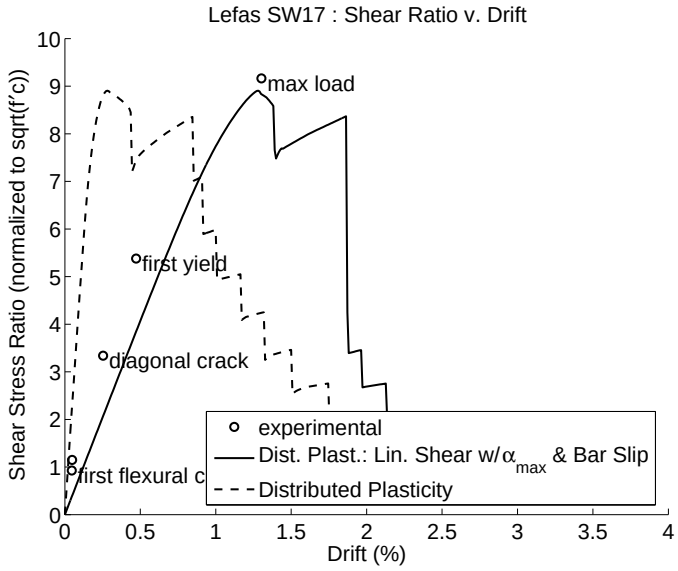

Figure M.247: Pushover of Beam-Column Element with Bar-Slip and Elastic Shear Calibrated to Maximum Displacement – Lefas SW17

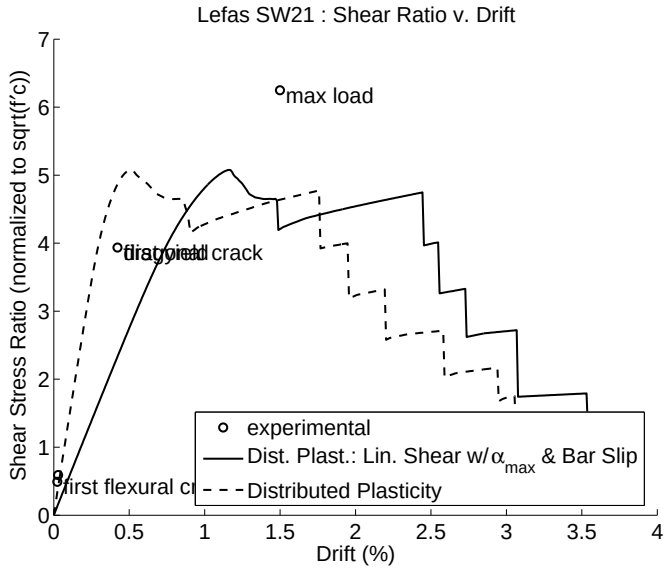

Figure M.248: Pushover of Beam-Column Element with Bar-Slip and Elastic Shear Calibrated to Maximum Displacement – Lefas SW21

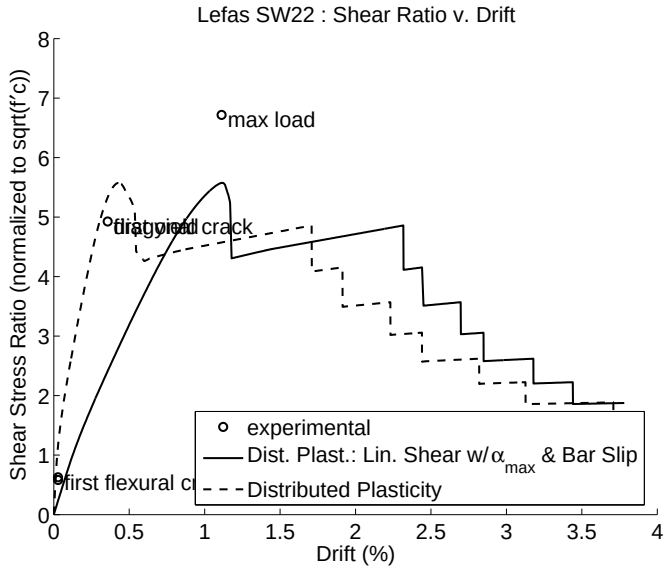

Figure M.249: Pushover of Beam-Column Element with Bar-Slip and Elastic Shear Calibrated to Maximum Displacement – Lefas SW22

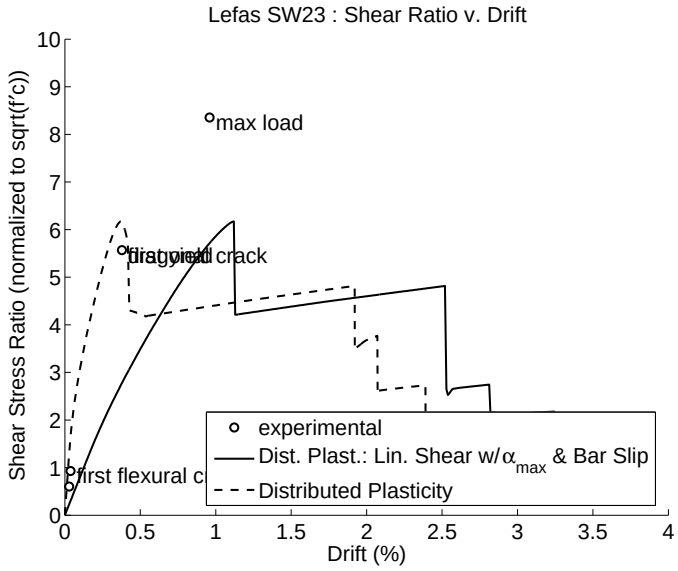

Figure M.250: Pushover of Beam-Column Element with Bar-Slip and Elastic Shear Calibrated to Maximum Displacement – Lefas SW23

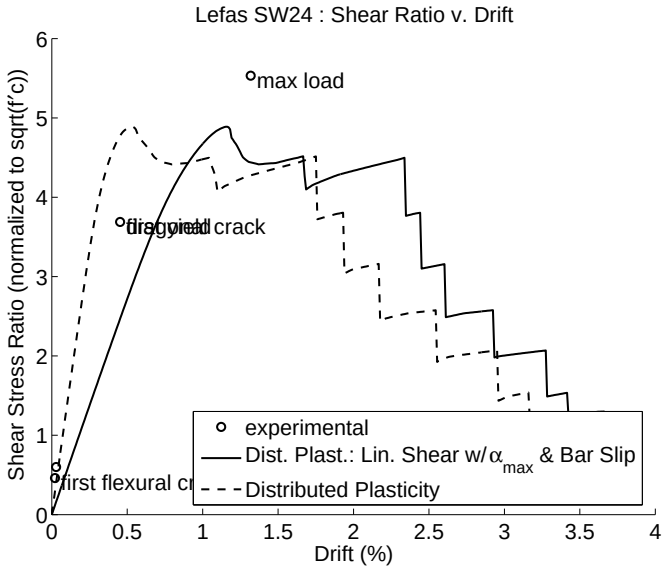

Figure M.251: Pushover of Beam-Column Element with Bar-Slip and Elastic Shear Calibrated to Maximum Displacement – Lefas SW24

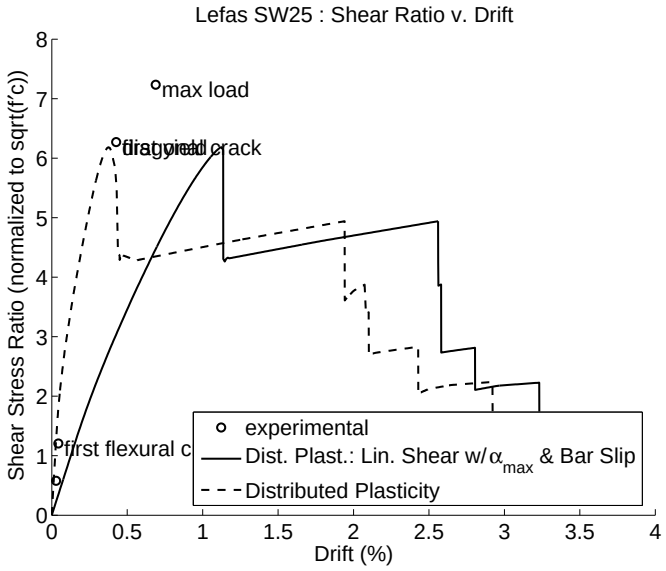

Figure M.252: Pushover of Beam-Column Element with Bar-Slip and Elastic Shear Calibrated to Maximum Displacement – Lefas SW25

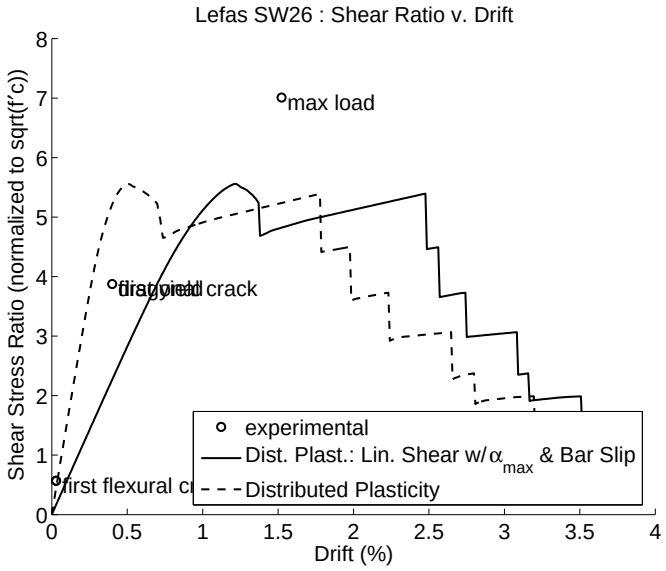

Figure M.253: Pushover of Beam-Column Element with Bar-Slip and Elastic Shear Calibrated to Maximum Displacement – Lefas SW26

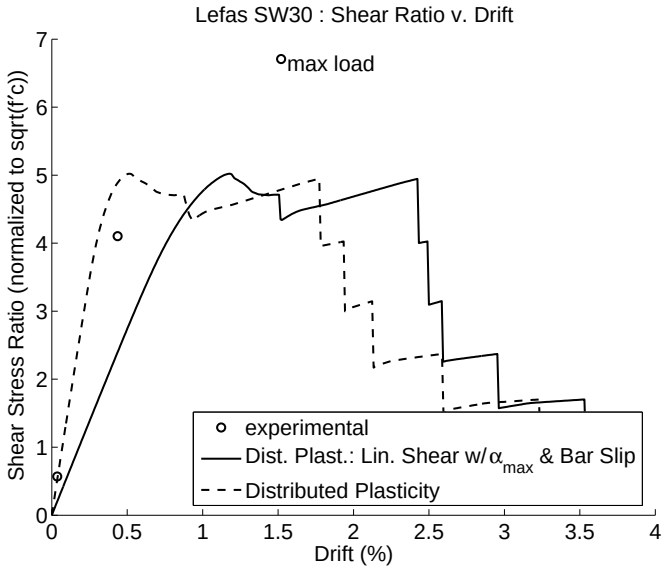

Figure M.254: Pushover of Beam-Column Element with Bar-Slip and Elastic Shear Calibrated to Maximum Displacement – Lefas SW30

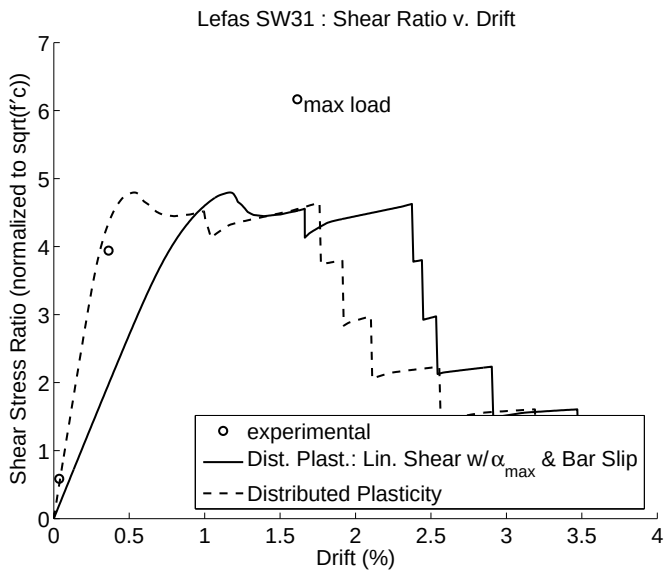

Figure M.255: Pushover of Beam-Column Element with Bar-Slip and Elastic Shear Calibrated to Maximum Displacement – Lefas SW31

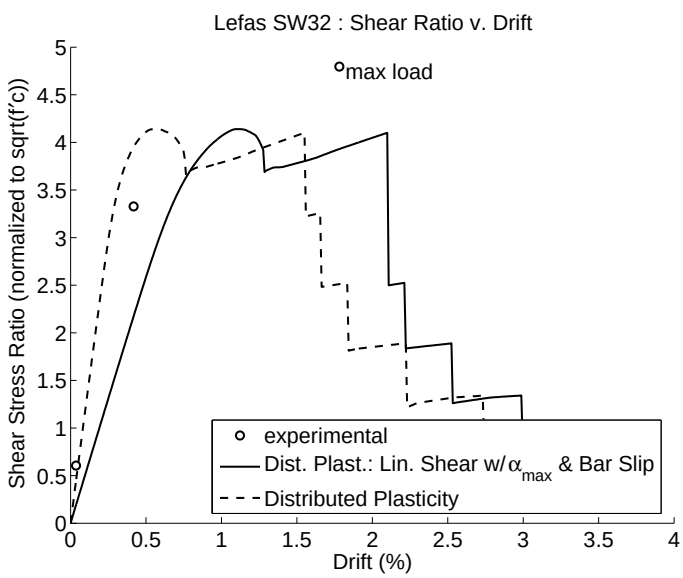

Figure M.256: Pushover of Beam-Column Element with Bar-Slip and Elastic Shear Calibrated to Maximum Displacement – Lefas SW32

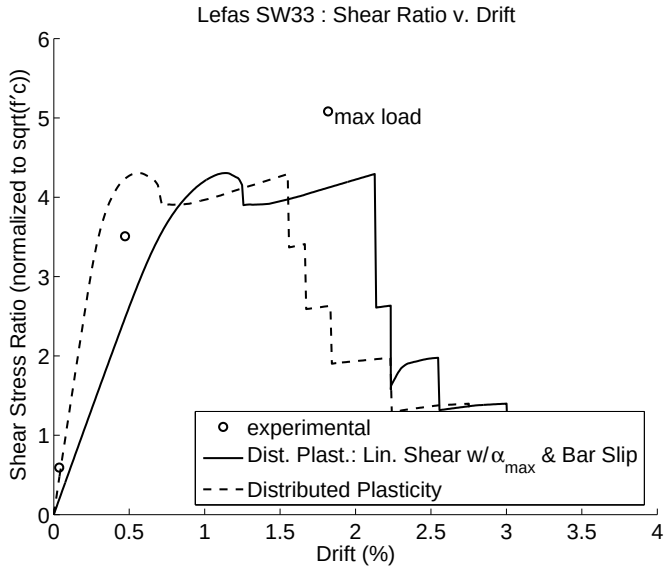

Figure M.257: Pushover of Beam-Column Element with Bar-Slip and Elastic Shear Calibrated to Maximum Displacement – Lefas SW33

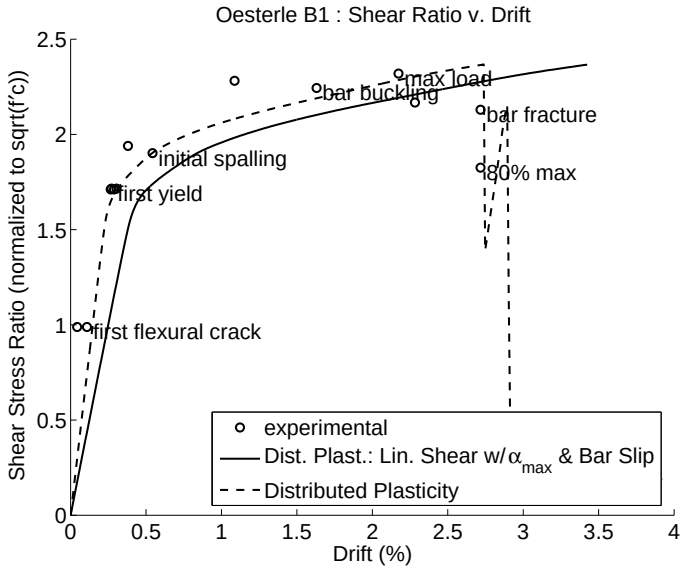

Figure M.258: Pushover of Beam-Column Element with Bar-Slip and Elastic Shear Calibrated to Maximum Displacement – Oesterle B1

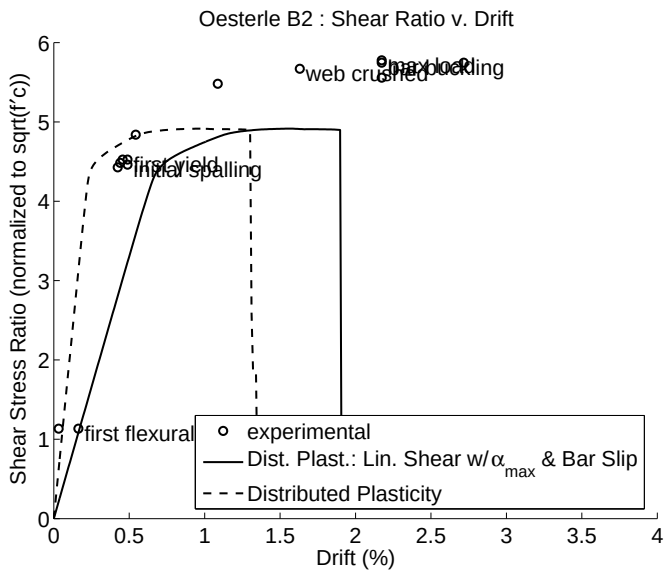

Figure M.259: Pushover of Beam-Column Element with Bar-Slip and Elastic Shear Calibrated to Maximum Displacement – Oesterle B2

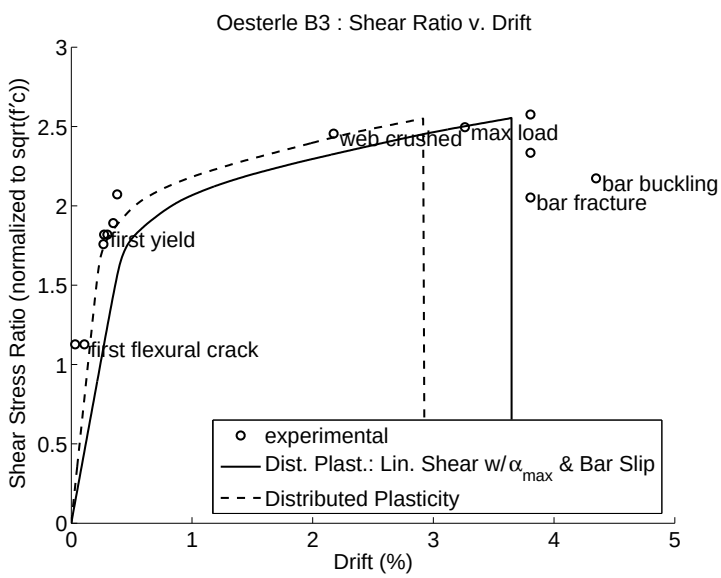

Figure M.260: Pushover of Beam-Column Element with Bar-Slip and Elastic Shear Calibrated to Maximum Displacement – Oesterle B3

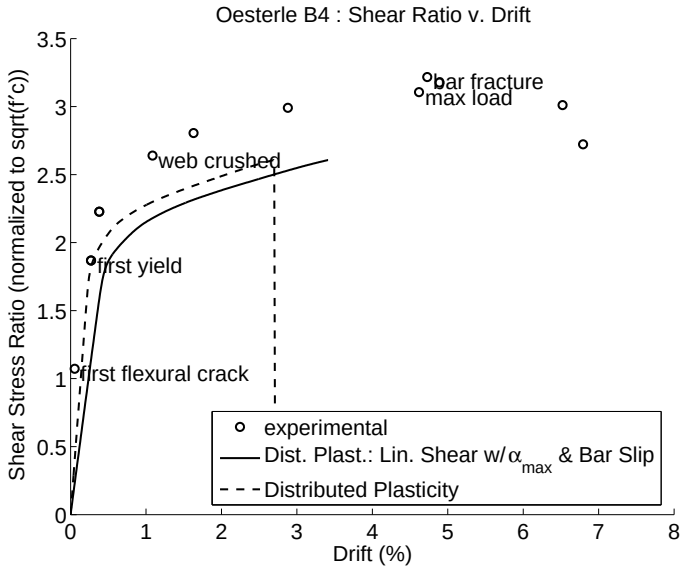

Figure M.261: Pushover of Beam-Column Element with Bar-Slip and Elastic Shear Calibrated to Maximum Displacement – Oesterle B4

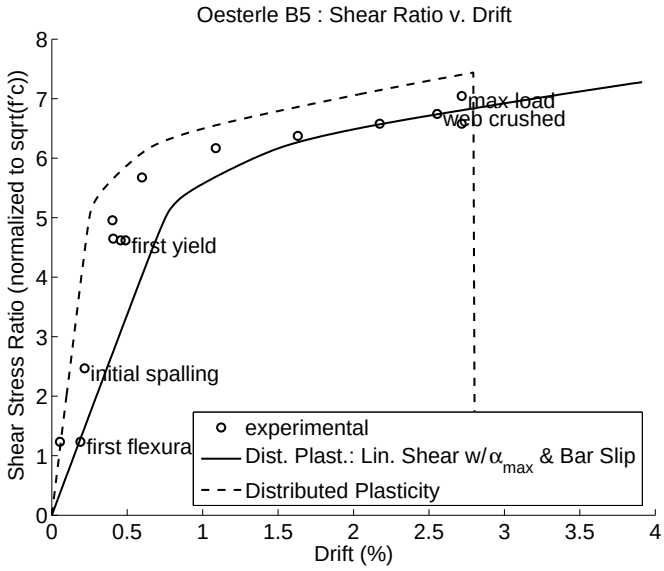

Figure M.262: Pushover of Beam-Column Element with Bar-Slip and Elastic Shear Calibrated to Maximum Displacement – Oesterle B5

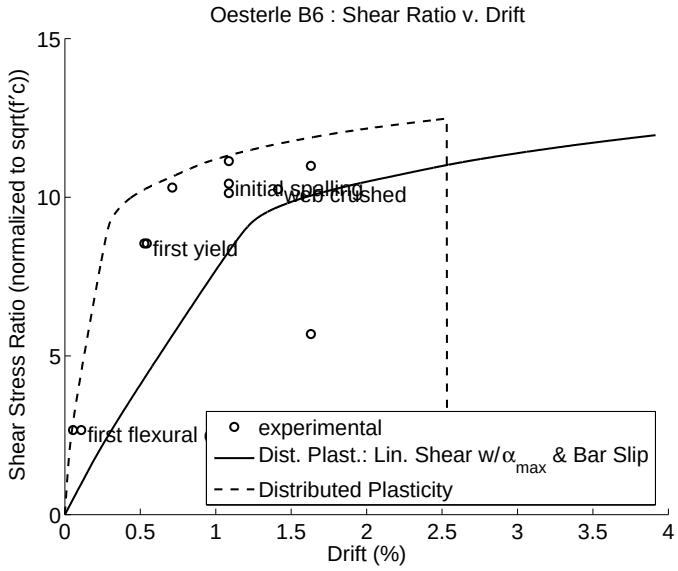

Figure M.263: Pushover of Beam-Column Element with Bar-Slip and Elastic Shear Calibrated to Maximum Displacement – Oesterle B6

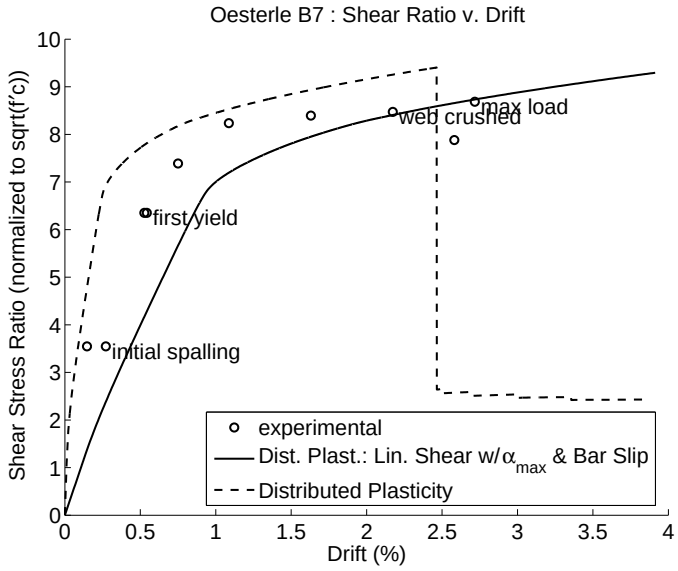

Figure M.264: Pushover of Beam-Column Element with Bar-Slip and Elastic Shear Calibrated to Maximum Displacement – Oesterle B7

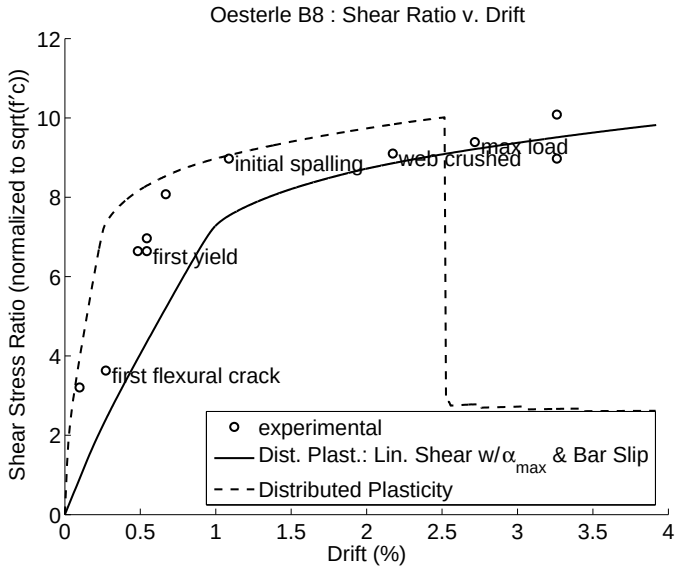

Figure M.265: Pushover of Beam-Column Element with Bar-Slip and Elastic Shear Calibrated to Maximum Displacement – Oesterle B8

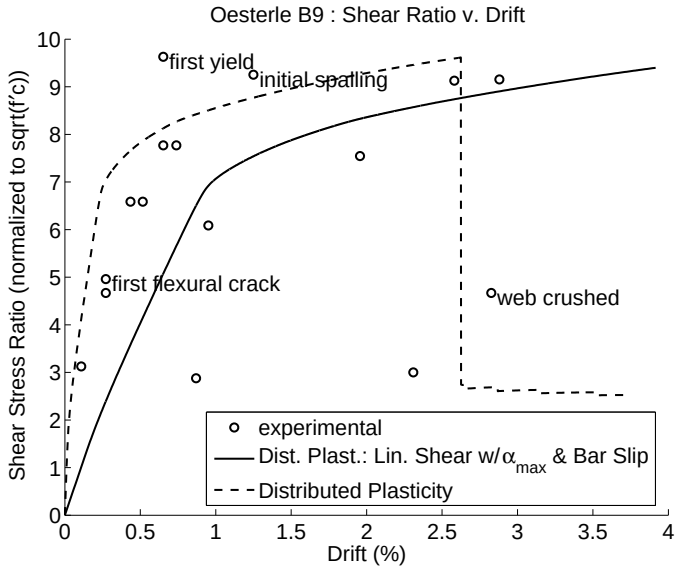

Figure M.266: Pushover of Beam-Column Element with Bar-Slip and Elastic Shear Calibrated to Maximum Displacement – Oesterle B9

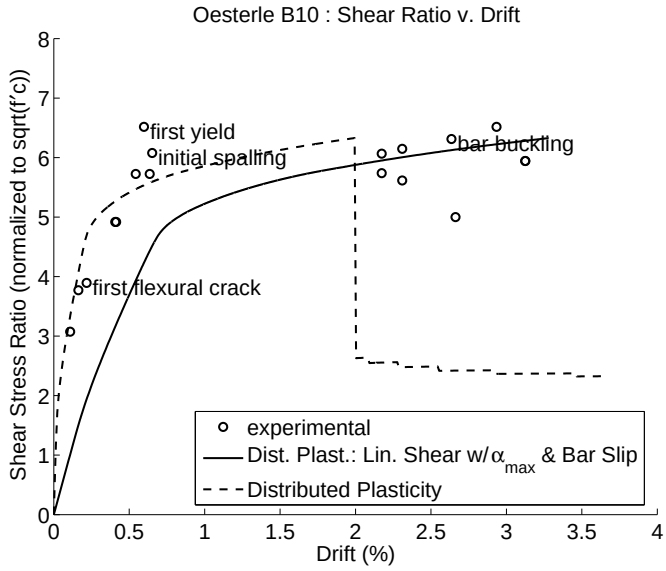

Figure M.267: Pushover of Beam-Column Element with Bar-Slip and Elastic Shear Calibrated to Maximum Displacement – Oesterle B10

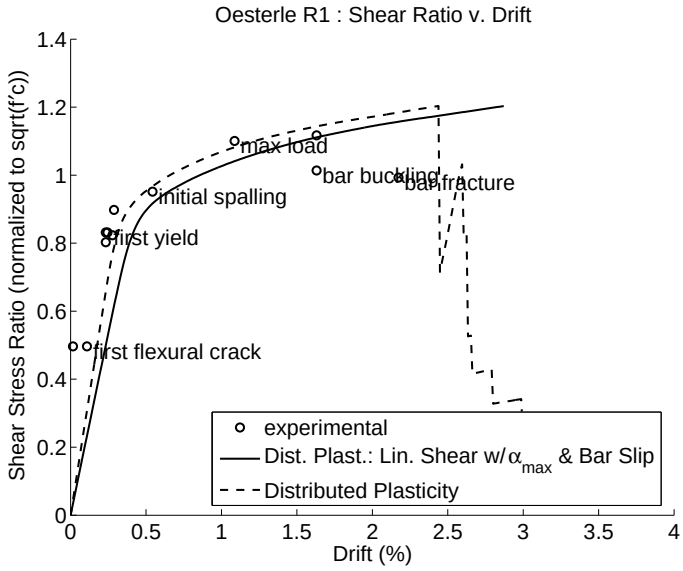

Figure M.268: Pushover of Beam-Column Element with Bar-Slip and Elastic Shear Calibrated to Maximum Displacement – Oesterle R1

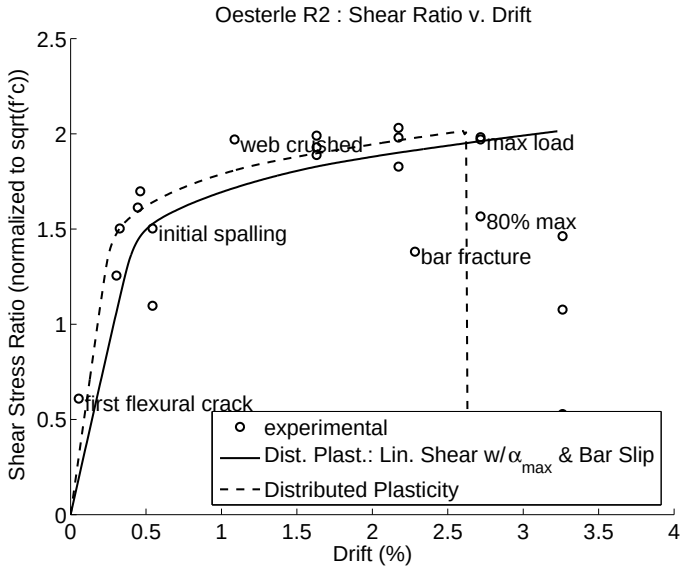

Figure M.269: Pushover of Beam-Column Element with Bar-Slip and Elastic Shear Calibrated to Maximum Displacement – Oesterle R2

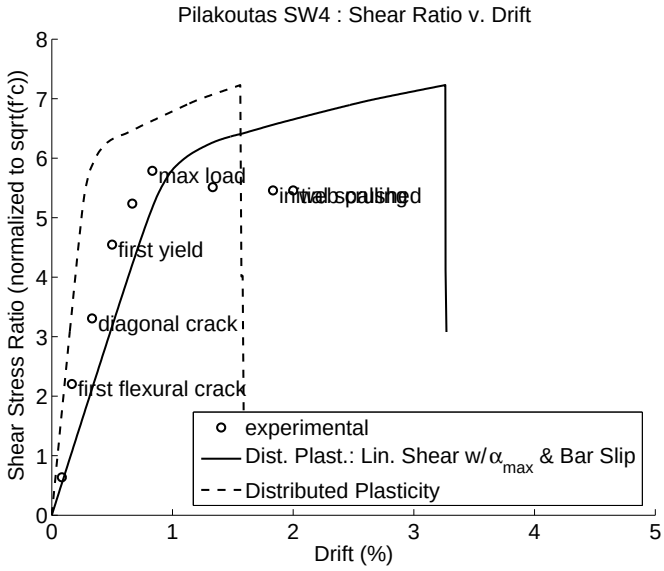

Figure M.270: Pushover of Beam-Column Element with Bar-Slip and Elastic Shear Calibrated to Maximum Displacement – Pilakoutas SW4

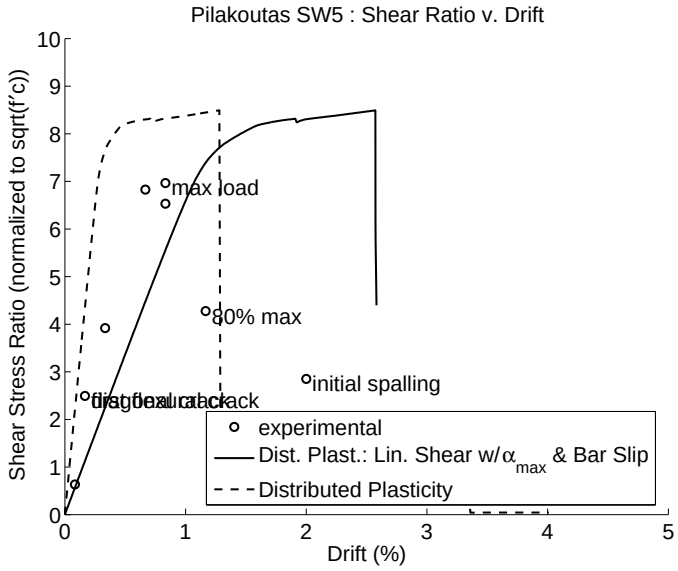

Figure M.271: Pushover of Beam-Column Element with Bar-Slip and Elastic Shear Calibrated to Maximum Displacement – Pilakoutas SW5

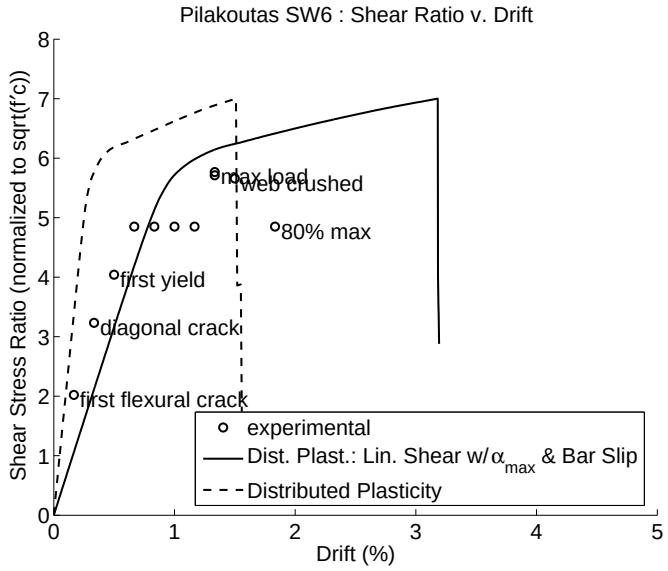

Figure M.272: Pushover of Beam-Column Element with Bar-Slip and Elastic Shear Calibrated to Maximum Displacement – Pilakoutas SW6

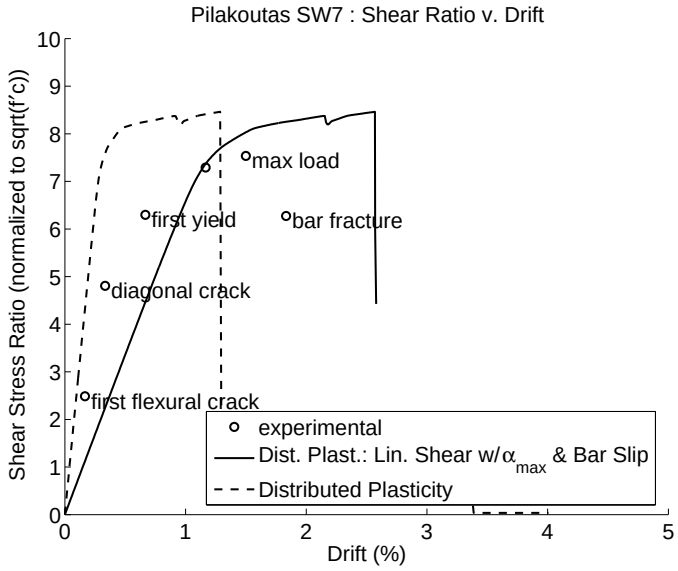

Figure M.273: Pushover of Beam-Column Element with Bar-Slip and Elastic Shear Calibrated to Maximum Displacement – Pilakoutas SW7

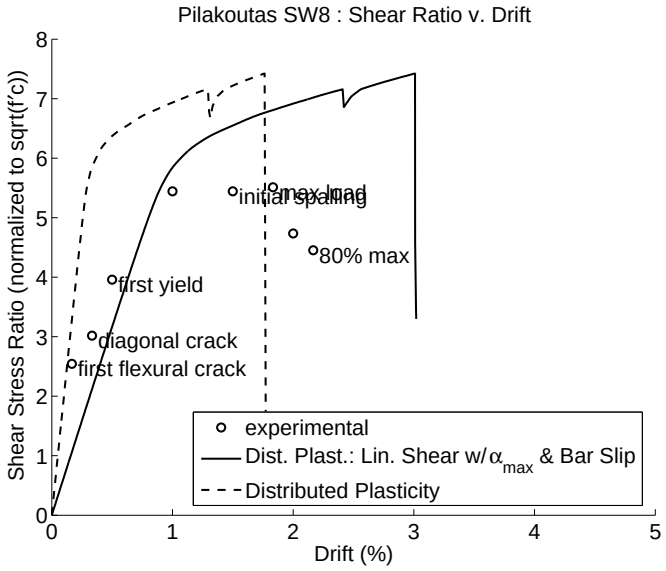

Figure M.274: Pushover of Beam-Column Element with Bar-Slip and Elastic Shear Calibrated to Maximum Displacement – Pilakoutas SW8

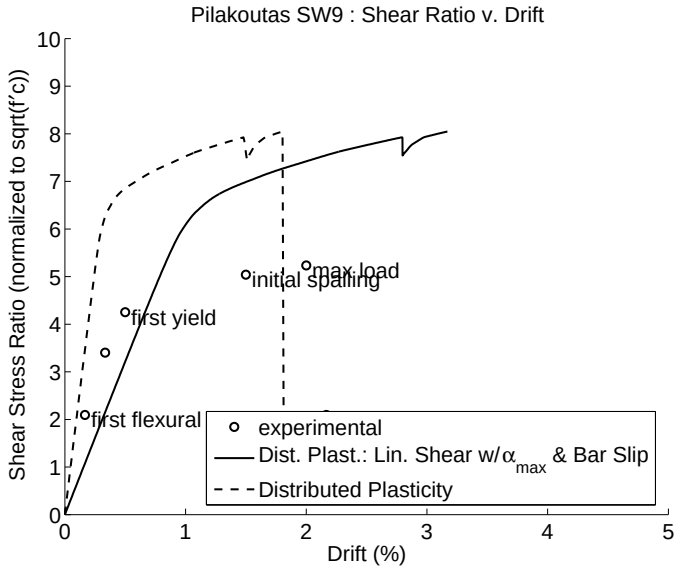

Figure M.275: Pushover of Beam-Column Element with Bar-Slip and Elastic Shear Calibrated to Maximum Displacement – Pilakoutas SW9

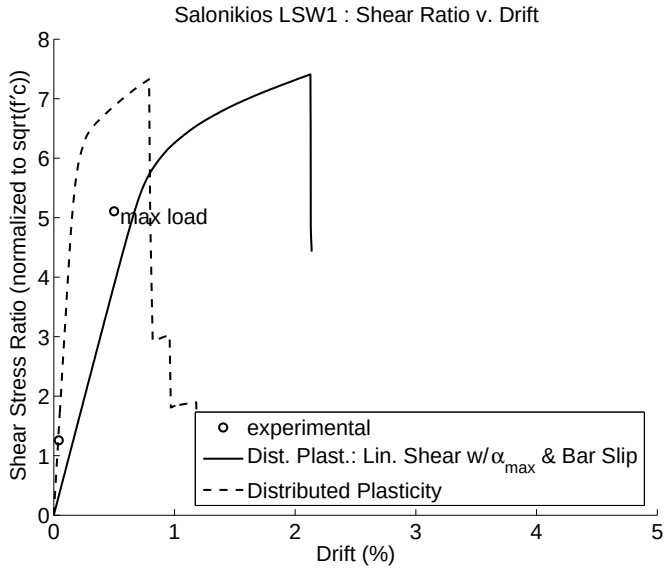

Figure M.276: Pushover of Beam-Column Element with Bar-Slip and Elastic Shear Calibrated to Maximum Displacement – Salonikios LSW1

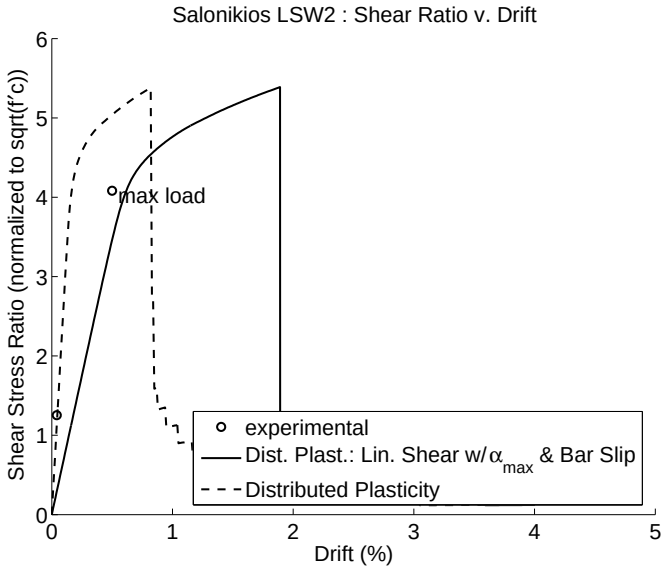

Figure M.277: Pushover of Beam-Column Element with Bar-Slip and Elastic Shear Calibrated to Maximum Displacement – Salonikios LSW2

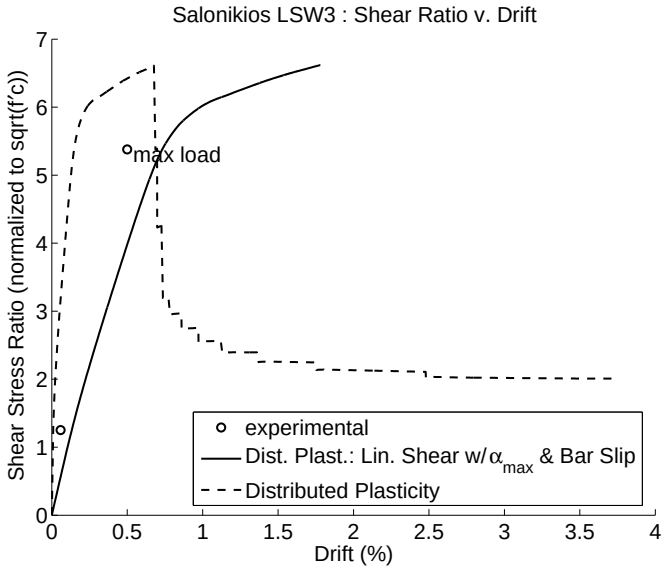

Figure M.278: Pushover of Beam-Column Element with Bar-Slip and Elastic Shear Calibrated to Maximum Displacement – Salonikios LSW3

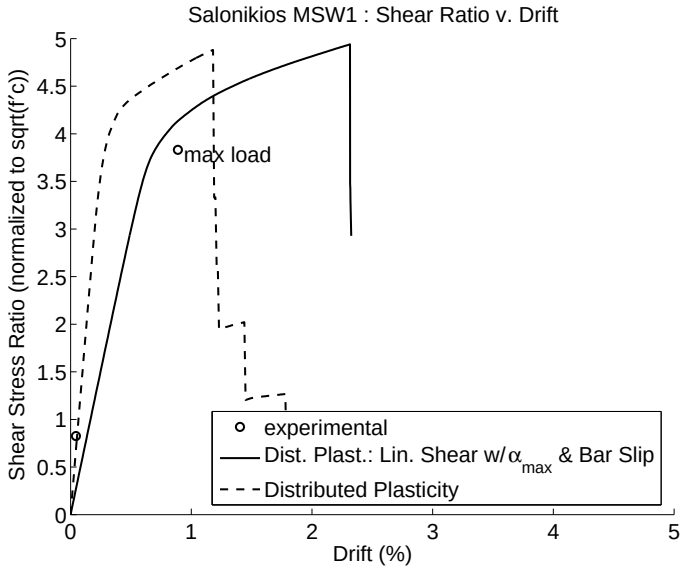

Figure M.279: Pushover of Beam-Column Element with Bar-Slip and Elastic Shear Calibrated to Maximum Displacement – Salonikios MSW1

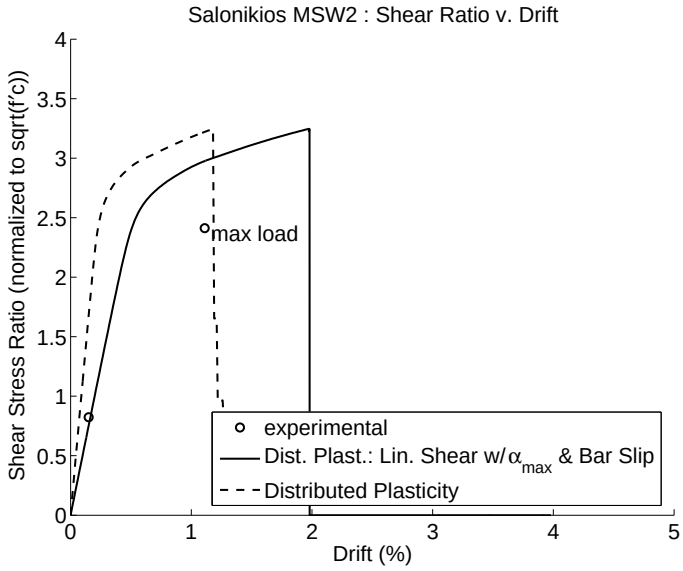

Figure M.280: Pushover of Beam-Column Element with Bar-Slip and Elastic Shear Calibrated to Maximum Displacement – Salonikios MSW2

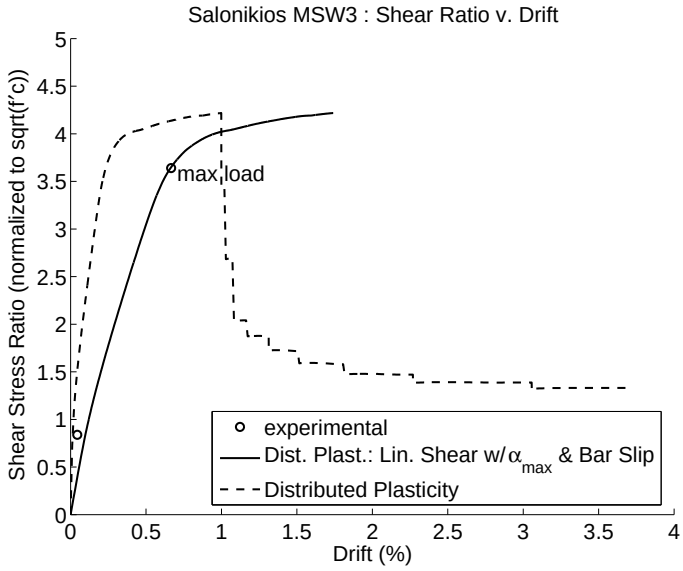

Figure M.281: Pushover of Beam-Column Element with Bar-Slip and Elastic Shear Calibrated to Maximum Displacement – Salonikios MSW3

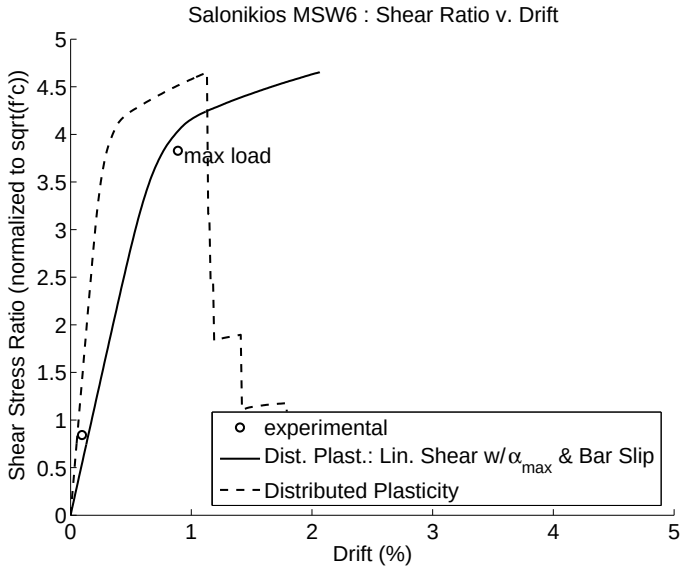

Figure M.282: Pushover of Beam-Column Element with Bar-Slip and Elastic Shear Calibrated to Maximum Displacement – Salonikios MSW6

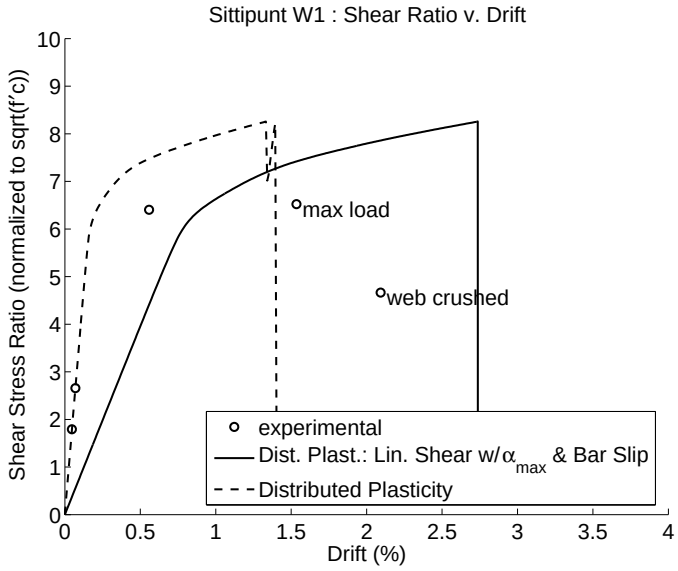

Figure M.283: Pushover of Beam-Column Element with Bar-Slip and Elastic Shear Calibrated to Maximum Displacement – Sittipunt W1

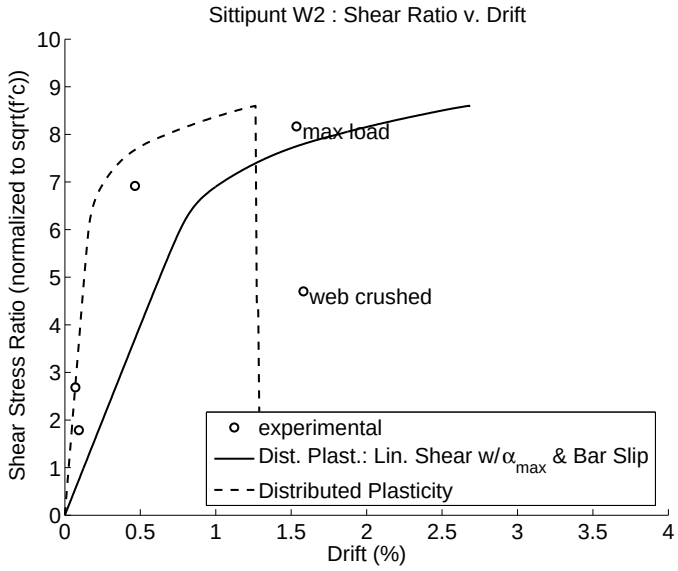

Figure M.284: Pushover of Beam-Column Element with Bar-Slip and Elastic Shear Calibrated to Maximum Displacement – Sittipunt W2

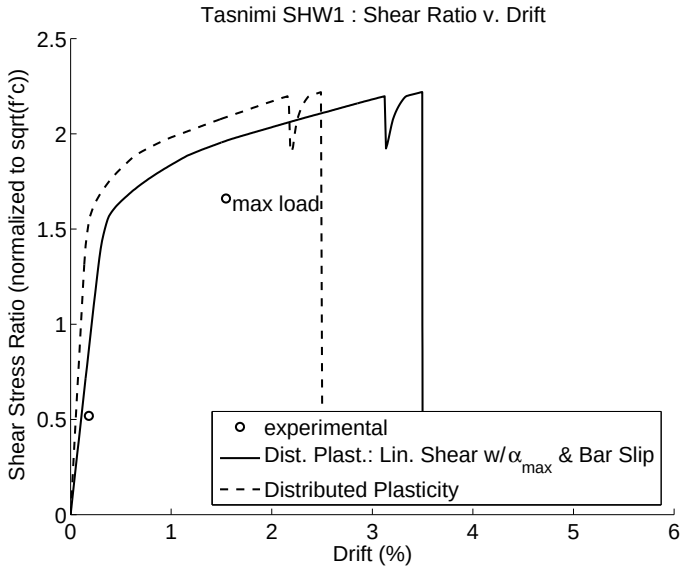

Figure M.285: Pushover of Beam-Column Element with Bar-Slip and Elastic Shear Calibrated to Maximum Displacement – Tasnimi SHW1

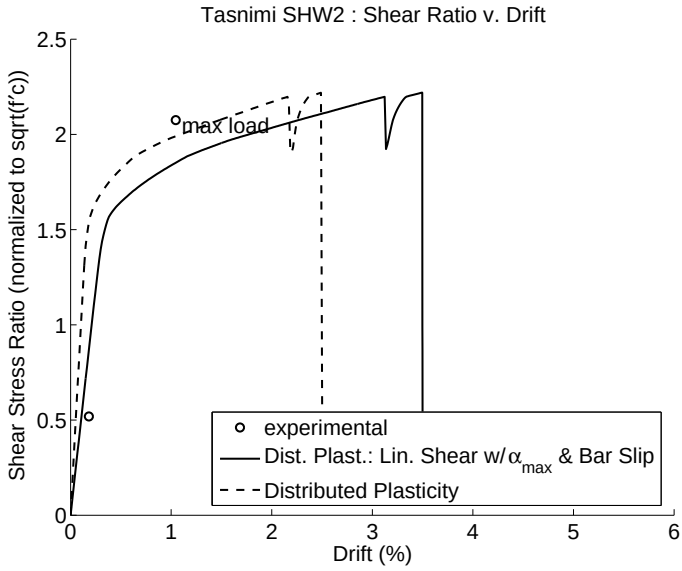

Figure M.286: Pushover of Beam-Column Element with Bar-Slip and Elastic Shear Calibrated to Maximum Displacement – Tasnimi SHW2

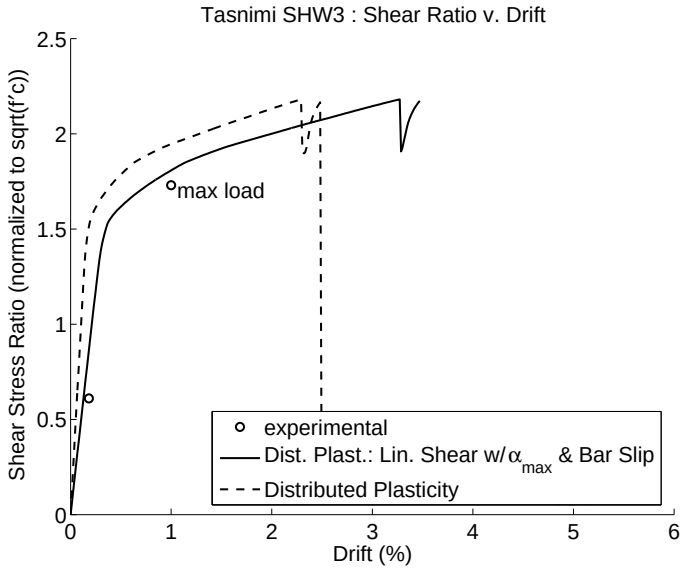

Figure M.287: Pushover of Beam-Column Element with Bar-Slip and Elastic Shear Calibrated to Maximum Displacement – Tasnimi SHW3

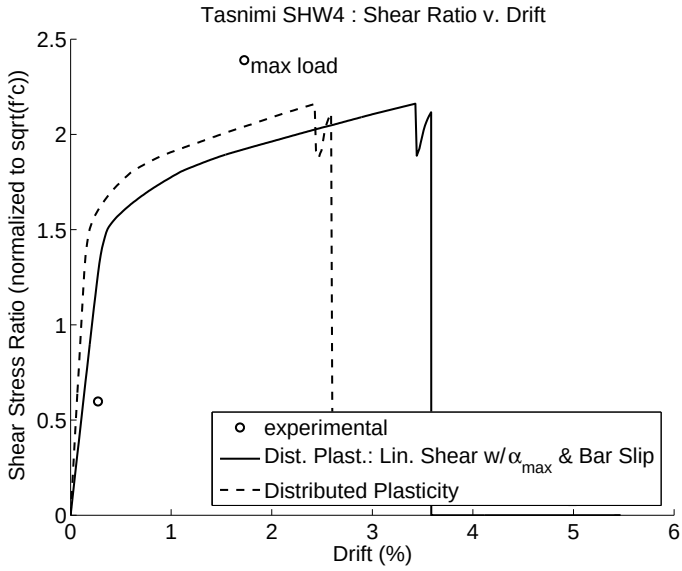

Figure M.288: Pushover of Beam-Column Element with Bar-Slip and Elastic Shear Calibrated to Maximum Displacement – Tasnimi SHW4

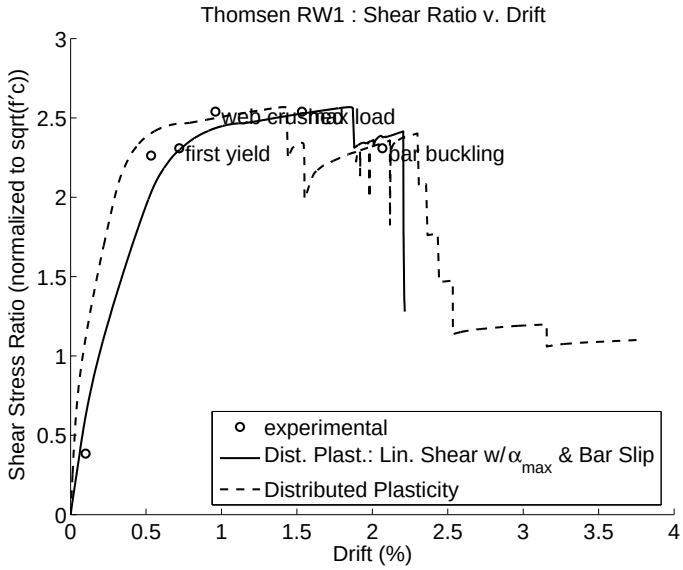

Figure M.289: Pushover of Beam-Column Element with Bar-Slip and Elastic Shear Calibrated to Maximum Displacement – Thomsen RW1

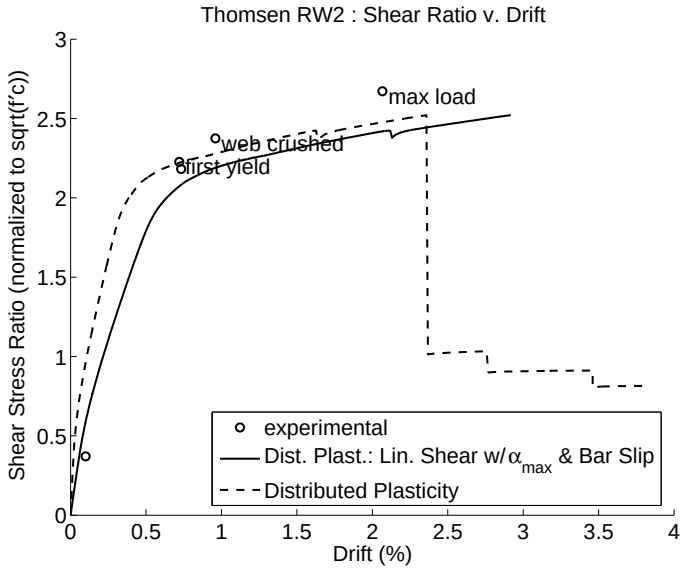

Figure M.290: Pushover of Beam-Column Element with Bar-Slip and Elastic Shear Calibrated to Maximum Displacement – Thomsen RW2

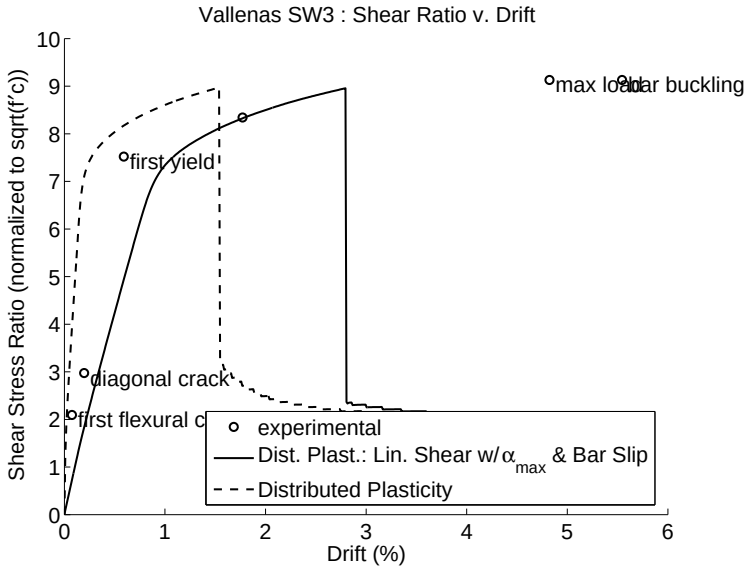

Figure M.291: Pushover of Beam-Column Element with Bar-Slip and Elastic Shear Calibrated to Maximum Displacement – Vallenas SW3

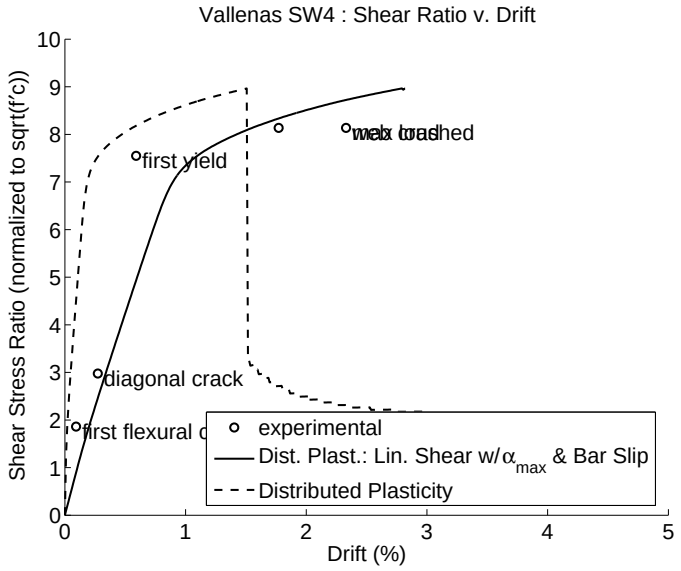

Figure M.292: Pushover of Beam-Column Element with Bar-Slip and Elastic Shear Calibrated to Maximum Displacement – Vallenas SW4

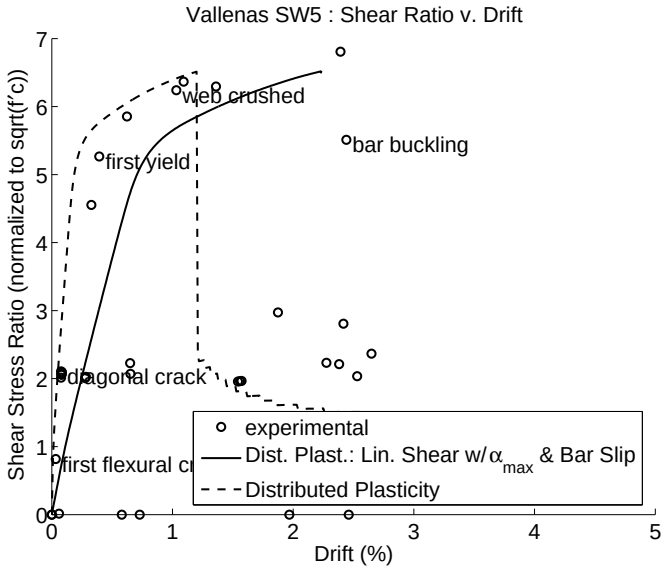

Figure M.293: Pushover of Beam-Column Element with Bar-Slip and Elastic Shear Calibrated to Maximum Displacement – Vallenas SW5

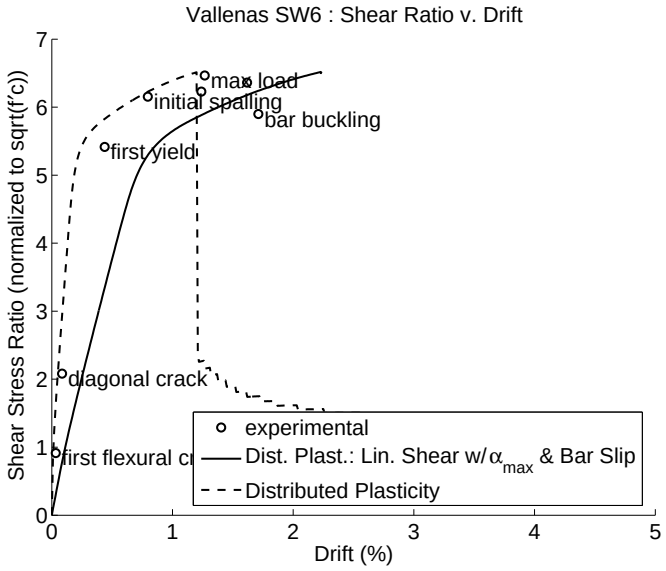

Figure M.294: Pushover of Beam-Column Element with Bar-Slip and Elastic Shear Calibrated to Maximum Displacement – Vallenas SW6

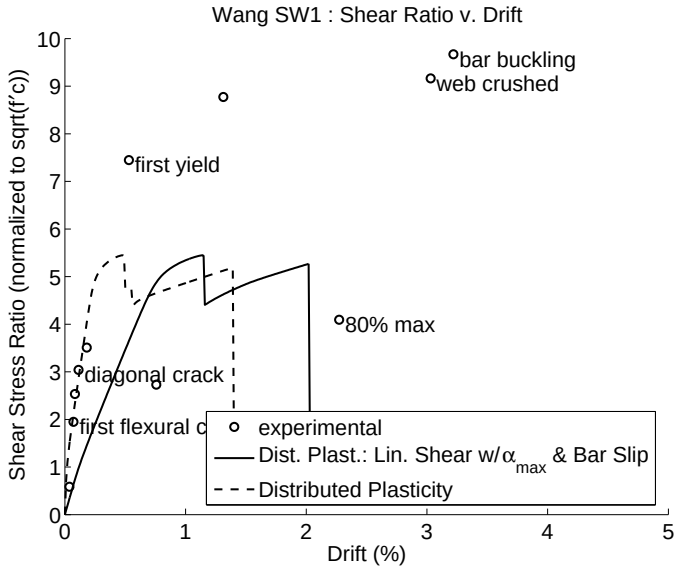

Figure M.295: Pushover of Beam-Column Element with Bar-Slip and Elastic Shear Calibrated to Maximum Displacement – Wang SW1

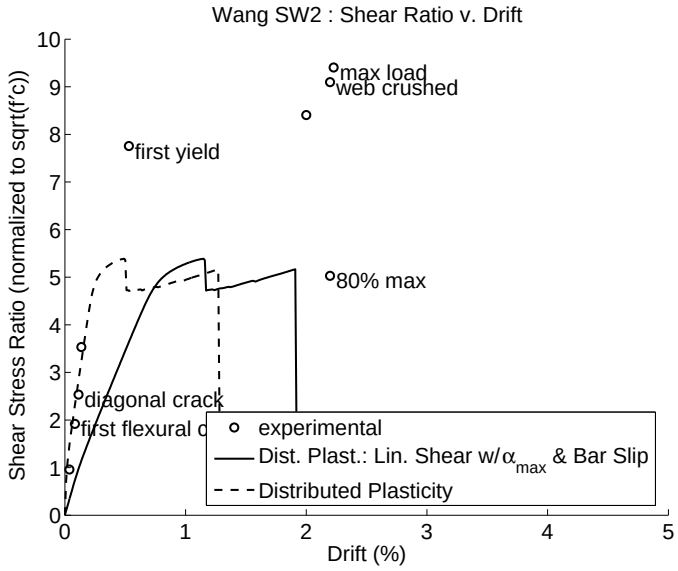

Figure M.296: Pushover of Beam-Column Element with Bar-Slip and Elastic Shear Calibrated to Maximum Displacement – Wang SW2

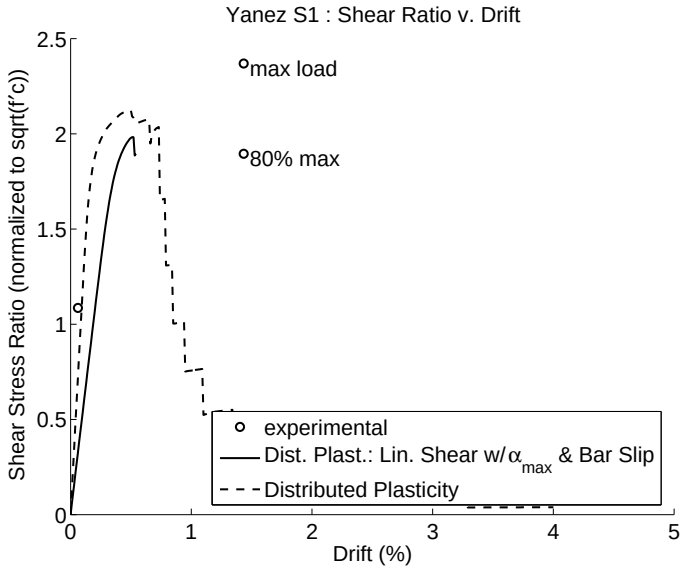

Figure M.297: Pushover of Beam-Column Element with Bar-Slip and Elastic Shear Calibrated to Maximum Displacement – Yanez S1

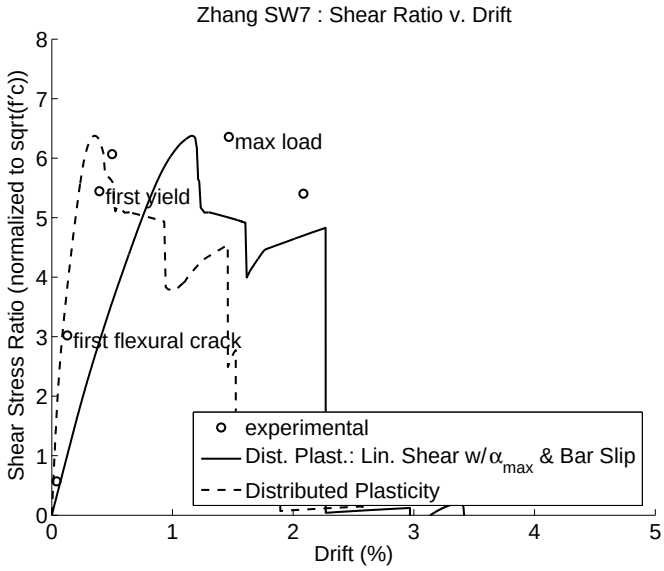

Figure M.298: Pushover of Beam-Column Element with Bar-Slip and Elastic Shear Calibrated to Maximum Displacement – Zhang SW7

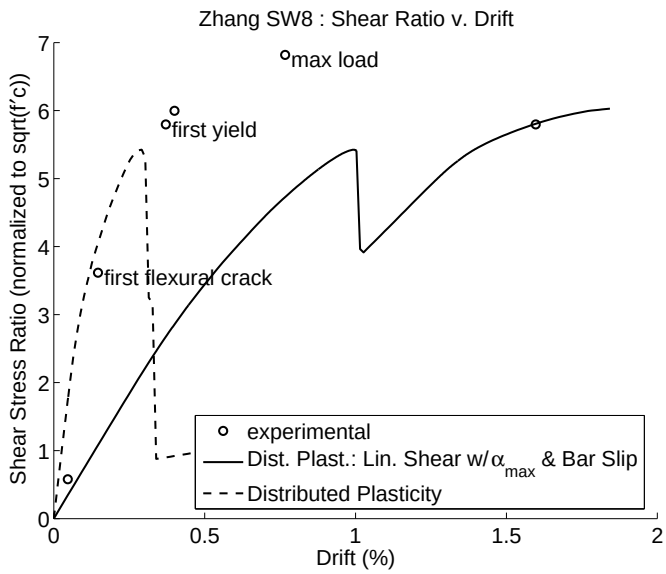

Figure M.299: Pushover of Beam-Column Element with Bar-Slip and Elastic Shear Calibrated to Maximum Displacement – Zhang SW8

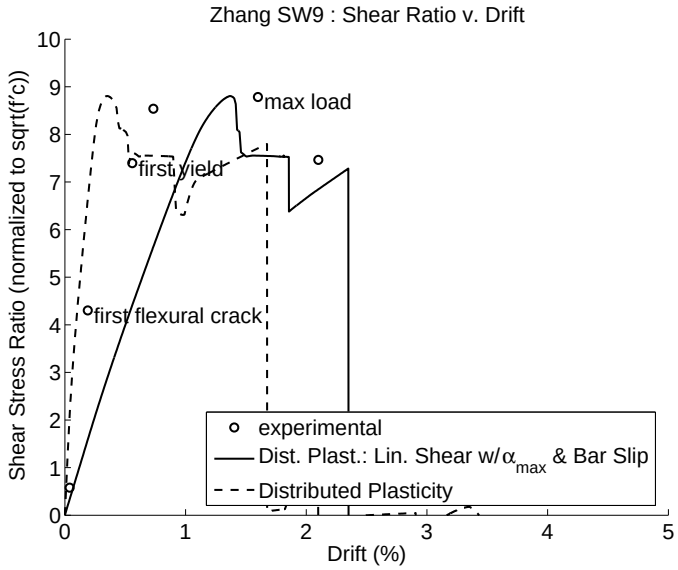

Figure M.300: Pushover of Beam-Column Element with Bar-Slip and Elastic Shear Calibrated to Maximum Displacement – Zhang SW9

Appendix N

EFFECTIVE SHEAR MODEL PREDICTION ERROR CHANGE COMPARED TO DESIGN PARAMETER FIGURES

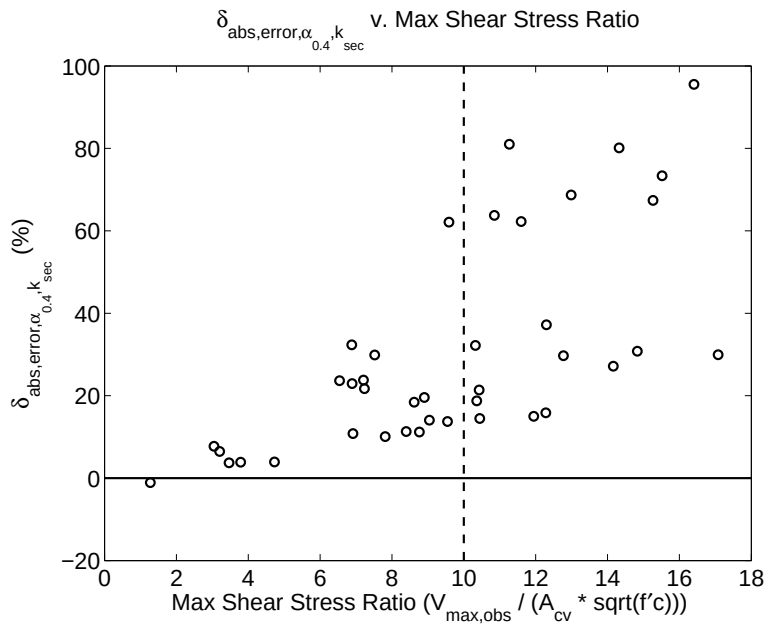

Figure N.1: Elastic Shear Secant Stiffness Absolute Error Change v. Max Shear Stress Ratio

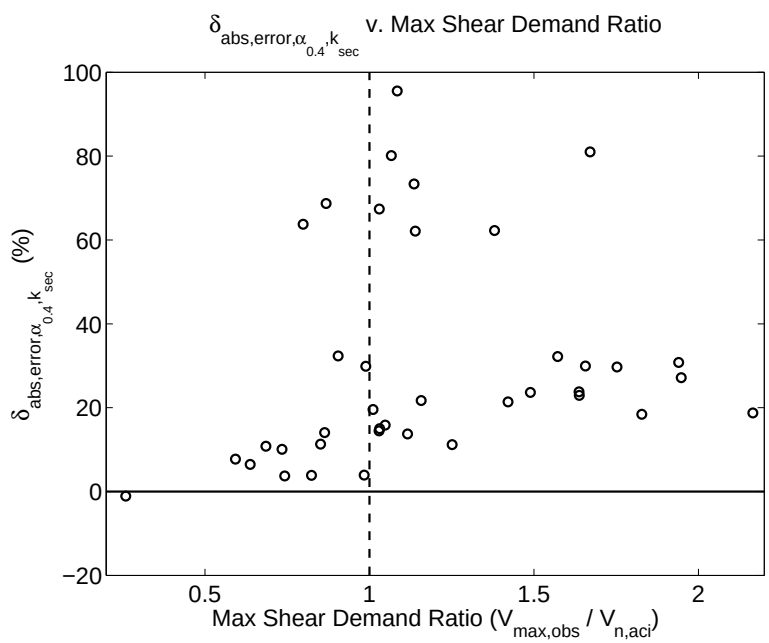

Figure N.2: Elastic Shear Secant Stiffness Absolute Error Change v. Max Shear Demand Ratio

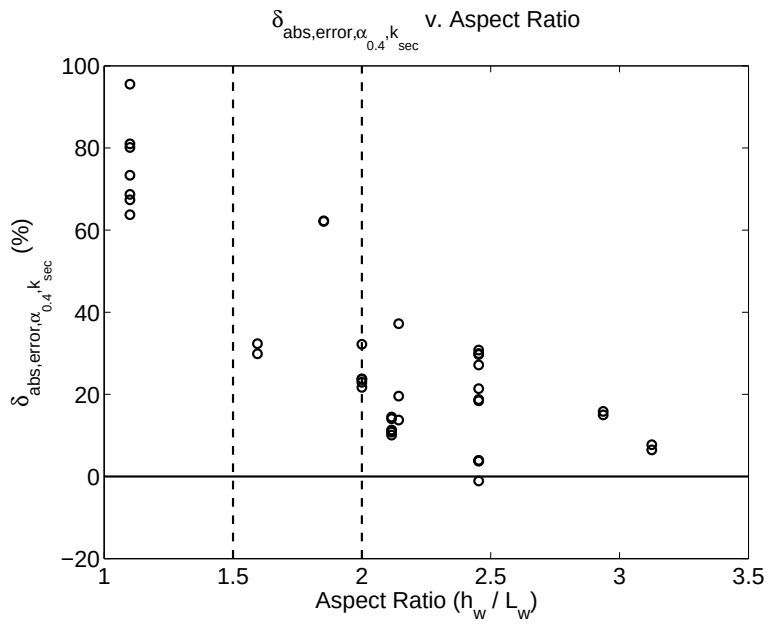

Figure N.3: Elastic Shear Secant Stiffness Absolute Error Change v. Aspect Ratio

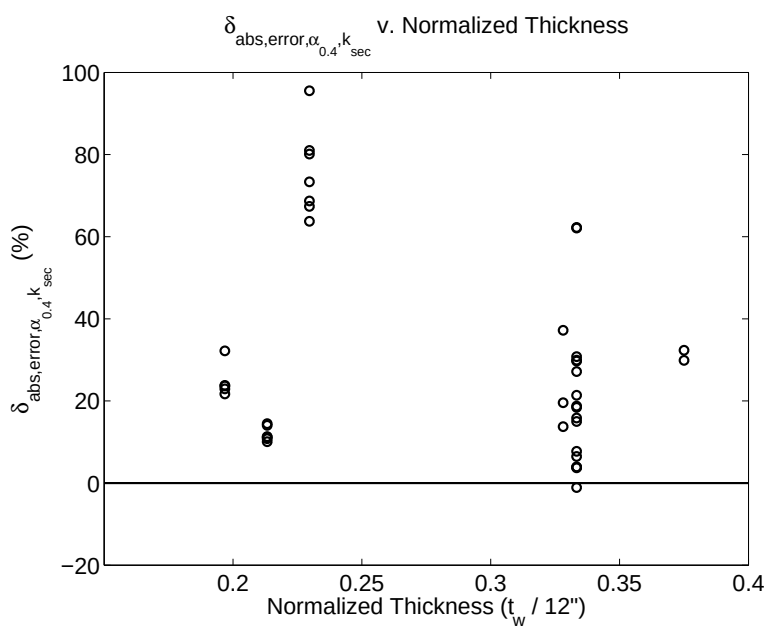

Figure N.4: Elastic Shear Secant Stiffness Absolute Error Change v. Normalized Thickness

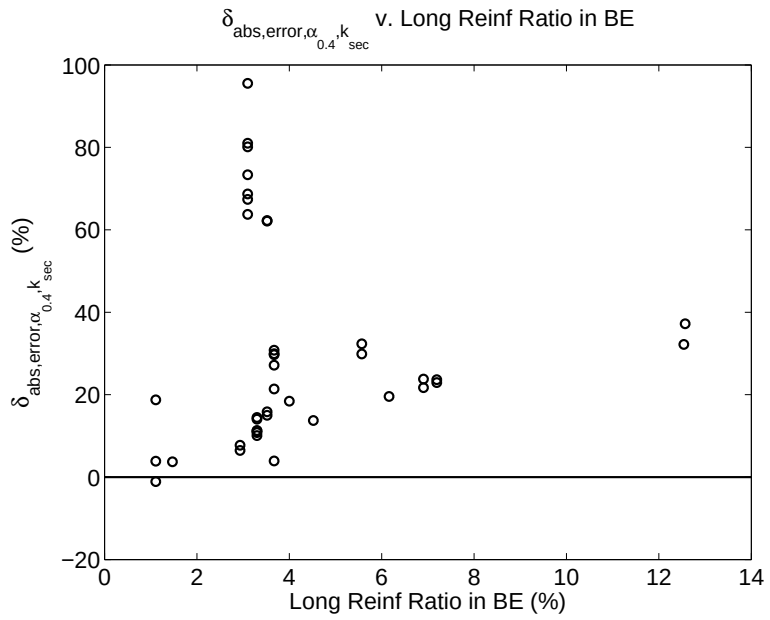

Figure N.5: Elastic Shear Secant Stiffness Absolute Error Change v. Long Reinf Ratio in BE

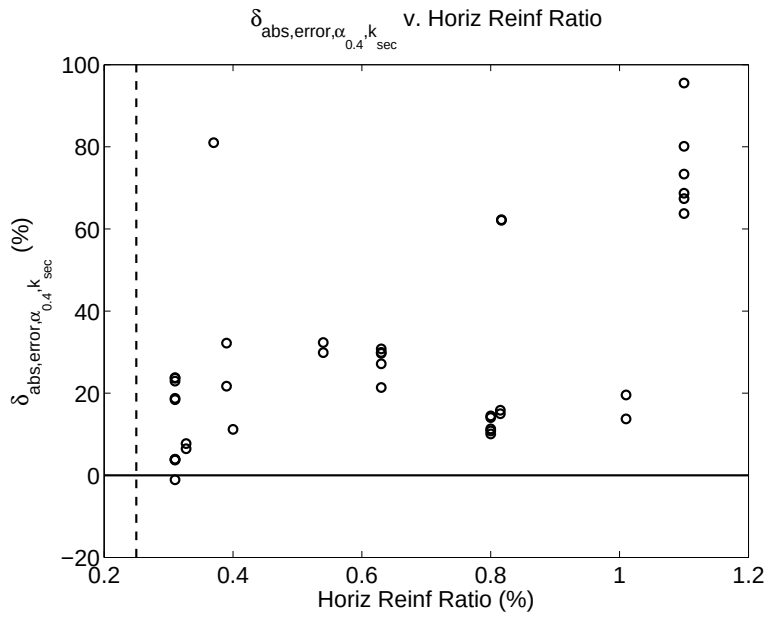

Figure N.6: Elastic Shear Secant Stiffness Absolute Error Change v. Horiz Reinf Ratio

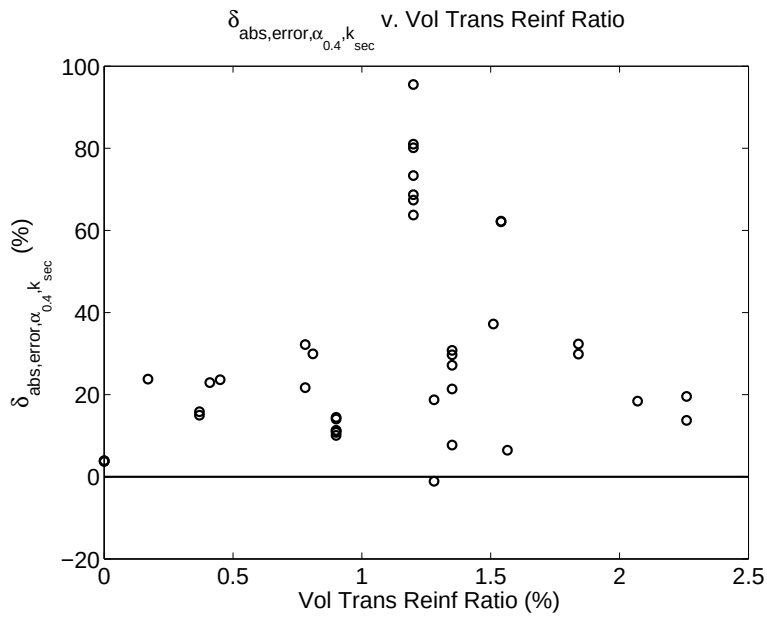

Figure N.7: Elastic Shear Secant Stiffness Absolute Error Change v. Vol Trans Reinf Ratio

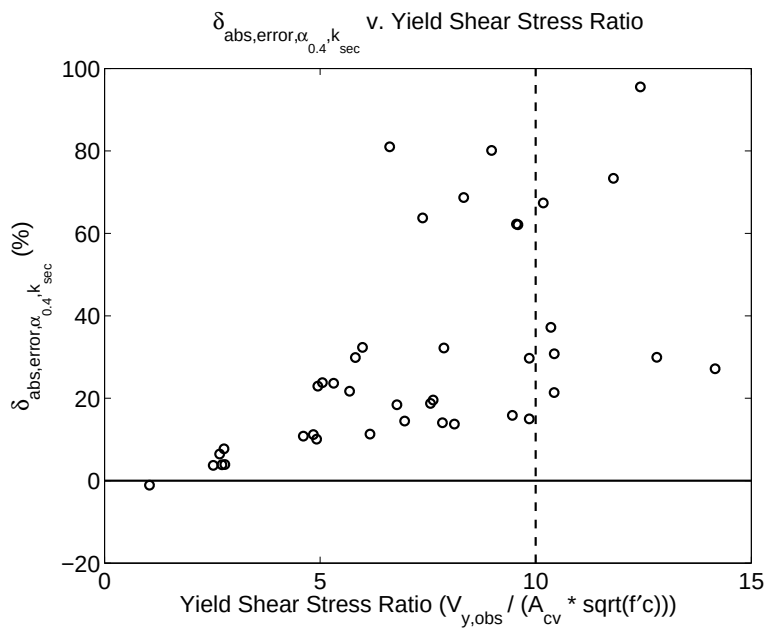

Figure N.8: Elastic Shear Secant Stiffness Absolute Error Change v. Yield Shear Stress Ratio

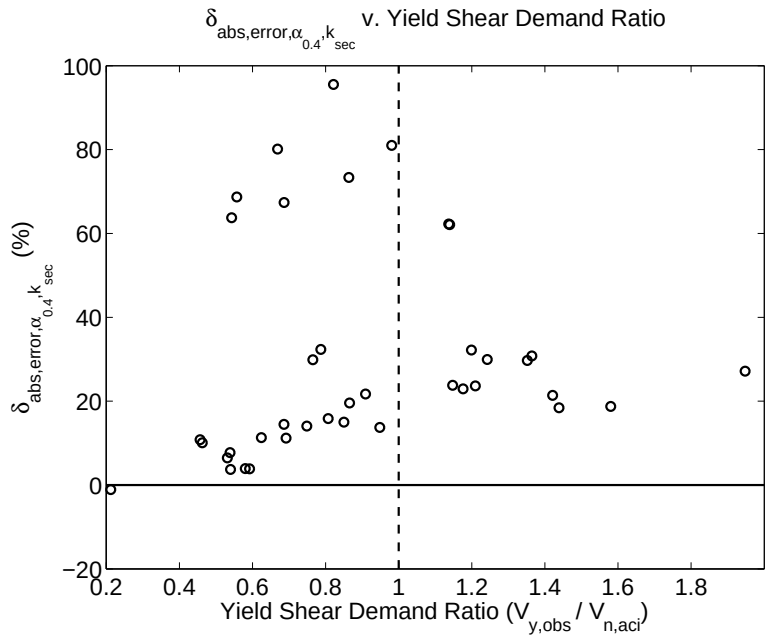

Figure N.9: Elastic Shear Secant Stiffness Absolute Error Change v. Yield Shear Demand Ratio

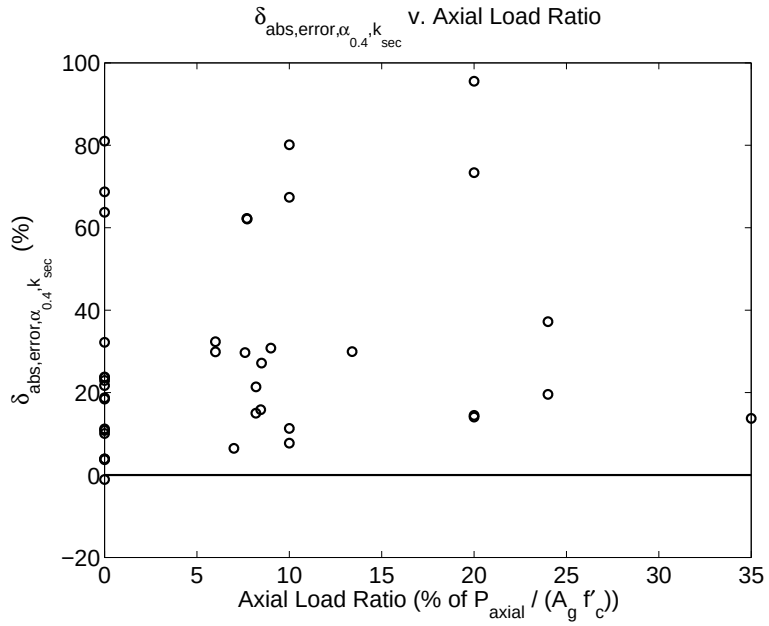

Figure N.10: Elastic Shear Secant Stiffness Absolute Error Change v. Axial Load Ratio

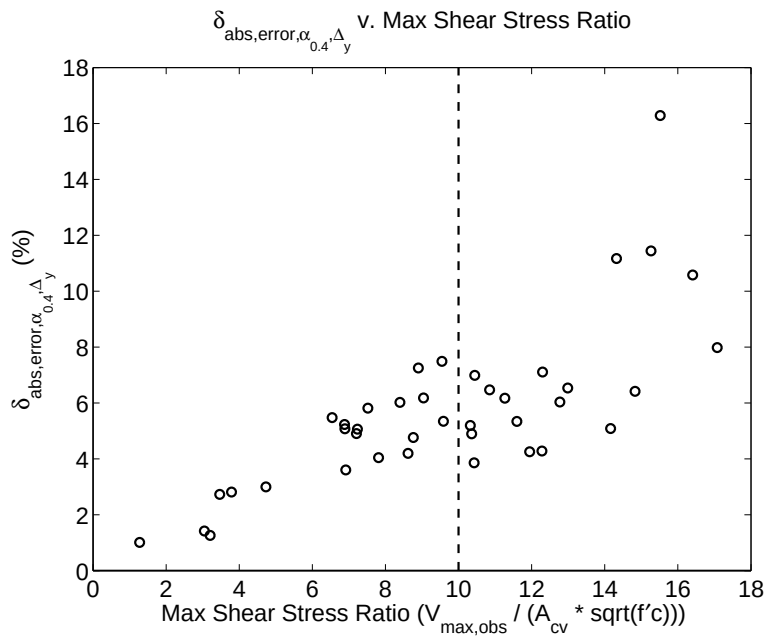

Figure N.11: Elastic Shear Yield Displacement Absolute Error Change v. Max Shear Stress Ratio

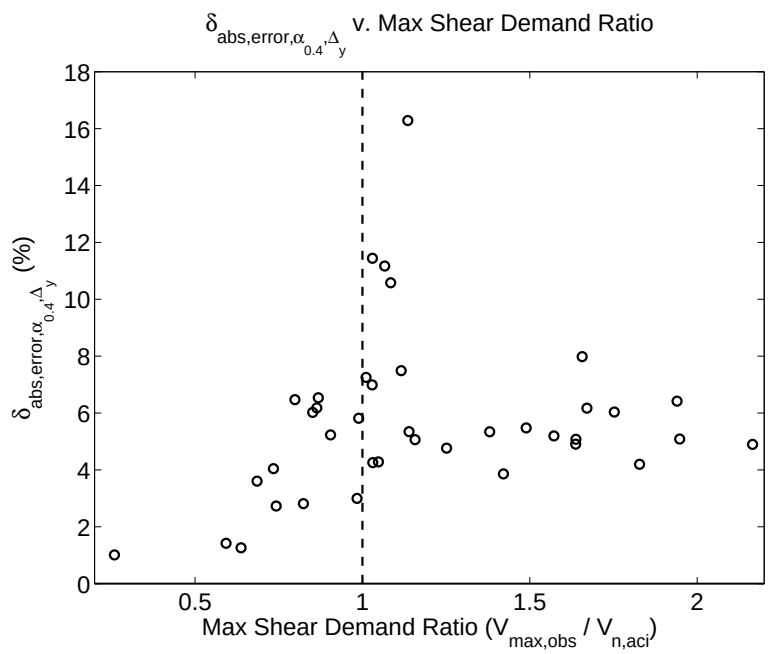

Figure N.12: Elastic Shear Yield Displacement Absolute Error Change v. Max Shear Demand Ratio

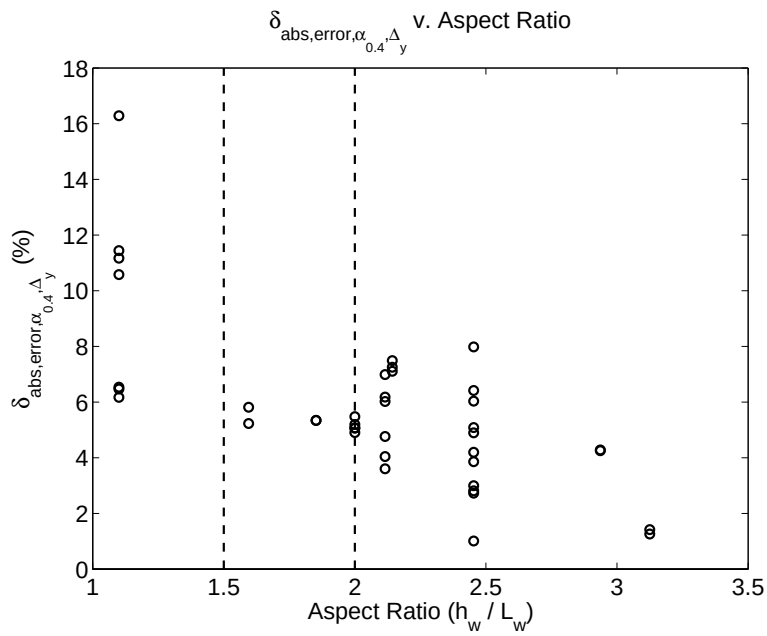

Figure N.13: Elastic Shear Yield Displacement Absolute Error Change v. Aspect Ratio

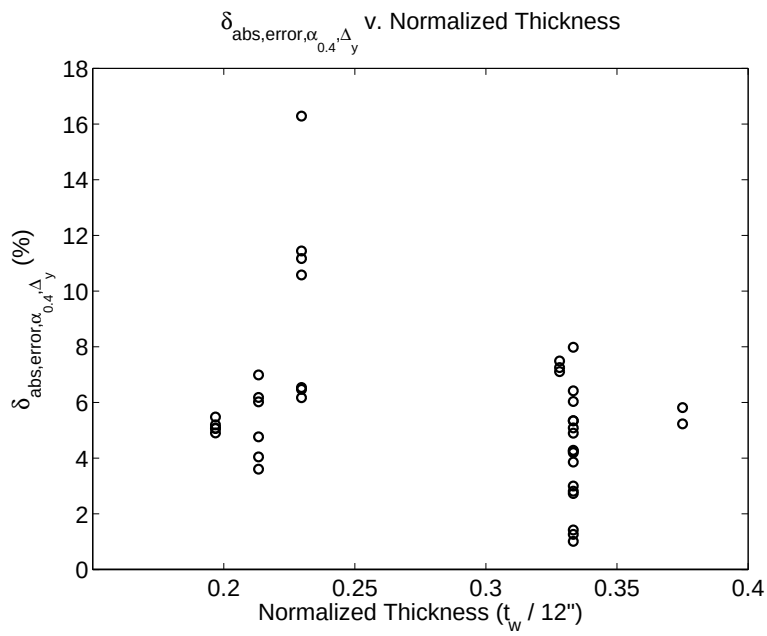

Figure N.14: Elastic Shear Yield Displacement Absolute Error Change v. Normalized Thickness

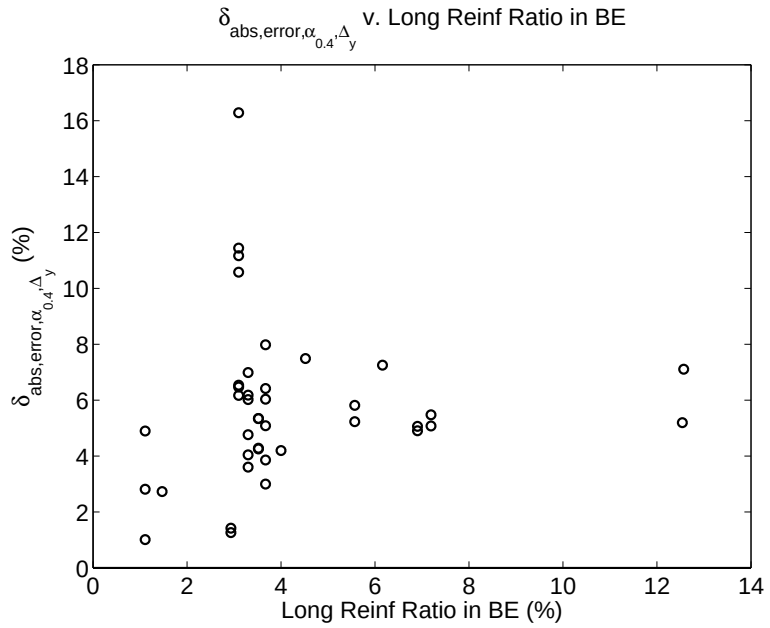

Figure N.15: Elastic Shear Yield Displacement Absolute Error Change v. Long Reinf Ratio in BE

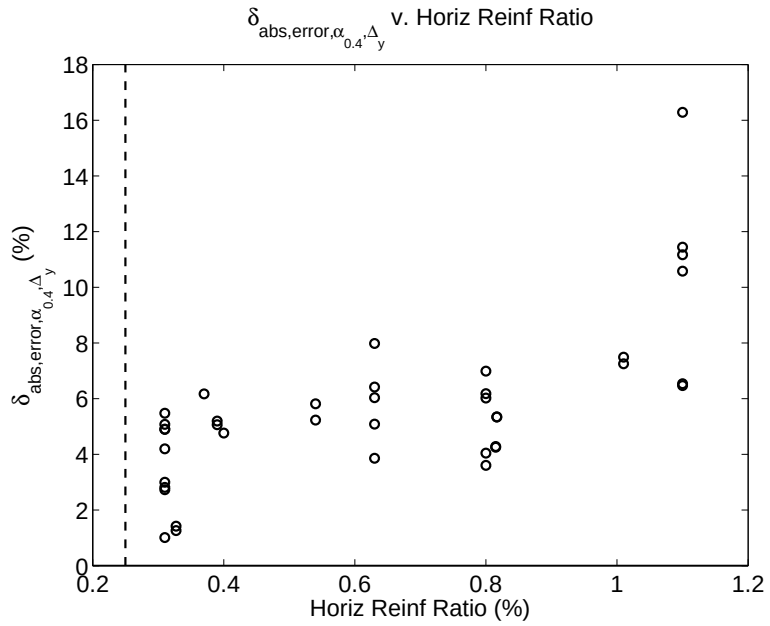

Figure N.16: Elastic Shear Yield Displacement Absolute Error Change v. Horiz Reinf Ratio

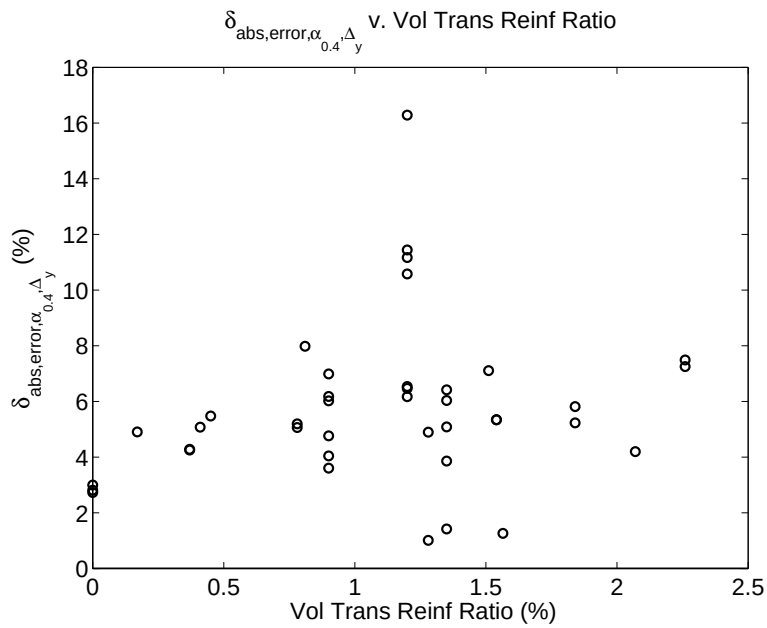

Figure N.17: Elastic Shear Yield Displacement Absolute Error Change v. Vol Trans Reinf Ratio

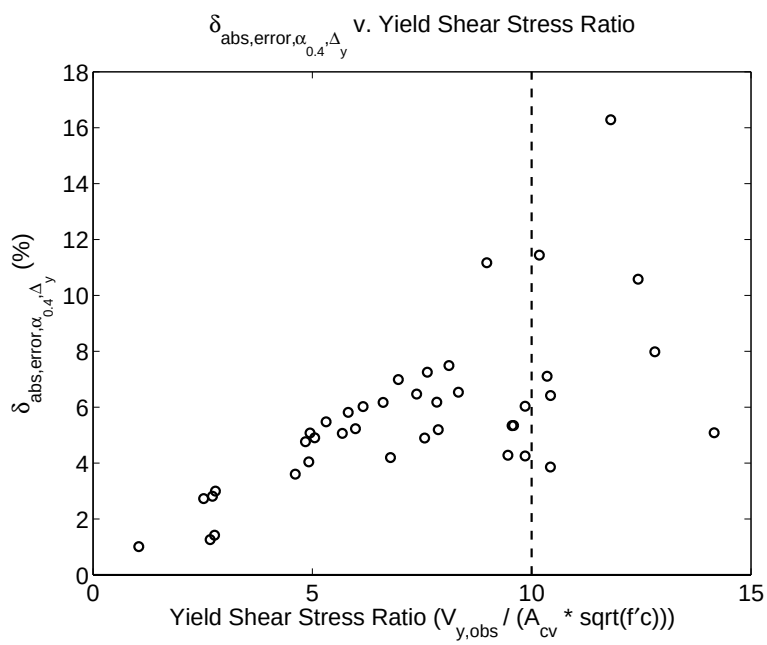

Figure N.18: Elastic Shear Yield Displacement Absolute Error Change v. Yield Shear Stress Ratio

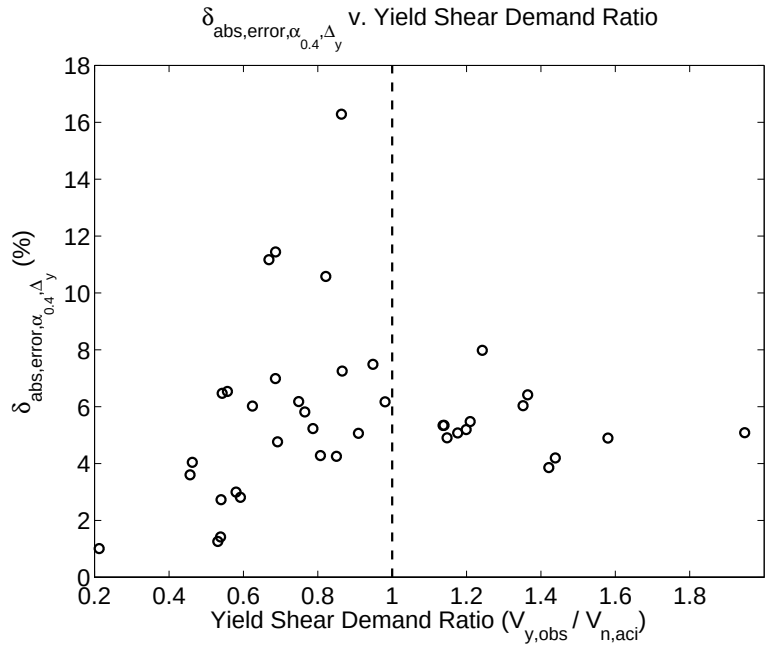

Figure N.19: Elastic Shear Yield Displacement Absolute Error Change v. Yield Shear Demand Ratio

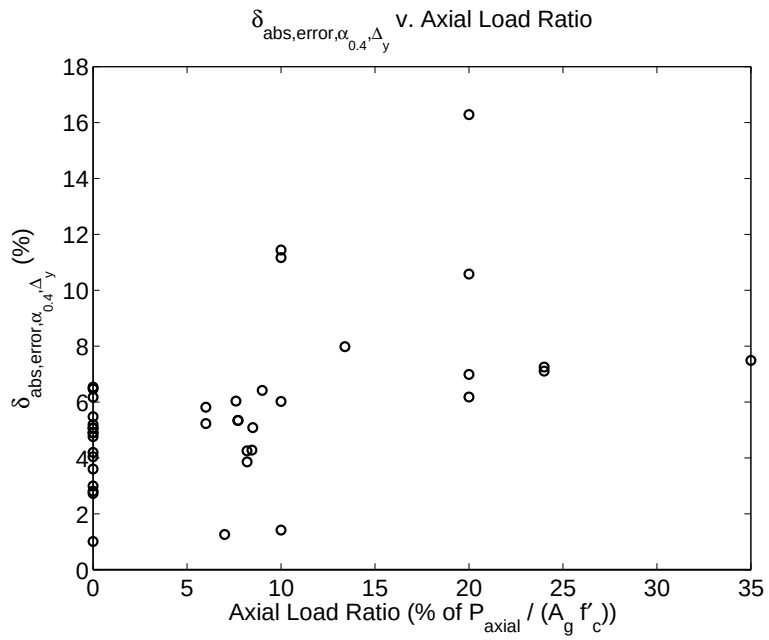

Figure N.20: Elastic Shear Yield Displacement Absolute Error Change v. Axial Load Ratio

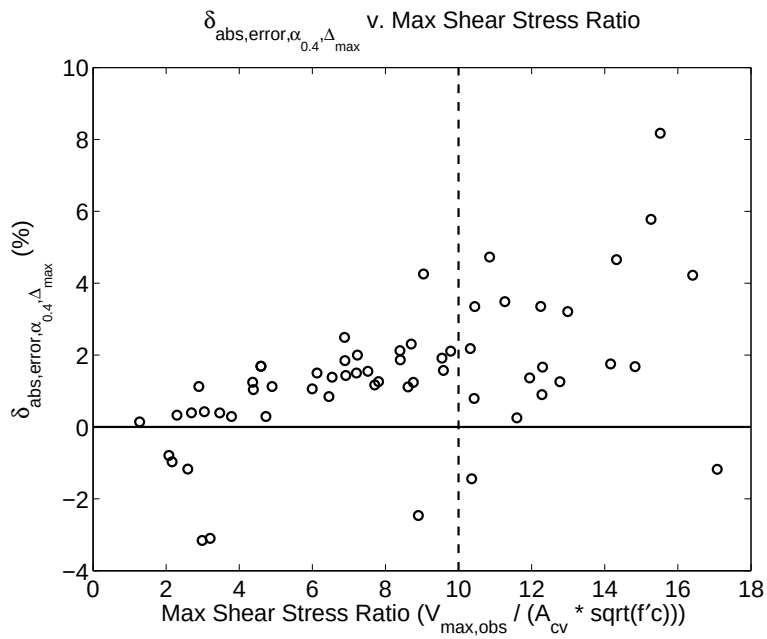

Figure N.21: Elastic Shear Max Displacement Absolute Error Change v. Max Shear Stress Ratio

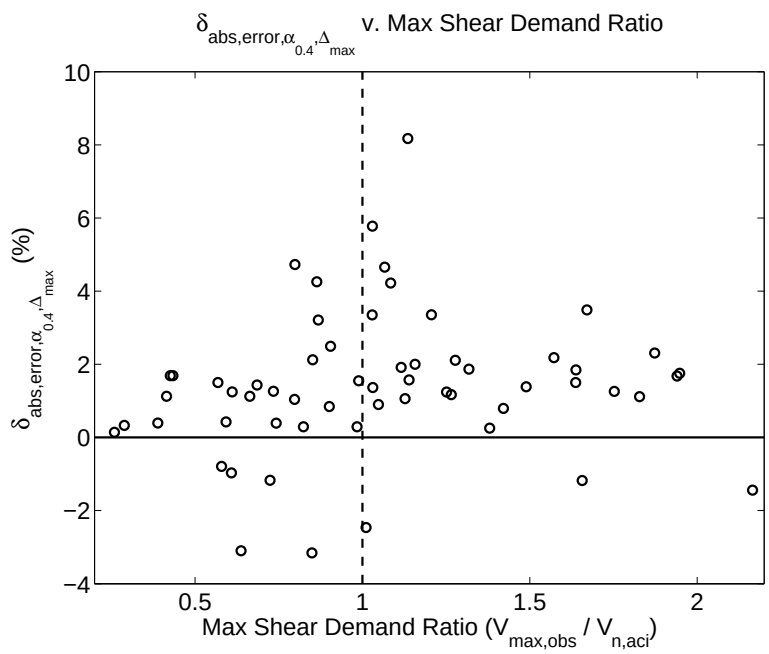

Figure N.22: Elastic Shear Max Displacement Absolute Error Change v. Max Shear Demand Ratio

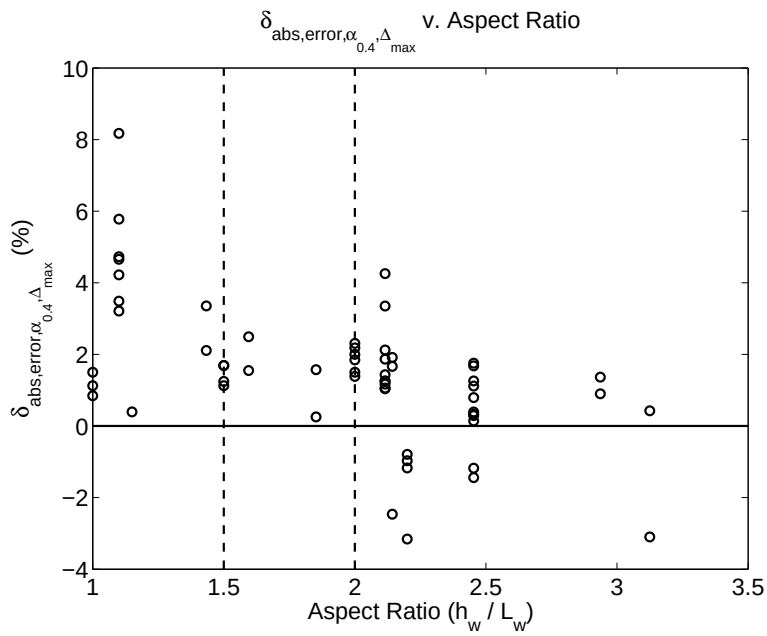

Figure N.23: Elastic Shear Max Displacement Absolute Error Change v. Aspect Ratio

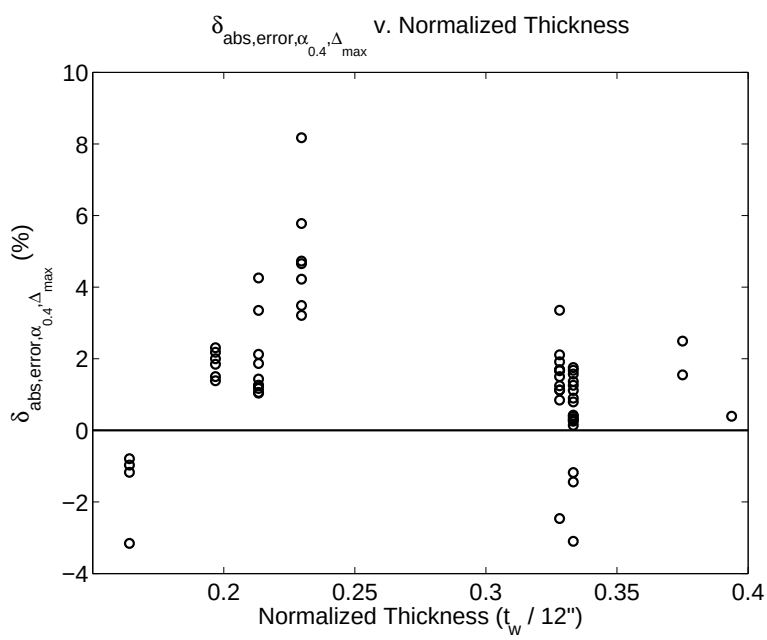

Figure N.24: Elastic Shear Max Displacement Absolute Error Change v. Normalized Thickness

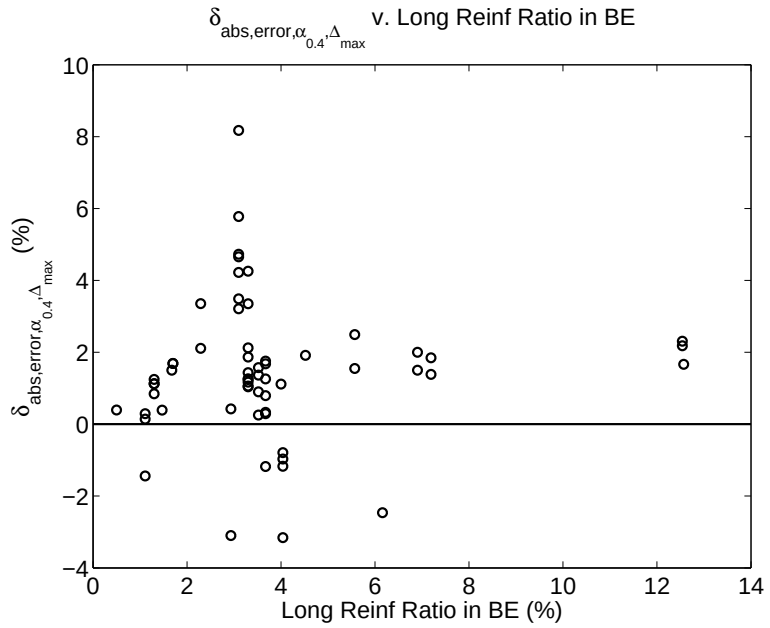

Figure N.25: Elastic Shear Max Displacement Absolute Error Change v. Long Reinf Ratio in BE

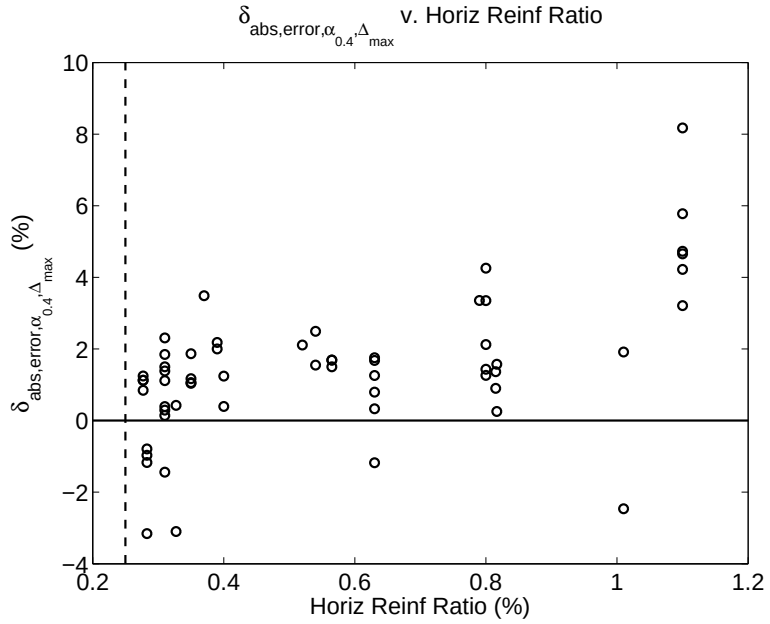

Figure N.26: Elastic Shear Max Displacement Absolute Error Change v. Horiz Reinf Ratio

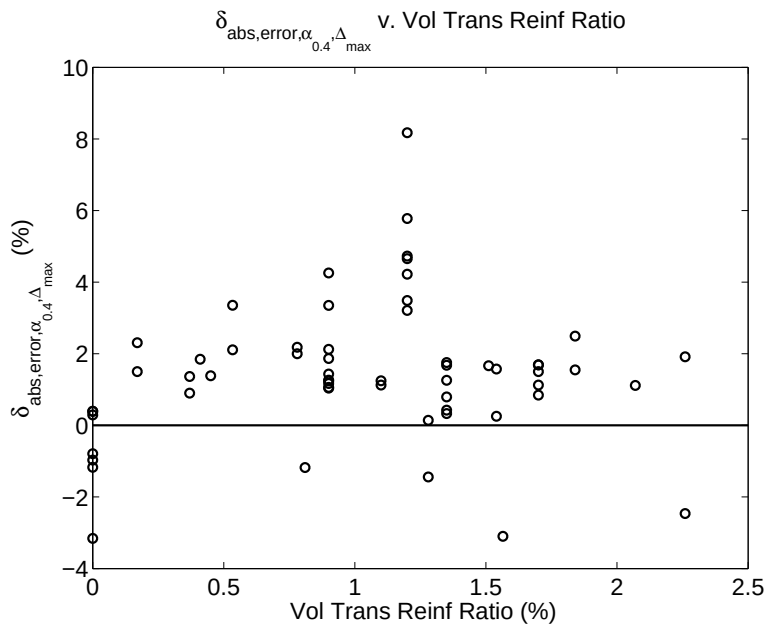

Figure N.27: Elastic Shear Max Displacement Absolute Error Change v. Vol Trans Reinf Ratio

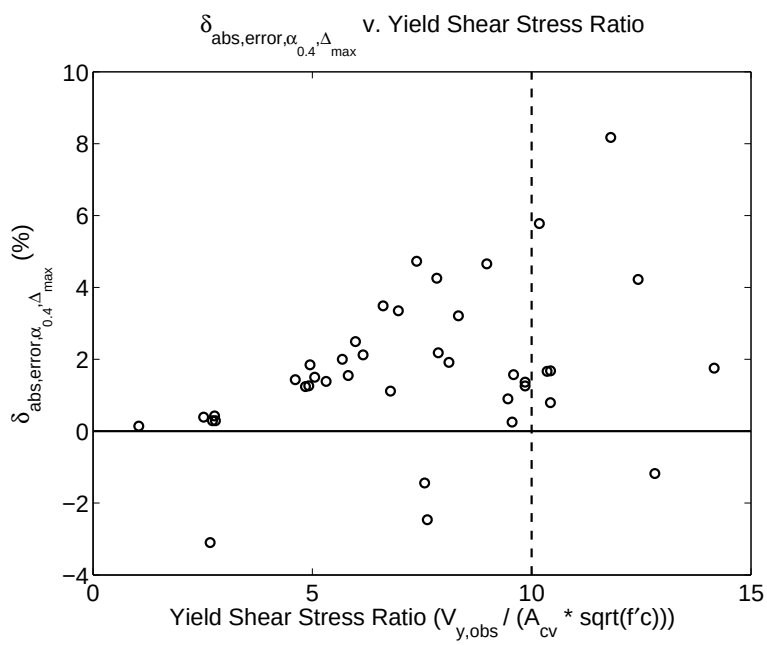

Figure N.28: Elastic Shear Max Displacement Absolute Error Change v. Yield Shear Stress Ratio

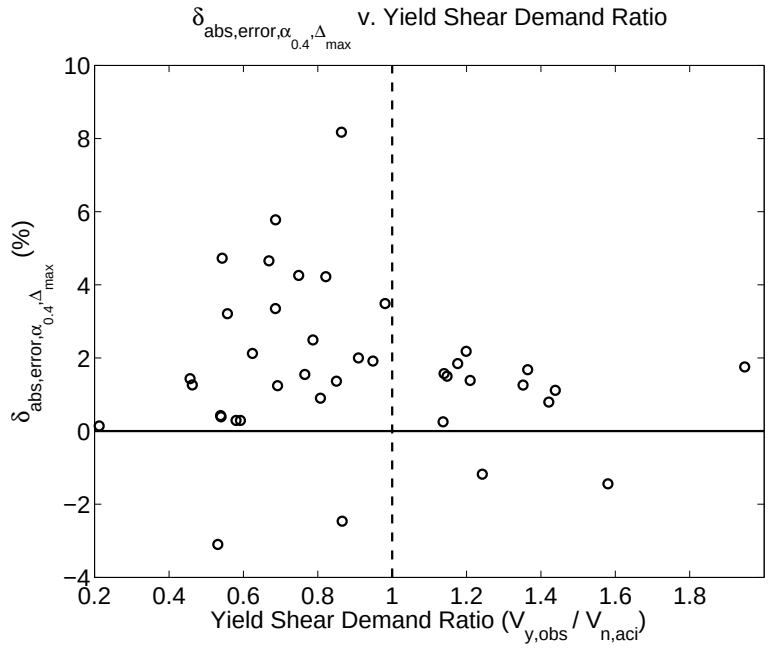

Figure N.29: Elastic Shear Max Displacement Absolute Error Change v. Yield Shear Demand Ratio

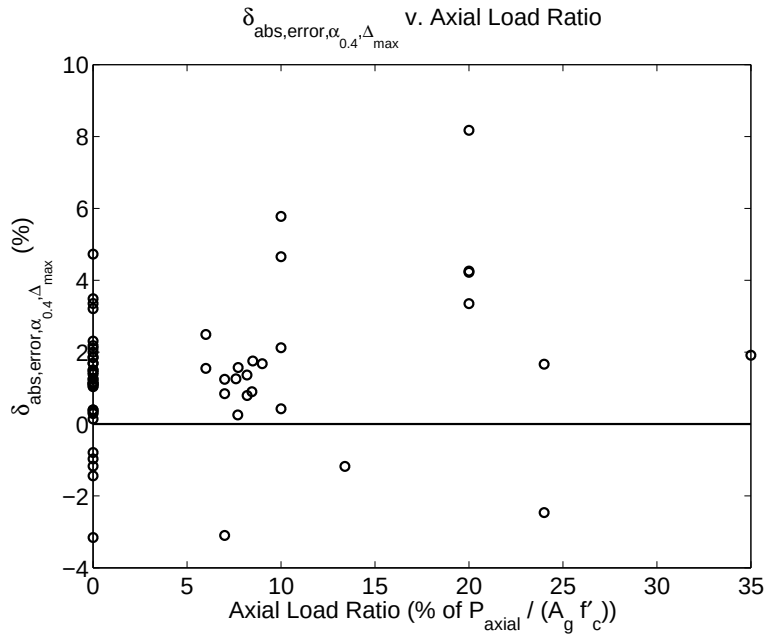

Figure N.30: Elastic Shear Max Displacement Absolute Error Change v. Axial Load Ratio

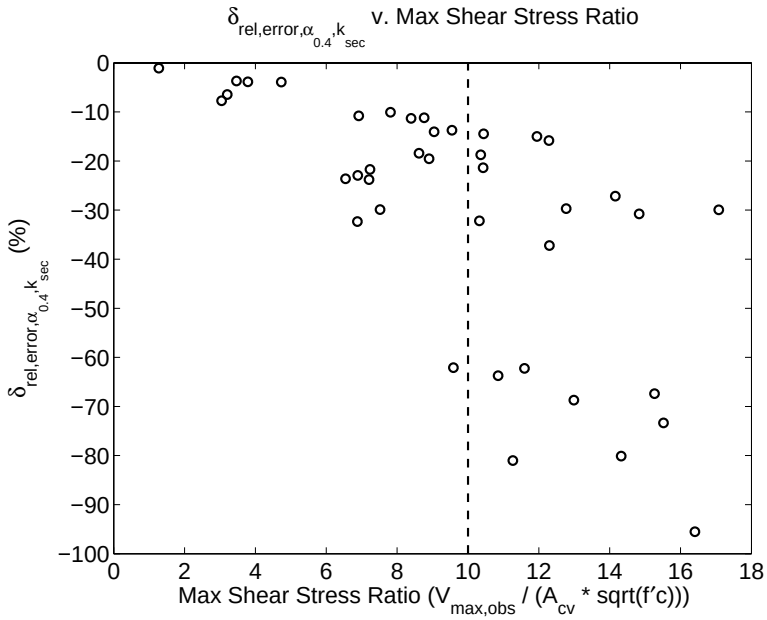

Figure N.31: Elastic Shear Secant Stiffness Relative Error Change v. Max Shear Stress Ratio

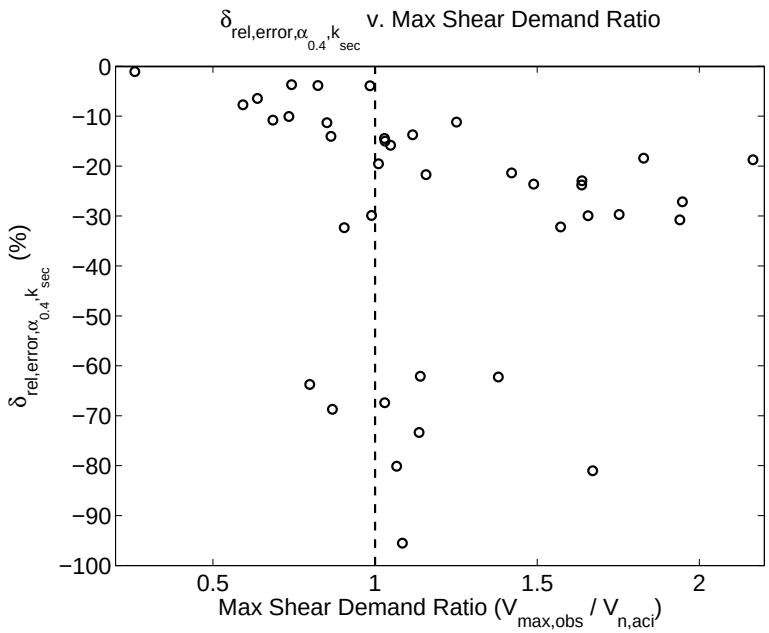

Figure N.32: Elastic Shear Secant Stiffness Relative Error Change v. Max Shear Demand Ratio

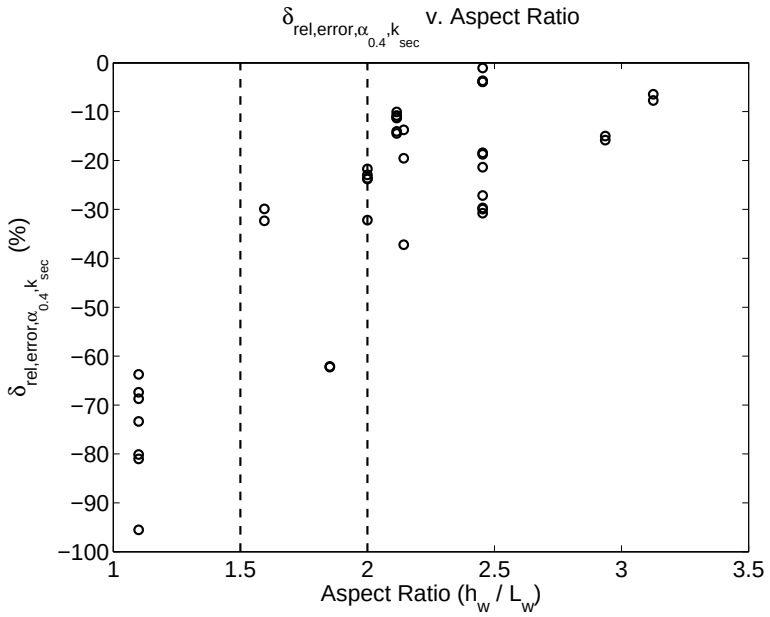

Figure N.33: Elastic Shear Secant Stiffness Relative Error Change v. Aspect Ratio

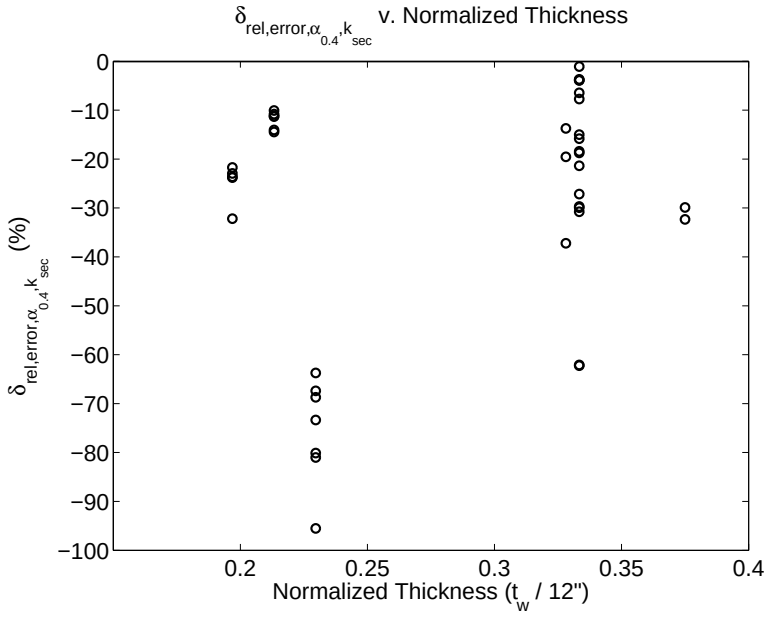

Figure N.34: Elastic Shear Secant Stiffness Relative Error Change v. Normalized Thickness

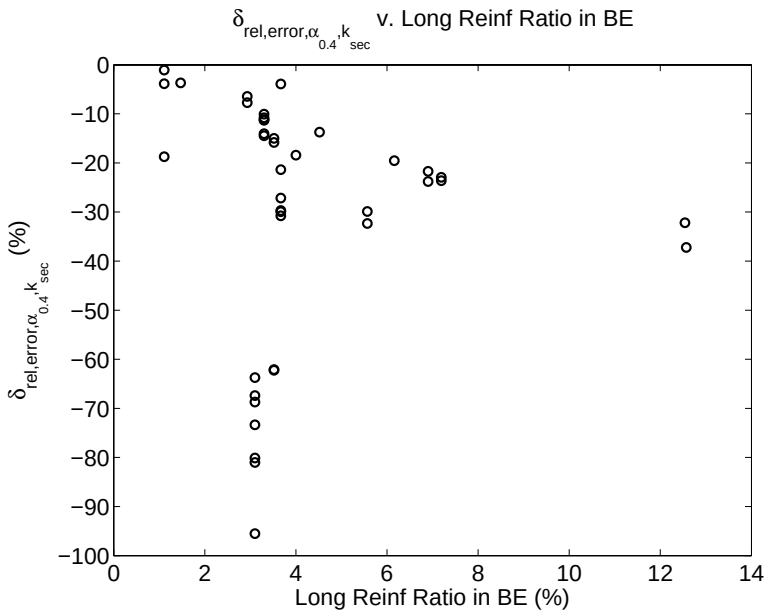

Figure N.35: Elastic Shear Secant Stiffness Relative Error Change v. Long Reinf Ratio in BE

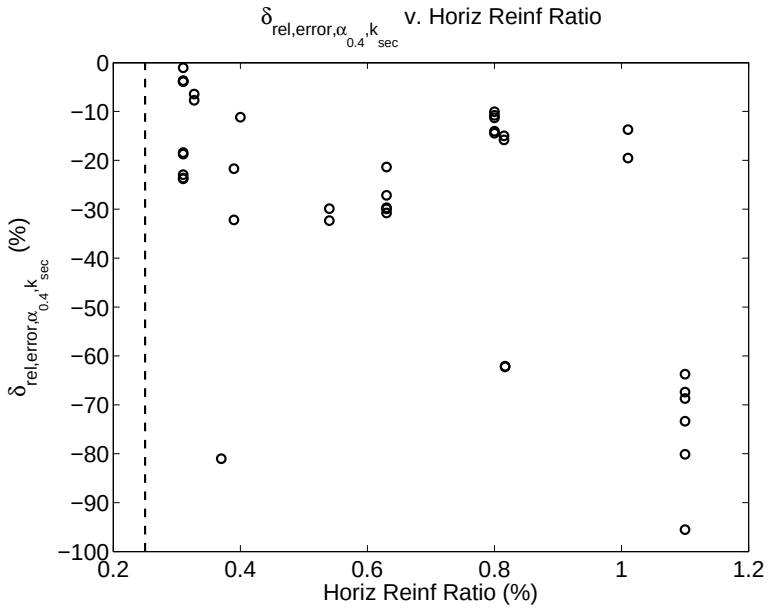

Figure N.36: Elastic Shear Secant Stiffness Relative Error Change v. Horiz Reinf Ratio

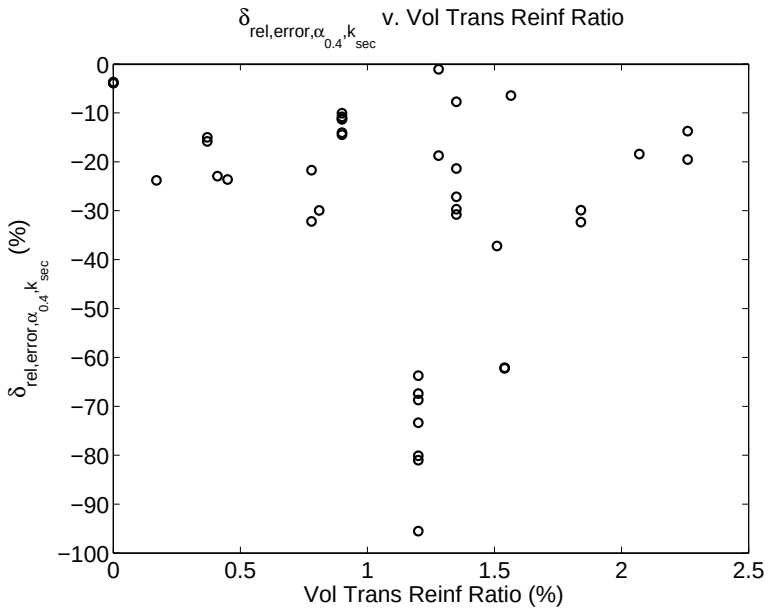

Figure N.37: Elastic Shear Secant Stiffness Relative Error Change v. Vol Trans Reinf Ratio

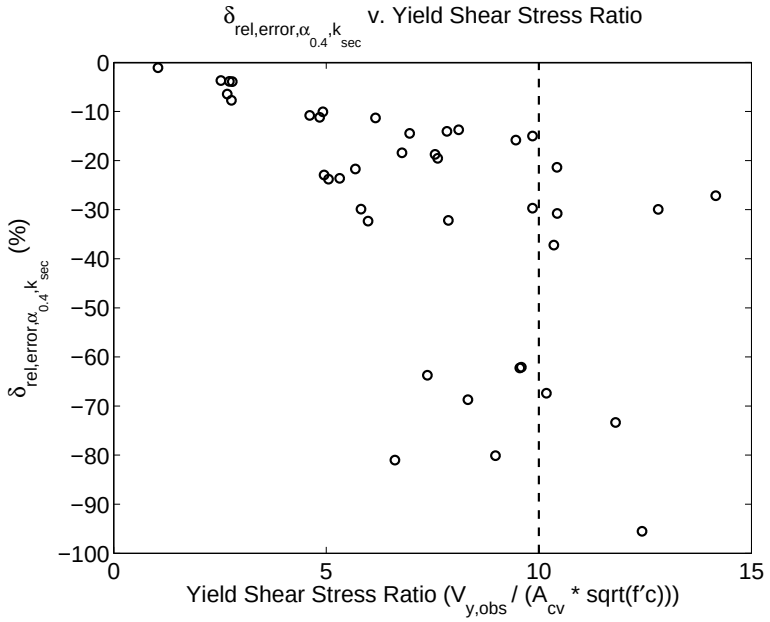

Figure N.38: Elastic Shear Secant Stiffness Relative Error Change v. Yield Shear Stress Ratio

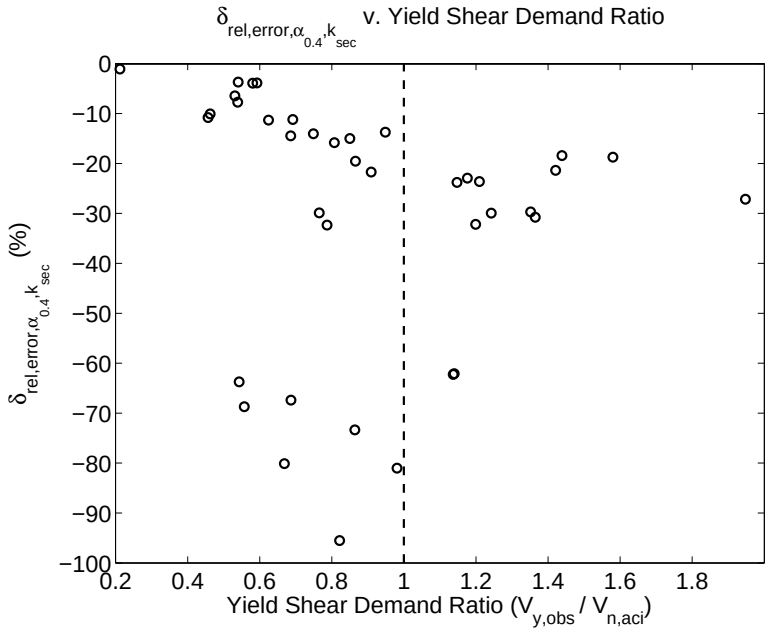

Figure N.39: Elastic Shear Secant Stiffness Relative Error Change v. Yield Shear Demand Ratio

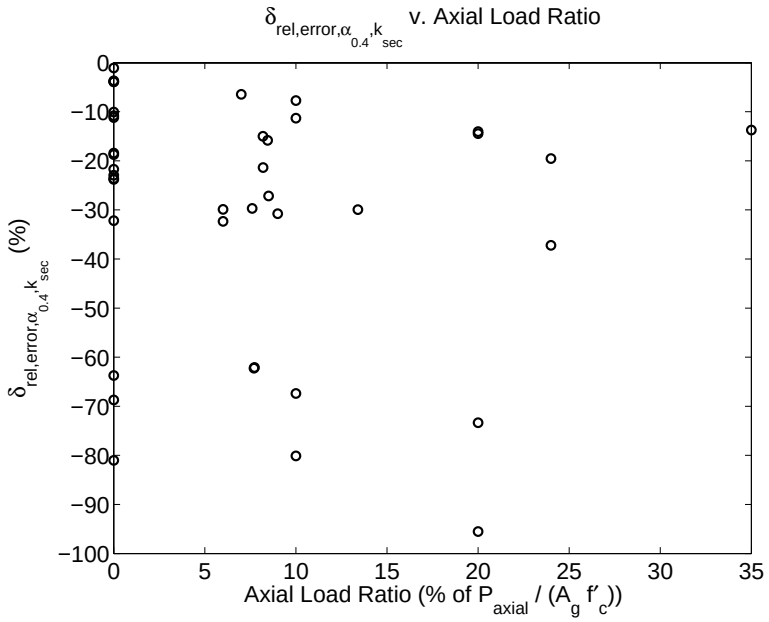

Figure N.40: Elastic Shear Secant Stiffness Relative Error Change v. Axial Load Ratio

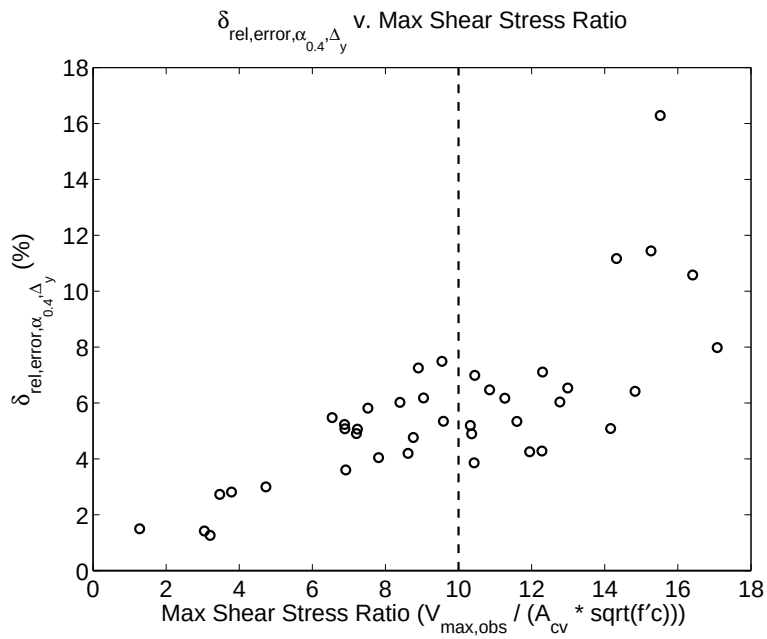

Figure N.41: Elastic Shear Yield Displacement Relative Error Change v. Max Shear Stress Ratio

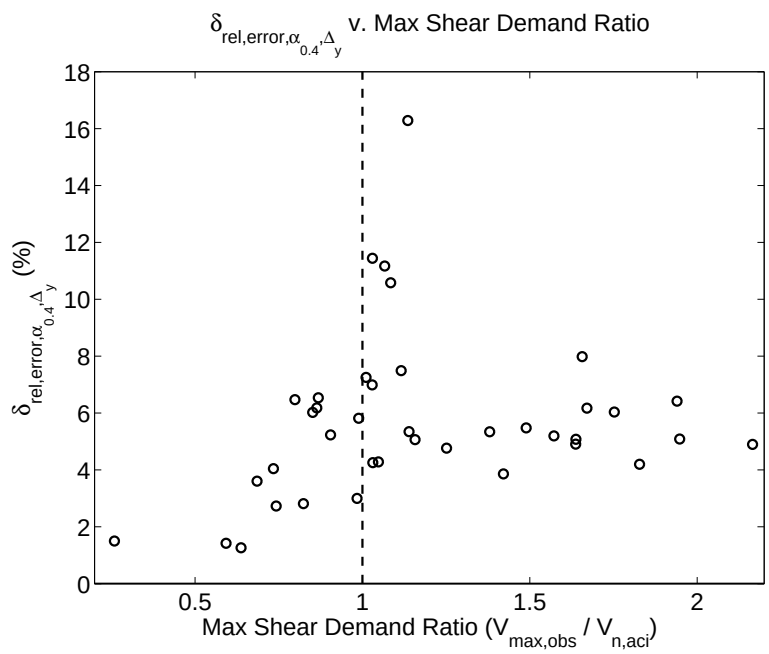

Figure N.42: Elastic Shear Yield Displacement Relative Error Change v. Max Shear Demand Ratio

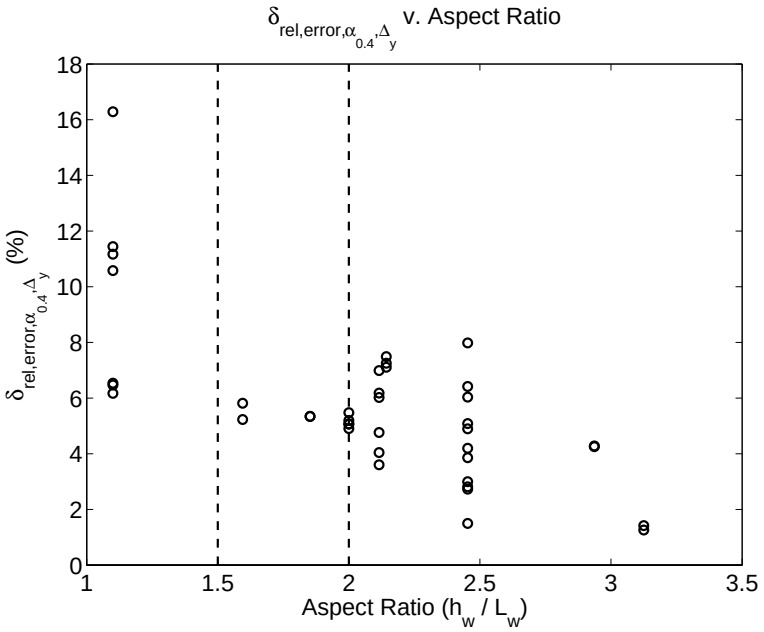

Figure N.43: Elastic Shear Yield Displacement Relative Error Change v. Aspect Ratio

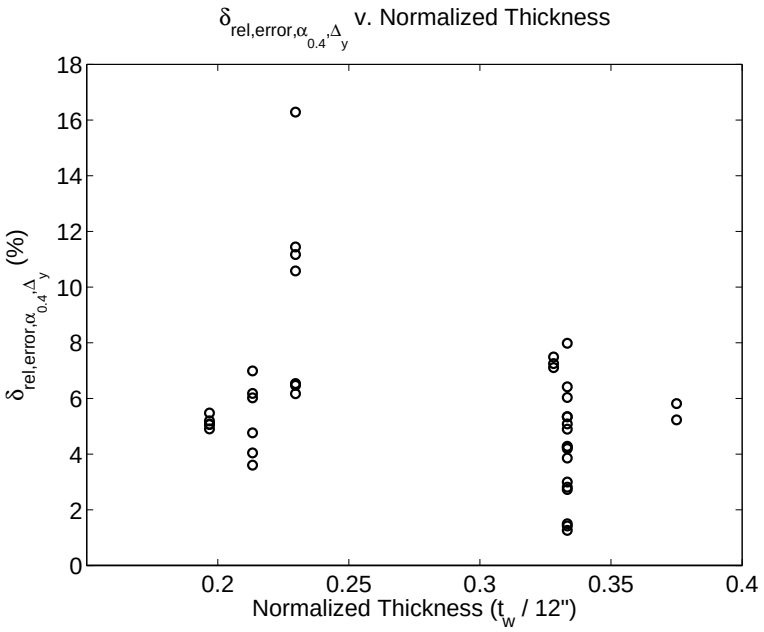

Figure N.44: Elastic Shear Yield Displacement Relative Error Change v. Normalized Thickness

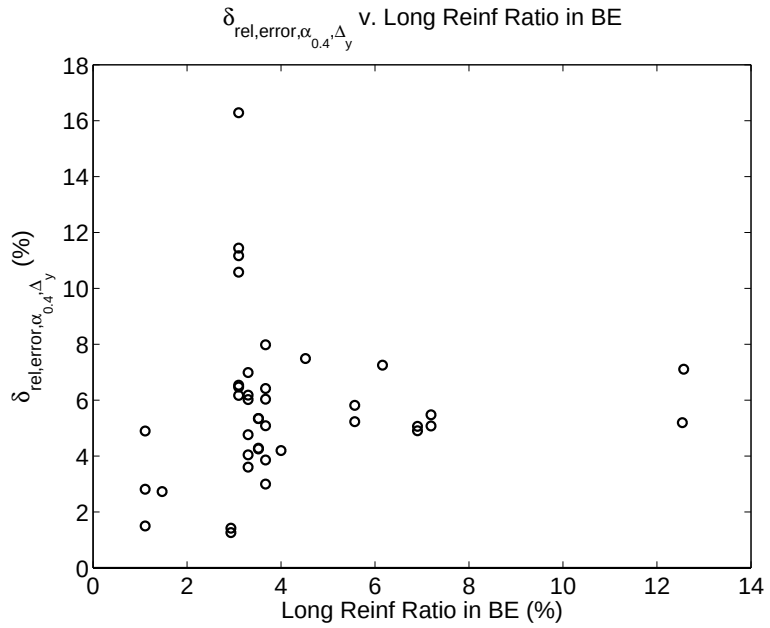

Figure N.45: Elastic Shear Yield Displacement Relative Error Change v. Long Reinf Ratio in BE

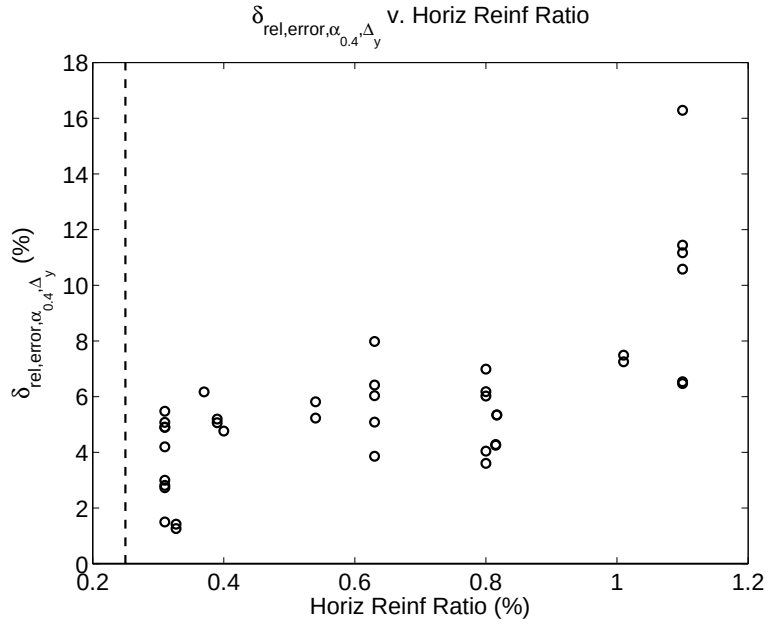

Figure N.46: Elastic Shear Yield Displacement Relative Error Change v. Horiz Reinf Ratio

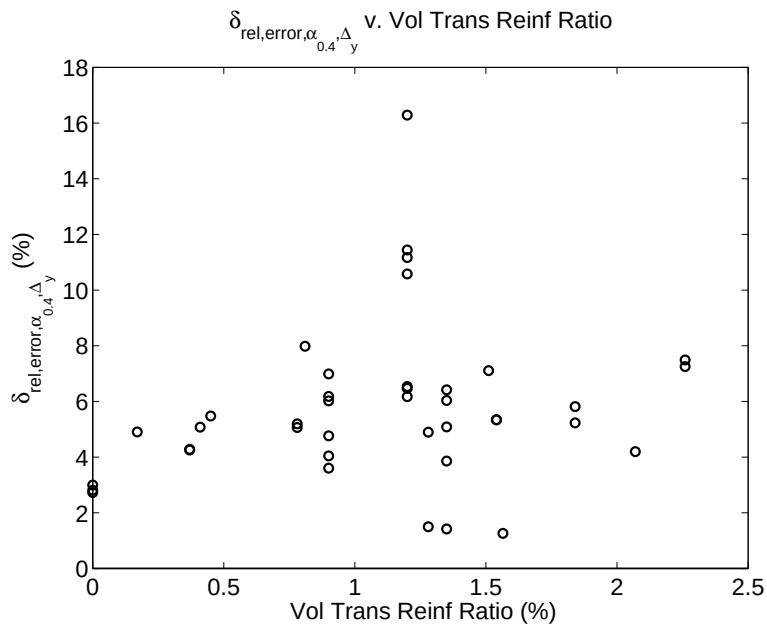

Figure N.47: Elastic Shear Yield Displacement Relative Error Change v. Vol Trans Reinf Ratio

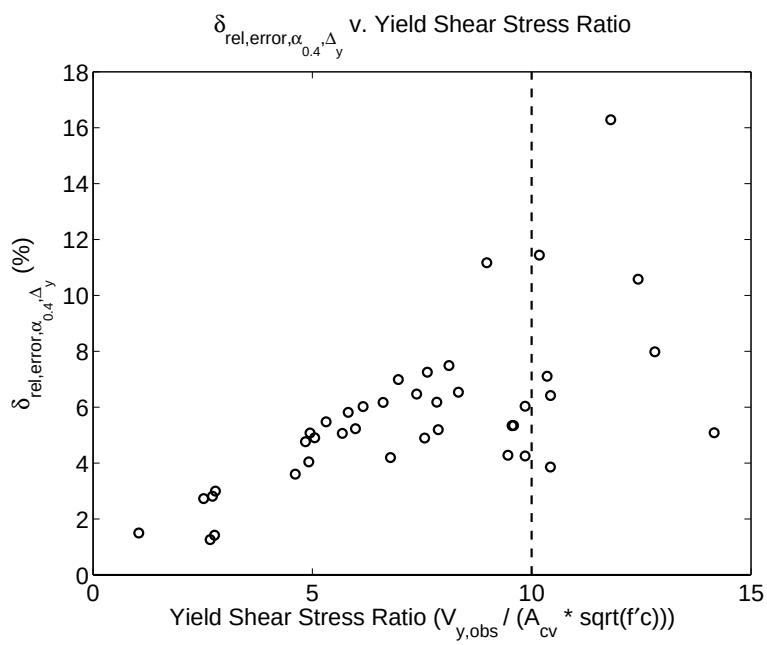

Figure N.48: Elastic Shear Yield Displacement Relative Error Change v. Yield Shear Stress Ratio

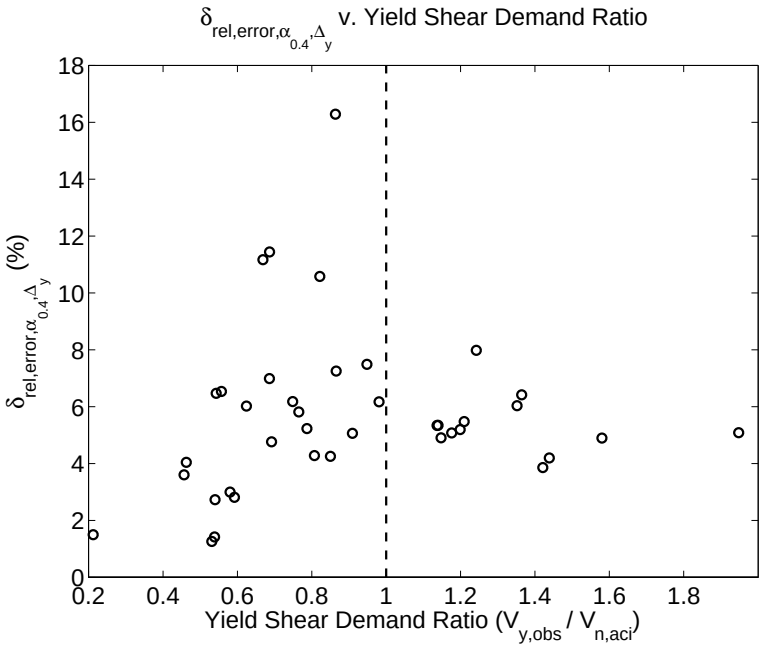

Figure N.49: Elastic Shear Yield Displacement Relative Error Change v. Yield Shear Demand Ratio

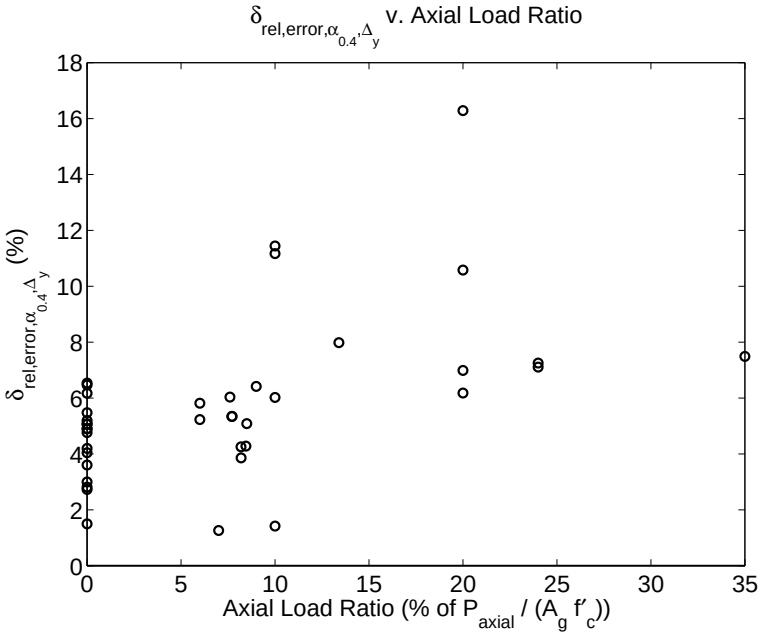

Figure N.50: Elastic Shear Yield Displacement Relative Error Change v. Axial Load Ratio

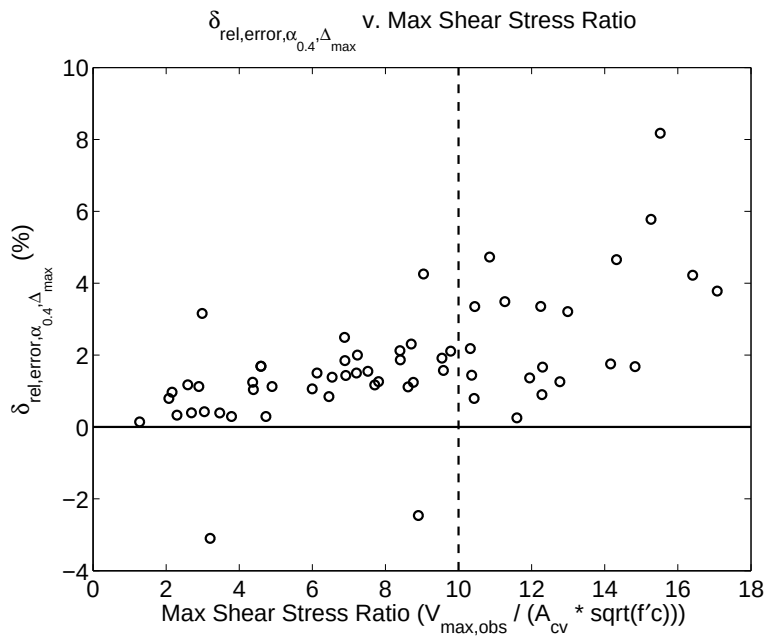

Figure N.51: Elastic Shear Max Displacement Relative Error Change v. Max Shear Stress Ratio

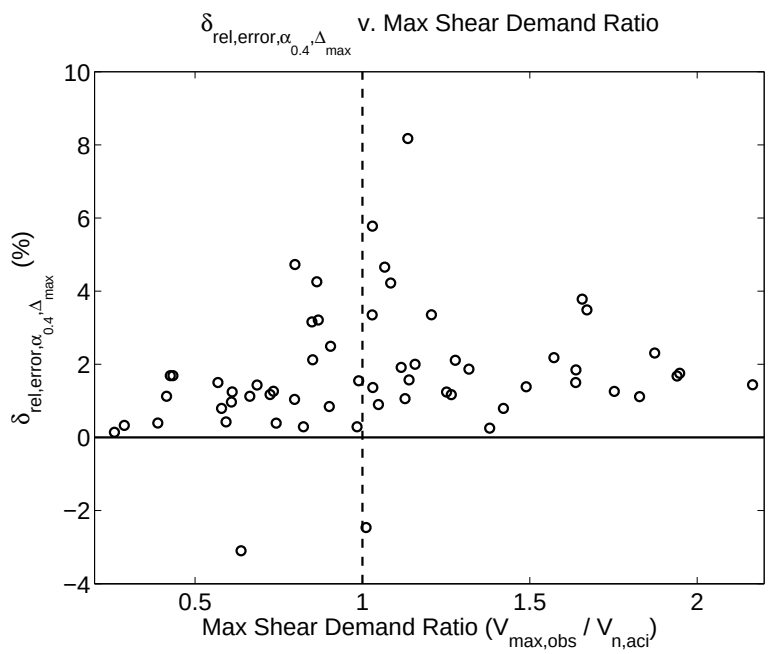

Figure N.52: Elastic Shear Max Displacement Relative Error Change v. Max Shear Demand Ratio

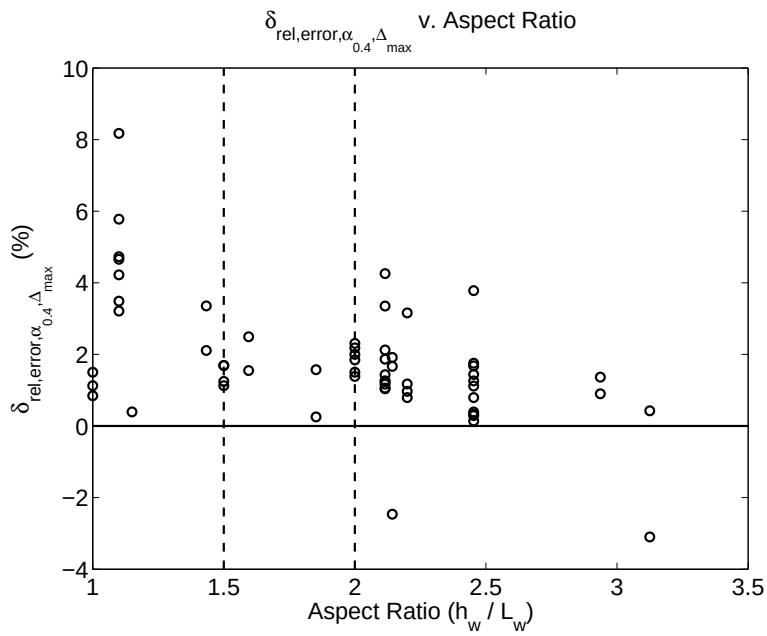

Figure N.53: Elastic Shear Max Displacement Relative Error Change v. Aspect Ratio

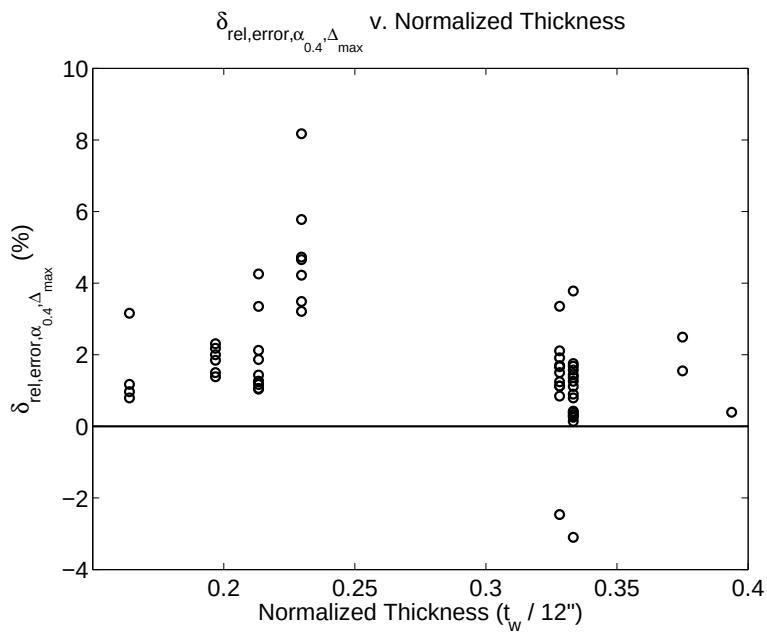

Figure N.54: Elastic Shear Max Displacement Relative Error Change v. Normalized Thickness

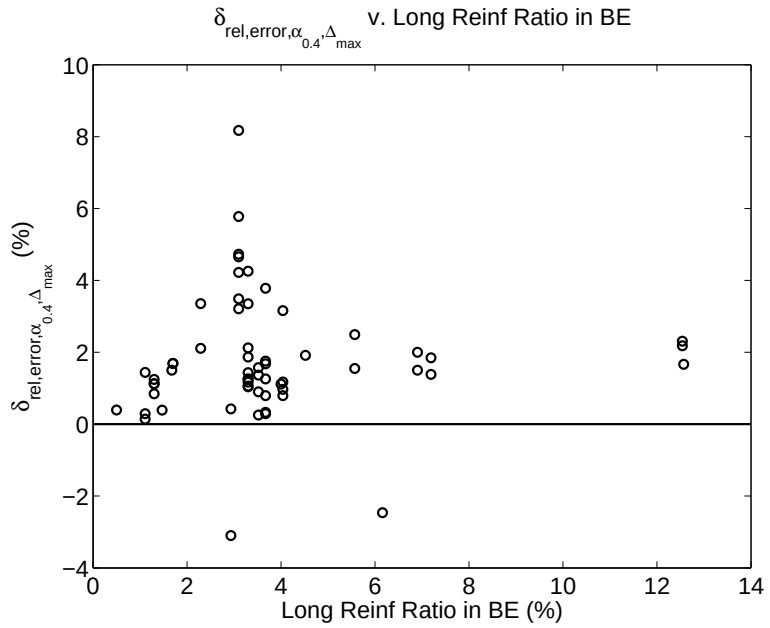

Figure N.55: Elastic Shear Max Displacement Relative Error Change v. Long Reinf Ratio in BE

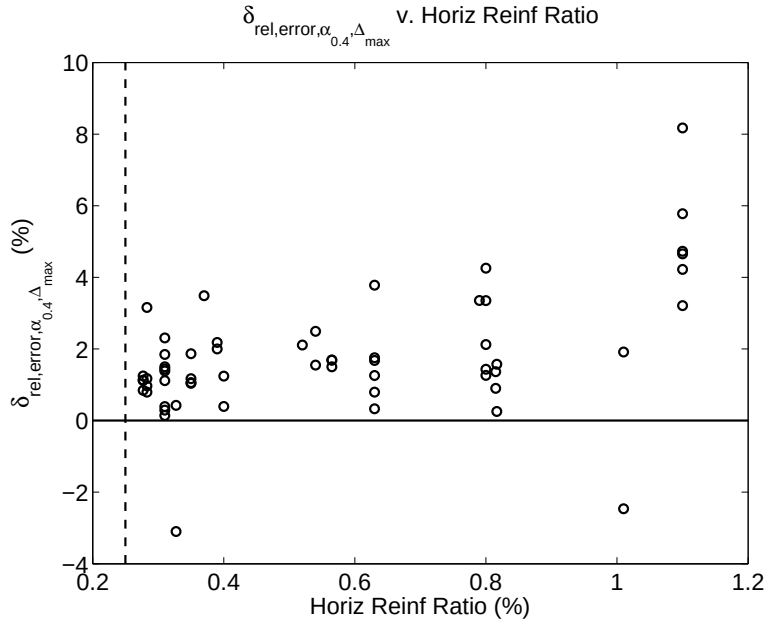

Figure N.56: Elastic Shear Max Displacement Relative Error Change v. Horiz Reinf Ratio

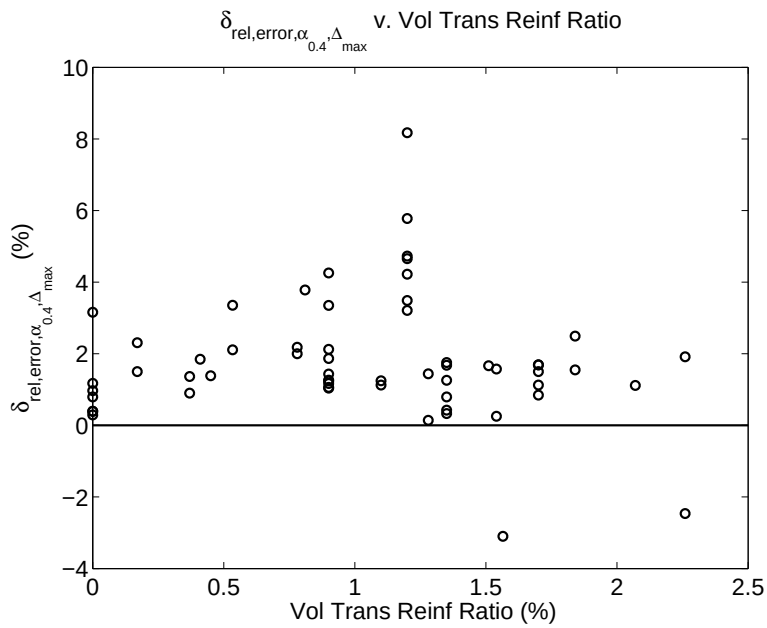

Figure N.57: Elastic Shear Max Displacement Relative Error Change v. Vol Trans Reinf Ratio

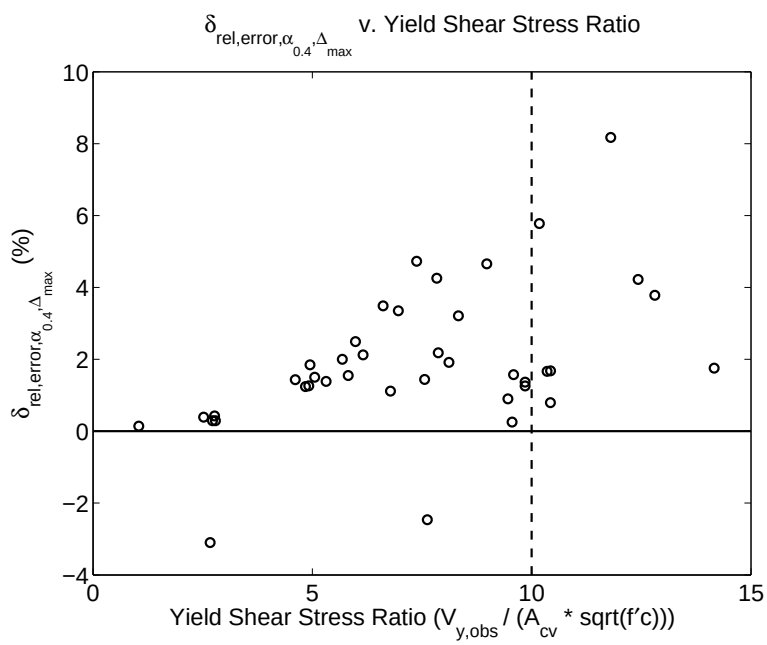

Figure N.58: Elastic Shear Max Displacement Relative Error Change v. Yield Shear Stress Ratio

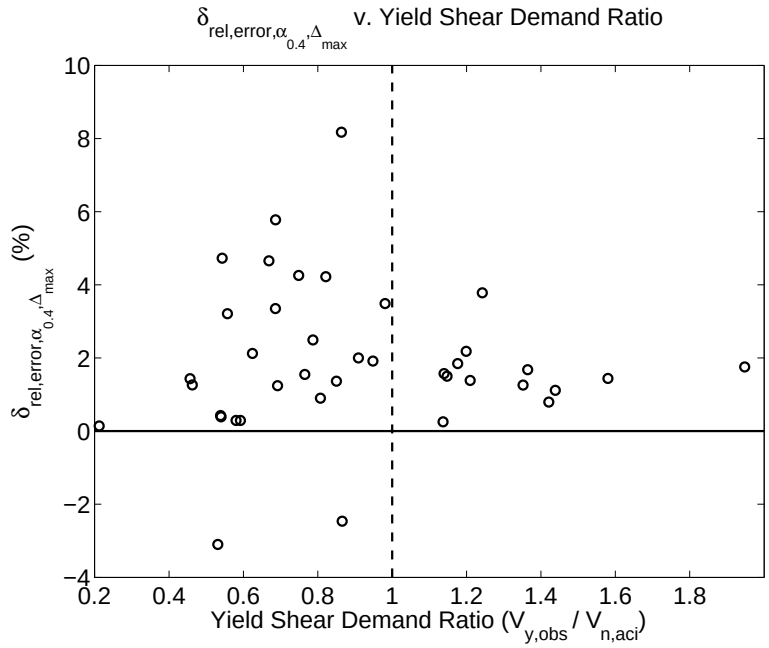

Figure N.59: Elastic Shear Max Displacement Relative Error Change v. Yield Shear Demand Ratio

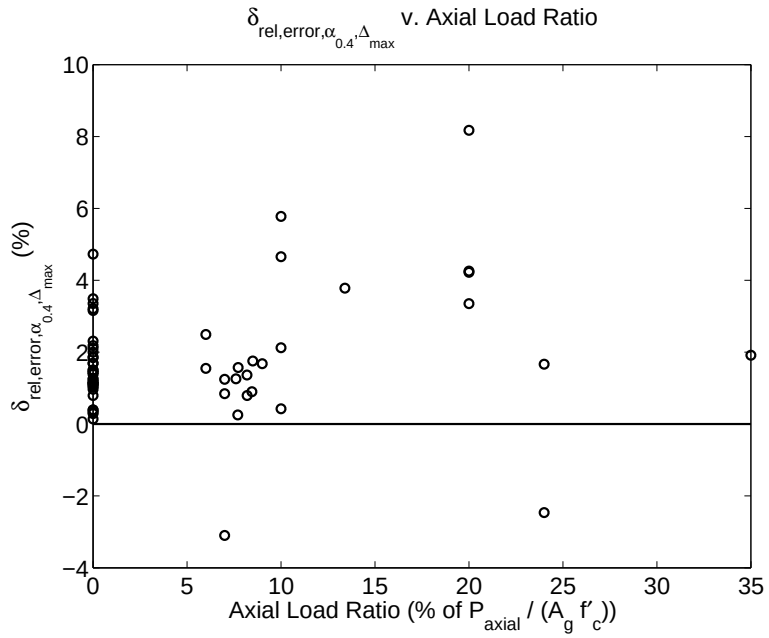

Figure N.60: Elastic Shear Max Displacement Relative Error Change v. Axial Load Ratio

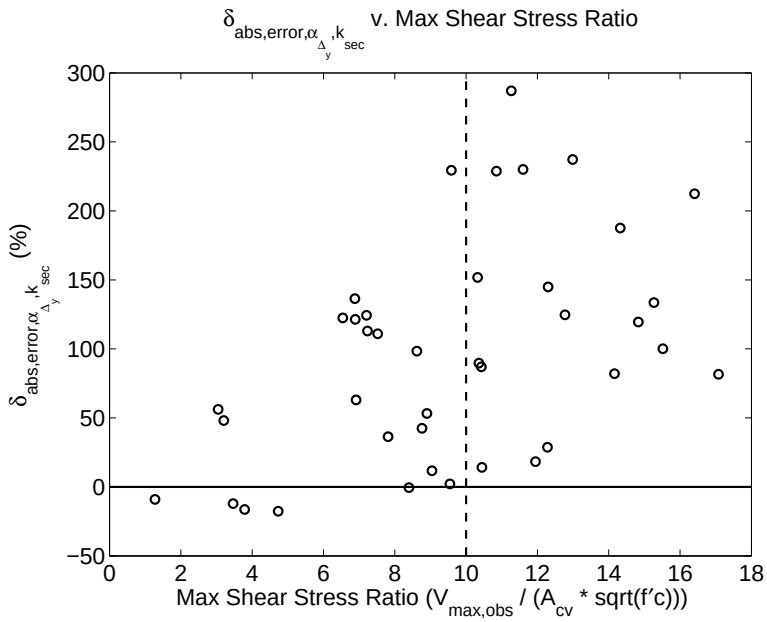

Figure N.61: Effective Shear Calibrated to Yield Displacement Secant Stiffness Absolute Error Change v. Max Shear Stress Ratio

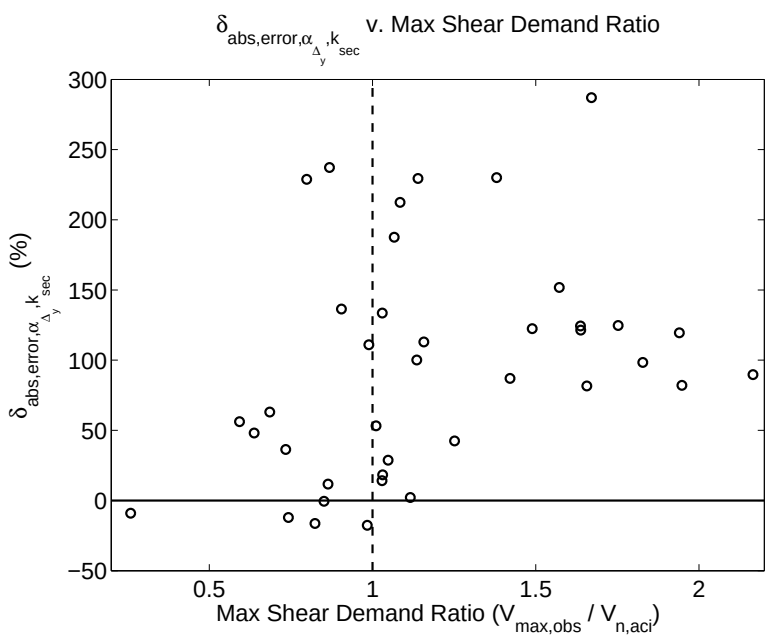

Figure N.62: Effective Shear Calibrated to Yield Displacement Secant Stiffness Absolute Error Change v. Max Shear Demand Ratio

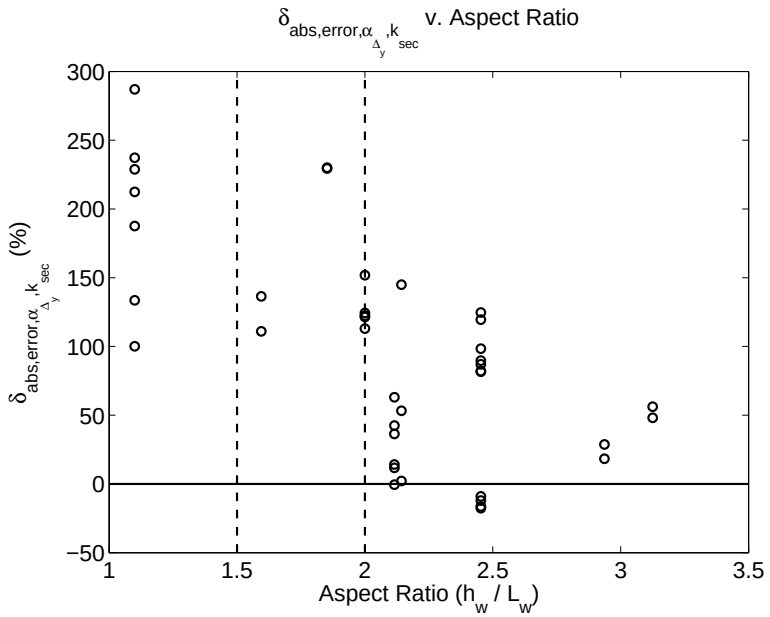

Figure N.63: Effective Shear Calibrated to Yield Displacement Secant Stiffness Absolute Error Change v. Aspect Ratio

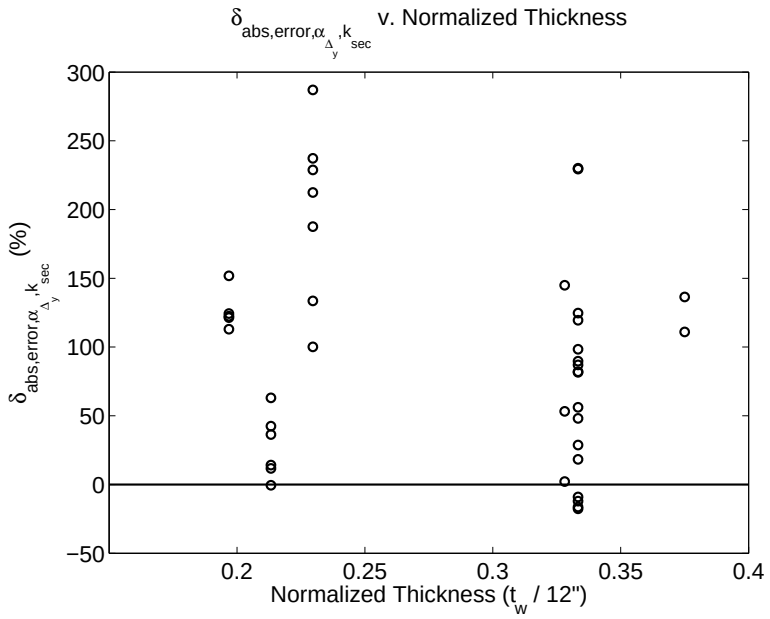

Figure N.64: Effective Shear Calibrated to Yield Displacement Secant Stiffness Absolute Error Change v. Normalized Thickness

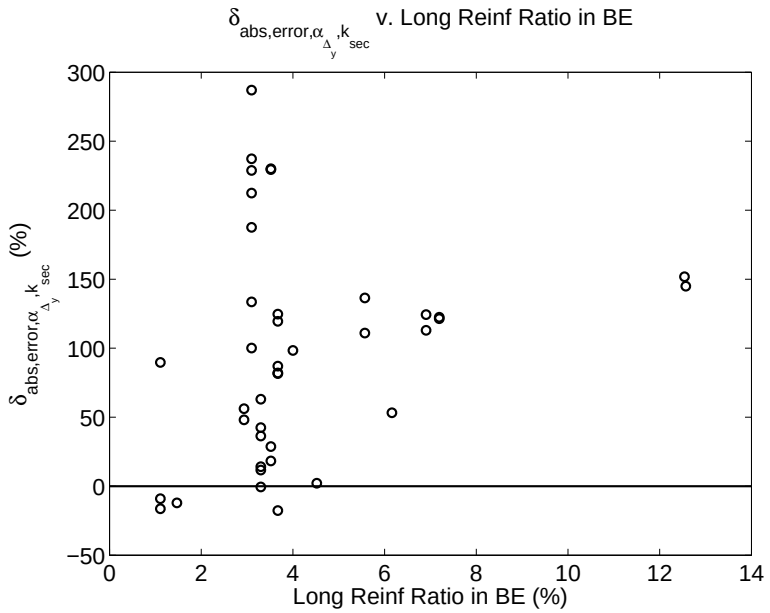

Figure N.65: Effective Shear Calibrated to Yield Displacement Secant Stiffness Absolute Error Change v. Long Reinf Ratio in BE

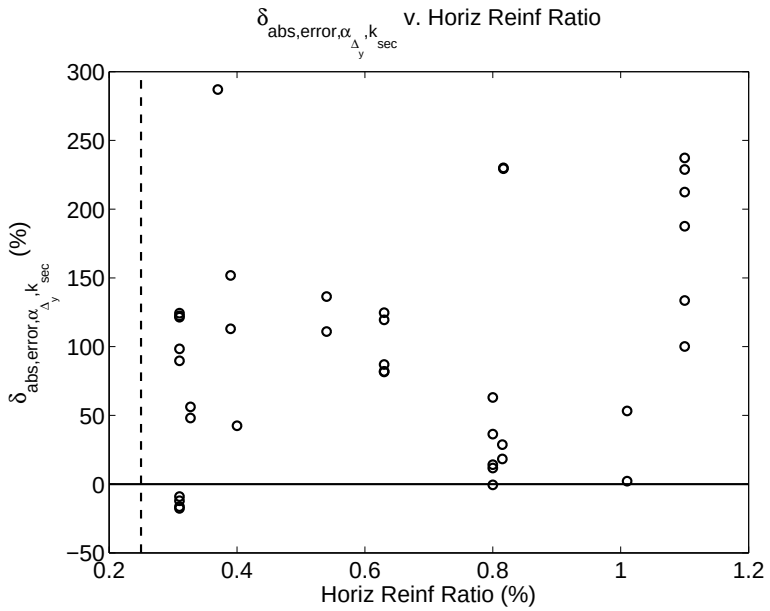

Figure N.66: Effective Shear Calibrated to Yield Displacement Secant Stiffness Absolute Error Change v. Horiz Reinf Ratio

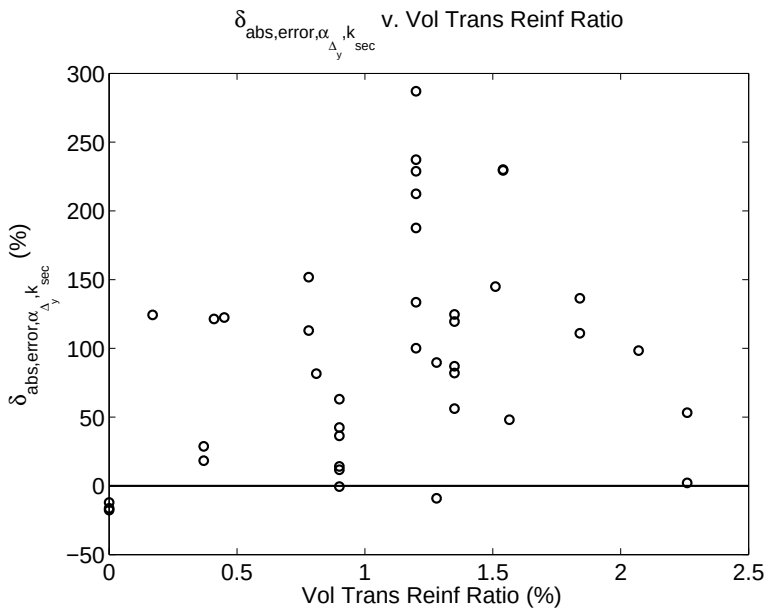

Figure N.67: Effective Shear Calibrated to Yield Displacement Secant Stiffness Absolute Error Change v. Vol Trans Reinf Ratio

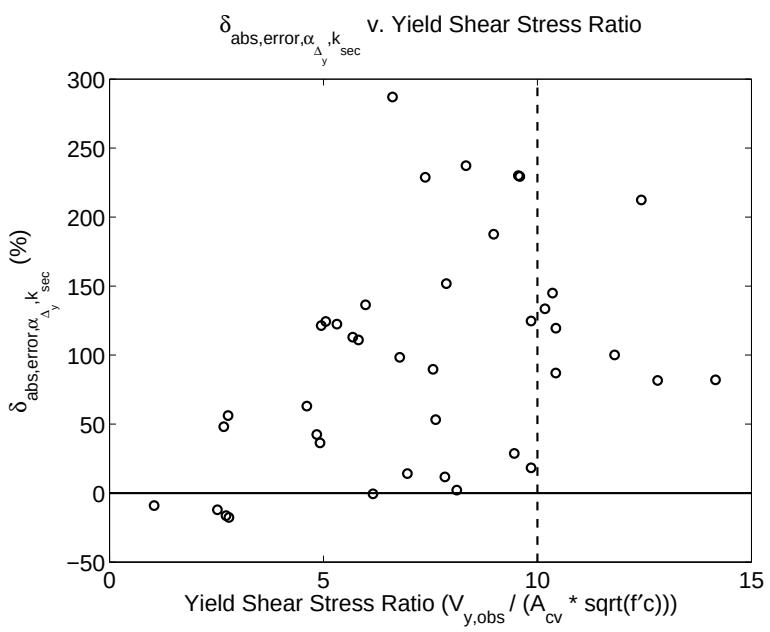

Figure N.68: Effective Shear Calibrated to Yield Displacement Secant Stiffness Absolute Error Change v. Yield Shear Stress Ratio

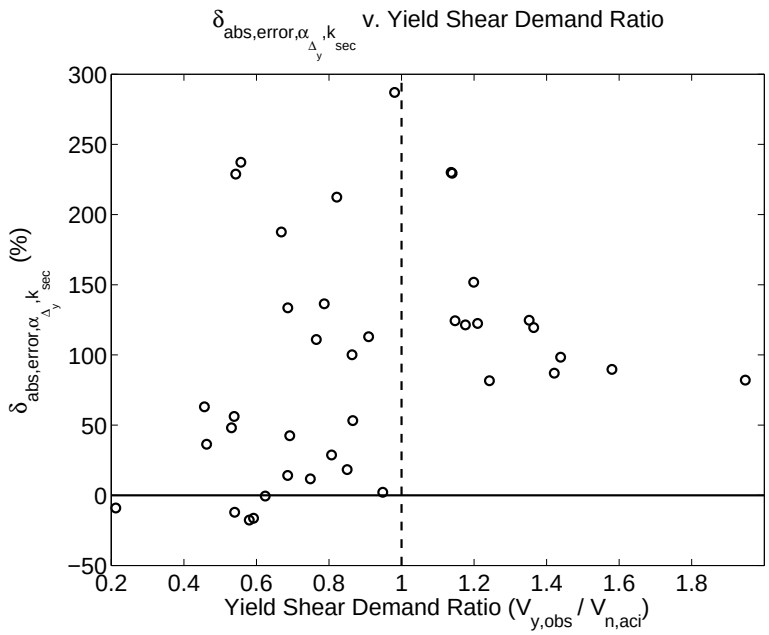

Figure N.69: Effective Shear Calibrated to Yield Displacement Secant Stiffness Absolute Error Change v. Yield Shear Demand Ratio

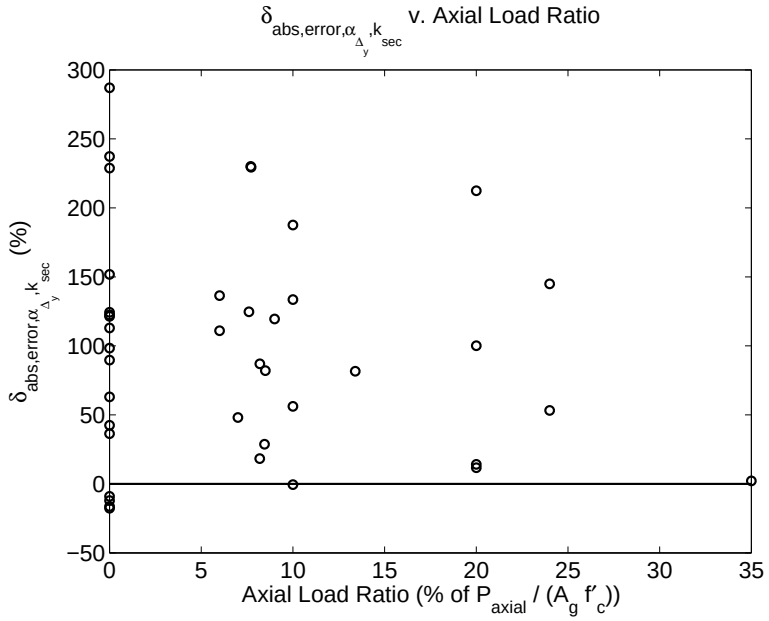

Figure N.70: Effective Shear Calibrated to Yield Displacement Secant Stiffness Absolute Error Change v. Axial Load Ratio

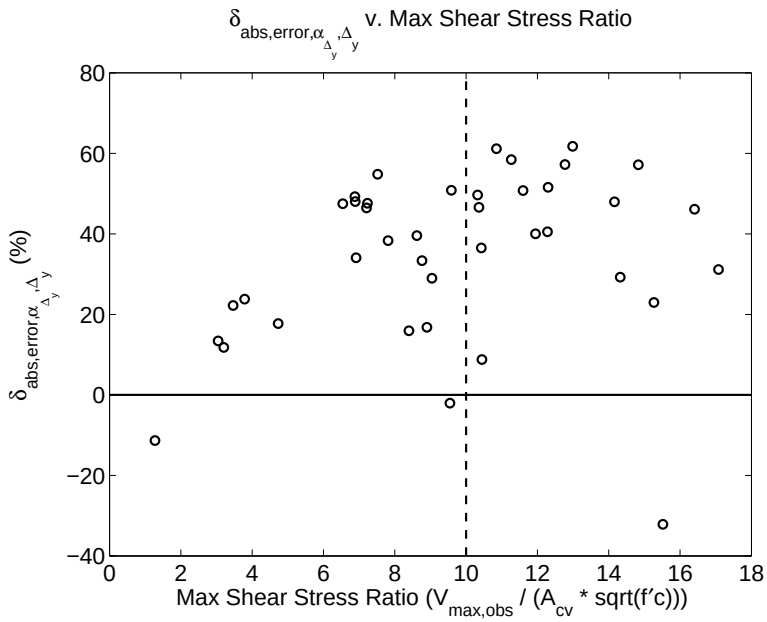

Figure N.71: Effective Shear Calibrated to Yield Displacement Yield Displacement Absolute Error Change v. Max Shear Stress Ratio

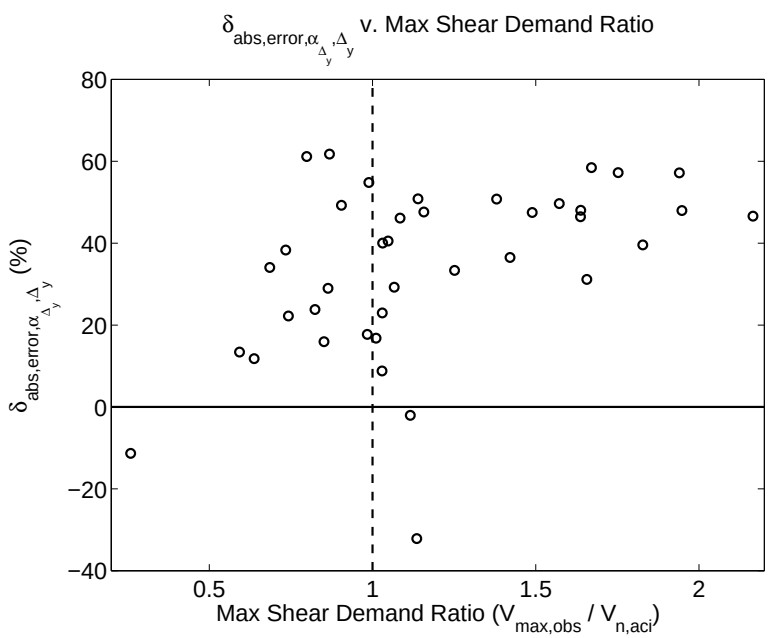

Figure N.72: Effective Shear Calibrated to Yield Displacement Yield Displacement Absolute Error Change v. Max Shear Demand Ratio

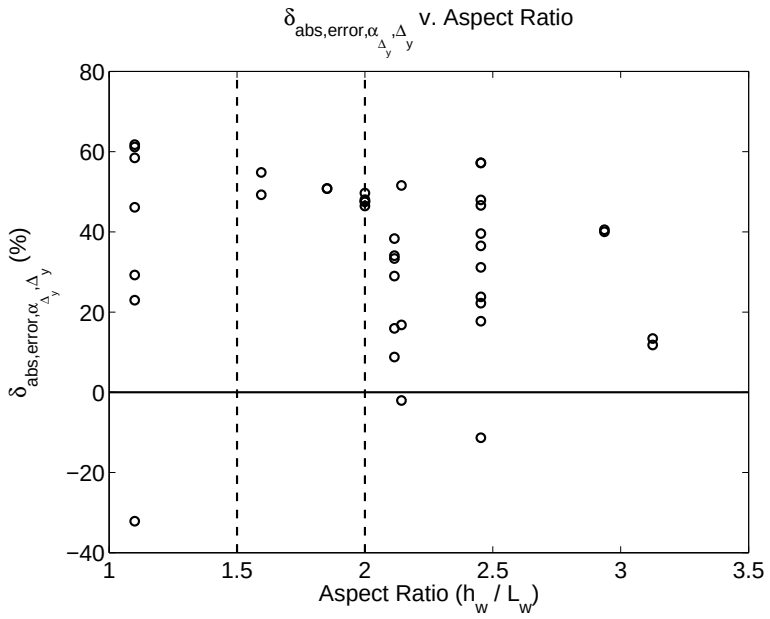

Figure N.73: Effective Shear Calibrated to Yield Displacement Yield Displacement Absolute Error Change v. Aspect Ratio

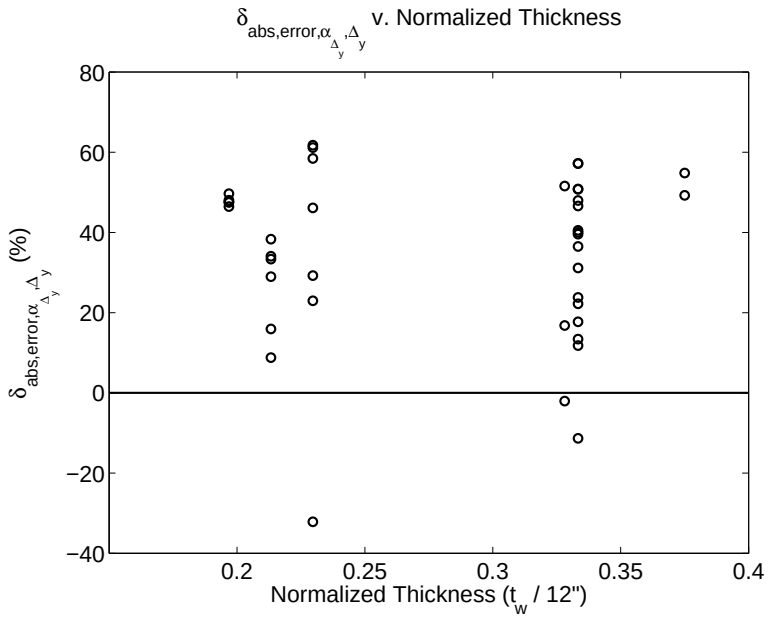

Figure N.74: Effective Shear Calibrated to Yield Displacement Yield Displacement Absolute Error Change v. Normalized Thickness

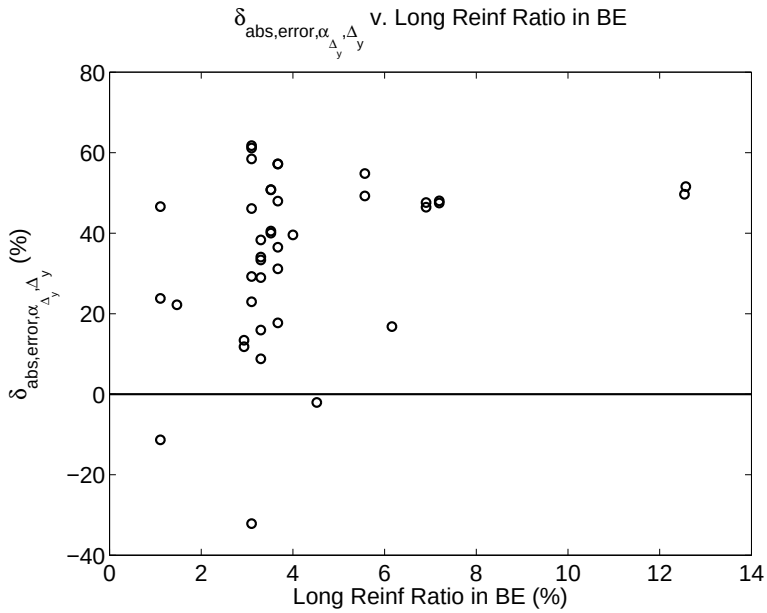

Figure N.75: Effective Shear Calibrated to Yield Displacement Yield Displacement Absolute Error Change v. Long Reinf Ratio in BE

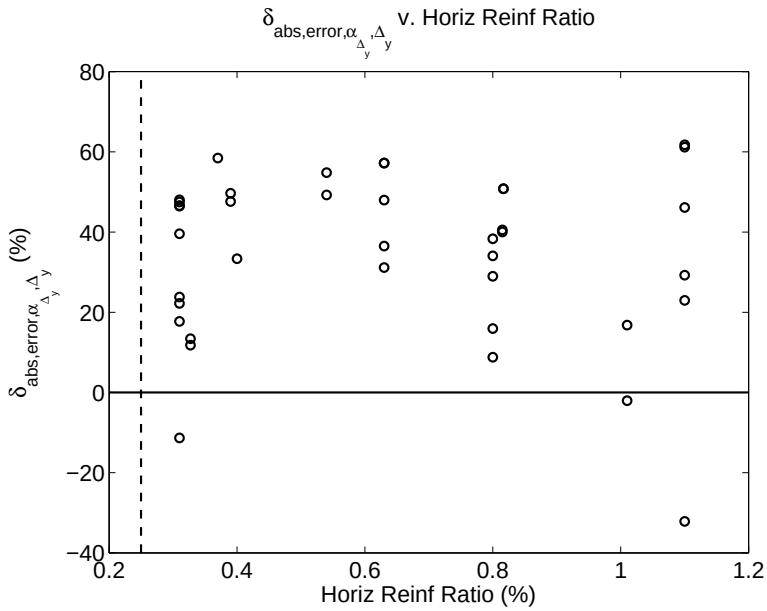

Figure N.76: Effective Shear Calibrated to Yield Displacement Yield Displacement Absolute Error Change v. Horiz Reinf Ratio

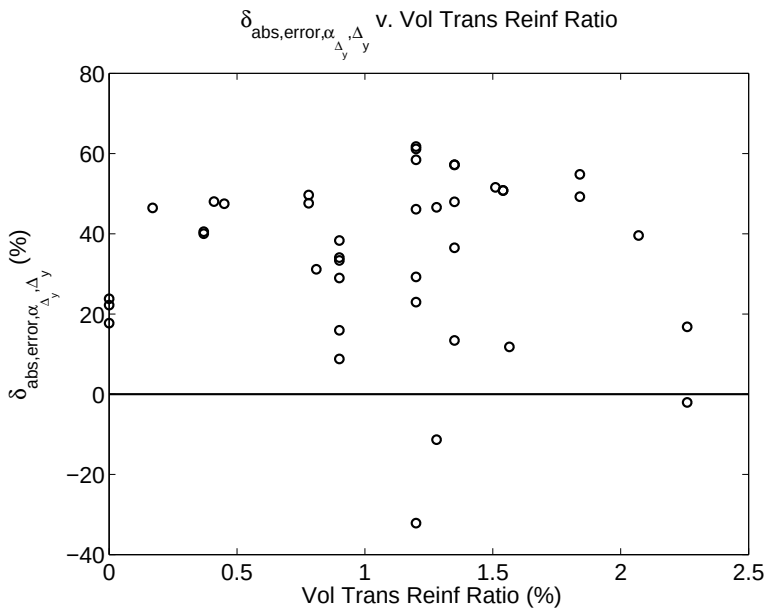

Figure N.77: Effective Shear Calibrated to Yield Displacement Yield Displacement Absolute Error Change v. Vol Trans Reinf Ratio

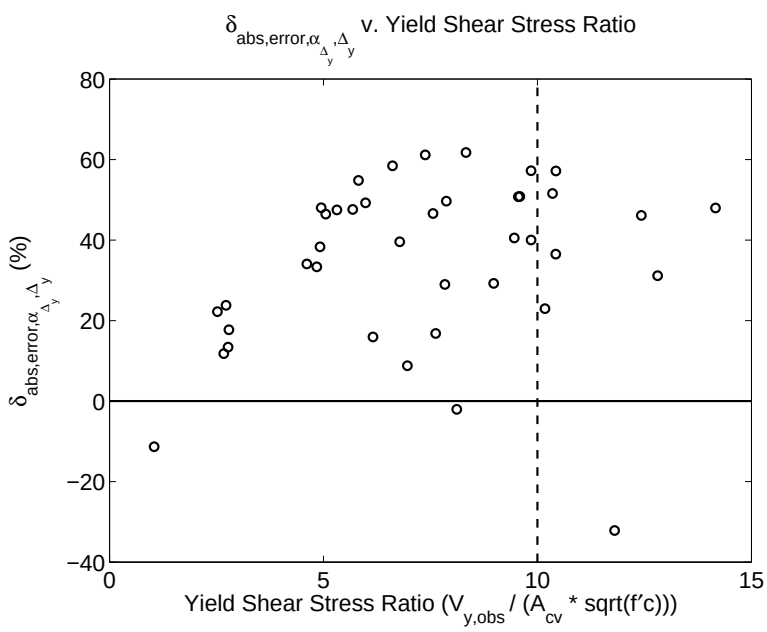

Figure N.78: Effective Shear Calibrated to Yield Displacement Yield Displacement Absolute Error Change v. Yield Shear Stress Ratio

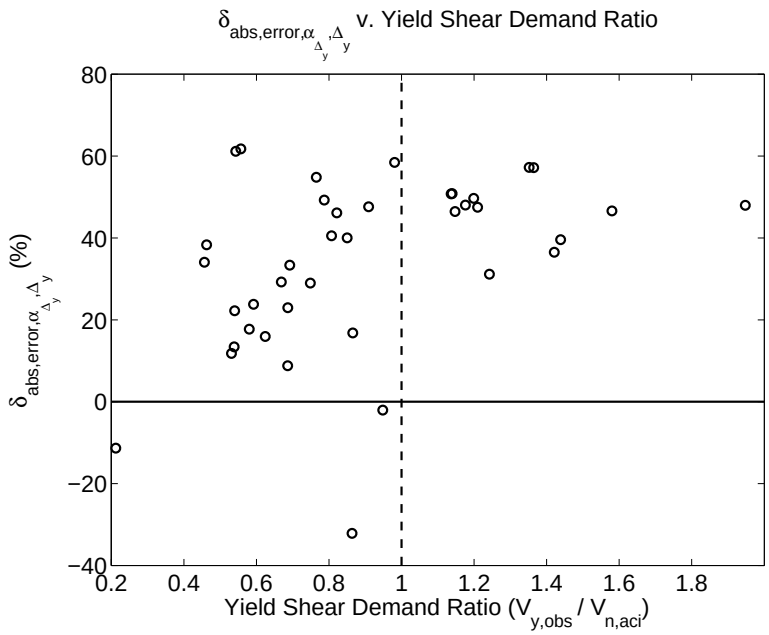

Figure N.79: Effective Shear Calibrated to Yield Displacement Yield Displacement Absolute Error Change v. Yield Shear Demand Ratio

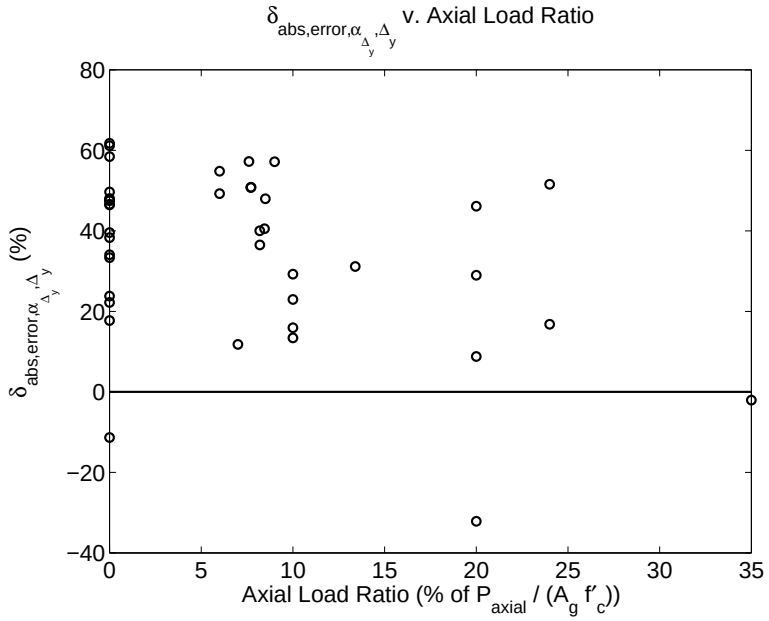

Figure N.80: Effective Shear Calibrated to Yield Displacement Yield Displacement Absolute Error Change v. Axial Load Ratio

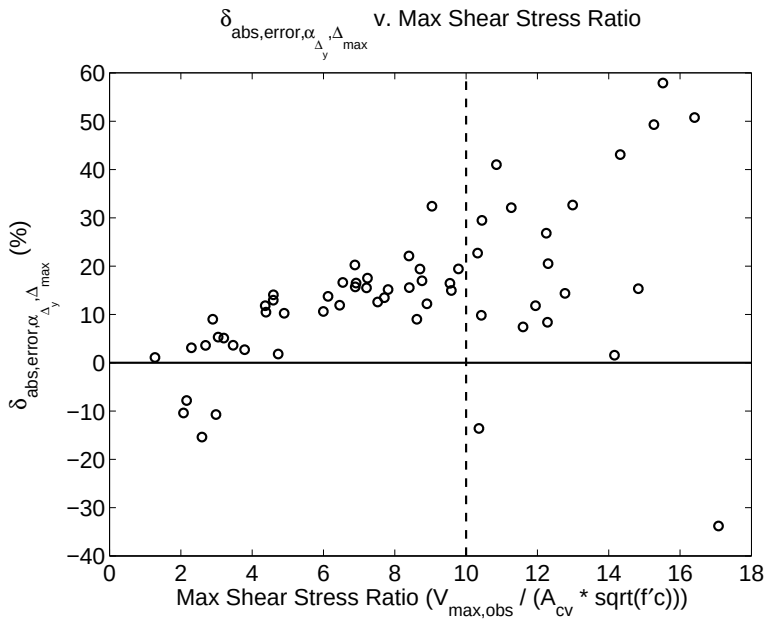

Figure N.81: Effective Shear Calibrated to Yield Displacement Max Displacement Absolute Error Change v. Max Shear Stress Ratio

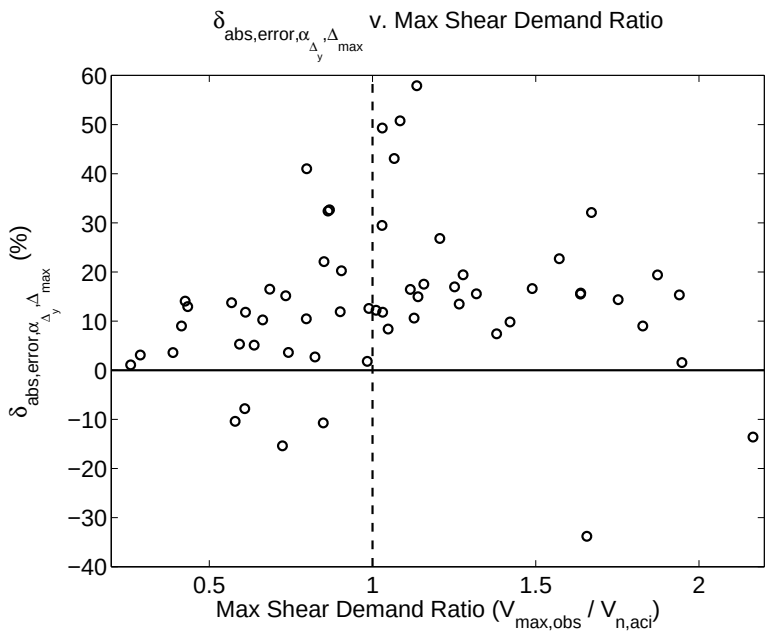

Figure N.82: Effective Shear Calibrated to Yield Displacement Max Displacement Absolute Error Change v. Max Shear Demand Ratio

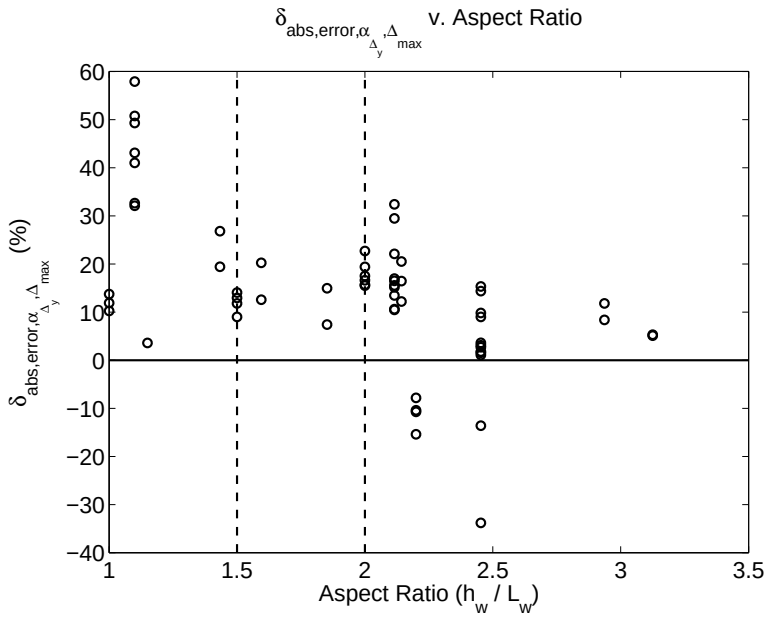

Figure N.83: Effective Shear Calibrated to Yield Displacement Max Displacement Absolute Error Change v. Aspect Ratio

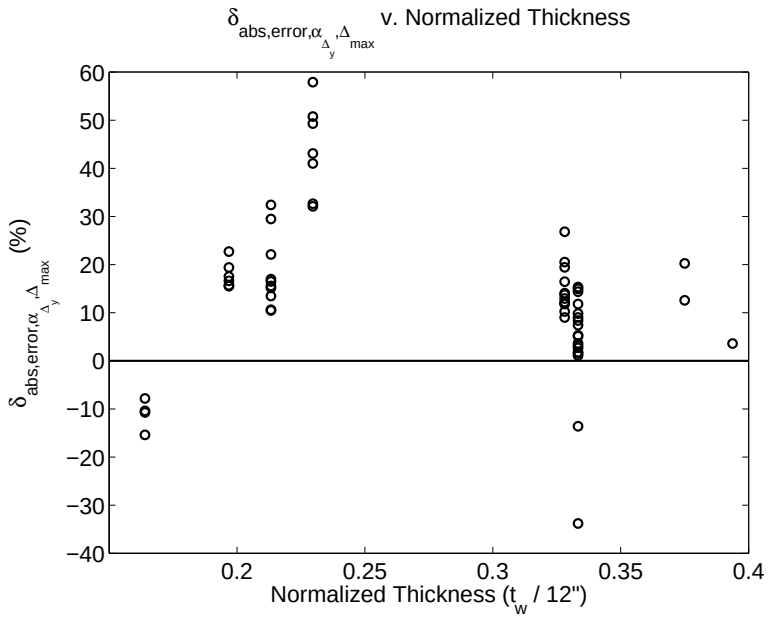

Figure N.84: Effective Shear Calibrated to Yield Displacement Max Displacement Absolute Error Change v. Normalized Thickness

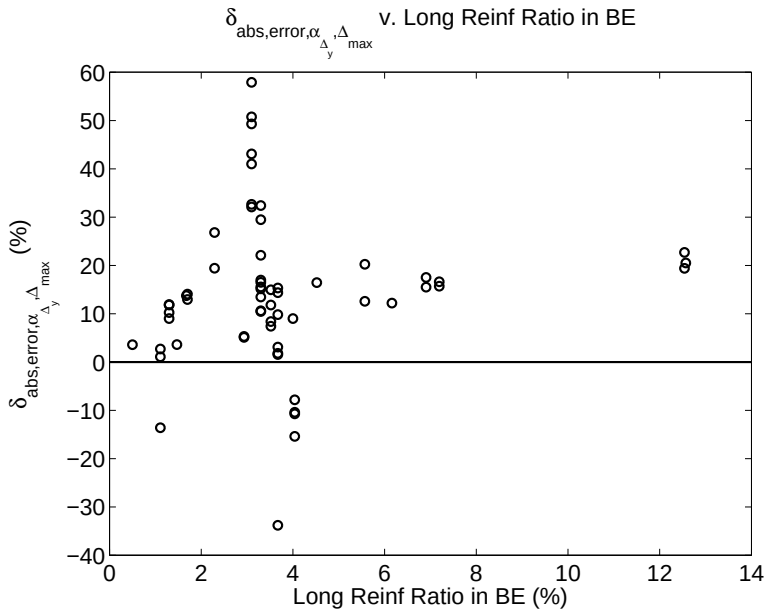

Figure N.85: Effective Shear Calibrated to Yield Displacement Max Displacement Absolute Error Change v. Long Reinf Ratio in BE

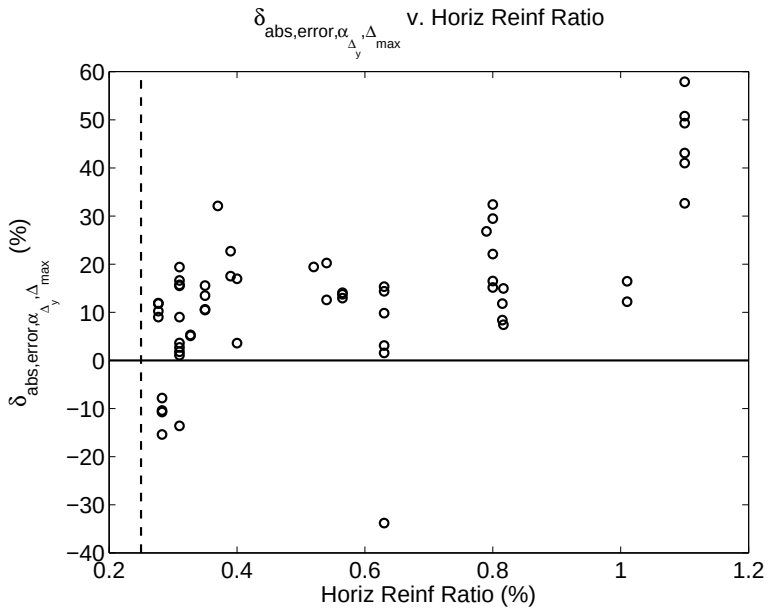

Figure N.86: Effective Shear Calibrated to Yield Displacement Max Displacement Absolute Error Change v. Horiz Reinf Ratio

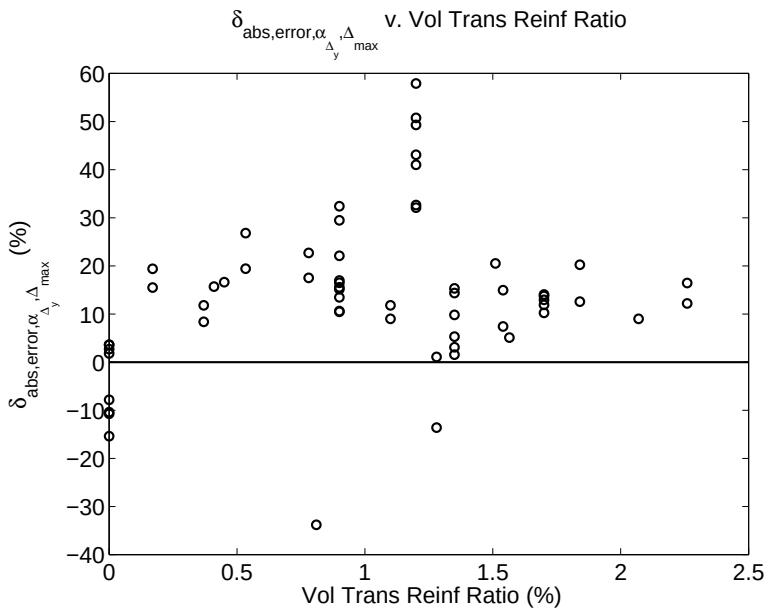

Figure N.87: Effective Shear Calibrated to Yield Displacement Max Displacement Absolute Error Change v. Vol Trans Reinf Ratio

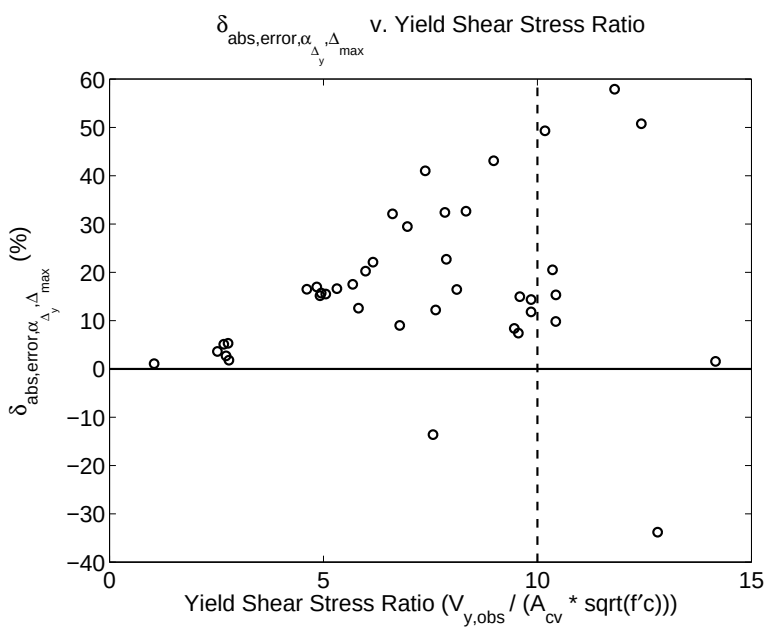

Figure N.88: Effective Shear Calibrated to Yield Displacement Max Displacement Absolute Error Change v. Yield Shear Stress Ratio

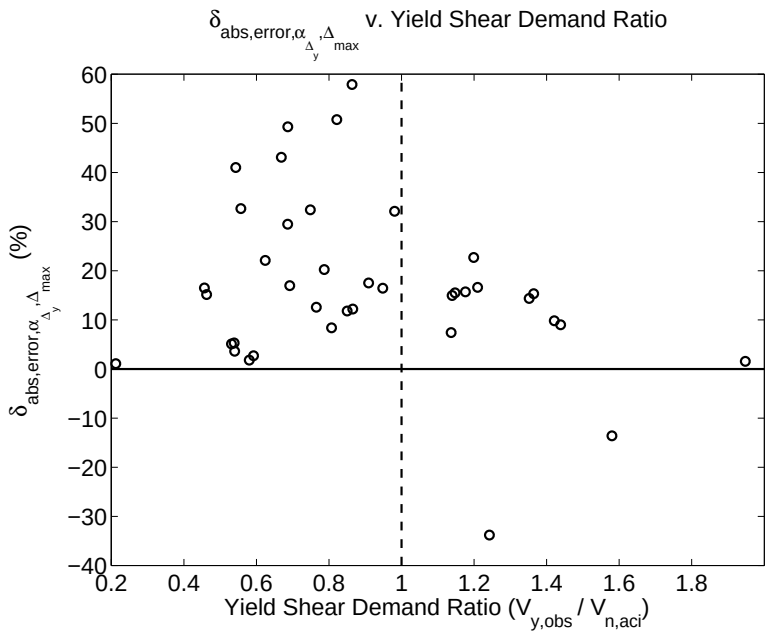

Figure N.89: Effective Shear Calibrated to Yield Displacement Max Displacement Absolute Error Change v. Yield Shear Demand Ratio

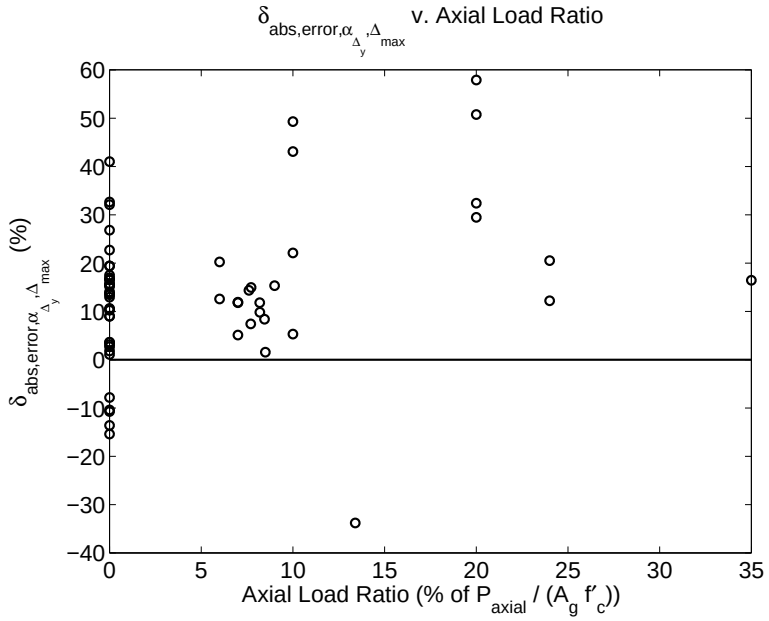

Figure N.90: Effective Shear Calibrated to Yield Displacement Max Displacement Absolute Error Change v. Axial Load Ratio

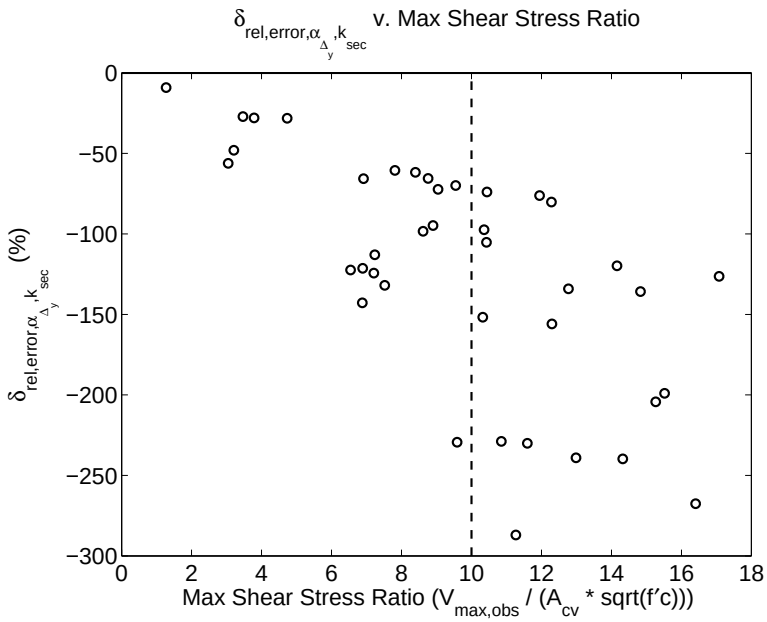

Figure N.91: Effective Shear Calibrated to Yield Displacement Secant Stiffness Relative Error Change v. Max Shear Stress Ratio

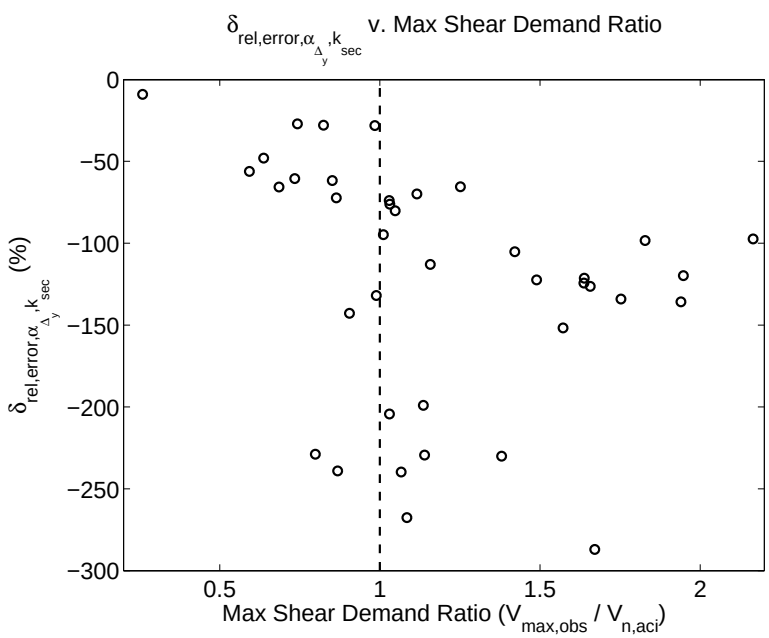

Figure N.92: Effective Shear Calibrated to Yield Displacement Secant Stiffness Relative Error Change v. Max Shear Demand Ratio

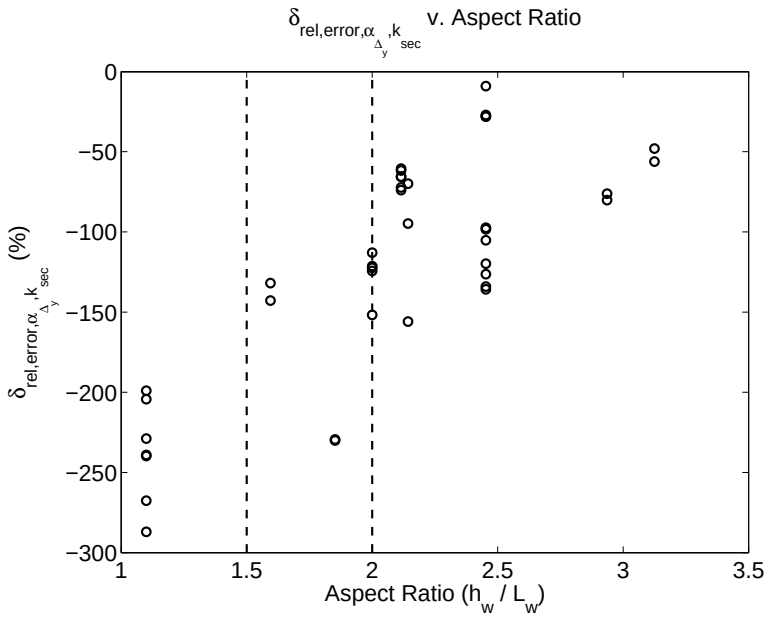

Figure N.93: Effective Shear Calibrated to Yield Displacement Secant Stiffness Relative Error Change v. Aspect Ratio

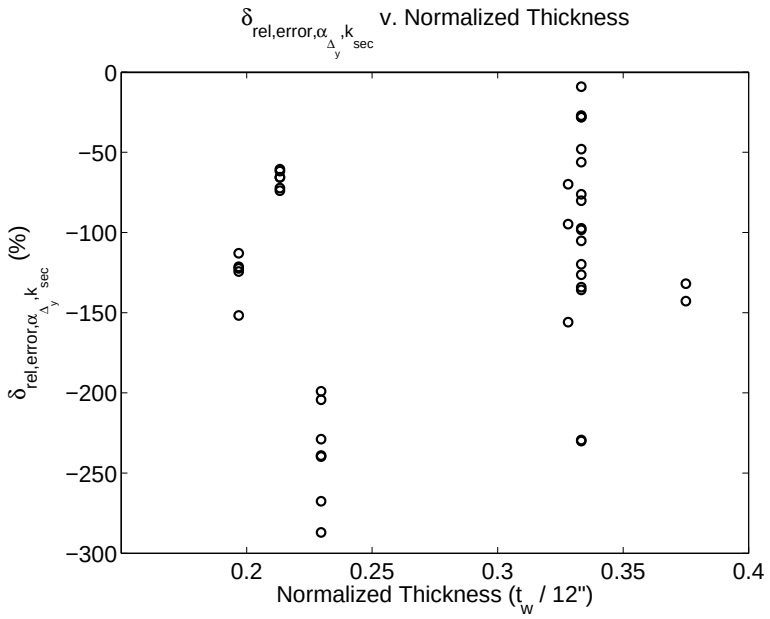

Figure N.94: Effective Shear Calibrated to Yield Displacement Secant Stiffness Relative Error Change v. Normalized Thickness

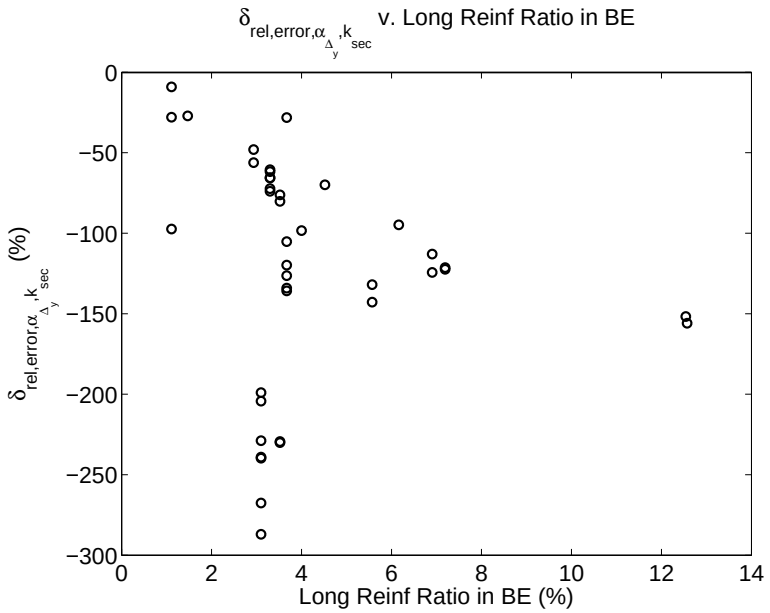

Figure N.95: Effective Shear Calibrated to Yield Displacement Secant Stiffness Relative Error Change v. Long Reinf Ratio in BE

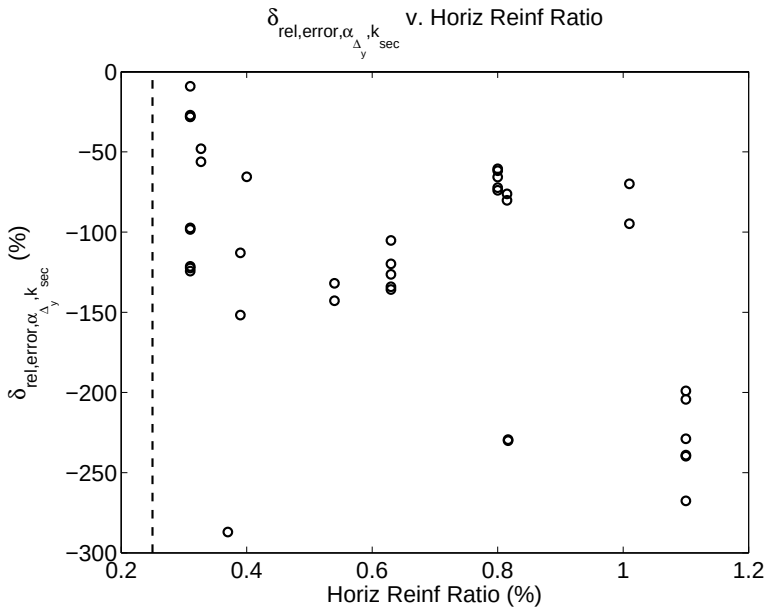

Figure N.96: Effective Shear Calibrated to Yield Displacement Secant Stiffness Relative Error Change v. Horiz Reinf Ratio

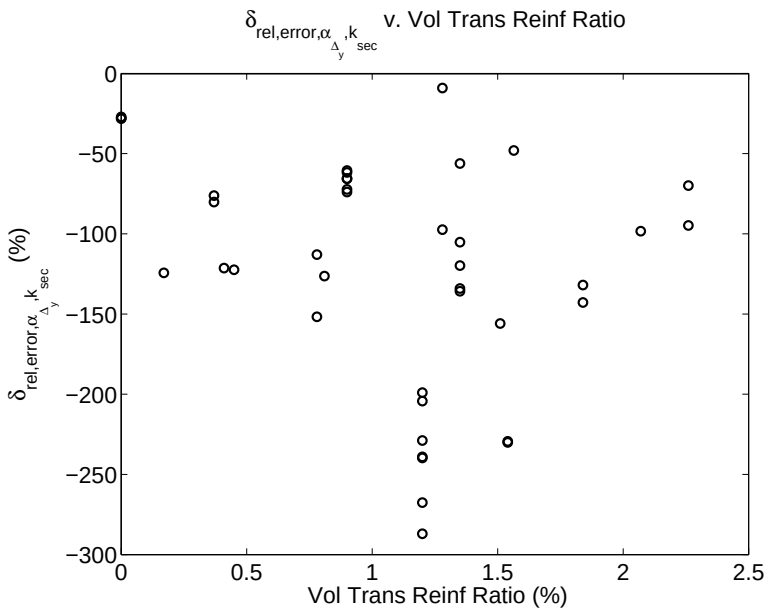

Figure N.97: Effective Shear Calibrated to Yield Displacement Secant Stiffness Relative Error Change v. Vol Trans Reinf Ratio

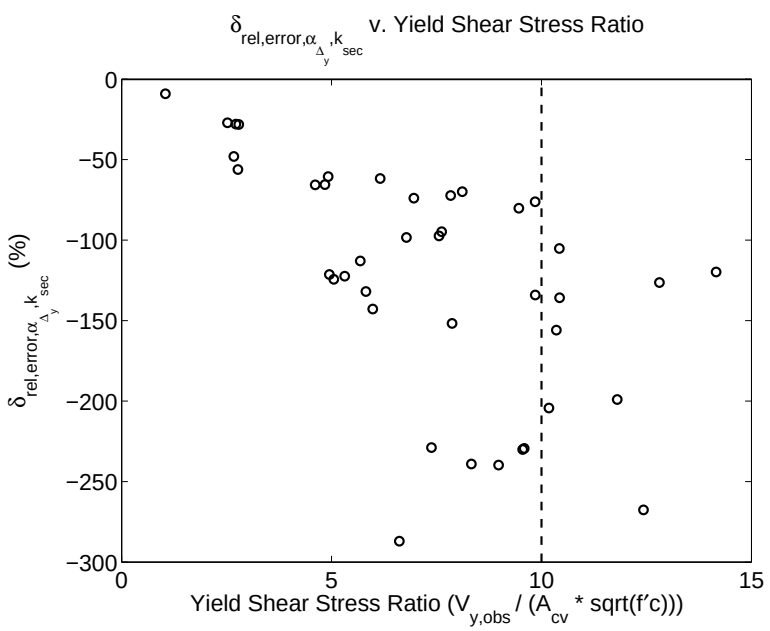

Figure N.98: Effective Shear Calibrated to Yield Displacement Secant Stiffness Relative Error Change v. Yield Shear Stress Ratio

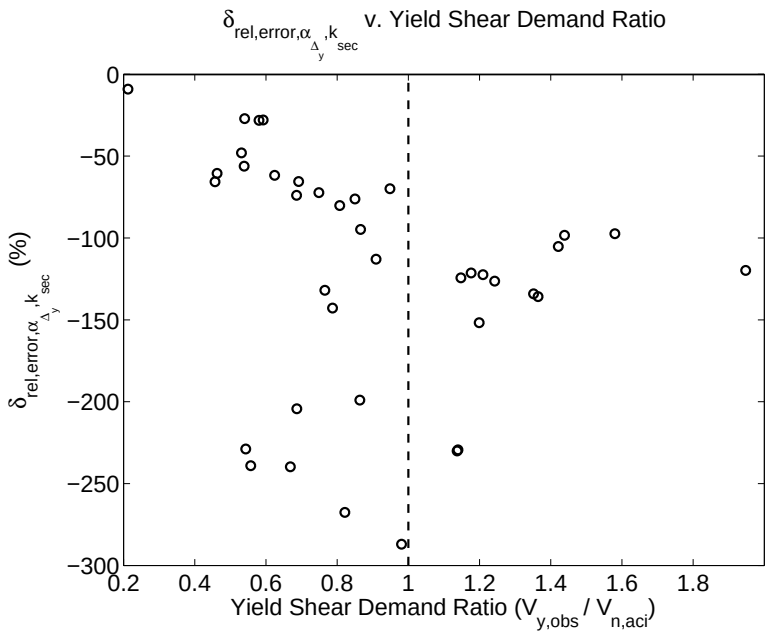

Figure N.99: Effective Shear Calibrated to Yield Displacement Secant Stiffness Relative Error Change v. Yield Shear Demand Ratio

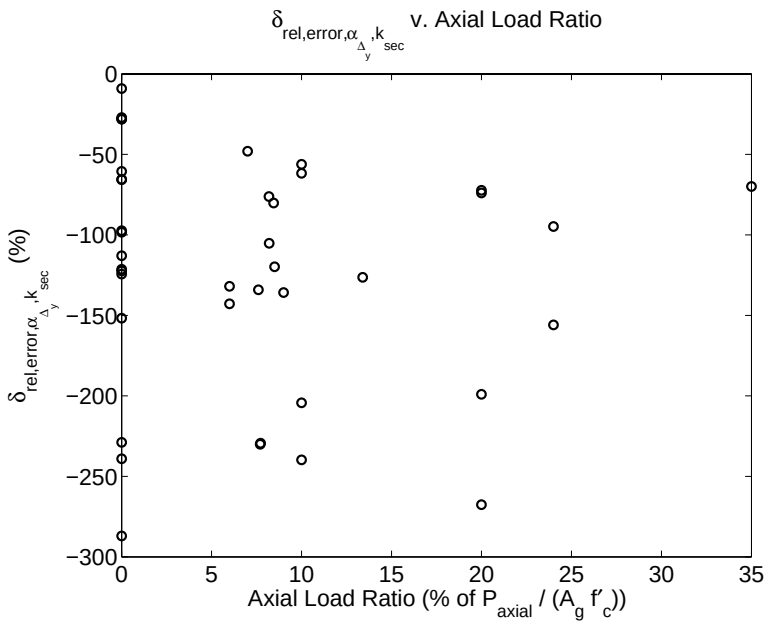

Figure N.100: Effective Shear Calibrated to Yield Displacement Secant Stiffness Relative Error Change v. Axial Load Ratio

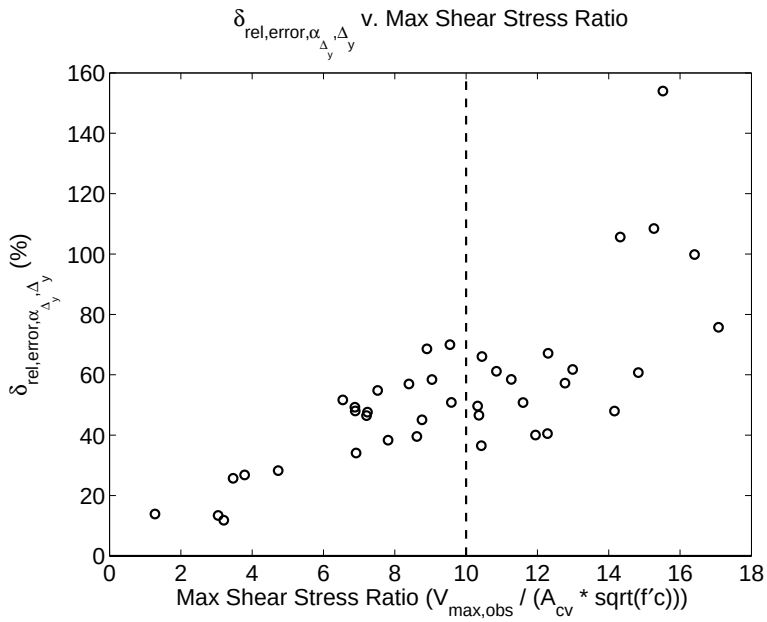

Figure N.101: Effective Shear Calibrated to Yield Displacement Yield Displacement Relative Error Change v. Max Shear Stress Ratio

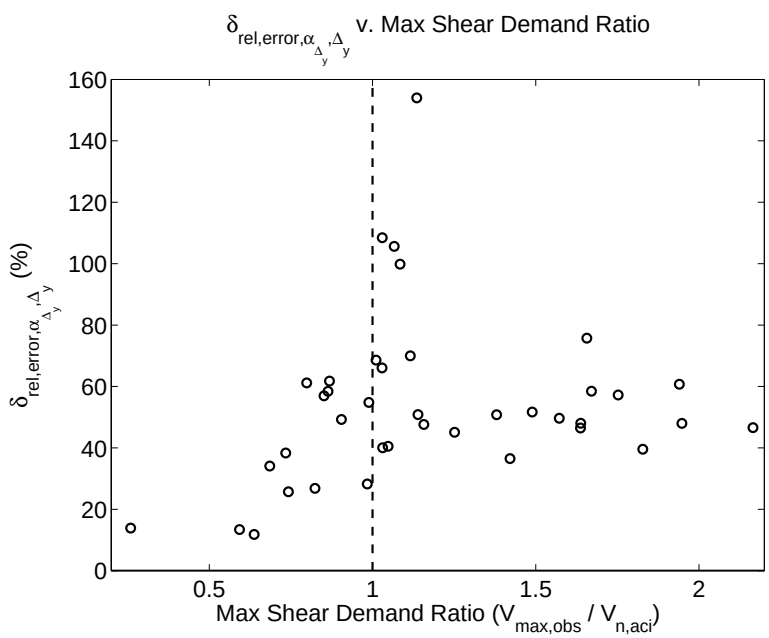

Figure N.102: Effective Shear Calibrated to Yield Displacement Yield Displacement Relative Error Change v. Max Shear Demand Ratio

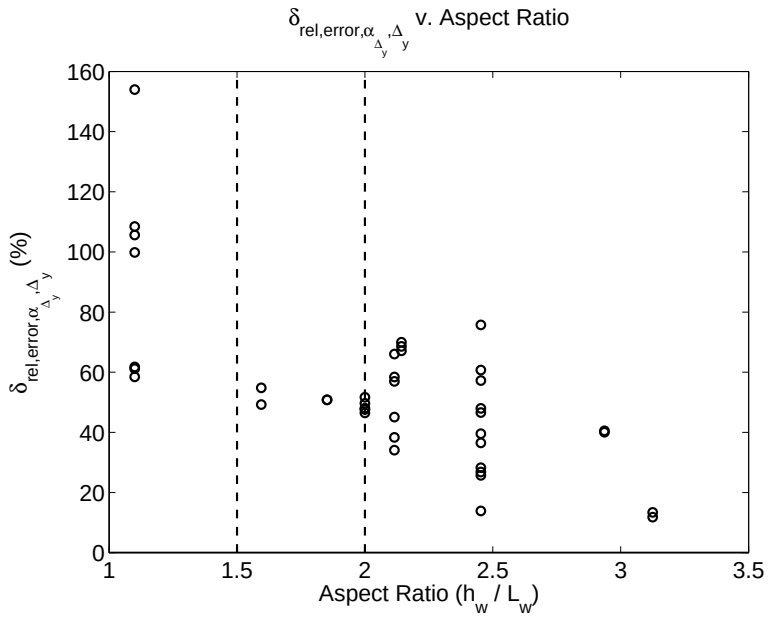

Figure N.103: Effective Shear Calibrated to Yield Displacement Yield Displacement Relative Error Change v. Aspect Ratio

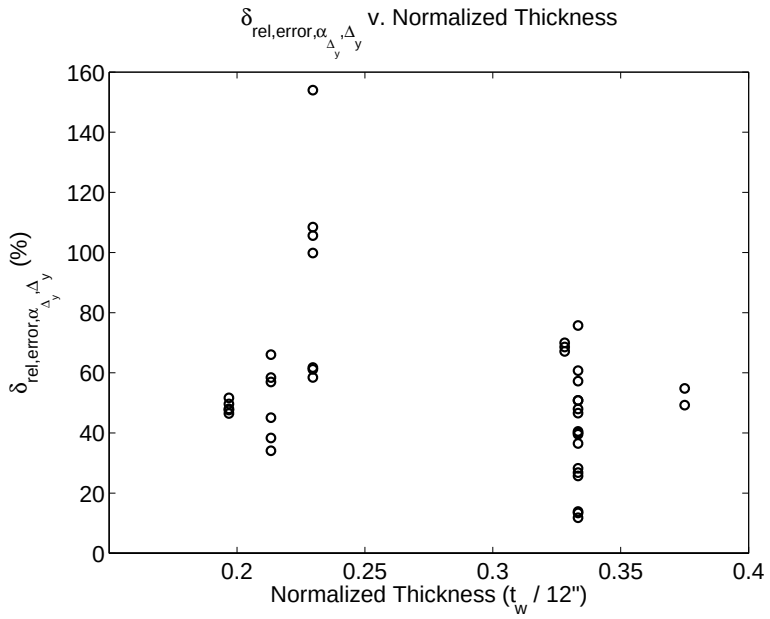

Figure N.104: Effective Shear Calibrated to Yield Displacement Yield Displacement Relative Error Change v. Normalized Thickness

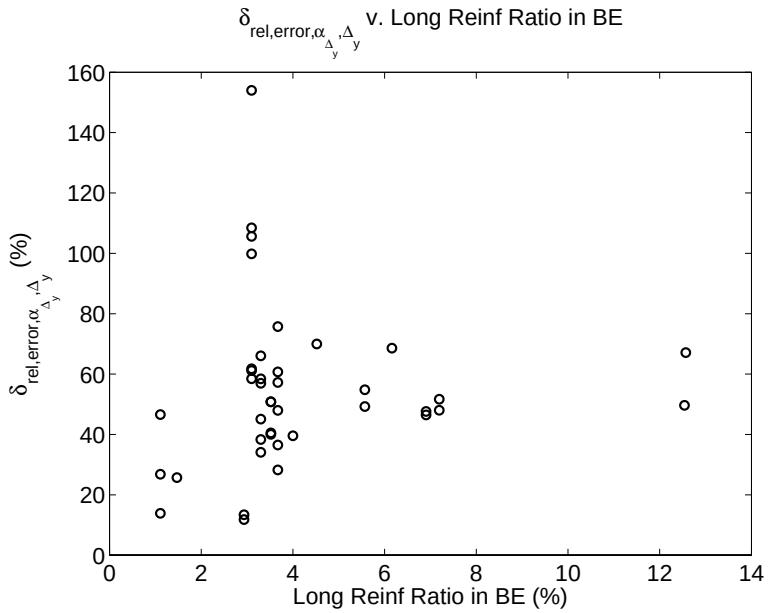

Figure N.105: Effective Shear Calibrated to Yield Displacement Yield Displacement Relative Error Change v. Long Reinf Ratio in BE

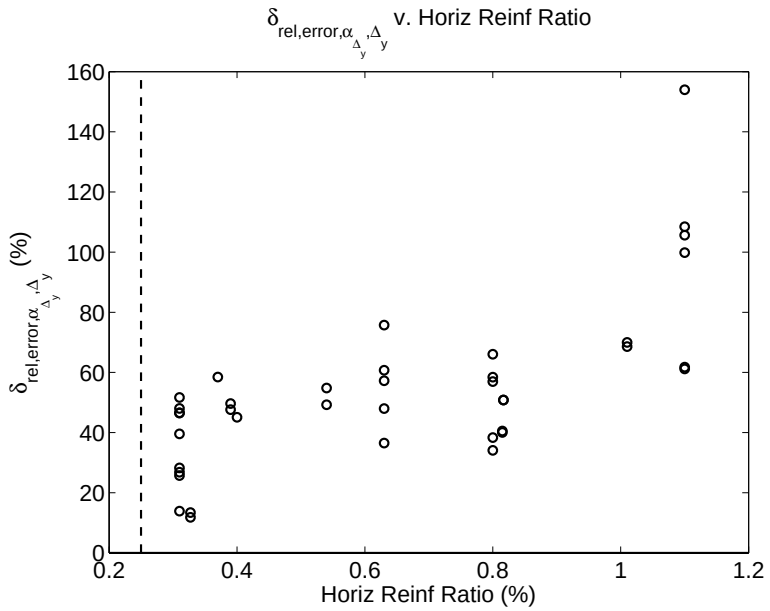

Figure N.106: Effective Shear Calibrated to Yield Displacement Yield Displacement Relative Error Change v. Horiz Reinf Ratio

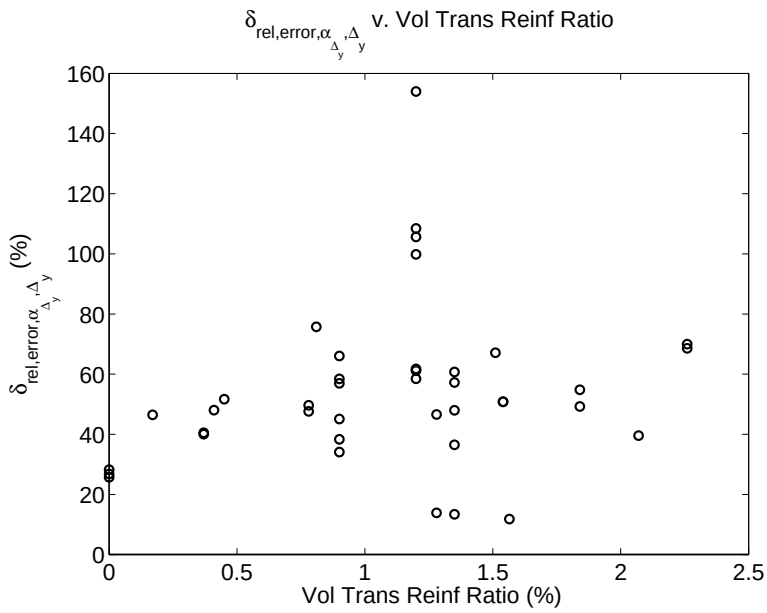

Figure N.107: Effective Shear Calibrated to Yield Displacement Yield Displacement Relative Error Change v. Vol Trans Reinf Ratio

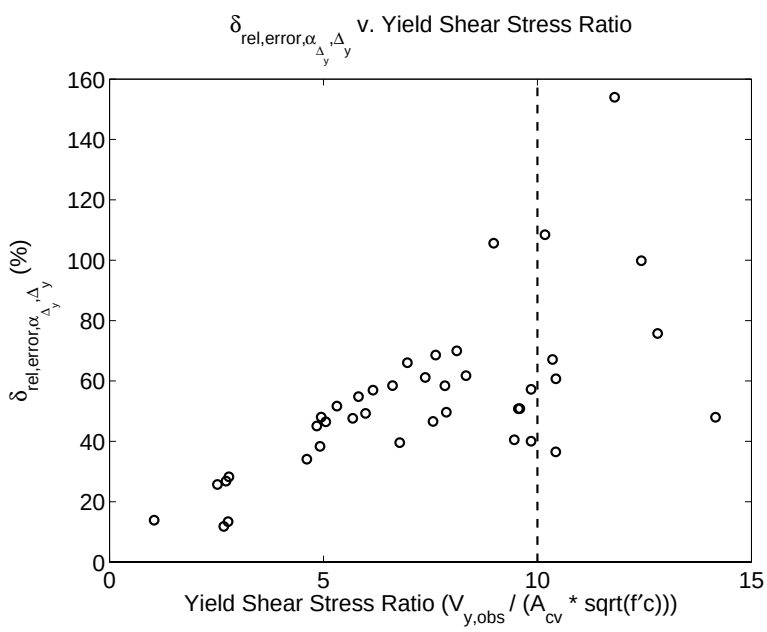

Figure N.108: Effective Shear Calibrated to Yield Displacement Yield Displacement Relative Error Change v. Yield Shear Stress Ratio

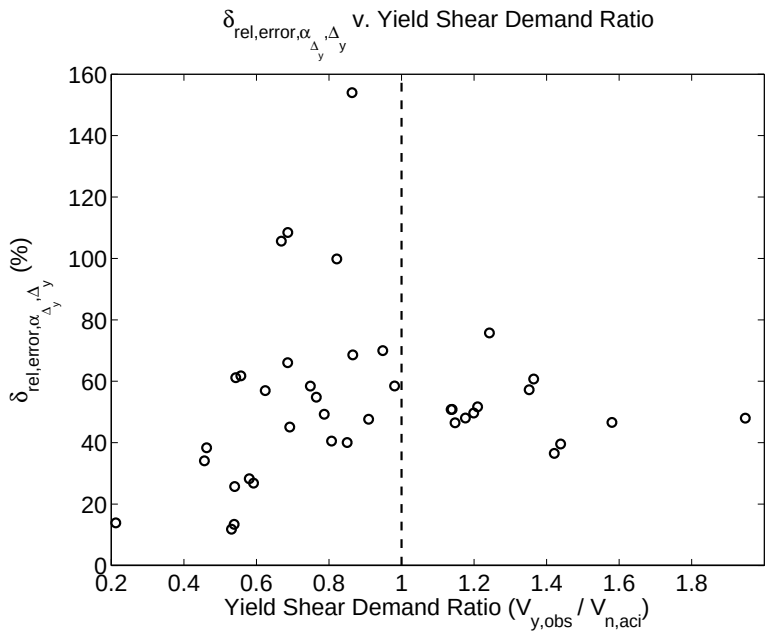

Figure N.109: Effective Shear Calibrated to Yield Displacement Yield Displacement Relative Error Change v. Yield Shear Demand Ratio

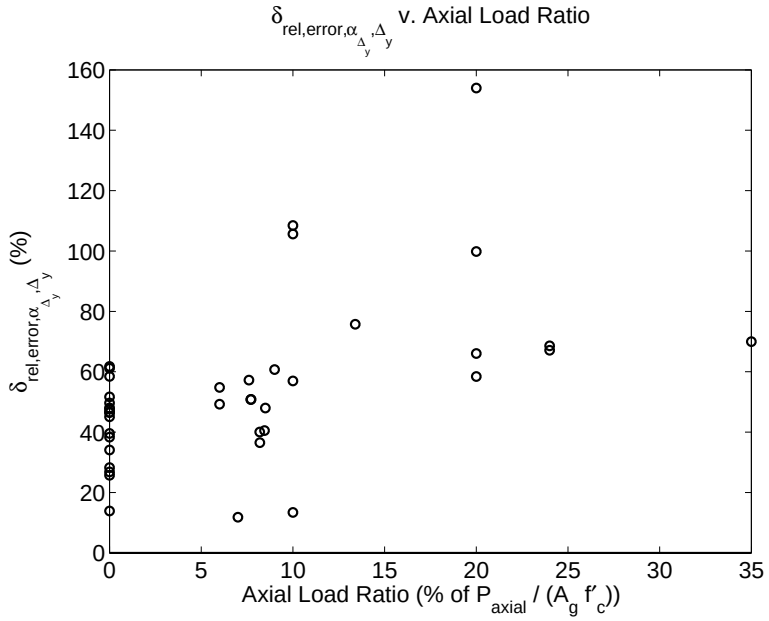

Figure N.110: Effective Shear Calibrated to Yield Displacement Yield Displacement Relative Error Change v. Axial Load Ratio

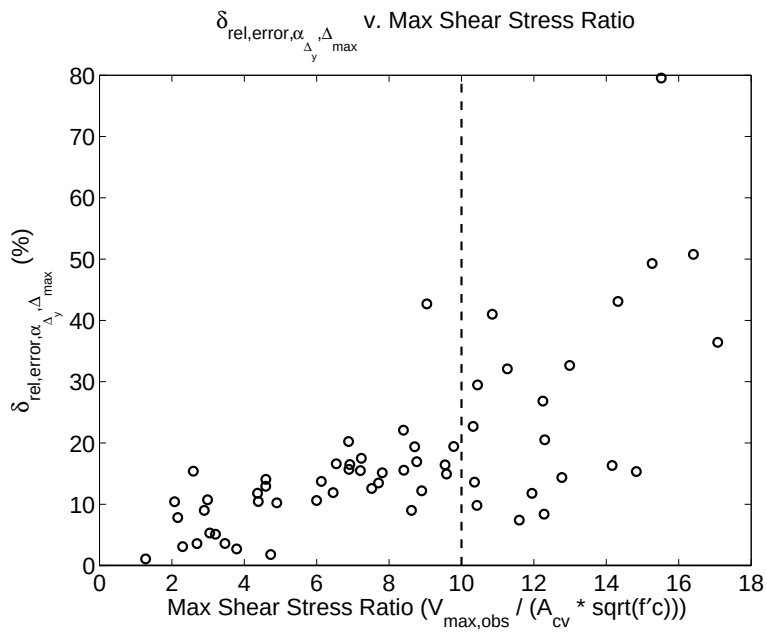

Figure N.111: Effective Shear Calibrated to Yield Displacement Max Displacement Relative Error Change v. Max Shear Stress Ratio

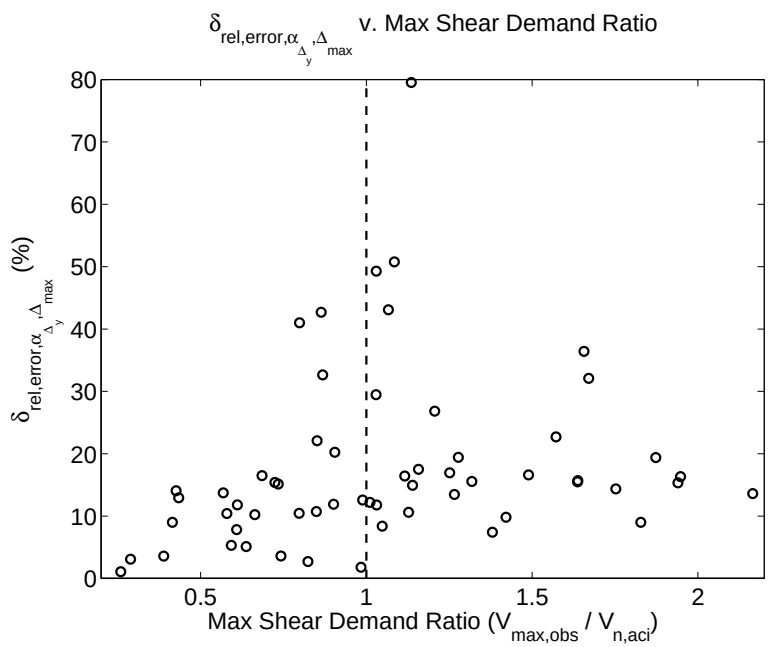

Figure N.112: Effective Shear Calibrated to Yield Displacement Max Displacement Relative Error Change v. Max Shear Demand Ratio

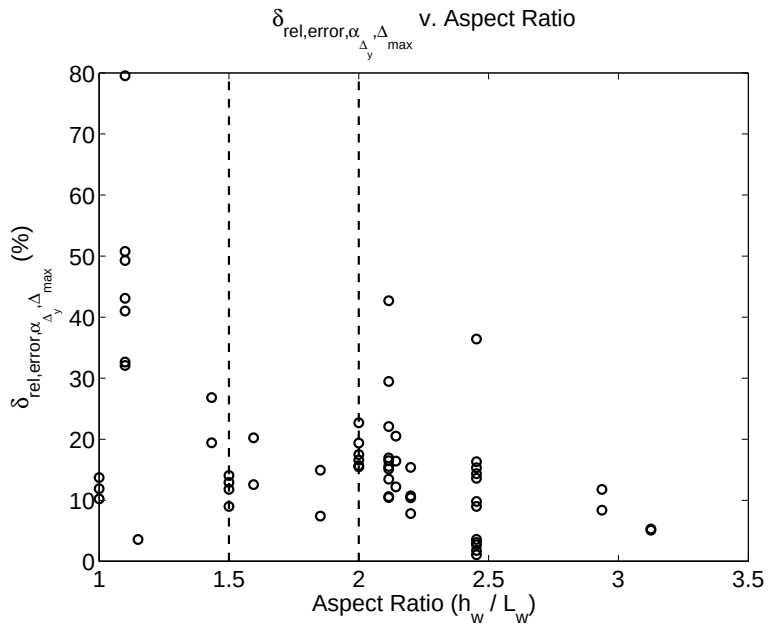

Figure N.113: Effective Shear Calibrated to Yield Displacement Max Displacement Relative Error Change v. Aspect Ratio

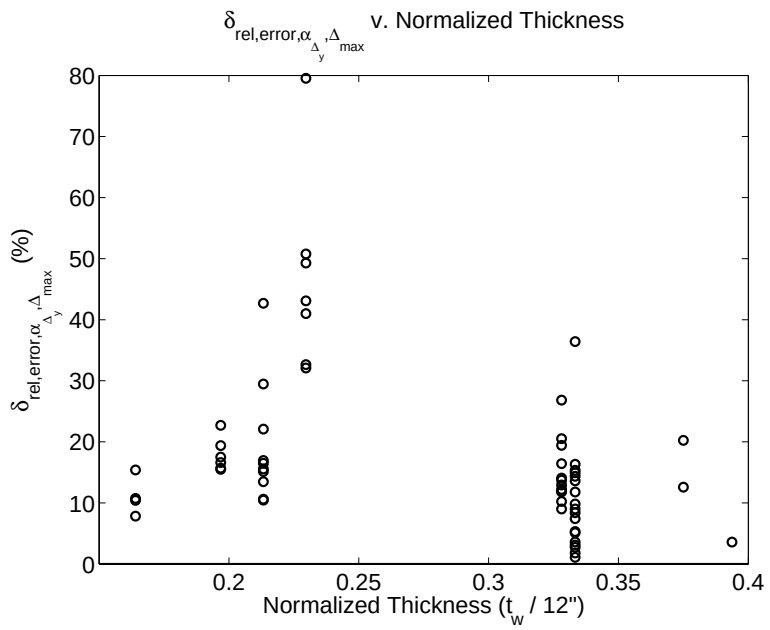

Figure N.114: Effective Shear Calibrated to Yield Displacement Max Displacement Relative Error Change v. Normalized Thickness

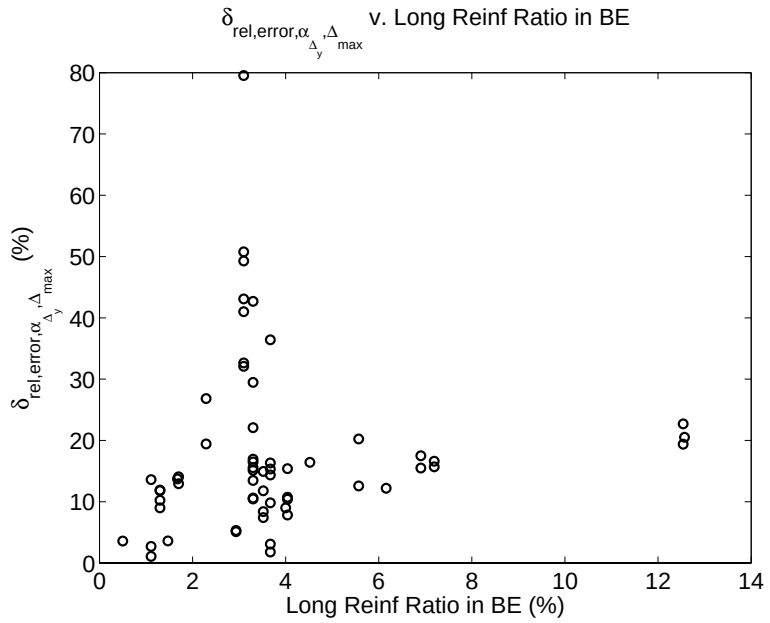

Figure N.115: Effective Shear Calibrated to Yield Displacement Max Displacement Relative Error Change v. Long Reinf Ratio in BE

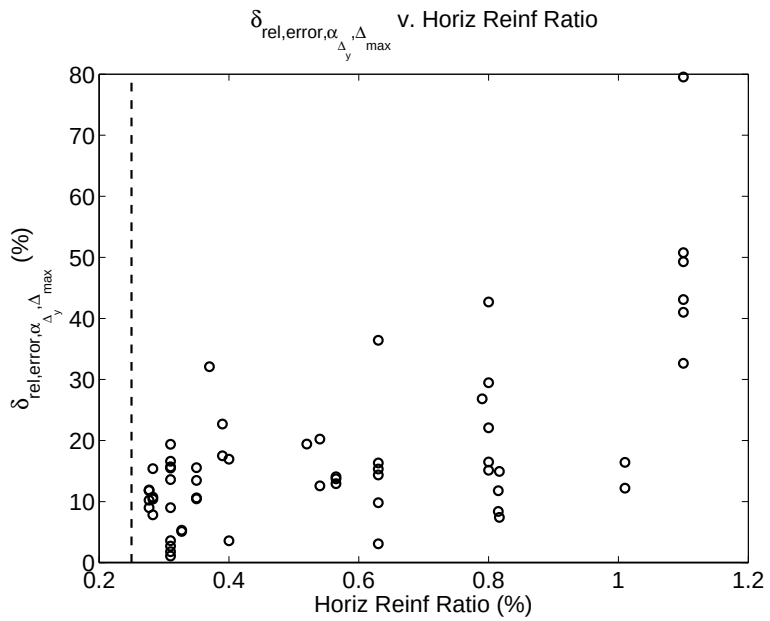

Figure N.116: Effective Shear Calibrated to Yield Displacement Max Displacement Relative Error Change v. Horiz Reinf Ratio

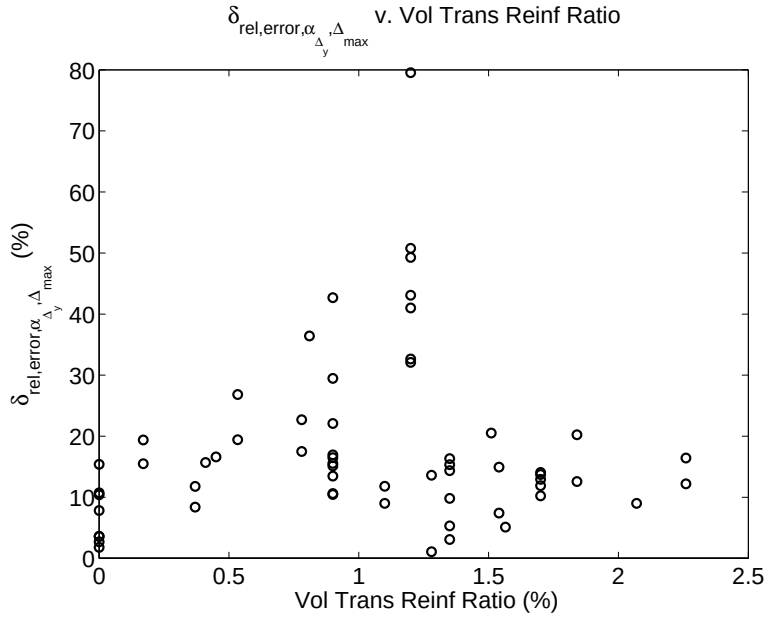

Figure N.117: Effective Shear Calibrated to Yield Displacement Max Displacement Relative Error Change v. Vol Trans Reinf Ratio

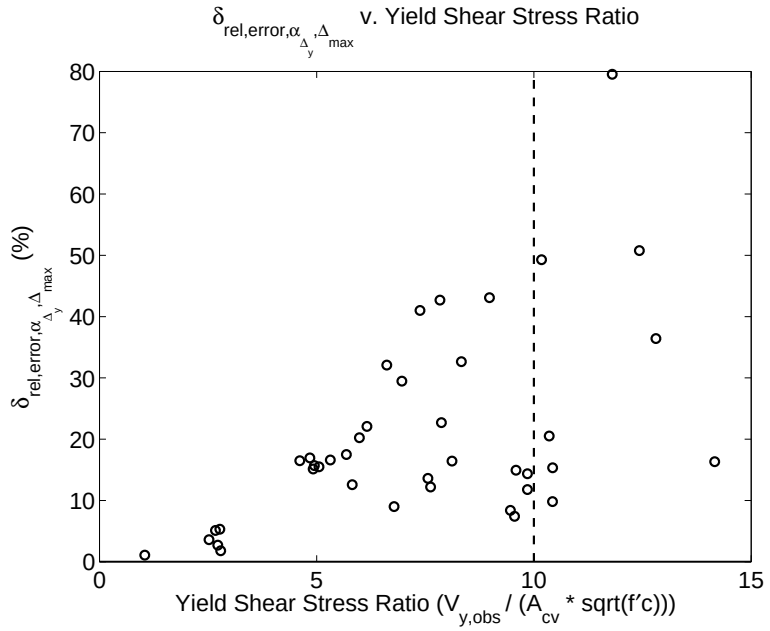

Figure N.118: Effective Shear Calibrated to Yield Displacement Max Displacement Relative Error Change v. Yield Shear Stress Ratio

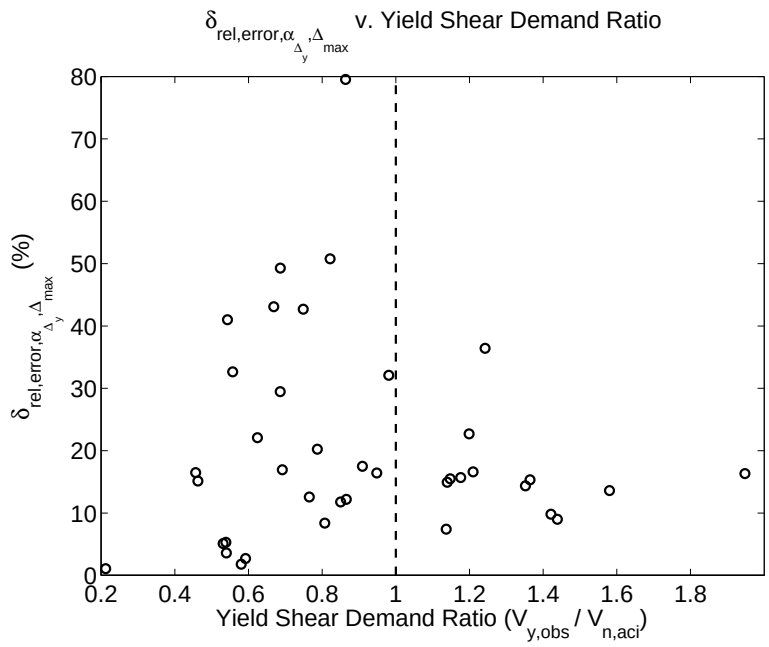

Figure N.119: Effective Shear Calibrated to Yield Displacement Max Displacement Relative Error Change v. Yield Shear Demand Ratio

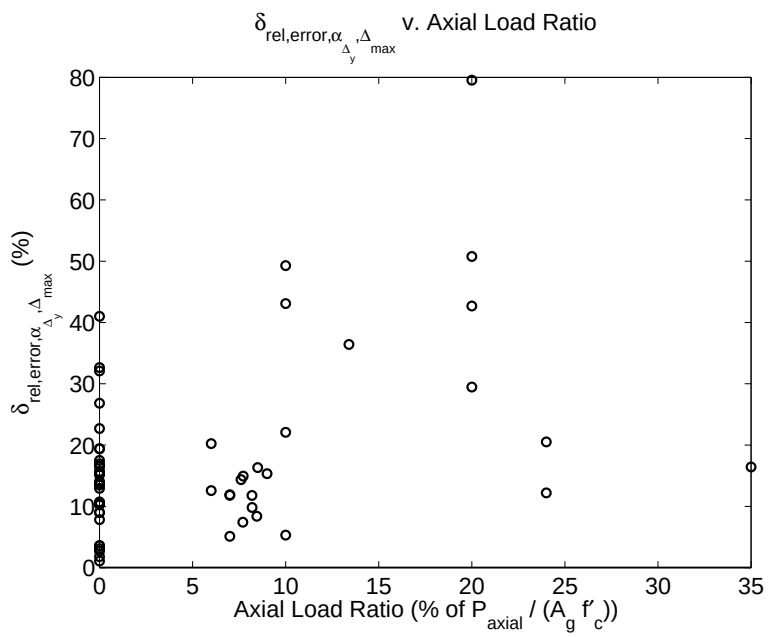

Figure N.120: Effective Shear Calibrated to Yield Displacement Max Displacement Relative Error Change v. Axial Load Ratio

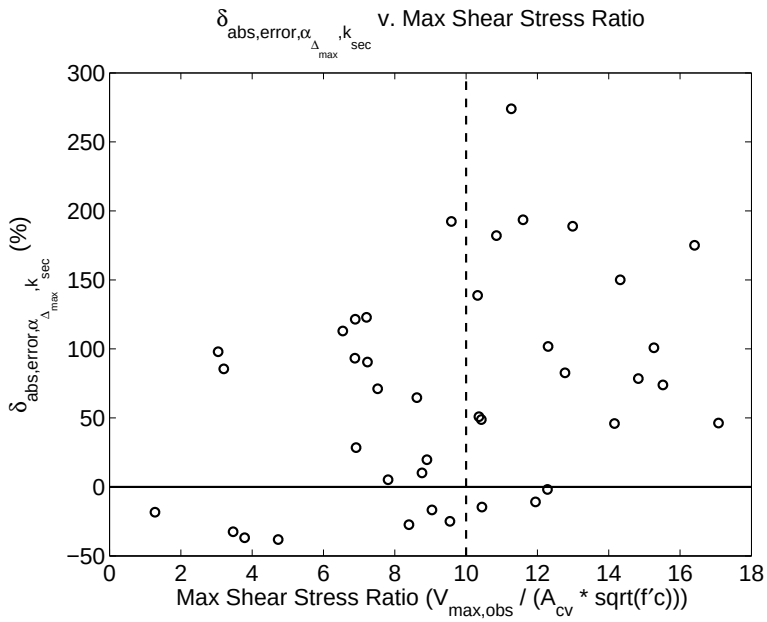

Figure N.121: Effective Shear Calibrated to Max Displacement Secant Stiffness Absolute Error Change v. Max Shear Stress Ratio

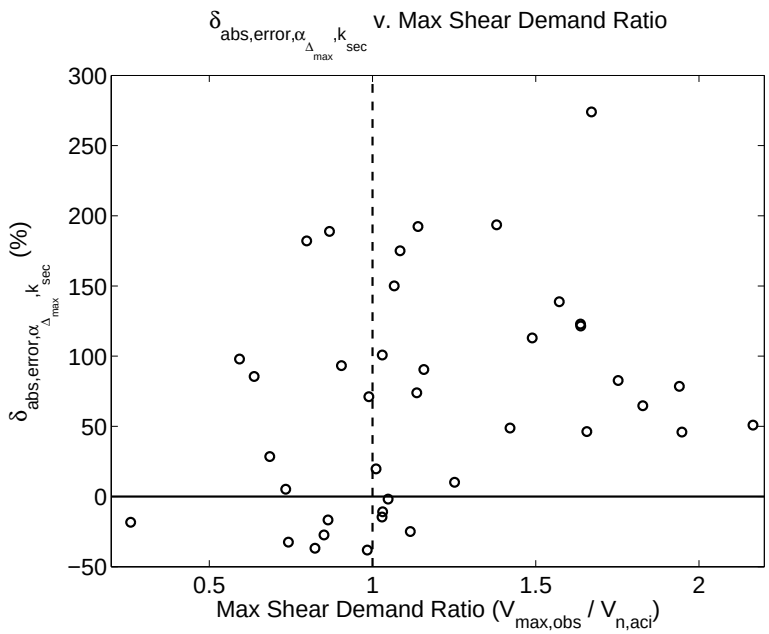

Figure N.122: Effective Shear Calibrated to Max Displacement Secant Stiffness Absolute Error Change v. Max Shear Demand Ratio

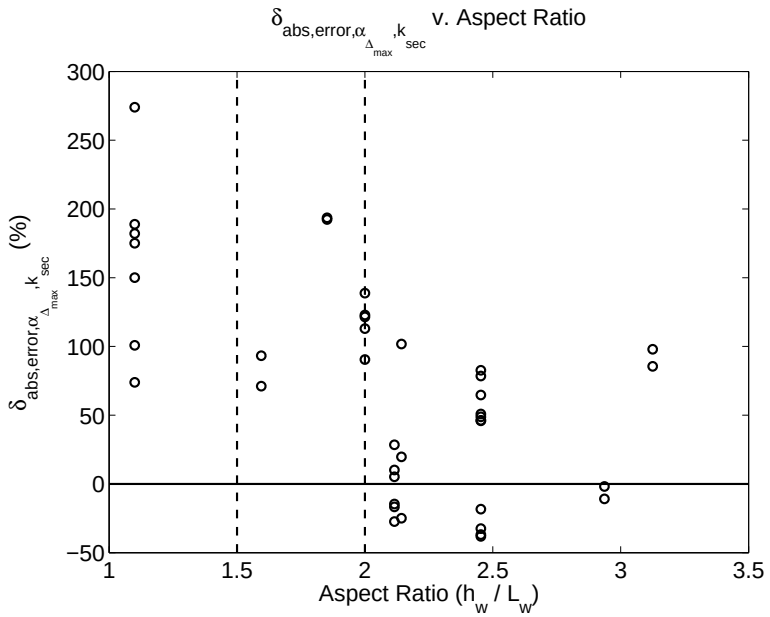

Figure N.123: Effective Shear Calibrated to Max Displacement Secant Stiffness Absolute Error Change v. Aspect Ratio

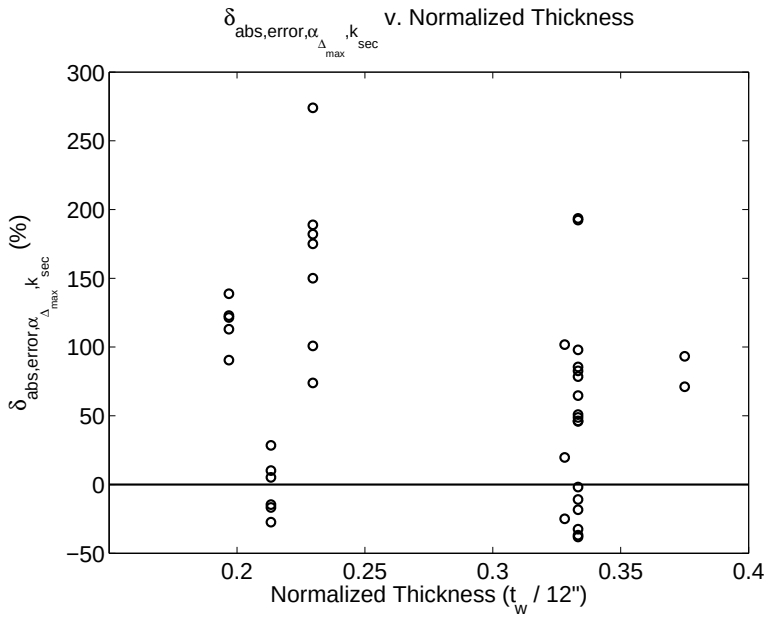

Figure N.124: Effective Shear Calibrated to Max Displacement Secant Stiffness Absolute Error Change v. Normalized Thickness

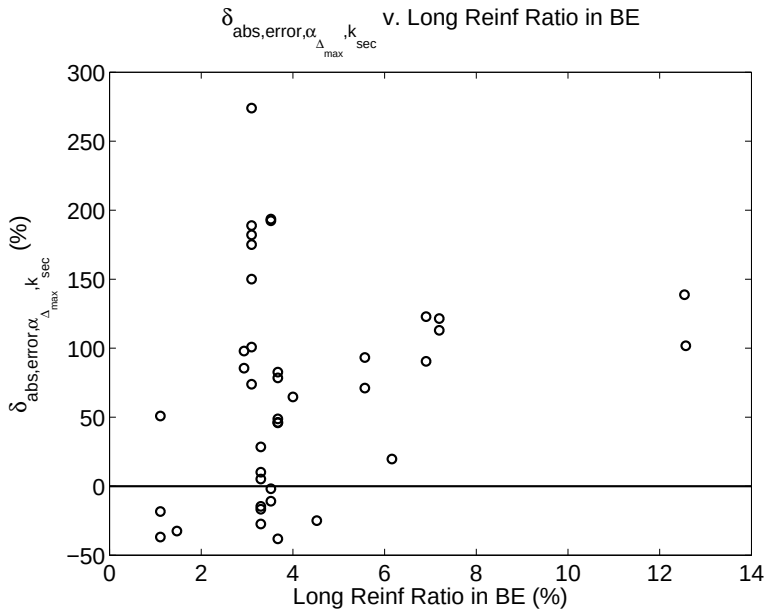

Figure N.125: Effective Shear Calibrated to Max Displacement Secant Stiffness Absolute Error Change v. Long Reinf Ratio in BE

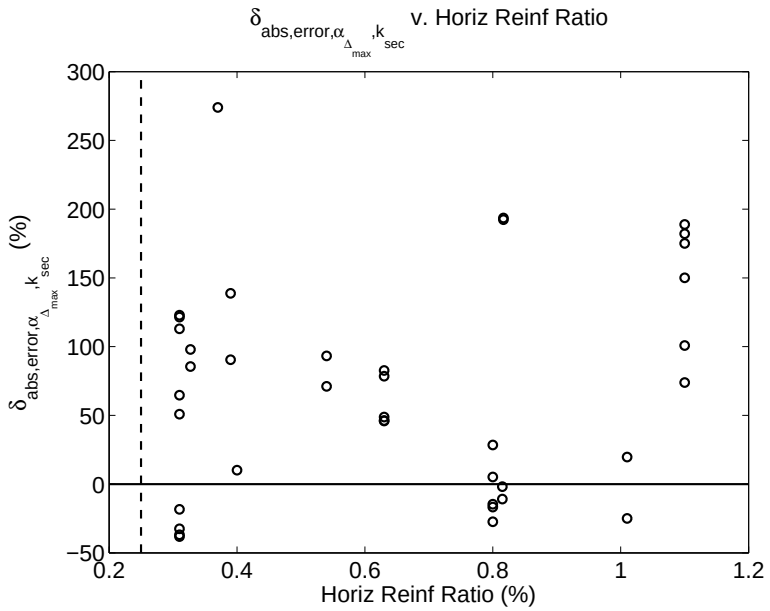

Figure N.126: Effective Shear Calibrated to Max Displacement Secant Stiffness Absolute Error Change v. Horiz Reinf Ratio

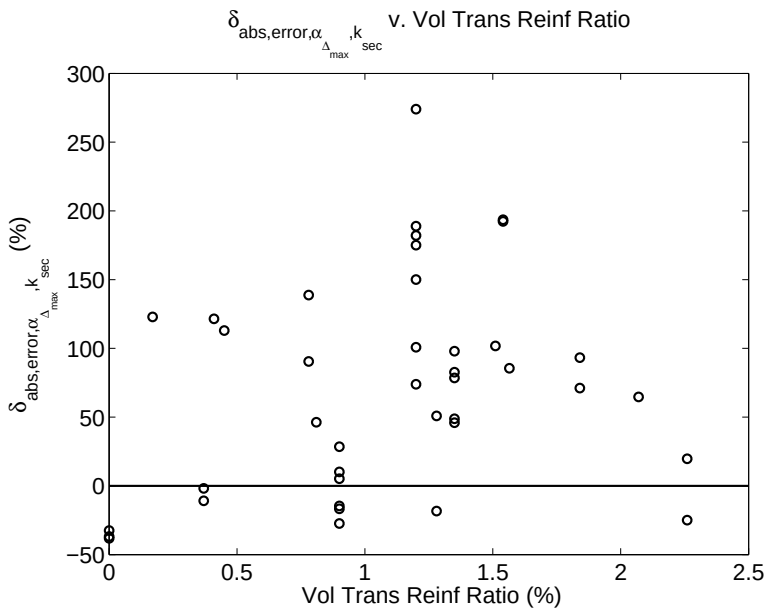

Figure N.127: Effective Shear Calibrated to Max Displacement Secant Stiffness Absolute Error Change v. Vol Trans Reinf Ratio

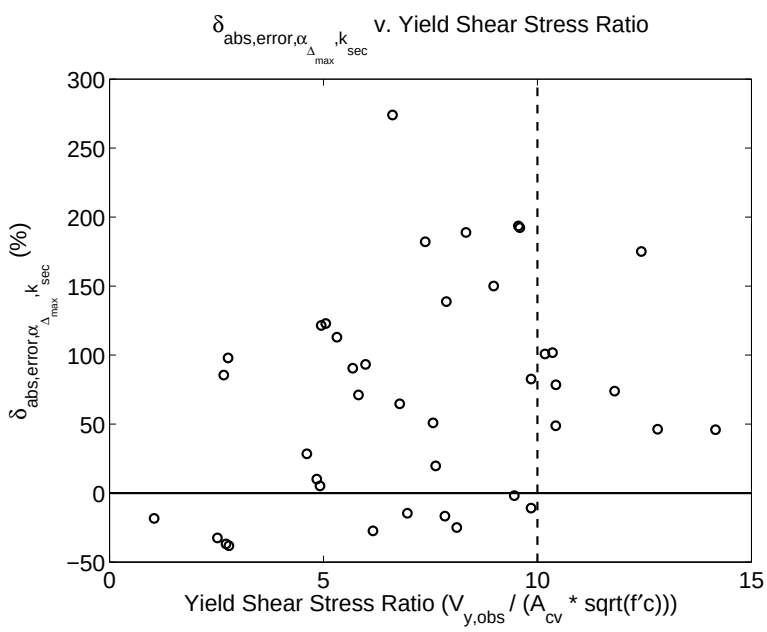

Figure N.128: Effective Shear Calibrated to Max Displacement Secant Stiffness Absolute Error Change v. Yield Shear Stress Ratio

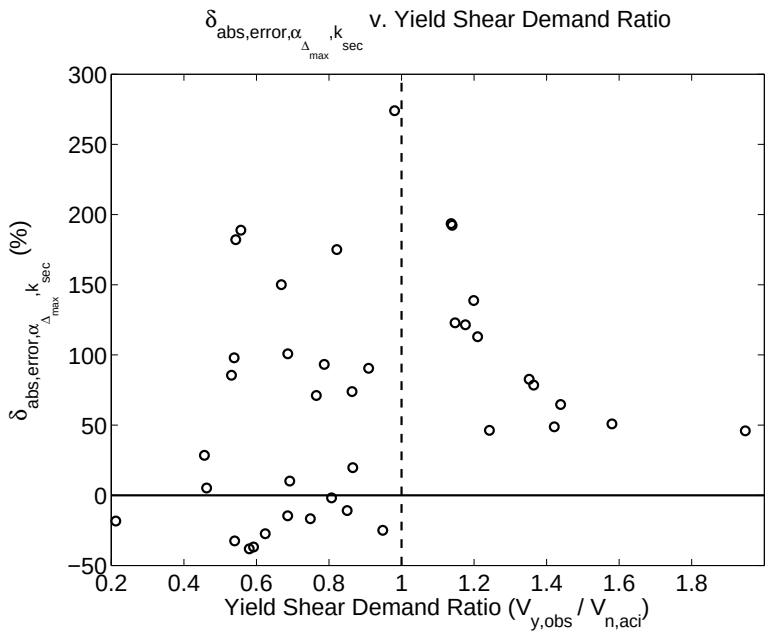

Figure N.129: Effective Shear Calibrated to Max Displacement Secant Stiffness Absolute Error Change v. Yield Shear Demand Ratio

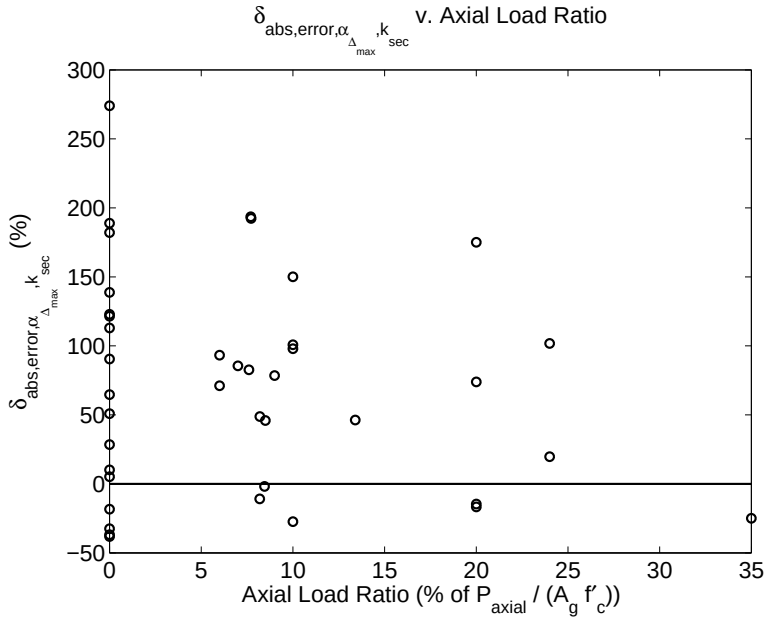

Figure N.130: Effective Shear Calibrated to Max Displacement Secant Stiffness Absolute Error Change v. Axial Load Ratio

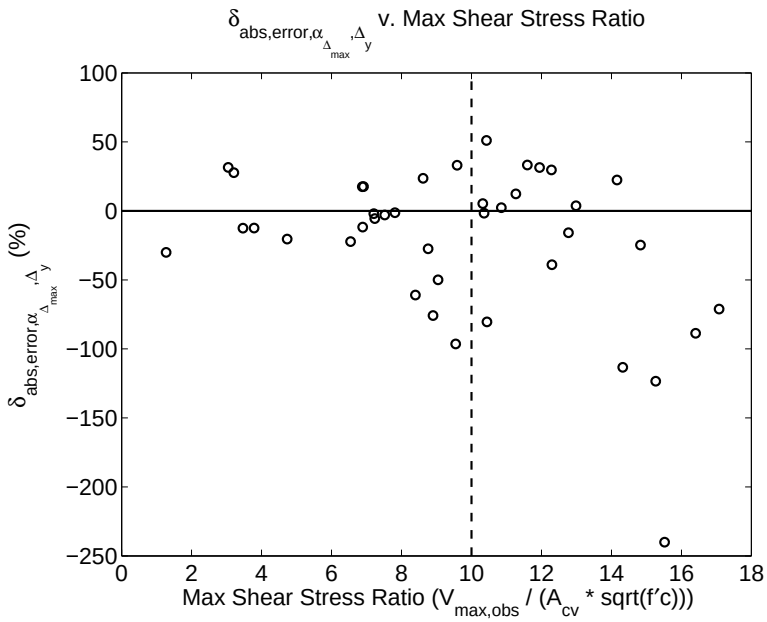

Figure N.131: Effective Shear Calibrated to Max Displacement Yield Displacement Absolute Error Change v. Max Shear Stress Ratio

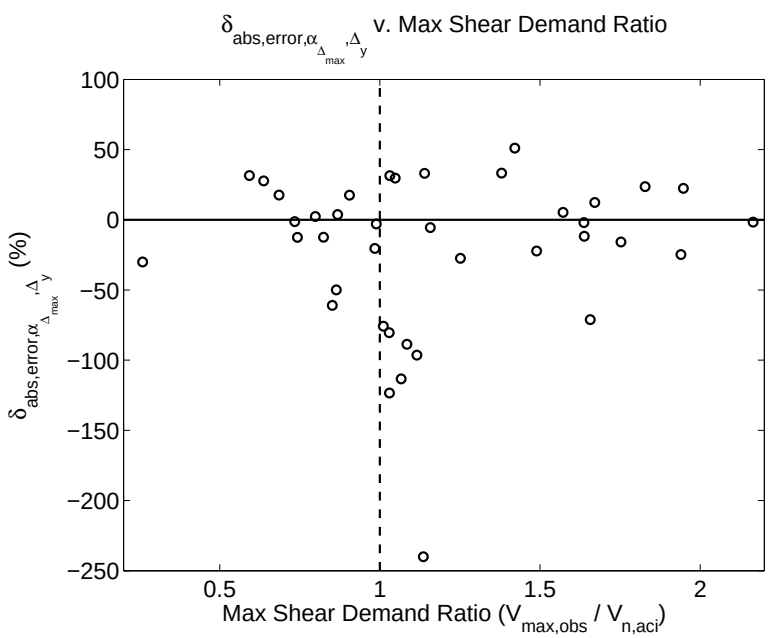

Figure N.132: Effective Shear Calibrated to Max Displacement Yield Displacement Absolute Error Change v. Max Shear Demand Ratio

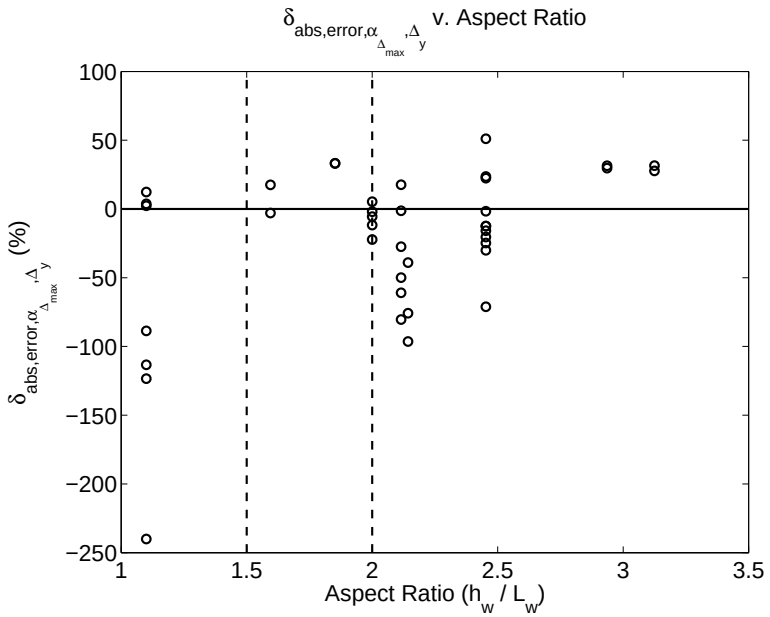

Figure N.133: Effective Shear Calibrated to Max Displacement Yield Displacement Absolute Error Change v. Aspect Ratio

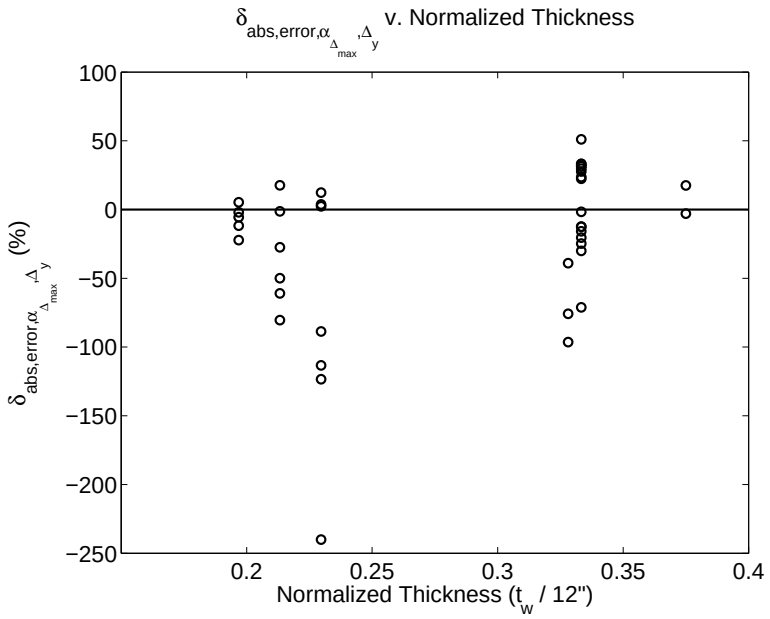

Figure N.134: Effective Shear Calibrated to Max Displacement Yield Displacement Absolute Error Change v. Normalized Thickness

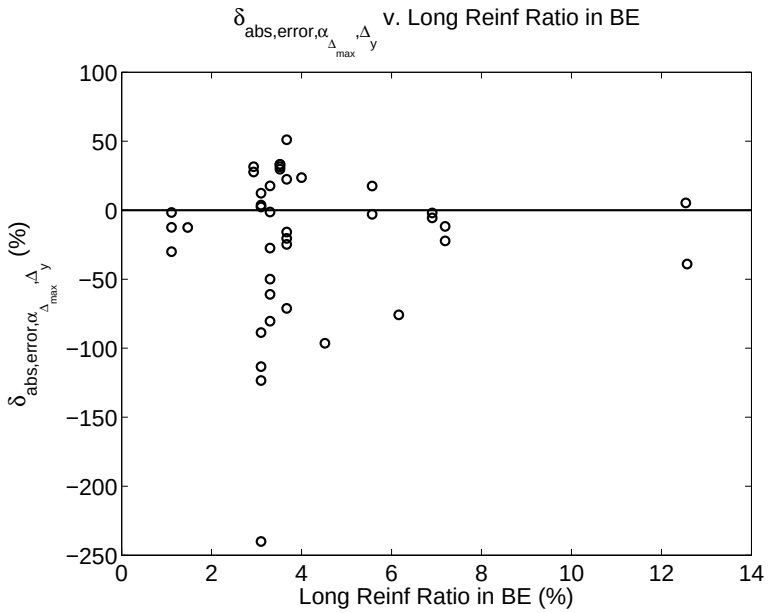

Figure N.135: Effective Shear Calibrated to Max Displacement Yield Displacement Absolute Error Change v. Long Reinf Ratio in BE

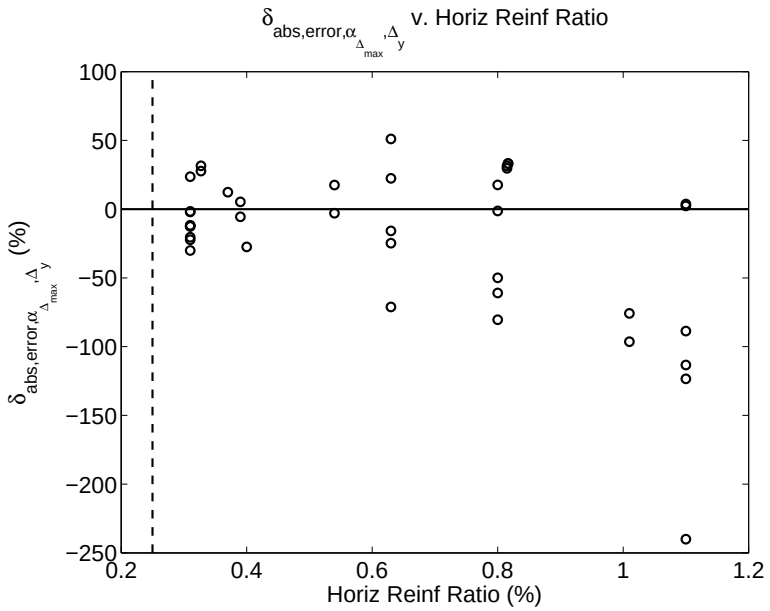

Figure N.136: Effective Shear Calibrated to Max Displacement Yield Displacement Absolute Error Change v. Horiz Reinf Ratio

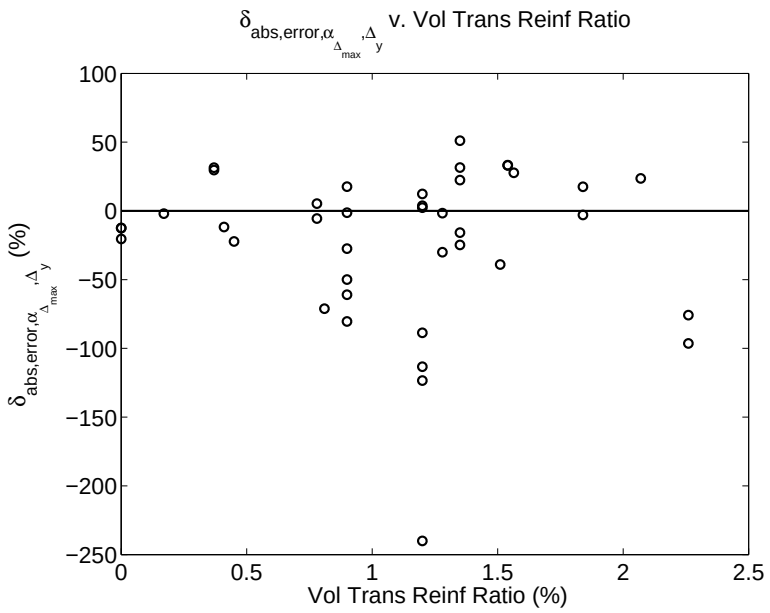

Figure N.137: Effective Shear Calibrated to Max Displacement Yield Displacement Absolute Error Change v. Vol Trans Reinf Ratio

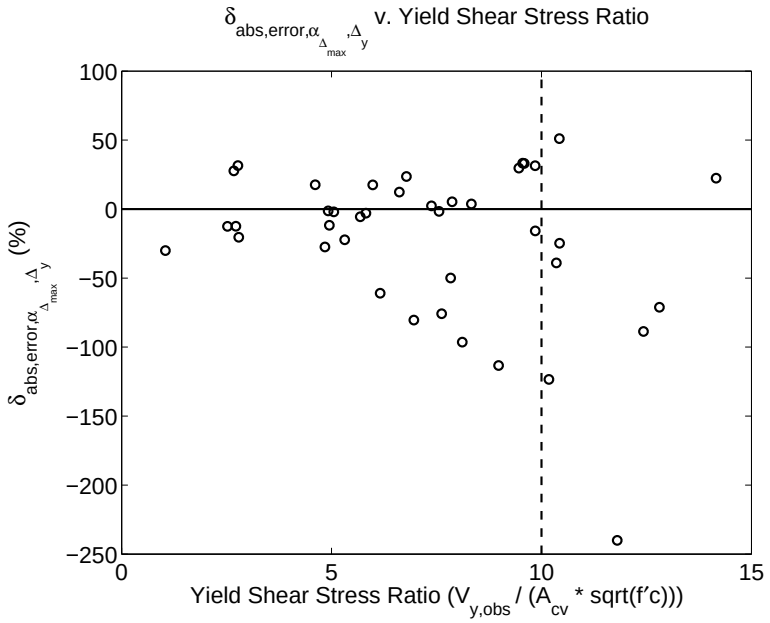

Figure N.138: Effective Shear Calibrated to Max Displacement Yield Displacement Absolute Error Change v. Yield Shear Stress Ratio

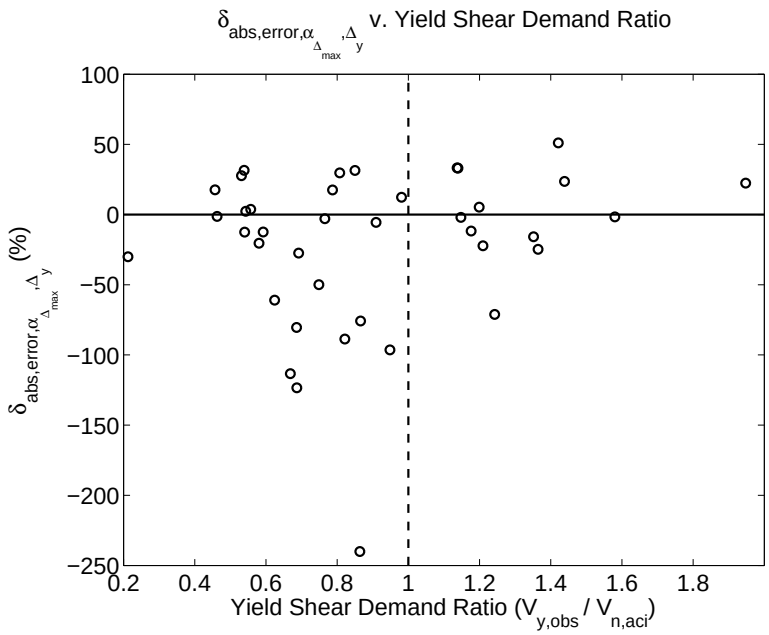

Figure N.139: Effective Shear Calibrated to Max Displacement Yield Displacement Absolute Error Change v. Yield Shear Demand Ratio

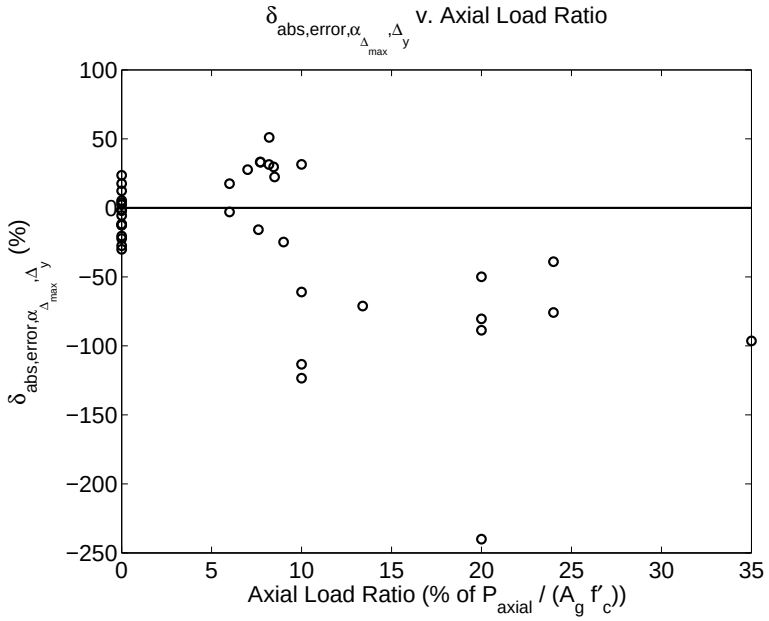

Figure N.140: Effective Shear Calibrated to Max Displacement Yield Displacement Absolute Error Change v. Axial Load Ratio

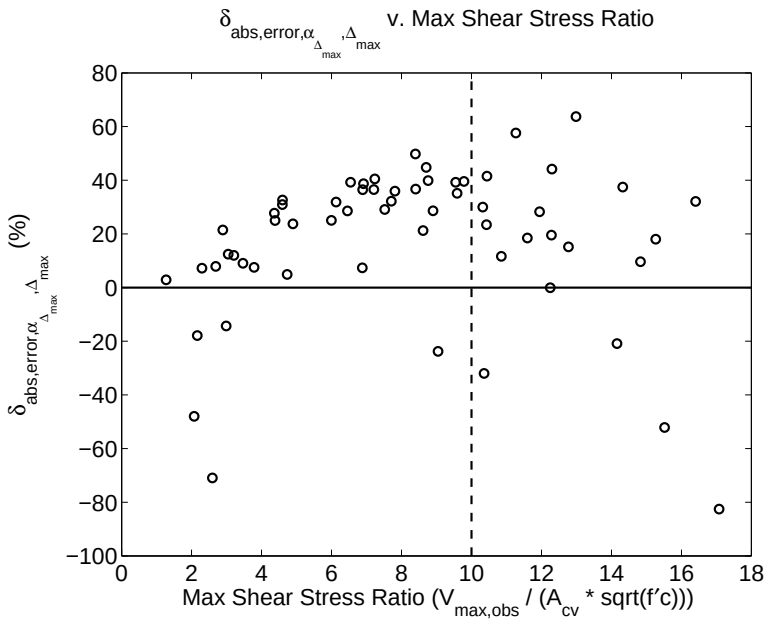

Figure N.141: Effective Shear Calibrated to Max Displacement Max Displacement Absolute Error Change v. Max Shear Stress Ratio

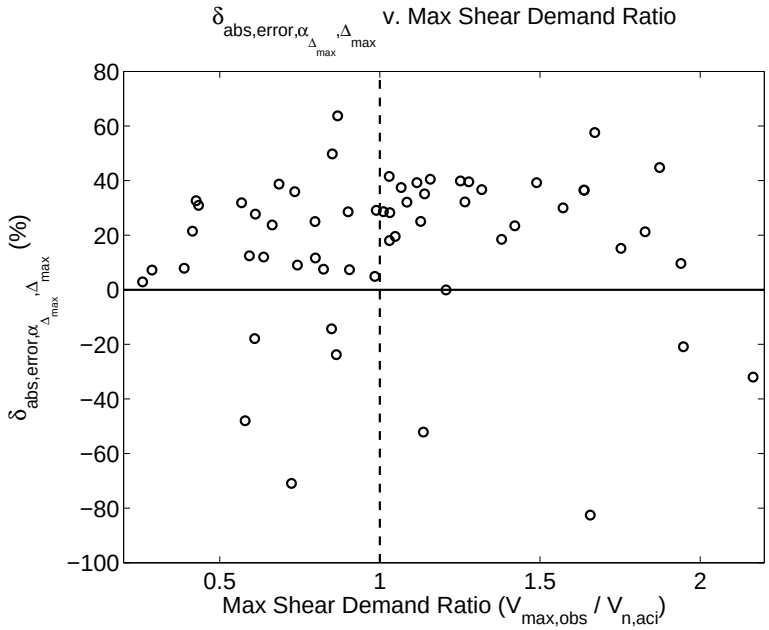

Figure N.142: Effective Shear Calibrated to Max Displacement Max Displacement Absolute Error Change v. Max Shear Demand Ratio

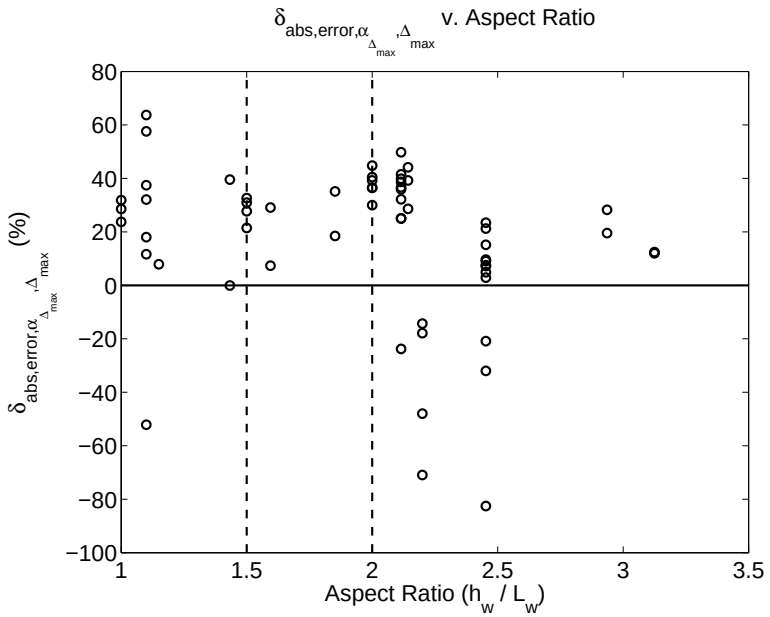

Figure N.143: Effective Shear Calibrated to Max Displacement Max Displacement Absolute Error Change v. Aspect Ratio

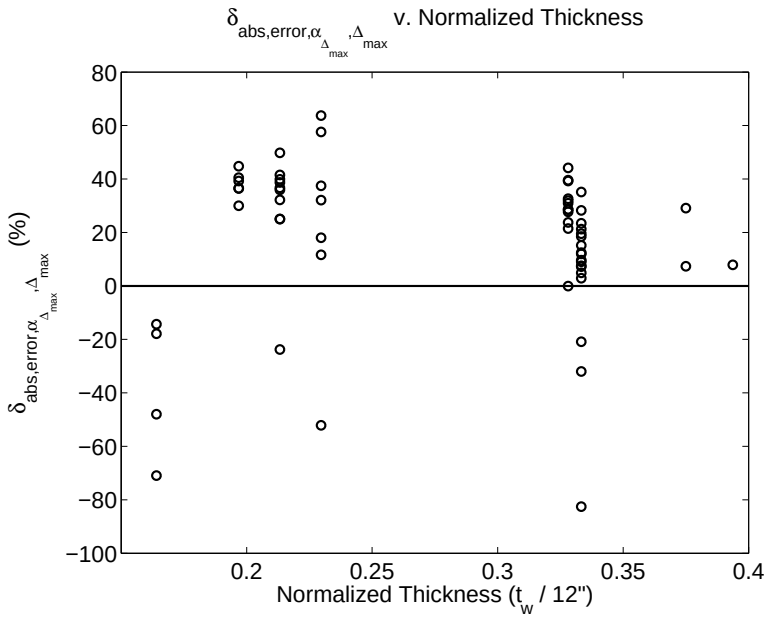

Figure N.144: Effective Shear Calibrated to Max Displacement Max Displacement Absolute Error Change v. Normalized Thickness

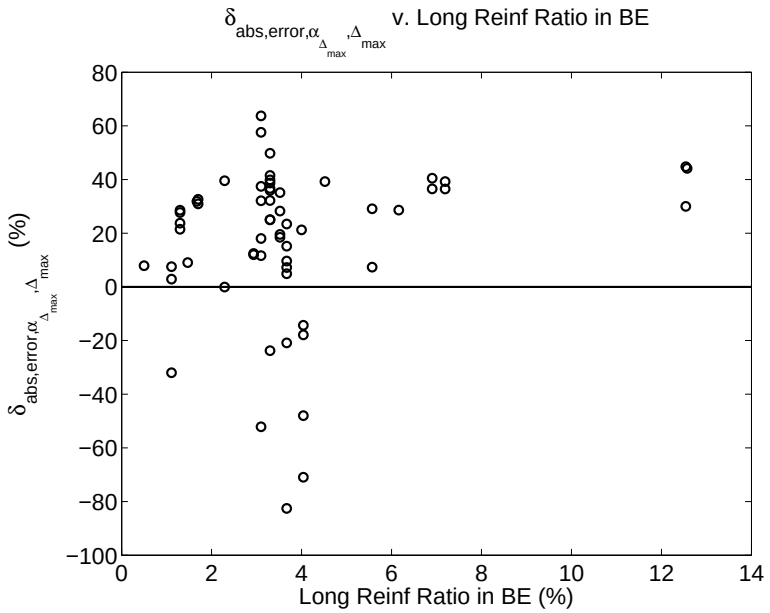

Figure N.145: Effective Shear Calibrated to Max Displacement Max Displacement Absolute Error Change v. Long Reinf Ratio in BE

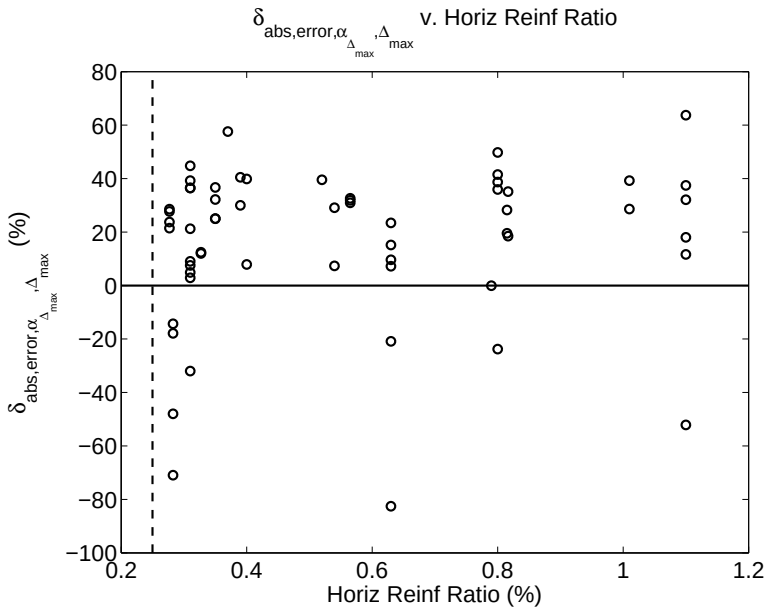

Figure N.146: Effective Shear Calibrated to Max Displacement Max Displacement Absolute Error Change v. Horiz Reinf Ratio

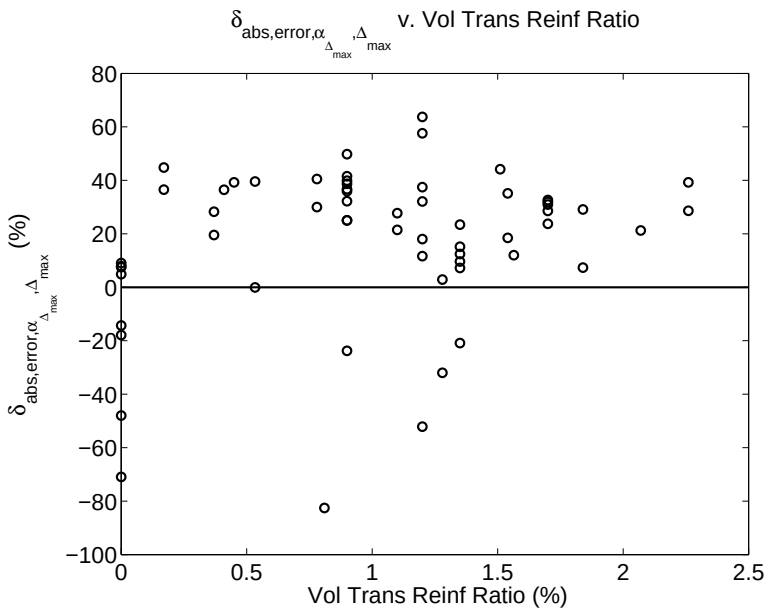

Figure N.147: Effective Shear Calibrated to Max Displacement Max Displacement Absolute Error Change v. Vol Trans Reinf Ratio

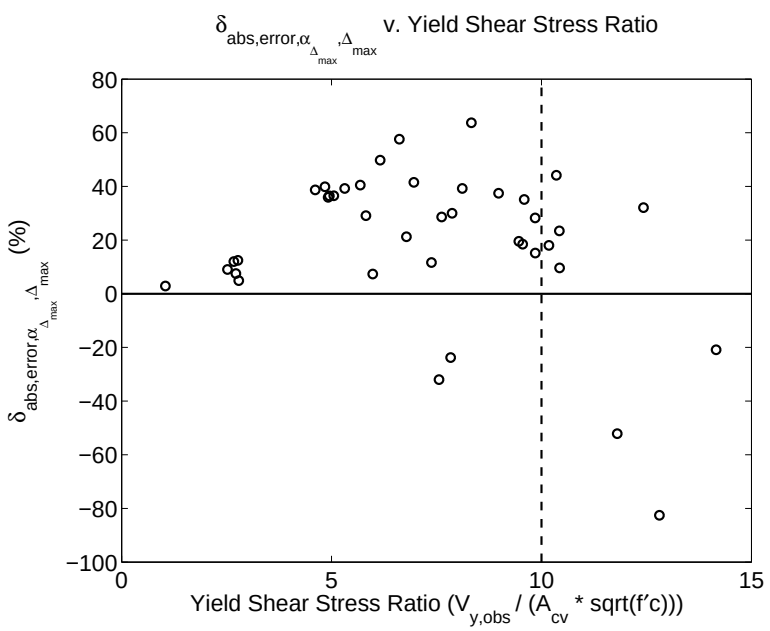

Figure N.148: Effective Shear Calibrated to Max Displacement Max Displacement Absolute Error Change v. Yield Shear Stress Ratio

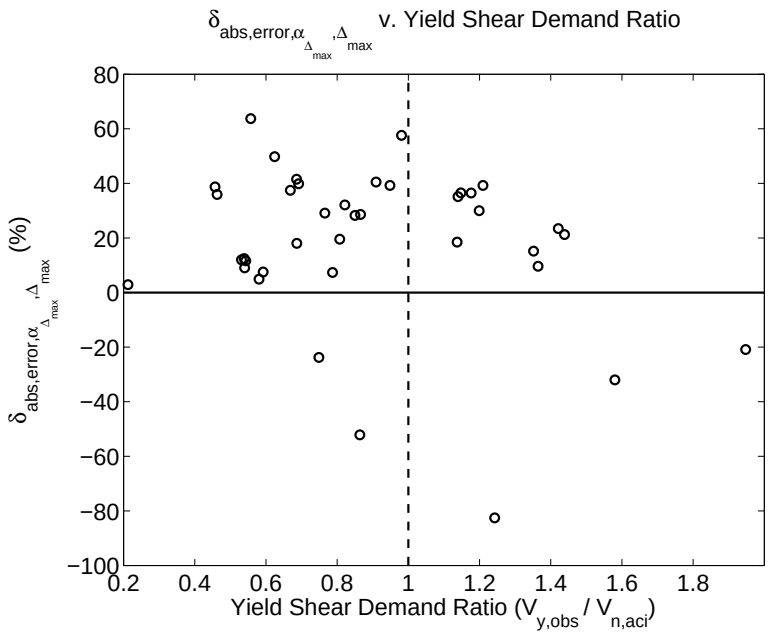

Figure N.149: Effective Shear Calibrated to Max Displacement Max Displacement Absolute Error Change v. Yield Shear Demand Ratio

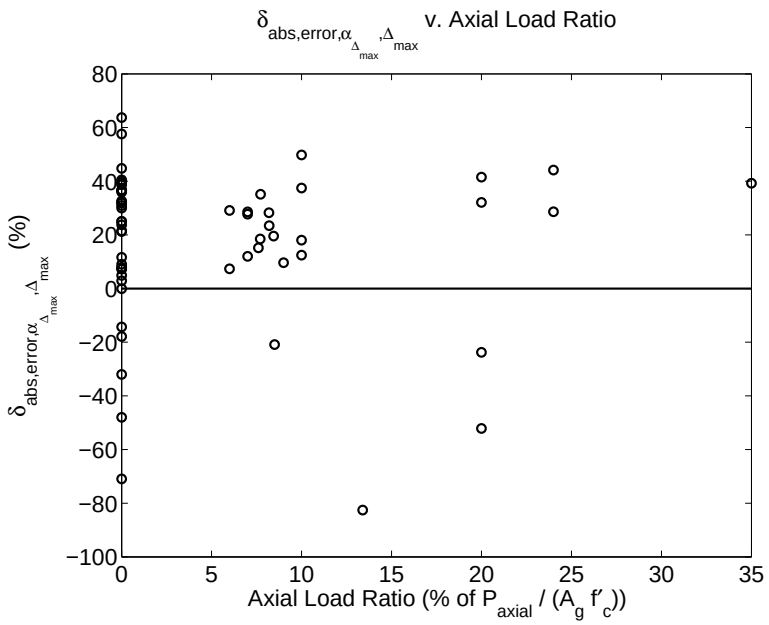

Figure N.150: Effective Shear Calibrated to Max Displacement Max Displacement Absolute Error Change v. Axial Load Ratio

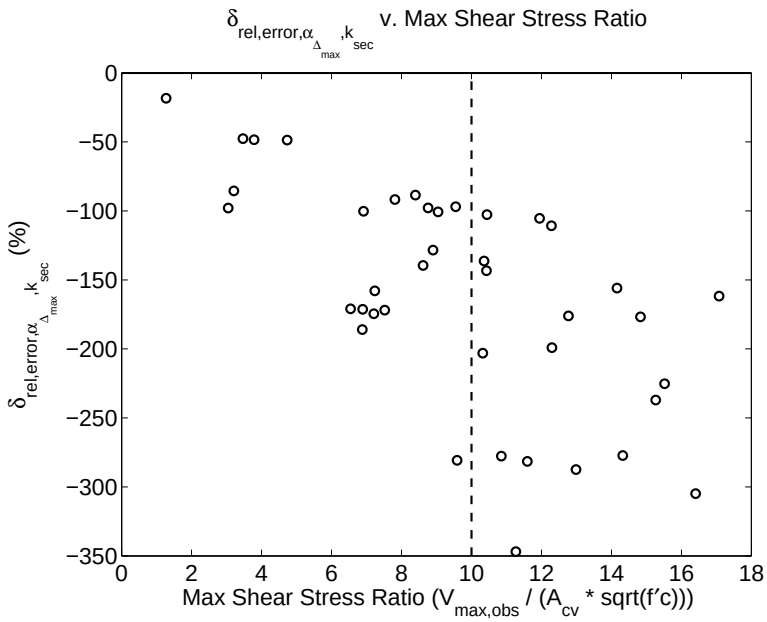

Figure N.151: Effective Shear Calibrated to Max Displacement Secant Stiffness Relative Error Change v. Max Shear Stress Ratio

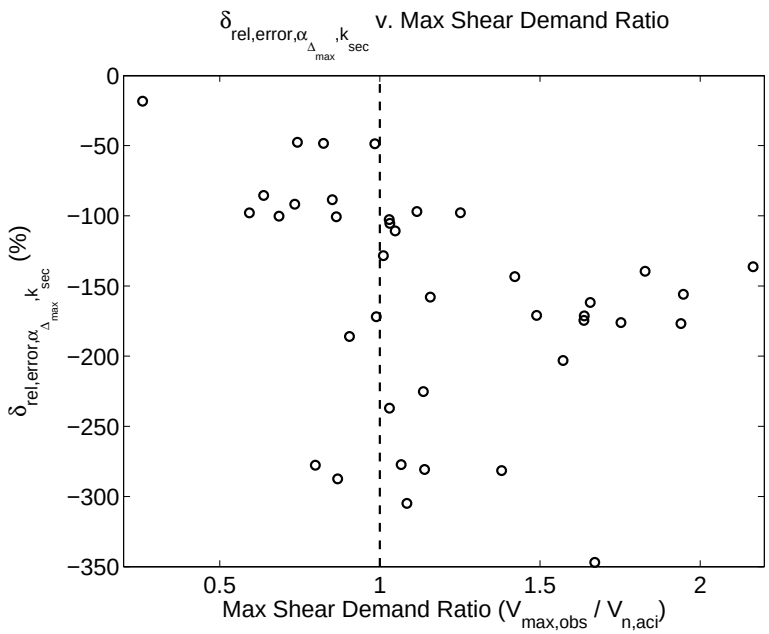

Figure N.152: Effective Shear Calibrated to Max Displacement Secant Stiffness Relative Error Change v. Max Shear Demand Ratio

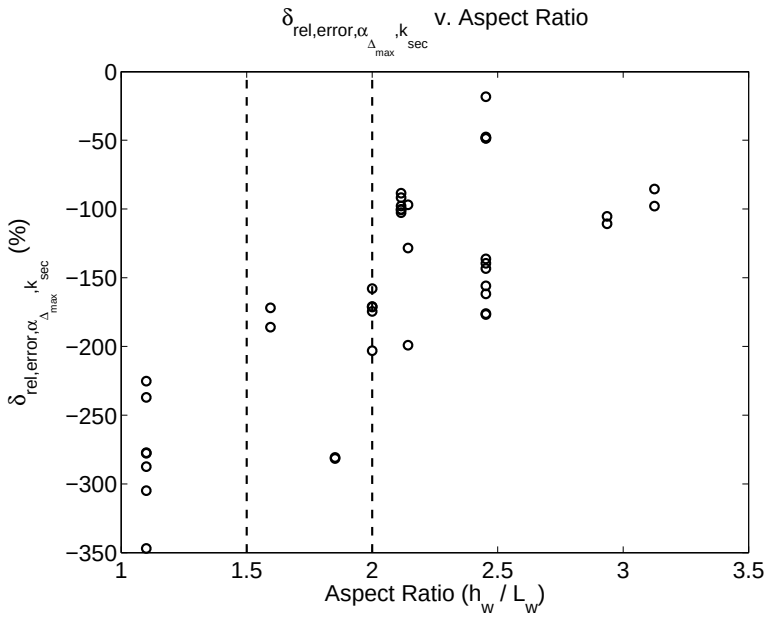

Figure N.153: Effective Shear Calibrated to Max Displacement Secant Stiffness Relative Error Change v. Aspect Ratio

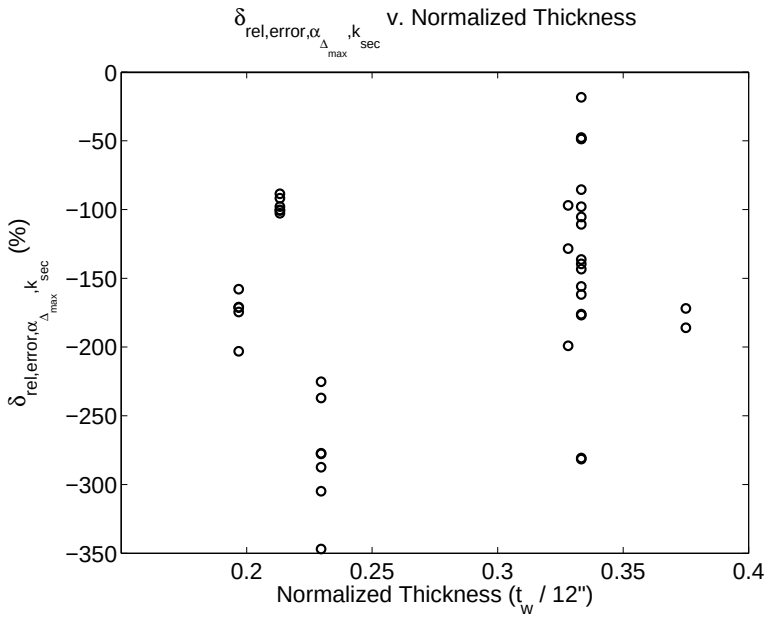

Figure N.154: Effective Shear Calibrated to Max Displacement Secant Stiffness Relative Error Change v. Normalized Thickness

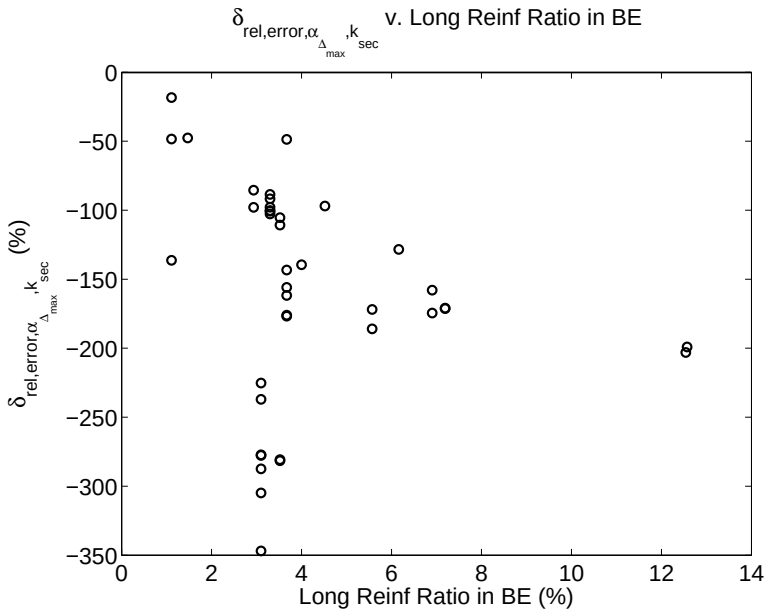

Figure N.155: Effective Shear Calibrated to Max Displacement Secant Stiffness Relative Error Change v. Long Reinf Ratio in BE

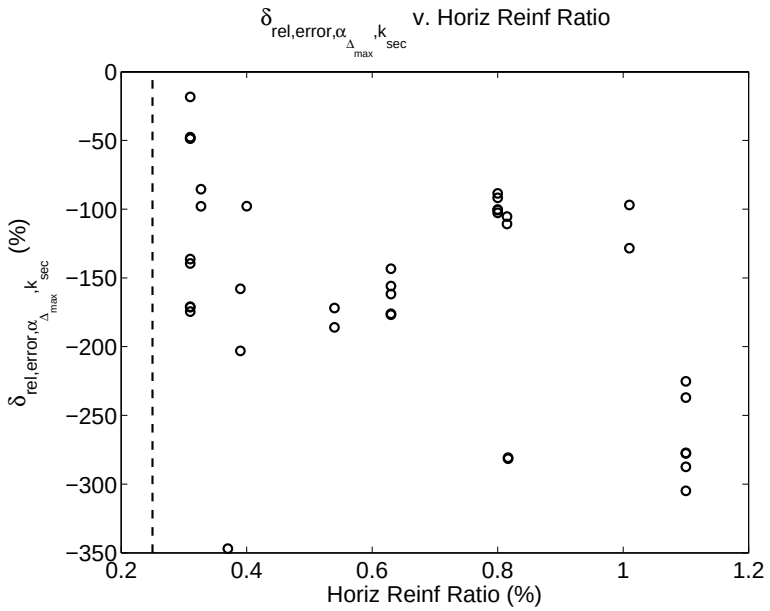

Figure N.156: Effective Shear Calibrated to Max Displacement Secant Stiffness Relative Error Change v. Horiz Reinf Ratio

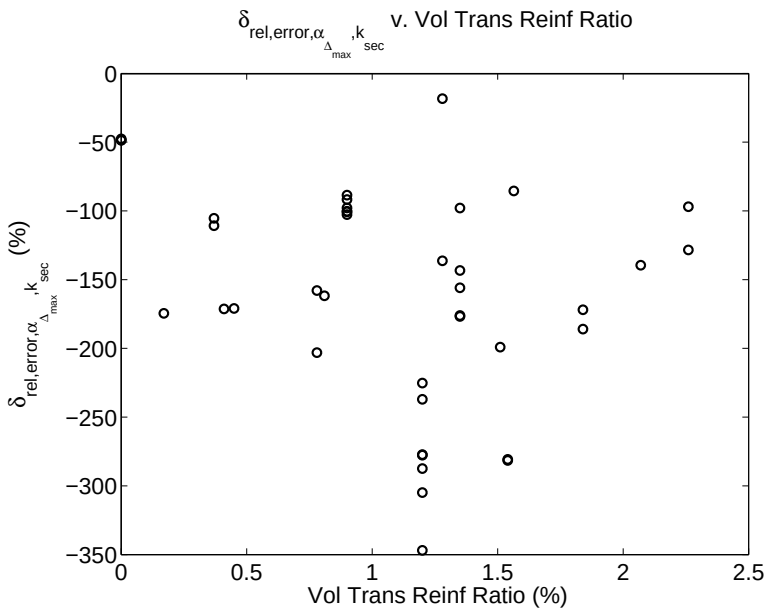

Figure N.157: Effective Shear Calibrated to Max Displacement Secant Stiffness Relative Error Change v. Vol Trans Reinf Ratio

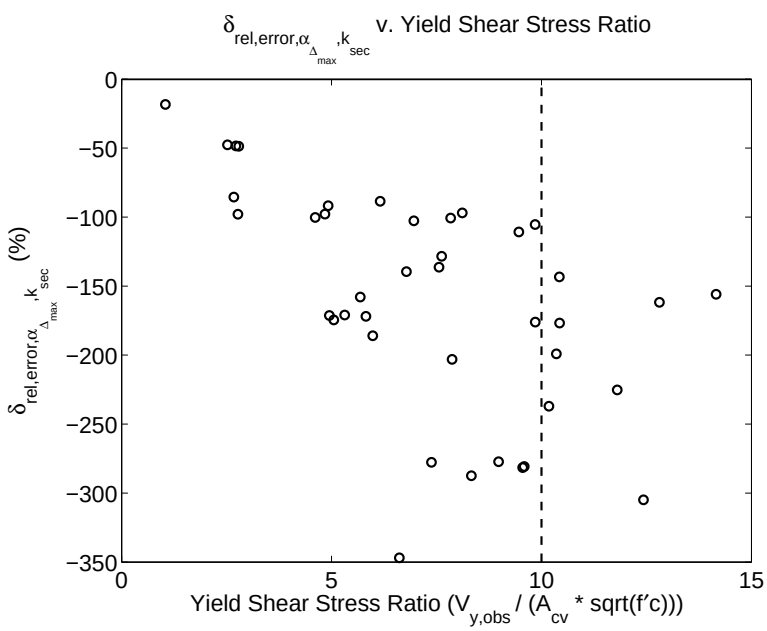

Figure N.158: Effective Shear Calibrated to Max Displacement Secant Stiffness Relative Error Change v. Yield Shear Stress Ratio

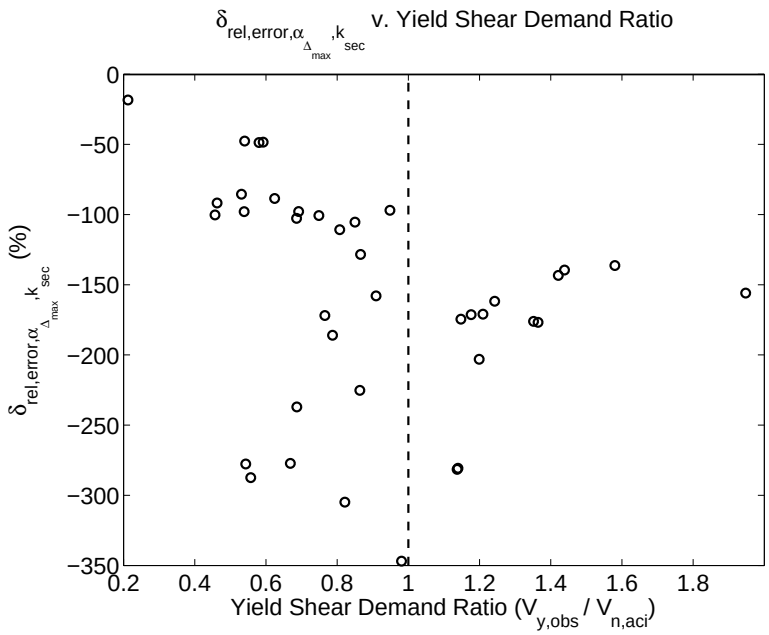

Figure N.159: Effective Shear Calibrated to Max Displacement Secant Stiffness Relative Error Change v. Yield Shear Demand Ratio

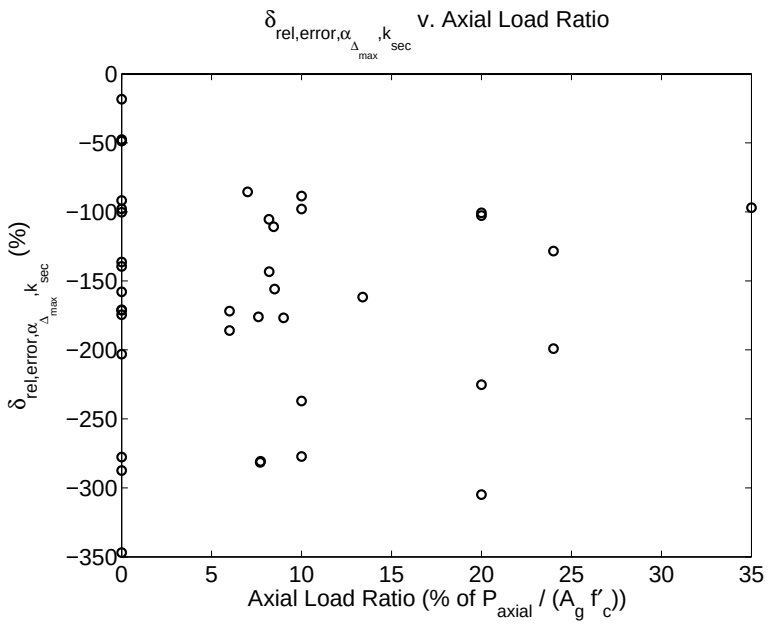

Figure N.160: Effective Shear Calibrated to Max Displacement Secant Stiffness Relative Error Change v. Axial Load Ratio

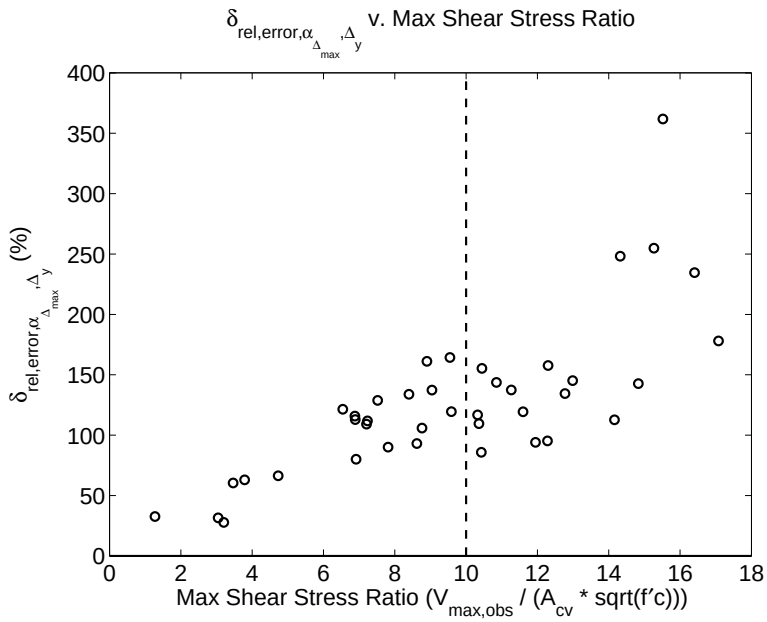

Figure N.161: Effective Shear Calibrated to Max Displacement Yield Displacement Relative Error Change v. Max Shear Stress Ratio

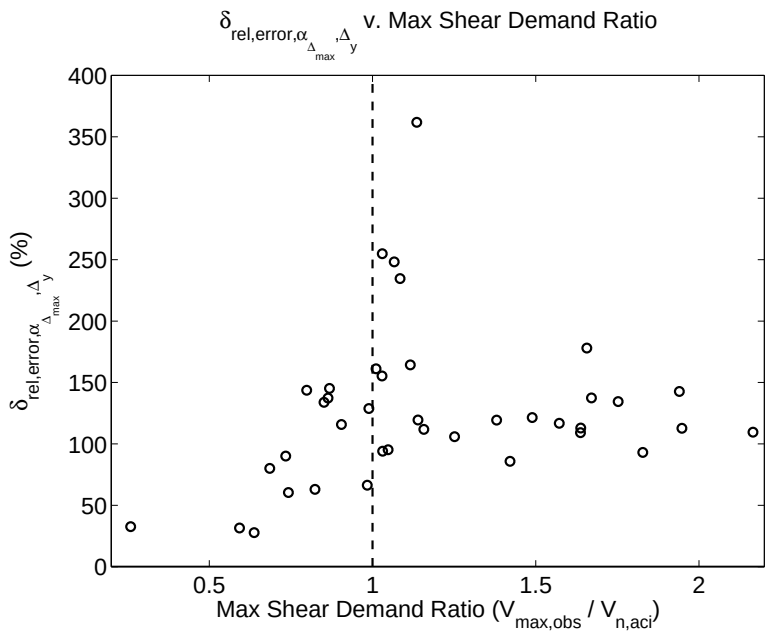

Figure N.162: Effective Shear Calibrated to Max Displacement Yield Displacement Relative Error Change v. Max Shear Demand Ratio

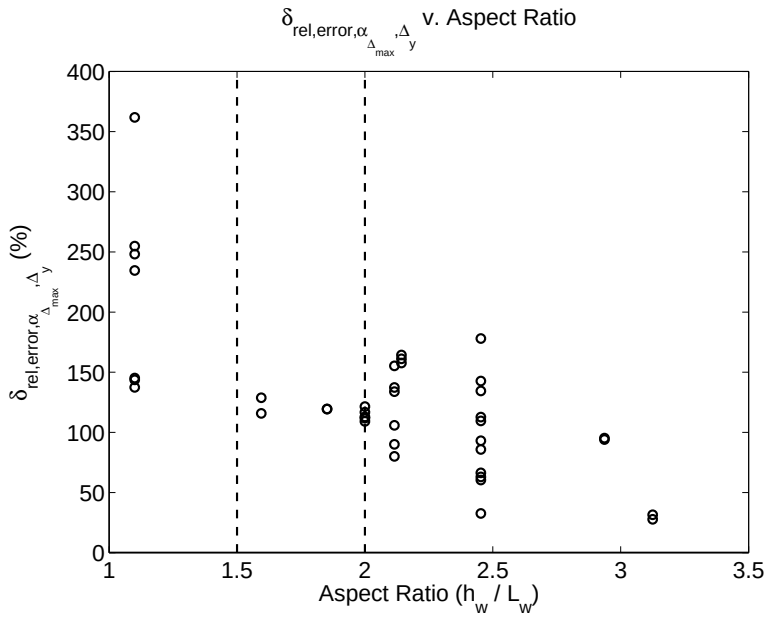

Figure N.163: Effective Shear Calibrated to Max Displacement Yield Displacement Relative Error Change v. Aspect Ratio

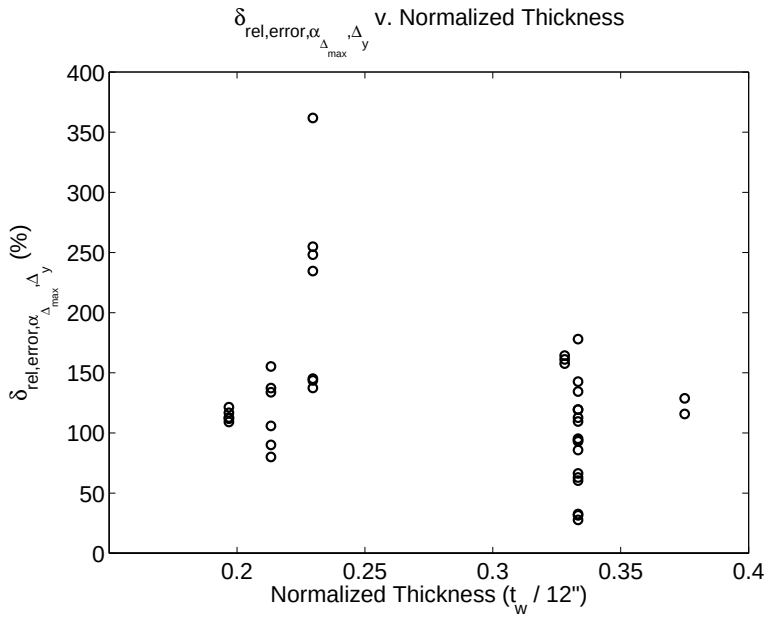

Figure N.164: Effective Shear Calibrated to Max Displacement Yield Displacement Relative Error Change v. Normalized Thickness

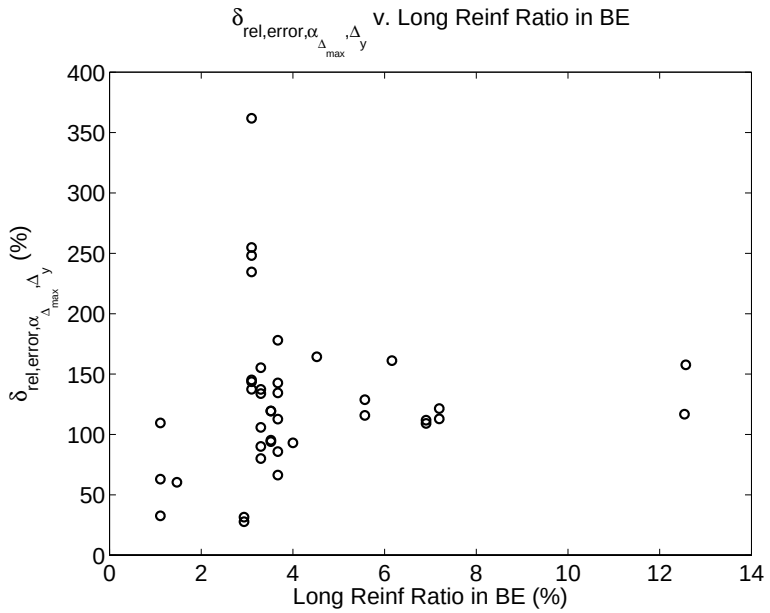

Figure N.165: Effective Shear Calibrated to Max Displacement Yield Displacement Relative Error Change v. Long Reinf Ratio in BE

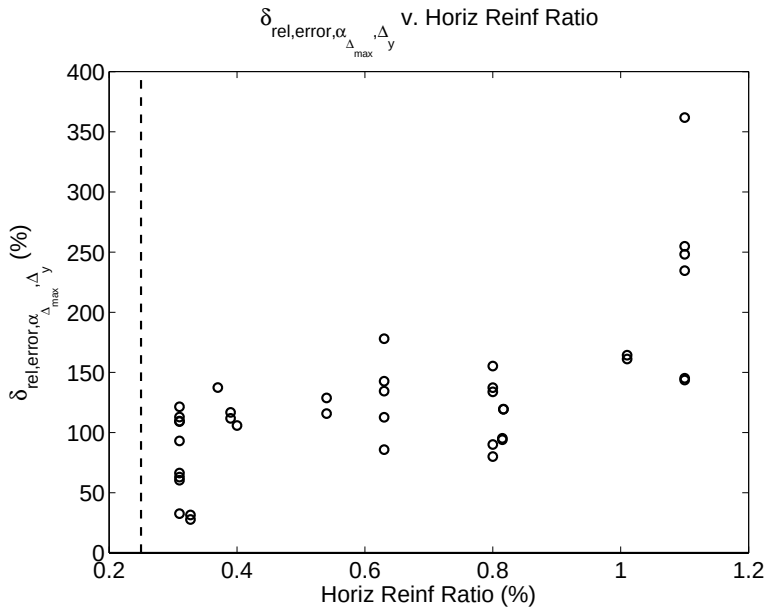

Figure N.166: Effective Shear Calibrated to Max Displacement Yield Displacement Relative Error Change v. Horiz Reinf Ratio

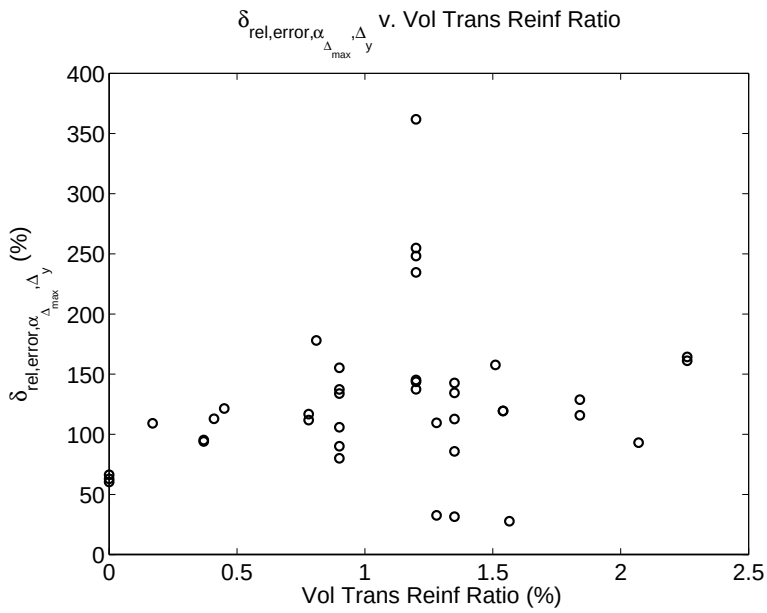

Figure N.167: Effective Shear Calibrated to Max Displacement Yield Displacement Relative Error Change v. Vol Trans Reinf Ratio

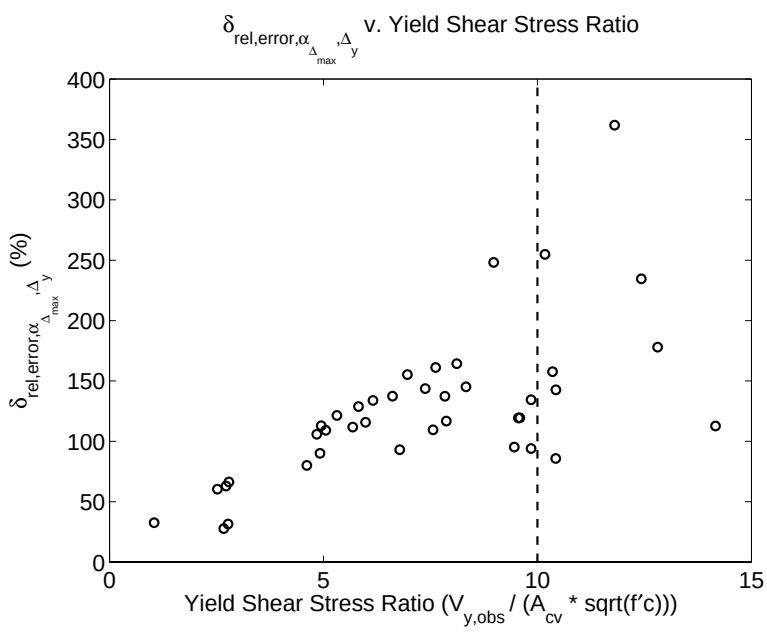

Figure N.168: Effective Shear Calibrated to Max Displacement Yield Displacement Relative Error Change v. Yield Shear Stress Ratio

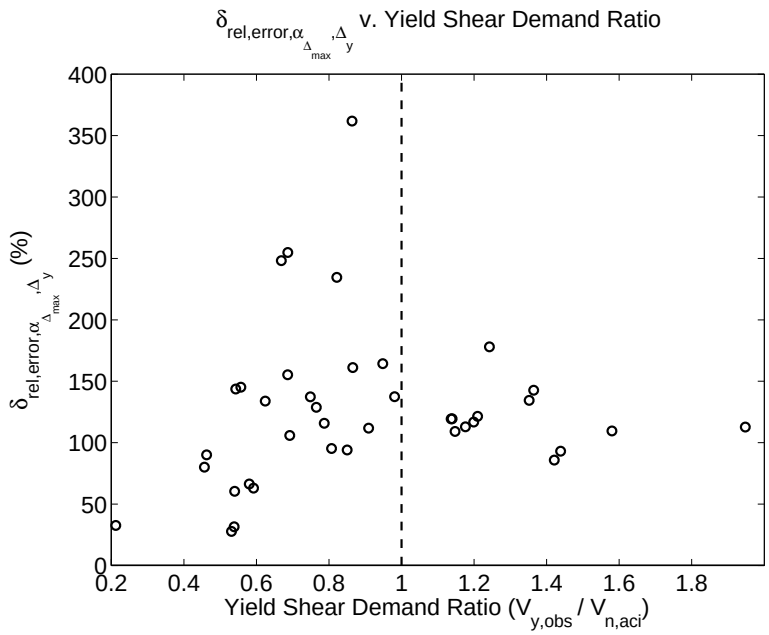

Figure N.169: Effective Shear Calibrated to Max Displacement Yield Displacement Relative Error Change v. Yield Shear Demand Ratio

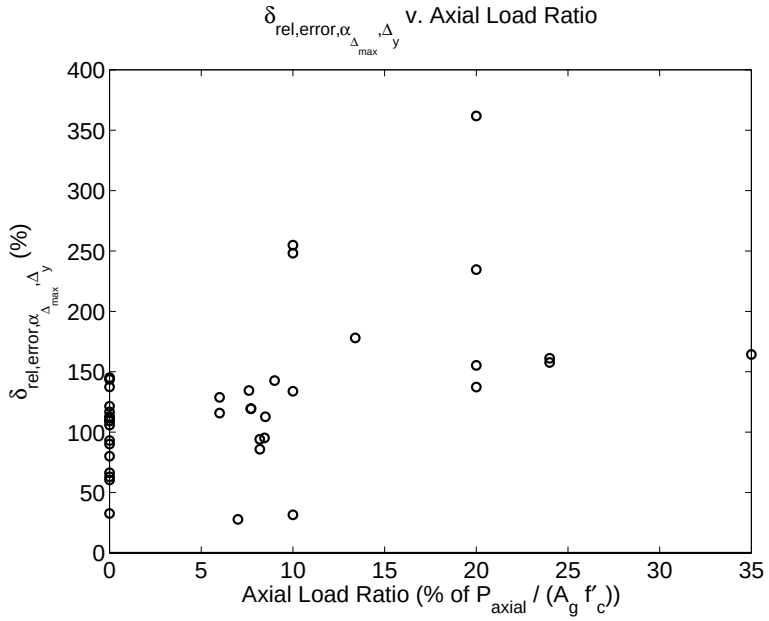

Figure N.170: Effective Shear Calibrated to Max Displacement Yield Displacement Relative Error Change v. Axial Load Ratio

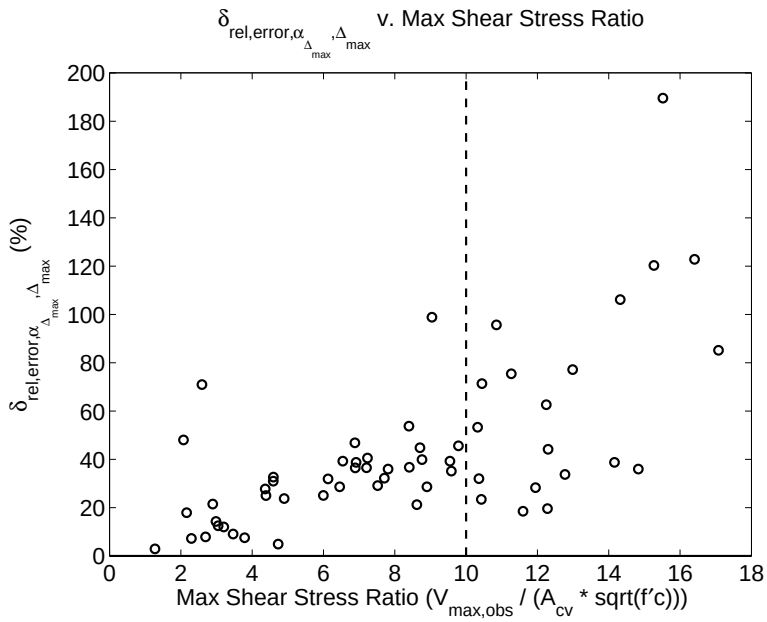

Figure N.171: Effective Shear Calibrated to Max Displacement Max Displacement Relative Error Change v. Max Shear Stress Ratio

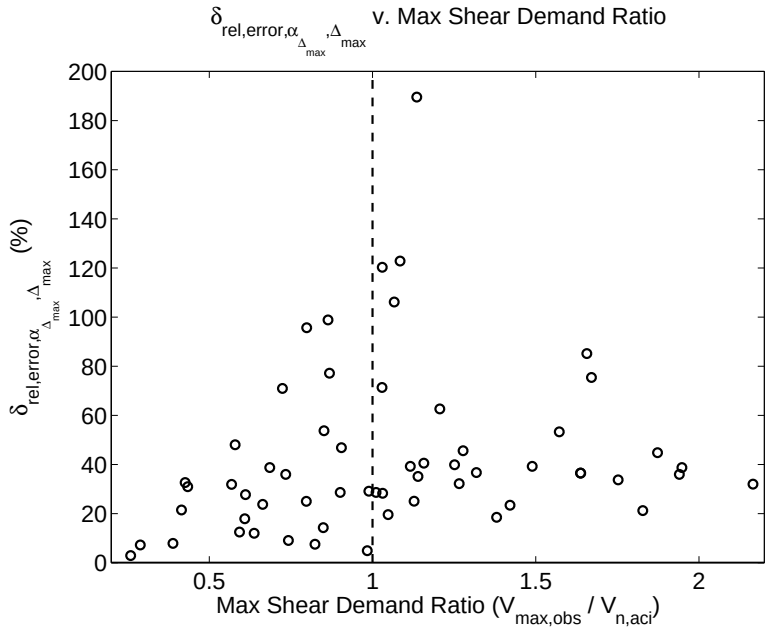

Figure N.172: Effective Shear Calibrated to Max Displacement Max Displacement Relative Error Change v. Max Shear Demand Ratio

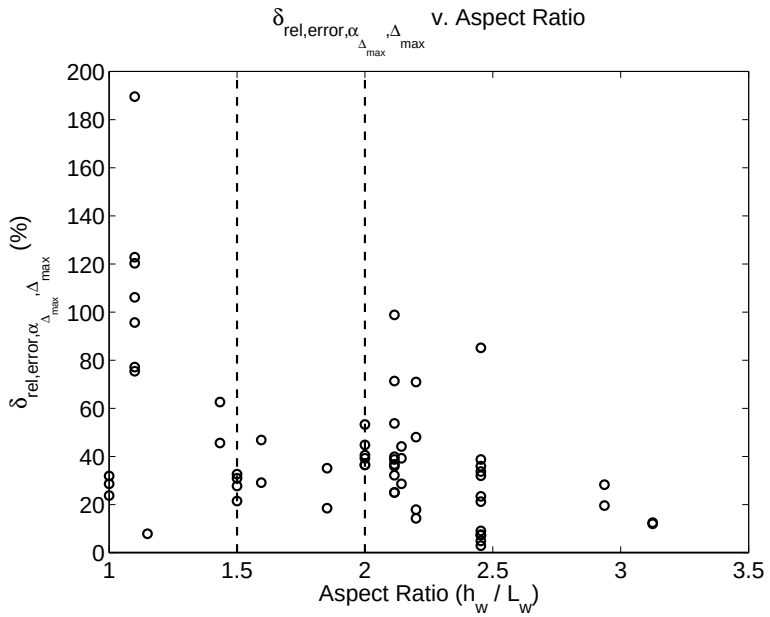

Figure N.173: Effective Shear Calibrated to Max Displacement Max Displacement Relative Error Change v. Aspect Ratio

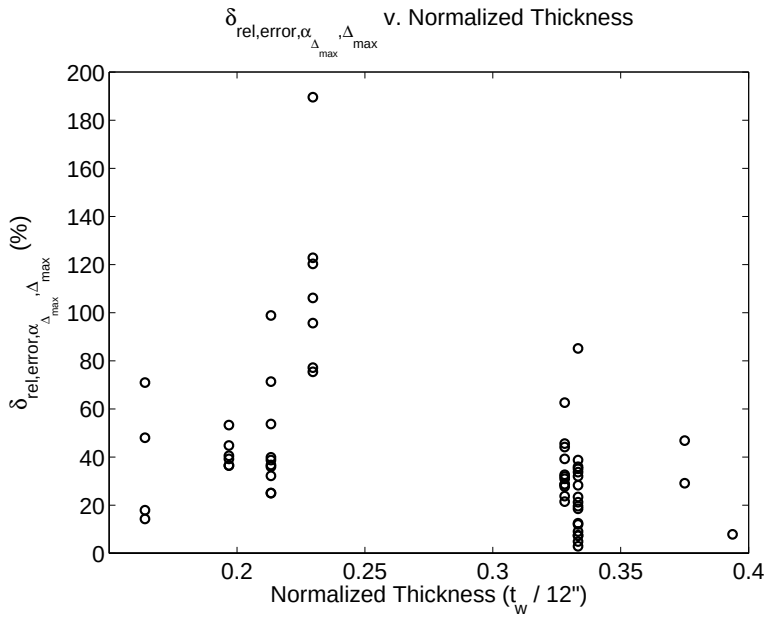

Figure N.174: Effective Shear Calibrated to Max Displacement Max Displacement Relative Error Change v. Normalized Thickness

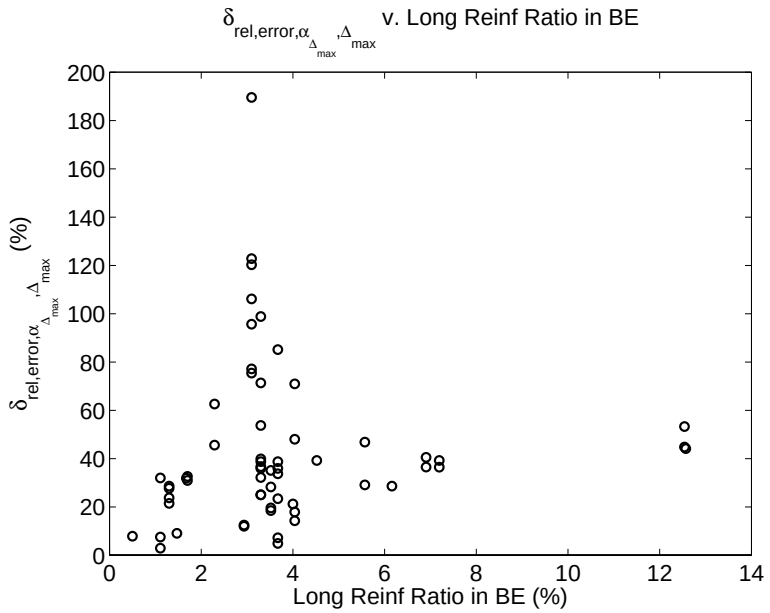

Figure N.175: Effective Shear Calibrated to Max Displacement Max Displacement Relative Error Change v. Long Reinf Ratio in BE

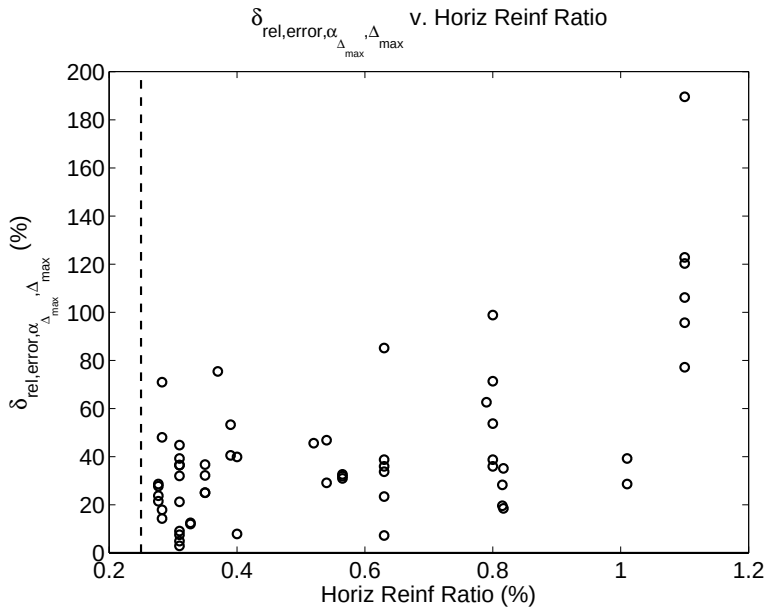

Figure N.176: Effective Shear Calibrated to Max Displacement Max Displacement Relative Error Change v. Horiz Reinf Ratio

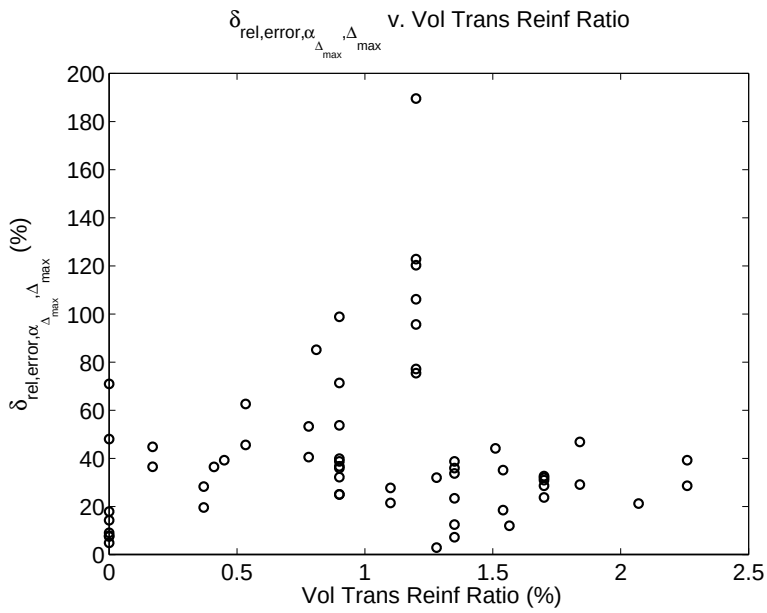

Figure N.177: Effective Shear Calibrated to Max Displacement Max Displacement Relative Error Change v. Vol Trans Reinf Ratio

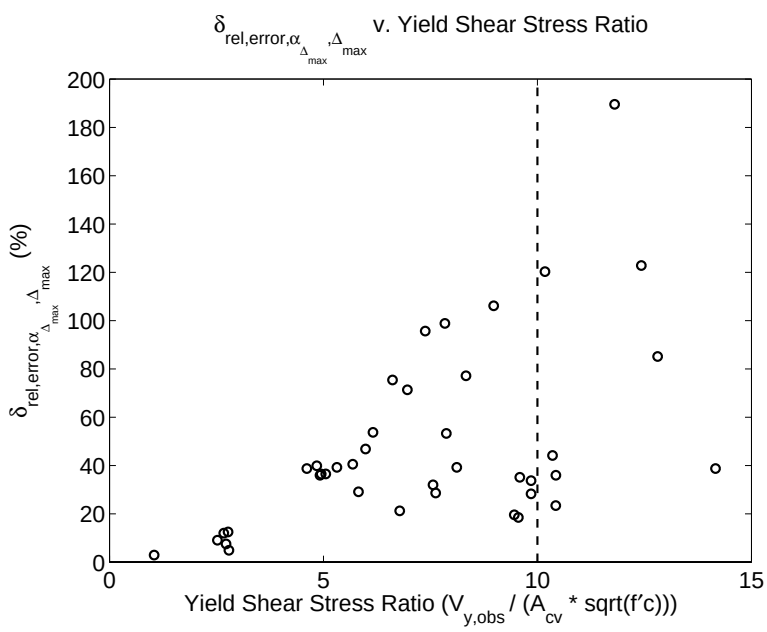

Figure N.178: Effective Shear Calibrated to Max Displacement Max Displacement Relative Error Change v. Yield Shear Stress Ratio

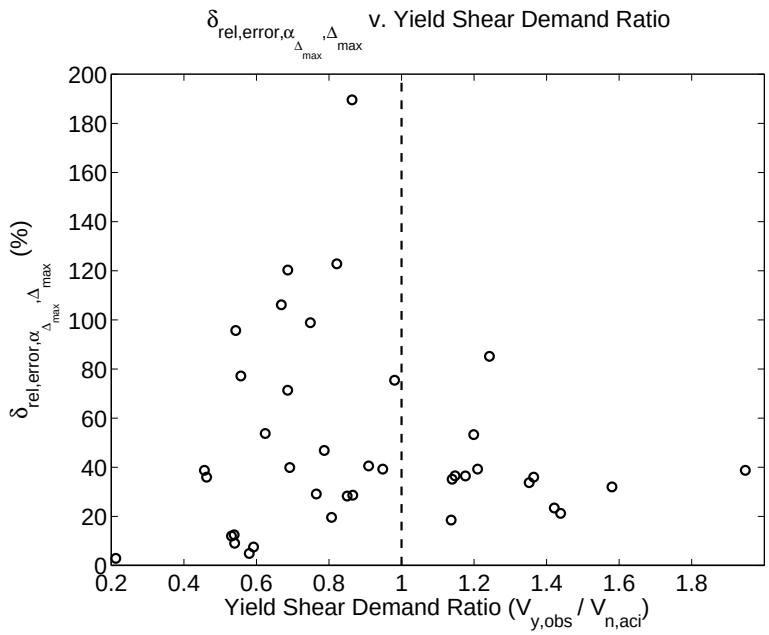

Figure N.179: Effective Shear Calibrated to Max Displacement Max Displacement Relative Error Change v. Yield Shear Demand Ratio

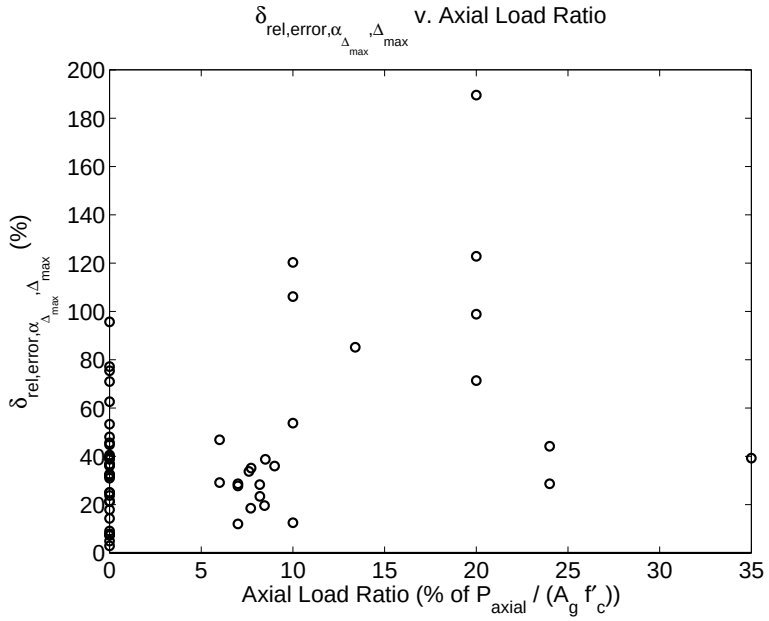

Figure N.180: Effective Shear Calibrated to Max Displacement Max Displacement Relative Error Change v. Axial Load Ratio

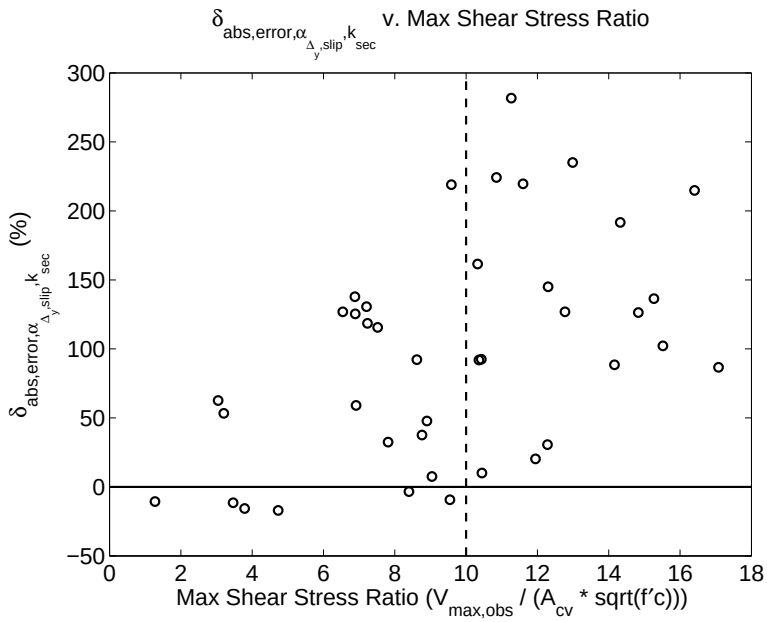

Figure N.181: Effective Shear Calibrated to Yield Displacement With Slip Secant Stiffness Absolute Error Change v. Max Shear Stress Ratio

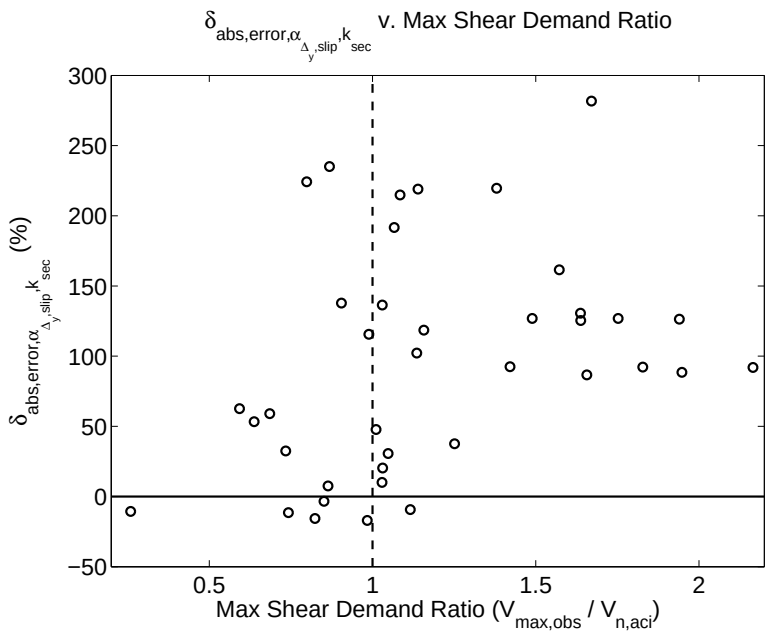

Figure N.182: Effective Shear Calibrated to Yield Displacement With Slip Secant Stiffness Absolute Error Change v. Max Shear Demand Ratio

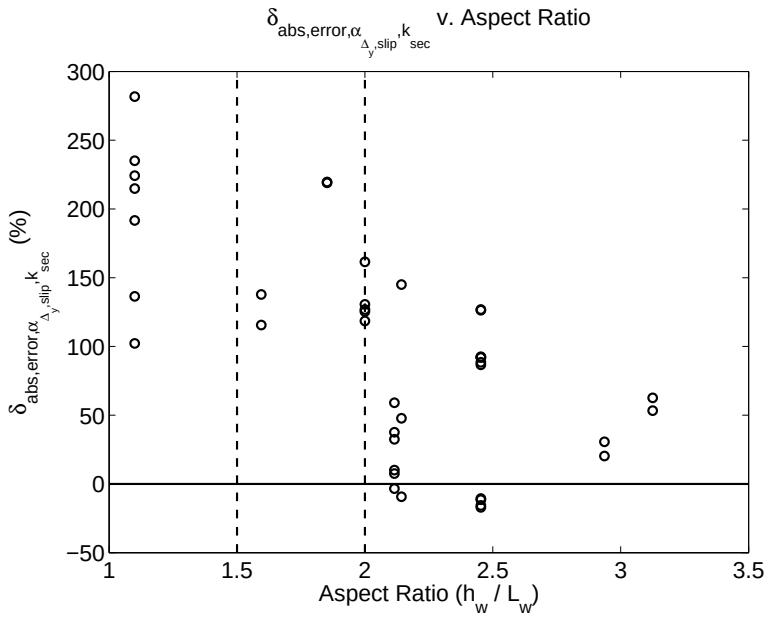

Figure N.183: Effective Shear Calibrated to Yield Displacement With Slip Secant Stiffness Absolute Error Change v. Aspect Ratio

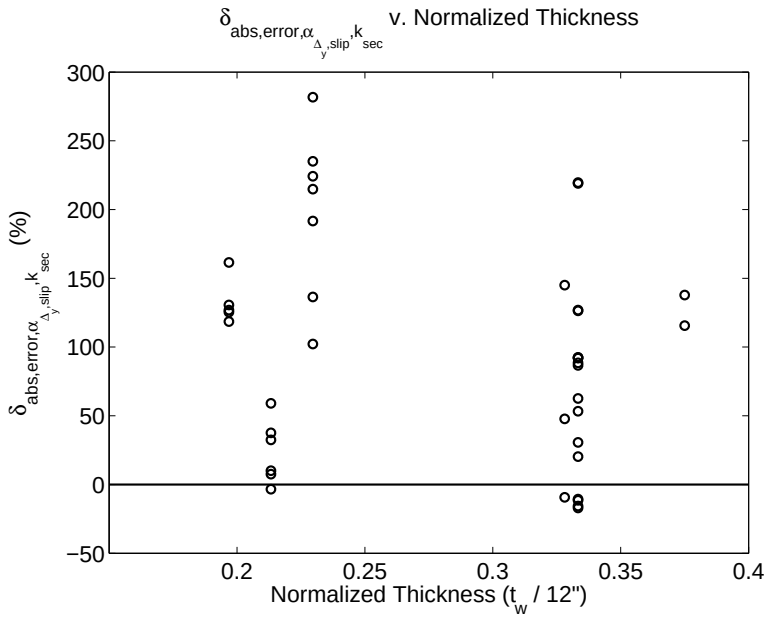

Figure N.184: Effective Shear Calibrated to Yield Displacement With Slip Secant Stiffness Absolute Error Change v. Normalized Thickness

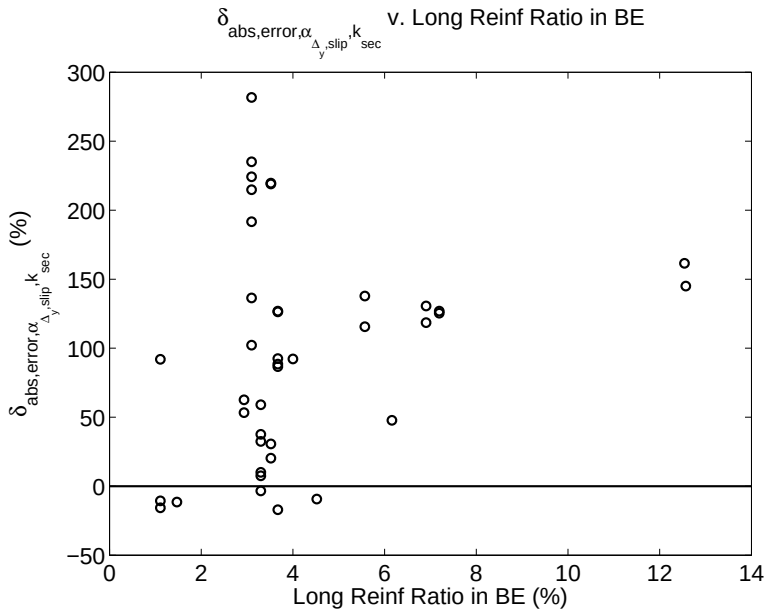

Figure N.185: Effective Shear Calibrated to Yield Displacement With Slip Secant Stiffness Absolute Error Change v. Long Reinf Ratio in BE

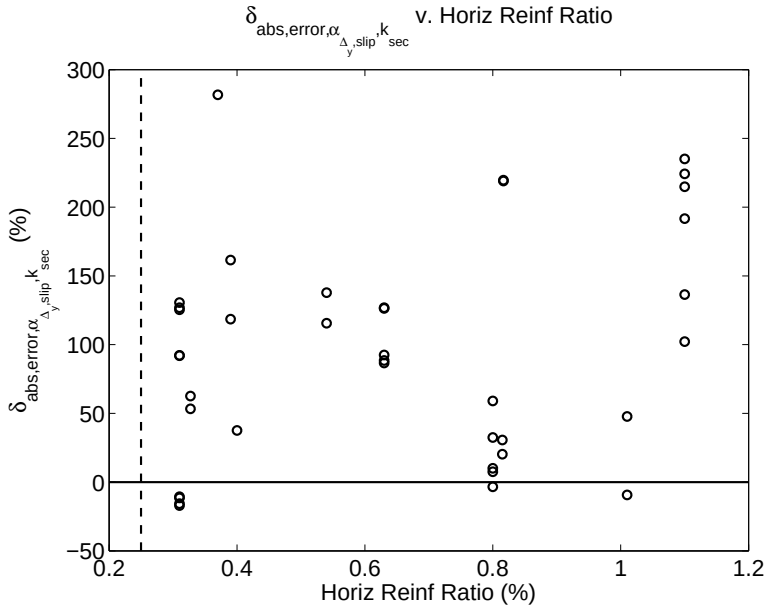

Figure N.186: Effective Shear Calibrated to Yield Displacement With Slip Secant Stiffness Absolute Error Change v. Horiz Reinf Ratio

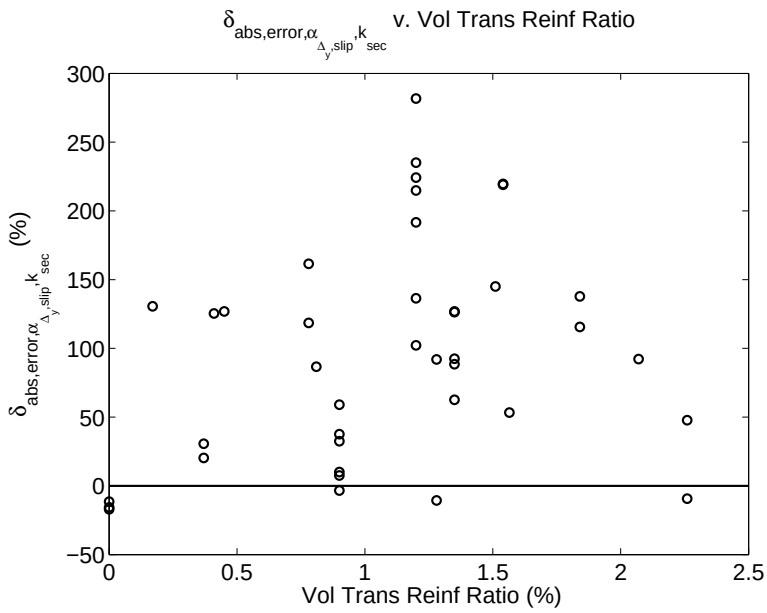

Figure N.187: Effective Shear Calibrated to Yield Displacement With Slip Secant Stiffness Absolute Error Change v. Vol Trans Reinf Ratio

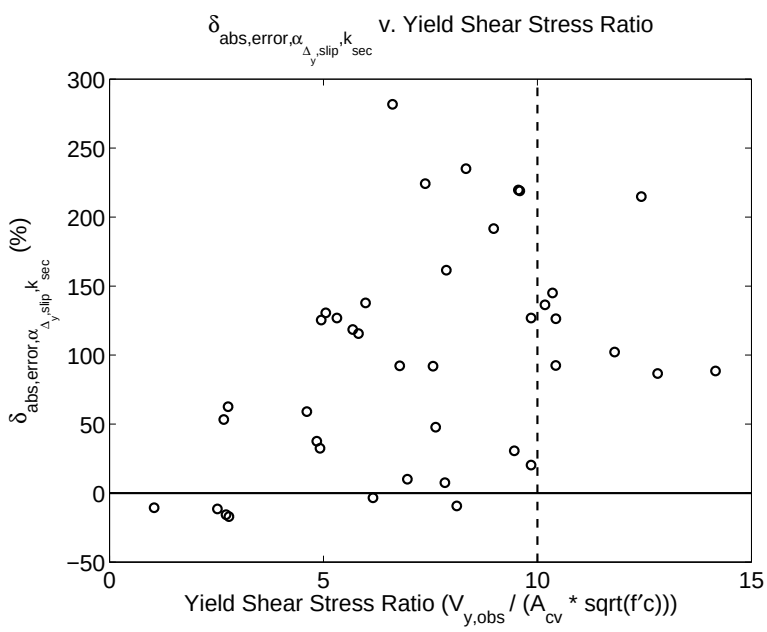

Figure N.188: Effective Shear Calibrated to Yield Displacement With Slip Secant Stiffness Absolute Error Change v. Yield Shear Stress Ratio

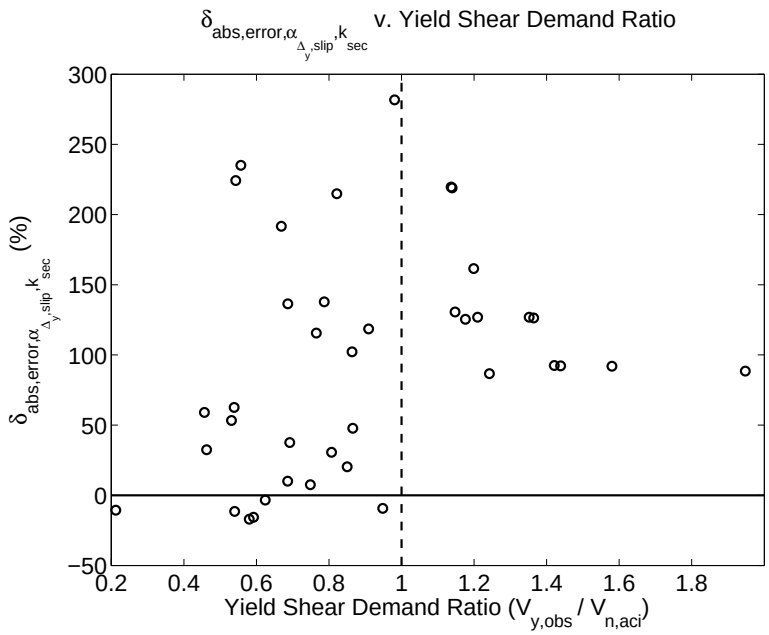

Figure N.189: Effective Shear Calibrated to Yield Displacement With Slip Secant Stiffness Absolute Error Change v. Yield Shear Demand Ratio

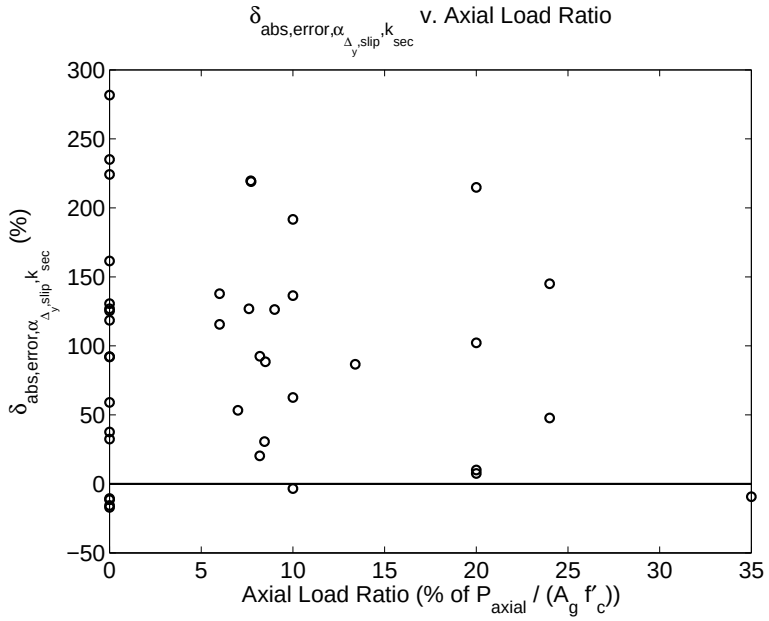

Figure N.190: Effective Shear Calibrated to Yield Displacement With Slip Secant Stiffness Absolute Error Change v. Axial Load Ratio

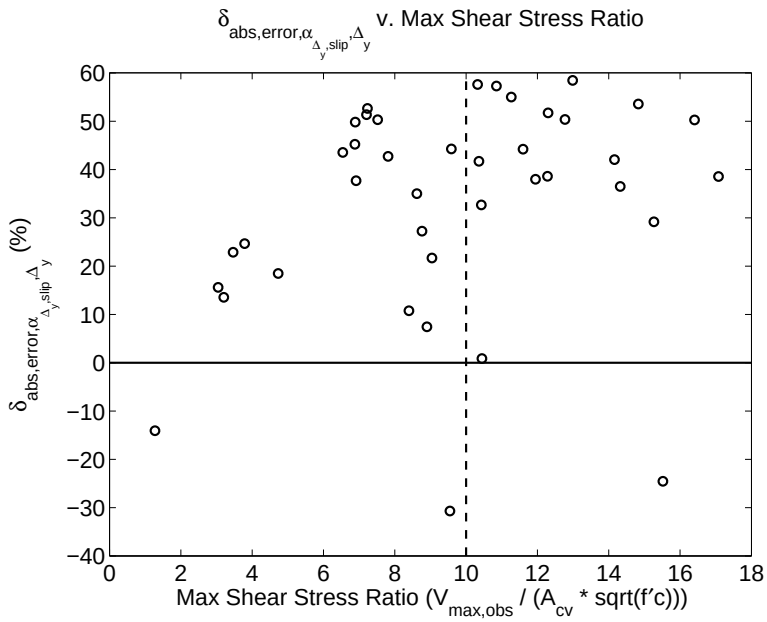

Figure N.191: Effective Shear Calibrated to Yield Displacement With Slip Yield Displacement Absolute Error Change v. Max Shear Stress Ratio

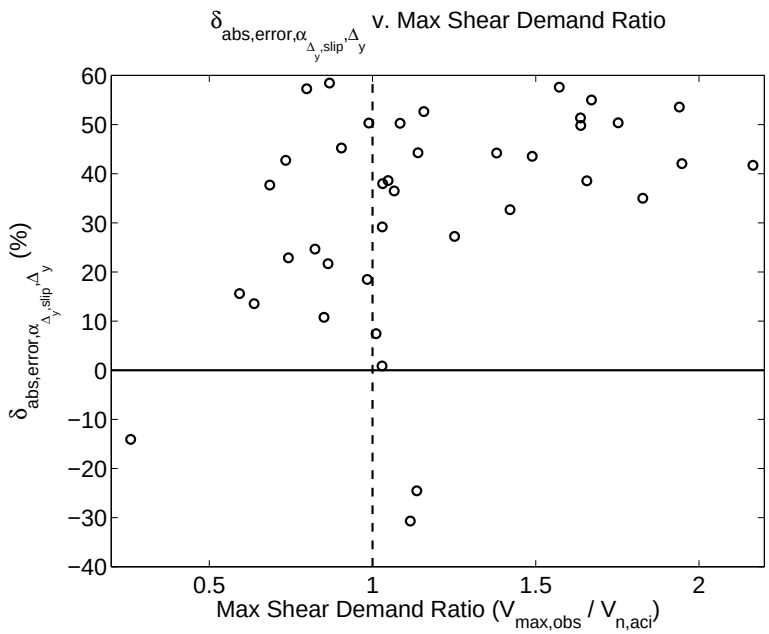

Figure N.192: Effective Shear Calibrated to Yield Displacement With Slip Yield Displacement Absolute Error Change v. Max Shear Demand Ratio

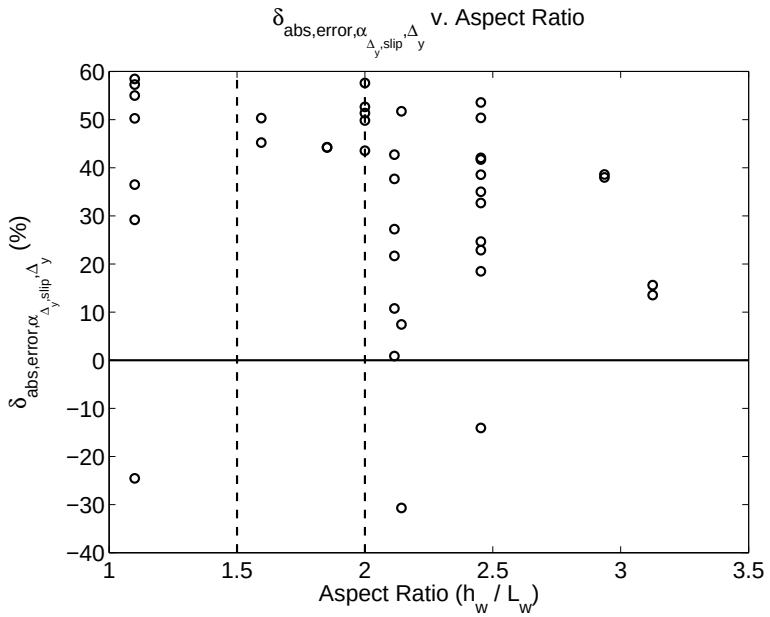

Figure N.193: Effective Shear Calibrated to Yield Displacement With Slip Yield Displacement Absolute Error Change v. Aspect Ratio

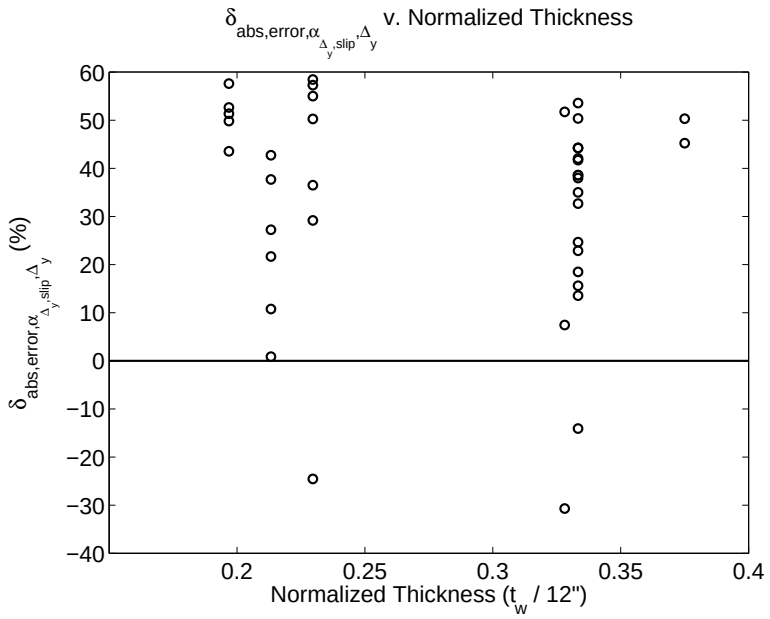

Figure N.194: Effective Shear Calibrated to Yield Displacement With Slip Yield Displacement Absolute Error Change v. Normalized Thickness

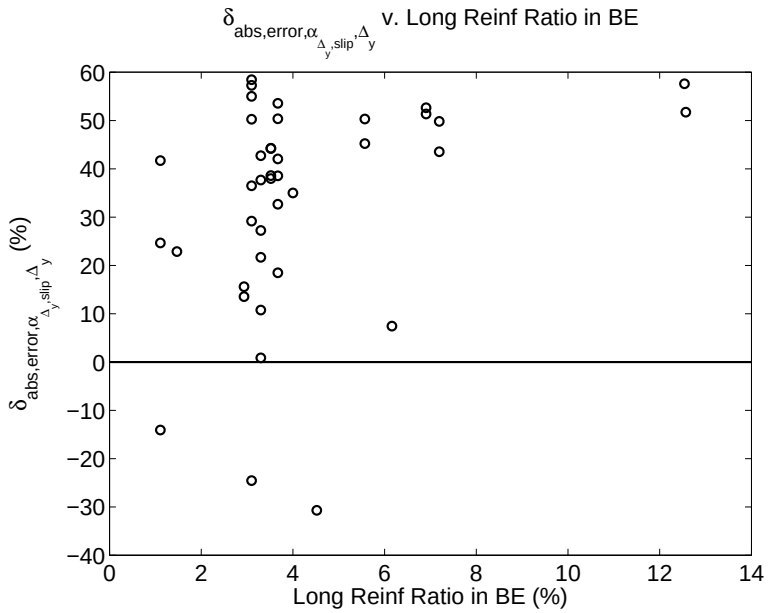

Figure N.195: Effective Shear Calibrated to Yield Displacement With Slip Yield Displacement Absolute Error Change v. Long Reinf Ratio in BE

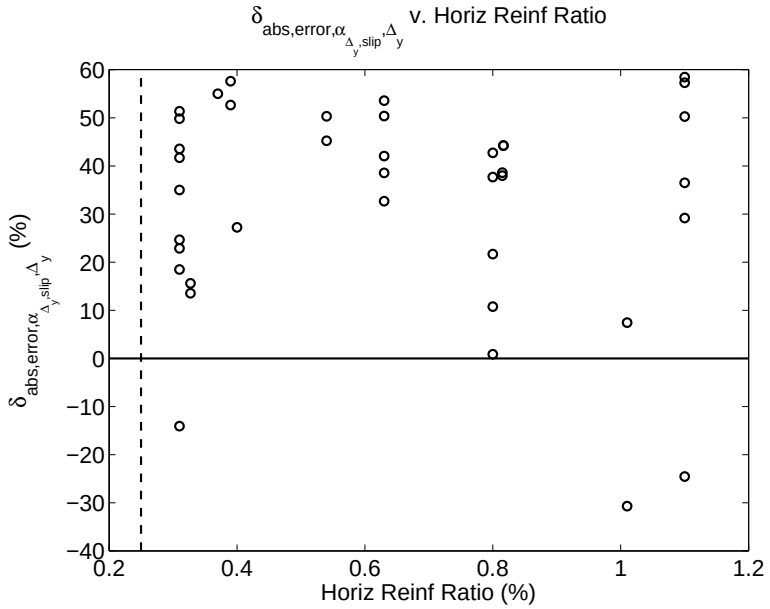

Figure N.196: Effective Shear Calibrated to Yield Displacement With Slip Yield Displacement Absolute Error Change v. Horiz Reinf Ratio

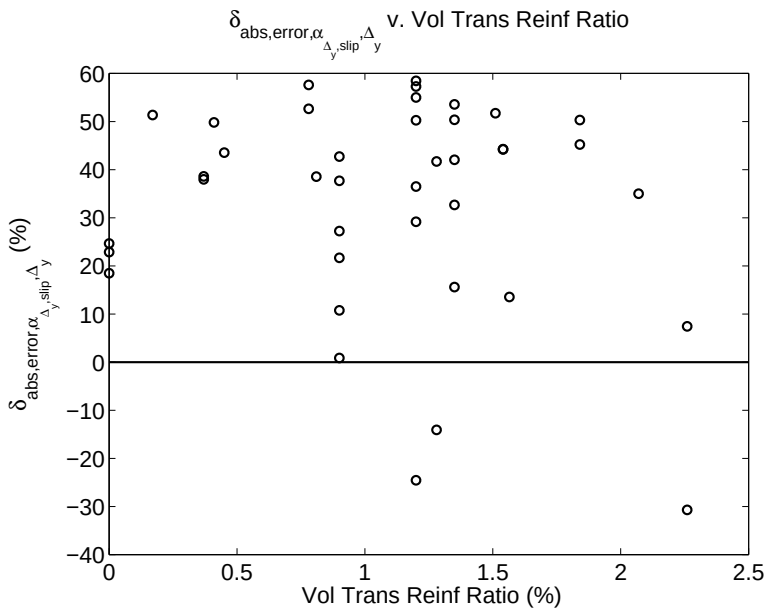

Figure N.197: Effective Shear Calibrated to Yield Displacement With Slip Yield Displacement Absolute Error Change v. Vol Trans Reinf Ratio

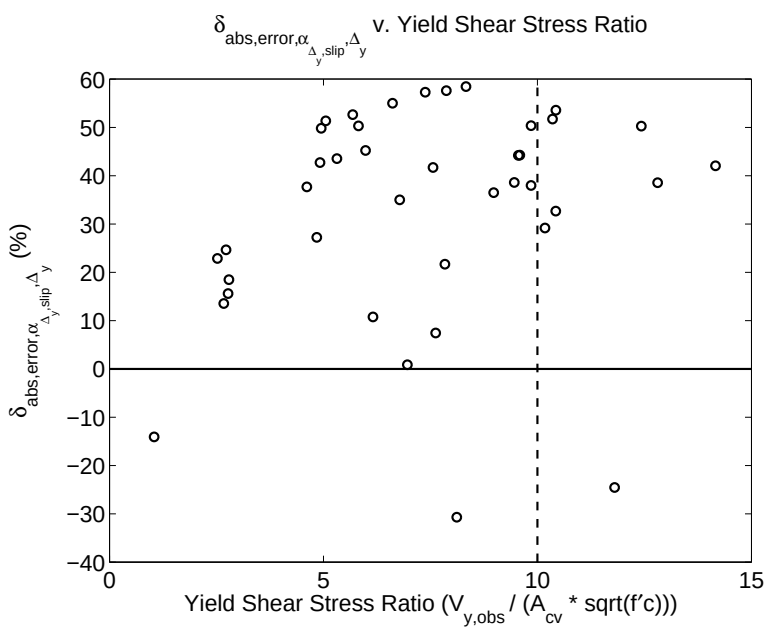

Figure N.198: Effective Shear Calibrated to Yield Displacement With Slip Yield Displacement Absolute Error Change v. Yield Shear Stress Ratio

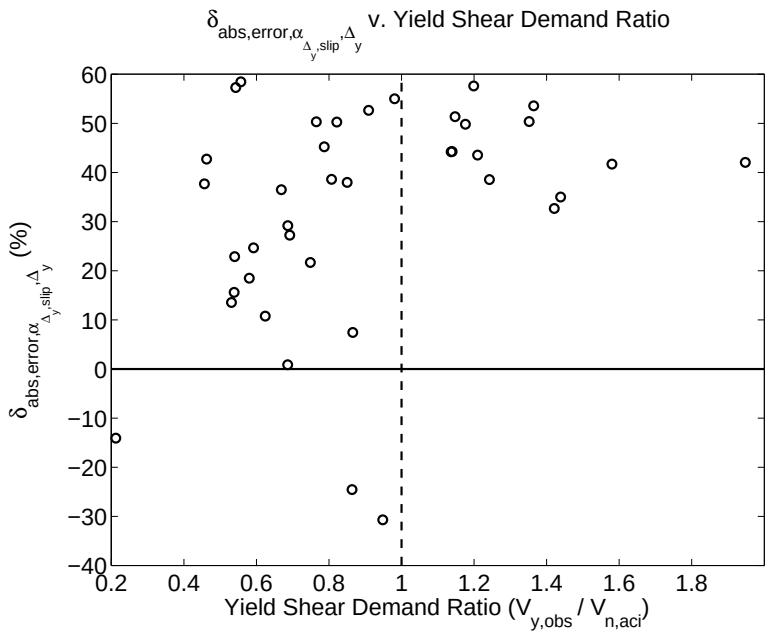

Figure N.199: Effective Shear Calibrated to Yield Displacement With Slip Yield Displacement Absolute Error Change v. Yield Shear Demand Ratio

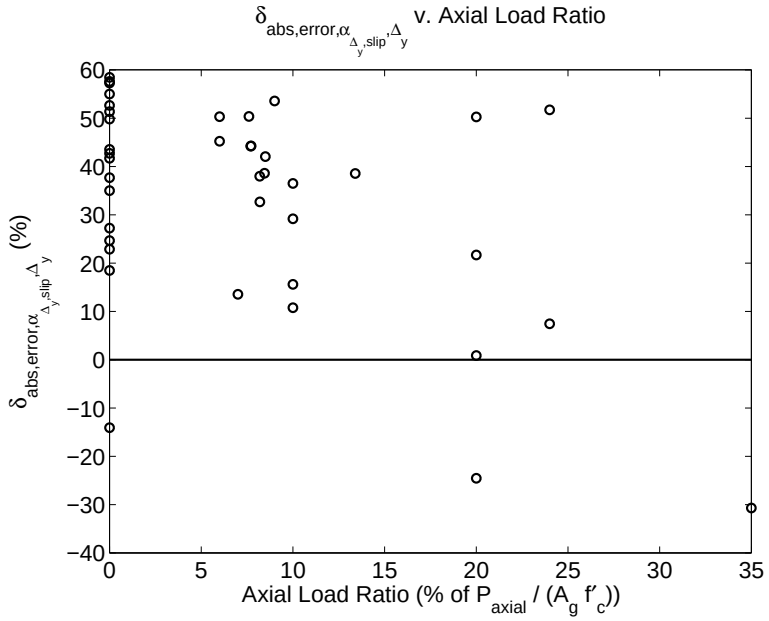

Figure N.200: Effective Shear Calibrated to Yield Displacement With Slip Yield Displacement Absolute Error Change v. Axial Load Ratio

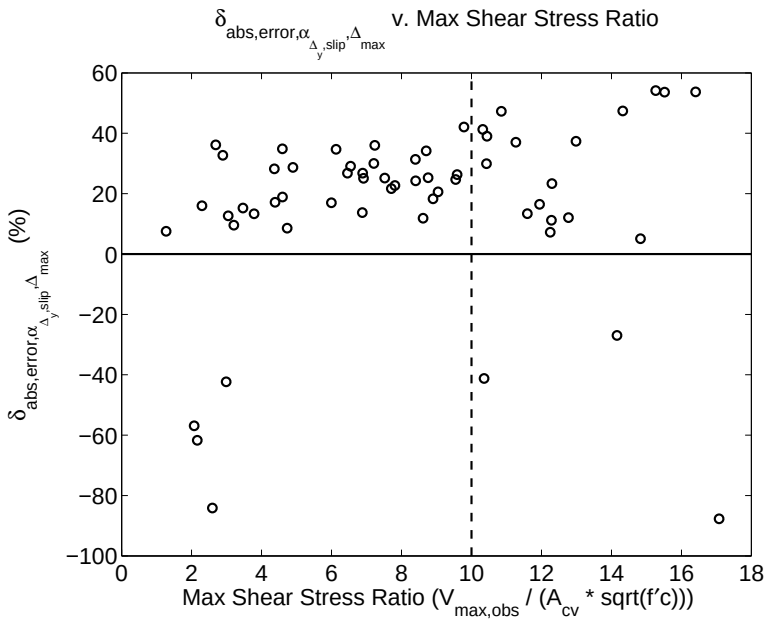

Figure N.201: Effective Shear Calibrated to Yield Displacement With Slip Max Displacement Absolute Error Change v. Max Shear Stress Ratio

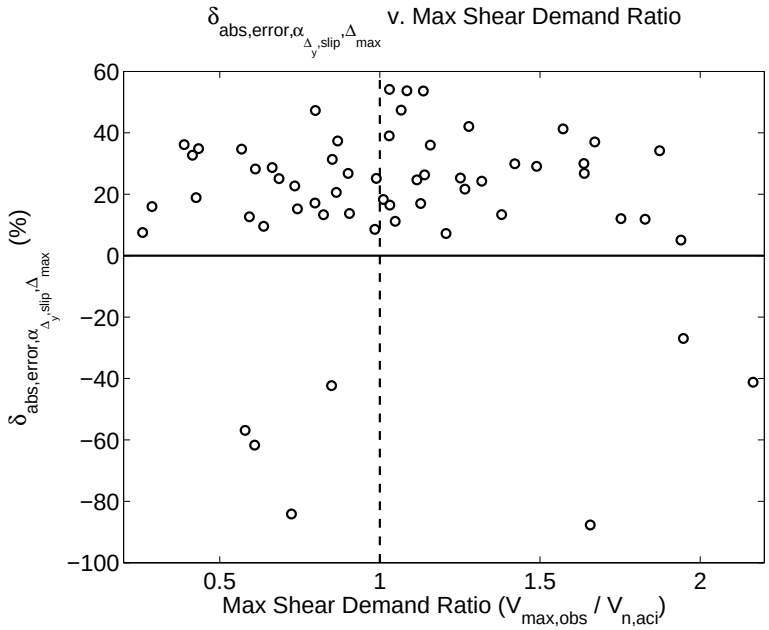

Figure N.202: Effective Shear Calibrated to Yield Displacement With Slip Max Displacement Absolute Error Change v. Max Shear Demand Ratio

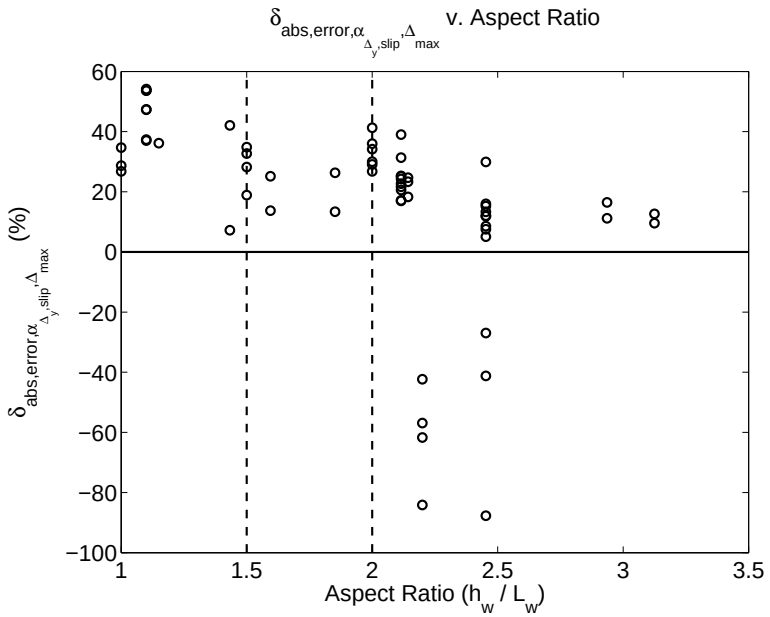

Figure N.203: Effective Shear Calibrated to Yield Displacement With Slip Max Displacement Absolute Error Change v. Aspect Ratio

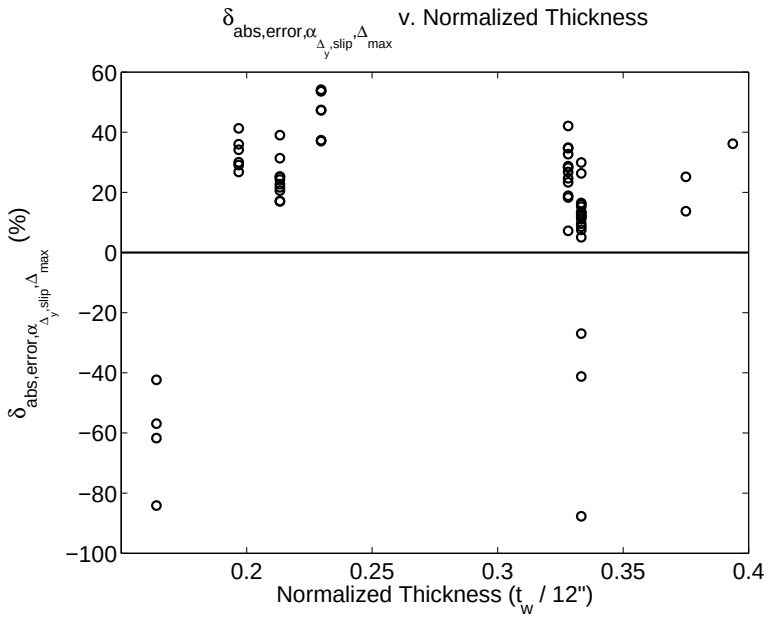

Figure N.204: Effective Shear Calibrated to Yield Displacement With Slip Max Displacement Absolute Error Change v. Normalized Thickness

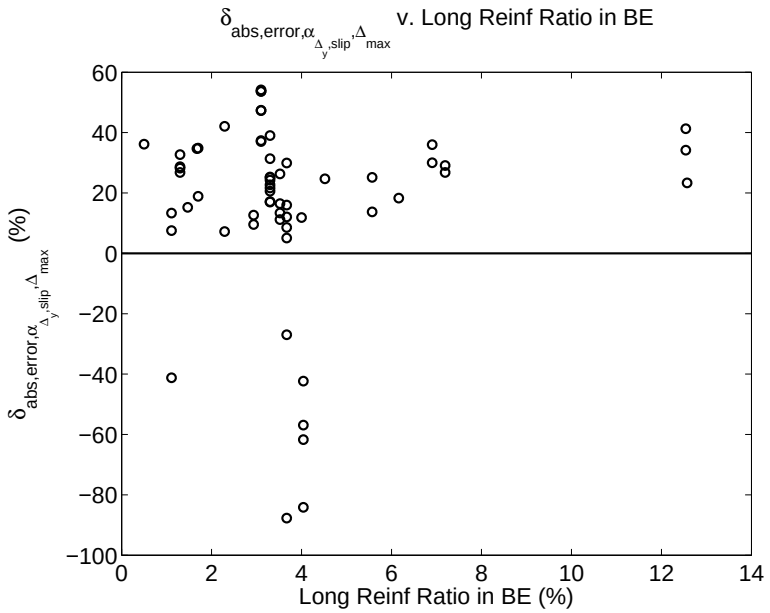

Figure N.205: Effective Shear Calibrated to Yield Displacement With Slip Max Displacement Absolute Error Change v. Long Reinf Ratio in BE

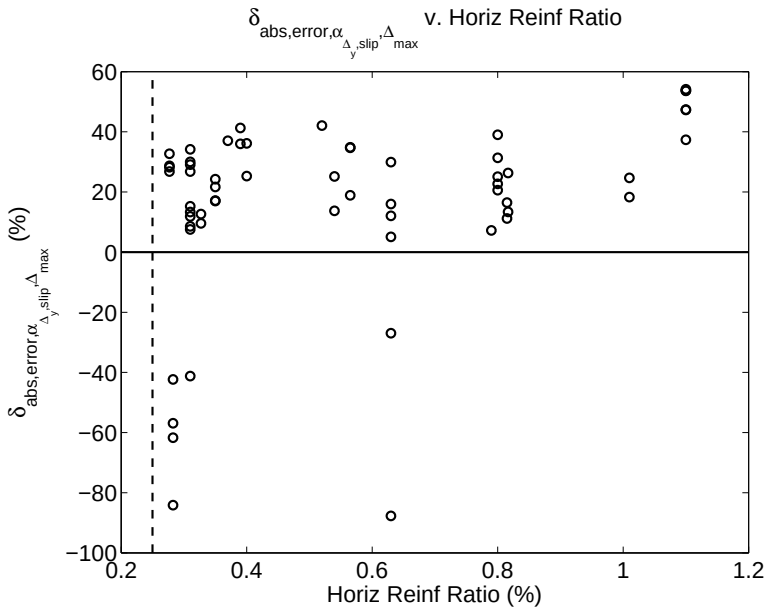

Figure N.206: Effective Shear Calibrated to Yield Displacement With Slip Max Displacement Absolute Error Change v. Horiz Reinf Ratio

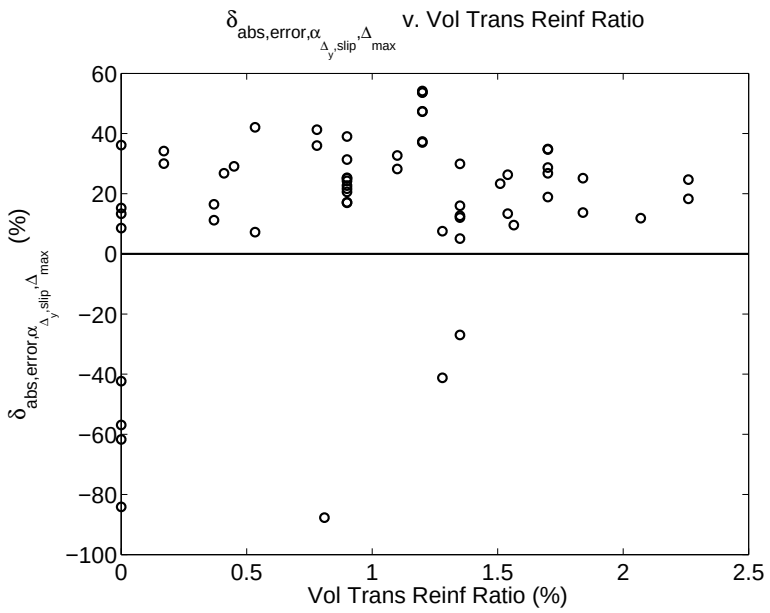

Figure N.207: Effective Shear Calibrated to Yield Displacement With Slip Max Displacement Absolute Error Change v. Vol Trans Reinf Ratio

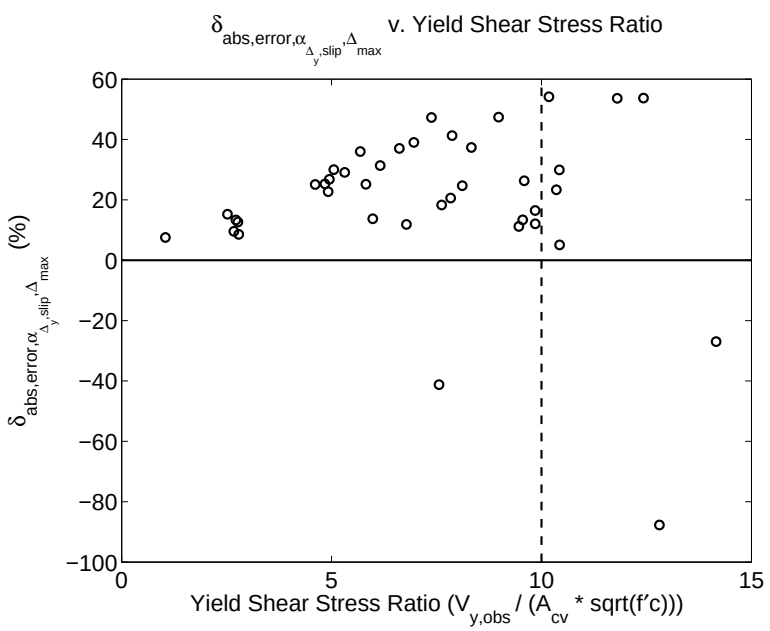

Figure N.208: Effective Shear Calibrated to Yield Displacement With Slip Max Displacement Absolute Error Change v. Yield Shear Stress Ratio

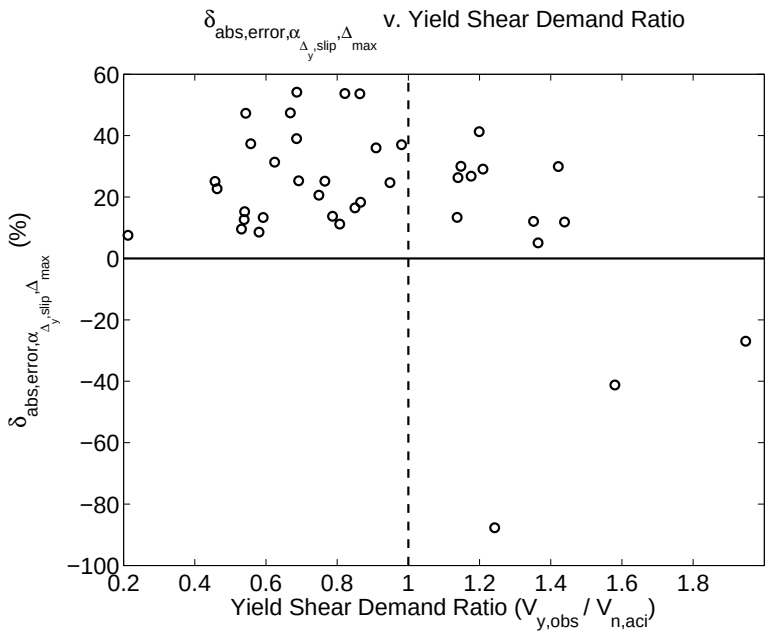

Figure N.209: Effective Shear Calibrated to Yield Displacement With Slip Max Displacement Absolute Error Change v. Yield Shear Demand Ratio

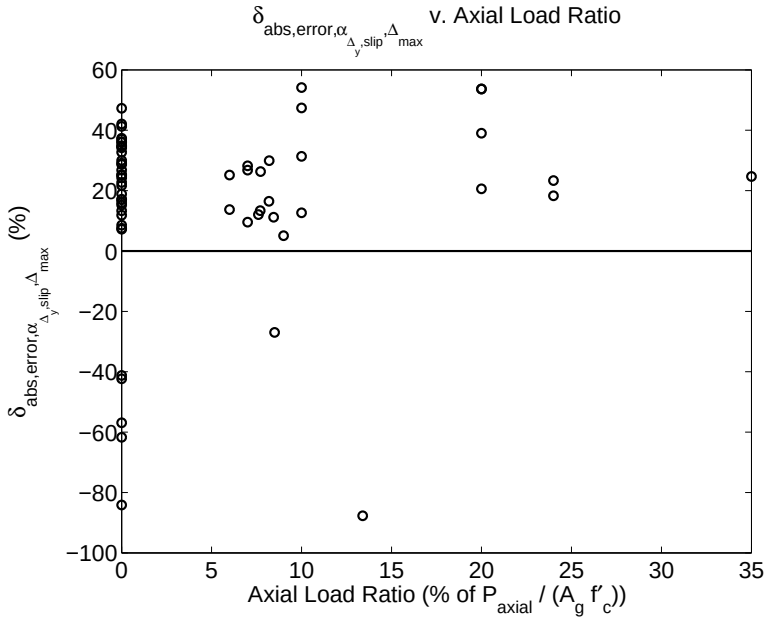

Figure N.210: Effective Shear Calibrated to Yield Displacement With Slip Max Displacement Absolute Error Change v. Axial Load Ratio

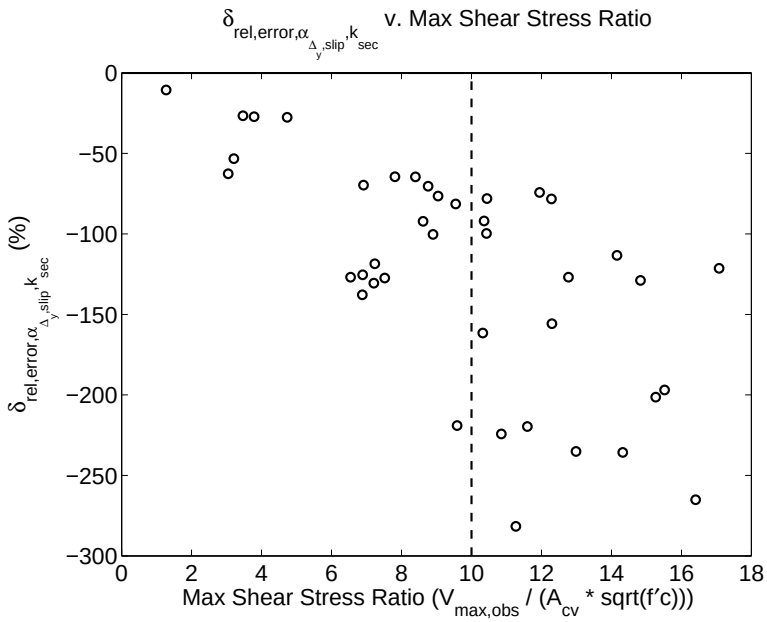

Figure N.211: Effective Shear Calibrated to Yield Displacement With Slip Secant Stiffness Relative Error Change v. Max Shear Stress Ratio

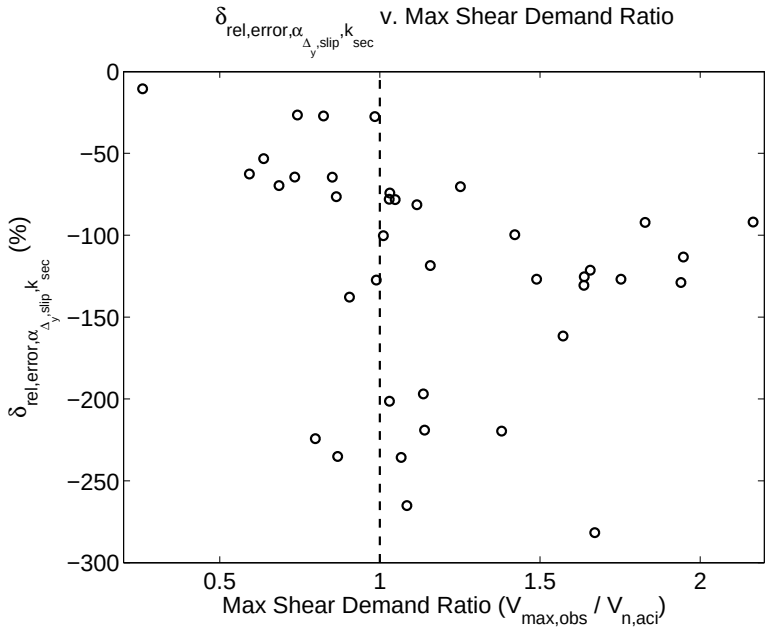

Figure N.212: Effective Shear Calibrated to Yield Displacement With Slip Secant Stiffness Relative Error Change v. Max Shear Demand Ratio

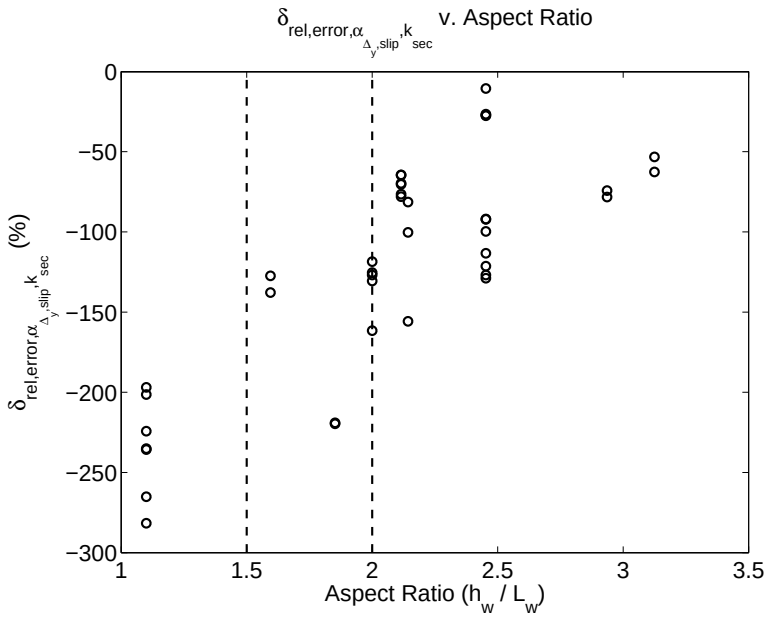

Figure N.213: Effective Shear Calibrated to Yield Displacement With Slip Secant Stiffness Relative Error Change v. Aspect Ratio

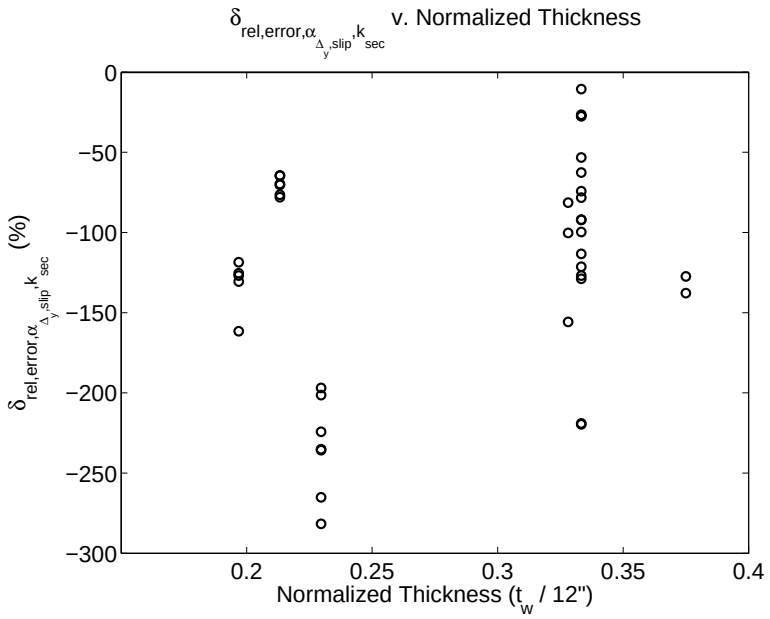

Figure N.214: Effective Shear Calibrated to Yield Displacement With Slip Secant Stiffness Relative Error Change v. Normalized Thickness

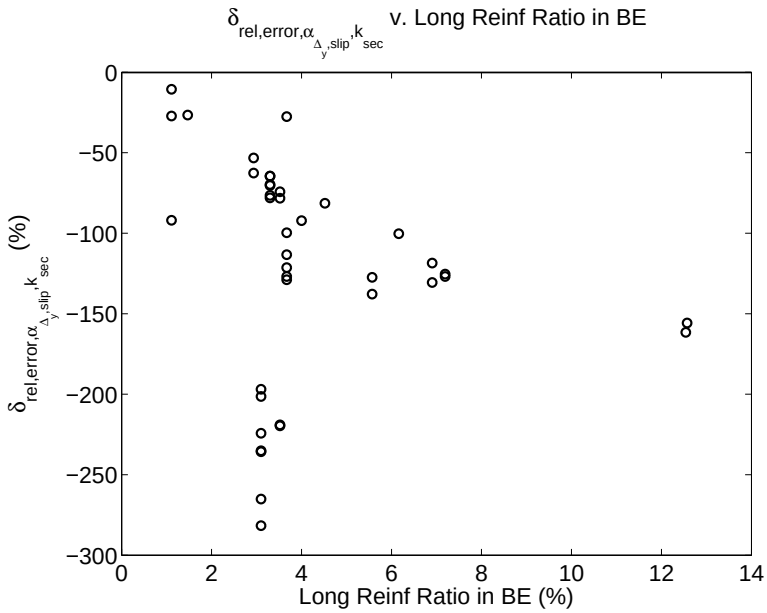

Figure N.215: Effective Shear Calibrated to Yield Displacement With Slip Secant Stiffness Relative Error Change v. Long Reinf Ratio in BE

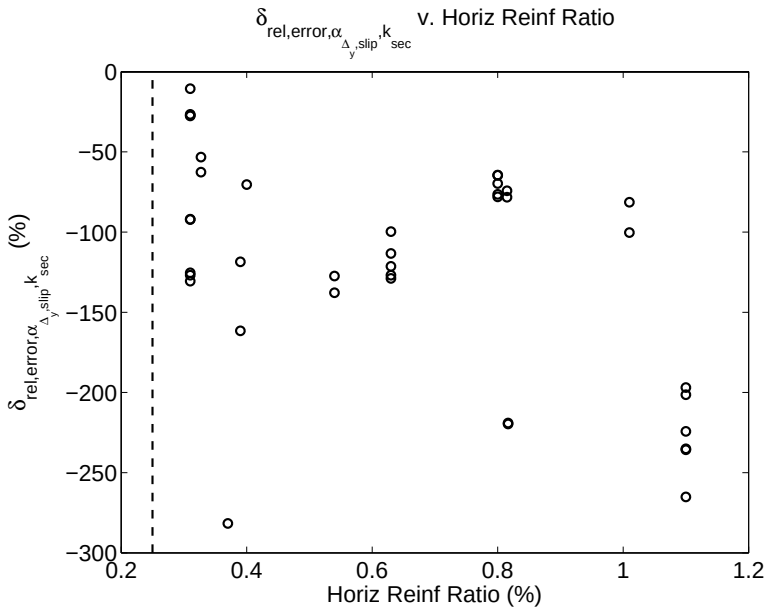

Figure N.216: Effective Shear Calibrated to Yield Displacement With Slip Secant Stiffness Relative Error Change v. Horiz Reinf Ratio

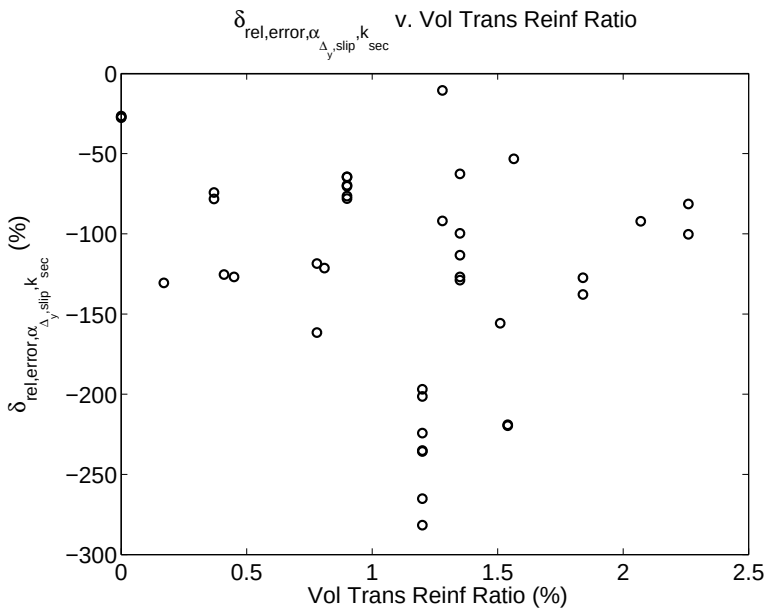

Figure N.217: Effective Shear Calibrated to Yield Displacement With Slip Secant Stiffness Relative Error Change v. Vol Trans Reinf Ratio

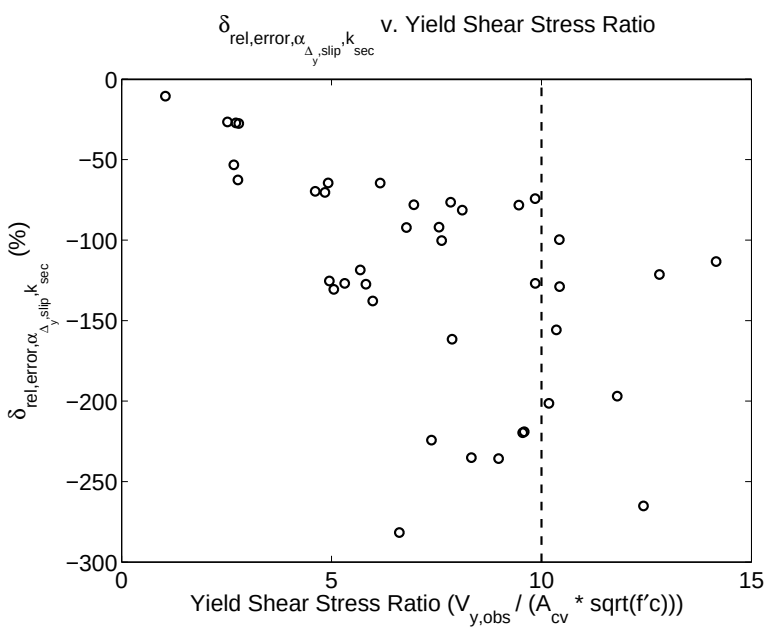

Figure N.218: Effective Shear Calibrated to Yield Displacement With Slip Secant Stiffness Relative Error Change v. Yield Shear Stress Ratio

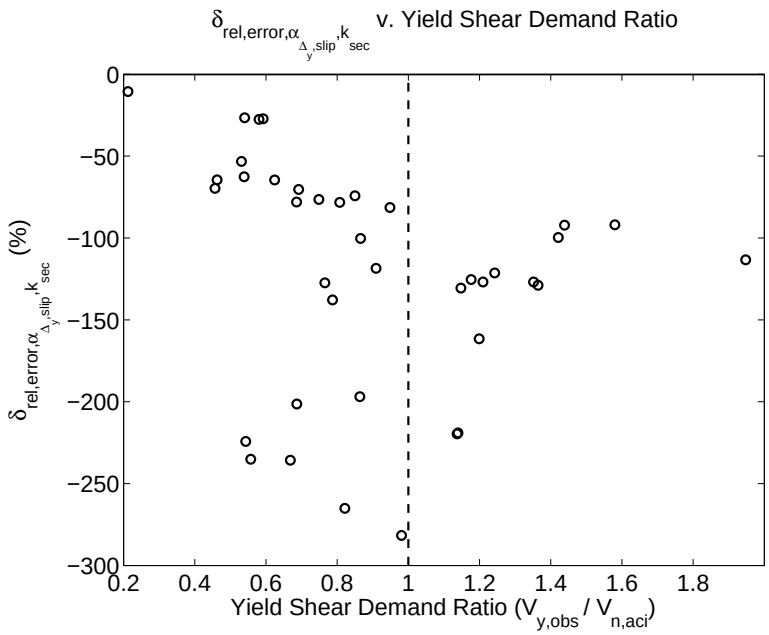

Figure N.219: Effective Shear Calibrated to Yield Displacement With Slip Secant Stiffness Relative Error Change v. Yield Shear Demand Ratio

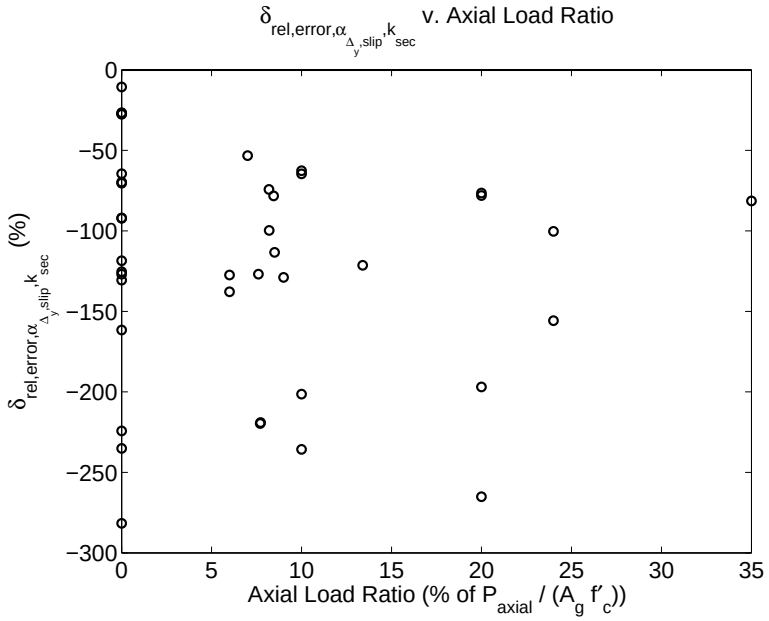

Figure N.220: Effective Shear Calibrated to Yield Displacement With Slip Secant Stiffness Relative Error Change v. Axial Load Ratio

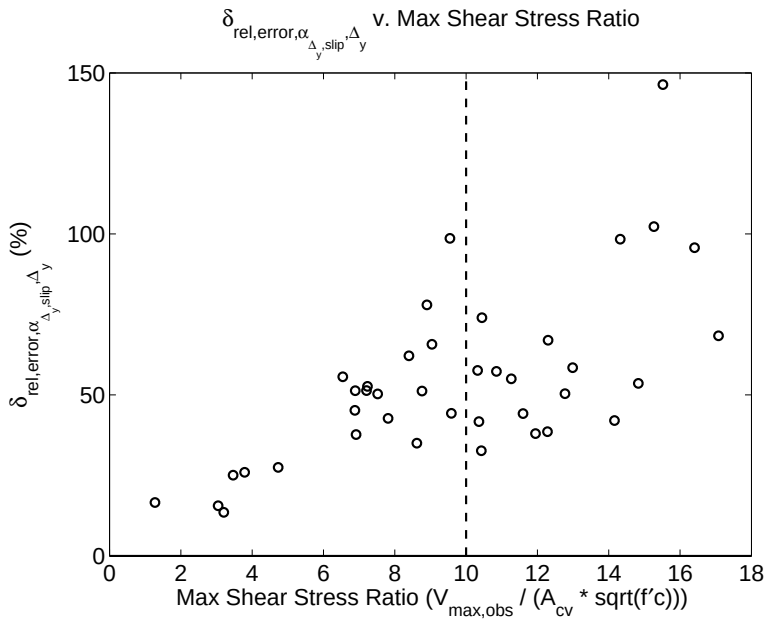

Figure N.221: Effective Shear Calibrated to Yield Displacement With Slip Yield Displacement Relative Error Change v. Max Shear Stress Ratio

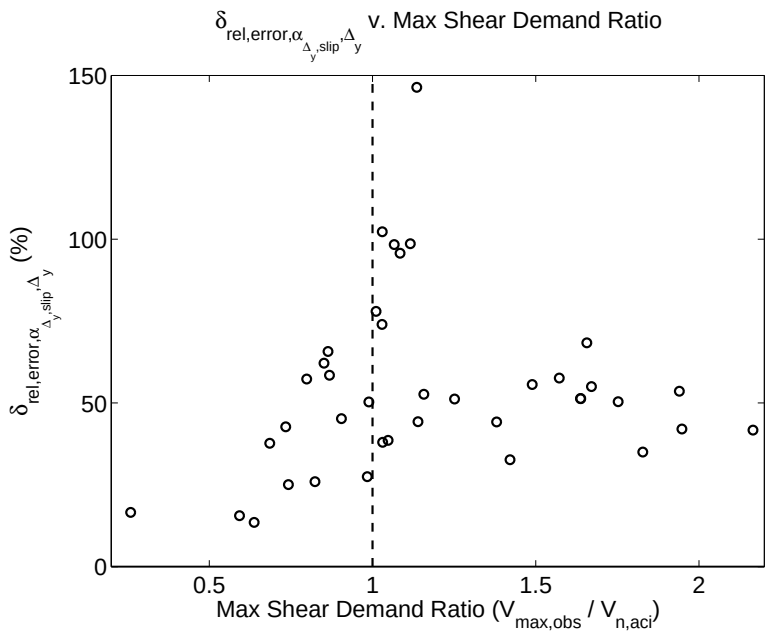

Figure N.222: Effective Shear Calibrated to Yield Displacement With Slip Yield Displacement Relative Error Change v. Max Shear Demand Ratio

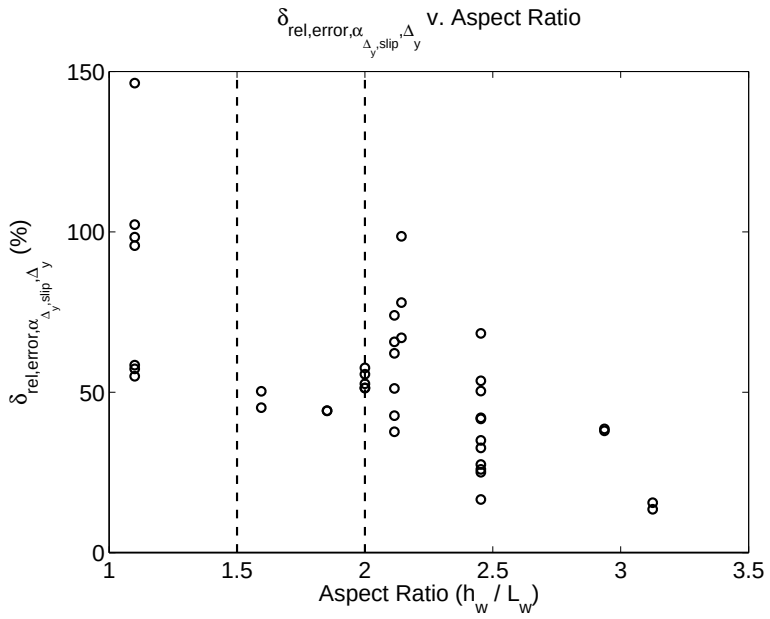

Figure N.223: Effective Shear Calibrated to Yield Displacement With Slip Yield Displacement Relative Error Change v. Aspect Ratio

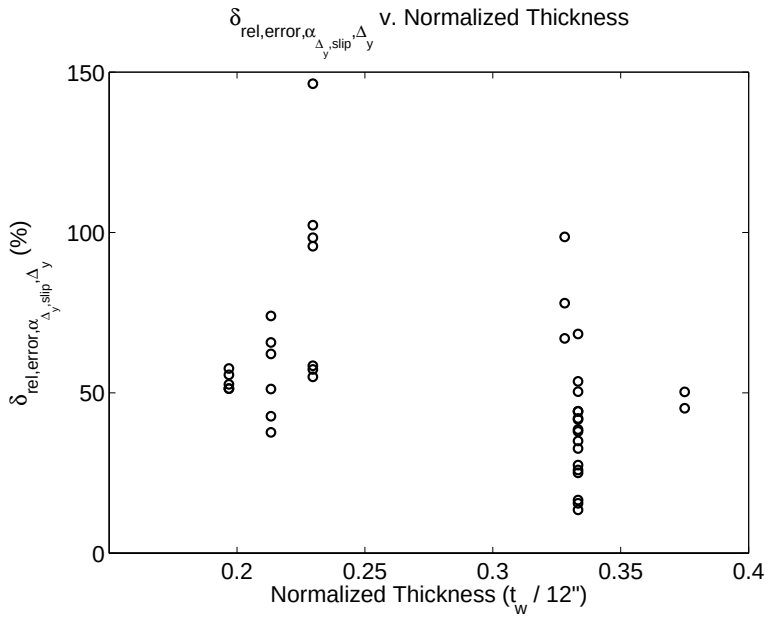

Figure N.224: Effective Shear Calibrated to Yield Displacement With Slip Yield Displacement Relative Error Change v. Normalized Thickness

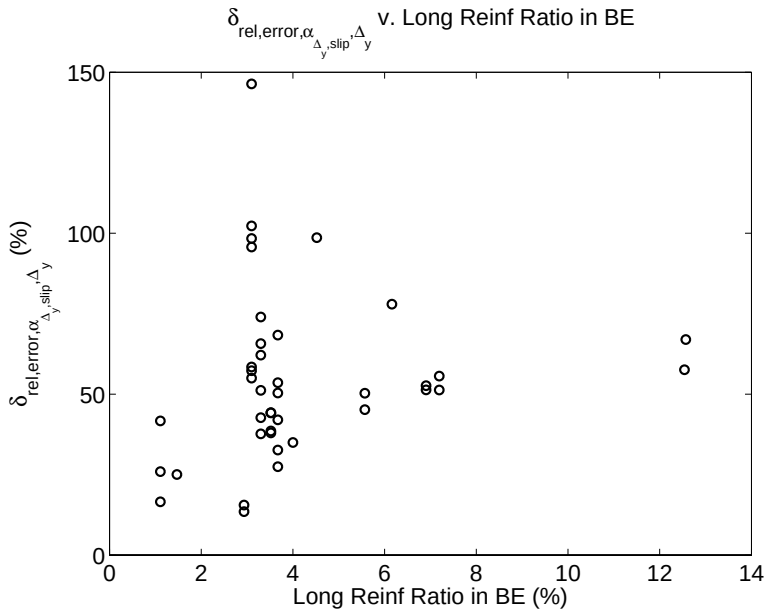

Figure N.225: Effective Shear Calibrated to Yield Displacement With Slip Yield Displacement Relative Error Change v. Long Reinf Ratio in BE

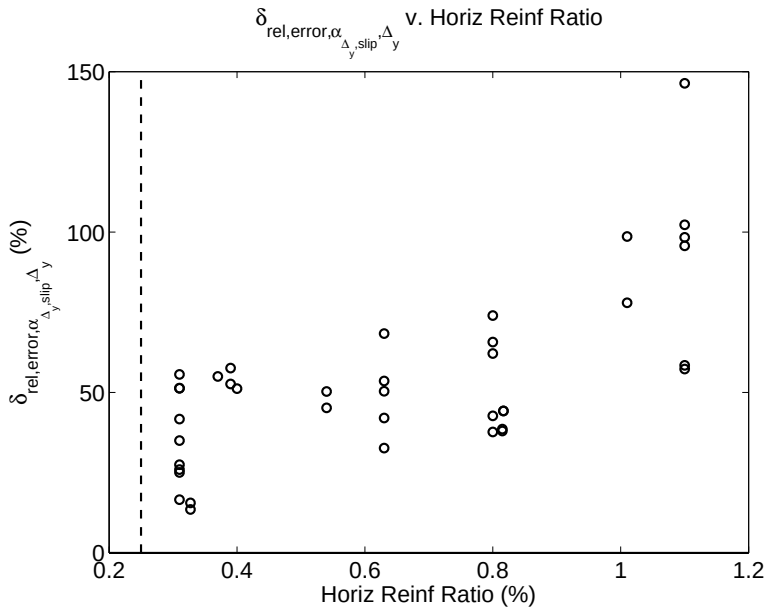

Figure N.226: Effective Shear Calibrated to Yield Displacement With Slip Yield Displacement Relative Error Change v. Horiz Reinf Ratio

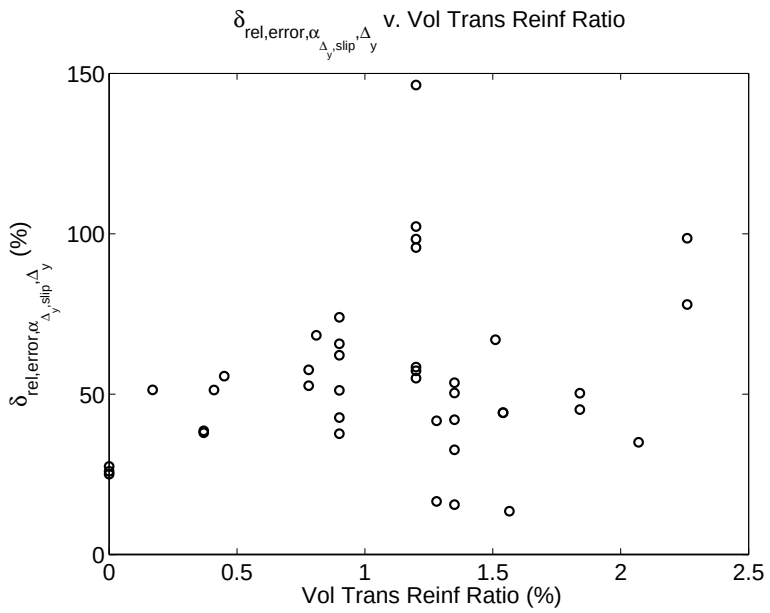

Figure N.227: Effective Shear Calibrated to Yield Displacement With Slip Yield Displacement Relative Error Change v. Vol Trans Reinf Ratio

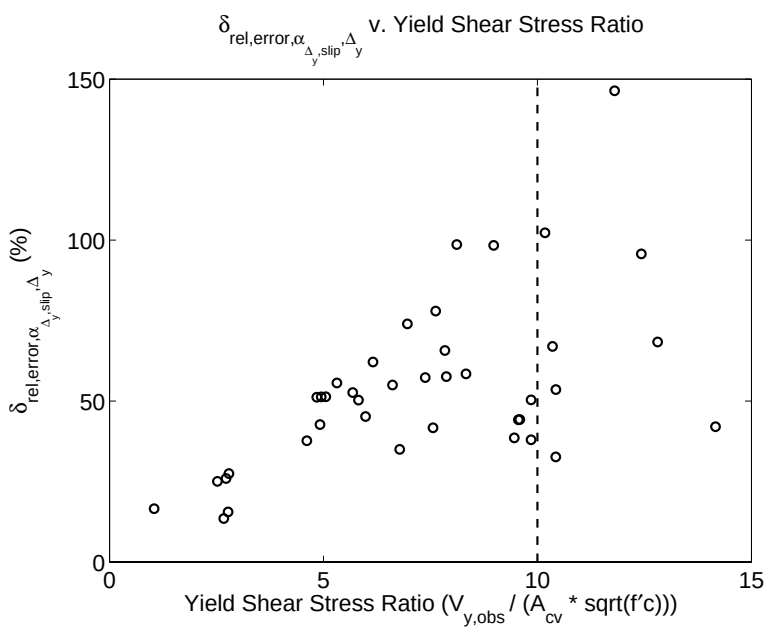

Figure N.228: Effective Shear Calibrated to Yield Displacement With Slip Yield Displacement Relative Error Change v. Yield Shear Stress Ratio

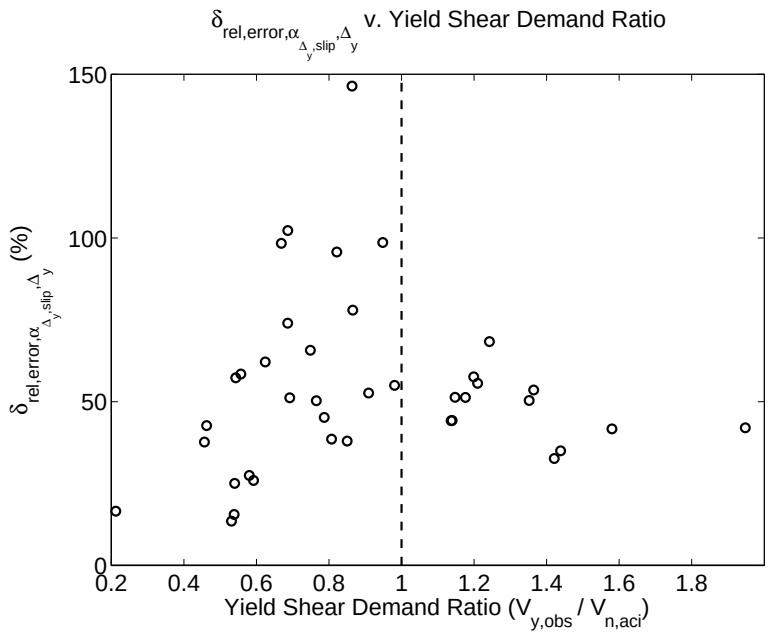

Figure N.229: Effective Shear Calibrated to Yield Displacement With Slip Yield Displacement Relative Error Change v. Yield Shear Demand Ratio

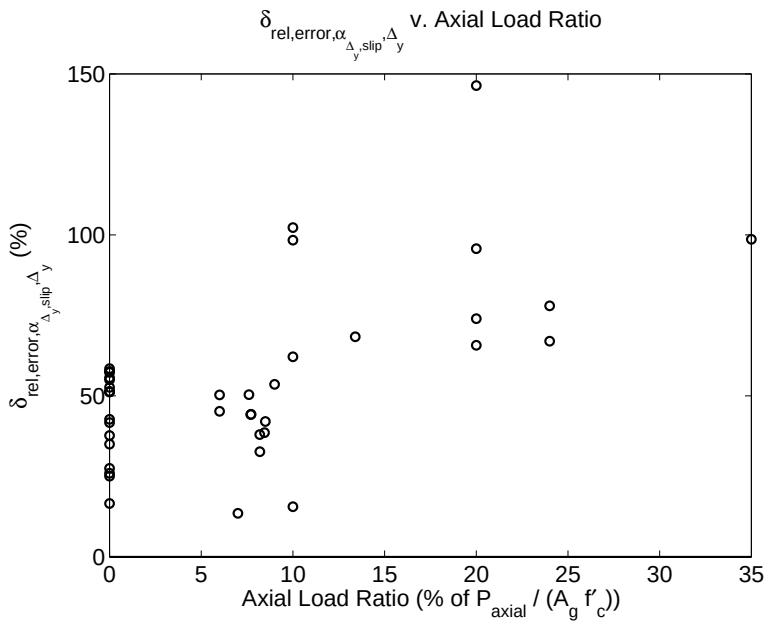

Figure N.230: Effective Shear Calibrated to Yield Displacement With Slip Yield Displacement Relative Error Change v. Axial Load Ratio

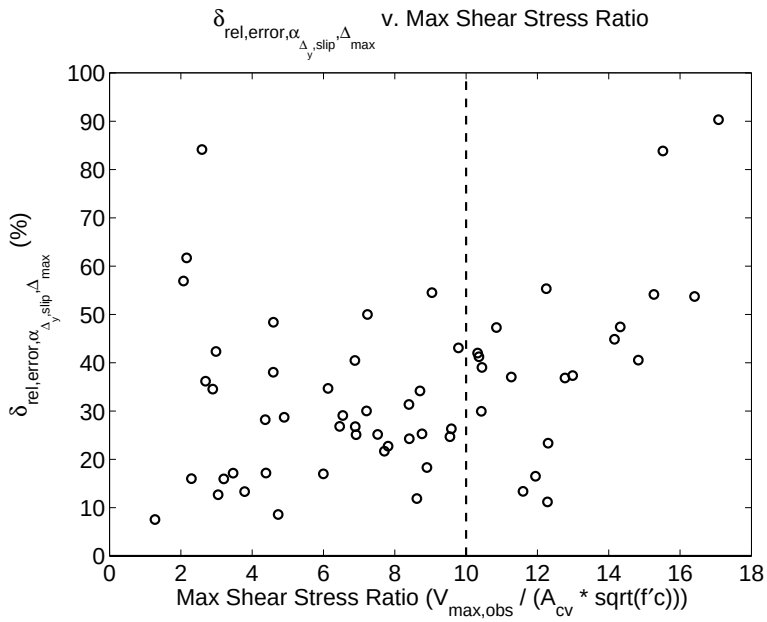

Figure N.231: Effective Shear Calibrated to Yield Displacement With Slip Max Displacement Relative Error Change v. Max Shear Stress Ratio

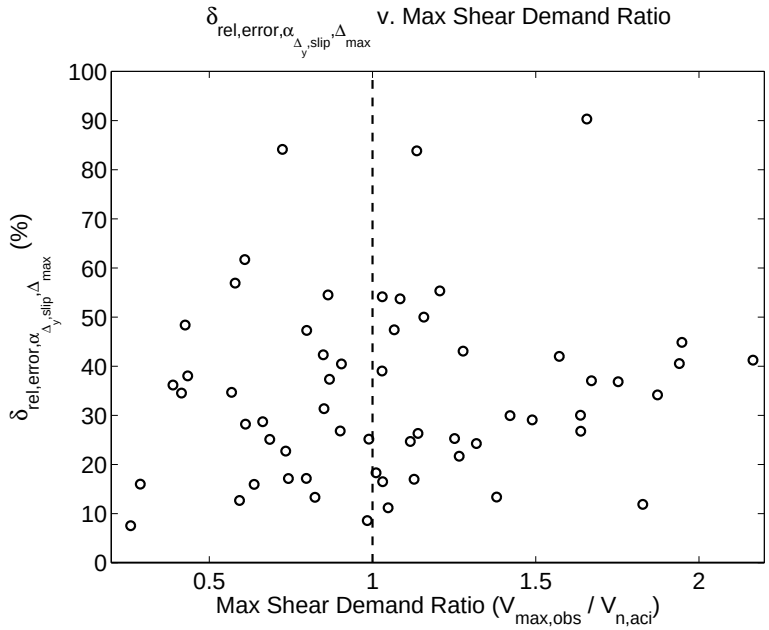

Figure N.232: Effective Shear Calibrated to Yield Displacement With Slip Max Displacement Relative Error Change v. Max Shear Demand Ratio

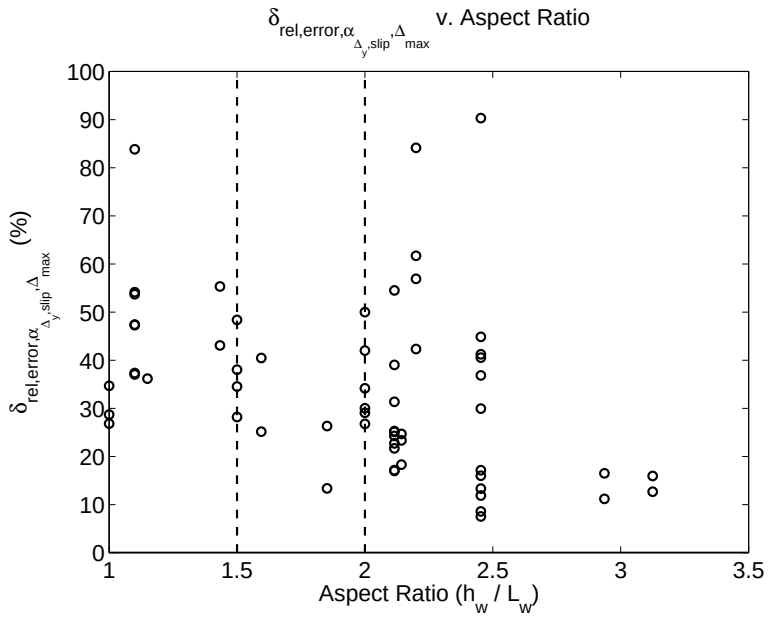

Figure N.233: Effective Shear Calibrated to Yield Displacement With Slip Max Displacement Relative Error Change v. Aspect Ratio

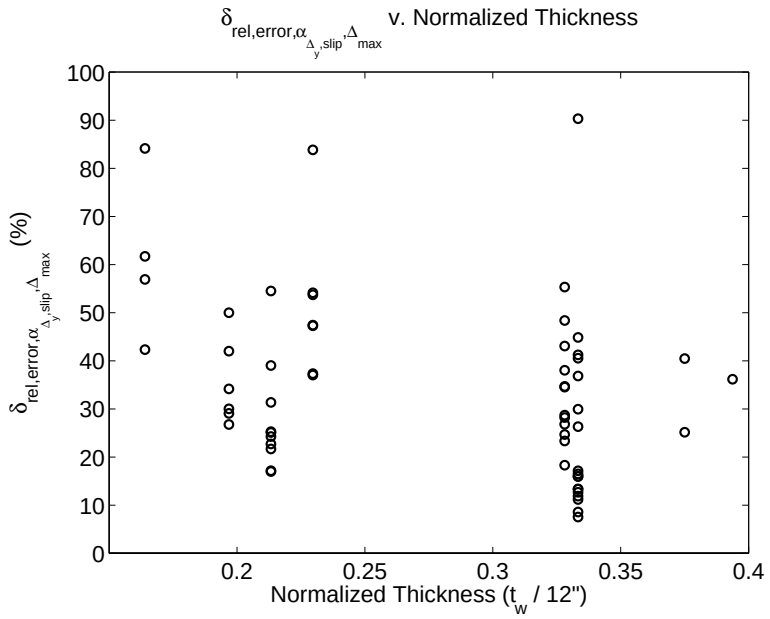

Figure N.234: Effective Shear Calibrated to Yield Displacement With Slip Max Displacement Relative Error Change v. Normalized Thickness

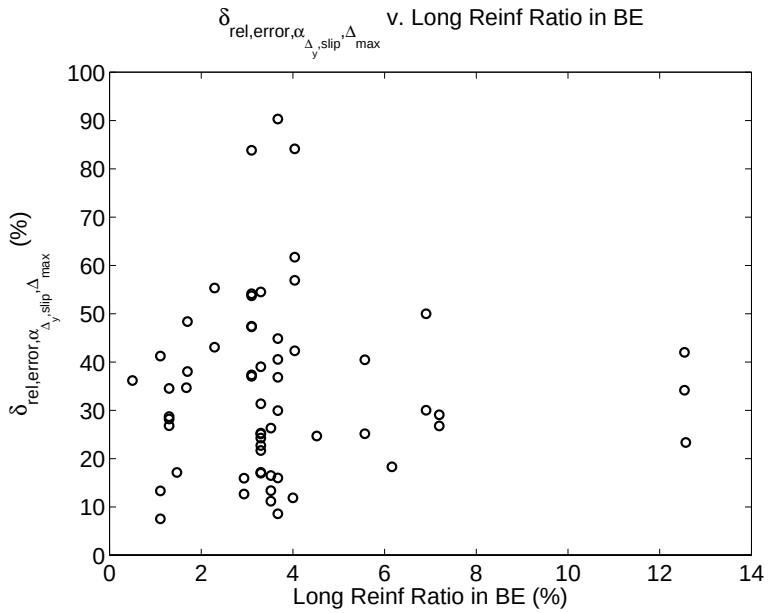

Figure N.235: Effective Shear Calibrated to Yield Displacement With Slip Max Displacement Relative Error Change v. Long Reinf Ratio in BE

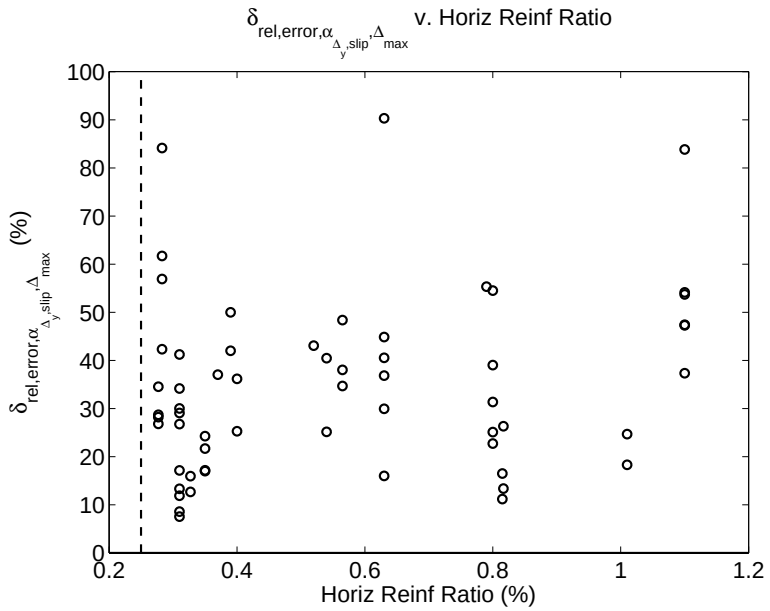

Figure N.236: Effective Shear Calibrated to Yield Displacement With Slip Max Displacement Relative Error Change v. Horiz Reinf Ratio

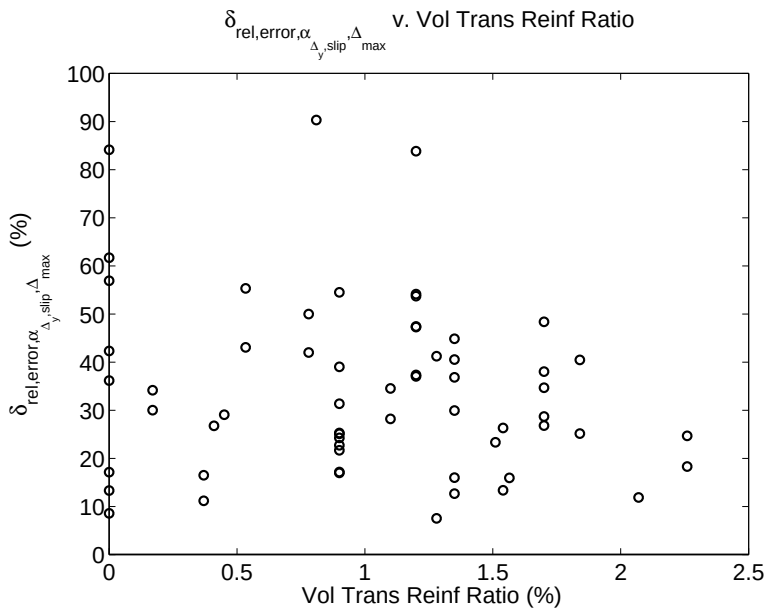

Figure N.237: Effective Shear Calibrated to Yield Displacement With Slip Max Displacement Relative Error Change v. Vol Trans Reinf Ratio

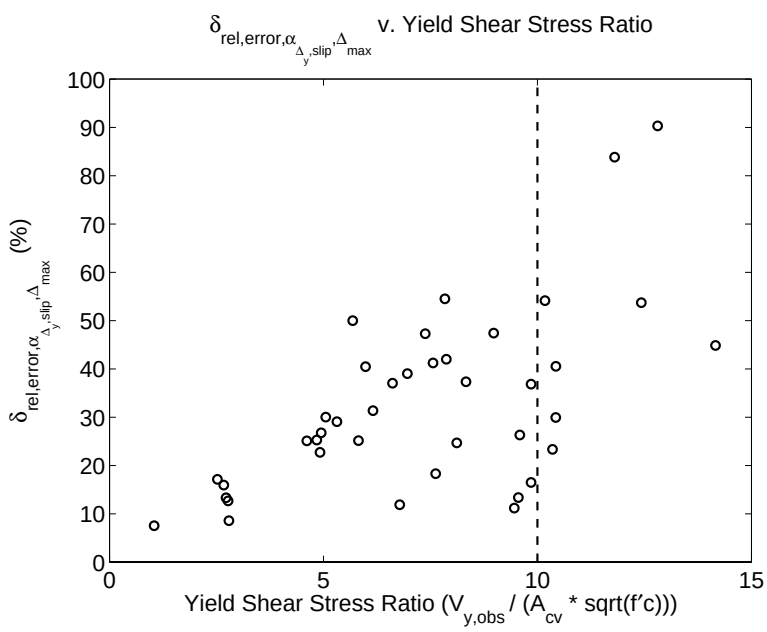

Figure N.238: Effective Shear Calibrated to Yield Displacement With Slip Max Displacement Relative Error Change v. Yield Shear Stress Ratio

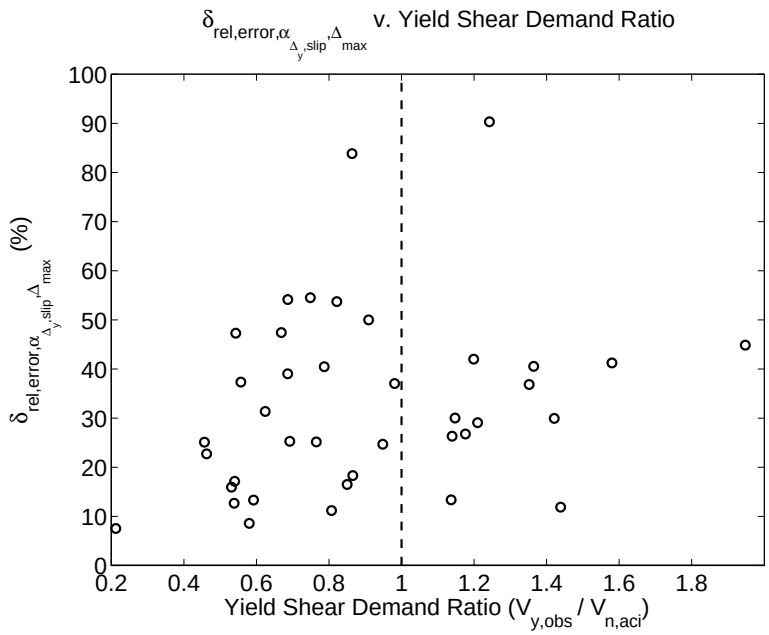

Figure N.239: Effective Shear Calibrated to Yield Displacement With Slip Max Displacement Relative Error Change v. Yield Shear Demand Ratio

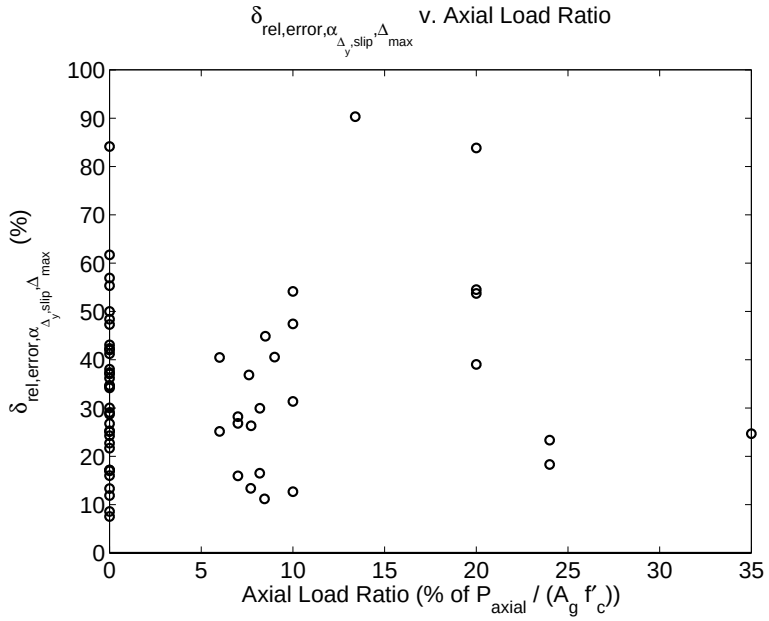

Figure N.240: Effective Shear Calibrated to Yield Displacement With Slip Max Displacement Relative Error Change v. Axial Load Ratio

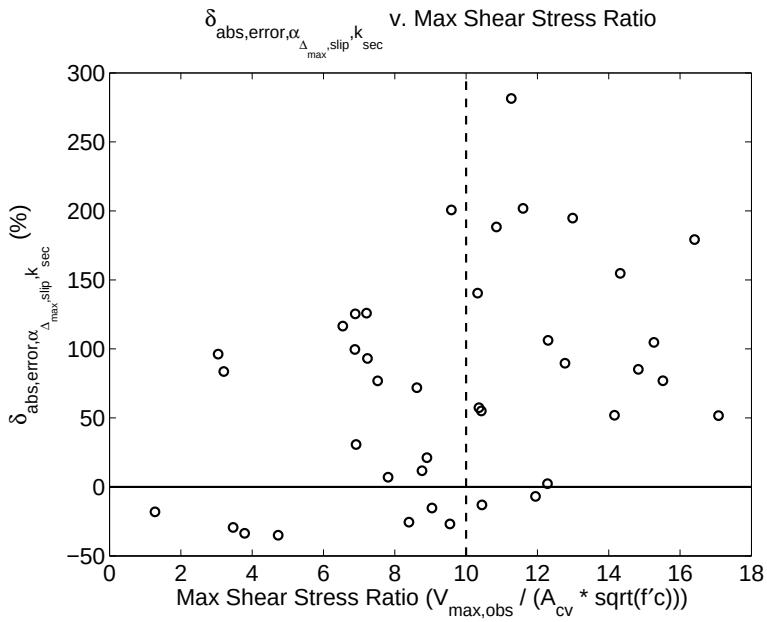

Figure N.241: Effective Shear Calibrated to Max Displacement With Slip Secant Stiffness Absolute Error Change v. Max Shear Stress Ratio

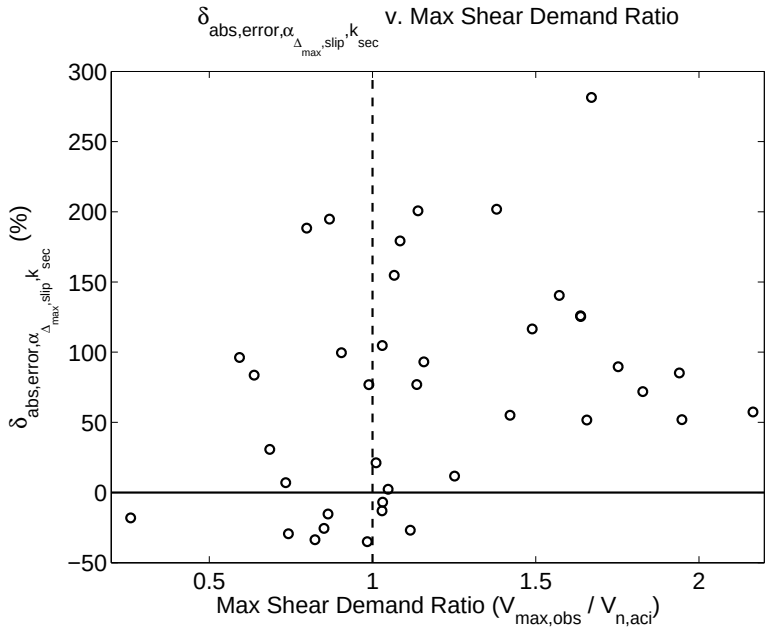

Figure N.242: Effective Shear Calibrated to Max Displacement With Slip Secant Stiffness Absolute Error Change v. Max Shear Demand Ratio

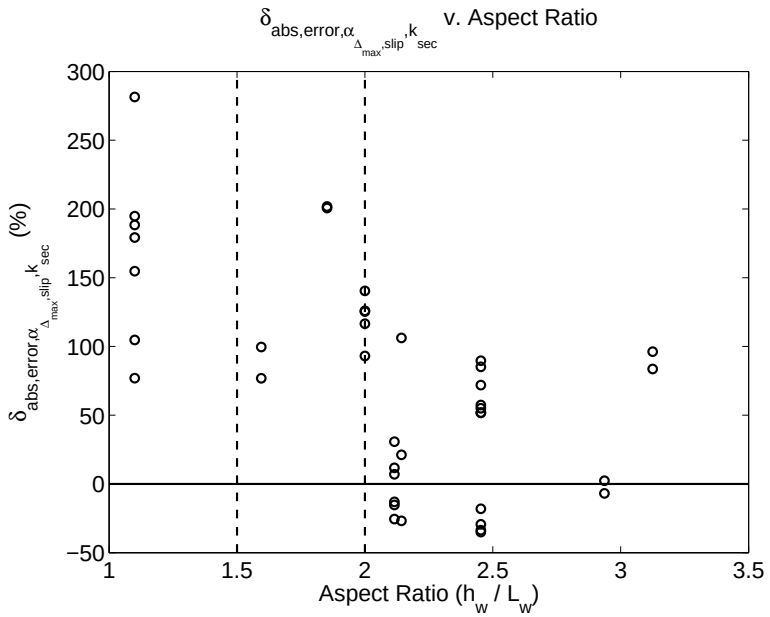

Figure N.243: Effective Shear Calibrated to Max Displacement With Slip Secant Stiffness Absolute Error Change v. Aspect Ratio

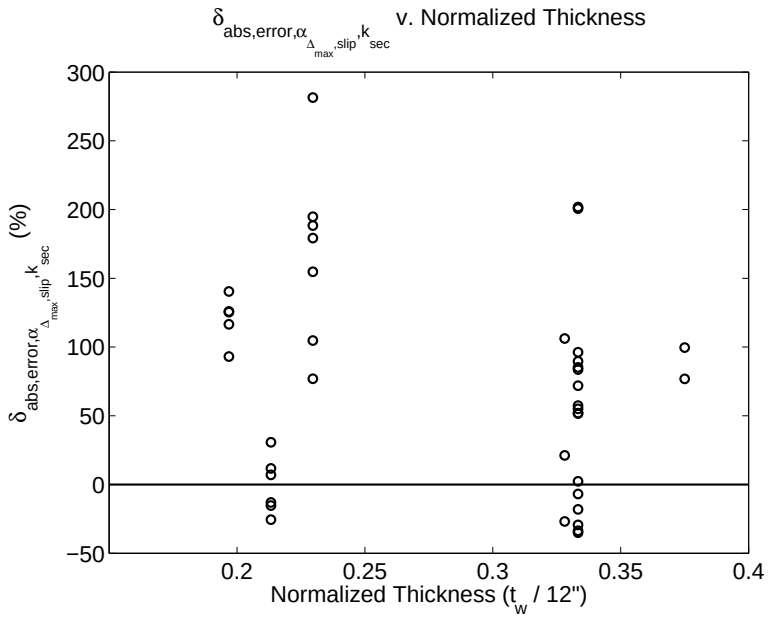

Figure N.244: Effective Shear Calibrated to Max Displacement With Slip Secant Stiffness Absolute Error Change v. Normalized Thickness

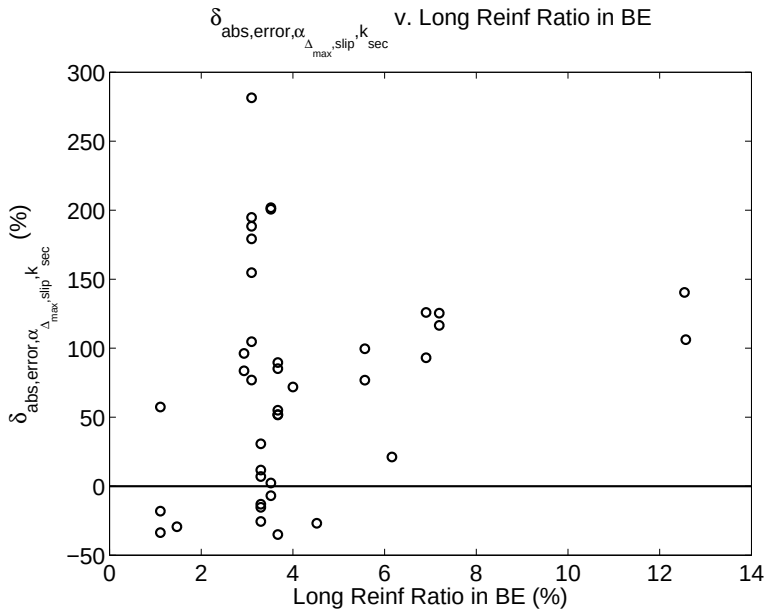

Figure N.245: Effective Shear Calibrated to Max Displacement With Slip Secant Stiffness Absolute Error Change v. Long Reinf Ratio in BE

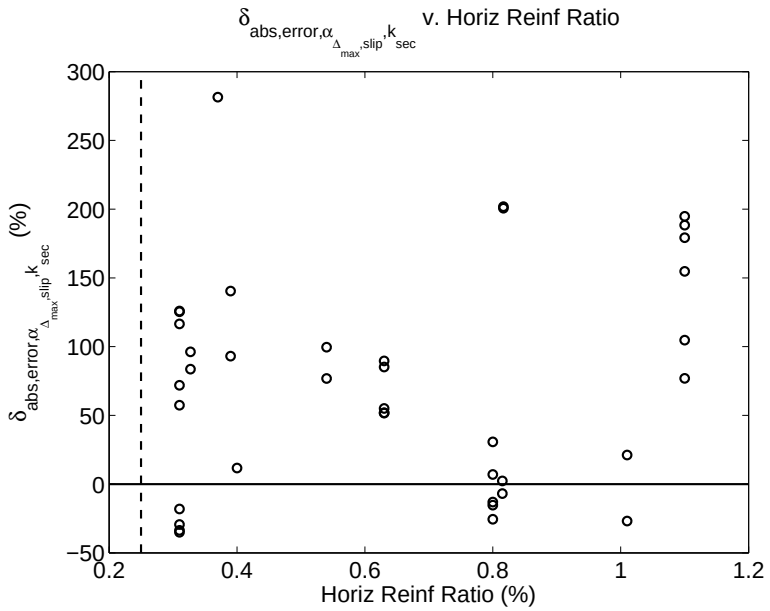

Figure N.246: Effective Shear Calibrated to Max Displacement With Slip Secant Stiffness Absolute Error Change v. Horiz Reinf Ratio

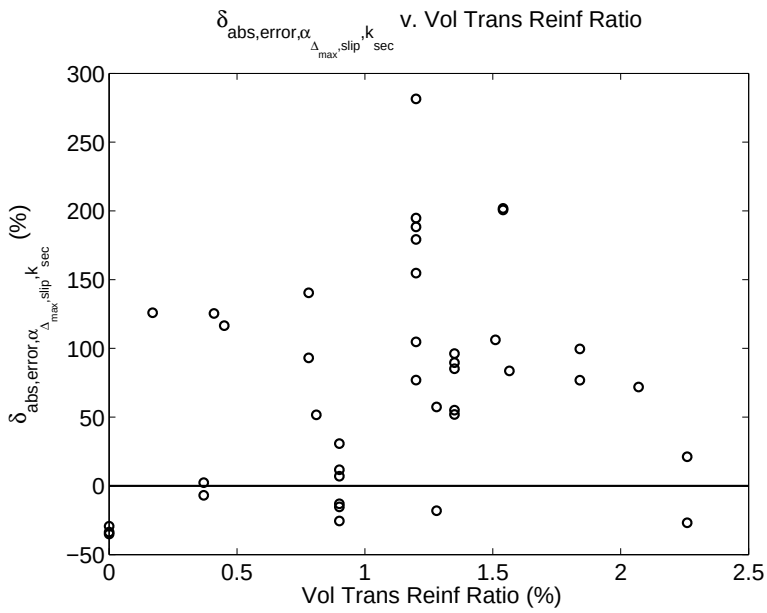

Figure N.247: Effective Shear Calibrated to Max Displacement With Slip Secant Stiffness Absolute Error Change v. Vol Trans Reinf Ratio

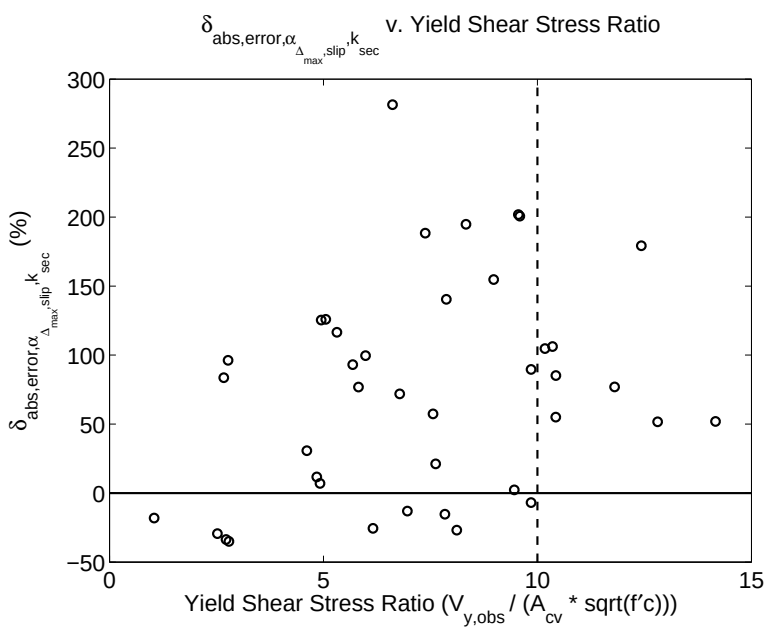

Figure N.248: Effective Shear Calibrated to Max Displacement With Slip Secant Stiffness Absolute Error Change v. Yield Shear Stress Ratio

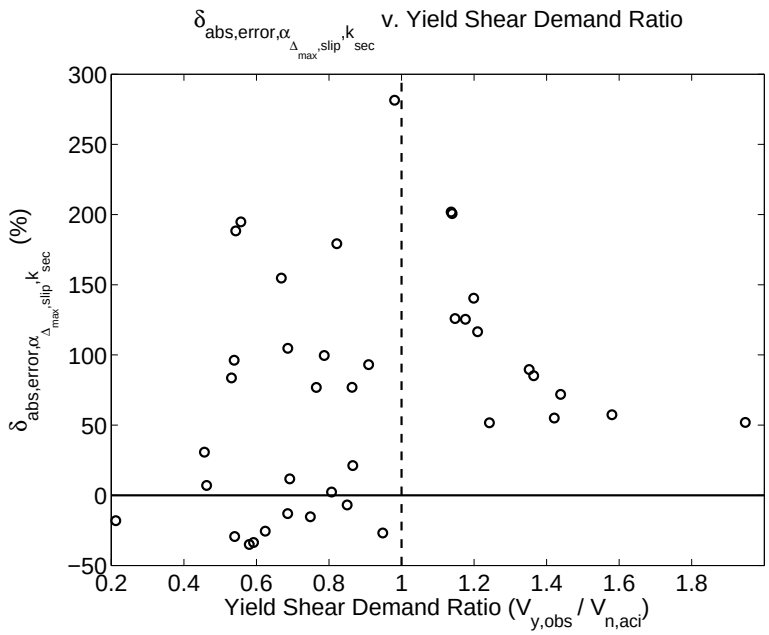

Figure N.249: Effective Shear Calibrated to Max Displacement With Slip Secant Stiffness Absolute Error Change v. Yield Shear Demand Ratio

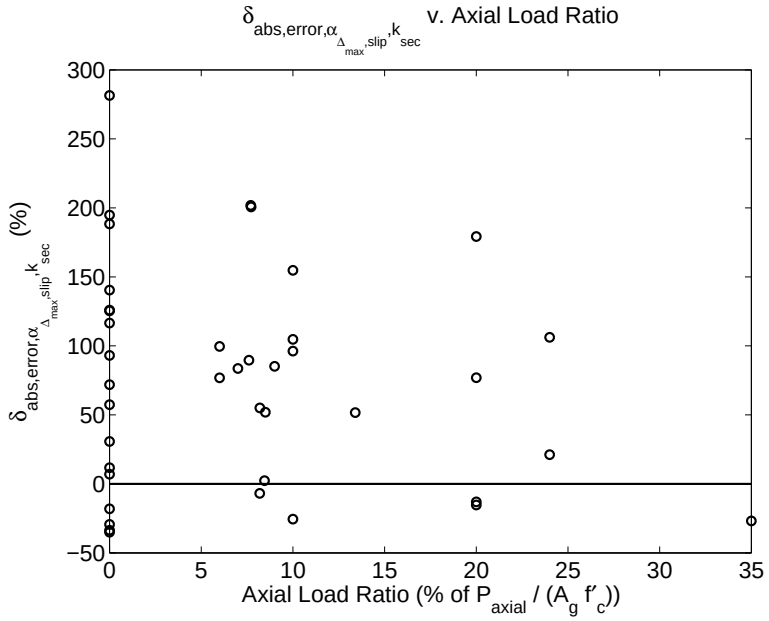

Figure N.250: Effective Shear Calibrated to Max Displacement With Slip Secant Stiffness Absolute Error Change v. Axial Load Ratio

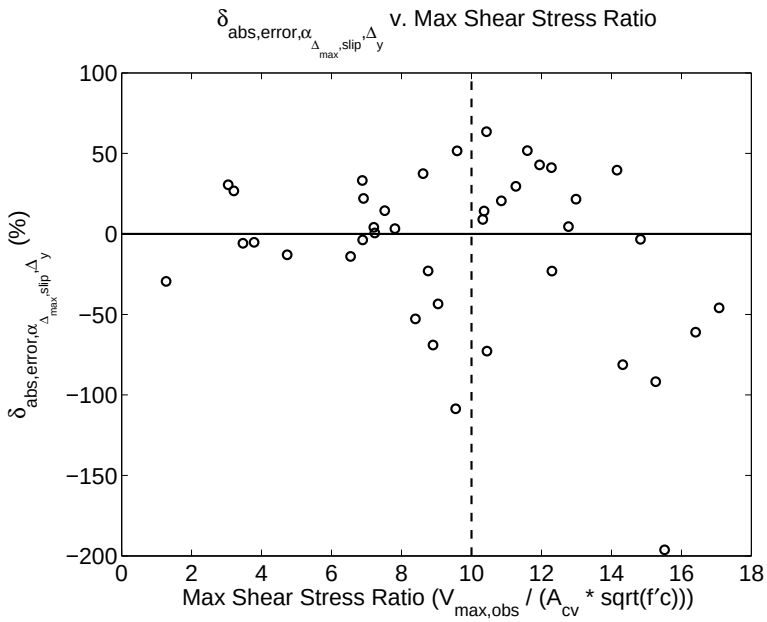

Figure N.251: Effective Shear Calibrated to Max Displacement With Slip Yield Displacement Absolute Error Change v. Max Shear Stress Ratio

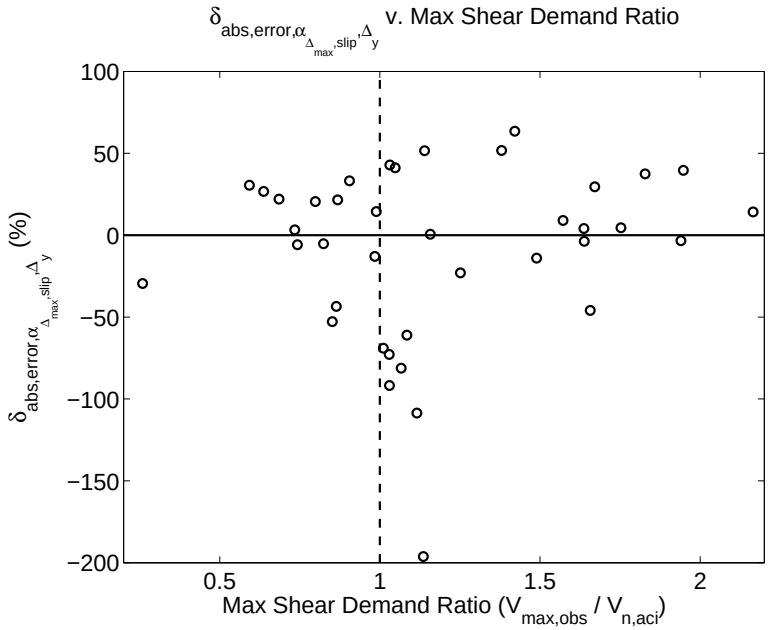

Figure N.252: Effective Shear Calibrated to Max Displacement With Slip Yield Displacement Absolute Error Change v. Max Shear Demand Ratio

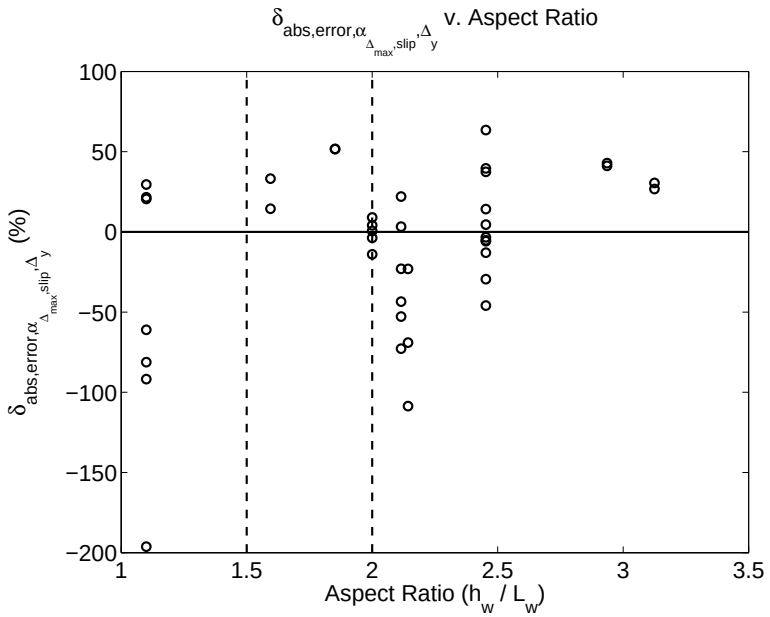

Figure N.253: Effective Shear Calibrated to Max Displacement With Slip Yield Displacement Absolute Error Change v. Aspect Ratio

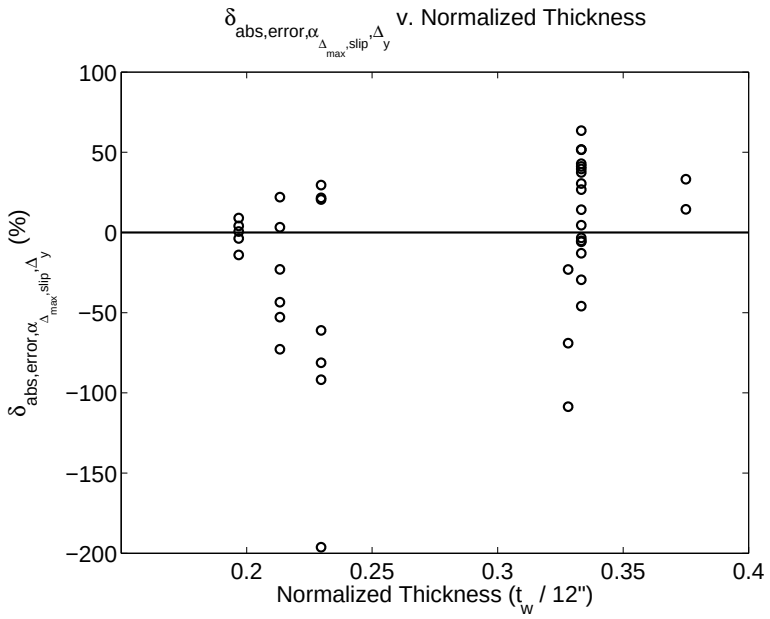

Figure N.254: Effective Shear Calibrated to Max Displacement With Slip Yield Displacement Absolute Error Change v. Normalized Thickness

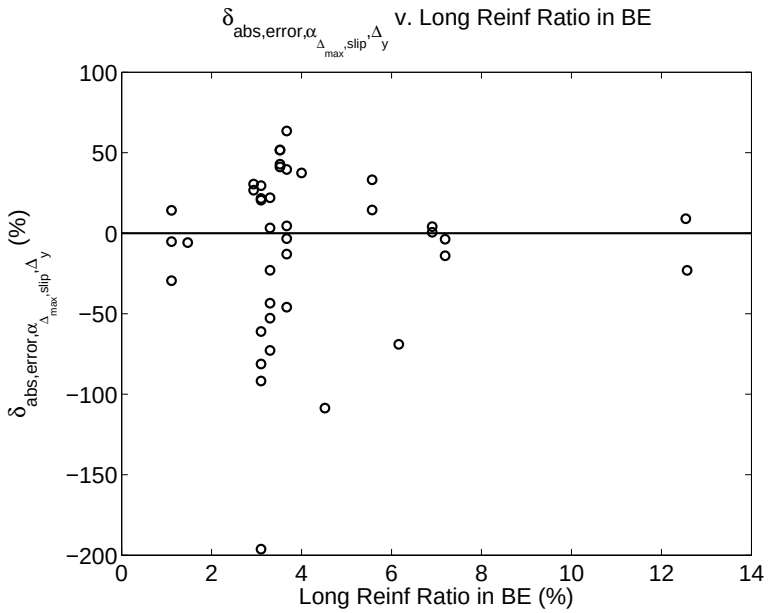

Figure N.255: Effective Shear Calibrated to Max Displacement With Slip Yield Displacement Absolute Error Change v. Long Reinf Ratio in BE

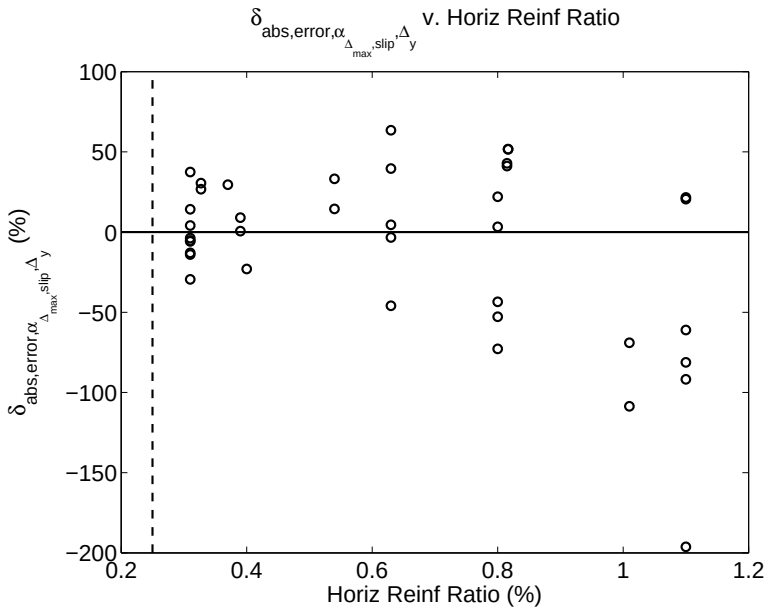

Figure N.256: Effective Shear Calibrated to Max Displacement With Slip Yield Displacement Absolute Error Change v. Horiz Reinf Ratio

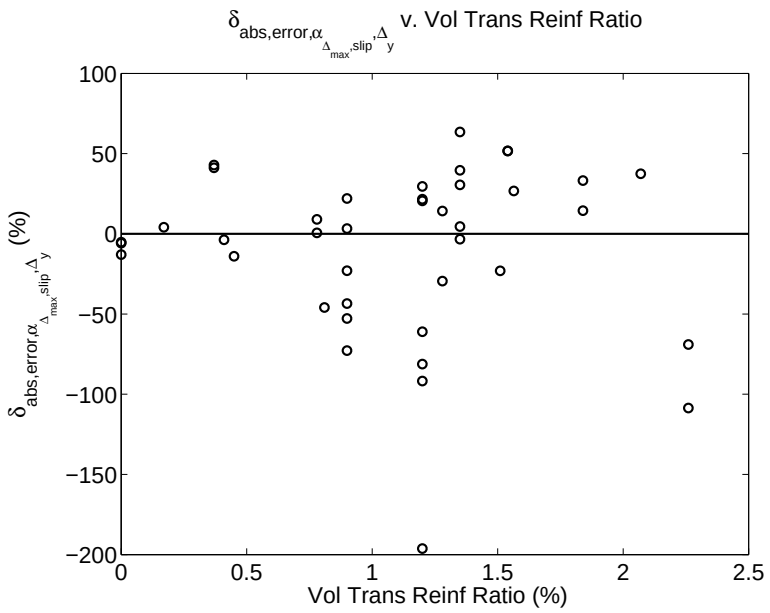

Figure N.257: Effective Shear Calibrated to Max Displacement With Slip Yield Displacement Absolute Error Change v. Vol Trans Reinf Ratio

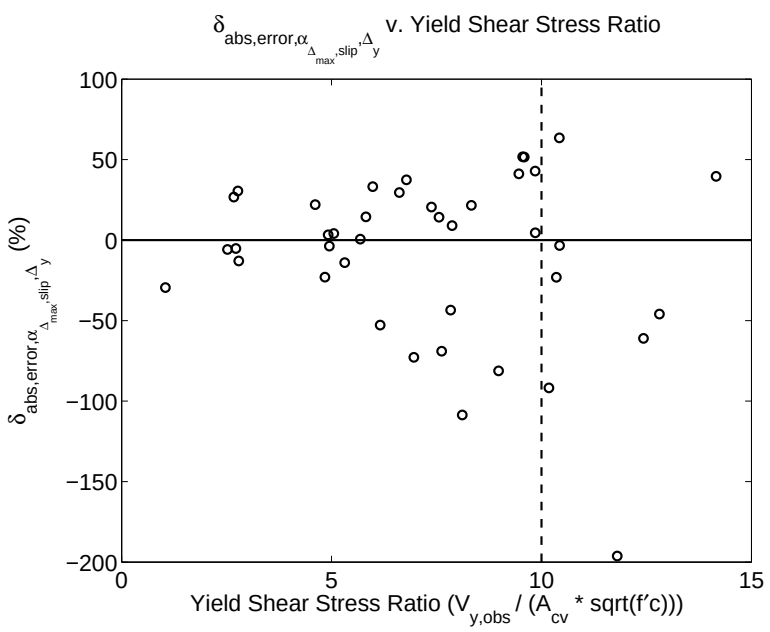

Figure N.258: Effective Shear Calibrated to Max Displacement With Slip Yield Displacement Absolute Error Change v. Yield Shear Stress Ratio

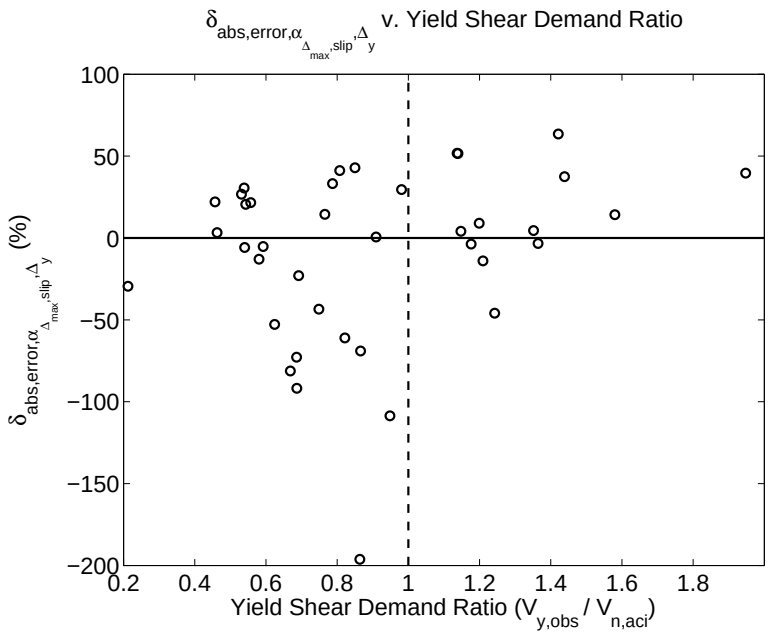

Figure N.259: Effective Shear Calibrated to Max Displacement With Slip Yield Displacement Absolute Error Change v. Yield Shear Demand Ratio

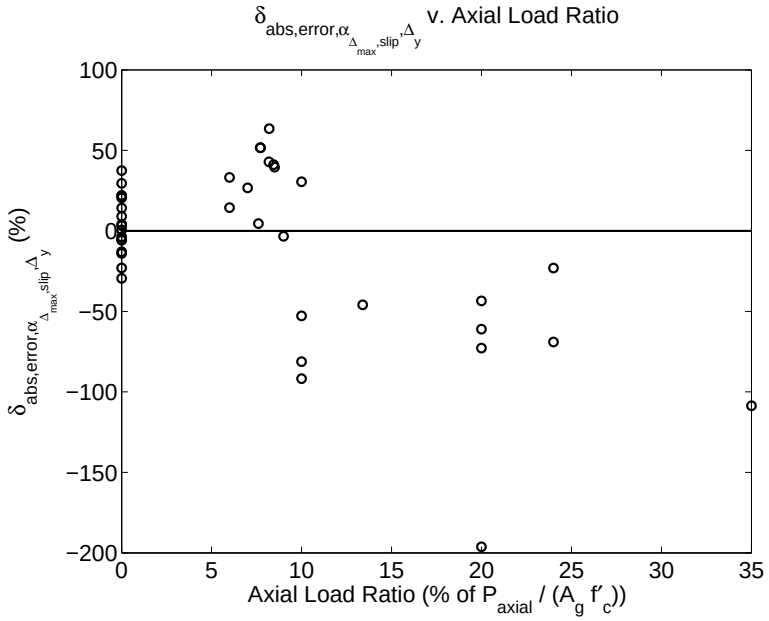

Figure N.260: Effective Shear Calibrated to Max Displacement With Slip Yield Displacement Absolute Error Change v. Axial Load Ratio

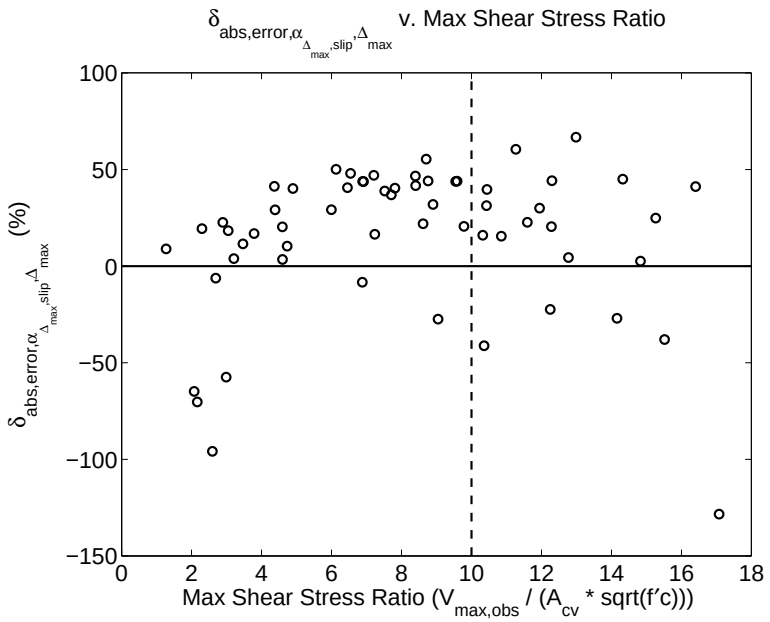

Figure N.261: Effective Shear Calibrated to Max Displacement With Slip Max Displacement Absolute Error Change v. Max Shear Stress Ratio

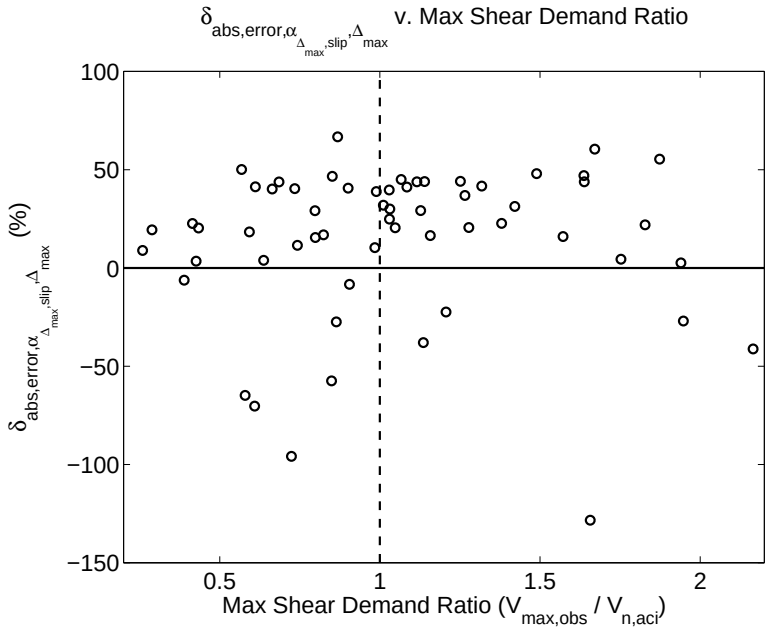

Figure N.262: Effective Shear Calibrated to Max Displacement With Slip Max Displacement Absolute Error Change v. Max Shear Demand Ratio

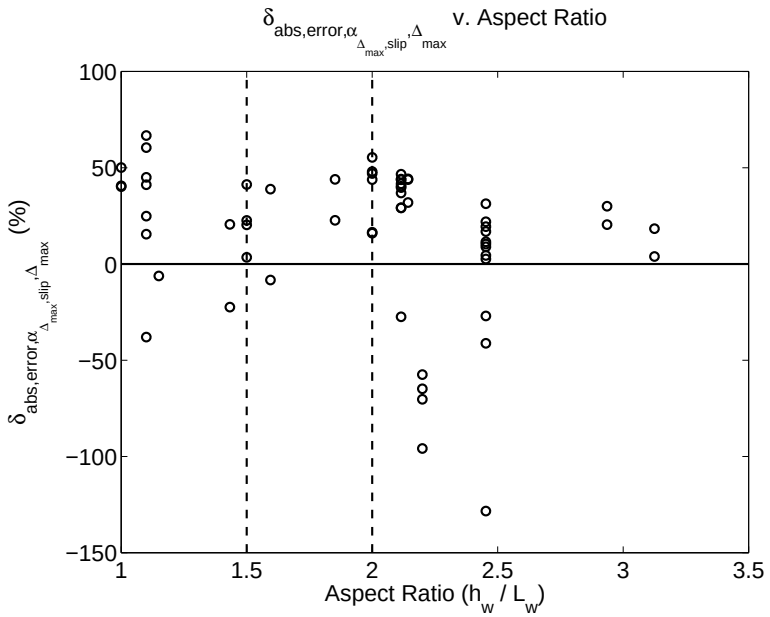

Figure N.263: Effective Shear Calibrated to Max Displacement With Slip Max Displacement Absolute Error Change v. Aspect Ratio

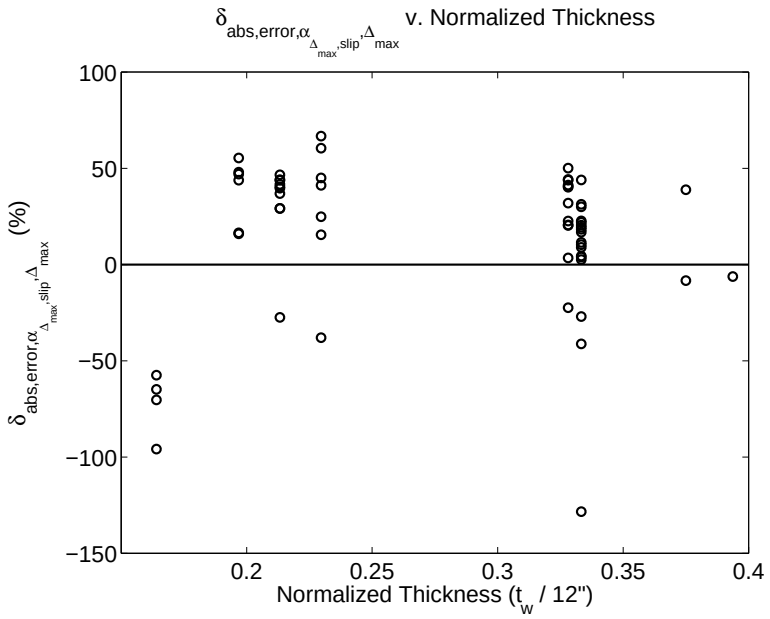

Figure N.264: Effective Shear Calibrated to Max Displacement With Slip Max Displacement Absolute Error Change v. Normalized Thickness

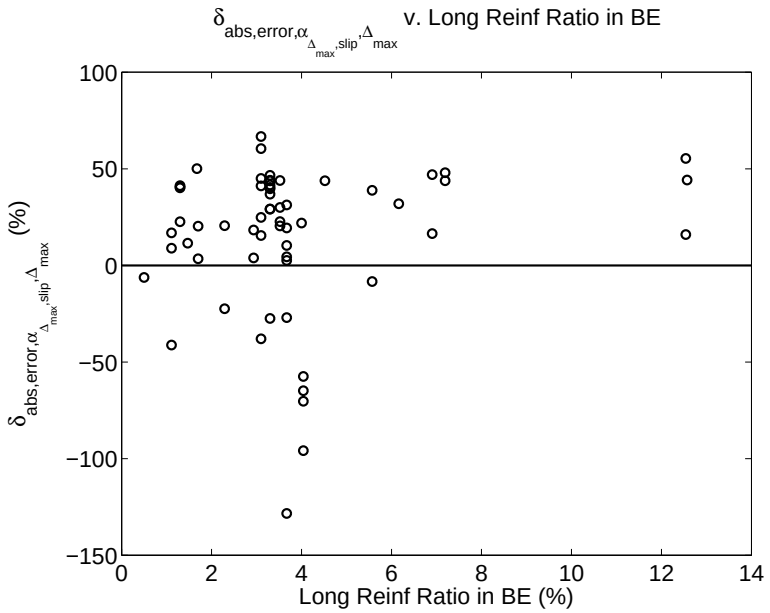

Figure N.265: Effective Shear Calibrated to Max Displacement With Slip Max Displacement Absolute Error Change v. Long Reinf Ratio in BE

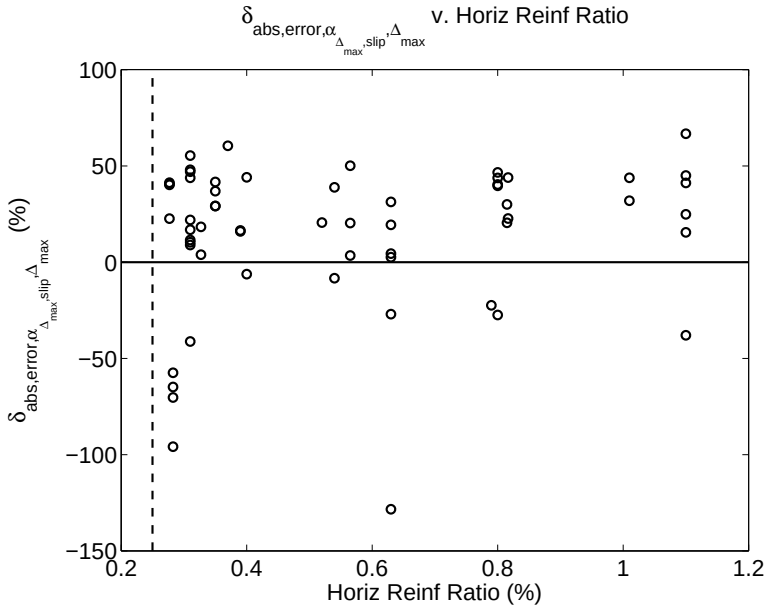

Figure N.266: Effective Shear Calibrated to Max Displacement With Slip Max Displacement Absolute Error Change v. Horiz Reinf Ratio

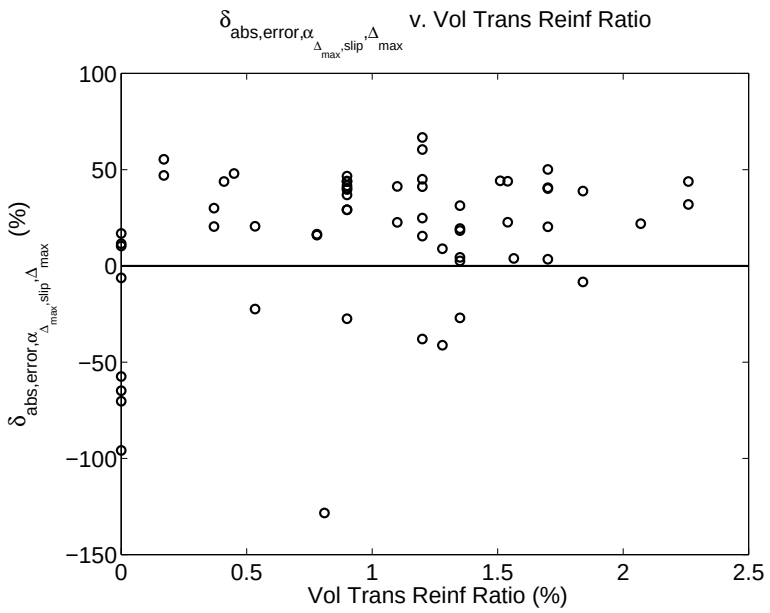

Figure N.267: Effective Shear Calibrated to Max Displacement With Slip Max Displacement Absolute Error Change v. Vol Trans Reinf Ratio

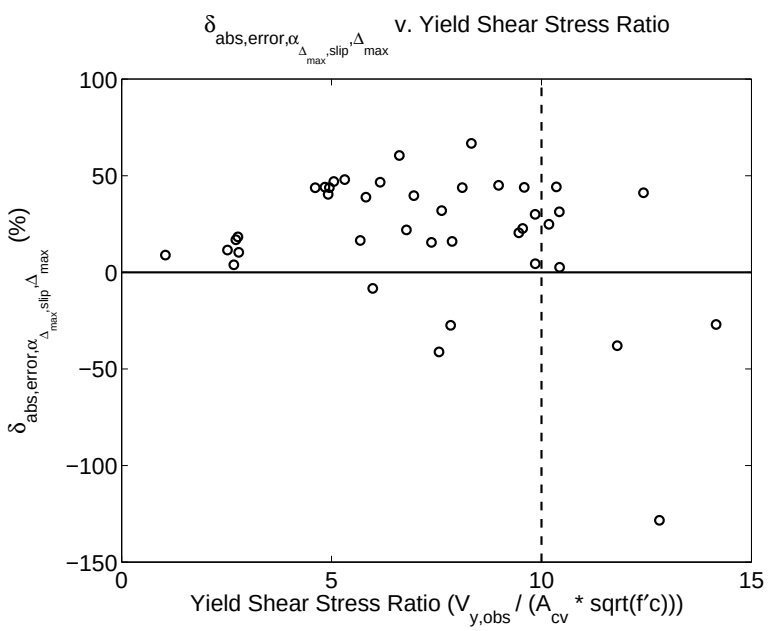

Figure N.268: Effective Shear Calibrated to Max Displacement With Slip Max Displacement Absolute Error Change v. Yield Shear Stress Ratio

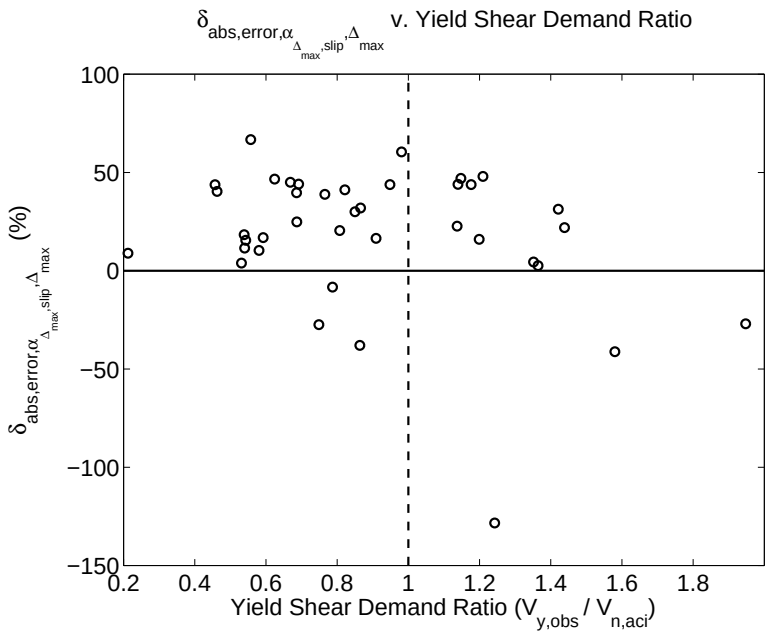

Figure N.269: Effective Shear Calibrated to Max Displacement With Slip Max Displacement Absolute Error Change v. Yield Shear Demand Ratio

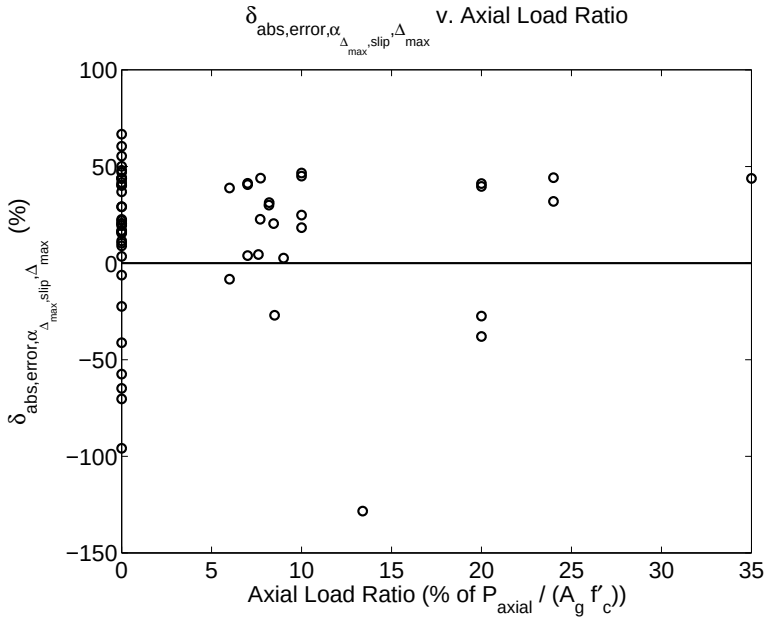

Figure N.270: Effective Shear Calibrated to Max Displacement With Slip Max Displacement Absolute Error Change v. Axial Load Ratio

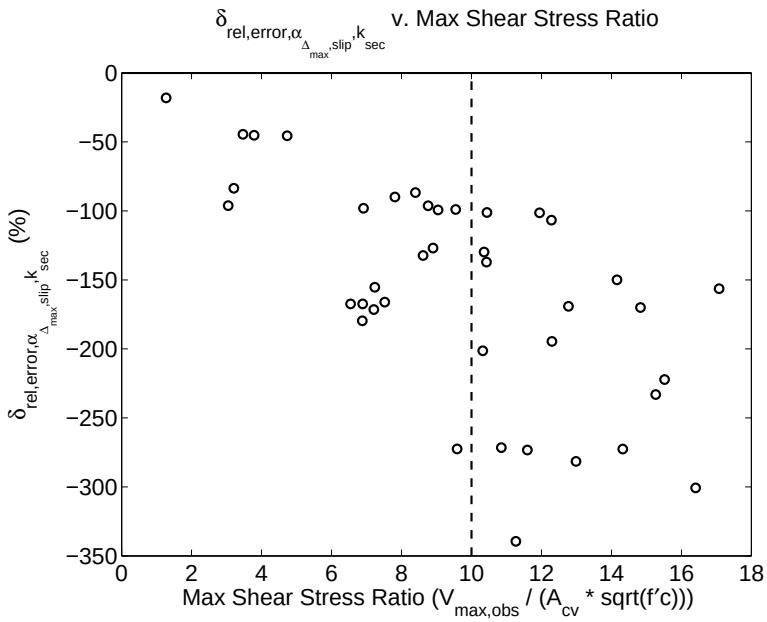

Figure N.271: Effective Shear Calibrated to Max Displacement With Slip Secant Stiffness Relative Error Change v. Max Shear Stress Ratio

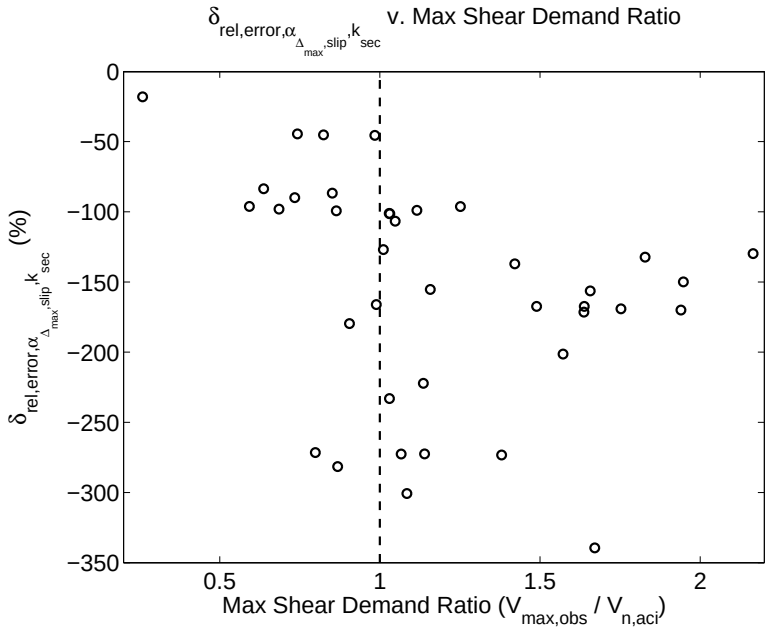

Figure N.272: Effective Shear Calibrated to Max Displacement With Slip Secant Stiffness Relative Error Change v. Max Shear Demand Ratio

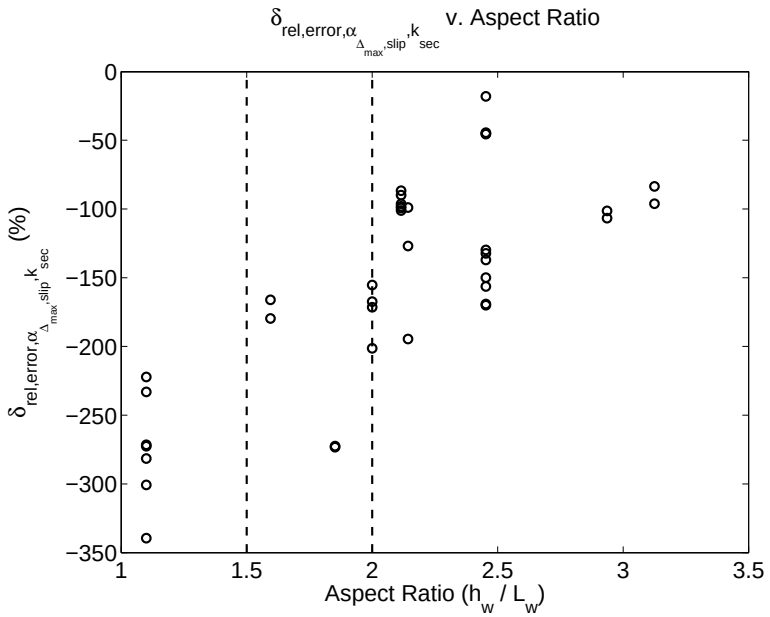

Figure N.273: Effective Shear Calibrated to Max Displacement With Slip Secant Stiffness Relative Error Change v. Aspect Ratio

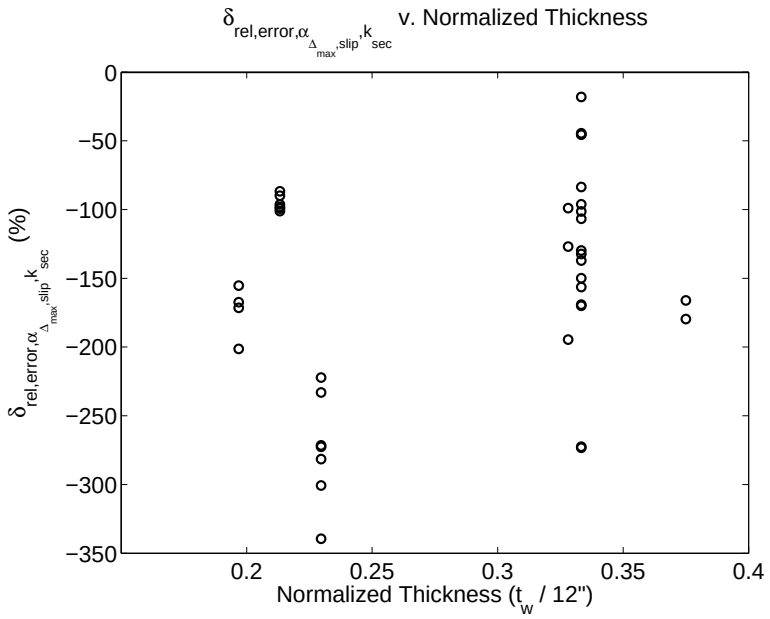

Figure N.274: Effective Shear Calibrated to Max Displacement With Slip Secant Stiffness Relative Error Change v. Normalized Thickness

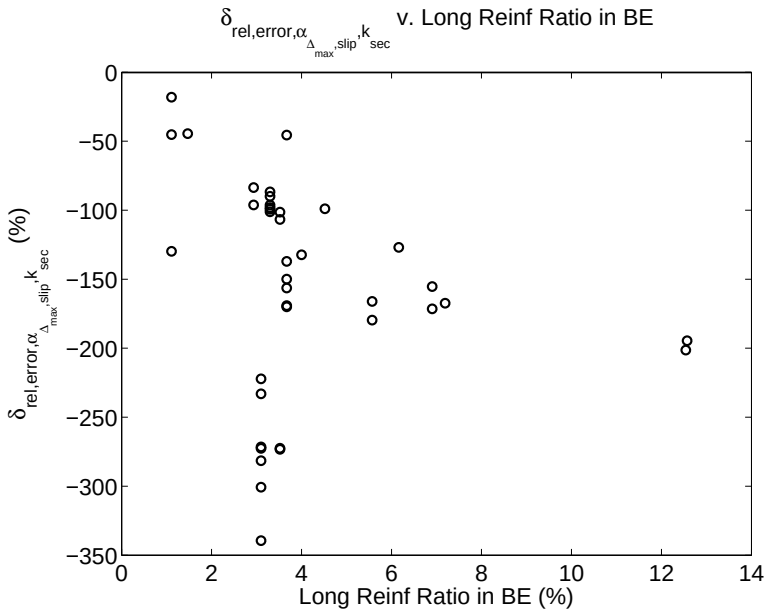

Figure N.275: Effective Shear Calibrated to Max Displacement With Slip Secant Stiffness Relative Error Change v. Long Reinf Ratio in BE

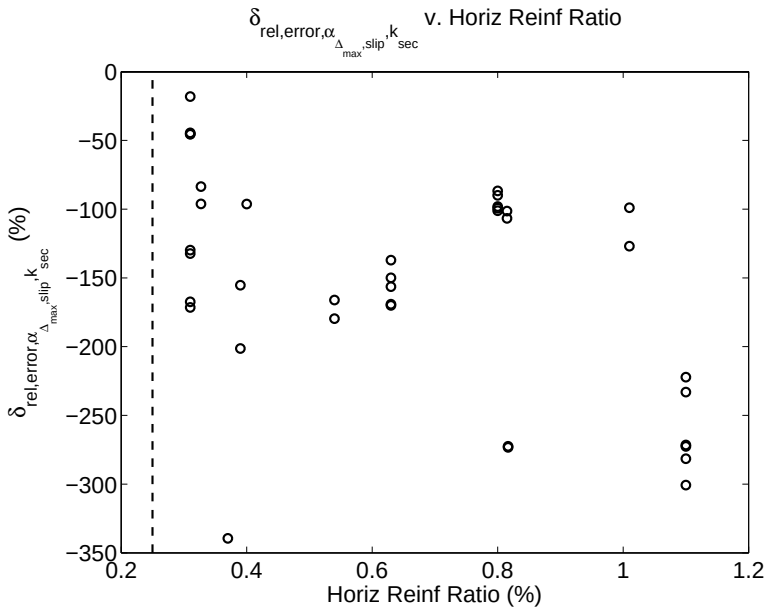

Figure N.276: Effective Shear Calibrated to Max Displacement With Slip Secant Stiffness Relative Error Change v. Horiz Reinf Ratio

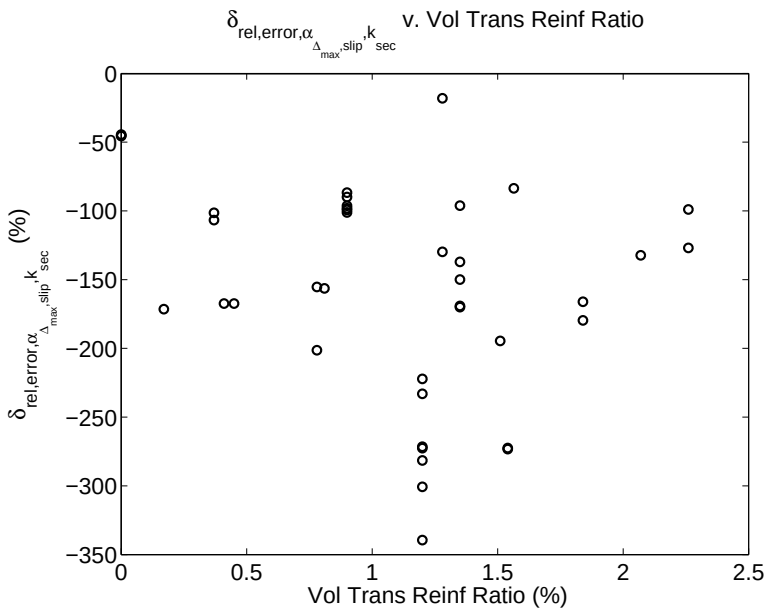

Figure N.277: Effective Shear Calibrated to Max Displacement With Slip Secant Stiffness Relative Error Change v. Vol Trans Reinf Ratio

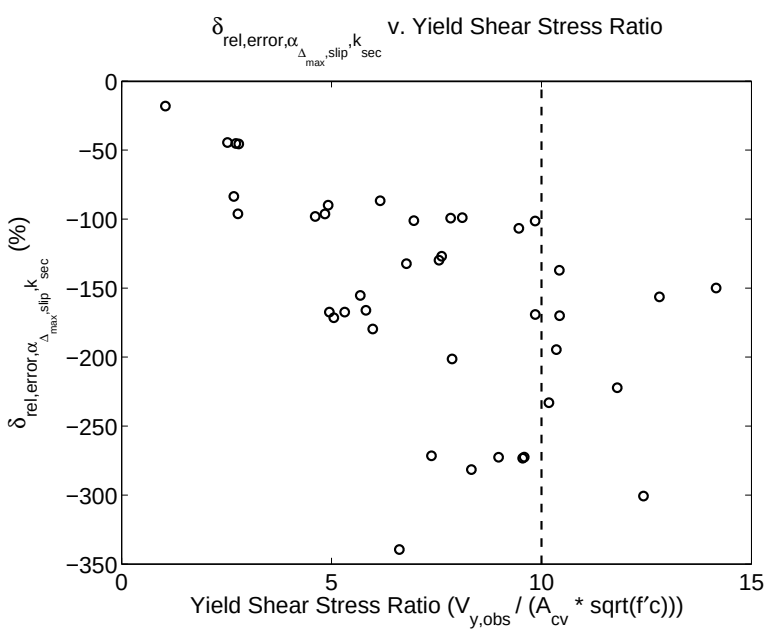

Figure N.278: Effective Shear Calibrated to Max Displacement With Slip Secant Stiffness Relative Error Change v. Yield Shear Stress Ratio

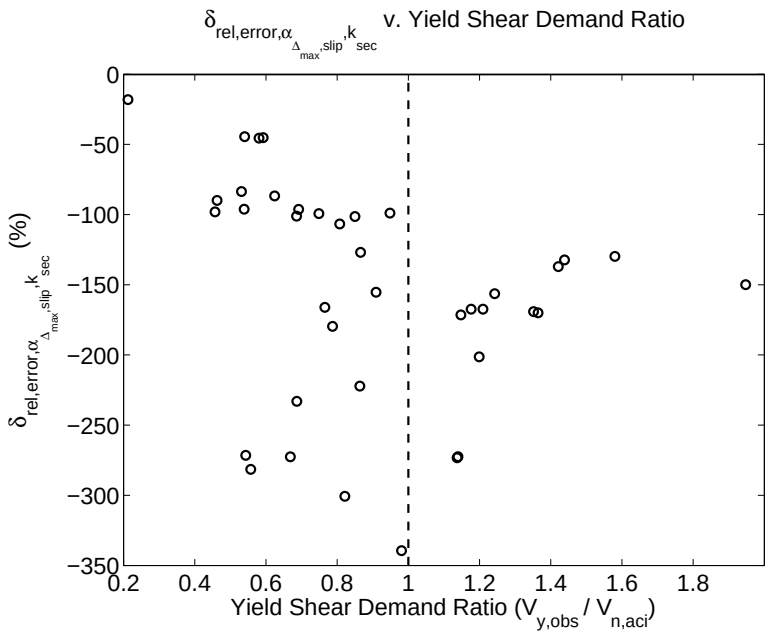

Figure N.279: Effective Shear Calibrated to Max Displacement With Slip Secant Stiffness Relative Error Change v. Yield Shear Demand Ratio

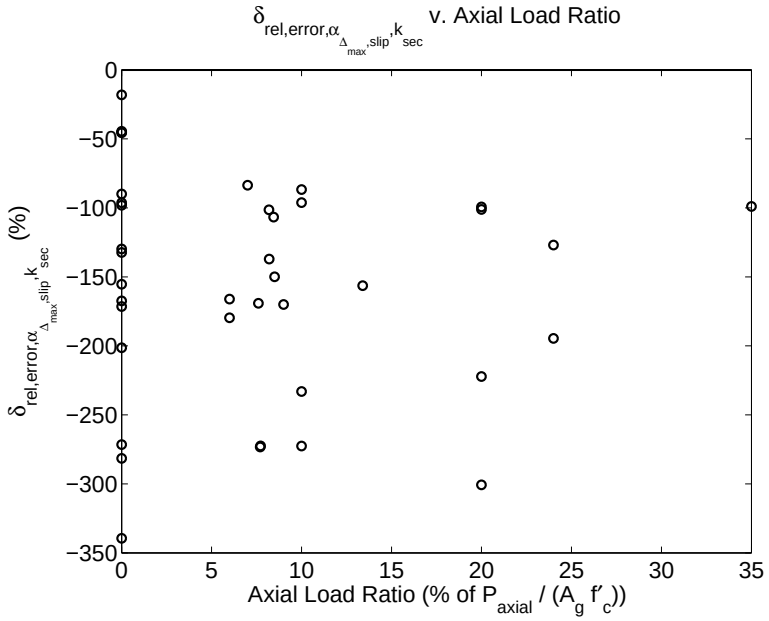

Figure N.280: Effective Shear Calibrated to Max Displacement With Slip Secant Stiffness Relative Error Change v. Axial Load Ratio

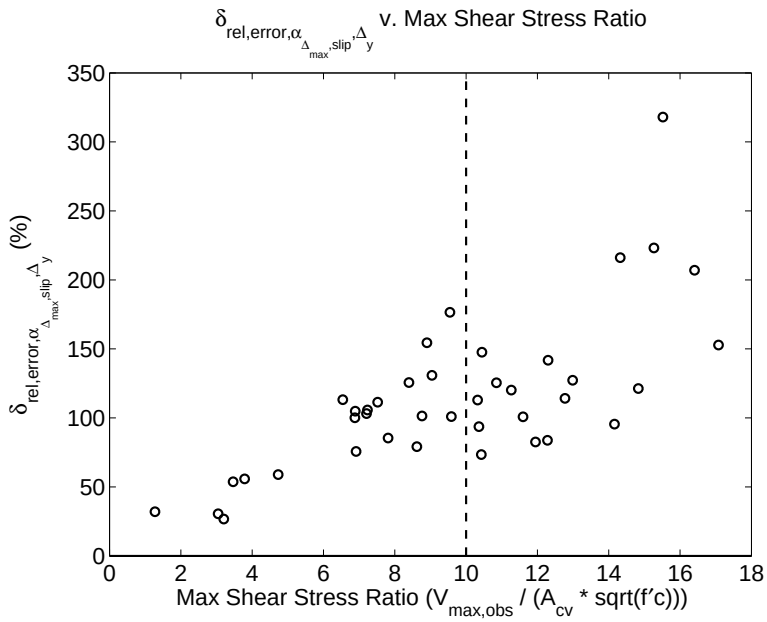

Figure N.281: Effective Shear Calibrated to Max Displacement With Slip Yield Displacement Relative Error Change v. Max Shear Stress Ratio

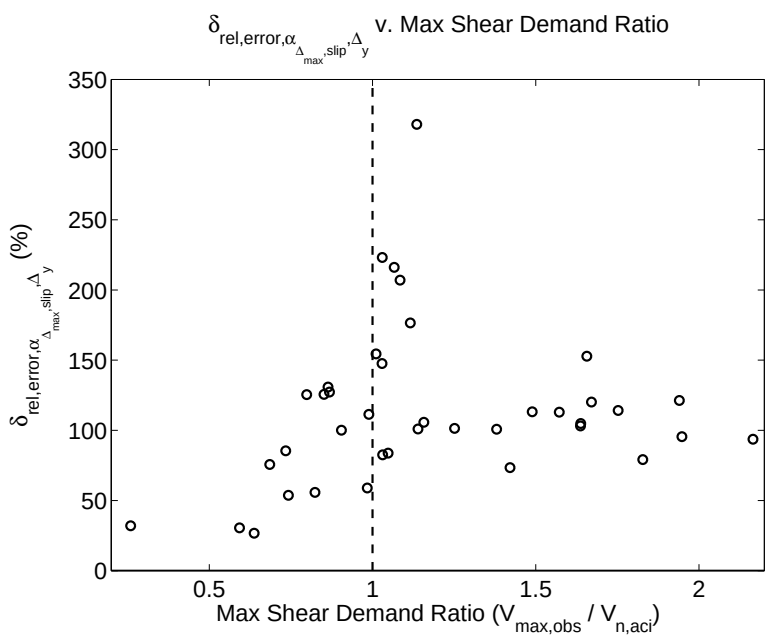

Figure N.282: Effective Shear Calibrated to Max Displacement With Slip Yield Displacement Relative Error Change v. Max Shear Demand Ratio

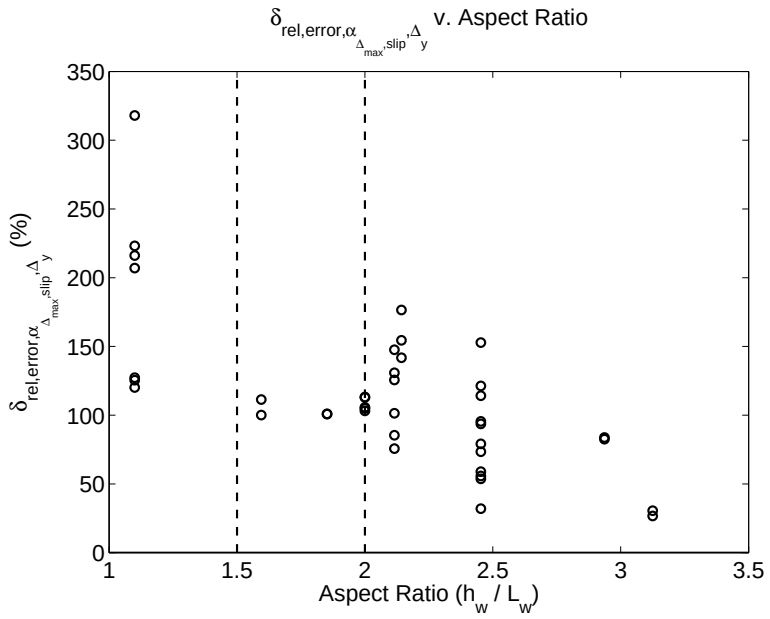

Figure N.283: Effective Shear Calibrated to Max Displacement With Slip Yield Displacement Relative Error Change v. Aspect Ratio

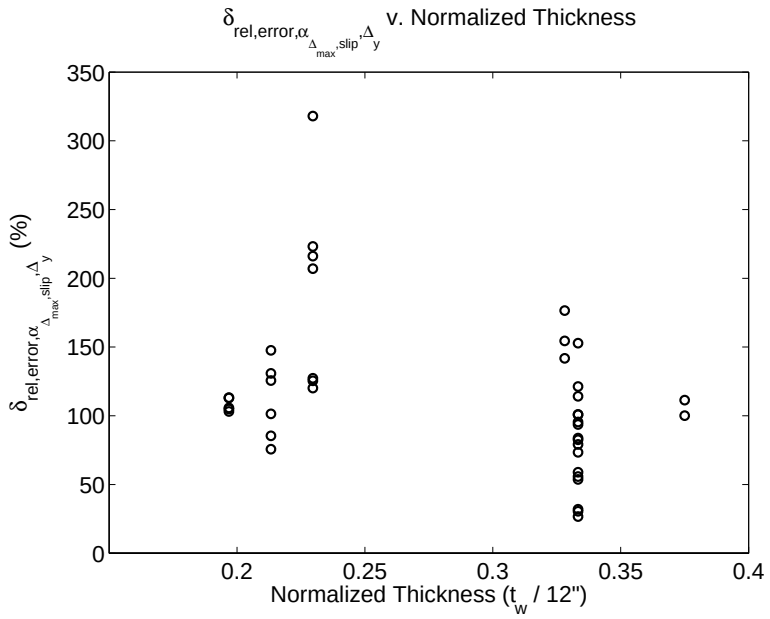

Figure N.284: Effective Shear Calibrated to Max Displacement With Slip Yield Displacement Relative Error Change v. Normalized Thickness

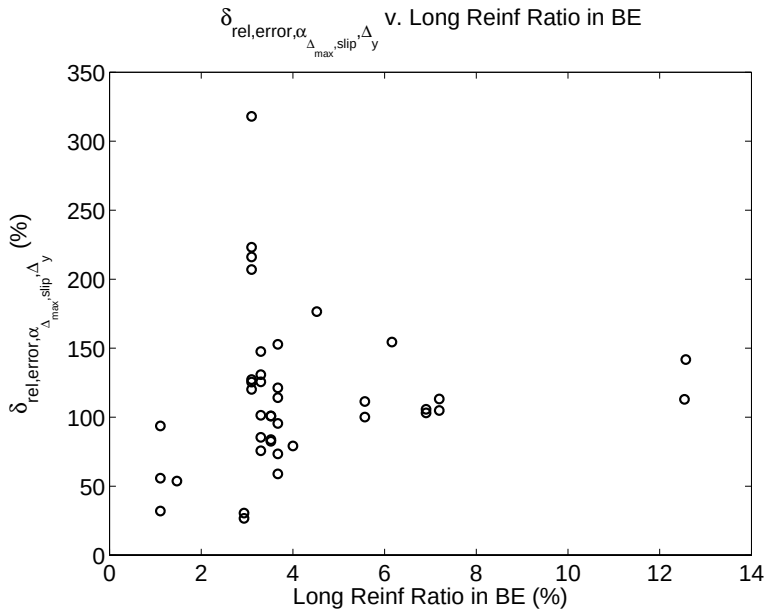

Figure N.285: Effective Shear Calibrated to Max Displacement With Slip Yield Displacement Relative Error Change v. Long Reinf Ratio in BE

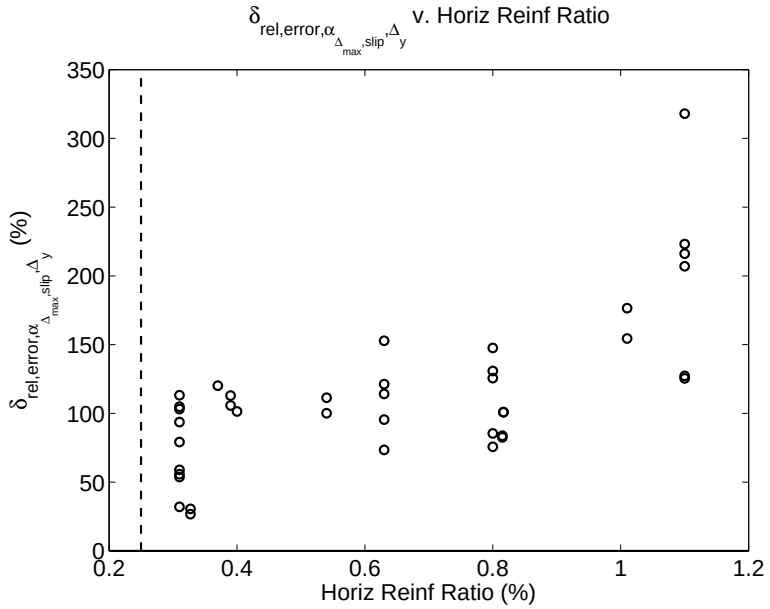

Figure N.286: Effective Shear Calibrated to Max Displacement With Slip Yield Displacement Relative Error Change v. Horiz Reinf Ratio

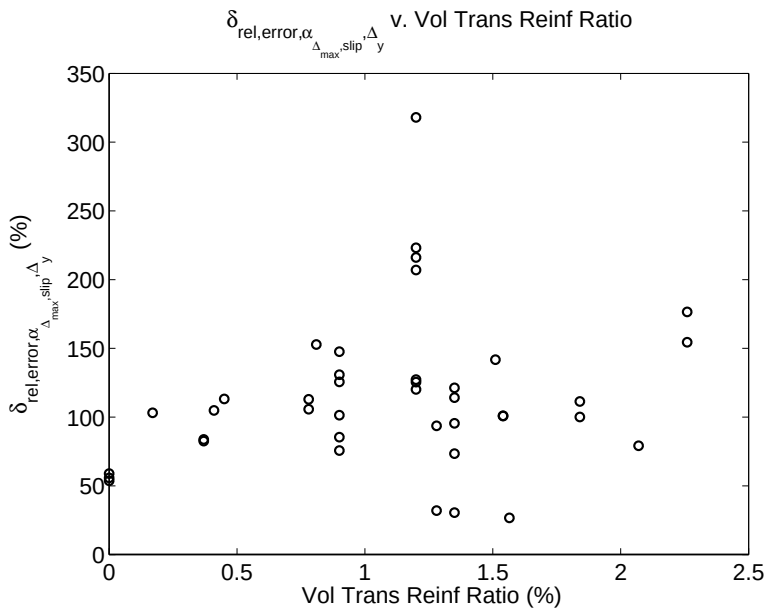

Figure N.287: Effective Shear Calibrated to Max Displacement With Slip Yield Displacement Relative Error Change v. Vol Trans Reinf Ratio

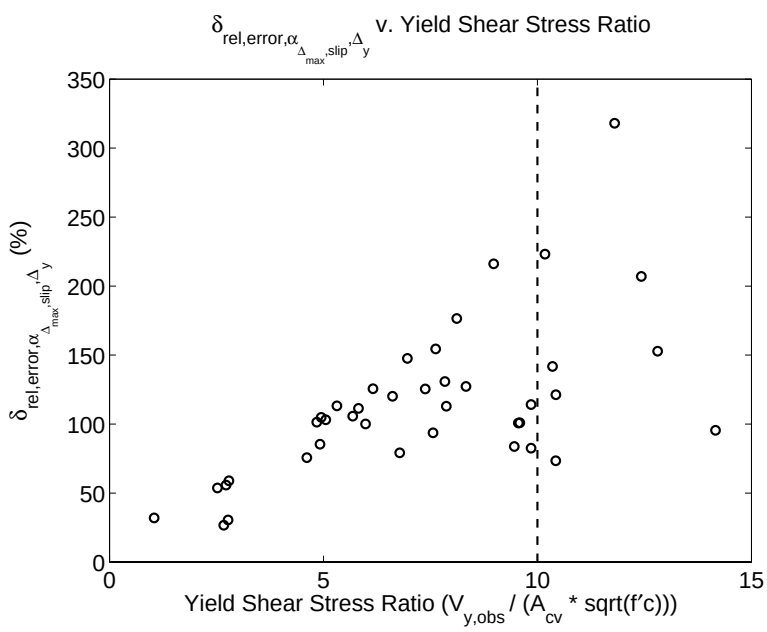

Figure N.288: Effective Shear Calibrated to Max Displacement With Slip Yield Displacement Relative Error Change v. Yield Shear Stress Ratio

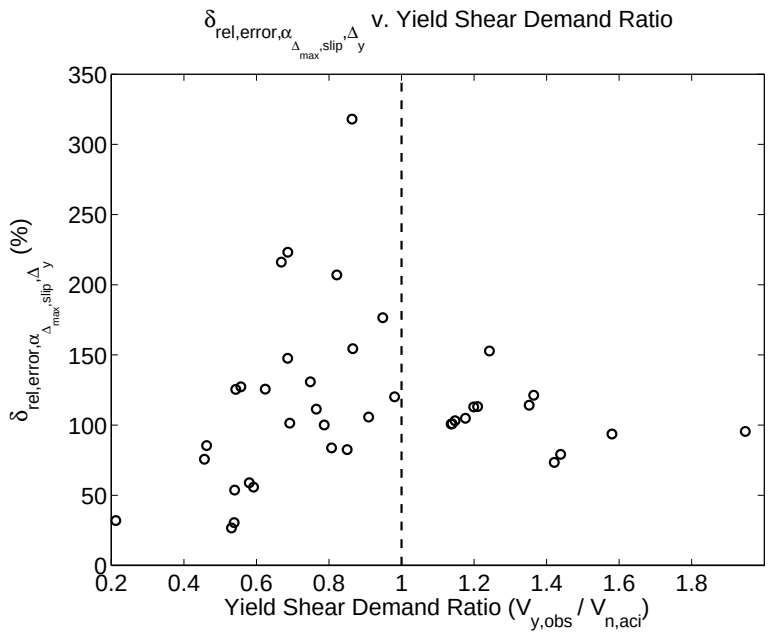

Figure N.289: Effective Shear Calibrated to Max Displacement With Slip Yield Displacement Relative Error Change v. Yield Shear Demand Ratio

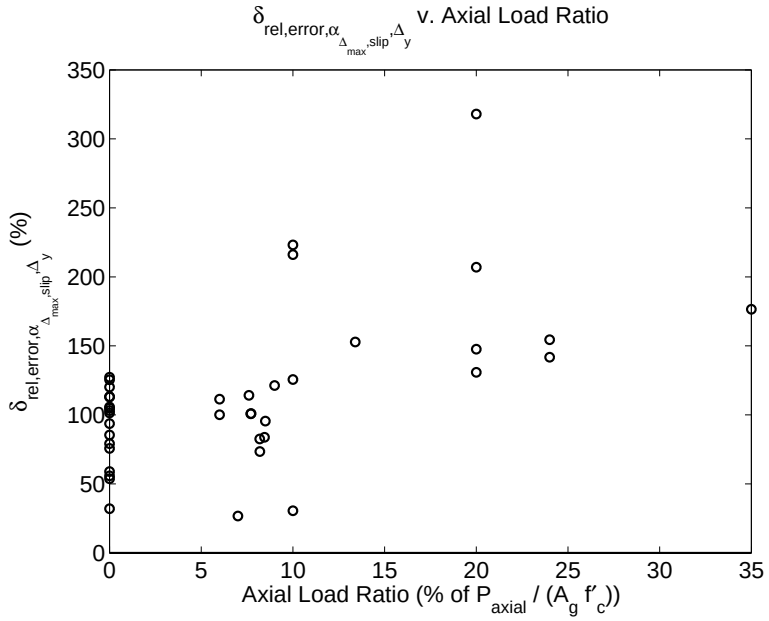

Figure N.290: Effective Shear Calibrated to Max Displacement With Slip Yield Displacement Relative Error Change v. Axial Load Ratio

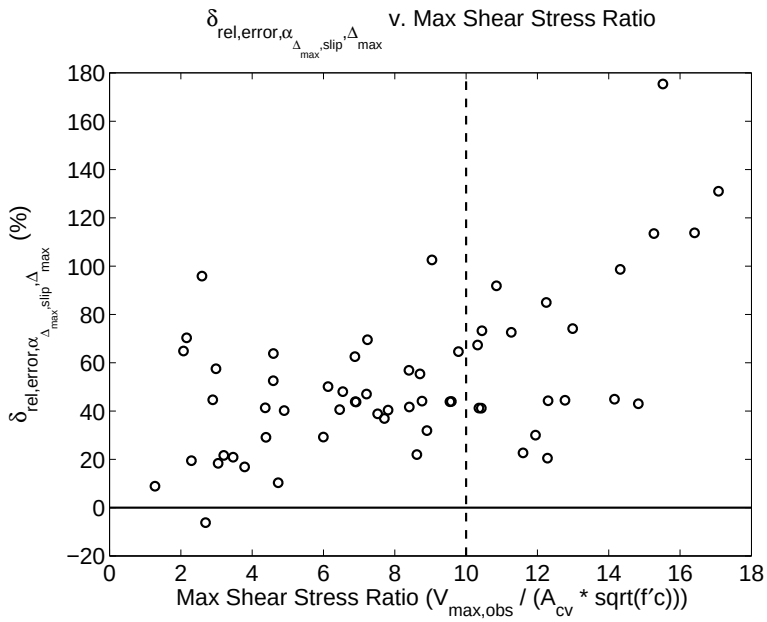

Figure N.291: Effective Shear Calibrated to Max Displacement With Slip Max Displacement Relative Error Change v. Max Shear Stress Ratio

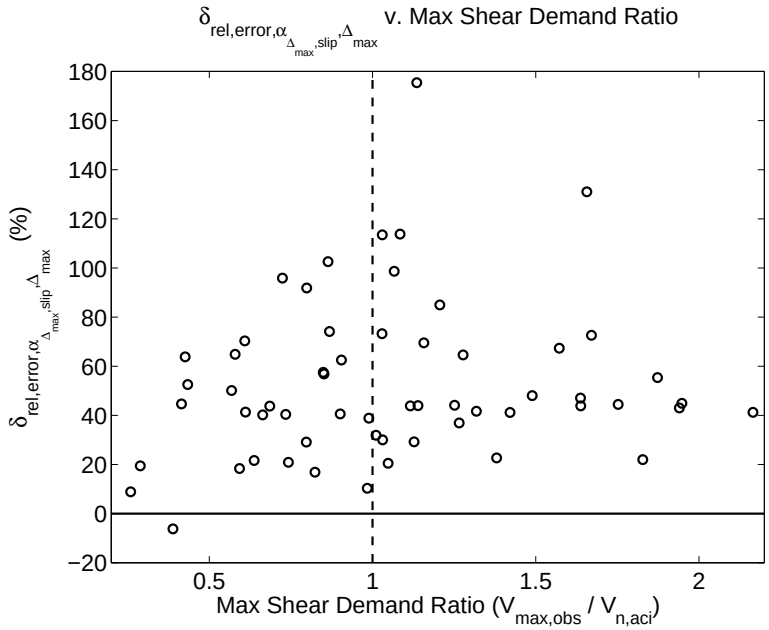

Figure N.292: Effective Shear Calibrated to Max Displacement With Slip Max Displacement Relative Error Change v. Max Shear Demand Ratio

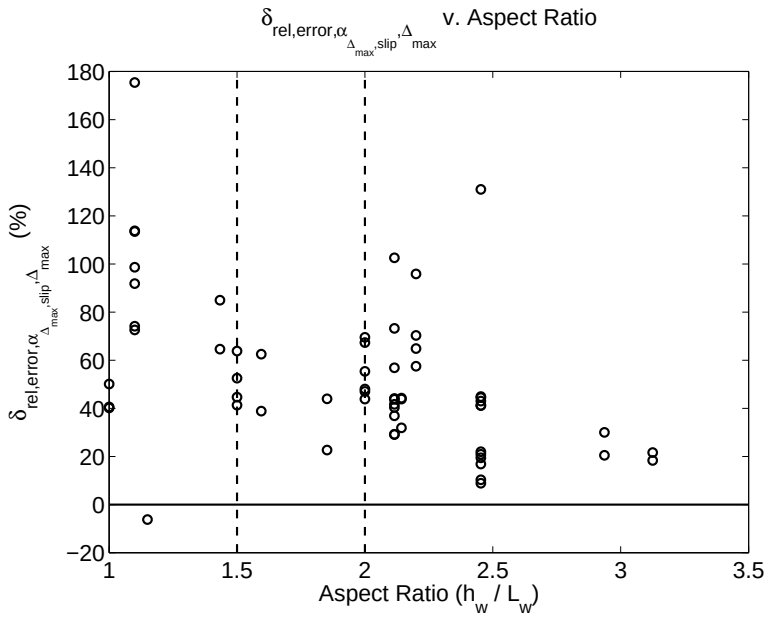

Figure N.293: Effective Shear Calibrated to Max Displacement With Slip Max Displacement Relative Error Change v. Aspect Ratio

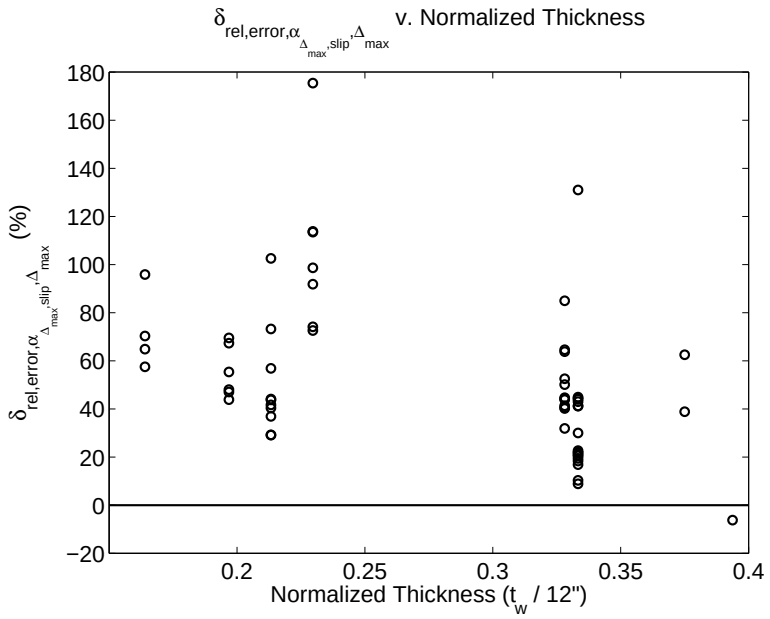

Figure N.294: Effective Shear Calibrated to Max Displacement With Slip Max Displacement Relative Error Change v. Normalized Thickness

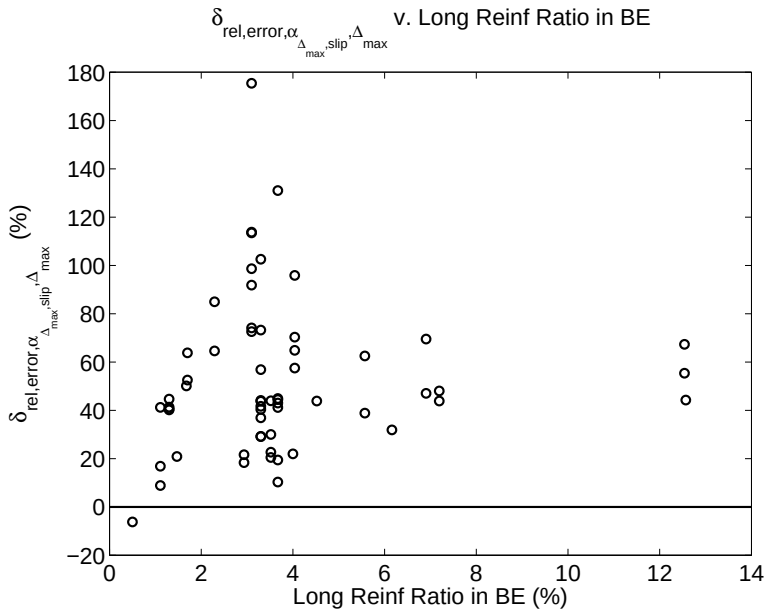

Figure N.295: Effective Shear Calibrated to Max Displacement With Slip Max Displacement Relative Error Change v. Long Reinf Ratio in BE

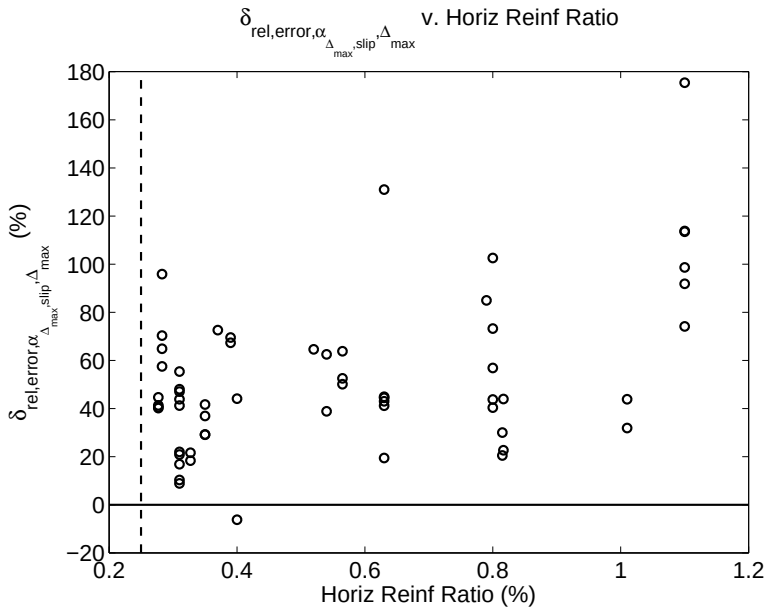

Figure N.296: Effective Shear Calibrated to Max Displacement With Slip Max Displacement Relative Error Change v. Horiz Reinf Ratio

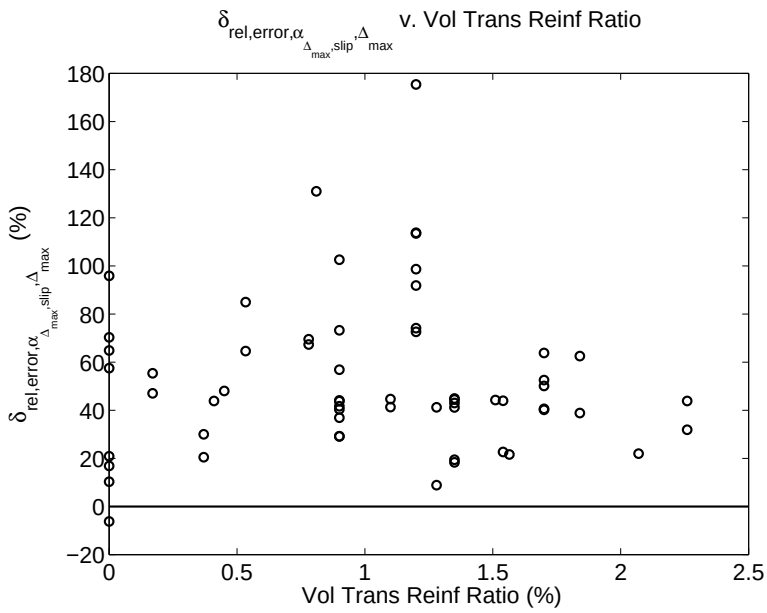

Figure N.297: Effective Shear Calibrated to Max Displacement With Slip Max Displacement Relative Error Change v. Vol Trans Reinf Ratio

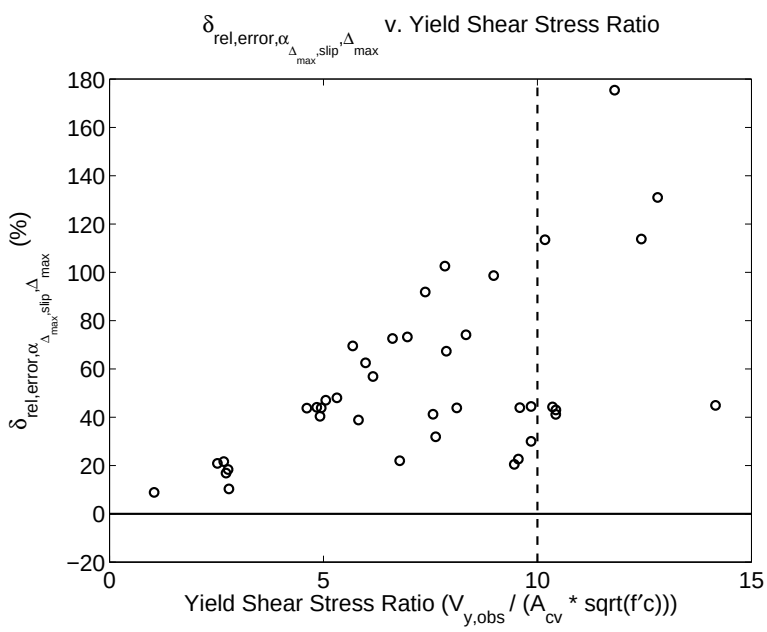

Figure N.298: Effective Shear Calibrated to Max Displacement With Slip Max Displacement Relative Error Change v. Yield Shear Stress Ratio

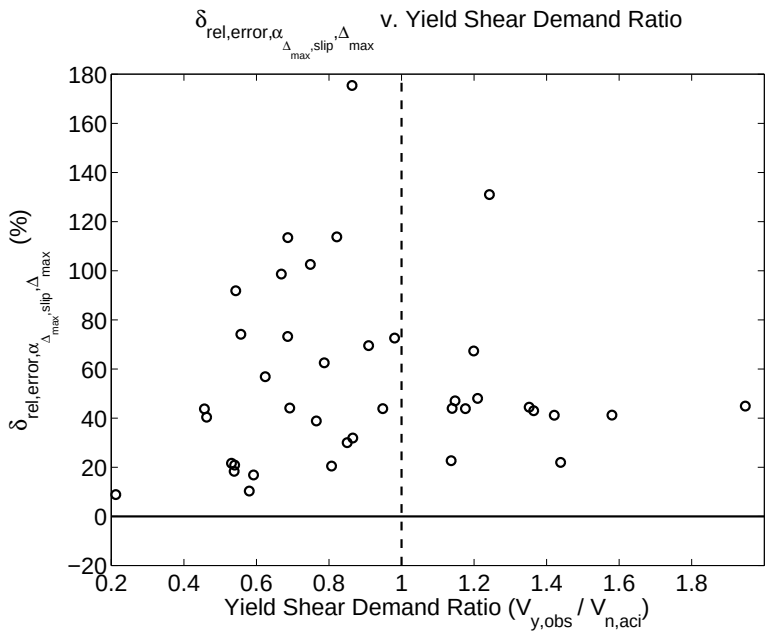

Figure N.299: Effective Shear Calibrated to Max Displacement With Slip Max Displacement Relative Error Change v. Yield Shear Demand Ratio

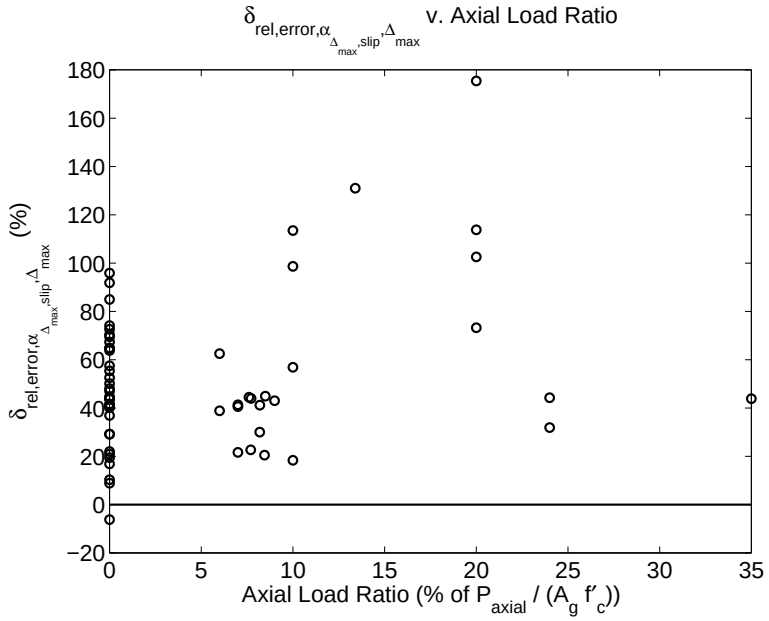

Figure N.300: Effective Shear Calibrated to Max Displacement With Slip Max Displacement Relative Error Change v. Axial Load Ratio